Table 44. Identification of B lineage cells in spleen

Subpopulation	Marker combination	References
T1	$B220^{pos}$ / $CD21^{low}$/ $CD23^{low/neg}$ / $IgD^{low/neg}$ / IgM^{high}	[1134, 1144, 1145]
	$B220^{pos}$ / $CD23^{neg}$ / IgM^{high} / $AA4.1^{pos}$	[1116]
T2	$B220^{pos}$ / $CD21^{high}$ / $CD23^{pos}$/ $IgD^{low/neg}$ / IgM^{high}	[1134]
	$B220^{pos}$ / $CD23^{pos}$ / IgM^{high} / $AA4.1^{pos}$	[1116]
	$B220^{pos}$ / $CD21^{high}$ / $CD23^{pos}$ / IgD^{high} / IgM^{high}	[1144]
T3	$B220^{pos}$ / $CD23^{pos}$ / IgM^{low} / $AA4.1^{pos}$	[1116]
FO	$B220^{pos}$ / $CD21^{intmed}$ / $CD23^{high}$ / IgD^{pos} / IgM^{intmed}	[1133, 1134]
	$B220^{high}$ / $CD23^{pos}$ / IgM^{low} / $AA4.1^{neg}$	[1132]
	$CD19^{intmed}$ / $CD1d^{intmed}$ / $CD23^{pos}$ / $CD43^{neg}$ / IgM^{low} / IgD^{high} / $CD5^{neg}$	[1146]
MZ	$B220^{pos}$ / $CD21^{high}$ / $CD23^{low/neg}$ / $IgD^{low/neg}$ / IgM^{high}	[1133, 1134, 1144]
	$CD9^{pos}$ / $CD21^{pos}$ / $CD23^{neg}$ / IgD^{low} / IgM^{high}	[1132]
	$CD19^{intmed}$ / $CD1d^{high}$ / $CD21^{high}$ / $CD23^{neg}$ / $CD43^{neg}$ / IgM^{high} / IgD^{low} / $CD5^{neg}$	[1146, 1147]
B-1	IgM^{high} / $CD43^{pos}$ / $IgD^{low/neg}$ / $CD23^{low/neg}$	[1132]
	$CD19^{pos}$ / $B220^{low}$ / $CD43^{pos}$ / $CD23^{neg}$ / $AA4.1^{neg}$	[1118, 1148]
B-1a	$CD19^{pos}$ / IgM^{pos} / $CD43^{pos}$ / $CD5^{pos}$	[1149, 1150]
	$CD19^{high}$ / $CD1d^{intmed}$ / $CD23^{neg}$ / $CD43^{pos}$ / IgM^{high} / IgD^{low} / $CD5^{pos}$	[1146]
B-1b	$CD19^{pos}$ / IgM^{pos} / $CD43^{pos}$ / $CD5^{neg}$	[1149]
	$CD19^{high}$ / $CD1d^{intmed}$ / $CD23^{neg}$ / $CD43^{pos}$ / IgM^{high} / IgD^{low} / $CD5^{neg}$	[1146]
Memory	$antigen^{pos}$, $CD73^{low}$ / $CD80^{low}$ / $CD273^{low}$	[1138–1143]
	$antigen^{pos}$, $CD73^{hi}$ / $CD80^{hi}$ / $CD273^{hi}$	
	$antigen^{pos}$, $CD73^{hi}$ / $CD80^{low}$ / $CD273^{low}$	
	$antigen^{pos}$, $CD73^{low}$ / $CD80^{hi}$ / $CD273^{hi}$	
	*$antigen^{pos}$, $CD73^{hi}$ / $CD80^{low}$	
GC	$CD19^{pos}$ / $B220^{pos}$ / $CD38^{neg}$ / $GL7^{pos}$	[1151, 1152]
	$B220^{pos}$ / $GL7^{pos}$ / Fas^{pos}	[1134]
	$B220^{pos}$ / $GL7^{pos}$ / PNA^{pos}	[1153]

*$Antigen^{pos}$ = cells are specific for the immunizing (memory) antigen

the binding of the BCR to its cognate antigen, allowing the B cells to acquire higher affinity. The process of class switch recombination (CSR), also known as isotype switching, is mediated by the same enzyme and leads to the replacement of the Cμ heavy chain by either Cγ, Cε, or Cα, resulting in the expression of IgG, IgE, or IgA, respectively [1182].

The selection of B cell clones with enhanced affinity to their cognate antigen occurs in the LZ of the GC and is mediated

Table 45. Identification of regulatory B cell subsets[a)]

Subpopulation	Marker combination	References
Breg	$CD5^{pos}$ / $CD19^{high}$ / $CD1d^{high}$ / $CD21^{high/intmed}$ / $CD23^{pos/neg}$ / $CD43^{neg}$ / IgM^{high} / $IgD^{low/intmed}$	[1146]
T2-MZP	$CD19^{pos}$ / $CD21^{high}$ / $CD23^{high}$ / IgM^{high} / HSA^{high} / $CD1d^{high}$ /IL-10 ^{pos}	[1162, 1168, 1169]
MZ	$CD19^{pos}$ / $CD21^{high}$ / $CD23^{neg}$ / IL-10^{pos}	[1170, 1171]
B10	$CD5^{pos}$ / $CD1d^{high}$ / $CD19^{pos}$ / IL-10^{pos}	[1156, 1163, 1172]
Tim-1^{+} cells	Tim-1^{pos} / $CD19^{pos}$ / IL-10^{pos}	[1173, 1174]
Plasma cells	$CD138^{pos}$ / $B220^{pos}$ / MHC-II^{low} / IL-10^{pos}	[1164, 1166]
Plasmablasts	$CD138^{pos}$ / $CD44^{high}$ / IL-10^{pos}	[1165]
Natural regulatory PCs	$CD19^{pos/neg}$ / $B220^{neg}$ / LAG-3^{pos} / $CD138^{high}$ / IL-10^{pos}	[1167, 1175]

a)including "regulatory plasma cells"

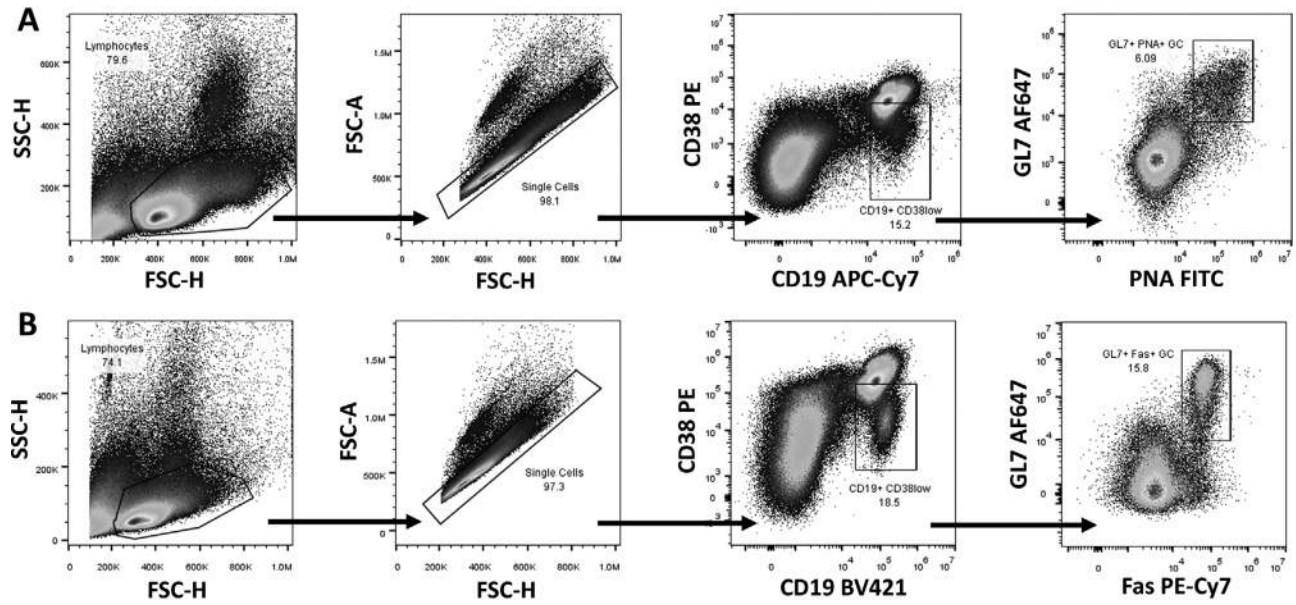

Figure 141. Two gating strategies for the identification of murine splenic GC B cells from single cell suspensions by flow cytometry. C57BL/6 mice were immunized with sheep red blood cells (SRBC) and analyzed on d10 post-immunization. In (A) GC B cells were stained as being $CD19^+$ $CD38^{low}$ and $GL7^+$ PNA^+. In (B) GC B cells were stained as being $CD19^+$ $CD38^{low}$ and $GL7^+$ Fas^+. Both variants unambiguously help to identify GC B cells.

by two cell types: follicular dendritic cells (FDCs) capture antigen in the form of immune complexes that is presented to B cells [1183]. Antigen-specific B cells internalize antigen and load it onto MHCII peptides for the presentation to T follicular helper (T_{fh}) cells. Besides FDCs, these are the other class of cells that mediate selection of high-affinity B cell clones. It has been proposed that peptide-MHCII density on GC B cells is the limiting factor that leads to positive survival signals by T_{fh} cells [1179]—that means the higher the affinity of the BCR of the B cell, the more antigen it will capture, internalize and finally present to T_{fh} cells. However, Yeh et al. have shown that halving peptide-MHCII density on B cells does not alter selection of high-affinity B cell clones but rather their initial entry into early GCs [1184] and therefore the precise mechanism for

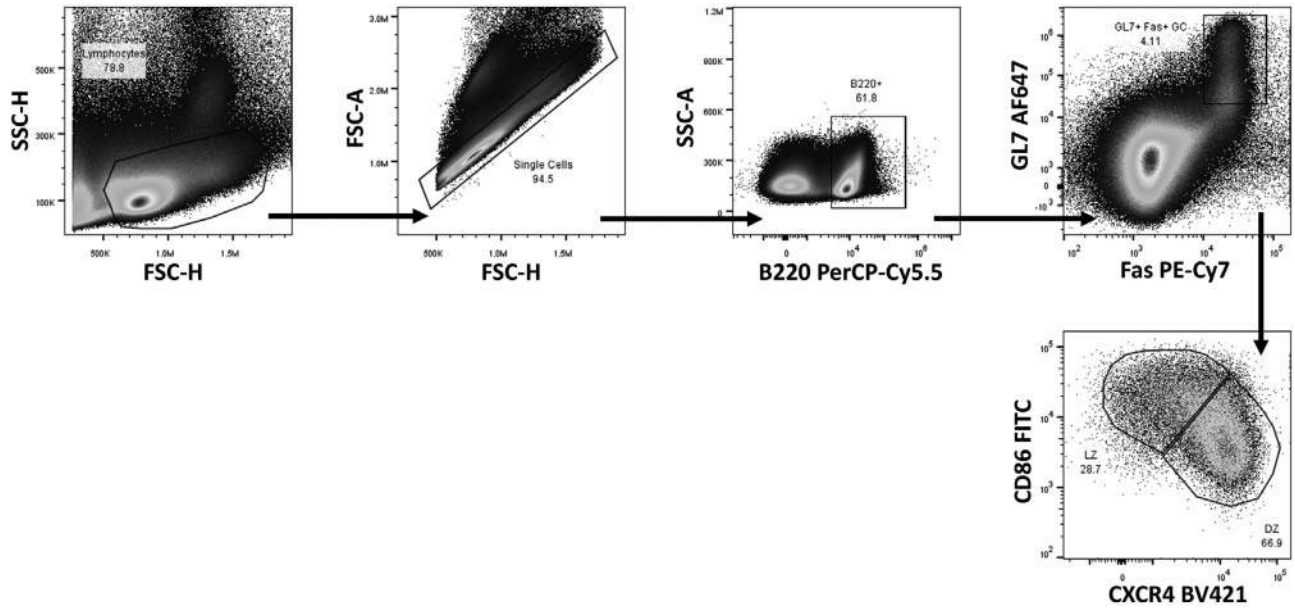

Figure 142. Staining of murine splenic GC B cells from single cell suspensions to identify GC subpopulations by flow cytometry. C57BL/6 mice were immunized with sheep red blood cells (SRBC) and analyzed on d10 post-immunization. The GC can be divided into the dark zone (DZ, $CXCR4^{hi}$ $CD86^{low}$) and the light zone (LZ, $CXCR4^{low}$ $CD86^{hi}$) and can be distinguished by their respective surface makers.

positive selection of high-affinity B cells within the LZ still remains unclear.

B cells can then either leave the GCs to become memory B cells [1185, 1186] or plasma cells [1187, 1188] or cycle back to the dark zone to undergo further rounds of division and somatic hypermutation to increase affinity even more [1189, 1190]. See also Chapter VI Sections 2.1 Murine B cells and their subsets, incl Breg cells and 3.1 Murine Ab-secreting plasmablasts and plasma cells.

2.2.3 Step-by-step sample preparation. For the generation of single cell splenocytes, spleens of mice were harvested and crushed through a 100 μM nylon mesh filter and finally resuspended in FCM buffer (PBS, 2% FCS, 2 mM EDTA). Lysis of erythrocytes was performed at room temperature for 5 min, cells were washed two times and Fc-blocking solution was added (20 min at 4°C). Finally, cells were incubated with FCM buffer containing respective directly conjugated Abs (20 min at 4°C) and resuspended in FCM buffer for analysis. All centrifugation steps were performed at 400 × *g* and 4°C for 8 min.

2.2.4 Materials. FCM buffer: PBS (137 mM NaCl + 2.7 mM KCl + 4.3 mM Na_2HPO_4 + 1.4 mM KH_2PO_4, pH 7.3), 2% FCS (PAN Biotech), 2 mM EDTA (Lonza).

Erythrocyte lysis buffer: 0.15 M NH_4Cl, 0.02 M HEPES, 0.1 mM EDTA.

Fc-blocking solution: CD16/32 mAb (clone 2.4G2, Hölzel Diagnostika) in FCM buffer.

Antibodies: Anti-mouse Abs that were used for FCM analysis: CD19 APC-Cy7 (clone 1D3, BioLegend), CD19 BV421 (clone 6D5, BioLegend), B220 PerCP-Cy5.5 (clone RA3-6B2, BioLegend), CD38 PE (clone 90, BioLegend), PNA FITC (Vector Laboratories), GL7 AF647 (clone GL7, BioLegend), Fas PE-Cy7 (clone Jo2, BD Biosciences), CD86 FITC (clone GL1, eBioscience), and CXCR4 BV421 (clone, L276F12, BioLegend). FCM analysis was performed on a Cytoflex instrument (Beckman Coulter) and FlowJo v10.5.3 analysis software (FlowJo, LLC).

2.2.5 Data analysis: Germinal Center B cells. Although the sample preparation leads to a single cell suspension, doublets can occur through cell–cell interactions (which can be reduced by adding EDTA to the FCM buffer) and can be easily excluded from the analysis by a plot that shows FSC Height versus Area (Fig. 141A). The lymphocytes gate should not be too stringent, as GC B cells tend to be larger in size. In order to stain for murine GC B cells, we suggest to use the markers CD19 or B220, CD38, GL7, and either PNA (Fig. 141A) or Fas (Fig. 141B). (See also Chapter VI Section 2.1, why to use CD19 or B220). In contrast to human GC B cells, murine GC B cells show reduced expression of the surface marker CD38 and can be gated accordingly [1191]. Here, it is important to set a larger gate for CD38 to not exclude any GC B cells, since these cells tend to have varying CD38 expression levels. Further, the rat mAb GL7 that reacts with a sialic acid glycan moiety called Neu5Ac [1152], previously reported as a marker for polyclonally activated B and T cells [1192], can be used in the staining protocol. In addition, the plant lectin peanut agglutinin (PNA) from *Arachis hypogaea* with specificity for terminal galactosyl residues on cell surface oligosaccharides [1193] has been shown to bind GC B cells and can be used to specifically identify these cells [1194–1196]. Instead of using PNA (see "pitfalls"), the Fas receptor (CD95, Apo-1) can be used to identify GC B cells (Fig. 141B), which is highly upregulated in these cells [1197].

With the mentioned four colors, CD19 or B220, CD38, GL7, and either PNA (Fig. 141A) or Fas (Fig. 141B), GC B cells can unambiguously be identified. Since GC B cells also downregulate IgD [1194, 1198, 1199], this is an additional marker that can be added to the staining protocol.

Pitfalls

One pitfall of the staining in Fig. 141A is that the PNA signal is downregulated quite fast if the time between staining and measurement of the samples is long (own observation). Constantly keeping samples on ice however helps to counteract this downregulation.

2.2.6 Data analysis: Germinal Center B cell subpopulations. The GC has a certain microanatomic structure that can be divided into the DZ, where B cell proliferation and somatic hypermutation take place, and a LZ, where selection of high-affine B cell clones occurs. In order to stain for these two zones, GC B cells are first stained as described in the section "Murine Germinal Center B cells" above (Fig. 141).

CD86 (also known as B7-2) is a surface protein that is expressed on activated B cells [1200, 1201] and has a costimulatory function for T cell proliferation [1202]. Together with the chemokine receptor CXCR4, that has been shown to be important for GC organization [1203], Victora et al. used the combination of CD86 and CXCR4 to differentiate DZ cells ($CXCR4^{hi}$ $CD86^{low}$) from LZ cells ($CXCR4^{low}$ $CD86^{hi}$) [1204]. The staining for DZ/LZ cells is shown in Fig. 142.

Pitfalls

A pitfall of this staining is the difficulty to set an accurate gate for the DZ/LZ, since these two populations are not clearly separable from each other by FCM. Especially if fluorochromes for CXCR4 and CD86 are used that are known for fluorescence spillover, proper compensation is very important to not distort DZ/LZ ratios. See also Chapter II Section 1 Compensation.

2.3 *Human B cells and their subsets*

2.3.1 Overview. B cells represent the Ab-producing cells developing from naïve B cells to Ab-secreting PC. One feature of B cells is their capacity to differentiate upon antigen dependent and independent stimulation to Ab secreting cells, also called plasma cells. The stages of B cell differentiation share several common features between the human and the rodent immune system. In this section, we focus on human B cells.

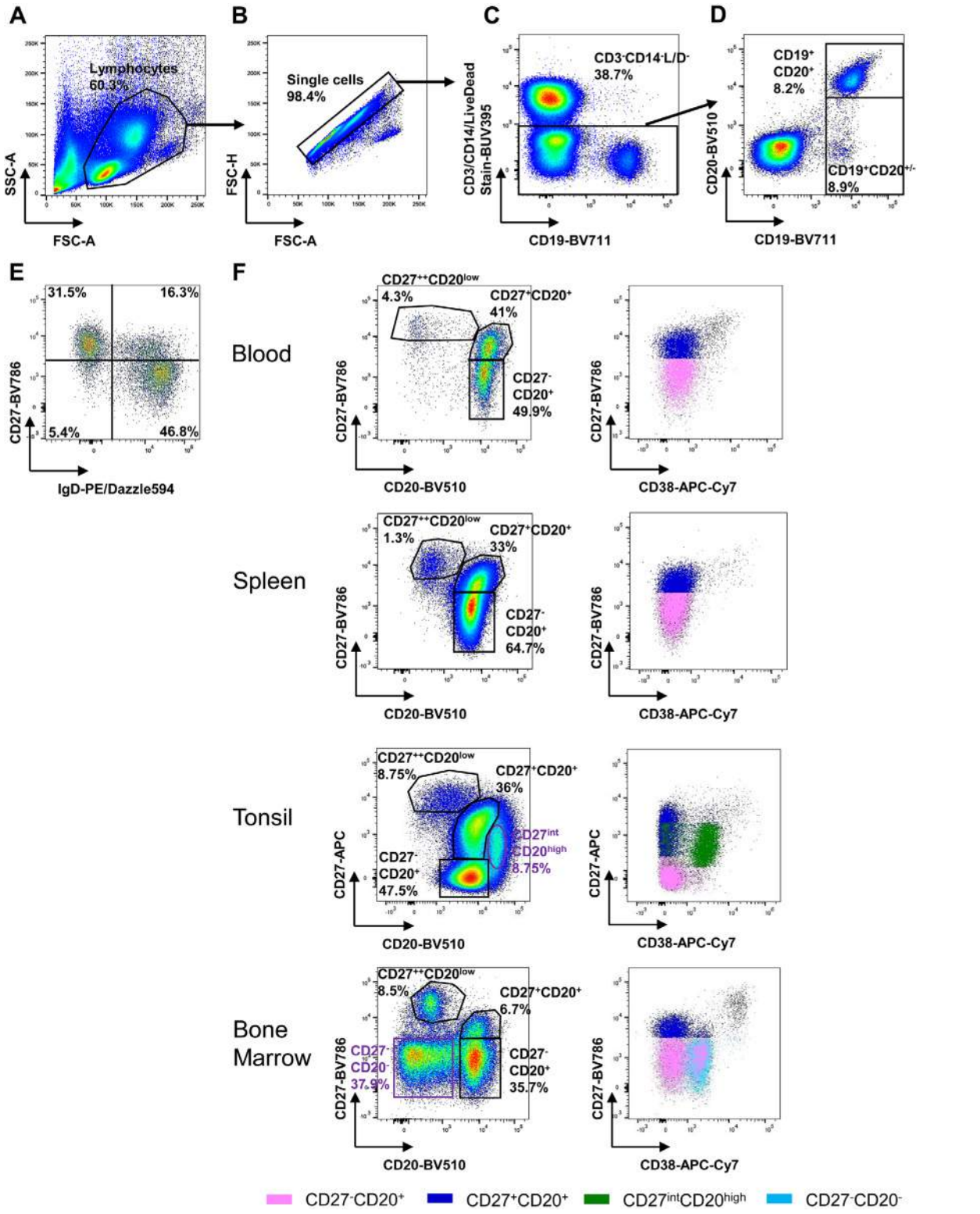

Figure 143. Gating strategy for the identification of human B cells. (A–E) Gating example for peripheral blood: (A) Lymphocytes are identified by their light scattering properties. (B) Exclusion of doublets. (C) Cells positive for CD3 and CD14 and DAPI stained dead cells are excluded. (D) B cells are identified by their expression of CD19 and CD20 including $CD20^{low}$ plasmablasts. (E) B cell subsets are discriminated by CD27 and IgD: $CD27^{-}IgD^{+}$ naïve B cells, $CD27^{+}IgD^{+}$ pre-switch memory B cells, $CD27^{+}IgD^{-}$ switched memory B cells, $CD27^{-}IgD^{-}$ B cells containing switched memory B cells. (F) B cell subsets discriminated by CD27 and CD20 in peripheral blood, spleen, tonsil, and bone marrow: conventional naive B cells are $CD27^{-}$ $CD20^{+}$ (containing $CD27^{-}$ memory B cells) memory B cells $CD27^{+}$ $CD20^{+}$ and plasmablasts $CD27^{++}$ $CD20^{low}$. Cell subsets defined by CD27 and CD20 expression were color-coded and depicted in a CD27 versus CD38 plot (pink: $CD27^{-}CD20^{+}$ B cells, dark blue: $CD27^{+}CD20^{+}$ B cells, green (only in tonsil): $CD27^{int}CD20^{high}$, turquois (only in bone marrow): $CD27^{-}CD20^{-}$).

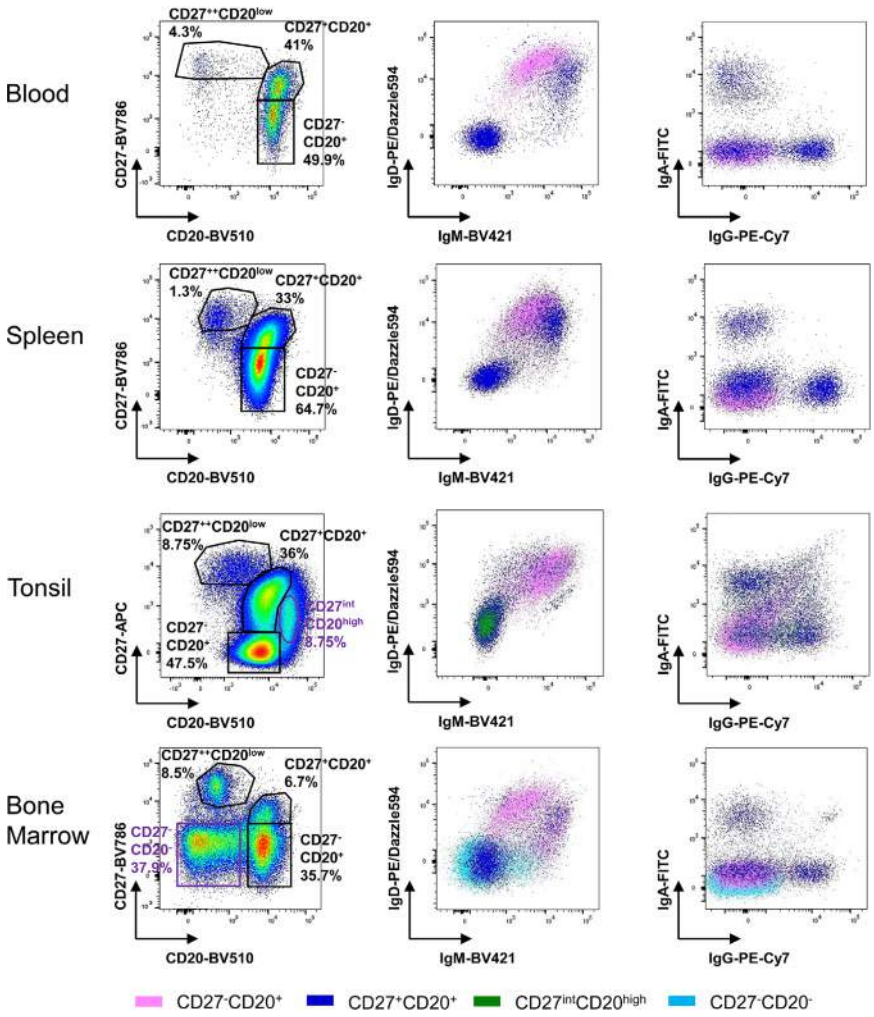

Figure 144. Ig isotype expression of B cell subsets in different human tissues. Gating strategy is the same as depicted in Figure 143A–D. B cell subsets discriminated by CD27 and CD20 in peripheral blood, spleen, tonsil and bone marrow: conventional naive B cells are $CD27^-$ $CD20^+$ (containing $CD27^-$ memory B cells) memory B cells $CD27^+$ $CD20^+$ and plasmablasts $CD27^{++}$ and $CD20^{low}$. Cell subsets defined by CD27 and CD20 expression were color-coded and depicted in a IgD versus IgM and IgA versus IgG plot to show Ig surface expression of each subset (pink: $CD27^-CD20^+$ B cells, dark blue: $CD27^+CD20^+$ B cells, green (only in tonsil): $CD27^{int}CD20^{high}$, turquois (only in bone marrow): $CD27^-CD20^-$).

2.3.2 Introduction. To identify B cells, the B cell specific molecules CD19 and/or CD20 serve as specific surface markers (Fig. 143). CD19 is a B cell surface molecule expressed at the time of immunoglobulin heavy chain rearrangement [1205], CD20 is expressed by all mature B cells beyond the pro B cell stage in the bone marrow and disappears on the surface of mature plasma cells [1206, 1207]. For further discrimination of B cell developmental stages, combinations of additional markers such as CD27, CD38, CD23, CD77, and expression of surface Igs are used. Immature $CD19^+$ B cells in the bone marrow express high levels of CD38 and variable levels of CD20 and IgM, which increase with their further differentiation (Figs. 143F and 144) [1208]. $CD38^{++}$ $CD20^{++}$ immature B cells express IgM and IgD, leave the bone marrow and become $CD38^{++}$ $CD24^{++}$ $CD10^+$ transitional B cells [1208]. Naïve B cells express IgM and IgD and are $CD27^-$ and $CD38^-$, they comprise about 60% of B cells in the peripheral blood (Figs. 143F and 144) [1209, 1210]. After antigen encounter and T cell help, memory B cells and Ab-secreting plasma cells are generated in the germinal center reaction. Human memory B cells (mBCs) can be identified by the expression of CD27 and carrying of mutated Ig VDJ gene rearrangements [1209, 1211]. In the peripheral blood, between 30 and 40% of circulating B cells express CD27 (Fig. 143F, Fig. 144) [1209, 1212]. PC carry distinct FSC and SSC characteristics, express high levels of CD27 and lack the expression of CD20 but are also highly positive for CD38 and partially $CD138^{++}$ [1213]. A $CD19^-$ PC population is uniquely enriched in the bone marrow [1214].

An alternative staining protocol of $CD20^+/CD19^+$ B cells has applied co-staining of CD38 and IgD together with CD77 and CD23 to mark differentiation stages of B cells in human tonsils [1215]. CD23 is a low-affinity Fcε receptor and associated with the activation of B cells. It was found to be co-expressed with IgM and IgD in the tonsil and in peripheral blood but not with IgA and IgG and hence is lost during isotype class-switching [1216]. CD77 is strongly expressed by germinal center B cells and can be used to differentiate centroblasts from centrocytes [1215, 1217]. In this protocol, naive IgD^+ $CD38^-$ B cells are separated by CD23 into Bm1 ($CD23^-$) and Bm2 ($CD23^+$) B cells. IgD^- $CD38^+$ germinal center B cells can be further discriminated into $CD77^+$ centroblasts (Bm3) and $CD77^-$ centrocytes (Bm4). IgD^- $CD38^-$ B cells comprise the memory compartment (Bm5).

The expression of IgD can be used as a marker to further discriminate certain naïve and memory B cell populations. $CD19^+$ $CD20^+$ B cells can be separated in a CD27 versus IgD dot plot (Fig. 143E). In this regard, naïve B cells express IgD and are $CD27^-$. Further quadrants represent different subsets of memory B cells: in detail, $CD27^+$ IgD^+ are memory B cells that mostly express high levels of IgM and carry somatic mutations of their V(D)J rearrangements, whereas $CD27^+$ IgD^- memory B cells are class-switched and also carry somatic mutations [1209]. Interestingly, the $CD27^-$ IgD^- B cell subset appears to be very heterogeneous and contains IgA- and IgG-expressing cells [1218, 1219]. It has been shown that this phenotypic population contains a memory B cell subset expressing CD95 with an activated phenotype, which is especially enhanced in patients with systemic lupus erythematosus (SLE) and correlated with disease activity and serologic abnormalities, whereas healthy donors only show minor frequencies of $CD95^+$ cells [1220]. Among other disturbances, B cells lacking expression of the complement receptor CD21, which is part of a signaling complex, together with CD19 have been reported to be expanded in patients with SLE [1221, 1222]. An overview of markers expressed on different B cell subsets can be found in Table 47.

2.3.3 Step-by-step sample preparation. Depending on the starting material, different methods for cell isolation can be applied. A common start is to isolate mononuclear cells (MNCs) by density gradient centrifugation (see also Chapter IV Section 1.2 Pre-enrichment by physical properties). When starting with tissue, a lysate of the minced material can be layered over the Ficoll (e.g., GE Healthcare) solution, when starting with blood, this is carried out with a mixture of blood and PBS according to the manufacturer's instructions. After collecting the MNC layer and subsequent washing steps, the number of isolated cells can be assessed and one can start with the staining procedure or further experiments. The washing buffer should be chosen according to the following experiments, for example PBS containing a carrier protein like BSA (e.g., 0.1–0.5%) for staining or medium for subsequent stimulation experiments. One should be aware that using EDTA in wash buffers might have an effect on following stimulation experiments by chelating calcium ions. For basic staining of B cells, $1–2 \times 10^6$ MNCs should suffice as input. For analysis of antigen-specific cells, a higher input number might be useful.

For further applications, enrichment of B cells, e.g., by MACS® technology (Miltenyi) might be necessary (see Chapter IV Section 1.3 Pre-enrichment by immunological properties). Depending on the experiment planned after enrichment, an approach with untouched cells of interest (negative selection) can be applied (e.g., B cell isolation kit II). If specific subpopulations are desired, a positive selection might be required. MACS® sorting gives high purities, nonetheless the purity check of the desired fraction by FCM staining should be performed.

A different approach for staining starting with peripheral blood is a lysis protocol of red blood cells (see also Chapter IV Section 2.5 Erythrocyte lysis, e.g., with BD PharmLyse, Qiagen EL buffer). After erythrocyte lysis and washing, the obtained cell suspension can be stained.

Depending on the application, blocking of Fc receptors can be useful prior to staining. One should be aware that Ig staining might not work after adding Fc blocking reagents to cell suspensions. Most manufacturers recommend surface staining at 4°C for 15–30 min but some molecules might require different staining conditions.

For intracellular staining, isolated MNCs can be lysed and permeabilized directly or after stimulation experiments to assess for example phosphorylation of intracellular proteins (see Chapter III Section 5: Cell fixation and permeabilization for flow cytometric analyses). There are different protocols and reagents available depending on the intracellular location of the antigen to be stained (e.g., BD, Biolegend, eBioscience and others). For antigens in the cytoplasm, a less harsh permeabilization buffer can be used than for example for antigens located in the nucleus. Blood or tissue lysates can also be prepared for intracellular staining directly (whole blood staining) by lysis and permeabilization and stained after washing steps. Twenty to 60 minutes at room temperature are frequently used for intracellular staining. One should be aware that some epitopes might be destroyed after lysis and permeabilization and thus may not be identified. This should be validated for each application.

2.3.4 Materials.

1. Ficoll Paque (GE Healthcare)
2. PBS (Biochrom)
3. Staining buffer (PBS/0,5% BSA/EDTA (Miltenyi autoMACS® Rinsing Solution/MACS® BSA Stock Solution))
4. Buffers for cell permeabilization (e.g., Phosflow Lyse/Fix Buffer (BD Biosciences), Phosflow Perm Buffer II (BD Biosciences))
5. Buffers for erythrocyte lysis (e.g., Lysing Buffer (BD PharmLyse ™ BD Biosciences, Buffer EL (Qiagen)),
6. Anti-Mouse Ig, κ/Negative Control Compensation Particles Set (BD Biosciences)
7. Live/Dead stain (e.g., DAPI (Molecular Probes) or LIVE/DEAD Fixable Dead Cell Stain Kit, (Invitrogen))
8. Instrument: LSR Fortessa X-20 (BD Biosciences)
9. Fluorescently labeled mAbs (Table 46):

2.3.5 Gating for human B cells subsets. After MNC preparation or lysing whole blood, lymphocytes should be gated according to their scatter properties and by the exclusion of doublets and dead cells from the analysis (Fig. 143A–C). In order to detect plasma cells simultaneously, the initial FSC/SSC gating should be larger and not limited to a conventional lymphocyte gate [1213].

When gating on $CD19^+$ B cells, $CD3^+$ T cells and $CD14^+$ monocytes need to be excluded. If these cells are not of further interest, they can be assigned to a so called "dump channel" with CD3 mAb and CD14 mAb together with other markers for cells that should be excluded from subsequent analyses, e.g., CD16/CD56

Table 46. Fluorescently labeled monoclonal antibodies used for the stainings in Figs. 143 and 144

Fluorophore	Marker	Manufacturer	Clone	Isotype
BUV395	CD3	BD	UCHT1	mouse IgG1κ
BUV395	CD14	BD	M5E2	mouse IgG2aκ
BV711	CD19	BD	SJ25C1	mouse IgG1κ
BV510	CD20	Biolegend	2H7	mouse IgG2bκ
BV786	CD27	BD	L128	mouse IgG1κ
APC-Cy7	CD38	Biolegend	HIT2	mouse IgG1κ
BV421	IgM	BD	G20-127	mouse IgG1κ
PE-Dazzle594	IgD	Biolegend	IA6-2	mouse IgG2aκ
PE-Cy7	IgG	BD	G18-145	mouse IgG1κ
FITC	IgA	Chemicon	M24A	mouse IgG1

mAb for NK cells. One approach frequently applied is to gate on $CD3^-$ $CD14^-$ $DAPI^-$ cells (Fig. 143C) and, in a subsequent step, identification of $CD19^+$ and $CD20^{+/-}$ cells (Fig. 143D). This gating permits reliable identification of $CD20^+$ B cells and additionally of $CD20^{low}$ plasmablasts. For the analysis of B cell subsets, a classical combination using CD27 and CD20 of $CD19^+$ B cells has been established. Using CD27, a number of B cell subsets can be identified independent of the expressed Ig subclasses. As a result, conventional $CD27^-$ $CD20^+$ naïve B cells, $CD27^+$ $CD20^+$ mBCs, including both preswitched and class-switched memory B cells, as well as $CD27^{++}$ $CD20^{low}$ PBs can be identified (Fig. 143F). While the distribution of these subsets can vary between different diseases with slight variations [1223], it has been demonstrated that CD27 can serve as a reliable marker for human healthy controls memory B cells, since CD27-expressing B cells differentiate timely into Ab-secreting cells after stimulation and carry somatic mutations in their immunoglobulin V regions [1209, 1211]. Of note, this gating strategy will not allow to identify class-switched B cells that lack the expression of CD27 [1218, 1219] and occur at higher frequencies among patients with systemic autoimmune diseases

When comparing the CD27 versus CD20 plot in the different tissues (Fig. 143F), an additional population has been found in the tonsil and another population in the bone marrow compared to peripheral blood and spleen. In the tonsil, a subset expressing high levels of CD20, intermediate levels of CD27 and CD38 expression appears in this plot and represent germinal center B cells that lack IgD expression [1224]. In the bone marrow, an additional population positive for CD19 but lacking the expression of CD20 and CD27 can be found. These B cells express CD38, do not show surface IgD expression and low to no IgM surface expression (Fig. 144) and represent immature B cells [1225].

2.3.6 Pitfalls.

1. Blocking Fc receptor prior to staining might interfere with staining of immunoglobulins on B cells
2. Choose an appropriate buffer for cell isolation: Buffers containing EDTA can decrease effects of stimulation by chelating calcium ions

2.3.7 Summary Table.

Table 47. Phenotypic differentiation of human B-lineage cell subsets based on their characteristic expression of surface markers

B cell population ($CD19^+$)	Phenotype/Subphenotype
Transitional	
T1+T2	$CD24^{++}CD38^{++}CD10^+CD27^-IgM^{++}$
Naive	
Resting	$CD24^{+/-}CD38^{+/-}CD27^-IgM^{++/+}$ $IgD^{++}CD21^+CD95^-$
Activated	$CD24^-CD38^-CD27^-IgM^{++}IgD^{++}$ $CD21^-CD95^+MTG^+$
Memory (Ki^-67^-)	
Preswitched	$IgM^+IgD^{+/-}CD27^+CD1c^+$
Switched	$IgG/IgA^+CD27^+CD21^+$
Atypical memory	
a) Double negative	IgD^-CD27^-
b) activated double negative	$IgD^-CD27^-CD95^+$
c) Syk^{++}	$IgD^{+/-}CD27^-CD95^{+/-}CD21^{+/-}$ $CD38^-MTO^-Syk^{++}$
d) tissue-resident	$IgM/IgG/IgA^+CD27^-FcRL4^+$
Marginal Zone	
Spleen	$IgD^+IgM^+CD27^{++}CD21^{++}CD1c^+$
Circulating	$IgD^+IgM^+CD27^+CD1c^+$
Ab secreting cells	
Circulating	
PB	$CD38^{++}CD27^{++}CD138^-Ki^-67^+$
PC	$CD38^{++}CD27^{++}CD138^{+/-}Ki^-67^{+/-}$
Bone marrow	
a) $CD19^+$ PC	$CD19^+CD38^{++}CD27^{++}CD138^+$ Ki^-67^-
b) $CD19^-$ PC	$CD19^-CD38^{++}CD27^{++}CD138^+$ Ki^-67^-

2.4 *Human B cells recognizing defined (auto)antigens*

2.4.1 Overview. Detection of human antigen-specific B cells has been challenging mainly due to their low frequency and the potential biases introduced by their ex vivo expansion. Naive B cells present with a diverse BCR repertoire that is usually of low avidity to the antigen. Upon antigen challenge, naive B cells undergo processes of somatic hypermutation, class switch recombination, and selection giving rise to memory B cells with high-avidity BCRs and PCs secreting highly specific Abs. Memory B cells and long-lived plasma cells are responsible for generation and maintenance of serologic memory. In some conditions, serum Ab titers correlate with the frequency of antigen-specific memory B cells in the circulation [1226, 1227]. Here, we present two recently established methodologies to identify human antigen-specific B cells by FCM.

2.4.2 Introduction. The identification of human antigen-specific B cell populations by FCM has become an extremely valuable

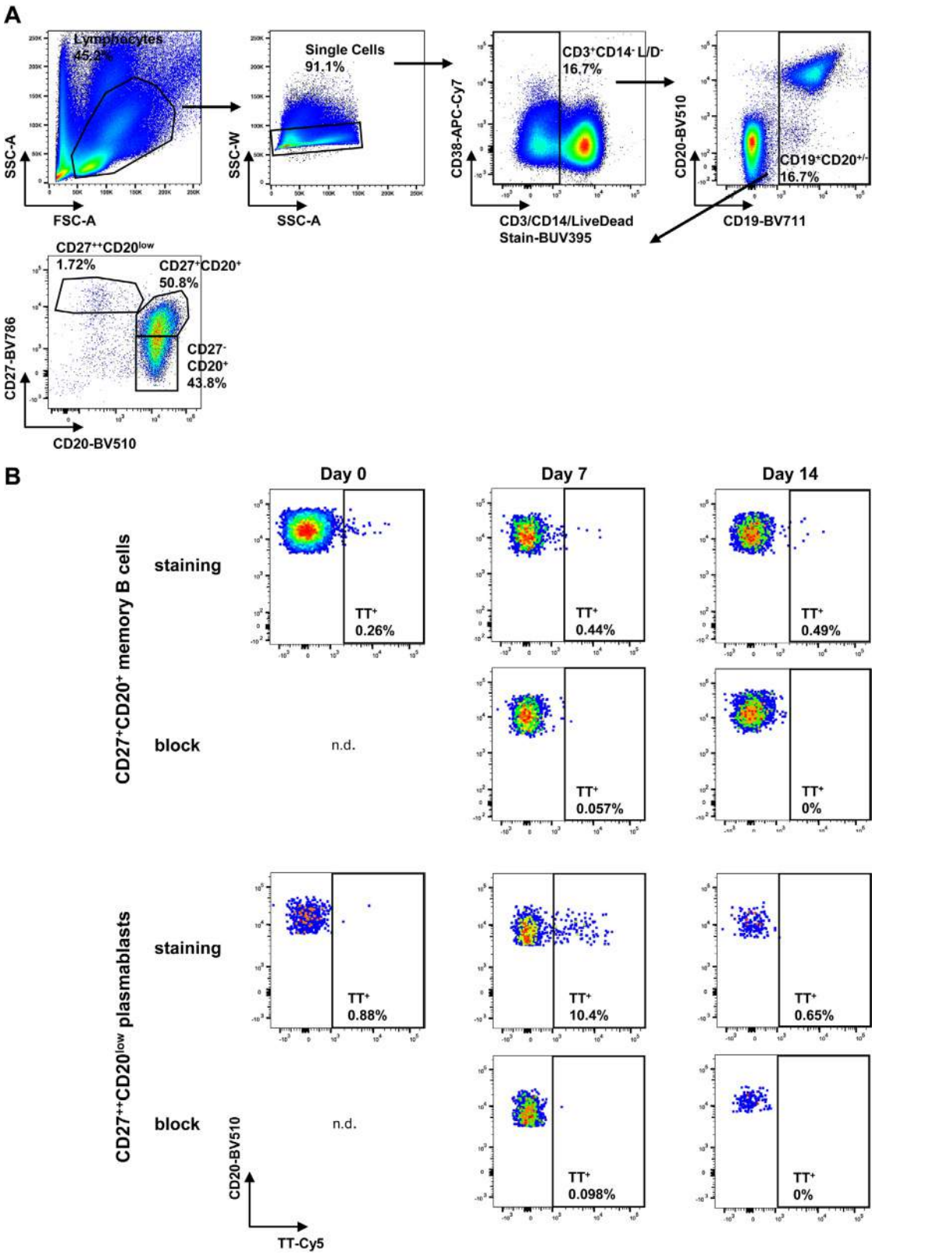

Figure 145. (A) After gating on lymphocytes, doublets, and in the subsequent gating step, $CD3^+$ T cells, $CD14^+$ monocytes, and dead cells are excluded. B cells including $CD20^{low}$ plasmablasts are gated by their CD19 and CD20 expression. Conventional naïve and memory B cells and plasmablasts are identified by using CD20 and CD27. (B) Identification of TT-specific memory B cells and plasmablasts before (day 0) and after TT vaccination (day 7 and day 14) in peripheral blood. Staining and block with unlabeled TT are shown.

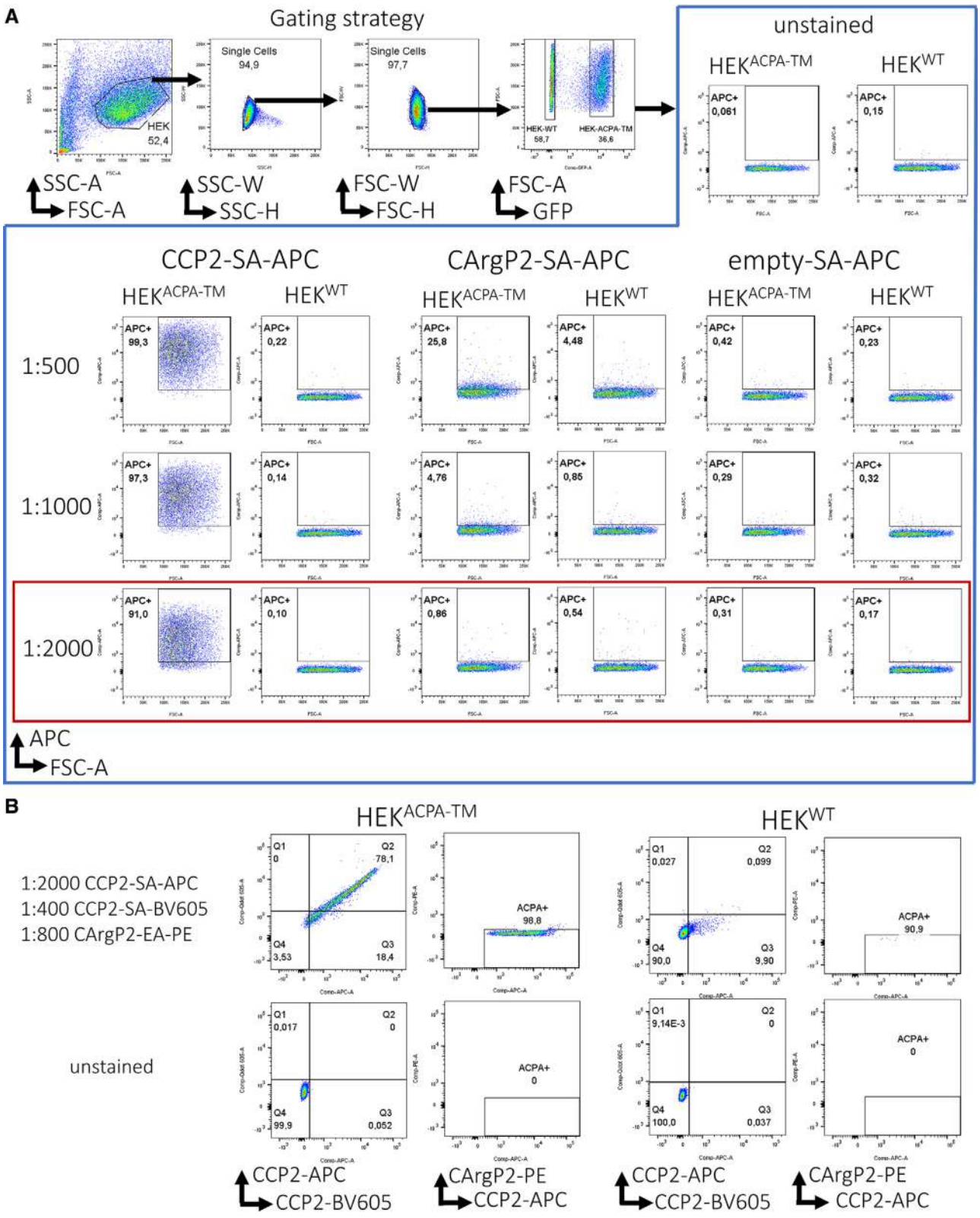

Figure 146. Determining optimal concentrations of multimerized antigen-tetramers for staining. (A) titration of CCP2-SA-APC, CArgP2-SA-APC, and of "empty" streptavidin APC tetramers on ACPA-expressing HEK 293T (HEK-ACPA^{TM}) and wild-type HEK 293T (HEK^{WT}) cells. Gates are based on unstained controls. The red square marks the optimal concentration of CCP2-SA-APC. (B) Staining of HEK-ACPA^{TM} and HEK^{WT} cells with combinatorial CCP2 and CArgP2 tetramers.

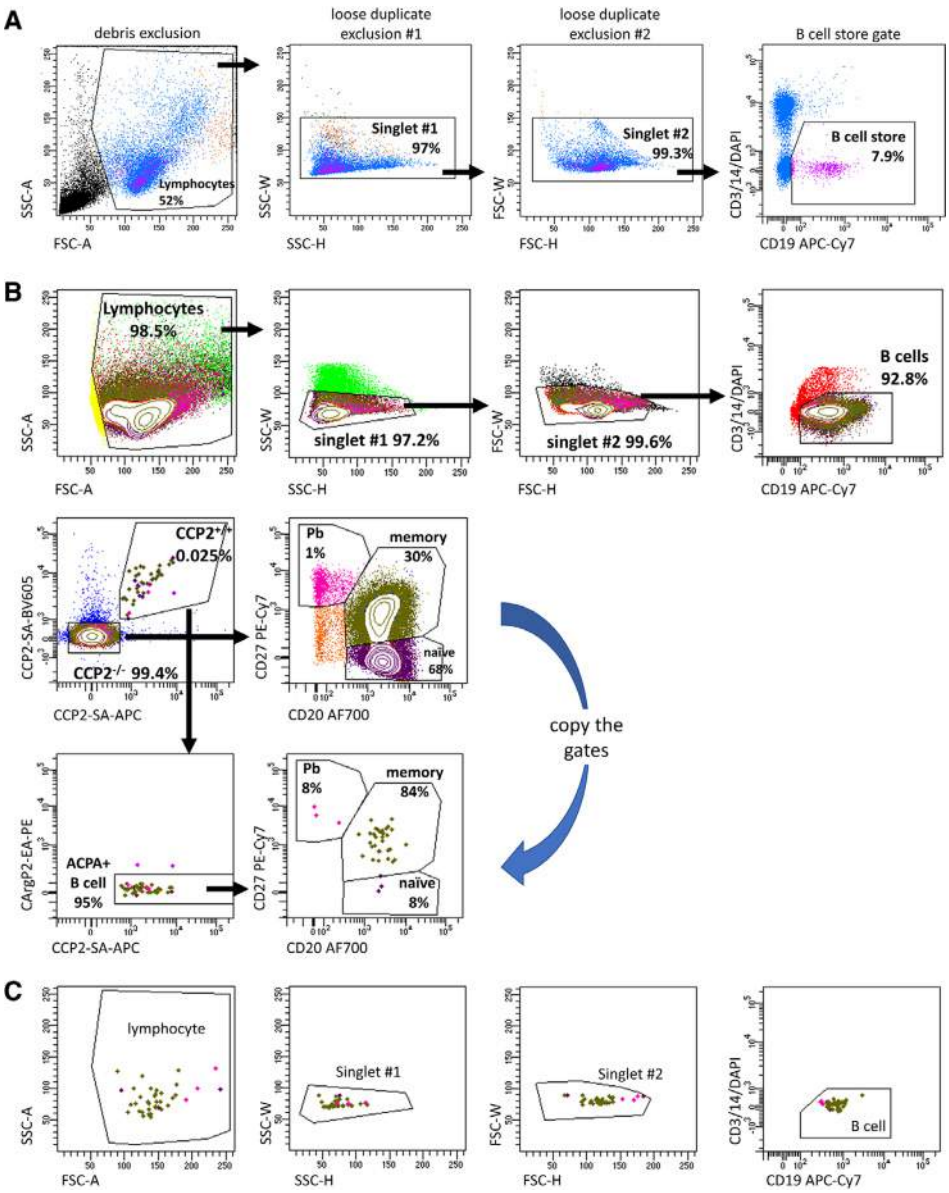

Figure 147. Gating strategy to identify ACPA-expressing B cells. (A) Setting up a "B cell store gate" that will be used during sample measurement to store data in order to obtain a manageable size of data to be analyzed. (B) Gating strategy to identify ACPA-expressing B cell subsets. The CD20 versus CD27 gates for ACPA-expressing B cells are copies of the same gates from the CCP2$^{-/-}$ population. (C) Back-gating of ACPA-expressing B cells as an additional measure of control to verify cell size and granularity within the large pool of PBMC-derived B cells.

tool for a detailed understanding of both protective and autoreactive human immune responses. Depending on the research questions, antigen-specific B cell responses can be analyzed and monitored upon vaccination, during "steady state," in different diseases including different disease stages, phases of treatment, and in different compartments of the human body [1228–1231]. It allows for the phenotypic analysis of antigen-induced B cells by assessing various markers on the cell surface and inside the cell. In combination with cell sorting, it also allows subsequent analysis, such as transcriptomic profiling by single cell-based ("next generation") sequencing techniques. Furthermore, it is possible to analyze antigen-specific B cell receptor (BCR) repertoires, to obtain full-length BCR sequences for mAb generation, and to perform functional studies of isolated single B cells or B cell populations, which includes the generation of immortalized, antigen-specific B cell clones [1232, 1233]. This wealth of possibilities permits unprecedented insights into human B cell biology; it requires, however, particular care and adherence to relevant and tedious control steps to ensure that the antigen-specific B cell populations identified by FCM, which are frequently very rare, indeed represent the antigen-specific B cell population of interest. Here, we provide a detailed description of the necessary considerations prior to starting out, the technological possibilities, approaches and necessary tools, and the relevant steps for performing experiments. We do so by using two examples of human antigen-specific B cell responses: (i) a vaccine-induced, high-avidity immune response identified by direct labeling of antigen with a fluorescent dye; and (ii) an autoreactive, low-avidity B cell response identified in an autoimmune disease setting using biotinylated self-antigens tetramerized with fluorescently labeled streptavidin molecules. In general, the examples described aim at identifying antigen-specific B cells within a polyclonal B cell repertoire to the highest validity. This implies

that strong emphasis is placed on the exclusion of nonspecific background signals and on several steps aimed at the verification of antigen-specificity. Notably, certain research questions might not require this strive for purity but can be answered by mere enrichment of the antigen-specific cell population. In other cases, such as single-cell transcriptomics, purity is crucial. In both cases, it is important to consider a number of general aspects before choosing the most suitable technical approach.

2.4.3 General considerations before starting out.

2.4.3.1 Estimated frequency of the antigen-specific B cell population of interest. In contrast to murine studies, in which the spleen and other lymphoid organs are readily accessible, most attempts to identify antigen-specific human B cells will need to rely on peripheral blood. In this compartment, $CD19^+$ B cells comprise around 4% of total PBMCs in adult healthy individuals (See also ChVI Section 2.3 Human B cells and their subsets). Frequencies of antigen-specific B cell populations, however, can be very low (<0.01% of total B cells). In an ideal setting, this requires, for example, 1×10^6 B cells to identify 100 antigen-specific B cells, and hence, a starting population of 25×10^6 PBMCs. In other compartments such as bone marrow, tonsils, or spleen, $CD19^+$ B cells are more frequent (mean of 19% in BM, 33% in the spleen, 43% in tonsils [1234]), as might be the frequency of antigen-specific subsets. Depending on the compartment studied, it can be important to estimate the expected frequency of the antigen-specific B cell population in order to determine the amount of starting material required for the identification of a minimum number of antigen-specific cells. This can be achieved by culturing ex vivo isolated PBMC or pre-enriched B cells in limiting dilution, followed by the assessment of antigen-specific B cell presence by either ELISA or ELISPOT [1235, 1236]. These approaches will likely underestimate the number of antigen-specific B cells in the circulation, but will provide a minimum estimate of the cell numbers that can be expected. In addition, this initial estimate can provide information on isotype usage of the antigen-specific B cell response to be studied, and allow determining whether the frequency of circulating, antigen-specific B cells correlates with serum titers of the corresponding Abs. This, in turn, will help in selecting donors and, hence, increase the yield of antigen-specific B cells for the eventual assessment.

2.4.3.2 Expected phenotype of the cell population of interest. Next, to determining compartmental frequencies, it can be relevant to use additional phenotypic markers in the eventual panel that allow to more specifically select the B cell subpopulation in which the antigen-specific cells are expected. For example, markers could identify the isotype or the Ig subclass that appears to be most prominent for the Ig produced by PC measured by ELISA. Also, if IgM-expressing B cells are to be identified, low-affinity antigen binding can be expected, which in turn indicates that multimerization of antigens can be helpful to increase the fluorescent signal. Other antigen-specific responses, for example, might be enriched in IgG4 expressing B cells, which allows to significantly narrow the cell numbers that need to be studied (see also Chapter VI Section 2.3 Human B cells and their subsets). The identification of plasma cells that lack surface Ig expression, on the other hand, might require an intracellular staining approach. If the expression of such phenotypic characteristics is known, these should be incorporated in the staining panel and included in the frequency estimation described above.

2.4.3.3 Source of cells. In general, any single cell suspension that contains B cells, whether derived from peripheral blood, bone marrow, spleen, tonsils, or solid tissues, can be assessed for the presence of antigen-specific B cells. Limitations are caused by the frequency of the antigen-specific population of interest, and by the viability of cells (including pre-analytical treatment, i.e., shipment). Freezing cells, for example, is likely to compromise the plasmablast compartment, while naïve and memory B cells are less sensitive (See also Chapter III Section 4.6 Freezing cell samples). Pre-enrichment of B cells from larger populations by positive or negative selection can increase the percentage of antigen-specific B cells and shortens the time required on the flow-cytometer; it can, however, also compromise B cell subsets, depending on the isolation technique used. Therefore, due to the usually very low frequency of antigen-specific B cell populations, we recommend—whenever possible—using fresh, directly ex-vivo isolated B cells or B-cell containing suspensions such as PBMC as a starting point. This will minimize the loss of antigen-specific cells during work-up. For certain B cell populations and research questions, however, the use of frozen cells can be acceptable [1237].

2.4.3.4 Choice of antigen. In most cases, the antigen used for flow-cytometric assessment will be the antigen for which reactivity has been demonstrated in serum ELISA measurements or epitope mapping studies, or which has been used for inducing the immune response in, for example, vaccination studies. Both peptide and protein antigens are possible candidates. Protein antigens might be preferred in case of conformational epitopes; in addition, proteins are more likely to carry multiple epitopes, which increases the chance for higher avidity interactions with the BCRs. However, protein synthesis usually requires cells or expression systems and purification steps after which impurities (such as LPS) can remain that can influence and confound binding properties and introduce nonspecific background signals. Peptides are easier to synthesize to high purity and contain one or more, sometimes synthetic, defined epitopes. Small sequence modifications can easily be introduced to generate nonbinding control peptides. However, peptides are usually too short to build appropriate 3D epitopes or structures that crosslink BCRs and, hence, monomeric peptides are usually insufficient for B cell identification. Therefore, peptide antigens are multimerized by generating either biotin–streptavidin tetramer complexes, or by coupling peptides to dextran backbones or other scaffolds using click-chemistry.

2.4.3.5 Choice of fluorescent labels. In general, and in particular for low-avidity B cell immune responses, it is strongly recommended to reserve at least two fluorescent channels in a given staining panel for the identification of ultra-low frequency antigen-specific B cells. For reasons described below, identification of antigen-specific B cells by double-positivity for two identical yet differentially labeled antigens significantly reduces nonspecific background signals and, hence, the risk for misinterpretation of fluorescent signals as antigen-specific cells. This concept of a dual labeling approach has been described in detail elsewhere, an example is provided bellow [1230, 1238, 1239]. We recommend using fluorescent dyes with emission spectra that show no or very little spectral overlap in order to reduce the need for extensive compensation. Use of single label antigens might suffice for certain, high avidity B cell responses in combination with blocking studies (see below), but additional measures should then be taken to demonstrate staining specificity, in particular in cases in which blocking with access, unlabeled antigen is incomplete.

2.4.3.6 Establishing positive and negative controls. To ensure the highest reliability, we strongly recommend the use of both positive and negative controls in the establishment of antigen-specific staining approaches. In the specific setting described here, controls need to be established at two levels:

1. Control cells that do or do not express the BCR of choice. Such cells allow determining the specificity of antigen binding, the use of optimal concentrations of labeled antigen or antigen-multimers, and the degree of nonspecific background binding. Furthermore, they allow controlling for variations between batches of labeled antigens and can be used to determine the sensitivity of the approach to detect antigen-specific cells within a larger pool of cells. Such control cells are particularly useful during the experimental setup phase of antigen-specific staining approaches aimed at identifying very low-frequency B cells. However, they maintain their relevance also once protocols have been established. Examples for control cells include B cell hybridomas that have maintained cell surface Ig expression [1240], immortalized human B cell clones of known specificity [1232, 1233], or cell lines transfected with mAb sequences with or without the transmembrane domain of IgG [1230]. An example of the latter option using HEK293T cells is provided below. Non-transfected cells or cells with known specificity to an unrelated antigen can serve as negative controls.
2. Control populations of donors that do or do not harbor the antigen-specific B cell population of interest. In disease settings, these should include matched healthy donors but also disease controls [1230]. In this context, a particular point for careful consideration lies in the possibility that control donors might harbor naïve B cells in their unmutated repertoire that specifically recognize the antigen of interest. Such recognition patterns have been described for nuclear autoantigens and studies suggest that healthy individuals harbor a considerable proportion of mature naïve B cells capable of recognizing autoantigens. For protective antigens, vaccinated donors can be analyzed as a control. Secondary vaccinations, e.g., with Tetanus Toxoid (TT), give rise to antigen-specific plasmablasts and memory B cells, which can be analyzed 1 and 2 weeks after vaccination, respectively [1241]. FCM is limited in the possibility to discern whether such staining signals reflect true antigen-specific B cells or nonspecific interaction between labeled antigens and cell surfaces by, for example, hydrophobic interaction or charge. If positive signals are observed in control donors in FCM, we highly recommend that additional measures be taken to determine/verify antigen specificity. Possible steps to do so are described below.

2.4.3.7 Verification of antigen-specificity. Different direct and indirect measures are available to determine whether fluorescent signals detected by FCM indeed identify B cells that specifically bind the antigen of interest via the BCR. Given that detection of ultra-low frequency B cells requires the assessment of large cell numbers of a given total B cell pool, it is almost inevitable that also nonspecific background signals are detected. Using a dual staining approach as described above significantly reduces such non-specific signals but does not suffice as a single argument to claim antigen-specificity. Additional options include:

1. Blocking (also called competition) experiments in which the binding of fluorescently labeled antigens to the BCR is blocked by an excess of unlabeled antigen. Note that an excess of unlabeled antigen should completely block the fluorescent signal. If this is not the case, nonspecific interaction between the labeled antigen and the cell cannot be excluded and additional verification steps (see below) should be taken. This method can also be applied in a stepwise approach with increasing amounts of unlabeled antigen where the increase of competing for binding sites results in a gradual decrease of labeled antigen occupying the BCR.
2. Single cell isolation by FCM followed by immediate cell lysis, mRNA isolation, and BCR sequencing using published protocols; alternatively, single cells can be cultured with relevant stimuli followed by the assessment of supernatants for the production of total and antigen-specific Ig by ELISA [1242]. Cells obtained from supernatants containing antigen-specific Ig can subsequently be lysed followed by mRNA isolation and BCR sequencing. In both cases, full-length BCR sequences can be obtained by primer-binding bias-free PCR protocols, which can subsequently be used for mAb expression [1243]. Note that it can be extremely useful during experimental setup to use the "index sort" function for single cell isolation protocols as this option allows to identify the localization of antigen-specific cells in the FCM dot plot.

Together, verification of antigen specificity is crucial as this step is, in the end, the only way to determine whether cells identified by FCM indeed represent the cell population of interest. Next to blocking experiments, the ultimate golden standard relies on

single cell isolation followed by BCR cloning and monoclonal Ab expression.

2.4.4 Step-by-step sample preparation.

1. Identification of a vaccine-induced, high-avidity immune response identified by direct labeling of antigen with a fluorescent dye

In order to detect B cells specific for a certain antigen, we here make use of the ability of B cells to bind the proteins they recognize through the BCR in a 3D manner. To illustrate this approach, we provide an example of the detection of TT-specific human memory B cells and plasmablasts in the circulation at several time points before and after TT vaccination (Fig. 145). Vaccination can be a highly useful tool in the initial setup of the staining procedure, but will not be available to aid the detection of autoreactive B cells described below. Nonetheless, the technological approach presented in this example has also successfully been used for the detection of autoreactive B cells [1244]. Therefore, the example provided can be seen as a template, which can be adapted to the identification of other antigen-specific B cell responses with similar characteristics.

In order to assure specificity of the staining, we show how the fluorescent signal in the same sample can be blocked with unconjugated protein used in excess. This methodology has been used successfully to analyze B cells specific for TT [1241, 1245]; cholera toxin B (CTB) [1246]; Keyhole Limpet Hemocyanin (KLH) [1227]; and Pentraxin-3 (PTX-3) [1244]. The possibility to down-titrate binding of antigen-specific cells (competitive assay principle) has long been recognized to ensure specificity.

Notes:

1. As discussed above, antigen-specific B cells are found at very low frequencies in the circulation; therefore, it is crucial to start with more input cells/blood that one would usually do to stain B cell subsets. The input depends on the estimated frequency of the antigen-specific B cells in the population of interest.
2. For sample preparation and staining of naive, memory B cells, and plasmablasts (see section 2 - B cells and their subsets).
3. For intracellular staining, permeabilize and fix the cells (see Section III.5: Cell fixation and permeabilization for flow cytometric analyses).

Steps:

1. Preparation of fluorescently labeled antigens. The fluorescently labeled antigens should be titrated (see ChIII Sect Titration: Determining optimal reagent concentration) independently for surface and intracellular detection. (Note: for intracellular staining usually a smaller quantity of labeled antigen is sufficient).
2. Upon sample preparation, wash cells twice with PBS before incubation with fluorescently labeled antigen.
3. Divide the sample in two: incubate half of the cells with fluorescently labeled antigen and the second half with unconjugated antigen. Incubate both at 4°C for 15–30 min.
4. Wash with PBS and prepare for acquisition on a flow cytometer of choice.

2. Identification of an auto-reactive, low-avidity B cell response identified in an autoimmune disease setting using biotinylated peptide self-antigens tetramerized with fluorescently labeled streptavidin molecules.

The example provided demonstrates the identification of B cells directed against citrullinated protein antigens in patients with rheumatoid arthritis (RA). Citrullination represents the posttranslational modification of arginine residues in a given protein to the amino acid citrulline. The citrulline-directed, auto-reactive B cell response is a hallmark of this disease and can be detected in >70% of patients by serum measurement of anti-citrullinated antigen Ig reactivity in ELISA. The humoral immune response uses all Ig isotypes and is, on the polyclonal level, of remarkably low avidity [1247]. Circulating, antigen-specific B cells in peripheral blood are expected at a frequency of ~1:10 000 total B cells and can comprise naïve and memory B cells as well as plasmablasts and plasma cells [1230, 1235, 1236]. Specific antigen recognition is determined by BCR binding to citrullinated antigens but not to the arginine-containing peptide control variants. A biotinylated, cyclic citrullinated peptide (CCP2) and its arginine control variant (CArgP2) are used for specific detection. HEK293T cells that express, in membrane-bound form, a mAb that specifically recognizes the citrullinated peptide antigen of choice ($HEK^{ACPA\text{-}TM}$), serve as controls during experimental setup [1230]. Note that this example can be seen as a template, which can be adapted to the identification of other antigen-specific B cell responses with similar characteristics.

1. Generating biotinylated peptide-avidin tetramers.

1. Incubate biotinylated peptides in excess with fluorescently labeled streptavidin or extravidin overnight at 4°C. The molar ratio between peptide and streptavidin should exceed 4:1.
   Note: In the example provided, six different peptide tetramers have been generated.
   - CCP2-biotin coupled to APC-labeled streptavidin (CCP2-SA-APC)
   - CArgP2-biotin coupled to APC-labeled streptavidin (CArgP2-SA-APC)
   - CCP2-biotin coupled to BV605-labeled streptavidin (CCP2-SA-BV605)
   - CArgP2-biotin coupled to BV605-labeled streptavidin (CArgP2-SA-BV605)
   - CCP2-biotin coupled to PE-labeled extravidin (CCP2-EA-PE)
   - CArgP2-biotin coupled to PE-labeled extravidin (CArgP2-EA-PE)
2. Remove unlabeled peptide with Bio-Spin® Columns with Bio-Gel® P-30. This will trap the free peptide in the gel and release peptide–streptavidin tetramers in the flow through. The removal of unlabeled peptides is crucial to avoid binding competition between unlabeled and labeled antigen during staining.

3. Store the labeled antigen tetramers at 4°C. In case of longer storage times (weeks to months), perform regular testing of the stability of the tetramers and fluorescent signal by using the positive/negative control cells (see below).

2. Determining optimal concentrations of multimerized antigen-tetramers for staining.

Notes:

- The optimal concentration of labeled peptide tetramers to be used for staining needs to be determined by titrating the labeled antigens on a fixed number of positive and negative control cells. Here, $HEK^{ACPA\text{-}TM}$ cells are used as positive control; non-transfected HEK293T wild-type cells (HEK^{WT}) serve as negative controls.
- For each tetramer, use the concentration at which the positive control stains highly positive and the negative control is negative.
- Combine the differentially labeled peptide tetramers at their optimal concentration to stain the positive ($HEK^{ACPA\text{-}TM}$) and negative (HEK^{WT}) control cells and determine whether a double positive population emerges in the diagonal of a FCM dot plot (Fig. 146). Should the double positive population deviate from the diagonal, adjust the concentrations of differentially labeled peptide tetramers accordingly until the double positive population falls into the diagonal. No signals should fall into this diagonal upon staining of the negative control cells.
- Upon determination of the optimal concentrations of labeled peptide tetramers to use, it can be helpful to spike positive control cells ($HEK^{ACPA\text{-}TM}$) in different numbers into healthy donor PBMC and to determine by subsequent antigen-specific staining whether the predetermined optimal concentrations remain optimal in a mixed population of cells.

Steps:

1. Prepare serial dilutions of peptide tetramers and of "empty"-labeled avidin molecules.
2. Stain a fixed number (here: 2×10^5) of positive and negative control cells with labeled peptide tetramers diluted in FCM buffer to 20 μL staining volume. Incubate for 30 minutes at 4°C.
3. Wash cells twice with FCM buffer and suspend in 100 μL FCM buffer for analysis on a flow cytometer.
4. In the example, CCP2-SA-APC tetramers at a dilution of 1:2000 stain >90% of $HEK^{ACPA\text{-}TM}$ cells, and less than 1% of HEK^{WT} cells (Fig. 146A). At the same concentration, CArgP2-SA-APC control tetramers show minimal background staining. Also, the empty labeled streptavidin molecules give minimal background at all concentrations. Therefore, a dilution of 1:2000 for this particular batch of CCP2-SA-APC tetramers is chosen for the subsequent combinatorial staining.
5. Perform similar titrations for BV605 and PE-labeled tetramers to obtain optimal dilutions for the subsequent combinatorial staining. To decide which concentration of CArgP2-EA-PE tetramers to use, choose the concentration at which CCP2-EA-PE tetramers give the highest signal and CArgP2-EA-PE tetramers minimal background $HEK^{ACPA\text{-}TM}$ cells.
6. In the example, dilutions of 1:2000 are optimal for CCP2-SA-APC, 1:400 for CCP2-SA-BV605, and 1:800 for CArgP2-EA-PE tetramers for the combinatorial staining. This combination identifies $HEK^{ACPA\text{-}TM}$ cells positive for CCP2-SA-APC and CCP2-SA-BV605 in the upper-right quadrant of the CCP2-APC versus CCP2-BV605 dot plot, while the CCP2 double positive population remains negative in the PE control channel (Fig. 146B). Also, no APC/BV605 double positive signal is observed for HEK^{WT} cells.

3. Staining of a sample containing human antigen-specific B cells.

Notes:

- Given the very low frequency of antigen-specific, ACPA-expressing B cells in the circulation, we here used 50 mL of freshly drawn peripheral blood as starting material.
- Here, we deliberately chose to stain whole PBMC and not to enrich B cells by subsequent isolation techniques in order not to compromise B cell subpopulations such as plasmablasts.
- In the example provided, DAPI is used to identify and exclude dead cells.
- We assume in this example that all labeled mAbs and their respective isotype control Abs have been titrated and tested in appropriate FMO-stainings to determine optimal concentrations. These steps are necessary but not mentioned in the description below.

Steps:

Identification of ACPA-expressing B cells in a peripheral blood sample of an ACPA-positive rheumatoid arthritis patient.

1. Isolate PBMC from a peripheral blood sample using Ficoll-Paque gradient centrifugation following standard protocols. Count the isolated PBMCs.
2. Suspend the PBMCs at 8×10^6 cells per 100 μL in FCM buffer in a 15 mL tube and stain with the fluorescently labeled Abs/streptavidin tetramers for 30 min on ice protected from light. In the example, we used: CD3 Pacific Blue (PB), CD14 Pacific Blue (PB), CD19 APC-Cy7, CD20 AF700, CD27 PE-Cy7, CCP2-SA-BV605, CCP2-SA-APC, and arginine peptide control CArgP2-Extravidin-PE at the appropriate concentrations.
   The emission wavelength of Pacific Blue is used in this example as a "dump channel" in which markers are combined that identify cells that are to be excluded from further analysis.
3. Add 1ml FCM buffer and centrifuge the cells for 5 min at 1500 rpm on ice.
4. Repeat the washing step at least two times.
5. Resuspend the cell pellet with 100 μL FCM buffer and transfer to an FCM tube (we use Micronic tube MP32022). Keep the sample on ice and in the dark at all times.
6. To compensate for spectral overlap between fluorescent dyes, we employ compensation beads (BD Biosciences) that bind to mouse IgG (provided that all of the fluorescently labeled

Abs used are of a murine IgG isotype). The beads are used to compensate for CD3 PB, CD19 APC-Cy, CD20 AF700, and CD27 PE-Cy7 spectral overlaps. For the tetramers, however, surrogate murine IgG that is conjugated with BV605, APC, and PE are used to allow fluorescence compensation using beads.

7. Set up a flow cytometer of choice (here: BD LSRFortessa) that allows simultaneously detecting and discriminating fluorescent signals from PB, APC-Cy7, AF700, PE-Cy7, BV605, APC, and PE dyes. For the analysis, we here used BD FACSDIVA software (version 8.0.2).
8. Perform fluorescence compensation using single-stained compensation beads and apply the compensation setup to the whole experiment.
9. Add 100 μL of 200 nM DAPI to the cell suspension (leading to a final concentration of 400 nM).
10. Place the sample into the cytometer and record 50 000 events. Put the sample back on ice and keep protected from light.
11. Place gates in a Global Worksheet of the DIVA program on the cell populations as follows (Fig. 147a):
    (a) In the FSC-A versus SSC-A plot, make an inclusive gate containing lymphocytes and monocytes to include plasmablasts that are larger in size and more granular than other subsets of B cells.
    (b) Subsequently, exclude duplicates using SSC-H versus SSC-W and FSC-H and FSC-W plots. The gates for duplicate exclusion should not be strict at this moment.
    (c) Lastly, in a PB versus CD19-APC-Cy7 plot, gate loosely on CD19 positive cells that are PB-negative. This gate is referred to as "B cell Store" (Fig. 147A).
12. Click "Next Tube" on the Acquisition Dashboard of the BD FACSDIVA workspace.
13. In the Acquisition Dashboard, choose "B cell Store" for both Stopping and Storage Gates. Set 10 000 000 events for both "Events to Record" and "Maximum Events to Display." This step is necessary to obtain a manageable size of data to analyze the antigen-specific cell population of interest (here: ACPA-expressing B cells).
14. Place the sample back into the flow cytometer. Record the "B cell store" and adjust the threshold rate to a maximum of 20 000 events/s. Measure the sample until it is finished.
15. Store the data appropriately.

2.4.5 Materials. Purified or Biotinylated peptide or protein antigens of choice depending on the protective/auto-reactive B cell response(s) to be studied.

- Fluorescently labeled streptavidin and/or extravidin molecules, e.g., BV605-streptavidin (Biolegend, catalog nr.: 405229), APC-labeled streptavidin (Invitrogen, catalog nr.: S32362), and PE-labeled extravidin (Sigma–Aldrich, catalog nr.: E4011-1ml).
- Fluorochrome for labeling of respective antigen, e.g. Cy5
- Bio-Spin® Columns with Bio-Gel® P-30 (BIO-RAD, catalog nr.: 732–6006)

Table 48. Fluorescently labeled monoclonal antibodies used in the example provided

No.	Marker	Clone	Fluorophore	Supplier	Catalog number
1	CD3	UCHT1	PB	BD	558117
2	CD14	M5E2	PB	BD	558121
3	CD19	Sj25C1	APC-Cy7	BD	557791
4	CD20	2H7	AF700	Biolegend	302322
5	CD27	M-T271	PE-Cy7	BD	560609

Table 49. Abs used as "surrogate" Abs for the compensation of avidin-tetramer derived fluorescent signals

No.	Marker	Clone	Fluorophore	Supplier	Catalog number
1	CD56	HCD56	BV605	Biolegend	318333
2	CD4	SK3	APC	BD	345771
3	CD8	RPA-T8	PE	BD	555367

- PBS
- BSA (Sigma–Aldrich, catalog nr.: A7906-1KG).
- FCM buffer (PBS, 0.5% BSA and 0.02% Azide)
- DAPI (Invitrogen, catalog-nr.: D1306)
- Fluorescently labeled mAbs (all Abs used in the present example are of mouse origin, expressed as IgG isotypes and directed against the respective human proteins, Table 48):
- Fluorescently labeled Abs to be used as "surrogate" Abs for the compensation of avidin-tetramer derived fluorescent signals (all Abs used in the example provided are murine Abs expressing the IgG_1 isotype directed against the respective human proteins indicated, Table 49):
- BD™ CompBeads anti-mouse Ig, κ (BD Biosciences, Catalog nr.: 51-90-9001229)
- BD™ CompBeads negative control (BD Biosciences, Catalog nr.: 51-90-9001291)
- Instrument: BD LSRFortessa (BD Biosciences)
- Software: BD FACSDIVA version 8.0.2 (BD Biosciences),
- Appropriate positive and negative control cells (here: $HEK^{ACPA\text{-}TM}$ and HEK^{WT}).

2.4.6 Data analysis/gating.

1. Identification of a vaccine-induced, high-avidity immune response identified by direct labeling of antigen with a fluorescent dye

Analysis and gating for the example provided are straightforward. B cell subsets can be gated as described in Section 2 B cells and their subsets. Following this step, fluorochrome specific plasmablasts, memory B cells, and naive B cells can be determined as shown for plasmablasts and memory B cells in Fig. 145.

2. Identification of an auto-reactive, low-avidity B cell response identified in an autoimmune disease setting using biotinylated peptide self-antigens tetramerized with fluorescently labeled streptavidin molecules

1. Open the experiment file using BD FACSDIVA version 8.0.2 (BD Biosciences)
2. Check and adjust the compensation of spectral overlap according to standard procedures.
3. Create a new "Normal Worksheet" in the file that stored only the "B cell store" gate, gate lymphocytes, single cells, and live B cells strictly (Fig. 147B)
4. Starting from the "live single B cell gate," create a CCP2-SA-BV605 versus CCP2-SA-APC plot to identify $CCP2^{+/+}$ and $CCP2^{-/-}$ populations. Place a gate around those $CCP2^{+/+}$ cells that strictly fall into the diagonal.
5. Display the cells identified in this gate (the $CCP2^{+/+}$ population) in a CCP2-SA-APC versus CArgP2-Extravidin-PE plot and place a gate on the CArgP2-PE negative population. These cells represent the antigen-specific B cell population of interest (i.e., ACPA-expressing B cells).
6. In the CCP2-SA-BV605 versus CCP2-SA-APC plot, place a gate on the $CCP2^{-/-}$ population, create a CD20-AF700 versus CD27-PE-Cy7 plot and gate on naïve ($CD20^{+}CD27^{-}$), memory ($CD20^{+}CD27^{+}$) and plasmablast ($CD20^{-}CD27^{high}$) subsets of these avidin-tetramer negative B cells.
7. From the gate identifying the ACPA-expressing B cell population (the $CCP2^{+/+}$ $CArgP2^{-}$ population), create a CD20-AF700 versus CD27-PE-Cy7 plot. Copy the gates identifying naïve ($CD20^{+}CD27^{-}$), memory ($CD20^{+}CD27^{+}$) and plasmablast ($CD20^{-}CD27^{high}$) subsets from the avidin-tetramer negative B cell population to the plot displaying the ACPA-expressing B cell population. This step is taken as it can be difficult to define the gates for these B cell subsets on the basis of very few cells. Therefore, copying the gates from a larger population (the avidin-tetramer negative B cells) to the antigen-specific B cell population (the ACPA-expressing B cells) is necessary for further analysis.
8. In the given example, the majority of ACPA-expressing B cells displays a memory ($CD20^{+}CD27^{+}$) phenotype, while avidin-tetramer-negative B cells mostly fall in the naïve B cell gate ($CD20^{+}CD27^{-}$) (Fig. 147B).
9. As an additional step of control, perform "back-gating" of the ACPA-expressing B cell population. Should some cells fall at the edge of the gates identifying lymphocytes, single cells, and live B cells, adjustment of these gates might be necessary to minimize the possibility that doublets or otherwise nonspecifically stained cells are misinterpreted (Fig. 147C).

2.4.7 Pitfalls.

- Be aware that the quality of the fluorescent signal of the labeled avidin-tetramers decreases overtime. Take along a staining control using the positive and negative control cells with each sample to control for such signal decay and/or an increase of non-specific background staining.
- The fluorochrome itself can be recognized by B cells giving rise to false positive signals; this can be overcome by using the same antigen labeled with a second fluorochrome, as described.

2.4.8 Top tricks.

- During setup and once a cell population has been identified that meets the criteria of antigen-specific cells delineated above, subsequent verification of antigen-specificity is indispensable. Please refer to the section "Verification of antigen-specificity" in the introduction for details on how antigen-specificity can be determined, and refer to [1230], supplementary data section, for examples.
- For differential labeling of antigens, we recommend using fluorescent dyes with emission spectra that show no or very little spectral overlap in order to reduce the need for extensive compensation.

2.4.9 Summary Table. See Summary Table 47 of Chapter VI Section 2.3 Human B cells and their subsets.

2.5 *Human regulatory B cells*

2.5.1 Overview. B cells play a key role in immune responses through the production of Abs, antigen presentation to other immune cells, and production of cytokines. Suppressive cytokines, such as IL-10, play a pivotal role in controlling inflammation and immune tolerance. Importance of regulatory B cells (Bregs) producing suppressive cytokines was described in murine models and in several human diseases. Depending on the disease studied or on the in vitro stimulation, different functional Breg subsets were described. Detailed characterization of individual Breg subsets, therefore, can improve our understanding of regulation of immune responses. This section describes a method for detection of individual Breg subsets in human PBMC samples. This panel can be considered a basis in which additional markers can be included to interrogate their expression among the different Breg subsets.

2.5.2 Introduction. The existence of B cells with regulatory function (Breg) was first proposed in studies using B cell-depleted rodents, which showed reduced suppressive capacity of the lymphocyte fraction and were unable to recover from experimental autoimmune encephalitis [1248–1250]. Later, Mizoguchi et al. [1251] and Fillatreau et al. [1252] demonstrated that B cells can suppress immunity through production of immunosuppressive cytokines.

Bregs is an umbrella term used for immunosuppressive B cells [1253]. Bregs were often described in the context of chronic inflammatory diseases and in human they are mostly characterized

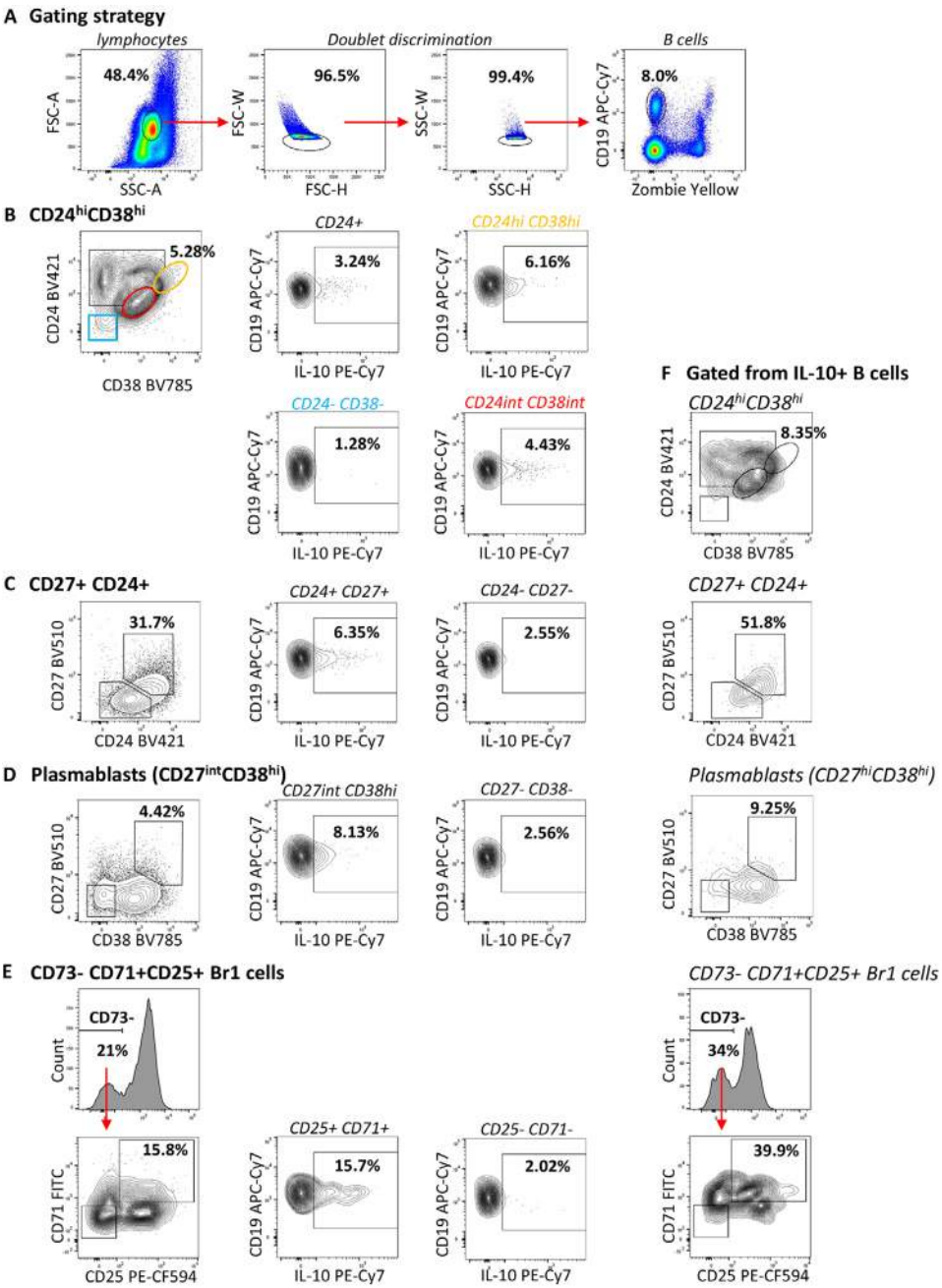

Figure 148. Identification of regulatory B cell subsets from CpG-stimulated PBMC. PBMC from healthy female adult subject cultured for 72 h with media alone or media containing 1μM CpG-ODN 2006. Before staining, cells stimulated for 5 h with 25 ng/mL PMA and 1 μg/mL Iono and for the last 2 h with 10 μg/mL Brefeldin A. Cells harvested and surface and intracellular antibody stainings performed. Total viable B cells gated from lymphocytes after doublet discrimination (A). Breg subsets gated from viable single $CD19^+$ B cells (B–E). IL-10^+ B cells gated from (B) $CD19^+$ $CD24^{high}$ $CD38^{high}$ B cells, (C) B10/pro-B10 cells ($CD19^+$ $CD24^{high}$ $CD27^+$), (D) suppressive plasmablasts ($CD19^+$ $CD27^{int}$ $CD38^+$), and (E) $CD19^+$ $CD73^-$ $CD25^+$ $CD71^+$ B cells. Breg subsets gated from IL-10^+ $CD19^+$ B cells based on surface markers showing enrichment of IL-10^+ B cells (F).

by production of the suppressive cytokine IL-10 [1162, 1253]. Generally, expression of IL-10 has been a very useful marker for B cells with suppressive phenotype [1162, 1253]. However, several Breg-related surface markers can be either down- or upregulated upon stimulation, making it difficult when Breg subsets are compared among different stimulatory environments [1162]. For example, CD25 and CD71 are often upregulated in activated B cells [1254, 1255] and they are widely used also as activation markers. Another activation marker, CD38, is expressed in naïve B cells and plasmablasts (the main IL-10 producing subsets) but is downregulated when naïve B cells develop into memory B cells [1256]. Furthermore, CD1d can be downregulated upon stimulation [1254]. In contrast to regulatory T cells, no Breg-specific transcription factor could be identified so far [1162]. Furthermore, the high diversity of B cell subsets with suppressive capacity strongly suggests that there is not one single lineage of B cells giving rise to Bregs but that there are precursors from various stages of B cell ontogeny that gain suppressive phenotype in response to stimulation.

In mice, Bregs were reported to act mainly via production of suppressive cytokines IL-10, IL-35, and TGF-β [1162] and inhibitory receptors such as LAG-3 [1167]. IL-10 can suppress production of pro-inflammatory cytokines by antigen presenting cells and induce T regulatory cells [1165, 1257]. IL-35 was reported

Table 50. Human B cell subsets

Name	Marker	Suppressor molecules	Induction	Associated disease
Immature B cells	$CD19^+$ $CD24^{high}$ $CD38^{high}$ $CD1d^+$	IL-10	CD40 ligation	Suppressive role in RA, SLE and CHB virus infection [1277–1279]
B10/pro-B10 cells	$CD19^+$ $CD24^{high}$ $CD27^+$ $CD48^{high}$ $CD148^{high}$	IL-10	CpG-ODN, LPS (+ CD40 ligation)	Various autoimmune diseases [1280].
Br1 cells	$CD19^+$ $CD73^-$ $CD25^+$ $CD71^+$ B cells	IL-10, IgG4, PD-L1	CpG-ODN	Allergen tolerance [1255]
Suppressive plasmablasts	$CD19^+$ $CD27^{int}$ $CD38^+$	IL-10, immunoglobulins	CpG-ODN + IL-2, IL-6, and IFN-α/γ	Healthy subjects [1165]
Suppressive plasma cells	$CD138^+$	IL-10	n/a	Multiple sclerosis lesions [1281]

to inhibit T helper 1 (Th1) cell responses [1159], while TGF-β can inhibit APCs and induce apoptosis in Th1 cells as well as bring on anergy in $CD8^+$ T cell [1258, 1259]. In murine spleen, $CD19^+$, $CD21^{hi}$ $CD23^{hi}$ CD24hi B cells (T2-MZP cells) [1168, 1169, 1260, 1261] and $CD19^+$, $CD21^{hi}$ $CD23^-$ B cells (MZ B cells) [1170, 1262, 1263] were found suppressing $CD4^+$ and $CD8^+$ T cells while inducing Tregs. Similarly, IL-10-producing $CD1d^{high}$ $CD5^+$ B cells (B10) were found in the spleen, suppressing $CD4^+$ T cells, dendritic cells (DC), as well as monocytes thereby playing a protective role in a plethora of mouse models including EAE [1264, 1265], lupus [1266], myasthenia-gravis [1267], collagen-induced arthritis [1268], colitis [1269], allergic inflammation [1270, 1271], and contact hypersensitivity [1272]. In spleen, also $CD19^+$ TIM-1^+ B cells were identified, suppressing $CD4^+$ T cells [1173, 1273]. Interestingly, suppressive phenotype was also found among B cells of later differentiation stages, such as $CD138^+$ $CD44^{hi}$ plasmablasts [1165], $CD138^+$ MHC-11^{lo} $B220^+$ plasma cells [1159, 1274] and LAG-3^+ plasma cells [1167]. Suppressive plasmablasts were found in LN, suppressing $CD4^+$ T cells and DCs [1165] while IL-10 and IL-35 secreting plasma cells were found in spleen, suppressing effector $CD4^+$ T cells as well as neutrophils and NK cells [1159, 1274]. LAG-3^+ plasma cells, in addition to LAG-3 also expressed additional inhibitory receptors, including CD200, PD-L1, and PD-L2 [1167]. A common characteristic among all the above-mentioned murine Breg subsets is their capability to produce of IL-10 [1162].

In this section, we focus on human Breg cell subsets (see Table 50 for a summary of human B cell subsets). The first data that indicated a potential role for regulatory B cells in humans came from the reports of new onset of colitis and psoriasis after CD20 mAb treatment with rituximab [1275, 1276]. In human Bregs, regulatory function is mainly conferred via secretion of IL-10. IL-10 can be produced by naïve B cells [1255, 1277–1280], plasmablasts [1165] from the blood and plasma cells from tissue [1281] while it is unclear which subset is the most potent producer. IL-10 can be induced from peripheral human B cells by ligation of TLR9 (using CpG-ODN) [1165, 1255, 1280] or CD40 [1277, 1280] in vitro. Bregs originating from immature $CD19^+$ $CD24^{high}$ $CD38^{high}$ B cells were found in blood and in inflamed tissue having a suppressive role in rheumatoid arthritis (RA), systemic lupus erythematosus (SLE), and chronic hepatitis B (CHB) virus infection [1277–1279]. These cells suppress Th1, TH17 cells, and virus-specific $CD8^+$ T cells while inducing Tregs [1277–1279]. Suppressive B10/pro-B10 cells ($CD19^+$ $CD24^{high}$ $CD27^+$ $CD48^{high}$ $CD148^{high}$) were found in blood suppressing $CD4^+$ T cells, monocytes, and DCs [1280]. B10/pro-B10 cells regulate innate immunity and are upregulated in patients with various autoimmune diseases [1280]. IL-10-producing $CD19^+$ $CD73^-$ $CD25^+$ $CD71^+$ Bregs play an important role in developing tolerance to allergens. This subset was shown to mature at increased frequency into plasma cells that secrete the suppressive Ab isotype IgG4 [1255]. In addition, $CD27^{int}$ $CD38^+$ plasmablasts derived either from naïve immature B cells or naïve mature B cells suppress effector $CD4^+$ T cells and DCs by expressing IL-10 [1165]. Recently, it was shown that in multiple sclerosis lesions, plasma cells (but not B cells) produced large amounts of suppressive IL-10 [1281]. An FCM panel was described combining several Breg-associated markers, including CD19, CD1d, CD5, CD24, CD25, CD38, CD71, CD73, and IL-10 [1254]. This allows to identify $CD24^{hi}$ $CD38^{hi}$ IL-10^+ Bregs (Fig. 148B), $CD73^-$ $CD25^+$ $CD71^+$ IL-10^+ Bregs (Fig. 148E), and a $CD5^+$ $CD1d^{high}$ IL-10^+ Breg subset, which was mainly described in mice. In humans, CD1d was also reported to more expressed in regulatory B cell subsets [1280, 1282]. Here, we included CD27, a marker for memory B cells, which allows additional distinction of $CD19^+$ $CD24^{high}$ $CD27^+$ B10/pro-B10 cells (Fig. 148C) and $CD19^+$ $CD27^{int}$ $CD38^+$ suppressive plasmablasts (Fig. 148D). These Breg subsets show enrichment for IL-10-producing B cells compared to total IL-10 producing B cells (Figure 149).

2.5.3 Step-by-step sample preparation. This staining protocol is optimized for human peripheral B cells. PBMCs were isolated from heparinized blood of healthy individuals by density gradient centrifugation (Biochrom, Berlin, Germany). Isolated PBMC were directly plated and stimulated for 72 h with CpG-ODN. Before staining, cells were incubated with PMA and Iono (5 h) and Brefeldin A (2 h), followed by viability staining with zombie

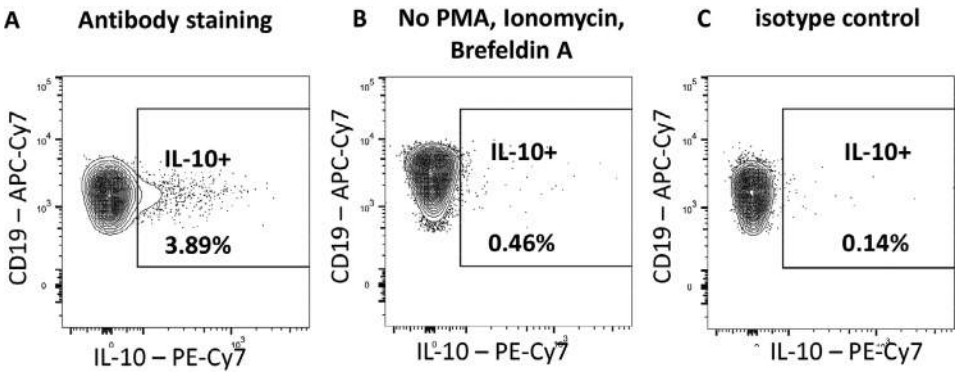

Figure 149. IL-10 staining and control stainings. PBMC cultured for 72 h with media alone or media containing 1 μM CpG-ODN 2006. The last 5 h before staining, PBMC additionally stimulated with 25 ng/mL PMA and 1 μg/mL ionomycin and for the last 2 h with 10 μg/mL Brefeldin A (A and C) or medium control (B). IL-10$^+$ B cells gated from single viable CD19$^+$ B cells. Upstream gating was performed as in Fig. 148. Anti-IL-10 antibody staining (A) after stimulation with PMA, Iono, and Brefeldin-A or (B) without stimulation and (C) isotype control staining.

yellow viability dye (Biolegend, San Diego, CA) and staining for surface markers with the Abs listed in Table 51 in staining buffer. Cells were washed, permeabilized, and Ab staining for intracellular IL-10 was performed. Then, samples were washed and measured on a BD LSR Fortessa with BD FACSDiva Software Version 8.0.1 and analyzed using Flowjo version 10.4.

Detailed protocol:

1. Collect fresh blood in heparinized containers (BD vacutainer 170 I.U. of lithium heparin)
2. Isolate PBMC:
   (a) Dilute blood samples at a 1:1 ratio with PBS supplemented with 2 mM EDTA.
   (b) For each 30 mL of diluted blood prepare a tube of Biocoll. Add 15 ml of Biocoll separating solution (room temperature) to a 50 mL blood-sep-filter tube. Spin down 1 min at 1100 × *g* to collect the Biocoll at the bottom of the tube below the filter.
   (c) Slowly add 30 mL of diluted blood to each filter tube and centrifuge the tubes at 800 × *g* for 20 min at 18°C and no break at end of program.
   (d) Collect the interphases and pool up to two interphases and transfer them to a new 50 mL centrifugation tube. Fill up tube with PBS supplemented with 2 mM EDTA. Centrifuge tubes at 780 × *g* for 10 min at 18°C.
   (e) Remove supernatant and resuspend cell pellet in 2 mL PBS supplemented with 2 mM EDTA. Pass cells through a 70 μM cell strainer into a new 50 mL centrifugation tube. Fill up tube with PBS supplemented with 2 mM EDTA. Centrifuge tubes at 220 × *g* for 10 min at 4°C.
   (f) Discard supernatant and resuspend PBMC in 5 mL of complete RPMI (cRPMI; RPMI 1640 medium supplemented with MEM Vitamin Solution, penicillin, streptomycin, kanamycin, MEM Non-essential Amino Acid Solution, Sodium pyruvate solution (Sigma-Aldrich Chemie GmbH), and 10% heat-inactivated FCS (Sigma–Aldrich Chemie GmbH).
3. Count PBMC and plate two million PBMC at concentration of 1 million/mL in cRPMI in 12-well tissue culture plate.

Table 51. Antibodies

Marker	Label	Clone	Manufacturer	Product number	Dilution
CD38	BV785	HIT2	Biolegend, San Diego, CA, USA	303530	1:50
CD27	Brilliant Violet 510	L128	BD Biosciences, Pharmingen, San Diego, CA, USA	563092	1:33
CD24	Brilliant Violet 421	ML5	Biolegend, San Diego, CA, USA	311122	1:40
CD71	FITC	CY1G4	Biolegend, San Diego, CA, USA	334104	1:20
CD25	PE-CF594	M-A251	BD Biosciences, Pharmingen, San Diego, CA, USA	562403	1:40
CD1d	PE	51.1	eBioscience, Affymetrix Inc., San Diego, CA, USA	12-0016-42	1:40
CD19	APC-Cy7	HIB19	Biolegend, San Diego, CA, USA	302218	1:100
CD73	APC	AD2	Biolegend, San Diego, CA, USA	344006	1:40
IL-10	PE-Cy7	JES3-9D7	Biolegend, San Diego, CA, USA	501420	1:200
Isotype ctrl	PE-Cy7	RTK2071	Biolegend, San Diego, CA, USA	400416	1:200

4. Stimulate PBMC with 1 μM CpG ODN 2006 or medium (control) for 72 h.

2.5.4 Materials.

Reagent	Product number	Manufacturer
BD vacutainer 170 I.U. of lithium heparin	367526	BD, Plymouth, UK
Blood separation filter tube	03-7100SI	Dacos, Esbjerg N, Denmark
Biocoll	L 6115	Biochrom, Berlin, Germany
BD Falcon 70 μM cell strainer	431751	BD Biosciences, Franklin Lakes, NJ, USA
Cell culture medium:		
RPMI-1640 Medium, with sodium bicarbonate and L-glutamine	R8758-500ML	Sigma–Aldrich Chemie GmbH
Fetal calf serum (FCS)	F7524	Sigma–Aldrich Chemie GmbH
MEM Vitamin Solution (100×)	M6895-100ML	Sigma–Aldrich Chemie GmbH
Penicillin-Streptomycin (100×)	P4333-100ML	Sigma–Aldrich Chemie GmbH
Kanamycin (100×)	15160-047	GIBCO, Paisley, UK
MEM Nonessential Amino Acid Solution (100×)	M7145-100ML	Sigma–Aldrich Chemie GmbH
Sodium pyruvate solution	S8636-100ML	Sigma–Aldrich Chemie GmbH
TPP® tissue culture plates, 12-well plate, polystyrene	Z707775-126EA	Sigma–Aldrich Chemie GmbH
CpG ODN 2006		MicroSynth, Balgach, Switzerland
PMA	P-8139	Sigma–Aldrich Chemie GmbH
Ionomycin	I9657-1MG	Sigma–Aldrich Chemie GmbH
Brefeldin A	B7651	Sigma–Aldrich Chemie GmbH
FCM staining buffer:		
PBS		GIBCO, Paisley, UK
2 mM EDTA		
BSA	A3294-500G	Sigma–Aldrich Chemie GmbH, Buchs, Switzerland
Zombie Yellow™ Fixable Viability Kit	423104	Biolegend, San Diego, CA, USA
Fixation/Permeabilization Solution Kit	554714	BD Biosciences, Pharmingen, San Diego, CA, USA

5. Harvest PBMC and spin down (300 × *g*, 10 min).
6. Staining for FCM:
   (a) Briefly vortex cell pellet and stain cells with 100 μL of Zombie yellow viability dye diluted 1:100 in staining buffer. Incubate 20 min at room temperature in dark. Wash once with 1 mL of staining buffer.
   (b) Stain cells with Abs specific for surface markers listed in Table 51 in a total staining volume of 100 μL. Incubate 15 min at 4°C in dark. Wash once with 1 mL of staining buffer.
   (c) Briefly vortex the cell pellet and resuspend with 250 μL of Fixation/Permeabilization solution (BD Biosciences, 554714) for 20 min at 4°C.
   (d) Wash the cell pellet two times with 1 mL BD Perm/Wash™ buffer (BD Biosciences, 554714).
   (e) For intracellular staining of IL-10, dilute Ab in 50 μL BD Perm/Wash™ buffer. As isotype staining control for IL-10, use isotype control Ab in equal concentration. Incubate 30 min in the dark at 4°C.
   (f) Wash the cells two times with 1 mL BD Perm/Wash™ buffer (BD Biosciences, 554714).
7. Resuspend cell pellet in 200 μL staining buffer and measure sample.

2.5.5 Data analysis. We first gate on lymphocytes in FSC versus SSC, followed by doubled discrimination (Fig. 148A). From single cells we gate on viable (Zombie Yellow negative) $CD19^+$ B cells. Total IL-10^+ cells are gated from viable B cells (Fig. 149A). B cells can be sub-gated into $CD24^+$ $CD38^+$ IL-10^+ Bregs (Fig. 148B), $CD19^+$ $CD24^+$ $CD27^+$ B10/pro-B10 cells (Fig. 148C), $CD19^+$ $CD27^{int}$ $CD38^+$ suppressive plasmablasts (Fig. 148D), and $CD73^-$ $CD25^+$ $CD71^+$ IL-10^+ Bregs (Fig. 148E). These four Breg subsets contain increased percentage of IL-10^+ B cells compared to total IL-10 producing B cells (Figs. 148B–E and 149A). Alternatively, when we gate Breg subsets based on their surface marker expression from total IL-10^+ B cells, we find that these Breg subsets are enriched among total IL-10^+ B cells (Fig 148F). However, even though IL-10^+ B cell are enriched among gated Breg subsets, there are also other IL-10-producing B cells, which are not falling into a described Breg gate. Also, Breg subsets are overlaping to some extent.

2.5.6 Pitfalls. Some of the surface expressed proteins used as markers for Bregs are also known as general activation markers. Depending on the stimulation used, surface markers of Bregs therefore might be up- or downregulated. For example, upon

stimulation with CpG or BCR ligation+CD40L for 72 h, it was seen that while number of $CD19^+$ $CD73^-$ $CD25^+$ $CD71^+$ B cells (Br1 cells) showed a tendency to be increased among total IL-10 producing B cells, $CD19^+$ $CD24^+$ $CD38^+$ B cells and $CD19^+$ $CD1d^+$ $CD5^+$ B cells were decreased [1254]. Therefore, it is important to carefully consider the length of the stimulation period when performing in vitro stimulation of regulatory B cells.

2.5.7 Top tricks. Depending the exact research question and on the flow cytometer available, several other Abs can be included to the panel. Since B cells sometimes produce inflammatory cytokines (e.g., TNF) together with IL-10 [1283], it can be useful to include Abs for exclusion of inflammatory cytokine-producing cells.

2.6 *Human immunoglobulin heavy chain isotypes*

2.6.1 Overview. B cells play a key role in immune responses through the production of Abs. Detailed characterization of individual subsets of B cells that have switched to distinct Ig heavy chain isotypes can improve our understanding of the development of humoral immune responses. This section describes a method for detection of individual Ig heavy chain expressing B cells in human PBMC samples. This panel can be considered a basis in which additional markers can be included to interrogate their expression among the different B cell subsets.

2.6.2 Introduction. B cells develop in the bone marrow and are released into the circulation, after which they mature predominantly in the spleen to become mature naive B cells. Mature B cells can be roughly divided into two subsets: conventional follicular B cells (frequently referred to as B-2 cells) and non-conventional extrafollicular B cells (including B-1 cells, which have been mainly characterized in the mouse, and marginal zone (MZ) B cells) [1284, 1285].

Extrafollicular B cells mount thymus-independent (TI) humoral responses, which are rapidly induced in response to conserved microbial carbohydrate or glycolipid structures. These responses often result in the production of polyspecific low-affinity IgM Abs, and typically do not involve somatic hypermutation or class switch recombination (CSR) [1286]. T-independent CSR and somatic hypermutation have been reported [1287]. Follicular B cells participate in thymus-dependent (TD) responses. These cells interact with follicular helper T (Tfh) cells in germinal centers, which are mainly found in secondary lymphoid organs [1288]. Follicular B cells that receive T cell help (through CD40L and cytokines) will become germinal center B cells and upregulate BCL6 and activation-induced deaminase expression, and will undergo CSR and somatic hypermutation [1286, 1289]. The B cells that emerge from such a germinal center reaction will either become circulating memory B cells or plasma cells. Some plasma cells will home to the bone marrow where they can survive for many years as long-living immunoglobulin-secreting plasma cells [1290].

B cell activation to T-cell dependent antigens requires BCR stimulation and CD40 ligation. Antigens can be captured directly by B cells or can be presented by follicular DCs in the lymphoid follicles. BCR stimulation is typically mediated through binding of a specific antigen to the BCR leading to internalization, processing and presentation of antigenic peptides in MHC class II molecules. Antigens are presented to $CD4^+$ T cells, which are activated in this manner. Activated $CD4^+$ T cells upregulate CD40L and secrete cytokines. The type of cytokines that are produced by these T cells depends on how these cells were primed as naïve T cells. CD40-CD40L interaction and the local cytokine milieu provide the second signal that is required for efficient B cell activation including proliferation, CSR, and plasma cell differentiation.

Abs are identical to the BCR of the B cell from which they originate, with the exception of a C-terminal sequence that anchors the molecule to the cell membrane. As a result, Abs are secreted and do not form surface-bound receptors. Abs have a functionally polarized structure, with on one side the Fab region harboring a hypervariable region, which is responsible for antigen binding, and on the other side a constant Fc region. The structure of the constant region determines the effector function of the Ig. Abs are typically classified according to the isotype of their heavy chain. Humans have nine major Ig heavy chain isotypes: IgM, IgD, IgG1, IgG2, IgG3, IgG4, IgA1, IgA2, and IgE [1291] while there are eight murine Ig isotypes: IgM, IgD, IgG1, IgG2a, IgG2b, IgG3, IgA and IgE [1291]. Each of these Ab isotypes mediates distinct functions through interaction with specific receptors on effector cells and serum factors.

Each Ig molecule consists of two heavy (IgH) and two light chains, both of which contain variable (V) and constant (C) regions. The region of the heavy chain that determines antigen-specificity is made up by the variable (V_H), diversity (D), and joining (J_H) segments that are rearranged during early B cell development to form a VDJ cassette or V-region. The V-region is located upstream of the CH exons. The C region of the IgH chain determines the isotype of the Ig. In mature naïve B cells, the V-region is linked to the constant region of the μ chain (Cμ) [1292]. Consequently, mature naïve B cells express surface IgM and, as a result of alternative splicing, IgD as their BCR. A population of IgM^-IgD^+ class switched B cell has been reported. These cells are primarily found in secondary lymphoid organs and are not readily detected in peripheral blood [1293].

Upon activation, naïve IgM^+IgD^+ B cells can undergo CSR, resulting in a change of the heavy chain isotype of the produced immunoglobulin, while its antigen-specificity is retained. Non-switched B cells are $CD19^+$ and express IgM and IgD on their cell surface (Fig. 150A and B). The nonswitched IgM^+IgD^+ B cell population contains transitional B cells, Naïve mature B cells, and IgM^+CD27^+ memory B cells. The staining procedure outlined below is designed for detection of human immunoglobulin heavy chain isotypes expressed as BCRs on B cells.

2.6.3 Step-by-step sample preparation. This staining procedure is designed for human peripheral B cells. PBMCs were isolated

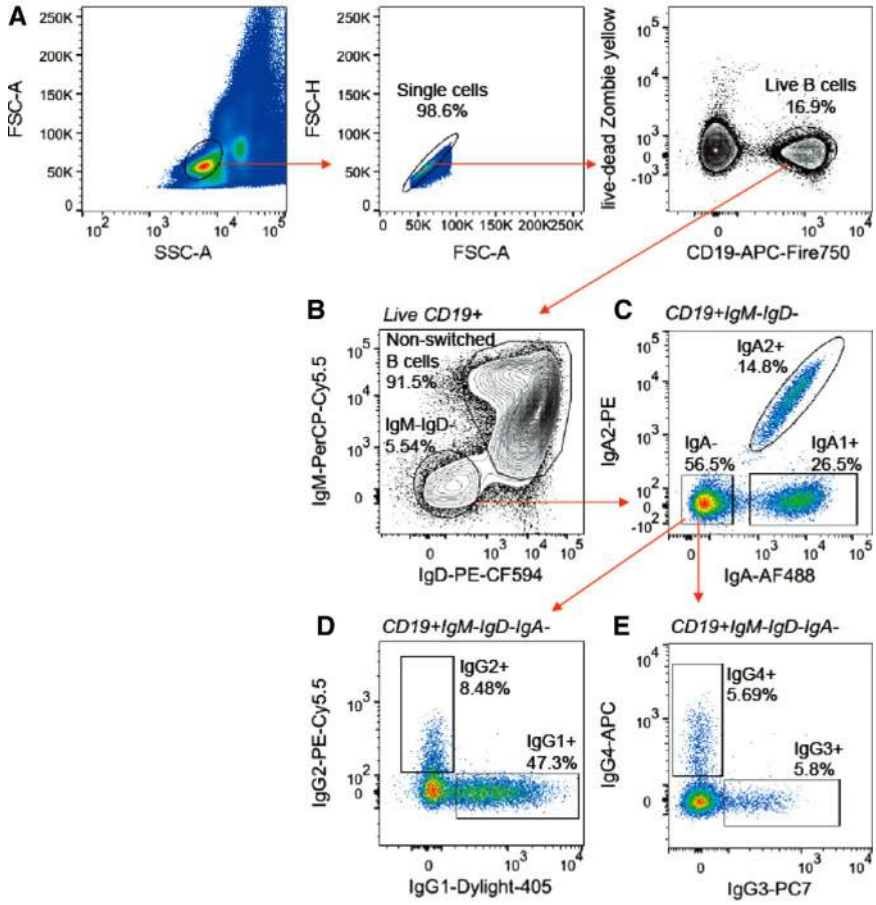

Figure 150. Identification of B cells expressing different Immunoglobulin heavy chain isotypes in a human PBMC sample (healthy individual age 47, male). (A) Lymphocytes were identified based on their FSC and SSC, Doublet exclusion was performed on FSC-H vs FSC-A, and B cells were gated as $CD19^+$ and zombie yellow (viability dye) negative. (B) Nonswitched B cells (IgD^+) and class-switched (IgM^-IgD^-) were gated. (C) Within the IgM^-IgD^- population, IgA^+ B cells, $IgA2^+$, and IgA^- cells can be distinguished. $IgA1^+$ B cells were defined as IgA^+IgA2^-. (D and E) IgA^- B cell were further differentiated based on expression of IgG1, IgG2 (D), IgG3, and IgG4 (E).

from heparinized blood of healthy individuals by density gradient centrifugation (Biochrom, Berlin, Germany). PBMC were counted and stained in PBS with zombie yellow viability dye (Biolegend, San Diego, CA). Samples were washed and incubated with antibodies listed in Table 52 and measured on a BD LSR Fortessa with BD FACSDiva Software Version 8.0.1 and analyzed using Flowjo version 10.4.

Detailed protocol:

1. Collect fresh blood in heparinized containers (BD vacutainer 170 I.U. of lithium heparin)
2. Isolate PBMC:
   (a) Dilute blood samples at a 1:1 ratio with PBS supplemented with 2 mM EDTA.
   (b) For each 30 mL of diluted blood prepare a tube of Biocoll. Add 15 mL of Biocoll separating solution to a 50 mL blood-sep-filter tube. The Biocoll should be at room temperature. Spin down 1 min 1100 × *g* to collect the Biocoll at the bottom of the tube.
   (c) Slowly add 30 mL of diluted blood to each filter tube and centrifuge the tubes at 800 × *g* for 20 min at 18°C and no break at end of program.
   (d) Collect the interphases and pool up to two interphases and transfer them to a new 50 ml centrifugation tube. Fill up tube with PBS supplemented with 2 mM EDTA. Centrifuge tubes at 780 × *g* for 10 min at 4°C.
   (e) Remove supernatant and resuspend cell pellet in 2 mL PBS supplemented with 2 mM EDTA. Pass cells through a 70 µM cell strainer into a new 50 mL centrifugation tube. Fill up tube with PBS supplemented with 2 mM EDTA. Centrifuge tubes at 220 × *g* for 10 min at 4°C.

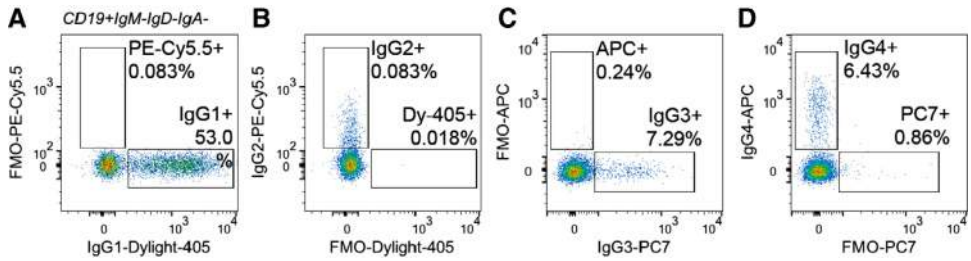

Figure 151. FMO controls for IgG subclasses. (A) FMO for IgG1-Dylight-405. (B) FMO for IgG2-PE-Cy5.5. (C) FMO for IgG4-APC. (D) FMO for IgG3-PC7. Upstream gating was performed as in Fig. 150.

(f) Discard supernatant and resuspend PBMC in 5 ml PBS supplemented with 2 mM EDTA.
3. Count PBMC and use between one and five million PBMC per staining.
4. Stain cells with Zombie yellow viability dye. Incubate 20 min at 4°C in dark. Wash 1x with staining buffer
5. Stain cells with Abs listed in Table 53 in a total staining volume of 100 μL. Incubate 15 min at 4°C in dark. Wash 1x with staining buffer
6. Stain cells with Streptavidin-PC7, incubate 15 min at 4°C in dark. Wash 1x with staining buffer.
7. Resuspend cells in 200 μL staining buffer and measure sample.

2.6.4 Materials.

Table 52.

Reagent	Manufacturer
Biocoll	Biochrom, Berlin, Germany
Blood separation filter tube	Dacos, Esbjerg N, Denmark
BD Falcon 70 μM cell strainer	BD Biosciences, Franklin Lakes, NJ, USA
Staining buffer: PBS + 2 mM EDTA + 2% BSA	Sigma, St Louis, MO, USA

2.6.5 Data analysis. B cells that undergo CSR will lose expression of IgM and IgD and can be gated as $CD19^+IgM^-IgD^-$ (Fig. 150B). A major fraction of the switched B cell compartment consists of IgA^+ B cells, which can be subdivided into $IgA1^+$ and $IgA2^+$ B cells. Here, we used an Ab against total IgA to identify all IgA^+ B cells combined with an anti-IgA2 Ab to separate $IgA2^+$ and $IgA2^-$ (i.e., $IgA1^+$) B cells (Fig. 150C). The IgA^- B cells can be further separated into $IgG1^+$, $IgG2^+$, $IgG3^+$, and $IgG4^+$ B cells (Fig. 150D and E), of which the $IgG1^+$ population is the most abundant (Fig. 150D). IgE^+ B cells are hardly detectable in healthy individuals and this population is not shown in this analysis. Expression of most Ig heavy chain isotypes, with the exception of IgM and IgD on non-switched B cells, is mutually exclusive. Thus a class-switched (IgM^-IgD^-) B cell will only express a BCR with one immunoglobulin heavy chain isotype. FMO controls for IgG subclasses are shown in Fig. 151.

2.6.6 Pitfalls. This protocol has been established for staining of PBMC samples. It may be applicable to other material such as tonsil, or other tissue-derived single cell suspensions. Cell suspensions from B cell rich tissues such as tonsils may require optimization of the antibody dilutions. Also when staining more than five million PBMCs, the amount of antibodies and/or the staining volume may need to be adjusted.

To the best of our knowledge, the heavy chain isotype-specific Abs that were used in this staining panel have do not cross-react with other isotypes. We did not observe significant populations of cells that were double positive for more than one Ig heavy chain isotype (other than IgM and IgD double positive non-switched cells). This can be easily confirmed by plotting every heavy chain isotype against every other.

2.6.7 Top tricks. This panel can be extended by adding selected surface markers of interest to study, in detail, the different heavy stain isotype-switched B cell subsets. The addition of fluorescently labeled antigens to the panel allows the measurement of the distribution of antigen-specific B cells among different heavy chain isotypes as we have demonstrated before [1294].

2.6.8 Summary table.

B cell population ($CD19^+$)	Phenotype (all $CD19^+$)	Expected frequency range within total CD19+ B cells	Expected frequency range within parent population
Non-switched	IgM^+IgD^+	40-95%	40-95%
IgA1-switched	$IgM^-IgD^-IgA^+IgA2^-$	2-10%	10-40%
IgA2-switched	$IgM^-IgD^-IgA^+IgA2^+$	1-5%	5-20%
IgG1-switched	$IgM^-IgD^-IgA^-IgG1^+$	5-10%	40-70%
IgG2-switched	$IgM^-IgD^-IgA^-IgG2^+$	0.5-6%	5-30%
IgG3-switched	$IgM^-IgD^-IgA^-IgG3^+$	0.2-1%	3-15%
IgG4-switched	$IgM^-IgD^-IgA^-IgG4^+$	0.01-1%	0.1-8%

3 Ab-secreting cells (plasmablasts and plasma cells)

3.1 *Murine Ab-secreting plasmablasts and plasma cells*

3.1.1 Overview. Plasma cells are terminally differentiated B lineage cells that secrete large amounts of Abs, a key step in establishing effective adaptive humoral immunity against pathogens and other toxic substances. After being activated in either a T cell-dependent or T cell-independent manner, B cells proliferate and initiate a transcriptional program (controlled by e.g., Irf4 and Blimp1) to adapt to the challenge of secreting enormous quantities of Abs. The induction of the plasma cell program begins with the transition of activated B cells to the proliferating plasmablast stage, where Ab secretion starts. Ab-secreting cells enter the blood stream, migrate to effector sites or survival niches, e.g., in the bone marrow, spleen, gut, or sites of inflammation and develop into mature, nondividing plasma cells. Some of these cells may

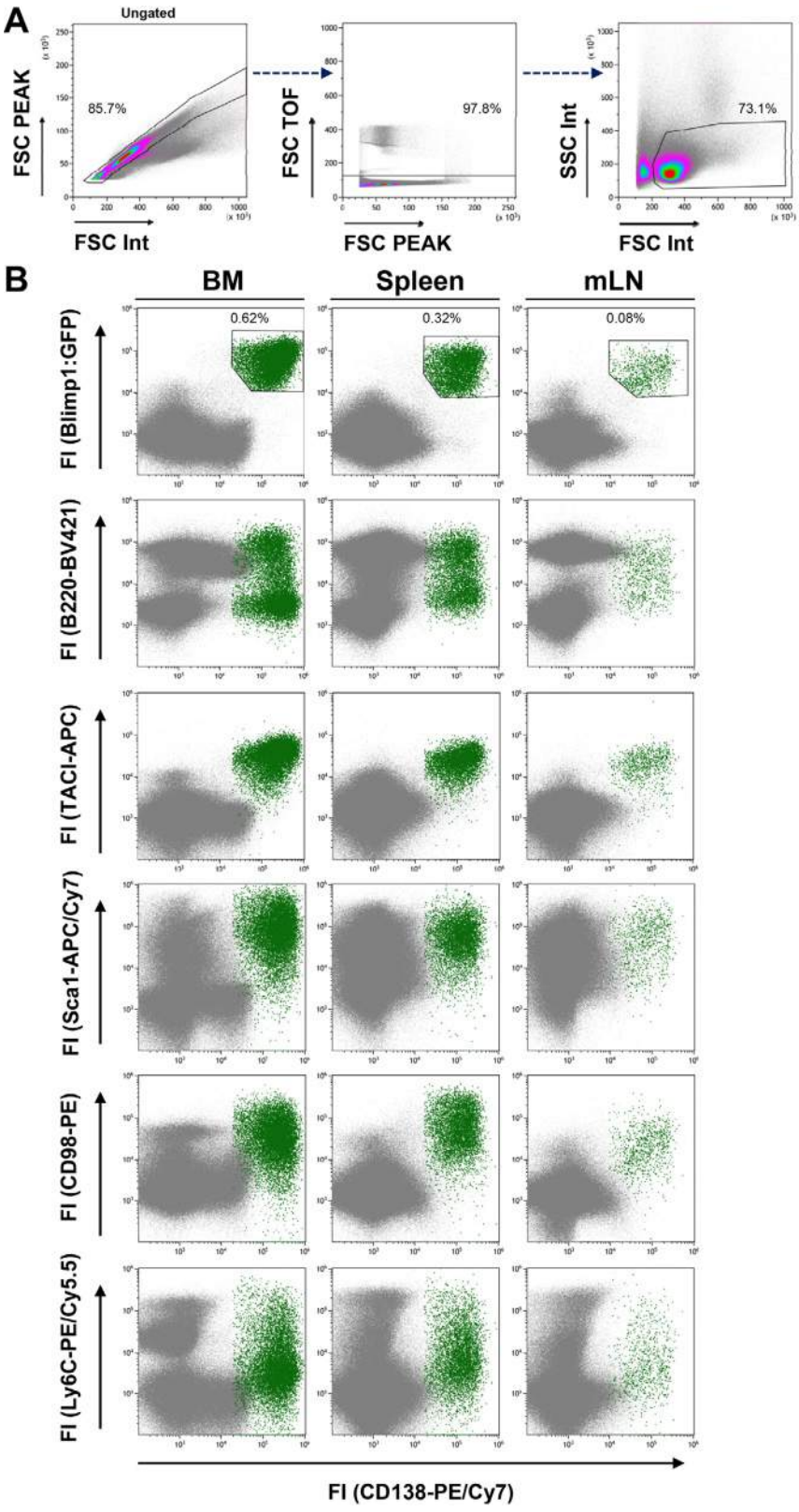

Figure 152. Comparison of common two-color flow cytometric analyses of plasma cell populations. (A) Exemplary gating strategy for single extended lymphocytes in spleen. (B) Single cell suspensions from bone marrow (BM), spleen and mesenteric lymph nodes (mLN) of Blimp1:GFP-reporter mice were isolated and stained as described with Abs against CD138 and one additional surface marker indicated on the y-axis. The Blimp1:GFP^{hi}/CD138^{hi} gate was used as the reference gate for the plasmablast/plasma cell populations and events in this gate are highlighted in green in the following plots.

Table 53. Antibodies and other reagents used for staining

Antibody	Clone	Species reactivity	isotype	Company	Dilution
IgA-AF488	Polyclonal	Human	polyclonal goat IgG	Jackson Immunoresearch, West Grove PA, USA	1:1500
IgA2-PE	REA995	Human	human IgG1	Miltenyi biotec, Bergisch Gladbach, DE	1:100
IgG1-Dylight405*	HP6188	Human	mouse IgG2b,k	Sanquin, Amsterdam, NL	1:1000
IgG2-PE/Cy5.5*	HP6014	Human	mouse IgG1,k	Sanquin, Amsterdam, NL	1:1000
IgG3-biotin* (followed by Streptavidin-PC7	HP6095	Human	mouse IgG1,k	Sanquin, Amsterdam, NL	1:1000
IgG4-APC	SAG4	Human	mouse IgG1,k	Cytognos, Salamanca, Spain	1:400
IgM-PerCP/Cy5.5	MHM-88	Human	mouse IgG1,k	Biolegend, San Diego, CA, USA	1:100
IgD-PE-CF594	IA6-2	Human	mouse IgG2a,k	BD Biosciences, Franklin Lakes, NJ, USA	1:35
CD19-APC/FIRE750	HIB19	Human	mouse IgG1,k	Biolegend, San Diego, CA, USA	1:100
CD27-BV510#	L128	Human	mIgG1,k	BD Biosciences, Franklin Lakes, NJ, USA	1:100
CD38-BV786#	HIT2	Human	mIgG1,k	Biolegend, San Diego, CA, USA	1:100
Zombie yellow viability dye	–	–	–	Biolegend, San Diego, CA, USA	1:100
Streptavidin-PC7	–	–	–	Biolegend, San Diego, CA, USA	1:2000

*These antibodies were labeled using lightning link labeling kits from Novus Biologicals, Centennial, CO, USA.
#These antibodies were included in the staining panel but are not applied in the gating strategy shown in Fig. 150.

persist for weeks up to years and continuously provide protective as well as pathogenic Abs. The following chapter will provide an overview of surface markers and detailed protocols to identify proliferating plasmablasts and nondividing plasma cells in various murine lymphatic tissues by FCM.

3.1.2 Introduction. Ab-secreting cells are a heterogeneous population ranging from very early proliferating (i.e., plasmablasts) to late nondividing and long-lived Ab-secreting cells (i.e., plasma cells); see also Chapter VI Section 3.2 Human Ab-secreting cells. Utilizing the Blimp1:GFP-reporter mouse line, which is frequently used to detect Ab-secreting cells [1295], we tested the efficiency of different surface marker combinations and gating strategies to distinguish plasmablasts from early and late plasma cells with a single staining panel.

Maturation of proliferating early Ab-secreting plasmablasts into resting long-lived plasma cells is accompanied by an increased abundance of immunoglobulins (Ig), Blimp1, CD138 (Syndecan-1), Transmembrane activator, and CAML interactor (TACI) and B cell maturation antigen (BCMA), while B cell-specific surface proteins such as CD19, CD20, MHCII, and B220 are downregulated [1296]. Combinations of these markers can be used to track the various subsets of Ab-secreting cells. In addition, Blimp1-reporter mouse lines (e.g., Blimp1:GFP) represent a handy tool to identify Ab-secreting cells by FCM or fluorescence microscopy. However, there are several limitations to consider when using the Blimp1:GFP reporter mouse. Most importantly, the GFP reporter signal alone is not sufficient for a reliable analysis of plasmablasts/plasma cells because Blimp1 is also produced by other immune cells, e.g., effector T cell subsets in the spleen and other lymphatic and nonlymphatic tissues [1297]. In addition, the knock-in of the GFP reporter cassette into the *Prdm1* gene (encodes Blimp1) results in an inactive *Prdm1* allele [1295]. Furthermore, in contrast to formaldehyde fixation the fluorescence of the GFP molecule is abolished by methanol/ethanol-based fixation protocols. Finally, the Blimp1:GFP reporter mouse might either be not available, or it might be too time consuming to cross the *Prdm1* reporter allele into other transgenic lines or disease mouse models. Therefore, alternative surface staining protocols to detect Ab-secreting cells on a single-cell basis by FCM have been developed.

As plasma cells produce large amounts of Igs, surface CD138 staining together with staining of intracellular Ig-kappa and Ig-lambda light chains was considered the gold standard for identifying Ab-secreting cells by FCM for many years [1298, 1299]. However, this protocol does not allow sorting of live cells. This can be accomplished by using a combination of a variety of other surface markers. Among the available markers, CD138 is most commonly used to analyze plasma cells, albeit its expression is not restricted to Ab-secreting cells. Therefore, CD138 staining with the detection of Blimp1-reporter expression, e.g., in the Blimp1:GFP mouse [1295], is frequently used as a reference staining to detect murine plasma cells. However, to allow the detection of Ab-secreting cells in mice that do not carry a Blimp1 reporter allele, CD138 staining together with a surface markers, e.g., TACI [1300], Sca-1 [1301], CD98 [1302], Ly6-C [1303], and B220 [1304], have been described in recent years. A caveat is that most of these double-stainings do not differentiate between early dividing plasmablasts and late nondividing plasma cells.

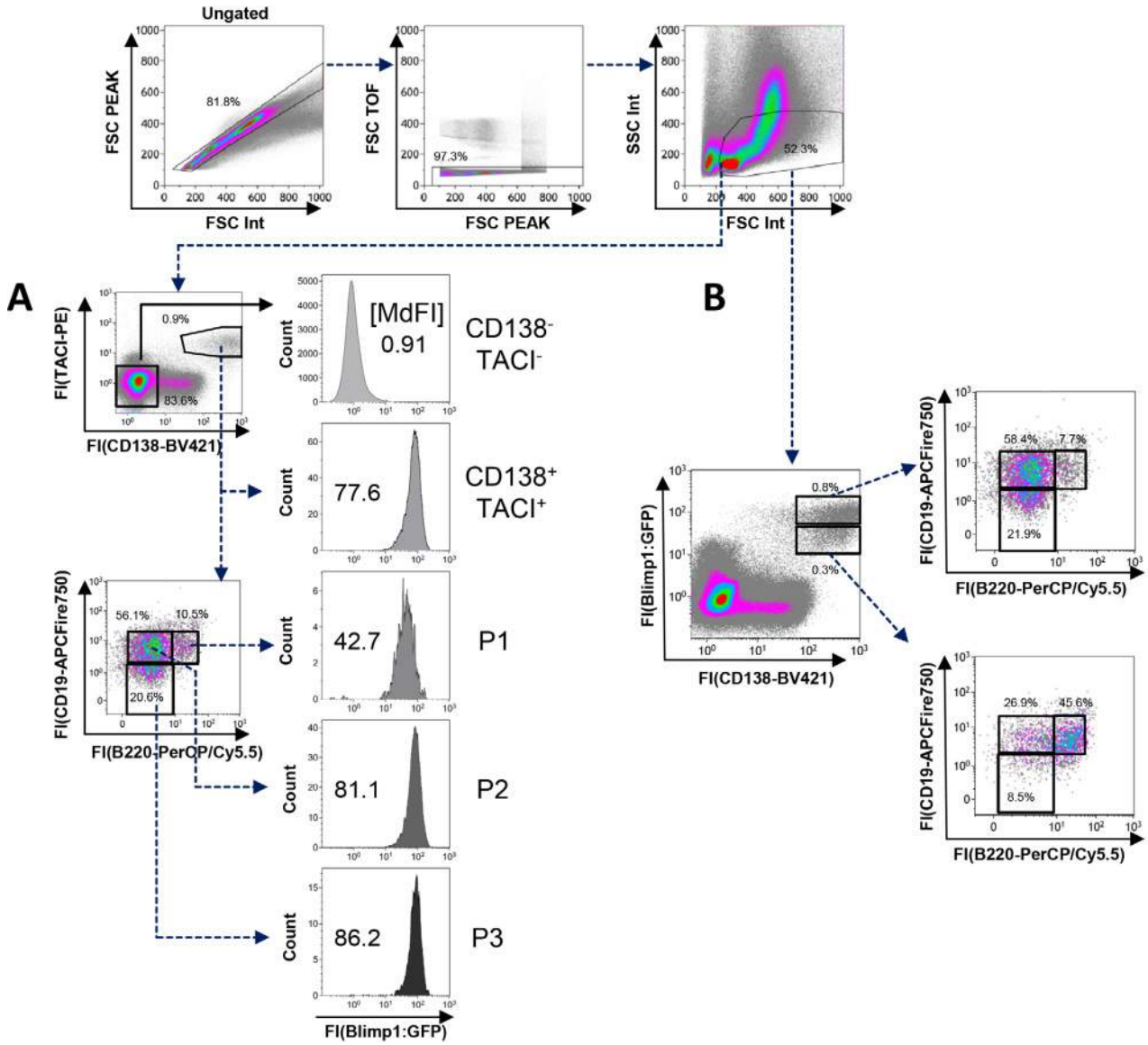

Figure 153. Flow cytometric distinction between plasmablasts, early- and late mature plasma cells. Single cell suspensions from the bone marrow (femur and tibia) of Blimp1:GFP-reporter mice were analyzed for their surface expression of CD138, TACI, CD19, and B220. Viable cells were defined using FSc/SSc characteristics. (A) $CD138^+/TACI^+$ cells and subpopulations defined on their B220 and CD19 abundance were analyzed for their Blimp1:GFP-expression (MdFI: Median fluorescence intensity); MdFI values are indicated in the depicted histograms. CD19 and B220 surface expression was used to further subdivide the $CD138^+TACI^+$ population (P1: $CD19^+/B220^+$; P2: $CD19^+/B220^{low}$; P3: $CD19^{low}/B220^{low}$). $CD138^{-/-}TACI^-$ cells were used as a negative control for Blimp1:GFP-expression. (B) $Blimp1:GFP^+/CD138^+$ cells were divided based on their fluorescence intensities in high-expressing population ($CD138^{high}/Blimp1:GFP^{high}$) and low- expressing population ($CD138^+/Blimp1:GFP^+$). These two subpopulations are further subdivided based on heterogeneous CD19/B220 expression.

To distinguish dividing plasmablasts from nondividing plasma cells, analysis of the proliferation marker Ki-67 can be useful. However, for staining of Ki-67, cells have to be fixed and permeabilized, which is incompatible with cell viability [547, 1214]. Another frequently used method to analyze Ab-secreting cells in mice is the treatment with the nucleotide analog BrdU (bromodeoxyuridine) or EdU (5-Ethynyl-2'-deoxyuridine) via the drinking water [1305, 1306]. In combination with additional surface markers such as CD138, this allows to (i) distinguish between BrdU/EdU-positive proliferating plasmablasts or freshly differentiated plasma cells and previously generated BrdU/EdU-negative mature plasma cells, as well as (ii) the tracking of BrdU/EdU-positive mature resting plasma cells over time.

Although the combined analysis of B220 and CD138 has also been used to identify plasmablasts and plasma cells for many years, the recently published four-color staining including CD138, TACI, B220, and CD19 is superior in separating proliferating plasmablasts from early and late plasma cell subsets because it (1) does not require intracellular Ki67-staining or a plasma cell reporter-mouse line, (2) it clearly excludes CD138-positive B cell

progenitors in the bone marrow (Fig. 153A), and (3) it allows the sorting of viable plasma cell subsets [547].

3.1.3 Step-by-step sample preparation.

3.1.3.1 Bone marrow. Bones (e.g., femurs, tibiae, humeri, vertebrae) were isolated, cleaned from surrounding tissue, and crushed with mortar and pestle in PBS + 2% FCS or RPMI 1640 medium supplemented with 10% FCS (R10). Residual bone fragments were removed by using a 70 μm cell strainer or decapped and flushed with 27G cannula and PBS + 2%FCS or R10. The bone marrow suspension was subsequently centrifuged at 300 × *g* for 5 min at 4°C. The pellet was resuspended in RBC-lysis buffer and incubated for 5 min at room temperature. Lysis was stopped by addition of PBS + 2% FCS or R10 medium, and the cell suspension was filtered through a 30 μm mesh filter.

3.1.3.2 Spleen. The spleen was isolated, cleaned from surrounding tissue, and gently disrupted in PBS + 2% FCS or R10 through a 70 μm cell strainer using the plunger of a 2 mL syringe. The cells were pelleted by centrifugation at 300 × *g* for 5 min at 4°C, resuspended in RBC-Lysis buffer and incubated for 5 min at room temperature. The lysis was stopped by addition of PBS + 2% FCS or R10 medium, and the cell suspension was filtered through a 3 0μm mesh filter.

3.1.3.3 Mesenteric lymph node. Mesenteric lymph nodes (typically about 4) were isolated and cleaned from surrounding fatty tissue. The lymph nodes were then gently disrupted in PBS + 2% FCS or R10 medium through a 70 μm cell strainer using the plunger of a 2 mL syringe.

3.1.3.4 Staining protocol. Cells from organ suspensions were pelleted by centrifugation at 300 × *g* for 5 min at 4°C, resuspended in PBS + 2% FCS and adjusted to a density of 2×10^7 cells/mL. A total of 4×10^6 cells from each tissue were washed in PBS + 2% FCS + 0.05% $NaN_3$and pelleted at 300 × *g* for 5 min at 4°C. To avoid unspecific binding, cell pellets were resuspended in 50 μL of unlabeled CD16/32 mAb (1:100 in PBS + 2% FCS + 0.05% NaN_3) and blocked for 15 min on ice (or 5 min at room temperature). Cells were washed again in PBS + 2% FCS + 0.05% $NaN_3$and centrifuged at 300 × *g* for 5 min at 4°C. The pellet was then resuspended in 50 μL PBS + 2% FCS + 0.05% NaN_3containing the respective fluorochrome-coupled Abs and incubated for 20 min on ice in the dark. After staining, the cells were washed twice with PBS + 2% FCS + 0.05% NaN_3 and centrifuged at 300 × *g* for 5 min at 4°C. The pellet was resuspended in PBS + 2% FCS + 0.05% NaN_3 for flow cytometric analysis.

3.1.4 Materials.

- Dulbecco's PBS
- FCS, heat-inactivated (56°C, 1 h)
- Sodium azide (NaN_3)
- Falcon® 70 μm cell strainer (Becton Dickinson)
- CellTrics® 30 μm filter (Sysmex)
- Red blood cell (RBC) lysis buffer (BioLegend, product number 420301)
- Gallios flow cytometer (Beckman Coulter)

Antigen	Fluorochrome	Supplier	Clone	Identifier
B220 (CD45R)	BV421	BioLegend	Ra3-6b2	103251
B220 (CD45R)	PerCP/Cy5.5	ThermoFisher	Ra3-6b2	103236
CD16/32	unlabeled	eBioscience	93	14-0161-86
CD19	APC/Fire750	BioLegend	6D5	115558
CD98	PE	BioLegend	RL388	128207
CD138 (Sdc1)	PE/Cy7	BioLegend	281-2	142514
CD138 (Sdc1)	BV421	BioLegend	281-2	142507
Ly6-C	PerCP/Cy5.5	ThermoFisher	HK1.4	45-5932-82
Sca-1 (Ly6-A/E)	APC/Cy7	BioLegend	D7	108125
TACI (Tnfrsf13b)	APC	ThermoFisher	eBio8F10-3	17-5942
TACI (Tnfrsf13b)	PE	ThermoFisher	eBio8F10-3	12-5942

3.1.5 Gating and analysis. In Fig. 152, we compared the presence or absence of one additional commonly used surface markers on $CD138^+$ cells to the $CD138^+$/Blimp1:GFP^+ reference population in bone marrow, spleen, and mesenteric lymph node. CD138 together with a B cell marker, e.g., B220 [1304], is the most commonly used staining protocol to distinguish between early dividing plasmablasts ($CD138^+/B220^+$) and mature $CD138^+/B220^-$ plasma cells (Fig. 152B, first row). However, without the addition of a Blimp1:GFP reporter (Fig. 152B, second row), it is difficult to clearly separate bone marrow $B220^+/CD138^+$ plasmablasts from $B220^+$ pro-B/pre-B cells with a moderate staining for CD138 [1097, 1307]. The detection of the survival receptor TACI on $CD138^+$ cells prevents these problems because almost all Blimp1:GFP-positive cells are included within a clearly separated $TACI^+/CD138^+$ population (Fig. 152B, compare row 1 with row 3 and [547]). CD98 and Sca-1 can also be used in conjunction with CD138 staining to detect Ab-secreting cells in bone marrow and spleen, but these populations are more

diffuse, and especially in the lymph node, are interspersed by cells outside of the CD138$^+$/Blimp1:GFP$^+$ reference gate (Fig. 152B rows 4 and 5). These protocols might be improved by the use of "dump" markers, e.g., F4/80 and CD4/CD8 as suggested by Wilmore et al. [1301]. Despite being described as a plasma cell marker, in our hands Ly6C is not suitable for the detection of all Ab-secreting cells, as it is not ubiquitously expressed in the Blimp1$^+$/CD138$^+$ plasmablast/plasma cell population (compare row 1 with row 6 in Fig. 152B). Therefore, the combination of CD138 and TACI staining is a robust protocol to detect a clearly separated plasmablast/plasma cell population in very high concordance with the CD138$^+$/Blimp1:GFP$^+$ reference across all analyzed lymphatic organs.

The double staining strategies described in Fig. 152 do not discriminate plasmablasts and plasma cells. Therefore, it is necessary to add additional surface markers. For example, the inclusion of the B cell markers CD19 and B220 into the TACI/CD138 staining protocol resulted in three sub-populations. All three subsets (P1–P3) were Blimp1:GFP-positive with a stepwise increase in the abundance of Blimp1:GFP fluorescence from P1 to P3 (Fig. 153A), indicating an increase in maturity from the P1 (dividing plasmablasts) to the P2 (early predominantly nondividing plasma cell) and the P3 (late nondividing plasma cells) subpopulation. While the B220$^+$/CD19$^+$ P1 population contains a high frequency of proliferating (Ki-67$^+$) cells, most of the cells in the subpopulations P2 and P3 are mature Ki-67-negative resting plasma cells [547]. In the spleen of non-immunized mice, the P1- and P2- subpopulations are dominant, while in the bone marrow the CD19$^-$/B220$^-$ P3 population is most prevalent.

In humans, CD19-negative plasma cell subpopulations have been described [1214]. However the biological origin and functional differences between the CD19$^+$ and CD19$^-$ plasma cell subpopulations remain largely unclear [1308].

3.1.6 Pitfalls and top tricks. To guarantee a reliable flow cytometric analysis of plasma cells in mice, some points should be considered. As mentioned before, other cells express markers used for detecting plasmablast/plasma cells such as Blimp1 (T cells) or CD138 (pro-B /pre-B cells). Therefore, strategies to identify plasma cells based on only one marker should be avoided. In addition, plasma cells express markers usually associated with other cell types (e.g., Ly6C [1303], CD11c [1309], CD56 [1310]). Therefore, care has to be taken when using "dump" gate markers. Furthermore, methanol/ethanol-based fixation methods will often result in a loss of the GFP-reporter signal. A prefixation step can prevent the leakage of cytosolic GFP and enable the retention of GFP fluorescence in a co-staining for cytosolic/nuclear antigens [522].

TACI/CD138 staining is also sensitive to different fixation strategies, e.g., formaldehyde fixation. In addition, TACI harbors protease cleavage sites (shedding) [1311] and can, therefore, be degraded when enzymes, e.g., collagenases are used to dissociate tissues. Plasma cells are also quite sensitive to mechanical stress due to their enlarged cytoplasm; therefore, vortexing of the samples should be avoided and cell pellets should rather be resuspended by finger tipping the reaction tube or careful pipetting.

Higher abundance of Blimp1 and CD138 is associated with a more mature stage of plasma cell differentiation [1295, 1296]. As demonstrated in Fig. 153B, the CD138$^+$/Blimp1:GFP$^+$-population in the bone marrow of mice contains two clearly separated subpopulations, CD138$^+$/Blimp1:GFP$^+$cells and CD138^{high}/Blimp1:GFP^{high} cells. Analysis of CD138 and B220 abundances revealed that the CD138$^+$/Blimp1:GFP$^+$population still expresses surface B220, while the majority of the CD138^{high}/Blimp1:GFP^{high} cells is negative for surface B220. Therefore, cells gated on Blimp1:GFP and CD138 contain early and late plasma cells.

In the bone marrow of unimmunized mice, frequencies of plasma cells range between 0.4 and 0.6% of viable cells, while frequencies in spleen and lymph nodes vary between 0.3 and 0.5% and 0.1 and 0.2%, respectively. Therefore, at least 1×10^6 events (optimally 3–4 $\times$ 10^6 events) should be acquired during the flow analysis in order to collect a sufficient number of events in the plasma cell gate for valid conclusions. As plasma cells have a larger cell size compared to other lymphocytes, the regularly used "lymphocyte gate" in the FSC/SSC plot has to be extended.

The paradigm of plasma cell differentiation includes the termination of membrane-bound IgH chain and a switch toward the production of only the soluble form of the B cell receptor. However, Pinto and colleagues found that human plasma cells still express functional IgM and IgA receptors on the cell surface, overturning the dogma of complete membrane-BCR loss upon plasma cell differentiation [1312]. We and others confirmed this finding in mice, i.e., almost all IgM- and IgA-producing CD138$^+$/TACI$^+$-plasmablasts and mature plasma cells present these IgH-isotypes as BCRs on their cell surface [547, 1166]. In contrast, IgG-producing mature plasma cells have lost the expression of surface IgG. Therefore, one could determine the frequency of IgH-isotype-expressing plasmablasts/plasma cells by including the detection of surface IgM and IgA in the previously described four-color staining (see Fig. 153).

3.2 *Human antibody-secreting cells*

3.2.1 Overview. Plasma cells (PC) are terminally differentiated B lymphocytes specialized on large-scale Ab production and secretion. PC are implicated in both protective and pathogenic humoral immunity, and, as long-lived cells, in humoral memory. Thus, they are being studied as therapeutic targets for the treatment of Ab-mediated diseases and as biomarkers for B cell activation in various clinical settings such as infection, inflammation, and vaccination.

In this chapter, we describe human ASC analyses by FCM. The vast majority of PC and their immediate precursors, the plasmablasts (PB), are characterized by high expression of CD27 and CD38, low or no expression of CD20, and variable expression of CD19, HLA-DR, and CD138. PB/PC represent approximately 0.01–1% of leukocytes in different tissues, and phenotypical

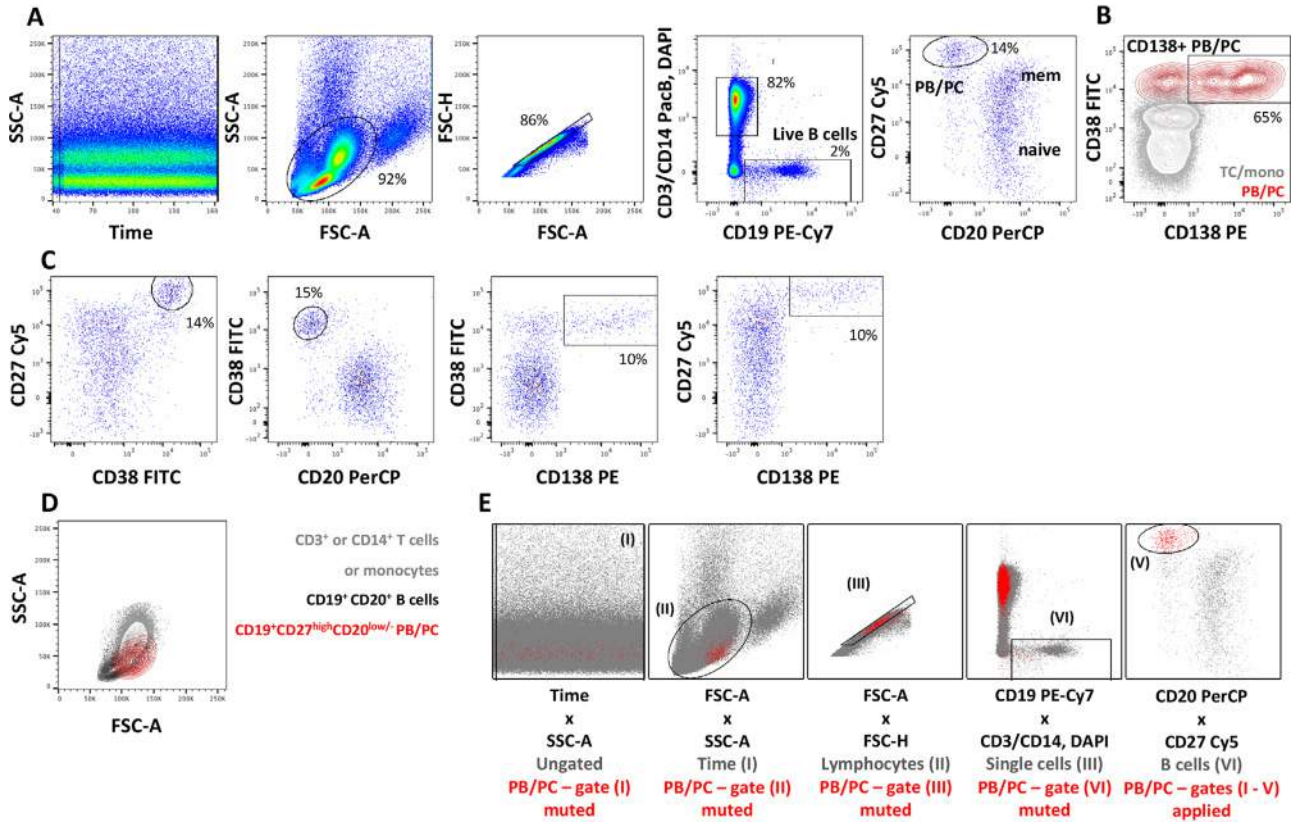

Figure 154. Representative gating strategy and analysis of human peripheral blood PB/PC. Whole blood from a patient with systemic lupus erythematosus (SLE) was diluted with PBS at room temperature, and subjected to density gradient centrifugation over Ficoll (GE Healthcare, Uppsala, Sweden) to isolate PBMC. Active SLE patients exhibit significant B lymphopenia, with increased frequencies and absolute numbers of PB/PC in peripheral blood [1246, 1315]. PBMC were washed with PBS/0.2% BSA, and stained at 4°C for 15 min with a cocktail of the following mAbs: CD19 (clone SJ25C1, BD), CD27 (clone 2E4; Sanquine), CD20 (L27, BD), CD14 (M5E2, BD), CD3 (UCHT1, BD), CD38 (HIT2, BD), CD138 (B-B4, Miltenyi Biotec). Cells were washed with PBS/0.2% BSA. DAPI was added prior to acquisition of the sample on a BD FacsCANTO II instrument for dead cell labeling. In total, 300 000 events were collected. (A) Gating strategy. Data were analyzed for changes of scatter or fluorescence parameters over the time of data acquisition, and optionally gated to remove parts of the acquisition that show irregular or discontinuous cytometric patterns. Then, a large light scatter parameter gate was used to identify lymphocytes and monocytes. FSC^{high} cells represent doublets and were excluded. SSC^{high} cells correspond to remaining granulocytes, likely low density granulocytes described before in SLE [1332] that were co-enriched along with PBMC. Next, cell aggregates were removed by gating on cells showing closely correlating area and height values of the FSC signal. Most cell doublets are characterized by a relatively increased FSC-area vs. FSC-height ratio. Live B cells were detected by staining for CD19, and exclusion of T cells, monocytes and dead cells according to CD3, CD14, and DAPI staining. Note that the B cell gate captures $CD19^{dim}$ cells, which can be strongly enriched for PB/PC. CD19 expression itself is subject to regulation in, e.g., autoimmune conditions [1328, 1333], so that boundaries of the CD19 B cell gate should be carefully validated. $CD19^+CD3^-CD14^-DAPI^-$ B cells were then analyzed for CD20 and CD27 expression, revealing $CD20^+$ subsets of naive and memory B cells besides PB/PC with a $CD27^{high}CD20^{low/-}$ phenotype. In this (SLE) sample, PB/PC are detectable at increased frequencies; normal donors show commonly less than 2% PB/PC among $CD19^+$ B cells. (B) PB/PC were then analyzed for expression of CD38 and CD138. Virtually all $CD27^{high}CD20^{low/-}$ gated PB/PC (red) expressed high levels of CD38, and two thirds expressed CD138. $CD3^+$ T cells and $CD14^+$ monocytes not expressing CD138 and containing very few $CD38^{high}$ cells are shown for comparison (grey). (C) As an alternative to the PB/PC gating shown in (A-B), total PB/PC, or $CD138^+$ PB/PC can be gated in various combinations of the markers CD20, CD38, CD27 and CD138, with consistent results. (D) PB/PC show a unique FSC and SSC profile distinct from that of total lymphocytes, B lymphocytes, and monocytes. (E) Backgating confirms the validity of the gating strategy. In particular, it shows that the entire PB/PC subsets was included during light scatter gating, some PB/PC events were excluded as doublets, and that significant amounts of T cells and/or monocytes share the $CD27^{high}CD20^{-/low}$ phenotype of PB/PC and may contaminate this population unless careful CD19 gating and DUMP channel exclusion is employed. An example for the detection of blood PB/PC by icIg staining is published in ref. [1322].

characteristics of PB/PC are associated with tissue origin, maturity level, and clinical context. Their low frequency, variable phenotype, and their uncommon light scatter properties should be considered when analyzing PB and PC by FCM.

3.2.2 Introduction. Plasma cells are terminally differentiated B cells capable of continuous production of Ab [1313]. Next to their immediate precursors, the PB, they are the only cells of the body that secrete Ab and contribute the vast majority of Ig detectable in serum and mucosal secretions. Thus, PC (also termed plasmacytes, plasmocytes, or named according to detection assays other than FCM: spot-forming cells (SFC), Ab-secreting cells (ASC), Ab-forming cells (AFC), plaque-forming cells (PFC), or Ig-secreting cells (ISC)) are the foundation and the cellular correlates of humoral immunity by secreting specific, commonly adaptively shaped Abs that neutralize or opsonize pathogens.

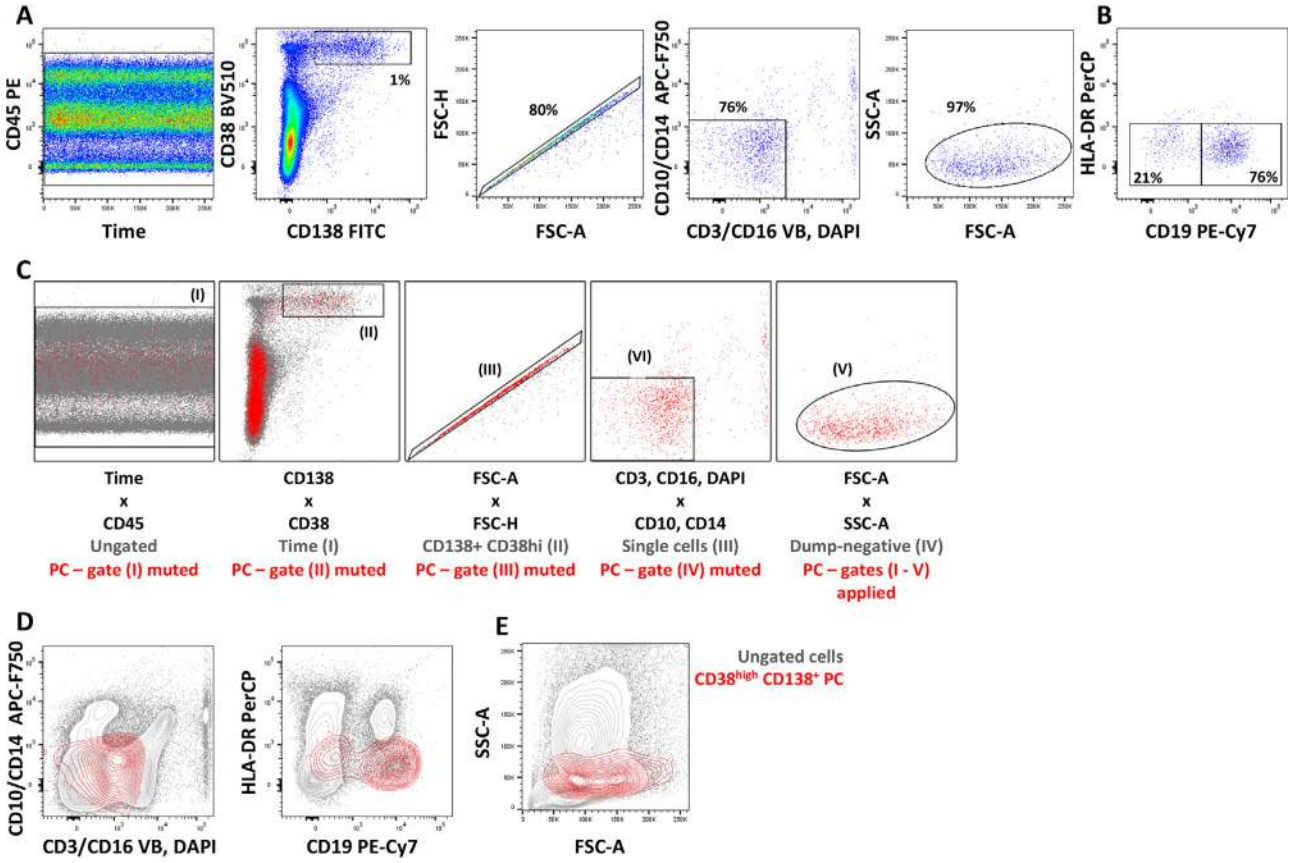

Figure 155. Representative gating strategy and analysis of human bone marrow PC. Bone marrow (BM) cells were flushed from a femoral head piece of a healthy donor using PBS/0.2% BSA/5 mM EDTA buffer and mononuclear cells were isolated via density gradient centrifugation over Ficoll. BM cells were washed with PBS/0.2% BSA/5 mM EDTA and stained at 4°C for 15 min with a cocktail of the following Abs:CD3-VioBlue (BW264/56, Miltenyi), CD16-VioBlue (REA423, Miltenyi), CD38-BV 510 (HIT2, BioLegend), CD138-FITC (44F9, Miltenyi), CD45-PE (HI30, BioLegend), HLA-DR-PerCP (L243, BioLegend), CD19-PE-Cy7 (HIB19, BioLegend), CD10-APC-Fire 750 (HI10a, BioLegend), CD14-APC-Fire 750 (M5E2, BioLegend). Cells were then washed with PBS/0.2% BSA/5 mM EDTA and stained with DAPI for later dead cells exclusion prior to acquisition of the sample on a MACS® Quant Analyzer. (A) Analytical gating strategy. Time/CD45 visualization confirms the stability of the cytometric measurement over time. Time frames showing discontinuous data should be excluded. As PC exhibit particular light scatter and background fluorescence properties, the $CD138^+CD38^{high}$ PC population was gated first, followed by cell aggregate exclusion and gating on $CD3^-$, $CD16^-$, $CD10^-$, $CD14^-$, and $DAPI^-$ cells, for exclusion of dead cells and cell types potentially contaminating the gated PC population. Then, the FSC-A/SSC-A plot reveals that PC show a broader light scatter value distribution than typical lymphocytes, which is in agreement with their increased size and ellipsoid shape. Should the FSC-A/SSC-A plot reveal remaining FSC^{low} and/or SSC^{low} cell debris or electronic artifacts, these should be excluded by gating at this step. (B) Human BM PC consistently display distinct populations with either high or low to no expression of CD19 [1214, 1324]. The absence of HLA-DR expression confirms at large the absence of PB [1245, 1322], and remaining $HLA\text{-}DR^+$ PB are excluded. (C) Backgating analyses of the procedure shown in (A). (D) Comparison of antibody staining and light scatter properties of total $CD138^+CD38^+$ BM PC vs total, ungated BM mononuclear cells. PC exhibit increased background fluorescence signals compared to other cells (possibly integrating cell size effects, autofluorescence, and nonspecific binding of labelled antibodies) stressing that subset gating should be adjusted at the level of PC rather than at global levels. Consistent with their increased size, nonspherical shape, and high organelle content, BM PC show a FSC/SSC pattern distinct from that of other BM cells.

So-called long-lived or memory PC can gain longevity and directly contribute to immune memory by long-term secretion of specific Ab [1305, 1314], a phenomenon termed humoral (or serological) memory.

Plasma cells are of interest to medical and biological research in various regards. Vaccines are tailored to induce long-lasting and specific Ab titres that result from the generation and persistence of vaccine-specific PC. On the other hand, PC are also the source of pathogenic Abs in autoimmune diseases and humoral transplant rejection, and constitute a potential therapeutic target in these conditions. Furthermore, the abundance of PB and PC in the peripheral blood serves as a biomarker for acute B cell responses in systemic autoimmune disease such as SLE [1315, 1316]. Upon vaccination and infection, especially antigen-specific PB are expanded in the blood [1214, 1246, 1317–1319]. The diagnosis, treatment, monitoring, and research in lymphoid tumors recapitulating PC features and biology, such as multiple myeloma, monoclonal gammopathy of undetermined significance (MGUS), reactive plasmacytoma, or Morbus Waldenstrom, are commonly associated with PC analyses by FCM.

Technically, antigen-specific PC can serve as a template for cloning Abs for new biomedical assays, diagnostics or therapeutic purposes. Furthermore, PC are investigated in a number of interrelated biological contexts such as apoptosis and survival

mechanism(s), large-scale protein production, and balancing the consequential cellular stress, transcriptional reprogramming, cell adhesion, and homing.

3.2.3 Activated B cells become plasma cells. Upon activation of B cells by B cell antigen receptor (BCR) stimulation by antigen, by cytokines, TLR ligands, cognate T cells, or combinations thereof, they start proliferating and differentiating into PB, or memory B cells. In vivo, this activation can target naïve, or antigen-experienced memory B cells, and leads to B cell differentiation within germinal centers (including somatic hypermutation and class-switching of Ig gene rearrangements, or in follicular or extrafollicular processes. In line with the observation that the differentiation of PB is fairly easy to mimic in vitro by different stimuli [1320, 1321], PB differentiation appears as the default differentiation pathway upon B cell activation.

Once formed, PB may either reside at the site of their generation (such as spleen or lymph nodes), or emigrate and transit via the blood to PC deposits in the gut lamina propria (LP) or the bone marrow (BM), or die. Immunization studies have been particularly useful for determining PB dynamics and biology in man [1214, 1245, 1246, 1313, 1319, 1322]. While PB and PC types are common in lymphoid tissues such as spleen and BM [1214, 1313], and are present at very low frequencies in peripheral blood at all times [1322], additional PB specific for the vaccination antigen appear in the blood as a sharp peak approximately 1 week after intramuscular or subcutaneous immunizations [1241, 1245]. Their presence in blood lasted longer when the immunization was applied via mucosal routes [1323]. At the PB stage circulating in peripheral blood, the cells have already started to secrete antibody that is detectable by Elispot assays [1245], express the proliferation marker Ki-67 [1214, 1322], and migrate along gradients of the chemokines CXCL12 and/or CCL28 (using CXCR4 and CCR10, respectively), navigating them into their BM or mucosal niches.

Besides primary and secondary lymphoid tissues including mucosa-associated lymphoid tissues, PB/PC can also be found at different sites under pathological conditions, such as inflammation (brain, cerebrospinal fluid, kidney, joints, and synovial fluid [1214], or in the form of multiple myeloma metastases.

3.2.4 Detection of PB and PC according to unique cell-surface receptor expression profiles. In the blood, PB and PC express the unique phenotype $CD19^{+}CD27^{high}CD38^{high}$ and show low or no expression of CD20 [1213, 1322, 1324]. CD138, often referred to as a PC marker, is expressed to only variable extents in the blood [1324, 1325] (Figure 154). Besides $CD38^{high}$ PB/PC, a minor $CD38^{low}$ subset has been defined in tonsils [1326], and CD27-negative differentiation stages have been described in in vitro studies [1327]. Blood PB/PC can show downregulated, yet still present levels of the B cell marker CD19 [1328]. During steady-state, PB/PC make up about 1% of peripheral blood B cells. One week after immunization, antigen-specific PB circulating in blood express high levels of HLA-DR, distinguishing them from HLA-DR^{low} cells sharing the typical $CD19^{+}CD27^{high}$ phenotype, but being non-migratory and non-proliferating, thus resembling BM PC [1313, 1322]. Taken together, blood PB and PC can be well distinguished from other B cells and other leukocytes according to their unique cell-surface marker expression profile. However, as all mentioned markers alone are also expressed by other cell types or B cell differentiation stages, multiple markers need to be co-stained to obtain a PB/PC population (i) that covers most of the PB/PC present in the sample under normal conditions and (ii) is sufficiently pure to permit their reliable quantification and phenotypical characterization. PC in deposit tissue such as the bone marrow (BM) express intermediate to high levels of CD138, usually very high levels of CD38 (a molecule that candidates as a therapy target for depletion of malignant PC in patients with MM [1329], lack CD20 expression, and show low or no expression of HLA-DR. Notably, CD19 is differentially expressed among mature BM and LP PC, and $CD19^{-}$ PC show consistent features of PC that have reached an exceptionally mature state [1214, 1330, 1331]. A representative analysis of human BM PC is shown in Fig. 155.

3.2.5 Detection of PB/PC according to high expression of intracellular Ig and by cellular affinity matrix assay. Apart from cell-surface staining, PB and PC can be detected by staining intracellular Ig (icIG) [1322]. Consistent with large-scale Ab production by PB and PC, they accumulate large amounts of it in their cytoplasm, and intracellular flow cytometric staining without prior in vitro stimulation and/or secretion inhibition yields high signal intensities that are suitable to distinguish $icIg^{high}$ PB/PC from Ig^{+} B cells, which do not express extraordinarily high levels of icIg and to which anti-Ig Abs bind mainly via their cell-surface Ig (BCR). Fixation with 1.5% formaldehyde solution and mild permeabilization with 0.1–0.5% saponin solution is sufficient to permit detection of icIg in PB/PC.

The above cell-surface markers, IgD, and intracellular (ic)IgM, icIgA, and icIgG, were combined in an optimized multicolor panel (OMIP) for the detection of PB/PC [1334].

Furthermore, affinity matrix technology has been developed to cytometrically capture PB and PC according to their ability to secrete Ab, thus providing access to live and functional PB/PC [621, 1326]. Abs capturing the Ig of interest are immobilized on the cell surface, and the cell suspension is short-term cultured to permit antibody secretion by PB/PC. The secreted antibody is bound by the cell-bound capture antibody and detected by a second, fluorochrome-labeled anti-Ig antibody, which specifically stains the cells that have secreted Ig during the culture phase.

Activated B cells undergoing PC differentiation gradually downregulate the expression of the membrane B cell receptor, and start to secrete the soluble form of Ab. At the PB stage in the blood, cell-surface IgM^{+}, and IgA^{+} PB are detectable, and cell-surface IgG is also expressed at least after recent vaccination, as evidenced by specific cell-surface binding of fluorescently labeled antigen) [1241] Notably, cell-surface BCR is not detectable

anymore in mature IgG^+ PC, while IgM^+, and IgA^+ PC in deposit tissues can maintain expression of cell-surface Ig [1312, 1335].

3.2.6 Receptors expressed by plasma cells. Besides Ig of different classes and subclasses, PB and PC, or their subsets express receptors and transcription factors that are implicated in their survival, maturity, and homing, such as, for example, the cytokine receptors IL-6R (CD126), BCMA, and TACI, selectins, integrins, and chemokine receptors such as CD62L, $\alpha4\beta1$, and $\alpha4\beta7$ integrins, CXCR4, CXCR3, CCR9, and CCR10, transcription factors BLIMP-1, IRF4, and the anti-apoptotic protein Bcl-2 [1214, 1245, 1313, 1324, 1330, 1336, 1337]. Notably, highly mature PC lose expression of PAX5, leading to the expression of a number of receptors that are typically absent from B lineage cells such as CD56, CD28, and CCR2 [1214, 1338].

3.2.7 Light scatter properties of plasma cells. PB and PC exhibit a unique morphology reflecting their role as protein factories. They show an enlarged cytoplasm with expanded Golgi apparatus and endoplasmatic reticulum content, and an eccentrically located nucleus. Coherently, PB/PC show increased FSC/SSC light scatter signals, and a broader distribution, compared to small lymphocytes (Figs. 154 and 155). This entails an important caveat when analyzing PB/PC in routine immune profiling studies in which gating strategies start off from a small lymphocyte gate. Any gating performed "upstream" of the PB/PC gate should be carefully checked for unwanted selection against PB/PC fractions. The increased cell size may also lead to increased fluorescent background signal of PB/PC compared to smaller lymphocytes (Figs. 154 and 155), thus, control staining (such as isotope controls if helpful, or FMO controls) should always be evaluated on the same PB/PC fraction that is subject to analysis.

3.2.8 Sample preparation. Flow cytometric assessment of PB/PC is commonly performed from single-cell suspensions obtained by either red blood cell lysis of whole blood, density gradient centrifugation to obtain mononuclear cells (such as PBMC), or tissue cell suspensions obtained by protocols tailored for individual tissue types. Since collagenase treatment has been shown to liberate additional fractions of PC from tonsillar tissue compared to mechanical processing alone [1339], digestion protocols can be considered to retrieve PC or certain fractions of PC. It should be noted that different enzymes used for this purpose may differently impact on the detectability of different cell-surface receptors, including the above mentioned used to detect human PC. PB/PC tend to die rapidly during longer preparation protocols and when cultured in the absence of survival promoting cytokines. Thus, keeping cells cool and working quickly is key. Protocols should be kept short to avoid excessive death of PB/PC after preparation, and dead cell detection and exclusion should be performed.

When analyzing rare fractions of PB/PC such as antigen-specific cells, PB/PC may be pre-enriched for FCM analyses by magnetic cell sorting, e.g., by depleting large, unwanted sample fractions such as granulocytes, T cells, and monocytes, etc., or by direct enrichment of $CD138^+$ cells. One should carefully choose depletion markers (and DUMP channel markers) as mature PC subsets (and especially malignant PC) can express markers like CD28, CCR2, and CD56 commonly associated with T cells, monocytes, or NK cells, respectively.

Live-cell cryopreservation using standard procedures and media such as FCS/DMSO impacts on detection of PB/PC. Usually, after freezing and thawing, frequencies of PB/PC are much lower compared to fresh cell preparations, and the detection of some receptors including CD138 have been described to be impaired after cryopreservation [1340].

Since PB/PC are commonly found at low to very low frequency in cell suspensions, the separation of PB/PC from cells that share elements of the PC phenotype is key, and the use of carefully designed DUMP channels is advised. For example, PBMC contain high frequencies of $CD27^{high}$ expressing T cells that may contaminate the $CD19^{dim}/CD27^{high}$ PB/PC gate unless T cells are excluded from the analysis. Since PB/PC are infrequent in many cell suspensions from primary tissue, care must be taken to acquire suitable total cell numbers, which ensure that sufficient PB/PC are recorded for the desired statistical analysis.

Generally, it must be stressed that, to deliver accurate results, PB/PC analyses require careful experimental and cytometric setup and validation that can be very specific to a certain project (considering what readout parameters are to be measured), tissue specific phenotypes and sample logistics.

4 Innate lymphoid cells

4.1 *Overview*

This section will give an overview on the flow cytometric strategy to gate on different subsets of tissue-derived innate lymphoid cells (ILCs) in humans and mice. While only murine small intestine and human tonsils are representatively shown, the use of master transcription factors in combination with established surface markers can be generally used across different tissues to identify ILC subsets.

4.2 *Introduction*

During the past years, an emerging family of $CD45^+$ innate lymphoid cells (ILCs) has been described in both mouse and man. $CD45^+$ ILCs lack rearranged antigen receptors as well as lineage (Lin) markers typically expressed on T cells, B cells, or dendritic cells (DCs) [1341]. ILCs can be classified into distinct groups according to the expression of surface markers, transcription factors and effector cytokines (reviewed in ref. [1342]). ILC1 express T-box transcription factor T-bet (T-bet) and produce IFN-γ in response to IL-12 and IL-18 or activating receptor engagement, thus contributing to the response against viruses and intracellular pathogens [1343–1346]. ILC2 express GATA binding protein-3 (GATA3), produce IL-13 and IL-5 in response

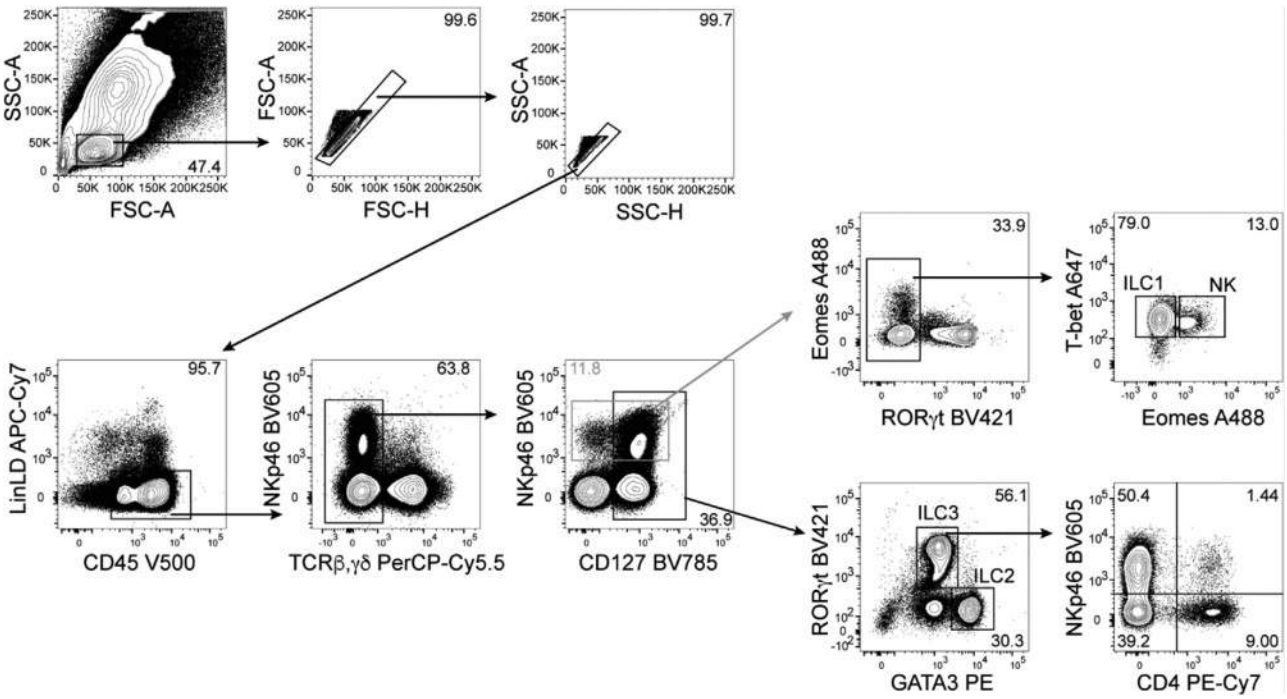

Figure 156. Identification of murine SI LP ILCs. Representative gating strategy of ILCs derived from the small intestinal (SI) lamina propria LP of 6-week-old C57BL/6 mice. Mononuclear cells (MCs) were prepared as previously described [1350]. Cells were gated as viable (LD^-), $B220^-$ $CD11c^-$ $Gr\text{-}1^-$ $F4/80^-$ $Fc\varepsilon R1\alpha^-$ (Lin^-) $CD45^+$ $TCR\beta^-$ $TCR\gamma\delta^-$ and either as $NKp46^+$ (grey gate) $T\text{-}bet^+$ $Eomes^-$ ILC1, $Eomes^+$ $T\text{-}bet^+$ NK cells or as $CD127^+$ (black gate) $GATA3^+$ $ROR\gamma t^-$ ILC2 and $ROR\gamma t^+$ $GATA3^{lo}$ ILC3 which can be further separated according to NKp46 and CD4 expression.

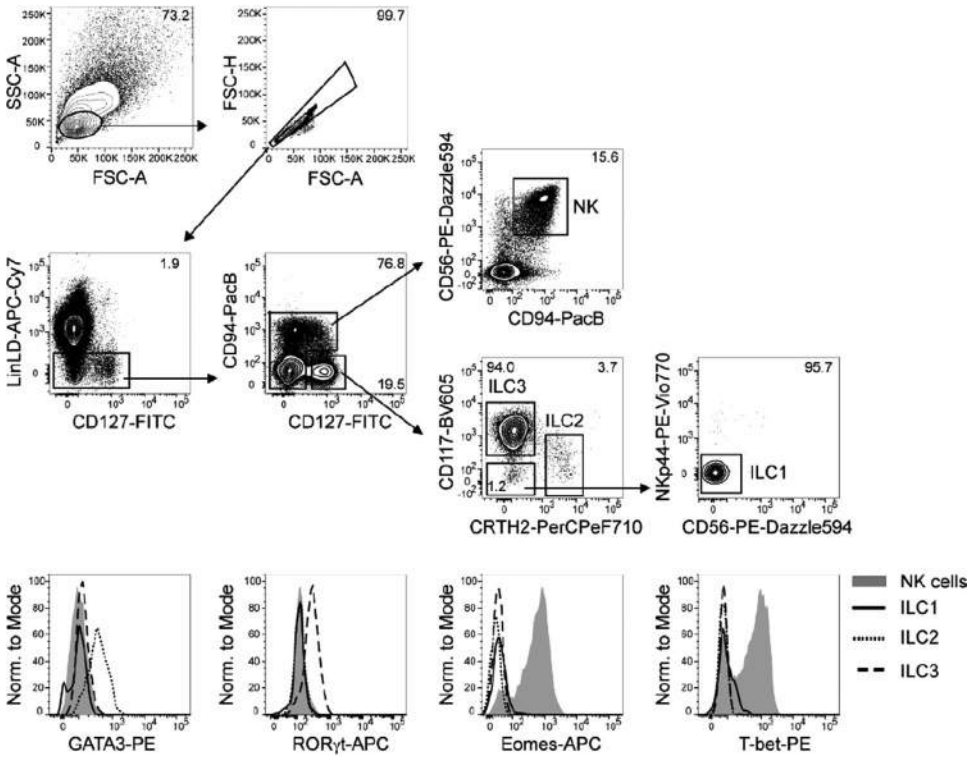

Figure 157. Identification of human tonsil ILCs. Representative gating strategy (upper panel) and expression of transcription factors (lower panel) of human tonsil ILCs. After magnetic depletion of $CD3^+$ cells, cells were gated as viable (LD^-), $CD3^-$ $CD14^-$ $CD19^-$ $Fc\varepsilon RI\alpha^-$ $CD123^-$ $CD11c^-$ $BDCA3^-$ (Lin^-) and either $CD94^+$ $CD127^{-/lo}$ $CD56^+$ NK cells; $CD94^-$ $CD127^{hi}$ $CD117^+$ $CRTH2^-$ ILC3; $CD94^-$ $CD127^{hi}$ $CD117^{+/lo}$ $CRTH2^+$ ILC2; or $CD94^-$ $CD127^{hi}$ $CD117^-$ $CRTH2^-$ $NKp44^-$ $CD56^-$ ILC1.

to IL-25, IL-33, and Thymic stromal lymphopoietin (TSLP) and contribute to the defense against helminthic infections as well as to the pathogenesis of allergic inflammation [1347]. ILC3 express retinoic acid receptor (RAR)-related orphan receptor RORγt, and produce IL-17 and/or IL-22 in response to IL-1β and IL-23 or activating receptor engagement. ILC3 include both fetal-derived lymphoid tissue-inducer (LTi) cells (considered as a distinct subset [1342]) and post-natal ILC3; LTi are required for the embryonic development of lymph nodes and Peyer's patches, while ILC3 contribute after birth to defense against extracellular pathogens, containment of commensals, epithelial tissue homeostasis, and regulation of inflammatory disorders, such as IBD and psoriasis [1348]. As such, ILC1, ILC2, and ILC3 show similarities with $CD4^+$ T helper (Th) subsets Th1, Th2, and Th17 and mirror the functional analogies between natural killer (NK) cells and adaptive $CD8^+$ cytotoxic T lymphocytes (CTL) [1341, 1349]. Accordingly, the International Union of Immunological Societies (IUIS) now recognizes five related innate lymphoid subsets: NK cells, ILC1, ILC2, ILC3, and LTi cells [1342].

4.3 *Step-by-step sample preparation*

For isolation of murine SI LP MCs a previously described protocol was used [1350]: residual fat tissue, Peyer's Patches and feces were removed, and the intestine was cut open longitudinal and washed with PBS. After clearing, tissue was cut into pieces of 1 cm length and digested with a lamina propria dissociation kit (Miltenyi), according to the manufacturer's instructions. Lymphocytes were further enriched on a 40%/80% Percoll gradient.

Written informed consent was obtained from all patients prior to sample acquisition and experiments have been approved by the Ethics Committee of the Charité Medical University, Berlin (EA2-078-16, EA1/149/1). Mononuclear cells (MCs) from human tonsils were isolated from patients undergoing tonsillectomy as previously described [1351]. After mashing and density gradient centrifugation using Ficoll-Paque PLUS, ILCs were enriched by using magnetic cell depletion of $CD3^+$ T cells with CD3 mAb microbeads and LD columns (Miltenyi) according to the manufacturer's instructions.

4.4 *Materials*

Flow cytometry:

Phenotypic analysis of murine lymphocytes was performed using the following Abs reactive to murine surface or intracellular antigens: eFluor780 Fixable Viability Dye, APC-eFluor780 anti-FcεRIα (MAR-1), PerCP-Cy5.5 anti-TCRβ (H57-597), PerCP-eFluor710 anti-TCRγδ (GL-3), eFluor660 anti-T-bet (4B10), Alexa488 anti-Eomes (Dan11mag) (eBioscience); APC-Vio770 anti-B220 (RA3-6B2), PE anti-GATA3 (REA174) (Miltenyi); APC-Cy7 CD11b mAb (M1/70), CD11c mAb (N418), anti-Gr-1 (RB6-8C5), anti-F4/80 (BM8), BV785 CD127 mAb (A7R34), BV605 anti-KLRG1 (2F1/KLRG1), BV711 CD4 mAb (RM4-5), PE-Cy7 anti-NKp46 (29A1.4) (BioLegend); V500 CD45 mAb (30F11), and BV421 anti-RORγt (Q31-378) (BD).

Staining for transcription factors was performed using the Foxp3 Transcription factor staining buffer set (eBioscience) according to manufacturer's instructions and cells were immediately analyzed. Flow cytometric analysis was performed by using BD LSRII or Fortessa employing FACSDiva Software (BD Biosciences), and data were analyzed by using FlowJo software (Tree Star).

Phenotypic analysis of human lymphocytes was performed using the following Abs reactive to human surface or intracellular antigens: eFluor780 Fixable Viability Dye, APC-eFluor780 CD14 mAb (61D3), CD19 mAb (HIB19), CD3 mAb (SK7), CD123 mAb (6H6), eFluor660 anti-Eomes (WD1928), PE anti-T-bet (eBio4B10), or anti-GATA-3 (TWAJ), PE-Cy7 anti-T-bet (eBio4B10), APC anti-RORγt (AFKJS-9) (eBioscience); APC - Vio770 CD141 mAb (AD5-14H12), anti-FcεRIα (CRA1), and CD11c mAb (MJ4-27G12), Fitc CD127 mAb (MB15-18C9), PE-Dazzle594 CD56 mAb (HCD56), PE-Vio770 NKp44 (2.29) (Miltenyi Biotec); BV605 CD117 mAb (104D2), PerCP-Cy 5.5 anti-CRTH2 (BM16), Pacific Blue CD94 mAb (XA185) (conjugated in house).

4.5 *Data analysis*

How can we identify these different NK cell and ILC subsets in different tissues from different species? The analysis of NK cells is described in the NK chapter by Moretta et al., where readers can find more details (See also Chapter VI Section 5 Natural Killer cells). ILCs are present in diverse organs as tissue-resident cells but are also detected in the circulation [1346, 1352]. In mouse small intestinal (SI) lamina propria (LP), all ILCs, namely NK cells, ILC1, ILC2, and ILC3 could be described [1345, 1353]. In Fig. 156 a gating strategy for murine ILCs derived from SI LP is shown; however, it should be stressed that ILC populations are not equally distributed in all organs and display some tissue-specific phenotypic differences. Combination of intranuclear staining of master transcription factors, namely T-bet (expressed on ILC1, NK cells and a subset of murine ILC3), Eomes (NK cells), RORγt (ILC3), and GATA3 (ILC2) together with NKp46 and CD127 (IL-7Rα) (Figure 156) or CD90 (not shown) enables identification of ILC subsets in all organs analyzed. Among SI LP $CD45^+$ Lin^- cells, NKp46 (or NK1.1) can be expressed not only on NK cells but also on ILC1 and a subset of ILC3. Thus, staining of transcription factors is helpful to dissect their identity (see also Chapter V Section 13 Transcription factors). It has been proposed that SI LP NK cells can be defined as $NKp46^+$ $ROR\gamma t^-$ $T\text{-}bet^+$ $Eomes^+$ cells, while ILC1 are $NKp46^+ROR\gamma t^-$ $T\text{-}bet^+$ $Eomes^-$ cells [1345] (Figure 156). However, a population of cytotoxic $NKp46^+$ $ROR\gamma t^-$ $T\text{-}bet^+$ $Eomes^+$ intraepithelial ILC1 has been also described [1354]. Moreover, the analysis of NK/ILC1 in different mouse compartments revealed a high degree of phenotypic and functional complexity [1346, 1355], suggesting that distinction between NK and ILC1 cells might be more challenging.

ILC2 and ILC3 are enriched among SI LP CD45$^+$ Lin$^-$ CD127$^+$ lymphocytes and can be identified after intranuclear staining of GATA3 and RORγt as GATA3^{hi} RORγt$^-$ ILC2 and of GATA3^{lo} RORγt$^+$ ILC3 (Figure 156) [1353, 1356]. Surface markers such as ST2 (IL-33R), CD25, ICOS, or KLRG1 have also been commonly used to identify ILC2 [1353, 1357, 1358]. As previously mentioned, expression of these markers slightly varies in different compartments.

SI LP RORγt$^+$ ILC3 can be dissected into three major subsets according to NKp46 and CD4 expression (Figure 156), namely CD4$^+$ ILC3, which functionally and phenotypically resemble fetal LTi and preferentially produce IL-17 and IL-22; NKp46$^+$ ILC3, which expand postnatally, co-express RORγt and T-bet and produce IL-22 and IFN-γ; and CD4$^-$ NKp46$^-$ ILC3, which actually represent a heterogeneous population of CCR6$^+$ cells (related to LTi) and CCR6$^-$ ILC3, co-expressing RORγt and T-bet, similar to NKp46$^+$ ILC3 [1359–1361]. As it has been shown that ILC3 can be plastic in vivo, and downregulate RORγt expression while acquiring NK/ILC1-cell features such as T-bet expression and IFN-γ production, the use of RORγt fate mapping (RORγt^{fm}) can be helpful to distinguish ex-ILC3 (RORγt^{fm+} RORγt$^-$ T-bet$^+$) from ILC1 [1361, 1362]. Although this distinction is conceptually important, ex-ILC3 behave functionally similar to NK/ILC1 cells.

In humans, ILCs have been documented in several tissues and in the circulation, although a larger characterization has been performed in tonsils, where all ILC subsets have been described

Table 54. Selection of important markers for flow cytometry analysis of mouse and human ILC

	Mouse					Human				
	NK cells	CD127$^+$ ILC1	ILC2	NCR$^-$ ILC3	NCR$^+$ ILC3	NK cells	CD127$^+$ ILC1	ILC2	NCR$^-$ ILC3	NCR$^+$ ILC3
Marker										
CD127	–	+	+	+	+	lo/-	+	+	+	+
CD117	lo/-	–	+	–	lo	lo/-	–	+/–	+	+
CD25	–	lo	+	+	ND	+/–	lo	+	+/–	lo
IL-23R	–	lo/-	ND	+	+	lo	+/–	lo	+	+
IL-17RB	–	–	+	–	–	–	lo/-	+	ND	–
ST2	–	–	+	–	–	–	ND	+	ND	–
IL-1R1	–	lo	ND	+	+	+/–	lo/-	lo	+	+
CCR6	–	–	–	+/–	–	–	+	+	+	+
RANKL	lo/-	ND	ND	+	+	–	ND	ND	+	+
CRTH2	ND	ND	ND	ND	ND	–	–	+	–	–
ICOS	–	ND	+	ND	+	–	–	+	ND	+
NK1.1/CD161	+	+	–	–	lo/-	+/lo	+	+	+	+
CD56	NA	NA	NA	NA	NA	+	–	–	+/–	+/–
CD94	+/–	ND	+/–	–	+/–	+/–	–	–	–	–
CD16	+/–	ND	–	–	–	+/–	–	–	–	–
NKp30	NA	NA	NA	NA	NA	+	ND	+/lo	+/–	+
NKp44	NA	NA	NA	NA	NA	+[a]	–	–	–	+
NKp46	+	+	–	–	+	+	–	–	+/–	+
Ly49/KIR	+/–	lo	–	–	–	+/–	–	–	–	–
CD57	NA	NA	NA	NA	NA	+/–	ND	ND	ND	ND
CD27	+/–	+	–	–	–	+/–	+	–	–	–
CD11b	+/–	–	–	ND	ND	+/–	ND	ND	ND	ND
Perforin	+	lo	–	–	–	+	–	–	–	–
Transcription factors										
T-bet	+	+	–	+/–	+	+	+	–	–	–
Eomes	+	–	–	–	+	+	–	–	–	–
RORγt	–	–	–	+	+	–	–	–	+	+
GATA3	–	lo	+	lo	lo	lo/-	lo/-	+	lo/-	lo/-
Cytokines										
IFNγ	+	+	-/lo	-/lo	-/lo	+	+	–	–	–
IL-22	–	–	+	+	+	–	–	lo	lo/-	+
IL-17	–	–	–	+/–	–	–	–	–	+	–
IL-13	–	–	+	–	–	lo	–	+	–	lo
IL-5	–	–	+	–	–	–	–	+	–	–

+ Indicates high expression, - indicates no expression, +/– indicates bimodal expression, lo indicates low expression, a indicates expression on activated cells, ND indicates not determined, and NA indicates not applicable according to published reports [1344–1347, 1350, 1353, 1354, 1356–1365, 1367, 1374–1384]

[1354, 1363–1365]. In tonsils, magnetic depletion of $CD3^+$ T cells and of $CD19^+$ B cells is recommended for better detection of ILCs, due to their low frequency. After pre-enrichment and further gating on Lineage negative cells, staining of CD94 and CD127 enables the identification of NK cells, as $CD94^{+/lo}$ $CD127^{neg/lo}$ $CD56^+$ cells, which express high levels of T-bet and Eomes, and of other ILCs enriched among Lin^- $CD127^{hi}$ $CD94^-$ cells (Fig. 157).

It has been proposed that staining of CD117 (the receptor for stem cell factor, c-kit) and CRTH2 (prostaglandin D2 receptor chemoattractant receptor-homologous molecule expressed on T helper type 2 cells) facilitates identification of ILC3 and ILC2 in tonsils [1366]. ILC3 are enriched among $CD117^+$ $CRTH2^-$ cells and express NKp44 and RORγt, while lacking T-bet and Eomes [1365, 1367]. ILC2 are enriched among $CD117^{-/lo}$ $CRTH2^+$ cells and express GATA-3, while lacking T-bet and Eomes (Figure 157) [1364, 1365]. Among Lin^- $CD127^{hi}$ $CD94^-$ $CD117^-$ $CRTH2^-$ cells, a population of ILC1 has been described that lacks NKp44 and CD56 and is enriched in the SI LP of patients affected with inflammatory bowel diseases [1365]. This population displays only low amount of T-bet protein expression (Figure 157). In line with mouse data, additional populations of NK cells/ILC1 subsets with different phenotypic characteristics have been described in human tissues, including tonsils [1354, 1368–1371], making the selection of markers for the identification of NK/ILC1 quite challenging.

Recently, a human $CD117^+$ $NKp44^-$ ILC subset was identified in peripheral blood and in tissues that represents a "naïve" ILC precursor [1372]. This population was able to give rise to all ILC subsets in vitro and in vivo and did not express signature transcription factors associated with mature ILCs (T-bet, Eomes, GATA-3, RORγt). Accordingly, CD117 staining on human ILCs should not be equated with ILC3 identification but should additionally include markers such as NKp44.

Notably, the resolution of transcription factor staining in humans is not as good as in murine tissues and, therefore, combined staining of the above-mentioned surface markers is highly recommended in order to reliably gate on different human ILC subsets. However, as for their murine ILC counterparts, tissue-specific differences of surface markers should be taken into account as it has been shown for expression of CRTH2 for lung ILC2 [1373]. A selection of markers shown to be expressed by human and/or mouse ILC subsets is depicted in Table 54 (see also ref. [1342]).

5 Natural killer cells

5.1 *Overview*

NK cells represent a first fundamental line of defense against tumors and virus infected cells. In this section, we describe for both humans and mice, the most important strategies used to isolate and identify their subpopulations in an unequivocal manner.

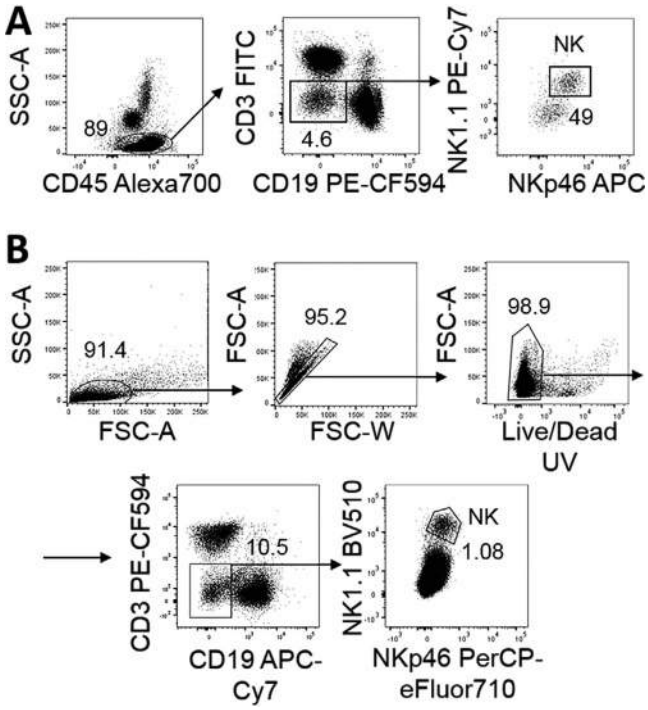

Figure 158. Identification of NK cells in the blood and spleen of C57BL/6 mice. Whole blood (A) was stained in BD Trucount tubes and analyzed after red blood cell lysis. Lymphocytes were gated among $CD45^+$ leucocytes based on their morphology and, after exclusion of $CD3^+$ T cells and $CD19^+$ B cells, NK cells were gated as $NK1.1^+NKp46^+$ cells. For the analysis of spleen NK cells (B), due to extraction techniques, doublets and dead cells need to be gated out. $CD3^+$ T cells and $CD19^+$ B cells were excluded and NK cells were gated as $NK1.1^+NKp46^+$ splenocytes.

5.2 *Murine NK cells*

5.2.1 Introduction. Mouse NK cells are commonly identified by FCM by the expression of the surface markers NK1.1, NKp46, and CD49b. The lack of expression of the T cell marker CD3 is used to exclude from the NK cell gate contaminating T cell subsets, such as NKT cells and NK-like T cells, that express NK1.1 and NKp46 respectively [1385]. In blood and spleen NK cells represent the most abundant innate lymphoid cell (ILC) subset, and the expression of NKp46 and NK1.1 is sufficient to identify them (Fig. 158). However, these NK markers vary depending on the mouse strain. NK cells from C57B/6 and SJL mice can be identified by NK1.1 expression, while in other mouse strains, such as BALB/c, NK cells display no reaction to the widely used anti-NK1.1 Ab PK136, because of allelic variations in Nkrp1b and Nkrp1c [1386]. In this case, NK cells can be identified only with CD49b and NKp46.

Even if mouse NK cells share many characteristics with human NK cells, it is not easy to identify functionally comparable NK cell subpopulations in the two species. Indeed, mouse NK cells lack the expression of human NK cell surface markers, including CD56 and some activating and inhibitory receptors. Murine NK cells lack KIRs, but express structurally divergent lectin-like Ly49 receptors that are functionally equivalent to the human KIRs and recognize MHC class I molecules. Most mouse Ly49 receptors recognize the

Table 55. Human- and mouse-specific and shared NK cell receptors

Receptor	Ligand	Human	Mouse
KIR2DL1 (CD158a)	Group 2 HLA-C	X	
KIR2DL2, KIR2DL3 (CD158b1, -b2)	Group 1 HLA-C, some group 2 HLA-C and some HLA-B	X	
KIR3DL1 (CD158e1)	HLA-Bw4	X	
KIR2DS1 (CD158h)	HLA-C2	X	
KIR2DS4 (CD158i)	Some HLA-C1 and HLA-C2, HLA-A11	X	
KIR2DL4 (CD158d)	HLA-G	X	
Ly49A (Klra1)	H2-Dd, H2-Dk, H2-Ld, H2-Db, H2-Kb, H2-Dp, H2-M3		X
Ly49C (Klra3)	H2-Db, H2-Kb, H2-Dd, H2-Kd, H2-Dk		X
Ly49E (Klra5)	Urokinase plasminogen		X
Ly49G (Klra7)	H2-Dd, H2-Kd, H2-Ld, H2-Db, H2-Dk, H2-Dr		X
Ly49I (Klra9)	H2-Kb, H2-Kd, H2-Dk, H2-Kk, m157 (MCMV)		X
Ly49D (Klra4)	H2-Dd, H2-Dr, Dsp2		X
Ly49H (Klra8)	m157 (MCMV)		X
Ly49P (Klra16)	H2-Dd, H2-Dk, m04 (MCMV)		X
NKG2A (CD159A)/CD94	HLA-E (human), Qa-1b (mouse)	X	X
NKG2C (CD159C)/CD94,	HLA-E (human), Qa-1b (mouse)	X	X
NKG2D (CD314)	Human: MICA/B, ULBP1, ULBP2, ULBP3, ULBP4, ULBP5, ULBP6 Mouse: RAE-1a, RAE-1b, RAE-1d, RAE-1e, RAE-1g, H60a, H60b, H60c, MULT1	X	X
KLRG1	E-, N-, and R-cadherin	X	X
NKp46 (NCR1; CD335)	CFP (properdin), hemagglutinin, PfEMP1	X	X
NKp30 (NCR3; CD337)	B7-H6, BAT3	X	
NKp44 (NCR2; CD336)	21spe-MLL5	X	
NKp80 (KLRF1)	AICL (activation-induced C-type lectin)	X	
DNAM-1 (CD226)	Nectin-2, PVR	X	X
2B4 (CD244)	CD48	X	X

classical MHC class I molecules H2-K and –D/L, while Ly49H and Ly49I recognize the MHC class I-related m157 molecule encoded by cytomegalovirus (CMV). The CD94/NKG2 heterodimer is conserved between mouse and human and, in mice, it recognizes the non-polymorphic Qa-1. The activating receptor NKG2D is also conserved between the species, and it is triggered by stress-induced MHC class I-related ligands retinoic acid early inducible (RAE)-1 and, in mice, the minor histocompatibility complex H60. Among the natural cytotoxicity receptors (NCRs), NKp30, and NKp44 are not expressed in mice, while NKp46 is considered to be the most specific NK cell marker, as it is expressed by all NK cells in mammals (Table 55) [1385].

Analogously to human NK cells for which the levels of CD56 and CD16 expression are used to define the maturation from immature $CD56^{bright}$ $CD16^{-}$ NK cells to mature $CD56^{dim}$ $CD16^{+}$ cells [1387], CD27 and CD11b expressions are used to identify several murine NK cell maturation steps. Immature NK cells are $CD11b^{low}$ $CD27^{high}$, then they mature into double-positive $CD27^{+}CD11b^{+}$ cells and, finally, into fully mature $CD27^{low}$ $CD11b^{high}$ NK cells (Table 56). This developmental program is associated with the acquisition of NK cell effector functions [1376]. Both $CD27^{+}$ and $CD27^{-}$ subsets express equivalent levels of activating Ly49 receptors and CD94/NKG2 receptors, but $CD27^{-}$ NK cells contain higher levels of inhibitory Ly49s.

Recently, using high-throughput single-cell-RNA-seq, the gene expression of human and murine NK cells from spleen and blood was analyzed at the single cell level. In this study, two major NK cell subsets transcriptionally similar across organ and species were identified: it was shown a correspondence between the $CD27^{-}CD11b^{+}$ and the $CD27^{+}CD11b^{-}$ mouse NK cell subsets and the $CD56^{dim}$ and $CD56^{bright}$ human NK cell subsets, respectively [1388]. Moreover, this study revealed spleen- and blood-specific NK cell signatures common in both species, highlighting the importance of the organ of origin in the definition of a cell population.

While in blood and spleen NK cells represent the most abundant ILC subset, in tissues, there are high proportions of the other ILCs subsets, which are largely tissue-resident. CD127 is classically used to identify ILCs and distinguish them from NK cells, as it is not expressed by NK cells of liver, intestine, skin, uterus, salivary gland, bone marrow, or lymph nodes. However, CD127 is expressed by NK cells in the thymus and in some spleen populations, and it is not expressed by liver and intraepithelial gut ILC1s. Thus, the phenotypic characterization of tissue-resident NK cells is more complicated and requires the analysis of additional markers. In particular, NK cells share many features with ILC1s, they both produce IFN-γ as the main cytokine and require Tbet for this function. However, while NK cells require Eomes for their

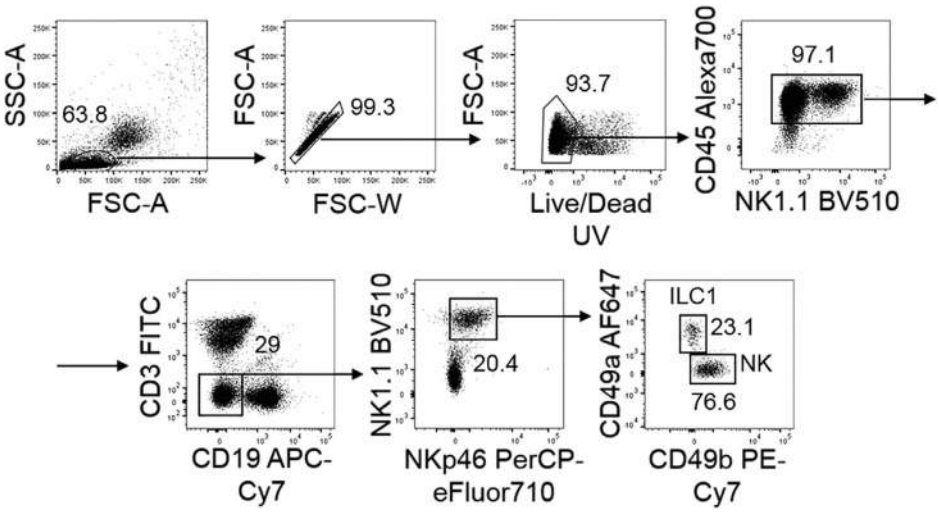

Figure 159. Identification of liver NK cells in C57BL/6 mice. After Percoll density gradient centrifugation of single cell suspension obtained scratching the liver, lymphocytes were analyzed. Doublets, dead cells, $CD45^-$ cells, $CD3^+$ T cells, and $CD19^+$ B cells were sequentially excluded. Among $NK1.1^+NKp46^+$ cells NK cells were gated as $CD49b^+CD49a^-$ cells, and distinguished from $CD49b^-CD49a^+$ ILC1s.

development process, ILC1s develop in the absence of this transcription factor. Moreover, ILC1s are generally noncytotoxic and express lower levels of perforin compared to NK cells [1342]. Regardless these developmental and functional differences, ILC1s have some phenotypic markers in common with NK cells (see Chapter VI Section 4 Innate lymphoid cells), including NK1.1 in mice and NKp46 in both humans and mice. In the liver, for example, to distinguish these two populations, it is useful to include additional markers such as CD49b, exclusively expressed by NK cells in mice, and CD49a and TRAIL, preferentially expressed by ILC1s in both humans and mice (Fig. 159). Recently, CD200R has been shown to be an additional marker to distinguish ILC1s from NK cells in mice (Table 56) [1389].

In addition to ILC1s, NK cells share the expression of some markers with ILC3s. In mice ILC3s are dependent on RORγt for their development and function [1381] and two subsets can be distinguished on the basis of NKp46 expression: NCR^+ and NCR^- ILC3s. As NK cells and NCR^+ ILC3s both express NKp46, the analysis of the expression of the transcription factors RORγt and Eomes can be useful to distinguish them (Figure 160, See also Chapter VI Section 4 Innate lymphoid cells).

Unlike NK cells, ILC2s are characterized by the capacity to produce type 2 cytokines. They contain larger amounts of the transcription factor GATA3 compared to the other ILC subsets but upon activation can express high levels of KLRG1, an inhibitory receptor also expressed by mature NK cells [1390].

For the identification and distinction of NK cells from other ILCs by FCM, it must be considered that, like T helper cell subsets, ILC subsets also display a certain degree of plasticity. For example, fate mapping and adoptive transfer studies in mice have shown that gut $CCR6^-NKp46^-$ ILC3s can convert into IFN-γ producing $NK1.1^+NKp46^+$ ILC1s via a $CCR6^-NKp46^+$ intermediate through a decrease in RORγt expression and parallel increase in Tbet [1362, 1391].

5.2.2 Step-by step sample preparation. Cell isolation: Spleens and livers were scratched through 70 and 100 μm cell strainers, respectively. Liver lymphocytes were isolated on a 37.5–67.5% Percoll gradient. For isolation of small intestine lamina propria cells, intestines were cut longitudinally, then transversally in 2–3 cm pieces, thoroughly rinsed with PBS, and shaken for 30 min in PBS containing 10% FBS, 15 mM Hepes and 5 mM EDTA to remove intraepithelial and epithelial cells. Intestines were then digested with collagenase VIII (300 UI/mL) in complete RPMI for 45 min at 37°C under agitation, and lamina propria lymphocytes were isolated on a 40–100% Percoll gradient. Whole blood was analyzed using BD Trucount tubes according to the manufacturer's instructions (BD Biosciences) [1392].

5.2.3 Materials. The following Abs were used and/or are suggested for the surface and intracellular staining of mouse NK cells:

BD Biosciences: CD45.2 AlexaFluor700 (1:200, clone 104), CD3 PE CF594 (1:100, clone 145-2C11), CD19 PE CF594 (1:200, clone 1D3), NK1.1 BV510 (1:50, clone PK136), CD49a AlexaFluor647 (1:400, clone Ha31/8), CD11b BV510 (1:400, clone M1/70), NKp46 BV421 (1:50, clone 29A1.4), TCRb FITC (1:400, clone H57-597), granzyme B PE (1:50, clone GB11), Rorγt PE (1:100, clone Q31-378), CD107a FITC (1:60, clone 1D4B), Fc block CD16/CD32 (1:200, clone 24G2);

eBiosciences: NKp46 PerCP-eFluor710 (1:50, clone 29A1.4), CD49b PE-Cy7 (1:200, clone DX5), Eomes APC (1:100, Dan11mag);

Biolegend: IFN-g BV421 (1:100, clone XMG1.2), CD19 APC-Cy7 (1:200, clone 6D5), NKp46 APC (1:50, clone 29A1.4), NK1.1 PE-Cy7 (1:50, clone PK136), CD3 FITC (1:100, clone 145-2C11), CD19 FITC (1:100, clone 6D5).

Dead cells were identified using the fixable blue dead cell stain kit (Invitrogen). For surface staining cells, Abs were diluted in PBS 5 mM EDTA (Euroclone). For intracellular staining, cells were fixed and permeabilized with an intracellular staining kit (eBioscience). Flow cytometric data were acquired with a BD LSR II flow cytometer equipped with FACS DIVA software (BD Biosciences), and analyzed by using FlowJo software (FlowKo, LLC).

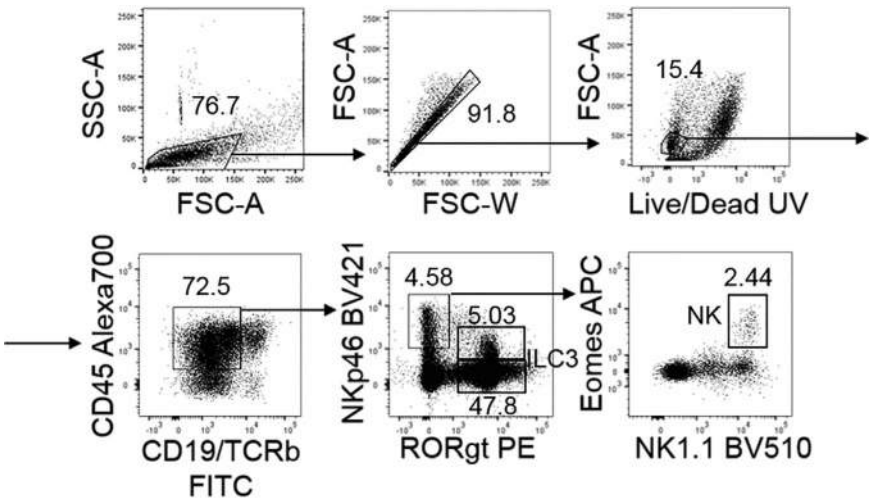

Figure 160. Identification of small intestine lamina propria NK cells in C57BL/6 mice. After enzymatic digestion and Percoll density gradient centifugation, single cell suspension obtained from the small intestine was analysed. As in figure 159, doublets, dead cells, $CD45^-$ and $CD19^+$ B cells were sequentially excluded. T cells were gated out based on their expression of TCRβ. $ROR\gamma t^+$ cells represent ILC3s, which can be further distinguished in NCR^+ and NCR^- ILC3s. Among $ROR\gamma t^-$ $NKp46^+$ cells, NK cells are gated as $NK1.1^+Eomes^+$ cells.

Table 56. Key markers for murine NK cell identification and characterization

Marker	Expression
NK lineage	
NK1.1 (CD161)	Surface
NKp46 (NCR1; CD335)	surface
CD49b	Surface
T-bet	Nucleus
Distintion from other ILCs	
IL7Rα (CD127)	Surface, ILC1, ILC2, ILC3
CD49a	Surface, ILC1
CD200R	Surface, ILC1
TRAIL	Surface, ILC1
Eomes	Nucleus, NK cells
Rorγt	Nucleus, ILC3
Development/ maturation stages	
CD27	Surface, immature NK cells
CD11b (Mac-1/CD18)	Surface, mature NK cells
KLRG1	Surface, mature NK cells
CD43	Surface, mature NK cells
CXCR6	Surface, "memory" NK cells in the liver

5.2.4 Pitfalls. When including CD11b in cytometry panels to exclude myeloid cells from the analysis, it must be taken into account that mature murine NK cells express this marker too. Therefore, one must check carefully that $NK1.1^+$ and/or $NKp46^+$ $CD11b^+$ cells do not get excluded in the associated gating strategy.

5.3 *Human NK cells*

5.3.1 Introduction. Natural killer (NK) cells were described over 40 years ago as cells capable of killing tumor cells without prior sensitization. They are lymphoid cells derived from hemopoietic stem cells (HSCs) [1393, 1394] and belong to the innate immunity cell family. In contrast to T and B cells, NK cells do not express receptors encoded by rearranging genes and they play a major role in innate immunity as both effector and regulatory cells, participating in the first line of defense against pathogens and tumors. Notably, NK-cell-susceptible tumors are primarily those lacking or expressing insufficient amounts of MHC class I molecules (missing-self hypothesis) [1395]. Another requirement for NK-cell-mediated tumor cell killing is the surface expression of a series of different stress-induced structures [1396]. The NK cell function appears to complement the cytolytic T cell–mediated MHC-I-dependent activity [1397].

The recognition of MHC class-I is mediated by a family of receptors termed Killer Ig-like receptors (KIRs), by the NKG2A/CD94 heterodimer and by LIR-1 (CD85j). In particular, NKG2A/CD94, expressed early during the process of NK cell maturation, recognizes the nonclassical HLA-E molecule [1398, 1399] while KIRs, expressed at later stages of NK cell maturation, recognize allelic determinants of HLA-A -B or -C [1400, 1401]. Other non-HLA-related inhibitory receptors including Siglec7 (CD328), PD1 (CD279), and IRP60 (CD300a) may be expressed at the surface of NK cells (see Tables 57 and 58). In most instances, the NK receptors that mediate their activation upon binding to target cells are non-HLA-specific and recognize cell stress-induced molecules. These receptors include NKp30, NKp44, and NKp46 (which constitute the natural cytotoxicity [NCR] family), NKp80, 2B4 (CD244), and NKG2D [1402–1404]. Of note, activating isoforms of KIRs also exist [1405]. While inhibitory KIRs are characterized by immune-receptor tyrosine-based inhibition motif (ITIM) domains in their long intracytoplasmic tail, the various activating receptors bear a short intracytoplasmic tail and are associated with signaling polypeptides containing immune-receptor tyrosine-based activating motifs (ITAM) domains [1406]. A fundamental activating receptor is also CD16, the low affinity Fcγ receptor, which binding to IgG complexes mediates the Ab-dependent cell-cytotoxicity (ADCC). In resting conditions, the bright expression of CD16 is restricted to mature NK cells.

Among peripheral NK cells, two major subsets have been identified on the basis of the cell surface density of CD56 molecules (neural cell adhesion molecule, N-CAM). $CD56^{bright}$ ($CD3^-CD56^{++}CD16^{-/+}$) represent approximately 10% of the

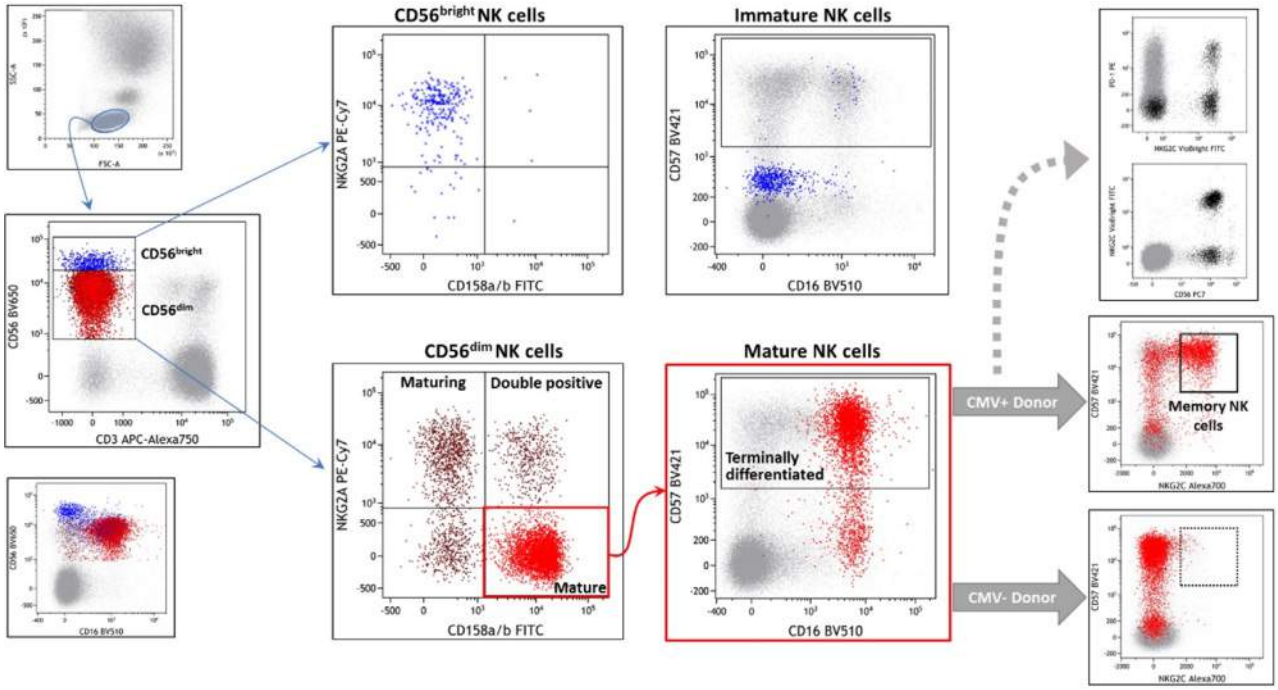

Figure 161. In this PB samples, lymphocytes are first gated based on their physical parameters (upper left grey dot plot) then human NK cells can be identified for their CD56 surface expression and lack of CD3. The CD56^{bright} NK subpopulation (in blue) is positive for NKG2A, negative for KIRs and CD57 while CD16 can be either negative or dimly expressed (as shown). NKG2A and KIR surface expression allows three subpopulations of CD56^{dim} NK cells (in red), namely "maturing" (NKG2A^{+}KIR^{-} in dark red), "double positive" (NKG2A^{+}KIR^{+} in dark red) and "mature" (NKG2A^{-}KIR^{+} in light red), to be identified. To discriminate among these CD56^{dim} maturation steps, we used a cocktail of anti-KIR (clones: EB6B, GL183, Z27) that did not include anti-LIR1, for this reason in the dot plot also a double negative population is present. Among the mature population (in light red), CD57 molecule is expressed on the, so called, "terminally differentiated" NK cells. In CMV positive donors, a percentage of this latter population could also express NKG2C representing the so called "memory NK cells." Recently it has been demonstrated that in some CMV positive individuals a fraction of the NKG2C subset can also express PD1. Percentage of subpopulation are not specified because they are extremely diverse among different individuals and do not give additional information to the gate strategy.

circulating PB NK cells while they prevail in secondary lymphoid organs (liver, synovial fluid and decidua). CD56^{dim} (CD3^{-}CD56$^{+/-}$ CD16^{++}) cells are largely predominant (~90%) in PB NK cells. They derive from CD56^{bright} NK cells, as revealed by different studies in vitro (differentiation from HSC) and in vivo after HSC transplantation [1407, 1408]. Moreover, the existence of a third NK cell population totally lacking CD56 has been widely demonstrated both on virus infected patients and, more rarely, on healthy donors. This population is characterized by a reduced expression of NCRs and, in in vitro studies, by a poor cytotoxic activity [1409–1412].

5.3.2 CD56^{bright} NK cells. In resting conditions all CD56^{bright}, in contrast to CD56^{dim}, NK cells are poorly cytolytic but secrete cytokines, primarily IFN-γ and TNF-α and express both high (CD25) and intermediate (CD122/CD132) affinity IL-2 receptors and c-Kit (CD117), rendering them highly susceptible to IL-2–induced cell proliferation [1413, 1414]. Moreover, CD56^{bright} NK cells express high levels of both CD62L [1415] and CXCR3 which, together with the surface expression of CCR7, dictates their preferential homing into secondary lymphoid organs [1416–1418] Notably, although poorly cytotoxic under resting conditions, CD56^{bright} NK cells may acquire cytolytic activity comparable to that of CD56^{dim} cells upon stimulation with cytokines, such as IL-2, IL-12, IL-15. While CD56^{bright} NK cells express CD94/NKG2A (i.e., the receptor for HLA-E) they lack KIRs. Regarding activating NK receptors, CD56^{bright} cells express higher levels of NKp46 and NKp30 than CD56^{dim} cells, while CD56^{bright} cells lack or express low amounts of CD16.

5.3.3 CD56^{dim} NK cells. CD56^{dim} NK cells under resting conditions express granules containing perforin and granzymes, and display cytolytic activity. Until recently, CD56^{dim} NK cells were mainly associated with cytotoxicity while cytokine production was thought to be confined to the CD56^{bright} subset. However, more recently, it has been shown that, upon stimulation via activating receptors, CD56^{dim} NK cells rapidly release cytokines such as IFN-γ- and TNF-α (even more efficiently than CD56^{bright} cells) and chemokines such as MIP-1β and MIP-1α [1419, 1420]. In contrast to CD56^{bright} NK cells, the CD56^{dim} population is phenotypically heterogeneous. Thus, as shown in Fig. 161, NKG2A versus KIR expression allows identification of three distinct subset of human NK cells that recapitulate the consecutive steps of PB NK cell maturation to be distinguished.

Table 57. Human NK cell inhibitory and activating receptors

Receptor	Ligand	CD56^{bright}	CD56^{dim}
Activation			
NKG2C (CD159a)	HLA-E	–	Subsets
NKG2D (CD314)	MIC-A - MIC-B - ULPBs	All PB NK cells	
KIR2DS1 (CD158h)	HLA-C2	–	Subsets
KIR2DS2/3 (CD158j)	???	–	Subsets
KIR2DL4 (CD158d)	HLA-G	–	Subsets
KIR2DS4 (CD158i)	HLA-A*11 and some HLA-C	–	Subsets
KIR2DS5 (CD158f)	???	–	Subsets
KIR3DS1 (CD158e1)	HLA-Bw4, HLA-F	–	Subsets
NKp30 (CD337)	B7-H6 - BAG6/BAT3	++	+
NKp44 (CD336)	21spe-MLL5, Nidogen 1	On activated NK cells	
NKp46 (CD335)	CFP (properdin), haemagglutinin, PfEMP1	++	+
NKp80	AICL	+	+
DNAM1 (CD226)	Nectin-2 (CD112), PVR (CD155)	+	+
2B4 (CD244)	CD48	All PB NK cells	
NTB-A (CD352)	NTB-A (CD352)	All PB NK cells	
CRACC/CS1 (CD319)	CRACC/CS1 (CD319)	All PB NK cells	
Tactile (CD96)	PVR (CD155)	All PB NK cells	
FcγRIII (CD16)	IgG	–/+	+/++
Inhibition			
NKG2A/KLRD1 (CD159a/CD94)	HLA-E	+	Subsets
KIR2DL1 (CD158a)	HLA-C2	–	Subsets
KIR2DL2/3 (CD158b)	HLA-C1, few HLA-C2	–	Subsets
KIR2DL4 (CD158d)	HLA-G	–	Subsets
KIR2DL5 (CD158f)	???	–	Subsets
KIR3DL1 (CD158e1)	HLA-A-Bw4 and HLA-B-Bw4	–	Subsets
KIR3DL2 (CD158k)	HLA-A*03 and *11	–	Subsets
ILT2/LIR-1 (CD85J)	Different MHC-I alles	–	Subsets
PD-1 (CD279)	PDL1 (CD274) and PDL2 (CD273)	–	Subsets
Siglec-7 (CD328)	Ganglioside DSGb5	Most of PB NK cells	
IRP60 (CD300a)	α-herpes virus Pseudorabide virus Phosphatidylserine Phosphatidylethnolamine	+	+
TIGIT	PVR (CD155)	PB NK cells	

The "maturing" population (NKG2A$^+$KIR$^-$) is characterized by the NKG2A$^+$/KIR$^-$ phenotype, similar to that of CD56^{bright} cells, while the "mature" population expresses the NKG2A$^-$KIR$^+$ phenotype. An intermediate step of maturation is identified by the "double positive" NKG2A$^+$KIR$^+$ cells [1377, 1387]. The unidirectional nature of NK cell differentiation is further supported by the presence of CD57 on the surface of the "terminally differentiated" NK subset. When compared with the CD57-negative counterpart, the NKG2A$^-$KIR$^+$CD57$^+$ population shows a decreased surface expression of NKp30 and NKp46, and a reduced proliferative potential, possibly as the result of downmodulation of IL-2Rβ (CD122) and IL-18Rα (CD218a) [1377, 1379].

In CMV-positive healthy donors, it is possible to identify an additional subset of mature cells that expresses CD57 and the activating HLA-E-specific receptor NKG2C dimerizing with CD94 [1421]. This subset appears to contain cells endowed with an adaptive/memory-like capability (i.e., clonal expansion, prompt response to restimulation, and epigenetic modification including that of the intracytoplasmic FcεRγ chain) [1411, 1422, 1423]. Recent data have shown that, in CMV positive individuals, a fraction of CD57 positive cells may also express PD-1 [1412].

The recruitment of CD56^{dim} NK cells to inflamed peripheral tissues is driven by several chemokines and homing receptors including, for example, CXCR1, CX3CR1, and in certain subsets CD62L and CXCR3^{low} also [1416].

5.3.4 NK cells present in decidua. During the first trimester of pregnancy, NK cells represent the main lymphoid population (50–70%) in human decidua where they bear a unique phenotypic and functional profile. Their phenotypic features resemble to an extent those of CD56^{bright} PB NK cells; however, in addition to

Table 58. Other human NK cell receptors

Receptor	Ligand	CD56^{bright}	CD56^{dim}
Adhesion			
LFA-1 (CD11a/CD18)	ICAM-1, ICAM-2, ICAM-3	−/+	++
LFA-2 (CD2)	CD15, CD58, CD59	Most of mature NK cells	
LFA-3 (CD58)	CD2, CD48, CD58	Most of mature NK cells	
MAC-1 (CD11b/CD18)	iC3b, C4b, ICAM-1, fibrinogen	Most of circulating NK, up-regulated upon activation	
ICAM-1 (CD54)	LFA-1, MAC-1	++	+/−
N-CAM (CD56)	???, FGFR	++	+
HNK-1 (CD57)	???	−	Subsets
L-Selectin (CD62L)	GLyCAM-1 MadCAM-1	++	Subsets
Cytokine /Chemokine receptors			
IL-2Rα (CD25)	IL-2	+	−
IL-2Rβ/IL-2Rγ (CD122/CD132)	IL-2 AND IL.15	Almost all PB NK cells	
c-Kit (CD117)	SCF (KL)	+	−
IL7Rα (CD127)	IL-7	+	−
CXCR1 (CD181)	CXCL8 (IL-8)	−	+
CXCR2	IL8-RB	−	+
CXCR3 (CD183)	CXCL9, CXCL10, CXCL11	++	Subsets
CXCR4 (CD184)	CXCL2	Subsets of PB NK cells	
CCR5 (CD195)	RANTES, CCL3 (MIP1α) and CCL4 (MIP1β)	Subsets of PB NK cells	
CCR7 (CD197)	CCL19, CCL21	+	−
IL-18R (CD218a)	IL-18	++	+
ChemR23	Chemerin	−	+
CX3CR1	Fraktaline	−	+
Death Receptors			
Fas/APO-1 (CD95)	Fas ligand (CD95L)	Activated NK cells They induce target apoptosis	
Fas ligand (CD95L)	Fas/APO-1 (CD95)		
CD40L (CD154)	CD40		
TRAIL (CD253)	DR4 (TRAIL-R1), DR5 (TRAIL-R2)		
Other surface molecules			
LAMP1 (CD107a)	—	Briefly expressed on NK cell surface after degranulation	
LAMP2 (CD107b)	—		
LAMP3 (CD63)	—		
TNFRSF7 (CD27)	CD70	+	−

the NKG2A^{high}NKp30^{high}NKp46^{high} surface phenotype, they also display characteristics of CD56^{dim} NK cells including high expression of KIR and lytic granules. Of note, in contrast to PB NK cells, the 2B4 (CD244) receptor on decidual NK cells displays a strong inhibitory (and not activating) activity, similar to that seen in NK cell precursors [1424], that renders this population poorly cytolytic [1425, 1426] [Moreover, in contrast to PB NK cells, decidual NK cells release a unique set of cytokines, including IL-8 (CXCL8), VEGF, CXCL12 (stromal-derived factor–1 [SDF-1α]), and IFN-γ–inducing protein 10 (IP-10, CXCL10), that play a pivotal role in tissue remodeling (i.e., placenta development processes) and neo-angiogenesis [1427].

5.3.5 NK cells present in lymph nodes. In normal conditions, NK cells are present in lymph nodes where they occupy the T-cell areas [1428]. They are consistently CD56^{bright}CD16^{neg}KIR^{neg} and lack perforin and granzymes. In contrast to PB CD56^{bright} NK cells, lymph node NK cells do not express CCR7 or CD62L. Concerning the NCR family, lymph node NK cells express low levels of NKp46 and may lack NKp30. Remarkably, however, upon IL-2 activation, lymph node NK cells may express KIRs and CD16, and upregulate NCR [1428, 1429].

5.3.6 Step-by-step sample preparation. PB NK cell surface staining:

1. Put 100 μL of heparinized whole blood in a sample tube
2. Add 50 μL of Brilliant Stain Buffer to each tube
3. (a) To study PB subpopulations, add the following antibodies: CD158a FITC (10 μL) CD158b FITC (10 μL), CD158e FITC

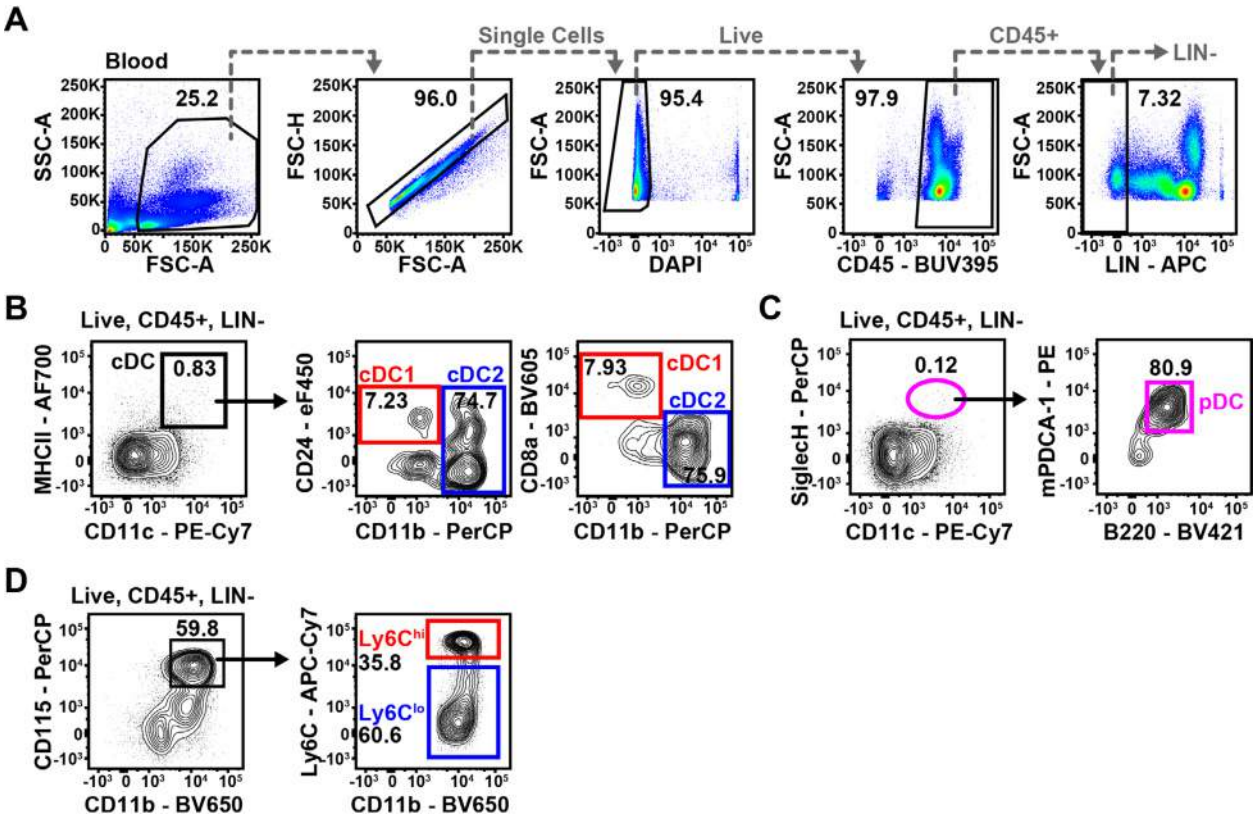

Figure 162. Flow cytometric analysis of mouse blood DCs and monocytes. Example for basic gating strategy from FSC-A/SSC-A, over doublet exclusion and gating on Live, CD45$^+$ LIN$^-$ cells (defined as CD3/CD19/CD49b/Ly6G$^-$) on a blood sample (A), as used for all tissues. Conventional DCs are identified as CD11c^{hi}MHCII$^+$ cells and can be divided into cDC1 (CD8/CD24$^+$CD11b$^-$, red gates) and cDC2 (CD8$^-$CD11b$^+$, blue gates) (B). Plasmacytoid DCs are identified as CD11c^{int}SiglecH$^+$ and can be further purified by gating on B220$^+$mPDCA-1$^+$ cells (pink gates; C). Monocytes are identified as CD115$^+$CD11b$^+$ cells and can be further divided into Ly6C^{lo} and Ly6C^{hi} monocytes (blue and red gates, respectivley; D).

(5 µL), CD279 PE (10 µL), CD159a PE-Cy7 (3 µL), NKG2C A700 (3 µL), CD3 APC-A750 (3 µL), CD57 BV421 (3 µL), CD16 BV510 (3 µL), CD56 BV650 (3 µL).

(b) To study only NKG2C/PD1 co-expression this simpler cocktail can be used: NKG2C VioBright FITC, CD279 PE (10 µL), CD56 PC7 (3 µL) CD3 APC-A750 (3 µL).

4. Incubate 20 min at 4°C.
5. After incubation, lyse sample in 2 mL of Pharm Lyse^{TM}, for 5–8 min
6. Centrifuge 5 min at 1300 rpm
7. Discard supernatant
8. Resuspended in 300 µL of PBS for acquisition.

5.3.7 Materials. Pharm Lyse^{TM} and Brilliant Stain buffer are from Becton Dickinson (San Josè, CA), PBS is from (Sigma–Aldrich).

Beckman Coulter: CD3 APC or APC-Alexa Fluor 750 (UCHT1, IgG1), CD56 PC7 (N901), CD158a PE (EB6B, IgG1), CD158b PE (GL183), CD158e FITC or PE (Z27, IgG2a), CD159a PE-Cy7 (Z199 IgG2b), NKp30 (Z25, IgG1), NKp44 (Z231, IgG1) NKp46 (BAB281, IgG1), NKp80 (MA152, IgG1) NKG2D (ON72, IgG1).

Becton Dickinson: CD16 BV510 (3G8, IgG1), CD56 BV650 (NCAM16.2, IgG2b), CD57 BV421 (NK-1, IgM), CD158b (CH-L, IgG2b).

Miltenyi: PD1 PE (PD1.3.1.3, IgG1), NKG2C VioBright FITC (REA205, Ig1).

R&D System: NKG2C Alexa Fluor 700 (134591, IgG2a).

Flow cytometric data were acquired with a BD LSR II flow cytometer equipped with FACS DIVA software (BD Biosciences), and analyzed by using Kaluza software (Beckman Coulter).

5.3.8 Top Tricks. When using many different Brilliant Violet fluorochromes in the same sample, in order to avoid aspecific interactions between these polymer dyes, it is better to add always Brilliant Stain Buffer to the sample before adding the conjugated mAbs.

While for PD1 detection in human T cells most of commercial mAb clones are equally good, when working with human NK cells the situation is totally different. In our experience, the best clone to discriminate PD1 positive NK cells is PD1.3.1.3 conjugated with PE.

6 Mononuclear phagocytes: Monocytes, macrophages, and dendritic cells

6.1 *Overview*

This chapter aims to provide basic guidelines for researchers interested in analyzing mononuclear phagocytes that include monocytes, macrophages, and dendritic cells. We describe here processing and FCM-staining techniques for various murine and human tissues such as blood, bone marrow, spleen, lung, skin, intestine, or lymph nodes. Furthermore, this chapter provides basic gating strategies as well as tips and tricks and background information for each tissue in order to easily identify the various subpopulations of monocytes, macrophages, and dendritic cells.

6.2 *Introduction*

Both mouse and human lymphoid and non-lymphoid tissues contain a high number of mononuclear phagocytes, innate myeloid cells that play crucial roles in homeostasis as well as host–pathogen interactions. This pool is composed of monocytes, macrophages, and dendritic cells (DCs). Ontogeny, heterogeneity and specific functions of these cells have been extensively described in various recent reviews (e.g., [1430–1435]).

Briefly, the murine DC compartment is currently divided into classical DCs (cDCs) and plasmacytoid DCs (pDCs), with cDCs being further subdivided into cDC1 ($CD11b^-$ $CD8^+$ in lymphoid tissues or $CD11b^-$ $CD103^+$ in non-lymphoid tissues) or cDC2 ($CD8/CD103^-$ $CD11b^+SIRP\alpha^+$ cells) [1433, 1436, 1437] (Table 60). While all cDCs express high levels of CD11c and MHCII across tissues, pDCs are rather $CD11c^{int}$ cells that are characterized by the expression of markers such as SiglecH, B220, and mPDCA-1, while lacking expression of CD11b. Note that the dendritic cell nature of pDCs is currently being challenged as recent studies have reported that pDCs arise rather from a lymphoid lineage [1438–1440]. Langerhans cells (LCs) are epidermal-specific antigen presenting cells that were originally classified as members of the DC family as they express CD11c, CD11b, and MHCII and shown to migrate to lymphoid organs. However, LCs were shown to be more of fetal macrophage origin, hence, these cells are now rather classified as the resident macrophages of the epidermis [1441–1443]. Monocytes are also heterogeneous and have been categorized into two subsets: inflammatory $CXCR1^{hi}CCR2^-CD62L^-CD43^{hi}Ly6C^{lo}$ and patrolling $CX3CR1^{int}CCR2^+CD62L^+CD43^{lo}Ly6C^{hi}$ monocytes [1444, 1445]. $Ly6C^{hi}MHCII^{lo}$ monocytes recruited in tissues in steady state continually differentiate into $Ly6C^{lo}MHCII^{hi}$ macrophages, a phenomon referred to as the monocyte to macrophage "waterfall," mostly described in the gut and skin [1446, 1447].

Human mononuclear phagocytes also include cDCs, namely $CD1c^+$ cDC2 and $CLEC9A^+XCR1^+CADM1^+CD141^+$ cDC1; $CD123^+$ pDCs; monocyte-derived cells (termed $CD14^+$ cells here) and tissue-resident macrophages [1431, 1448, 1449]. We have recently described cDC progenitors in the blood, namely pre-DC [1450], that were previously included into the classic $HLA\text{-}DR^+CD123^+$ pDC gate. Similar to mouse, in humans, monocytes can be distinguished into $CD14^{hi}CD16^-$ classical versus $CD14^{lo}CD16^+$ non-classical monocytes [1451], that are the equivalent of the inflammatory $CXCR1^{hi}CCR2^-CD62L^-CD43^{hi}Ly6C^{lo}$ and patroling $CX3CR1^{int}CCR2^+CD62L^+CD43^{lo}Ly6C^{hi}$ monocytes, respectively, with an additional minor population of $CD14^+CD16^+$ intermediate monocytes.

The efficient processing of both mouse and human tissues is highly valuable to properly characterize tissue-associated mononuclear phagocytes in steady state or inflammation. Here, we explain techniques for the enrichment and FCM-based identification of all mononuclear phagocyte populations across a number of mouse and human tissues.

6.3 *Materials*

6.3.1 Mouse tissue processing materials.

6.3.1.1 General reagents and materials.

Reagent	Manufacturer	Catalog number
Bovine Serum Albumin, lyophilized powder (BSA)	Sigma–Aldrich	A2058
Collagenase IV	Sigma	C5138
DAPI	Life Technologies	D1306
Dispase	Gibco	17105041
DNase I	Roche	10104159001
Dulbecco's Phosphate Buffered Saline (PBS)		
Dithiothreitol (DTT)	Gold Biotechnology	DTT50
Foetal Bovine Serum (FBS)	Serana	S-FBS-SA-015
n-mouse serum	Sigma-Aldrich	M5905-10ML
n-rat serum	Sigma-Aldrich	R9759-10ML
1× RBC Lysis Buffer	eBioscience	00-4333-57
RPMI 1640	HyClone	SH30255.01

Prepare:

- RPMI 1640 containing 10% FBS (or FCS)
- FCM buffer: 0.5% w/v BSA + 2 mM EDTA in 1X PBS
- FCM staining buffer (as used for indicated tissues): 1% n-mouse serum + 1% n-rat serum in FCM buffer
- Digestion buffer (solution **1**): 0.2 mg/ml collagenase IV + 0.03 mg/ml DNase I in RPMI + 10% FBS/FCS
- Fine scissors and forceps/tweezers
- 5 mL FCM tubes, round bottom, polystyrene
- Six-well/12-well plates for harvesting tissues/digestion of tissues
- 15 mL/50 mL conical tubes
- 70 μm cell strainer

6.3.1.2 Additional materials for mouse bone marrow processing.

- 25 G needles and 20 mL syringes to flush bone marrow

6.3.1.3 Additional materials for mouse lung processing.

- 70 μm nylon mesh sheet—cut into approximately 1 × 1 cm squares
- 18 G blunt needles and 3 mL syringes for dissociation

6.3.1.4 Additional reagents and materials for mouse intestine processing.

- Six-well plates: one well per mouse for harvesting; one well per mouse for digestion of small intestine and one well per mouse for digestion of large intestine
- Beaker of cold PBS (keep on ice)
- Metal trays or petri dishes for various washing steps
- Three 50 mL centrifuge tubes for each small intestine and colon sample (four if the epithelial compartment is to be isolated for analysis as well)
- Epithelium dissociation solution (50 mM EDTA + 100 μL 20 mM DTT in PBS)
- Digestion solution **1** (0.2 mg/mL collagenase IV, 0.03 mg/mL DNase in RPMI + 10% FCS)
- Digestion solution **2** (0.4 mg/mL collagenase IV, 0.03 mg/mL DNase in RPMI + 10% FCS)
- 70 μm cell strainers
- Percoll* (see * in chapter)

6.3.1.5 Additional reagents and materials for mouse skin (ears) processing.

- Dispase solution (4 U/mL in RPMI 1640)
- Six-well plate for Dispase incubation
- 12-well plate for digestion incubation
- Digestion solution **1** (0.2 mg/mL collagenase IV, 0.03 mg/mL DNase in RPMI + 10% FCS)
- Flat clean surface for separating dorsal and ventral halves, and epidermis from dermis
- 70 μm nylon mesh sheet—cut into approximately 6 × 6 cm squares

6.3.1.6 Additional reagents for mouse lymph node (LN) processing.

- Digestion solution **3**: 0.4 mg/mL collagenase IV + 0.06 mg/mL DNase I in RPMI + 10% FBS/FCS (2× concentrated digestion buffer/solution **1**)
- 25 G needles and 1 mL syringes for dissociation of LNs for digestion
- 70 μm nylon mesh sheet—cut into approximately 6 × 6 cm squares

6.3.2 Abs for murine mononuclear phagocyte identification.

Antibody	Fluorochrome	Clone	Provider	Cat #
CD3ε	APC	145-2C11	BioLegend	100312
CD8α	BV605	53-6.7	BioLegend	100744
CD11b	BV650	M1/70	BioLegend	101259
CD11c	PE-Cy7	N418	BioLegend	117318
CD11c	BV605	N418	BioLegend	117334
CD16/32	Pure	2.4G2	BD	553142
CD19	APC	eBio1D3	eBioscience	17-0193-82
CD24	eFluor 450	M1/69	eBioscience	48-0242-82
CD45	BUV395	30-F11	BD	564279
CD49b	APC	DX5	BioLegend	108909
CD64 / FcγRI	PE	X54-5/7.1	BD	558455
CD64 / FcγRI	BV711	X54-5/7.1	BioLegend	139311
CD103	APC	2E7	eBioscience	17-1031-82
CD115	PerCP	AFS98	eBioscience	46-1152-82
CD172α	Biotin	P84	BioLegend	144006
CD317/m-PDCA-1	PE	eBio97	eBioscience	13-1721-82
B220/CD45R	BV421	RA3-6B2	BioLegend	103240
CCR2	FITC	FAB5538F	R&D	475301
CX3CR1	PE	SA011F11	BioLegend	149006
EpCAM	BV605	G8.8	BioLegend	118227
F4/80	Biotin	BM8	BioLegend	123106
F4/80	PE-CF594	T45-2342	BD Horizon	565613

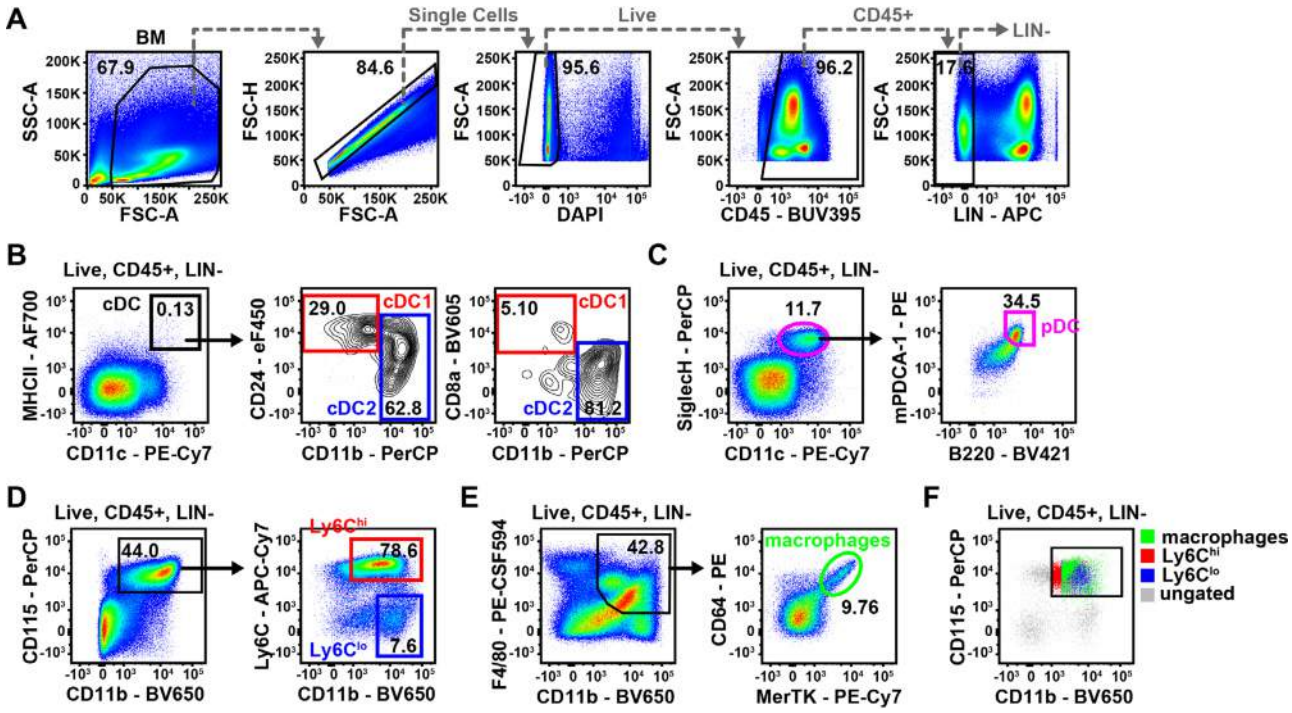

Figure 163. Flow cytometric analysis of mouse bone marrow DCs, macrophages, and monocytes. Example for basic gating strategy from FSC-A/SSC-A, over doublet exclusion and gating on Live, CD45$^+$ LIN$^-$ cells (defined as CD3/CD19/CD49b/Ly6G$^-$) on a BM sample (A). Conventional DCs are identified as CD11c^{hi}MHCII$^+$ cells and can be divided into cDC1 (CD8/CD24$^+$CD11b$^-$, red gates) and cDC2 (CD8$^-$CD11b$^+$, blue gates) (B). Plasmacytoid DCs are identified as CD11c^{int}SiglecH$^+$B220$^+$mPDCA-1$^+$ cells (pink gates; C). Monocytes are identified as CD115$^+$CD11b$^+$ cells and can be further divided into Ly6C^{lo} and Ly6C^{hi} monocytes (blue and red gates, respectivley; D), while macrophages can be gated as CD11b$^+$F4/80$^+$ (green gate; E). Backgating of monocyte and macrophage populations, that were gated independently of CD115 expression, onto CD115 versus CD11b expression confirms CD115 as a valid marker for these populations (F).

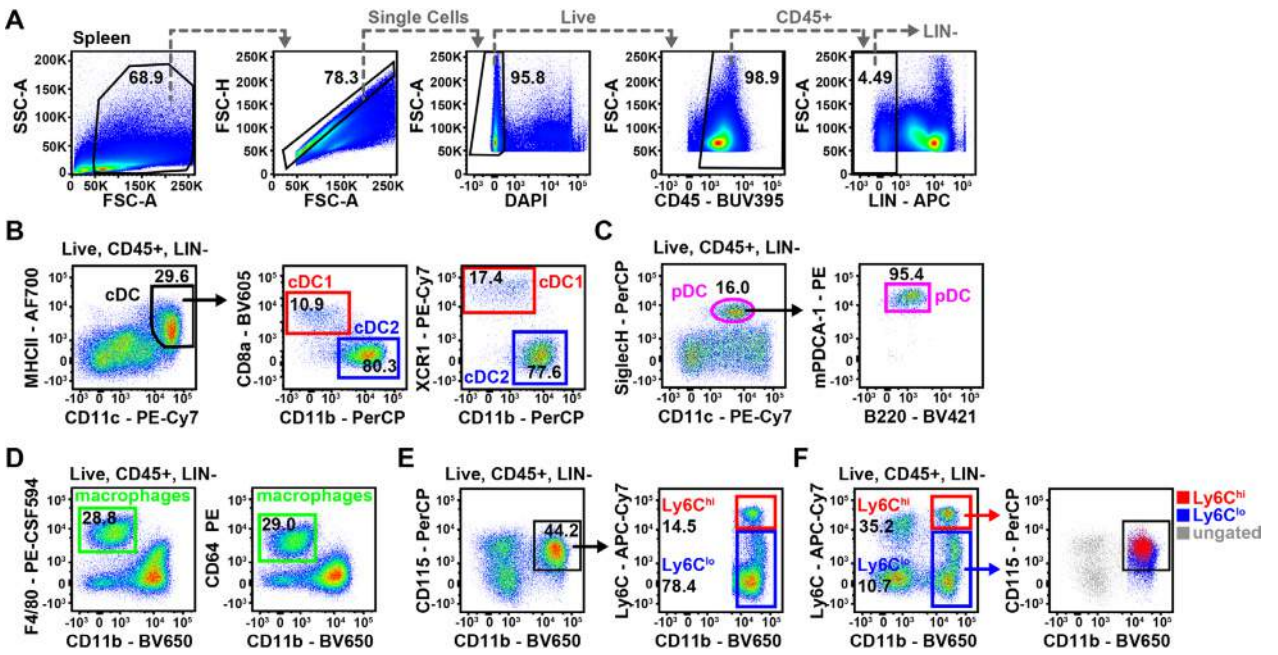

Figure 164. Flow cytometric analysis of mouse spleen DCs, macrophages, and monocytes. Example for basic gating strategy from FSC-A/SSC-A, over doublet exclusion and gating on Live, CD45$^+$ LIN$^-$ cells (defined as CD3/CD19/CD49b/Ly6G$^-$) on a spleen sample (A). Conventional DCs are identified as CD11c^{hi}MHCII$^+$ cells and can be divided into cDC1 (CD8$^+$/XCR1$^+$CD11b$^-$, red gate) and cDC2 (CD8$^-$CD11b$^+$, blue gate) (B). Plasmacytoid DCs are identified as CD11c^{int}SiglecH$^+$ but can also be identified by using B220 or mPDCA-1 (pink gates; C). Red pulp macrophages are identified as CD11b^{lo}F4/80$^+$ or CD11b^{lo}CD64$^+$ (green gate; D). Monocytes are identified as CD115$^+$CD11b$^+$ cells and can be further divided into Ly6C^{lo} and Ly6C^{hi} monocytes (blue and red gates, respectivley; E). Backgating of Ly6C^{lo} and Ly6C^{hi} monocytes that were gated independently of CD115 expression confirms CD115 as a valid marker for both populations (F).

Antibody	Fluorochrome	Clone	Provider	Cat #
MerTK	PE-Cy7	DS5MMER	Invitrogen	25-5751-82
MHCII	Alexa Fluor 700	M5-114.15.2	BioLegend	107622
Ly6C	APC-Cy7	HK1.4	BioLegend	128026
Ly6G	APC	1A8	BioLegend	127614
SiglecF	BV421	E50-2440	BD	562681
SiglecH	PerCP-Cy5.5	551	BioLegend	129614
XCR1	PE	ZET	BioLegend	148204
Streptavidin	PE-Cy7		BioLegend	405206
Streptavidin	PE-CF594		BD	562284
Streptavidin	PerCP-Cy5.5		BioLegend	405214

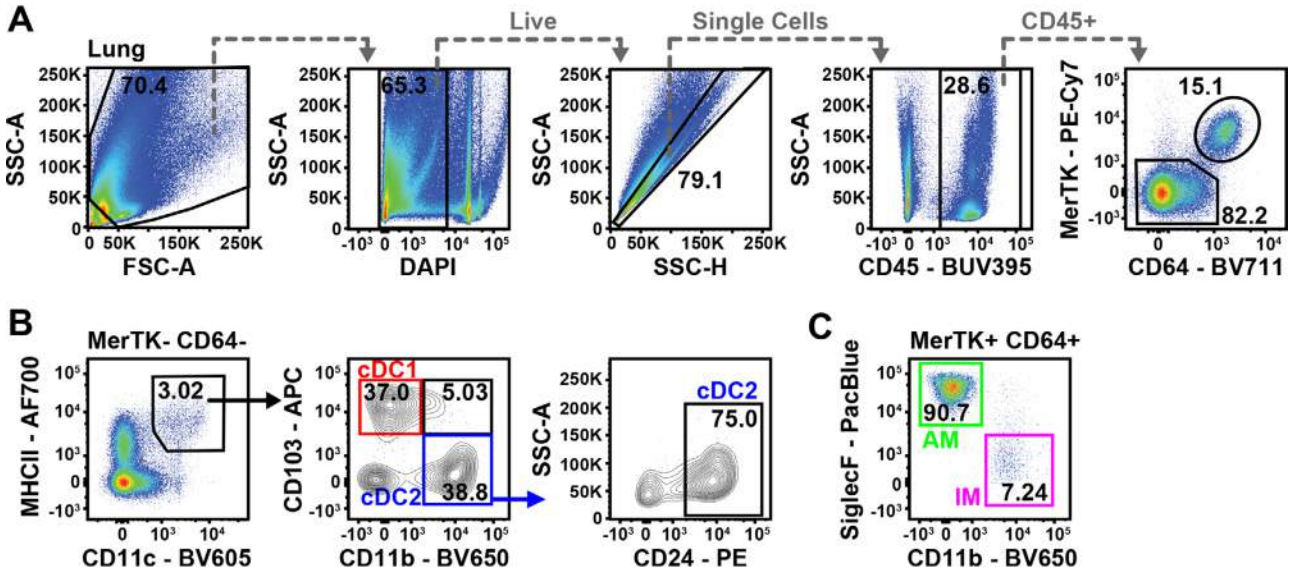

Figure 165. Flow cytometric analysis of mouse lung macrophages and DCs. Example for basic gating strategy from FSC-A/SSC-A, over doublet exclusion and gating on Live, CD45$^+$ cells on a lung sample (A). Conventional DCs are gated as MerTK$^-$ CD64$^-$ MHCII$^+$ CD11c$^+$ before being identified for cDC1 (red) and cDC2 (blue) (A and B). Macrophages are first gated as MerTK$^+$ CD64$^+$ cells, before being separated into SiglecF$^+$ CD11b$^-$ Alveolar Macrophages (AM, green) and SiglecF$^-$ CD11b$^+$ Interstitial Macrophages (IM, pink) (A and C).

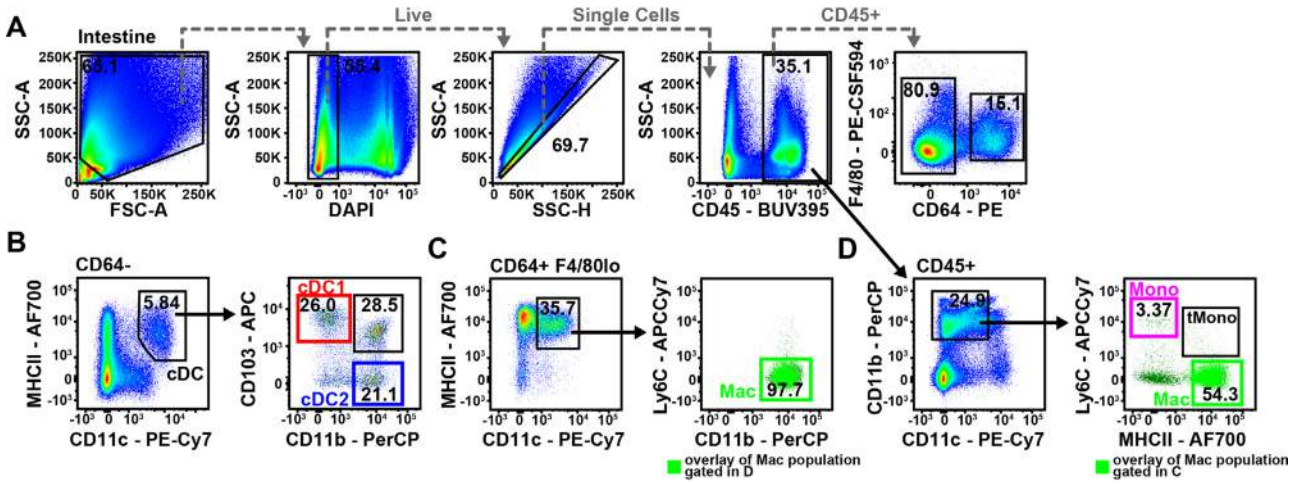

Figure 166. Flow cytometric analysis of mouse small intestine macrophages and DCs. Example for basic gating strategy from FSC-A/SSC-A, over doublet exclusion and gating on Live, CD45$^+$ cells on a small intestine sample (A). Conventional DCs are gated as CD64$^-$ MHCII$^+$ CD11c$^+$ before being identified as CD103$^+$ CD11b$^-$ cDC1 (red), CD103$^-$ CD11b$^+$ cDC2 (blue), and CD103$^+$ CD11b$^+$ "double positive" cDC2 (black) (B). Macrophages can be identified as CD64$^+$ F4/80^{lo} MHCII$^+$ CD11c$^+$ CD11b$^+$ (green) (C) or alternatively can be gated from the CD11b$^+$ CD11c^{lo} population. From this gate cells can be split into Ly6C^{hi} MHCII$^-$ monocytes (pink), Ly6C$^+$ MHCII$^+$ transitional monocytes (tMono, black) and Ly6C$^+$ MHCII$^+$ macrophages (green; D).

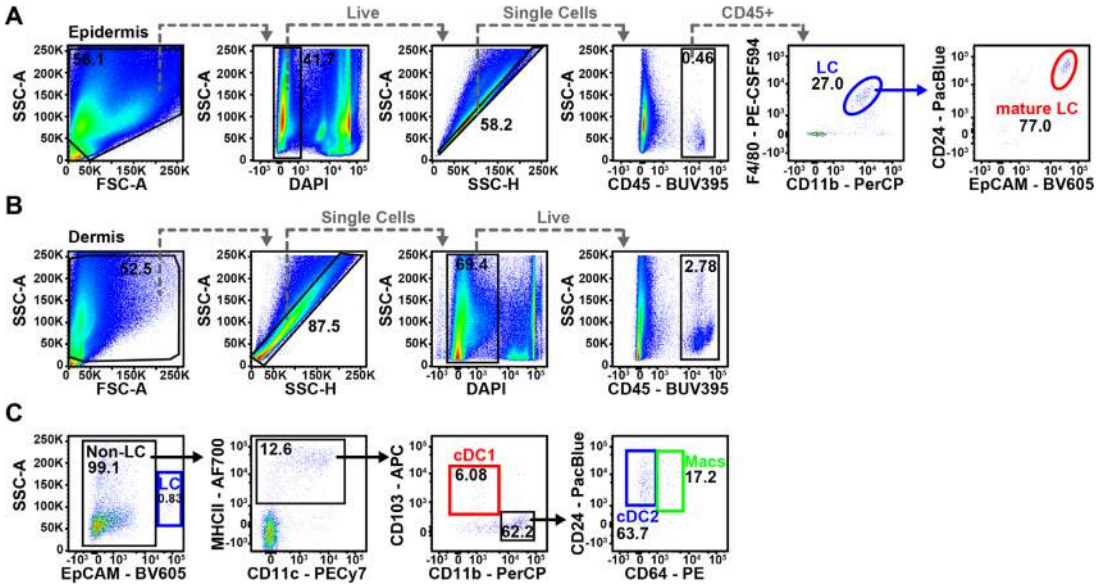

Figure 167. Flow cytometric analysis of mouse skin macrophages and DCs. Example for basic gating strategy from FSC-A/SSC-A, over doublet exclusion and gating on Live, CD45$^+$ cells on an epidermis sample (A). Langerhans cells (LC) are mainly found in the epidermis and are gated as F4/80$^+$ CD11b$^+$ (blue), while mature LC can be further identified by being CD24$^+$ EpCAM$^+$ (red; A). Example for basic gating strategy from FSC-A/SSC-A, over doublet exclusion and gating on Live, CD45$^+$ cells on a dermis sample (B). Conventional DCs are gated as EpCAM$^-$ MHCII$^+$ CD11c$^+$ before being identified as CD103$^+$ CD11b$^-$ cDC1 (red) or CD24$^+$ CD11b$^+$ cDC2 (blue; C) Within this last gate macrophages can be identified as CD64$^+$ cells (green; C).

6.3.3 Human tissue processing materials.

6.3.3.1 General reagents and materials.

Reagent	Manufacturer	Catalog number
Collagenase IV	Sigma	C5138
Worthington's Collagenase, Type IV	Worthington Biochemical	LS004188
DNase I	Roche	10104159001
Dulbecco's Phosphate Buffered Saline (PBS)		
Ficoll-Paque	GE Healthcare	17-1440-02
FCS	Sigma–Aldrich	F2442
L-Glutamine	Sigma–Aldrich	G7513-100ML
LIVE/DEAD^{TM} Fixable Blue Dead Cell Stain Kit	Life Technologies	L23105
Penicillin-Streptomycin	Sigma–Aldrich	F4333
1× RBC Lysis Buffer	eBioscience	00-4333-57
RPMI 1640	HyClone	SH30255.01

Prepare:

- FCM buffer: 2% FCS + 2 mM EDTA in PBS + 0.05% Azide in 1× PBS
- Digestion solution: 0.2 mg/mL collagenase + 0.05 mg/mL of DNase I in RPMI1640 + 10% FCS.

6.3.4 Antibodies for human mononuclear phagocyte identification. see Table 59.

6.3.5 General Remarks.

- All staining procedures in this chapter are described for staining in 5 mL FCM polystyrene tubes (in "lab slang": FACS tubes) but alternatively one may choose to do the staining in 96-well round or V-bottom plates. **Note**: This is very convenient when handling larger numbers of samples (or for in vitro assays where cells where cultured in these plates) but will increase the risk of cross-contamination during staining/washing steps!
- In general, we recommend aspirating any supernatant after centrifugation steps, as this will yield consistent staining results. An alternative method is to discard the supernatant by simply pouring it out. This usually results in a higher loss of cells (as compared to aspirating) and may leave an unknown volume of residual supernatant in the tube that might affect staining efficiency and therefore results! **Fun Fact**: We calculated the time it takes to aspirate larger numbers of FCM tubes containing ~2 mL of buffer. Result: 5 min for 100 tubes ($n = 3$ experiments with 70 to 130 tubes each, SEM ±1 min).
- It is highly recommended to count cell numbers wherever possible (ideally after RBC lysis), so one can calculate absolute numbers of individual cell populations per tissue, once the data are obtained. Depending on your lab

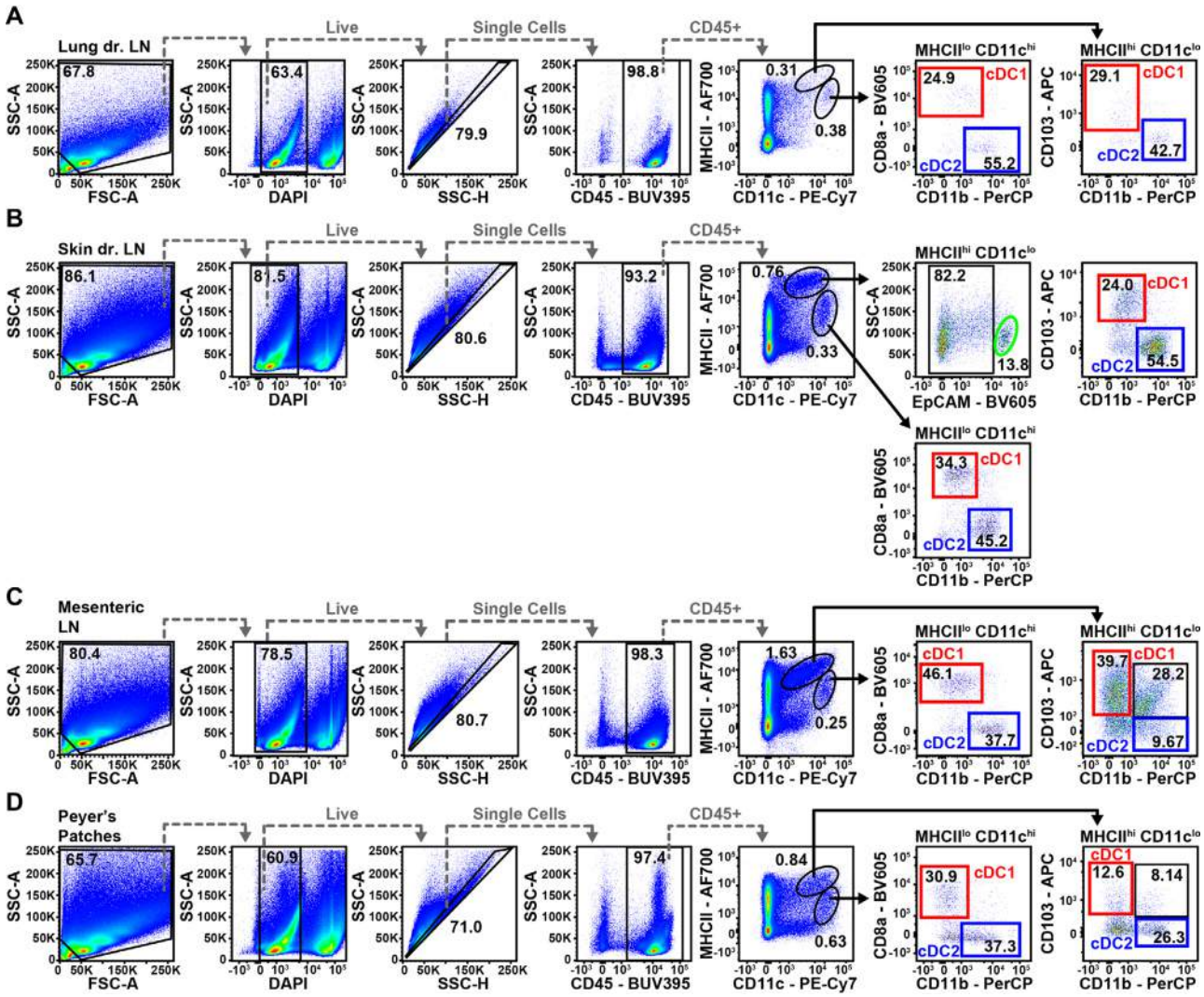

Figure 168. Flow cytometric analysis of mouse lymph node macrophages and DCs in steady-state. Example for basic gating strategy from FSC-A/SSC-A, over doublet exclusion and gating on Live, CD45$^+$ cells on lung draining (dr.) LN sample (A), skin draining LN sample (B), mesenteric LN sample (C) and for Peyer's Patches (D). Generally, migratory cDCs express higher levels of MHCII but lower levels of CD11c on their surfaces as compared to lymphoid resident cDCs (MHCII^{lo} CD11c^{hi}). Lymphoid-resident cDC1 are further gated as CD8$^+$ CD11b$^-$ (red), cDC2 as CD8$^-$ CD11b$^+$ (blue) (A–D). Migratory cDC1s (MHCII^{hi} CD11c^{lo}) can be identified by their subsequent expression of CD103 (red) while migratory cDC2s are identified as CD103$^-$ CD11b$^+$ (blue; A–D). The skin dr. LN migratory fraction further consists of EpCAM$^+$ Langerhans cells (green; B). In the mesenteric LNs and Peyer's Patches the migratory cDC2 population can be divided into CD103$^-$ CD11b$^+$ cDC2 (blue) and CD103$^+$ CD11b$^+$ "double positive" cDC2 (black; C and D).

or institute you might have access to, e.g., Neubauer chambers for manual counting, to automatic cell counters or be able to include cell counting beads to your sample (e.g., Count-Bright Absolute Counting Beads, Invitrogen, catalog number C36950). All methods are equally fine and should be chosen by the researcher fitting to their experimental setup/question. We simply recommend to use the same method for all related experiments to gain comparable and consistent results.

- Ab concentrations/dilutions stated in the protocols are meant as a guideline for first-time users and can be used as a starting point. Alternatively, check the manufacturer's recommendations when trying a new Ab. Ideally, the exact concentration needed should be determined by titration.
- Be aware that EDTA may interfere with the staining quality specifically for lectin receptors and you may opt to use an EDTA-free staining buffer.
- In the protocols, 1350 rpm equals roughly 400 × *g*.

6.4 *Step-by-step sample preparation for mouse tissues*

6.4.1 Step-by-step sample preparation for mouse blood DCs and monocytes.

1. Collect blood (e.g., from the heart, retro-orbital plexus, facial vein, etc.) and immediately transfer into a sample tube containing either PBS + 10 mM EDTA or heparin (e.g., from Sigma–Aldrich, catalog number H3393). This will prevent

Table 59. Primary and secondary antibodies for staining of human DCs and monocytes/macrophages in different tissues

Target Molecule	Fluoro chrome	Isotype	Clone	Dilution	Provider	Cat#	Target Cell	Target Tissue
Primary ab								
CADM1	Purified	chicken IgY	3E1	1/400	MBL	CM004-3	cDC1	Bl, Sp, Lu, Sk*
CD1a	AF700	mouse IgG2a	NA1/34-HLK	1/20	Novus Bio	NB100-64852AF700	LCs	Sk
CD1c	PE/Cy7	mouse IgG1	L161	1/200	Biolegend	331516	cDC2	Bl, Sp, Lu
CD1c	BV421	mouse IgG1	L161	1/20	Biolegend	331526	cDC1, cDC2	Sk
CD3	BV650	Mouse IgG2a	OKT3	1/20	Biolegend	317324	T cell	Bl, Sp, Lu, Sk
CD5	BV711	mouse IgG1	UCHT2	1/20	BD Biosciences	563170	Early pre-DC	Bl
CD11c	BV605	mouse IgG1	3.9	1/20	Biolegend	301636	cDC2	Sk, Bl, Sp, Lu
CD14	BV711	mouse IgG2a	M5E2	1/20	Biolegend	301838	DCs, Mac	Sk
CD14	ECD	mouse IgG2a	RMO52	1/10	Beckman Coulter	IM2707U	DCs, Mo	Bl, Sp, Lu
CD16	APC/Cy7	mouse IgG1	3G8	1/40	Biolegend	302018	Mo/Mac, NK cell	Bl, Sp, Lu, Sk
CD19	BV650	mouse IgG1	HIB19	1/20	Biolegend	302238	B cell	Bl, Sp, Lu, Sk
CD20	BV650	mouse IgG2b	2H7	1/20	Biolegend	302336	B cell	Bl, Sp, Lu, Sk
CD26	PE/Cy7	mouse IgG2a	BA5b	1/20	Biolegend	302714	cDC1, cDC2	Sk
CD26	PE	mouse IgG2a	BA5b	1/20	Biolegend	302706	cDC1, cDC2	Bl, Sp, Lu
CD45	V500	mouse IgG1	HI30	1/20	BD Biosciences	560777	DCs, Mo/Mac	Bl, Sp, Lu, Sk
CD123	BUV395	mouse IgG2a	7G3	1/40	BD Biosciences	564195	pDC, early pr-DC	Bl, Sp, Lu
CD169 (Siglec-1)	PE/eFluor610	mouse IgG1	7-239	1/20	eBioscience	61-1699-42	Early pre-DC	Bl
HLADR	BV786	mouse IgG2a	L243	1/20	Biolegend	307642	DCs, Mo/Mac	Bl, Sp, Lu, Sk
SIRPa (CD172a)	Purified	mouse IgG1	DH59B	1/400	King Fischer Biotech Inc	WS0567B-100	LCs	Sk
Secondary ab								
anti-Chicken IgY	Alexa Fluor 647	Donkey Fab'2	N/A	1/200	Jackson Immunore-search	703-606-155	cDC1	Bl, Sp, Lu, Sk

* Bl, blood; Sp, spleen; Lu, lungs; and SK, skin.

blood from coagulating. Place tubes on ice till further processing.
2. Centrifuge at 1350 rpm, 4°C for 4 min.
3. Carefully aspirate supernatant. Try to avoid aspirating the blood and containing cells, as the pellet will be rather fluid.
4. Resuspend pellet in 2 mL of RBC lysis buffer, incubate for 5 min at room temperature.
5. After 5 min stop reaction by adding 10 mL of FCM buffer.
6. Centrifuge at 1350 rpm, 4°C for 4 min.
7. Carefully aspirate supernatant. **Tip**: If the pellet still contains a lot of red blood cells, you might want to repeat RBC lysis step a second time for 3 min. Try avoiding further RBC lysis rounds, as the lysis buffer is very harsh on your immune cells.
8. Resuspend pellet in FCM buffer and transfer 1–10 $\times$ 10^6 cells to FCM tube for cell surface staining.
9. Centrifuge at 1350 rpm, 4°C for 4 min, aspirate supernatant.
10. Prepare blocking buffer (FCM buffer + 1:50 rat/mouse serum or purified CD16/32 (FC-block)) and cocktail containing all Abs required (dilution as recommended by manufacturer, or 1:100) for primary staining, store in the dark on ice or at 4°C.
11. Add 25 μL of blocking buffer to the pellet, vortex, incubate for 10–15 min in the dark, at 4°C. This will help prevent unspecific binding of subsequently used antibodies.
12. Add 25 μl of Ab cocktail* to the cell suspension, vortex, incubate for 15–30 min in the dark, at 4°C.
13. Add 2–3 mL of FCM buffer to the cell suspension to wash off Ab cocktail.
14. Centrifuge at 1350 rpm, 4°C for 4 min, aspirate supernatant.
15. Optional: If required, add secondary Ab, e.g., fluorochrome-conjugated Streptavidin (dilution 1:300 usually is sufficient), vortex, incubate for 15 min in the dark, at 4°C. Wash off with 2–3 mL of FCM buffer, centrifuge at 1350 rpm, 4°C for 4 min, aspirate supernatant.
16. Resuspend pellet in ~200 μL of FCM buffer containing DAPI (1:200).
17. Proceed to analyze sample on flow cytometer. **Note**: Filter sample using a 70 μm nylon mesh/cell strainer prior acquisition to avoid clogging of the analyzer.

*Staining Abs: CD45 (30-F11), F4/80 (BM8), CD64/FcγRI (X54-5/7.1), MHC Class II IA/IE (M5/114.15.2), CD11c (N418), CD11b (M1/70), Ly6C (HK1.4), CD115 (AFS98), CD24 (M1/69), CD3 (145-2C11), CD19 (eBio1D3), CD49b (DX5), Ly6G (1A8), mPDCA-1 (eBio97), SiglecH (551), B220 (RA3-6B2). Lineage (LIN) consists of CD3, CD19, CD49b (alternatively NK1.1), and Ly6G.

6.4.1.1 Gating for mouse blood DCs and monocytes (Fig. 162). Gating from single, live, $CD45^+$ LIN^- cells:

- Dendritic cells: $CD64^-$, $F4/80^-$, $MHCII^+$, $CD11c^+$

cDC1: $CD8\alpha^+/CD24^+$ $CD11b^-$
cDC2: $CD8\alpha^-$ $CD11b^+$

- pDCs: $CD11c^{int}$ $CD11b^-$ $SiglecH^+$ $mPDCA\text{-}1^+$ $B220^+$
- Monocytes: $CD115^+$ $CD11b^+$ $Ly6C^{lo/hi}$

Table 60. Phenotypic characterization of DC subsets in mouse and human tissues

	Peripheral or Migratory cDC1		Lymphoid-resident cDC1		cDC2		Plasmacytoid DCs		Early pre-DC
Marker	Mouse	Human	Mouse	Human	Mouse	Human	Mouse	Human	Human
CD4	–	+	–	+	+	+	+/–	+	+
CD8a	–	–	+	–	–	–	+/–	+/– *2	–
CD9		+		+		+	+/–	+	+
CD11b	–	–	–	–	+	(gut +)	0	–	–
CD11c	+	lo/-	++	lo/-	+	+	int	–	+/–
CD24	+	–	+	–	+	–	–	–	–
CD26	+	+	+	+	+	+ (bl –/+)	+	+	+
CD45	+	+	+	+	+	+	+	+	+
CD64	–	–	–	(spl +)	–	+/–	–	–	–
CD80	+/– *2	–		–	+/– *2	(mat +)	+/– *2	–	–
CD86	+/– *2	+		lo/+	+/– *2	+	+/– *2	lo/+	+
CD103	+	- (gut+)	–	+	–/+ *1	- (gut +)	–	–	–
CD115	–	–	–	–	–	–	–	–	–
CD117	–	+	–	+	–	–	–	–	–
CD169		–		–		–		–	+
CD172a	–	–	–	–	+	+	+	+	int
B220	–	–	–	–	–	–	+	n/a	n/a
CADM1	+	+	+	+	–	–	–	–	–
CCR7	+/– *2	+/– *2	+/– *2	+/– *2	+/– *2	+/– *2	lo/+ *2	+	–
CCR9							+/–		
Clec9a	+	+	+	+	–	–	+/–	–	–
EpCAM	–	–	–	–	–	–	–		
F4/80	–		–	n/a	–/+	n/a	–	n/a	n/a
mPDCA-1	–	–	–	–	–	–	+	n/a	n/a
MHCII *3	+	+	+	+	+	+	+/– *2	+	+
Langerin	- (der +)	–	–	–	–	–	–	–	–
Ly6C	–	–	–	–	–	–	+/–	n/a	n/a
Ly49Q							+/–	n/a	n/a
XCR1	+	–	+	–	–	–	–	–	–
IRF4	–	–	–	–	+	+	+	+	+
IRF8	+	+	+	+	–	–	+	+	+
CD1a	n/a	- (der +)	n/a	–	n/a	- (der +)	n/a	–	–
CD1c	n/a	- (der +)	n/a	–	n/a	+	n/a	–	–
CD14	n/a	–	n/a	–	n/a	–/+	n/a	–	–
CD16	n/a	–	n/a	–	n/a	–	n/a	–	–
CD123	n/a	–	n/a	–	n/a	–	n/a	+	+
CD141	n/a	+	n/a	+	n/a	–	n/a	–	int
CD303	n/a	–	n/a	–	n/a	–	n/a	+	+
CD304	n/a	–	n/a	–	n/a	–	n/a	+	+

bl, blood; der, dermis; int, intermediate; sple, spleen; mat, mature.
n/a: gene coding this protein absent in this species
Not defined
*1: $CD103^+$ $CD11b^+$ DP cDC2 population of gut, mesenteric LN, and Peyer's patches
*2: + upon activation
*3: HLA-DR in humans

Table 61. Phenotypic characterization of monocytes/macrophages in mouse and human tissues

	Classical Monocyte		Intermediate Monocyte		Non-classical Monocyte		Macrophages	
Marker	Mouse	Human	Mouse	Human	Mouse	Human	Mouse	Human
CD11b	+	hi		+	+	lo	+/−	+ (skin)
CD14	(+)	hi		+	(+)	lo		+ (skin
CD16	lo	−		+	+	+		lo/- (skin)
CD43	lo	+		+	hi	+		+
CD45	+	+		+	+	+	+	+
CD62L	+	lo		lo/-	−	−	−	
CD64	−	+		+	−	lo/-	+	+
CD115	+	lo		hi	+	int	+	+
CD169	+/−	+/−			+/−	+/−	+	+
CCR2	+	hi		int	−	−	+/−	−
CX3CR1	int	lo		int	hi	hi	+	
F4/80	−	n/a		n/a	−	n/a	+	n/a
HLA-DR		+		hi		lo		+ (skin)
MerTK	+/−				+/−		+	+
Ly6C	hi	n/a		n/a	lo	n/a	−	n/a
Lyve-1	−				−		+/−	

n/a: gene coding this protein absent in this species
Not defined

6.4.1.2 Top tricks and pitfalls.

- Additionally to CD11b and Ly6C other monocyte marker may be included for further/more detailed separation of Ly6C^{hi} and Ly6C^{lo} monocytes, such as, e.g., CX3CR1, CCR2, or TremL4 (see Table 61; [1452]).

6.4.2 Step-by-step sample preparation for mouse bone marrow DCs, monocytes, and macrophages.

1. Remove femur and tibia from euthanized mouse and, using scissors, free bones from surrounding muscle tissue and tendons. **Tip**: Use a paper towel to gently remove tissue that is stuck to the bones. This will also make it easier to detach the knee to separate femur and tibia, and to detach the foot from the tibia—use a turning/rotating motion to gently remove the foot/knee without breaking the bone.
2. Place clean bones in ice-cold PBS in a six-well plate, on ice, till all tissues have been harvested.
3. To flush out the bone marrow: take bones out of PBS, e.g., place on the inside of the lid of your six-well plate and carefully cut off a tiny bit at both ends of the bone.
4. Fill a 20 ml syringe with ice-cold FCM buffer. Use a 23 G needle to flush out the bone marrow, directly into a 15 mL or 50 mL conical tube. **Note**: This needle size should fit into most mouse bones, allowing to sufficiently flush out all the bone marrow but other G sizes will work just as well. **Tip**: For best results flush bone from both sides, moving the needle up and down within the bone while flushing.
5. Centrifuge at 1350 rpm, 4°C for 4 min.
6. Aspirate supernatant.
7. Thoroughly suspend pellet in about 1 mL of RBC lysis buffer, incubate for 3 min at room temperature. **Note**: You want to reach a single cell suspension at this step to ensure proper RBC lysis. Make sure you have no BM "pieces" left.
8. After 3 min stop reaction by adding 10 mL of FCM buffer. **Note**: You may want to filter the single cell suspension using a 70 μm nylon mesh/cell strainer to remove lose bone particles and clumps.
9. Centrifuge at 1350 rpm, 4°C for 4 min.
10. Resuspend pellet in ice-cold FCM buffer and transfer 1–10 × 10^6 cells to FCM tube for cell surface staining.
11. Centrifuge at 1350 rpm, 4°C for 4 min, aspirate supernatant.
12. Prepare blocking buffer (FCM buffer + 1:50 rat/mouse serum or purified CD16/32 (FC-block)) and cocktail containing all Abs required (dilution as recommended by manufacturer, or 1:100) for primary staining, store in the dark on ice or at 4°C.
13. Add 25 μL of blocking buffer to the pellet, vortex, incubate for 10–15 min in the dark, at 4°C. This will help prevent unspecific binding of subsequently used Abs.
14. Add 25 μl of Ab cocktail* to the cell suspension, vortex, incubate for 15–30 min in the dark, at 4°C.
15. Add 2–3 mL of FCM buffer to the cell suspension to wash off Ab cocktail.
16. Centrifuge at 1350 rpm, 4°C for 4 min, aspirate supernatant.
17. Optional: If required, add secondary Ab, e.g., fluorochrome-conjugated Streptavidin (dilution 1:300 usually is sufficient), vortex, incubate for 15 min in the dark, at 4°C. Wash off with 2–3 mL of FCM buffer, centrifuge at 1350 rpm, 4°C for 4 min, aspirate supernatant.
18. Resuspend pellet in ~200 μL of FCM buffer containing DAPI (1:200).

19. Proceed to analyze sample on flow cytometer. **Note**: Filter sample using a 70 μm nylon mesh/cell strainer prior acquisition to avoid clogging of the analyzer.

*Staining Abs: CD45 (30-F11), F4/80 (BM8), CD64/FcγRI (X54-5/7.1), MHC Class II IA/IE (M5/114.15.2), CD11c (N418), CD11b (M1/70), Ly6C (HK1.4), CD115 (AFS98), MerTK (DS5MMER), CD24 (M1/69), CD3 (145-2C11), CD19 (eBio1D3), CD49b (DX5), Ly6G (1A8), mPDCA-1 (eBio97), SiglecH (551), B220 (RA3-6B2). LIN consists of CD3, CD19, CD49b (alternatively NK1.1), and Ly6G.

6.4.2.1 Gating for mouse bone marrow DCs/monocytes/macrophages (Fig. 163). Gating from single, live, $CD45^+$ LIN^- cells:

- Dendritic cells: $CD64^-$, $F4/80^-$, $MHCII^+$, $CD11c^+$

cDC1: $CD8\alpha^+/CD24^+$ $CD11b^-$
cDC2: $CD8\alpha^-$ $CD11b^+$

- pDCs: $CD11c^{int}$ $CD11b^-$ $SiglecH^+$ $mPDCA\text{-}1^+$ $B220^+$
- Macrophages: $F4/80^+$ $CD11b^+$ $MerTK^+$ $CD64^+$
- Monocytes: $CD115^+$ $CD11b^+$ $Ly6C^{lo/hi}$

6.4.2.2 Top tricks and pitfalls.

- Cytokine receptors such as CSF-1R (CD115) are often shed off if samples are treated too harsh or processed over long periods or even internalized. Avoid receptor shedding/internalization by working quickly and keeping samples chilled.
- If working with frozen/thawed bone marrow samples one may incubate the freshly thawed samples in RPMI1640 for 6 h at 37°C to allow for proper expression of cell surface receptors. This will improve staining results.
- When gating on pDCs in the bone marrow, it is advisable to include SiglecH, mPDCA-1 and B220, as SiglecH also labels pDC progenitors, which either do not or only express low levels of B220 and mPDCA-1 yet.
- Inclusion of CD117 into the panel, followed by gating on $CD117^-$ LIN^- cells prior the monocyte gating can lead to a better resolution of these populations.

6.4.3 Step-by-step sample preparation for mouse spleen DCs, monocytes, and macrophages.

- Harvest spleen from euthanized mouse and place in ice-cold PBS in a six-well plate, on ice, till all tissues have been harvested.
- Prepare digestion buffer (as described in reagents list), keep at room temperature.
- Aliquot 2 mL of digestion buffer into a fresh well in a six-well plate.
- Take spleen out of PBS, quickly dry off on clean paper towel, if necessary remove fat and place spleen in digestion buffer.
- Use fine tweezers (or scissors) to tear spleen into very fine pieces.
- Incubate in digestion buffer at 37°C for 30 min.
- Stop digestion by adding 3 mL of PBS + 10 mM EDTA.
- Carefully, but thoroughly, pipette spleen suspension up and down using either a 5 mL pipette or a 18 G needle with a 5 mL syringe, up to 20 times to gain a single cell suspension.
- Transfer spleen cell suspension over a 70 μm nylon mesh/cell strainer into a 50 mL conical tube.
- Centrifuge at 1350 rpm, 4°C for 4 min.
- Aspirate supernatant.
- Thoroughly suspend pellet in about 1 mL of RBC lysis buffer, incubate for 3 min at room temperature.
- After 3 min stop reaction by adding 10 ml of FCM buffer.
- Centrifuge at 1350 rpm, 4°C for 4 min.
- Resuspend pellet in ice-cold FCM buffer and transfer 1–10 × 10^6 cells to FCM tube for cell surface staining.
- Centrifuge at 1350 rpm, 4°C for 4 min, aspirate supernatant.
- Prepare blocking buffer (FCM buffer + 1:50 rat/mouse serum or purified CD16/32 (FC-block)) and cocktail containing all Abs required (dilution as recommended by manufacturer, or 1:100) for primary staining, store in the dark on ice or at 4°C.
- Add 25 μL of blocking buffer to the pellet, vortex, incubate for 10–15 min in the dark, at 4°C. This will help prevent unspecific binding of subsequently used antibodies.
- Add 25 μL of Ab cocktail* to the cell suspension, vortex, incubate for 15–30 min in the dark, at 4°C.
- Add 2–3 mL of FCM buffer to the cell suspension to wash off Ab cocktail.
- Centrifuge at 1350 rpm, 4°C for 4 min, aspirate supernatant.
- Optional: If required, add secondary Ab, e.g., fluorochrome-conjugated Streptavidin (dilution 1:300 usually is sufficient), vortex, incubate for 15 min in the dark, at 4°C. Wash off with 2–3 mL of FCM buffer, centrifuge at 1350 rpm, 4°C for 4 min, aspirate supernatant.
- Resuspend pellet in approximately 200 μL of FCM buffer containing DAPI (1:200).
- Proceed to analyze sample on flow cytometer. **Note**: Filter sample using a 70 μm nylon mesh/cell strainer prior acquisition to avoid clogging of the analyzer.

*Staining Abs: CD45 (30-F11), F4/80 (BM8), CD64/FcγRI (X54-5/7.1), MHC Class II IA/IE (M5/114.15.2), CD11c (N418), CD11b (M1/70), Ly6C (HK1.4), CD115 (AFS98), CD8α (53-6.7), XCR1 (ZET), CD3 (145-2C11), CD19 (eBio1D3), CD49b (DX5), Ly6G (1A8), mPDCA-1 (eBio97), SiglecH (551), B220 (RA3-6B2). LIN consists of CD3, CD19, CD49b (alternatively NK1.1), and Ly6G.

6.4.3.1 Gating for mouse spleen DCs/monocytes/macrophages. Gating from single, live, $CD45^+$ LIN^- cells:

- Dendritic cells: $CD64^-$, $F4/80^-$, $MHCII^+$, $CD11c^+$

cDC1: CD8α$^+$ CD11b$^-$ or XCR1$^+$ CD11b$^-$
cDC2: CD8α$^-$ CD11b$^+$

- pDCs: CD11c^{int} CD11b$^-$ SiglecH$^+$ mPDCA-1$^+$ B220$^+$
- Macrophages: F4/80$^+$ CD11b$^+$
- Monocytes: CD115$^+$ CD11b$^+$ Ly6C$^{lo/hi}$

6.4.3.2 Top tricks and pitfalls.

- Note that this protocol will yield mainly red pulp macrophages, while other splenic macrophages subsets such as marginal zone macrophages are more difficult to isolate. These can be better identified by inclusion of a Tim4 Ab into the panel [1453].
- cDC1 traditionally were identified using CD8α but we highly recommend the use of XCR1 instead, as this marker is more specific than CD8α and yields a better discrimination of cDC1 from cDC2 (as can be seen in **Figure** 164) [1437, 1454, 1455].

6.4.4 Step-by step sample preparation of mouse lung macrophages/DCs.

1. Thoroughly perfuse freshly euthanized mouse intracardially with cold PBS, and harvest lungs into a 12-well plate containing cold PBS, on ice.
2. Place individual lung samples into 1.5 mL microcentrifuge tube containing 500 μL of digestion solution **1**.
3. Mince lung into small pieces using fine scissors (in the tube).
4. Transfer to 12-well plate containing additional 1–1.5 mL digestion solution (final volume 1.5–2 mL of digestion solution **1**).
5. Incubate at 37°C for 30 min.
6. Homogenize minced and digested sample using a 18 G syringe needle and 3 mL syringe and filter through 70 μm cell strainer (you may use the syringe plunger to push tissue through the strainer) into 50 mL conical tube.
7. Wash remaining cells from strainer with 20 mL FCM buffer.
8. Centrifuge at 400 × *g* for 5 min, at 4°C
9. Lyse any remaining erythrocytes by resuspending cell pellet in 500 μL of RBC lysis buffer for 3 min, at room temperature. Then stop reaction by topping up with FCM buffer.
10. Centrifuge at 400 × *g* for 5 min, at 4°C
11. Resuspend pellet in FCM buffer.
12. Filter cell suspension again through a 70 μm cell strainer to remove any clumps that may have formed after erythrocyte lysis and transfer cells to FCM tube.
13. Resuspend the appropriate number of cells (e.g., 1–10 × 10^6 cells) in FCM staining buffer (see 6.2.2.1) containing the required Abs* and incubate in the dark at 4°C.
14. Wash with FCM buffer.
15. Centrifuge at 400 × *g* for 5 min, at 4°C
16. Resuspend cells in an appropriate amount of FCM buffer.
17. Filter with 70 μm nylon mesh into a new (clean) FCM tube and analyze sample in FCM cell sorting machine.

*Staining Abs: CD45 mAb (30-F11), CD64/FcγRI mAb (X54-5/7.1), SiglecF (E50-2440), MerTK (DS5MMER), MHC Class II IA/IE mAb (M5/114.15.2), CD24 (M1/69), CD11c mAb (N418), XCR1 mAb (ZET) or CD103 mAb (2E7), SIRPα/CD172a mAb (P84) or CD11b mAb (M1/70), and Ly6C mAb (HK1.4).

6.4.4.1 Gating for mouse lung macrophages/DCs. Gating from single, live, CD45$^+$ cells:

- Alveolar macrophages (AMs): CD64$^+$, MerTK$^+$, SiglecF$^+$, CD11b$^-$
- Interstitial macrophages (IMs): CD64$^+$, MerTK$^+$, SiglecF$^-$, CD11b$^+$
- Dendritic cells: CD64$^-$, MerTK$^-$, MHCII$^+$, CD11c^{hi}

cDC1: XCR1/CD103$^+$, SIRPα/CD11b$^-$
cDC2: XCR1/CD103$^-$, SIRPα/CD11b$^+$, CD24$^+$

6.4.4.2 Top tricks and pitfalls.

- The two major macrophage populations in the mouse steady-state lung are the AMs and IMs. They express MerTK$^+$ CD64$^+$, but can also be differentiated from each other according to differences in SiglecF, MHCII, CD11c, and CD11b expression. Further markers like Lyve-1 and others (not included in the example FCM plots) have been shown to be very useful for AM versus IM discrimination [1456, 1457].
- In addition, if the configuration of the used flow cytometer allows for it, a "blank" channel (e.g., the FITC channel) is useful for discriminating "auto-fluorescent" AMs from non-autofluorescent IMs.
- Note that "aggressive" perfusion can lead to loss of alveolar resident cells.
- Two major conventional DC subsets in the lung are cDC1 and cDC2. cDC1s express XCR1 and CD103, while cDC2s express CD172α/SIRPα or CD11b, and CD24 [1437, 1456, 1458]. A minor fraction of CD103/CD11b-double-positive cDC2 can be found as well (Figure 165).

6.4.5 Step-by-step sample preparation of mouse intestinal macrophages/DCs.

1. From a freshly euthanized mouse, open up the abdominal cavity by dissecting through the skin and peritoneal membrane in a line along the ventral midline.
2. Remove the intestinal tract by dissecting the small intestine just after the pyloric sphincter, dissecting the colon by sectioning it as caudally as possible, and then carefully lift the intestines out while severing any places of attachment to the abdominal cavity and other organs.
3. Place the dissected intestine into six-well plate with cold PBS on ice. **Note**: At this point you may retrieve the mesenteric LNs from the mesenteric fat for analysis, if desired.

4. Remove as much attached mesenteric fat from intestines as possible, pulling the fat from one end and following through to the other end until the intestines have been linearized.
5. Follow the following steps for cleaning the fecal content of small intestine and colon, respectively:
   (a) For the small intestine: Dissect just above the caecum, retrieve the Peyer's Patches that lie along the length of the intestine by either cutting or plucking them (they can be analyzed separately or discarded), open the lumen lengthwise with scissors, and wash away fecal content from the opened small intestine in a beaker containing cold PBS before sectioning washed small intestine into 0.5–1 cm long pieces and placing into 50 m conical tube.
   (b) For the colon: Separate away from the cecum (discard the cecum), use two pairs of forceps to squeeze solid fecal content out of the lumen, open the lumen lengthwise wish scissors, and wash away remaining fecal content from the opened colon in beaker containing cold PBS before placing washed colon into a 50 mL conical tube.
6. Add 25 mL of cold PBS into the 50 mL conical tube with the washed intestinal sections and place on ice while completing previous steps for other samples.
7. Vigorously shake the intestinal sections in 50 mL conical tube with cold PBS to get rid of the mucus for around 10 s each round (four rounds with fresh cold PBS each round for small intestine, only once for colon).
8. Put the washed pieces into a new 50 mL conical tube and keep on ice while completing the wash step(s) for other samples.
9. When all samples are ready, add 10–12.5 mL of epithelial dissociation buffer to each sample and incubate for 20 min at 37°C in an orbital shaker set to 250 rpm.
   (a) During this incubation prepare two Petri dishes, one clean and the other filled with cold PBS, and 1.5 mL microcentrifuge tubes with 300–500 μL of digestion buffer **1** (for small intestine) or digestion buffer **2** (for colon).
   (b) If the epithelial compartment is to be retained, prepare the additional 50 mL conical tubes and cell strainers for collection.
10. Dilute epithelium dissociation buffer with 25 mL of cold PBS and shake vigorously for 10 s in the 50 mL conical tube.
11. Pour out the tube contents into the first clean Petri dish (or through a cell strainer into an additional 50 mL conical tube if the epithelium compartment is to be retained for further analysis).
12. Transfer the pieces to the second Petri dish with cold PBS and move them around to wash away traces of DTT/EDTA and epithelium cells.
13. Dry briefly on a piece of tissue before transferring the tissue pieces to the 1.5 mL microcentrifuge tube with the appropriate digestion buffer.
14. Mince tissue into small pieces with fine scissors, and then pour into six-well plate, washing out the remaining tissue from the microcentrifuge tube with digestion solution **1** (to a final volume of 2.5–3 mL in the well).
15. Incubate for 45 min at 37°C. **Note**: Some protocols state that agitation at this step will enhance the digestion process but usually this does not have any effect on digestion efficiency.
16. Homogenize minced digested sample with 18 G syringe needle and 3 mL syringe and filter through a 70 μm cell strainer (you may use the syringe plunger to push tissue through the strainer) into the final 50 mL conical tube.
17. Centrifuge at 400 × *g* for 5 min, at 4°C.
18. If cell pellet is still loose after centrifugation, repeat step 17.
19. Resuspend pellet in FCM buffer* (see Top Tricks and Pitfalls below)
20. Resuspend the appropriate number of cells in FCM staining buffer (see 6.2.2.1) containing the Abs*[1], incubate in the dark at 4°C.
21. Wash with FCM buffer.
22. Centrifuge at 400 × *g* for 5 min, at 4°C.
23. Resuspend cells in an appropriate amount of FCM buffer.
24. Filter with 70 μm nylon mesh into a new, clean FCM tube and analyze sample using a FCM cell sorting machine.

*[1]Staining Abs: CD45 mAb (30-F11), F4/80 mAb (BM8), CD64/FcγRI mAb (X54-5/7.1), MHC Class II IA/IE mAb (M5/114.15.2), CD11c mAb (N418), CD103 mAb (2E7), CD11b mAb (M1/70), Ly6C mAb (HK1.4).

6.4.5.1 Gating for intestinal macrophages/DCs. Gating from single, live, $CD45^+$ cells:

- Macrophages (Mac): $CD64^+$, $F4/80^{lo}$, $CD11b^+$, $CD11c^{lo}$, $Ly6C^-$, $MHCII^+$
- Monocytes (Mono): $CD11b^+$, $CD11c^{lo}$, $MHCII^-$, $Ly6C^+$
- Transitional Monocytes (tMono): $CD11b^+$, $CD11c^{lo}$, $MHCII^+$, $Ly6C^+$ [1459]
- Dendritic cells: $CD64^-$, $MHCII^+$, $CD11c^+$

cDC1: $CD103^+$, $CD11b^-$
cDC2: $CD103^-$, $CD11b^+$
DPs: $CD103^+$, $CD11b^+$

6.4.5.2 Top tricks and pitfalls.

- *At this point, some protocols opt to perform a 45/65% [1460] or 45/70% [1461] Percoll separation to further enrich for macrophages and DCs while removing debris. However, in our experience (and previously reported by [1462], cell yield is greatly reduced when this step is performed.
- The processing of both small intestine and large intestine for the purpose of analyzing macrophages/DCs in the lamina propria (LP) is detailed here. There are little to no macrophages/DCs in the gut epithelium compartment at steady state, hence in this protocol the dissociated epithelium is normally discarded. However, if desired, simple modifications that are mentioned here can be made to the protocol to retain the dissociated epithelium for separate analysis

- The intestinal LP contains a substantial population of eosinophils; exclusion of these can be achieved by inclusion of SiglecF (an eosinophil-specific marker) and CD64 (LP macrophage specific) into the panel. Monocyte-derived macrophages can be further gated using Ly6C [1463].
- Tim4 can be a useful marker to be added, for further delineation of macrophage populations [1453].
- There are three main subsets of lamina propria DCs: cDC1, cDC2, and an intestine-specific subset of "double positive" $CD103^+$ $CD11b^+$ DP cDC2 (Fig. 166). While in some publications intestinal cDC1 are delineated from cDC2 using XCR1 and SIRPα [1437], these markers alone are not sufficient to delineate the DP cDC2 fraction from the $CD103^-$ $CD11b^+$ cDC2.
- In general, inclusion of a lineage channel containing B, T, or neutrophil markers (e.g., CD19, CD3, Ly6G, respecitively) and gating on LIN^- cells prior gating on mononuclear phagocytes might lead to a cleaner separation of these populations and will lower the risk of contamination with other cell types.

6.4.6 Step-by-step sample preparation of mouse skin (ears).

1. Harvest ears from euthanized mouse by dissection with a fine scissors.
2. The following steps depend if total skin is analyzed, or if the epidermis and dermis are analyzed separately:
   (a) If processing total skin, proceed to place ears directly into digestion solution 1 and mince into small pieces using a pair of fine scissors, and then proceed on with step 7.
   (b) If analyzing the epidermis and dermis separately proceed on to step 3.
3. Using two pairs of fine forceps, split each ear into dorsal and ventral halves to expose the inner dermal layer.
4. Float the ear halves dermis side down in 3 mL of Dispase solution/well in 6-well plate, ensuring that they are sufficiently spread out on the solution surface.
5. Incubate for 1 h at 37°C.
6. Place each ear half on a suitable clean flat surface (polystyrene dish or lid, stainless steel tray, or a dark ceramic tile are all suitable) dermis side down.
7. In order to separate epidermis and dermis, carefully scrape the epidermis from the dermis using forceps and wash the dermis thoroughly in PBS or medium to remove any remaining epidermis.
8. Using forceps, place tissues into microcentrifuge tubes containing 500 μL digestion solution **1**, and mince into small pieces with fine scissors.
9. Pour out the cut up tissue into a 12-well plate and wash remaining minced tissue into same well using an additional 1 mL of digestion solution **1** (final volume 2 mL)
10. Incubate for 1 h at 37°C.
11. Homogenize with 3 mL syringe and 18 G needle and siphon it through 70 μm nylon mesh into FCM tube, using a 1 mL pipette tip as a funnel.
12. Centrifuge at 400 × *g* for 5 min, at 4°C.
13. Resuspend the cell pellet in FCM staining buffer (see 6.2.2.1) containing the Abs*, incubate in the dark at 4°C.
14. Wash with FCM buffer.
15. Centrifuge at 400 × *g* for 5 min, at 4°C.
16. Resuspend cells in an appropriate amount of FCM buffer.
17. Filter with 70 μm nylon mesh into a new, clean FCM tube, and analyze sample using a FCM cell sorting machine.

*Staining Abs: CD45 mAb (30-F11), F4/80 mAb (BM8), CD64 mAb (X54-5/7.1), MHC Class II IA/IE mAb (M5/114.15.2), CD11c mAb (N418), XCR1 mAb (ZET) or CD103 mAb (2E7), SIRPα/CD172a mAb (P84) or CD11b mAb (M1/70), EpCAM mAb (G8.8).

6.4.6.1 Gating for mouse skin macrophages/DCs. Gating from single, live, $CD45^+$ cells:

- LCs: $F4/80^+$, $CD11b^+$, $EpCAM^+$
- Dendritic cells: $MHCII^+$, $CD11c^+$

cDC1 – $CD103^+$, $CD11b^-$
cDC2 – $CD103^-$, $CD11b^+$, $CD24^+$, $CD64^-$

- Macrophages (Mac): $CD64^+$, $CD11c^{lo}$, $MHCII^+$

6.4.6.2 Top tricks and pitfalls.

- This protocol can be used for analysis for total skin, or the epidermis and dermis separately. However, each method comes with its own drawbacks. Total skin preparations tend to have significantly less Langerhans cells (LCs) but better yield of DCs. Separation of the epidermis and dermis has good yield of LCs in the epidermal compartment, but results in a decreased yield of dermal DCs in the dermal compartment.
- Various methods whereby different enzymes are used for processing mouse skin have been reported [1464–1466]. The effect certain enzymes can have on the surface expression of some markers should be considered.
- LCs are the main macrophage population in the epidermis. LCs express numerous markers including F4/80, CD11b, EpCAM, Langerin, and CD24 [1467, 1468]. However, EpCAM alone is sufficient to distinguish them from other $CD45^+$ cells in the skin if there are limitations to machine configuration.
- Do note that some populations of mouse DCs express Langerin as well [1467]. The dermis may contain some migratory LCs and these can be identified using EpCAM [1469] before gating for dermal cDC1 and cDC2 (Fig. 167).

6.4.7 Sample preparation of mouse LNs.

1. Harvest lymph nodes of interest from euthanized mouse into 12-well plate with 1 mL of RPMI + 10% FCS in each well.

2. Add 1 mL of 2× concentrated digestion solution **1** (=digestion solution **3**; hence, the final digestion solution will be 1× working concentration).
3. Tear apart lymph nodes in the well and digestion solution using two 25 G needles mounted on 1 mL syringes.
4. Incubate for 30 min at 37°C.
5. Homogenize with 3 mL syringe and 18 G needle and siphon it through 70 μm nylon mesh into FCM tube, using a 1 mL pipette tip as a funnel.
6. Centrifuge at 400 × *g* for 5 min, at 4°C.
7. Resuspend the cell pellet in FCM staining buffer (see Section 6.3.1.1) containing the Abs*, incubate in the dark at 4°C.
8. Wash with FCM buffer
9. Centrifuge at 400 × *g* for 5 min, at 4°C.
10. Resuspend cells in an appropriate amount of FCM buffer
11. Filter with 70 μm nylon mesh into a new, clean FCM tube and analyze sample using a FCM cell sorting machine

*Staining antibodies: CD45 mAb (30-F11), MHC Class II IA/IE mAb (M5/114.15.2), CD11c mAb (N418), XCR1 mAb (ZET), or CD103 mAb (2E7) and CD8α mAb (53-6.7), SIRPα/CD172a mAb (P84) or CD11 mAb (M1/70).

Additional staining Abs: EpCAM mAb (G8.8) for skin draining LNs.

6.4.7.1 Gating for mouse LN DCs. Gating from single, live cells:

- Migratory DCs: $CD45^+$, $MHCII^+$, $CD11c^+$
- Migratory cDC1: XCR1/$CD103^+$, SIRPα/$CD11b^-$
- Migratory cDC2: XCR1/$CD103^-$, SIRPα/$CD11b^+$
- Migratory LCs: $EpCAM^+$
- Migratory intestinal DP cDC2: $CD103^+$, SIRPα/$CD11b^+$
- Lymphoid resident DCs: $CD45^+$, $MHCII^+$, $CD11c^+$
  Lymphoid resident cDC1: XCR1/$CD8a^+$, SIRPα/$CD11b^-$
- Lymphoid resident cDC2: XCR1/$CD8a^-$, SIRPα/$CD11b^+$

6.4.7.2 Top tricks and pitfalls.

- This protocol is used to digest all LNs including Peyer's patches.
- As LNs are small pieces of tissue, we opted to do digest the LNs in the same well they are harvested into, to avoid the need to transfer LNs into a separate plate for digestion.
- Also, as LNs are highly concentrated in lymphocytes, it is recommended not to stain too many cells (especially in the case of mesenteric LNs and Peyer's patches) to avoid saturating the Ab staining mix.
- Further, inclusion of a lineage channel containing, e.g., B, T, NK cell, or neutrophil markers (e.g., CD19, CD3, CD49b/NK1.1, or Ly6G, respecitively) and gating on LIN^- cells prior gating on mononuclear phagocytes might lead to a cleaner separation of these populations and will lower the risk of contamination with other cell types.
- Mouse lymph nodes at steady-state contain two fractions of conventional DCs. The first fraction are migratory DCs that come from the peripheral tissues and express high levels of MCHII and lower levels of CD11c, and can be further split into cDC1 and cDC2 subsets using similar markers used for gating peripheral tissue DCs [1430]. The second fraction are lymph node resident conventional DCs, which express high levels of CD11c and lower levels MHCII, are also comprised of cDC1 and cDC2, and are gated using either XCR1 or CD8a, and SIRPα or CD11b for cDC1 and cDC2, respectively [1430] (Figure 168).

6.5 *Step-by-step sample preparation for human tissues*

6.5.1 Step-by-step sample preparation for human blood DCs, monocytes, and macrophages. Critical: This protocol is designed for 10 ml of human blood. If working with lower blood volumes ensure to keep the appropriate ratio for blood versus PBS versus Ficoll-paque.

1. Aliquot 10 mL of Ficoll-paque (pre-warmed to RT) into a 50 mL conical tube.
2. Dilute 10 mL of blood with PBS to a final volume of 40 mL.
3. Carefully layer the 40 mL of diluted blood on top of the Ficoll-Paque layer.
4. Centrifuge at 1800 × *g* for 25 min, at room temperature. Critical: set centrifuge to acceleration = 0 - 1 and brake = 0 - 1.
5. Collect the PBMC layer, which is found at the Plasma (PBS)–Ficoll interface, and transfer it into a 50 mL conical tube. Top up with PBS to a final volume of 50 mL.
6. Centrifuge at 365 × *g* for 5 min, at 4°C. Critical: set centrifuge to maximum acceleration and maximum brake.
7. Aspirate the supernatant.
8. Re-suspend the pellet in 1 mL of RBC lysis buffer, incubate for 5 min, at room tempertaure in the dark.
9. Top up with PBS to a final volume of 50 mL
10. Centrifuge at 365 × *g* for 5 min, at 4°C.
11. Aspirate the supernatant and re-suspend the pellet (which contains the immune cells) in 1 mL of PBS.
12. Transfer cells into a 1.5 mL microcentrifuge tube, perform cell count, and proceed with staining protocol as described in **6.4.5**.

6.5.2 Step-by-step sample preparation for human spleen DCs, monocytes, and macrophages.

1. Prepare 20 mL of digestion buffer (see Section 6.3.3.1).
2. Transfer spleen sample into 2 mL microcentrifuge tube containing 0.5 mL of the digestion solution. Using a small sterile pair of scissors mince spleen tissue into small pieces.
3. Transfer the tissue suspension into one well of a six-well plate and add on 4 mL (per well) of the digestion solution.
4. Incubate for 1 h at 37 °C.

5. Pipette up and down –six to eight times with a 10 mL disposable transfer pipette in order to disrupt the remaining tissue/gain a single cell suspension, and transfer suspension over a 70 μm cell strainer into a 50 mL conical tube. Rinse the well with PBS and add to cell suspension in the 50 mL conical tube (via filter; to ensure minimum cell loss). Adjust the volume of the suspension with PBS to a total of 50 mL.
6. Centrifuge at 365 × *g* for 5 min, at 25°C.
7. Aspirate supernatant and re-suspend the pellet in 40 mL of PBS, to achieve a proper dilution of the spleen cell suspension.
8. Aliquot 10 mL of pre-warmed (room temperature) Ficoll-paque into a new (clean) 50 mL conical tube.
9. Carefully transfer the 40 mL of the diluted spleen cell suspension as a top layer onto the 10 mL of pre-warmed (room temperature) Ficoll-paque.
10. Follow steps 4–12 from Chapter 6.5.1 (Sample preparation for human blood DCs, monocytes and macrophages).

6.5.3 Step-by-step sample preparation for human lung DCs, monocytes, and macrophages.

1. Follow Steps 1–7 from Chapter 6.5.2 (Sample preparation for human spleen DCs, monocytes, and macrophages).
2. Then, follow Steps 4–12 from Chapter 6.5.1 (Sample preparation for human blood DCs, monocytes and macrophages).

6.5.4 Step-by-step sample preparation for human skin (epidermis) DCs, monocytes, and macrophages. Critical: Skin should be immediately immersed in RPMI1640 upon collection and incubated on ice until further processing.

1. Cut skin into strips (1 × 5–10 cm) using disposable scalpels, in a large petri dish.
2. Cover circular Styrofoam with a rubber mat and place a sterile silicon mat on top.
3. Pin down the skin longitudinally at one end with 2 × 25 G needles, keeping it stretched while pulling down from the other end.
4. Shave skin using a Goulian knife by applying a side-to-side slow motion, to make it thinner. Critical: Blades should not be re-used (to avoid contamination).
5. Spread shaved strips in a 15 cm Petri dish containing 50 mL of RPMI1640 supplemented with: 10% FCS, 1% L-glutamine, 1% Pen/Strep, 0.8 mg/mL Worthington's collagenase (1×), and 0.05 mg/mL DNase.
6. Cut the skin strips into pieces of 1 cm^2 and incubate them for a minimum of 18 h, at 4°C.
7. Pipette up and down for about –eight to ten times using a 10 mL disposable transfer pipette, in order to disrupt the epidermis and dermis layers. Filter through a 70 μm cell strainer into a 50 mL conical tube. Rinse the Petri dish with PBS and add through filter to cell suspension to ensure minimum loss of cells.
8. Adjust volume of the skin cell suspension with PBS, to a total of 50 mL.
9. Follow steps 6–12 from Chapter 6.5.1 (Sample preparation for human blood DCs, monocytes, and macrophages).

6.5.5 Staining for human DCs and monocytes/macrophages from different tissues. *Notes*:

- The following protocol is used for staining DCs and monocytes/macrophages (optimal 1–5 × 10^6 cells/tube for staining) isolated from human blood (see Section 6.5.1), spleen (see Section 6.5.2), lungs (see Section 6.5.3), and skin (see Section 6.5.4).
- For Abs and reagents, see Table 59
- Staining can be performed either in a 1.5 mL microcentrifuge tube or a V-shaped 96-well plate (non-culture-treated).

1. Aliquot required number of cells, and centrifuge at 650 × *g* for 2 min, at 4°C.
2. Aspirate/discard the supernatant and re-suspend the cell pellet in 1 mL of PBS containing Live/Dead blue dye (1:1000), incubate for 20 min, at 4°C in the dark.
3. Add human AB serum or FCS, at a final dilution of 5%, and incubate for 15 min, at 4°C in the dark, in order to block FC receptors on the immune cells and to neutralize free Live/Dead molecules that bind protein N-terminal amines. **Tip**: During the incubation time for steps 2 and 3 prepare the Ab pre-mix at final dilutions as described in Table 59.
4. Add 200 μL of FCM buffer and centrifuge at 650 × *g* for 2 min, at 4°C.
5. Aspirate/discard the supernatant and re-suspend the cell pellet in 50 μL of Ab pre-mix. Incubate for 30 min, at 4°C in the dark.
6. Add 200 μL of FCM buffer, and centrifuge at 650 × *g* for 2 min, at 4°C.
7. Aspirate/discard the supernatant, then:
   (a) For staining monocytes/macrophages: proceed to step 9.
   (b) For staining DCs: since a purified Ab is used to stain CADM1 you will need to perform an additional staining step, as described in step 8 before proceeding to step 9.
8. Re-suspend the cell pellet in 50 μL of FCM buffer containing anti-Chicken-IgY-Alexa-Fluor 647. Incubate for 15 min, at 4°C. Then add 200 μL of FCM buffer and centrifuge at 650 × *g* for 2 min, at 4°C. Aspirate/discard the supernatant.
9. Re-suspend the cell pellet in 200–400 μL of FCM buffer, filter through a 70 μm cell strainer into a new (clean) FCM tube and analyze using a suitable flow cytometer.

6.5.6 Gating strategies for identification of human DCs and monocytes/macrophages in tissues. As depicted in Figs. 169 and 170, a similar gating strategy is adopted for human blood, spleen, and lung samples to characterize their cDC1, cDC2, as well as classical monocytes (cMo), intermediate monocytes (iMo) and non-classical monocytes (ncMo) subsets. We also recently described

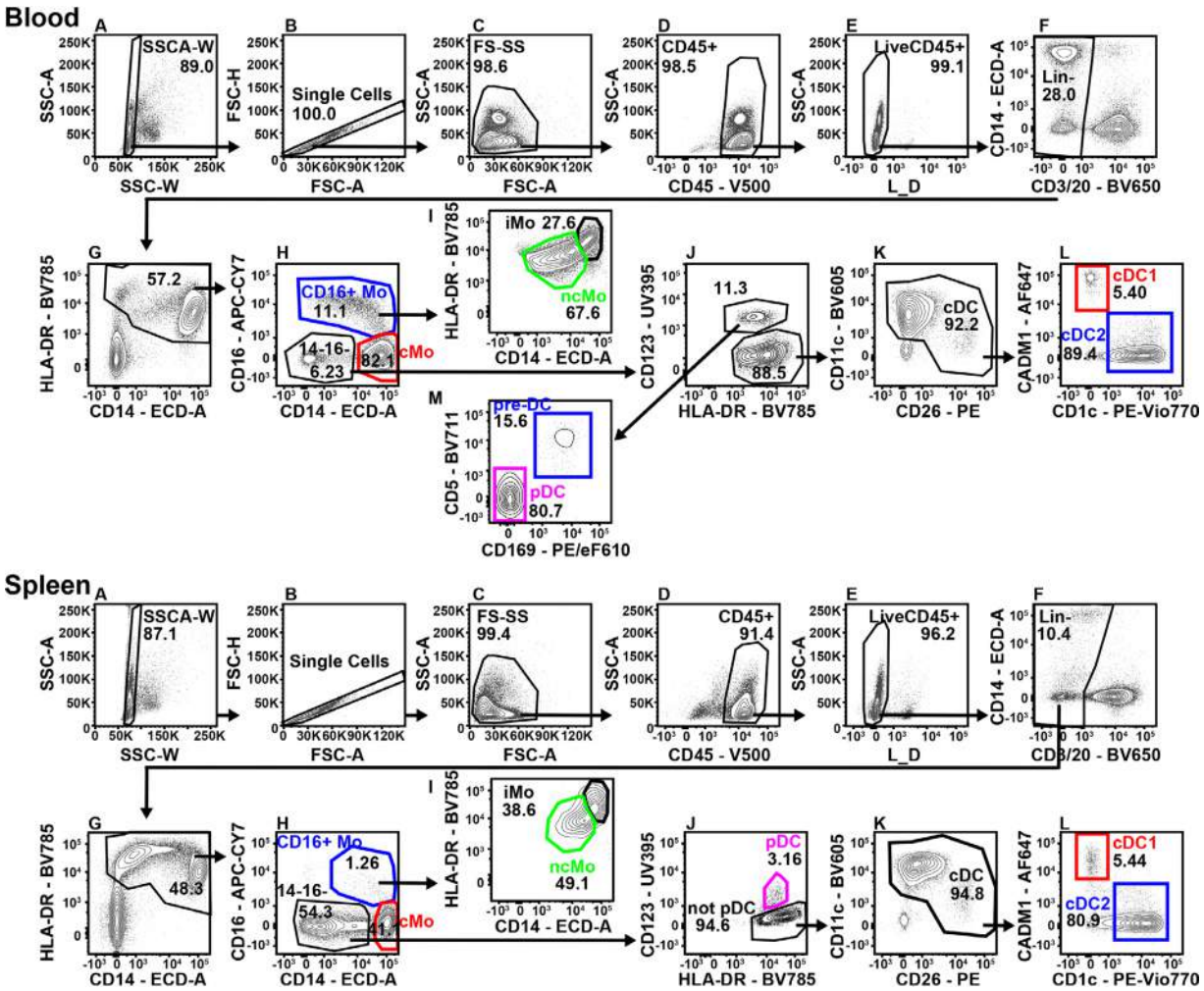

Figure 169. Gating strategies for flow cytometric analysis of human DCs and monocytes in blood and spleen. *For blood and spleen*: (A) Exclusion of doublets, (B) exclusion of doublets, (C) identification of cells based on their Forward and Side Scatter profile, (D) gating on CD45$^+$ cells, (E) exclusion of Live/Dead$^+$ dead cells, (F) gating on Lin(CD3/CD19/CD20)$^-$ cells, and (G) gating on HLA-DR$^+$ cells. (H) Gating on CD14$^{-/lo}$ CD16$^-$ DCs, CD14$^{-/+}$ CD16$^+$ monocytes and identification of CD14^{hi} CD16$^-$ classical monocytes (cMo). (I) Identification of HLA-DR$^{lo/+}$ CD14$^{lo/+}$ nonclassical monocytes (ncMo) and HLA-DR^{hi}CD14^{hi} intermediate monocytes (iMo). *For Blood*: (J) Gating on HLA-DR$^+$ CD123$^+$ cells for identification of early pre-DCs and pDCs as well as HLA-DR$^+$ CD123$^-$ cDCs. (K) Gating on classical DCs (cDC) based on expression of CD11c and CD26 (exclusion of CD11c$^-$ CD26$^-$ non-cDCs). (L) Identification of CD1c$^-$ CADM1$^+$ cDC1 and CD1c$^+$ CADM1$^-$ cDC2 (M) Identification of CD123$^+$ CD5$^+$ CD169$^+$ pre-DCs and CD123$^+$ CD5$^-$ CD169$^-$ pDCs. *For spleen*: (J) Identification of HLA-DR$^+$ CD123$^+$ pDCs. (K) Gating on classical DCs (cDC) based on expression of CD11c and CD26 (exclusion of CD11c$^-$ CD26$^-$ non-cDCs). (L) Identification of CD1c$^-$ CADM1$^+$ cDC1 and CD1c$^+$ CADM1$^-$ cDC2.

cDC progenitors in the blood, namely early pre-DC [1450], that fall into the pDC gate and their respective gating is thus described for human blood. A distinct gating strategy is also used to define Langerhans cells (LCs) and macrophages in addition to cDC1, cDC2, and pDC in the skin.

In the blood, spleen and lungs, DCs are identified by gating on CD45$^+$Lin$^-$ (CD3$^-$CD20$^-$) HLADR$^+$CD14$^{-/lo}$CD16$^-$ cells, among which cDC1 is identified as CD1c$^{-/lo}$CD11c$^-$CD123$^-$CADM1$^+$ and cDC2 as CD1c$^+$CD11c$^+$CD123$^-$CADM1$^-$. In addition, for blood, a unique gate is added to define CD123$^+$CD5$^-$CD169$^-$ pDC and the recently described human cDC progenitors, that is CD123$^+$CD5$^+$CD169$^+$ early pre-DC [1450], while the spleen and lungs' pDCs are defined as HLADR$^+$CD123$^+$. Moreover, cMo in the blood, spleen, and lungs are initially identified by gating on CD45$^+$Lin$^-$HLADR$^+$CD14^{hi}CD16$^-$ cells, while CD45$^+$Lin$^-$HLADR$^{lo\text{-}hi}$CD14$^{lo\text{-}hi}$CD16$^+$ cells are further classified into two subsets of HLA-DR$^{lo/+}$CD14$^{lo/+}$ ncMo and HLA-DR^{hi}CD14^{hi} iMo.

In the skin, DCs are identified by gating on CD45$^+$Lin$^-$(CD3$^-$CD19$^-$CD20$^-$)HLADR$^+$CD14$^-$CD16$^-$ cells, among which LCs are defined as CD1a^{hi}CD11c$^{-/lo}$ cells, while CD1a$^{-/+}$CD11c$^{-/+}$ non-LCs are classified as two subsets of CD1c$^+$CD11c$^-$SIRPα$^-$CADM1$^+$ cDC1 and CD1c$^+$CD11c$^+$SIRPα$^+$CADM1$^-$ cDC2. In addition, skin macrophages are identified by gating on CD45$^+$Lin$^-$HLADR$^+$CD14$^+$CD16$^{-/lo}$ cells.

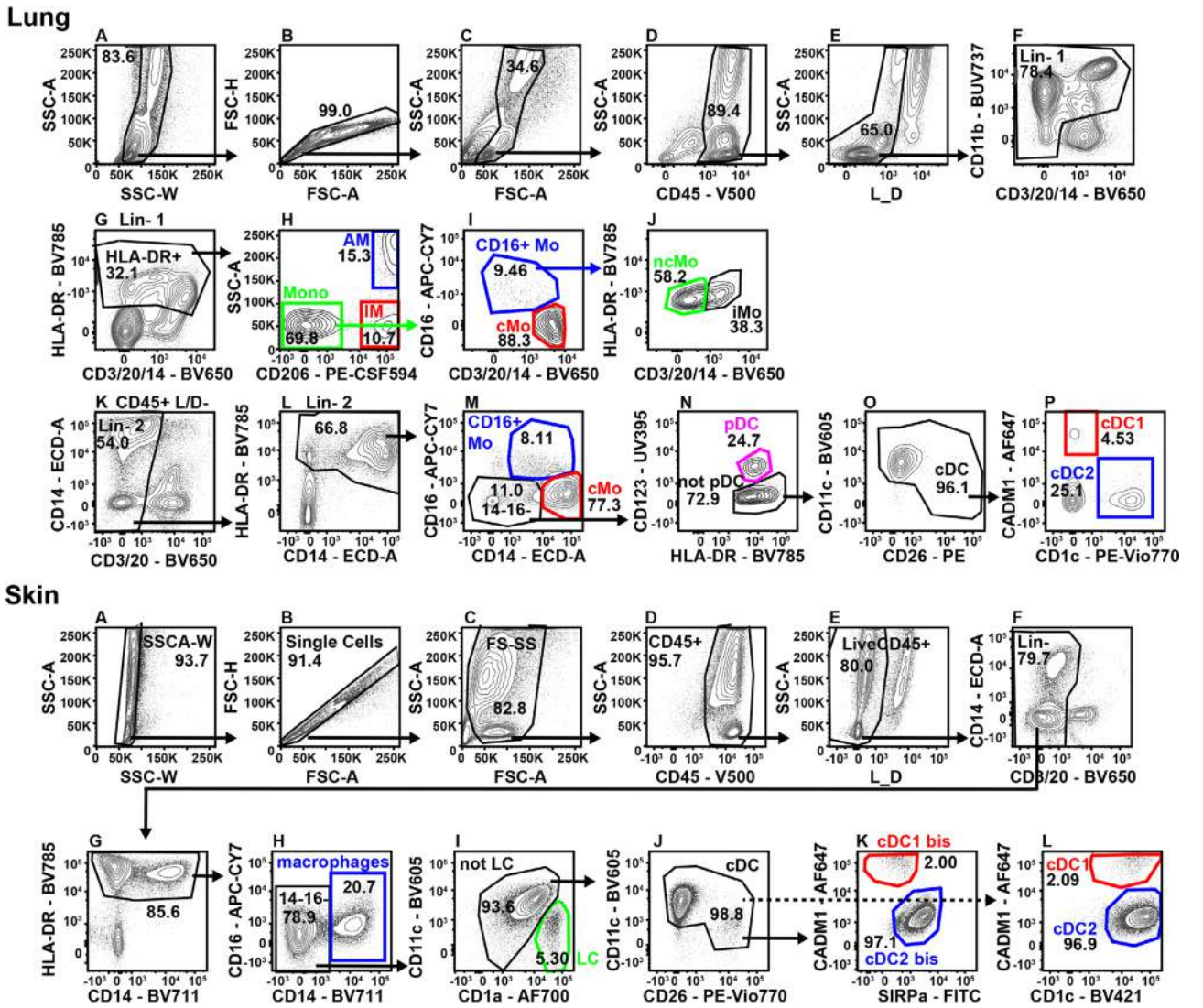

Figure 170. Gating strategies for flow cytometric analysis of human DCs and monocytes in lung and skin. *For lung and skin*: (A) Exclusion of doublets, (B) exclusion of doublets, (C) identification of cells based on their Forward and Side Scatter profile, (D) gating on CD45$^+$ cells, (E) exclusion of Live/Dead$^+$ dead cells, (F) gating on Lin(CD3/CD19/CD20)$^-$ cells, and (G) gating on HLA-DR$^+$ cells. *For lung*: (H) Gating on SSC-A^{hi} CD206^{hi} alveolar macrophages (AM) (blue), SSC-A^{lo} CD206^{hi} interstitial macrophages (IM) (red) and SSC-A^{hi} CD206$^-$ monocytes. (I) Monocytes are divided into CD14$^+$ CD16$^-$ classical monocytes (cMo) (red) and CD16+ monocytes (blue), and from there (J) into HLA-DR^{lo} CD14^{lo} non-classical monocytes (ncMo) and HLA-DR^{lo} CD14$^+$ intermediate monocytes (iMo). (K) Gating on LIN- cells and (L) HLA-DR$^+$ cells. (M) Gating on CD14$^{-/lo}$ CD16$^-$ DCs (and also CD14$^{-/+}$ CD16$^+$ monocytes (blue) and identification of CD14^{hi} CD16$^-$ classical monocytes (cMo; red)). (N) Identification of CD123$^+$ pDCs. (O, P) Gating on classical DCs (cDC) based on expression of CD11c and CD26 (exclusion of CD11c$^-$ CD26$^-$ non-cDCs) and identification of CD1c$^-$ CADM1$^+$ cDC1 and CD1c$^+$ CADM1$^-$ cDC2. *For Skin*: (H) Identification of CD14$^+$ CD16$^{-/lo}$ macrophages, (I) Identification of CD1a^{hi} CD11c$^{-/lo}$ Langerhans cells (LCs), (J) Gating on cDC based on expression of CD11c and CD26, (K) Identification of SIRPα$^-$ CADM1$^+$ cDC1 and SIRPα$^+$ CADM1$^-$ cDC2, (L) Alternative way to identify CD1c$^{-/+}$ CADM1$^+$ cDC1 and CD1c$^+$ CADM1$^-$ cDC2 if using the same strategy as the other organs.

6.6 *Pitfalls*

First, generating qualitative FCM data requires proper combinations of fluorochromes/markers. It should be avoided to use Abs binding co-expressed markers conjugated with fluorochromes that have a lot of fluorescence spill-over into channels in which they are detected. Second, analyzing DC and monocyte/macrophages by FCM requires using more than ten Abs and thus complexifies the definition of a correct compensation matrix. Third, when analyzing FCM data using manual gating, a major challenge is to avoid dropping out cells of interest along the gates. To facilitate these two latter critical aspects of FCM data analysis, an initial manual gating should be done to define major DC and monocyte subsets.

Then, using a compatible software (Diva, Kaluza, and eventually Flow Jo), n dot plot (for an n color FCM panel) should be defined (fluorochrome A on the *x*-axis vs. all the other fluorochromes on the *y*-axis) all displaying CD45$^+$ cells with all

the DC and monocyte subsets overlayed (each having a defined color). This will allow the proper setting of "all fluorochromes-the A fluorochrome" compensations. When all "fluorochrome X-fluorochrome A" compensations are properly set, the next fluorochrome must be displayed on the *x*-axis, and so on, until all fluorochromes have been properly compensated.

Once compensations are properly set, two methods can be used for analysis, manual gating or unsupervised dimensionality reduction, latter being the most reliable method.

For manual gating, the different cell subsets must be displayed in all gates defined to reach them by "back gating" to ensure that each of them are present at all steps of the gating strategy. To ensure that all populations can be properly visualized in all gates, back gated cell subsets should be ordered by count, with the rarest populations displayed above all the other cell subsets.

A major drawback of manual gating is that gates are defined based on one (histogram) or two markers' (dot plot) expression, which in some cases does not allow the proper separation of cell populations that share overlapping phenotypes. Thus, unsupervised dimensionality reduction is now becoming the gold standard method to avoid this, since it reduces all dimensions (one marker = one dimension) into a 2D or 3D space. Machine learning-based algorithms such as t-SNE [144], or UMAP [1470]; [1470, 1471] combined with clustering algorithms [1450, 1472, 1473] allow the proper identification and separation of cell subsets by integrating all markers analyzed. When performing dimensionality reduction on a very heterogeneous population, such as total $CD45^+$ leukocytes, minor cell subsets will not be finely resolved, such as DC subsets. Thus, dimensionality reduction can be first done on total $CD45^+$ cells using a dimensionality reduction method such as UMAP that contrary to tSNE, allows the analysis of millions of cells (events). As an illustration, total Live $CD45^+$ cells from the same FCM data of human blood, spleen, and lung from Fig. 169 and 170 were analyzed using the UMAP algorithm (Fig. 171A–C). The same manual gating strategy was applied and for each step, the corresponding populations were overlayed on the UMAP space, demonstrating that manual gating leads to minor contaminations as illustrated by cells falling into the dashed black delimited regions (Fig. 171A). We next plotted major cell subsets defining markers expression as meaning plots to guide the unsupervised delineation of all major mononuclear cell subsets (Fig. 171B–C). In the UMAP bidimensional space obtained, $Lin^-HLA\text{-}DR^+$ cells (DC and monocyte/macrophages) were not clearly resolved and thus, were gated and reanalyzed with both the UMAP and t-SNE dimensionality reduction algorithm together with the Phenograph clustering algorithm to obtain a higher resolution of the cells comprised in this gate (Fig. 171D–F). Analysis of the expression of DC and monocyte/macrophage markers allowed the delineation of Phenograph clusters corresponding to DC and monocyte/macrophage subsets (Fig. 171D,E), and to compare the relative phenotype and distribution of cell subsets in the blood, spleen, and lung (Fig. 171E–F). This subgating can be done again in a particular subpopulation of the second dimensionality reduced space obtained to further increase the resolution of discrete cell populations.

7 Granulocytes

7.1 *Neutrophils, eosinophils, and basophils*

7.1.1 Overview. This chapter aims to provide guidelines for researchers interested in analyzing polymorphonuclear leucocytes. We describe a gating strategy to distinguish different subsets of PMNs via FCM staining for human and murine blood samples. Furthermore, we provide a simple method to examine phagocytosis via FCM staining as well as basic tips and tricks for handling neutrophils appropriately to prevent activation.

7.1.2 Introduction. Granulocytes are highly granular cells with a distinct lobed nuclear morphology. They can further be divided in basophils (0.5–1% of WBC), eosinophils (1–3% of WBC) and neutrophils (50–70% of WBC). Neutrophils exert potent antibacterial functions and are involved in inflammatory diseases (see also Chapter VI Section 7.2 Bone marrow and umbilical cord blood neutrophils), whereas basophils and eosinophils help to control parasitic infections and contribute to allergic reactions. Granulocytes are rapidly recruited to sites of infection, providing robust early microbial control. This feature is essential for the survival of the host, however, comes with the need for special arrangements when working with isolated granulocytes: All instrumentation and buffers/media need to free of LPS and other pathogen-associated molecular patterns (PAMPS) to prevent undesired activation. Further, granulocyte exhibit a relatively short life span of only a few hours to a few days and are sensitive to inappropriate treatment, for example, harsh physical handling or high concentrations of calcium. It is advisable to work rapidly, reduce manipulation steps that could mechanically activate the cells and use the cells immediately upon isolation. Therefore, it is necessary to use optimized protocols for the dissociation of different tissues to prepare single cell suspensions for FCM. The easiest way to obtain granulocytes for analysis is to use whole blood (human or mouse) and perform lysis of erythrocytes.

7.1.3 Step-by-step sample preparation. Successful FCM analysis requires high quality single cell suspensions. Minimal manipulation of the cells is essential for the quality of both Ab and cell death staining. Human granulocytes are abundantly present in peripheral blood and can be isolated via density centrifugation or analyzed as a subpopulation of total leukocytes. Note that some inflammatory disorders are characterized by low density granulocytes that colocalize with PBMCs during density centrifugation. In mice, granulocytes can be obtained from peritoneal lavage, i.e., after intraperitoneal injection of thioglycolate, whole blood, or bone marrow (see Isolation Chapter VI: Section 8 Murine bone marrow stromal cells). In some cases, enrichment for granulocytes might be necessary and this can be achieved via density gradient centrifugation (see Chapter IV Section 1.2 Pre-enrichment by physical properties) or negative selection via magnetic beads (see Chapter IV Section 1.3 Pre-enrichment by immunological

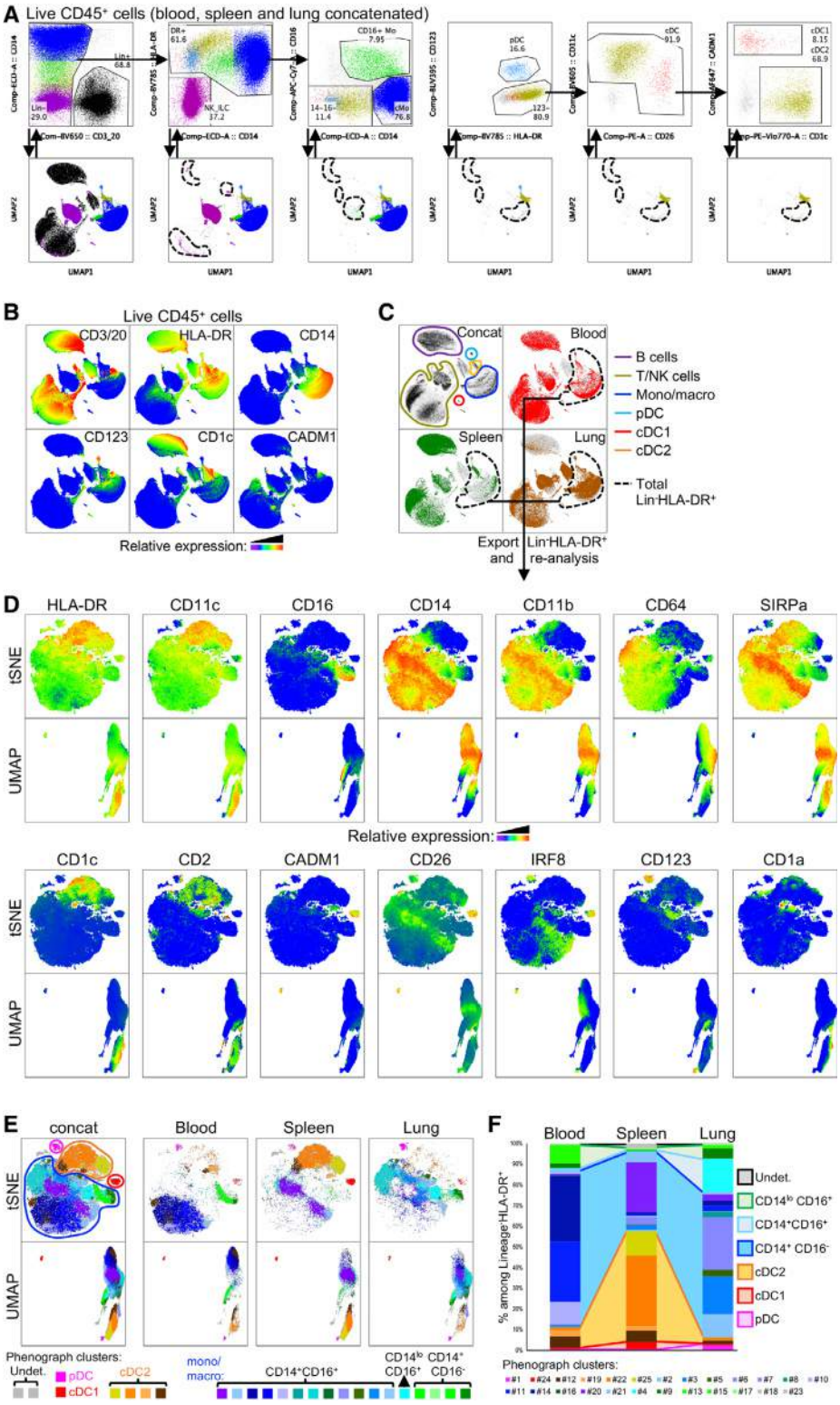

Figure 171. Unsupervised analysis of human DCs and monocyte/macrophages in different tissues. Lin$^-$HLA-DR$^+$ cells from Blood, Spleen and Lung data from Figures 169 and 170 were analysed using two dimensionality reduction methods, Uniform Manifold Approximation and Projection (UMAP) and t-Distributed Stochastic Neighbor Embedding (t-SNE) combined with the Phenograph automated clustering method. (A) Manual gating strategy of the concatenated data obtained from blood, spleen and lung starting from Live CD45$^+$ cells. The upper panels show the different steps of the manual gating strategy and the lower panels show the projection of each step of the gating strategy into a UMAP space. (B) Meaning pots of lineage-defining markers overlayed on the UMAP plot. (C) UMAP plot showing the concatenated data obtained in the three organs (upper left panel), in the blood (red, upper left panel), in the spleen (green, lower left panel) and in the lung (brown, lower right panel) where Lin$^-$HLA-DR$^+$ cells are defined. (D) Meaning pots of the relative expression of all parameters overlayed on the tSNE and UMAP plots of the concatenated data (blood, spleen and Lung) from Lin$^-$HLA-DR$^+$ cells exportes as shown in (C). (E) Visualisation of phenograph clusters overlayed on the tSNE and UMAP plots of the concatenated data (left panel), or of each individual sample. Clusters corresponding to pDC (pink), cDC1 (red), cDC2 (yellow = enriched in DC2 to brown -= enriched in DC3 [1474, 1475], CD14$^+$CD16$^-$ (blue to purple), CD14$^+$CD16$^+$ (cyan), CD14^{lo}CD16$^+$ (green) monocyte/macrophages, and three minor undetermined clusters are shown. (F) Frequencies of Phenograph clusters defined in (B) regrouped by cell subsets defined in (B).

properties). For FCM analysis, the initial cell suspension should be depleted of erythrocytes (e.g., short hypotonic lysis with water, ammonium chloride treatment, or use of commercially available RBC lysis buffers).

7.1.3.1 Flow cytometric characterization of human and murine granulocytes. Staining can either be performed before or after lysis of RBC. In the protocol described below, lysis of erythrocytes was performed prior to Ab staining. Due to the abundant expres-

sion of Fc receptors on granulocytes, use of an Fc block is strongly advised.

1. A total of 100 μL of human or murine whole blood is pelleted via centrifugation at 300 × *g* for 5 min. The cell pellet is resuspended in a small volume and subjected to lysis with hypotonic water (900 μL) for 20 s to lyse erythrocytes. Physiological osmolality is re-obtained by addition of 100 μL of 10× PBS.
2. Cells are pelleted via centrifugation at 300 × *g* for 5 min and resuspended in 100 μL HBSS (with 2% heat inactivated FCS and Fc block). The samples are incubated for 15 min on ice.
3. Cells are pelleted via centrifugation at 300 × *g* for 5 min and resuspended in 100 μL HBSS (with 2% heat inactivated FCS and Abs). The samples are incubated for 30 min on ice in the absence of light.
4. One milliliter of HBSS (with 2% heat inactivated FCS) is added to the suspension and cells are pelleted via centrifugation at 300 × *g* for 5 min, resuspended in an appropriate volume of HBSS (with 2% heat inactivated FCS) and subjected to FCM analysis.

7.1.3.2 Flow cytometric detection of cell death in human granulocytes. Human granulocytes can easily be obtained via density gradient centrifugation of human blood. Several different protocols have been published, with some involving dextran sedimentation of RBCs. The protocol we describe here omits the lengthy dextran sedimentation step without affecting the purity of the granulocyte fraction.

1. A total of 20 mL of anti-coagulated blood is diluted with 15 mL PBS and gently layered on top of 15 mL Lymphoflot. Cells are separated via centrifugation at 300 × *g* for 30 min without break. The granulocytes layer directly on top of the RBCs (whitish veil) and are collected and washed once in PBS. Note that this fraction contains mainly neutrophils and eosinophils, whereas basophils sediment in the PBMC fraction.
2. The cell pellet is resuspended in 200 μL of PBS. Hypotonic lysis of erythrocytes is performed by addition of 36 mL of ice-cold water for 20 s. Physiological osmolality is re-obtained by addition of 4 mL of 10× PBS.
3. The granulocytes are resuspended in RPMI-1640 supplemented with 100 U/mL penicillin/streptomycin, 2 mM glutamine, and 10% heat-inactivated FCS and 25 mM HEPES at a concentration of 2 × 10^6 cells/mL and cultivated at 37°C/5% CO_2. Due to the short life span of granulocytes, detectable cell death will occur in less than 12 h.
4. Cell death is assessed by harvesting of cells via centrifugation at 300 × *g* for 5 min and resuspension at a concentration of 1 × 10^6 cells/mL in HBSS supplemented with 2% heat inactivated FCS, 100 ng/mL PI, and 1 μg/mL ANX-V. Staining is performed on ice for 30 min.
5. Without an additional washing step, samples are directly subjected to FCM analysis. Note that washing is not recommended as this can result in the loss of subcellular particles and compromise integrity of apoptotic cells.

7.1.3.3 Flow cytometric detection of particle uptake in human granulocytes.

1. A total of 20 mL of anti-coagulated blood is diluted with 15 mL PBS and gently layered on top of 15 mL Lymphoflot. Cells are separated via centrifugation at 300 × *g* for 30 min without break. The granulocytes layer directly on top of the RBCs (whitish veil) and are collected and washed once in PBS. Note that this fraction contains mainly neutrophils and eosinophils, whereas basophils sediment in the PBMC fraction.
2. The cell pellet is re-suspended in 200 μL of PBS. Hypotonic lysis of erythrocytes is performed by addition of 36 mL of ice-cold water for 20 s. Physiological osmolality is re-obtained by addition of 4 mL of 10× PBS.
3. The granulocytes are re-suspended in in HBSS supplemented with 2% heat inactivated FCS. A total of 20 μg/mL micro monosodium urate crystals and 250 μg/mL Lucifer Yellow are added and cells are incubated at 37°C/5% CO_2 for various time points.
4. Cells are collected and without additional washing directly subjected to FCM analysis.

7.1.4 Materials.

7.1.4.1 Reagents. HBSS, calcium, magnesium, no phenol red (ThermoFisher Scientific, 14025050)
Lymphoflot (Bio-Rad, #824012)
Lucifer Yellow CH (ThermoFisher Scientific, L453)
RPMI 1640 Medium (ThermoFisher Scientific, 21875034)
L-Glutamine (ThermoFisher Scientific, 25030081)
Penicillin–Streptomycin (ThermoFisher Scientific, 15140122)
HEPES (ThermoFisher Scientific, 15630056)
Fetal Calf Serum (Biochrom, S 0115)
Propidium iodide (Sigma, P4170)
Anx-V-FITC (Immunotools, 31490013)
Human TruStain FcX™ (Biolegend, 422301)
TruStain FcX™ PLUS (anti-mouse CD16/32) (Biolegend, 156603)

7.1.4.2 Instruments/Software.

GALLIOS flow cytometer (Beckman-Coulter)
Kaluza Analysis Software (Beckman-Coulter)
Prism 7 (Graphpad)

7.1.5 Data Analysis. Differential light scattering of cells depending on the size and morphology is useful to discriminate subsets of cells. The SSC is considered to be an indicator for the internal structure of the cell (e.g., nuclear morphology) and the FSC

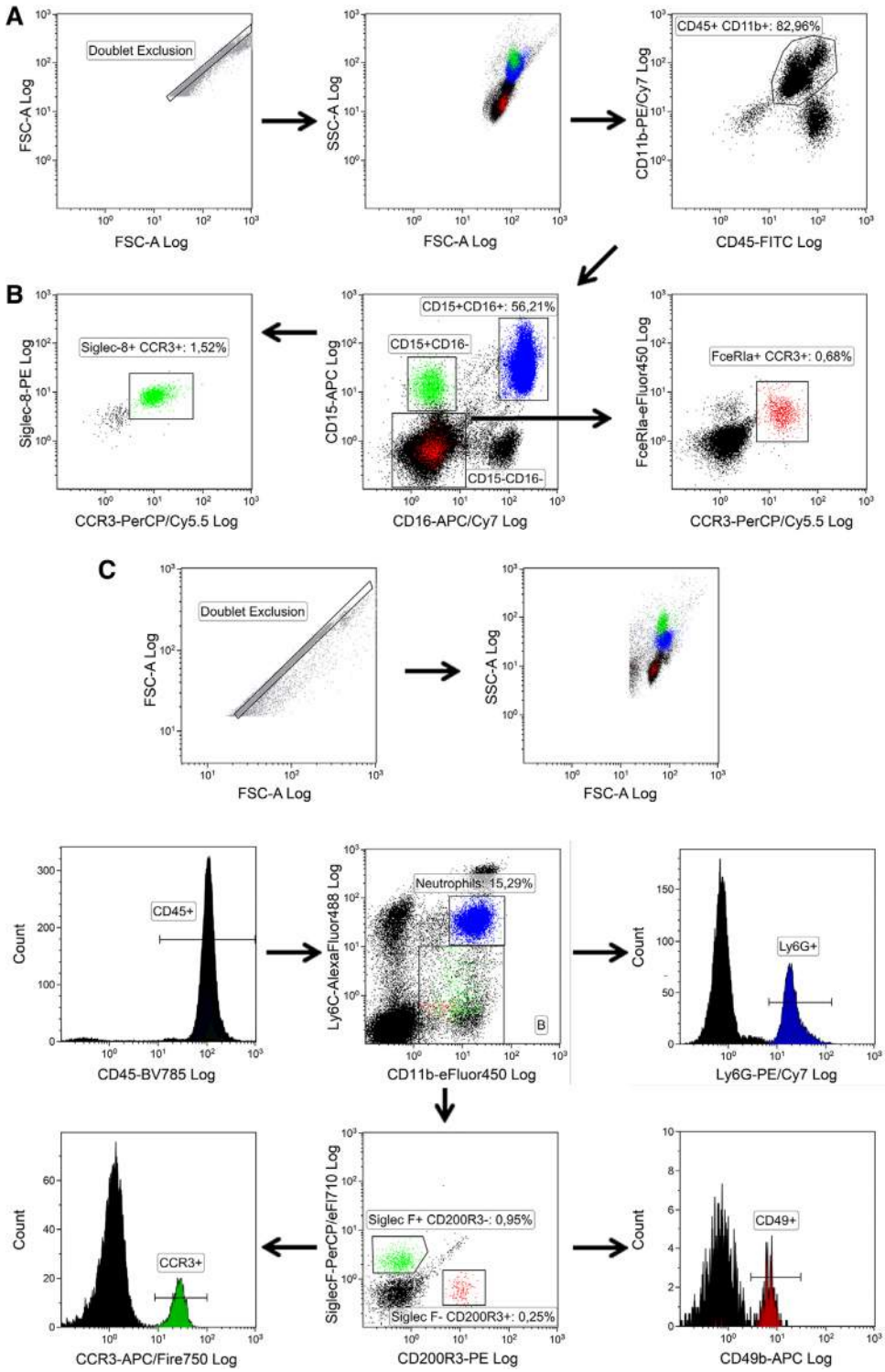

Figure 172. Discrimination of granulocyte subpopulations. (A) Human cells were displayed in a SSC versus FSC dot plot to show the location of eosinophils (green, high SSC), neutrophils (blue, high SSC), and basophils (red, low SSC). (B) Human cells were stained with Abs against CD45, CD11b, CD15, CD16, CCR3, Siglec-F, and FcεRIα. $CD45^+/CD11b^+$ cells were gated on CD15 versus CD16 to distinguish granulocyte subpopulations. $CD15^+/CD16^+$ cells were determined as neutrophils, $CD15^+CD16^-$ were further designated as eosinophils by their expression of Siglec-8 and CCR3, and the $CD15^-/CD16^-$ population was depicted in a FcεRIα versus CCR3 plot to identify the double positive basophil fraction. (C) $CD45^+$ murine cells were gated on CD11b/Ly6C to display the $CD11b^+/Ly6^{int}$ population that was further analyzed using Ly6G to identify neutrophils (blue). $CD11b^+/Ly6C^{neg\text{-}low}$ cells were gated on Siglec-F versus CD200R3 and were subsequently analyzed for expression of additional cell subset markers. CD200R3-cells expressing Siglec-F and CCR3 were designated as eosinophils (green) and Siglec-F-cells were marked as basophils (red) supported by their expression of CD200R3 and CD49b.

Table 62. List of Abs used for characterization of human granulocyte populations

Target	Fluorophore	Supplier	Cat#	Clone	Host	Isotype	Cross-Reactivity
CCR3	PerCp/Cy5.5	BioLegend	310717	5E8	Mouse	IgG2b, κ	None
CD11b	PE/Cy7	BioLegend	301321	ICRF44	Mouse	IgG1, κ	Yes
CD15	APC	BioLegend	301907	HI98	Mouse	IgM, κ	Yes
CD16	APC/Cy7	BioLegend	302017	3G8	Mouse	IgG1, κ	Yes
CD45	FITC	BioLegend	304005	HI30	Mouse	IgG1, κ	Yes
FcRε1	eFluor450	eBioscience	14-5899-82	AER-37	Mouse	IgG2b, κ	None
Siglec-8	PE	BioLegend	347103	7C9	Mouse	IgG1, κ	None

reflects cellular size. Since both human and murine neutrophils and eosinophils have a multi-lobulated nucleus, they exhibit a high SSC signal, with eosinophils showing a slightly higher signal in this parameter. The nuclear morphology of basophils is less complex and therefore they are found among the lymphocyte population and cannot be distinguished in such manner (Fig. 172A). Furthermore, changes in SSC and FSC may also represent other morphological features of various cellular processes (e.g., phagocytosis, cell death). These changes can also be detected in this manner as described below in this section. It is recommended to start your analysis with excluding doublets by gating on FS PEAK Log versus FS INT Log to prevent an impact of doublets on, e.g., population frequencies. Then, to detect either human or murine granulocytes, it is useful to start with a staining for CD45 to define WBCs accompanied by the simultaneous staining for CD11b. These two markers together with FSC and SSC features are enough to roughly narrow down granulocytes from whole blood preparations (Fig. 172A and C). Human neutrophils are the most abundant cell type within the granulocyte family. They can be further distinguished from other granulocytes by their positivity for both CD15 and CD16. Eosinophils are positive for CD15, but do not express CD16. Additional staining for CCR3 and Siglec-8 allows a specific detection of eosinophils. Basophils neither express CD15 nor CD16; therefore staining with anti-FcεRIα identifies them in the $CD15^{neg}/CD16^{neg}$ population (Fig. 172B).

Murine neutrophils and eosinophils are CD11b positive and exhibit an intermediate to low expression of Ly6C. Neutrophils are detected as Ly6G positive cells, whereas eosinophils are identified by their expression of CCR3 and Siglec-F. Basophils also show positivity for CD11b, but have only a low expression of Ly6C. They can be further identified by the expression of CD200R3 and CD49b (Fig. 172C).

Especially in the context of inflammatory infiltrates it is sometimes necessary to further determine neutrophil viability. During the resolution of inflammation, neutrophils undergo apoptosis, mediate anti-inflammatory and immunosuppressive effects, and secrete factors that prevent the additional influx of neutrophils. Apoptosis and necrosis can be detected by a combination of PI and fluorophore-conjugated ANX-V. PI is a DNA-intercalating substance that only enters cells that have lost their membrane integrity (necrotic cells and NETotic cells). ANX-V binds to phosphatidylserine exposed by cells undergoing apoptosis (Fig. 173A). If granulocytes have been purified prior to the L/D analysis, no Ab staining is needed. However, if more than one cell type is present, the cell death staining should be supplemented with an Ab combination allowing the identification of granulocytes as mentioned above. FCM allow the simultaneous use of multiple fluorophores. If such an instrument is available, the classical apoptosis staining deploying ANX-V-conjugates and PI can be supplemented with two additional dyes (e.g. Hoechst33342 and 1,1′,3,3,3′,3′-hexamethylindodicarbo-cyanine iodide (DilC1(5)) that allow a more detailed characterization of cell death. This staining takes into account the condition of the nucleus and the mitochondrial membrane potential, respectively, and can also be deployed for live-cell imaging [2256, 2257].

Further, neutrophils show a strong capacity to take up particulate matter. If confronted with nanoparticles or small-sized monosodium urate crystals, neutrophils engulf these particles and respond in an appropriate manner. Since such material cannot be easily conjugated with fluorophores, one has to rely on other methods to monitor their uptake. Soluble dyes, such as Lucifer

Table 63. List of Abs used for characterization of murine granulocyte populations

Target	Fluorophore	Supplier	Cat#	Clone	Host	Isotype	Cross-Reactivity
CCR3	APC/Fire750	BioLegend	144521	J073E5	Rat	IgG2a, κ	None
CD11b	eFluor450	eBioscience	48-0112-82	M1/70	Rat	IgG2b, κ	Yes
CD45	BV785	BioLegend	103149	30-F11	Rat	IgG2b, κ	None
CD49b	APC	BioLegend	108909	DX5	Rat	IgM	None
CD200R3	PE	BioLegend	142205	Ba13	Rat	IgG2a, κ	None
Ly6C	AlexaFluor 488	BioLegend	128021	HK1.4	Rat	IgG2c, κ	None
Ly6G	PE/Cy7	BioLegend	127617	1A8	Rat	IgG2a, κ	None
Siglec-F	PerCP-eFluor710	eBioscience	46-1702-82	1RNM44N	Rat	IgG2a, κ	None

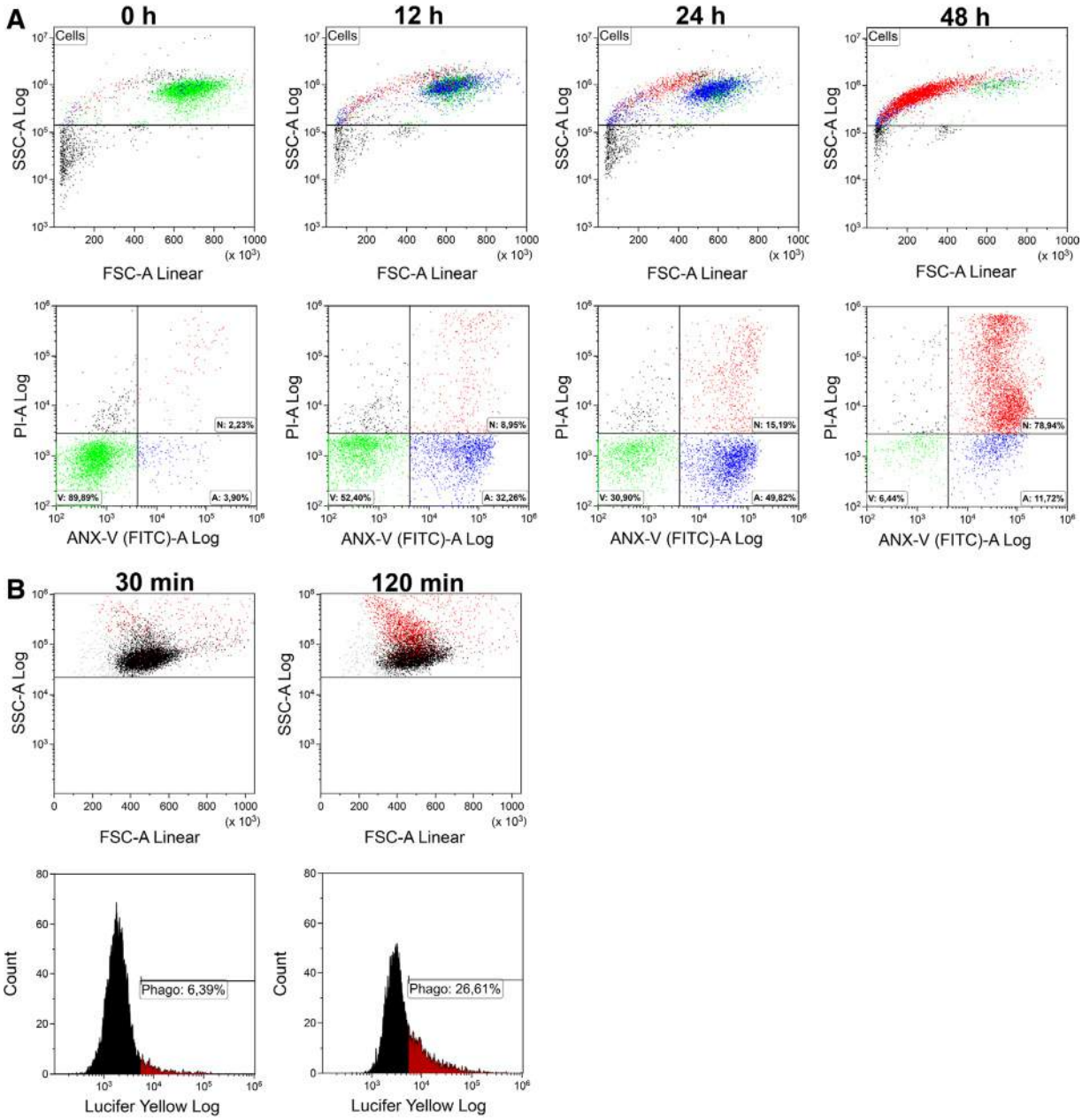

Figure 173. Apoptosis detection and uptake of nanoparticles in purified human granulocytes. (A) Granulocytes were cultivated at 37°C/5% CO_2 for indicated time points and stained according to the cell death protocol. Subsequently, they were subjected to FCM analysis. During apoptosis, granulocytes shrink and increase in granularity, as indicated by a decrease in FSC and an increase in SSC. Viable cells (V) first start to expose ANX-V-FITC and become apoptotic (A), before they lose their plasma membrane integrity and become necrotic as indicated by PI-positivity (N). Note that in the N-gate the population high in PI reflects cells without the loss of nuclear content. In contrast, the population low in PI reflects cells with a subG1 DNA content, which is considered a hallmark of apoptosis. (B) A total of 20 μg/mL micro monosodium urate crystals and 250 μg/mL Lucifer Yellow were added to the granulocytes and the suspension was incubated at 37°C/5% CO_2 for the time points indicated. Subsequently, FCM analysis was performed. The increase in Lucifer Yellow (in red) is restricted to the population of cells that increase in granularity. Therefore, the simultaneous increase in Lucifer Yellow and SSC can be used to monitor the uptake of nanoparticles by granulocytes.

Yellow, can be added together with the prey that will subsequently be co-ingested during phagocytosis. In addition, the uptake of particulate matter tends to increase the complexity of the phagocyte. As shown in Fig. 173B, the increase in SSC and in Lucifer Yellow strongly correlates. Combined observation of both represents a feasible method for addressing such questions.

7.1.6 Pitfalls and top tricks.

- Neutrophil released from the BM are following a circadian rhythm [1476]. To ensure the highest comparability, neutrophils from different donors (murine and human) should be isolated roughly at the same time of the day.

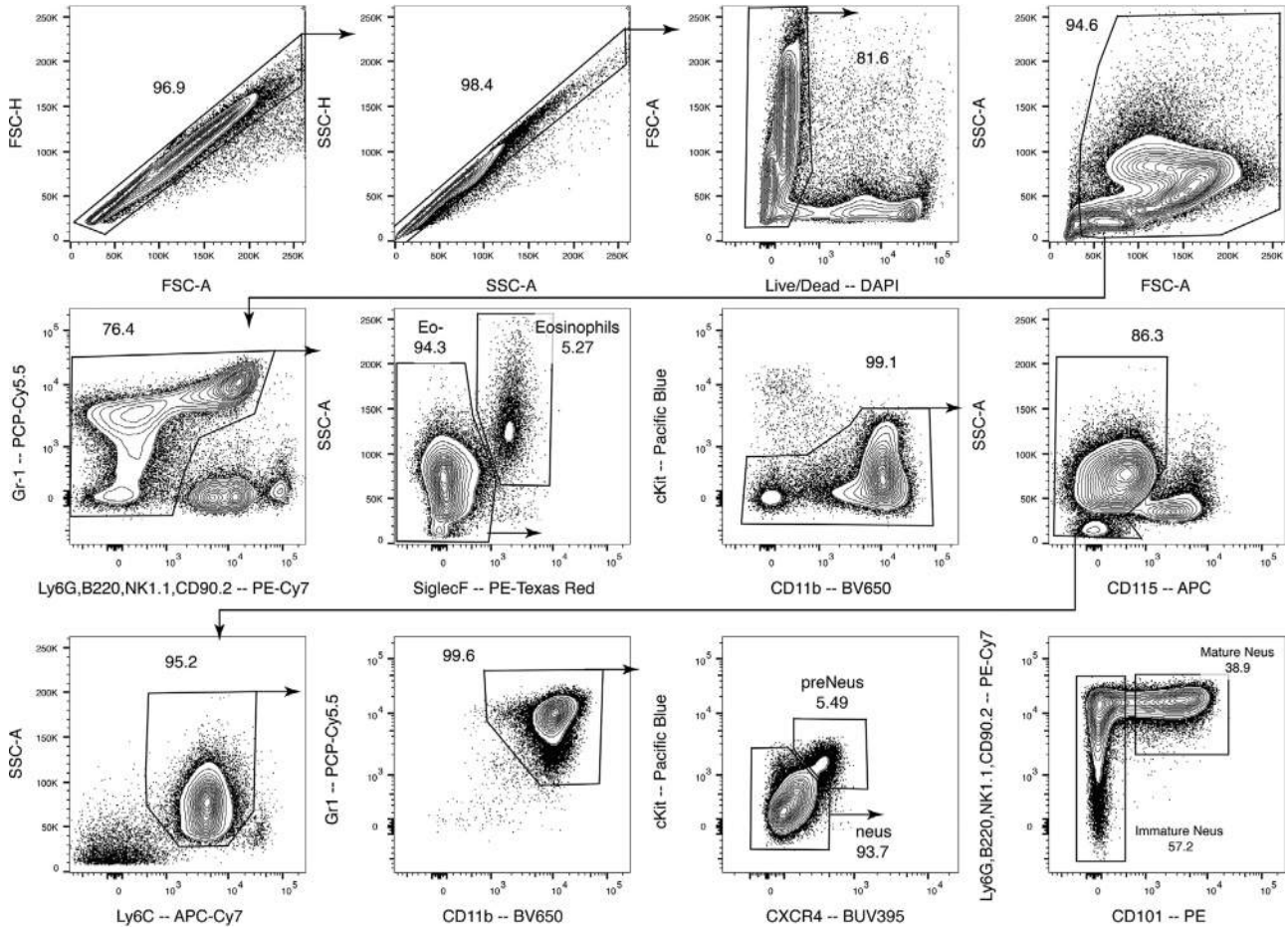

Figure 174. Flow cytometric analysis of murine bone marrow neutrophil subsets. Samples are first gated to exclude doublets and dead cells. Debris are also excluded based on FSC and SSC information. Lineage positive cells (T, B, and NK cells) are then excluded followed by the exclusion of eosinophils and monocytes. Ly6C is then used to further remove any Ly6C^{hi} and Ly6C^{lo} monocyte contamination. Gr-1 and CD11b gates for total bone marrow neutrophils. cKit and CXCR4 is used to gate proliferative pre-neutrophils and CD101 distinguishes mature neutrophils from immature neutrophils.

- When FCM analysis is performed, proper arrangements are necessary to prevent neutrophil adhesion. Neutrophils show a tendency to adhere under serum free conditions, to glass or adhesive plastic surfaces and especially fast in response to stimulation.
- Neutrophils are susceptible to changes in pH and readily form NETs even under mildly alkaline conditions. Buffers should be checked for pH prior to use. RPMI and HBSS can be supplemented with HEPES to stabilize the pH [1477].
- Neutrophils have a very limited life time. They undergo full blown apoptosis in less than 24 h. In addition, several stimuli induce the formation of neutrophil extracellular traps. Although it is possible to detect NETs as material with very high SSC, FCM is not robust enough to quantify NETs. Furthermore, NETs tend to aggregate and form material that cannot be collected by standard needles.
- Phagocytic uptake of particles alters the morphology of a variety of cell types. It is therefore not advisable to identify granulocyte populations only by SSC.
- Activation of leucocytes is usually accompanied by shedding or membrane renewal consequently changing their phenotype (e.g., CD16 downregulation).
- L/D stainings deploying ANX-V must be performed in the presence of at least 2 mM calcium, since binding of ANX-V to phosphatidylserine is calcium-dependent. Avoid washing to prevent loss of subcellular particles and impairment of apoptotic cell integrity.
- Granulocytes express a variety of Fc receptors. To prevent false-positive staining's and to reduce the background fluorescence, we advise to always block unspecific bindings with 2% FCS and to prevent Fc-mediated Ab binding via the use of an Fc blocking agent.

7.2 *Bone marrow and umbilical cord blood neutrophils*

7.2.1 Overview. The developmental pathway of neutrophils has been recently investigated with great interest [1478–1480]. However, there is still no universally accepted characterization of

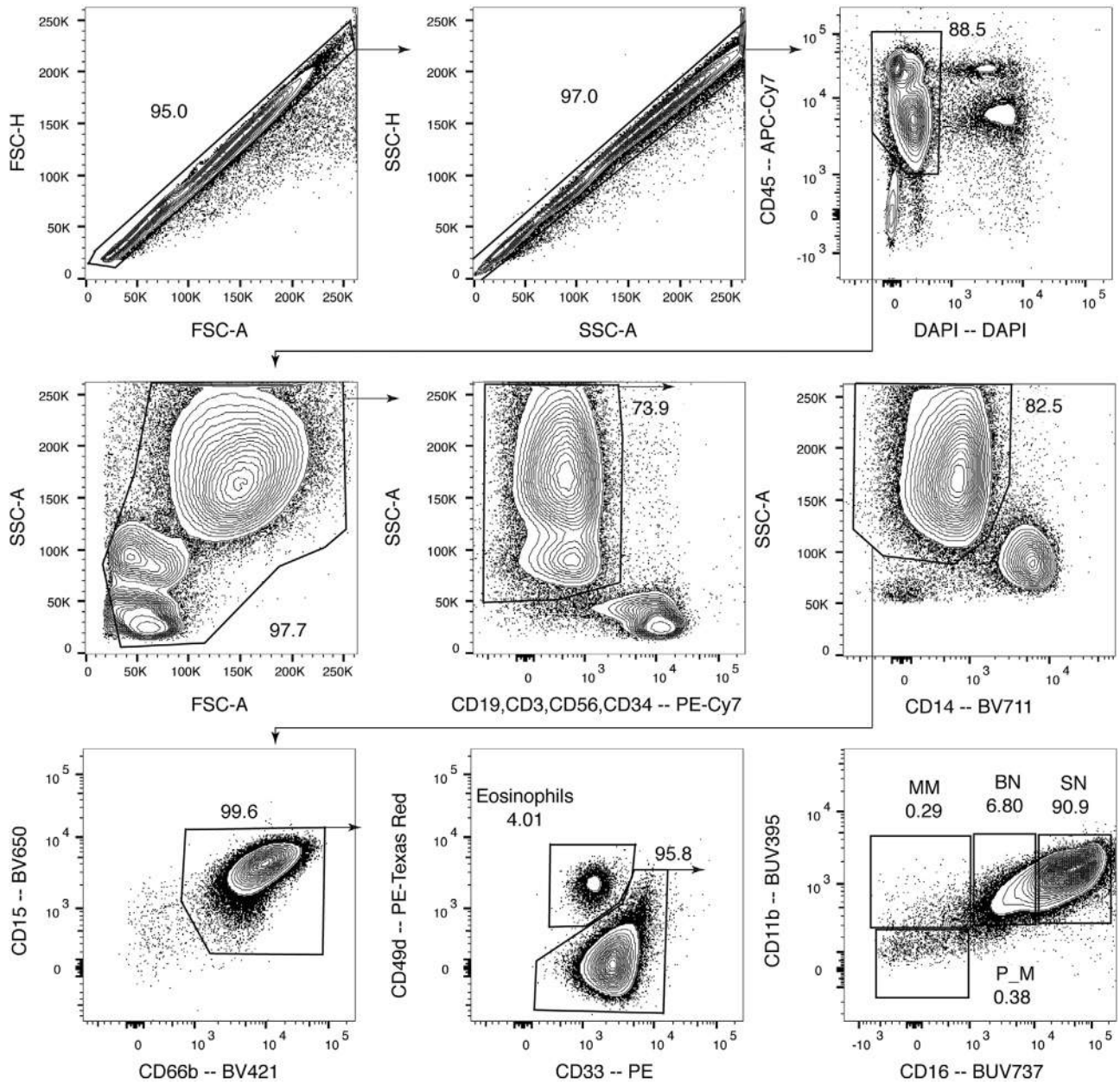

Figure 175. Flow cytometric analysis of human umbilical cord blood neutrophil subsets. Similarly, to the mouse neutrophil subsets, doublets, and dead cells are first excluded, followed by the exclusion of $CD45^-$ cells and debris. Lineage cells and $CD14^+$ conventional monocytes are excluded before total granulocytes are gated with CD15 and CD66b. From there, eosinophils are excluded before gating on the classical nomenclature of neutrophil subsets using CD11b and CD16. P_M = Promyelocytes and Myelocytes, MM = Meta-myelocytes, BN = Band cells, SN = Segmented neutrophils. Gating is adapted from ref. [1487, 1494].

neutrophils by FCM. Moreover, tissues such as bone marrow and spleen contain multiple cell types, which may share overlapping surface markers that can lead to contamination and improper identification. Here, we propose an FCM framework to identify and isolate pure populations of neutrophil subsets, which can be generally applied to most tissues in mice and human. We provide the necessary surface markers, reagents, and tips for successful characterization of neutrophil subsets.

7.2.2 Introduction. Granulocytes are the granule-producing branch of the myeloid cell lineage that includes neutrophils, eosinophils, and basophils [1481]. Neutrophils represent the large majority of granulocytes and are involved in a myriad of immune functions and diseases [1482–1484]. Flow cytometric analysis and characterization of neutrophils has been performed over 20 years ago [1485]. The stages of granulopoiesis—myeloblasts, promyelocytes, myelocytes, metamyelocytes, band cells, and hyper-segmented neutrophil—have been characterized

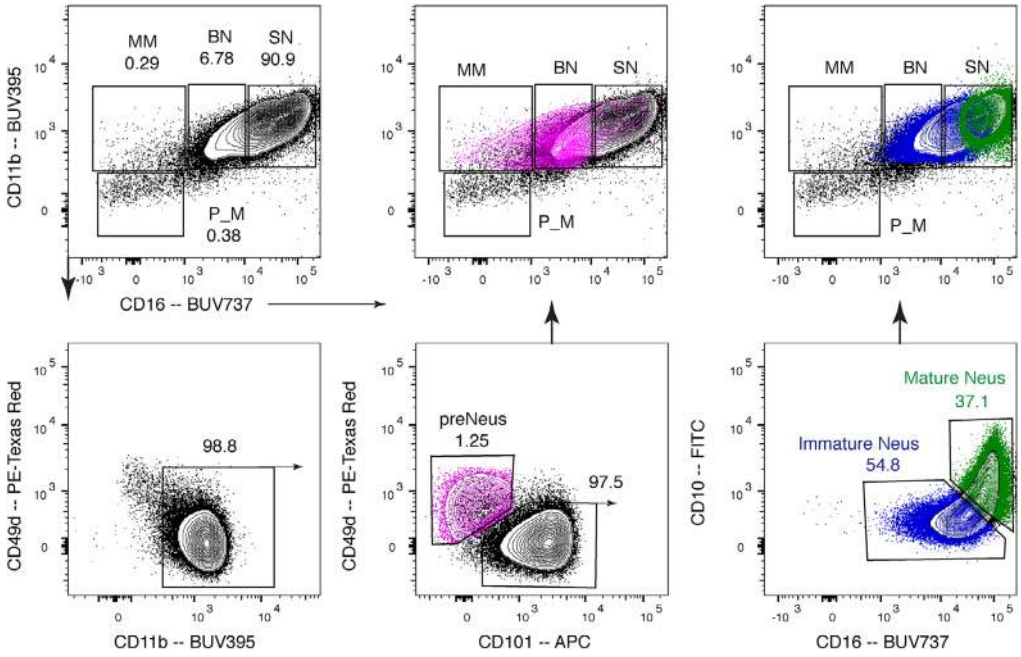

Figure 176. Potential improvements to classical nomenclature and gating. Using proliferation as a marker, total neutrophils can be first gated (according to Figure 175) before gating on proliferative CD11b^{+} preNeus using CD101 and CD49d as shown previously [1478]. The remaining non-proliferative pool of neutrophils can be separated with CD10 as described recently [1489].

by the use of markers such as CD11b, CD15, and CD16. Traditionally, these analyses were performed by correlating surface marker expression levels with the morphological characteristics of the different stages of terminal granulopoiesis [1486, 1487].

Recently, neutrophil heterogeneity in disease has been of a growing interest with the introduction of neutrophil subsets with the underappreciated roles previously [1484, 1488, 1489]. Many of these reports suggest an immature phenotype of granulocytes [1480, 1490–1492], suggesting the importance of investigating neutrophil function in relation to the various developmental stages.

Therefore, understanding the stages of neutrophil maturation provides a firm foundation to study these novel functions of neutrophils. Indeed, recent evidence shows how clearly defined subsets of neutrophils can specifically perform distinct functions that influence the disease progression of arteriosclerosis [1493]. In this section, we provide guidelines in analyzing neutrophil subsets characterized by their distinct functions and the roles they play during inflammatory states [1478].

Table 64. Most important markers for FCM analysis of human and murine granulocytes. All cell types were first gated on CD45 and CD11b positivity

Cell type	Human	Mouse
Neutrophil	CD15^{pos}, CD16^{pos}, CD66b^{pos}	Ly6C^{int}, Ly6G^{pos}
Eosinophil	CD15^{pos}, CD16^{neg}, Siglec-8^{pos}, CCR3^{pos}	Ly6C$^{low/int}$, Siglec-F^{pos}, CCR3^{pos}
Basophil	CD15^{neg}, CD16^{neg}, CD117^{neg}, *FcεRIα^{pos}, CCR3^{pos}, *CD203c^{pos}	Ly6C^{low}, CD200R3^{pos}, CD49b^{pos}, *FcεRIα^{pos}

* These markers were not used in our analysis, but are valid markers for the given cell types.

7.2.3 Step-by-step sample preparation.

7.2.3.1 Step-by-step sample preparation of murine bone marrow neutrophils.

1. Isolate femur bone with a scalpel by dislocating ball–socket joint at the hip. Detach kneecap joint connecting the tibia. Clean off muscle tissue and cut off the ball of the femur to create an opening.
2. Using a 1mL syringe with a 19-gauge needle containing 1 mL wash buffer (PBS + 2% FCS + 2 mM EDTA), flush marrow out through the opening into a 15 mL falcon tube containing 1 mL of buffer. Aspirate and repeat twice. Flush marrow from the opposite end. Aspirate and repeat twice.
3. Filter suspension through a 70 μM strainer to remove clumps and bone chips. Wash strainer with 4 mL of buffer. Centrifuge cells at 4°C, 400 × *g* for 5 min.
4. Discard supernatant and re-suspend pellet with 1 mL of buffer. Aliquot a fraction out for staining purposes. One-fifth is typically adequate.
5. Wash and centrifuge sample aliquot with buffer. Discard supernatant and re-suspend cells in 50 μL blocking buffer. Add 50 μL

of staining buffer with the Abs (See Tables 63 and 64). Incubate at 4°C for 30 min.
6. Add 2 mL of wash buffer and centrifuge. Discard supernatant.
7. Lyse erythrocytes with 200 μL 1× RBC lysis buffer for 3 min. Wash.
8. Re-suspend in wash buffer, add DAPI, and filter sample before acquisition.

#Gating: pre-Neutrophils are defined as Lin^- $Gr\text{-}1^+$ $CD11b^+$ $cKit^{hi}$ $CXCR4^{hi}$ cells. Immature Neutrophils are defined as Lin^- $Gr\text{-}1^+$ $CD11b^+$ $cKit^-$ $CXCR4^{lo}$ $CD101^-$ cells. Mature Neutrophils are defined as $Gr\text{-}1^+$ $CD11b^+$ $Ly6G^+$ $CD101^+$ cells (See Fig. 174).

7.2.3.2 Step-by-step sample preparation of human bone marrow neutrophils.

1. Collect donor bone marrow aspirate in heparin saline containing ACD-A (acid-citrate-dextrose formula A).
2. Wash sample aliquot with 2 mL of 1× PBS. Centrifuge at 4°C, 400 × *g* for 5 min. Discard supernatant. Perform cell count.
3. Using 5 million cells, block Fc-receptors using purified anti-human CD16/32 Ab for 30 min at 4°C. Add staining buffer containing Abs (see Tables 62 and 64). Incubate at 4°C for 30 min.
4. Wash sample with PBS and centrifuge at 4°C, 400 × *g* for 5 min. Discard supernatant.
5. Lyse erythrocytes with 500 μL 1× RBC lysis buffer for 3 min. Wash.
6. Add DAPI and acquire cells.

7.2.3.3 Step-by-step sample preparation of human cord blood neutrophils.

1. Lyse erythrocytes with 1 mL of 1× RBC buffer for every 100 μL of cord blood. Incubate at room temperature for 6 min or until sample becomes translucent.
2. Neutralize with 1× PBS. Centrifuge at 4°C, 400 × *g* for 5 min.
3. Using 5 million cells, block Fc-receptors using purified anti-human CD16/32 Ab for 30 min at 4°C (See Table 64). Add staining buffer containing Abs. Incubate at 4°C for 30 min.
4. Wash sample with PBS and centrifuge at 4°C, 400 × *g* for 5 min. Discard supernatant. Add DAPI and acquire cells (See Figs. 175 and 176 for gating strategies).

7.2.3.4 Materials.

General reagents.

- Dulbecco's PBS with calcium and magnesium
- Wash buffer: PBS with 2% heat-inactivated FCS and 2 mM EDTA.
- 70 μM Cell-strainer mesh
- 1× RBC lysis buffer (eBiosciences)

Staining reagents for murine neutrophils

Table 64. List of antibodies used for characterisation of neutrophil subsets

Marker	Fluorophore	Supplier	Catalog number	Clone	Host	Isotype
CD101	PE	eBioscience	12-1011	Moushi101	Rat	IgG2a, κ
Siglec-F	PE-Texas Red	BD Biosciences	562757	E50-2440	Rat	IgG2a, κ
Ly6G	PE-Cy7	Biolegend	127618	1A8	Rat	IgG2a, κ
B220	PE-Cy7	eBioscience	25-0452	53-6.7	Rat	IgG2a, κ
NK1.1	PE-Cy7	eBioscience	25-5941	PK136	Mouse	IgG2a, κ
CD90.2	PE-Cy7	eBioscience	25-0902-82	53-2.1	Rat	IgG2a, κ
Gr-1	PerCP-Cy5.5	eBioscience	45-5931-80	RB6-8C5	Rat	IgG2b,κ
cKit	SB436	eBioscience	62-1171	2B8	Rat	IgG2b, κ
CD11b	BV655	Biolegend	101259	M1/70	Rat	IgG2b, κ
CD115	APC	eBioscience	61-1152	AFS98	Rat	IgG2a, κ
Ly6C	APC/Cy7	eBioscience	47-5932	HK1.4	Rat	IgG2a, κ
CXCR4	Biotin	eBioscience	13-9991-80	2B11	Rat	IgG2b, κ
Streptavidin	BUV395	BD Biosciences	564176	–	–	–

Staining reagents for human neutrophils

Marker	Fluorophore	Supplier	Catalogue Number	Clone	Host	Isotype
CD10	FITC	Biolegend	312208	HI10a	Mouse	IgG1, κ
CD33	PE	Biolegend	303404	WM53	Mouse	IgG1, κ
CD49d	PE-Texas Red	BD Biosciences	563645	9F10	Mouse	IgG1, κ
CD3	PE-Cy7	Biolegend	300420	UCHT1	Mouse	IgG1, κ
CD19	PE-Cy7	eBioscience	25-0199	HIB19	Mouse	IgG1, κ
CD56	PE-Cy7	Biolegend	318318	HCD56	Mouse	IgG1, κ
CD34	PE-Cy7	Biolegend	343516	581	Mouse	IgG1, κ
CD66b	BV421	BD Biosciences	562940	G10F5	Mouse	IgM, κ
CD15	BV655	BD Biosciences	564232	HI98	Mouse	Ig2M, κ
CD14	BV711	Biolegend	301838	M5E2	Mouse	IgG2a, κ
CD101	APC	Biolegend	331010	BB27	Mouse	IgG1, κ
CD45	APC-Cy7	Biolegend	304014	HI30	Mouse	IgG1, κ
CD16	BUV737	BD Biosciences	564434	3G8	Mouse	IgG1, κ
CD16/32	Purified	BD Biosciences	564219	2.4G2	Mouse	IgG2b, κ
CD11b	BUV395	BD Biosciences	563839	ICRF44	Mouse	IgG1, κ

Flow Cytometer. All experiments were performed on a LSRII flow cytometer with a 365, 405, 488 nm, 561, and 640 nm configuration (BD Bioscience). Filters: 379/34(365) for BUV395; 740/35(365) for BUV737; 450/50(365) for DAPI; 530/30(488) for FITC or AF488; 685/35(488) for PerCP-Cy5.5; 450/50(405) for BV421 or SB436; 525/50(405) for BV510 or V500; 660/20(405) for BV650; 710/40(405) for BV711; 800/50(405) for BV785; 585/15(561) for PE; 610/20(561) for PE-Texas Red; 780/60(561) for PE-Cy7; 675/20(640) for APC or AF647; 730/45(640) for AF700; 780/60(640) for APC-eF780 and APC-Cy7.

7.2.3.5 Pitfalls.

- Human neutrophils are sensitive to Ficoll, and will change the expression of certain markers. For example, Ficoll will down-regulate CD49d expression that prevents the isolation of proliferative preNeus from immature Neus.
- Besides Ficoll, temperature can affect marker expression. Therefore, keep cells on ice throughout sample preparation as markers like CD115 will down-regulate.

Eosinophils can be a big source of contamination as they share many markers like CD15 and CD11b with neutrophil subsets. They are $CD101^{+}CD49d^{+}CD16^{-}$ and express Siglec-8. Gating them out is essential, especially in eosinophilic patient samples.

7.2.3.6 Top tricks.

- In certain inflammatory conditions, such as a bacterial challenge, neutrophils may lose Ly6G expression. Make use of SSC information and Ly6C expression level to gate for neutrophils.
- Perform titration of Abs for optimal staining index. Typically, 0.25 μL is used for mouse Abs for one-fifth of femur marrow and 2 μL per 5 million cells is used for human Abs.
- Bone marrow composition in tibias, humeri, pelvis, and sternum are similar to the femur. Therefore, use these bones if large numbers of neutrophils are required for sorting purposes.
- Gr-1 labels both Ly6G and Ly6C. When staining, use twice the amount of Ly-6G to prevent competitive binding by Gr-1.

7.2.3.7 Table summary of neutrophil subset phenotypes in mouse and human.

Neutrophil Subset	Mouse	Human
Pre-Neutrophils	$CD115^{-}SiglecF^{-}Gr\text{-}1^{hi}CD11b^{+}CXCR4^{hi}cKit^{hi}Ly6G^{lo}CD101^{-}$	$CD66b^{+}CD15^{+}CD49d^{lo}CD101^{-}CD16^{+}CD10^{-}$
Immature Neutrophils	$CD115^{-}SiglecF^{-}Gr\text{-}1^{hi}CD11b^{+}CXCR4^{lo}cKit^{lo}Ly6G^{-/+}CD101^{-}$	$CD66b^{+}CD15^{+}CD49d^{-}CD101^{+}CD16^{++}CD10^{-}$
Mature Neutrophils	$CD115^{-}SiglecF^{-}Gr\text{-}1^{hi}CD11b^{+}CXCR4^{lo}cKit^{lo}Ly6G^{+}CD101^{+}$	$CD66b^{+}CD15^{+}CD49d^{-}CD101^{+}CD16^{++}CD10^{+}$

Classical Human Nomenclature	Markers
Promyelocyte/Myelocyte	$CD66b{+}CD15{+}CD11b^{-}$ $CD16^{-}$
Metamyelocyte	$CD66b{+}CD15{+}CD11b^{+}$ $CD16^{-}$
Band Cells	$CD66b{+}CD15{+}CD11b^{+}$ $CD16^{+}$
Segmented Neutrophil	$CD66b{+}CD15{+}CD11b^{+}$ $CD16^{++}$

8 Murine bone marrow stromal cells

8.1 *Overview*

The bone marrow (BM) stroma plays a critical role in the maintenance of hematopoietic homeostasis. The ability to isolate BM stromal cells at high efficiency is critical to maximize cell recovery and reproducibility of the isolation procedure. In this section, we describe the processing of BM samples through sequential enzymatic digestion and the gating strategy used to identify stromal and mesenchymal stem cells (MSCs).

8.2 *Introduction*

The bone marrow stroma is composed of non-hematopoietic cells responsible for the structural organization of the marrow cavity where they support blood cell development. Early work by Friedenstein et al. has shown that stromal cells could be distinguished from hematopoietic cells by their adherence to plastic culture dish and their ability to form fibroblastic colonies (called CFU fibroblasts or CFU-F) when plated at clonal density [1495]. Subsequently, a single CFU-F was shown to generate heterotopic ossicles when transplanted in vivo [1496]. These studies paved the way to our understanding of how BM stromal cells regulate developmental and steady-state hematopoiesis. MSCs located at the top of the stromal hierarchy can self-renew and differentiate into bone, fat, and cartilage [1497]. MSC populations are found in distinct perivascular niches where they regulate hematopoietic stem and progenitor functions through the action of cell-bound or secreted cytokines [1498]. In the developing mouse marrow, CD45$^-$ Tie2$^-$ Thy1.1$^-$ CD105$^+$ CD51$^+$ progenitors undergo endochondral ossification and contribute to the formation of the BM cavity by promoting vascularization and the formation of an hematopoietic stem cell (HSC) niche [1499]. In the adult mice BM, MSCs can be labeled by GFP in Nestin-GFP transgenic mice, wherein Nestin-GFP$^+$ cells contain all CFU-F activity or mesensphere formation capacity of the BM [1500]. Nestin-GFP^{bright} cells mark periarteriolar stromal cells that are significantly associated with quiescent HSCs and secrete niche factors such as Cxcl12 and Stem Cell Factor (SCF) that contributes to HSC localization and maintenance [1501]. Nestin-GFP$^+$ cells also highly overlap with stromal cells expressing the Leptin receptor [1502], Cxcl12-abundant reticular (CAR) cells [1503] or Prx-1-cre cells [1504] that have also been described as regulators of hematopoietic stem and progenitors functions. Lineage tracing has also revealed the osteogenic and stromal contribution of MSCs during development [1505]. Furthermore, skeletal stem cells found in the periosteum of long bones have been shown to contribute to bone formation at steady state or after injury [1506–1508].

To study murine BM stromal cells populations, cell surface markers have been proposed to facilitate their identification, but many of these markers are expressed on cultured cells and may differ from freshly isolated stromal cells [1509]. In addition, distinct stromal cell populations can be extracted depending on the isolation methods. Sequential digestion of BM plugs results in efficient extraction of stromal cells with MSC activity [1510]. CD51$^+$ PDGFRa$^+$ CD45$^-$ Ter119$^-$ CD31$^-$ cells comprise most of detectable BM MSC activity isolated from flushed BM plugs and can reconstitute an ectopic HSC niche when transplanted under the kidney capsule [1511]. Crushed bone can result in an enrichment of PDGFRa$^+$ Sca-1$^+$ CD45$^-$ Ter119$^-$ CD31$^-$ MSCs [1512, 1513] or skeletal stem cells expressing Gremlin1 [1514] and CD200 [1506]. While a hierarchal organization for skeletal stem cells and downstream progenitors responsible for cartilage, bone, and stromal cell generation has been proposed [1506], it remains unclear how the bone-associated skeletal stem cells and BM-associated MSCs relate to each other. Therefore, the isolation method (enzymatic treatments, bone crushing, or flushing) will influence the content and heterogeneity found within the stromal cell fraction.

8.3 *Step-by-step sample preparation*

The stromal fraction of the BM is classically defined by the absence of CD45 (hematopoietic), Ter119 (erythroid) and CD31 (endothelial) marker expression. CD45$^-$ Ter119$^-$ CD31$^-$ or triple-negative cells (TNCs) are known to contain stromal cells as well as hematopoietic cells [1515]. In order to isolate BM stromal cells, femurs or tibias from mice can be cut below the metaphysis toward the epiphysis and the BM is flushed out as an intact plug using syringe with 21G (femur) or 25 ½ G (tibia) needle containing digestion buffer (collagenase type IV 2 mg/mL and dispase 1 mg/mL in HBSS). While CD45, CD31, Ter119, and CD51 epitopes have been shown to be resistant to cell digestion [1515], it is important to compare the sensitivity of each marker to be tested on digested cells and undigested or flushed cells. BM plugs are sequentially digested three times for 10 min at 37°C. The supernatant, which contains cells released by the digestion process, is collected after each digestion and pooled into a 50 mL tube containing ice-cold FCM buffer (PBS, EDTA 2 mM, BSA 0.1%) to prevent any loss of cell surface markers or cell viability. Following the digestion process, enzymatically dissociated cells can be centrifuged and the pellet can be subjected to RBC lysis. Cells are then filtered through a 100 μm cell strainer to remove any clumps prior to staining for FCM analysis. For cell sorting, it is recommended to perform CD45$^+$ cells depletion using microbeads directly conjugated with CD45 mAb (Miltenyi Biotec) that will enrich for TNCs. After incubation with CD45 microbeads the cell suspension is washed, pelleted and resuspended in 500 μL FCM buffer. Cells are applied to a column (Miltenyi Biotec) coupled with a magnet which will retain CD45$^+$ hematopoietic cells. Cells are eluted by washing the column with 2 × 1mL of FCM buffer and can be used for antibody staining (Table 65) for 15 min at 4°C. Stained cells are washed and resuspended in FCM buffer containing a viability dye such as DAPI or 7-AAD.

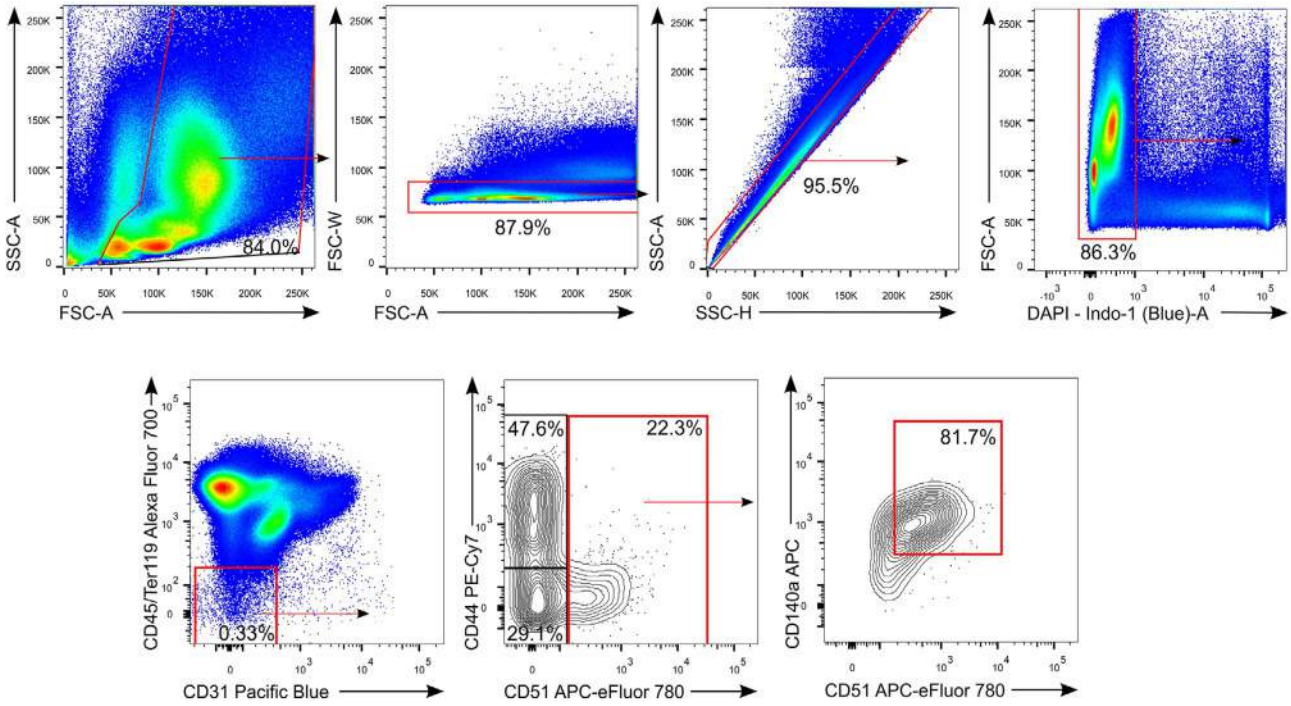

Figure 177. Gating strategy for murine BM stroma. Live single cells are separated using CD45, Ter119, and CD31 markers (left panel). Gated TNCs are then analyzed for their expression of stromal marker CD51 and for excluding hematopoietic cells by using CD44 (middle panel). MSC populations can be found within CD51$^+$ TNCs where PDGFRα expression can be detected (right panel).

Table 65. Antibodies to analyze mouse bone marrow stromal cells

Antibody	Fluorochrome	Clone	Company
CD45	Alexa Fluor 700	30-F11	BioLegend
Ter119	Alexa Fluor 700	Ter-119	BioLegend
CD31	Pacific Blue	390	BioLegend
CD51	Biotin	RMV-7	eBioscience
CD44	PE-Cy7	IM7	eBioscience
PDGFRα	APC	APA5	eBioscience
Streptavidin	APC-eFluor 780	–	eBioscience

8.4 *Materials*

8.4.1 Animals. Adult mice such as C57BL/6 (8–12 weeks old).

8.4.2 Reagents.

1. Collagenase type IV (Gibco, Cat #17104019)
2. Dispase (Gibco, Cat #17105-041)
3. Ammonium chloride (Sigma, Cat #A4514)
4. DAPI (Sigma, Cat #D9542)

8.4.3 Solutions.

1. HBSS (Corning, Cat #21-023-CV)
2. FCM buffer (PBS 1×, EDTA 2 mM, BSA 0.1%)
3. RBC lysis buffer (NH_4Cl 0.17 M, $KHCO_3$ 0.01 M, EDTA 0.1 mM)
4. Digestion buffer (Collagenase IV 2 mg/mL, Dipase II 1 mg/mL in HBSS)
5. DAPI (0.05 μg/mL in FCM buffer)

8.4.4 Equipment.

1. 1 mL syringe with 21G × 1 needle (for femurs) or 25 G × 5/8 needle (for tibias)
2. 100 μM cell strainer (Falcon, Cat #08-771-19)
3. CD45 microbeads, mouse (Miltenyi Biotec, Cat #130-052-301)
4. MACSR® LS column (Miltenyi Biotec, Cat #130-042-401)
5. QuadroMACSR® separator (Miltenyi Biotec, Cat #130-090-976)
6. FCM cell sorter (at least five colors and equipped with UV laser)

8.5 *Data analysis*

When using adult mice, TNCs represent approximately 0.5% of total single live BM cells (Figure 177). The TNC fraction contains mostly hematopoietic cells (~85%), which are found in the CD44$^+$ CD51$^-$ and CD44$^-$ CD51$^-$ TNCs. Gating on CD51$^+$ cells allows the separation of bona fide stromal cells from hematopoietic TNCs, while MSCs can be further selected by gating on CD51$^+$ PDGFRa$^+$ TNCs (Fig. 177). Cell surface markers such as CD200, Thy-1, and 6C3 can be used to distinguish among cartilage, bone, and stromal cells when samples are made from crushed bones [1499, 1506, 1513]. Consistency in the processing of BM plugs should limit the variation in the frequency of isolated TNCs or MSCs.

8.6 *Pitfalls*

In the event that additional markers are to be included in the gating strategy, their sensitivity to the enzymatic digestion should be addressed. Samples should be analyzed as soon as possible after processing and staining since digested BM cells have a higher tendency of clumping together than undigested samples.

8.7 *Top tricks*

To ensure equal digestion throughout all samples, first harvest all bones and place on ice, in PBS. Then, flush the first sample with digestion buffer and directly put at 37°C. Start timer for the first 10 min of incubation and proceed with the second sample and so on. A constant digestion incubation time is critical in order to avoid overdigestion which could result in a loss of cell surface markers, and to reduce variation among samples.

9 Hematopoietic Stem Cells

9.1 *Overview*

This chapter deals with the characterization, isolation, and preparation of murine and human hematopoietic stem cells (HSCs).

9.2 *Introduction*

Throughout life of mice and humans the major site of HSCs is bone marrow [1516–1518]. HSCs are thought to reside in cellular niches [1519–1521], generated by environmental non-hematopoietic stromal cells of mesenchymal and endothelial origin (See Chapter VI Section 8 Murine bone marrow stromal cells) and of other, hematopoietic cells, which ensure their quiescence and longevity and their capacity to proliferate and/or differentiate to more lineage restricted progenies. This proliferation and differentiation continuously regenerates, and thereby maintains the differentiated compartments of erythroid, myeloid, and lymphoid cell lineages. Differentiation can occur in a hierarchical order from LT-HSC to ST-HSC, to erythroid and megakaryocytic progenitors and to lymphoid–myeloid progenitors (LMPP, MPP) and from them to common lymphoid progenitors (CLP) and common myeloid progenitors (CMP). These progenies give rise to erythrocytes, megakaryocytes, and platelets, monocytes, macrophages, and granulocytes, and to lymphoid cells (T- and B-, dendritic, innate, and natural killers and innate lymphoid cells). A part of the generation of myeloid and erythroid cells can be initiated directly from a special subpopulation of HSCs. Under stress, such as a bacterial or viral infection, this direct differentiation to granulopoiesis, erythropoiesis, and the development of megakaryocytes and platelets is increased and accelerated directly from HSC [1522–1524].

Transplantation of HSC into suitably recipient hosts populates all HSC and progenitor compartments in bone marrow of the host and regenerates erythroid, myeloid, and lymphoid compartments with donor-derived cells to normal sizes.

9.3 *Murine hematopoietic stem cells*

The first part of this chapter describes the methods for adult murine hematopoietic stem cells.

In mice, HSCs are generated during embryonic development, first extra-embryonically from cells in yolk sac, then from cells in the embryonic aorta-gonad-mesonephros area via hemangioblasts, which are common progenitors of vascular endothelium and hematopoietic cells [1525, 1526]. These early progenitors seed into fetal liver and fetal thymus to generate first, transient waves of hematopoiesis. Shortly before birth, the developing marrow of bone becomes the site, where HSC find an environment for their life-long residence, hematopoietic renewal and differentiation capacities [1527].

HSCs are identified by FCM, based on surface-marker expression. One set of fluorescent mAb combinations, and the FCM profiles of the stained bone marrow cells is given in Fig. 178. HSCs are found in the 0.1% of all $CD45^+$ bone marrow cells, which do not yet express the markers of differentiated hematopoietic cells, i.e., of $F4/80^+$/$Mac1^+$ monocytes and macrophages, $Gr1^+$ granulocytes, $CD11c^+$ dendritic cells, $CD4^+$/$CD8^+$/$CD3^+$ T cells, $CD5^+CD19^+B220^+$ B cells, $NK1.1^+$ NK cells, and $Ter119^+$ erythrocytes. Thus, they are "lineage-negative" (Lin-. L). The absence of these antigens and expression of CD45 is necessary to identify the hematopoietic population within the lineage-negative (Lin^-) cells of the bone marrow. On the other hand, HSC express Sca-1 (S) and c-Kit (K), thus are called LSK-cells.

Furthermore, differences in surface expression of the CD150 and CD48 "SLAM" markers allow to distinguish long-term self-renewing HSCs and transiently reconstituting multipotent progenitors [1531–1533]. Thus, a Lin^-c-Kit^+Sca-$1^{+-}CD150^+CD48^-$ population contains mainly long-term self-renewing HSCs, a Lin^-c-Kit^+Sca-1^+ $CD150^+CD48^+$ population mainly transiently self-renewing multipotent progenitors, and a Lin^-c-Kit^+Sca-$1^+CD150^-CD48^+$ population mainly non-self-renewing multipotent progenitors [1531–1533]. Their functions have been determined by transplantation analyses. These three distinct populations vary with each stage in the progression toward lineage commitment in their frequency, engraftment-kinetics, self-renewal potential, cell-cycle status, gene expression, and lineage distribution of the mature cells they can generate in vivo.

In the bone marrow of 2–3 month-old mice between 1 and 3×10^3 LSK, $CD150^+CD48^-$ cells remain in a non-proliferating, cell cycle Go-resting state for life [1534, 1535].

Barcoding of these early progenitors shows that most of them have clone sizes of less than ten cells, and most of them retain these small clone sizes, because they divide at best once a year in the life of a mouse [1534, 1535]. A part of this HSC population can be transplanted, remarkably even as single (e.g. $CD45.1^+$) HSC with carrier ($CD45.2^+$) bone marrow cells into lethally irradiated (ideally histocompatible CD45.1xCD45.2) recipients. They home

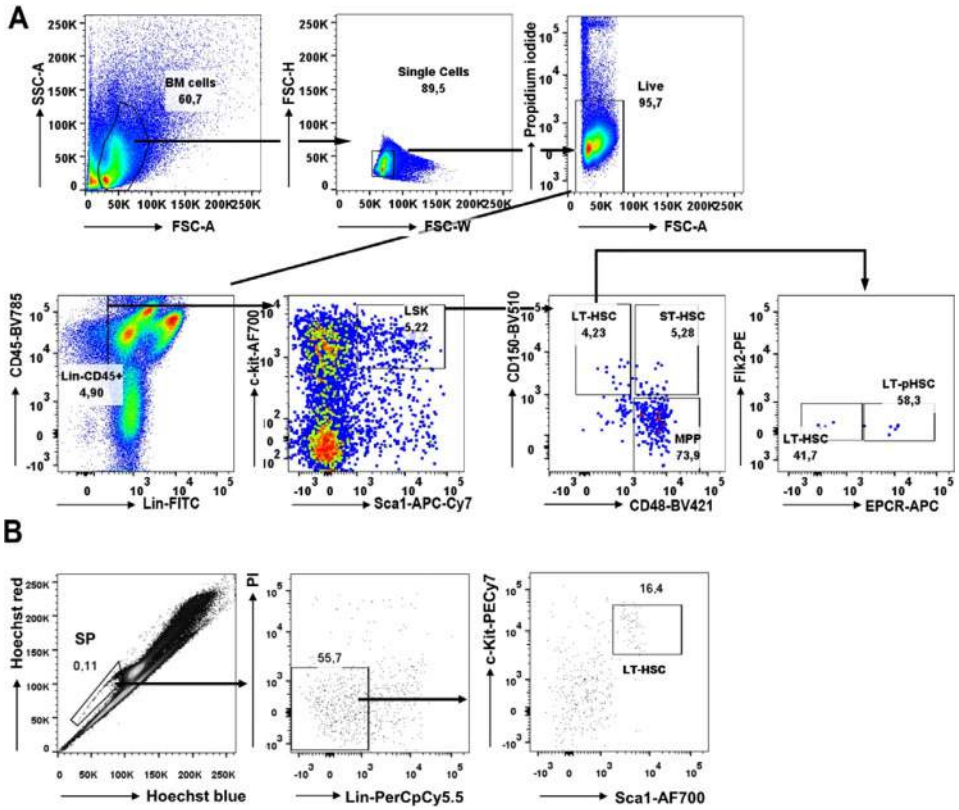

Figure 178. Gating strategy of mouse hematopoietic stem cells. Phenotypic characterization of mouse bone marrow derived HSCs. LSK cells were identified as c-kit$^+$ Sca1$^+$ cells within the CD45$^+$ Lin- compartment. LT-HSCs were further identified as CD150$^+$ CD48$^-$, ST-HSCs as CD150$^+$ CD48$^+$, and MPPs as CD150$^-$ CD48$^+$cells. LT-pHSCs can be further characterized as Flk2$^-$EPCR$^+$ (CD201) population within the CD150$^+$ CD48$^-$ gate. Gating for all colors were set according to the isotype control staining (not shown). Forward and side scatter voltages can be increased to dissect bone marrow cell populations into more differentiated subpopulations, differing in size and density (see general introduction).

to bone marrow and then repopulate all HSC compartments, all hematopoietic progenitors and all mature cell lineages, except of the long-lived resident myeloid cells generated from fetal liver progenitors during embryonic development [1536]. These HSC are called long-term repopulating (LT-HSC). Upon transplantation LT-HSC can home back to bone marrow into special niches near hypoxic areas of arteriolar vascular endothelium and barcoding reveals a smaller number of these LT-HSC with much larger clone sizes [1522].

Between 4 and 8 $\times$ 10^3 HSC are lin-sca1$^+$c-kit$^+$CD150$^+$CD48$^+$ HSC, which are in active G1-S-G2-M cell cycle, renewing their HSC state by symmetric or asymmetric cell divisions. In asymmetric cell divisions a fraction of them can enter differentiation to more mature states of hematopoietic developments. When transplanted, these HSC repopulate all different lymphoid and myeloid cell lineages in subsiding waves, again without populating the embryonically derived resident myeloid cell lineages. They do not repopulate the LT-HSC. Since they repopulate the transplanted host only for a short time, they are short-term active HSC (ST-HSC). ST-HSCs have also been described to be lin-sca1+c-kit+CD150$^-$CD48$^-$ cells [1534]. The relationship of these "SLAM"-negative HSC to the double "SLAM"-positive ST-HSC remains to be investigated.

HSC can be mobilized to enter blood circulation. They might differentiate in the periphery or pick up intracellular infections, such as *Mycobacterium tuberculosis*, and then use their exceptionally efficient capacity to return to bone marrow and become again resident in their niches [1537].

9.3.1 Isolation of murine HSCs. The first step in the preparative isolation of adult mouse HSCs from BM is the erythrolysis with hypothonic ACK (ammonium-chloride-potassium) solution. The next step usually consists of removing mature cells that express "lineage" (Lin) antigens specific to terminally differentiated blood cells, including F4/80$^+$/Mac1$^+$ monocytes and macrophages, Gr1$^+$ granulocytes, CD11c$^+$ dendritic cells, CD4$^+$/CD8$^+$/CD3$^+$ T cells, CD5$^+$CD19$^+$B220$^+$ B cells, NK1.1$^+$ NK cells, and Ter119$^+$ erythrocytes. HSC are then enriched from the remaining cells as Lin$^-$ CD45$^+$ cells that express combinations of cell surface markers, c-Kit and Sca1. Multipotent hematopoietic progenitors, purified as LSK (Lin$^-$ c-Kit$^+$Sca-1$^+$) make up <0.1% of nucleated BM cells. They contain all multipotent progenitors in mice [1538–1541]. However, they are still heterogeneous, containing transiently reconstituting multipotent progenitors in addition to long-term reconstituting HSCs.

The differences in "SLAM"-marker expression between long-term self-renewing HSCs and transiently reconstituting multipotent progenitors permit the separation and independent isolation of these different progenitor populations [1531–1533] as Lin$^-$c-Kit$^+$Sca-1$^+$ CD150$^+$CD48$^-$, mainly long-term self-renewing (LT-)HSCs, Lin$^-$c-Kit$^+$Sca-1$^+$ CD150$^+$CD48$^+$, mainly transiently renewing HSC (ST-HSC), and Lin$^-$c-Kit$^+$Sca-1$^+$ CD150$^-$CD48$^+$, mainly non-renewing multipotent progenitors (MPP), as characterized by transplantation analyses. These three distinct populations vary with each stage in the progression toward lineage commitment in their frequency, engraftment-kinetics, self-renewal

potential, cell-cycle status, gene expression, and lineage distribution of the mature cells they can generate in vivo.

However, "SLAM"-defined cells themselves are still heterogeneous populations in which HSCs represent, at most, 20% of all cells. Further enrichment of LT-HSCs can be achieved by the purification of SLAM-defined cells that express high levels of EPCR (CD201) [1542]. The expression of CD34 and Flk2 further defines the ST-HSC and MPP sub-populations, respectively [1543, 1544] (Fig. 178A). Although transiently reconstituting multipotent progenitors are enriched in the $CD34^+$ fraction, they usually are not purified based on CD34 expression. Rather, the current purification protocols are based on the LSK, SLAM, and endothelial protein C receptor (EPCR) expression patterns of these HSCs and progenitors.

Alternatively, HSCs can be isolated due to their hypoxia-induced high expression of the multidrug transporter proteins MDR1 and ABCG2, thus, cells that retain only low levels of DNA dyes, such as Rhodamine-123 (Rho123) and Hoechst 33342. $Rho123^{lo}$ or $Hoechst^{lo}$ cells ("side population," SP cells), and that are $Lin^-c\text{-}Kit^+Sca\text{-}1^+$ are nearly pure populations of long-term reconstituting HSCs [1545, 1546] (Fig. 178B).

It should be kept in mind, that all these purified HSC populations are still a heterogeneous collection of cells, when their functions are considered. Thus, it is believed that myeloid-biased HSCs express higher levels of CD150 and efflux Hoechst 33342 more efficiently than lymphoid-biased HSCs. They also exhibit higher self-renewal ability as demonstrated by serial transplantation of BM cells from primary recipients into secondary hosts. Quantitative analyses of the frequencies of single HSC/progenitors for a given function "in vitro" or "in vivo" (e.g., as done with single cells) should be attempted to define their potencies [1547] or [1522] or [1548] or [1549–1551].

9.3.2 Materials.

1. Adult mice such as C57BL/6, typically, 6- to 10-week-old mice are used for the isolation of HSCs.
2. Staining medium: PBS Solution (1xPBS) with 0.5% BSA fraction V, 2 mM EDTA, without azide.
3. Nylon screen (40 μm nylon mesh) to filter the cells after isolation.
4. 10-mL syringes with 25-gauge needles to flush marrow out of femurs and tibias.
5. Use 15-mL tubes to stain BM cells. Abs described in this protocol are available from eBioscience and BioLegend.
6. Lineage-marker Abs: anti-Mac1/CD11b (M1/70), anti-Gr1 (RB6-8C5), anti-Ter119 (TER-119), CD19 mAb (6D5), anti-B220 (RA3-6B2), CD5 mAb (53-7.3), CD3ε mAb (145-2C11), CD11c mAb (N418), CD4 mAb (GK1.5), CD8 mAb (53-6.7), and anti-NK1.1 (PK136). Note that all Abs should be titrated before use, and used at dilutions that brightly stain antigen positive cells without nonspecific staining.
7. Anti-CD45 (30-F11), anti-Flk2 (A2F10), anti-EPCR/CD201 mAb (RCR-16), anti-Sca-1 (D7), anti-c-kit (ACK2), CD150 mAb (TC15-12F12.2), CD34 mAb (RAM34), and CD48 mAb (HM48-1).
8. SP buffer (PBS, 2% FCS, 2 mM HEPES buffer; GIBCO, Life Technologies), Hoechst 33342 (5 μg/mL, Molecular Probes, Life Technologies).
9. A viability dye such as PI or 7-AAD.

9.4 *Human hematopoietic stem cells*

In this chapter we provide an overview on the identification and isolation of human hematopoietic stem cells (HSCs) from different sources (see Fig. 179 for identification of HSCs from BM).

9.4.1 Isolation of human HSCs. Primary sources of human HSCs are human bone marrow, G-CSF-mobilized blood, umbilical cord blood, and fetal liver. Human HSCs can also be isolated from immune-deficient mouse models engrafted with primary human HSCs.

Isolation from human sources: Mononuclear cells are prepared from human bone marrow, peripheral blood, or umbilical cord blood using Ficoll-Paque density gradient centrifugation (e.g., 3–5 mL bone marrow for 1–10 $\times$ 10^7 MNCs or 15–20 mL cord blood for 1–15 $\times$ 10^7 MNCs). After collection of the MNCs, cells are washed three times in PBS/2% FCS. If the cell pellet is very red after two washes of the MNCs, a RBC lysis may be performed (5 minutes in ACK lysing buffer).

Isolation from mouse recipients: Bone marrow cell suspensions are prepared as outlined above (See Chapter V Section 9.3.1 Isolation of murine HSCs).

Perform Ab staining in PBS/2% FCS (100 μL Ab mix for 1–2 $\times$ 10^7 MNCs) for 40 min at 4°C. Refer to Table 66 for a list of the antibodies. Wash cells once in PBS/2% FCS and resuspend in appropriate volume of PBS/ 2% FCS containing a viability dye such as DAPI, PI, or Sytox Green.

Filter cells prior to analysis through a 40 μm filter.

Analyze cells on a flow cytometer or cell sorter with at least eight-color capability.

Gatings to determine positivity are performed using FMO. Isotype controls are used to show that no unspecific binding is observed in the chosen gates.

HSCs from all sources display a similar pattern of surface marker expression and can therefore be isolated using the same panel of antibodies (See Table 66). Like murine HSCs, human HSCs do not express antigens of mature blood cell lineages (Lin^-). Further, the glycoprotein Thy-1 (CD90) has been shown to be expressed on human HSCs [1552, 1553]. But other than this, there is not much correspondence of cell surface markers identifying HSCs in mice and humans.

The most important surface marker used to enrich human hematopoietic progenitor cells (HPCs) is the glycoprotein CD34, which is expressed on HSCs and committed progenitors but not mature blood cells [1554]. In mice, LT-HSCs do not express CD34 whereas ST-HSCs and progenitors are $CD34^+$ [1543, 1555].

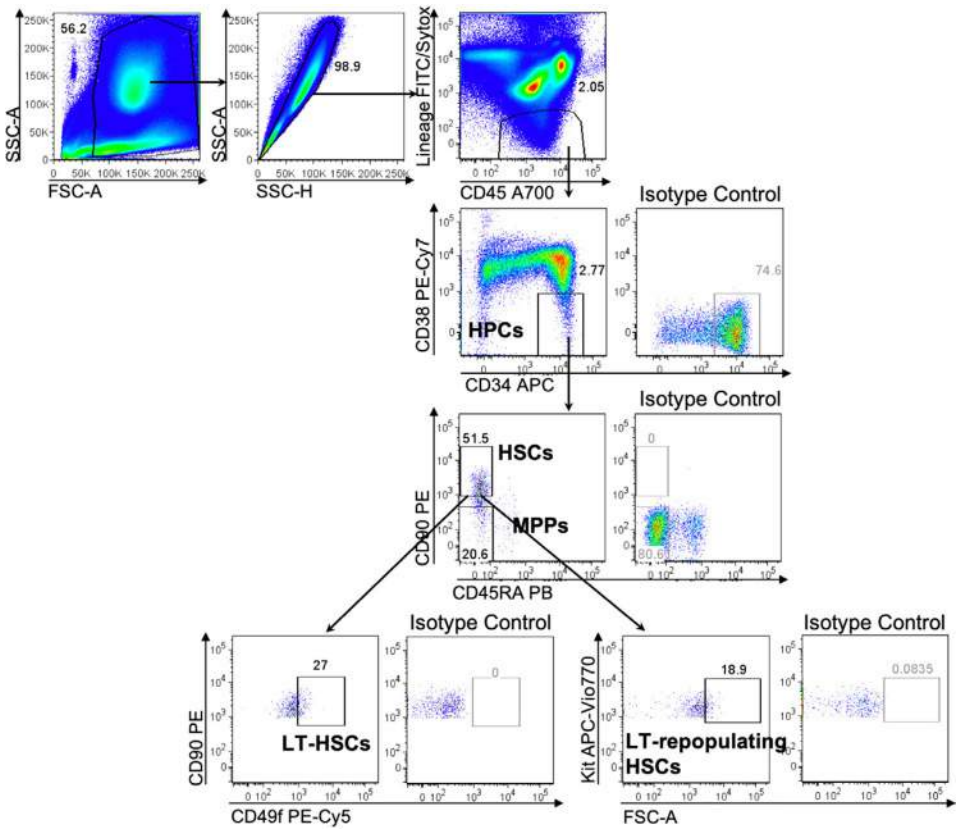

Figure 179. Phenotypic characterization of HSCs from human BM. HSPCs were identified as CD34$^+$ CD38$^-$ cells within the CD45$^+$ Lin$^-$ compartment. HSCs were identified as CD34$^+$ CD38$^-$ CD90$^+$ CD45RA$^-$ cells and MPPs as CD34$^+$ CD38$^-$ CD90$^-$ CD45RA$^-$ cells [1528, 1529]. LT-HSCs can be identified using CD49f [1529] or Kit (CD117) (Cosgun et al., [1530]). Gatings for CD38, CD90, CD49f, and Kit were performed according to isotype controls, which are depicted in the right side of each plot.

CD34-enriched cells from human bone marrow or mobilized peripheral blood are frequently used in clinical stem cell transplantation [1556]. However, HSC activity has also been reported in the CD34$^-$ population of human cord blood and bone marrow, even though those cells are extremely rare [1557–1559].

However, CD34 expression alone does not provide an accurate measure of HSCs because also hematopoietic progenitor cells are positive for CD34, and additional markers are required to identify and isolate the most primitive HSCs [1560]. Multilineage reconstitution in vivo models in combination with FCM allowed to further separate the Lin- CD34$^+$ population using markers that are differentially expressed on immature and more differentiated cells. Bhatia et al. showed that the CD38$^-$ fraction of CD34$^+$ human bone marrow and cord blood cells was highly enriched for cells with the ability to repopulate immune-deficient mice [1561]. Limiting dilution analysis showed that one in 617 purified CD34$^+$ CD38$^-$ cells was able to engraft in a NOD/SCID mouse for at least 8 weeks. Ten years later, Majeti et al. showed that Lin$^-$ CD34$^+$ CD38$^-$ human bone marrow and cord blood cells could be further subdivided using the cell surface markers CD90 and CD45RA [1528]. They identified Lin$^-$ CD34$^+$ CD38$^-$ CD90$^+$ CD45RA$^-$ cells as HSCs with long-term repopulation capacity for up to 30 weeks with as few as ten transplanted cells being able to engraft NOG newborn mice. Purified Lin$^-$ CD34$^+$ CD38$^-$ **CD90$^-$** CD45RA$^-$ cells were also capable of long-term multilineage engraftment in immunodeficient mice, but more cells were required to achieve engraftment and the cellular output per transplanted stem cell was lower. Secondary transplantations showed that CD90$^+$ HSCs generated secondary transplants at a significantly higher frequency than CD90$^-$ cells. Thus, Majeti and colleagues postulated that human HSCs with long-term repopulation and self-renewal capacity are contained within the Lin$^-$ CD34$^+$ CD38$^-$ CD90$^+$ CD45RA$^-$ population of human cord blood and bone marrow cells whereas Lin$^-$ CD34$^+$ CD38$^-$ **CD90$^-$** CD45RA$^-$ cells mainly contain the less primitive multipotent progenitors [1528].

The group of John Dick identified CD49f (VLA-6) as an additional marker for human long-term HSCs using limiting dilution assays and single-cell transplantation into NSG mice [1562]. They showed that one of ten Lin$^-$ CD34$^+$ CD38$^-$ CD90$^+$ CD45RA$^-$ CD49f$^+$ cells had long-term repopulation activity and could be serially transplanted, representing the most purified population of human HSCs to date. Recently, the laboratory of Claudia Waskow showed that human HSCs with increased long-term repopulating activity could be further enriched by high expression of the Kit receptor on the cell surface of CD34$^+$ CD38$^-$ CD90$^+$ CD45RA$^-$ human HSCs [1530]. Transplanted Lin$^-$ CD34$^+$ CD38$^-$ CD90$^+$ CD45RA$^-$ Kit^{hi} cord blood cells led to a human chimerism of around 60% in peripheral blood for up to 30 weeks and an increased frequency of human HPCs in bone marrow of recipient mice compared to Lin$^-$ CD34$^+$ CD38$^-$ CD90$^+$ CD45RA$^-$ Kit^{lo} cells (22% blood chimerism). Whether HSCs with long-term repopulation potential within the CD49f$^+$ and the Kit^{hi} HSC populations are overlapping remains to be shown in future studies. The

Table 66. Abs used for the identification of human cell types

Antibody	Clone	Conjugate	Supplier	
CD2	RPA-2.10	FITC	eBioscience	Lineage mix
CD3	HIT3a	FITC	eBioscience	
CD10	SN5c L4-1A1	FITC	eBioscience	
CD11b	CBRM1/5	FITC	eBioscience	
CD14	61D3	FITC	eBioscience	
CD15	HI98	FITC	eBioscience	
CD16	CB16	FITC	eBioscience	
CD19	HIB19	FITC	eBioscience	
CD56	MEM188	FITC	eBioscience	
CD235a	HIR2	FITC	eBioscience	
CD34	581	APC	BioLegend	
CD38	HIT2	PE-Cy7	eBioscience	
CD45	HI30	Alexa Fluor® 700	BioLegend	
CD45RA	HI100	eFluor® 450	eBioscience	
CD49f	GoH3	PE-Cy5	BD Biosciences	
CD90	5E10	PE	BD Biosciences	
CD117	A3C6E2	APC Vio770	Miltenyi	
Isotype Controls				
Mouse IgG1 κ	MOPC-21	PE	BioLegend	
Mouse IgG1 κ	P3.6.2.8.1	PE-Cy7	eBioscience	
Rat IgG2a κ	eBR2a	PE-Cy5	eBioscience	
Mouse IgG1 κ		APC Vio770	Miltenyi	

Table 67. Cell surface phenotype for the identification of human HSPC populations

HPC population ($CD45^+$ Lin^-)	Phenotype/ subphenotype	Reference
HPCs	$CD34^+$ $CD38^-$	[1561]
HSCs	$CD34^+$ $CD38^-$ $CD90^+$ $CD45RA^-$	[1528]
MPPs	$CD34^+$ $CD38^-$ $CD90^-$ $CD45RA^-$	[1528, 1529] add PMID 26541609
LT-HSCs	$CD34^+$ $CD38^-$ $CD90^+$ $CD45RA^-$ $CD49f^+$	[1562]
LT-HSCs	$CD34^+$ $CD38^-$ $CD90^+$ $CD45RA^-$ $CD117^{hi}$	[1530]

different cell surface phenotypes of human HSPC populations are summarized in Table 67.

Another marker, which was only lately proposed to identify a subset of human HSCs in cord blood, is the EPCR [1563]. The group of Guy Sauvageau showed that only $EPCR^+$ $CD34^+$ but not $EPCR^-$ $CD34^+$ cord blood cells were able to engraft secondary NSG recipients. Interestingly, EPCR can also be used to identify murine bone marrow and fetal liver HSCs [1542, 1564]. However, it remains unknown whether EPCR is also expressed on human bone marrow and mobilized blood HSCs.

To discriminate human from murine HSCs in a humanized mouse model, Abs specific for murine and human CD45 need to be used. The high amount of RBCs in samples of any source may result in background dots. To avoid that, a gate can be set on Ter119 and CD235 negative cells to exclude mouse or human erythrocytes, respectively.

9.4.2 Materials.

1. Source of adult human HSCs such as bone marrow, G-CSF mobilized peripheral blood or umbilical cord blood, or humanized mice.
2. Ficoll-Paque solution (d = 1.077) (e.g., Biocoll separating solution, Biochrom)
3. PBS containing 2% FCS
4. Optional: ACK lysing buffer
5. Flow cytometer able to measure FITC, PE, PE-Cy7, PE-Cy5, APC, Alexa Fluor700, Alexa Flour780, and Pacific Blue (eFluor 450)

9.4.3 Pitfalls.

1. The quality of primary samples may differ depending on the donor, the way of extraction, and the used anti-coagulant. Thus, frequencies of HSCs might not always be comparable between specimens.
2. If there is no clear cell fraction after Ficoll-Paque density gradient centrifugation, check whether the centrifuge break was set to 0 or 1.

9.4.4 Top tricks.

1. Try to use samples as fresh as possible to obtain a high HSC yield.
2. Dilute bone marrow or blood with PBS (1:1 to 1:2) prior to Ficoll-Paque density gradient centrifugation.
3. To avoid surplus hours at the sorting machine, you can enrich human $CD34^+$ cells with magnetic beads prior to staining and sorting.

10 Tumor cells

10.1 *Overview*

The FCM-based characterization of tumors is instrumental for the improvement of existing, and the development of novel, therapeutic strategies against all types of cancers [1565]. The various alterations involved in malignant transformation are elegantly summarized in "Hallmarks of cancer—the next generation" by Hanahan and Weinberg 2011 [1566].

Many of the proteins involved in transformation mechanisms can be detected using FCM. The most relevant examples are summarized in this section, detailing the surface expression of hematopoietic, epithelial, endothelial, and neuroectodermal markers for the classification of tumor cells according to their cellular origin. Importantly, flow cytometric analysis of surface receptors associated with the tissue of origin is helpful for a detailed characterization of solid and hematopoietic tumor types with respect to their surface expression of growth factor receptors, as well as molecules important for the interaction with immune effectors cells, such as MHC molecules as ligands for T cells, as well as adhesion molecules. The most common strategies for the definition and characterization of human and murine tumor cells are presented, along with several practical examples.

10.2 *Introduction*

Tumor cells are derived from nontransformed cells of either hematopoietic, epithelial, endothelial, neuroectdermal, or mesenchymal origin, resulting from a sophisticated process of malignant transformation. Therefore, the origin of a tumor cell indicates which markers are suitable for its flow cytometric characterization. Since hematopoietic tumor cells, i.e., leukemias and lymphomas, are derived from their non-malignant counterparts, they retain expression of the pan-leukocyte marker CD45, originally defined as the leukocyte common antigen (LCA). In this section, the definition of subsets of leukemias and lymphomas will be briefly mentioned in the context of EuroFlow (http://euroflow.org/usr/pub/pub.php), a consortium developing novel flow cytometric diagnostic tests. Solid tumor cells, on the other hand, do not express hematopoietic markers and therefore the absence of CD45 can be used to discriminate solid tumor cells from all hematopoietic cells, including progenitor cells (HCS, see Chapter VI Section 9: Hematopoietic stem cells [1567]). In the case of tumor tissue preparations, this basic discrimination of solid tumor cells from hematopoietic cells is especially helpful because it represents the first step for a detailed characterization of solid tumor cells.

10.2.1 Hematological malignancies. The classification of leukemias and lymphomas can be guided by FCM and the procedure has been harmonized, standardized and successfully integrated into the clinical immunophenotying routine [1568]. Of note, the EuroFlow (www.euroflow.org) consortium, represented and headed by Jacques M. van Dongen, has designed panels for n-dimensional flow cytometric immunophenotyping of leukemias and lymphomas. Beyond the staining and gating protocols, the group has developed novel computerized evaluation procedures for the characterization and quantification of human hematopoietic malignancies. The EuroFlow guidelines represent the gold standard of hematopoietic malignancy immunophenotyping (http://euroflow.org/usr/pub/pub.php). For research laboratories working on hematopoietic malignancies in patients, it is important to mention that virtually all hematopoietic malignancies are accompanied by a disturbed distribution of the lymphocyte subsets in peripheral blood. Therefore, a detailed knowledge of the "normal" distribution of leukocytes in healthy individuals is instrumental for the analysis of the influence of malignant cells on hematopoiesis and immune function. To this end, "The ONE Study" group guided by Birgit Sawitzki and Edward Geissler has established an advanced FCM panel for human immune-cell phenotyping in order to define the distribution of the most important T-cell, B-cell, NK-cell and monocyte, dendritic cell subsets in healthy individuals [1569]. In addition, the International Society for Advancement of Cytometry (ISAC, https://isac-net.org/), the CIP consortium (CIMT immunoguiding program, https://www.cimt.eu/about-cip-1) of the Cancer Immunotherapy Consortium (CIMT, http://www.cimt.eu), the International Clinical Cytometry Society (ICCS, http://www.cytometry.org/web/index.php), the Federation of Clinical Immunology Societies (FOCIS, http://www.focisnet.org/) represent other initiatives that aim to harmonize and standardize protocols for immunophenotyping, primarily of human peripheral blood. The tremendous efforts of these consortia to establish guidelines, protocols and tools for the quantification of leukocytes, tumor cells, and immune responses will be instrumental not only for research projects but also for future clinical studies, in particular those with immunological endpoints.

10.2.2 Solid tumors. Due to their origin from a given tissue, solid tumor cells are not, or only at very low frequencies, present as circulating tumor cells in the blood, rather being located in the primary or metastatic tumor tissue. Since tumor tissue comprises a peculiar "contexture" of tumor cells, stroma, endothelial, and other parenchymal cells, as well as infiltrating immune cells, it

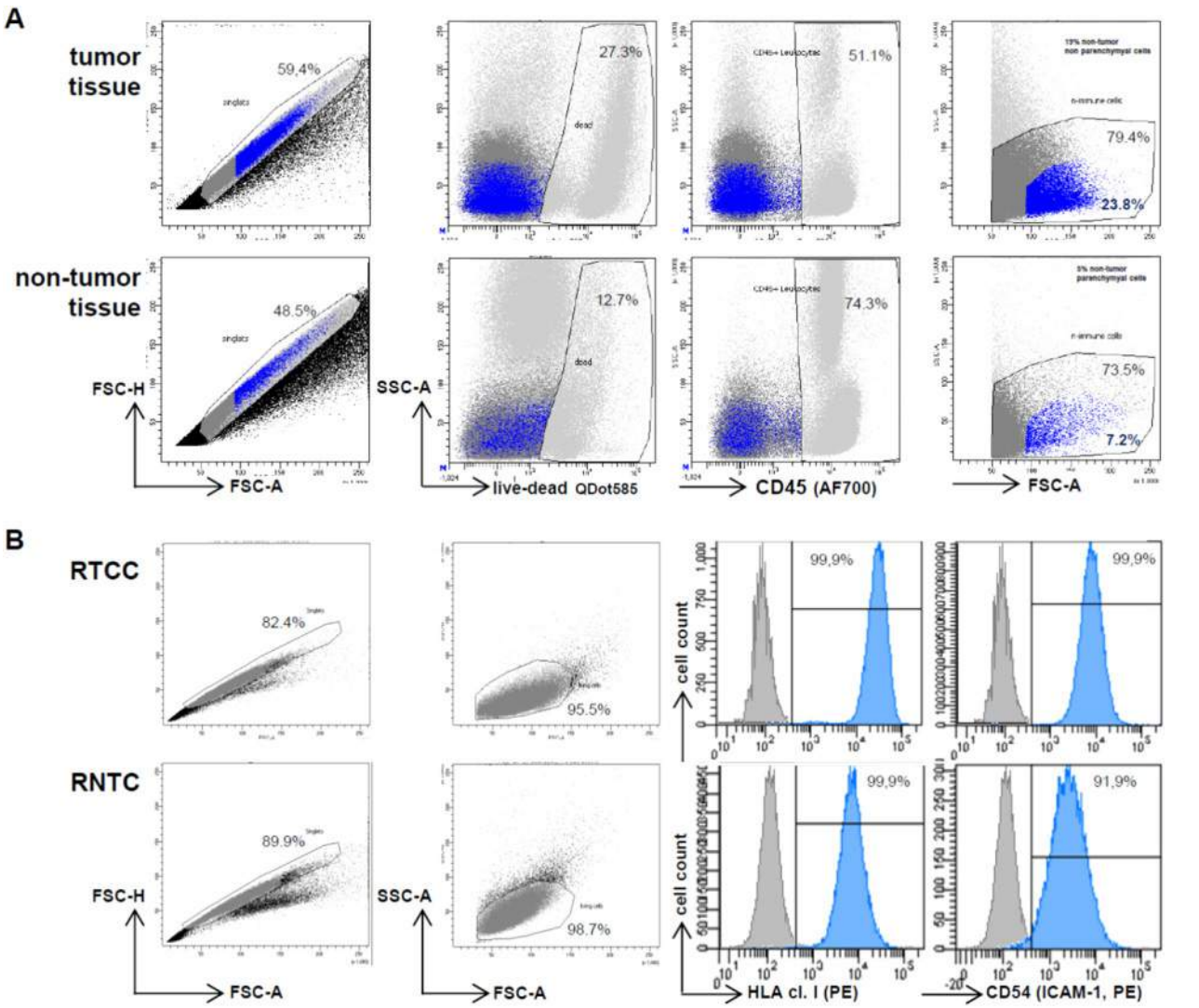

Figure 180. Single cell preparations from human tumor versus nontumor tissues and characterization of human tumor versus nontumor epithelial cells. (A) Human tumor (upper row) and adjacent nontumor tissue (lower row) was obtained as surplus tissue in the course of a pulmonary tumor resection with informed consent (MHH number 1747). After tissue digestion, single cells were stained with a live/dead dye (QDot585) and anti-human CD45 (Alexa-Fluor700) mAb. The hierarchical gating strategy starts with exclusion of doubles and aggregates in the FSC-A/FSC-H plot, followed by exclusion of dead cells in the QDot585/SSC-A plot and leukocytes, i.e., CD45-positive cells in the CD45/SSC-A plot. The remaining living CD45-negative single cells are shown in the FSC-A/SSC-A plot and in the blue gate, epithelial cells including tumor cells in the tumor tissue, can be identified according to their relative size and granularity. (B) A renal tubular cancer cell (RTCC) and the corresponding nontumor tubular cell line (RNTC) derived from tumor and adjacent non-tumor tissue of the same patient are compared with respect to surface expression of the following markers: HLA class I (mAb W6/32) and the adhesion molecule ICAM-1 (CD54, mAb gp89). All primary mAb are mouse IgG2a and were stained with a goat-anti-mouse PE-labeled secondary Ab.

is important to discriminate the tumor cells from all the non-malignant cells by tailored FCM panels.

This chapter will give an overview on suitable surface markers to use for the characterization of human and murine tumor cells.

10.3 *Procedure for the staining of surface markers for the characterization of solid tumor cells*

For the establishment of FCM panels for hematopoietic and solid tumors, it is helpful to start with tumor cell lines that available from research groups, several vendors, and the ATCC (American Type Tissue Collection, https://www.lgcstandards-atcc.org/). Recommended surface antigens for FCM staining of human solid tumor cells are listed in Table 68 and for murine tumor cells in Table 69. The procedures for cell staining, fixation, sample acquisition, data analysis, and visualization are identical to the general recommendations for direct and indirect surface marker staining and the intracellular staining protocols, which are presented in Chapters I: Cytometry equipment, Chapter II: Setup – Instrument setup and quality control and Chapter III: Before you start: Reagent and sample preparation, experimental design.

Table 68. Collection of surface molecules for staining of human solid tumor cells

Antigen	Molecules/synonyms	Antibodies/clones (selection)
HLA class I	all HLA-A, -B, -C, -G, -E alleles	W6/32, HC10
	beta$_2$-microglobuline, β_2m	HB28, B2M-01, 2M2
HLA class II	HLA-DR	L243
	HLA-DQ	TÜ169, SK10
	HLA-DP	B7/21
NKG2D ligands	MICA	clone #159227
	MICB	clone #236511
	ULBP1	clone #170818
	ULBP2	clone #165903
	ULBP3	clone #166510
ICAM-1	CD54	9H21L19, LB-2, gp98
VCAM	CD106	51-10C9
Ep-CAM	CD326	EBA-1, 9C4, 22HCLC
VE-cadherin	CD144	BV13, 55–7H1, BV9
E-cadherin	CD234	36/E-cadherin, 5HCLC, 67A4
EGFR	HER1	EGFR.1, H11, 199.12
PDGFR	CD140a (alpha chain)	AlphaR1, 16A1
	CD140b (beta chain)	28D4, 18A2, Y92
c-Met	HGF-receptor	3D6, ebioclone97
Pan-cytokeratin	pan-cytokeratin	C-11, PAN-CK
Cytokeratin 18	CK18	CK2, C-04, DC10, AE1, E431-1
Cytokeratin 8	CK8	K8.8, 5D3, C-43, M20
CD99	MIC2; single-chain type-1 glycoprotein	TÜ12, 3B2/TA8, EPR3096

Table 69. Collection of surface molecules for staining of murine solid tumor cells

Antigen	Molecules/synonyms	Antibody/clone (selection)
MHC class I	MHC class I, all H-2 molecules	M1/42
	H-2K	K^d+D^d (ab131404);
	H-2D	D^d (ab25590)
	H-2L	K^b (ab93364)
	beta$_2$-microglobuline, β_2m	S19.8
MHC class II	I-A, I-E	M5/114.15.2
NKG2D ligands	Rae-1γ	CX1
	H60	MAB1155
	MULT1	MULT1 (5D0)
ICAM-1	CD54	YN1/1.7.4
VCAM	CD106	429
Ep-CAM	CD326	G8.8
VE-cadherin	CD144	ab33168, MC13.3
E-cadherin	CD234	DECMA-1, M168
EGFR	HER1	EP38Y
PDGFR	CD140a (alpha chain)	APA-5
	CD140b (beta chain)	APB-5
c-Met	HGFR	ebioclone7, EP1454Y
Pan-cytokeratin	pan-cytokeratin	C-11, ab9377, AE1/AE3
Cytokeratin 18	CK18	6-19
Cytokeratin 8	CK8+CK18	EP1628Y
CD24		J11d, M1/69, 30-F1
CD34		RAM34, MEC14.7, MAB6518
CD44		IM7
CD133		13A4, 315-2C11

10.3.1 Preparation of tissue, staining of samples, and gating strategy. The staining protocols for human or murine tumor cell lines, or tumor cells derived from fresh tumor tissue after enzymatic digestion, follow the general recommendations summarized in Chapters I to III. With respect to mechanical dissociation for instance, by Gentle-MACS® procedures, and enzymatic digestion, the protocols do not differ between human or murine tumor tissue. The experimental protocols presented Chapter III Section 3 "Preparation of Single Cell Suspensions" are recommended using enzymatic digestion with DNAse, collagenase, and/or hyaluronidase, which are known not to affect surface expression of the molecules listed in Tables 68 and 69. In brief, after enzymatic digestion of tumor tissue, Ficoll or Percoll density centrifugation and optional lysis of erythrocytes, the resulting single cell suspensions should be comprised of tumor cells, endothelial cells, fibroblasts, and infiltrating immune cells. Ideally, these cells should be immediately applied to flow cytometric analyses using the FCM staining protocols provided in Chapters I to III for single cell suspensions but they can also be cryopreserved in liquid nitrogen as living cells for later analyses but the potential instability of some surface markers should be taken into account. Below some examples of staining protocols are provided in more detail (10.3.2 to 10.3.4).

10.3.2 Direct and indirect staining of surface molecules expressed by solid tumor cells isolated from tissue or in vitro culture. Single cell suspensions from tumor tissue:

After preparation of single cell suspensions (see Chapters I to III) from tumor tissue, solid tumor cells, for instance carcinoma cells of epithelial origin, can be detected by a FCM panel, using the CD45 marker to exclude hematopoietic cells, in combination with epithelial markers for the identification of carcinoma cells. In the following protocol, steps a or b should be followed depending on the indicated circumstances. Steps indicated by a number only are common for all circumstances.

1a. Staining strategy for single cell suspensions derived from tumor tissue:

Single cell suspensions of tumor tissue should be stained first with the unlabeled mAb that is specific for the surface molecule of interest on the tumor cells, followed by the respective sec-

ondary mAb and finally a directly labeled CD45 Ab to exclude hematopoietic cells. Figure 180A, 10.3.2 shows single cell preparations from human tumor tissue and the nontumor tissue counterpart, stained with CD45 to discriminate between leukocytes and parenchymal cells. Details of the gating strategy are given in section 10.3.4.

1b. Staining strategy for cultured tumor cells:

Cultured adherent tumor cells are detached and singularized by washing with 5 mL PBS followed by treatment with 0.05% trypsin/0.02% EDTA solution (1 mL per T25 culture flask) for 2–5 min, gentle shaking, and detachment by adding 5 mL medium (RPMI1640 + 5% heat-inactivated FBS).

2. The cell count of the single cell suspension is determined using trypan blue solution for discrimination of dead cells.
3. A total of 1×10^5 cells of the tumor suspension or 1×10^5 cultured tumor cells for each tube are pelleted by centrifugation ($800 \times g$, 5 min) in FCM tubes and resuspended (15 s vortex) in PBS or FCM buffer (PBS, 1% FBS, 0.1% Na-azide).

4a. For indirect staining, unlabeled mAb or isotype control mAb solutions (previously titrated for each antigen to determine the optimum concentration to use) are added in a volume of 50 μL to the single cell suspensions for 30 min at 4°C. After washing twice with 500 μL PBS or FCM buffer, and vortexing, goat-antimouse Ab solutions labeled with FITC, PE, APC, pacific blue, or other fluorochromes (100 μL of dilutions between 1:100 and 1:200) are added for 30 min at 4°C in the dark. Many reagents (e.g., fixable live/dead dyes such as the frequently used Zombie-series) cannot be used with FCM buffer but require PBS instead.

4b. For direct staining, cells are resuspended in 50 μL FCM buffer and directly labeled titrated mAb (usually 1–5 μL) are added for 30 min at 4°C in the dark.

5. After two washing steps with 500 μL PBS or FCM buffer, cell suspensions are stained with a titrated directly labeled CD45 Ab for 30 min at 4°C in the dark for the exclusion of hematopoietic cells.
6. After three washing steps, cells are resuspended in 150 μL FCM buffer if measured immediately or in FCM fixation buffer (PBS, 1% FCS, 1% paraformaldehyde) and stored at 4°C until measurement.
7. Exclusion of dead cells without cell fixation is highly recommended, for instance by live/dead staining with 2 μL PI stock solution (20 μg/mL PI, PE channel) that requires immediate acquisition of the cells. Other live/dead staining protocols for instance using 7AAD or other live/dead fluorochromes are available in different colors. Most protocols recommend staining for 10 to 15 min and washing steps are according to the manufacturer's instructions.

An example of the comparison between human renal tubular cancer cells (RTCC) and renal nontumor tubular cells (RNTC) from the same individuum is shown in Fig. 180B (10.3.2). Surface expression of HLA class I, CD155, CD166, and CD54 was compared between tumor (RTCC) and renal nontumor tubular epithelial cells (RNTC) showing indeed some differences in the density of these molecules.

10.3.3 Detection of circulating tumor cells in the peripheral blood and bone marrow. The detection of circulating tumor cells in the peripheral blood and bone marrow has clinical relevance for several forms of carcinomas and sarcomas in terms of disease staging and treatment response [1570]. Although molecular methods such as real-time PCR of tumor-specific mRNA expressed by carcinoma, sarcoma, or melanoma tumor cells, and so on, recently called "real time liquid biopsy," have a higher sensitivity compared to FCM, FCM is still valid for the quantification and characterization of circulating cancer cells [1571]. Under nonmalignant conditions, cells of epithelial, mesenchymal, or neuroectodermal origin cannot be detected in blood or bone marrow aspirates. However, the process of metastasis formation is associated with dissemination of malignant cells through the blood stream and bone marrow. Therefore, disseminating cancer cells are detectable in these compartments but at very low frequencies that are close to the detection limit of <0.01% cells within the gate for living cells. Hence, enrichment techniques such as Ab -based magnetic positive or negative selection are used to increase the sensitivity of detection. For the quantification of tumor cells, the direct or indirect staining protocol outlined in 10.3.2 can be combined with the CD45 marker for the exclusion of all leukocytes. The epithelial markers Ep-CAM (CD326) or cytokeratin 18 (CK18) are suitable markers for the detection of carcinoma cells. For sarcomas, the mesenchymal marker (CD99) is recommended and for the detection of melanoma cells, growth factor receptors like c-Met or PDGF-R are appropriate markers, and although not tumor-specific are characteristic for the tissues of origin.

10.3.4 Gating strategy for the identification of tumor cells. The hierarchical gating strategy should follow the recommendations shown in Fig. 180A 10.3.2. starting with FSC-A/FAC-H to exclude doublets and cell aggregates but taking into account the different sizes for leukocytes and the non-immune cell fractions containing tumor cells as well as other cell types. In this FSC-A/FSC-H gate, dead cells should be excluded by live/dead staining (in this case with a QDot585 dye). In the case of staining tumor cells in single cell suspensions derived from tumor tissue, leukocytes should be excluded by gating only on single cells negative for CD45 in the plot showing CD45 versus SSC-A. Then, the non-immune (CD45-negative) cells are displayed in a FSC-A/SSC-A plot to allow detection of the postulated tumor cell proportion, which can be further identified by surface markers of interest, for example, EGFR for carcinoma cells using histogram or dot plot images depending on the marker combinations. In Fig. 180B, renal tubular cancer cells (RTCC) are compared to renal nontumor tubular epithelial cells (RNTC) with respect to expression of HLA class I, CD155 (poliovirus receptor), CD166 (ALCAM), ICAM-1 (CD54) molecules (Figure 180B). Although pairs of tumor vs.

non-tumor cells from one individuum are rare, they allow a comparison of the expression density of several surface markers involved in immune recognition like HLA class I or adhesion molecules (CD54).

10.4 *Specific recommendations for human and murine solid tumors*

Details of suitable antigens and the respective mAbs are given in Table 68 for human tumor cells and Table 69 for murine tumor cells.

In contrast to leukemias and lymphomas, solid tumor cells are classified according to their originating cell type, i.e., tumor cells derived from (i) epithelial cells are defined as carcinoma cells, (ii) mesenchymal cells as sarcoma cells, (iii) neuroendocrine tumors are defined as originating from endocrine glands, and (iv) neuroectodermal tumors are defined as originating from neuroectodermal cells of the skin or brain. This classification is identical for all species, such as humans, nonhuman primates, dogs, cats, and rodents. Although many solid tumor cells can express a variety of tumor-associated antigens (TAA), including cancer-testis (CT), carcinoembryonal (CEA), and neo-antigens, most of these antigens are not suitable for flow cytometric characterization of tumor cells due to either their poor expression, intracellular localization or simply the lack of specific Abs [1572, 1573]. Therefore, the characterization of solid tumor cells relies on surface markers associated with their tissue origin, in combination with exclusion markers for hematopoietic cells such as CD45.

The induction of tumor-specific immune responses can result in immune escape mechanisms through which the tumor cells aim to evade their recognition and elimination by effector cells, in particular T cells and NK cells. One frequent mechanism of immune evasion is mediated by loss or downregulation of major histocompatibility complex (MHC) or human leukocyte antigen (HLA) class I molecules because, in the absence of MHC class I molecules, recognition of tumor cells by T cells is prevented. Mutation or deletion of beta-2-microglobulin ($ß_2$m), leading to MHC class I-deficiency, represents a major tumor escape strategy occurring in vivo in cancer patients, as well as in murine tumor models. Thus, MHC class I (mouse H-2) or HLA class I (human) surface staining by FCM is highly recommended for all immunological experiments with solid tumor cells [1574]

In addition to T cells, NK cells can also recognize tumor cells but via other receptor/ligand interactions. Expression of ligands for NK-cell receptors, for instance NKG2D ligands (NKG2DL), are important for recognition by the activating NKG2D receptor and for the sensitivity of tumor cells to NK cell-mediated recognition and tumor-cell elimination [1575]. NKG2D (CD314) belongs to the group of activating receptors that are conserved between humans, nonhuman primates, and rodents and are expressed by NK and $CD8^+$ T cells. In contrast to NKG2D, MHC class I molecules, human HLA-C in particular, serve as inhibitory ligands for NK cells by specific binding to inhibitory receptors of the killer-immunoglobulin–like (KIR) or C-type lectin (CD94/NKG2A) families. Thus, NK-cell recognition of tumor cells is regulated by a balance between activating and inhibitory signals derived from interactions with the respective ligands on the surface of tumor cells. In order to investigate the immunogenicity of tumor cells, it is therefore, recommended to determine the surface expression of NKG2D ligands on human or mouse tumor cells (Tables 68 and 69). Moreover, these ligands for T-cell and NK-cell receptors can be modulated during tumorigenesis, for instance MHC class I and NKG2D are targeted by oncogenic signaling via mutated MAP kinase signaling [1576].

In addition, surface expression of adhesion molecules such as ICAM-1, and VCAM should also be included in the flow cytometric characterization of solid tumor cells due to their increased expression upon development of metastases in human tumors and mouse models and, thus, their relevance for T-cell and NK-cell activation, as well as for the formation of metastases. Besides these surface molecules, which are commonly expressed by non-malignant as well as malignant cells of both hematopoietic and parenchymal origin, solid tumor cells can be also characterized by cell fate markers. For instance, splice variants of CD44, especially CD44v6, have a long-standing and controversial history as potential "tumor stem cell" markers, together with the hematopoietic stem cell markers CD34, CD133 with a recent revival of CD24 as potential prognostic marker for some carcinomas [1577, 1578]. A selection of the most relevant human cancers, grouped into carcinomas, sarcomas, neuroectodermal tumors, and their tumor biology, "the hallmarks of cancer," is given below with the respective recommendation for their flow cytometric characterization.

10.4.1 Human carcinomas. Carcinomas, i.e., epithelial tumors, represent the most frequent human cancers [1579] and their malignant transformation is often based on "driver mutations" in growth factor receptors, receptor tyrosine kinases in particular, as well as their downstream signaling pathways. For the identification of carcinoma cells, epithelial markers such as CK18 and CK8 are useful, although they have to be detected by intracellular staining procedures [1580]. In addition, epithelial cells selectively express growth factors such as epidermal growth factor receptor (EGFR), platelet-derived growth factor receptor (PDGFR), fibroblast growth factor receptor (FGFR), Her-2, c-Met, and others [1581]. These surface receptors often directly contribute to tumorigenesis by carrying "tumor-driving mutations" in their signaling domains; providing constitutive proliferative signals independently of the availability of growth factors. Therefore, these receptors can be useful for the identification and characterization of tumor cells in terms of their growth factor receptor repertoire. Importantly, the intracellular protein vimentin serves as a specific marker for the discrimination of tumor cells from fibroblasts.

Some of the most frequent human carcinomas are listed in Table 70 together with their originating epithelial cell type [1579, 1582–1587].

Table 70. Overview of the most frequent human carcinomas

Carcinoma tissue	Most frequent form of carcinoma	Originating cell	Reference
Lung cancer	Non-small cell lung cancer (NSCLC)	Type I / II alveolar epithelial cells	[1579]
Breast cancer	Mammary carcinoma	Epithelial cells of the milk duct	[1582]
Colon cancer	Colorectal carcinoma (CRC)	Epithelial cells of inner mucosal layer	[1579]
Prostate cancer	Prostate carcinoma	Epithelial basal cells of the prostate	[1583]
Liver cancer	Hepatocellular carcinoma (HCC)	Hepatocytes	[1579]
Stomach cancer	Stomach carcinoma	Epithelial cells transformed by H. pylori	[1579]
Cervical cancer	Cervical carcinoma	Cervical epithelial cells after HPV infection	[1584]
Esophagus cancer	Esophagus carcinoma	Epithelial cells lining the oesophagus	[1585]
Bladder cancer	Bladder carcinoma	Transitional epithelium of the bladder wall	[1586]
Pancreatic cancer	Pancreatic carcinoma	Endocrine ductal epithelial cells	[1587]
Kidney cancer	Renal cell carcinoma (RCC)	Proximal tubular epithelial cells	[1579]
Ovarian cancer	Ovarian carcinoma	Ovarian tubal-type epithelium	[1579]
Squamous cancer	Squamous cell carcinoma	Epithelial cells of skin or glands	[1579]

10.4.2 Human sarcomas. Mesenchymal tumors, i.e., sarcomas [2254], develop from tissue cells originating from mesenchymal progenitors and manifest primarily in soft tissue like fat, muscle, tendons, nerve or connective tissue cells, blood and lymph vessels, or fibroblasts (Table 71). The family of osteosarcomas, including Ewing osteosarcomas, comprises a severe form of juvenile sarcoma with manifestations preferentially in the bone, bone marrow, and organs like the lung or, in rare occasions, the kidney. For the flow cytometric detection of Ewing sarcoma cells in the peripheral blood of patients, CD99, the MIC2 gene product, which is normally expressed by osteoclasts and leukocytes, has been proposed in conjunction with the absence of CD45 [1588]. Kaposi's sarcoma represents a virally induced form of sarcoma mediated by the human herpesvirus 8 (HHV8), also called Kaposi's sarcoma-associated herpesvirus (KSHV). The viral HHV8 genome contributes to dysregulation and tumorigenesis by its manipulation of mechanisms regulating viral latency and lytic replication [1589]. For bone and soft tissue sarcomas, dysregulation of the Hippo signaling pathway has been shown to affect several surface receptors including EGFR, E-cadherin, CD44, and tight junctions indicating that oncogenic signaling can impinge on the stability of these surface receptors as markers for sarcoma cells [1590].

10.4.3 Human neuroectodermal tumors. Neuroectodermal tumors, i.e., malignant cells derived from neuroectodermal cells, belong to less prevalent but life-threatening cancers such as melanoma (black skin cancer) and several forms of brain cancer (Table 72). In malignant melanoma, melanocytes originating from neuroectodermal cells acquire "driver" mutations in components of the MAK kinase signaling, most frequently in the BRaf kinase (with the highest prevalence being the $BRaf^{V600E}$ mutation) or in the upstream NRas GTPase [1591]. Although these mutations cannot directly be utilized for the FCM of melanoma cells, their mutation status may have an impact on the recognition by T-cells and NK-cells [1592, 1593]. Since melanoma cells do not express unique tumor-associated surface molecules, there are no specific FCM panels available for the discrimination of malignant

Table 71. Overview of the most frequent human sarcomas

Sarcoma tissue	Mesenchymal tumor	Originating cell	Reference
Ewing sarcoma	Ewing's sarcomas (bone, bone marrow, lung, kidney)	Soft tissue cell of the respective organ	[1587, 1588]
Kaposi's sarcoma	Soft tissue sarcoma	Induced after infection with HHV-8	[2254]

Table 72. Overview of the most frequent human neuroectodermal tumors

Tumor tissue	Neuroectodermal tumor	Originating cell	Reference
Black skin cancer	Malignant melanoma	Melanocytes of the skin	[1589–1591]
Brain cancer	Gioblastoma, glioma	Glial cells of the brain	[1592, 1593]
Brain cancer	Astrocytoma	Astrocytes of the brain	[1594]

melanoma cells from melanocytes. However, melanoma cells can be detected in single cell suspensions of tumor tissue, by combinations of ICAM-1, MUC18/MCAM (CD146) and the exclusion of CD45.

Several forms of brain cancers are derived from neuroectodermal cells including some of the most aggressive brain tumors like glioblastoma with the malignant cells being derived from glial cells [1594]. Besides their poor MHC expression, glioblastoma cells utilize a broad selection of immune evasion strategies that are in part responsible for their aggressive nature and the resulting poor survival of glioma patients [1595]. Other forms of brain tumors are represented by astrocytomas, a group of differentially graded variants, i.e., diffuse, polycystic, and anaplastic astrocytoma with different degrees of aggressiveness. For gliobastoma, the GD2 and CD90 antigens are accepted as tumor-associated surface molecules for FCM and also as targets for chimeric antigen-specific T cell (CAR-T cell) therapeutic strategies. Due to the lack of additional, reliable and tumor-specific surface markers for FCM, molecular characterization, i.e., expression profiling, is currently used for a more detailed classification at the level of gene profiles, signaling pathways, and regulatory networks. Despite these molecular analyses, the cellular origin is still controversial ranging from stem cell-like precursors to neuronal stem cells [1596].

10.5 *Characterization of murine tumor cells*

For the flow cytometric characterization of murine tumor cells, both hematopoietic tumors like mouse leukemias and lymphomas, and solid tumors like carcinomas of the mouse breast, liver, or colon, melanomas, or sarcomas, the same recommendations can be applied as outlined above for human tumor cells. Since the numerous mouse tumor models cannot be discussed here comprehensively, only general remarks are provided regarding FCM of murine tumor cells. Mouse solid tumor cells are also classified into carcinomas, sarcomas, and neuroectodermal tumors according to their originating tissue. Therefore, the same surface molecules can be utilized for their characterization by FCM as are listed in Table 69 showing a selection of known mAbs for mouse antigens. In addition, the protocols do not differ from the general protocols of direct, indirect surface and intracellular staining (Chapters I to III). Furthermore, the protocol in section 10.3.2 can also be used for staining of murine tumor cells. In the case of unlabeled mAbs, the secondary mAb needs to be adapted to the species of the mAb, rat or goat for instance, and then, fluorochrome-labeled goat-anti-rat or rabbit-anti-goat secondary antibodies have to be utilized for indirect FCM.

Final remarks: The recent clinical advances in immunotherapy of human solid tumors could only be achieved using sophisticated preclinical mouse models. Since the early days of transplanted tumor cells into immunodeficient mice, numerous elegant mouse models with spontaneously developing tumors based on germline or inducible mutations have been developed over the past decade [1597]. More recently, humanized mouse models utilizing severely immunodeficient mice reconstituted with human peripheral or even hematopoietic stem cells have gained tremendous insight into immune recognition of human tumor cells, escape mechanisms and opened the door for new therapeutic approaches that finally made their way into clinical application [1598].

10.6 *Pitfalls*

The major pitfalls in the characterization of tumor cells are the selection of surface antigens suitable for either the discrimination between tumor and nonmalignant cell or the definition of their antigenicity, respectively. Since many tumor cells maintain their overall surface expression profile and rather modulate the density of certain surface receptors or ligands, it is highly recommended to perform a rather broad analysis of their receptor and ligand profile with standardized protocols that allow a quantitative assessment for each surface molecule. In Fig. 180B, the quantitative differences between a tumor and nontumor renal epithelial cell line as shown with respect to HLA class I and ICAM-1 (CD54) expression. In the case of single cell preparations derived from fresh tissue, it is important to include live/dead staining in combination with an exclusion of leukocytes in order to identify tumor cells that may represent a minor cell type within the entire complex tumor tissue. Therefore, a stepwise hierarchical gating strategy is instrumental for the identification of tumor cells.

10.7 *Top tricks*

In the context of tumor cell analyses, one of the top tricks is the direct comparison of tumor versus nontumor samples, i.e., tissue or cell lines because the genetic alterations in the course of malignant transformation result in a gradient of changes rather than in an on/off situation for most surface markers. Therefore, a side by side analysis of tumor and nontumor samples allows a direct comparison of the expression levels of the marker of interest and, hence, this facilitates the interpretation of general or even individual changes associated with tumor development or progression, respectively. Addition of genetic analyses can of course further

improve tumor cell and tissue characterization at the molecular level.

11 Human plasma cells in multiple myeloma

11.1 *Overview*

Multiple myeloma is defined by the accumulation of monoclonal plasma cells in the bone marrow and usually preceded by non-malignant monoclonal gammopathy of undetermined significance. FCM can accurately identify multiple myeloma cells, associated immune phenotypes, and confirm clonal expansion by detection of immunoglobulin light chain restriction. The technology can critically contribute to initial diagnostics, definition of disease heterogeneity, risk stratification, selection of targeted therapeutics, decisions in clinical trials, and detection of minimal residual disease among others.

11.2 *Introduction*

Plasma cells are terminally differentiated B cells and the major source of circulating soluble Abs. Plasma cell differentiation is thought to be driven by B cell receptor–target antigen affinity [689, 1599]. Upon stimulation, B cells can proliferate and increase in size, a process referred to as becoming a B cell blast. B cell blasts that secrete Ab are termed plasmablasts. Plasma cells are plasmablasts without proliferation [1600] and circulate in the peripheral blood of healthy individuals at very low frequencies (<0.1% of PBMCs).

More than 90% of plasma cells are so-called long-lived plasma cells, which are assumed to arise from germinal centers. In contrast, short-lived plasma cells can develop independent from germinal centers and consequently mostly lack somatic hypermutations [689, 1214, 1599, 1601].

Multiple myeloma is defined by the accumulation of monoclonal plasma cells in the bone marrow. In contrast to plasma cells from healthy individuals, in multiple myeloma, (epi-)genetic aberrations are assumed to restore proliferative capacity in variable proportions of plasma cells, enabling malignant clonal expansion [1602]. Their substantial number of somatic hypermutations and completed class switch recombination suggest that malignant transformation of plasma cells occurs at the (post) germinal center stage of B cell development [1603–1605]. Consequently, immunoglobulin gene sequences can act as unique molecular barcodes for disease tracking at the single cell level [1606]. In the clinical setting, immunoglobulin light chain restriction can indicate clonal plasma cell expansion.

Multiple myeloma uniquely programs its microenvironment to support tumor growth [1607], and to protect from T cell responses [1608] and chemotherapeutics [1609–1611]. Microenvironmental features in combination with (epi-)genetic aberrations [1612–1616] result in intra- and interclonal diversity of the malignant plasma cells including their expression of aberrant (surface) molecules.

FCM can accurately identify multiple myeloma cells, associated immune phenotypes, and confirm clonal expansion by detection of Ig light chain restriction. The technology can critically contribute to initial diagnostics, definition of disease heterogeneity, risk stratification, selection of targeted therapeutics, decisions in clinical trials, and detection of minimal residual disease among others. In this section, we present a basic FCM panel and give technical advice for the reliable identification of plasma- and multiple myeloma cells in human bone marrow. The experimental setup can serve as a possible foundation for individual design of detailed immunological studies of the plasma cell compartment.

11.3 *Step-by-step sample preparation*

1. Collect bone marrow samples, use EDTA as in vitro anticoagulant (1.2–2.0 mg EDTA/mL bone marrow sample).
2. Filter the bone marrow sample through cell strainer with 100 μm pore size (Falcon).
3. Pipette 100 μL of bone marrow blood into a FCM tube.
4. Add 2 mL lysing solution and incubate for 10 min.
5. Wash three times: add 2 mL wash medium, re-suspend, centrifuge for 3 min at 420 × *g*, and aspirate supernatant.
6. Vortex to fully re-suspend the cell pellet.
7. Add mAbs for surface staining: 3 μL CD138 (V500C, MI15, BD Biosciences), 3 μL CD19 (PECy7, HIB19, BD Biosciences), 3 μL CD45 (V450, 2D1, BD Biosciences), 5 μL CD38 (PE, HB-7, BD Biosciences), and 5 μL CD56 (FITC, NCM16.2, BD Biosciences).
8. Incubate for 15 min in the dark at room temperature.
9. Add 100 μL of Reagent A (FIX&PERM Cell Fixation and Permeabilization Kit, Nordic-MUbio) and incubate for 15 min in the dark at room temperature.
10. Wash once: add 2 mL wash medium, re-suspend, centrifuge for 3 min at 420 × *g*, aspirate supernatant.
11. Add 100 μL of Reagent B (FIX&PERM Cell Fixation and Permeabilization Kit, Nordic-MUbio).
12. Add mAbs for intracellular staining: 3 μL kappa light chain (APC, TB28-2, BD Biosciences) and 3 μL lambda light chain (APC-H7, 1-155-2, BD Biosciences).
13. Incubate for 15 min in the dark at room temperature.
14. Wash once: add 2 mL wash medium, re-suspend, centrifuge for 3 min at 420 × *g*, and aspirate supernatant.
15. Resuspend cells in sheath fluid for immediate analysis.

11.4 *Materials*

11.4.1 Media and buffers.

Wash medium: 100 mL 10× PBS (Gibco) + 900 mL Aqua dest (Braun)
FIX&PERM Cell Fixation and Permeabilization Kit, Nordic-MUbio
Lysing solution: Lysing Solution 10x Concentrate (BD FACS™)

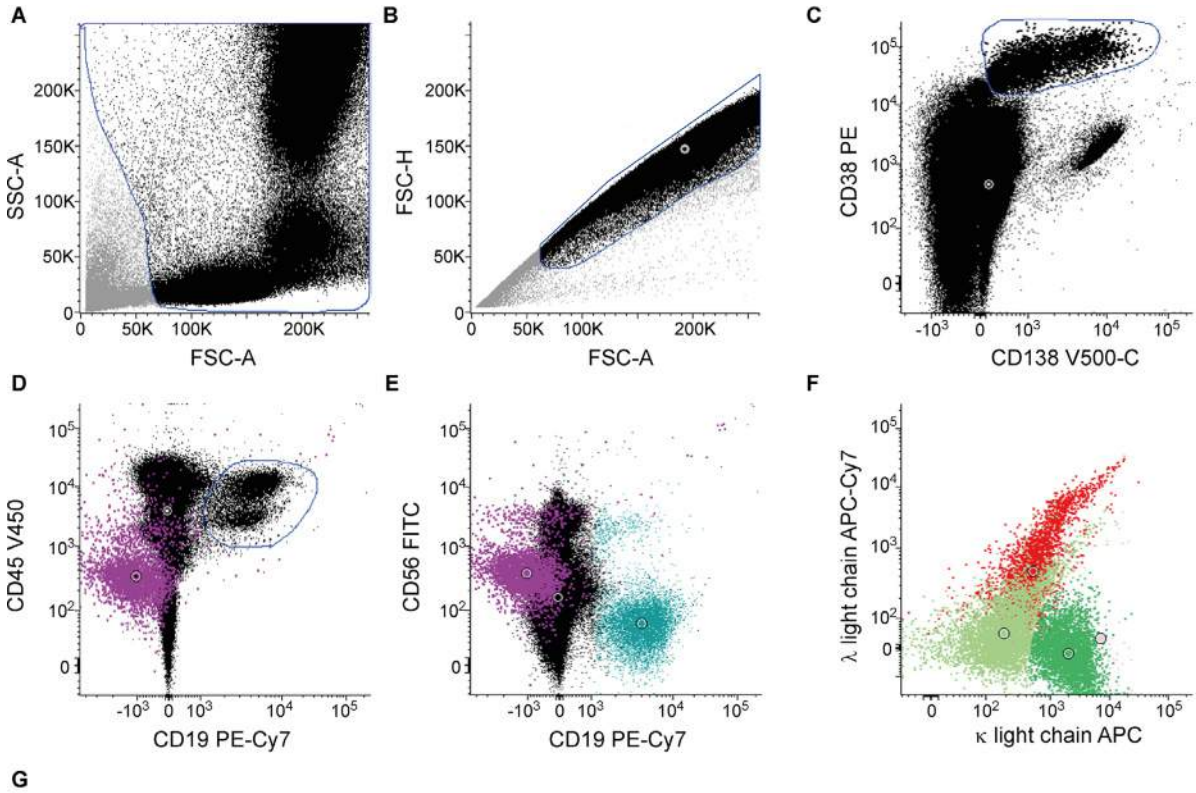

G

Population	Events	Freq. of parent (%)	Freq. of total (%)
Events	511576		
Other events	69205	13.5	13.5
Nucleated cells	442371	86.5	86.5
Other nucleated cells	430920	97.4	84.3
Plasma cells	3215	0.73	0.63
Normal plasma cells κ light chain	86	2.70	0.02
Normal plasma cells λ light chain	0	0.00	0.00
Abnormal plasma cells	3129	97.3	0.61
B cells	8236	1.90	1.60
B cells κ light chain	3443	41.8	0.67
B cells λ light chain	4792	58.2	0.94

Figure 181. Identification of aberrant plasma cells in human multiple myeloma bone marrow. Plasma cells are defined as the CD38- and CD138-positive population (gate shown in C, purple in D and E) among leukocytes (black) after exclusion of debris (A) and doublets (B). No live/dead staining is performed. Aberrant plasma cells in this sample are partially CD56-positive, homogeneously negative for CD19 and CD45-low (D and E). Moreover, aberrant plasma cells do show immunoglobulin light chain restriction (in this case lambda, indicated in red, F), which ultimately characterizes them as abnormal plasma cells. As an internal comparison, B cells (gate shown in D) present characteristic CD19 and heterogeneous kappa/lambda expression (F). The hierarchy of defined populations as well as absolute and relative numbers of events are shown in (G). Open circles indicate population centers. Gating was performed with Infinicyt™ Flow Cytometry Software. SSC-A, side scatter area; FSC-A, forward scatter area; FSC-H, forward scatter height.

11.4.2 Monoclonal antibodies.

11.4.2.1 Surface staining.

CD138 (V500C, MI15, BD Biosciences)
CD19 (PECy7, HIB19, BD Biosciences)
CD45 (V450, 2D1, BD Biosciences)
CD38 (PE, HB-7, BD Biosciences)
CD56 (FITC, NCM16.2, BD Biosciences)

11.4.2.2 Intracellular staining.

kappa light chain (APC, TB28-2, BD Biosciences)
lambda light chain (APC-H7, 1-155-2, BD Biosciences)

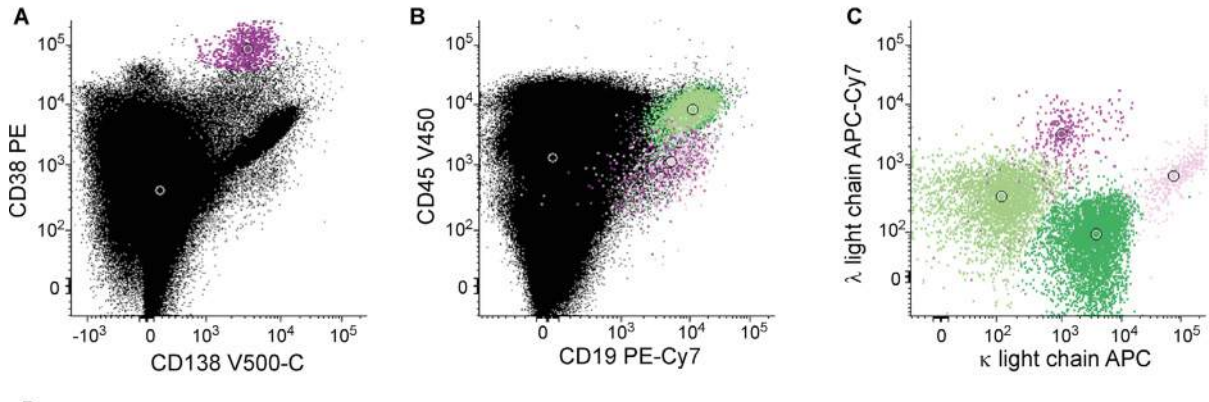

D

Population	Events	Freq. of parent (%)	Freq. of total (%)
Events	1077360		
Other events	396895	36.8	36.8
Nucleated cells	680465	63.2	63.2
Other nucleated cells	670980	98.6	62.3
Plasma cells	726	0.11	0.07
Normal plasma cells κ light chain	428	59.0	0.04
Normal plasma cells λ light chain	298	41.0	0.03
Abnormal plasma cells	0	0	0.0
B cells	8759	1.30	0.82
B cells κ light chain	5353	61.1	0.50
B cells λ light chain	3406	38.9	0.32

Figure 182. Identification of non-malignant plasma cells in human bone marrow. An example of a normal plasma cell population is shown. The gating strategy for identification of single nucleated cells, plasma cells, and B cells as well as color coding are identical to Fig. 181. Plasma cells are defined as the CD38- and CD138-positive population (purple, A) among leukocytes (black). Normal plasma cells usually express CD19 and CD45 (B) in combination with heterogeneous kappa/lambda light chain expression (C). The hierarchy of defined populations as well as absolute and relative numbers of events are shown in (D). Open circles indicate population centers. Gating was performed with Infinicyt™ Flow Cytometry Software. SSC-A, side scatter area; FSC-A, forward scatter area; FSC-H, forward scatter height.

11.4.3 Flow cytometer. All experiments were performed on a BD FACSLyric (BD Biosciences).

11.5 *Data analysis/gating*

FCM can identify plasma and multiple myeloma cells by forward/side scatter characteristics in combination with uniquely high expression of CD38 and CD138 (Fig. 181A–C) [1617–1619]. While CD45 and heterogeneous CD19 expression indicate different maturation states of normal plasma cells [1618, 1620], the identification of malignant plasma cells can be complicated by considerable variation in marker expression between and within individual patients. For example, phenotypes frequently associated with multiple myeloma cells (absence of CD19 and expression of CD56, example in Fig. 181D and E) can also be part of nonmalignant differentiation [1214, 1330, 1331, 1621]. The detection of Ig light chain restriction (Fig. 181F) can help identifying clonal expansion in most cases [1622] but may be technically challenging (intracellular staining, low target cell numbers, absence of light chain expression). In comparison to normal plasma cells that do not show light chain restriction (Fig. 182) the light chain restriction on aberrant plasma cells is particularly convincing.

11.6 *Pitfalls*

11.6.1 FCM underestimates the number of plasma cells in bone marrow aspirates. Although, providing key information on plasma cell clonality and aberrant phenotype, FCM consistently underestimates the number of plasma cells in bone marrow samples compared to morphological assessment [1623]. This might result from an increased fragility of plasma cells compared to other leukocytes, loss of plasma cells during sample preparation, hemodilution, and a discrepancy in content of plasma cells in different samples (first versus subsequent pulls during bone marrow aspirate collection). As an accurate plasma cell quantification is crucial for diagnosis of plasma cell disorders, a morphologic assessment of bone marrow smears and/or histopathological evaluation of bone marrow biopsies should be performed. However, providing an immediately available lower limit estimate and differentiating between

normal and aberrant plasma cells, FCM is a powerful method in first diagnosis and determination of minimal residual disease.

11.6.2 mAbs used in multiple myeloma treatment can interfere with flow cytometric analysis. As CD38 is frequently expressed on a high percentage of normal and aberrant plasma cells, immunotherapeutical approaches in multiple myeloma target CD38 with mAbs, such as daratumumab, isatuximab (SAR650984), MOR03087 (MOR202) and Ab79 [1623–1625]. Recent studies have shown that CD38 mAb treatment, in particular daratumumab, can interfere with diagnostic plasma cell detection caused by a long-term CD38 saturation leading to an absence of CD38-positive events [1626, 1627]. As plasma cells are identified as CD38 and CD138-positive cells, CD38 mAb treatment might lead to false negative results in plasma cell detection. It can be assumed that also further therapeutically used mAbs directed against plasma cell surface antigens that are crucial for detection of plasma cells (e.g., CD138) may also interfere with flow cytometric analysis. Therefore, bone marrow samples from patients treated with mAbs should also be evaluated by morphologic techniques as aspirate smears and immunohistopathology. Moreover, alternative plasma cell-specific antigens, as SLAMF7, or intracellular transcription factors, as BLIMP1 and IRF4, might be used for plasma cell identification in FCM [1621, 1628, 1629]. Furthermore, CD27 and CD81 expression indicates different maturation stages of normal plasma cells and might be helpful in detection of an aberrant phenotype (Table 73) [1618, 1620].

11.7 *Top tricks: Focus on minimal residual disease detection*

Minimal residual disease (MRD) is defined as a small number of malignant plasma cells that persist after treatment. MRD represents the treatment efficacy, is highly predictive for outcome and is considered as the major cause of relapse in multiple myeloma [1631, 1632]. Multicolor FCM is one of the available MRD detection methods that can reach a sensitivity of up to 10^{-5}–10^{-6}. The simultaneous detection of multiple sets of surface and intracellular markers enables reliable and fast identification of multiple myeloma cells making FCM an indispensable tool in basic research and clinical diagnostics alike. The high-throughput characterization of millions of cells in a reasonable amount of time allows minimal residual disease detection with high sensitivity comparable to next generation sequencing [1633]. Similarly to the detection of aberrant plasma cells at first diagnosis the antigen panel for MRD detection includes CD38, CD138, CD45, CD19, kappa, and lambda light chains. However, assessment of $>10^6$ nucleated cells is crucial to reach adequate MRD sensitivity levels. Moreover, high level of standardization with regard to used Abs, sample preparation and measurement and data analysis is crucial. The Multiple Myeloma MRD Kit, a EuroFlow™ approach to monitor MRD by FCM, offers a ready-to-use solution for sensitive and accurate MRD detection [1633]. Automatic software tools lead to an automated identification of cell populations and aberrant plasma cells offering high levels of standardization. These approaches are expected to overcome heterogeneity of MRD detection protocols [1634] across different FCM laboratories and provide reliable MRD data particularly within clinical trials.

11.8 *Summary table*

Table 73. Frequent immunophenotypes of normal and aberrant plasma cell populations

Plasma cell population	Frequent phenotype
Normal	Positive: CD38, CD138, CD319 (SLAMF7) Usually positive: CD19, CD45, CD27, CD81 Usually negative: CD56 Immunoglobulin light chain restriction: none
Aberrant	Positive: CD38, CD138, CD319 (SLAMF7) Usually positive: CD56 Usually negative: CD19, CD45, CD27, CD81 Immunoglobulin light chain restriction: yes

References: [1621, 1630].

12 Brain/neural cells

12.1 *Overview*

In contrast to peripheral immune cells, the application of FCM for cells from the central nervous system (CNS) is most often not the method of choice. It is limited mainly due to the lack of CNS cell-specific markers, high lipid content (through myelin), and the high integration of cells within the parenchyma. Preparing brain homogenates without severely damaging cells and their processes has proven technically challenging and special caution has to be taken toward keeping the integrity of the antigens during tissue digestion. For any of the non-hematopoietic cells of the CNS, FCM sorting and subsequent culturing therefore requires specific protocols and is facilitated by the use of reporter mouse lines. Yet FCM can also be a useful tool if the expression of genes or proteins directly after isolation are of interest [1635] but also in the analysis of resident microglia or infiltrating and nonparenchymal myeloid cells. Another complication of FCM analysis of CNS-resident cells, however, is the identification of pan-neuronal, astrocyte, microglia, and oligodendrocyte markers due to the common origin of many CNS cells as well as the regional and intracellular heterogeneity of the CNS [1636]. Different cell types, species, and even regions and age of the brain will need different dissociation protocols. We here provide three exemplary approaches for tissue preparation and subsequent FCM of brain cells. Two protocols describe the isolation of murine CNS cells and one outlines the isolation of nuclei, yet we advise to establish individual tissue dissociation procedures to account for cell-, region-, age-, and species-specific requirements.

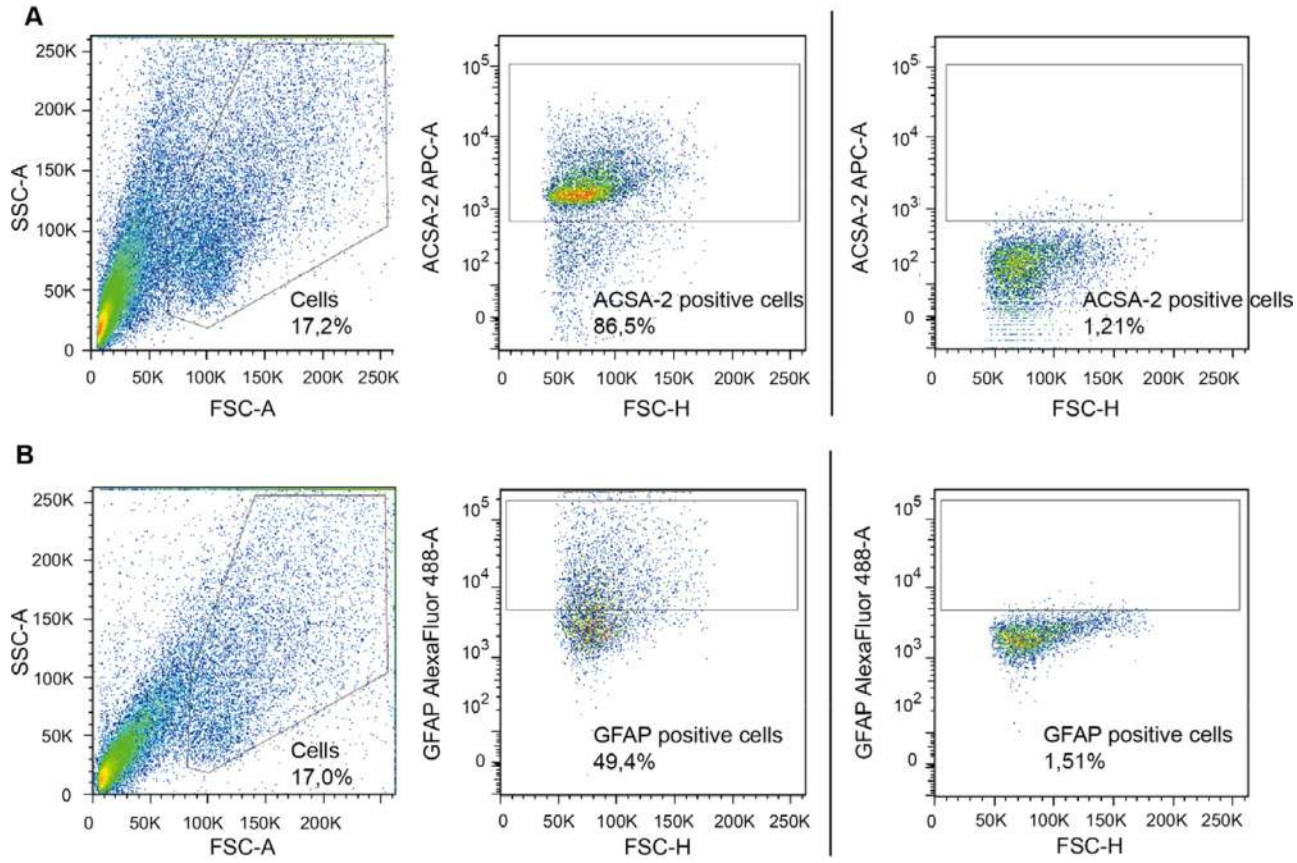

Figure 183. FCM analysis of murine neonatal astrocytes. (A) Neonatal astrocytes were harvested and stained with the cell surface marker ACSA-2 (recombinant human anti-mouse, APC-conjugated, 1:10 dilution, Miltenyi Biotec). (B) Neonatal astrocytes were harvested, fixed in 2% PFA and permeabilized in 0.5% saponin. Cells were stained with the intracellular marker GFAP (mouse monoclonal, Alexa Fluor-488-conjugated, 1:20 dilution, BD Biosciences). Ab gates were based on unstained controls for each Ab as shown on the far right. A total of 10 000 cells of the SSC-A/FSC-A gate were set as a stopping point during FCM. FSC and SSC axes are linear, fluorochrome axes are log.

12.2 *Introduction*

The human and rodent CNS, which include the brain and spinal cord, are composed of many various cell types that together orchestrate brain metabolism, neuronal signal transduction, and all bodily functions. The primary difference between the human brain and that of other species is the enormous expansion of the neocortex (with its neurons) relative to total brain volume [1637].

Neurons are the primary components of the CNS and transfer chemical and electrical signals throughout the central and peripheral nervous systems. Depending on region and function, several neuronal subtypes exist [1638]. Next to the subsets of neuronal cells, the CNS is also composed of glia cell populations. The cells belonging to the glial compartment are oligodendrocytes, astrocytes and microglia. Oligodendrocytes are cells that form myelin sheaths around neurons, insulating the neuronal processes to enable fast electric signal transduction (reviewed in ref. [1639]). Astrocytes are the most numerous cells in the CNS that have essential roles in its development, homeostasis, and disease contexts. Astrocytes are linked via vast intercellular networks, yet despite this global connectivity, astrocytic microenvironments are formed within specific brain regions or within astrocytic subpopulations (reviewed in ref. [1640]). Neurons, astrocytes, and oligodendrocytes all originate from neural stem cells (NSCs) with patterned migration and maturation phases during development (reviewed in ref. [1641]). Microglia as well as perivascular and subdural meningeal macrophages, on the other hand, originate from hematopoietic stem cells in the yolk sac that migrate to the brain throughout development [1642, 1643]. Microglia are the innate immune cells of the brain and constantly surveil the CNS parenchyma for pathogens and cellular changes.

12.2.1 Astrocytes. FCM sorting can be used to obtain astrocytes from neonatal to adult tissue. Depending on the downstream application of the sorted astrocytes (culturing, freezing, etc.), some considerations need to be kept in mind. Most cell surface Abs found on astrocytes are not cell-specific and often also found on NSCs, oligodendrocytes, and/or neurons. Additionally, only few fluorochrome-conjugated FCM Abs are commercially available (see summary table at the end of the chapter). A suitable Ab for FCM sorting both neonatal and adult murine astrocyte is ATP1B2/ACSA-2 [1644, 1645]. Labeling of intracellular markers such as GFAP requires cell permeabilization and is therefore not

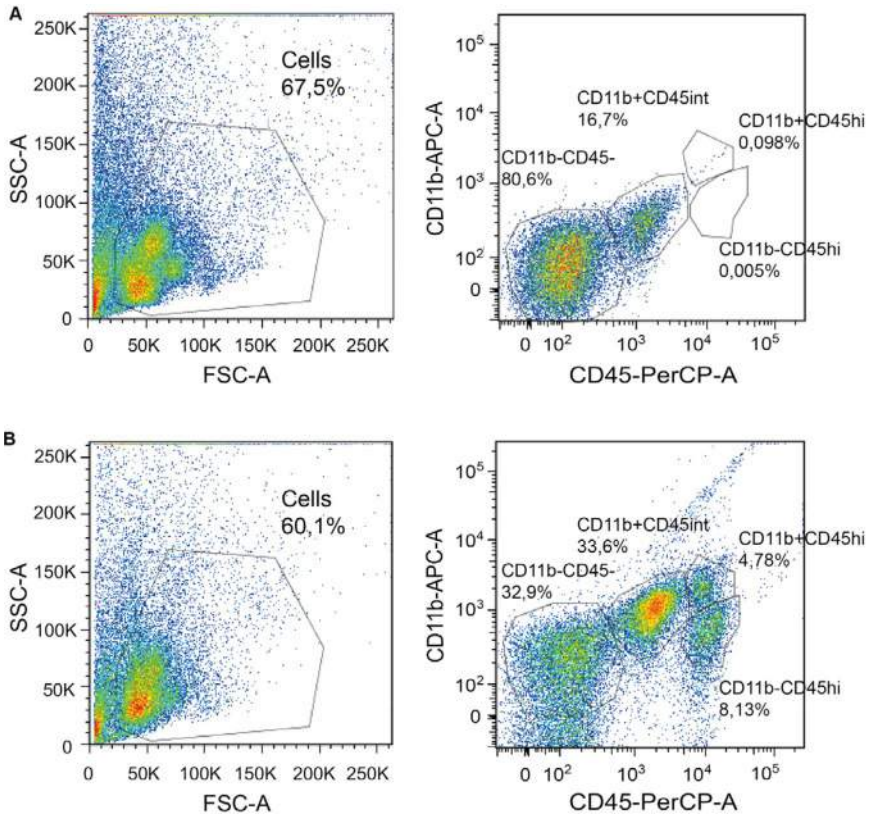

Figure 184. FCM strategy for the classification of brain-resident microglia and infiltrating macrophages and lymphocytes. (A) Analysis of brain cell suspension from a non-immunized wild-type mouse via CD45 and CD11b marker expression. (B) Analysis of monocyte-derived macrophages, infiltrating lymphocytes, and microglia in a mouse immunized with MOG35-55 at chronic phase. Cell populations were distinguished by CD45 and CD11b expression levels with macrophages showing CD11b positive, CD45 high expression ($CD11b^{+}CD45^{hi}$), microglia showing CD11b positive, CD45 intermediate expression ($CD11b^{+}$,$CD45^{int}$), infiltrating lymphocytes showing CD11b negative, CD45 high expression ($CD11b^{-}CD45^{hi}$) and non-leukocytes being CD11b and CD45 negative (CD11b-CD45-). Abs used: rat anti-mouse CD45, PerCP-conjugated, 1:200 clone 30-F11, Biolegend; rat anti-mouse CD11b, APC-conjugated, 1:400 clone M1/70, Biolegend. A total of 100 000 cells of the SSC-A/FSC-A gate were set as a stopping point during FCM. FSC and SSC axes are linear, fluorochrome axes are log.

suitable for subsequent culture. Combining different Abs can also assist in generating pure astrocyte populations and even distinguish between astrocytic subpopulations. For example, [1646]) identified astrocyte populations based on Aldh1l1 expression combined with CD51, CD71, and/or CD63 cell surface expression, which showed clear regional specificities. Mouse lines containing fluorescent labeling of astrocytes also provide a useful tool for FCM (Table 74). Currently, the Aldh1l1-EGFP reporter line [1647] is the only line labeling solely mature astrocytes in the mouse brain. All other lines are therefore only useful in astrocyte enrichment and contamination by other neural cell types needs to be considered.

12.2.2 Neurons. Neurons are cells that are very sensitive to isolation methods. Traditionally, neurons have been isolated from late-embryonal or early-postnatal murine brain tissue with culture conditions removing contaminating glial cells. This method provides a large number of cells; however, still faces the risk of contamination by other cell types. To obtain purer cultures, FCM sorting of neuron-labeled reported mice can be used [1666–1668].

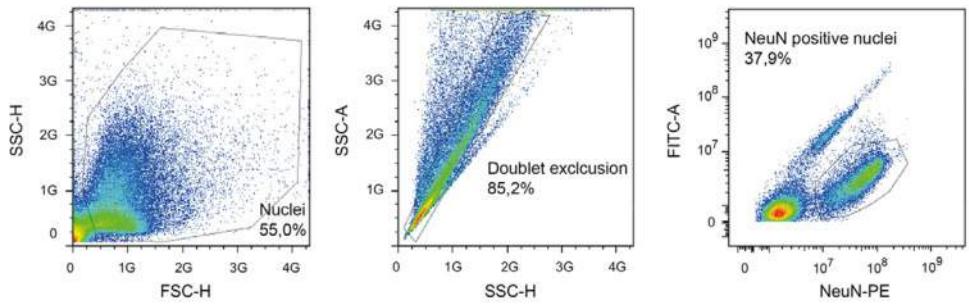

Figure 185. Fluorescence-activated nuclear sorted analysis of nuclei prepared from human surgical brain tissue. Nuclei were prepared from frozen adult brain tissue (>100 mg), stained with nuclear marker NeuN (monoclonal mouse anti-NeuN, clone A60, 1:1000 and PE-conjugated goat anti-mouse IgG 1:1000) and submitted to sorting. Gating for identification of NeuN-PE positive neuronal and non-neuronal cell populations or respective nuclei was based on the first 20 000 events. FITC fluorescence was included to identify and exclude autofluorescent nuclei. FSC and SSC axes are linear, fluorochrome axes are log.

Table 74. List of all astrocyte- and microglia- targeted fluorescent reporter lines. Modified from ref. [1648] with permission

Reporter gene	CNS cells targeted	Reference
Aldh1l1	Astrocytes	[1635, 1647]
GFAP	Astrocytes + NSCs But not expressed in all astrocytes/different expression levels	[1649–1652]
SLC1A3 (GLAST/EAAT1)	Astrocytes + NSCs	[1653, 1654]
SLC1A2 (GLT1/EAAT2)	Astrocytes + ependymal cells	[1653–1655]
Vimentin	Astrocytes + NSCs	[1656]
CX3CR1	Microglia, NK cells, monocytes, dendritic cells and some macrophages	[1657, 1658]
Sall1	Microglia	[1659]
Iba1/Aif1	Microglia, macrophages, other leukocytes	[1660]
CSF1R	Microglia, macrophages, other leukocytes	[1661]
CD11b	Microglia, macrophages, other leukocytes	[1662]
TMEM119	Mature microglia	The Jackson Laboratory #031823
CD45	Microglia, macrophages, other leukocytes	[1663]
CD68	Phagocytic microglia, macrophages	[1664, 1665]

Again, this is only possible with neonatal tissue and thus only certain aspects of neuronal development and physiology can be analyzed using this technique.

Limited neuronal cell surface markers and their respective Abs exist. CD24 labeling has been used for neuronal cell sorting, however sorting procedures dramatically decrease cell integrity and viability of neurons. Thus, FCM sorting of neurons for cell culture from both adult murine and human tissue is not possible. Reports exist that describe tissue fixation for subsequent analysis of cytoplasmic or nuclear neuronal proteins or genes [1669]. Another method to analyze neurons is via nuclei sorting that has proven successful for many applications including genetic [1670, 1671], epigenetic [1672], transcription factor, or gene expression profiling [1638]. The Akbarian method of neuronal nuclei isolation provides a useful alternative to analyzing neurons [1673].

12.2.3 Oligodendrocytes. The study of oligodendrocytes has provided valuable insights into neuronal signal transduction and its changes in disease settings. Especially in demyelinating diseases such as multiple sclerosis (MS) the relationship between myelin sheath integrity and neuronal health has become apparent. As with other brain cells, oligodendrocytes have traditionally been analyzed in vitro and a plethora of culture protocols exist [1674–1677]. Based on varying medium supplements and other culture conditions, it is thus possible to grow each of the oligodendrocyte subsets and maturation stages ranging from oligodendrocyte precursors cells (OPCs) to pre-myelinating and mature oligodendrocytes. Again, these cultures are derived from neonatal brain and contain multiple cell types. FCM is mainly used to enrich oligodendrocytes from these cultures and only very few studies are published using FCM [1678] or immunopanning [1679] to isolate oligodendrocyte lineage cells from the CNS directly and reduced yield and viability need to be considered. An overview of oligodendrocyte markers available for FCM can be found at the end of the chapter. Additionally, oligodendrocyte reporter mice are also available such as EGFP-labeled CNP mice [1680], Olig2 mice [1656], and NG2 mice [1681].

12.2.4 Microglia. Microglia are CNS-resident phagocytes that are distinct from macrophages originating in the periphery. To date, microglia have been distinguished from other CNS or myeloid cells by FCM sorting mainly based on CD45 expression levels. Non-myeloid CNS cells are CD45-negative, while perivascular macrophages or infiltrating myeloid cells and leukocytes show CD45 high expression. Microglia on the other hand can be sorted by selecting for intermediate CD45 expression (CD45 int) in the combination with CD11b [1682]. However, it needs to be considered that CD45 expression may change due to activation of the cells. Similar to other CNS cells, the same limitations regarding the need of tissue dissociation and myelin removal hold true for microglia, yet the overlap with antigens shared with other glial/neuronal cell types is not very extensive. The main challenge therefore is not to separate microglia from other CNS cells but from macrophages originating in the periphery. Microglial expression of the fractalkine receptor, CX3CR1 and CCR2, overcame some of these limitations. CX3CR1, however, is also highly expressed by circulating monocytes ($Ly6C^{lo}$) and other tissue resident macrophages [1657, 1658]. Only recently, new microglia-specific markers such as Tmem119 were identified, enabling robust selection of mature microglia independent of activation status in humans and in mice [1683]. Reporter lines for microglia/myeloid cells also exist for facilitating FCM sorting (Table 74). Mass cytometry, or CyTOF, has also proven a very successful tool in characterizing heterogeneity of human and murine CNS-specific myeloid

and microglial cell populations in both health and disease based on expression profiles of up to 50 cell and functional markers [1684–1688].

12.3 *Step-by-step brain preparation*

12.3.1 From integrated cells to a single cell suspension (example for glial cells). Obtaining single cell suspensions from adult brain tissue can be challenging due to the vast extension of cellular processes within the brain parenchyma that upon disruption can influence cell viability and morphology. The commercially available Neural Tissue Dissociation Kit (NTDK, Miltenyi Biotec) or Adult Brain Dissociation Kit (ABDK, Miltenyi Biotec) provide gentle methods to homogenize rodent brain tissue for downstream applications such as cell enrichment and/or culture. The NTDK is recommended for dissociation of neonatal mouse tissue and adult mouse tissue with subsequent microglia isolation. Use of the ABDK is recommended for dissociation of adult mouse tissue with subsequent astrocyte, neuron, or oligodendrocyte isolation. A list of Abs available can be found at the end of this chapter.

Detailed protocol:

1. Obtain fresh mouse brain tissue and store in HBSS without Ca^{2+} and Mg^{2+} (for NTDK) or D-PBS supplemented with glucose, sodium pyruvate, CaCl, and MgCl (D-PBS (w), for ABDK). For microglia isolation from adult tissue, perfuse mouse brain with PBS before dissociation.
2. Transfer 400–1000 mg neural tissue into C tube (Miltenyi Biotec) and add NTDK or ABDK enzyme mixes according to manufacturer's protocol.
   (a) For neonatal murine tissue and murine adult microglia use NTDK
   (b) For murine adult astrocytes, neurons, and oligodendrocytes use ABDK
3. Run the samples on the gentleMACS® with heaters (Miltenyi Biotec):
   (a) Neonatal murine cells: 37C_NTDK_1.
   (b) Murine adult cells: Program 37C_ABDK_01
4. Resuspend cell suspensions and pass through a 70 μM cell strainer placed on a 50 mL tube.
5. Wash cell strainer with 10 mL HBSS with Ca^{2+} and Mg^{2+} (for NTDK) and 10 mL D-PBS (w) (for ABDK).
6. Centrifuge samples at 300 × *g* for 10 min, 4°C and remove the supernatant.
7. Resuspend pellet according to kit used:
   (a) NTDK: Resuspend in buffer and volume required for further applications.
   (b) ABDK: Resuspend in D-PBS (w) according to input material and transfer to 15 mL tube
      i) 400–500 mg tissue: 3100 μL D-PBS (w)
      ii) 800–1000 mg tissue: 6200 μL D-PBS (w)
8. (ABDK only) Add cold Debris Removal Solution depending on input material, mix well, and overlay very gently with 4 mL of D-PBS (w). Centrifuge at 3000 × *g* for 10 min, 4°C with full acceleration and brake.
   (a) 400–500 mg tissue: 900 μL
   (b) 800–1000 mg tissue: 1800 μL
9. (ABDK only) Aspirate the top two phases and fill up with D-PBS to a final volume of 15 mL. Invert tube three times.
10. (ABDK only) Centrifuge samples at 1000 × *g* for 10 min, 4°C with full acceleration and brake.
11. (ABDK only) Discard supernatant and resuspend cell pellet in 1 mL 1× Red Blood Cell Removal Solution (diluted in ddH2O). Incubate for 10 min at 4°C.
12. (ABDK only) Add 10 ml cold PBS + 0.5% BSA and centrifuge samples at 300 x g for 10 min, 4°C.
13. (ABDK only) Remove the supernatant and resuspend pellet in buffer and volume required for further applications.

12.3.2 From integrated cells to a single cell suspension 2 (example for immune cells). Depending on the immune cell subtype of interest different Percoll-based protocols are available that can additionally be combined with enzymatic digestion, whilst the resistance of antigens to digestion enzymes needs to be considered and protocols optimized accordingly. We present here a rapid, easy and cheap protocol not requiring enzymatic digestion that is suitable for the isolation of the majority of peripheral immune cells as well as microglia.

Detailed protocol:

1. Mechanically dissociate neural tissue using a 70 μm nylon cell strainer and the plunger of a 5 mL syringe into 15 mL tubes containing complete RPMI medium or HBSS.
2. Centrifuge at 400 × *g* for 10 min at 4°C.
3. Aspirate supernatant and vortex pellet.
4. Add 6 mL 37% Percoll (dissolved in Percoll mix, recipe in table with materials) to each tube at room temperature.
5. Resuspend pellet thoroughly by repeated pipetting.
6. Spin in swinging bucket centrifuge at 2800 × *g*, 20 min, no brake, at room temperature. It is important to use a centrifuge in which the buckets swing out a full 90° to ensure good separation of the myelin layer.
7. Aspirate myelin, take care to clean the sides of the tube.
8. Aspirate Percoll solution, down to ~500 μL and do not break up the pellet, as you are trying to dilute the residual Percoll.
9. Add 6 mL complete medium (or HBSS) (1st wash).
10. Centrifuge at 400 × g for 10 min at 4°C.
11. Completely aspirate medium, vortex pellet, add 10 mL complete medium (2nd wash).
12. Centrifuge at 400 × *g* for 10 min at 4°C.
13. Resuspend in FCM Fc-block (see materials table) for 15 min and count a diluted fraction of cells (e.g., for a mouse brain, resuspend in 1 mL FCM Fc-block, for a single murine spinal cord, use 0.5 mL).

14. Wash the cells in medium and subsequently stain with Abs as desired.
15. Following antibody stain, cells may be fixed in 4% paraformaldehyde (Electron Microscopy Science) for 10 min at room temperature. Following a wash step the cells can be resuspended and stored at 4°C until measurement.

12.3.3 From integrated cells to nuclei (example for neurons). This method can be used to extract nuclei from >100 mg of fresh or frozen human cortical tissue. Immunotagging with an anti-NeuN Ab robustly stains human cortical neuron nuclei for subsequent FCM sorting. Other cell populations beyond neurons can be captured the same way (e.g., astrocytes, oligodendrocytes) if specific nuclear antigens are known and respective Abs available. Other methods to study single neurons in the adult human brain include the use of microfluidic devices as the Fluigdime C1 and ultra-high-throughput droplet-based technologies [1689].

Detailed protocol:

1. Chill a clean B-type 7 mL pestle on ice and add 5 mL of lysis buffer (see materials section). Note: Lysis buffer can be prepared on day prior to sorting, but DTT should be added fresh on the day of use.
2. Cut 100—500 mg fresh-frozen human surgical or postmortem brain tissue and transfer to lysis buffer in homogenizer. Homogenize tissue on ice using pestle.
3. Put 8 mL sucrose cushion buffer in a Beckman Ultra-clear 14 × 95 mm centrifuge tube.
4. Note: Tube size and type have to fit with the ultracentrifuge and rotor system used (here, e.g., Beckmann OPTIMA XE – 90 ultracentrifuge and SW-40Ti rotor).
5. Carefully overlay homogenized sample on top of sucrose cushion without mixing the two solutions.
6. Centrifuge for 2 h in pre-chilled swing-out rotor at 4°C, 30 000 × *g*.
7. After centrifugation, put tube on ice and carefully remove supernatant. Add 500 μL of 3 mM $MgCl_2$ in PBS and let stand on ice. After 10 min very gently re-disperse pellet. Note: Do not vortex nuclei. Always keep nuclei on ice.
8. Pass nuclei suspension through a 40 μM cell strainer into a clean 1.5 mL tube and dilute with 3 mM $MgCl_2$ in PBS. Keep a fraction for manual counting.
9. Add mouse anti-NeuN Ab (1:1000), Goat anti-Mouse IgG (H+L) Secondary Ab, PE-conjugated (1:1000), and incubate for at least 30 min at 4°C on a rotator.
10. Manual counting of a fraction of nuclei and quality control with bright field microscopy.
11. Proceed to sorting.

12.4 *Materials*

12.4.1 Cell suspension (glial protocol).

Reagent	Manufacturer
OctoMACS® with Heaters	Miltenyi Biotec
Adult Brain Dissociation Kit	Miltenyi Biotec
Neural Tissue Dissociation Kit (P)	Miltenyi Biotec
C tubes	Miltenyi Biotec
HBSS with Ca^{2+} and Mg^{2+} (NTDK only)	Life technologies
HBSS without Ca^{2+} and Mg^{2+} (NTDK only)	Life technologies
D-PBS with 0.55 mM glucose, 0.033 mM sodium pyruvate, 0.9 mM CaCl, 0.49 mM MgCl (pH 7.2, keep cold) (ABDK only)	–
PBS + 0.5% BSA (pH 7.2, keep cold)	–

12.4.2 Cell suspension (immune cell protocol).

Reagent	Manufacturer
Cell Strainer size 70 μm Nylon	BD Falcon
5 mL syringe	BD Falcon
15 mL tubes	BD Falcon
Complete RPMI medium (5% FCS, Penicillin/Strepdavidine, b-Mercapto) or HBSS	Sigma
37% Percoll (100% Percoll mixed with respective amount of mastermix of 45 mL 10× PBS, 3 mL 0.6 N HCl, 132 mL H_2O, pH 7–7.2 filter sterilized)	Sigma
FCM Fc-block (to a given volume of FCM buffer add 50 μg/mL rat IgG and 1 μg/mL CD16/CD32 mAb	eBioscience

12.4.3 Nuclei preparation (neurons).

Reagent	Specifications
7 mL Dounce tissue grinder	Wheaton #357542
Lysis buffer	0.32M Sucrose, 5 mM $CaCl_2$, 3 mM $MgAc_2$, 0.1 mM EDTA, 10 mM Tris-HCL pH 8, 1 mM fresh DTT, 0.1% Triton X100
Sucrose cushion buffer	1.8 M Sucrose, 3 mM $MgAc_2$, 10 mM Tris-HCL pH 8, 1 mM fresh DTT
Beckman ultra-clear 14 × 95mm centrifuge tube	Beckman Coulter #344060
3 mM MgCl2 in PBS	–
40 μM nylon cell strainer	BD Falcon
Mouse anti-NeuN Ab, Clone A60 (1:1000)	Millipore
Goat anti-Mouse IgG (H+L) Secondary Ab, PE (1:1000)	

12.5 *Data analysis/gating*

Fig. 183 provides representative FCM blots of neonatal murine astrocytes labeled with the cell surface marker ACSA-2 (Fig. 183A) and the intracellular marker GFAP (Fig. 183B). For the intracellular GFAP stain, cells were fixed in 2% PFA and permeabilized with 0.5% saponin.

12.6 *Microglia (human/mouse)*

To analyze microglia and macrophages, brain tissue from a mouse immunized with MOG35-55 peptide in the chronic phase of experimental autoimmune encephalomyelitis (EAE) and tissue from non-immunized mice was mechanically dissected and myelin removed via Percoll layering as described in the step-by-step preparation. Fig. 184 provides representative FCM blots of gating strategies for macrophages (CD11b positive, CD45 high expression), microglia (CD11b positive, CD45 intermediate (int) expression), infiltrating lymphocytes (CD11b negative, CD45 high expression), and non-leukocytes (CD11b negative, CD45 negative expression). In contrast to non-immunized mice, where only brain-resident microglia and some perivascular macrophages are present (Fig. 184A), infiltrating macrophages and lymphocytes are present in MOG35-55 immunized mice (Figure 184B).

12.7 *Neurons*

Figure 185 shows a representative blot of fluorescence-activated nuclear sorted nuclei prepared from human surgical brain tissue. Nuclei were prepared from frozen adult brain tissue and stained with the neuronal nuclear marker NeuN. FITC fluorescence was included in order to select for autofluorescence.

12.8 *Pitfalls*

As already mentioned in the introduction, the low yield and reduced cell viability are challenging when wanting to FCM sort CNS cells. Cell purity is also an issue in the CNS as cell markers are often expressed by more than one cell type and are region specific. Since neurons, astrocytes and oligodendrocytes share the same precursor, many cell markers are shared between them. Microglia and peripheral myeloid cells also share many of the same cell surface markers, that change during activation state and/or pathology and which need to be carefully selected for.

Special attention should be also paid during analysis of antigens on the surface of microglia/macrophages and astrocytes as unspecific binding via Fc receptors or membrane absorption can create false positive results. These cells do express different Ig Fc receptors. By incubating cells in the presence of blocking reagents, Fc receptor-mediated binding of Igs can be suppressed. Blocking can be performed by purified Igs, serum, or purified CD16/32, but also different commercial special blocking solutions are available or included in kit protocols. When Fc receptors itself are of interest as antigen it has to be checked whether the used blocking approach enables a detection after blocking. Besides binding to Fc receptors membrane adsorption can generate false positive results. Fast processing, repeated washing steps as well as addition of EDTA and BSA to the buffer solutions are helping to reduce unwanted membrane adsorption (see Chapter V Section 5: Surface Parameters).

In some experiments, microglia and/or macrophages can affect the analysis/sorting of other cells from the CNS. In setups where the focus is, e.g., on astrocytes, nonspecific Ab binding can be reduced by an additional microglia/macrophage depletion step.

Additionally, myelin debris can lead to essential problems during data acquisition and labeling of cells with Abs and protocols need to be adapted accordingly [1690, 1691]. This is especially important for the analysis of adult white matter regions. Through high myelin content, clogging of the instruments may occur and cells of interest might not be detectable in the sample. Therefore, we highly recommend including an effective but gentle myelin removal step when analyzing CNS tissue with FCM.

When wanting to analyze human tissue, it needs to be taken into account that it can only be obtained from very limited fresh biopsies or from postmortem autopsies. Fresh healthy controls are therefore not available and in the case of autopsy material, a high postmortem interval can dramatically reduce tissue quality.

12.9 *Top tricks*

In the past, the study of CNS resident cells has largely relied on ex vivo slice cultures, histological means or the in vitro culture of neonatal cells. FCM analysis was traditionally used only on microglial cells that show similar expression of cell surface markers to peripheral myeloid cells. Advances in brain dissociation techniques and the vast array of reporter mice have made the analysis of other brain cells amenable to methods such as FCM, MACS®, immunopanning, and single cell or nuclear sequencing. Each of these methods has limitations with regards to cell viability, purity, yield, and Ab availability. It is thus essential to choose the most appropriate method depending on the scientific question.

For studies using neonatal murine CNS tissue, obtaining enriched cell suspensions from mixed cultures or by FCM/MACS®, offers a high yield of cells, however cultures may be contaminated by other CNS cells. Additionally, some cells only reach maturity at late postnatal stages and these cultures thus contain many precursor cells. Here, selecting the appropriate cell culture medium before FCM sorting may help in selecting for a specific cell type [1692]. Obtaining adult cells from murine brain or cells from human tissue is best achieved using gentle dissociation techniques. Enriched cell populations can then be generated by FCM or MACS®, yet reduced cell viability, yield, and Ab availability need to be considered. CyTOF also offers a high-throughput technique for analyzing cells of myeloid origin including microglia on a single-cell level. For mouse tissue, reporter lines are a valuable tool for FCM sorting of specific cell populations. When interested in isolating more than one cell type, immunopanning is a suitable method since all cells are sequentially purified from whole brain suspensions [1693]. Neuron isolation of both adult murine

and human tissue remains challenging to this day. A suitable alternative when interested in gene expression or nuclear proteins/transcription factors is nuclei sorting via FCM, which also is applicable to immunolabeled neurons and methods such as single-nuclei RNA sequencing.

12.10 *Summary table (Table 75)*

Table 75. Selection of molecules that discriminate subpopulations of brain cells

Antigen	Cells targeted	Species reactivity	Cellular compartment	Company
ACSA-2	Astrocytes	Mouse	Cell surface	Miltenyi Biotec
SLC1A3 (GLAST/EAAT1)	Astrocytes + NSCs	Human, Mouse, Rat	Cell surface	Miltenyi Biotec
SLC1A2 (GLT-1/EAAT2)	Astrocytes + ependymal cells	Human, Mouse, Rat	Cell surface	Biorbyt
ITGAV (CD51)	Specific astrocyte populations	Mouse/Human	Cell surface	BD Biosciences/ Biolegend
CD63	Specific astrocyte populations	Mouse/Human	Cell surface	eBioscience/BD Biosciences
CD71	Specific astrocyte populations	Mouse, Human	Cell surface	BD Biosciences
GFAP	Astrocytes + NPCs	Human, Mouse, Rat	Intracellular	BD Biosciences
AQP4	Astrocytes + ependymal cells	Human, Mouse, Rat	Cell surface	Biorbyt
CD45	Microglia, macrophages, other leukocytes	Mouse, human	Cell surface	eBioscience
CD11b	Microglia, macrophages, other leukocytes	Mouse, human	Cell surface	eBioscience
CD68	Phagocytic microglia, macrophages	Mouse, human	Intracellular	eBioscience
CX3CR1	Microglia, NK cells, monocytes, dendritic cells and some macrophages	Mouse, human	Cell surface	Biolegend
Tmem119	Mature microglia	Mouse, human	Cell surface	Abcam
Iba-1 (AIF-1)	Microglia, macrophages, other leukocytes	Mouse, human	Intracellular	Abcam
NG2/AN2	OPCs	Human, Mouse	Cell surface	Miltenyi Biotec
CD140a (PDGFRα)	OPCs	Human, Mouse	Cell surface	Miltenyi Biotec
GalC/O1	Pre-myelinating and mature oligodendrocyte	Human, Mouse, Rat	Cell surface	Merck
O4	Pre-myelinating and mature oligodendrocytes	Human, Mouse, Rat	Cell surface	Miltenyi Biotec
MOG	Mature oligodendrocytes	Mouse, Rat	Cell surface	Merck
CNPase	Mature oligodendrocytes	Human	Cell surface	Merck
Nestin	NSCs	Human, Mouse, Rat	Intracellular	R&D systems
NeuN	Neurons	Human, Mouse, Rat	Nuclear	Merck
CD24	Neurons and peripheral cells	Human, Mouse, Rat	Cell surface	Biolegend
Thy-1	Neurons	Human	Intracellular	Biolegend
Tuj-1 (beta III tubulin)	Neurons	Human, Mouse, Rat	Intracellular	R&D systems

13 Cells from liver

13.1 *Overview*

The section gives a short introduction into the unique immunological milieu of the liver and the different hepatic immune cells of the innate and adaptive immune system. Moreover, this section provides detailed protocols for isolation and subsequent staining of hepatic immune cells from murine and human liver tissue.

13.2 *Introduction*

The liver is an organ that exerts both metabolic and immunological functions. Due to a dual blood supply, the liver receives blood from the hepatic artery as well as from the portal vein containing gut-derived food and microbial antigens. There are unique hepatic immune regulatory mechanisms, which induce tolerance against innocuous antigens including nutrients and microbiome-derived degradation products like LPS. The liver is a site of primary T-cell activation mediated by local conventional and unconventional antigen-presenting cells, such as liver sinusoidal endothelial cells, which promote tolerance by induction of T-cell anergy and apoptosis as well as generation and expansion of Tregs. The tolerogenic properties of the liver ensure the maintenance of local

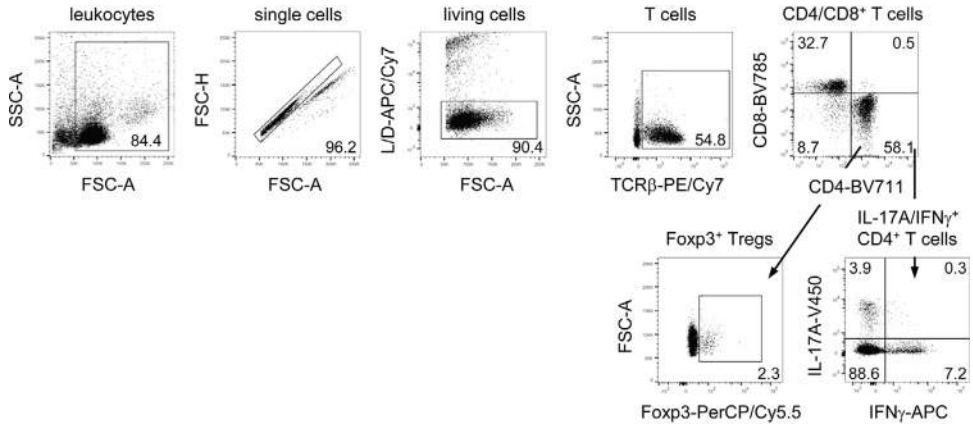

Figure 186. Gating strategy for T-cell populations in the murine liver. Hepatic leukocytes from *TNFR1*$^{-/-}$ x *Mdr2*$^{-/-}$ mice, which develop chronic liver inflammation, were used for analysis. Single cells were discriminated from doublets by plotting FSC-A against FSC-H. To exclude dead cells, a fixable dead cell staining was performed. Hepatic leukocytes were stained with anti-TCRβ-PE/Cy7 (H57-597; BioLegend), BV711 CD4 mAb (RM4-5; BioLegend), BV785 CD8 mAb (53-6.7; BioLegend), anti-Foxp3-PerCP/Cy5.5 (FJK-16s; ThermoFisher Scientific), anti-IL-17A-V450 (TC11-18H10; BD Pharmingen), and anti-IFNγ-APC (XMG1.2; ThermoFisher Scientific) Abs to distinguish between TCRαβ$^+$ CD4$^+$ T cells, TCRαβ$^+$ CD8$^+$ T cells, CD4$^+$ Foxp3$^+$ Tregs, and CD4$^+$ T cells expressing IFN-γ and/or IL-17A.

and systemic immune tolerance, but they also contribute to the persistence of hepatic viral infections and tumor metastasis. However, the liver is also able to mount effective immune responses against pathogens. The liver consists of parenchymal cells (hepatocytes and cholangiocytes) and non-parenchymal cells comprising liver sinusoidal endothelial cells, hepatic stellate cells, and various immune cell populations belonging to the innate and adaptive immune system. The quantitative and qualitative composition of hepatic immune cells markedly differs from secondary lymphoid organs. The majority of hepatic DCs display an inactive phenotype. Moreover, the liver contains the largest population of resident macrophages, termed Kupffer cells, and there is an increased proportion of hepatic NK cells, NKT cells, and γδ T cells compared to secondary lymphoid organs [1694–1698].

To study the complex network of hepatic immune cell populations in healthy and diseased liver, flow cytometric analysis is the best validated method. In this section, we provide detailed protocols for the isolation of leukocytes from murine and human liver as well as for surface and intracellular/intranuclear hepatic leukocyte staining. In the murine section, we further provide Ab panels for the analysis of T cells, Tregs (Fig. 186), NK cells, NKT cells, γδ T cells (Fig. 187), and macrophage subsets (Fig. 188). In the human section, we provide Ab panels for the analysis of NK cells (Fig. 189), T cells (Fig. 190), and myeloid cells (Fig. 191). The phenotypic markers in T-cell and NK-cell subsets, and monocytes and macrophages are summarised in Tables 75 and 76 respectively.

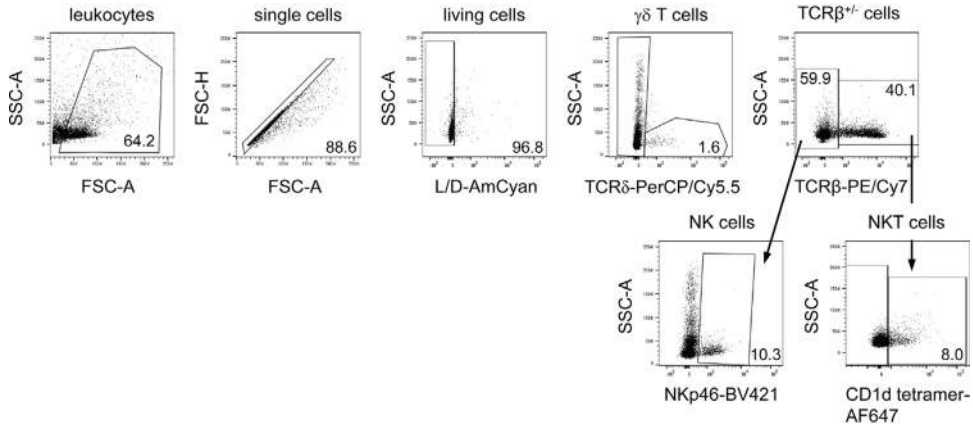

Figure 187. Gating strategy for NK cells, NKT cells, and γδ T cells in the murine liver. Hepatic leukocytes from *Mdr2*$^{-/-}$ mice, which develop chronic liver inflammation, were used for analysis. Single cells were discriminated from doublets by plotting FSC-A against FSC-H. To exclude dead cells, a fixable dead cell staining was performed. Hepatic leukocytes were stained with anti-TCRβ-PE/Cy7 (H57-597; BioLegend), anti-TCRδ-PerCP/Cy5.5 (GL3; BioLegend), anti-NKp46-BV421 (29A1.4; BioLegend), and CD1d tetramer-AF647 (NIH Tetramer Core Facility) Abs to distinguish between TCRαβ$^-$ TCRγδ$^+$ T cells, TCRαβ$^+$ CD1d tetramer$^+$ NKT cells, and TCRαβ$^-$ NKp46$^+$ NK cells.

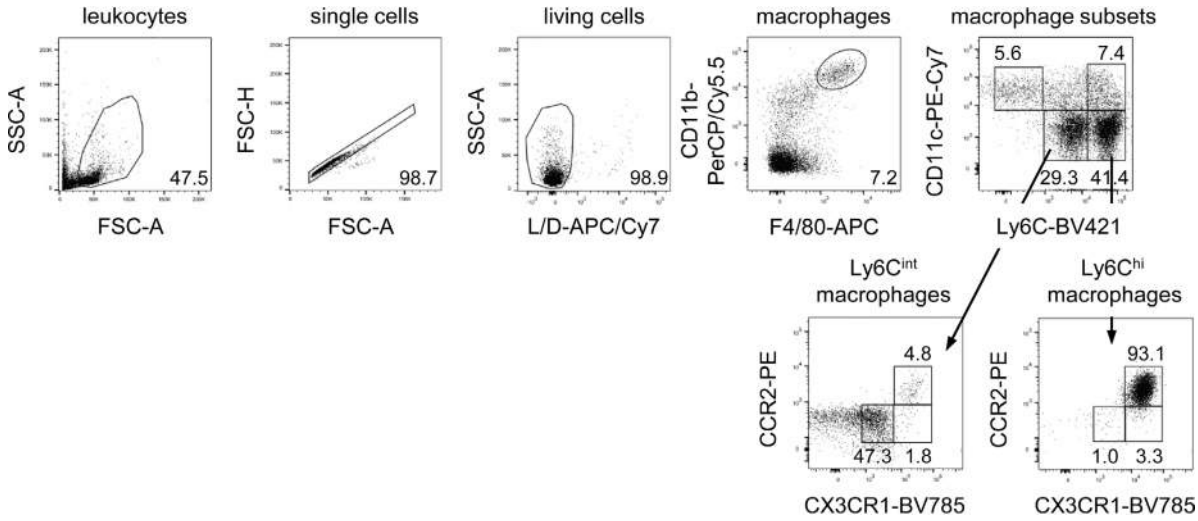

Figure 188. Gating strategy for macrophage subsets in the murine liver. Hepatic leukocytes from naive C57Bl/6 mice were used for analysis. Single cells were discriminated from doublets by plotting FSC-A against FSC-H. To exclude dead cells, a fixable dead cell staining was performed. Hepatic leukocytes were stained with PerCP/Cy5.5 CD11b mAb (M1/70; BioLegend), anti-F4/80-APC (BM8; BioLegend), PE/Cy7 CD11c mAb (N418; BioLegend), anti-Ly6C-BV421 (AL-21; BD Pharmingen), anti-CCR2-PE (475301; R&D Systems), and anti-CX3CR1-BV785 (SA011F11; BioLegend) Abs. CD11b$^+$ F4/80$^+$ macrophages can be further divided into CD11c$^-$ Ly6C^{int}, CD11c$^-$ Ly6C^{hi}, CD11c$^+$ Ly6C$^-$, CD11c$^+$ Ly6C^{int}, and CD11C$^+$ Ly6C^{hi} subsets, which differ from each other by distinct expression of the chemokine receptors CCR2 and CX3CR1.

13.3 *Murine*

13.3.1 Protocol for liver tissue harvest and leukocyte isolation.

Reagents

- 1× HBSS (for 1 L): 403 mg KCl, 53 mg $Na_2HPO_4 \times 2\ H_2O$, 54 mg KH_2PO_4, 353 mg $NaHCO_3$, 191 mg $CaCl_2 \times 2H_2O$, 102 mg $MgCl_2 \times 6\ H_2O$, 148 mg $MgSO_4 \times 7\ H_2O$, 8.006 g NaCl, 1.11 g D-glucose-monohydrate
  Add ddH_2O and adjust to pH 7.2–7.4; filtrate solution through 0.22 μm filter
- Liver Digest Medium (ThermoFisher Scientific)
- Liver Perfusion Medium (ThermoFisher Scientific)
- ACK-lysis buffer (for 1 L): 8.25 g NH_4Cl, 1 g $KHCO_3$, 29.2 mg EDTA
  Add ddH_2O and adjust to pH: 7.2-7.4
- Percoll^{TM}, density 1.130 g/mol (GE Healthcare)
- 10× PBS (for 1 L): 80 g NaCl, 11.6 g $Na_2HPO_4 \times 2H_2O$, 2 g KH_2PO_4, 2 g KCl
  add dH_2O and adjust to pH7.2–7.4; autoclave
- 7.5% $NaHCO_3$ in ddH_2O
- Heparin 5000 I: E/mL (Ratiopharm)
- ddH_2O
- Percoll solution A: 3.70 mL Percoll, 0.29 mL 10× PBS, 0.05 mL 7.5% $NaHCO_3$
- Percoll working solution (10 mL; for one liver): Add 6 mL HBSS and 0.2 mL Heparin to Percoll solution A and store it at room temperature
- 4% PFA

Equipment

- CO_2/O_2 vaporizer
- Styrofoam pad
- 70% EtOH v/v
- Half-curved blunt microsurgery scissors
- Curved forceps
- Falcon^{TM} Cell Strainer, 100 μm (Fisher Scientific)
- Petri dishes with scratched bottom

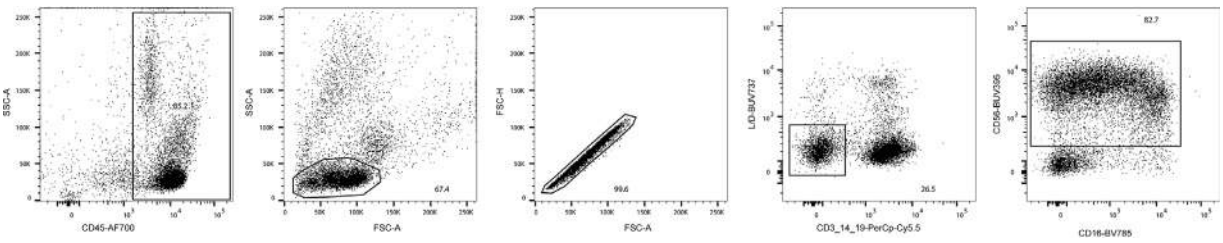

Figure 189. Gating strategy to identify NK cells in cells derived from the human liver. Hepatic leukocytes from individuals undergoing liver resection due to liver tumor metastases were used after leukocyte purification (see 16.3.1). Gating on CD45$^+$ cells (anti-human CD45; 2D1; AF700; Biolegend) was performed followed by standard leukocyte size gating and doublet exclusion. T cells, B cells, monocytes, and dead cells were excluded by employing a fixable dead cell staining (LIVE/DEAD Blue; Invitrogen) as well as Abs against CD3 (anti-human CD3; UCHT1; PerCP-Cy5.5; Biolegend), CD14 (anti-human CD14; HCD14; PerCP-Cy5.5; Biolegend), and CD19 (anti-human CD19; HIB19; PerCP-Cy5.5 Biolegend). CD56 (anti-human CD56; HCD56; BUV395, BD Biosciences) and CD16 (anti-human CD16; EG8; BV785; Biolegend) were used to identify NK cells.

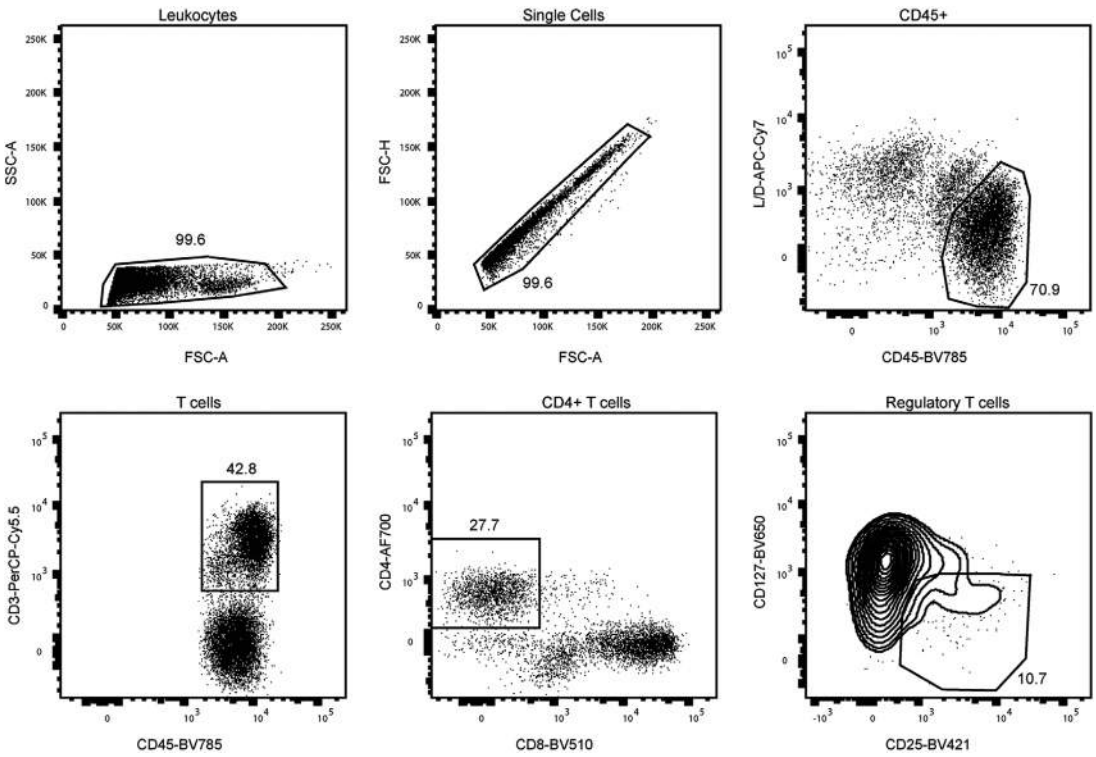

Figure 190. Gating strategy to identify T cells in cells derived from the human liver. Hepatic leukocytes from individuals undergoing liver resection due to liver tumor metastases were used without leukocyte purification (see 16.3.1). Leukocytes were exported in and subsequently analyzed. Gating on standard leukocyte sized cells, followed by doublet exclusion and gating on CD45$^+$ cells (anti-human CD45; HI30; BV785; Biolegend). CD3$^+$ T cells (antihuman CD3; OKT3; PerCP-Cy5.5; Biolegend) and subsequently CD4$^+$ and CD8$^+$ (anti-human BV510; RPA-T8; BV510; Biolegend) T cells were identified. Finally, regulator T cells were identified through CD127 (antihuman CD127; A019D5; BV650; Biolegend) and CD25 (antihuman CD25; BC96; BV421; Biolegend). We would like to thank Tobias Poch and Gloria Martrus for providing the T cell and myeloid cell flow plots.

- 50 mL centrifugation tube
- 15 mL centrifugation tube
- 2 mL syringes
- Centrifuge (Eppendorf 5810R)
- Optional:
  - Histology cassettes
  - 1.5 mL centrifugation tubes with safe lock
  - Liquid nitrogen

Procedure

- Place the mice into the CO_2/O_2 vaporizer and anesthetize by gently flowing the chamber*
- Once the mice are anesthetized, euthanize the animal by cervical dislocation, and confirm death
- Place the mouse on a styrofoam pad with the ventral side upward and fix the animal
- Spread the abdomen with 70% EtOH and open the abdomen by making an incision in the cranial direction
- Flap the skin to the side and fix with a needle
- Take blood by cardiac puncture (~1 mL) to prevent contamination with peripheral blood cells Alternatively, the liver can be perfused in situ as described in Blom et al. [1699]
- Push the intestine sideward by using the blunt end of a forceps to get access to the liver
- Optional: if no blood sampling is required, in situ perfusion of the liver is recommended, using liver perfusion media or PBS
  - Perfuse the liver by gently injecting Liver Perfusion Media or PBS into the vena cava
  - The liver becomes blanched and swollen
  - Cut the portal vein, once the liver is swollen. Blood and media should visibly flow from the vein
  - Continue perfusion with a total volume of 10 mL
- Remove the gall bladder**
- Remove the liver and transfer it into 5 mL HBSS; store at room temperature
- Discard the HBSS and transfer the liver on a scribed petri dish
- Homogenize the liver by rubbing over the scribed surface using the pistil of a 2 ml syringe
- Fill ~5 mL of HBSS (room temperature) into the petri dish and transfer the homogenate into a 100 μm cell strainer placed on a 50 mL centrifugation tube. Alternatively, digestion of smashed liver tissue might improve cellular recovery, especially from fibrotic or cirrhotic livers as this procedure degrades extracellular matrix components, to which immune cells might adhere.
  - If choosing liver digestion, take up the smashed homogenate in 10 mL Liver Digest Medium and transfer it into a fresh 50 mL centrifugation tube
  - Incubate the cells for 30 min at 37°C
- Mince the homogenate through the cell strainer and wash with HBSS (room temperature) thereby removing fatty debris

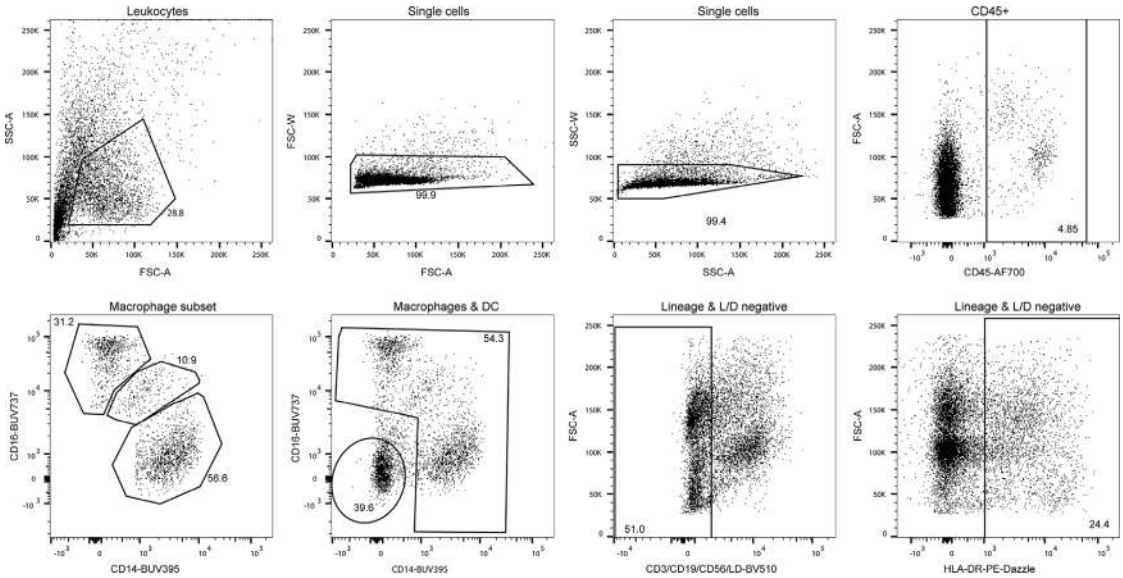

Figure 191. Gating strategy to identify myeloid cells in cells derived from human liver. Hepatic leukocytes from individuals undergoing liver resection due to liver tumor metastases were used without leukocyte purification (see 16.3.1). Gating on standard leukocyte sized cells, followed by doublet exclusion and gating on CD45$^+$ cells (antihuman CD45; HI30; AF700; Biolegend). Gating on HLA-DR$^+$ cells (antihuman HLA-DR; L243; PE-Dazzle; Biolegend) followed by lineage (antihuman CD3; UCHT1; BV510/antihuman CD19; HIB19; BV510/antihuman CD56; HCD56; BV510; all Biolegend) and L/D negative gating. Finally macrophages, dendritic cells and macrophage subsets were identified using CD14 (antihuman CD14; MΦP9; BUV395; BD Biosciences) and CD16 (antihuman CD16; 3G8; BUV737; BD Biosciences). We would like to thank Tobias Poch and Gloria Martrus for providing the T cell and myeloid cell flow plots.

- Fill up with HBSS to ~20–25 mL and centrifuge for 5 min at 500 × *g*, room temperature
- Carefully discard the supernatant and re-suspend the pellet in 10 mL 37% Percoll working solution
- Transfer the Percoll suspension into a 15 mL centrifugation tube and centrifuge for 20 min at 800 × *g*, room temperature
  Caution: Switch off the brake to assure proper assembly of the different phases
- Leukocytes and erythrocytes are pelleted on the bottom of the tube. Remove the upper, light brown layer, which contains hepatocyte debris and carefully discard the supernatant
- For erythrocyte lysis, re-suspend the pellet in 3 mL ACK-lysis buffer and transfer the suspension into a fresh 50 mL centrifugation tube
- Incubate the cells for 3 to 5 min at room temperature and stop the reaction by adding 12 mL cold HBSS
- Centrifuge for 5 min at 500 × *g*, 4°C
- Discard the supernatant and re-suspend the pellet in 1 mL cold HBSS
- Determine the cell number
- Centrifuge for 5 min at 500 × *g*, 4°C
- Discard the supernatant and re-suspend the pellet in an appropriate volume of HBSS, depending on the amount of FCM-panels, which are designated for analysis***

*If whole blood is required for analysis of hepatic enzyme activity, euthanize the animals by intravenous injection of a mixture of ketamine (120 mg/kg), xylazine (16 mg/kg), and heparin (8333 I:E/kg). Harvest blood by cardiac puncture as this allows a high yield and does not interfere with subsequent procedures such as liver perfusion. Caution: This treatment requires a specific approval according to national laws and institutional regulations.

**If liver tissue is used for histology (i) or RNA isolation (ii), take little pieces for each procedure prior to removal of the liver.

(i) Cut a piece of 1–2 cm^2 and transfer into a histology cassette; fix tissue in 4% PFA
(ii) Cut 2 to 3 small pieces of liver tissue and transfer into a 1.5 mL centrifugation tube with safe lock; immediately shock freeze tissue in liquid nitrogen and subsequently store the samples at -20°C***200 µL HBSS per FCM panel is recommended. Caution: For analysis of cell populations with rare frequency, such as ILCs, a maximum of three different FCM panels per liver is recommended.

13.3.2 Protocol for hepatic leukocyte staining. Reagents

- 1× PBS, optional 1× PBS/1% FCS (v/v)
- RPMI 1640 media (ThermoFisher Scientific)
- PMA, ionomycin, brefeldin A (all Sigma Aldrich), monensin (BioLegend)
- TruStain FcX™ (anti-mouse CD16/32) Antibody (Fc-receptor blocking solution; BioLegend)
- LIVE/DEAD™ Fixable Red Dead Cell Stain Kit or LIVE/DEAD™ Fixable Aqua Dead Cell Stain Kit (both ThermoFisher Scientific)
- Antibodies (see staining panels)
- Foxp3/Transcription Factor Staining Buffer Set (ThermoFisher Scientific)
- ddH_2O

Equipment

- 96-well microtiter plate, v-bottom (Nunc™)
- Centrifuge (Eppendorf 5810R)
- FCM tubes
- Flow cytometer BD LSR Fortessa™
    - Laser: violet (405 nm), blue (488 nm), green (561 nm), red (640 nm)
    - Filter: 530/30(488) for FITC and AF488, 695/40(488) for PerCP/Cy5.5, 780/60(561) for PE/Cy7, 582/15(561) for PE, 780/60(640) for APC/Cy7, 670/14(640) for APC and AF647, 450/50(405) for BV421 and V450, 525/50(405) for AmCyan, 710/50(405) for BV711, 785/60(405) for BV785

Procedure

Note: the following protocol is described in the absence of protein carrier such as FCS. However, the addition of protein carrier (i.e., 1% FCS (v/v)) to the blocking and extracellular staining solutions might improve cellular vitality and reduce unspecific binding of the respective Abs.

- Transfer the cells into a 96-well microtiter plate
- Centrifuge for 5 min at 500 × *g*, 4°C; discard supernatant
- Prepare a working solution of 5 μg/mL Fc-receptor block in 1× PBS and store it at 4°C*
- To block unspecific Ab binding, incubate the cells in 50 μL Fc-receptor blocking solution/well for 10 min at 4°C
- Fill 150 μl 1× PBS to each well and centrifuge for 5 min at 500 x g, 4°C; discard supernatant
- For detection of death cells, prepare a live/dead staining solution in 1× PBS*
- Add 50 μL live/dead staining solution/well and re-suspend the cells
- Incubate for 30 min at 4°C in the dark**
- Fill 150 μL 1× PBS/well and centrifuge for 5 min at 500 × *g*, 4°C; discard supernatant
- For detection of surface molecules, prepare an Ab solution in 1× PBS* and re-suspend the cells in 50 μL Ab solution/well
- Incubate for 30 min at 4°C in the dark
- Fill 150 μL 1× PBS/well and centrifuge for 5 min at 500 × *g*, 4°C; discard supernatant
- Repeat the washing step
- If no intracellular staining is required, take up the cells in 150 μL PBS/well and proceed to flow cytometric analysis
- Note: For detection of cytokines and transcription factors, an intracellular and intranuclear Ab staining is required. For cytokine expression analysis, a re-stimulation of cells is recommended prior to cell staining. Incubate the cells in RPMI 1640 medium supplemented with 10% FCS, PMA (20 ng/mL) and Iono (1 μg/mL) for 5 h. After 30 min, add brefeldin A (1 μg/mL) and/or monensin (2 μM) to the cell culture medium.
  Monensin impairs protein secretion by blocking the Na^{++}/H^{+} transport from the Golgi apparatus while brefeldin A causes a re-shuttling of proteins from the Golgi apparatus to the endoplasmic reticulum. Overall, this results in intracellular aggregation of proteins and thus, cellular stress, which might impact cellular viability. Although both methods allow subsequent analysis of produced cytokines, it is recommended to do previous literature search in order to select the respective transport inhibitor for the specific cytokine.
- Prepare a Fixation/Permeabilization working solution by mixing 1 volume Fixation/Permeabilization concentrate with three volumes Fixation/Permeabilization diluent (Foxp3/Transcription Factor Staining Buffer Set)
- Add 100 μL Fixation/Permeabilization working solution/well, immediately re-suspend the cells and incubate for 30 min at 4°C in the dark***
- Prepare 1× Permeabilization Buffer by mixing one volume 10× Permeabilization buffer (Foxp3/ Transcription Factor Staining Buffer Set) with nine volumes ddH_2O
- Fill 150 μL 1× Permeabilization Buffer/well and centrifuge for 5 min at 500 × *g*, 4°C***; discard supernatant
- Repeat the washing step
- Prepare an antibody solution in 1x Permeabilization Buffer and re-suspend the cells in 50 μl Ab solution/well
- Incubate for 30 min at 4°C in the dark***
- Add 150 μl 1× Permeabilization Buffer/well and centrifuge for 5 min at 500 × *g*, 4°C; discard supernatant
- Repeat the washing step
- Take up the cells in 150 μL 1× PBS and proceed to flow cytometric analysis or store at 4°C in the dark. The staining is stable for at least three days.
- Prior to acquisition, re-suspend the cells in the 96-well microtiter plate and transfer them into flow cytometry-tubes supplemented with 150 μl 1x PBS

*Solution can be prepared on the day before and stored at 4°C in the dark

**To our experience, LIVE/DEAD™ Fixable Red Dead Cell Stain Solution can be directly added to the antibody cocktail without an additional incubation step. However, we cannot recommend this for the LIVE/DEAD™ Fixable Aqua Dead Cell Stain Solution.

***Incubation at 4°C is approved for detection of Foxp3 and cytokines. If staining of other transcription factors, such as T-Bet, Eomes, GATA3, or RORγt is required, all incubation and washing steps should be performed at room temperature.

13.4 *Human*

13.4.1 Protocol for hepatic leukocyte isolation. Reagents

- OptiPrep Density Gradient Medium (e.g., Sigma–Aldrich)
- R10 (RPMI+10% FBS+1% Pen/Strep)
- PBS or HBSS
- ACK Lysing Buffer (e.g., Biozym)
- Freezing solution (90% FBS+10% DMSO)

Equipment

- Petri dish

- Tweezers
- Scalpel
- gentleMACS®
- gentleMACS® tubes
- Cell strainers (300/200/100/70/40 μm)
- 15/50 mL conical tubes
- 1.5 mL Eppendorf tubes
- Cryo tubes
- 10 mL syringes

Procedure

Sample preparation

- Obtain fresh liver tissue and transport on 4°C to the lab for further downstream processing immediately[a]
- Weigh liver piece in petri dish
- Cut Liver into pieces of ~5 × 5 × 5 mm
- Split up into —four to six C-Tubes[b] (in general 5 g per C-Tube works best)
- Add 1–2 mL of R10

Mechanical dissociation

- Put tubes onto gentleMACS® (should go in easy) and hash for 36 s[c]
- Remove tubes from machine (do not twist!)
- Remove pieces stuck in hashing blades with a pipette tip
- Repeat procedure five times

Serial Filtering

- Pour contents through 300 μm strainers into a 50 mL conical and push hashed liver through filter carefully with the plunger of a syringe
- Pour the 300 μm filtered content through a 200 μm cell strainer into a new 50 mL conical
- Pour the 200 μm filtered content through a 100 μm cell strainer into a new 50 mL conical
- Pour the 100 μm filtered content through a 70 μm cell strainer into a new 50 mL conical
- Pour the 70 μm filtered content through a 40 μm cell strainer into a new 50 mL conical
- Fill up to 50 mL with PBS or Hank's

Sample assessment

- Centrifuge 10 min/500 × *g*/room temperature, discard supernatant
- Resuspend pellet in 10 mL of R10
- Count cells[d,g]
- Move on to lymphocyte purification

Lymphocyte purification

- Distribute the (remaining, see [d]) cells into 50 mL conicals (1 tube per ~10^9 cells)
- Fill up to 50 mL with PBS/Hank's
- Centrifuge 4 min/40 × *g*/room temperature
- Transfer supernatant carefully with 25 mL Pipette to 50 mL conical, discard pellet
- Fill up to 50 mL with PBS/Hank's
- Centrifuge 4 min/40 × *g*/room temperature
- Transfer supernatant carefully with 25 mL Pipette to 50 mL conical, discard pellet
- Fill up to 50 mL with PBS/Hank's
- Centrifuge 4 min/500 × *g*/room temperature
- Discard supernatant
- Fill up to 50 mL with PBS/Hank's
- Centrifuge 4 min/500 × *g*/room temperature
- Discard supernatant
- Resuspend each pellets in PBS at a final volume of 4.5 mL
- Pipette 25 mL of OptiPrep™* (2.5 mL each) into 15 mL conicals (1 tube per ~10^9 cells)
- Add the 4.5 mL of cell suspension per tube and mix it by carefully pipetting up and down (avoid any bubbles)
- Layer 1 mL of PBS above the OptiPrep suspension
- Centrifuge 20 min/400 × *g*/room temperature **without brake**[e]
- Carefully take erythrocyte/leukocyte containing interphases and pool them
- Fill up to 50 mL with PBS/Hank's
- Centrifuge 4 min/500 × *g*/room temperature → discard supernatant
- Resuspend pellet (redish) in 3 mL ACK lysis buffer and incubate for 3 min/room temperature
- Fill up to 50 mL with PBS/Hank's
- Centrifuge 5 min/500 × *g*/room temperature discard supernatant
- Resuspend pellet (should be white) in 10 mL R10
- Count cells

Move forward to perform either direct staining's of the isolated leukocytes or cyro preserve[f,g] them for later use

[a]If liver tissue is used for histology (i) or RNA isolation (ii), take little pieces for each procedure prior to weighting the tissue depending on the size we would recommend storing tissue pieces in

(i) In 4% PFA as well as Tissue-Tek™ (depending on the planned procedures)
(ii) In cyro-tubes and freeze immediately at –80°C

[b]For the mechanical dissociation of the tissue, we use a gentleMACS™ Octo Dissociator, other means of mechanical dissociation could also be viable, but have not been tested with this procedure.

[c]We refrain from using any enzymes during the mechanical dissociation as in our experience this leads to alterations in or loss of expression of surface proteins (e.g., CD56) without leading to improvements in cell yield or higher viability

[d]Depending on cell yield storing 10 aliquots of 1.5 × 10^7cell in 1 mL of freezing medium can be performed. The following procedure has been tested:

- Centrifuge 1.5 × 10^8 cells at 5 min/500 × *g*/room temperature, discard supernatant

- Resuspend pellet in freezing medium for a final concentration of 1.5×10^7 cells/mL
- Pipette cells into 10 cryo tubes
- Put tubes into precooled stratacooler (4°C) and store at –80°C for 24 h before transferring into liquid nitrogen

[e]Adhering to basic density centrifugation protocol is relevant for this step. Use minimum acceleration and no brakes on the centrifuge.

[f]Cyro preservation of isolate leukocytes can be performed at this step (see also [d]):

- Centrifuge 5 min/500 × *g*/room temperature discard supernatant
- Resuspend pellet in freezing medium for a final concentration of 1×10^7 cells/mL
- Pipette cells into cryo tubes (1 mL each)
- Put tubes into precooled stratacooler and store at –80°C for 24 h before transferring into liquid nitrogen

[g]Cells stored at these points have been successfully used for both phenotypical as well as functional analysis. When using cells stored without leukocyte purification step[d], we advise using a method of depleting dead cells (e.g., EasySep™ Dead Cell Removal (Annexin V) Kit) as well as resting the cells before functional assessment.

13.4.2 Protocol for hepatic leukocyte staining. Reagents

- 1× PBS
- LIVE/DEAD™ Fixable Dead Cell Stain Kit
- Antibodies (see staining panels)
- Foxp3/Transcription Factor Staining Buffer Set (or comparable)
- ddH_2O

Equipment

- 96-well microtiter plate, u- or v-bottom
- Centrifuge
- FCM tubes
- Flow cytometer BD LSR Fortessa™
    - Laser: ultraviolet (355), violet (405 nm), blue (488 nm), green (561 nm), red (633 nm)
    - Filter: 740/35, 380/14 for 355; 780/60, 710/40, 675/50, 610/20, 586/15, 525/50, 450/50 for 405; 710/40, 530/30, 488/10 for 488; 780/60, 670/30, 610/20, 586/15 for 561; 780/60. 730/45, 670/14 for 633

Procedure

Continued from 16.3.1 or after thawing of cryo-preserved samples

Surface staining

- Transfer the cells into a 96-well microtiter (preferably u- or v-bottom) plate
- Centrifuge for 5 min/500 × *g*/room temperature, discard supernatant
- Fill add 150–200 µL 1× PBS to each well and centrifuge for 5 min at 500 × *g*, discard supernatant
- For detection of surface molecules, prepare an Ab master mix in PBS and re-suspend the cells in 100 µL Ab solution/well[a,b]
- Incubate for 30 min/4°C in the dark
- Fill 150–200 µL PBS/well and centrifuge for 5 min/500 × *g*/room temperature, discard supernatant
- Repeat the washing step
- Resuspend the cells in 150 µL PBS/well and proceed to flow cytometric analysis[c]

Intracellular staining[d]

- Add 100 µL of Fixation/Perneabilization working solution per well, resuspend the cells, and incubate for 30 min at 4°C in the dark[e]
- Add 150 µL 1× Permeabilization Buffer/well and centrifuge for 5 min/500 × *g*/4°C; discard supernatant
- Repeat the washing step
- Prepare the Ab solution for intracellular staining in Permeabilization Buffer and re-suspend the cells in 100 µL Ab solution/well
- Incubate for 30 min at 4°C in the dark
- Add 150 µL Permeabilization Buffer/well and centrifuge for 5 min/500 × *g*/4°C; discard supernatant
- Repeat the washing step
- Resuspend the cells in 150 µL PBS/well and proceed to flow cytometric analysis, alternatively stained cells can be keep at 4°C in the dark

[a]The use of Ab master mixes is recommend, these can be prepared either fresh before the experiments or prepared beforehand and stored at 4°C in the dark. Preparation beforehand should be tested and validated against freshly prepared master mixes for each panel. The volume of the antibody master mix added might be modified based on panel size or cell numbers.

[b]In our experience, LIVE/DEAD Fixable Viability Dye's can be added directly to the Ab master mix and stained simultaneously. Alternatively, an additional staining and washing step can be included beforehand:

- For detection of death cells, prepare a live/dead staining solution in PBS
- Add 50 µL live/dead staining solution/well and re-suspend the cells
- Incubate for 30 min at 4°C in the dark
- Fill 150 µL PBS/well and centrifuge for 5 min/500 × *g*/4°C; discard supernatant

[c]Alternatively and depending on time-to-flow, we can recommend fixing the cells with 100 µL 4%PFA for 20 min at 4°C (or similar fixation reagents, e.g., BD CellFIX™) before washing once

and resuspending in 150 µL PBS. Keep stained cells at 4°C in the dark until proceeding to flow cytometric analysis

[d]For dection of cytotoxic properties, cytokines and transcription factors, an intracellular and intranuclear Ab staining is required. Some functional properties of immune cells might only be detectable after stimulation with the appropriate stimulus (e.g., target cells, cytokines). In general we add protein transport inhibitors containing Monensin and Brefeldin A (e.g., GolgiStop™ & GolgiPlug™, BD Bioscience) after 1 h of stimulation for the rest of the stimulation period.

[e]We have tested and successful used a number of different fixation and permeabilization reagents, e.g., BD Fixation/Permeabilization Solution Kit, eBioscience Intracellular Fixation & Permeabilization Buffer Set, FIX & PERM™ Cell Permeabilization Kit or Foxp3/Transcription Factor Staining Buffer Set (ThermoFisher Scientific). Following the provided protocols, all of those yield satisfying results. Depending on the panel and staining used testing of different reagents is recommend.

13.5 *Summary of immune cell subsets in murine and human liver*

Table 76. Phenotypic marker molecules of murine and human T-cell and NK-cell subsets according to references [1342, 1700–1703]

Mouse							Human						
Cell surface	CTL	T_h	T_{reg}	γδ	NK	NKT	Cell surface	CTL	T_h	T_{reg}	γδ	NK	NKT
CD45	+	+	+	+	+	+	CD45	+	+	+	+	+	+
CD3	+	+	+	+	−	+	CD3	+	+	+	+	−	+
CD4	−	+	+	+/−	−	+/−	CD4	−	+	+	+/−	−	−
CD8	+	−	−	+/−	−	−	CD8	+	−	−	+/−	−	−
CD25	+/−[i]	+/−[i]	+[i]	+	+/−[i]	−	CD25	+/−[i]	+/−[i]	+	+	+/−[i]	−
CD107a	+	−	−	−			CD107a	+	−	−	−	+/−[i]	−
CD127	+/−	+/−	+	+	−	+	CD127	+/−	+/−	+	+	−	+
CD1 specific	−	−	−	+	−	+	CD1 specific	−	−	−	+	−	+
FasL	+	−	−	−	+/−	−	FasL	+	−	−	−	−	−
NK1.1	−	−	−	+	+	+	CD56	−	−	−	+	+	+
NKp46	−	−	−	−	+	+	CD335	−	−	−	−	+	+
NKG2D	−	−	−	+	+	+	CD314	−	−	−	+	+	+
TCRαβ	+	+	+	−	−	+	TCRαβ	+	+	+	−	−	+
TCRγδ	−	−	−	+	−	−	TCRγδ	−	−	−	+	−	−
TRAIL	+	−	−		+	−	TRAIL	+	−	−	−	+	−
Surface activation/exhaustion markers													
CD44[ii]	+	+	+	+	−	+	CD45RO[ii]	+	+	+	+	−	+
CD69[iii]	+/−	+/−	+/−	+/−	−	−	CD69	+/−	+/−	+/−	+/−	+/−	−
CD62L[iv]	+/−	+	+/−	−	−	−	CD62L	+/−	+	+/−	−	−	−
PD-1[v]	+/−	+/−	+	+/−	+/−	+/−	PD-1	+/−	+/−	+	+/−	+/−	+/−
Secreted cytokines													
GZMB	+	−	−	+	+	+	GZMB	+	−	−	+	+	+
IFNγ	+	+	−	+	−	+	IFNγ	+	+	−	+	−	+
IL-5	−	+	−	−	−	−	IL-5	−	+	−	−	−	−
IL-10	−	−	+	+	−	+	IL-10	−		+	+	−	+
IL-13	−	+	−	−	−	+	IL-13	−	+	−	−	−	+
IL-17A	−	+	−	+	−	−	IL-17A	−	+	−	+	−	−
Perforin	+	−	−	+	+	−	Perforin	+	−	−	+	+	−
TNFα	+	+	−		−	+	TNFα	+	+	−		+/−[i]	+
Transcription factors													
Eomes	+	−	−	−	+	+	Eomes	+	−	−	−	+	+
Foxp3	−	−	+	−	−	−	Foxp3	−	−	+	−	−	−
GATA3	−	+[vi]	−	−	−	−	GATA3	−	+[vi]	−	−	−	−
RORyt	−	+[vi]	−	+	−	−	RORyt	−	+[vi]	−	+	−	−
T-bet	+	+[vi]	−	+	+	+	T-bet	+	+[vi]	−	+	+/−	+

[i]Expressed following activation; downregulated on effector Tregs
[ii]Low expression by naive T cells
[iii]Early activation marker
[iv]Expressed on naive and central memory T cells; downregulated on effector T cells
[v]Expressed by activated and/or exhausted T cells
[vi]Depending on Th subset

Table 77. Phenotypic marker molecules of murine and human monocyte and macrophage subsets according to references [1444, 1704–1707]

Mouse						Human					
Cell surface	Mo	M1	M2	KC	DC	Cell surface	Mo	M1	M2	KC	DC
CD45	+	+	+	+	+	CD45	+	+	+	+	+
CD11b	+	+	+	+	+/−	CD11b	+	+	+	+	+/−
CD11c	−	−	−	−	+	CD11c	+	+	−	−	+
CD80	−	+	+	low	+	CD80	−	+	+	low	+
CD86	+	+	+	−	+	CD86	+	+	+	−	+
CD206	+	−	+	+	+/−	CD206	+	−	+	+	+/−
F4/80	+	+	+	+	low	CD14	+	high	+	+	+/−
IL-4Rα	+	−	+	ND	ND	IL-4Rα	+	−	+	ND	−
Ly6c	+	high	low	low	+/−	CD16	+/−	−	high	+	−
MHC-II	+	+	+	+	+	HLA-DR	+	+	+	+	+
PDL-1	−	−	+	+	−	PDL-1	−	−	+	+	−
Chemokine receptors											
CCR2	+/−	+	+/−	−	−	CCR2	+/−	high	low	−	−
CCR5	+	+	+	ND	ND	CCR5	+	+	+	ND	−
CX_3CR_1	+/−	+/−	+	−	+/−	CX_3CR_1	−	low	high	−	+/−
Secreted cytokines											
IL-6	−	+	−	−	+	IL-6	−	+	−	−	+
IL-10	−	−	+	+	+/−	IL-10	−	−	+	+	+/−
IL-12	−	+	−	−	+	IL-12	−	+	−	−	+
TNF-α	−	+	−	−	+	TNF-α	−	+	−	−	+

Mo, monocytes; M1, inflammatory Mo-derived macrophages; M2, alternatively activated Mo-derived macrophages; KC, Kupffer cells; ND, not detected

13.6 *Pitfalls*

Albeit sampling of whole blood by cardiac puncture minimizes the risk of contamination, this can further be reduced by in situ perfusion of liver tissue prior to organ isolation. Additionally, incubation of liver homogenate in Liver Digest Medium may reduce intercellular junctions and thus, increase the total recovery of immune cells within the tissue. If choosing additional incubation in digestion medium, the incubation time should not be prolonged as this might impact cell viability and shed surface molecules from the cells of interest and thus, might cause false results during analysis.

13.7 *Top tricks*

If performing cellular stimulation for subsequent analysis of intracellular effector cytokines, the choice of the respective transport inhibitor should be considered. For instance, brefeldin A is recommended to block intracellular transport of murine IL-6, IL-12, or TNF-α, while monensin is recommended to impair secretion of IL-10, IL-5, or GM-CSF. Please compare the recommendations of pharmaceutical companies for the right choice of transport inhibitors.

14 Porcine cells

14.1 Overview. This chapter will introduce FCM for immune cells of the pig (*Sus scrofa*) with a strong focus on T-cell phenotypes and myeloid cells. Best practice staining examples and step-by-step sample preparations are provided, mainly for blood-derived cells. Protocols describe the isolation of porcine immune cells from blood and spleen, however, we advise to establish individual tissue dissociation protocols to account for age-, cell-, and organ-specific differences. Phenotypes of immune cells present in lymphatic and nonlymphatic organs are briefly described and referenced.

14.2 Introduction. Pigs represent an excellent model for various human diseases, in particular infectious diseases [1708]. Exploitation of the pig as human-relevant model but also the study of pig diseases requires a detailed knowledge of the pig's immune system and adequate detection tools. In contrast to SPF mice, but comparable to human individuals, conventionally raised pigs are exposed to persistent and non-persistent pathogens, diverse food and environmental antigens and are routinely vaccinated. Therefore, the pig's immune system undergoes similar priming processes as observed in humans.

For flow cytometric assessment of porcine immune cells, recent updates summarize available reagents reacting with porcine CD markers including pig-specific mAbs and polyclonal Abs, but also cross-reactive mAbs from different species [1709, 1710]. In addition, a website listing Abs specific

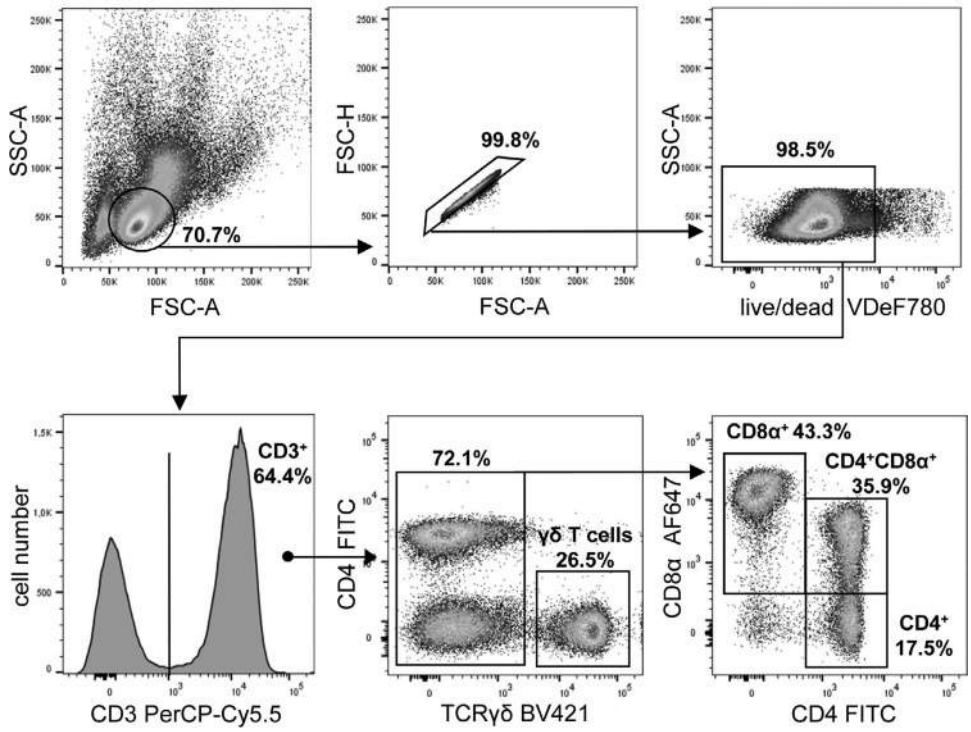

Figure 192. Identification of $CD4^+$, CD4CD8α double-positive, conventional $CD8^+$, and γδ T cells in porcine peripheral blood. Lymphocytes are identified based on the forward (FSC) and side (SSC) scatter. Single cells are discriminated from doublets by plotting FSC area against height. Dead cells are excluded by a viability dye and total $CD3^+$ T cells (mAb clone BB23-8E6-8C8) are gated further. γδ T cells are identified by mAb PPT16. Remaining T cells can be considered as αβ T cells (currently no TCR-αβ-specific mAb available). Within this subpopulation, cells can be distinguished on their expression of CD4 (mAb clone 74-12-4) with $CD4^+$ T cells separating into a $CD8\alpha^+$ population (mAb clone 11/295/33) and $CD8\alpha^-$ population. $CD3^+TCR\text{-}\gamma\delta^-CD4^-CD8\alpha^{high}$ cells represent conventional $CD8^+$ T cells. Data are generated from defrosted PBMC from an animal of approximately 6 months of age.

for porcine immune-related molecules (but also for cattle, sheep, goat, horse and chicken) has been launched in 2019 (https://www.immunologicaltoolbox.co.uk/). According to the human CD nomenclature, currently listing 419 human CD markers, 359 corresponding orthologous swine CD proteins have been identified [1710]. However, many CD orthologs have been identified based on genomic data, but still lack species-specific functional description or specific Abs and imply an urgent need for developing pig specific immune reagents. As a major remark, anti-human CD mAb cross-reactivity to porcine immune cell molecules should be experimentally defined (see Chapter VI Section 15 Cross-reactive Ab clones).

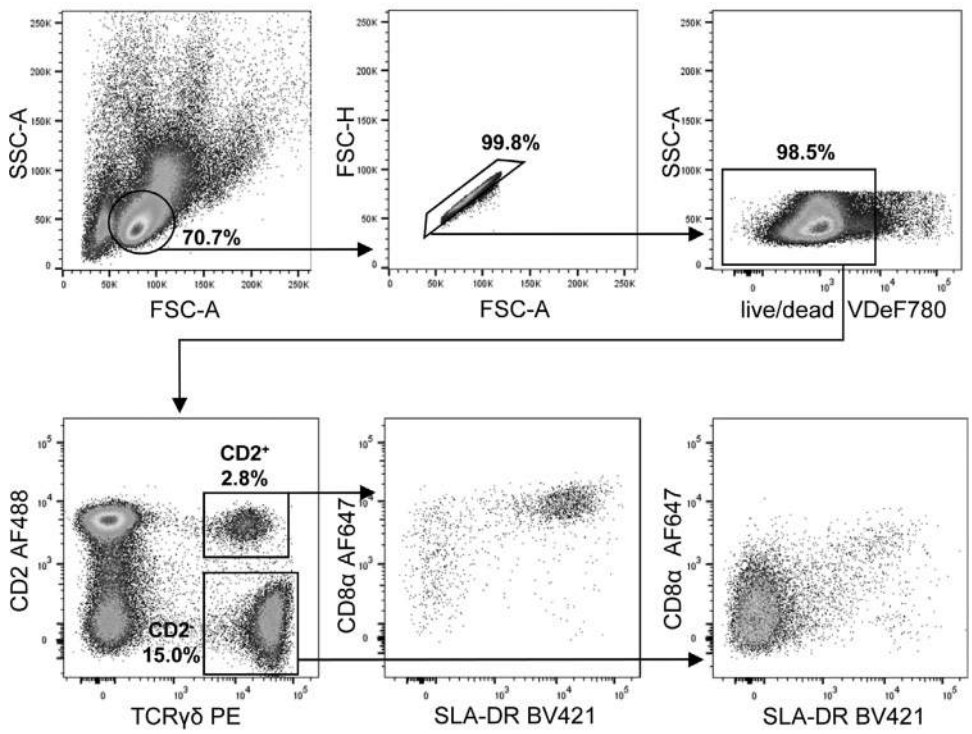

Figure 193. Identification of porcine γδ T-cell subpopulations in peripheral blood. Lymphocytes are identified based on the forward and side scatter. Single cells are discriminated from doublets by plotting FSC area against height. Dead cells are excluded by a viability dye. Two subsets of γδ T cells (mAb clone PGBL22A) can be distinguished in the pig by their CD2 expression (mAb clone MSA4). The majority of $CD2^+$ γδ T cells express CD8α (mAb clone 11/295/33) and SLA-DR (mAb clone MSA3). In contrast, the majority of $CD2^-$ γδ T cells have a CD8α/SLA-DR double-negative phenotype. Data is generated from defrosted PBMC from an animal of approximately 6 months of age.

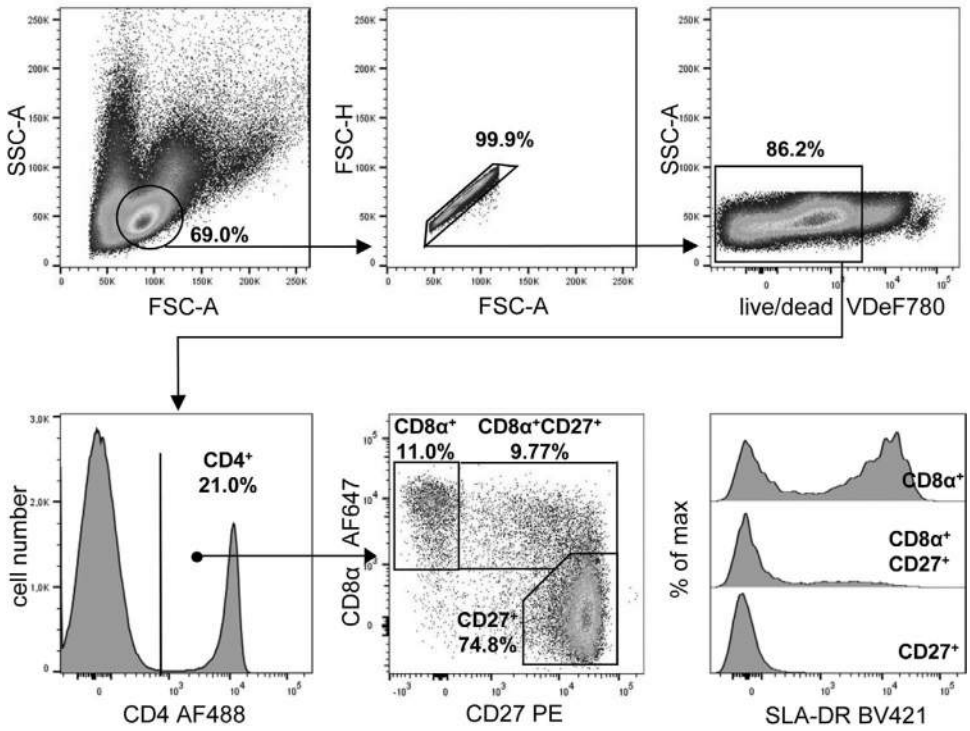

Figure 194. Identification of porcine $CD4^+$ T-cell subpopulations in peripheral blood. Lymphocytes are identified based on the forward and side scatter. Single cells are discriminated from doublets by plotting FSC area against height. Dead cells are excluded by a viability dye and cells were gated on $CD4^+$ cells (mAb clone 74-12-4) for further analysis. Naïve $CD4^+$ T cells are defined as $CD8\alpha^-$ $CD27^+$ (mAb clone CD8α 11/295/33; mAb clone CD27 b30c7), while $CD8\alpha^+CD27^+$ cells represent central memory cells and $CD8\alpha^+CD27^-$ effector memory cells in the pig. Different SLA-DR expression patterns (mAb clone MSA3) of the three subsets are shown in the histograms. Data is generated from freshly isolated PBMC from an animal of approximately 2.5 months of age.

Porcine CD marker expression as compared to humans and mice include several peculiarities such as

(i) The expression of CD8αα homodimers and MHC-II (swine leukocyte antigen-DR) molecules on activated or memory CD4 T cells [1711–1713],
(ii) Major subsets of NK cells that lack CD335 (NKp46) [1714],
(iii) Expression of CD33 on neutrophils and monocytes [1715],
(iv) Varying levels of CD45RA expression on plasmacytoid DCs (pDCs) [1716]
(v) Siglec-10 expression on B cells [1717].
(vi) The high abundance of peripheral γδ T cells, ranging from ~8 to 57% within total peripheral blood lymphocytes (PBL) [1718].

14.3 Porcine T cells. Porcine T cells from peripheral blood can be identified by gating on lymphocytes according to scatter, excluding doublets and dead cells and gating on $CD3^+$ cells. Compared to humans, pigs have a high proportion of circulating γδ T cells identified by mAbs recognizing the constant region of porcine TCR-δ chain or TCRγδ-associated CD3 molecules (Fig. 192). Pig γδ T-cell numbers are highest in young animals and decrease with age [1719]. The different porcine γδ T-cell subsets currently known are phenotypically divided based on CD2 expression into $TCR\gamma\delta^+CD4^-CD8\alpha^-CD2^-$ γδ T cells and $TCR\gamma\delta^+CD4^-CD8\alpha^{-/+}CD2^+$ γδ T cells [1720, 1721] (Fig. 193). Current studies suggest that similar to human γδ T cells, $CD2^+$ γδ T cells can be activated either in direct response to PAMPs via TLRs or upon APC interaction [1722, 1723], secrete various cytokines involved in pathogen defense analogous to porcine αβ T cells and partially express MHC-II molecules on their surface [1724] (Fig. 193). In addition, cytotoxic activity, antigen- and MHC-independent, is reported for $TCR\gamma\delta^+CD4^-CD8\alpha^{low}CD2^+$ γδ T cells (H. [1725, 1726]). The role of $TCR\gamma\delta^+CD4^-CD8\alpha^-CD2^-$ γδ T cells is less clear since those cells remain unresponsive for antigenic stimuli tested so far. More recently, it was shown that these cells express high levels of GATA-3, but the functional relevance of this phenotype is not clear yet [1727].

Porcine $CD4^+CD8\alpha^+$ T cells recall antigens in a MHC-II dependent manner and increase strongly in number over life time [1728, 1729]. CD8α expression on porcine Th cells is therefore perceived as marker for activated and memory T helper cells. While naïve, porcine Th cells are defined as $CD4^+CD8\alpha^-CD27^+$, differential expression of CD27 on $CD4^+CD8\alpha^+$ defines terminally differentiated effector memory cells ($CD4^+CD8\alpha^+CD27^-$) and central memory cells ($CD4^+CD8\alpha^+CD27^+$) (Fig. 194) [1713]. Additional markers that have been investigated to characterize differentiation of activated/memory Th cells are CD45RC and SLA-DR (MHC-II) but there is currently no unifying differentiation model based on all four molecules (i.e., CD8α, CD27, CD45RC,

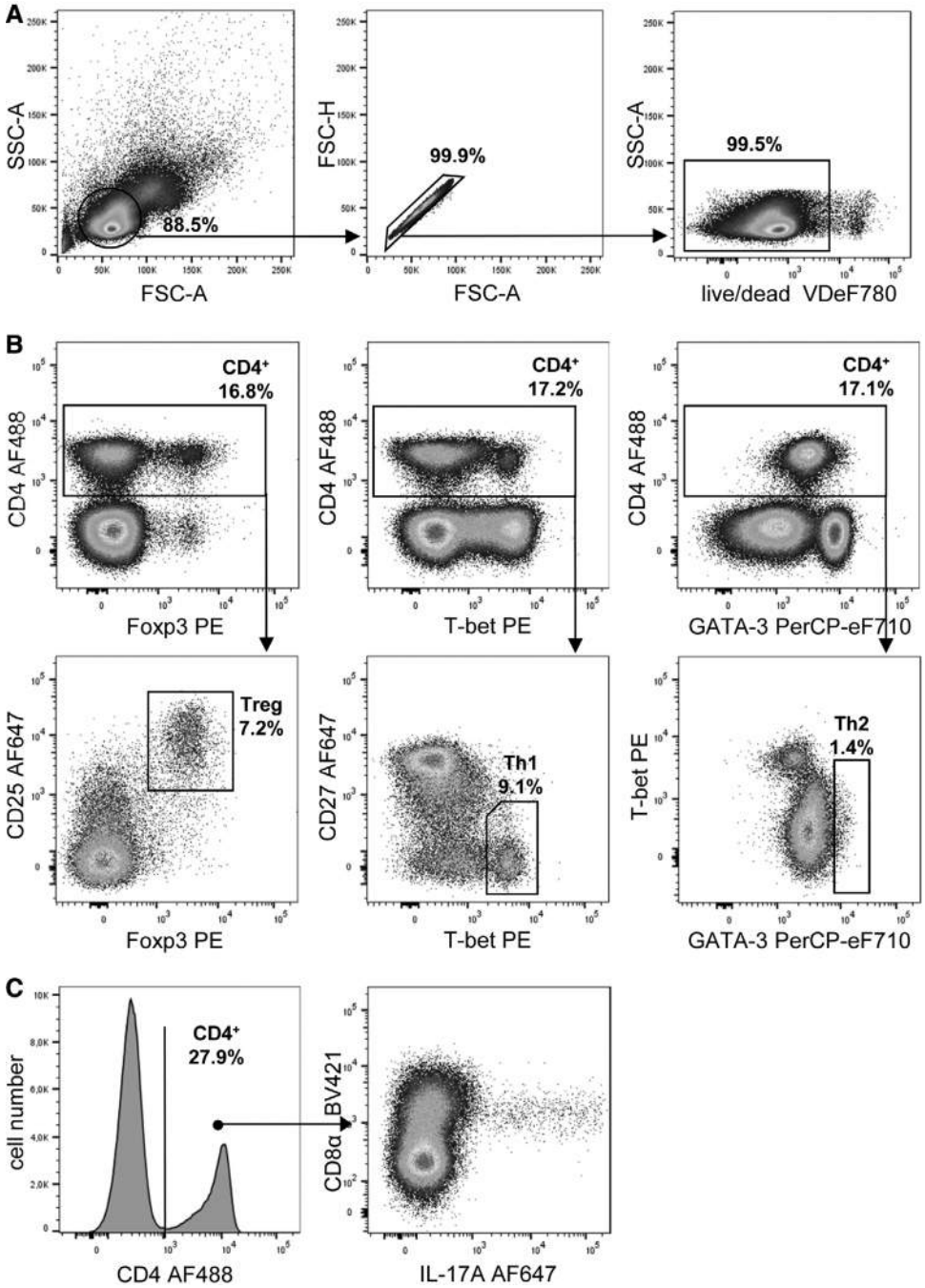

Figure 195. Functional subsets of porcine CD4$^+$ T cells can be identified based on expression of master transcription factors using cross-reactive mAbs developed against mouse and human. (A) Lymphocytes are identified based on the FSC and SSC. Single cells are discriminated from doublets by plotting FSC area against height. Dead cells are excluded by a viability dye. (B) Following surface staining of CD4 (mAb clone 74-12-4), cells were fixed and permeabilized to perform intranuclear transcription factor staining. Master transcription factors are used to identify distinct CD4$^+$ subsets: Tregs – Foxp3$^+$ (cross-reactive mAb clone FJK-16s) with CD25^{high} expression (mAb clone 3B2), Th1 – T-bet$^+$ (cross-reactive mAb clone 4B10) that are mainly negative for CD27 (mAb clone b30c7), Th2 –GATA- 3$^+$T-bet$^-$ (cross-reactive mAb clone TWAJ). (C) CD4$^+$ Th17 cells can be identified by their IL-17A expression (cross-reactive mAb clone SCPL1362) after PMA/ Ionomycin stimulation for 4 h. Data was generated from defrosted PBMC of healthy, uninfected pigs of approximately 6 months of age.

and SLA-DR) (Fig. 194). While all CD4$^+$ T cells have a CD27$^+$ phenotype in newborn piglets, a distinct subpopulation of CD45RC$^-$ cells could already be detected in neonates [1730].

Porcine CD4$^+$ T-cell subsets can be further discriminated using cross-reactive mAbs against master transcription factors. Treg cells are identified by Foxp3/CD25 co-expression [1731] (Fig. 195). T-bet expression correlates with the capacity for IFN-γ production and appears to be suitable to identify Th1 cells [1729]. GATA-3 expression is inducible in a subset of porcine CD4$^+$ T cells in vitro by ConA + IL-4 stimulation and in vivo after helminth

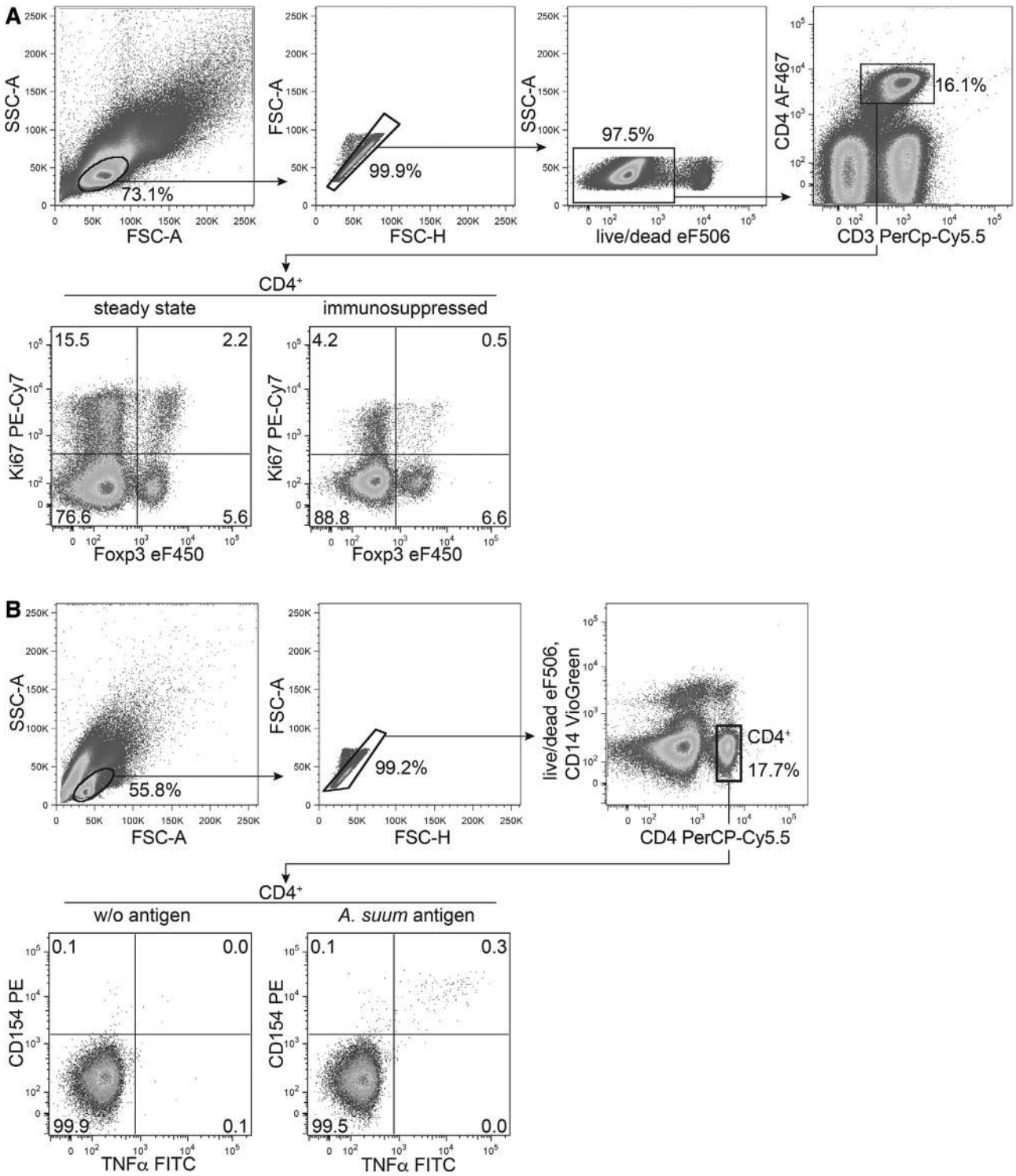

Figure 196. Proliferation- and activation-associated markers of porcine CD4$^+$ T cells. Porcine CD4$^+$ T cells are identified according to the gating strategies shown. (A) Nuclear staining of Ki-67 and Foxp3 using cross-reactive mAbs (mAb clone Ki-67 SolA15, mAb clone Foxp3 FJK-16s) before (left) and after (right) cyclophosphamide and methylprednisolone induced immunosuppression of a piglet aged 8 weeks. (B) PBL from an *Ascaris suum* infected pig (9 days post-infection) were subjected to short-term stimulation (7h) with *Ascaris suum* larval worm antigen (40 μg/mL) (right), or left untreated (left), followed by intracellular staining of CD154 (CD40L) using a cross-reactive mAb (mAb clone 5C8). Data is generated from fresh PBMC from an animal of approximately 3 month of age.

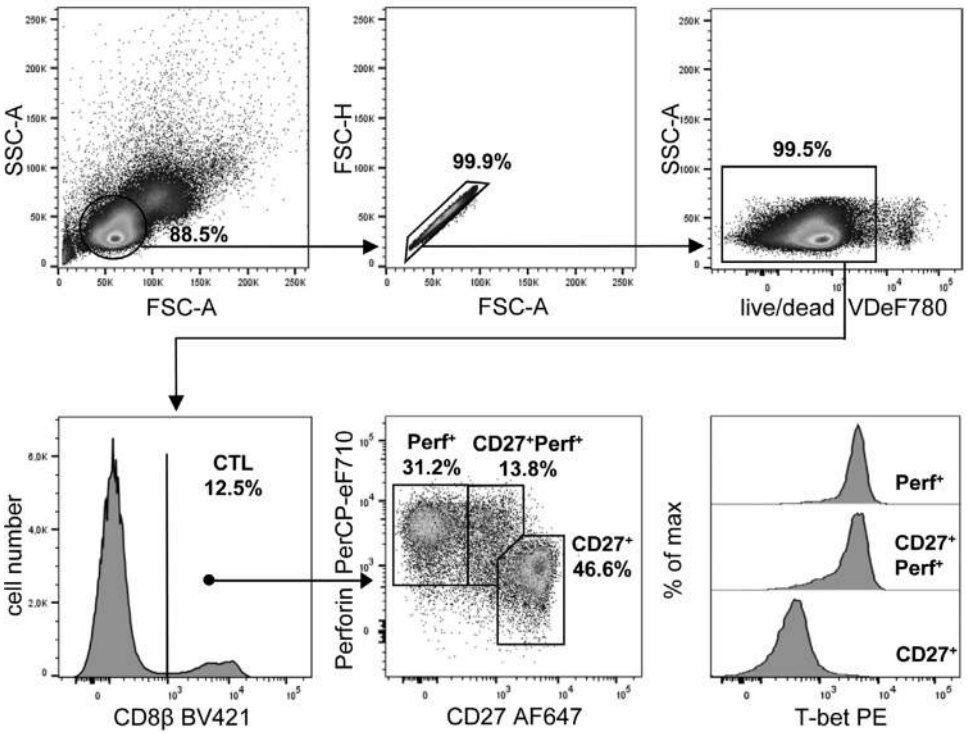

Figure 197. Identification of porcine $CD8^+$ T cells in peripheral blood. Lymphocytes are identified based on the forward and side scatter. Single cells are discriminated from doublets by plotting FSC area against height. Dead cells are excluded by a viability dye and porcine $CD8^+$ T cells are gated as $CD8\beta^+$ cells (mAb clone PPT23). Three subsets can further be identified on the basis of CD27 (mAb clone b30c7) and perforin expression (cross-reactive mAb clone δG9). Both, perforin$^+$CD27^{dim} and perforin$^+$CD27$^-$ $CD8^+$ T cells express T-bet. Data is generated from defrosted PBMC from an animal of approximately 6 months of age.

infection [1732]. However, in pigs kept under conventional housing conditions, the frequency of GATA-3$^+$ $CD4^+$ T cells is quite low. Instead, the majority of naïve $CD4^+$ T cells express low levels of GATA-3 (Fig. 195) [1729]. Th17 cells can be identified by intracellular cytokine staining with various cross-reactive anti-human IL-17A mAbs (Fig. 195 and Chapter VI 15). Nuclear staining using cross-reactive anti-mouse Ki-67 mAb identifies proliferating porcine cells [1733] (Fig. 196).

The CD4 T-cell activation marker CD154 (CD40L) is upregulated shortly (5–16 h) after TCR-dependent antigen encounter and is, also in porcine $CD4^+$ T cells, found to be co-expressed with cytokines [1734]. An anti-human cross-reactive mAb reactive to CD154 can be used to identify antigen-reactive porcine $CD4^+$ T cells by intracellular staining (Fig. 196) [1734].

In contrast to the abundant expression of CD8αα homodimers on subsets of $CD4^+$ and γδ T cells, porcine $CD8^+$ T cells with the capacity to differentiate into CTLs express CD8αβ heterodimers and hence can be identified by using mAbs against CD8β. Alternatively, they can be identified by a $CD3^+$TCR-γδ$^-$$CD4^-$ $CD8\alpha^{high}$ phenotype (Fig. 192). Perforin expression can be identified by cross-reactive anti-human mAbs and perforin expression has been suggested to identify antigen-experienced $CD8^+$ T cells. T-bet shows a clear positive correlation with perforin expression and ex vivo time course studies with aging pigs suggest that a lack of CD27 expression identifies terminally differentiated CTLs [1730] (Fig. 197).

Porcine T-cell development in the thymus follows the phenotypic pattern described in other vertebrates, with $CD4^-CD8\alpha^-$ thymocytes representing the most immature stage, followed by a $CD4^+CD8\alpha^+$ phenotype and further development into $CD4^+CD8\alpha^-$ and $CD4^+CD8\alpha^+$ thymocytes [1711, 1719]. The more immature phenotypes express high levels of GATA-3 [1729]. TCR-γδ T cells separate already in the thymus into a $CD2^+$ and $CD2^-$ subset [1735]. In lymph nodes, T cells with a naïve phenotype dominate, whereas in non-lymphatic organs effector (memory) phenotypes are enriched [1736]. Recently, tissue-resident memory T cells were described in porcine lung tissue and bronchoalveolar lavage [1737]. Abs for porcine CD103 are currently not available and pig-specific mAbs for CD69 were described just recently [1738] but are not yet commercialized. All reagents and Abs for porcine T-cell stainings shown in Figs. 192 to 197 are listed in Table 78.

14.4 Porcine NK cells and B cells. In contrast to NK cells in humans and mice, porcine NK cells are small dense lymphocytes [1739, 1740]. Porcine NK cells can be found within the $CD3^-CD16^+$ subset of lymphocytes, representing non-T and non-B cells. Up to date, no pan-NK cell marker exists in swine as the activating receptor NKp46 (CD335, NCR1) that is proposed as marker for NK cells across mammalian species [1741], is differentially expressed in pigs. Three distinct NK-cell subsets can be identified on the basis of their NKp46 expression: NKp46$^-$, NKp46$^+$, and $NKp46^{high}$ [1714, 1742] (Fig. 198). $NKp46^{high}$ NK cells are more abundant in spleen and non-lymphatic organs compared to blood and show a reduced or lacking expression of CD8α (dim/-) compared to the NKp46- and NKp46$^+$ $CD8\alpha^+$ subsets [1714, 1742, 1743]. All porcine NK-cell subsets express perforin, CD2, and CD27. For the latter, a positive correlation to

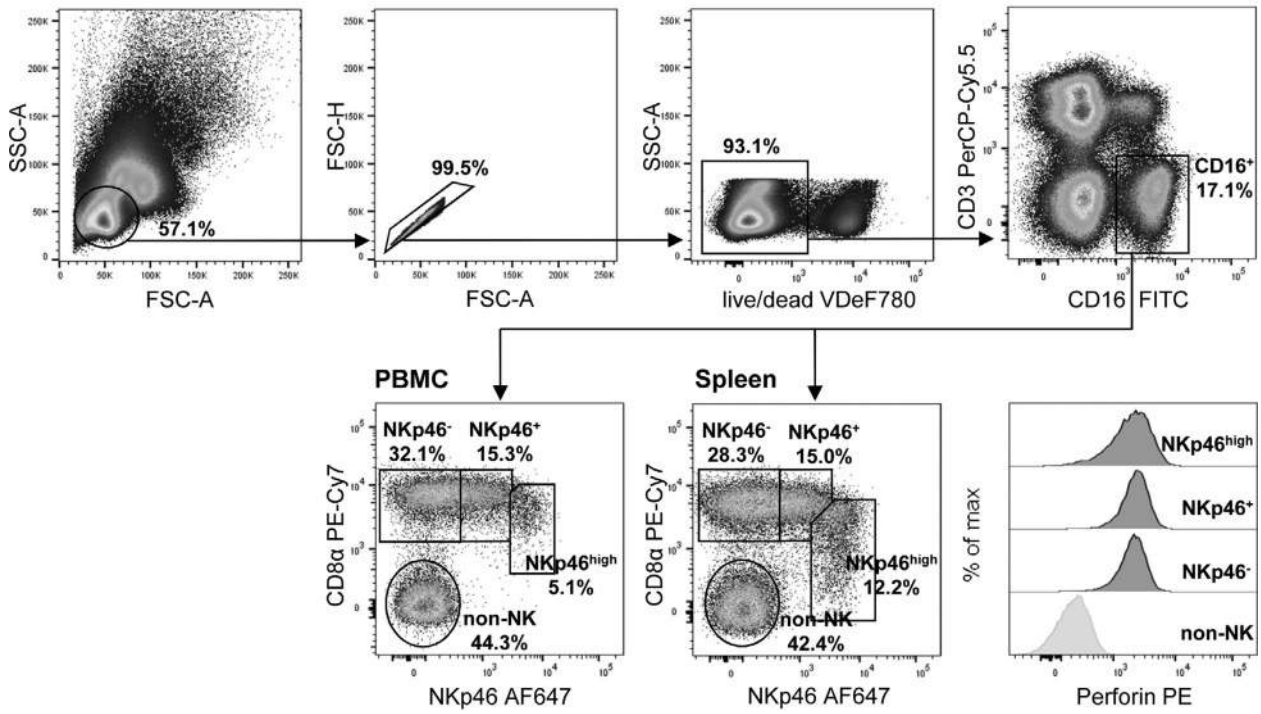

Figure 198. Identification of porcine NK cells in cells isolated from peripheral blood and spleen. Lymphocytes are identified based on the forward and side scatter. Single cells are discriminated from doublets by plotting FSC area against height and dead cells are excluded by a viability dye. $CD3^-CD16^+$ non-T and non-B cells (mAb clone CD3 B23-8E6-8C8; mAb clone CD16 G7) are further gated on three NK-cell subsets on the basis of their different CD8α (mAb clone 11/295/33) and NKp46 (mAb clone VIV-KM1) expression in blood as well as spleen. Perforin expression (cross-reactive mAb clone δG9) can be detected in all three NK-cell subsets in contrast to $CD8\alpha^-NKp46^-$ non-NK cells. Data is generated from defrosted PBMC and lymphocytes isolated from spleen of an animal of approximately 6 months of age.

NKp46 expression is described [1742]. In contrast to human NK cells that show a functional dichotomy of the $CD16^{bright}CD56^{dim}$ (higher cytotoxicity) and $CD16^{dim/-}CD56^{bright}$ (higher potential to produce cytokines) subsets, porcine $NKp46^{high}CD8\alpha^{dim/-}$ NK cells have the highest capacity for both functions [1742].

Up to date, a detailed phenotypic and functional analysis on porcine B cells is hampered due to the lack of a pan-B cell marker like CD19 as used in humans and mice. For the detection of total porcine B cells a cross-reactive mAb against CD79α can be used [1744] (Fig. 199). As the mAb recognizes a cytoplasmic epitope, fixation and permeabilization of the cells is required prior to CD79α staining with this mAb, excluding subsequent functional analyses with sorted B cells. Furthermore, no species-specific or cross-reactive mAbs for the identification of distinct functional B-cell subsets like transitional B cells and plasma cells/plasmablasts (e.g., CD38 and CD138) are available. In humans, CD27 is used to distinguish memory from naïve B cells, whereas in the pig, no CD27 expression was detected on B cells [1745]. Cross-reactive mAbs against CD21 have been used to distinguish more mature ($CD21^-$) from less mature B cells ($CD21^+$) in the pig [1746]. Monoclonal Abs against IgM, IgG, and IgA [1747] can also be used in FCM and recently IgM^+CD21^- B cells have been proposed to represent B1-like B cells [1748]. Interestingly, this cell population also express high levels of CD11R1 and CD11c, markers that are also found in high levels on myeloid cells [1748]. Intracellular staining for Ig-molecules, to identify plasma cells and memory B cells, has not been thoroughly applied yet in the phenotyping of porcine B cells. All reagents and Abs for porcine NK- and B-cell staining shown in Figs. 198 and 199 are listed in Table 79 and 80.

14.5 Porcine myeloid cells. Although common features are found between mononuclear phagocytes of mice, humans, and pigs, each species has its own features in terms of marker expression and subset function [1749]. Only recently, cross-species similarities were addressed by, e.g., cross-species transcriptome comparison [1750] and phenotypic differences were investigated at the protein and transcriptome level to identify different dendritic cell (DC) and macrophage subsets in swine [1751–1753].

The porcine equivalents of conventional DCs (cDC) cDC1, cDC2, and plasmacytoid DCs (pDCs) in the peripheral blood can be discriminated from monocytes by the absence of CD14 expression as follows: cDC1 are $CD14^-CD172a^{low}CADM1^+$ cells, cDC2 are $CD14^-CD172a^{high}CADM1^+$ cells, and pDCs are $CD14^-CD172a^+CADM1^-CD4^+$cells (Fig. 200) (based on the results and gating described in ref. [1752]). The phenotypic characterization of porcine blood cDC1 revealed species-conserved features such as high surface expression of CD135, CADM1, CD205, low levels of CD172a, and a lack of CD115 [1752]. Opposing to murine DC, where CD11b is used as a cDC2-specific marker,

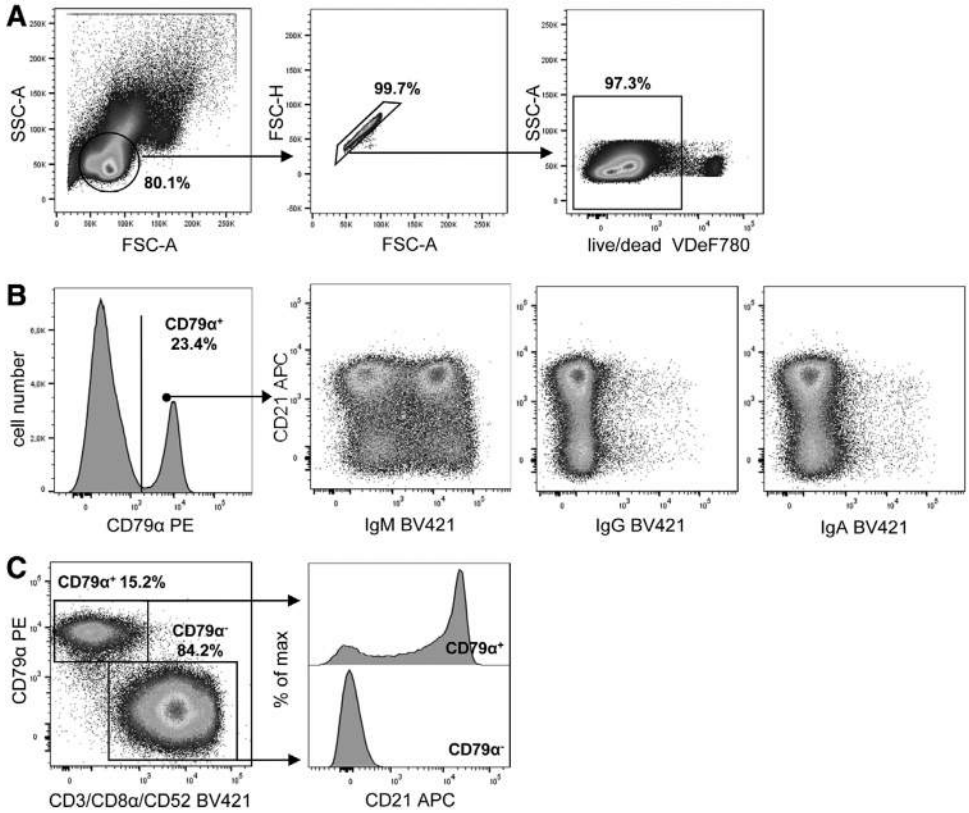

Figure 199. Identification of porcine B cells in peripheral blood. (A) Lymphocytes are identified based on the forward and side scatter. Single cells are discriminated from doublets by plotting FSC area against height and dead cells are excluded by a viability dye. (B) CD79α$^+$ B cells (cross-reactive mAb clone HM57) within live PBL can be further analyzed for expression of CD21 (cross-reactive mAb clone B-ly4), IgM (mAb clone K52 1C3), IgG (mAb clone 23.7.1b) and IgA (mAb clone K61 1B4). A comprehensive functional characterization of the various porcine B-cell subsets has not been performed so far. (C) Bulk staining for CD3 (mAb clone PPT3), CD8α (mAb clone 11/295/33), and CD52 (mAb clone 11/305/44) in combination with a co-staining for CD79α and CD21 shows that CD79α$^+$ B cells are CD3$^-$CD8α$^-$CD52$^-$ but contain CD21$^-$ and CD21$^+$ cells. Non-B cells (CD3$^+$CD8α$^+$CD52$^+$) are CD21$^-$. Data is generated from freshly isolated PBMC from an animal of approximately 6 months of age.

porcine CD11R1 (equivalent to murine and human CD11b) is highly expressed on circulating cDC1 and cDC2 [1752]. The phenotypic characterization of the porcine blood cDC2 subset is difficult as different markers (e.g., CD163, CSF1R) are expressed also on porcine monocytes, but the lack of the porcine monocyte-specific marker CD14 and high FLT3 expression approved these as DCs [1752]. Species-specific characteristics of porcine cDC2 are reflected by the high surface expression of CD1.1 (equivalent to CD1a [1754]), which is restricted to dermal cDC2 in humans [1755], and CADM1, which is a feature of other mammalian cDC1 subsets [1756]. Like in other species, the porcine pDC subset (typically CD4$^+$SLA-DR^{low}CD80/86^{low}), produces high amounts of type I IFNs after virus stimulation [1716] and produces high amounts of cytokines following TLR ligand stimulation (e.g., IL-12p35 after CpG stimulation) compared to the porcine cDC subsets. Similar to human pDC, porcine pDC express CD303 (BDCA-2), and CD304 (BDCA-4) [1752].

In contrast to human monocyte classification based on CD14 and CD16, and mouse monocyte classification based on Ly6C$^{+/-}$, porcine monocytes can be identified as CD14$^+$CD172a$^+$ mononuclear leukocytes that can be further divided into different subpopulations based on the expression levels of CD163, SLA-DR, and CD14 (Fig. 201) [1757, 1758]. Two major subpopulations of blood monocytes have been described in pigs (CD14^{high}CD163$^-$ SLA-DR$^-$ and CD14^{low}CD163$^+$SLA-DR$^+$) that show differences in CD11a, wCD11R1 (α-integrins), CD29 (integrin β1), CD49d (integrin α4), CD61 (integrin β3), CD80/86, and CD1a expression [1757, 1759, 1760] and also differ in chemokine receptor expression of CX3CR1 and CCR2 [1761]. So far state of the art is that these cells divide into distinct subsets in the bone marrow, thereafter circulating monocyte subpopulations represent different maturation stages and comprise distinct functional capacities [1758, 1762, 1763]. Compared to mouse, gene expression profiles suggest that porcine blood-derived monocyte subsets are close to human monocytes as certain genes (e.g., CD36, CLEC4E, TREM-1 expressed in human monocytes) were selectively expressed in pig monocyte subsets [1759]. The same profiles revealed also that the pig CD14^{low}CD163$^+$ cells are actually equivalent to intermediate human monocytes (CD14^{high}CD16$^+$), and that there is no CD14$^+$CD16$^+$ "nonclassical" population [1759]. Porcine

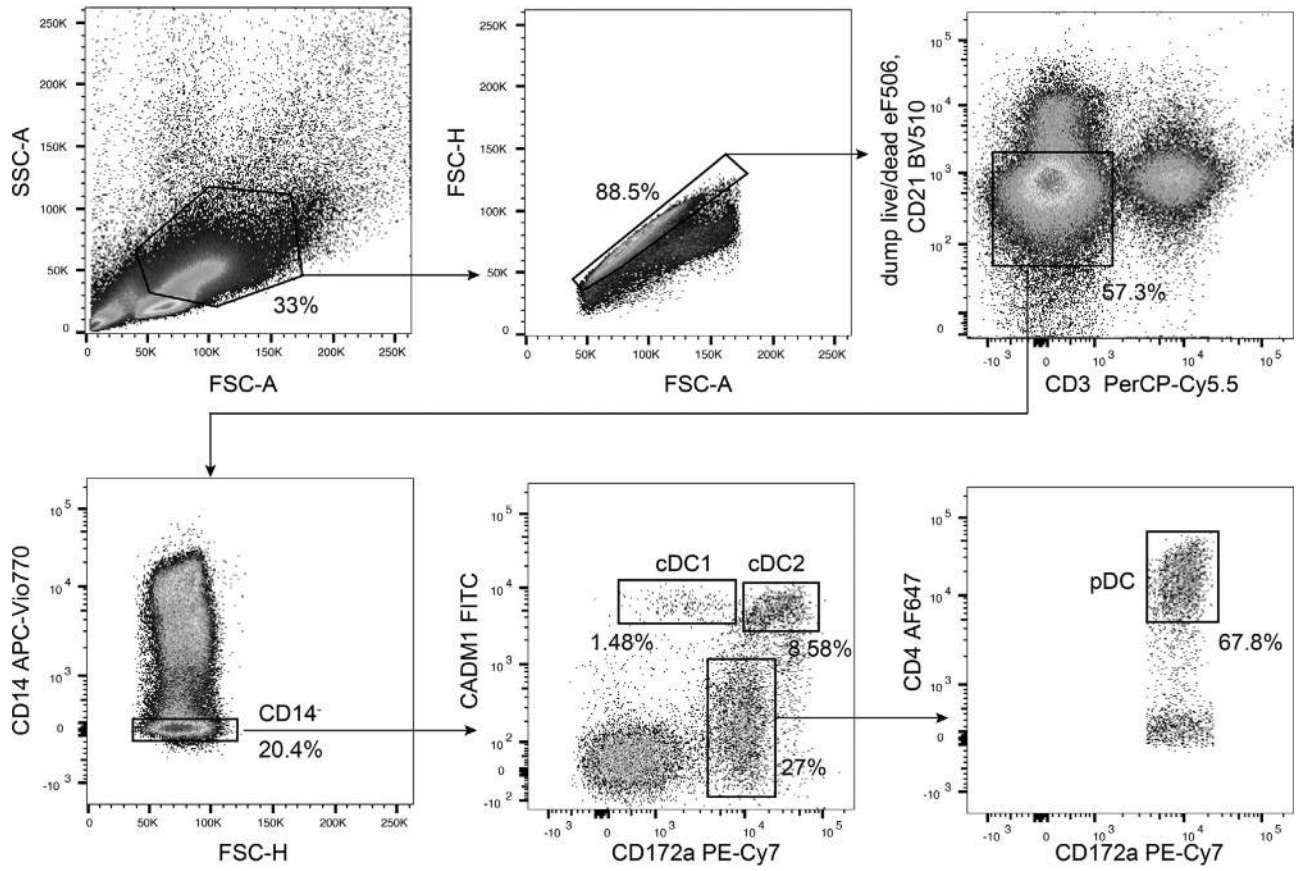

Figure 200. Identification of porcine conventional dendritic cells (cDC) and plasmacytoid dendritic cells (pDC) in peripheral blood. Large mononuclear cells are identified based on FSC and SSC. Single cells are discriminated from doublets by plotting FSC area against height. Dead cells are excluded by a viability dye combined with a dump channel for exclusion of porcine CD21$^+$ B cells (mAb clone B-ly4). Viable CD3$^-$ non-T cells (mAb clone BB23-8E6-8C8) can be further discriminated from porcine monocytes by the absence of CD14 expression (mAb clone TÜK4). Subsequently, three different DC subsets can be identified based on the expression of CD172a (mAb clone 74-22-15), CADM1 (mAb clone 3E1) and CD4α (mAb clone 74-12-4) as follows: cDC1 are CD14$^-$ CD172a^{low}CADM1$^+$ cells, cDC2 are CD14$^-$CD172a^{high}CADM1$^+$ cells and pDC are CD14$^-$ CD172a$^+$CADM1$^-$CD4$^+$cells. Data are generated from fresh PBMC of a sow of approximately 2 years of age.

CD14^{high}CD163$^-$ monocytes likely correspond to classical monocytes (CD14^{high}CD16$^-$) in humans [1762]. However, cross-species subset comparison of blood monocytes among human, bovine, murine, and pig cells using transcriptomics indicated that CD163-based discrimination of porcine monocytes into classical and non-classical monocytes might need to be reevaluated [1750, 1764]. CD14 expression can also be found at lower levels on granulocytes in the pig [1762]. Of note, porcine granulocytes are also positive for CD172a and some mature B cells can be induced to express low levels of CD172a after antigen stimulation [1762, 1765].

Quite recently, the phenotypic characterization of lung tissue resident DC and macrophage network segregated porcine mononuclear phagocytes as follows: conventional cDC1 (MHCII^{++}CD172a$^-$CD163$^-$CD1$^-$CADM1$^+$CD14$^-$) and cDC2 (MHCII^{++}CD172a$^+$CD163$^-$CD1^{low}CADM1^{low}CD14$^-$), inflammatory monocyte-derived DCs (MHCII^{++} CD172a$^+$CD163^{low}CD1$^-$CADM1$^+$CD14$^-$), monocyte-derived macrophages (MHCII^{++}CD172a$^+$CD163^{int}CD1$^-$CADM1^{low}CD14$^+$), and alveolar macrophage-like cells/interstitial macrophages (MHCII^{++}CD172a$^+$CD163^{++}CD1$^-$CADM1$^-$CD14$^-$) and alveolar macrophages (MHCII^{++}CD172a$^+$CD163^{++}CD1$^-$CADM1$^{-/low}$ CD14$^-$) [1753, 1766, 1767]. This nomenclature is based on the origin and the function of the myeloid cells [1768], and offers the advantage to assign one single name per DC/Macrophage subpopulation for all the species facilitating trans-species comparisons [1753, 1766]. The FLT3-dependent cDC being Sirpα (CD172a) negative or low are named cDC1 in the pig lung and correspond to the BDCA3$^+$ cDC and CD103$^+$ cDC in human and mouse, respectively [1753, 1766]. Referring to the BDCA1$^+$ and CD11b$^+$ DC subset in human and mouse, the CD172a^{++}/CD11b$^+$ cDC in the porcine respiratory tract are named cDC2 [1753]. Porcine alveolar macrophages express high levels of CD172a, CD163, CD169, CD16, and SLA-II molecules, whereas CD14 and CD11R1 expression is minimal or negative on alveolar macrophages [1762]. Moreover, CD203a (originally clustered as SWC9) is expressed widely in porcine macrophage populations with notably high levels on alveolar macrophages, but is not expressed on monocyte populations [1762]. Like in other

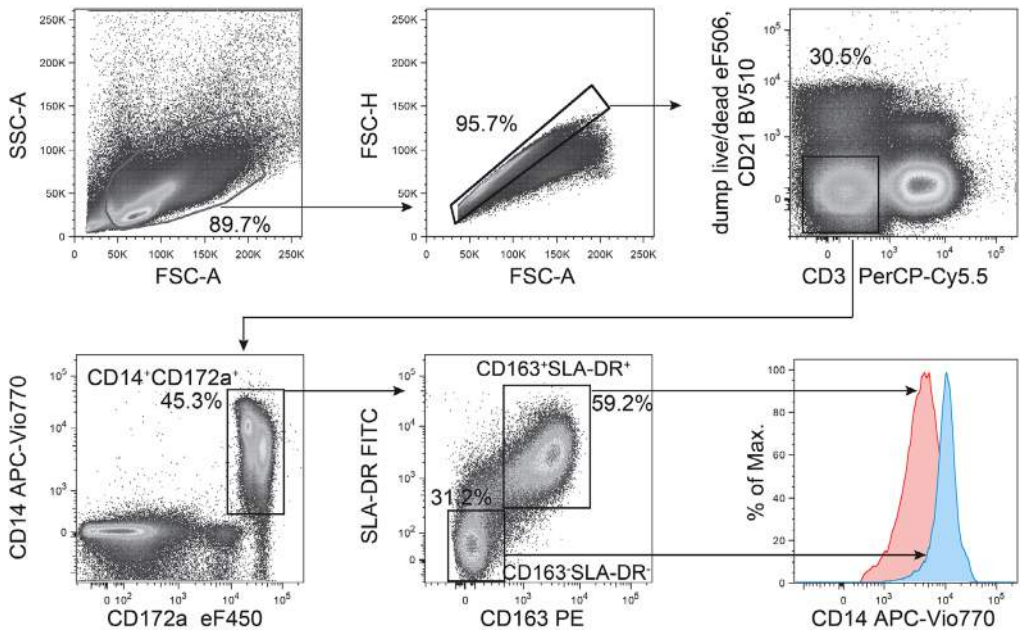

Figure 201. Identification of porcine monocyte subsets in peripheral blood. Mononuclear cells are identified based on the forward and side scatter. Single cells are discriminated from doublets by plotting FSC area against height. Dead cells are excluded by a viability dye combined with a dump channel for exclusion of porcine CD21$^+$ B cells (cross-reactive mAb clone B-ly4). Monocytes can be further discriminated from viable CD3$^-$ non-T cells (mAb clone BB23-8E6-8C8) as CD14$^+$CD172a$^+$ cells (mAb clone CD14 TÜK4; mAb clone CD172a 74-22-15). Different monocyte subsets can be identified based on the expression of CD163 (mAb clone 2A10/11) and SLA-DR (mAb clone 2E9/13). The histogram shows CD14 expression (mAb clone TÜK4) of the two monocyte subsets representing the major "steady-state" subsets (CD14^{high}CD163$^-$SLA-DR$^-$ and CD14^{low}CD163$^+$SLA-DR$^+$) in porcine peripheral blood. Data is generated from fresh PBMC of a sow of approximately 2 years of age.

species, alveolar macrophages of the pig are also highly autofluorescent [1753]. Contrary to porcine alveolar macrophages those in mice do not express MHC-II and are all negative for CD11b [1456], whereas human alveolar macrophages widely express CD11b and MHC-II [1769]. Porcine alveolar macrophage-like cells are pulmonary intravascular macrophages that have not been observed yet at steady-state in mice or non-human primates, and have nearly the same phenotype like porcine alveolar macrophages [1767, 1770]. Interstitial CD169$^-$ macrophages are a prominent cell type in human lung tissue, whereas CD169$^+$ macrophages are located in the alveolar space/airway, defining them as alveolar macrophages [1771]. Whether this CD169$^-$ negative macrophage population in the human lung refers to the porcine alveolar macrophage-like cells is not resolved yet.

In the skin of pigs, similar to humans, the classical DC subsets of epidermal Langerhans cells (LC) and dermal DC are found [1772]. Dermal DC can be divided into three main subsets according to their CD163 and CD172a expression: CD163$^-$CD172a$^-$, CD163$^+$CD172a$^+$, and CD163^{low}CD172a$^+$ that differ in the expression of CD16, CD206, CD207, CD209, and CADM1 [1772]. Based on comparative transcriptomics, phenotypic analysis, and functional studies, Marquet and colleagues proposed the allocation of porcine dermal DC to those of the human system as follows: the porcine CD163$^-$CD172a$^-$ subset corresponds to the human CD141$^+$ dermal DC subset, the porcine CD163^{low}CD172a$^+$ subset to the human CD1c$^+$ dermal DC, and the porcine CD163$^+$CD172a$^+$ subset to the monocyte-derived human CD14$^+$ dermal DC subset.

In porcine tonsils, plasmacytoid DC (CD172a^{low}CD4$^+$MHCII^{low}) and conventional DC (cDC1, CD172a$^{-/low}$CADM1^{++}MHCII^{++} and cDC2, CD172a^{++}CD14$^-$CD163$^-$MHCII^{++}CADM1^{low}) but also monocyte-derived cells (CD172a^{++}CD163$^-$CD14$^+$MHCII^{++}) and macrophage-like cells (CD172a^{++}, CD163$^+$CD14$^-$MHCII^{++}) have been identified [1751]. Compared to blood, not all tonsil-resident cDC1 and cDC2 cells express the C-type lectin receptor DEC205 [1773]. All reagents and Abs for porcine myeloid cell staining shown in Figs. 200 and 201 are listed in Table 81.

For analyzing neutrophils, eosinophils and basophils in porcine whole blood, granulocytes are identified based on their high SSC and FSC properties and expression of CD172a. To separate between them, SWC8, a marker defined by the International Workshop on Swine Leukocyte Differentiation Antigen (A. [1774]), SWC1 (now identified being porcine CD52 [1775]) and the antigens 2B2 and 6D10 [1776] can be used. Mature neutrophils in blood express CD172a$^+$SWC8^{++}CD52$^+$6D10$^+$2B2$^+$CD14$^+$, whereas mature eosinophils are CD172a$^+$SWC8^{++}CD52$^-$6D10$^-$2B2$^+$CD14$^-$ and mature basophils will identify as CD172a$^+$SWC8$^-$ CD52$^+$6D10$^-$2B2$^+$CD14$^-$ [1762].

Table 78. Reagents and Abs for T-cell staining

Reagent/antibody	Clone	Manufacturer
Mouse anti-pig CD2 - Alexa Fluor® 488	MSA4	In house[1]
Mouse anti-pig CD3 - PerCP-Cy™5.5	BB23-8E6-8C8	BD Biosciences
Mouse anti-pig CD4	74-12-4	In house[2]
Mouse anti-pig CD4 - FITC	74-12-4	BD Biosciences
Mouse anti-pig CD4 - Alexa Fluor® 647	74-12-4	BD Biosciences
Mouse anti-pig CD8α - Alexa Fluor® 647	11/295/33	In house[3]
Mouse anti-pig CD8α - Biotin	11/295/33	In house[4,5]
Mouse anti-pig CD8β - Biotin	PPT23	In house[4,6]
Mouse anti-human CD14 - VioGreen	TÜK4	Miltenyi Biotec
Mouse anti-pig CD25	3B2	In house[7]
Mouse anti-pig CD27	b30c7	BioRad
Mouse anti-pig CD27 - Alexa Fluor® 647	b30c7	In house[8]
Mouse anti-pig TCRγδ	PGBL22A	Kingfisher Biotech
Mouse anti-pig TCRγδ - Biotin	PPT16	In house[4,9]
Mouse anti-pig SLA-DR - Biotin	MSA3	In house[4,10]
Mouse anti-human Perforin - PerCP-eFluor710	δG9	ThermoFisher Scientific
Rat anti-mouse Foxp3 - PE	FJK-16s	ThermoFisher Scientific
Rat anti-mouse Foxp3 - eFluor™ 450	FJK-16s	ThermoFisher Scientific
Mouse anti-human T-bet - PE	4B10	ThermoFisher Scientific
Rat anti-human/ mouse GATA-3 - PerCP-eFluor710	TWAJ	ThermoFisher Scientific
Mouse anti-human IL-17A - Alexa Fluor® 647	SCPL1362	BD Biosciences
Mouse anti-human TNFα - FITC	MAb11	BD Biosciences
Rat anti-mouse Ki-67 - PE-Cy7	SolA15	ThermoFisher Scientific
Mouse anti-human CD154 - PE	5C8	Miltenyi Biotec
Goat anti-mouse IgG1 - PE	–	SouthernBiotech
Goat anti-mouse IgG2b - Alexa Fluor® 488	–	ThermoFisher Scientific
Streptavidin - Brilliant Violet 421™	–	BioLegend
Fixable Viability Dye eFluor™ 780	–	ThermoFisher Scientific
Fixable Viability Dye eFluor™ 506	–	ThermoFisher Scientific

[1]Conjugation with Alexa Fluor® 488 Protein Labeling Kit (ThermoFisher Scientific); non-conjugated mAb available from Kingfisher Biotech
[2]Commercially available from BD Biosciences
[3]Conjugation with Alexa Fluor® 647 Protein Labeling Kit (ThermoFisher Scientific); mAb commercially available from BD Biosciences
[4]Biotinylation with EZ-LinkTM Sulfo-NHS-LC-Biotin (ThermoFisher Scientific)
[5]Alternative mAb clone 76-2-11 available from BD Biosciences and ThermoFisher Scientific
[6]Non-biotinylated mAb commercially available from Bio-Rad
[7]mAb commercially available from Bio-Rad (clone name K231.3B2)
[8]Conjugation with Alexa Fluor® 647 Protein Labeling Kit (ThermoFisher Scientific); mAb commercially available from Bio-Rad
[9]mAb currently not commercially available, alternative clone: PGBL22A, available from Kingfisher Biotech
[10]mAb commercially available from Kingfisher Biotech

14.6 Step-by step-sample preparation.

14.6.1 General comments. Blood samples from pigs are most commonly taken by venipuncture from the external jugular vein and require fixation but no sedation. Terminal blood samples are obtained intracardially under deep anesthesia and Lithium–Heparin or Sodium–Heparin as anticoagulants are recommended with respect to the duration of large animal dissections.

14.6.2 Step-by-step sample preparation of porcine PBMC.

1. Draw blood and transfer to an anti-coagulant containing tube.
2. Dilute blood 1:2 in 0.9% sodium chloride solution or PBS.
3. Carefully overlay Pancoll (e.g. Pancoll human, Cat# P04-601000 by PAN-Biotech, density 1.077 g/mL) with diluted blood in a ratio of 1:3.
4. Centrifuge at room temperature at 800 × *g* without brake for 20 min.
5. Collect interphase, transfer to new tube and wash with 0.9% sodium chloride solution or PBS.
6. [optional] Perform erythrocyte lysis (for example using 3 mL ACK lysis buffer at RT for 3 min).
7. Wash with staining buffer.
8. Pellet cells (300 × *g*, 4°C, 6 min) and discard supernatant.

14.6.3 Step-by-step sample preparation of porcine lymphocytes from spleen.

1. Cut dissected spleen into small pieces.
2. Mechanically dissociate tissue pieces by forcing through a sieve and rinse with PBS.

3. Centrifuge at 4°C at 350 × *g* and discard supernatant.
4. Resuspend cells in 20 mL PBS and force through a cell strainer (70 μm).
5. Carefully overlay Pancoll (for example Pancoll human, Cat# P04-601000 by PAN-Biotech) with cell suspension in a ratio of 1:3.
6. Centrifuge at room temperature at 800 × *g* without brake for 20 min.
7. Collect interphase, transfer to new tube and wash twice with PBS at 300 × *g*, 4°C, 6 min and discard supernatant.

14.6.4 FCM staining of porcine leukocytes from blood and spleen.

1. Transfer up to 2 × 10^6 cells into a 96-well conical or U-bottom shaped plate.
2. Centrifuge the plate at 300 × *g* at 4°C for 3 min.
3. Aspirate or decant supernatant.
4. [optional] For blocking of Fc receptors add 1:200 to 1:500 diluted mouse serum (in staining buffer) for 5 min at 4°C or use 10% porcine plasma in PBS staining buffer.
5. [optional] Add True-Stain Monocyte Blocker™ according to the manufacturer's instruction.
6. Add a max of 30 μL surface staining mix per well and incubate for 15 min at 4°C.
7. Two washing steps: add up to 200 μL staining buffer and centrifuge the plate at 300 × *g* at 4°C for 3 min and aspirate or decant supernatant.
8. [optional] Add secondary reagents as described above including the two washing steps.
9. [optional] Add Fix/ Perm reagent for 20 min at 4°C, following two washing steps in permeabilization buffer as described above.
10. [optional] Add mAbs specific for intracellular or intranuclear antigens for 20 min at 4°C, following two washing steps in permeabilization buffer as described above.

N.B. If unlabeled and directly-conjugated Abs with identical isotypes are used in the same sample, a sequential staining should be performed: After labeling with unconjugated primary mAb and isotype-specific dye-conjugated secondary Abs, free binding sites should be blocked by whole mouse IgG molecules (typically 2 μg per sample, vendor: Jackson ImmunoResearch).

14.7 Materials. Flow cytometer:

- FACSCanto II flow cytometer
- FACSAria III sorter (both BD Biosciences)

Media and buffers:

- RPMI+AB: RPMI 1640 (PAN-Biotech) supplemented with 100 U/mL Penicillin, and 100 μg/mL Streptomycin (PAN-Biotech)

Table 79. Reagents and Abs for NK-cell staining

Reagent/antibody	Clone	Manufacturer
Mouse anti-pig CD3 - PerCP-Cy™5.5	BB23-8E6-8C8	BD Biosciences
Mouse anti-pig CD8α - Biotin	11/295/33	In house[1]
Mouse anti-pig CD16 - FITC	G7	BioRad
Mouse anti-pig NKp46 - Alexa Fluor® 647	VIV-KM1	In house[2]
Mouse anti-human Perforin - PE	δG9	ThermoFisher Scientific
Streptavidin - PE-Cy7	–	ThermoFisher Scientific
Fixable Viability Dye eFluor™ 780	–	ThermoFisher Scientific

[1]Biotinylation with EZ-Link™ Sulfo-NHS-LC-Biotin (ThermoFisher Scientific), alternative mAb clone 76-2-11 available from BD Biosciences and ThermoFisher Scientific
[2]Conjugation with Alexa Fluor® 647 Protein Labeling Kit (ThermoFisher Scientific), mAb commercially available from Bio-Rad

Table 80. Reagents and Abs for B-cell staining

Reagent/Antibody	Clone	Manufacturer
Mouse anti-pig CD3	PPT3	In house
Mouse anti-pig CD8α	11/295/33	In house
Mouse anti-human CD21 - APC	B-ly4	BD Biosciences
Mouse anti-pig CD52	11/305/44	In house[1]
Mouse anti-human CD79α - PE	HM57	Dako
Mouse anti-pig IgM	K52 1C3	Bio-Rad
Mouse anti-pig IgA	K61 1B4	Bio-Rad
Mouse anti-pig IgG	23.7.1b	ThermoFisher Scientific
Rat anti-mouse-IgG1 - Brilliant Violet 421™	RMG1-1	BioLegend
Goat anti-mouse-IgG2a - Brilliant Violet 421™	–	Jackson Immuno Research
Goat anti-mouse-IgG2b - Brilliant Violet 421™	–	Jackson Immuno Research
Fixable Viability Dye eFluorTM 780	–	ThermoFisher Scientific

[1]mAb commercially available from Bio-Rad

- cRPMI: Complete RPMI 1640 (PAN-Biotech) supplemented with 10% FCS (PAN-Biotech), 100 U/mL Penicillin, and 100 μg/mL Streptomycin (PAN-Biotech)
- cIMDM: Complete IMDM (PAN-Biotech) supplemented with 10% FCS (PAN-Biotech), 100 U/mL Penicillin, and 100 μg/mL Streptomycin (PAN-Biotech)
- ACK lysis buffer: 150 mM NH4Cl, 10 mM $KHCO_3$, and 0.1 mM Na_2EDTA
- Fixation and Permeabilization reagents: for detection of intracellular cytokines: Fixation/Permeabilization solution kit (BD Biosciences); For detection of intranuclear molecules and per-

Table 81. Reagents and Abs for the staining of mononuclear phagocytes

Reagent/antibody	Clone	Manufacturer
Mouse anti-pig CD163 – PE	2A10/11	BioRad
Chicken anti-human CADM1 - FITC	3E1	MBL
Mouse anti-human CD21 - BV510	B-ly4	BD Biosciences
Mouse anti-pig CD3 - PerCP-Cy™5.5	BB23-8E6-8C8	BD Biosciences
Mouse anti-pig CD4 - Alexa Fluor® 647	74-12-4	BD Biosciences
Mouse anti-human CD14 - APC-Vio770	TÜK4	Miltenyi Biotec
Mouse anti-pig CD172a - Biotin	74-22-15	SouthernBiotech
Mouse anti-pig SLA-DR - FITC	2E9/13	BioRad
Streptavidin - PE-Cy®7	–	ThermoFisher Scientific
Streptavidin - eFluor™ 450	–	ThermoFisher Scientific
eBioscience™ Fixable Viability Dye eFluor™ 506	–	ThermoFisher Scientific
True-Stain Monocyte Blocker™	–	BioLegend®

forin: Foxp3/Transcription factor staining buffer set (ThermoFisher Scientific)
- Staining buffer: PBS (PAN-Biotech) supplemented with 2 mM EDTA and 0.5% BSA (AppliChem) or PBS (PAN-Biotech) supplemented with 10% porcine plasma

In vitro stimulation

- PMA (50 ng/mL) and Ionomycin (500 ng/mL, both Sigma–Aldrich) for 4 h in combination with Brefeldin A (GolgiPlug, BD Biosciences, 1 μg/mL)
- Antigen preparation of selected pathogens for antigen induced T-cell responses (in total 6–8 h, in titrated concentrations (e.g., 25–80 μg/mL) and for 4 h in combination with Brefeldin A (Brefeldin A solution, 1000×, ThermoFisher Scientific)

14.8 Data Analysis. Flow cytometric analysis was performed by using FACSCanto II flow cytometer and FACSAria III sorter employing FACSDiva Software v6.1.3 (BD Biosciences), and data were analyzed by using FlowJo software v9.9.4 and v10.5 (FlowJo, LLC).

14.9 Pitfalls.

- Be aware that CD8α does not identify conventional $CD8^+$ T cells per se, but is also expressed on CD4 T cells, NK cells, and subsets of γδ T cells.
- Keep in mind the strong age-dependency of the expression of several porcine markers (e.g., CD8α, MHC-II).
- Porcine monocytes do not separate from peripheral blood lymphocytes by FSC/SSC properties as clearly as human monocytes.
- Carefully test cross-reactivity of anti-human or anti-murine Abs before use (see also section 15.6).

14.10 Top tricks.

- If working with frozen/thawed samples we advise to incubate freshly thawed samples in cRPMI overnight at 37°C to improve cytokine responses after subsequent stimulation.

Summary of major porcine immune cell subpopulations

γδ T-cell populations	Phenotype/sub-phenotype
	$TCR\gamma\delta^+CD4^-CD8^-CD2^-$
	$TCR\gamma\delta^+CD4^-CD8^{-/+}CD2^+$
$CD4^+$ T-cell populations	Phenotype/sub-phenotype
Naïve	$CD4^+CD8\alpha^-CD27^+$
Effector-memory	$CD4^+CD8\alpha^+CD27^-$
Central-memory	$CD4^+CD8\alpha^+CD27^+$
Treg	$CD25^{high}Foxp3^+$
Th1	$Tbet^+$
Th2	$GATA3^{high}$
$CD8^+$ T-cell populations	Phenotype/sub-phenotype
Naïve	$CD3^+TCR\text{-}\gamma\delta^-CD4^-CD8\alpha^{high}CD8\beta^+CD27^+perforin^-$
Effector-(memory)	$CD3^+TCR\text{-}\gamma\delta^-CD4^-CD8\alpha^{high}CD8\beta^+CD27^{-/dim}perforin^+$
NK-cell populations	Phenotype/sub-phenotype
highly activated	$CD3^-CD8\alpha^{dim}CD16^+NKp46^{high}$
less activated	$CD3^-CD8\alpha^+CD16^+NKp46^{-/+}$
B-cell populations	Phenotype/sub-phenotype
Naïve	$CD79\alpha^+CD21^+IgM^+$
B-1	$CD79\alpha^+CD21^-IgM^{++}$
Class-switched memory	$CD79\alpha^+CD21^{-/+}IgG^+/IgA^+$
Myeloid populations in blood	Phenotype/sub-phenotype
Monocytes	$CD14^+CD16^+CD163^{+/-}CD135^-$
Steady state	$CD14^{++}CD163^{-/low}$
	$CD14^{low}CD163^{+/++}$
Inflammatory	$CD14^{low}CD163^+SLA\text{-}DR^-$
cDC1	$CD14^-CD172a^{low}CADM1^+CD4^-wCD11R1^+CD135^+$
cDC2	$CD14^-CD172a^+CADM1^+CD4^-CD115^+wCD11R1^+CD135^+CD1^+$
pDC	$CD14^-CD172a^+CADM1^-CD4^+CD135^+CD123^+CD303^+$

Myeloid populations in lung	Phenotype/sub-phenotype
Alveolar macrophages	SLA-DR^{++}CD172a^{+}CD163^{++}CD1^{-} CADM1$^{-/low}$CD14^{-}
Pulmonary intravascular macrophages	SLA-DR^{++}CD172a^{+}CD163^{++}CD1^{-} CADM1^{-}CD14^{-}
Monocyte-derived macrophages	SLA-DR^{++}CD172a^{+}CD163^{int}CD1^{-} CADM1^{low}CD14^{+}
Monocyte-derived DC	SLR-DR^{++}CD172a^{+}CD163^{low}CD1^{-} CADM1^{+}CD14^{-}
cDC1	SLA-DR^{++}CD172a^{-}CD163^{-}CD1^{-} CADM1^{+}CD14^{-}
cDC2	CD14^{-}CD172a^{+}CADM1^{+}CD4^{-} CD115^{+}wCD11R1^{+}CD135^{+}CD1^{+}
pDC	CD14^{-}CD172a^{+}CADM1^{-}CD4^{+} CD135^{+}CD123^{+}CD303^{+}

Myeloid populations in tonsils	Phenotype/sub-phenotype
Macrophages	CD172a^{++}CD163^{+}CD14^{-}MHCII^{+}
Monocyte-derived DC	CD172a^{++}CD163^{-}CD14^{+}MHCII^{++}
cDC1	SLA-DR^{++}CD172a$^{low/-}$CD4^{-}CADM1^{++} CD14^{-}CD163^{-}
cDC2	SLA-DR^{++}CD172a^{++}CD4^{-}CADM1^{low} CD14^{-}CD163^{-}
pDC	SLA-DR^{low}CD172a$^{low/-}$CD4^{+}CADM1^{-} CD14^{-}CD163^{-}

Myeloid populations in skin	Phenotype/sub-phenotype
Langerhans cells	CD172a^{+}CD1^{+}CD16^{-}CD163^{-}CADM1^{+} CD207^{+}MHCII^{+}
Dermal DC	CD163^{-}CD172a^{-}CD16^{-}CD206^{-}CADM1^{+}
	CD163^{+}CD172a^{+}CD1^{+}CD14^{+}CD16^{+} CD209^{low}CD206^{low}
	CD163^{low}CD172a^{+}CD1^{+}CD14^{low}CD16^{low}

Granulocyte populations in blood	Phenotype/sub-phenotype
Neutrophils	CD172a^{+}SWC8^{++}CD52^{+}6D10^{+}2B2^{+}CD14^{+}
Eosinophils	CD172a^{+}SWC8^{++}CD52^{-}6D10^{-}2B2^{+}CD14^{-}
Basophils	CD172a^{+}SWC8^{-}CD52^{+}6D10^{-}2B2^{+}CD14^{-}

15 Cross-reactive Ab clones

15.1 Overview. The testing of existing mAbs for reactivity with orthologous molecules in species different from the one the Ab was originally raised for is a frequent task to overcome limitations in the toolbox of available mAbs. This section provides an outline how experiments for cross-reactivity testing should be performed and what pitfalls might be encountered.

15.2 Introduction. For immunophenotyping studies in mice and humans researchers can choose from a large variety of mAbs specific for cluster of differentiation (CD) molecules, but also cytokines, transcription factors, and molecules involved in signal transduction. However, when it comes to other animal species this collection is severely diminished. One possibility to overcome this limited availability of mAbs is to test already existing mAbs for cross-reactivity with the orthologous molecule of the species under investigation. Although this might sound like a simple and straightforward task, like with any other immunophenotyping experiment, certain problems and pitfalls might be encountered. Hence, this chapter will give an outline for solid and successful cross-reactivity testing.

In the framework of the 8th Human Leukocyte Differentiation Antigen Workshop (HLDA8) a community-based effort was undertaken to identify commercially available mAbs for cross- reactivity with 17 different animal species, ranging from more frequently studied ones like swine, dog, or cattle up to more "exotic" species like mink and carp. This study revealed that for the typical cell membrane-located CD-molecule, the likelihood of cross-reactivity even within mammalian species is relatively low. A few exceptions applied to this observation, including mAbs against CD18, CD29, or CD49d, all forming either α or β-chains of integrins, or the cartilage link protein CD44 [1777, 1778].

15.3 General considerations on cross-reactivity testing. This study was far from being comprehensive and hence new tests for cross-reactivity are a frequent task if species different from mice and humans are studied. Work from our team and others on the cross-reactivity of mAbs with various porcine immune-related molecules revealed certain approaches that can be used not only to identify cross-reactive mAbs but also to scrutinize specific binding to the molecule of interest (see Fig. 202 for a general overview). In a first step commercially available Abs for the molecule of interest need to be identified. Online search tools like "biocompare" (https://www.biocompare.com/Antibodies/) or "antibodypedia" (https://www.antibodypedia.com/) might be helpful for this task, but the online catalogs of established producers for FCM-approved Abs are also a good source. Numerous Ab data sheets from the respective companies do provide information on cross-reactivity but such statements should be treated with caution as the claim of cross-reactivity is frequently based on sequence alignments and lacking solid experimental testing (see also Fig. 205 for an example). Under ideal circumstances, references are provided that demonstrate the claimed cross-reactivity, allowing a further scrutiny of the Ab.

If no information on cross-reactivity is provided, sequence alignments comparing the amino acid sequence of the target antigen in the species under investigation with the sequence of the species the Ab is specific for give a first indication of the likelihood of cross-reactivity. Our empirical observations show that homology rates below 75% usually indicate a low probability for cross- reactivity. However, for some Abs the sequence of the immunogen is provided in the data sheet, allowing a more focused

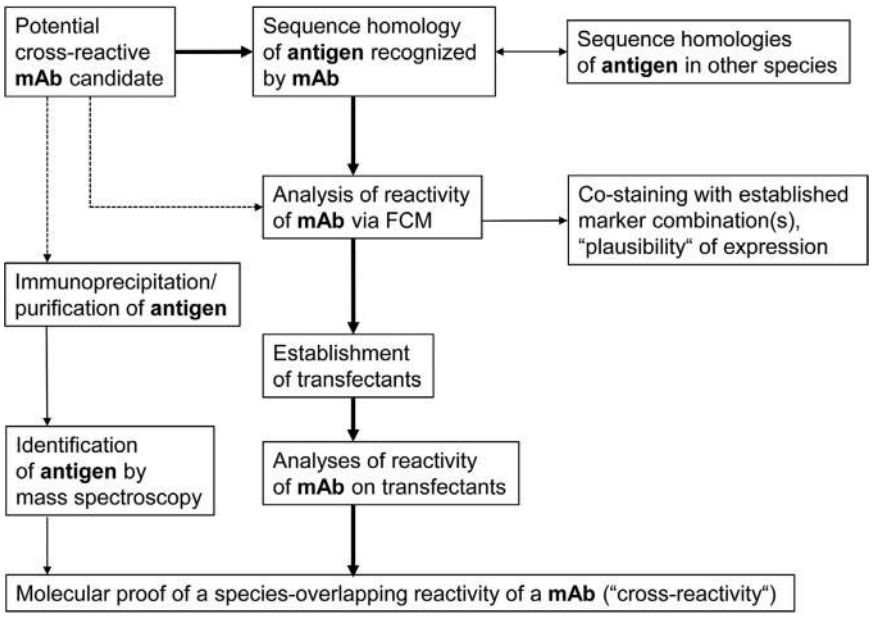

Figure 202. Strategies on cross-reactivity testing for mAbs for FCM. After identification of mAb candidates for cross-reativity testing, sequence homology analyses, ideally for the immunogen used to generate the Ab, will provide a first prognosis of the likelihood of cross-reactivity testing. Homologies higher than 90% indicate a good chance for cross-reactivity. High homology of target antigens across several species increases the likelihood of cross-reactivity further (typical examples: transcription factors or molecules involved in signal transduction). FCM staining experiments with the Ab under investigation in combination with an established marker or larger marker panels helps to evaluate cross-reactivity. As a final proof for cross-reactivity, cells transfected for expression of the target antigen should be generated and tested. Alternatively, the mAb candidate might be tested for its suitability in immunoprecipitation and precipitates can be subjected to mass spectroscopy for the identification of the target antigen.

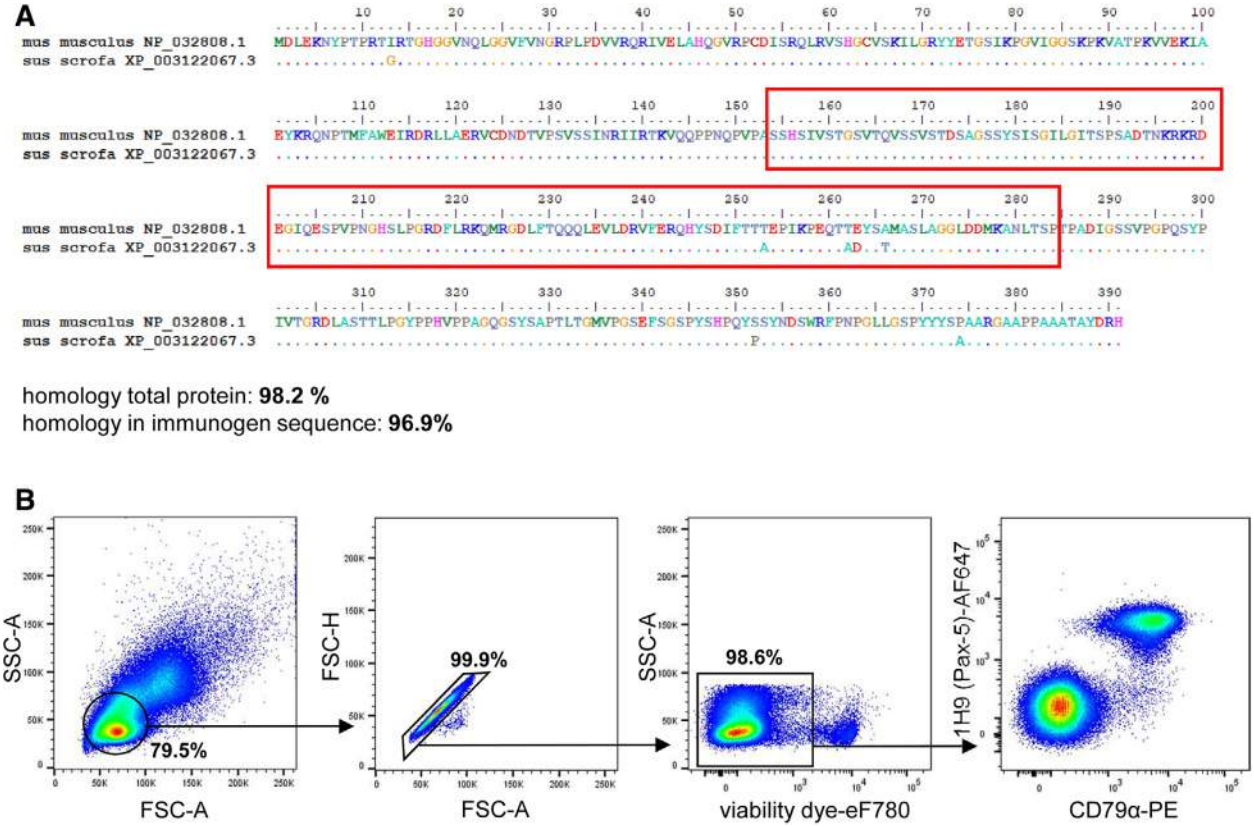

Figure 203. Test of anti-mouse Pax-5 mAb for cross-reactivity with the porcine orthologue. (A) Protein sequence alignment of murine (NCBI accession no. NP_032808.1) and porcine (NCBI accession no. XP_003122067.3) Pax-5 sequence. The homology of Pax-5 between the two species is 98.2%. The anti-mouse Pax-5 mAb clone 1H9 (BD Biosciences, catalogue no. 562814) is derived from an immunization of mice with recombinant mouse Pax-5 protein spanning amino acid residues 154–284. The alignment of the region of the immunogen is framed in red and has a homology of 96.9% between the two species. (B) Test of anti-mouse Pax-5 mAb on porcine PBMC. Lymphocytes were gated according to their light scatter properties and single cells are discriminated from doublets by plotting FSC area against height. Dead cells are excluded by a viability dye. The anti-Pax-5 mAb was tested in combination with a CD79α-specific mAb for the staining of porcine B cells, as Pax-5 is expressed from the pro-B to the mature B cell stage and only repressed during terminal plasma cell differentiation [1779]. A distinct co-staining of both mAbs is observed, indicating cross-reactivity of the 1H9 mAb clone with porcine Pax-5. The final proof of cross-reactivity still needs to be obtained by testing the mAb on cells transfected with recombinant porcine Pax-5.

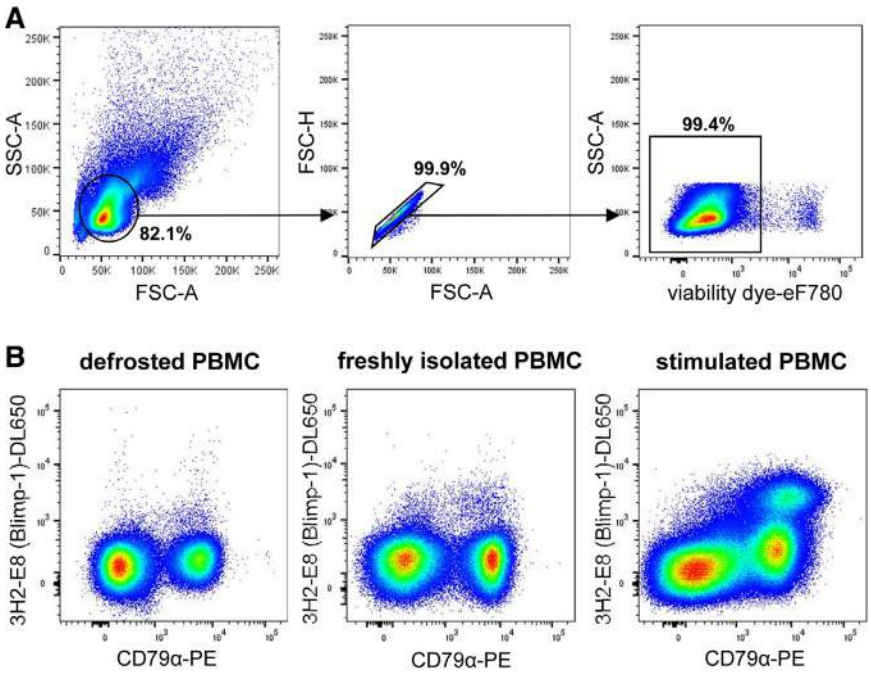

Figure 204. Test of anti-mouse Blimp-1 mAb for cross-reactivity with the porcine ortholog. For the anti-mouse Blimp-1 mAb clone 3H2-E8 (ThermoFisher Scientific, catalogue no. 13207588) cross-reactivity to the porcine protein is indicated on the data sheet. Flow cytometric analyses of the mAb on porcine PBMC were performed. (A) Lymphocytes were gated according to their light scatter properties and single cells are discriminated from doublets by plotting FSC area against height. Dead cells are excluded by a viability dye. The gating strategy is shown for freshly isolated PBMC and is representative for all experiments shown. (B) The anti-Blimp-1 mAb was tested in combination with a CD79α-specific mAb for staining of porcine B cells, as the transcription factor Blimp-1 is known to be essential for the generation of plasma cells [1781]. Only obscure staining patterns were observed when analyses were performed on defrosted cells. A more distinct population of porcine Blimp-1$^+$CD79α$^+$ B cells was detected with freshly isolated cells. For further analyses on the cross-reactivity of clone 3H2-E8, PBMC were stimulated with the TLR7/8 agonist resiquimod (R848, 2.5 mg/ml) as TLR-mediated activation is described to promote expression of Blimp-1 [1782, 1783]. After three days of in vitro stimulation, a clear increase in Blimp-1$^+$CD79α$^+$ B cells was detected. The final proof of cross-reactivity still needs to be obtained by testing the mAb on cells transfected with recombinant porcine Blimp-1.

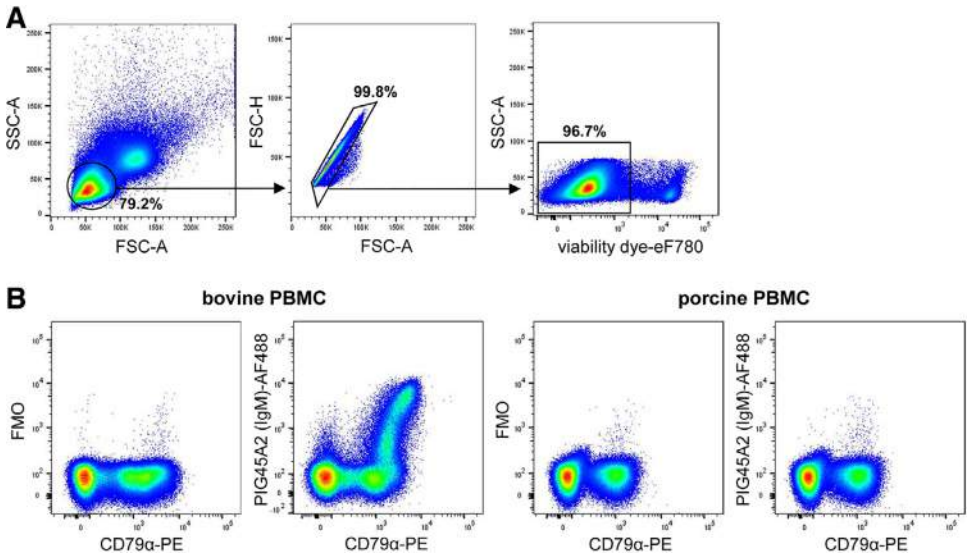

Figure 205. Test of anti-bovine IgM mAb for cross-reactivity with the porcine orthologue. For the anti-bovine IgM mAb clone PIG45A2 (Kingfisher Biotech, catalogue no. WS0620B-100) cross- reactivity to the porcine protein is indicated on the Kingfisher Biotech data sheet. (A) Porcine and bovine lymphocytes were gated according to their light scatter properties and single cells are discriminated from doublets by plotting FSC area against height. Dead cells are excluded by a viability dye. A representative gating strategy for bovine PBMC is shown. (B) The anti-IgM mAb was tested in combination with a CD79α-specific mAb for staining of either bovine or porcine B cells. A clear IgM-specific staining was obtained with the mAb on bovine B cells in contrast to a FMO control by using only secondary antibodies. No clear difference in the staining of the anti-IgM mAb on porcine B cells in comparison to the FMO control could be observed. The same staining patterns were obtained by different concentrations of the anti-IgM mAb (data not shown).

sequence alignment. High homology rates here (> 90%) are usually a strong indicator of Ab cross-reactivity. An example on this given in Fig. 203A. According to the data sheet for the anti-mouse paired box protein-5 (Pax-5) mAb clone 1H9, distributed by BD Biosciences, the immunogen used for its generation spanned the amino acid residues 154 to 284 of the murine Pax-5 sequence. This part of the murine sequence has a homology of 96.9% with the corresponding porcine Pax-5 sequence. Of note, also the entire murine Pax-5 sequence has 98.2% homology with porcine Pax-5, suggesting in general a high likelihood that anti-murine Pax-5 Abs will cross-react with porcine Pax-5. Indeed, this Ab showed a clear co-staining with CD79α$^+$ porcine B cells (see further details below and Fig. 203B).

Sequence alignments are also helpful to get a first impression on the likelihood of Ab cross-reactivity between closely related species e.g. within the families of Bovidae or Suidae. However, this requires that sequence data is available at all. If sequence data is lacking or the sequence alignments reveal a number of amino acid changes in the region of interest (for example the binding site of the mAb) carefully performed experiments for cross-reactivity testing become inevitable, as described in the following.

15.4 Practical guidelines for cross-reactivity testing. In any case, once one or several Ab candidates have been identified for cross-reactivity testing, first FCM experiments become inevitable. Prudent planning is required, since negative results will be frequently encountered. This leads to the question whether the Ab under investigation is indeed not cross-reactive or whether other conditions may have caused a failure of the experiment. Hence, one important aspect is to make sure that cells used in the experiment have a high likelihood to express the molecule of interest. For example, if Abs specific for homing markers from the gut tissue are investigated, leukocytes isolated from the intestine should be used. Similarly, chemokine receptor expression might be affected by freezing/ thawing procedures or the staining temperature [1780]. Additionally, particular cell subsets can be more affected by freezing/ thawing procedures than others, e.g. plasma cells. Therefore, here likewise testing on freshly isolated cells is highly recommendable. If the subset to be stained with the putative cross-reactive mAb is very small or likely to be expected on activated cells, *in vitro* stimulation of cells prior to staining can also increase the likelihood of a positive result. An example on these phenomena is shown in Fig. 204. The anti-mouse B lymphocyte–induced maturation protein-1 (Blimp-1) mAb clone 3H2-E8 was tested for cross-reactivity with its orthologous molecule in swine. With thawed porcine PBMC only a small and somewhat obscure positively stained subset was found (Fig. 204B, left plot). With freshly isolated PBMC, a more distinct subset of CD79α$^+$ that co-stained with the anti-Blimp-1 mAb became visible. Finally, in porcine PBMC, which were *in vitro* stimulated with the Toll-like receptor (TLR) 7/8 agonist resiquimod, a clear CD79α$^+$ putatively Blimp-1 double-positive subset was observed.

To ensure that the tested Ab is of sufficient quality, especially when encountering negative results, we frequently test it in parallel on cells from the species the Ab has been raised for. In this way, potential doubts on the quality of the mAb or the overall performance of the staining procedure can be ruled out. An example on this is shown in Fig. 205. The anti-bovine IgM mAb clone PIG45A2, distributed by Kingfisher Biotech, is claimed to be cross-reactive with porcine IgM in the Ab data sheet. Hence, we tested the Ab on bovine and porcine PBMC in parallel. Whereas in bovine PBMC a clear IgM/CD79α double-positive population was observed, with porcine PBMC putatively IgM$^+$ cells were on the level of an FMO-control, which was only stained with the isotype-specific secondary Ab (Fig. 205B). Hence, anti-bovine IgM mAb clone PIG45A2 does not seem to cross-react with its porcine orthologue.

In a comparable way, also positive findings for a newly tested mAb should be thoroughly questioned. One first approach is to test putatively cross-reactive mAbs from the very beginning (i.e. already during the initial titration) in combination with other established mAbs that allow the identification of phenotypes on which expression of the target antigen is expected. For example, for a target antigen that is expected to be expressed only by B cells, a co-staining with pan-B cell-specific mAbs allows a first assessment whether the cells stained by the putatively cross-reactive mAb are indeed labeled in a specific manner. As shown in Fig. 203B, the anti-mouse Pax-5 mAb clone 1H9 was tested in combination with CD79α, an anti-human mAb that cross-reacts with CD79α in multiple mammalian species [1744]. As expected from the high sequence homology between murine and porcine Pax-5 (Fig. 203A), a clear CD79α$^+$ putatively Pax-5 double-positive subset was observed. In the same manner, also in Figures 204 and 205 a co-staining against CD79α was performed in order to test Abs against Blimp-1 and IgM for their reactivity with porcine B cells (see also above for further details).

Once the optimal quantity or dilution of the mAb under investigation has been established, more complex phenotyping experiments should be performed to ensure that the stained cell populations match with phenotypes identified in more thoroughly studied species like human or mouse. Like for any other experiment, investigations with cells from several animals of the new species and different lymphatic and non-lymphatic organs should be performed to further scrutinize the obtained results. Nevertheless, it should be noted that expression patterns for particular immune-related molecules might not be completely conserved between different species. Examples for this would be the abundant expression of CD8αα homodimers on porcine NK cells as well as substantial subsets of CD4 and γδ T cells [1784], a phenomenon not seen in the corresponding human or mouse lymphocyte subsets. Likewise, differently from human or mouse T cells, MHC-II molecules are frequently expressed on activated and memory T-cell subsets in pigs [1712, 1785].

From a pedantic view, the aforementioned experimental strategies do not provide the final proof of cross-reactivity. This proof can be achieved by cloning and recombinant expression of the species-specific protein in a cell line with the subsequent analysis in immunofluorescence staining as performed to demonstrate the cross-reactivity of mAbs against porcine and ovine Foxp3 [1786, 1787] as well as porcine Helios [1788]. Also, Abs against

Table 82. Abs cross-reacting with porcine immune-related non-CD molecules in FCM[1]

Molecule	Species Ab was raised for	Clone name	Vendor(s)	References
Transcription factors				
Eomes	human	WD1928	ThermoFisher Scientific	[1729]
Foxp 3	mouse/ rat	FJK-16s	ThermoFisher Scientific	[1786]
GATA-3	human/ mouse	TWAJ	ThermoFisher Scientific	[1732]
Helios	human/ mouse	22F6	BioLegend	[1788]
T-bet	human	eBio4B10	ThermoFisher Scientific	[1732]
Cytokines				
IFN-γ	cattle	CC302	Bio-Rad	[1791]
IL-17A	human	SCPL1362	BD Biosciences	[1724]
TNF-α	human	MAb11	BioLegend	[1792]
Miscellaneous				
Ki-67	human	B56	BD Biosciences	[1793]
Perforin	human	δG9	BD Biosciences, ThermoFisher Scientific	[1740]

[1] Table is not claimed to be complete

ovine TNF-α [1789] and bovine and ovine IL-17A [1790] have been tested in this way. Similar experiments are currently under way in our laboratory to confirm the cross-reactivity of the anti-mouse Pax-5 mAb 1H5 and anti-mouse Blimp-1 mAb 3H2 2E8 with the respective porcine orthologs. However, it is important to state that numerous cross-reactive Abs, which are in use in the pig (and in other species), have not been tested in this way. Indeed, in those cases where the amino acid sequence of the immunogen used to raise the Ab is known and has a 100% identity to the orthologous sequence of the species under investigation, the testing on a recombinant protein is irrelevant. For all other cases, the authors of this chapter strongly recommend a testing on recombinant proteins in order to achieve the highest possible quality standards. Finally, an alternative approach to prove cross-reactivity is an immunoprecipitation of the target antigen by the putatively cross-reactive mAb and subsequent analysis of the precipitate by mass spectroscopy.

15.5 Examples on cross-reactive mAbs in pigs. Pigs have received increasing interest as a large animal model in recent years [1708], which has also resulted in publications on the knowledge of CD-molecule expression in porcine leukocytes, including listings of available mAbs to study their expression [1709, 1710]. Moreover, very recently a website was launched that lists currently available mAbs not only for the pig but also cattle, sheep, goat, chicken, horse, cat, and some fish species: https://www.immunologicaltoolbox.co.uk/. Cross-reactive mAbs are also interspersed in these sources of information, but should be treated with caution since several of these mAbs have not been scrutinized according to the guidelines above. In addition, these publications do not cover intracellular molecules, which are also of high relevance in immunophenotyping. Hence, Table 82 provides a list of miscellaneous molecules that are not CD-molecules and for which mAbs that cross-react with the porcine orthologue have been identified.

Table 83. Reagents and Abs used for cross-reactivity testing

Reagent/ Antibody	Clone	Manufacturer
Mouse anti-human CD79α - PE	HM57	Dako
Rat anti-human/ mouse Pax-5 - AlexaFluor® 647	1H9	BD Biosciences
Mouse anti-human/ mouse Blimp-1 - DyLight650	3H2-E8	ThermoFisher Scientific
Mouse anti-bovine sIgM	PIG45A2	Kingfisher Biotech
Goat anti-mouse IgG2b - AlexaFluor® 488	–	ThermoFisher Scientific
Fixable Viability Dye eFluor™ 780	–	ThermoFisher Scientific

15.6 Step-by-step sample preparation.
Step-by-step sample preparation of porcine PBMC

1. Draw blood and transfer to an anti-coagulant containing tube.
2. Dilute blood 1:2 in PBS (PAN-Biotech)
3. Carefully overlay Pancoll (for example Pancoll human, Cat# P04-601000 by PAN-Biotech) with diluted blood in a ratio of 1:3.
4. Centrifuge at room temperature at 800 × *g* without brake for 20 min.
5. Collect interphase, transfer to new tube and wash twice with PBS at 300 × *g*, 4°C, 6 min and discard supernatant.
6. Wash with staining buffer
7. Pellet cells (300 × *g*, 4°C, 6 min) and discard supernatant.

Step-by-step FCM staining of porcine leukocytes from blood and spleen

1. Transfer up to 2 × 10^6 cells into a 96-well conical or U-bottom shaped plate.

2. Centrifuge the plate at 300 × *g* at 4°C for 3 min. Aspirate or decant supernatant.
3. Add a max of 30 μL surface staining mix per well and incubate for 15 min at 4°C.
4. Two washing steps: add up to 200 μL staining buffer and centrifuge the plate at 300 × *g* at 4°C for 3 min and aspirate or decant supernatant.
5. Add secondary reagents as described above including the two washing steps.
6. Add Fix/ Perm reagent for 20 min at 4°C, following two washing steps in permeabilization buffer as described above.
7. Add mAbs specific for intracellular or intranuclear antigens (Table 83) for 20 min at 4°C, following two washing steps in permeabilization buffer as described above.

Materials
Flow cytometer:

- FACSCanto II (BD Biosciences)

Media and buffers:

- cRPMI: complete RPMI 1640 (PAN-Biotech) supplemented with 10% FCS (Sigma-Aldrich), 100 U/mL Penicillin, and 100 μg/mL Streptomycin (PAN-Biotech)
- Fixation and Permeabilization reagents for detection of intranuclear molecules: Foxp3/ Transcription factor staining buffer set (ThermoFisher Scientific)
- Staining buffer: PBS (PAN-Biotech) supplemented with 10% porcine plasma (in house preparation) for freshly isolated or thawed cells and PBS (PAN-Biotech) supplemented with 3% FCS (Sigma–Aldrich) for cells that were cultivated in vitro

In vitro stimulation

- TLR7/8 agonist resiquimod (R848, 2.5 mg/mL, InvivoGen) for 3 days

VII Data handling, evaluation, storage and repositories

1 Data analysis

1.1 *Introduction*

During the last decade, the field of FCM has gone through a number of revolutionary, technological advances that have resulted in a wide array of novel single-cell platforms. These include classical, multiparameter FCM, mass cytometry, spectral FCM, imaging FCM, and imaging mass cytometry, to name only a few (See Chapter VIII: Advanced techniques in, and management of, FCM). Many of these novel technologies generate large and/or high-dimensional data sets, which cannot be analyzed adequately anymore using the classical, manual analysis techniques. For example, current flow and mass cytometers can measure tens of parameters, while techniques such as imaging FCM are producing several hundreds of parameters at the single cell level. In addition, manual analysis techniques, such as manual gating to identify cell populations, have a number of important limitations [1794]. These include the fact that they are hard to reproduce, are subjective and biased, and are inefficient when exploring high-dimensional parameter spaces [599]. In addition, manual analysis is very time consuming when analyzing large cohorts of samples.

To mitigate these limitations of manual analysis, computational techniques can be used to take full advantage of the power of high-dimensional cytometry data analysis [1795]. However, this does not mean computational techniques completely replace the manual analysis. Rather, they should be considered as complementary tools that offer new insights, and performing an additional, manual inspection is still good practice as a quality control check. Computational methods can be used at several stages of the data analysis pipeline, including storage of the well-annotated data in repositories, during data cleaning and pre-processing, and for different types of analyses such as data visualization, population identification, and biomarker detection. Figure 206 presents an overview of the different stages of the data analysis pipeline where computational techniques can be used. Crucial to all these data analysis techniques is the fact that data should be of the best quality, and thus care should be taken to correctly design the experiment, take into account all the appropriate controls, and generate the data in such a way that is suited for all the computational analyses to be performed afterward.

A wide variety of methods from the fields of statistics, data mining, and machine learning is used to extract knowledge from cytometry data [1796]. These techniques can be broadly categorized into two groups: unsupervised learning and supervised learning strategies. Unsupervised learning techniques are descriptive models that aim at better characterizing the data, and are typically used to explore the structure of the data. These include techniques such as dimensionality reduction, clustering, and trajectory inference. Briefly, dimensionality reduction techniques aim at transforming the original, high-dimensional data set to a lower-dimensional space, often two or three dimensions, where it is easy to visually appreciate the structure in the data. This would, for example, allow detecting population structures, outliers, batch effects, or other trends present in the data. Clustering and trajectory inference methods aim to look for specific structures present in the data. Clustering techniques typically look for groups of cells (clusters) that are similar within a group, but different between groups, and mostly assume groups are well separated. Trajectory inference methods on the other hand rather look for structures that behave more like gradients, e.g., cells smoothly transitioning between different stages of a developmental process. These gradients should not necessarily be linear gradients, but can include branching processes and cycles as well.

Supervised methods take another approach to data analysis, and are typically used to construct predictive models. In this case, one wants to relate the cellular data to an outcome variable of interest, for example, the disease status of a patient, or the cell type of a particular cell of interest. Different types of supervised

methods exist, the most important of which are classification techniques, regression techniques, and techniques for survival analysis. The typical use of these methods is to construct a model based on data for which the outcome variable is already known, which is referred to as training the model. Such a trained model can later be used to predict the outcome variable for new data, not seen before.

1.2 *Cell-population analysis: Data preprocessing, manual and automated gating, and quality control*

1.2.1 Overview. Manual analysis is still an important component of FCM experiments in many labs, however, automated methods for identifying cell subpopulations in FCM data have proliferated rapidly [1797]. As manual gating is inherently subjective, it is important to follow defined protocols to improve analysis reproducibility. Preprocessing of data is necessary to remove errors and establish the appropriate data transformation parameters. Gating decisions should carefully consider different types of controls, and populations represented as a shoulder of a larger population should be analyzed with caution. Back-gating is critical for determining whether the initial gates are appropriate for the final subpopulation being analyzed, instead of being appropriate for the majority populations.

1.2.2 Complementary manual and automated analysis methods. FCM data analysis presents a complex problem because of recent rapid increases in the number of parameters measured, and because of some peculiarities of flow data. Current datasets include 20 or more parameters even by conventional fluorescence cytometry, and other methods yield 35 or more channels. Traditional bivariate gating (manually drawing boundaries on sequential two-parameter plots) can still be performed on high-dimensional data sets, but this becomes progressively more time consuming and less thorough as the parameter number increases. The current generation of flow cytometers is capable of simultaneously measuring 50 characteristics per single cell. These can be combined in 3^{50} possible ways using traditional bivariate gating, resulting in a massive data space to be explored [1798]. There has been rapid development of unsupervised clustering algorithms, which are ideally suited to biomarker discovery and exploration of high-dimension datasets [599, 1795, 1796, 1799–1804], and these strategies are described in more detail in Chapter VI, Section 1.2. However, the directed identification of specific cell populations of interest is still critically important in flow analysis for providing "reality checks" for the results returned by different algorithmic strategies, and for the generation of reportable data for clinical trials and investigations. This is the approach used by investigators who prefer to continue manual gating for consistency with previous results, now complemented by the availability of supervised cell population identification methods. This section will describe common issues in this type of analysis, in three stages: preprocessing, gating, and postprocessing (Fig. 207).

1.2.3 Principles of analysis.

1. **Preprocessing flow data in preparation for subpopulation identification**:

***Batch effects*:** FCM data are difficult to standardize between batches analyzed days or months apart, because cytometer settings can change with time, or reagents may fade. Imperfect protocol adherence may also lead to changes in staining intensity or machine settings. Such variations need to be identified, and where possible corrected. In addition to batch variation, individual outlier samples can occur, e.g., due to temporary fluidics blockage during sample acquisition. Identification of these changes can be performed by detailed manual examination of all samples. However, this involves evaluating the MFI between samples after gating

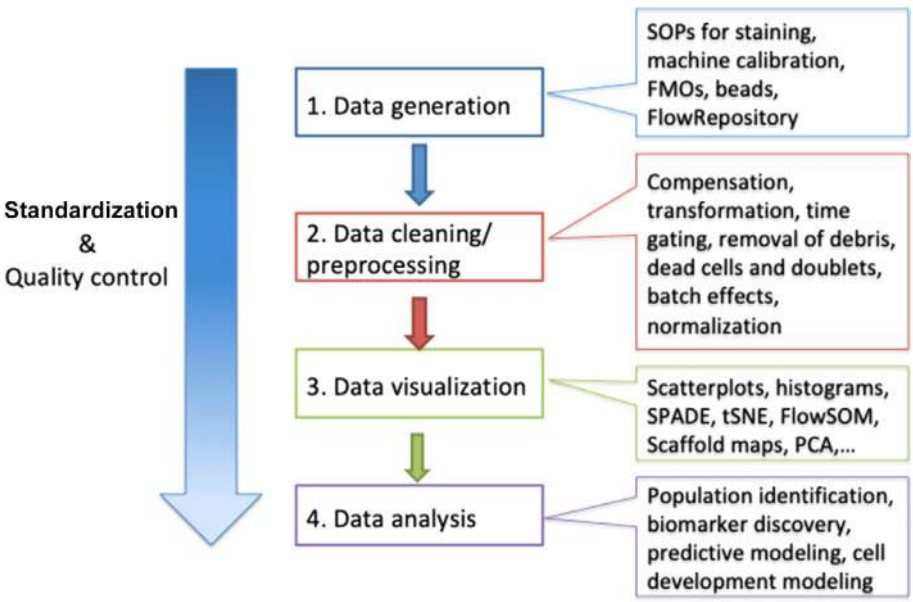

Figure 206. Computational methods offer great potential to automate many stages in the analysis of cytometry data. For every stage, computational pipelines can greatly contribute to standardization and quality control, leading to better standards in the FCM field.

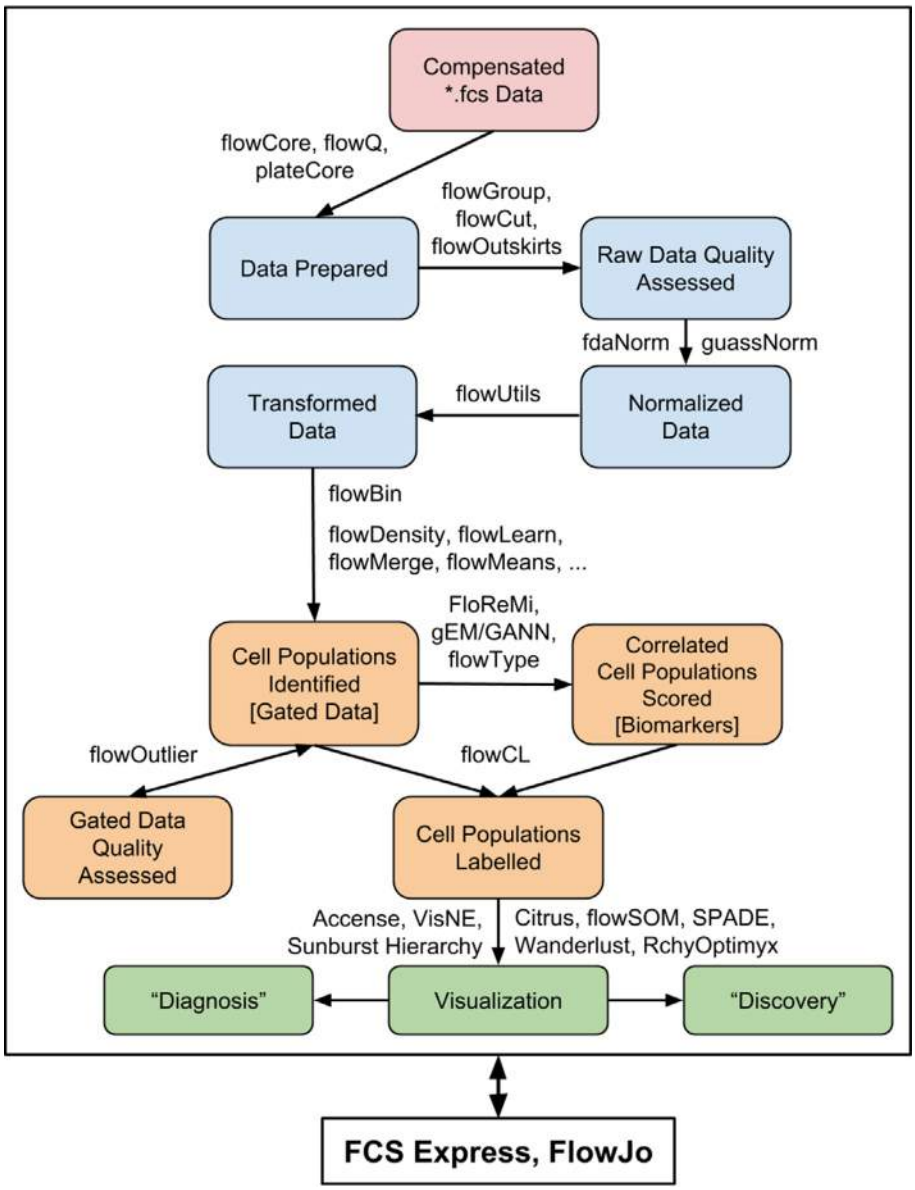

Figure 207. Typical analysis workflows in FCM for the identification of specific cell populations of interest by either manual of automated analysis. Analysis usually starts with several preprocessing steps on compensated data, including quality assessment, data normalization, and data transformation (blue boxes). Preprocessing is followed by identifying cell populations of interest (orange boxes), and finally visualization and interpretation (green boxes).

down to meaningful subpopulations. For high-dimensional data, this is difficult to perform exhaustively by manual analysis, and is more easily achieved by automated methods. As an example, samples from a study performed in two batches, on two cytometers, were analyzed by the clustering algorithm SWIFT [1801, 1805], and the resulting cluster sizes were compared by correlation coefficients between all pairs of samples in the study (Fig. 208). The most consistent results (yellow squares) were seen within samples from one subject, analyzed on 1 day and one cytometer. Samples analyzed on the same day and cytometer, but from different subjects, showed the next smallest diversity (compare subjects 1 vs. 2, and 4 vs. 5). Weaker correlations (blue shades) occurred between samples analyzed on different days, or different cytometers. Similar batch effects are seen in data sets from many labs. These effects should be addressed at two levels: experimental and computational. At the experimental level, day-to-day variation can be minimized by stringent adherence to good protocols for sample handling, staining, and cytometer settings (see Chapter III, Sections 1 and 2). For multisite studies, cross-center proficiency training can help to improve compliance with standard protocols. If shipping samples is possible, a central laboratory can reduce variability in the staining and flow cytometer settings. Clearly, performing a study in a single batch is ideal, but in many cases this is not possible.

***Ameliorating batch effects during analysis*:** At the analysis level, some batch effects can be reduced during further analysis. In experiments in which batch effects occur due to variability in staining or cytometer settings, algorithms for reducing this variation by channel-specific normalization have been developed (below). Batch effects due to other causes may be more difficult to correct. For example, increased cell death is another potential batch problem that is not completely solved by just gating out dead cells, because marker levels on other subpopulations can also be altered before the cells die.

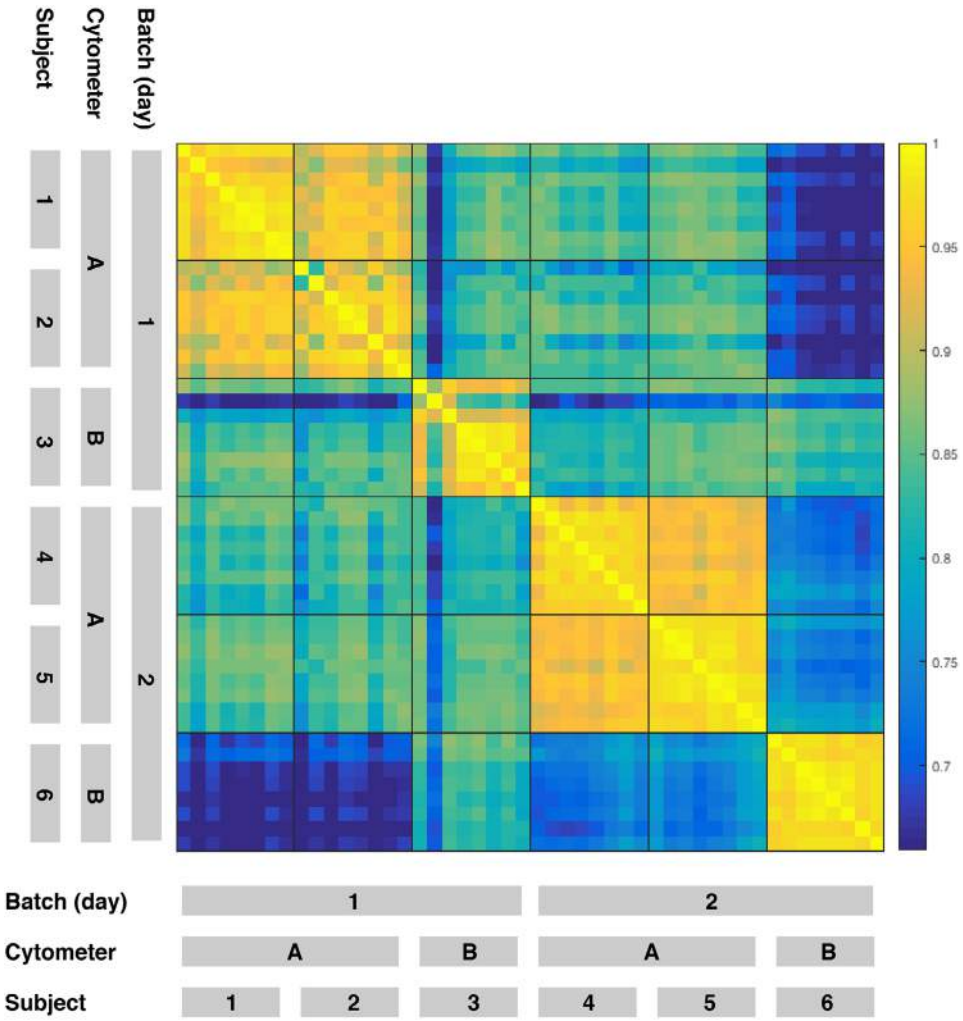

Figure 208. Quality control analysis to detect batch effects. Eight sequential blood samples each from six subjects were analyzed by FCM, clustered using the SWIFT algorithm, and Pearson correlation coefficients in the number of cells per cluster were calculated between all pairs of subjects. Samples were analyzed for 2 days, and on two identically configured LSR-II cytometers. Data files can be found here: https://flowrepository.org/id/FR-FCM-ZZ8W

***Curation of datasets*:** In some datasets, curating names and metadata may be necessary, especially when following the MIFlowCyt Standard (See Chapter VIII Section 3 Analysis presentation and publication (MIFlowCyt)). The manual entry error rate can be greatly reduced by using an automated Laboratory Information Management System (e.g., FlowLIMS, http://sourceforge.net/projects/flowlims) and automated sample data entry. As manual keyboard input is a major source of error, an LIMS system can achieve a lower error rate by minimizing operator input through automated data input (e.g., by scanning 2D barcodes) or pre-assigned label choices on pull-down menus. Although compensation is conveniently performed by automated "wizards" in popular FCM analysis programs, this does not always provide the best values, and should be checked by, e.g., $N \times N$ displays showing all possible two-parameter plots. Further information on compensation can be found in [60]. CyTOF mass spectrometry data needs much less compensation, but some cross-channel adjustment may be necessary in case of isotope impurities, or the possibility of M+16 peaks due to metal oxidation [1806].

In some data sets, further data curation is necessary. Defects at specific times during data collection, e.g., bubbles or changes in flow rate, can be detected and the suspect events removed by programs such as flowClean [1807]. Furthermore, compensation cannot be performed correctly on boundary events (i.e., events with at least one uncompensated channel value outside the upper or lower limits of its detector) because at least one channel value is unknown. The upper and lower detection limits can be determined experimentally by manual inspection or by programs such as SWIFT [1801]. The investigator then must decide whether to exclude such events from further analysis, or to keep the saturated events but note how this may affect downstream analysis.

***Transformation of raw flow data*.** Fluorescence intensity and scatter data tend to be log-normally distributed, often exhibiting highly skewed distributions. Flow data also typically contain some negative values, mainly due to compensation spreading but also partly because of subtractions in the initial collection of data. Data transformations (e.g., inverse hyperbolic sine, or logicle) should be used to facilitate visualization and interpretation by reducing fluorescence intensity variability of individual events within similar subpopulations across samples [1808]. Several transformation methods are available in the package flowTrans [1809], and should be evaluated experimentally to determine their effects on

the data with regard to the automated methods used and further downstream analysis.

***Registration/normalization of fluorescence intensity values*:** Normalization between data sets with regard to fluorescence intensities can be accomplished either by adjusting gates (i.e., manually specified filters or probabilistic models designed to enumerate events within defined regions of the data) between samples, or by moving sample data closer to the gates via fluorescence intensity registration. Auto-positioning "magnetic" gates can reconcile slight differences between samples in programs like FlowJo (Tree Star) and WinList (Verity Software House), but large shifts in subpopulation locations are difficult to accommodate. Several semi-automated methods of fluorescence intensity registration are available (e.g., fdaNorm and gaussNorm [1810, 1811]). These attempt to move the actual data-points across samples to similar regions, thus allowing gates to be applied to all samples without adjustment. Both fdaNorm and gaussNorm register one channel at a time, and do not address multidimensional linkages between biological sub-populations. The methods further require pregating to expose subpopulation "landmarks" (peaks or valleys in 1D histograms) to register effectively. However, this "global" approach does not adequately capture the semantics of biologically interesting rare subpopulations that are often obscured by high-density data regions. A recent extension [1811] of the fdaNorm method attempts to address this shortcoming by tightly integrating "local" (subpopulation specific) registration with the manual gating process, thus preserving the multidimensional linkages of rare subpopulations, but still requiring a hierarchy of manual gates derived from a reference sample. Fully automated fluorescence intensity registration methods are in development.

2 Identification of subpopulation sizes and properties by gating

***Sequential bivariate gating*:** Once data preprocessing steps are complete, users can identify cell populations using manual analysis or one or more of more than 50+ automated gating algorithms currently available [599, 1812]. Sequential gating in 2D plots is the standard method for manual analysis. Rectangular gates are convenient for well-separated sub-populations, but more subtle gates are often required, e.g., elliptical gates to define subpopulations in close proximity, or "spider" gates (available in FlowJo) to allow for fluorescence spreading due to compensation. The sequence of gates can be important because the desired subpopulation may be visualized more effectively by particular marker combinations.

***Back-gating*:** A critically important step for gating high-dimensional data is to **optimize the gates using back-gating**, which involves examining the cell subpopulations that satisfy all but one of the final gates. This procedure is performed for each gate in turn, and is critically important because small cell subpopulations may be defined by boundaries that are different from the boundaries of bulk subpopulations, e.g., stimulated cytokine-producing T cells display less CD3 and CD4 than unstimulated T cells, so setting the $CD3^+$ and $CD4^+$ gates on the bulk T-cell subpopulation will give suboptimal gates for the stimulated T cells (Fig. 209). Back-gating partly compensates for the inability of manual gating to use all dimensions simultaneously, as can be achieved in algorithmic clustering.

***Validation of gated or clustered sub-populations*:** Another critical issue is to **examine the final gated sub-populations** carefully, using prior knowledge and expectations from the biology. Figure 210 illustrates the importance of detailed examination using three artificial samples—a negative control that has no positive cells in either dimension (left); a positive sample that has small subpopulations of A+B– and A–B+ cells (middle); and a sample that has no obvious positive subpopulations, but has a slightly increased fluorescence intensity resulting in cells appearing in the A+B– and A–B+ gates (right). If the results of gating are accepted blindly, then samples 2 and 3 will be evaluated as having similar A+B– and A–B+ responses, whereas examination of the plots suggests a very different interpretation. Biological insight is also very useful—if a large subpopulation appears to be positive for a marker that is usually expressed only on a minor subpopulation, it should be suspected that there is an unusually high background for that marker on some cells and further experiments should be done to confirm the specificity of binding.

A limitation of manual gating in sequential two-dimensional plots is that two sub-populations may not be fully resolved in any combination of two dimensions, even though the sub-populations are fully resolved if all dimensions are considered simultaneously (which is only possible by algorithmic analysis). Thus in manual gating, it is sometimes necessary to make choices based either on recovering the largest number of the target cells (wider gates, at the expense of increased contamination), or identifying cells with the most certainty (narrower gates, at the expense of some loss of positive cells).

Another limitation of manual gating in sequential 2D plots is that human subjectivity has been identified as a primary source of variation within analyzed results [609, 1804]. Automated analysis methods have reached a state where they can now provide a solution to the challenge of analyzing big sets of FCM data. If chosen and used with care, many of these automated tools show as good, or even better, as well as more consistent analytic results compared with those performed by "human" users [1795, 1802, 1813, 1814].

Automated gating algorithms can be categorized as supervised or unsupervised. Supervised approaches to cell population identification incorporate user knowledge into the algorithm at various points. As such, supervised approaches are especially beneficial when users have project-specific expectations (e.g., target cell populations of interest, based on an existing gating strategy the user is trying to replicate). The most general type of supervised learning is where the method takes as input one or few training sample(s) in which all cells are manually gated and assigned to a cell population. This sample(s) trains a classification model that then classifies the cells of similar ungated samples. Examples of models tested in this category include the neural network [1815], support vector machine [1816], and hierarchical agglomerative hierarchy construction [1817]. On the other hand, OpenCyto [1818] and flowDensity [1819] approach the problem

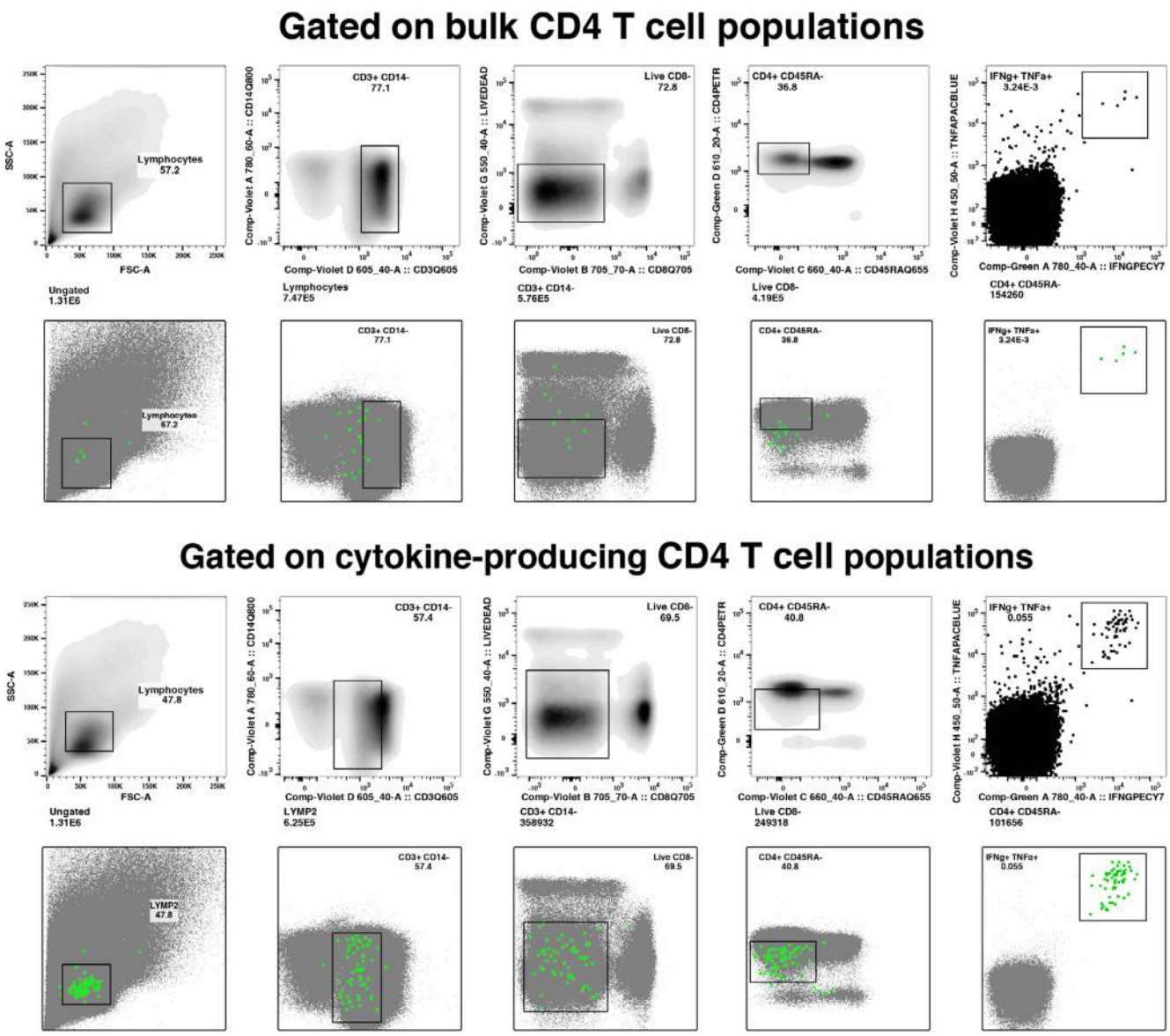

Figure 209. Importance of back-gating for minor subpopulations. A sample from the study described in Fig. 207 was stimulated in vitro with influenza peptides, and cytokine-producing cells were then identified by Intracellular Cytokine Staining and FCM. The top row shows the sequential gating of memory CD4 T cells ($CD3^+CD4^+CD8^-CD14^-$ Live $CD45RA^-$), using gates appropriate for the bulk memory population. However, backgating in FlowJo (row 2) shows that these gates do not capture many of the CD4 T cells secreting cytokines in response to the influenza peptides. Adjusting the gates by back gating results in much better identification of the stimulated, cytokine-expressing T cells that have slightly different values for several parameters (rows 3 and 4). The negative control sample contained zero cells in the final $TNF\alpha^+$ $IFN\gamma^+$ gate. Data files can be found here: https://flowrepository.org/id/FR-FCM-ZZ8H

by mimicking the manual gating process. Machine learning methods such as flowLearn aim to automate the parameterization of supervised methods [1820]. Users can specify everything from desired gate characteristics to the dimensions on which the algorithm should gate. Users can even provide a single or few gated samples for the algorithm to learn gate characteristics from ref. [1820]. When using machine-learning methods, these samples must have similar fluorescent value and shape distributions as their ungated counterparts for the methods to work [1815, 1820]. The development of machine learning approaches for supervised gating is still in its infancy, but holds great potential to ease the burden of automating the identification of specific cell populations of interest based on a prescribed gating hierarchy. The resulting gates can then be extracted, plotted, and adjusted until they are satisfactory. Since the plots produced can be specified to match a gating strategy, they can easily be used to communicate with those who are not familiar with the computational aspects of analysis. Moreover, comprehensive analysis of state-of-the-art supervised algorithms through the FlowCAP effort has shown that these approaches produce unbiased results and can reduce

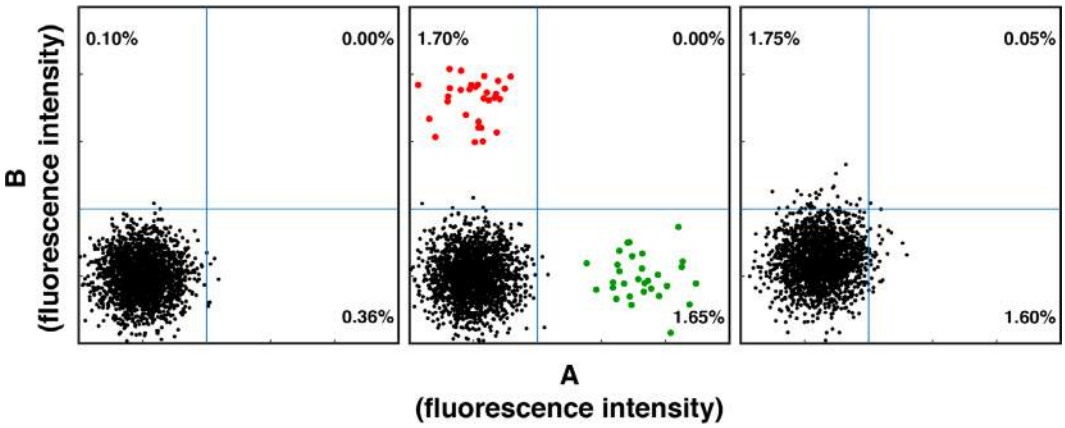

Figure 210. Model data illustrating the very different interpretations of two samples with similar proportions of cells in a positive gate. Left: A double-negative (A–B–) population with a random normal distribution is modeled. Middle: Two extra small sub-populations with random normal distributions are added to the A–B– sub-population. The red and green subpopulations contain few cells, but are well-separated from the A–B– population. Right: The "negative" subpopulation has been shifted slightly, but no distinct smaller subpopulations are present.

analysis variability by up to 94% compared with that occurring with manual analysis [1802]. Given the inputs required, it is ideal to have a well-made or established gating strategy in hand when operating these methods, as indicated in refs. [1802, 1821].

While supervised algorithms take into account user specified cell populations, unsupervised algorithms, such as flowMerge [1800] and flowMeans [1822], "cluster" or group cells with similar fluorescent intensities for similar groups of markers directly in high-dimensional space. In contrast with supervised methods, unsupervised methods often do not require user input. However, many methods do allow users to tweak results by changing few global parameter(s), such as the number of cell populations expected. Clustering procedures are great for discovering new natural cell populations which can then be manually validated and gated for using optimized gating strategies generated by tools such as GateFinder [1823] (convex hull gates) and HyperGate [147] (rectangular gates)—note that these are also good for finding optimized gates that may differ for sorting and gating purposes. These approaches are described more fully in the Clustering section (Chapter VII section 1.5).

Regardless of whether manual or automated gating is used to identify cell populations, careful examination of the results on test data sets through examination of familiar bivariate scatter plots is necessary to validate the results. Dimensional reduction tools such as *t*-distributed stochastic neighbor embedding [144, 1824] can be helpful in this regard. Tools for examining the output of automated methods are built in to programs such as FLOCK and SWIFT, and available as plugins in FlowJo, Cytobank, and FCS Express.

For scientists interested in adopting automated methods, collaboration with bioinformaticians is perhaps the quickest path to explore. Learning how to use the algorithms is another option. The most comprehensive library of FCM analysis tools built to date can be found on R/Bioconductor [599]. Although not the most user-friendly choice, R uses a command-line interface to provide a powerful foundation for many data mining and statistical computational tools. A subset of Bioconductor tools are available and can be integrated with more user friendly graphical user interfaces [1825] such as FlowJo, CytoBank [1826], FCSExpress, SPICE [1827], and GenePattern [1828].

With the growing amount of data becoming available, automated analysis is becoming an essential part of the analysis procedure [1829]. Only by taking advantage of cutting-edge computational abilities will we be able to realize the full potential of data sets now being generated.

***Description of final sub-populations*:** The final subpopulations identified by analysis are identified mainly by their fluorescence intensities for each marker. For some markers, e.g., CD4 on T cells, the positive cells comprise a log-symmetrical, clearly separated peak, and the center of this peak can be described by the geometric mean, the mode, or the median with very similar results. However, if a positive peak is incompletely separated from negative cells, the fluorescence values obtained by these methods can vary substantially, and are also highly dependent on the exact positioning of a manual gate. If a subpopulation is present as a shoulder of a larger, negative peak, there may not be a mode, and the geomean and median may have substantially different values.

3 Post-processing of subpopulation data: Comparison of experimental groups and identification of significantly altered subpopulations.

Regardless of the primary analysis method, the output of most FCM analyses consists of the sizes (cell numbers) and MdFIs of many cell subpopulations. Differences between samples (e.g., in different groups of a clinical study) can be performed by standard statistical analysis, using methods appropriate for each particular study. It is very important to address the problem of multiple outcomes, and this is even more critical in high-dimensional datasets because the potential number of subpopulations is very large, and so there is a large potential multiple outcome error. By automated

analysis, hundreds or even thousands of subpopulations can be identified [1801, 1805], and manual analysis also addresses similar complexity even if each subpopulation is not explicitly identified. As in the analysis of microarray and deep sequencing data, it is important to consider the false discovery rate, using a strong multiple outcomes correction such as the Benjamini–Hochberg strategy [1830] or alternative strategies [1831]. Applying corrections to data from automated analysis is relatively easy because the total number N of subpopulations is known [1832], but it is very difficult to identify N for manual bivariate gating, because a skilled operator exploring a dataset will consider many subpopulations before intuitively focusing on a smaller number of "populations of interest." To avoid errors in evaluating significance due to multiple outcomes in manual gating, strategies include: performing the exploratory gating analysis on half of the data, and calculating the statistics on the other half; or performing a confirmatory study with one or a few predictions; or specifying the target subpopulation before starting to analyze the study.

Comprehensible visualizations are essential for the communication, validation, exploration, and discovery of possibly significant cell populations. In conjunction with cell population identification algorithms, visualization is an often overlooked but essential part of the discovery and diagnosis process (see green box in Fig. 207).

Visualization can be a challenge for unsupervised clustering algorithms, as it is difficult for users to comprehend the cell populations identified in high-dimensional space. Therefore, dimension reduction is increasingly being applied to map multidimensional (i.e., samples using more than two markers) results onto a 2D plane for viewing. For instance, the SPADE algorithm colors and connects significant, structurally similar immunophenotypes together in the form of a minimum spanning tree, or a tree-like form [1804]. Dimensionality reduction techniques such as those based on *t*-distributed stochastic neighbor embedding arrange cell populations in a way that conserves the spatial structure of the cell populations in high-dimensional space (See Chapter VII Section 1.4 Dimensionality reduction). This way, users get a more representative view of cluster distributions [1833]. However, these and some other dimensionality reduction methods do not explicitly identify and partition cells into subpopulations. Other methods, such as PhenoGraph [2252] and Cytometree [2250], opt to combine all the analysis processes—segmenting cells into their phenotypically similar subpopulations, which are then labeled and visualized—without loss in performance and accuracy [1814].

Conversely, RchyOptimyx [1834, 1835], gEM/GANN [1836], and FloReMi [1837] use already-labeled samples (e.g., subject has or does not have a certain disease) to extract and display only the cell populations that most significantly discriminate between the differently labeled samples. These cell populations can then be used as indicators, and thus one can target these cell populations, when determining the label of future samples [1813]. Such visualizations aim to focus in on only the most important data structures present to facilitate human interpretation of the data. A comprehensive review of the available visualization algorithms is covered in ref. [1838].

1.3 *Artificial intelligence in FCM*

Since the advent of the first computing devices, scientists have been fascinated by the possibility to use these machines to mimic the remarkable capacities of the human brain. The broad field of artificial intelligence (AI) spans a wide variety of different techniques to represent knowledge and infer new knowledge from it. For FCM data analysis, the machine learning field, a subfield of AI that focuses on learning models from data, can be considered the most relevant. These techniques include the various types of supervised and unsupervised learning that we have discussed earlier. However, some novel types of machine learning approaches are making their way into the single cell field, most notably the novel types of deep learning approaches.

Deep neural networks are a recent development in the AI field [1839], building further on the classical techniques of neural networks that have already been proposed in the 1950's [1840]. Deep neural networks further build on classical neural networks, but include a much larger number of feature transformations that allow them to make high-level abstractions that are useful for model learning. These networks have been shown particularly suited to work on image types of representations [1841]. Therefore, deep learning methods are suitable models for different types of cytometry where image data is produced [1842], such as imaging FCM [1843] and imaging mass cytometry [1844].

However, deep learning models are generally applicable, and recent work in the field has shown promising results, such as the CellCNN network [1845], an adaptation of convolutional neural networks (CNNs) for cytometry data, or DeepCyTof [1846], a deep learning framework for automated gating. As the number of deep learning papers on single-cell data has recently exploded in the literature, it can be expected that also many of these new techniques will be applicable for FCM data, including novel methods for batch effect correction, data visualization, and automated cell type identification.

1.4 *Dimensionality reduction*

Visual data exploration is a powerful tool for hypothesis generation. Traditionally, FCM data are being visualized by a set of 2D scatter plots, where in each plot two of the available markers are selected and plotted against each other on the two axes of the plot. With the increasing number of markers provided by novel acquisition techniques [31, 1847] pairwise analysis becomes infeasible. Instead, so-called dimensionality reduction techniques aim to visualize the data by finding a low-dimensional representation that preserves as much structure as possible from a high-dimensional input. In the context of FCM, the original high-dimensional space is formed by treating each marker as a dimension.

However, unless the original data is of low-dimensional nature, embedded in the high-dimensional space, the dimensionality-reduced representation cannot preserve all existing structure. A number of approaches with different goals with regard to the preserved structure have been employed in single-cell analy-

sis. The most common ones are Principal Component Analysis (PCA) [1848], t-distributed stochastic neighbor embedding (t-SNE) [144], and very recently Uniform Manifold Approximation and Projection (UMAP) [1471].

1.4.1 PCA. PCA is a well-known technique that has been used early on for cytometry analysis [1849, 1850]. In short, PCA uses a set of linear transformations, on the original high-dimensional space, such that the axes of main variation (the principal components) in the data are mapped to the axes of the resulting space in order of the amount of variation. For visualization in a 2D scatterplot, the two principal components with the highest variation are then chosen as the axes of the plot and the other components are simply projected onto the given 2D plane. The resulting mapping preserves relative distances, however, due to its rigid transformations, it cannot faithfully represent nonlinear structure, typically present in single-cell cytometry data [1824].

1.4.2 t-Distributed stochastic neighbor embedding. Recently, t-SNE was established as the gold standard for dimensionality reduction of cytometry data. Introduced into the field under the name viSNE [1824], it is implemented in a plethora of widely used cytometry analysis platforms such as Cytobank [1851], Cytosplore [1852], or cytofkit [1853]. t-SNE is a nonlinear dimensionality reduction technique and as such has largely different goals than the above described PCA. Instead of using only transformations that conserve relative distances, t-SNE aims at preserving local neighborhoods. For a detailed description of the mathematical background of t-SNE, we refer to the original publication [144]. In short, t-SNE first computes local neighborhoods in the high-dimensional space. Such neighborhoods are described by low pairwise distances between data points, for example in Euclidean space. Intuitively, the size of these neighborhoods is defined by the perplexity parameter. In a second step, t-SNE iteratively optimizes the point placement in the low-dimensional space, such that the resulting mapping groups neighbors of the high-dimensional space into neighborhoods in the low dimensional space. In practice, cells with a similar expression over all markers will group into “islands" or visual clusters of similar density in the resulting plot while separate islands indicate different cell types (Fig. 211). When interpreting the resulting t-SNE maps, it is important to understand that the optimization only preserves relative distances within these islands, while the distances between islands are largely meaningless. While this effect can be softened, by using large perplexity values [1854], this hampers the ability to resolve fine-grained structure and comes at large computational cost.

The perplexity is only one of several parameters that can have major impact on the quality of a final t-SNE embedding. Wattenberg et al. provide an interactive tool to get a general intuition for the impact of the different parameters [1855]. In the context of FCM rigorous parameter exploration and optimization, particularly for large data, has been carried out recently by Belkina et al. [1856].

While t-SNE has gained wide traction due to its ability to effectively separate and visualize different cell type in a single plot, it is limited by its computational performance. The exact t-SNE implementation becomes computationally infeasible with a few thousand points [1857]. Barnes Hut SNE [1858] improves on this by optimizing the pairwise distances in the low dimensional space only close data points exactly and grouping large distance data points. A-tSNE [1859] only approximates neighborhoods in the high-dimensional space. FIt-SNE [1860] also uses approximated neighborhood computation and optimizes the low dimensional placement on a grid in the Fourier domain. All these techniques can also be combined with automated optimal parameter estimation [1856].

1.4.3 Uniform Manifold Approximation and Projection. As a result of these optimizations, t-SNE embeddings for millions of data-points are feasible. A similar technique called UMAP [1471] has recently been evaluated for the analysis of cytometry data [1470]. UMAP has similar goals as t-SNE, however, also models global distances and, compared to the exact calculation, provides a significant performances improvement.

While UMAP as well as optimized t-SNE methods provide the possibility to show millions of points in a single plot, such a plot will often lack detail for fine-grained structures, simply due to the limited visual space. Hierarchical SNE [1861] builds a hierarchy on the data, respecting the nonlinear structure, and allows interactive exploration through a divide and conquer approach. It has been adapted and tested with cytometry data in Cytosplore [1862].

Generally, dimensionality reduction provides means to visualize the structure of high-dimensional data in a 2D or 3D plot, however it does not provide automated cell classification or clustering. For biological interpretation or quantification, the dimensionality reduced data needs to be augmented with additional information and tools. viSNE [1824] allows to overlay a single marker as color on each of the plotted cells. Multiple plots with different markers overlayed can then be used to interpret the biological meaning of each cell and manually gate. It has been shown that t-SNE relates to spectral clustering [1863], meaning that visual clusters in the t-SNE embedding can be extracted using automatic clustering techniques as is being done with tools like ACCENSE [1864], or mean shift clustering implemented in Cytosplore [1852] where the resulting clusters can also directly be inspected in standard visualizations such as heatmaps.

1.5 *Clustering*

To identify subpopulations of cells with similar marker expressions, most researchers apply hierarchical gating, an iterative procedure of selecting subpopulations based on scatter plots showing two markers at a time. To automate the detection of cell populations, clustering algorithms are well suited. These algorithms do not make any assumptions about expected populations and take all markers for all cells into account when grouping cells with

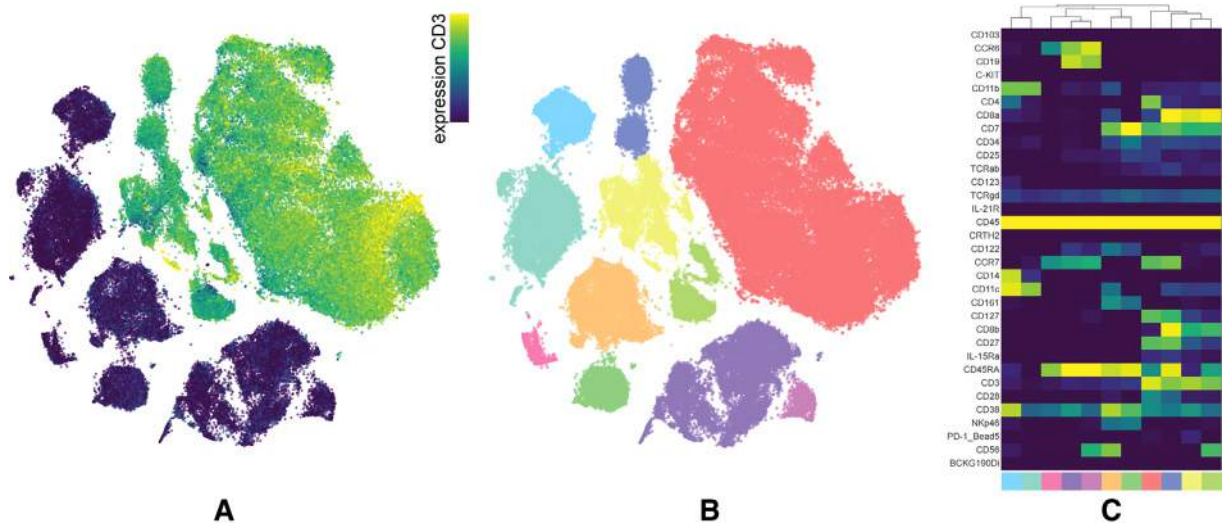

Figure 211. A t-SNE embedding of a mass cytometry dataset consisting of 100.000 cells. Each dot represents a cell. The typical islands of similar cells can be seen. Color overlay in (A) represents expression of one marker, in (B) identified islands of similar cells and the median expression for all markers/islands as a heatmap in (C).

similar marker expressions. The results correspond with cell populations, like typically obtained by manual gating, but without any assumptions about the optimal order in which markers should be evaluated or which markers are most relevant for which subpopulations, allowing the detection of unexpected populations. This is especially valuable for bigger panels, as the possible amount of 2D scatter plots to explore increases quadratically.

The first time a clustering approach was proposed for cytometry data was in 1985, by Robert F. Murphy [1865]. Since then, many clustering algorithms have been proposed for cytometry data and benchmark studies have shown that in many cases they obtain solutions very similar to manual gating results [1795, 1814].

From the many clustering algorithms proposed, several types can be distinguished. Model-based tools try to identify clusters by fitting specific models to the distribution of the data (e.g., flowClust, flowMerge, FLAME, immunoclust, Aspire, SWIFT, BayesFlow, flowGM), while others rather try to fit an optimal representative per cluster (e.g., kMeans, flowMeans, FlowSOM). Some use hierarchical clustering approaches (Rclusterpp, SPADE, Citrus), while others use an underlying graph-structure to model the data (e.g., SamSPECTRAL, PhenoGraph). Finally, several algorithms use the data density (e.g., FLOCK, flowPeaks, X-shift, FlowGrid) or the density of a reduced data space (ACCENSE, DensVM, ClusterX). Overall, these algorithms make different assumptions, and it is important to understand their main ideas to have a correct interpretation of their results.

All these clustering algorithms belong to the group of unsupervised machine learning algorithms, meaning that there are no example labels or groupings given for any of the cells. Only the measurements of the flow cytometer and a few parameter settings (e.g., the expected number of clusters) are given as input to the algorithm. It should be noted that most clustering algorithms thus only identify groups of cells with similar marker expressions, and do not yet label the subpopulations found. The researcher still needs to look at the descriptive marker patterns to identify which known cell populations the clusters correspond with. Some tools have been developed which can help with this, such as GateFinder [146] or MEM [1866]. Alternatively, if the user is mainly interested in replicating a well-known gating strategy, it would be more relevant to apply a supervised strategy instead of a clustering approach (e.g., making use of OpenCyto [1818] or flowLearn [1820]).

One important aspect of an automated cell population clustering is choosing the number of clusters. Several clustering tools take the number of clusters explicitly as input. Others have other parameters that are directly correlated with the number of clusters (e.g., neighborhood size in density based clustering algorithms). Finally, there also exist approaches that will try several parameter settings and evaluate which clustering was most successful. In this case, it is important that the evaluation criterion corresponds well with the biological interpretation of the data. In those cases where the number of clusters is not automatically optimized, it is important that the end user does several quality checks on the clusters to ensure they are cohesive and not over- or under-clustered.

1.6 *Integration of cytometric data into multiomics analysis*

While FCM enables detailed analysis of cellular systems, complete biological profiling in clinical settings can only be achieved using a coordinated set of omics assays targeting various levels of biology. Such assays include, transcriptomics [1867–1869], proteomics [1870–1872], metabolomics analysis of plasma [1873–1875], serum [1876–1878] and urine [1879, 1880], microbiome analysis of various sources [1881], imaging assays [1882, 1883],

data from wearable devices [1884], and electronic health record data [1885]. The large amount of data produced by each of these sources often requires specialized machine learning tools. Integration of such datasets in a "multiomics" setting requires a more complex machine learning pipeline that would remain robust in the face of inconsistent intrinsic properties of these high throughput assays and cohort specific variations. Such efforts often require close collaborations between biorepositories, laboratories specializing in modern assays, and machine learning consortiums [1795, 1813, 1886, 1887].

Several factors play a key role in integration of FCM and mass cytometry data with other high-throughput biological factors. First, much of the existing data integration pipelines are focused on measurements of the same entities at various biological levels (e.g., genomics [1867, 1888] profiled with transcriptomics [1869] and epigenetics [1889] analysis of the same samples). FCM, being a cellular assay with unique characteristics, lacks the biological basis that is shared among other popular datasets. This makes horizontal data integration across a shared concept (e.g., genes) challenging and has inspired the bioinformatics subfield of "multiomics" data fusion and integration [1890–1893]. In order to facilitate meaningful sample subgroup discovery and to uncover between-modality correlations, recently developed methodologies apply a variety of existing machine learning techniques, such as, matrix factorization and latent space modeling [1894, 1895], graph-based analysis [1896, 1897], consensus clustering [1898], and canonical correlation analysis [1899]. The implementation of principled multiomics analysis techniques therefore help to reveal the joint biological system and crosstalk between all measured biological datasets.

A second consideration for integration of FCM data with other omics modalities is the targeted nature of FCM. While FCM typically produces fewer measurements compared to genomics, transcriptomics, and proteomics datasets, the panel of markers measured is often carefully curated to target key cell types and signaling pathways. Therefore, if FCM data are simply combined with other high-throughput and high-content data modalities, the predictions will be primarily driven by the larger datasets [1900]. This is further complicated by the facts that large untargeted datasets often include highly correlated measurements (e.g., a large number of gene expressions measured from the same biological pathway). Therefore, an FCM data set, despite its smaller size, may have a higher information context than traditional untargeted assay. An example of this is demonstrated in a recent study of normal pregnancy in which a mass cytometry data set, despite its relatively small number of cell types and signaling pathways measured, required a higher number of principal components to account for 90% variance than large microbiome and transcriptomics datasets with tens of thousands of measurements [1901]. Therefore, computationally accounting for not only the number of measurements but also the redundancy of the measurements is of critical importance when integrating FCM data with other omics platforms [1901–1903].

1.7 *Modeling cell dynamics using trajectory inference*

While automated population identification techniques, such as the ones based on clustering, often make the assumption that cell populations are well separated in the space defined by all markers, trajectory inference methods intent to model dynamic biological processes. In this case, the assumption is made that differences between populations might not be well separated, but rather can be modeled as a continuum. This continuum then represents different stages, e.g., of a cell developmental process, and when sufficient cells are present in the different stages of the continuum, a model can be learned to represent this gradient. The first method to describe this novel class of techniques, Wanderlust [1904], was applied to mass cytometry, but since the advent of single-cell sequencing techniques the field of trajectory inference methods has exploded and currently more than 70 techniques are available [1905]. Many of these techniques have been developed for single-cell transcriptomics data, but often they can be applied equally well to cytometry data.

An example of the result of a trajectory inference method applied to a dataset of reprogramming fibroblasts is presented in Fig. 212. Here the black, bifurcating curve represents the model, where MEF cells either develop further to neurons or to myocytes [1906]. As cell developmental processes can be quite complex, e.g., resulting in very complex tree structures, accurately reconstructing the underlying topology of the trajectory is a very complex and challenging computational problem.

Conceptually, trajectory inference methods (sometimes also referred to as pseudo-temporal ordering methods) typically consist of two steps: a dimensionality reduction step, and a trajectory modeling step [1907]. Since many methods exist to perform either of those steps, a wide variety of combinations is available, and the current next challenge in the field is to compare these methods and find out which ones work best for which situation, providing a biological user with guidelines on good practices in the field [1905], along with novel ways of extracting dynamics of the system under investigation [1908].

2 Statistics for flow cytometry

2.1 *Background*

One of the attributes of cytometric systems is that a large number of cells can be analyzed. However, the data sets produced are just a series of numbers that need to be converted to information. Measuring large numbers of cells enables meaningful statistical analysis, which "transforms" a list of numbers to information.

At the most basic level, the objective of cytometric measurements is to determine if there is more than one population in a sample. In the case that two or more populations are completely separated, e.g., the subsets studied can be gated by virtue of phenotypic markers or easily separated by cluster analysis (for more

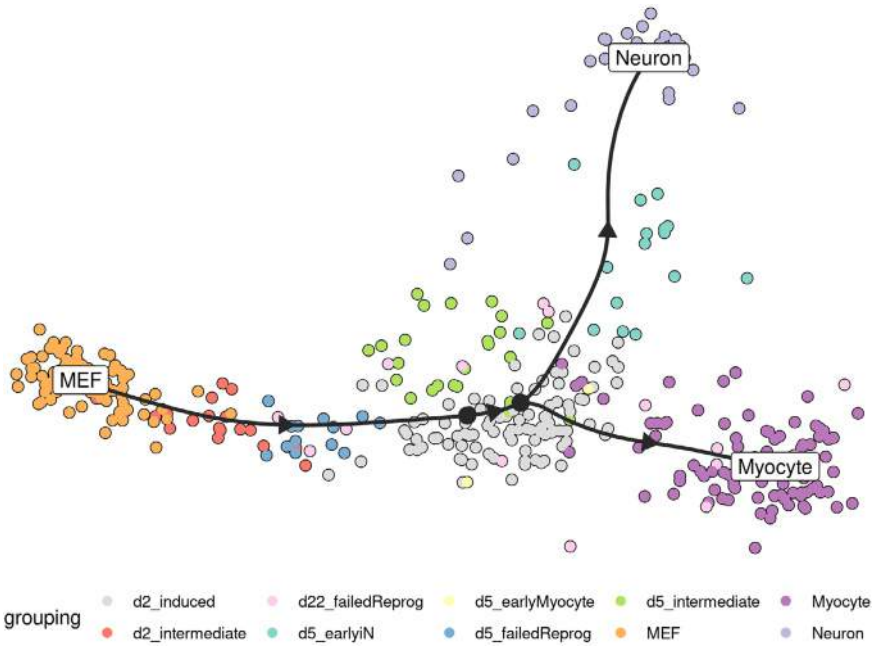

Figure 212. Example of a bifurcating trajectory, automatically constructed for a data set of reprogramming fibroblasts from ref. [1906].

detail please see Chapter VI Section 2: Automated data analysis: Automated FCM cell population identification and visualization), then the proportions of cells within each subset and additional measurement parameters for each subset can easily be calculated, and the analysis would be problem-free. However, problems arise when there is overlap between subsets, based on the parameters of the specific measurement, e.g., fluorescence or light scatter intensity.

Those performing DNA histogram cell-cycle cytometric analysis are accustomed to resolving the problem of overlap as this occurs at the G1:S and the S:G2+M interfaces of the histogram. G0, G1, S, and G2+M are phases during cell division and obviously have different DNA contents, which can be measured with DNA reactive fluorescent dyes by flow or image cytometry. A considerable body of analytical work has addressed this problem [1909–1912]. In contrast, relatively little such work has been carried out in immunocytochemical studies, where the time-honored method of resolving histogram data has been to place a delimiter at the upper end of the control and then score any cells above this point as (positively) labeled. This approach can lead to large errors and is best overcome by improvements in reagent quality to increase the separation between labeled and unlabeled populations in a cytometric data set, or by the addition of extra independent measurements like additional fluorescence parameters [1795]. But, this may not always be possible and any subset overlap needs to be resolved. See Chapter VII Section 1.2 that discusses data analysis and display. The tools available to resolve any subset overlap in mixed populations require an understanding of (i) probability, (ii) the type of distribution, (iii) the parameters of that distribution, and (iv) significance testing. An overlapping immunofluorescence example is shown below in subsection 3.6-Immunofluorescence example Table 91. Additionally the use of statistical methods for drawing conclusions at the level of data, derived from cytometric measurements, is essential, but not covered here specifically.

2.2 *Probability*

Qualitative statements on probability are not very useful for quantitative analysis of cytometric data, which are affected by variability of sample collection, sample preparation, sampling, measurement imprecision, and variability in manual or automated data analysis. Statistics allows us to derive quantitative probabilities from cytometric data, especially as many data points are generally measured in FCM. Probability designated with a *p*-value has a measurement range of zero, or absolutely impossible, to unity, or absolute certainty. Very few events, if any, occur with a *p*-value at these extremes. "The sun will rise tomorrow," is a statement with a *p*-value very close to unity. In contrast, "Man, one day, will run the 100 meters in 1 second," has a *p*-value of zero.

2.3 *Types of distributions*

There are many distributions but those most commonly encountered in the biological sciences are the Gaussian, binomial, and Poisson distributions.

2.3.1 The Gaussian distribution. The Gaussian distribution (error function, "normal" distribution) is a bell-shaped curve symmetrical about a mean value with the following formula

$$Y = \frac{1}{\sigma\sqrt{2\pi}} e^{-(X-X)^2/2\sigma^2} \quad (1)$$

where σ is the SD and $\bar{X}$ is the mean of the distribution. Algorithms, based on the Gaussian distribution, have been used extensively for cell cycle analysis by FCM [1912].

2.3.2 The binomial distribution. The binomial distribution is concerned with occurrences of mutually exclusive events and is given by the formula

$$(p+q)^n = 1 \tag{2}$$

where p is the chance of something happening and q is the chance of that same something not happening. If we throw two regular six-faced dice, n in the binomial equation is 2 and this expands the equation to $p^2 + 2pq + q^2 = 1$. The chance of getting 2 threes on a single paired throw is $p^2 = (1/6)^2$, the chance of getting one three and any other number is 2 $pq = 2 \times 1/6 \times 5/6$ and the chance that neither die will be a three is $(5/6)^2$. Hence, the total probability is given by $((1/6) \times (1/6)) + (2 \times 1/6 \times 5/6) + ((5/6) \times 5/6))$, which sums to unity. Rosenblatt et al. describe the use of a binomial distribution based algorithm to optimize flow cytometric cell sorting [1913].

2.3.3 The Poisson distribution. The Poisson distribution is used to describe the distribution of isolated events occurring in a continuum, originally formulated by Poisson [1914]. A good example is the number of cells passing the analysis point in the cytometer per second. Clearly you cannot ask the question of how many cells did not pass the analysis point per second, so neither the Gaussian nor the binomial distributions can handle this type of problem. In order to use the Poisson distribution all we need is z, the average number of times the event occurs within the continuum, where the probability of observing the event n times, $p(n)$, is given by

$$p(n) = 2^n e^{-z}/n! \tag{3}$$

where $n!$ is factorial n. The notation for the whole distribution that sums to unity is

$$P = \sum_{n-0}^{n-\infty} Z^n e^{-s}/n! \tag{4}$$

The Poisson distribution is important in cytometric cell sorting purity for investigating coincidence in which there could be a possibility of two or more cells being in the analysis point simultaneously. Poisson statistics also applies to the measurement of low intensity signals, where just a few photons contribute to the measurement, and to the counting of rare subpopulations, discussed in some more detail below.

2.4 *Distribution parameters*

These include measurement of (i) central tendency namely, the mean, percentiles, median, and mode, and (ii) dispersion parameters namely, the mean deviation, variance, SD, and CV, wherein the last of these, the CV of limited statistical significance, is the SD divided by the mean.

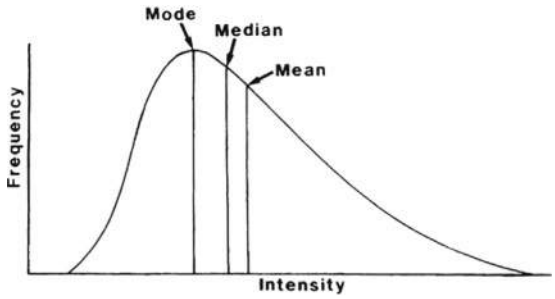

Figure 213. Measurements of central tendencies for cytometric intensity histograms. The curve is an ideal distribution, showing key measurements. Cytometric intensity histograms span a finite intensity range with a noisy curve and frequently with off-scale events at the lower and/or upper end(s) of the scale. Generally the median is the most robust measure, because the mean is heavily influenced by off-scale events and the mode by noise.

2.4.1 Central tendency. The goal of many cytometry measurements is the determination of the expression level of a given marker in a cell and its distribution in a cell population. The mean of a distribution is the sum of all the data points divided by the number of the values in the distribution. The *median* is the point in the distribution where half the data lie on either side; it is also known as the 50th percentile, the point, where 50% of the data has been accumulated. Twenty-fifth percentiles and 75th percentiles are also determined for distributions. The *mode* is the maximum frequency. But, this is an unreliable measurement of central tendency in cytometry for two reasons. First, the mode is meaningless if this is located in the first or last channel of the histogram. In some cases cytometry histograms have many off-scale events, which makes the fist or last channel in the histogram the highest point. Second, even though a large number of cells will have been sampled, the distribution is not continuous, due to the analog-to-digital conversion (ADC) step, i.e., intensity values are used as indices for incrementing histogram channels (e.g., 0 to 1023), and counting statistics as the SD of a count in a discrete "channel" is equal to the square root of the count (more below in Chapter VII Section 2.7: Rare cell analysis). Therefore, typical unsmoothed cytometry histograms are often very noisy. Any "noise" around the mode will give an erroneous result. The relationship between these parameters is shown in Fig. 213.

2.4.2 Dispersion parameters. Just as central tendency gives a measure of the overall "average" difference between Gaussian distributions, the dispersion parameters give a measure of the different spreads within and between those distributions.

The mean deviation is given by $\Sigma(X - \bar{X})$.
The variance, mean squared deviation, is given by $\Sigma(X - \bar{X})^2$.
The SD is given by $\sqrt{[\Sigma(X - \bar{X})^2]}$.

2.5 *Significance testing*

The central axiom in statistical theory is that the variance of the sum or difference of two independent and noncorrelated random variables is equal to the sum of their variances. These tests are designed to give a measure of how different two or more distributed populations might be.

The most commonly asked questions in cytometry are (i) is there more than one subset? and (ii) if there is more than one, how many cells are in each? This is far too naive a perspective, and with the statistical tools available we should be asking the following:

1. Is there more than one subset?
2. If there is more than one, how far "separated" are they?
3. What is the significance of that separation?
4. If the subsets are significantly separated, then what are the estimates of the relative proportions of cells in each ?
5. What significance can be assigned to the estimated proportions?

The statistical tests can be divided into two groups. (i) Parametric tests include the *SE of difference*, *Student's t-test*, and *variance analysis*. (ii) Non-parametric tests include the *Mann-Whitney U-test*, *Kolmogorov–Smirnov test*, and *rank correlation*.

2.5.1 Parametric tests. These may best be described as functions that have an analytic and mathematical basis where the distribution is known.

2.5.1.1 Standard error of difference. Every cytometric analysis is a sampling procedure as the total population cannot be analyzed. And, the SD of a sample, $\boldsymbol{s}$, is inversely proportional to the square root of the sample size, $\sqrt{N}$, hence the SEM, $\mathrm{SE_m} = \boldsymbol{s}/\sqrt{N}$. Squaring this gives the variance, V_m, where

$$V_\mathrm{m} = s^2/N \tag{5}$$

We can now extend this notation to two distributions with $\bar{X}_1$, $\boldsymbol{s}_1$, N_1, and $\bar{X}_2$, $\boldsymbol{s}_2$, N_2 representing, respectively, the mean, SD, and number of items in the two samples. The combined variance of the two distributions, $\mathrm{V_c}$, can now be obtained as

$$V_\mathrm{c} = (s_1^2/N_1) + (s_2^2/N_2) \tag{6}$$

Taking the square root of Equation (6), we get the SE of difference between means of the two samples. The difference between means is $(\bar{X}_1 - \bar{X}_2)$ and dividing this by $\sqrt{V_\mathrm{c}}$ (the SE of difference) gives the number of "standardized" SE difference units between the means; this standardized SE is associated with a probability derived from the cumulative frequency of the normal distribution.

2.5.1.2 Student's t-test. The approach outlined in the previous section is perfectly satisfactory if the number of items in the two samples is "large," as the variances of the two samples will approximate closely to the true population variance from which the samples were drawn. However, this is not entirely satisfactory if the sample numbers are "small." This is overcome with the *t*-test, invented by W.S. Gosset, a research chemist who very modestly published under the pseudonym "Student" [1915]. Student's *t* was later consolidated by Fisher [1916]. It is similar to the SE of difference but, it takes into account the dependence of variance on numbers in the samples and includes Bessel's correction for small sample size. Student's *t* is defined formally as the absolute difference between means divided by the SE of difference:

$$\text{Student's } t = \frac{|\bar{X}_1 - \bar{X}_2|\sqrt{N}}{\sigma} \tag{7}$$

When using Student's *t*, we assume the null hypothesis, meaning we believe there is no difference between the two populations and as a consequence, the two samples can be combined to calculate a pooled variance. The derivation of Student's *t* is discussed in greater detail in ref. [1917].

2.5.1.3 Variance analysis. A tacit assumption in using the null hypothesis for Student's *t* is that there is no difference between the means. But, when calculating the pooled variance, it is also assumed that no difference in the variances exists, and this should be shown to be true when using Student's *t*. This can first be addressed with the standard-error-of-difference method similar to Section 2.5.1.1 Standard Error of Difference, where $\mathrm{Var_s}$, the sample variance after Bessel's correction, is given by

$$\mathrm{Var_s} = \left\{\frac{(n_1 \times s_1^2) + (n_2 \times s_2^2)}{n_1 + n_2 - 2}\right\} \times \left\{\frac{1}{2n_1} + \frac{1}{2n_2}\right\} \tag{8}$$

The SE of the SD, $\mathrm{SE_s}$, is obtained as the square root of this best estimate of the sample variance (equation (8)). This is now divided into the difference between the two sample deviations.

The second method of addressing the variance analysis is to use the variance ratio [1918], designated the *F*-test by Snedcore [1919]. *F* is calculated as the ratio of the greater variance estimate of sample variance to the lesser estimate of sample variance. After Bessel's correction, we get the best estimate of the variances, σ^2, as,

$$\sigma^2 = \mathrm{Var_s} \times \left\{\frac{N}{N-1}\right\} \tag{9}$$

2.5.2 Nonparametric tests. These rely on ranking methods when there is no known, or suspected, distribution that can be assigned to samples being analyzed.

2.5.2.1 Mann–Whitney U. This problem was originally addressed by Wilcoxon [1920] and was later refined by Mann and Whitney [1921]. Consider two sets of data, the X-group and Y-group, containing 5 and 4 values respectively; these are illustrated in Table 84. These values have been ordered according to

Table 84. Comparison of two data sets X and Y in a rank analysis[a)]

Y-group			y_1			y_2		y_3	y_4
X-group	x_1	x_2		x_3	x_4		x_5		
Values	**3**	**7**	**9**	**15**	**23**	**31**	**36**	**44**	**51**
Rank	1	2	3	4	5	6	7	8	9

[a)] The values have been ordered according to magnitude in the third row with their rank position in the last row. The populations from which the data were drawn are shown in rows 1 and 2, the Y-group and X-group, respectively. It is clear that the Y-group is tending to be more to the right (greater magnitude) than the X-group, and the question is whether this arrangement could have occurred purely on a random basis. Reproduced with permission from ref. [1917].

magnitude in the third row with their rank position in the last row. The populations from which the data were drawn are shown in rows 1 and 2, the Y-group and X-group, respectively. It is clear that the Y-group is tending to be more to the right (greater magnitude) than the X-group, and the question is whether this arrangement could have occurred purely on a random basis. To do this, we determine how many x-values lie to the right of every y-value and sum the result to get U_y for the Y-group. There are three x-values (x_3, x_4, and x_5) to the right of y_1 and one x-value to the right of y_2, thus Uy sums to four. The same process is now carried out for the x-group to give $\boldsymbol{U}_x$ equal to 16. For small sample numbers, this procedure is satisfactory but it can be prohibitively time consuming for large samples for which the following expressions are used.

$$U_y = NxNy + \frac{Ny(Ny-1)}{2} - T_y$$
$$U_x = NxNy + \frac{Nx(Nx-1)}{2} - T_x \qquad (10)$$

Nx and Ny are the number of values in the X- and Y-groups, respectively, and T_y and T_x are the sums of the rank positions for the Y- and X-groups, respectively.

If the X- and Y-values are randomly distributed in the rank, the sum of the rank position T has a mean value of T and a variance of σ_T^2 given by the following expressions:

$$\bar{T}_x = \frac{Nx(Nx+Ny+1)}{2} \quad \text{and} \quad \bar{T}_y = \frac{Ny(Nx+Ny+1)}{2} \qquad (11)$$

These values of $\bar{T}_x$ and $\bar{T}_y$ will be identical if Nx and Ny are equal, but the variance, σ_T^2, will be the same irrespective of the numbers in each group and is given as

$$\sigma_{T^a} = \frac{NxNy(Nx+Ny+1)}{12} \qquad (12)$$

If both samples are large, >20, we take the values of T and $\bar{T}$ associated with the smaller of the pair of U-values, in this example the Y-group, to calculate the Z-statistic as follows:

$$Z = \frac{|T_y - \bar{T}_y|}{\sqrt{((NxNy(Nx+Ny+1))/12)}} \qquad (13)$$

The numerator in equation (13) represents the difference between the values of T for the Y-group and the mean, $\bar{T}$, that would be expected if the numbers were randomly distributed within the rank structure and the denominator is the square root of the variance. Hence, Z represents the observed deviation from the mean in SD units and the associated probability can be read off from the cumulative frequency of the normal curve because, for large samples, the Z-distribution approximates very closely to the Gaussian distribution.

Table 85. Part of the Mann–Whitney probability table example for the X-group size of Table 84 ($N_2 = 5$)[a)]

U	$N_1 = 1$	$N_1 = 2$	$N_1 = 3$	$N_1 = 4$	$N_1 = 5$
0	.167	.047	.018	.008	.004
1	.323	.095	.036	.016	.008
2	.500	.190	.071	.032	.016
3	.667	.286	.125	.056	.023
4		.429	.196	**.095**	.048
5		.571	.286	.143	.075
6			.393	.206	.111
7			.500	.278	.155
8			.607	.365	.210
9				.452	.271

[a)] Reproduced with permission from ref. [1917].

With small sample sizes, e.g., with less than 30 values, the Z-distribution does not approximate to a Gaussian curve, and Mann–Whitney computed the probabilities associated with U-values for different-sized samples. These data are arranged in tables for $N_2 = 3, 4, 5, 6$, and so on and within each table there are sample sizes for $N_1 = 1, 2, 3, 4, 5$ and so on versus the U-values and associated probabilities for the N_2 and N_1 sample sizes. The example for $N_2 = 5$ is shown in Table 85. The sample size of the X-group (N_2 in Table 85) is 5, and the associated U-value is 4. The number of data points in the Y-group is also 4, and hence, the probability that this distribution of data points in Table 84 is different can be read off as 0.095 in Table 85 and does not reach "significance" at the 1:20 level (0.05).

2.5.2.2 Kolmogorov–Smirnov statistic. In the Kolmogorov–Smirnov (K–S) statistic, D is a measure of the maximum vertical displacement between two cumulative frequency distributions. The one-tailed test compares an experimentally derived distribution with a theoretical cumulative frequency distribution and, the two-tailed test compares two experimentally derived distributions (for more detail, see Chapter 6 in ref. [1922]). In any biological system, a test sample should always be compared with a control, i.e., the two-tailed test, and this was first used in FCM by Young [1923].

The cumulative frequency distributions containing n_1 and n_2 cells in the control and test samples respectively can be calculated as follows for $i = 1 \leq 256$,

$$F_{n1}(i) = \sum_{j=1}^{j=i} f\ n1(j) \quad \text{and} \quad F_{n2}(i) = \sum_{j=1}^{j=i} f\ n2(j) \qquad (14)$$

Table 86. Kolmogorov–Smirnov (K–S) statistic critical values, D_c, with their associated p-values (probabilities)[a)]

D_c	1.0727	1.2238	1.3581	1.5174	1.6276	1.7317	1.8585	1.9525
p	0.200	0.100	0.050	0.020	0.010	0.005	0.002	0.001

[a)] Reproduced with permission from ref. [1917].

Table 87. Hypothetical results of the same determinations from two different laboratories[a)]

Sample	1	2	3	4	5	6	7	8	9	10
Lab A	.61	.23	.31	.11	.41	.19	.10	.03	.07	.17
Lab B	.54	.38	.42	.20	.36	.27	.21	.11	.14	.12

[a)] Reproduced with permission from ref. [1917].

These cumulative frequencies are now normalized to unity and the null hypothesis is assumed (i.e., both distributions are samples derived from the same population) where the probability functions $P_1(j)$ and $P_2(j)$ that underlie the respective frequency density functions (the histograms) $f\ n_1(j)$ and $f\ n_2(j)$ are samples assumed to be drawn from the same populations so that

$$P_1(j) = P_2(i), \quad -\infty \le j \le +\infty \tag{15}$$

The D-statistic is computed as the maximum absolute difference between the two normalized cumulative frequency distributions over the whole of the two distributions, where

$$D = \max_j |f\ n1(j) - f\ n2(j)| \tag{16}$$

As with the Mann–Whitney U, there is a variance, Var, associated with the assumed common population from which the two samples, containing n_1 and n_2 items, respectively, are drawn. This is given by

$$Var = \frac{(n_1 + n_2)}{n_1 \times n_2} \tag{17}$$

The SD s can now be found by taking the square root of this relationship, then dividing D by s gives D_{crit}, where

$$D_{\text{crit}} = \frac{\max |F_{n1} - F_{n2}|}{\sqrt{((n_1 + n_2)/(n_1 \times n_2))}} \tag{18}$$

This type of relationship, in which we divide a difference by a measure of dispersion, has been seen in all the other statistical tests described previously. Two-tailed critical D_c for large samples, along with their probabilities, are shown in Table 86.

2.5.2.3 Rank correlation. Correlation between two or more sets of measurements can be determined with Spearman's rank correlation coefficient [1924]. This enables an objective assessment to be made regarding the consistency between paired laboratory results as in the purely hypothetical data shown in Table 87.

When we look through these data, we find that both laboratories score sample 8 with the lowest results and in both cases these are ranked 1. Sample 9 from lab A has the next lowest value (0.07) and is ranked 2 but, it is sample 10 (0.12) that is ranked 2 in the lab B series, and these ranking positions are shown in Table 88.

Table 88. Ranking of the data from Table 87 with rank differences (d, and d^2)[a)]

Sample	1	2	3	4	5	6	7	8	9	10
Lab A	10	7	8	4	9	6	3	1	2	5
Lab B	10	8	9	4	7	6	5	1	3	2
Rank difference, d	0	–1	–1	0	2	0	–2	0	–1	3
d^2	0	1	1	0	4	0	4	0	1	9

[a)] Reproduced with permission from ref. [1917].

In terms of ranking alone, the two laboratories agree exactly for only four of the ten samples, namely 1, 4, 6, and 8. Spearman's rank correlation coefficient R is given by the expression:

$$R = 1 - \left\{ \frac{6\Sigma d^2}{n^3 - n} \right\} \tag{19}$$

Σd^2 is the sum of the squared rank differences and n is the number of samples; in our particular example, these values are 20 and 10, which gives $R = 0.8787$. This coefficient was designed to have a value of +1 if there is perfect ranking agreement and –1 where there is total ranking disagreement.

This value of 0.8787 for R would suggest that there is fairly close agreement between laboratories and where there are ten or more samples being compared we can use Student's t to assess the significance of comparison:

$$\text{Student's } t = R \times \sqrt{((n-2)/(1-R^2))} \tag{20}$$

which gives $t = 5.2$ with eight degrees of freedom associated with $P < 0.01$, which is highly significant and suggests there is close agreement between laboratories. However, this does not tell us anything about the quality of the "intersample" agreement from the two laboratories. This can be addressed by analysis of the differences in results from the laboratories as shown in Table 89.

The mean difference $\bar{X}$ is calculated by summing the data in the difference row and dividing by n, the number of samples, which gives –0.052. If there are no differences between laboratories, this mean value should not differ significantly from zero since any random differences should cancel out.

The variance, s^2, is calculated from the convenient relationship as

$$s^2 = \left(\Sigma X^2/n\right) - \bar{X}^2 \tag{21}$$

where $\mathbf{\Sigma}X^2$ is equivalent to $\mathbf{\Sigma}d^2 = 0.0824$ yielding $s^2 = 0.0055$. After Bessel's correction and using equation (6), we get Student's $t = 2.1$. This value of t, with nine degrees of freedom, does not quite reach the 5% probability level and we can conclude that the inter-laboratory differences are not significant. However, in a quality control exercise such as this, we would be justified in setting more stringent statistical criteria. If we now take a probability level of 0.1 for magnitude discrepancies between laboratories,

Table 89. Differences between values from Table 87 by subtracting Lab B results from those of Lab A

Sample	1	2	3	4	5	6	7	8	9	10
Lab A	0.61	0.23	0.31	0.11	0.41	0.19	0.10	0.03	0.07	0.17
Lab B	0.54	0.38	0.42	0.20	0.36	0.27	0.21	0.11	0.14	0.12
Sample difference, d	0.07	–0.15	–0.11	-0.09	0.05	–0.08	–0.11	–0.08	–0.07	0.05
d^2	0.0049	0.0225	0.0121	0.0081	0.0025	0.0064	0.0121	0.0064	0.0029	0.0025

which would be reasonable as we know they should be getting the same results, we must conclude there is something suspicious occurring in the generation of the results, which would require further investigation.

2.6 *An example of immunofluorescent staining in cytometry*

Figure 214 shows a histogram representation of weak staining of a small population. Statistical analysis of this datum must ask a number of questions.

First, is there any difference between these two datasets? This is addressed with a K–S analysis, which reveals that there is a maximum normalized vertical displacement of 0.0655 at channel 37 with 8976, N_1, and 8570, N_2, cells in the control and test sample, respectively (Fig. 215). K–S statistic gave $P < 0.05$, suggesting there is a statistical difference between the two datasets at the 1:20 probability level. The remaining data shown in this figure will become apparent later.

Second, can we establish the "meaning" of the discernible shoulder in the lower histogram of Fig. 214? This is addressed analytically using a concept derived from mechanics; namely, taking moments about a point. Imagine a weightless beam with two different weights hanging from the beam that will balance according to equation (22)

$$W_1(B - \bar{X}_1) = W_2(\bar{X}_2 - B) \tag{22}$$

where W_1 and W_2 are the "weights" hung from the beam, B is the balance point, and $\bar{X}_1$ and $\bar{X}_2$ are the distances of the respective weights from the balance point, B. On rearranging equation (22), we get

$$B = ((W_1\bar{X}_1) + (W_2\bar{X}_2))/(W_1 + W_2) \tag{23}$$

Let us suppose that the distances $\bar{X}_1$, $\bar{X}_2$, and B are known for a normalized total mass of unity, where $W_1 + W_2 = 1$. We can now calculate the relative proportion of W_2 by replacing W_1 with $(1.0 - W_2)$ in equation (23) and simplifying to give

$$W_2 = (B - \bar{X}_1)/(\bar{X}_2 - \bar{X}_1) \tag{24}$$

The "weight" in equation (24) that will now be referred to as "labeled cells," is defined by three distances namely, $\bar{X}_1$, $\bar{X}_2$, and B. $\bar{X}_1$ is the mean of the control unlabeled fraction, B is the mean of the test sample containing labeled and unlabeled cells,

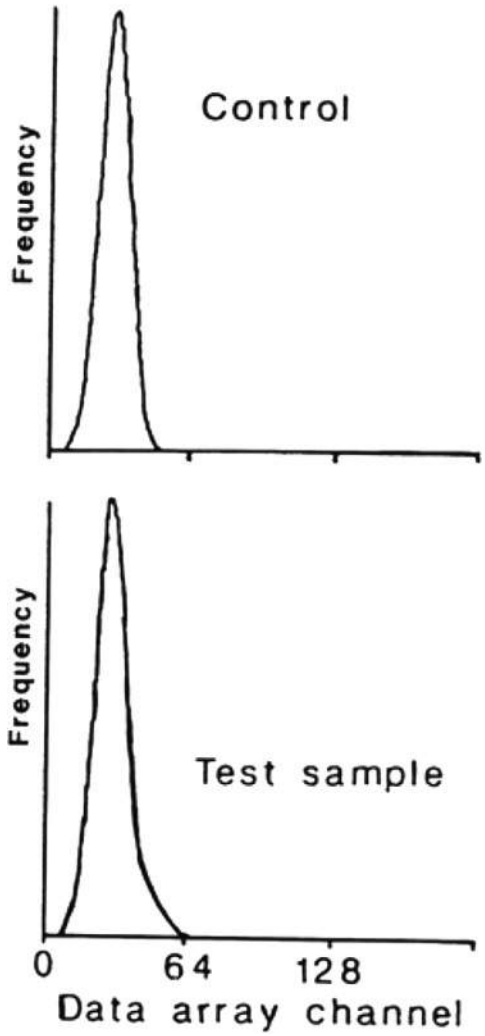

Figure 214. The histogram representation of fluorescence from a weak staining of a small (rare) population. The upper histogram shows an unstained control. A small shoulder from the staining of the rare population is visible in the lower histogram. Reproduced with permission from ref. [1925].

and both of these can be obtained directly from the experimental data. We now need to obtain $\bar{X}_2$, the mean of the labeled fraction, as follows:

It has been shown in ref. [1925] that the mean of the distribution obtained by subtracting the N_2 cumulative frequency from the cumulative frequency of N_1, is independent of the number of cells in N_1, and the mean of the subtracted distribution D_m, depicted in

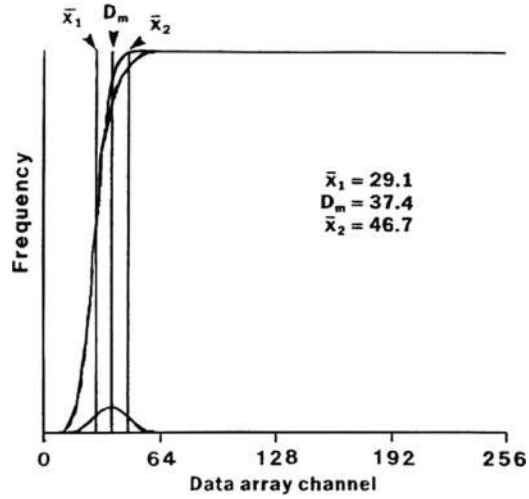

Figure 215. Cumulative frequencies from the two histograms in Fig. 214 and difference. Details on the calculation of $\overline{X1}$, $\overline{X2}$, and D_m are described in the text. Reproduced with permission from ref. [1925].

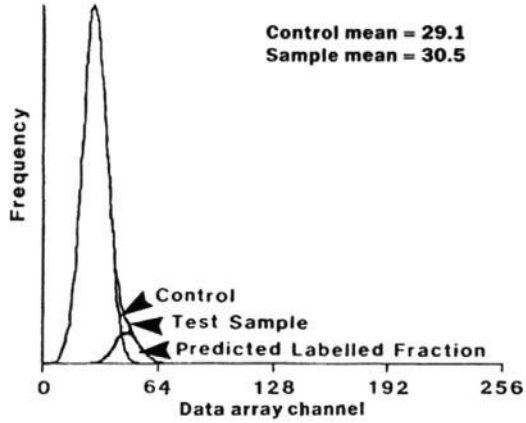

Figure 216. Result of the histogram analysis. The two original histograms and the calculated stained population are shown with population means. Reproduced with permission from ref. [1925].

Fig. 215, is exactly halfway between the means of N_1 and N_2. However, this applies to a continuous distribution and all cytometric distributions are not continuous due to the ADC conversion and a half channel correction must be applied to give the mean of the N_2 distribution as

$$\bar{X}_2 = (2.0 \times (D_m + 0.5)) - \bar{X}_1 \quad (25)$$

All the data have now been derived to calculate the proportion of cells in the N_2 distribution as W_2 from equation (24) by substituting the $\bar{X}_2$ of equation (25) and simplifying to give

$$W_2 = (B - \bar{X}_1)/(2.0 \times (D_m + 0.5 - \bar{X}_1)) \quad (26)$$

The data depicted in Fig. 214 were analyzed according to this ratio analysis of means to give $X_1 = 29.1$, $D_m = 37.4$ and $\bar{X}_2 = 46.7$ as shown in the figure and the predicted proportion in N_2 was 0.08. These data are shown in Fig. 216 where the control, test sample, and the predicted labeled fraction are labeled in the figure. The test sample results are shown Table 90. We now have to ask if this result is reasonable and what significance can be placed on the result.

2.6.1 K–S analysis. The cumulative frequency distributions of the control and test sample were re-analyzed over a range of ±3 SD about the mean of the predicted labeled distribution, X_2. With the number of cells involved, the K–S analysis showed that the two cumulative frequency distributions over this ±3 SD range had a probability of being different at the 99% confidence interval, $P < 0.01$.

2.6.2 Student's t. The results from the analysis of the test sample shown in Table 90 were also submitted to Student's t analysis (Chapter 7 in ref. [1917]). This gave $t = 65.58$ with 8568 degrees of freedom, $P < 0.001$.

Hence, we can present the results in probabilistic terms by saying the analysis was compatible with two subsets with means separated by 17.6 channels containing 92% and 8% of the population at the 99% confidence interval.

This analysis should only be used for symmetrical data sets with constant, or near constant, variance, and these data were chosen for illustration as they conformed to this condition. However, there are a number of other factors that should be considered, including positive skew that tends to be minimized with log-amplification as discussed elsewhere [1925]. Nevertheless, this analysis goes some way to producing a more statistically convincing method of presenting results of immunofluorescence data.

2.7 *Rare cell analysis*

Flow cytometric analysis of cell samples is often applied to characterize subsets of very low frequency, ranging from 1% to less than 1 ppm. In those cases, it is very important to understand the inherent variation when randomly sampling a small number of events. As mentioned above, the SD of a count is the square root of the number, e.g., when sampling from a cell/particle

Table 90. Results of the immunofluorescence analysis example, data from Watson [1925]

Test sample	Number of cells	proportion	Mean	Standard deviation
Unlabeled	7889, N_1	0.92	29.1,′X_1	6.69, s_1
Labeled	681, N_2	0.08	46.7,′X_2	7.13, s_2

Table 91. Illustration of potential interpretation problems, when counting extremely rare cells

Run	1	2	3	4
	11	11	9	9
	15	13	9	10
	15	13	11	7
	10	7	9	8
	5	8	9	7
Mean	11.2	10.4	9.4	8.2
St.Dev	4.1	2.8	0.9	1.3
Overall mean:	9.8			
Overall St.Dev:	2.7			

[a]The table shows integers from four different runs with five measurements each from a random number generator. This could reflect a study with four conditions with five replicates each. The table indicates a trend from run 1 to 4; however, all of the data is from the same distribution, and there is no change from runs 1 to 4 (generated with ROUND(NORMINV(RAND(),9,3),0) with a mean of 9.0 and an SD of 3.0 in MS Excel. The cumulative mean and SD from the 20 values approximate the real population numbers well.)

suspension several times a volume, which should contain four cells per particles the SD will be 2, the CV 50%.

If enough cells in the full sample are available, cytometric data acquisition should be continued until a number of cells is reached in the rare subset that assures the desired measurement precision—a feature available in most commercial data acquisition software. If not enough cells are available, care must be taken to not come to conclusions, which are not supported by the limited precision associated with limited acquisition.

Table 91 shows an example, where four consecutive determinations indicated a progressive change of a property; but all of the data are from the same distribution, and there is no change from series 1 to series 4 (the data is from a simulation with a Gaussian random number generator with a mean of 9.0 and a SD of 3.0). This issue is discussed in more detail in a paper by [196].

In certain cases the limitation of the imprecision of counting small numbers of cells can be overcome. For example, one can evaluate a bulk cell separation technology by dispensing a known number of cells into a sample, subjecting the sample to a separation process, and analyzing the total volumes of the resulting fractions.

2.8 *Measurements of central tendency. Arithmetic mean, geometric mean, median, and mode*

In order to accurately measure the average of a population, measurements of central tendency such as the arithmetic mean, geometric mean, median, and mode can be used. The arithmetic mean, often referred to as just mean, is the sum of all events divided by the total number of events. The geometric mean is the n^{th} root of the product of events. The median is the middle point in a number series, while the mode is simply the most common number. These measures of central tendency are applied to fluorescence intensity, generated by a flow cytometer to give the MFI, geometric MFI (gMFI), or MdFI. The mode is rarely appropriate as a single measure of central tendency and is not commonly used in this context.

2.9 *MFI, gMFI, MdFI which to use?*

Which of these measurements is appropriate is dependent on the distribution of the data itself. The MFI is appropriate where data has a normal (Gaussian) distribution. The gMFI is appropriate where data has a log-normal distribution, i.e., the logs of the raw data are normally distributed, but is influenced by outliers and cannot account for any values below zero that may be created during compensation. The median, on the other hand, is robust, i.e., it is not affected by the data distribution and is not strongly influenced by outliers. In practice, most fluorescence data collected on modern flow cytometers, is skewed and conforms to an approximately log-normal distribution, indicating that the gMFI and MdFI may be better choices than the MFI. For example, in the logarithmic number series 1, 10, 100, 1000, 10 000; the arithmetic mean is 1700, the geometric mean is 100, and the median is 100, indicating that the arithmetic mean is not appropriate for estimating the average of log-normally distributed data. While no one measurement may be suitable for all purposes, generally speaking, the MdFI is the most reliable and, as a result, is the basis for many machine calibration methods (BD Cytometer Setup and Tracking Application Guide V3.0 [41, 48]). However, while the MdFI is advantageous due to its insensitivity to extreme outlier events and skewness, this loss of sensitivity may also prove a disadvantage where outliers are of interest, in which case the gMFI is also a valid option. Use of MFI, despite its enduring popularity, is likely to be inappropriate unless the raw data is confirmed to have a normal distribution.

2.10 *Pitfalls*

Measurements of central tendency are useful to estimate the average of a unimodal population. However, when data is bimodal or multimodal (has two or more distinct populations), measurements of central tendency may be misleading. For example, if the data has two equally numbered populations centered at 0 and 1000, the average would be 500 despite there being no events in this area. In these situations, it is more effective to use gating to enumerate the percentage of cells in the different peaks rather than relying on measurements of average fluorescence.

3 Analysis presentation and publication (MIFlowCyt)

3.1 *Overview*

Basic research is often criticized to be non-reproducible. To ensure reproducibility of cytometry data, it is the aim of journals to express standards that data should be minimally provided to

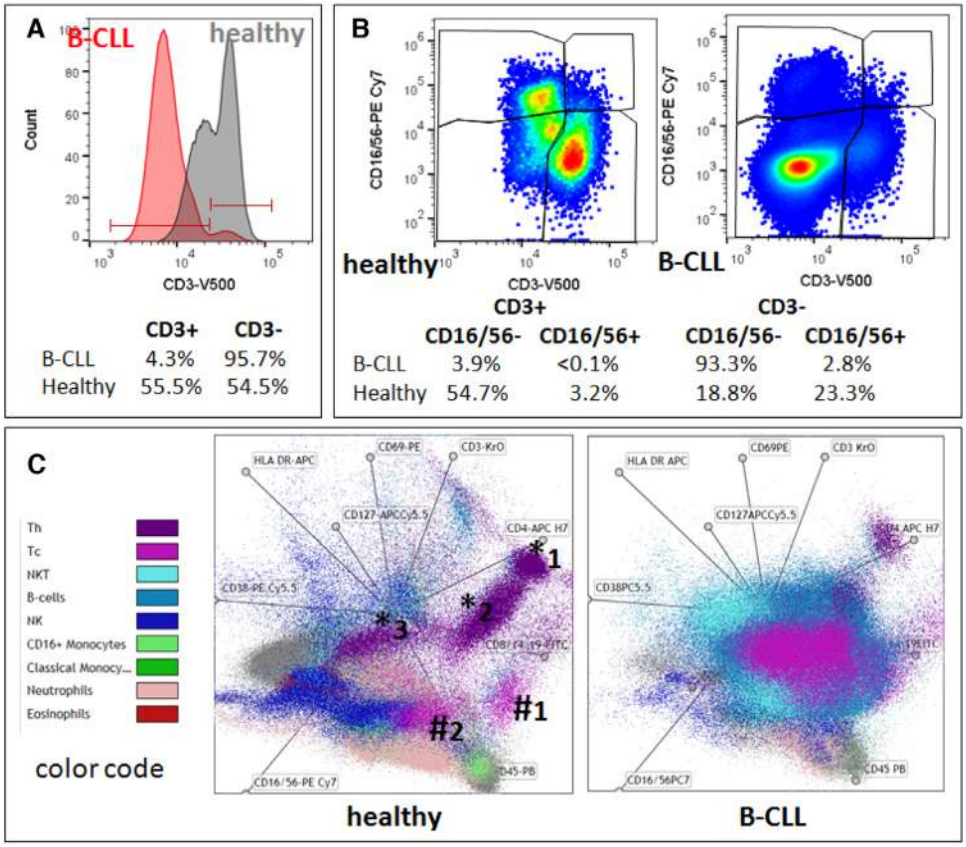

Figure 217. Uni-, bi-, and multi-parameter presentation of flow data. Comparison of two gender and age matched patients: a healthy one (67 years) and a patient with B-CLL (64 years). (A) 1D-Histogram presentation of CD3 expression on lymphocytes (red, B-CLL; grey, healthy), (B) 2D-Dot-plot presentation of CD3 expression on x-axis versus CD16/56 expression on y-axis, (C) multivariate presentation of expression of 13 different antibodies on ten colors (OMIP-023 [1926]) for nine different leukocyte subsets in a radar-plot. Abbreviations: B-CLL, B-cell chronic lymphocytic leukemia; Th, $CD4^+$ T-helper cell; Tc, $CD8^+$ cytotoxic T-cell; NK, natural killer cell. Data analysis: (A and B) FlowJo, V10.2; (C) Kaluza, Beckman-Coulter, V 1.1.

understand the paper and in the best case to reproduce these data. This section describes the MIFlowCyt standard, gives examples for good and current data visualization, and highlights the necessity of providing example data for the readers.

3.2 *Introduction*

The complexity of cytometric data requires careful consideration of how to display results in scientific presentations and publications in order to make them understandable "at a glance." To easily reproduce published cytometric experiments, the used methods and results need to be described and presented comprehensively.

By FCM, thousands of cells are acquired within seconds by gaining information of their scatter properties and expression of multiple markers. Manual analysis of these multidimensional and complex data requires special software skills, gating knowledge, time, and can be quite laborious. Manual gating is still considered by most cytometrists to be the "standard," although semi-automated algorithms exist (see Chapter VII, Sections 1 and 2). Some basic rules for data visualization allow presenting these data in a directly comprehensible format.

3.3 *Principles of the technique*

What data should be minimally displayed to fully understand research papers? First of all, the full gating strategy should be displayed so that data analysis strategy used is obvious to the reader. This display should also include the position of positive and negative controls and essential statistical information, such as the percentage of cells in the region or gate or event count. Axis legends should include the marker (e.g., antigen) and the dye used, and show the scaling (log/lin; Fig. 217). Simple experiments with one or two colors can be presented in 1D histograms; this allows easy comparison of the expression level of the marker of interest for different samples (positive, negative controls, and samples) in overlay histograms (Fig. 217A). Within these histograms, positive and negative populations can be easily distinguished from one another. For better comparison, the histograms should be normalized, i.e., the maximum values set to 100%.

More common is a display using 2D pseudocolor density plots (Fig. 217B). Plotting the expression of two markers against each other allows a more precise distinction of double negative, single positive, and double positive, as well as weakly or strongly labeled subsets. The 2D-plot presentation also helps to identify errors of

automated compensation for manual correction, as needed. Multicolor experiments are normally analyzed by a sequential gating strategy. A full gating strategy is performed in a step-by-step procedure (examples can be found in ref. [1926, 1927]). To analyze discrete populations such as T-cell subsets within blood samples in a first step CD45 negative red blood cells (CD45 expression vs. scatter) are excluded. Furthermore, only lymphocytes are gated based on their scattering (FSClow, SSClow). By exclusion of CD3 negative B cells (CD16/56$^-$) and NK cells (CD16/56$^+$) only CD3 positive cells will be analyzed in the next step. By the expression of CD16/56, NKT-cells (CD3 vs. CD16/56) can be excluded from T-cells. In a final step, CD4$^+$ T-helper cells and CD8$^+$ cytotoxic T cells (CD4 vs. CD8) can be analyzed. This process is strongly driven by a priori expectation and knowledge of the scientist analyzing the data. That means the scientists will expect, for example, to analyze within the T-cells at least four subsets: CD4$^+$ CD8$^-$ T-helper cells, CD8$^+$ CD4$^-$ cytotoxic T-cells, CD4$^+$ CD8$^+$ immature T-cells and CD4$^-$ CD8$^-$ mature T-cells. But within these subsets additional T-cell subsets might be neglected that will be taken into count by automated approached. Keep in mind that by using small (conservative) gates instead of overlapping gates, disease-specific cells might be excluded already in the first step of the analysis, or novel subsets might not be recognized. Analyzing data by the conventional step by step method in sequential 2D-plots has several drawbacks: for example, loss of information by the loss of rare cell subsets by pregating, and some marker combinations that might help to further subdivide a subset might not be analyzed. With the constant increase of the complexity of cytometric measurements and data (in the last year several standardized OMIP protocols with 28 colors became available; [1928]), there is also a need to develop new algorithms to analyze and visualize these complex data (see Chapter VII, Section 1.3.–1.6).

One example for a user-friendly visualization of multidimensional data at one glance is the radar plot (e.g., provided as a visualization tool in the Kaluza® software by Beckman–Coulter), which plots pregated subpopulations in a multiparameter way (Fig. 217C); this allows analysis of the heterogeneity of the pregated populations and to identify new subpopulations (For further details see Cossarizza et al. Eur J Immunol 2017, 47:1584-1797).

Besides manual analysis and their visualization, several methods exist to perform software-assisted, unsupervised, or supervised analysis [1838]. For example, using several open source R packages and R source codes often requires manual pregating, so that they finally work just as a semi-automated computational method. For identification of cell populations, for example, *FLAME* (suitable for rare cell detection based on clustering techniques), *flowKoh* (self-organizing map networks are produced), or *NMFcurvHDR* (density-based clustering algorithm) are available [1795]. Histograms (*2DhistSVM*, *DREAM–A*, *fivebyfive*), multidimensional cluster maps (*flowBin*), spanning trees (*SPADE*), and tSNE (stochastic neighbor embedding) maps are suitable visualization tools for sample classification [1795, 1838, 1929]. To find and identify new cellular subsets of the immune system in the context of inflammation or other diseases analysis in an

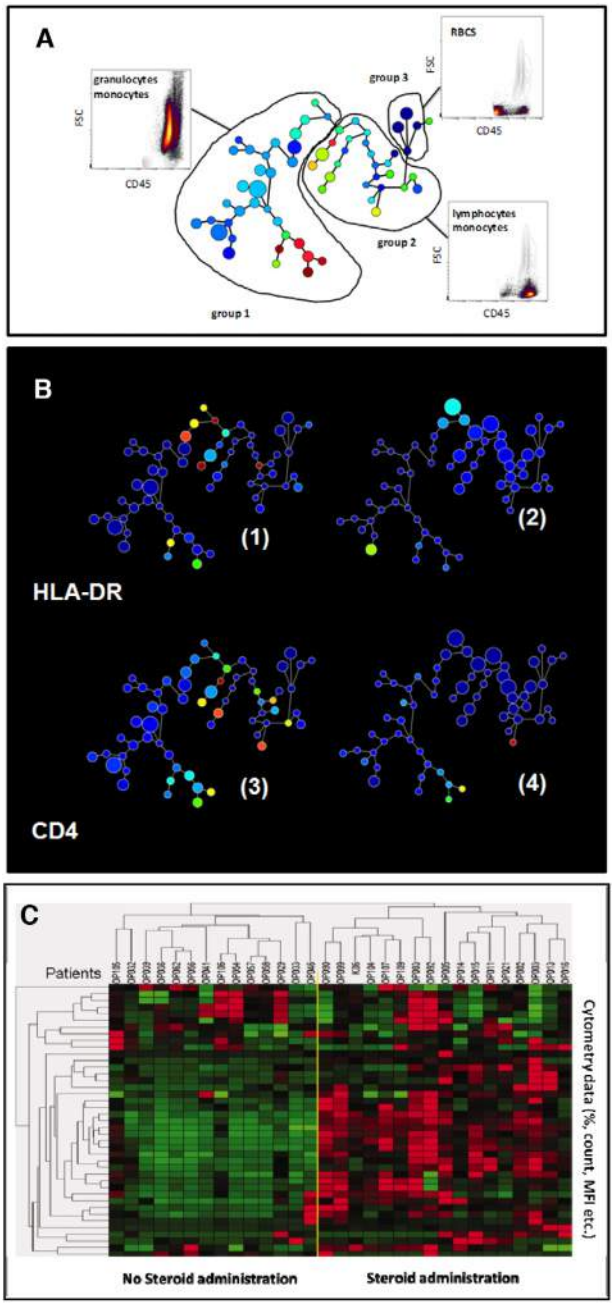

Figure 218. Semi-automated clustering and analysis of flow cytometric data by SPADE (Qui et al., 2011) and hierarchical clustering. (A) SPADE tree display and CD3 expression on blood cells from two male patients. Dot-plot analysis reveals groups of cluster (circles) belonging to the same cell type. (B) Color codes correlate with expression level from low (blue) to high (red) and size of the nodes correlate with cell frequencies. Data of (A) and (B) are from a healthy (B1 and 3; 67 years) and a B-CLL patient (B.2 and 4; 64 years). (C) Hierarchical clustering of flow-cytometry data to visualize and distinguish immune response of pediatric patients (columns) who underwent elective cardiovascular surgery with (left of the yellow line) or without synthetic steroid administration (right) before surgery. PBL were immunophenotyped at day 1 after surgery. FCM parameters (MFI and cell counts) are displayed horizontally. Red indicates relative upregulation and green relative downregulation of the respective parameter. Reproduced with permission from ref. [1931]. (SPADE analysis by Cytoscape, V 3.4.0, Nolan Lab; hierarchical clustering by free software Genes@Work).

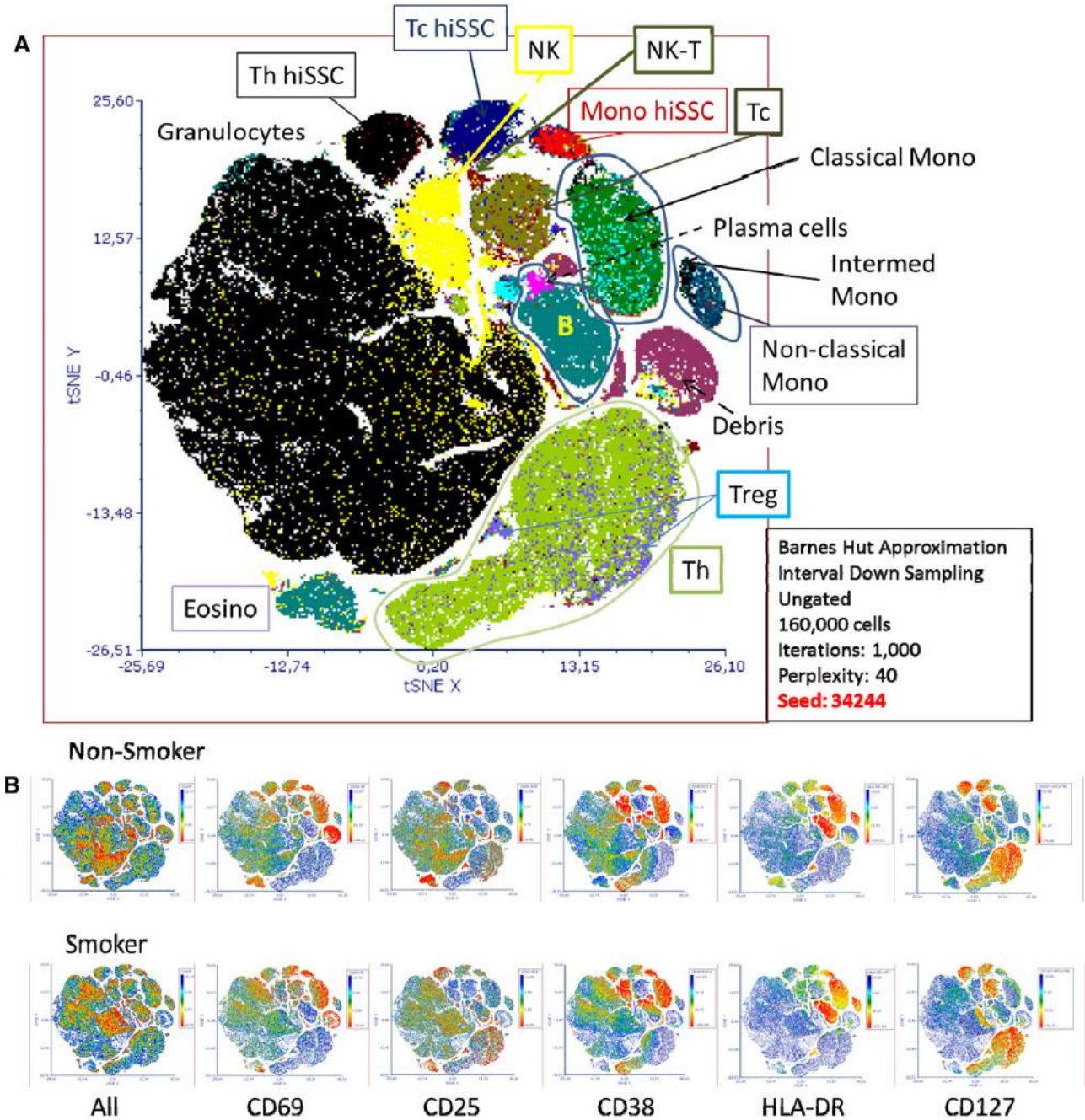

Figure 219. Semi-automated analysis of flow cytometry data by tSNE. (A) 16-Part differential of ten individuals (five smokers, five nonsmokers) by OMIP-23 (ten colors, 13 antibodies; [1926]) showing the location of regular T-helper (Th) and cytotoxic T-cells (Tc) with high side scatter (Th hiSSC, Tc hiSSC), T-regulatory cells (Treg), natural killer (NK), and NK-T cells on the tSNE map. Bottom left box contains information for calculating the tSNE plot. (B) Heat map display of expression level of 5 activation markers in nonsmokers and smokers and distribution of cell count (All). Scale bars right of each tSNE plot show color coding of fluorescence intensity or cell count levels. (Data of individuals from the LIFE study [1934]; data analysis by FCS Express V.6, De Novo Software.)

unsupervised manner, such as by SPADE (spanning-tree progression analysis of density-normalized data [1804]) can be a better approach.

SPADE is a density normalization, agglomerative clustering, and minimum-spanning tree algorithm that reduces multidimensional single cell data down to a number of user-defined clusters of abundant but also of rare populations in a color-coded tree plot. In near vicinity, nodes with cells of similar phenotype are arranged. Therefore, related nodes can be summarized in immunological populations determined by their expression pattern. SPADE trees are in general interpreted as a map of phenotypic relationships between different cell populations and not as a developmen-

tal hierarchical map. But finally SPADE tree maps help to (1) reduce multiparameter cytometry data in a simple graphical format with cell types of different surface expression, to (2) overcome the bias of subjective, manual gating, to (3) resolve unexpected, new cell populations, and to (4) identify disease-specific changes (Fig. 218A,B). Other ways for comprehensive analysis and display of complex data by unsupervised approaches can be found in ref. [1930] and include Heatmap Clustering (Fig. 218C, for details, see captions and ref. [1931]), viSNE/tSNE (Fig. 219 new) and Phenograph, and FlowSOM [1932] (Chapter VII, section 2, 3). Fig. 219 shows an example of tSNE display of immunophenotyping data (10 colors, 13 antibodies) from 10 individuals (five smokers, five nonsmokers). The position of the various leukocyte types in the tSNA map can be color coded based on their antigen expression from 2D dot-plots (Fig. 219A). As displayed in the Fig. 219A, sufficient information should be provided to reproduce the calculations. Then (Fig. 219B) for example antigen expression levels for the different patient groups can be visualized (for more detail see captions).

Data reduction and display aids also improved visualization of between group differences and generally different tools are used in combination to achieve this aim. A useful tool is hierarchical clustering cytometry data indicating by color differences [1931]; Fig. 218 and/or color intensity differences [1933] highly discriminative parameters. These can then be further visualized using SPADE or tSNE display. There are several new tools such as Phenograph, FlowSOM and others for patient or experiment group discrimination that are explained in detail elsewhere (Chapter VII, Section 1).

Finally, irrespective of which dimensionality approaches are used, it is essential that all preprocessing information is provided (pregating procedures, data normalization; see Chapter VII, Section 1.2) either with the graphs or as supplementary material. Also, authors should provide information of the calculation of the SPADE. tSNE, etc. graphs (e.g., n iterations, perplexity, n nodes, Fig. 218, Fig. 219). Also software tools used have to be named and in case of own development also made available for the readership.

Next to the appropriate illustration of flow cytometry data it is crucial that the essential details of flow experiments are displayed in order to allow others to accurately reproduce the experiments. Lack of reproducibility is of great concern in biomedical research and rough estimates say that up to 50% of the results published are not reproducible, meaning billions or trillions US$ of funding money lost [1935]. To reduce this problem, the MIBBI (Minimum Information for Biological and Biomedical Investigations) project was launched in 2008 [1936]. Its goal is to provide comprehensive checklists for different types of experiments so that all essential information for repeating the experiment is provided. Relevant for flow cytometry is MIFlowCyt (Minimum Information about a Flow Cytometry Experiment) [39]. These standards were defined by an international group of cytometry experts from bioinformatics, computational statistics, software development, and instrument manufacturers, from clinical and basic research. With this information, cross-experiment comparisons are possible. Several scientific journals, first of all *Cytometry Part A*, have adopted these regulations, but also journals from the Nature Publishing Group have accepted these standards. MIFlowCyt-compliant manuscripts should have a checklist table containing information on reagents, instrumentation, and experimental setup, including information on controls, gating strategies, among others (for details see ref. [39], Table 92). Importantly, it is required that original primary list-mode data are made publicly available in an open access data base such as the FlowRepository (See Chapter VII Section 4 Data repositories: Sharing your data). This allows others to analyze published data by alternative methods and better understand the published material. In the following manuscripts, you can find examples for MIFlowCyt checklists with different MIFlowCyt score values and original FCS data in the FlowRepository for Flow [1937, 1938] and mass cytometry [1939]. Since October 2018 MIFlowCyt compliance and reposition of original data are mandatory for *Cytometry Part A* publications [1940].

Although several *MIFlowCyt*-compliant manuscripts for flow data have been published in *Cytometry Part A*, comparable guidelines for image cytometry (e.g. *MIImaCyt*) have not been adapted so far [1941, 1942]. In order to improve the quality of polychromatic flow cytometry, a special publication type for multicolor flow cytometry protocols, Optimized Multicolor Immunofluorescence Panels (*OMIP*), was developed in *Cytometry Part A* [1943]. The central issue in multicolor flow cytometry is to demonstrate that the developed multiplexed panel has been optimized by testing different reagents and reagent combinations. Until now, over 50 different OMIPs have been published with the aims of (1) reducing the time to develop similar panels and (2) providing a starting point for the development of new panels, or (3) for optimizing existing ones. OMIPs present unique reagent combinations, document the developing progress, explain the final choice

Table 92. Important provided data for cytometric publications. (*part of MiFlowCyt)

Data set	Details
Sample/specimen	*Type*, source*, source treatment*, taxonomy, age*, gender*, phenotype*, genotype*, location**
Sample treatment	*Analytes*, Ab clone*, names/numbers*, manufacturer*, catalogue numbers**
Reagents	*Concentration, purity*
Controls	*Quality Control Measures*, FMOs*, Positive/negative control**
Instrument	*Manufacturer*, model*, configuration*, settings*, detector voltages*, optical filters**
Data analysis	*List-mode data file*, compensation*, gating*, flow repository data access code**

and should be useful to a wide range of readers. OMIPs are by nature MIFlowCyt compliant.

To avoid biases by manual analysis of high complex flow, data software tools are available that work partly operator independent. This stresses also the importance of the reproducibility in complex, (semi)-automated data analysis [1944]. O'Neill and Brinkman have suggested that certain data besides compensation, gating details and mathematical algorithms, should be shared for reproducible FCM bioinformatics [1945]. One major aim is to make FCM data easily accessible to the users by open-access databases for flow data (e.g., *FlowRepository*), as well as the code sources. A series of data sets have already been provided by the *FlowCAP* (Critical Assessment of Population Identification Methods) project, comparing different mathematical models and automated methods for analysis. The cytometry community has already made great steps toward reproducible research by standardizing instrumentation, measurement, and data analysis, but still looks forward to optimize the reproducibility in different cytometry fields.

3.4 *Advantages*

The major advantage of the MIFlowCyt concept is that each reader of MIFlowCyt-compliant manuscripts can access all necessary data so that experiments can be reproduced step by step as easily as cooking recipes, because the focus is on the transparency of scientific data.

Advanced data analysis tools offer the advantage of objective data evaluation that works completely user-independently. To be able to reproduce these analyzes, essential data such as the seeding cell must be provided.

3.5 *Pitfalls*

In order to be able to evaluate data by means of automated methods, it is necessary to pre-purify the data beforehand; this includes, for example, normalization or downsampling of data. On the one hand, these processes are time consuming and on the other hand, they can also be sources of error (data loss, data distortion), since a minimum of expert knowledge is necessary for the correct execution. The output of the visualized data subsequently requires a high manual effort to e.g. identify the populations. If high data sets are to be evaluated, the user is often limited to the computing power of the used device. And since not every user has a supercomputer with high computing power available, long times for the calculation can be expected or even multiple crashes of the software might be obtained before the optimal result is achieved. Since automated data visualization methods (SPADE, SNE, etc.) are stochastics, small changes in the initial algorithm setting will results in (sometimes totally) different maps or trees. For reproducibility, it is therefore important to document the exact setup of the algorithm (example see Fig. 219A).

Also, it is not always easy to meet the MIFlowCyt requirements. For example, the provision of original data is required. This can sometimes face a privacy problem. First, it is necessary to anonymize patient data, which in turn may require the presence of special software tools, which are however in the most cases open access. Sometimes the studies may be designed in such a way that it is not allowed to share data with third parties or to make it publicly available, so that the MIFlowCyt/Flowrepository requirements cannot be sufficiently met in all cases of manuscript submission.

4 Data repositories: Sharing your data

Scientific research is more data intensive and collaborative than ever before. Transparency and public availability of well annotated data is crucial for independent validation, verification, and extending research from prior results [1946]. The availability of primary data is therefore increasingly required by national policies, international regulatory bodies, scientific journals as well as research funding agencies [1947–1951].

In both, fluorescence-based and mass-based FCM, primary data is generally represented by FCS files that contain a matrix (table) of expression values of all measured "channels" (characteristics) of all particles (cells) analyzed by the instrument. These files should be properly annotated as per applicable domain-specific guidelines. In FCM, such guidelines are represented by the Minimum Information about a Flow Cytometry Experiment (MIFlowCyt) [39]. The MIFlowCyt standard includes recommendations about descriptions of the specimens and reagents included in the FCM experiment, the configuration of the instrument used to perform the assays, and the data processing approaches used to interpret the primary output data. In additional, the biosharing.org portal (Minimum Information for Biological and Biomedical Investigations (MIBBI) project) [1936] should be checked for extra requirements that may be applicable. MIBBI is a common portal to a group of nearly 40 checklists of Minimum Information for various biological disciplines.

Depositing data in a public repository is generally the recommended, and increasingly the required way of sharing FCM data. Below, we introduce four public repositories suitable for FCM data: Cytobank [1826, 1851] (http://www.cytobank.org/), FlowRepository [1941, 1952] (https://flowrepository.org/), ImmPort [1953, 1954] (https://immport.niaid.nih.gov), and ImmuneSpace [1955] (https://www.immunespace.org/). An overview with technical notes and highlighted features is provided in Table 93.

Cytobank is an online data analysis and management platform developed and hosted by Cytobank Incorporated. A community (basic) version of Cytobank provides free functionality including web access, data storage, experiment sharing, and basic online analysis. The Community version of Cytobank contains close to 300 public experiments (data sets). In addition, Cytobank offers paid Premium and Enterprise versions with advanced data analysis options (including SPADE [1804], t-SNE [144, 1824], and FlowSOM [1932]), better customer support, and dedicated computing resources. If your lab is using Cytobank already, then choosing its Community version presents a straightforward option of sharing

Table 93. Public repository sites: technical notes and highlighted features

Name	URLs and references	Technical notes and highlighted features
Cytobank	• http://www.cytobank.org/ • PMID: 24590675 • PMID: 20578106	• Free community version, requires registration • Web access • Advanced online data analysis options in paid versions
FlowRepository	• https://flowrepository.org/ • PMID: 22887982 • PMID: 22752950	• Free and open source, no registration required to download data • Web access, R library, FlowJo plugin • Full MIFlowCyt support • Basic online data analysis options • Integrated FCS de-identification (optional) • Recommended by Nature, Cytometry Part A and PLOS journals
ImmPort	• https://immport.niaid.nih.gov/ • PMID: 24791905	• Free, requires registration and approval • Web access • Data from dozens of assay types including cytometry • Online data analysis tools • Templates for data deposition, management and dissemination • Used mainly for NIAID/DAIT funded studies
ImmuneSpace	• https://www.immunespace.org/ • PMID: 24441472	• Free, requires registration • Web access, R library • Database and analysis engine that leverages ImmPort infrastructure • Exploring, integration and analyses of data across assays • Ontology support through standards-aware data templates • Used mainly for HIPC data

your data publicly. In addition, all versions of Cytobank give you the option of sharing data privately with your collaborators. A potential drawback of Cytobank is that public datasets can be set back to private—and thus "disappear."

FlowRepository is a public repository allowing researchers to deposit, annotate, analyze, share, and publish FCM data, mainly those associated with peer-reviewed manuscripts. The repository is provided free of charge by the International Society for Advancement of Cytometry. While FlowRepository was developed by extending Cytobank's code base, the two platforms drifted apart significantly over the past 8 years. However, there are still some common aspects allowing users of one system to adapt to the other easily. While Cytobank's platform offers more advanced data analysis options, FlowRepository focuses on data sharing and annotations, including a full support of MIFlowCyt. In addition, FlowRepository works closely with several scientific journals and allows for linking data with related publications. Unlike with most other repositories, users do not need to register in order to download public data from FlowRepository. They can do so anonymously by using a web-based interface, or from within the R statistical language using the FlowRepositoryR BioConductor library, or from within FlowJo using the FlowRepositoryServer plugin. At this point, FlowRepository contains over 1500 data sets from 1700 scientists and links to papers in 40 different journals. Half of the data sets are currently public and most of the remaining data are related to ongoing studies where underlying data will be released along with publication of the study results. Depositing data to FlowRepository is recommended by *Nature*, *Cytometry Part A*, and *PLoS* journals.

The Immunology Database and Analysis Portal (ImmPort) system provides an archive of immunology research data generated by investigators mainly funded through the National Institutes of Health (NIH), National Institute of Allergy and Infectious Diseases (NIAID), and Division of Allergy, Immunology, and Transplantation (DAIT). It is an extensive data warehouse containing an integration of experimental and clinical trial data generated by dozens of assay types, including 131 FCM and 24 CyTOF data sets. In addition, the ImmPort system also provides data analysis tools and it contains implicit knowledge and "best practices" for clinical and genomic studies in the form of ~50 templates for data deposition, management, and dissemination. ImmPort has been developed under the Bioinformatics Integration Support Contract (BISC) by the Northrop Grumman Information Technology Health Solutions team for the NIH NIAID/DAIT. If your research funding comes from this source and you are generating immunology data, you should deposit it in ImmPort. Immport's support for different

data types can be another reason to choose it if you are generating FCM data as well as data from different types of assays. A (free) registration and approval by DAIT is required in order to deposit and access data from ImmPort. A potential drawback of using this resource is that there can be a long delay in publication of deposited datasets.

ImmuneSpace is a database and analysis engine built by customizing the LabKey server for the Human Immunology Project Consortium (HIPC). ImmuneSpace can be used to find and explore studies, integrate, and analyze data across assays, and perform custom analysis directly from within R. ImmmuneSpace takes advantage of the infrastructure already developed for ImmPort, and in many cases, ImmuneSpace provides a new interface and new complimentary tools to data that are also available in ImmPort. Currently, ImmuneSpace can be used to access several large HIPC studies with FCM and CYTOF data. The typical data submission work flow consists of data submission to ImmPort using a set of standardized data templates. If you are a HIPC participant, then your data should be deposited to ImmuneSpace; otherwise, you can still use ImmuneSpace as a valuable resource of HIPC data and analysis tools.

If you are in a clinical setting, there is one important thing to consider before you start sharing your FCM data by depositing it in any of the repositories. Besides the expression matrix, FCS data files contain a segment with keyword/value pairs. Most of the keyword values keep basic information essential for the interpretation of the raw data matrix and acquisition settings related values. These include the number of acquired parameters, their names, acquisition voltage settings, the total number of events (particles), and many other keywords as specified in the FCS data file standard. In clinical settings, some of the keywords may include information that could be used to identify the subject that was the source to generate the data in the file. Such information has to be removed prior to sharing the data file in order to comply with patient privacy requirements as specified by the Health Insurance Portability and Accountability Act (HIPAA) [1956] in the United States and similar rules enforced by regulatory agencies in most other countries. Patient data must be properly protected and cannot be publicly shared; however, those rules generally do not apply as long as the data is properly de-identified. De-identification is the process of removing identifiers that could be used to identify an individual. Identifiers include items such as patient name, social security number, other public ID numbers, date of birth, and so on as specified by HIPAA and other applicable regulations. There are several standalone tools available for the de-identification of FCS files as listed, for example, in the FlowRepository Quick Start Guide (http://flowrepository.org/quick_start_guide).

There is widespread agreement in the biomedical research community that data sharing is a primary ingredient for ensuring that science is more transparent and reproducible [1957]. While FCM has lagged behind other technologies in this area, the recent availability of public repositories provides the means to satisfy this necessary component for data sharing and its long-term stewardship.

VIII Advanced techniques in, and management of, flow cytometry

1 Imaging flow cytometry

1.1 *Overview*

Imaging FCM (IFC) adds to the power of conventional FCM by also providing spatial and morphological information within the cell. IFC combines the statistical power and phenotyping capabilities of FCM with the image analysis of microscopy. The following section is an overview to the principles of the technology, the wide range of areas of research where it is utilized, detail into the experimental workflow and analysis, and finally any pitfalls to look out for and tips that may assist researchers based on experience with the platforms.

1.2 *Introduction*

IFC was first introduced in the late 1970's with a slit-scan cytometer [1958] and since then improvements to the original concept came slowly until the development of the ImageStream (Amnis Corp; now part of Luminex Corp) [1959]. Imaging cytometry also includes technologies such as laser scanning cytometry and high-throughput microscopy where cells are interrogated in situ on a slide [1960]. This is useful in circumstances where placing cells in laminar flow would disrupt their phenotype or where spatial context within tissue is important. The slit-scan cytometry technology has also been developed into a microfluidic imaging assay [1961] and, most recently, into a microfluidic chip capable of sorting cells [1962]. This section will focus on the ImageStream IFC.

1.3 *Principles of IFC*

In IFC, the cells enter the flow cell in much the same way as conventional FCM, where they are placed in a hydrodynamically focused flow cell. Cells are then illuminated by both LEDs, for bright-field images, and lasers, for fluorescent images, and this light is collected by the objective lens. The light then intersects with a spectral decomposition element, a stack of angled wide BP filters that separate the light based on wavelength into six individual channels (Fig. 220). On the ImageStream Mk-II, these filters are 457/45, 528/65, 577/35, 610/30, 702/85, and 762/35. The major difference in IFC is the use of charge-coupled device (CCD) detectors instead of PMTs. The six separated images are collected using time delay integration (TDI) technology. The CCD converts photons from images into photocharges on a pixel array containing 256 rows. With TDI, as the cell moves through the flow cell the information collected from the pixels from the first row are integrated into subsequent rows until the light leaves the detector. The collective images' pixel content is then formed from the pixels on the last row. For this technology to be successful, the

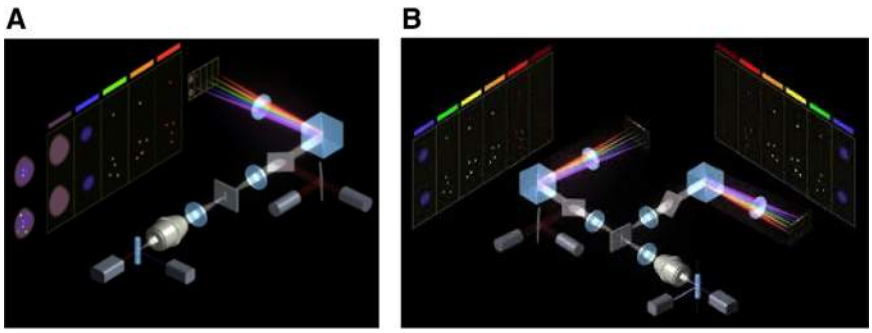

Figure 220. The optical layout of the ImageStreamX Mk-II one camera, six channel (A), and two camera, 12 channel (B) systems. Figure modified with permission from ref. [1959] and reproduced with permission from Luminex.

CCD camera must maintain synchrony with the flow cell speed. This is achieved by tracking the speed of 1 μ polystyrene beads (speedbeads) that continually run through the flow cell during operation. An advantage of using CCD detection with TDI is that cells can be running through the flow cell at high speed and will still produce a focused image thus allowing for image analysis of large numbers of cells per sample. In order to achieve 12 channels from which to image, the ImageStream Mk-II can be equipped with two CCD cameras (Fig. 220) and two spectral decomposition elements to which different lasers are directed toward, e.g., the 375, 488, and 561 nm lasers would be directed toward camera 1, while 405, 592, 642, and 730 nm lasers would be directed toward the second camera. The cameras capture sequential images from the cells allowing for fluorochromes emitting at the same wavelength but excited by different lasers to be interrogated sequentially. A bright-field image is taken on both cameras so that images can be accurately spatially correlated in analysis. To eliminate scatter from each of the lasers, narrow BP notch filters are placed in front of the cameras.

1.4 *Applications*

The applications of IFC are wide and varied. Not intended to be an exhaustive list, this section describes some of the most common applications to date. It is useful to remember that any research question that would be answered by microscopy or FCM could potentially be answered by IFC. The IDEAS software used to analyze ImageStream data contains a large number of possible image analysis parameter or "features" that may be applied based on the question.

IFC is particularly useful in cell signaling. Expression of proteins, such as transcription factors, that are part of signaling cascades are typically unchanged during activation. Instead, activation is determined by relocation of the transcription factor into the nucleus to initiate transcription of downstream targets. Staining the transcription factor of interest alongside the nucleus can determine activation based on "Similarity" of the two images. This information alongside the ability to simultaneously phenotype cells enables detection of heterogeneity of activation in subpopulations. Examples of cell signaling pathways studied in this way include NF-κB, NFAT, JNK, IRF, and STAT [1963–1969].

Phagocytosis has been extensively studied using this technology with phagocytes or macrophages stained for a particular marker, and the cell to be taken up stained with another [1970, 1971]. The level of "Internalization" can then be quantified. As the name suggests, internalization is performed by measuring the uptake of a protein/cell or other material into a specific cell. More recently, this feature has been utilized to determine exosome uptake into a cell [1972, 1973].

In addition to internalization, the protein/marker of interest can also be tracked to where in the cell it traffics to or whether it interacts with a specific marker in the cell. For example, dyes can be used to stain mitochondria, endosomes, and/or lysosomes and their 'Co-localization' with certain markers can be assessed. Co-localization uses a feature known as Bright Detail Similarity. This takes the brightest pixels (with a choice of radius of 3 or 7 pixels) of both markers and determines their similarity in spatial distribution, if they overlap, the value will be higher indicating co-localization [1974].

Since a bright-field image is collected by the ImageStream, changes in morphology can be studied. Chemotaxis is a good example when change in cell shape can be measured using its "Circularity." A normal monocyte would be circular, whereas one undergoing chemotaxis would have an irregular shape. The bright-field is also a useful parameter in the measurement of apoptosis. Those cells undergoing apoptosis will have a relatively higher contrast in their bright-field images than healthy cells. This can be combined with a DNA stain such as PI, DRAQ5, or DAPI where the area of the nucleus can also be measured, showing cells undergoing apoptosis with a lower nuclear area. Stains such as for caspases or Annexin-V can also be added to obtain information regarding the specific stage of the apoptotic process [1975, 1976].

Antigen presentation is central to the immune response and this event can be quantified using IFC. The antigen presenting cells and T cells are stained alongside actin. Those doublets that contain one of each cell and have a high actin expression concentrated at the "Interface" between the two are involved in the immune synapse [1977, 1978].

IFC can also be used to characterize cytotoxic immune synapses for multiparametric analysis of molecular mechanism involved in the cytotoxicity of human CD8 T-cells [668].

The extended depth of field (EDF) component of the ImageStream, where the focal plane can be expanded to 16 microns, makes analysis of small areas of fluorescence within

the cell possible. Fluorescent in site hybridization has been successfully adapted to cells in suspension, and recently with phenotyping, thus allowing measurement of numerical chromosomal aberrations in large number of cells, increasing the sensitivity of the assay [928, 1979].

A major advantage of IFC is the high volume of information available from the data acquired. Recently, researchers have begun to expand how this may be analyzed. An open source machine learning model has been developed (Cell Profiler Analyst), which can process hundreds of different features and morphological information in the thousands of data rich images [1980].

1.5 *Equipment*

The original ImageStream platform began with the IS-100 in 2004, followed by the ImageStream^X and most recently the third generation instrument; the ImageStream^X Mk-II. The ImageStream^X Mk-II can be configured for up to seven lasers (the standard 488, 375, 405, 561, 592, 642, and 730 nm) as well as the dedicated 785 nm laser for darkfield (side) scatter, and a dedicated 830 nm laser for autofocus. Most common configurations contain four or five of the seven lasers offered. There are 12 channels with up to ten fluorescent channels available. The Mk-II has a 40× magnification that has resolution of 0.5 μ/pixel. With the optional 60× magnification, this resolution increases to 0.3 μ/pixel making the Mk-II a potentially useful instrument in the emerging field of microvesicle research [1972, 1973]. The 60× magnification combined with the EDF function is useful when measuring small organelles such as mitochrondria, or small chromosomal spots by fluorescent in site hybridization -IS [928, 1979]. EDF extends the focal depth from 4 to 16 μ to allow for the entire cell (in most circumstances) or nucleus to be in focus [1981]. The EDF image is automatically deconvoluted in the analysis software resulting in a focused image. The Mk-II may also have the 20× magnification for larger cells/aggregates. The FlowSight (Amnis) is a more compact IFC with a 20× magnification only, with a resolution of 1 μ/pixel. It also has 12 channels but with a maximum of four lasers (the standard 488, 405, 561, and 642 nm). The lower resolution indicates that it is limited in its image analysis when compared to the Mk-II. A third cytometer from Amnis, part of Luminex Corp. is the CellStream. While not strictly an imaging flow cytometer since images cannot be saved, this instrument can save morphology data from the brightfield image during acquisition. The remaining sections will apply to the two camera Mk-II unless otherwise specified.

1.6 *Experimental workflow and acquisition*

For the daily start up, the ImageStream has a fluidics initialization routine and a quality control software suite (ASSIST) that checks that the instrument performance is within the factory-set margins. Any test that falls outside of these margins will be flagged and may require adjustments. Depending on the comfort level of the user, these adjustments can be made by the operator themselves or may require intervention by the manufacturer. For the latter, in many cases, troubleshooting and making adjustments can be performed remotely by establishing an internet screen sharing connection.

For the daily shutdown, the ImageStream has an instrument shutdown routine that soaks the fluidics with bleach and rinses it with water. The shutdown procedure ends by turning the electronics of the ImageStream off and optionally, the instrument can be instructed to shut down the computer workstation as well. Both the startup and shutdown procedures, once initiated, proceed automatically without the need of operator interaction.

The same rules for panel design that are applicable to conventional FCM apply to ImageStream cytometry. The proper balance between epitope density and fluorochrome intensity needs to be observed. The use of too many tandem conjugate dyes simultaneously should be avoided to reduce cross-excitation problems by multiple lasers. Single color controls need to be prepared for multicolor panels. Note that the volume of sample loaded can be as low as 20 up to 200 μL. Rule of thumb is to prepare the same cell number as would be prepared for conventional FCM; commonly between 0.5 and 1 x 10^6 cells per sample if possible. Since the standard sample acquisition rate is 1.2 μL/min, which is 20 nL/s, a concentration of 10^6 cells/mL would therefore only yield 20 total events/s. Therefore, following the staining procedure samples should be resuspended in 50 μL instead of 500 μL as is common in conventional FCM to achieve a much higher cell density; the higher the cell density, the faster the event rate. However, be careful not to exceed a cell density above ~30 × 10^6 cells/mL since this may lead to cavitation/bubble formation and loss of laminar flow (see Pitfalls section). When a sample is loaded, the INSPIRE acquisition software displays a volume gauge that shows how much acquisition time is left.

The single color controls are acquired with the bright-field LEDs and scatter laser off but with the full complement of lasers that are used for the experimental samples on and set at the laser outputs that will be used for the experimental samples. The number of events needed to be acquired for single color controls is low, commonly between 500 and 1000 positive events.

When desired, compensation can be applied during acquisition but this would only be necessary, for example, if acquisition gates are used based on a fluorescence intensity signal that may suffer highly from spectral overlap from a neighboring fluorochrome. For most applications, post-acquisition compensation is recommended.

During acquisition, acquisition gates can be set with the options to collect the desired number of events to include only events within the gate or include all events with the acquisition time determined by the number of events defined within the set acquisition gate. When setting the laser intensities saturation of the intensity signal should be avoided. This can be monitored with the "raw max pixel" parameter, which reaches saturation above the value of 4096.

If the detection channels of the designed panel are spread over both cameras (camera 1: channels 1–6 and camera 2: channels 7–12), and spatial correlative analysis is desired, the acquisition of two bright-fields (one in each camera) is required. The two

bright-field images are used by the software to spatially align the acquired images by each camera. The bright-field pairs can be selected not to interfere with the optimal detection wavelengths of the fluorochromes in the panel.

If SSC measurements are desired, the ImageStream uses a dedicated 785 nm laser for SSC. The SSC signal can be collected either in channel 6 (camera 1) or camera 12 (camera 2), the preferred choice of which is dependent on the fluorochromes used in the panel.

1.7 *Data analysis*

The acquisition of data with the ImageStream platform produces proprietary raw image files with a .rif extension. The data analysis is performed with the IDEAS software package. For multicolor experiments, a compensation matrix (.ctm file) is first calculated using appropriately acquired single color controls [1982]. IDEAS can then open a .rif file with a corresponding .ctm to produce a compensated image file (.cif) and a data analysis file (.daf). The IDEAS software has a separate work space area for the image gallery and one for data analysis in which single and dual parameter plots can be created using default or custom-made features and regions can be drawn on and applied to plots for which statistical information can be derived. The image gallery and the data analysis workspaces are interactively correlated in that images of interest can be clicked and their position in the data analysis plots be identified by a cursor and vice versa, that the image galley can display individual events or regional events of interest identified from the data analysis plots.

The most challenging part of introducing imaging FCM data analysis to someone who is familiar with conventional FCM is the concept of "masks"—defining the region of interest of an image (e.g., the nucleus, the cytoplasm, the immunological synapse region)—and "features"—what parameter is measured in that mask (e.g., intensity, co-localization, area). Although the software calculates numerous features related to size, location, shape, texture, and signal strength by default, these features are calculated for the default masks only. Commonly, a custom feature would be created depending on the specific experimental setup and analysis question. The software also by default will create several default masks (regions of interest), which in turn can be modified to suit the specific experimental setup and analysis question. The software has a guided analysis function (wizard) in which the user is guided through the sequential data analysis steps of creating masks and features for many of the most commonly used applications such as nuclear translocation, internalization, co-localization, immune synapse formation, and so on. A data analysis commonly follows a hierarchical gating strategy that starts with the identification of single cells that are in focus from which then various subpopulation can be derived and features can be calculated. Once the analysis strategy has been completed, this can be saved as an analysis template (.ist file) that can be applied to subsequent data files through batch processing.

Following data analysis, images can be exported as .TIFF files and data files of the parameters of interest as .fcs files, which then can be read in any FCM analysis software package. Of note, FCSExpress has the ability to directly read .daf files for use in its analysis package. It is important to be aware that any image analysis such as designing masks and features will still have to be done in the IDEAS software package before exporting as .fcs files or reading in the .daf files in FCSExpress.

1.8 *Advantages*

The obvious major advantage of imaging FCM is the added spatial information that is provided with the intensity parameters. That spatial information enables the study of co-localization, cellular redistribution, cell morphology beyond what is possible based in FSC and SSC only (e.g., shape), and verification that obtained signals are not artificial (e.g., a nuclear parameter should not be detected in the cytoplasm or cell membrane). Even with the study of events that are not dependent on spatial parameters, such as the study of exosomes, the inherent differences between sensitivity of the CCD cameras with detectors used in conventional FCM (PMTs) are advantageous.

1.9 *Pitfalls*

Not all panel designs that work well for FCM will work for imaging FCM (See Fig. 221). Among the main reasons for this are the vastly larger bandwidths for the collection filters used making spectral overlap correction more challenging; the use of so-called notch filters to block the scatter of the excitation lasers from reaching the detector that will also block the corresponding emission wavelengths of any fluorochrome; the fact that instead of the sensitivity of the detector, the output of the excitation laser is adjustable thus any intensity adjustment will affect all fluorochromes excited by the same laser; the colinear arrangement of the lasers that are directed to the same camera that prevents the application of laser-delays to discriminate between excitation sources.

Air bubbles should be eliminated from sample before loading. Bubbles can create a break in the sample volume loaded in the fluidics that the equipment will sense as a small volume (the volume detected is the first contiguous volume until a bubble is detected).

The acquisition is limited by the sample acquisition rate that in turn is dependent on the cell density of the sample. As a general rule of thumb, do not exceed a cell density of 30×10^6 cells/mL since too high of a cell concentration (dependent on size and stickiness of cells) will lead to cavitation/bubble formation and loss of laminar flow, leading to reduced sample recovery. Depending on the desired number of events to be acquired, long acquisition times may be necessary that requires one to take into consideration how long acquisition times at room temperature may affect the biological sample analyzed since no temperature control is applied once sample is taken up into injection syringe.

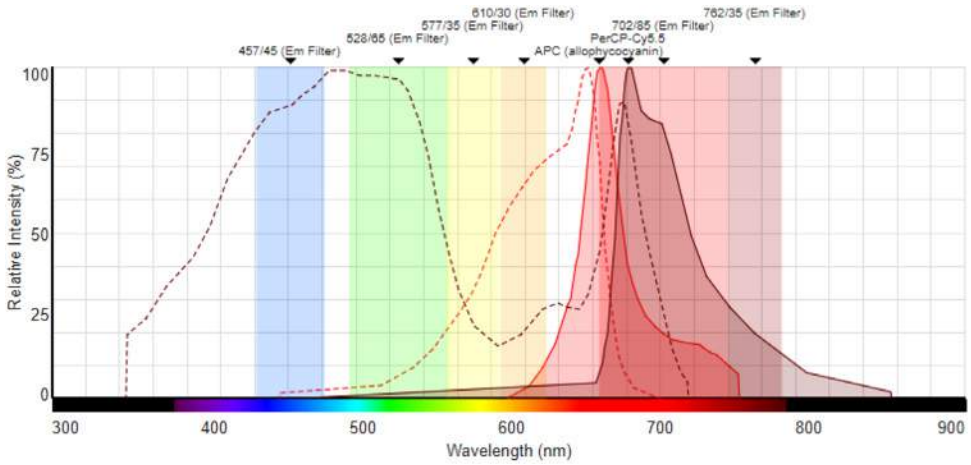

Figure 221. Excitation (broken lines) and emission spectra (solid lines) of APC and PerCP-Cy5.5 and BP emission filters used on the ImagestreamX MkII demonstrate that APC is suboptimally detected and therefore may appear less bright in a panel compared to the same panel acquired on a conventional flow cytometer that would typically be configured with a 660/20 BP. The problem is that by attempting to make the APC signal brighter by increasing the 642 laser output the cross-excitation of PerCP-Cy5.5 by the 642 laser is also increased making the compensation challenging. In this case, the use of AlexaFluor 647 instead of APC would be a suitable alternative.

1.10 *Top tricks*

- Data file sizes (and subsequent computer processing time) can be reduced by acquiring only images for the acquisition channels of interest to the experiment. Each omission of a channel will reduce the file size by ~10%. For example, a three-color experiment only requires the three fluorescence channels of interest, the scatter channel if desired, and two bright-field channels.
- When large numbers of cells are required for analysis, it is more efficient to acquire and analyze ten 10 000 event files than one 100 000 event file since for analysis all the information of the events within one file are stored in memory. Once the analysis is finished, the files can be merged into one if desired.
- When analysis of co-localization is required (for example, by calculating a similarity score), it is advisable to choose the fluorescent markers associated with the analysis to be on the acquisition channels within the same camera (within channels 1–6 or 7–12) for the most accurate assessment. For any other multicolor experiment, spread out the choice of fluorochromes evenly between the two camera systems.
- When studying signal transduction events (e.g., nuclear translocation of transcription factors), it is important to be aware that cell enrichment procedures that are very common to flow cytometric immunophenotyping (e.g., Ficoll density gradient separation or RBC lysis) can affect the activity of the signaling pathway especially those involved with stress response such as NF-κB.
- Displaying a graph of the raw max pixel intensity during the setup is helpful to determine that the laser powers are not set too high to a level where pixel saturation will occur (>4096).
- For accurate measurement of punctate images (e.g., spot counting), the optional EDF optics are necessary.
- The system should be flushed with 10% bleach after the use of dyes that stick to the fluidics tubing such as DAPI and PI. This is especially important when collecting the single color controls required to construct the compensation matrix.
- The algorithm used to calculate the compensation matrix for multicolor experiments requires information on all available channels. When the number of acquisition channels has been reduced during acquisition make sure that when acquiring the single color controls that all channels are being collected.
- For day-to-day consistency between ImageStream measurements, a standardized fluorescence intensity bead set should be acquired and laser settings adjusted so that the intensities are consistent between runs.
- In the experimental setup, include biological positive and negative controls, not just single-color and FMO compensation controls. This would be stimulated or unstimulated cells, i.e., in which you see populations positive or negative for the feature of interest (nuclear translocation, internalization, colocalization, immune synapse formation, etc.).

2 Barcoding in cytometric assays

2.1 *Overview*

Sample barcoding denotes a procedure in which distinct cell samples are stained with unique labels, pooled, and then further processed and acquired as a mixture of samples, often referred to as a "sample convolute." After acquisition of the convolute, data of the original samples are recovered by resolving the label signature used for sample tagging (Fig. 222). Barcoding allows for multiplexed analyses in FCM and mass cytometry. Importantly,

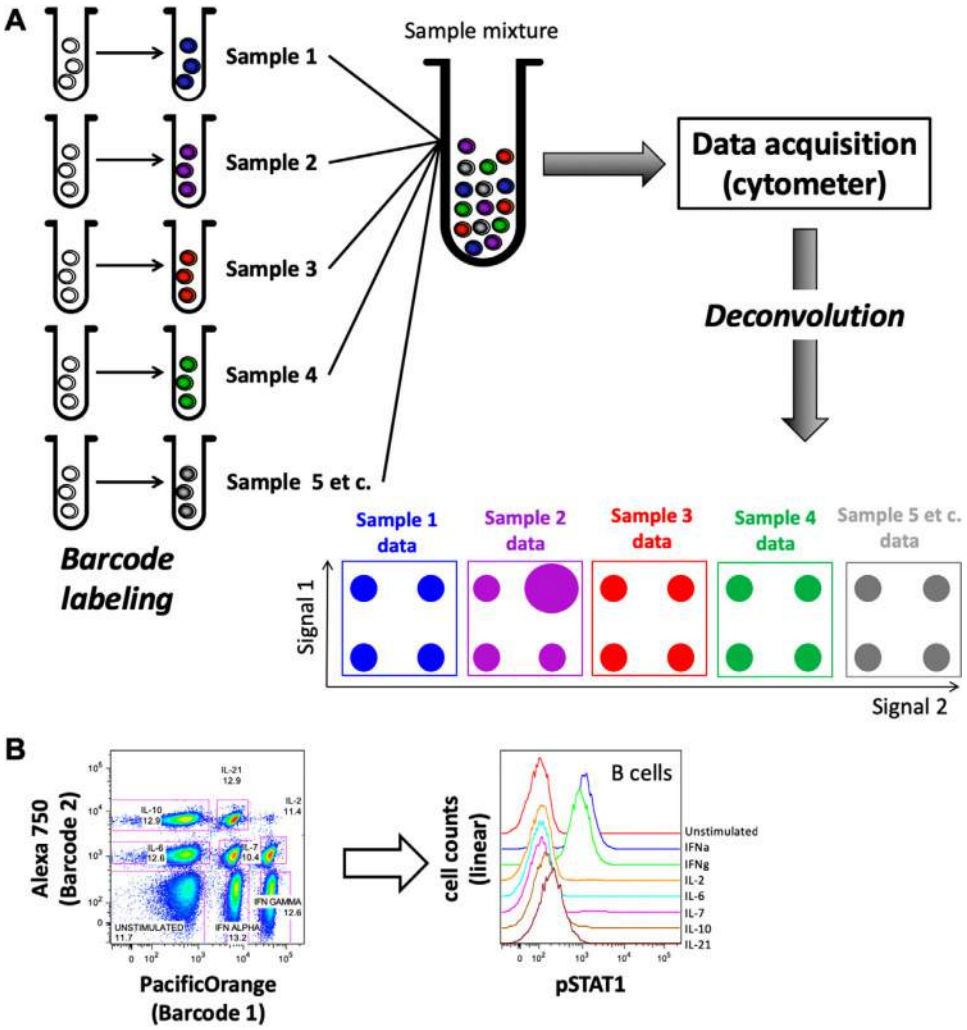

Figure 222. Workflow of cell sample barcoding for FCM and mass cytometry. (A) Schematic overview of sample barcoding. Individual reagents and reagent combinations are indicated by different color; schematic 2D plots are shown in the same corresponding colors. Individual sample properties are illustrated by staining patterns, the sample 2 plot depicting a pattern clearly deviating from the others. (B) Example of fluorescent sample barcoding for a Phospho-Flow experiment. PBMC were stimulated in vitro with eight different stimuli or controls, fixed with formaldehyde, and permeabilized with ice-cold methanol. Cells from each condition were barcoded using different concentrations and combinations of Alexa Fluor 750 and/or PacificOrange succinimidyl esters (eBioscience). Following the barcoding reaction, single samples were washed, pooled, and further stained for major lymphocyte lineage antigens and phosphorylated STAT3 in the pooled sample. After selecting $CD33^+$ monocytes by gating, the barcode was deconvoluted by gating in the two barcode dimensions. The left plot depicts the barcode labeling of all cells in that pool. Eight major populations corresponding to different stimulation conditions can be discriminated (indicated by gating). Cells of a given single sample group together as a "population" with homogeneous Alexa Fluor 750 and PacificOrange labeling, respectively. Annotations indicate stimulation conditions applied prior to barcoding, as well as the frequencies of gated populations. The similarity of these frequency values confirms that the pool contains similar amounts of cells from each barcoded condition. On the right side, the histogram overlay representation depicts pSTAT1 expression in the different stimulation conditions. pSTAT1 signal was induced in B cells treated with IFN-α and IFN- γ, but not or only minimally in the other conditions, which are visually indifferent in pSTAT1 signal from the "unstimulated" control. Data were generated by Patty Lovelace, HIMC, Stanford.

this contributes to harmonization of assay conditions, and reductions in the amount of wet work, technical errors resulting from pipetting and staining variability, and reagent consumption, as compared to preparing and acquiring multiple single samples. For example, minimizing the number of total pipetting steps means an overall reduction of pipetting error along the entire sample preparation, and since all individual samples are stained, washed, and optionally fixed and permeabilized in the very same sample tube, no sample-specific artifacts can arise from these procedures. This results in increased data consistency and robustness. After samples have been pooled, the assay is performed in a single vial, which reduces the complexity of sample preparation work and allows for sample acquisition with only a minimal need for manual interference. Compared to running multiple single samples, no instrument cleaning cycles are necessary when acquiring one barcoded convolute, thereby reducing instrument run-time. Similarly, barcoding practically excludes sample-to-sample carry-over, which can occur during one-by-one sample acquisition by the

cytometer. Barcoding of samples is particularly useful when high data consistency is required, e.g., when shifts in median signal are used as the assay readout, such as in the case of cell signaling studies. The reduction of unwanted noise in cytometric data by sample barcoding/pooling benefits the quality of results achieved with algorithmic data analyses, which require a high degree of technical data consistency [1794, 1983].

2.2 *Introduction—Benefits and caveats of cell sample barcoding*

Cytometric sample barcoding was first developed as intracellular barcoding for phospho-flow applications [1984]. Barcoding was later similarly applied to mass cytometry [1985] with two barcode staining intensity levels (present/absent) for each channel (see also Chapter VIII Section 3 Mass Cytometry). More recent efforts moved barcoding to earlier steps in the sample preparation protocol to extend the number of protocol steps that benefit from sample barcoding. Behbehani et al. [1986] introduced intracellular barcoding with only minimal permeabilization using 0.02% saponin buffer. Mei and colleagues and Lai et al. [1987–1989] used differently labeled CD45 Abs to achieve cell surface barcoding of PBMCs in mass cytometry. The concept has also been transferred to FCM [1990] using Abs against murine CD4 and B220.

While barcoding of samples has many benefits, it represents an additional step in the protocol, needs to be optimized on its own, and usually occupies cytometric channels that would be otherwise available to the measurement of target analytes. Preparation of larger barcoding reagent mixtures can be time consuming and require a high degree of precision. For larger studies, and to avoid errors and variability in barcoding from experiment to experiment, one should consider automating the generation of barcode reagent mixtures [1991], and/or to prepare them in batches that can be stored frozen or lyophilized. A drawback of using sample barcoding is that any error associated with only one or a few samples in the convolute will not be discovered until deconvolution, such as the lack of cells in a sample, unexpectedly low cell number, high frequency of dead cells, excess presence of debris, or contamination events such as erythrocytes in PBMCs. Additionally, errors in barcoding can result in issues during deconvolution, which can lead to the loss of some or all data of the barcoded sample convolute. When using unrestricted combinatorial barcoding schemes (Fig. 223), mishaps during barcode preparation result in miscoding of the sample(s), while with restricted schemes, only the miscoded sample will be lost in most of the cases.

2.3 *Barcoding schemes*

Principally, any number of samples can be processed as a barcoded sample convolute. The capacity of a barcoding scheme is determined by the number of cytometric channels reserved for barcode markers and the number of different signal intensity levels per channel. The simplest approach is to label each sample by one unique marker (Fig. 223A). By leveraging the capacity of some barcoding reagents to stain at different signal intensities when used at different dilutions in the assay [1984], more samples can be barcoded using the same number of channels, multiplying the capacity by the number of intensity levels used (Fig. 223B). This strategy is frequently used in FCM, while barcode labeling for mass cytometry assays typically makes use of two intensity levels (stained and unstained) to achieve robust barcode labeling. This is mainly due to the fact that (i) more channels are available in mass cytometry, and that resolution-limiting, lower sensitivity channels or reagents, e.g., in the palladium range are used for barcoding to keep higher sensitivity ones for analytical readouts. In combinatorial barcoding, samples are labeled by unique combinations of multiple markers rather than by a single marker (Fig. 223C). In a scheme with two intensities per channel (i.e., "positive" and "negative"), the capacity of such a scheme is 2^n. However, using the full combinatorial capacity entails certain limitations. Different barcode labels often compete for identical binding sites, leading to different barcode marker signal intensities. For example, a sample marked by one label usually exhibits higher signal than another sample where that label is one of four different labels. In addition, nonhomogeneous barcode labeling of a sample may limit or even entirely preclude the retrieval of the original sample cells from the barcoded convolute. Doublet events, containing differently barcoded cells (intersample doublets), can mimic cells of a third sample that carries the marker combination of the other two cells combined. This is especially relevant in mass cytometry, which lacks the light scatter parameters available in FCM, which are applicable for cell doublet removal. When occupying the full capacity of a combinatorial barcoding scheme, such issues can neither be reliably detected nor corrected. Mislabeled cells will be lost for analysis, and will contaminate another barcoded sample of the convolute.

As a consequence, a restricted combinatorial scheme has been developed, in which only unique combinations, with equal numbers of barcode labels per sample are used. This strategy allows for the detection of samples erroneously labeled by more or fewer of the fixed number of labels, thereby permitting exclusion of wrongly labeled cells, as well as virtually all intersample doublets [1988, 1992]. With identical numbers of barcoding channels, the capacity of restricted schemes is significantly lower, but this is justified by the removal of doublets, especially in mass cytometry. Technically, intrasample doublets are not removed by barcoding. However, with increasing numbers of samples barcoded and pooled, the likelihood of cell doublets being intersample (removed in restricted barcoding schemes) increases relative to intrasample doublets, and leads to indirect but significant reduction of intrasample doublets [1988]. The sample accommodation capacity of restricted barcoding schemes equals $n!/(k!(n - k)!)$, with n being the number of barcode channels and k being the number of labels per sample [1992]. Pascal's triangle provides quick visual access to the sample capac-

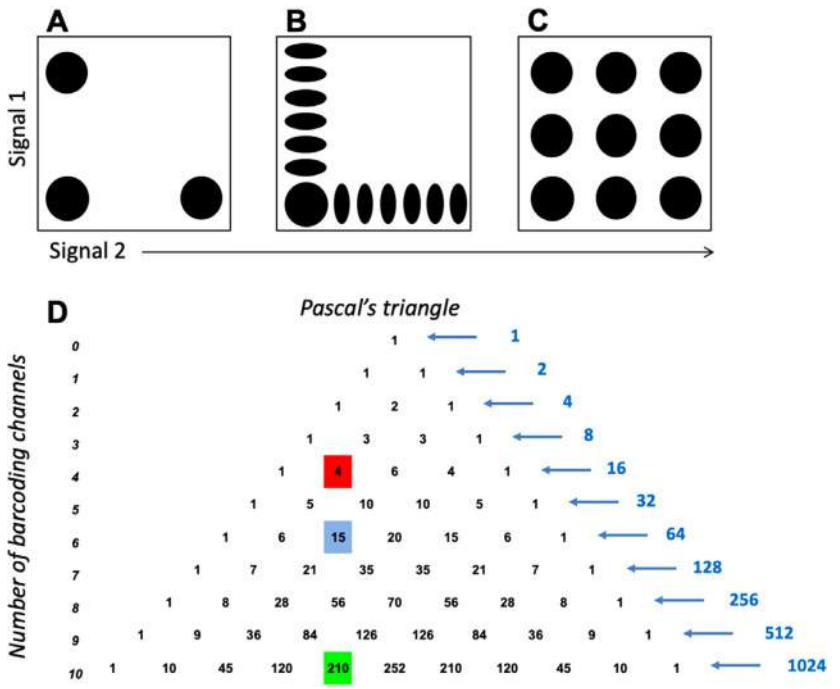

Figure 223. Barcoding schemes. (A–C) Schematic 2D dot plot representations of (A) three samples, each barcoded by presence or absence of one of two barcode labeling reagents, (B) 13 samples barcoded by gradually increasing label signals (six levels each) in two channels, or by the absence of a label, or (C) nine barcoded samples using a combinatorial barcoding scheme based on three intensity levels per channel. Circles/ellipses indicate different barcode-labeled samples. Note that the samples characterized by the absence of barcode labels (lower left populations), tend to accumulate insufficiently labeled cells of other samples and debris, and is therefore recommended not to be used for barcoding. (D) Pascal's triangle can be used as a tool for the construction of barcoding schemes. The line numbering indicates the number of barcode channels, and the ordering of numbers in each line reflects the number of labels per sample, not counting the "1." Different scenarios are indicated by the numbers highlighted. Four samples labeled by one marker each consumes four barcoding channels (red), dual barcode marker labeling in six channels (blue) can be used to barcode and pool 15 unique samples, and, in theory, 210 samples could be barcoded by quadruple combinations in ten cytometric channels (green). Blue numbers denote sums of each line that equal the capacity of unrestricted combinatorial barcoding schemes consuming the indicated number of barcoding channels.

ity of restricted and exhaustive combinatorial barcoding schemes (Fig. 223D).

2.4 *Establishing and validating barcoding schemes*

The effort required to establish sample barcoding for FCM or mass cytometry depends on the complexity of the desired scheme, and includes its development and validation. Development steps include the selection of the barcode scheme fitting the study's needs, the barcoding reagent type (depending on sample type, aspired protocol coverage, and the available mass/flow cytometer in combination with available dyes or mass-tags), the titration of barcoding reagents and the optimization of labeling conditions, which is especially key when more than two signal intensity levels per cytometric channel are desired. Optimal reagent concentrations and labeling conditions need to be experimentally determined, using the type and number of target cells the barcoding is finally intended for. This is specifically important when using intracellular, protein-reactive barcoding reagents, as these bind to proteins in a stoichiometric fashion, under commonly nonsaturating conditions, so that fluctuations in cell numbers (or protein content and composition), buffer composition, incubation time, and temperature can lead to differing barcode label staining intensities, which can complicate deconvolution of data. It is important to use protein-free media for covalent barcode labeling to avoid reaction of barcode reagents with buffer proteins instead of cellular proteins. CD45 or other cell surface Ab-based barcoding operates at ideally saturating conditions, which make the barcode stainings more robust to small assay fluctuations, but leads to competition between Ab conjugates for target epitopes in the case of combinatorial barcoding, causing a decrease in barcode staining intensity depending on how many different Ab conjugates are combined on the same cell sample. It is therefore essential to incubate cells with premixed cocktails of barcoding Abs rather than adding barcoding reagents one by one to the cell suspension. Finally, cell washing conditions following the barcode labeling reaction prior to sample pooling have to be established. Careful washing of cells is required to minimize the carryover of barcode reagents into the sample pool. Remaining reagents can cause unwanted low-level labeling of all cells in the pool, which negatively impacts on cytometric resolution of barcode signals, thereby complicating deconvolution. More washing steps usually mean a better separation of barcode/labeled cells from unlabeled background but also cause greater cell loss due to removal of supernatant. In our hands, three to five washing cycles are usually sufficient to achieve a clean bar-

code staining pattern. As for covalent barcoding reagents, washing buffer should contain protein such as BSA or FCS, which serves to catch unbound barcode reagents. The barcoding reaction typically lasts 10–15 min.

Experiments such as the checkerboard test or the retrieval of sample-specific traits should be conducted, which address the reproducibility of results achieved by measuring the samples separately (without barcoding) [1985, 1987, 1992, 1993] to establish and validate sample barcoding protocols. Analyses of unique sample characteristics, such as the known lack of a certain cell population within PBMCs in individual samples, which are either run barcoded or separately must provide matching results. The checkerboard test is an extension of the above strategy that takes into account that many experiments involving sample barcoding are prepared in microtiter plates. When plotting data (e.g., cell frequencies or signal intensities) of samples with and without a known characteristic that have been plated in different orders, heatmap representations generate a characteristic checkerboard or similar pattern. It should also be confirmed that barcoding does not introduce systematic error, e.g., by interfering with the binding of specific probes post-barcoding, or due to spill-over between barcode marker and analyte-specific signals.

Barcoded sample convolutes typically contain unusually large amounts of cells that mandates titration of the post-barcoding Ab staining cocktail on the same amount of cells. Nevertheless, this generally still results in a several-fold reduction of Ab use per sample, especially if the staining volume of the convolute is kept to a minimum. Careful control of the staining volume is of course an important aspect of consistent staining results.

2.5 *De-multiplexing of barcoded data*

Original sample data can be extracted from barcoded, pooled samples by deconvolution through consecutive manual gating in standard FCM software, by Boolean gating for combinatorically barcoded samples [1988], or using scripts developed for that purpose [1992, 1994, 1995]. Debarcoding software can be developed in-house or retrieved from https://github.com/nolanlab/single-cell-debarcoder (accessed August 15, 2016) [1992], Premessa (https://github.com/ParkerICI/premessa), and has been implemented in the regular CyTOF software (Fluidigm). The better the cytometric separation of the barcoded samples from each other, the better the recovery of original sample cells in the deconvolution. When different cell types in a given sample show heterogeneous barcoding marker staining intensity, resulting in suboptimal cytometric separation in the barcode channels, one should consider separating those first (e.g., by gating for lineage markers), and then deconvoluting the data of different cell types separately.

2.6 *Barcoding reagents*

Different barcoding reagents have been explored. Usually, sample barcoding is achieved by covalently labeling cellular proteins with dyes or mass tags via reactive thiols or primary amines [1984–1986, 1992, 1996], or by Abs [1987–1990, 1997–1999]. In mass cytometry, lipid-reactive RuO_4 and OsO_4 have also been demonstrated as applicable for barcoding [1993]. Covalent labeling is usually used for barcoding of fixed and permeabilized cells, giving the reagent access to the cell interior with many more binding sites than present on the cell surface. In principle, dead cell labeling reagents that function by binding to the cellular protein content ("fixable" viability reagents) should work well as intracellular sample barcode labels. In flow cytometry, succinimidyl derivatives of fluorescent dyes such as PacificBlue™, PacificOrange™, or Alexa Fluor dyes [2000, 2001] are frequently applied [1984, 2002–2007]. In mass cytometry, thiol-reactive mDOTA loaded with lanthanide isotopes [1985, 1996], thiol-reactive BABE, or amine-reactive isothiocyanobenzyl-EDTA loaded with palladium isotopes [1986, 1992, 2008] have been used for intracellular barcoding. DNA intercalators (containing rhodium or iridium) are also candidates for intracellular barcode labels, as are cisplatins that are available in different formats holding isotopically enriched platinums [2009]. A commercial kit suitable for intracellular barcoding of up to 20 samples is available from Fluidigm. For intracellular barcoding, cells require fixation and at least "partial" permeabilization [1986] prior to barcode labeling, which limits the benefits of barcoding to subsequent steps in the protocol. Sample barcoding by Abs [1987–1989, 1998] is implemented earlier in sample preparation protocols. Because of this, more protocol steps—including surface staining of live cells—are performed on the barcoded sample convolute, facilitating the staining of fixation-sensitive markers in barcoded samples [1988]. When using Ab-based sample barcoding, choosing the right target is key. The selected Ab target should be stably and abundantly expressed by the cells of interest and should not be modified by the clinical or experimental conditions applied in the assay prior to sample barcoding. Since CD45 is expressed by all mature leukocytes circulating in blood, and particularly by lymphocytes and PBMCs at high levels, combinations of CD45-Ab conjugates have been used to barcode PBMCs in immune phenotyping experiments [1988]. For other cell types or conditions, such as immature leukocytes in thymus and BM, or malignant progenitors, using CD45 must be treated with caution, and different Ab targets might be more suitable, such as β2 microglobulin to capture leukocytes including $CD45^{low}$ neutrophils [2010], or by combined targeting of CD298 and β2 microglobulin to additionally capture tumor and stem cells [1997]. The use of multiple noncompeting Ab targets also increased the overall barcode signal intensity. It should be kept in mind that antibody labeling of live cells can induce biologically functional responses to Ab-based sample barcoding. Barcode labeling can be applied to fixed cells, if target epitopes are fixation-insensitive, which is the case for, e.g., CD45 (Mei et al., unpublished observation). Recently, barcoding of live and fixed cells by a tellurium compound was described [2011], expanding the available options for live-cell barcoding to situations in which cell-surface markers suitable for barcoding are not known or available. Another variation is ratiometric barcoding, in which signal

intensities relative to each other rather than discrete absence or presence of signals are used as barcode labels, and for deconvolution, removing the strict requirement for cytometric separation in each individual barcoding channel. While this has been demonstrated using lanthanide-coordinated polymer dots [2012, 2013], similar scenarios can be envisioned using different reagents. Ratiometric barcoding increases the barcoding capacity, but complicates the depletion of cell doublets through the application of barcoding.

2.7 *Application of cytometric barcoding to different cell types*

The decision regarding using cell-surface versus intracellular barcoding is usually determined by the overall study outline and protocol. For complex immune phenotyping of live cells, cell-surface barcoding prior to fixation will be more suitable. Intracellular barcoding is often used in signaling studies in which cell activation is stopped by fixation, and therefore all cytometric stainings are performed post-fixation. Sample barcoding has been frequently applied not only to human and mouse primary leukocytes, PBMCs, and cell lines, but also to platelets [2006], and erythrocytes [2007]. The technique is often used in cell signaling analysis using FCM and mass cytometry. Since the induction of phosphorylated states of intracellular signaling mediators is usually characterized by shifts in staining intensity/signal, which can be small and can therefore be affected by technical tube-to-tube variations, barcoding of sample aliquots that underwent different stimulation conditions and their pooling for joint acquisition and analysis is often employed to protect against such error and resulting misinterpretation. Fluorescent and/or mass-tag barcoding has been employed in B cell signaling studies [2014] and various other cell signaling studies [2001, 2004], in the characterization of the effects of pharmacological inhibitors on primary mouse and human immune cell subsets [1985, 2003], in the mapping of myeloid cells in mice [2008], in stem cell research [1992], and also in clinical immune monitoring [2015].

3 Mass cytometry

3.1 *Overview*

Mass cytometry takes advantage of metal-conjugated Abs and other metal-containing probes for cell characterization that are detected by time-of-flight mass spectrometry, providing a cytometric platform that is able to assess up to 135 parameters, ~50 of which are being used. It facilitates high-dimensional single-cell cytometry, especially in experimental setups where fluorescent spillover and autofluorescence are limiting in conventional FCM. This chapter outlines the principles, specifics, applications, advantages, and bottlenecks and of mass cytometry, and outlines workflow details promoting its successful implementation.

3.2 *Introduction*

Since its introduction in 2009 [2016], mass cytometry (or Cytometry by Time-Of-Flight technology, CyTOF) has pioneered a new era of high-dimensional single-cell analysis, surpassing the limits set by the availability of spectrally resolvable fluorochromes in conventional FCM [1849, 2017]. The innovative concept of mass cytometry is the use of stable rare earth metal isotopes of very high isotopic purity coupled to Abs or other target-specific probes for labeling of single-cell suspensions. These probes are characterized by and detected based on the metals' mass/charge ratios by inductively-coupled plasma time of flight mass spectrometry [2018]. Thereby, it is comparatively easy to perform single-cell cytometric experiments with currently more than 50 parameters in a single measurement in which typical obstacles inherent to fluorescence-based cytometry, such as spectral overlap/compensation and autofluorescence are absent or have only minimal, and manageable, impact.

3.3 *Mass cytometry in biomedical research*

Mass cytometry is ideally applied to research requiring high parametrization at single-cell resolution, e.g. for resolving cellular heterogeneity in complex mixtures of cells (such as blood or tissue cells); complex phenotypes of isolated cell types (such as T-cell subsets according to intracellular cytokine expression and chemokine receptor expression) [561, 1850, 2019]; or when a maximum of information is to be extracted from a given, limited sample, such as from certain cell cultures, fluids, tissue biopsies, children's or certain patients' blood samples [1688, 2015, 2020–2023]. While mass cytometry is able to assess many parameters from a single cell sample, the information gained by high parametrization needs to be balanced against the limited sample transmission efficacy of mass cytometry.

Metal-labeled Abs used in mass cytometry largely resist the methanol treatment that is used for permeabilization of cells in order to detect phosphorylated states of intracellular signaling mediators. Therefore, mass cytometry is a sought-after tool in cell signaling studies [1849, 1985, 2015]. Mass cytometry also facilitates large-scale immune monitoring and drug effect screening in clinical/translational research and systems immunology [1849, 1985, 2024]. To date, mass cytometry has been performed not only on leukocytes from different species including mouse, man, and nonhuman primates [2025], but also on cell lines and bacteria [2026, 2027], and has been used to track metal nanoparticles [2027, 2028]. Metal-containing polystyrene or Ab capture beads [1994, 2029] are used as internal standards in mass cytometry measurements and could potentially be modified to work as capture beads for serological analysis using the CyTOF platform, similar to fluorescence-based Luminex technology.

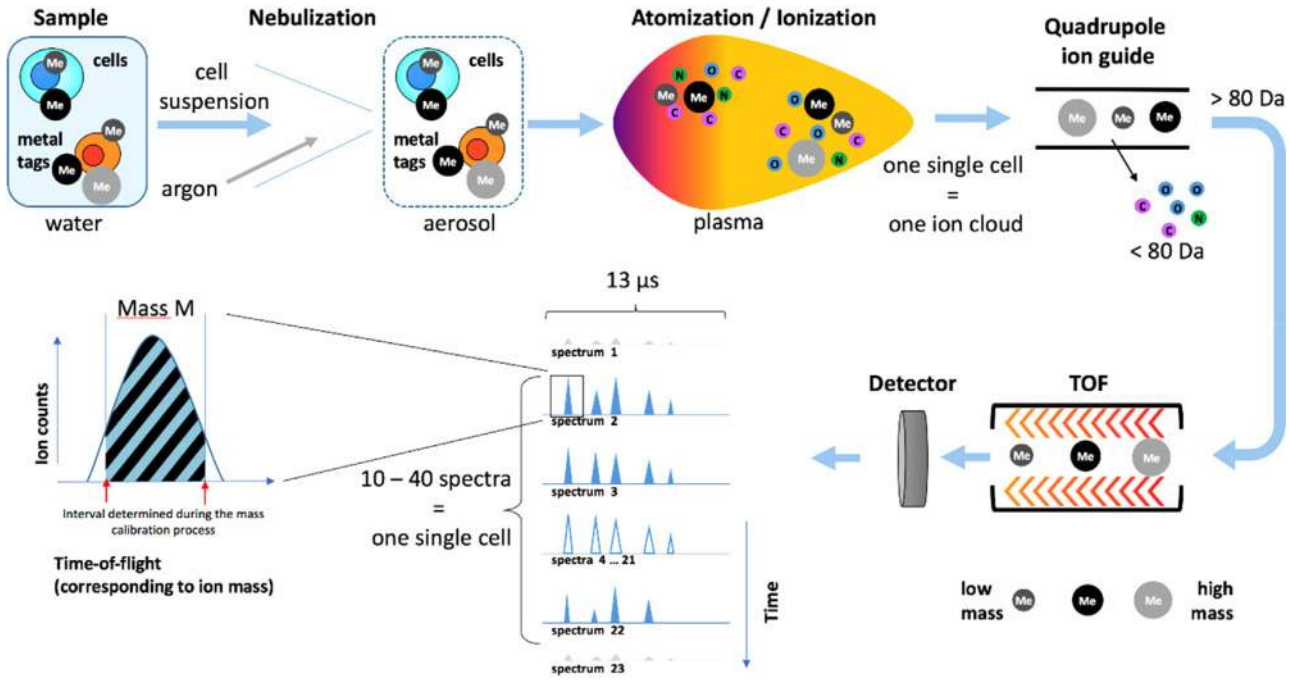

Figure 224. Schematic overview of a mass cytometric measurement. A suspension of cells stained with different rare-earth-metal-conjugated Abs (metal, Me, different sizes reflect different isotopically enriched metals) is injected into the CyTOF instrument. First, an aerosol of single-cell-carrying water droplets is generated by spray nebulization, which is then dried on the fly and introduced into the inductively-coupled argon plasma. In the hot plasma, cellular matter is completely atomized and ionized, resulting in the formation of a single ion cloud from each individual cell. Next, uncharged material and low weight ions (<80 Da), such as carbon (C), nitrogen (N), or oxygen (O) are removed from the ion cloud by quadrupole ion guides. The remaining heavier ions, including the rare earth metal ions are then separated by time-of-flight (TOF) analysis according to their mass-to-charge ratio, and analyzed for their abundance. An entire TOF spectrum is recorded every 13 µs, so that a single ion cloud is represented by a series of about 10–40 consecutive TOF spectra. The abundance of each atomic mass (defined by TOF windows) in each spectrum belonging to one cell is then integrated to yield a data format in which each cell event is assigned an ion count (similar to a "signal intensity") reflecting the amount of the respective metal-conjugated antibody that was bound to the cell.

3.4 *The mass cytometer: Cell introduction and signal detection*

The mass cytometer combines a cell introduction system with a mass spectrometer consisting of three basic components: the ion source, the ion analyzer, and the ion detector. Essential parts and steps of the measurement are summarized in Fig. 224. During a CyTOF measurement, single cells labeled with metal-tagged probes typically suspended in water are injected at a flow rate of 30 µL/min into a nebulizer. Using argon as a carrier gas, the nebulizer creates an aerosol that is guided into the mass cytometer. The nebulizer orifice of about 80–150 µm diameter limits in theory the size of cells or particles measurable by mass cytometry, while in practice, a large variety of primary cells and cell lines have been successfully analyzed. The CyTOF instrument utilizes an inductively-coupled argon plasma. At a plasma temperature of ~8000 K, injected cells traveling through the plasma are vaporized, and entirely disintegrate into their atomic, ionized constituents. Thus, each cell generates an ion cloud that expands by diffusion and charge repulsion and enters the vacuum of the mass cytometer. Afterward, the vast majority of matter is removed from these ion clouds: uncharged material is depleted by an electrostatic deflector, and low-weight ions, including those of elements abundant in organic material such as C, O, H, N, and Ar (serving as carrier gas), as well as ions carrying multiple charges, filtered out by a quadrupole ion guide. Only heavy-weight single-charged ions pass on to the time-of-flight (TOF) analyzer. There, ions are separated and identified by their flight time difference after acceleration in an electric field of a defined strength, in which all ions receive the same energy. Since the TOF of a given ion depends on its mass and on its charge, the charge has to be the same (+1) for all ions to correctly determine the mass an ion by its TOF. The velocity of lighter ions is higher and they reach the detector first, followed by heavier (and slower) ions, in the sequence of increasing ion mass.

The ion cloud of a given cell is measured in small portions, termed pushes. The CyTOF instrument performs 76 800 measurements (pushes) per second, which means that one mass spectrum is captured every 13 microseconds. Since the CyTOF technology is currently limited to detection of metal isotopes with high atomic mass, only the segment of the spectrum corresponding to atomic masses higher than 75 Da is taken in consideration. Typically, a single ion cloud is captured by ~10–40 spectra. An electron multiplier is used for ion detection and consists of a series of dynodes maintained at increasing potentials, resulting in serial amplification of the original signal. The output signal

of the detector is further amplified and subsequently digitized by an analog-to-digital converter. The spectra are then analyzed by two successive integration steps, to obtain information about the amount of metal associated with each ion cloud corresponding to a single cell event. The first integration is an area under curve calculated over an around 19–26 ns interval according to the region of a given mass spectrum and represents the intensity of the peak for a given isotope. The region used for the first integration is determined during the instrument setup procedure termed mass calibration, using a tuning solution. The second integration summarizes consecutive positive peaks corresponding to a single (cell) event. The signal with the maximum number of consecutive spectra is taken as reference to identify the spectra contributing to an ion cloud representing a single-cell event. Finally, the integrated signal intensities obtained for one cell in the different mass channels are converted into FCM standard (FCS) 3.0 format files. Thus, mass cytometric data can be viewed and analyzed manually using standard FCM software packages. However, considering the high complexity of mass cytometric data, manual data analysis is time consuming, subjective, and may miss much information contained in complex mass cytometric data. It is advisable to employ automated cell clustering, population identification, and dimensionality reduction techniques such as PCA or t-stochastic neighbor embedding (t-SNE)-based, UMAP, or similar methods [1470, 1794, 1983, 2030, 2031] for the analysis of high-content mass cytometry data (see also Section VI.1: Data analysis: An overview; and Section VI.5: Data repositories: Sharing your data). An important point to consider is that data analyses of a given study increasingly employ several algorithms organized in an analysis pipeline, very similar to an experimental procedure that needs to be described and annotated in appropriate detail [2032]. Finally, the technical identity of cell populations defined by mass cytometry in combination with, e.g., data clustering approaches can be validated by algorithms that break down high dimensionality into a lower dimensionality that can be handled by routine FCM analyzers, so that cell populations can be gated by conventional human-defined analysis [146, 147]. The same tools help to further characterize identified cell populations by providing a lead that markers to use for isolating them for further functional or molecular analyses.

3.5 *Equipment*

At present, Fluidigm Corp. is the only commercial provider of mass cytometry instruments and of almost all mass cytometry-tailored reagents. Mass cytometers can be run in a high-throughput manner by employing either an autosampler suitable for consecutive measurements of larger number of samples of limited sample size (from a 96-well plate), or an add-on device that permits acquisition of larger samples of any volume (Supersampler, Victorian Airship LLC), which is ideally used in combination with sample barcoding approaches (for more details, see Section VIII.2 Barcoding in cytometric assays). The latest mass cytometer version ("Helios") can sample volumes of up to 5 mL. A tube is placed in a chamber where an applied pressure drives the intermittently agitated sample from the tube to the injection line. More recent mass cytometer versions (CyTOF version 2 and Helios) do not necessarily require in-depth technical knowledge of mass spectrometry, as the daily tuning and instrument alignment is largely performed automatically. However, it is advisable to have the instrument maintained and managed by an expert operator. The installation of a mass cytometry platform usually requires the additional setup of air conditioning, an exhaust system, argon gas supply and an IT infrastructure suitable to store and manage mass cytometry data.

Mass cytometry has also been used for imaging of tissue sections stained with metal-conjugated Abs, similar to those used in immunofluorescence microscopy [1883, 2033, 2034] (see also Sections IMC and microscopy). The stained section is dissected into a series of vaporized samples corresponding to μm-sized tissue section spots by high-resolution laser ablation; these tissue section spots are then consecutively analyzed on a CyTOF instrument [1883]. The data of each spot reveal the amount of metal isotopes that was bound to the spot when the tissue section was stained with metal-tagged Abs. By plotting the single-spot data next to each other in the order they were ablated from the entire tissue section, highly multiplexed images are reconstructed. Similar data can be generated using an alternative approach, i.e., multiplexed ion beam imaging (MIBI) that, does not rely on the mass cytometry equipment discussed here [2035, 2214].

3.6 *Coping with bottlenecks in mass cytometry*

While the advantages of mass cytometry are striking for various applications, it should be noted that due to the destruction of the cells in the argon plasma, CyTOF instruments cannot recover the original cell sample for subsequent experiments. Instrument sensitivity, cell throughput, and overall recovery should be taken in consideration when planning a study involving mass cytometry. Cells labeled with metal-conjugated Abs usually deliver signal intensities sufficient for gating and quantitative analyses. Current mass cytometers have a manufacturer-specified dynamic range of 4.5 orders of magnitude, which is comparable to fluorescence-based FCM. The variability in sensitivity for the detection of different reporters is lower in mass cytometry compared with that in FCM [2017]. However, mass cytometry currently lacks reporters that provide a specifically "bright" signal such as PE in conventional FCM [2017], due to an upper limit of metal ions that can currently be loaded onto a probe (~140 lanthanide ions per Ab using MAXPAR labeling kits [1987]). In addition, of any 10 000 heavy metal ions of the CyTOF detection mass range injected, only about 3–10 are counted by the instrument [2036]. These limitations are in part compensated for by the lack of inherent biological background signal (no "autofluorescence") and minimal signal spillover, which both can negatively impact fluorescent FCM data (see also Chapter II Section 1.2 Principle of spillover and compensation for a complete discussion about spillover). However,

this principally does not protect from background signals due to nonspecific binding of metal-labeled probes to cells. Significant background binding of MAXPAR-labeled Abs has been reported for fixed eosinophils, which could be eliminated by pre-incubation of cells with heparin [2037]. The sensitivity could be improved by probes that carry more metal per specific probe, such as heavy metal nanoparticles [2038–2040].

The volume of a single-cell derived ion cloud expands by diffusion to ~2 mm in size, restricting the instrument's throughput to ~1000 cells per second. A lower throughput (<500 events per second) usually delivers data comprising fewer doublet events. Thus, in contrast to most fluorescence-based flow cytometers with event acquisition rates of usually up to 10 000 events/s, acquisition times in mass cytometry are significantly longer and might necessitate pre-enrichment of target cells prior to mass cytometric analysis [2041]. In addition, a CyTOF measurement recovers data for about 30–50% of the injected cells, while the remaining sample is lost, e.g., by accumulating on the walls of the spray chamber and injector. Mass cytometers need to be set up and tuned daily (procedure detailed in ref. [1806], and instrument manuals) to confer stable instrument performance during day-to-day operations, while only very minor variations, e.g., due to slightly differing oxide ratios may remain.

Generally, the implementation of standardized tuning, sample barcoding (described in greater detail in Chapter VIII Section 2 Barcoding in cytometric assays) [1985, 1988, 1992], signal normalization according to bead standards [2042], and spillover compensation [1994], and Ab cocktail cryopreservation [2043] secure the generation of high quality data in mass cytometry.

All above approaches however do not account for experimental variability at the time of sample biobanking. To further improve data consistency, sample banking and assay automation are actively pursued in the mass cytometry field (covered in Chapter VIII section 11 Sample banking and Section 12 High throughput screening). Concerns for potential batch effects introduced at the time of sample banking and their long-term storage are particularly relevant to mass cytometry, as algorithmic analyses are particular sensitive to batch effects, complicating and limiting the discovery of biological features. Since different cell types behave differently during, e.g., cryostorage procedures [2044], proper sample banking must be confirmed for individual target cell populations.

In addition, the inclusion of a reference sample, that is, an aliquot of cells isolated from a single batch of sample material similar in nature to the study material, spiked into a series of batches of jointly processed samples that belong to a given study [2045], inform about remaining staining, and measurement variability across batches and may serve for normalization of batch effects in the future.

Ring trials have been adopted as a means to analyze the comparability of mass cytometry data generated by on different instruments and locations, showing that sample and reagent distribution rather than individual instrument performance were determinants of variability [2046].

3.7 *Experimental workflow, reagents, and controls*

The experimental workflow for preparing mass cytometry assays is typically very similar to that for conventional FCM, except for the strict requirement of cell fixation and their resuspension in water or cell acquisition solution prior to acquisition on the CyTOF instrument. Briefly, cells are subjected to cell surface staining and optional dead cell label incubation, fixed (usually using formaldehyde), permeabilized, stained for intracellular antigens and DNA content, finally resuspended in water or commercially available cell acquisition solution, and optionally supplemented with normalization beads for injection into the mass cytometer. Cryostorage of stained cell samples has been explored to improve the logistics of assay preparation and acquisition [2047]. Cell-surface and intracellular sample barcoding solutions are available and can be applied prior to surface staining or after permeabilization, respectively. Protocols are available for in-depth surface marker-based immune phenotyping [2024, 2048, 2049], intracellular cytokine staining [1850], tetramer-based detection of antigen-specific T cells [561, 1850], cell signaling analyses based on the detection of phosphorylated signaling mediators [1849, 1985, 2015], in vitro proliferation assays [2050] and the detection of RNA in single cells [2051, 2052]. In addition, recent developments in mass cytometry reagents allow the single-cell assessment of global epigenetic modifications [2053]. As such, the EpiTOF (Epigenetic landscape-profiling using cytometry by time-of-flight) Ab panel allows the assessment of different classes of histone modifications and variants. Functional probes available for mass cytometry include 5-iodo-2-deoxyuridine for assessing cell proliferation [2050], enzymatic activity [2054], and a tellurium-based hypoxia probe [2055]. Wheat germ agglutinin (WGA) and osmium tetroxide staining were proposed as a proxy for cell size in mass cytometry [2056], besides ASCQ-Ru for cell volume respectively, which, in conjunction with the Celltracer software has been used to correct for confounding cell size effects in signaling studies [2057]. Further, osmium tetroxide has been used to stain functionalized polystyrene beads, making beads manufactured for conventional FCM readily detectable by mass cytometry (Budzinski et al., 2019). Ab-binding quantum simply cellular beads modified by this method have been used to determine antibody binding capacities of immune cells [2058], and to study receptor occupancy after mAb therapy [2059] by mass cytometry.

Mass cytometers do not measure the light scatter parameters usually employed in FCM for detection of cell events and separation of cell aggregates; cells (or any other particles) are solely detected by the metal associated with them. Nucleated cells are typically revealed by rhodium- or iridium-based DNA intercalators [2060], and probes specific to characteristic cell antigens can be envisaged to reveal non-nucleated cells such as erythrocytes or platelets [2061]. Doublet events can be minimized by (i) filtering cells prior to injection, (ii) avoiding high cell densities in the injected sample, (iii) excluding cell events with high DNA signal and/or high cell/event length parameter values by gating, or (iv) sample barcoding using a restricted barcoding scheme efficiently filtering out doublet events formed between cells of differently bar-

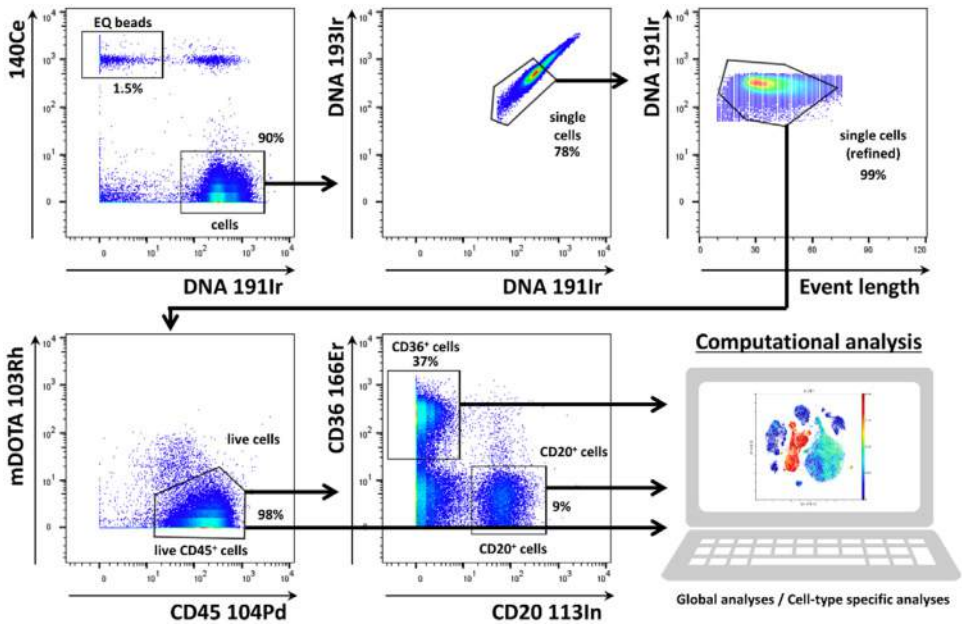

Figure 225. Typical gating strategy for PBMC analyzed by mass cytometry. Intact cells are identified by staining of DNA. Normalization beads elicit high signals in defined channels such as ^{140}Ce in the present example. Cells (unless stained with ^{140}Ce conjugated Abs) do not elicit high ^{140}Ce signals, and beads do not elicit high DNA/iridium signals. Events that appear in the upper right are cell-bead doublets, which could be either physical aggregates, or due to timely overlapping acquisition of two ion clouds with one cloud representing a cell, and the other one a bead event. Events not stained in either channel (lower left) are usually debris associated with metal amounts sufficient to be detected by the CyTOF instrument (first dotplot). Cell events are further restricted to events showing strongly correlating DNA signals according to their ^{193}Ir and ^{191}Ir staining. Both Ir isotopes almost equally contribute to the natural abundance iridium used in the DNA intercalator. Thus, signals are expected to correlate. Events with high iridium staining intensity are excluded since the DNA^{high} fraction is enriched for cell doublets. This procedure does not fully eliminate doublets but reliably reduces their presence when barcoding was not used to filter out doublets. However, back gating should be used to confirm that target cells are not excluded in this step (second dotplot). Gating according to "cell length" or "event length" is often employed in order to minimize the presence of doublets. The "length" parameter corresponds to the number of spectra that belong to a given event. Events labeled with large amounts of metal (and doublets) tend to show higher, and those with little metal tend to show lower "length" values. Upper and lower cell length boundaries are defined in the acquisition software. The length parameter is not indicative of cell size. Again, backgating should be employed to ensure that target cells are not excluded (third dotplot). Next, dead cells are excluded by gating on ^{103}Rh $^{low/-}$ cell events. High ^{103}Rh signals result from stronger labeling of dead cells by ^{103}Rh-mDOTA compared to live cells. PBMC identity is confirmed by CD45 staining (in-house ^{104}Pd conjugate, fourth dotplot), and CD36 and CD20 staining differentiate between monocytes/dendritic cells and B cells, respectively (in-house conjugates, fifth dotplot). Total cell events and/or select subsets are typically subjected to further computational analysis.

coded samples [1988, 1992]. Gaussian discrimination parameters have also been suggested for doublet identification and exclusion [2062]. Finally, DNA intercalators, cisplatin [2063], DCED-Pd [1997], or metal-loaded DOTA-maleimide [2048, 2064], are used for cell viability staining. A typical initial gating strategy is provided in Fig. 225.

The CyTOF instrument ("Helios" version) quantifies ions with atomic masses between 75 and 209, providing 135 channels. More than 50 of these can be used for detection metal-conjugated Abs, and additional channels accommodate DNA intercalators or dead cell detection. A central part of any mass cytometry experiment is Ab panel design, for which various mass tagged-Abs and predesigned panels are commercially available. Abs can be labeled in-house using commercial kits for lanthanides and indium isotopes, or according to published protocols with isotopes of palladium, yttrium, bismuth, and platinum [1987, 1988, 2047, 2065, 2066]. Moreover, metal-containing nanoparticles such as Qdots containing cadmium [1850, 2067] and silver nanoparticles [2038] have been successfully employed as mass tags for reporting binding of specific probes to cells. The design of mass cytometry panels is generally easier as compared to fluorescent flow cytometric panels of similar marker capacity, since signal spillover and sensitivity differences are comparably minor issues [2017]. However, the mere number of parameters and the implementation of quality control for Abs, as well as choosing appropriate Ab clones [2049] make panel design a significant effort. Panel design includes optimizing the pairing of specific probes with unique heavy metal isotopes considering instrument sensitivity for that particular isotope mass, target antigen abundance, and additionally potential signal spillover (see ref. [2068] for details). Signal spillover in mass cytometry can arise from (i) isotopic and elemental impurities of mass tags, (ii) between adjacent mass channels at high signal abundance (usually Mass (M) +1 spillover, but M-1 spillover is also possible), and (iii) because of metal oxide formation (M+16 spillover) [2049, 2068]. A careful panel design, an optimally tuned instrument and highly pure reagents, however, can minimize these spillovers to very low levels that are orders of magnitude lower than fluorescent spectral overlaps. In addition, residual spillover effects in mass cytometry and imaging mass cytometry data can be compensated [1994] using a nonnegative least square (NNLS)

approach [37] that applies correction at the single cell level and constrains data to signals higher than zero after compensation.

Isotype and FMO controls are typically used in conventional FCM experiments to distinguish between specific and background signal (for further detail see Section III.1 Controls: Determining positivity by eliminating false positives). In theory, isotype and FMO controls (termed in mass cytometry as Signal-minus-one or Metal-minus-one controls, SMO and MMO, respectively) are easily applicable to mass cytometry. However, the sole fact that, in mass cytometry, typical panels include approximately 40 Abs renders the routine and consistent realization of these controls laborious and complicated, and often unfeasible. Isotope controls require the use of an antibody with a matching isotype and the same amount of metal per antibody as the reagent that is to be controlled, and are presently not commercially available. As a result of these practical limitations, the SMO/MMO controls are either performed exemplarily or combined in a metal-minus-many (MMM) strategy, in which several rather than individual Ab conjugates are omitted during the staining procedure, e.g., a group of markers specific to a certain panel on the backbone lineage marker panel. In addition to these, biological controls are particularly adapted to mass cytometry, since they take advantage of the high dimensional level of the data. Counterstaining for multiple cell lineage markers in Ab conjugate evaluation experiments enables the identification of reference cell populations in the sample serving as positive and negative controls for a given Ab conjugate in the multitude of populations commonly identifiable by a 40-parameter panel. For example, B cells also present in the sample could be used as a negative control for a T-cell-specific marker. Ab titrations can also benefit from the high dimensional level of the data since multiple markers can be titrated concurrently across subsets defined by a backbone of lineage markers to facilitate assessment of the titration results on specifically gated populations of interest. Finally, mass cytometry data sets and their evaluation, especially by computational means, benefit from bundled, batch-wise sample processing, and data acquisition (as compared to processing samples individually) to achieve a high degree of data consistency.

Generally, experimental workflows for mass cytometry are typically very specific to individual studies, and many factors should be considered during the setup of mass cytometry studies [2069].

3.8 *Conclusions*

Mass cytometry is a recent hybrid technology employing principles of FCM and mass spectrometry. The core technology is rapidly developing along with bioinformatics and reagent chemistry, thereby creating a largely universal and extendable next generation platform for high-dimensional single-cell cytometry applied in translational research, systems biology, and biomarker discovery.

4 Combinatorial cytometry

Combinatorial cytometry is the subfield of cytometry, or single-cell analysis, whereby researchers describe, study, and model complex relationships between multiple combined cytometry samples exposed to varying stimuli, environment, treatment, and so on.

Examples include various techniques of multiplexing, such as fluorescence barcoding [1984], high-throughput cytometry, and cytometry-based compound screening [2070], as well as multiple computational techniques that combine multiple data files either during the data collection [2071] or post hoc in order to create multifactorial and multidimensional datasets to allow for analytical comparisons across properties not readily available or accessible via a single experiment [1795].

Combinatorial cytometry approaches have been implemented successfully with innovative mass cytometry (CyTOF) systems (For more information on the equipment and concept, see Section VIII.3 Mass cytometry) [2072], multispectral cytometry [31], multi-angle elastic light scatter cytometry [2073], high-throughput screening FCM [2070], and computational clinical and research cytometry of the immune system [2074–2076].

There is often a significant difference in the design of a traditional FCM and a high-throughput or high-content assay. This can be visualized in Fig. 226 where both traditional tube (or even plate based) FCM assays are performed, and high-throughput assays exclusively using 96 or 384 or larger plates. Using such large arrays of data creates a fundamental difference in how the data are both collected and analyzed. What is clear is that a high degree of organization and structure, complete with significant metadata is required to establish high-throughput or high-content FCM assay systems.

One of the key advantages of the combinatorial cytometry approach is the opportunity to employ advanced statistical and machine-learning methods, such as various techniques of clustering, supervised learning/classification, Bayesian techniques, and other state-of-the-art methodologies. On the other hand, combinatorial methodologies introduce complexity to the experimental planning and design. As a result, they may increase the cost of the experiential setup and heighten the risk of failure. Ultimately, the benefits of complex, information-rich "all-in-one" assays, must be balanced against the cost of assay development which is likely to be greater than that of performing assays using regular techniques.

Compound screening is a prime example of a combinatorial cytometry approach. Multiple multicolor flow-cytometry cell-stress assays can be rapidly executed in a sequential manner using an automated robotic sampler. The cellular populations are exposed to different concentrations of the compounds tested, but they can also be measured in different environments (different media) and/or at different times after exposure to the stress. The assay can scan a dense grid of possible combinations incorporating all the stress factors in various permutations. Consequently, a huge number of individual cytometry measurements may be required to complete the screen. It is self-evident that the key requirement for successful execution of such an assay is a well-defined, repeatable,

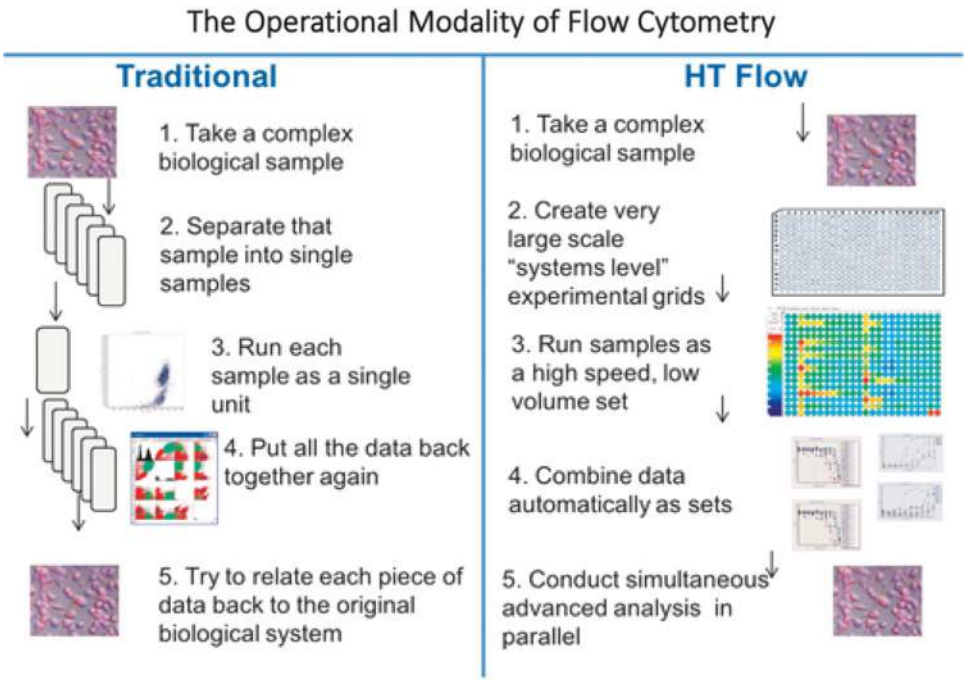

Figure 226. This is an example of how a traditional FCM assay might be designed using test tubes or even a 96-well plate assay. Because of the limitation in the number of tubes or samples that can be run by traditional instruments, it is not possible to create very large arrays. Using high-throughput cytometry, typical assays might be 384-well plates that can be processed in 10–20 min and produce a huge amount of data that can be processed using advanced statistical operations.

and reproducible assay layout (sample organization), which must be consistent throughout the entire cycle of experiments.

The assay sample organization defines the resultant data structure and organization as well, as schematically indicated in Fig. 227. A typical automated phenotypic assay executed using a cytometry screen would employ a 96- or even a 384-well layout that provides space for up to 32 drugs at 10 doses each, as well as negative and positive controls. Preparing such a layout in an automated, repeatable fashion allows glitch-free assay execution and subsequent feature extraction. Figure 228 shows a window of one example of a custom-built screening software package, *PlateAnalyzer*, which automatically outputs response curves and fits log-logistic models on the basis of the templates and gates predefined by an operator [2077]. Since such a system performs the operations involving up to 384 FCS files per plate, it is crucial that all the steps in the analytical procedure be fully automated and be executed without the need for any interactive operator input.

A screening system such as the one described above also relies on automated sample preparation and robotic liquid handling, as the probability of pipetting errors and inaccuracies is too high to allow for a manual assay setup. Automation of sample preparation not only ensures a high level of reproducibility, but also shortens the preparation time and guarantees that the minimal required amount of sample and reagents can be accommodated to make the assay more cost effective.

Opportunities for automated or semi-automated analysis of FC screens can be achieved using many available toolsets for FCM data processing. R-language for statistical computing is a commonly used environment for cytometrists who are interested in developing their own analysis tools and unique data processing pipelines. Combinatorial FCM incorporating dimensions of time, concentration, media, and other factors certainly expands the horizons for this field. Conversely, the availability of rapid development tools for custom design of data processing pipelines is a condition sine qua non for successful implementation of the described combinatorial and multifactorial approaches, see also Section VII.1 Data analysis an overview. When it is desirable to measure biological responses across multiple conditions (e.g., concentration, medium type, stress, temperature, time, etc.) with FCM, it is advantageous to approach the assay in an organized fashion. The technique is enabled by fast autosamplers, and informatics pathways aware of the multifactorial nature of the collected data as demonstrated in Fig. 227 where the differences in analysis of traditional flow data are compared with combinatorial analysis routines. These routines can be highly complex, but depend upon the ability to automatically extract features for all samples in the array.

Other examples of combinatorial cytometry are the well-known bead-based assays. Among those, cytokine assays are probably the most widely used and broadly accepted [2078]. In this technology, two to ten types of cytometry-compatible beads of various sizes (recognized by FCM by forward light scatter) can be dyed with increasing amounts of a tracer dye to encode their ability for capturing/measuring different analytes. For example, Fig. 228 shows 13 cytokines simultaneously recognizable by a commercially available FCM assay (any commercial plate could be entered into the

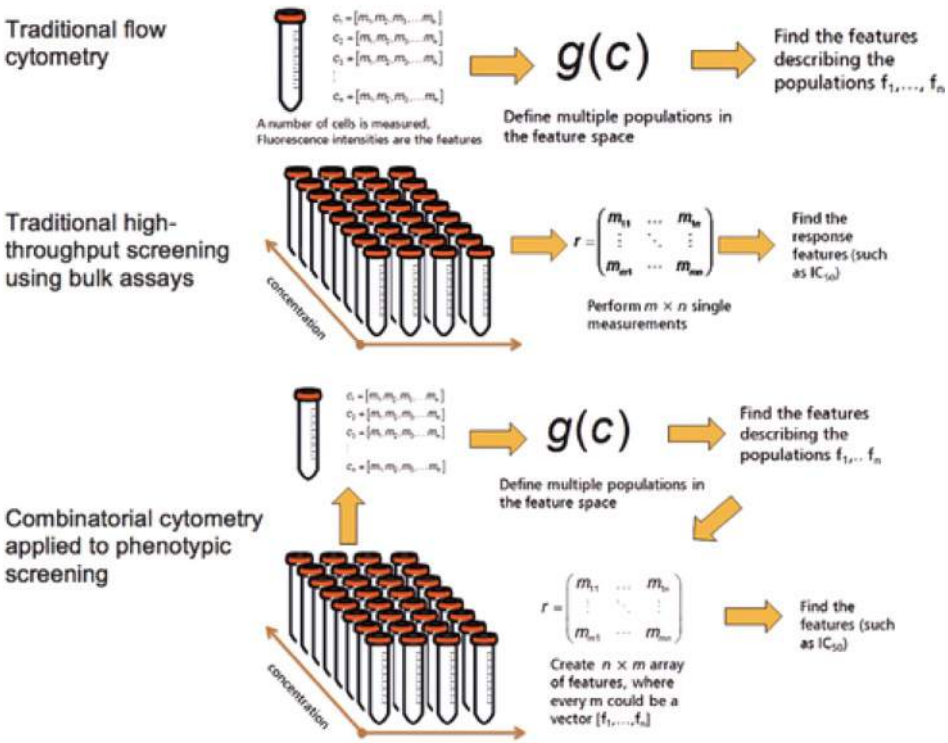

Figure 227. Combinatorial cytometry integrates the ideas of screening biological responses. Biological responses can be screened across multiple conditions (e.g., concentration, medium type, stress, temperature, time, etc.) with FCM. The technique is enabled by fast autosamplers, and informatics pathways aware of the multifactorial nature of the collected data.

Table 94. Cytokine assay reagents. This table shows the multiplex cytokine assay with bead location and target molecule. Using beads of different sizes, with increasing amount of bead fluorescence, many assays can be performed on very small samples of plasma (<15 μL). This example demonstrates how one particular kit (which uses beads identities as A4, A5 ....B2, B3, etc.) where each bead is associated with one particular analyte. Each of these beads are in a small size (A) or larger size (B) group. These are shown graphically in the upper right panel of Fig. 228

Target	Bead ID
IL-10	A4
IFN-g	A5
IL-5	A6
IL-2	A7
TNF-a	A8
CM-CSF	A10
IL-4	B2
IL-17F	B3
IL-9	B4
IL-17A	B5
IL-13	B6
IL-22	B7
IL-6	B9

system). In this system there are two bead sizes, and each bead type carries a different amount of target marker, in this case APC (see Table 94). Although the discussed technique employs only a 13-plex method, frequently up to 20 or 30 different cytokine tags can easily be simultaneously quantified in a minimal volume of plasma. If the organization of samples on multiwell plates is consistent, one can execute an automated data-processing task immediately after assay completion. Gating, recognition of different bead types, computation of calibration curves, and other necessary tasks can be executed automatically without operator intervention or a manual setup.

As mentioned before, multiplexing offers a huge advantage in terms of assay execution time and reagent/sample cost saving. As a result, the multiplexed bead assays allow researchers to identify concentration of analytes of interest in many samples essentially simultaneously. A dedicated software package (such as the PlateAnalyzer Cytokine edition in Fig. 229) provides the means to show all the calibration and to visualize the concentration of analytes across the entire plate. Such visualization techniques are commonly used for other combinatorial approaches in biomedical research and are equally valuable for FCM data.

A third example of a combinatorial cytometry technique is multispectral single-cell analysis. In contrast to traditional multicolor cytometry, which uses a dedicated detection channel for each fluorescent label in the hope of separating signals from multiple labels, the spectral system essentially acts as a superfast spectroscope connected to a flow cytometer. An approximation of the entire spectrum using about 30–40 bands for every cell is measured, and the data can be further processed via spectral unmixing techniques or directly used for spectral classification. There are a number of advantages to the spectral approach, mainly related to the less complex hardware as traditional optical filters are not utilized and neither are individual detectors. This approach creates a new opportunity for combining fluorescent probes that may not be feasible in conventional FCM [2079]. For example, dyes such as GFP and FITC can be used together because chemometric techniques to process spectral cytometry data can be utilized to classify and/or unmix the resultant signals. There are several excellent recent examples of this approach

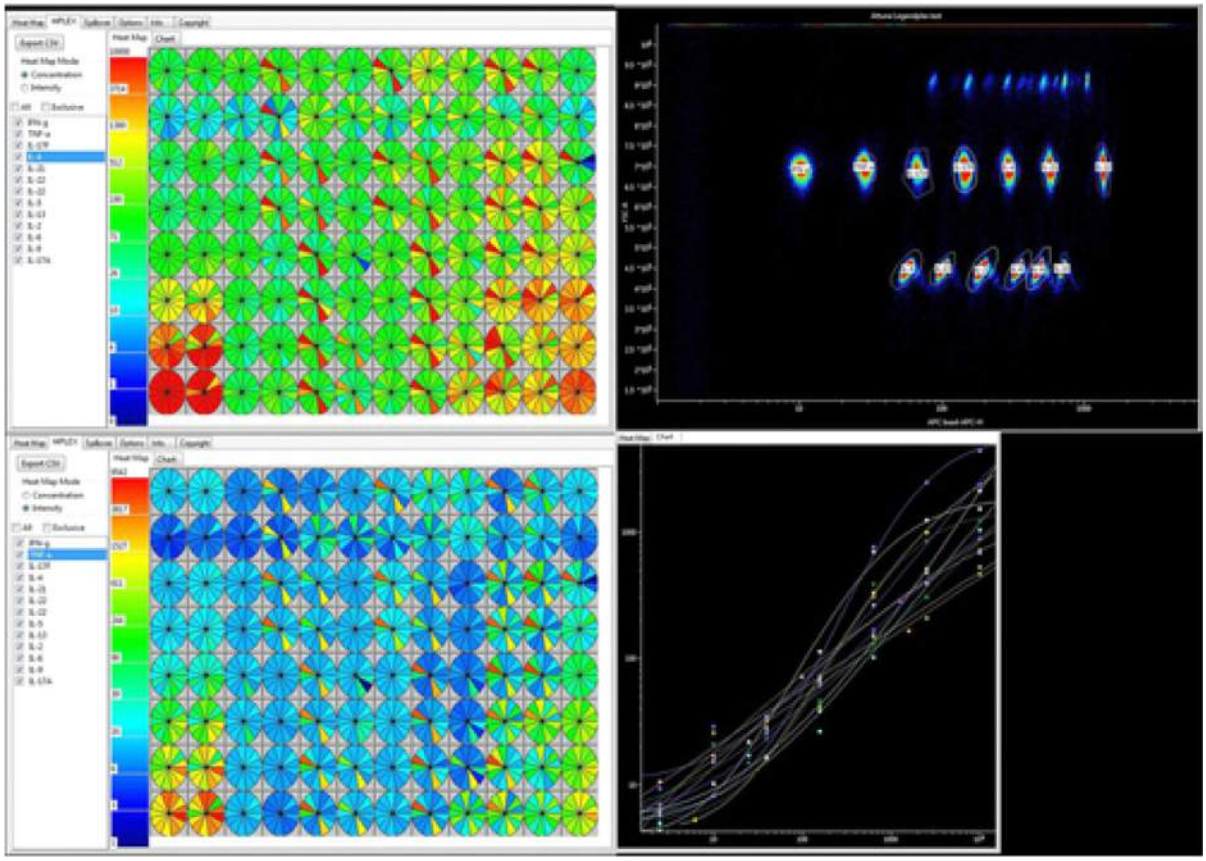

Figure 228. Automated processing of bead-based cytokine assay. Results obtained in a cytometric bead assay in graphical representation of the cytokine concentration in every well of the multi-well plate. Samples were run on an Attune NxT flow cytometer (ThermoFisher) using the instrument plate reader. On the left side of the figure is a list of the analytes used in the assay. In the center part of the figure is a 96-well plate layout showing a representation of each cytokine in a 13-piece pie chart. The colors represent the values in picograms per milliliter. The top right figure shows the bead populations used to define each cytokine. On the bottom left, the heat map describes the fluorescence intensity measurements for each well and each cytokine. The figure on the bottom right shows the standard curve derived from the standards run for this assay.

in FCM [32, 33] in which combinations of fluorescent proteins, together with a variety of fluorochromes, allowed a total of 11 markers to be used simultaneously and then separated by spectral unmixing.

A final example of combinatorial cytometry and one that demonstrates the extraordinary power of multiparameter datasets can be seen in data collected by the CyTOF technology and demonstrated in Fig. 230 (for an overview of the equipment, see Section VIII.3 Mass cytometry). This approach uses lanthanide-conjugated Abs, as opposed to the fluorescently labeled probes of a conventional FC system, and time-of-flight mass spectroscopy for analyzing single cells to produce information-rich population statistics [1849]. The final complexity of such data can be very high indeed, requiring innovative techniques for data processing and visualization. An ad hoc "what-if" analysis is possible using visual development environments allowing for interactive construction and modifications of data processing pipelines. A demonstration of such a pipeline, capable of tackling an input of 30–40 different biological parameters encoded by lanthanides, is represented in Fig. 230. The data processed in this example (courtesy of B. Bodenmiller, University of Zurich, Institute of Molecular Life Sciences) were produced by analyzing a bulk sample with seven lanthanide tags used to encode the position of individual subsamples in a 96-well plate. This experimental approach was applied to characterize human PBMC signaling dynamics and cell-to-cell communication, signaling variability between PBMCs from human donors, and the effects of various inhibitors on this biological system. For each inhibitor, 14 phosphorylation sites in 14 PBMC phenotypes were measured [1985].

The demonstrated data pipeline (or "logic map," in PlateAnalyzer terminology) can extract individual dose-response curves for the 14 phosphorylation states from each of the 14 cell phenotypes. This is a striking example of combinatorial FC analysis, which first creates relationships between different vectors of FC measurements and subsequently explores and quantifies these relationships. Where traditional cytometry is focusing on mapping individual cells in a multidimensional space of phenotypic descriptors, combinatorial cytometry looks at vectors of multidimensional measurements and explores the differences and similarities between those under various conditions.

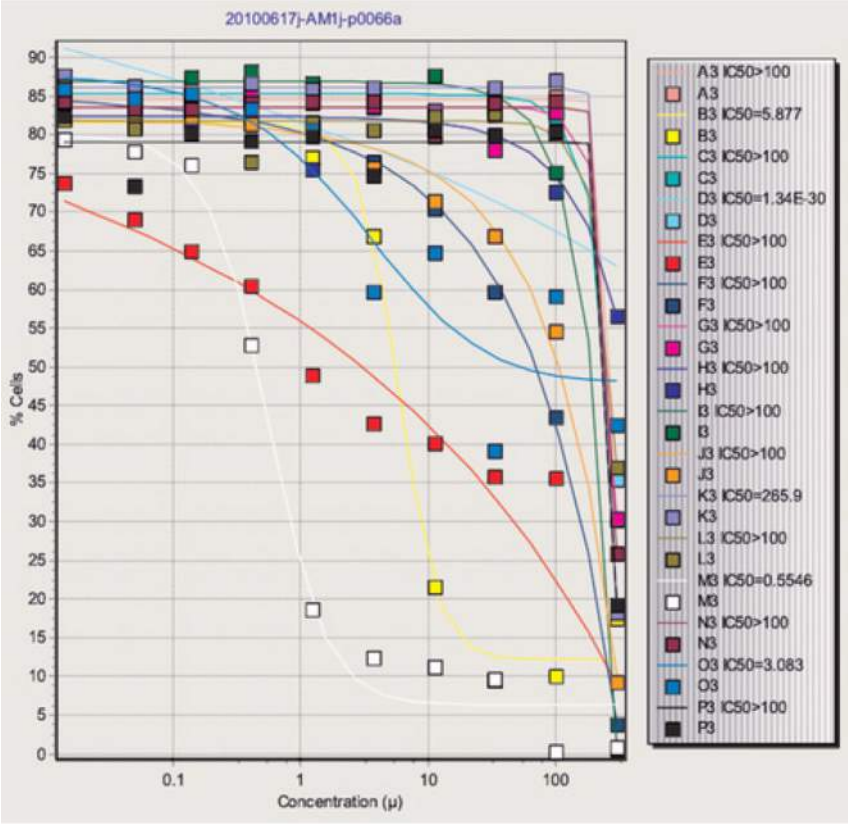

Figure 229. Response curves automatically produced from data extracted from multiple FCS files. Data across FCS files are collected using a robotic sampler connected to a flow cytometer. The PlateAnalyzer software recognizes the plate layout and creates response curves on the basis of pre-defined gates. Each curve results in an automatically calculated IC50 value as shown on the right side of the figure.

Conclusion. The key requirements for combinatorial cytometry are (i) well-defined reproducible assay layout, (ii) highly controlled, preferably automated, assay setup and preparation, (iii) data-collection method recognizing the relationships between the collected FCS files and organizing the measurements in higher-order data structures, and (iv) automated data analysis and reporting software. When this combination of tools is available, complex multiparameter and multifactorial experiment designs can be executed and the resultant data can be rapidly processed to produce

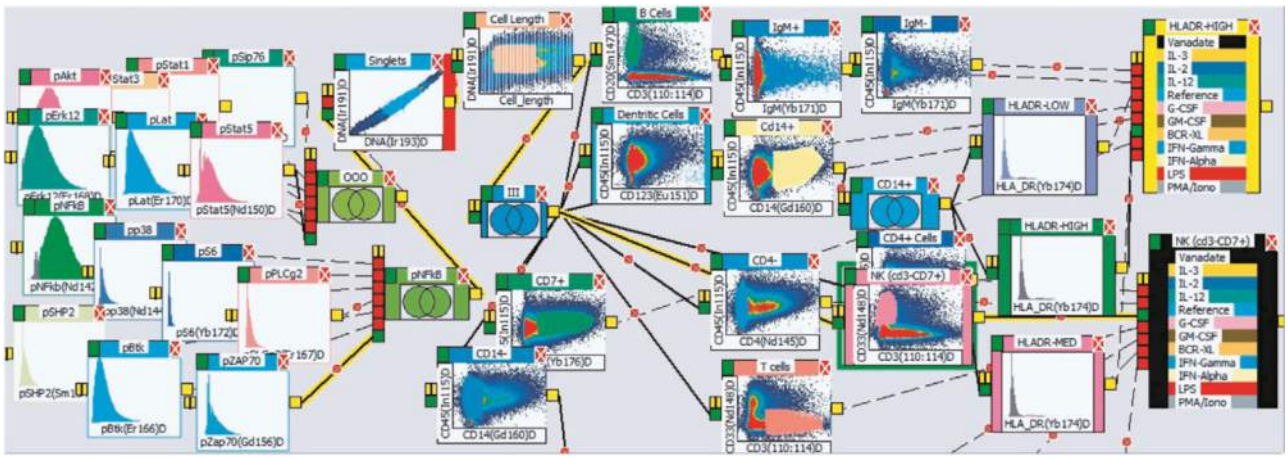

Figure 230. The pipeline design canvas of the PlateAnalyzer. This particular example of an analysis package (http://vault.cyto.purdue.edu) allows rapid development of data-processing maps for complex combinatorial cytometry experiments. In contrast to traditional FC software packages, all the operations are by definition applied to vectors or matrices of FCS files, rather than to individual datasets. On the left of the figure are shown histograms of each of the phosphorylated proteins in the assay, the central group identifies the phenotype of cells being evaluated, and the two boxes on the far right show the stimulating molecules (12 rows) each of which contains eight concentrations. Yellow lines show the active analysis connection pathway—i.e., the resulting dose response curves would be based on the phenotypic result of each component linked within this pathway. As an example in the figure, the phosphorylation state is ZAP70- and the phenotype is NK cells ($CD3^-$, $CD7^+$).

useful insight leading to mechanistic models of the studied biological systems.

5 High dimensional FCM

5.1 *Overview*

The characterization of the complex nature of immunological processes in health and disease requires multi-dimensionality as well as high resolution to detect all targets of interest. While the availability of novel technologies such as mass cytometry by time of flight (CyTOF) and single-cell RNA sequencing (sc-RNAseq) have greatly increased the number of features (protein and/or transcript) that can be measured at the single-cell level, fluorescence-based FCM remains a primary tool for immunophenotyping due to its low cost, high dynamic range, and high throughput. Furthermore, the most recent generation of instruments with five or even more spatially different laser lines allows the detection of 30 parameters, with up to 40 on the horizon (based on personal communication).

Though the general principles of experimental design have not changed (for review, see ref. [56]), reliable fluorescent panels of more than 10 parameters require not only a more thorough and systematic planning to ensure optimal resolution of all markers even at low Ag expression, but they also critically depend on validation and controls as a means to avoid misinterpretation of data. Within this section we describe a step-by-step approach for panel design based on the concept of the spillover spreading matrix (SSM), pointing out important considerations for fluorochrome–antigen combinations and address some of the most common misconceptions and caveats. In addition, we outline key steps in visual quality control of the obtained data to ensure a meaningful subsequent multidimensional data analysis.

5.2 *Introduction*

Most commonly, fluorescent flow cytometers dedicate one detector to the measurement of one fluorophore and use a compensation-based approach to correct for spectral overlap between the different fluorophores used. Improvements in electronics and the usage of multiple spatially separated laser lines have resulted in the latest generation of instruments that can measure up to 28 fluorescent parameters (such as the BioRad ZE5 or the BD FACSymphony) [2080]. In turn, spectral cytometry instruments have been developed that detect every single fluorochrome across all available detectors, thus measuring a complex composite spectrum for every cell, with individual signals being separated by spectral unmixing algorithms (originally developed at Purdue University and now commercialized by Sony Biotechnology as well as Cytek Biosciences) [33, 2081]. Currently, these instruments have reportedly been used for the measurement of up to 24 parameters. The availability of new dyes, dyes are presently limiting all fluorescent-based cytometers, will advance the field and push these limits toward 40, and possibly even beyond. While this section focuses on conventional, compensation-based FCM, most of the principles discussed are applicable to spectral cytometry as well.

Systematic panel design for a high-dimensional experiment requires multiple considerations. Inevitably, the used fluorochromes will show some degree of spectral overlap into more than one detector. The detector intended to capture the major emission peak of the respective fluorochrome is usually called the primary detector, and the secondary detector(s) is (are) the one(s) collecting the spillover. The mathematical process used to correct for spectral overlap is termed compensation [2082] (See Chapter II, Section 1- Compensation), and reports a percent value describing the relative fluorescence detected in the secondary detector compared to the primary detector. This signal portion is subtracted from the total signal detected in the secondary detector. A common misconception is that the magnitude of the compensation value is used as a representation for the amount of spectral overlap between fluorophores, while in fact the compensation value is highly dependent on detector voltages [2083].

The most useful metric in this context is the so-called spreading error, which was first described by the Roederer laboratory at NIH [38]. In short, the spreading error quantifies the spreading that the fluorochrome-positive population (in the primary detector) shows in any secondary detector. This increased spread (as measured by SD of the positive population) is sometimes erroneously attributed to compensation. In fact, compensation does not generate the spreading error, but rather makes it visible at the low end of the bi-exponential or logarithmic scale (Fig. 231a, left panel). Spreading error is a consequence of the imprecise measurement of fluorescent signals at the detector (typically a PMT), which show some variance due to the Poisson error in photon counting.

In short, there are three key aspects of spreading error that need to be considered for panel design: First, spreading error is proportional to signal intensity, i.e., the brighter a signal in the primary detector, the more pronounced the spreading error in the secondary detector will be (Fig. 231A, right panel). Second, spreading error reduces the resolution in the secondary detector, i.e., the detector that is collecting spillover (Fig. 231B). Third, spreading error is additive, i.e., if a detector collects spreading error from multiple different fluorophores, the overall loss of sensitivity will be more pronounced (Table 95).

Besides considering spreading error, which will be discussed in more detail in the next section, other relevant aspects of panel design include the relative expression level of target antigens per cell, co-expression of target markers, and the relative brightness of the used fluorochromes. Importantly, the consideration of spreading error is overall more relevant than fluorochrome brightness if dealing with co-expressed markers (Fig. 231C and D). Furthermore, for any high-dimensional fluorescence experiment the quality of single-stained controls is of utmost importance, thus these have to follow the four basic rules as described in detail in Chapter II Sections 1.3 (Measuring SOVs/compensation controls) and 1.4 (Compensation controls) and in ref. [165]. Finally, the chemical

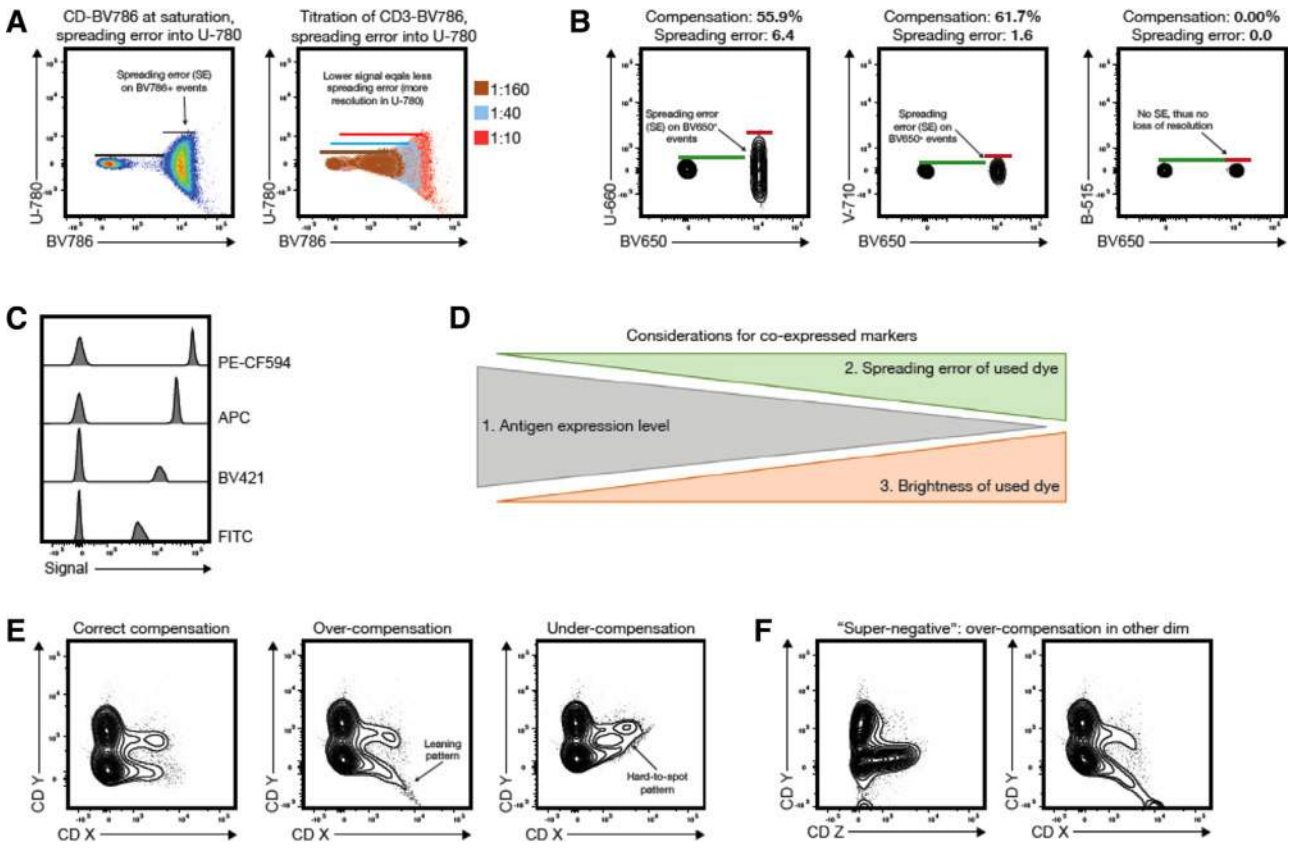

Figure 231. Spreading error and fluorochrome brightness in panel design and common compensation artifacts in quality control. (A) A typical example of spreading error is illustrated: BV786 shows significant spectral overlap in the U-780 detector (excitation by UV laser), which manifests as visible spread of the positive population. The relative loss of resolution on this population compared to the negatives is indicated by black bars on the left plot. Right plot shows how spreading error is proportional to signal intensity, and decreases with lower titers of the respective Ab. (B) The absolute compensation value and spreading error are not directly related, as exemplified for BV650+ events in different detectors (spreading error and compensation values for each combination are displayed above the plot). (C) Examples of staining intensities for different fluorochromes: FITC (dim), BV421 and APC (medium), and PE-CF594 (bright). Note that fluorochrome brightness can be instrument-specific. (D) Overview on the critical considerations for fluorochrome assignment for co-expressed markers. Highly expressed targets should preferably be paired with dim fluorochromes generating little spreading error. Dimly expressed (or unknown) targets should be paired with bright fluorochromes and utilize detectors that receive little spreading error. Numbers 1–3 indicate the relevance of the considerations. (E) and (F) show erroneous patterns that usually indicate incorrectly compensated data: (E) example of a correctly compensated plot, and respective over- and undercompensation of marker CD X into detector for CD Y. (F) Example of an incorrectly compensated population CD X (right plot) appearing as "super-negative" population if displayed against an unrelated detector measuring CD Z (left plot). The erroneous pattern is only visible if displayed against the detector measuring CD Y.

properties of the used dyes can impact complex panels, as unexpected dye–dye interactions or dye–cell/dye–buffer interactions can change the fluorescence spectrum of a given dye (also see *"Top tricks"* of this chapter). This aspect needs to be addressed by using appropriate controls, which will be discussed together with spreading error in the next section.

5.3 *Principles of the technique being described*

The SSM is a fundamental tool for successful panel design. It is specific for each instrument and provides comprehensive information on the relative contribution of any fluorochrome to spreading error in secondary detectors, and the relative loss of resolution in all the available detectors. As such, the SSM provides a way to tackle spreading error in a systematic manner. It is important to note that the extent of spreading error cannot be predicted from the corresponding value in the compensation matrix, which is exemplified in the plots displayed in Fig. 231B.

The SSM can be calculated from single-cell stained controls in a common data analysis package, FlowJo (version 10.4 and higher), or manually using the formulas provided by Nguyen et al. [38]. The information on spreading error obtained from the SSM can be translated into panel design in two ways: First, the SSM highlights individual fluorophore-detector pairs with high spreading error, which in turn should be used for mutually exclusive markers (e.g., CD3 and CD19) as in this case spreading error will not interfere with detection of either signal. Second, the SSM can be used to assess the additive loss of resolution in a secondary detector by calculating the column sums, and to assess the additive

Table 95. Example spillover spreading matrix (SSM)

Detector	B–530	B–710	R–670	R–710	R–780	U–379	U–570	U–610	U–660	U–740	U–800	V–450	V–470	V–570	V–610	V–655	V–710	V–780	YG–586	YG–610	YG–670	YG–780	Total spreading error
fluorochrome	(FITC)	(PerCPCy5.5)	(APC)	(AF700)	(APC–Cy7)	(BUV395)	(BUV563)	(BUV610)	(BUV661)	(BUV737)	(BUV805)	(BV421)	(BV510)	(BV570)	(BV605)	(BV650)	(BV711)	(BV785)	(PE)	(Pe–Tx)	(Pe–Cy5)	(Pe–Cy7)	contributed
FITC	0	0.599	1.07	0	0	0	0	0.356	0	0.729	0	0	0.396	0.449	0.455	0.386	0.24	0	1.37	1.06	0	0.296	7.406
PerCPCy5.5	0.247	0	2.24	4.18	1.91	0.223	0	0	0.275	2.92	1.76	1.72	0.465	0	4.92E–03	0.698	1.91	2.4	0	1.57	3.3	3.1	28.92292
APC AF700	0	1.09	0	2.78	1.29	0.0662	0.0775	0	0.268	0.889	0.486	0.361	0	0	0.183	0.905	0.55	0.433	0.811	0.391	4.28	1.23	16.0907
APC–Cy7	0.132	0.5	0.767	0	2.18	0.119	0.139	4.87E–04	0	1.62	0.738	0.44	0.143	1.99E–03	0	0.143	0.368	0.737	1.29	0.907	0.444	1.77	12.439477
	0.0822	0.231	0.847	0.639	0	0.0796	0.125	0.0848	0.132	0.747	2.06	0.974	0.0922	0	0.0874	0.196	0.142	1.33	0	0	0.507	5.49	13.8462
BUV395	0.896	0	0	0	0.861	0	0	0	0	0	0	0.624	0	1.39	0	0	0	0.709	0	0	1.5	0	5.98
BUV563	0.375	1.33	2.55	0	0	2.01	0	1.26	0.853	2.32	1.29	0.602	0.492	2.66	1.39	0.739	0.53	0.302	22.3	11.7	3.23	1.2	57.133
BUV610	0	2.22	3	1.15	0.442	1.34	0	0	0.781	3.34	1.97	0.517	4.11E–03	1.27	1.4	1.03	1.01	0.63	8.39	18.8	5.12	2.43	54.84411
BUV661	0	1.66	12.9	6.44	3.07	0.953	0	0.535	0	7.07	3.77	0.627	0.565	0.533	0.627	1.9	0.979	1.11	0	1.91	5.4	2.68	52.729
BUV737	0	0.519	0	1.72	1.22	0.182	0	0.194	0	0	2.17	0.347	0	0.242	0	0	0.337	0.605	1.97	1.07	0.649	0.816	12.041
BUV805	0.237	0	0.513	0	1.07	0.967	0	0.165	0	0.641	0	0.381	0	0.294	0.165	0.175	0	0.549	0.0998	0	0	0.849	6.1058
BV421 BV510	0	4.24E–03	0.738	0	0	0.123	0	0	0	0.576	0.19	0	0.632	0.182	0.214	0.157	0.132	0.118	0.264	0	7.97E–03	0.175	3.51321
BV570	0.207	0.235	0	5.15E–03	0.193	0.13	0.153	0.148	0.224	0	0	0.563	0	1.39	0.952	0.627	0.284	0.313	1.51	0.865	0	0.176	7.97515
BV605	0.205	0.749	1.27	0.534	0	0	0.223	0.485	0	1.37	0.416	1.48	0.386	0	2.76	2.03	0.695	0.761	7.75	4.02	1.59	0.794	27.518
BV650	0	0.927	2.23	0.449	0.466	3.11E–03	0	0.81	0.283	2.04	0.971	1.35	0.396	2.61	0	3.22	1.27	1.42	4.74	5.48	2.42	1.36	32.44511
BV711	0	0.889	0	1.38	0	0	1.15	0	1.18	3.71	1.28	1.36	1.15	1.64	1.12	0	1.5	1.65	0	0	0	1.57	19.579
BV785	0.839	1.61	1.27	3.72	1.86	0.784	1.1	0.584	0.638	3.77	3.15	2.54	0.914	1.32	0.62	0.655	0	3.59	0	3.28	0	1.85	34.094
	0	0.389	1.05	0.608	0.809	0.316	0	0.349	0	1.94	2.47	3.22	0.641	0	0.349	0.544	0.567	0	0	2.03	0.834	0.62	16.736
PE Pe–Tx	0.144	0.505	0.688	0.129	0	0.0902	0	0.153	0.161	0.505	0.18	0.338	0.113	1.44	0.81	0.465	0.239	0.225	0	3.32	1.16	0.382	11.0472
Pe–Cy5	0	1.09	0.552	0.455	0.124	1.01E–03	0	0.254	0.122	0.513	0.259	0.249	0.0573	0.511	0.736	0.597	0.531	0.282	3.4	0	2.06	1.08	12.87331
Pe–Cy7	0.0981	2.05	2.58	1.68	0.695	0.0638	0	0.101	0.0805	0.885	0.409	0.305	0.0746	0.158	0.151	0.681	1.07	0.446	1.52	0.683	0	2.07	15.801
	0.207	0.346	0.444	0.257	0.559	0.187	0.306	0	0	0.721	0.874	0.629	0.225	0	0	0.225	0	0.865	0	1.25	0.489	0	7.584
total SE collected	3.6693	16.94324	34.709	26.12615	16.749	7.63792	3.2735	5.479287	4.9975	36.306	24.443	18.627	6.74621	16.09099	12.02432	15.373	12.354	18.475	55.4148	58.336	32.99097	29.938	

Columns are to be interpreted as the detectors that are receiving spreading error. The value of the spreading error is relative and additive, i.e. a detector that is receiving spreading error from several fluorochromes is overall showing a higher loss in resolution. Examples as to how the SSM can be utilized during panel design are described in "experimental workflow".

contribution of spreading error from a single fluorochrome across all detectors by calculating the row sums. An example of a SSM and how to interpret it is shown in Table 95 and described in "*Experimental workflow*."

In many applications, researchers aim to target as many markers of interest on the same cell type as possible. Hence, for these applications, the antigen expression levels play an important role and need to be assessed beforehand—either experimentally or by utilizing published work. Useful resources in this context are optimized multicolor immunophenotyping panels (OMIPs) (See Chapter VIII, Section 3 Analysis presentation and publication (MIFlowCyt)), which usually show raw data of every Ab in their supplementary material [1943]. Using the information of antigen density, low-expression antigens should be detected in channels receiving little spreading error and fluorochromes generating large spreading error can be used for their detection, as this will decrease the relative spreading error (which is proportional to signal intensity). In turn, highly expressed antigens should be paired with fluorochromes generating little spreading error. Alternatively, one can assign highly expressed targets to detectors that receive a lot of spreading error, as a bright signal will typically still remain above the spreading error. A step-by-step approach for this process is outlined in the section *"Experimental workflow"* below.

In order to draw accurate conclusion and to avoid interpreting artifacts that result from spreading error, validation of Ab combinations and using the right controls is mandatory. In most cases, and especially for markers with unknown Ag expression levels FMO controls are required as they can help to identify gating boundaries, especially in detectors with spreading error [2084] (See Chapter III 1.2 Fluorescence spreading into the channel of interest: Fluorescence minus one controls before you start controls). However, it is important to note that FMO controls cannot account for unspecific binding of the Ab that it controlled for, which can cause a shift of the entire negative population in the fully stained sample that is absent in the FMO control. In this case, either a biological control is required, or one can use another cell type in the same experimental sample as a gating control. Isotype controls can serve the function to identify staining issues, especially when secondary Abs are used. Unstained controls have historically often been used to give information about the background autofluorescence of the measured cells, but these controls are of little use in most complex polychromatic experiments.

Finally, high-dimensional cytometry data can only partially be analyzed by traditional manual gating, but rather requires computational data analysis approaches. Prior to this, appropriate quality control and preprocessing of the data is mandatory, as specified below. For details on computational analysis techniques, we refer the reader to several recent reviews [1794, 1838, 1983] and to the corresponding section of the guidelines (see Chapter VII).

5.4 *Applications*

Multidimensional FCM with up to 30 parameters enables a deeper phenotyping and characterization of the immune system, which is required as cellular subsets require more and more mark-

ers for accurate definition [2085]. Besides basic research, clinical research can especially benefit from this analysis as a high amount of information can be extracted from limited, and thus precious, sample sources. Especially for longitudinal high-content immunomonitoring of big patient cohorts, multidimensional FCM serves a fast and highly sensitive tool to correlate responses and observe changes of treatment as the basis to predict outcome of the myriads of immunotherapeutic approaches to treat diseases. The computational approaches allow for interrogating large data sets generated in these types of studies and enable the unbiased analysis of the data, possibly leading to the detection of rare cell types and can be of predictive value for treatment outcome.

5.5 *Experimental workflow*

Here, we describe the key steps that should be taken for a systematic panel design approach.

1. Define the experimental hypothesis and the relevant cellular populations (e.g., $CD8^+$ T cells)
2. Make a list of lineage markers that are necessary for consistent identification of the populations of interest (e.g., CD3/CD8 and CD45 for $CD8^+$ T cells).
3. List all target markers of interest and categorize expected expression patterns and (if known) antigen density into low, medium, and high.
4. Generate an SSM on your instrument by running single-stained controls with all desired fluorochromes and calculating the SSM in FlowJo or another suitable analysis program.
5. Look for the three highest values in the SSM and assign the corresponding fluorochromes to mutually exclusive antigen targets, i.e., targets not expressed on the same cell (in our example SSM in Table 95 the most problematic pair would be BUV563 spread into the YG-586 PE detector).
6. Calculate the row sums in the SSM. The fluorophores with the lowest row sum overall contribute the least spreading error to your experiment—these should be assigned to your lineage markers, e.g., CD3 and CD8 for a CD8 T cell-centric analysis (in our example SSM in Table 95 this would be BV421 and BUV395).
7. Calculate the column sums in the SSM. The detectors with the lowest column sums receive the least amount of spreading error—these detectors are suitable for dim or unknown target markers (in our example SSM in Table 95 good examples would be the B-515 and V-510 detectors). Utilize bright fluorochromes for these antigens, if possible. The detectors with the highest column sums receive more spreading error—for these detectors perform preliminary experiments to assign target markers that deliver a bright enough signal to be above the spread (in our example SSM in Table 95 this would be YG-586 and YG-610 detectors). However, one has to keep in mind that there might be a single contribution that drives the total spreading error in a detector, and if not used on the target cell, this can improve the total spreading error received (e.g., in our example SSM in Table 95 the contribution of BUV661 and BUV563 to the YG-586 detector).
8. Run a test experiment including all relevant FMO controls. Perform data analysis and quality control as outlined in the next section.

5.6 *Data analysis*

For general concepts of computational analysis of high-dimensional single-cell data, we refer the reader to Chapter VII "Data handling, evaluation, storage and repositories" High dimensional FCM of the guidelines. Within this section, we focus primarily on quality control aspects prior to data analysis.

Most technical artifacts occur when samples are acquired over multiple days (i.e., batch effect), however, sometimes they also happen within one experiment due to the lack of appropriate controls or inconsistencies in instrument handling. In the authors experience, a common cause of artifacts in fluorescent cytometry is incorrect compensation, which in turn is mostly due to poorly prepared single-stained controls. To pinpoint such mistakes, visual inspection of N×N views of the final data should be performed, with N being the number of fluorescent parameters acquired, i.e., every marker against every marker. Within these plots, one should screen the data for typical erroneous patterns such as "leaning" triangular populations and "super-negative" events. Examples patterns are given in Fig. 231E and F.

Sometimes fluorescent signals vary across different experimental days or even within one experiment even though the same staining panel was applied. Correct data transformation can help to diminish this effect [2086]. Different transformation approaches such as the biexponential, arcsinh, and hyperlog display can be used, and the optimal transformation depends on the specific data and cannot always be computationally predicted [1808].

Dead cells, doublets or staining artifacts, e.g., by Ab aggregates, can appear as false positive data points or outliers in the analysis, potentially leading to wrong interpretation of the data. Thus, it is important to exclude these prior to unsupervised computational analysis by appropriate pregating or "data cleaning." Depending on the immunological question asked a pregating on the population of interest can be part of the preprocessing and may speed up the computational procedure of the analysis (e.g., per-gating and exporting of live singlet $CD45^+$ $CD3^+$ cells). Even though conventional manual gating may not be suitable to capture all the correlations between the up to 28 fluorescent parameters, it still serves as an important quality check before, during and after the computational data analysis.

5.7 *Advantages*

Thorough panel design, not only for multiparametric FCM panels, will award the researcher with robust and reproducible FCM data with a satisfying resolution also of dimly expressed markers. Even

though the optimization of a panel may appear time consuming and requires various controls to assure reliable interpretation, it will save time in the downstream analysis and interpretation of the generated data. Usage and correct interpretation of an SSM will improve the process tremendously. It may not be obvious at first, but cost will be reduced, as the unnecessary repetition of experiments due to non-interpretable data will be minimized.

5.8 *Pitfalls*

Pitfalls in high-dimensional fluorescent cytometry often arise from inappropriate planning of experiments and lack of controls. This can be avoided by systematic panel design and the inclusion of FMO controls as described above. Also, an inherent disadvantage is the necessity to obtain single-cell suspensions, which disrupts the natural architecture and interaction of cells in situ. Several emerging techniques allow high-dimensional cytometric measurements directly within tissues, as has been shown by Histocytometry [2087] or the recent commercial release of an imaging CyTOF system (Hyperion, Fluidigm) [1883].

5.9 *Top tricks*

1. It is important that the detector voltages of the used flow cytometer have been optimized using an appropriate technique. The most widely accepted approach for this is a voltage titration [48], which will determine the minimally acceptable voltage yielding optimal resolution for each detector. Voltages should not be adjusted solely for the purpose of lowering compensation values [2088].
2. To deal with spreading error beyond the above-mentioned approaches, one can utilize the fact that spreading error is directly proportional to the signal intensity. If assigning a fluorochrome to a lineage marker showing high and bimodal expression (e.g., CD8), one can utilize lower Ab titers (below saturating concentration) to lower the positive signal and in turn the spreading error generated. However, it is important to note that this approach requires consistent staining conditions in terms of cell numbers, staining temperature, and staining duration.
3. Many recent fluorochromes are based on organic polymers, which can under certain conditions show interaction due to their chemical properties. To alleviate this issue some manufacturers have released commercial buffers that are designed to minimize these unspecific interactions, and thus it is strongly encouraged to use these buffers whenever more than one polymer-based dye (e.g., all Brilliant Violet and Brilliant Ultra Violet dyes, SuperBright dyes, etc.) is included in a staining.
4. When performing experiments with staining and acquisition over several days, it is recommended to follow best practices for consistent setup of the used instrumentry [48] and to include a reference sample on every experimental day in order to detect irregularities in staining, compensation or transformation. These control samples can then be overlayed in histograms of all markers to visually control for the aforementioned errors. Should artifacts occur in the control samples, it might be useful to either exclude specific parameters or samples from the computational analysis.

6 Single cell genomics and cytometry

6.1 *Overview*

Cells for single-cell genomics are in almost all cases collected using FCM. FCM can be used to isolate cells of interest from more complex biological samples, to perform index sorting upstream of single-cell genomics workflows or to provide fluorescence intensity measurements from single cells, that can be merged into single-cell gene expression matrices as an additional layer of information. Here, we provide an overview on how FCM complements single-cell genomics technologies, together with a basic overview on currently available technologies.

6.2 *Introduction*

Single-cell technologies provide an unprecedented view on the complexity of biological systems, by uncovering how organisms are build up from single cells and how these cells are different. Classical bulk analysis tools analyze cell populations and consequently, a whole layer of biological processes stays invisible, like, for example, the presence of rare cell-types in tissues or gene-expression heterogeneity that can depend on highly time-resolved gene-expression bursts. Single-cell technologies depend on the separation of cells from tissues or cell culture and their sorting into separate reaction volumes, eventually containing a single cell per reaction. Then, DNA- or RNA-sequencing technologies are applied, specialized on low-input material. This allows to characterize the genome, epigenome, or transcriptome of each cell. Bioinformatic analysis, that takes into account the technical noise of sparse input material data, is used to extract biologically meaningful processes.

Although single-cell technologies can be technically challenging, advances in sample and library preparation methods have made single-cell analysis broadly available (Fig. 232):

1. **FCM-based multiwell plate methods**: Here, cells are sorted into multiwell plates and allow optional indexing of the sorted cells. Then, sequencing libraries are prepared from wells, most frequently using SMART-seq2 [2089]. Optionally, library preparation can be done using robotics, which increases throughput and at the same time, decreases batch effects [2090].
2. **Microfluidics- and nanowell-based methods** significantly increase throughput and decrease pipetting effort of single-cell transcriptomics. DropSeq [2091] and InDrop [2092] are frequently used and based on microfluidic chips that combine barcoded beads and cells within droplets. Especially

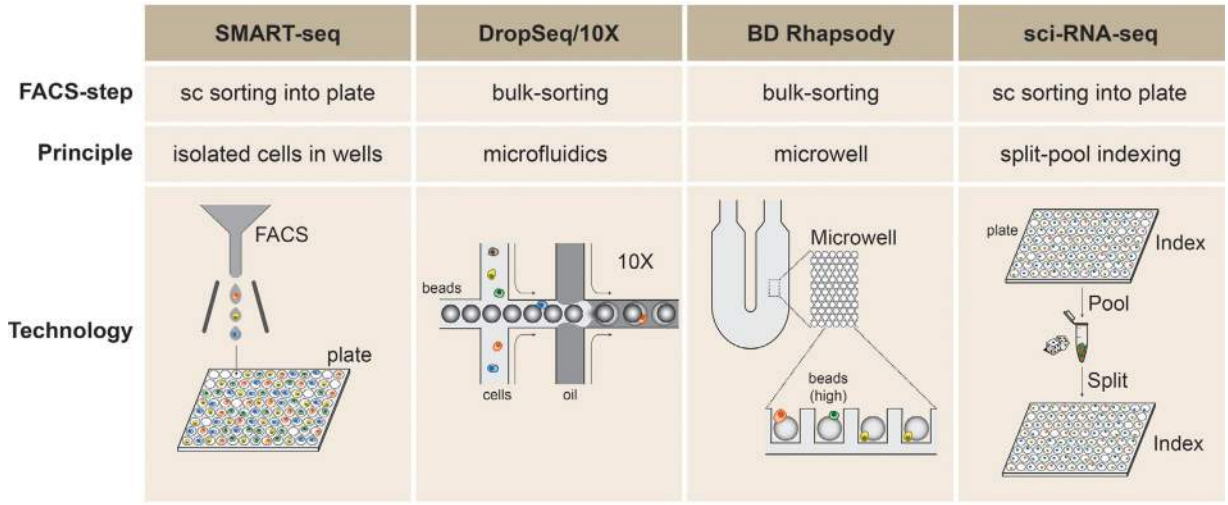

Figure 232. Examples of frequently used single-cell transcriptomics platforms. Comparison of different technologies for single-cell RNAseq, including SMART-seqs, DropSeq, 10× Chromium, BD Rhapsody and sci-RNA-seq. Basic differences are explained in the main text. Here, we only provide a collection of single-cell RNAseq methods to cover the key principles of the different technologies.

the invention of commercially available systems from 10× Genomics, Dolomite Bio, and 1Cell Bio, made these technologies broadly available. Nanowell-based systems process thousands of cells in a single step by depositing barcoded beads and cells into nanowells on a printed chip [2090, 2093]. These systems are commercially available, e. g., from BD Biosciences (Rhapsody), Fluidigm (C1), or Clontech (ICell8). Compared to microfluidics-based methods, nanowell systems have lower throughput, however, improved control over the deposition of beads and cells into wells using microscopy.

3. **FCM-based single-cell combinatorial indexing** uses a multistep barcoding strategy to increase throughput of single-cell RNAseq without the need to set up microfluidics and nanowell systems. Cells or nuclei are sorted into wells of a multiwell plate, indexed with a primary barcode, pooled, and sorted again into wells, followed by a secondary barcoding step. Consequently, each cell receives a unique combination of barcodes, enabling RNA-molecules to be assigned to individual cells [2094].

6.3 *Obtaining single cells for single-cell applications*

We will focus here on the application of FCM in combination with different single-cell transcriptomics technologies. FCM upstream of single-cell RNAseq library preparation allows to enrich for singlet cells (essential for any single-cell method) and if needed, to enrich for subpopulations of interest. These subpopulations may be viable cells, non-apoptotic cells, cells in a specific cell cycle phase, or cells expressing a sortable marker to enrich for specific or rare cell types.

1. True, viable, and non-apoptotic cells can be isolated using FCM. FCM markers and dyes are available, including Caspase 3/7 or AnnexinV for apoptosis and nonpermeable nucleic acid dyes for cell membrane permeability assessment or DNA staining. Cell separation from tissues or cell culture results in imperfect single-cell separation and enables efficient identification and isolation of singlets on an FSC/SSC plot. For such complex samples, including organ biopsies or whole embryos, it is possible to identify cells using a cell permeable DNA dye such as Hoechst 33342 or DRAQ5 [2095, 2096]. Figure 233 shows a DRAQ5 and singlet gating on *Drosophila* larvae neuronal stem cells, containing small cells that overlay with cellular debris and yolk particles.
In addition to nonviable cells, pro-apoptotic and apoptotic cells can be highly abundant in tissue preparations, but can be removed using FCM. Such stainings can be done using AnnexinV or Caspase3/7 [2097, 2098] (See Chapter V Biological assays Section 7 Measuring cell death mechanisms). Figure 234 shows example apoptosis staining in bone marrow and brain tissue preparations. The staining of pro-apoptotic cells is especially important, since these cells are difficult or impossible to distinguish from live cells computationally. Apoptosis is a biochemical process that can be initiated without prior changes in gene-expression that can be identified on transcriptome level (EMBL Genomics Core and Flow Cytometry Facility, unpublished data). There is no objection to combine the apoptosis staining with the viability stain on the same colour when the panel is tight (see Chapter V Section 7 for details). Importantly, we do not observe any influence of Hoechst, DAPI, or DRAQ5 stains on library preparation for RNAseq and single-cell transcriptome data quality.
2. Singlet gating is key to ensure that only single cells are analyzed, as multiple cells are difficult to filter out during bioinformatics analysis. The combination of sequential FSC and SSC height versus area pulse-shape analysis are reliable single cell gates [2099]. However, pulse-shape analysis-based singlet gates can become challenging when working with tissue material composed of diverse cell types (e.g., bone marrow, lung,

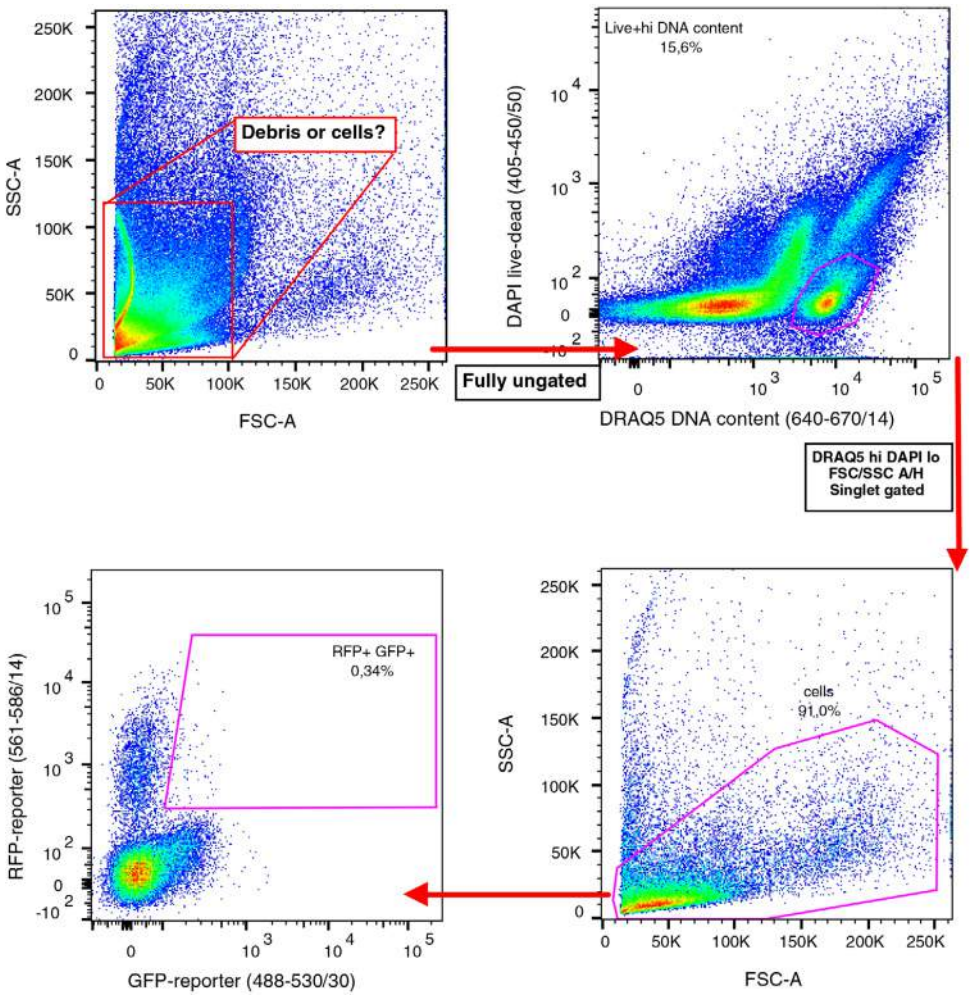

Figure 233. Cleaning up the scatter with a DNA stain resolves the masking of yolk and debris. Drosophila melanogaster larvae preparations were stained with 2μM/mL DRAQ5 to identify DNA containing particles from debris. Clear gates for fluorescence-reporter expressing cells can be drawn.

intestine, skin). In these cases, the scatter-based singlet gates (area vs. height) appear slightly spread and are often not efficient in isolating single cells. This scatter heterogeneity results from different optical densities, cell sizes, and shapes. To circumvent such limitations, the cell suspension can be stained with a cell permeable DNA dye (e.g., DRAQ5 or DAPI) and the signal is used for singlet gating (see Chapter V Biological assays Section 6 DNA synthesis, cell cycle, and proliferation). This method is independent of the scattering activity of cells, since DNA content is always the same. Implementing this strategy also allows to limit analysis to certain cell cycle phases, an often unwanted source of cellular heterogeneity important to consider during data analysis.

3. Gated cells should be of high purity and have a high chance to end up either in a microtiter-well or in the bulk sort tube for microfluidics/nanowell-based methods. Efficiency and purity of sorting depend on the sorting mode; therefore, it is important to select the best mode for the respective single-cell library preparation method. For microfluidics/nanowell-based methods, bulk sorts are done, based on sort modes ensuring purity of the sorted cells and fast sorting. Purity modes, however, suffer of reduced probability that the gated cell is actually sorted, because the mode does not take into account the actual position of the cell within the interrogated drop: If a cell is close to the edge of the interrogated drop, it can move into the neighboring drop during its travel time between detection and the actual drop charging (Fig. 235). Generally, purity modes that are run at an optimal sampling speed have an efficiency of 80 to 90%, i.e., the number of cells within the bulk sort tube will be only 80 to 90% of the assumed cell number [2100]. It is therefore important to count cells again after sorting and if necessary, to concentrate cells again. Injection of cells at defined concentration into microfluidics/nanowell-based devices is key to prevent doublet formation (too high cell density) or an unnecessary high number of empty droplets (too low cell density).
For microtiter-plate based methods, cells are sorted directly into the wells of a plate using a single-cell sorting mode. In most instruments, such modes implement a positional limitation for the cell to be in the center third of the drop, on top of the purity mask (Fig. 235). BD Aria systems use the phase mask scanning

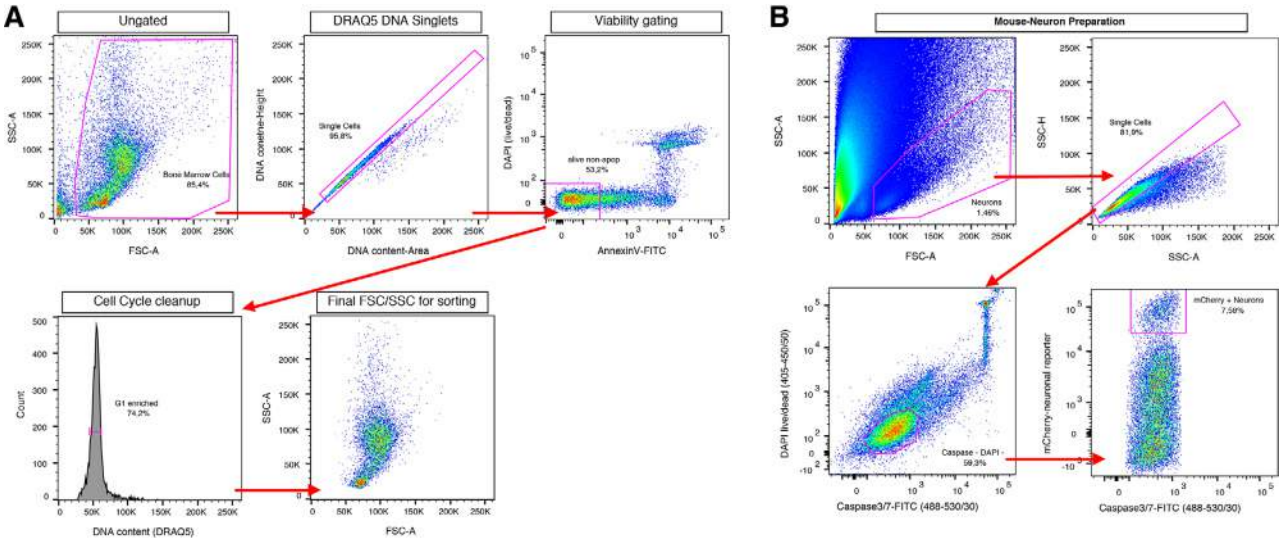

Figure 234. Advantage of combined apoptosis and viability stains upstream of single-cell RNAseq methods. (A) Scatterplots showing DRAQ5 staining (for singlet gating and cell cycle restriction) in combination with AnnexinV (apoptosis staining). Cells show a low frequency of dead cells when assessing cell death purely by staining membrane-permeability. However, adding AnnexinV or Capase3/7 probes reveals that the viability of the samples is rather mixed as many cells have started to become apoptotic. (B) High amount of pro- and late-apoptotic cells in dissected mouse brain tissue. In both cases, a significant number of non-perfectly viable cells would have been sorted for downstream sequencing if only simple live-dead staining with DNA-dyes was utilized.

the inside of the interrogated drop: If a cell falls within the phase mask, the drop will not be sorted due to a high risk of the cell moving into the leading or lagging drop (Fig. 235 and http://www.bdbiosciences.com/ds/is/others/23-6579.pdf). This results in a high probability of cells being sorted into the tube/well, but at the cost of a high number of aborted cell sorts due to phase mask violation (on average >50%) when using manufacturer's settings. Therefore, large bulk sorts are not operated using single-cell mode.

In addition to the sorting mode, the performance of sorters strongly depends on a perfect flow of the cells along the stream, which depends for example on sample properties including cell shape. One way to evaluate the machine derived drop delay for new or difficult to handle cell types is an easy to set up single-cell qPCR test, that is described in the Tips & Tricks section.

4. Both microfluidics-based (e.g., 10× Genomics) and nanowell-based (e.g., BD Rhapsody) single-cell transcriptomics solu-

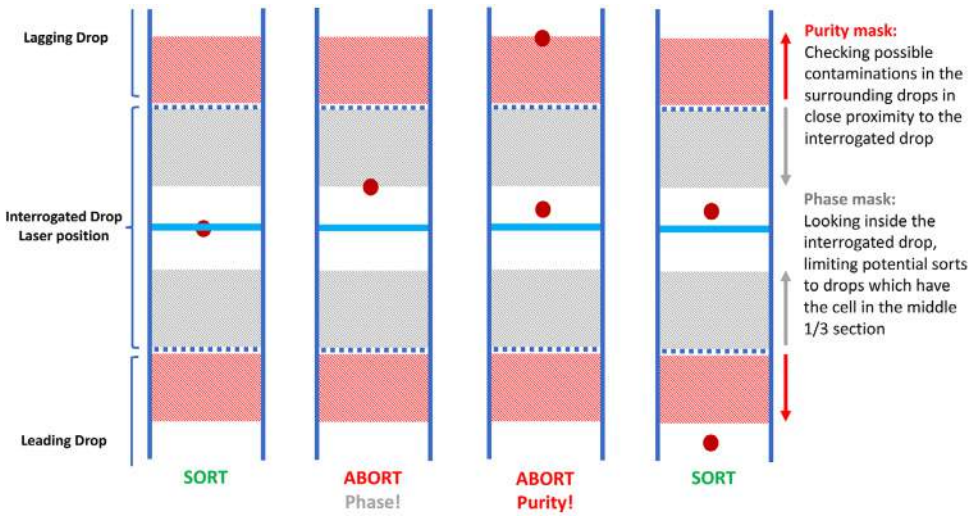

Figure 235. Technical details of different single-cell isolation modes. The single-cell mode in DiVa and FACSChorus includes a purity mask scanning the leading and lagging drop for contaminations plus a phase mask that scans the ends of the interrogated drop for the position of the cell of interest. Any violation of the purity or phase mask will lead to the termination of the drop. This results in a general loss of >50% of potential target cells—however, the mode has the highest precision for the cell to be delivered with the prospective drop while ensuring the purity and that only one cell is deposited.

tions use cell suspensions as input material that should fulfill the following requirements: (i) Cell viability must be high, ideally above 90%, as measured with a dye exclusion assay, e.g., Trypan blue (visual counting) or DAPI/Draq7 (FCM). Cell death inside the single-cell suspension and prior to droplet-generation results in ambient RNA that will be present in every droplet, reducing data quality. (ii) Only singlet cells should be present, as multiplets are packaged into droplets or wells at similar efficiency as singlet cells. (iii) Measurement of cell density should be exact and done directly before loading cells into the device. Loading too many cells results in a high multiplet rate, loading too less cells results in an unnecessary high number of empty droplets/wells and consequently, increases costs per cell. For 10× genomics, ideal cell density is between 600 and 1500 cells/μL. (iv) Cells should be suspended in a buffer like PBS or PBS + 0.04% (w/v) BSA and stored at 4°C until loading. Buffers that include residual RNase or DNase from upstream cell preparation should be replaced. Other buffers have been validated for different single-cell protocols (see respective manufacturers protocols), as for example DMEM + 10% FCS. Cell viability must be stable under these conditions, which can be tested in advance by prolonged incubation in the buffer and dye exclusion test before and after incubation. As cells settle fast, they should be mixed prior to loading. This can be done by pipetting or vortexing, depending on the cell type requirements. In case of longer runs, as often necessary when running DropSeq and other custom-built setups, cells can be constantly mixed using a magnetic mixer, preventing changes in injected cell concentration over time.

Of note, some cell types are more difficult to capture using microfluidics/microwell-based single-cell methods than others [2090, 2101]. Especially when working with complex tissues, this can result in underrepresentation of specific cell types and consequently, wrong conclusions regarding tissue biology. This is especially true using microfluidics- and nanowell-based methods, since it is not possible to see which types of cells are less efficiently packed into the reaction volumes. Here, it can make sense to do plate-based single-cell libraries using SMARTseq2.

6.4 *Applications*

Single-cell transcriptomics

Single cell transcriptome sequencing measures the expression level of polyadenylated transcripts within single cells. Furthermore, data contains transcript sequence information that can be used for structural variant analysis or the identification of splice-variants. Depending on the protocol and technology used, either whole transcripts or transcript 5' or 3'-ends are sequenced, with 3'-RNAseq being the most widely used technology for gene expression analysis.

Other single-cell omics technologies

Transcriptomes are highly informative, but alternative readouts reveal different views on cell-to-cell differences. These technologies include whole or targeted genome sequencing and epigenomics, for which both commercial and non-commercial platforms are available. Furthermore, proteomics and metabolomics are entering the single-cell field. Single-cell multiomics, i.e., the simultaneous analysis of two or more omics (e.g., genome and transcriptome) in the same cell, will become less technically challenging. Analyzing phenotypes on top of these -omics technologies, for example, by imaging-based FCM (see Chapter VIII Section 1 Imaging FCM) will become available in the future. Currently, these technologies suffer of low image quality, function at comparatively low throughput and depend on technically challenging setups that are not widely applicable.

CRISPR-screening technologies

CRISPR/Cas9 technologies can be combined with FCM and single-cell technologies, providing a powerful tool for large-scale functional genomics. CRISPR/Cas9-sgRNA libraries are applied to cells under conditions in which one cell expresses one sgRNA along with Cas9. The functional consequence of such a perturbation is then analyzed using simple or complex readouts: Simple readouts rely on FCM, e.g., by analysis of a fluorescent reporter or a proliferation dye. Then, sgRNA enrichment analysis within the binned and sorted populations is done by extracting genomic DNA and sequencing of the integrated sgRNA sequences. This allows conclusions on the influence of each sgRNA in the library on the respective phenotype. Even simpler, positive or negative selection screens analyze sgRNA enrichment after 1–3 weeks of growth with sgRNAs being either enriched or depleted depending on the function of the targeted gene. Complex readouts can be generated by coupling CRISPR/Cas9 with single-cell transcriptome readouts (CROP-Seq and similar methods). Here, the sgRNA sequence or a coupled barcode is sequenced along with the transcriptome, allowing to compute transcriptomic changes upon each perturbation in intermediate to high throughput.

6.5 *Data analysis*

Single-cell RNA sequencing (scRNA seq) development opened in the last couple of years new approaches to answer important questions in developmental biology [2102], cancer [2103], and neural network analysis [2104].

Detection and quantification of gene expression at single-cell level encompasses many challenges regarding data analysis. As an example, the very low starting material from a single-cell can lead to dropout genes in some cells and not in others. The stochastic nature of gene expression might imply an important cell-to-cell biological variability in single cell measurements although the specific cell is currently in a different expression cycle. These confounding factors, including variable detection sensitivity, batch effects, and transcriptional noise, complicate the analysis and interpretation of scRNA sequencing datasets.

Before using sequencing reads to extract valuable biological information, crucial considerations need to be put into the design of the experiment to lower at its minimum the impact of confounding elements and technical artifacts. These aspects have been discussed in detail in refs. [2090, 2105].

Analysis tools for bulk RNAseq have been first used and adapted to address the specific properties of scRNAseq data [1869, 2105]. Normalization is an essential first process in the global analysis workflow for scRNAseq due to high data variability and noise. The aim is to correct the biases introduced by gene expression dropouts, amplification, low library heterogeneity or batch effects (e.g., different platforms, time points, technical handling, reagent lots, etc.). External synthetic spike-in controls help to disentangle the technical noise from natural biological variability [2106]. Adaptation of formerly developed methods for bulk RNA sequencing could also be used [2107–2109]. More recent approaches are normalizing the data between sample [2110] or cell-based factors derived from the deconvolution of pool-based size factors [2111]. The popular R package Seurat integrates a comprehensive workflow from the quality assessment of each cell to analyze, exploring scRNA-seq data as well as integrating different datasets [2112].

The transcriptional landscape of a single cell can be compared based on co-expressed genes. Here, cells are grouped into clusters and marker genes, which are driving the expression signature of sub-clusters, are identified and annotated. Before the identification of cell clusters, visual exploration is usually achieved by dimensional reduction, where the dataset is projected to only a couple of dimensional spaces. Among these approaches, principal component analysis (PCA) [2113], t-SNE [2114], or UMAP [2115] are frequently used. Different clustering approaches and tools have been compared using a similarity index, i.e., the adjusted Rand index [144]. Annotation of differentially expressed (DE) genes between clusters allows biological hints on the nature of the subpopulation [145] and provides a comprehensive overview of the available DE methods. Finally, methods aiming to infer the differentiation trajectory of the clusters have been also compared in a comprehensive study [2116].We would also like to mention two interesting resources, listing software packages dedicated to the different scRNAseq applications (https://www.scrna-tools.org/ and https://github.com/seandavi/awesome-single-cell).

6.6 *Top tricks*

A simple single-cell qPCR protocol to test sorting efficiency prior to single-cell sequencing

Since single-cell sequencing can be cost-intensive and not all handling errors during sample preparation can be identified later during data analysis, We therefore provide a protocol allowing to check FCM instrument performance in advance, if using novel or difficult to sort cell types, This protocol was developed by the Stahlberg lab and is currently taught in the EMBO and EMBL single-cell trainings courses on single cell omics technologies [1905, 2117].

Testing whether the sort-stream hits the center of test tubes and microtiter plates is straight-forward. However, it is more difficult to validate if the drop-delay (as most frequently assessed with fluorescent beads) works with novel cell types or cells that show difficult behavior within the stream: Some cells, especially larger and more structured cells, have the tendency to tumble in the stream, slowing them slightly down due to potential drag. This could lead to a reduced number of positively seeded wells or to reduced cell numbers in a bulk sort. Sorting single cells into a multiwell-plate followed by qPCR of a highly expressed gene will give a precise measurement of sorting efficacy.

Protocol

Materials required:

- Human GAPDH primers:

  GAPDHv2_Fwd CCCACTCCTCCACCTTTGAC
  GAPDHv2_Rev GCCAAATTCGTTGTCATACCAGG

- BioRAD Hard-Shell® 96-Well PCR Plates, low profile, thin wall, skirted, red/clear #hsp9611
- TATAA SYBR® GrandMaster® Mix ROX - TA01R
- TATAA GrandScript cDNA Synthesis Kit - A103c (1000 rxn) A103b (200 rxn)
- CelluLyser™ Micro lysis buffer - H104
- RNAse and nucleotide free water

Procedure:

Cell sorting into plates

In addition to standard FCM calibration, the instrument needs to be calibrated to deposit cells in the center of each collection tube. This can be tested by sorting 10–20 beads/cells on plastic film covering the plate or by checking drop formation on the bottom of a hard-skirted BioRAD PCR plate (Fig. 236). In case of non-optically tracked arms, we suggest to check the calibration every second plate, because the sorting arm may be displaced over time. A too small volume of provided buffer (here: lysis buffer) increases the risk of a cell not reaching the buffer but sticking to the tube wall, while too large volumes might not work with downstream applications. We recommend sorting two wells with each ten cells (positive control), to include at least two wells that will intentionally not receive a cell (negative control) and the rest of wells with single cells.

PCR plates (96-well) with lysis buffer should be prepared in advance: We found that 5 μL of provided Cellulyser weak lysis buffer per well works well. Immediately after sorting into the plates, place the plate on carbon ice, and store at –80°C until proceeding with reverse transcription.

Reverse transcription

We have good experience with TATAA GrandScript cDNA synthesis Kit using a mix of oligo-dT and random hexamers. We generally use the following reverse transcription protocol (added directly to the frozen cells, per well): 2 μL 5× TATAA GrandScript RT reaction mix, 0.5 μL TATAA GrandScript RT enzyme, and 2.5 μL nuclease-free water (according to the manufacturer's instructions). The total volume per well is 10 μL. Reverse transcription is done using the following temperature profile: 22°C for 5 min, 42°C for 30 min, and 85°C for 5 min.

Quatitative PCR

GAPDH is highly and ubiquitously expressed and can be used to detect the presence of a single cells using qPCR amplification irrespective of the cell type. Normal qPCR-MIQE guidelines apply

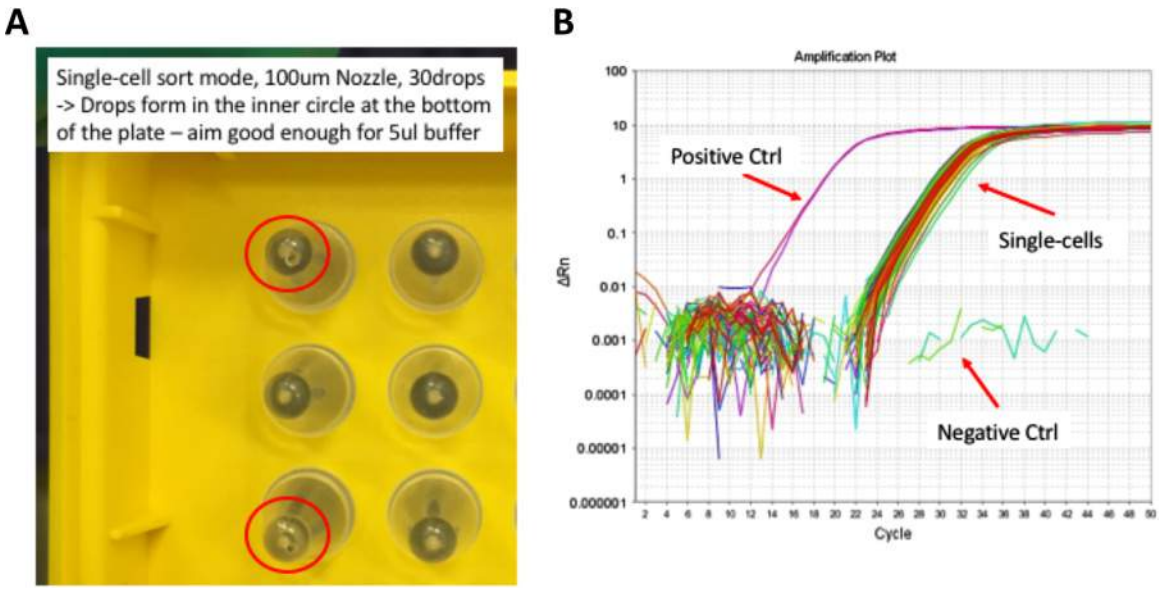

Figure 236. (A) Transparent hard-shell PCR plates can be used to check the correct deposition of sorted drops into 96-well PCR plates; controlling the aim at the bottom of the well is superior to only checking on a seal or lid above. (B) An example outcome of the single-cell qPCR protocol checking single-cell deposition of HeLa cells with GAPDH qPCR. Positive controls (ctrl) contained 10 cells per well, negative controls were empty wells. All single cells show formation of a specific PCR-product, indicating that all wells with expected single cells contained a single cell.

to the described qPCR assay For using a high number of amplification cycles due to low input material, consequently we suggest to check melt curves for byproducts and primer-dimers after PCR.

Dilute cDNA samples to a final volume of 30 µL with H_2O. Prepare qPCR reactions for a total volume of 10 µL per well: 5 µL qPCR 2×Mix, 0.4 µL 10 µM fwd/ref primer mix, 2.1 µl H_2O, 2.5 µL cDNA. A mastermix of qPCR 2×Mix, fwd/rev primer, and H_2O should be prepared. qPCR is run using SYBR Green ROX protocol for 50 cycles followed by melt curve: 30 s 95°C, 50× (5 s 95°C, 20 s 60°C, 20 sec 70°C), 65 °C to 95 °C with 0.5°C increment. Exemplary results are shown in Fig. 236.

7 Microbial cells

7.1 *Overview*

Recent insights into the impact of the microbiota for the environment and for human health has led to an explosion of research efforts to try to understand the role and mechanisms of bacteria, bacterial communities, and their products in regulating homeostasis and pathology. With the advent of high-throughput sequencing technologies, 16S rRNA gene amplicon sequencing and metagenomic approaches are widely applied to resolve the community structure while proteomic approaches are used to reveal functional relationships. However, these methods are still expensive, time consuming, and have high requirements for data analysis. FCM offers a fast and inexpensive alternative for the single-cell based characterization and analysis of microbial communities. Yet, flow cytometric measurement of microbial cells is still challenging and several issues that have to be considered will be discussed in this section. If done correctly, FCM of bacteria can surpass simple applications such as counting cells or determining live/dead cell states [2118].

7.2 *Introduction*

Complex microbial communities occur almost everywhere, from natural environments such as fresh water systems, marine environments and soil, to managed systems such as drinking water facilities or wastewater treatment plants, to the gut or skin of humans and animals. Recent research efforts have highlighted the importance of microbial communities, not only in the environment, where they are responsible for all biogeochemical processes, but also as integral part of multicellular organisms. As bacterial microbiota, they colonize all body surfaces and have been shown to educate the immune system but also play a crucial role in inflammatory diseases such as asthma, inflammatory bowel disease (IBD), and obesity.

Bacteria can vary up to two orders of magnitude in size, but 0.8 to 3 µm are common dimensions. Unlike eukaryotic cells, bacterial cells are not compartmentalized, i.e., they do not have organelles, allowing dyes to move freely in the cytoplasm unless they bind to specific structures such as DNA. This and the small volume of the bacteria can favor interactions of fluorescent dyes leading to loss of fluorescence intensity, making the simultaneous intracellular use of more than one or two dyes challenging. Most bacteria also have a cell wall that prevents the intracellular uptake of almost all larger probes such as Abs. The major challenge but also the major advantage of bacterial cytometry is the inability to grow many bacteria as pure culture. While “culturomics” has led to a large

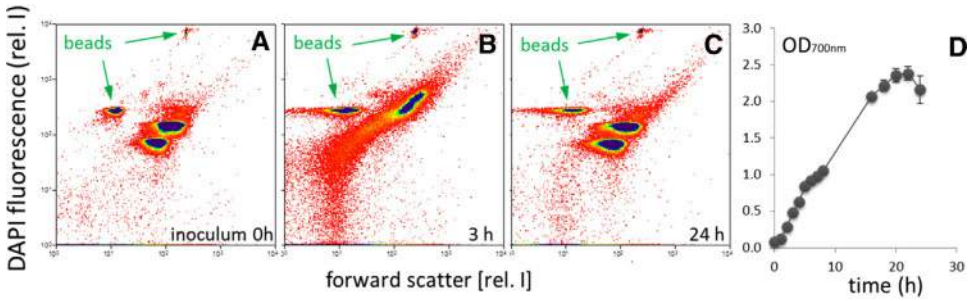

Figure 237. Flow cytometric analysis of cell states in pure cultures of *Escherichia coli* K12 grown on complex DSM 381 medium. Cells were sampled, treated with 2% PFA and fixed in 70% ice-cold ethanol. Following, cells were stained with a 0.24 μM DAPI solution and measured using a 355 nm Genesis CX laser (100 mW, both Coherent, Santa Clara, CA). Scatter was measured using a 488 nm Sapphire OPS laser (400 mW). 0.5 μm and 1 μm Fluoresbrite Microspheres (both Polysciences, 18339 and 17458, Warrington, PA, USA) were added to every sample as internal standards. A and C show nearly identical proliferation patterns during lag and stationary phases of growth. B shows the proliferation pattern (uncoupled DNA synthesis) in the log-phase. The right graph D shows the growth curve where samples were taken from 500 ml batch cultures with 200 ml medium for a time range of 24 hours. After a short lag phase the cells immediately started exponential growth which ended after about 20 hours.

increase in the number of bacteria that can be grown in culture, still many bacteria cannot. Lack of pure strains of bacteria precludes calibration and verification of specific staining. In addition, cells of the same bacterial strain change their physical and physiological properties depending on micro-environmental conditions and growth phase. Bacterial cells tend to be small in unfavorable growth conditions and increase in size during optimal growth conditions. While bacteria typically have one molecule of genomic DNA, some can have multiple copies of the same genomic DNA or have two or three genomic equivalents of different length and composition. The numbers of genomic DNA equivalents are also not evenly distributed among cells of a population as asymmetric cell division and uncoupled DNA synthesis is widespread among bacteria. The number of genomic DNA copies does not indicate the condition of the cell, as the cells often do not divide under stress conditions and retain the high copy number of genomic DNA [2119].

When considering these caveats, some of which can also be used as discriminating parameters, FCM is a well-suited method to study bacteria at the single-cell level. While the diversity of such natural communities can reach up to several thousands of different phylotypes per 1 g of sample, making cell type-specific labeling impossible [2120], approaches such as cytometric fingerprinting of natural microbial communities can be used to analyze community structures, complexity and alterations. New bioinformatics tools for quantitative and automatic evaluation of bacterial cytometric fingerprints are becoming available enabling the identification of subpopulations or sub-communities of interest for subsequent cell sorting and downstream analyses, such as NGS or proteomics approaches [2121, 2122].

7.3 *Applications*

A common application is the discrimination and enumeration of live bacteria using live/dead dyes. Both in biotechnology and in the environment changes in cell numbers can have major implications. Also recently, it has been shown that cell numbers are important for the standardization and normalization of 16S rRNA gene sequencing data [2123]. Flow cytometric applications achieving high resolution of light scatter and DNA content discrimination can be used to characterize and resolve complex microbial community structures, such as environmental microbiota or intestinal microbiota by generating community patterns.

There is a wealth of methods available to analyze states of cells in pure culture [2124]. Such methods are often used to describe segregated cell states of different activity. Besides the measurement of intracellular components also the determination of energy or growth states are in the focus to understand cell behavior. Especially in medicine, the detection of pathogens and their differentiation from other bacteria is desirable. Cell type labeling and cell proliferation can give information on active cell growth. Uncoupled and fast DNA synthesis can easily be visualized by FCM (Fig. 237B) and discriminated easily from non-growing cell states (Fig. 237A and C).

7.4 *Equipment*

Not all flow cytometers are suitable for the measurement of bacteria but we have good experiences with the BD Influx v7 Sorter and MoFlo Legacy cell sorters [2125]. Due to the small size the amount of dyes bacterial cells bind is significantly lower resulting in the generation of low number of photons when excited compared to eukaryotic cells. Thus, high laser power starting at 50 mW and going up to 400 mW lasers, highly sensitive PMTs for signal detection and clear tubes and water streams to provide low background signals are important prerequisites for the measurement of bacteria. Forward (information related to cell size) and side (information on granularity and surface structure) scatter signals of cells are best recorded at lower laser wavelengths (i.e., 350 nm or at least 488 nm). Using machines that lack sensitive scatter detection, using fluorescence of, e.g., nucleic acid stain as trigger signal for acquisition is an option. All solutions should be filtered (0.1 μm) before use. Samples isolated from natural environments may require a sensitive shaking or even an ultrasonic treatment

to dissolve flocs (see below). Samples should be filtered before measurement through a 50 μm mesh to avoid the clogging of the nozzle.

7.5 *Experimental workflow and acquisition*

When measuring viable bacterial cells by FCM, one has to be aware that some bacteria have generation times of only few minutes. Although bacteria are generally easy to handle, their physiological cell states can change from one minute to the next. Therefore, techniques that include fixation tend to be more robust. Several fixation methods have been described [2126]. In short, bacterial cells are incubated for 2% PFA at for 30 min at room temperature to stabilize the cell wall and finally fixed with 70% ice-cold ethanol. As this stage, samples are stable for weeks to month at –20°C. When staining methods are sensitive to PFA pretreatment cells can be stored stably in 20% glycerol at –20°C. Alternatively, samples can be stabilized for storage and shipping at ambient temperatures by infrared supported drying [2125]. However, it is crucial to test the optimal stabilization method for the samples in questions and the downstream application.

Bacterial communities can comprise cells of different sizes and shapes. Thus, classical doublet discrimination using, e.g., width signal versus height signal is not possible. For samples, where clumping of bacteria is expected, ultrasound sonification should be considered to resolve cellular aggregates. Also here, conditions of sonification have to be established for different types of samples to maintain cellular integrity. A typical treatment is exposure to 35 kHz and 80 W effective output power for 1 min in an ultrasonic bath to disband large cell aggregates [2125].

One also has to be aware that some bacteria can be permeable to otherwise cell-impermeable dyes, such as PI, and other bacteria very efficiently shuttle out otherwise cell-permeable dyes, such as SYTO9, easily resulting in false positives and negatives when looking at complex microbial communities [2123, 2124, 2127]. Again, the non-cultivability of many bacteria precludes the validation and calibration of such staining procedures. This applies also to other viability dye approaches, such as the measurement of membrane potential. Inhibition of the respiratory chain and depolarization of the membrane potential are important controls for this method, but is not feasible for all the different cell types in complex microbial communities.

Protocols should be optimized for staining all cells to mark and visualize each cell in a community. Good dyes for this are nucleic acid dyes such as DAPI used on fixed cells together with a cell wall permeabilizing detergent to allow quantitative penetration of DAPI through the cell wall [2125]. SYBR® Green I has also been described for staining of nucleic acids of viable cells [2128], although one should be aware of the above mentioned limitations. When available, specific Abs can be used to identify specific phylotypes in communities. Further differentiation of cell types in communities can be performed by the more qualitative approaches of fluorescent in situ hybridization (FISH) and lectin probes, while cell constituents such as lipid inclusion bodies can be stained by highly lipophilic dyes [2124].

A major limitation of microbial community cytometry as described here is the lack of any taxonomic or functional information in comparison to sequencing approaches, where cell phylotypes can be determined or genes with certain functions be detected or even metagenomics analyses be performed. To get a deeper insight, cell sorting can be used to separate interesting sub-communities [2122] or even single cells [2129] for further analyses by, e.g., NGS or proteomic technologies. Cell sorting not only provides access to bacteria that are currently not culturable, but also reduces background, as all cells outside of the sorted gates will not be included in downstream analyses increasing the resolution of the data obtained.

The positions of gates (subcommunities) to be sorted are still defined manually. Cell sorting should be done in the '1.0 Drop Pure' sort mode (BD Influx v7 Sorter). Between 500 000 and 5 000 000 cells within the selected gates should be sorted into tubes at rates from 200 up to 1000 cells/s. Sorted cells are harvested by two successive centrifugation steps (20 000 × *g*, 6°C, 20 min), and the cell pellets can be stored at –20°C for subsequent analyses [for proteomics: [2130]; for 16S amplicon profiling: [2122, 2131]].

7.6 *Data analysis*

High resolution FCM can resolve microbial community structures by generating community patterns. It is highly recommended to use a stain that labels every cell for this purpose. These communities are interpreted as pattern (see below post-processing of data) and are generally used to determine community dynamics and to allow for sort decisions.

To evaluate data as shown in Fig. 238, a master gate should be defined that contains all cell events excluding the beads (Fig. 238D). It is advisable to always measure the same number of cells. Usually 200 000 cells are sufficient for downstream analysis pipelines. For cytometric fingerprinting, a gate template has to be generated by marking all apparent sub-communities by a gate and combining all defined gates to the gate template (Fig. 238D and G). The gate template allows the determination of the cell number per gate across the different samples. The dynamic variation of community structure can then be described by quantifying the changes of events per gate [2132].

For the analysis of the cytometric microbial community fingerprint some evaluation tools are already available. FlowFP [2133, 2134] uses a geometrical grid as an alternative to cluster-based gating of FCM profiles. Alternatively, flowCHIC (cytometric histogram image comparison, http://www.bioconductor.org/packages/release/bioc/html/flowCHIC.html, [2135]), is also a grid-based algorithm that transforms 2D cytometric profiles (e.g., DAPI vs. FSC) into grey-scale images and compares the pixel density between two successive samples. FlowCybar (cytometric barcoding, http://www.bioconductor.org/packages/release/bioc/html/flow

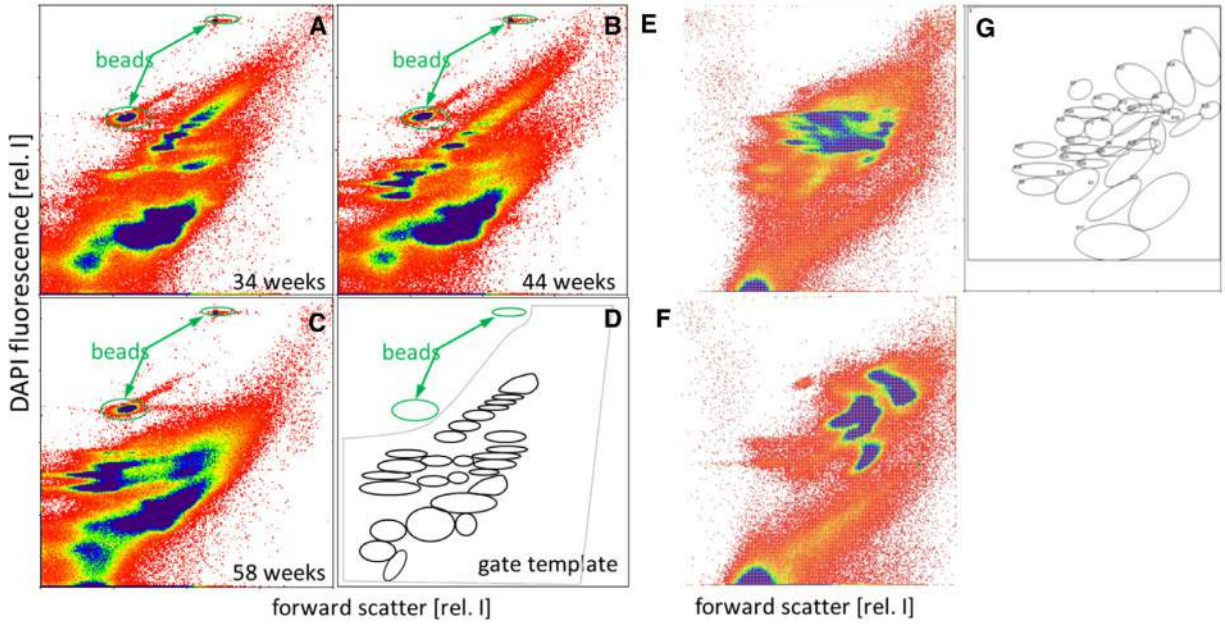

Figure 238. (A–D) A microbial community originating from a wastewater treatment plant cultivated in an aerobic and continuously operated bioreactor on a peptone medium for (A) 34, (B) 44, and (C) 58 weeks [2131], and (E–G) microbial community derived from a fecal sample of a mouse (E) before and (F) after induction of T cell-transfer colitis [2122]. Samples were taken and stained with a 0.24 μM DAPI solution and measured using a 355 nm Genesis CX laser (100 mW, Coherent, Santa Clara, CA, USA, MoFlo Legacy cell sorter, (Beckman Coulter, Brea, California, USA). Scatter was measured using a 488 nm Sapphire OPS laser (400 mW). Beads of sizes 0.5 μm and 1 μm Fluoresbrite Microspheres (both Polysciences, 18339 and 17458, Warrington, PA, USA) were amended into every sample as internal standards. A master gate (D and G: grey) was defined that comprised 200 000 cells for each measurement. Each upcoming subcommunity was marked by a gate in the three samples and a combined gate template generated (D and G: black ellipses). The three chosen samples show the highly diverse cytometric structure of the community and its evolution over time.

CyBar.html, [2132]) produces the cytometric fingerprint on the basis of the gate template as described that represents the microbial community structure by the number of clusters, the position of these clusters in the histogram, and the number of cells within each cluster. The direct comparison of cell abundance changes between gates with high and low cell numbers is facilitated by data normalization. FlowCybar can visualize variations of the cytometric fingerprint over time or in dependence on experimental/abiotic factors.

7.7 *Advantages*

- Relatively quick and cheap
- Absolute cell counts
- Sorting of bacteria for downstream genetic, proteomic, and functional analyses possible

7.8 *Pitfalls*

- Membrane-permeable DNA/viability dyes can be excluded or shuttled out by certain viable bacteria
- Taxonomic information requires FISH probes or specific antibodies
- Limited data analysis tools available
- Specific instrument requirements for high-resolution bacterial community structure measurements
- Standardization required for cross-sample comparison

7.9 *Top tricks*

The flow cytometer should be aligned before measurement using 1 μm or 2 μm beads that are fluorescent in the required range of light. In addition, we strongly advise to spike both 0.5 μm and 1 μm beads into each sample to guarantee comparability between samples. Creation of a gate template for these two types of beads and aligning the beads always inside the same gate template allows the comparison of data over weeks and months. It should be ensured that the beads lie outside of the cell populations to be analyzed (see Figs. 237 and 238). Beads, however, do not control for identical sample handling. When cells are stained using solutions in nanomolar concentration ranges, even small experimental variations result in handling-dependent changes of the fluorescence of the cells. To control for variations in handling, we recommend the additional use of a biological standard (with respective gate template). For this, fixed *Escherichia coli* cells that undergo the same procedure as the samples to be analyzed can be very helpful. For all published data, the cytometer setup and the applied standardizations should be specified together with the

experimental data deposited, for example, in the FlowRepository (https://flowrepository.org/).

8 Detailed and standardized methods to detect inflammasome assembly and activation in immune cells (FlowSight AMNIS)

8.1 *Overview*

Inflammasome is a multimeric protein platform involved in the regulation of inflammatory responses whose activity results in the production of IL-1β and IL-18.The evidences of inflammasome activation are the concentration of the inflammasome adapter protein apoptosis-associated speck like protein containing a caspase recruitment domain (ASC) into a single speck and a rapid lytic form of cell death termed pyroptosis. In this section, we will show inflammasome activation by ASC speck detection at single cell level using imaging cytometer technology by FlowSight.

8.2 *Introduction*

The inflammasomes are intracellular multimeric protein complexes, mainly expressed in myeloid cells, whose aggregation leads to the activation of the caspase-1 and the downstream secretion of three of its substrates, the proinflammatory cytokines IL-1β, IL-18 and gasdermin-D that in turn leads to pyroptotic cell death [2136–2138]. Nod-like receptors (NLRs), in particular, are cytoplasmic pattern recognition receptors that detect invading pathogens and initiate inflammasome-dependent innate immune responses. NLRs are activated by bacterial, fungal, or viral molecules that contain PAMPs, or by non-microbial danger signals (DAMPs) released by damaged cells [2139, 2140]. Upon activation, some NLRs oligomerize to form multiprotein inflammasome complexes that serve as platforms for the recruitment, cleavage, and activation of inflammatory caspases. At least four inflammasome complexes (NLRP1, NLRP3, IPAF, and AIM2) have been identified. These complexes contain either a specific NLR family protein or AIM2, the apoptosis-associated speck-like protein containing CARD (ASC) and/or the Cardinal adaptor proteins, and pro-caspases-1, 5 and 8 [2141, 2142]. NLRP3 is the best-characterized inflammasome; its formation requires multiple steps. In a priming step, transcriptionally active signaling receptors induce the NF-kB-dependent induction of NLRP3 itself as well as that of the caspase 1 substrates of the pro-IL-1β family [2143, 2144]. The NLRP3 is, at this stage, in a signaling incompetent conformation; this is modified upon a second signal which will result in the assembly of a multimolecular complex with ASC and caspase 1. Notably the inflammasome activation consists in the assembly of NLRP3 with ASC that in turn recruits procaspase-1 by its caspase recruitment domain (CARD) or procaspase-8 by pyrin domain (PYD) [2145] forming ASC speck [2146] and leading to caspases activation. The assembled ASC speck is the main feature of inflammasome formation and it occurs within minutes of activation, and it stabilizes, finally it is released into the intercellular space, collected by myeloid cells spreading inflammation [2147–2149]. Notably the resting myeloid cell show ASC protein diffuse in cytoplasm, after inflammasome activation the ASC shifts to form a speck.

The activated caspase-1 leads to the cleavage and release of bioactive cytokines including IL-1β and IL-18 and also of protein GSDMD causing membrane rupture and pyroptotic cell death [332]. The pyroptosis plays an important role in inflammatory response and its assessment could be of interest for therapeutic intervention (see Chapter V: Biological Applications, Section 7.4: Pyroptosis).

8.3 *Applications*

The assembly of a functional NLRP3 inflammasome complex results in the production of proinflammatory cytokines; although these cytokines have a beneficial role in promoting inflammation and eliminating infectious pathogens, mutations that result in constitutive inflammasome activation and overproduction of IL-1β and IL-18 were linked to inflammatory and autoimmune disorders [2150–2152]. A number of recent data strongly suggest that an excessive activation of the NLRP3 inflammasome can be observed as well in neurological diseases including multiple sclerosis as well as Parkinson's and Alzheimer's diseases, in which neuroinflammation plays a central role [2153–2157]. Indeed given that the neuroinflammation is the probable consequence of the activation of inflammasomes in immune cells that infiltrate the central nervous system, dampening of the inflammasome assembly could be beneficial in these diseases and could be envisioned as a possible therapeutic approach to these conditions. For these reasons, the quick and accurate evaluation of inflammasome assembly in peripheral immune cell could be a good methodology approach to monitoring inflammation in a number of diseases.

8.4 *Principles of the technique being described and Equipment*

Sester and colleagues performed an FCM method to detect ASC redistribution in myeloid cell defining speck formation by changes in fluorescence peak height and width [2156, 2157]. This protocol permits to define the true activated inflammasome by assessment ASC speck formation, because until then the detection of inflammasome, activation was made by monitor its end products, IL-1β or IL-18, or activated caspase-1 detection. Notably different pathways can secrete IL-1β and the methods to analyze caspase-1 activity are not always specific, in both cases the outcomes could be inflammasome independent. Despite to ASC speck formation microscopy analysis, used in the past, this methodology is faster, more accurate, and sensitive. Recently a better method to analyze simultaneously ASC speck and caspase-1 activity was performed by Amnis ImageStream^X [2158]. This protocol eliminates false

positive events detected by flow-cytometry method, by specific masks to select only single cell, excluding cells with nonspecific-like aggregation of ASC and also defining ASC speck size. Finally the study analyze the presence and distribution of active caspase-1, detected by FLICA spots, and ASC speck simultaneously, evaluating inflammasome activation.

In this section we show the analysis of inflammasome activation by FlowSight, performed utilizing ASC speck formation in LPS+Nig stimulated-THP1derived macrophage.

8.5 *Experimental workflow and acquisition*

8.5.1 THP1 cell differentiation. THP-1 human monocytes (IZSLER, Istituto Zooprofilattico Sperimentale della Lombardia e Dell'Emilia Romagna, IT) are grown in RPMI 1640 supplemented with 10% FBS, 2mM L- glutamine, and 1% penicillin (medium) (Invitrogen Ltd, Paisley, UK). To differentiate these cells into macrophages, THP-1 human monocytes are seeded in six-well plates at a density of 1.0×10^6 cells/well in medium that contained 50 ηM of PMA (Sigma–Aldrich, St. Louis, MO) and incubated for 12 h at 37°C in 5% CO_2.

THP1-derived macrophage culture and intracellular inflammasome protein staining

THP-1-derived macrophages are cultured with medium alone (negative control) or are incubated with LPS (1 μg/mL) (Sigma-Aldrich) for 2 h and Nigericin (Nig; 5 μM; Sigma–Aldrich) for the last 1 h.

THP-1-derived macrophages (1×10^6) are harvested by 0.05% (w/v) trypsin (Seromed, Biochrom KG) in **EDTA** solution for 5 min at 37°C, washed once in RPMI supplemented with 10% FBS, seeded in polystyrene round-bottom tubes (Falcon 2052, Becton Dickinson Labware, Franklin Lakes, NJ) and centrifuged for 10 min at 1500 rcf at 4°C. Tubes containing THP-1-derived macrophages are placed on ice; cell are permeabilized with 100 μL of Saponine in PBS (0.1%; Life Science VWR, Lutterworth, Leicestershire,LE) and 5 μL (25 μg/mL) of the PE-antihuman ASC (clone HASC-71, isotype mouse IgG1,Biolegend, San Diego, CA) mAbs are added to the tubes for 1 h at 4°C. Cells are then washed with PBS and centrifuged at 1500 rcf for 10 min at 4°C. Finally, cells are fixed with 100 μL of PFA in PBS (1%) (BDH, UK) for 15 min, washed with PBS, centrifuged at 1500 rcf for 10 min at 4°C, resuspended in 50 μL of iced PBS, and immediately analyzed by FlowSight.

8.5.2 Human peripheral monocyte cell cultures. PBMC (1×10^6/mL) are cultured in RPMI 1640 supplemented with 10% human serum, 2 mM L-glutamine, and 1% penicillin (Invitrogen Ltd, Paisley, UK) and incubated at 37°C in a humidified 5% CO_2 atmosphere for 2 h in a 12-well plate. After 2 h, non-adhering PBMCs are harvested and discarded; monocytes (adhering cells) are culture in medium alone (unstimulated) or primed with 2 μg/mL LPS for 2 h (Sigma–Aldrich, St. Louis, MO) before stimulation with Nigericine (5 μM) (Sigma–Aldrich) for 1 h at 37°C in a humidified 5% CO_2 atmosphere. Adhering cells (monocytes) are then collected by trypsin treatment and prepared for FlowSight analysis by immunofluorescence staining as THP1-derived macrophage (see above).

8.6 *Data analysis*

ASC-speck formation is analyzed by FlowSight (Amnis Corporation, Seattle, WA, USA) (see chapter VIII, Section 1 "Imaging flow cytometry").

8.6.1 FlowSight acquisition parameters. The FlowSight (MilliporeSigma) equipped with 488, and 642 nm lasers with two camera and twelve standard detection channels is used to acquire experimental samples using the INSPIRE software.

The flow rate is set to minimum and the objective magnification is set to 20x for all samples.

A multifluorophore-labeled sample (Flowsight Calibration Beads) is used to determine accurate laser and focus settings and avoid oversaturation.

Masks are defined region of interests that are computationally calculated by INSPIRE.

A mask defines a specific region of an image that can be used for specific feature calculations.

The saturation of an individual fluorophore in its corresponding channel is determined by plotting the Raw Max pixel feature for every channel.

Aspect ratio feature measures circularity, to distinguish between singlets, doublets, and cell clumps when used together with the area feature.

Area versus aspect ratio of the default mask on the brightfield is used during acquisition to ensure collection of single-cell events. A region is created to exclude debris and to record 2000 events for every sample.

For the compensation control, 1000 events for single-stained samples are acquired turning the Ch01 (brightfield) and Ch06 (side scatter) off.

All samples and controls are acquired as raw image files (.rif).

8.6.2 FlowSight image analysis. All sample and compensation analysis are performed using analysis software (IDEAS).

The IDEAS image analysis software allows quantification of cellular morphology and fluorescence at different cellular localizations by defining specific cellular regions (masks) and mathematical expressions that uses image pixel data or masks (feature).

Individual compensation controls of single-stained samples are loaded into the compensation wizard in IDEAS. A compensation matrix file (.ctm) is generated and applied to a positive control (nigericin-treated sample) raw data file (.rif) to generate both a compensated image file (.cif) and a corresponding data analysis file (.daf). A data analysis template (.ast) is developed by analyzing the.daf file of positive control sample. We applied the

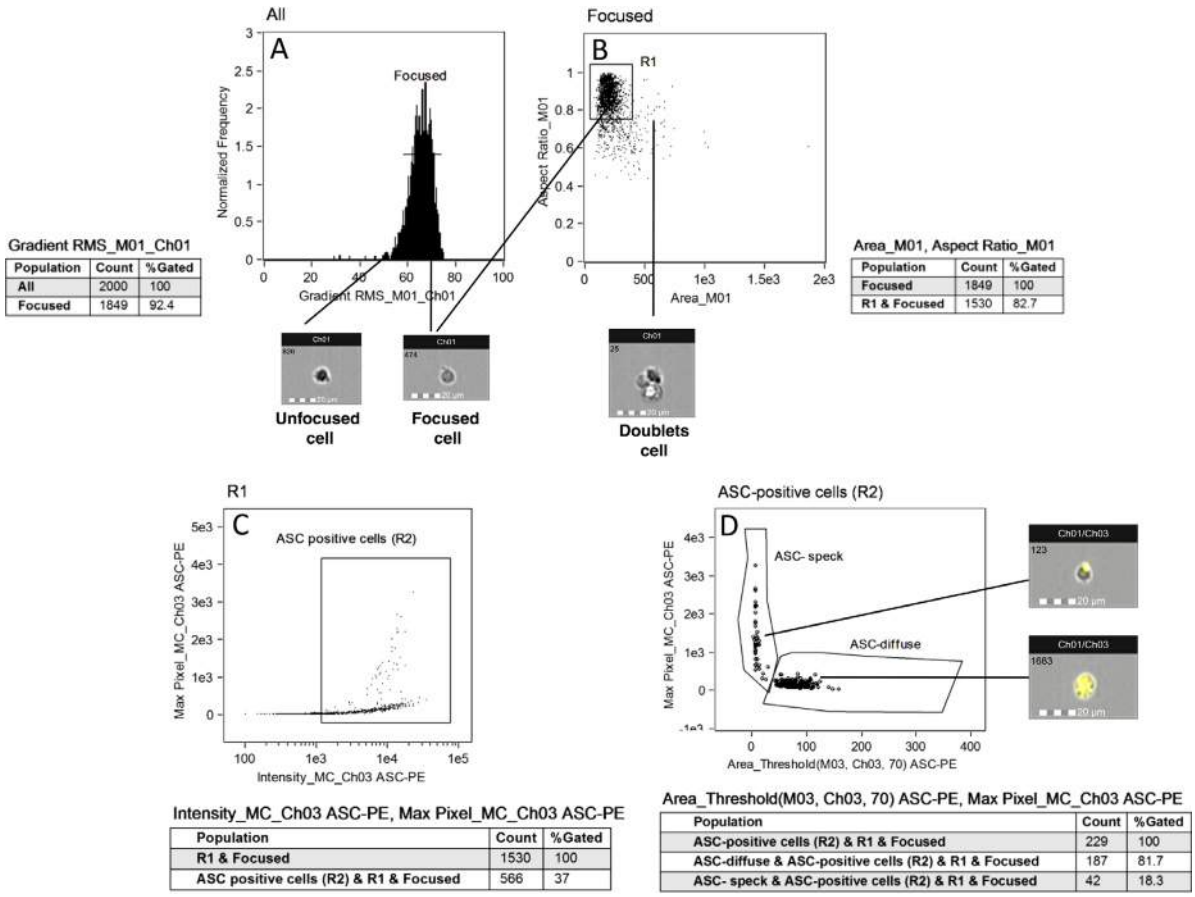

Figure 239. Representative images from unstimulated THP-1-derived macrophages (1×10^6). *Identifying focused cell* (A): The default mask (M Brightfield) used in acquisition does not discriminate between focused and unfocused cells; the object mask alows the exclusion of unfocused cell. *Identifying single cells* (B): Focused cells are plotted on AREA brightfield versus Aspect Ratio Brightfield scatterplot to exclude doublets cell. Events with an Aspect ratio of 0.6–1.0 and an area of 50–500 U representing single cell are selected (R1). *Identifying ASC positive cell* (C): Single cells (R1) are plotted on Max Pixel MC (Ch03) and intensity MC Ch03 scatterplot to indentify ASC positive cells (R2). *Identifying ASC speck* (D): ASC positive cell (R2) are plotted on Max Pixel MC (Ch03) versus Area threshold (M03,Ch03,70) scatter plot. This mask allows to discriminate between cells characterized by speck formation, in which a functional inflammasome complex is assembled, and cells with an ASC diffuse pattern.

template along with the compensation matrix to the rest of the experimental samples using the multiple file batch tool in IDEAS.

Focused cells

Unstimulated (cells kept in medium alone; Fig. 239) and LPS+Nig (Fig. 240)-stimulated THP-1-derived macrophages (1×10^6) are resuspended in 50 μL of PBS and analyzed by FlowSight.

The Gradient root mean square (RMN) of Brightfield channel is used to identify focused cells (Figs. 239A and 240A).

The focused cells are plotted on AREA bright field *vs*. Aspect Ratio Bright field scatterplot to exclude aggregates from single cells (R1) (Figs. 239B and 240B)

ASC speck mask

An intensity mask defined by Max Pixel MC (Ch03) *vs*. Intensity (Ch03) is created from the R1 gate to identify total ASC positive cells (Figs. 239C and 240C).

To define cell with ASC speck from cells with an ASC diffuse pattern a Threshold mask plotting Max Pixel MC (Ch03) *vs*. Area threshold (M03, Ch03,70) is created. This mask allows to separate within the population of ASC-fluorescent cells those with small area and high max pixel (ASC speck) from those with large area and low max pixel (ASC diffuse) (Figs. 239D and 240D).

8.7 *Advantages*

This protocol allows to identify quickly and in an extremely accurate way inflammasome activation at single cell level. The gate strategy identifying the different size and brightness of ASC fluorescence differentiates between cells with speck formation, in which a functional inflammasome complex is assembled, and cells characterized by an ASC diffuse pattern.

8.8 *Pitfalls/Top tricks*

Inflammasome activation leads to pyroptosis and release of ASC specks into extracellular space, to avoid cellular breakdown, it is essential to keep cells on ice after detachment by trypsinization and during the staining procedure.

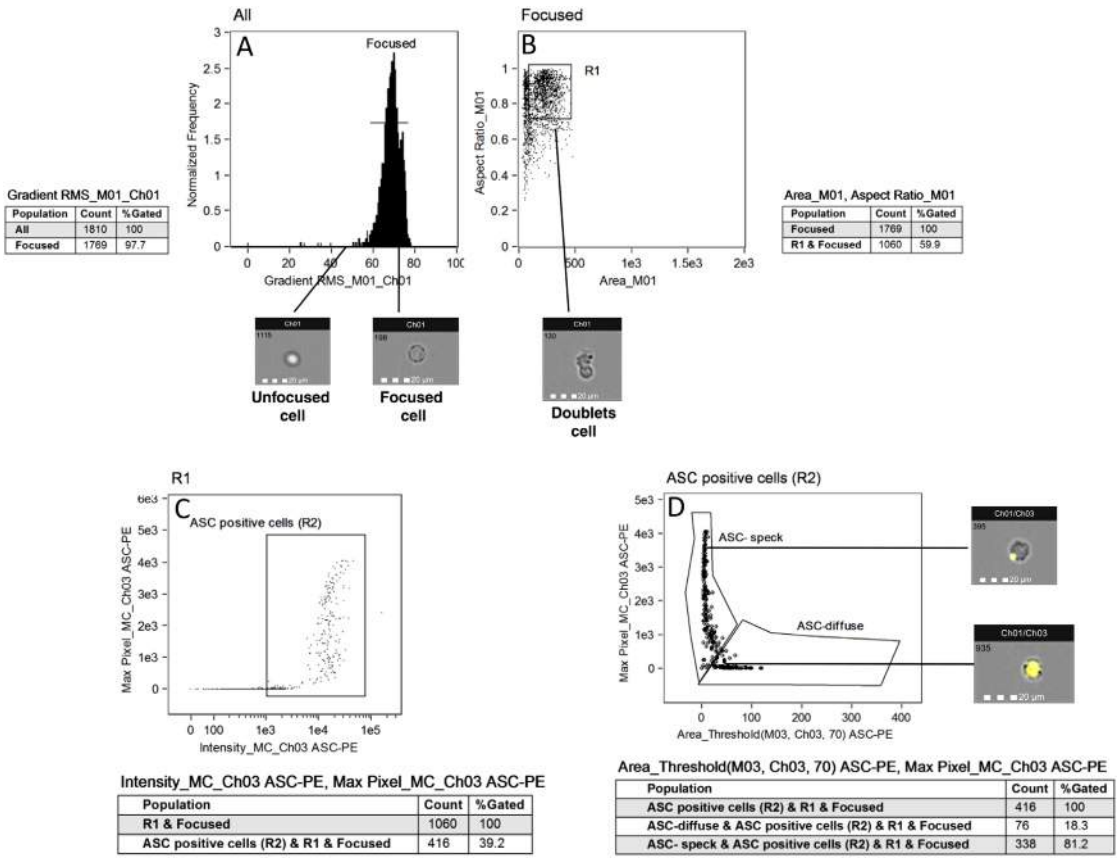

Figure 240. Representative images from LPS+Nig-stimulated THP-1-derived macrophages (1×10^6). *Identifying focused cell* (A): The default mask (M Brightfield) used in acquisition does not discriminate between focused and unfocused cells; the object mask alows the exclusion of unfocused cell. *Identifying single cells* (B): Focused cells are plotted on AREA brightfield versus Aspect Ratio Brightfield scatterplot to exclude doublets cell. Events with an Aspect ratio of 0.6–1.0 and an area of 50–500 U representing single cell are selected (R1). *Identifying ASC positive cell* (C): Single cells (R1) are plotted on Max Pixel MC (Ch03) and intensity MC Ch03 scatterplot to indentify ASC positive cells (R2). *Identifying ASC speck* (D): ASC positive cell (R2) are plotted on Max Pixel MC (Ch03) versus Area threshold (M03,Ch03,70) scatter plot. This mask allows to discriminate between cells characterized by speck formation, in which a functional inflammasome complex is assembled, and cells with an ASC diffuse pattern.

9 Multidrug resistance activity

9.1 *Overview*

Multidrug transporters, in particular MDR1, MRP1, and BCRP serve as independent biomarkers to monitor treatment efficiency and to support treatment decision in numerous clinical conditions, as the most prevalently used small molecule drugs are substrates of these efflux pumps.

Transporter activity measurement using fluorescent reporter substrates and transporter inhibitors is a simple and cost-effective assay that can be performed on primary cells or cell lines. Importantly, reagents used in transporter activity measurements are compatible with fluorescently labeled Abs, thus it is possible to perform the assay simultaneously on several cell types of interest.

9.2 *Introduction*

Multidrug resistance (MDR) transporters play an essential role in the extrusion of xenobiotics from the cell, however, small molecule drugs, like methotrexate (MTX), *Vinca* alkaloids, and other standard chemotherapeutics are also removed from target cells via these molecules. In the clinical routine, MDR1 (also known as P-gp, or ABCB1), MRP1 (also known as ABCC1), and BCRP (also known as ABCG2, or MXR) are the most important players in the development of resistance against these drugs [2159–2162].

Currently, qRT-PCR, immunohistochemistry, and Western blots are the most frequently used methods to determine the MDR transporter status in clinical samples. On the other hand, several polymorphisms affecting transporter function have been reported [2163, 2164]. Therefore, the relevance of quantitative description of these transporters is questionable. Transporter trafficking is affected by genetic variation. Therefore, FCM-based determination of cell surface expression of MDR transporters would be a significant progress [2165]. However, Abs recognizing the extracellular MDR1 and BCRP epitopes are conformation sensitive, making their accurate determination challenging [2166–2168]. Furthermore, the functional activity of these molecules still remains elusive.

Performing real-time transporter activity measurements using fluorescent reporter substrates is highly beneficial in the clini-

cal setting for personalized therapy and monitoring in certain hematologic malignancies and in autoimmune diseases, since the activities of MDR1, MRP1, and BCRP serve as biomarkers to predict the patient's response to small molecule therapy in treatment naïve conditions and during small molecule drug treatment [2169, 2170]. Furthermore, the determination of transporter activity is also relevant in cell lines in pharmaceutical research.

The following protocol provides a cost-effective method with a short turnaround time to determine MDR transporter activity. These measurements can be performed on various cell types, including cell lines, peripheral blood or bone marrow-derived cells.

9.3 *Principles of the technique being described*

Measuring the functional activities of MDR1, MRP1, and BCRP is based on the application of fluorescent transporter reporter substrates along with specific and pan-inhibitors of these transporters. Reporter substrates readily penetrate the cell membrane. Preferably, the non-fluorescent reporter substrate, such as calcein-AM, is cleaved by endogenous esterases to form a highly fluorescent derivative of the dye that becomes trapped in the cytoplasm due to its high hydrophilicity. However, many fluorescent substrates that are not cleaved by esterases are also used in drug discovery and in clinical practice, including mitoxantrone, Rhodamine 123, and Hoechst stains. The activity of the efflux transporters results in lower cellular accumulation of the fluorescent reporter dye. In cells expressing transporters the addition of specific inhibitors blocks dye exclusion activity of the relevant transporter and increases dye accumulation in the cells. In the absence of significant transporter activity, the net reporter substrate accumulation is faster in the cells due to a lack of transporter mediated efflux, which in turn is not influenced by the presence of an MDR transporter inhibitor [2171].

9.4 *Applications*

- **Basic research applications**: To characterize transporter biology and functionality, to study the pathobiology of transporter-mediated diseases, to test cell lines overexpressing multidrug transporters, to test drug–transporter interactions, and to examine drug or herb–drug interactions in the context of drug discovery and in the study of drug disposition
- **Cohort selection in Phase I trials**: Data show that up to 20% of healthy adults are characterized by high baseline transporter functions [2172]. Enrollment of these individuals in a Phase I trial may cause bias, which can be excluded by a preliminary screening of transporter function, saving cost and effort
- **Therapy tailoring to support personalized treatment**: Small molecule drugs are widely used in cancer and autoimmune diseases. As these drugs are removed from the target cell via multidrug transporters, transporter activity measurements would be highly beneficial at the time of diagnosis and during therapy to support treatment decisions

9.5 *Equipment*

The flow cytometer used for measurements does not require any special features. The lasers and channels applied for the detection of the fluorescent substrate depends on the specific fluorescent substrate molecule used. For example, the 488 nm laser and the 515 nm channel is recommended for calcein-AM while the 633 nm laser and the 684 nm channel is recommended for mitoxantrone. The configuration of the instrument will determine the number of additional cell surface markers that can simultaneously be used in order to identify individual cell subsets. In conclusion, no specific flow cytometer is required for running transporter activity measurements. The following assay is not suitable for high-throughput screening format.

9.6 *Experimental workflow and acquisition*

9.6.1 Sample preparation. Transporter activity measurements can easily be performed on human and rodent cell lines and primary cells. Importantly, transporter activity measurements require viable cells ($2–5 \times 10^6$) in good condition, not depleted of intracellular energy stores. ATP depletion tends to decrease the activity of membrane transporters and may lead to inaccurate results.

If primary human blood or bone marrow samples are used, K_3EDTA or Na-citrate is recommended to be used as anticoagulant, since other anticoagulants, e.g., heparine may interfere with transporter activity measurements. For collecting PBMCs, Ficoll density gradient centrifugation is suggested. Primary samples should be processed within six hours after drawing, as samples stored beyond 6 h may undergo serious ATP depletion, leading to inaccurate results. If samples are stored over 6 h, PI counterstaining is recommended to exclude dead cells. Blood samples should be stored at room temperature before testing. Do not freeze samples. Cells should be diluted in HBSS buffer.

9.6.2 Assay procedure. The specific steps of the procedure may vary depending on the instructions supplied by the manufacturer of the kit used. Here, we provide general considerations for the assays.

Prepare and measure samples under same inhibitor treatment and staining conditions in triplicates. *Mix cells thoroughly by gentle pipetting rather than vortexing to avoid forming bubbles in the test tube. Always include a control sample with no inhibitors applied. The concentrations of the respective inhibitors are specified in the manufacturer's instructions of the kit used. Samples are incubated at 37°C.*

To start the staining reaction, add the transporter reporter substrate into all tubes simultaneously. After incubation, stop reaction in all tubes simultaneously by rapid centrifugation (1 min at 2000 rpm) with rapid acceleration and deceleration. Discard supernatant

and stain resuspended cells with labeled Abs *if required. Stain cells with PI solution to demonstrate viability if necessary*.

9.6.3 Staining the cells with labeled cell surface Abs. For measuring transporter activities on your cell type of interest, the use of fluorescently labeled Abs are recommended. Both immunolabeling and conjugate labeling methodologies can be followed. Please note that some Abs may interfere with transporter activity measurements. To avoid such interference, the staining of cells with Abs as per the manufacturer's instructions should be carried out following the staining with the transporter reporter substrates. Cells must not be fixed or permeabilized. The necessary isotype controls or unlabeled cell controls should be used according to the manufacturer's instructions.

9.7 *Data acquisition*

Mix samples thoroughly before measurement and use only the viable cell population for data analysis. In case of using commercially available kits (e.g., the SOLVO MDQ Kit™), the assay contains internal standardization, thus the results will become independent from the PMT settings, whenever the acquisition occurs within the linear range of the equipment. However, samples belonging to the same assay must be measured using the same settings for PMT amplification.

9.8 *Data analysis*

Apply sequential gating strategy for the analysis (an example is provided in ref. [2173]). Within the desired cell subset gate, determine the corresponding geo-MFI values of the reporter substrate applied. For this, the inclusion of at least 10 000 cells within the desired cell subset gate is recommended.

9.8.1 Calculation of multidrug resistance activity factors. Take the median geo-MFIs of triplicate parallel measurements with and without the transporter inhibitors ("F" values). We provide an example below of the equations used to calculate multidrug resistance activity factor (MAF) values for each multidrug transporter, plus the composite activity of MDR1 and MRP1 (MAF_C) using the SOLVO MDQ Kit™. These calculations may differ when using other kit assays.

- $MAF_C = 100 \times (F_{MAX} - F_0) / F_{MAX}$
- $MAF_{MRP1} = 100 \times (F_{MRP1} - F_0) / F_{MAX}$
- $MAF_{MDR1} = MAF_C - MAF_{MRP1}$
- $MAF_{BCRP} = 100 \times (F_{MX} - F_B) / F_{MX}$

F_{MAX} and F_{MX} represent reporter substrate fluorescence (calcein and mitoxantrone, respectively) with inhibitors of MRP1 and MDR1 as well as of BCRP, respectively. F_0 represents fluorescence without inhibitors. F_{MRP1} represents reporter substrate fluorescence (calcein) with specific inhibitor of MRP1.

9.8.2 Expected results and interpretations. Theoretical MAF values can range between 0 and 100. The MAF_C found in normal PBMCs are in the range of 0–20, while in drug selected cell lines exhibiting extreme high levels of MDR1/MRP1 expression, the MAF_C values might be as high as 95–98. In case of hematological malignancies, the MAF_C values in tumor cell populations are usually found between 0 and 50, but in extreme cases, values can be as high as 70. Reference values of MAF values in $CD3^+$ lymphocytes were determined in a healthy population of 120 individuals [2173]. Importantly, MAF values are independent from gender. MAF_{MRP1} and MAF_{BCRP} are also independent from age, while MAF_C and MAF_{MDR1} showed a negative correlation with age in healthy adults.

9.9 *Advantages*

- **Functional data**: In contrast with other methods detecting the presence or absence of MDR transporters at relative gene expression or protein level, transporter activity measurements by FCM assess whether efflux transporters are functionally active.
- **Clinical application**: The assay works on both primary cells and cell lines. As little as 5 mL of peripheral blood is sufficient to study transporter activity in patient samples. A CE-IVD kit (SOLVO MDQ Kit™) is available for clinical use.
- **Short turnaround time**: Functional data can be obtained within 2 h following sampling as compared with much longer turnaround times of next generation sequencing methods. Moreover, a single sample can be measured cost-effectively without the need of batching multiple samples.
- **Cost effective**: Transporter reporter substrates and inhibitors are commercially available compounds that are far cheaper than Abs and reagents required for gene expression assays.
- **Flexible**: The use of fluorescent cell surface markers allows the simultaneous detection of transporter activity in various cell subsets of interest.

9.10 *Pitfalls*

- It is recommended to start the assay within 6 h after obtaining the primary sample to avoid depletion of intracellular ATP stores. Detection of dead cells with PI is recommended beyond this time limit.
- As timing of the staining steps is crucial in measuring transporter activity, the addition of the fluorescent reporter substrate to the samples should be take place within 20 s. Therefore, it is not recommended to start the reaction on more than 12 test tubes at the same time. Allow 2-min intervals between starting the reactions when multiple samples are measured. It is recommended to use a repeater pipette to add substrates and inhibitors to multiple test tubes.
- Sample measurement should preferably be performed immediately (within 2 h) after staining. Keep the samples on ice and protect them from light until the measurement.

9.11 *Top tricks*

- In case of cell lines growing adherently, trypsinization is a critical step to keep cell membranes intact: for this, trypsinization time should be established for the cell line of interest.

10 Index sorting

10.1 *Overview*

Index sorting records fluorescence information and scatter characteristics indexed for each individual sorted event. This technology is especially powerful when sorting single events and allows the retrospective identification of highly accurate multidimensional phenotypes.

10.2 *Introduction*

Fluorescence-activated cell sorting is broadly available and its applications reach from large-scale sorting of millions of cells into tubes to the targeted deposition of single events into multiwell plates or onto slides. For conventional sorting, target populations have to be defined before the sorting process involving more or less sophisticated gating strategies. The advantage of index sorting is that fluorescence data for each individual sorted event can be read out retrospectively. This technology, especially when applied as single cell sorting, is invaluable for specific research questions in which sorted events of interest can only be identified with downstream technologies. Most currently commercially available sorters are capable of index sorting.

We will illustrate the technology with one example combining 12 fluorescent parameter single T cell index sorting of a T lymphoblastic lymphoma sample with downstream single cell TCRαβ sequencing (Fig. 241).

10.3 *Principles of the technique being described*

Indexed fluorescence data and scatter characteristics are recorded for each single sorted event so they can be assigned retrospectively. Index sorting itself is not different from regular cell sorting except it has to be activated in the sorter software. After sorting, scatter characteristics and fluorescence data for each single event can be exported from the sorter software—usually as a table (comma separated list). Exported data have to be individually processed and, if desired, can be combined with data from downstream assays depending on the purpose of the experiment (see example in Fig. 241).

10.4 *Applications*

Index sorting has been applied in a variety of research areas including the isolation and characterization of single circulating tumor cells [2174], the determination of cell cycle states and immune phenotypes of stem cell populations [2175–2177], the combination of genotype with phenotype data in healthy and malignant B lineage cells [1606, 2178], the definition of the phenotypic range of individual T cell clones [2179–2181], and the determination of cell size in combination with microbial single cell genomics [2129], among others.

Table 96. Parameter panel for single cell index sorting in Fig. 241

Specificity	Clone	Fluorochrome	Vendor
CD8	RPA-T8	BV510	BioLegend
CD57	HCD574	FITC	BioLegend
PD-1	EH12.2H7	PerCP-Cy5.5	BioLegend
BTLA	J168-570	PE-CF594	BD Biosciences
TCRαβ	IP26	APC	BioLegend
CD45RA	HI100	AF700	BioLegend
CD25	CD25-4E3	PE-Cy7	Affymetrix
CTLA-4	BNI3	PE	Invitrogen
CCR7	G043H7	BV650	BioLegend
CD28	CD28.2	BV421	BioLegend
CD4	SK3	APC-Fire 750	BioLegend
live/dead		zombie yellow	BioLegend

As an example, we used index sorting to define the phenotypic range associated with clonal T cell expansion in one T lymphoblastic lymphoma lymph node (Fig. 241). The conventional approach would be to sort various T cell populations and sequence their TCR genes to detect clonal expansion. This approach is tedious and may not lead to the desired results due to shortcomings of 2D gating strategies for the definition of high-dimensional phenotypes ("Chapter VII: Data handling, evaluation, storage and repositories" and "Chapter VIII Section 5: High dimensional FCM"). Index sorting allows to stain with a multiparameter set of Abs (example in Table 96), randomly sort single T cells, sequence their TCRs, and retrospectively identify the multi-dimensional immune phenotype of each single cell belonging to the T cell clone of interest (Fig. 241).

Equipment

Most currently commercially available cell sorters are capable of index sorting. Sorting for the example in Fig. 241 was done using a FACSAria™ Fusion high-speed cell sorter equipped with a 70 μm nozzle and FACSDiva software version 8.02 (BD Biosciences). Sorter setup and preparation for index sorting does not differ from regular cell sorting with special attention on accurate drop delay ("Chapter II: Setup-Instrument setup and quality control," here). Single cells were sorted directly into 96-well plates prefilled with PCR buffer [2180].

Depending on the sorter hardware and target devices (e.g., 96-well plate), accurate and consistent mounting of the target device onto the robot can be difficult. Custom-made adapters and mounting plates onto 96-well racks can help to reduce alignment variability between plates [2176].

Experimental workflow and acquisition

Staining, preparation of single cell/particle suspensions, and the sorting process are identical to (single cell) sorting without

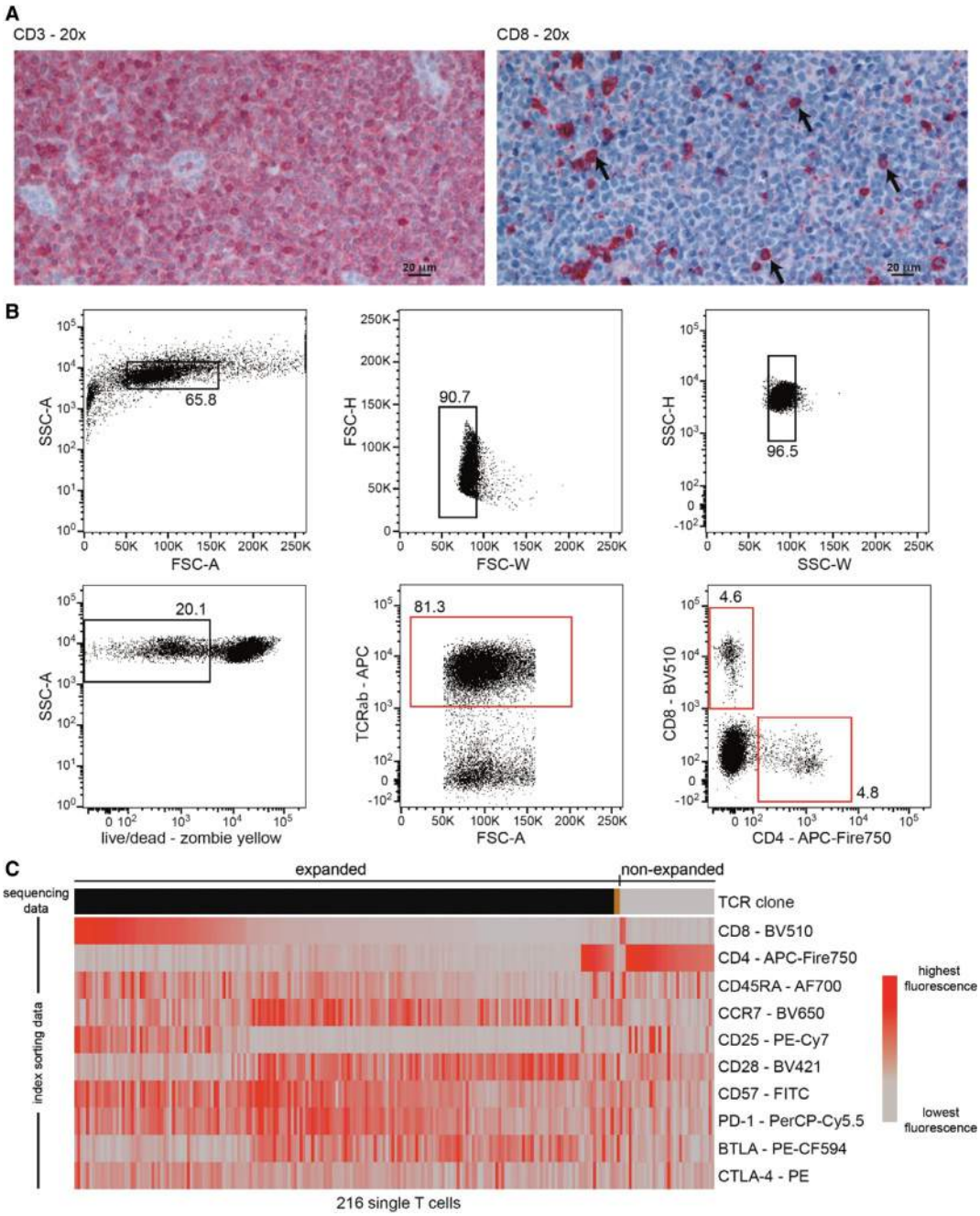

Figure 241. Determination of the phenotypic range of T lymphoblastic lymphoma cells as an application example for single cell index sorting. We combined 12 fluorescent parameter index sorting of αβ T cells with single cell TCRαβ sequencing of one single lymph node from a T lymphoblastic lymphoma patient. (A) Immunohistochemistry of a paraffin-embedded lymph node section demonstrates substantial infiltration with $CD3^+$ predominantly $CD8^-$ T lymphoblastic lymphoma T cells. $CD3^+$ (left image) or $CD8^+$ (right image) cells are stained in red. Polyclonal rabbit antihuman CD3 (A0452, Dako) and mouse antihuman CD8 (clone C8/144B, Agilent) were used for immunohistochemistry. Arrows in the right image point at single $CD8^+$ cells as examples. We aimed to determine the phenotypic range of T lymphoblastic lymphoma cells and asked whether interspersed $CD8^+$ T cells were polyclonal lymphoma-infiltrating T cells or part of the malignant clone. (B) Sequential gating for single cell index sorting of lymph node T cells. Upper row left: gating on lymphocytes; middle and right: gating on single cells by forward and side scatter characteristics. Lower row left: exclusion of dead cells; middle: gating on αβ T cells; right: gating on $CD4^+$ or $CD8^+$ T cells. Red indicates gates from which cells were ultimately sorted. (C) Combined paired TCRαβ sequencing and FCM data from cells sorted in (B). Single T cells are arranged in columns. The top bar color-codes TCRαβ CDR3 amino acid sequences; adjacent columns with the same color indicate expanded T cell clones. A clone was determined expanded if we detected at least two cells with identical TCRαβ CDR3 sequences. Grey indicates non-expanded T cells. FCM data were trimmed at the 2^{nd} and 98^{th} expression percentiles and scaled for each individual marker. While $CD4^+$ T cells were in parts polyclonal, the dominant proportion of $CD8^+$ T cells was part of the malignant clone. Data represent $n = 1$ experiment and illustrate an application example of index sorting. General findings on T lymphoblastic lymphoma biology cannot be concluded from these data. The lymph node and immunohistochemistry were provided by Martin-Leo Hansmann, Universitätsklinikum Frankfurt am Main, Dr. Senckenberg Institut für Pathologie, Germany.

index (see Chapter IV: Cell sorting). Index sorting has to be activated in the sorter software before starting the sorting process.

When sorting single events into multi-well plates or onto slides, special attention should be paid to plate targeting. Accurate plate alignment should be confirmed in regular intervals (e.g., after every fourth plate). Singlet gates should be defined stringently to reduce the chance of sorting doublets. Make sure to activate the "single cell mode" (or equivalent) in the sorter software when sorting single cells. It is recommended to run the sorter at a low flow rate (<200 events/s), which has been shown to improve the yield of rare events [2182].

Depending on the research questions and materials used, we recommend the inclusion of live/dead discriminatory dyes in the gating strategy.

For the example in Fig. 241B and C, cryopreserved cells from a lymph node sample of a T lymphoblastic lymphoma patient were stained with a 12 fluorescent parameter panel (Table 96). The panel included markers for the identification of major T cell differentiation states in combination with selected immune checkpoint molecules. Two-hundred single TCRαβ$^+$ cells were randomly index sorted into 96-well plates. Since CD4$^+$ and CD8$^+$ T cell frequencies were below 5% of all αβ T cells, we additionally sorted 88 CD4$^+$ T cells and 88 CD8$^+$ T cells. Paired TCRαβ sequences were obtained from a total of 216 T cells.

10.5 *Data analysis*

Index sort data can usually be exported from the sorter software as FCM standard (fcs) files or as tables (comma-separated values or equivalent). Detailed procedures for data export depend on the instrument manufacturer, software, and software versions. When exported as fcs files, index sort data can be visualized using commercially available software for FCM data visualization ("Chapter VII: Data handling, evaluation, storage and repositories"). If it comes to sub-setting of index sort data based on certain criteria, the combination with other data formats (e.g., single cell sequencing), data visualization as heatmaps and/or multidimensional plots, commercially available tools are rarely available. Data analysis involving programming/statistical computer languages such as R (https://www.r-project.org/) among others is the approach of choice, highly flexible and powerful but requires knowledge in (bio-) informatics.

10.6 *Advantages*

Index sorting makes exact scatter and fluorescence characteristics of each single sorted event available for downstream analyses and can help identifying multidimensional phenotypes where conventional sorting approaches are limited. With immune phenotypes being correct in >99% of sorted cells [2180], index sorting is one of the most accurate technologies for isolation and multidimensional phenotyping of single cells at the protein level.

10.7 *Pitfalls*

Currently, there are no ready-to-use software solutions that make the entire richness of index sort information available to users with limited access to advanced bioinformatics.

10.8 *Top tricks*

For single cell index sorting, accuracy of the assigned phenotypes is critical. In addition to general requirements for cell sorting ("Chapter II: Setup - Instrument setup and quality control" and "Chapter III: Before you start: Reagent and sample preparation, experimental design"), stringent gating on live single events and plate targeting are critical. Parameters that could indicate data inconsistency should be included whenever possible. For example, in healthy individuals, particular T cell clones show characteristic CD4/CD8 expression. The identification of CD4$^+$ T cells in an otherwise CD8$^+$ T cell clone could hint to data inaccuracy.

When sorting into multi-well plates, depending on the desired downstream applications and the type of sorted events, immediate centrifugation after sorting may increase yield.

11 Sample banking for FCM

11.1 *Overview*

Sample banking provides benefits for FCM, namely, that samples can be batched for a more efficient workflow and reduced sample-to-sample variability. The most common banking method involves cryopreservation of PBMC, and the principles to be followed are the same for FCM as for other downstream methods that require viable cells. Consideration should be given to optimization and standardization of the procedure, including time to processing. Alternatives to cryopreservation of PBMC include the use of transport stabilizers (Streck, Smart Tube) or methods for cryopreservation of whole blood/granulocytes. These systems can allow interrogation of cells depleted in the generation of PBMC; and the Smart Tube system captures functional readouts through stimulation of fresh whole blood prior to fixation/stabilization.

11.2 *Introduction*

With time after collection, biological samples begin to degrade with regard to their functions and phenotypic markers. Depending on the target function(s) or phenotype(s), this degradation may be on the order of hours or days. But running fresh samples immediately by FCM is often not logistically feasible. It is also not necessarily the best workflow choice for all studies, due to the inefficiency of running single samples, and the variability that can be introduced from day to day. Biobanking offers a good alternative to running fresh samples immediately after collection. By far the most common biobanking approach is cryopreservation of PBMC (or other sources of immune cells). This has the advantage

that cells can be viably stored for many years in liquid nitrogen or equivalent cryogenic storage [2183], allowing for many different types of assays to be performed downstream. An important disadvantage is the loss of granulocytes, which are generally removed by Ficoll density gradient centrifugation prior to cryopreserving the PBMC. Another limitation is the partial loss of certain labile cell-surface markers and some functional characteristics with cryopreservation, as well as differential recovery of certain subtypes of cells (discussed under "Principles" below). If these affected cells, markers, or functions are critical to the FCM assays being used, then an alternative strategy needs to be taken. This could include viable cryopreservation of whole blood/granulocytes, which may bring additional caveats in terms of cell viability and function; or activation/fix/freeze systems, which are ideal for capturing a functional and phenotypic state, but which limit the downstream applications. As such, the choice of whether and how to bank samples prior to FCM involves a set of trade-offs, in which the investigator needs to evaluate the factors of greatest importance for a particular study, as well as the logistical constraints, prior to picking a sample banking approach.

11.3 *Principles*

With any sample banking method, it is necessary to minimize pre-analytical variations in the collection, processing, and storage stages. The pre-analytical variations can be different depending on the type of biosample, the type of analyte, and the method of analysis. PBMC isolation methods based on density gradient centrifugation, for example, Ficoll-Paque, Lymphoprep, and cell preparation tubes (CPT, Becton Dickinson) show comparable cell counts and viability [2184], but the different handling of cells may affect their detailed phenotypes and functions. For example, compared to Ficoll-Paque density gradient centrifugation, Lymphoprep showed a higher SEB-induced cytokine response from human PBMC [2185]. CPT, on the other hand, have a potential for increased erythrocyte contamination [2185], though they provide an easier workflow than other methods. In general, the selection of a specific PBMC isolation technique, aside from the cost, should be based on the downstream analysis.

In addition to the choice of the PBMC isolation technique, key protocol factors (e.g., time to processing, buffer, DMSO mixing, cell density, freezing rate, transfer to LN2, and thawing) also play a role in good cryopreservation [2186, 2187].

The time delay between blood sampling and handling of the sample may affect the immune cell subsets, their function, and activation markers [2188]. A standardized processing time for all samples (which still preserves the desired functions and/or phenotypes) will give the most comparable results. In addition to the time interval between the collection and the processing, the time of day of blood collection may also play a role in the recovered phenotypes and functions, due to circadian effects (reviewed in ref. [2189]).

Tompa et al. [2190] compared fresh versus cryopreserved PBMC (stored for 6 or 12 months) for three different isolation techniques, analyzing the subsets of $CD4^+$, $CD8^+$, and $CD25^{hi}$ lymphocytes. In general, there was no influence of isolation method or long-term cryopreservation. However, slightly different subsets of cryopreserved PBMC were described, e.g., naive and early-differentiated $CD4^+$ and $CD8^+$ effector memory T cells were affected by isolation and cryopreservation. Another group has reported changes in $CD4^+CD25^+$ T cell numbers in HIV+ individuals as a result of cryopreservation [2191], highlighting the possibility of disease-specific affects. Minor differences in B and T cell numbers with Ficoll separation versus whole blood have also been reported [2192]. Finally, resting cells post-thaw can have differential effects on T cell fine phenotyping [2193, 2194].

Some investigators have made further efforts to optimize methods and implement quality control to achieve improved cell viability [2195]. Both the centrifugation and washing conditions can be varied and a higher DMSO concentration (15%) in the freezing medium can be beneficial. A controlled cooling rate of –1°C/min can be achieved in different ways and is discussed in a previous section (see Chapter III Section 4 Dead cell exclusion, cell viability, and sample freezing).

Once banked, samples need to be kept at a constant optimal temperature. Fluctuations from liquid nitrogen to vapor phase, or frequent exposure to ambient temperatures as samples are removed will degrade their viability. Even fixed samples stored using Smart Tube proteomic stabilizer become clumped when exposed to repeated temperature fluctuations or storage above –80°C. For this reason, it may be advantageous to separate locations of samples intended for long-term storage versus those to which frequent access is needed. Additionally, when working with open sample boxes to retrieve specimens, the use of a liquid nitrogen tray is recommended, to minimize temperature fluctuation. Similarly, shipping in nitrogen dry shippers is preferable to dry ice shipments of frozen PBMC; however, a single, short-term exposure to dry ice during shipping will not result in any noticeable sample degradation [2186].

Another important consideration whenever biobanking extends to larger numbers of samples and studies is inventory management software and protocols. There are several good software packages designed specifically for freezer/biobank management (e.g., LabVantage, CentraXX, STARLIMS, SMARTLIS, Freezerworks, Biobank, Open Specimen, etc.), and they have advantages over simple solutions such as spreadsheets. These advantages may include audit controls, study–subject–sample hierarchy definition, searchability, access control, and so on, depending upon the particular software. Consideration should also be given to protocols for sample annotation. For example, a naming scheme can be used that follows the format 01-002-03, where 01=the study ID, 002=the subject ID, and 03=the visit ID. Further suffixes can designate derivative sample types, e.g., PBMC, serum, and so on. When combined with a barcode and barcode readers, such systematic naming can aid in organization and retrieval efforts. Linking relevant clinical information, de-identified to meet privacy requirements, can further make searching for desired samples much faster.

Table 97. Markers affected by cryopreservation and/or whole blood stabilization*

Affected by PBMC cryopreservation	Affected by Smart Tube stabilization
CD62L [861, 2187, 2194, 2196]	CCR6 (our unpublished data)
CCR5 [861]	CXCR5 (our unpublished data)
PD-1 [2197]	CD11b (our unpublished data)
PD-L1 [2197]	CD16 (our unpublished data)
CD20b [2198]	CD45RA (our unpublished data)
CD45RO [2187]	CD127 (our unpublished data)
CD28 [2194]	

* These lists are not exhaustive, nor do we rule out the use of the listed markers in cryopreservation or whole blood stabilization protocols. Results will depend upon the antibody clone/epitope targeted, as well as the permeabilization conditions used.

11.4 *Applications*

We can divide approaches for FCM sample banking into three general categories. The first is to run all samples fresh without any banking. This avoids any loss of cells, markers, or functions and thus allows for the full gamut of FCM assays to be performed. However, it also carries logistical challenges that may make it impossible for many studies; and the workflow creates more sample-to-sample variability, assuming that sample collection is staggered (i.e., not all samples are collected at once). Finally, unless combined with another method, it means no samples are available for later assays that are yet to be determined.

A second approach involves viable cryopreservation of cells for later FCM analysis. For human blood samples, this usually means cryopreservation of PBMC. While there are protocols for viable freezing of granulocytes and/or whole blood, these tend to be associated with greater loss of viability and/or staining resolution. In any case, cryopreservation allows for any number of later assays to be performed, subject only to how many cells are available. It also avoids much of the variability inherent in fresh real-time analysis of individual samples, since samples can be batched and therefore results are more comparable. However, it also means potential loss of certain cell types, markers, or functions (see Table 97). For example, CD62L is known to be variably lost upon PBMC cryopreservation [861, 2196]. Certain chemokine receptors (e.g., CCR5, [861]) can also lose some staining intensity, as can PD-1 and PD-L1 [2197]. Monocytes and their associated antigen processing functions can be preferentially lost with cryopreservation, such that functional assays that rely on protein antigen processing will be significantly compromised [638].

Both of the above approaches may be combined with initial shipping of fresh samples from a collection to an analysis or processing site. Obviously, this increases sample degradation, in ways that may be variable depending upon time and temperature in transit, and so on. NK and B cell frequencies and functional capacity may be most vulnerable to shipping [2199]. However, this may be an unavoidable sacrifice in multicenter studies. Even in cases where each individual collection site could in theory perform cryopreservation, it may be preferable to ship samples to a single processing site where there is better control of the procedure [2199].

A final approach involves using a sample preservation method (generally some type of fixation) that allows for later FCM analysis, even though the cells are no longer viable. A simple example is a blood collection tube such as Cyto-Chex (Steck, Inc.), that fixes cells upon blood draw, and confers stability of major lineage epitopes (e.g., for assays like CD4 counting) for up to 1 week. A more complex example is the Smart Tube system (Smart Tube, Inc.), which allows for stimulation of fresh blood, followed by timed release of a stabilizer solution, after which samples can be stored at –80°C for later analysis. This system has been used for signaling studies, where signals degrade quickly after sample collection (e.g., Gaudilliere et al. [2015]). Similarly, investigators have performed erythrocyte lysis followed by fixation and freezing, for later staining and analysis of leukocyte counts [2200]. Such schemes require time-dependent work at the collection site, in terms of pipetting and freezing samples. They also compromise the staining of certain cell-surface epitopes, due to fixation. Of course, these systems preserve granulocytes as well as PBMC, which may be useful in certain studies. Finally, it goes without saying that the fixed cells are no longer useful for further stimulation or functional assays not previously anticipated.

When performing an animal study, it is often possible to synchronize sampling such that fresh parallel analysis of all samples at a given time point is feasible. However, if the intent is to compare longitudinal samples from the same animals, it may be preferable to cryopreserve or stimulate/fix/freeze samples, so that all timepoints from a given animal can be run in a single batch. This of course assumes that the readouts being assessed can be adequately preserved with such methods.

With clinical studies, the sample collection is almost always staggered with subject enrollment, so biobanking becomes even more attractive, to allow batching of samples for analysis. The exception, again, is if the cells, markers, and/or functions of interest can only be assessed in fresh cells. With multicenter clinical studies, the considerations become even more complex, as one needs to balance the advantages of well-controlled procedures at a single central lab with the reduced sample degradation of processing and/or assays done at multiple sample collection sites [2199]. Alternately, a central lab can provide SOPs, analysis templates, training, and so on, to collection sites that then perform the assays in parallel [2201]. Inclusion of replicate control samples into the workflow can help determine reproducibility in the context of such workflows [2202].

11.5 *Equipment*

The viability and concentration of isolated PBMCs are important for the planned analysis. Besides manual conventional cell counting with trypan blue (TB) and a hemacytometer, there are advanced methods for PBMC cell counting, which provide automated documentation options, e.g., Scepter™, CASY®, and

Countess™ II. However, these devices require specialized consumables that result in additional costs. Also, the accuracy of automated cell counting varies, and is still limited by factors such as cell density, erythrocyte contamination, and so on. Thus, the "Gold standard" remains the experienced laboratory professional and validation with manual cell counting using trypan blue stained cells. However, in a multicenter study with several employees working at different levels, automated counting instruments have a great advantage because the results remain consistent.

Among the aspects of PBMC processing and cell counting, the freezing conditions of PBMC on the survival of immune cells are crucial. The point should be made to avoid defrosting cysts as well as long storage at –70°C. If interim storage is necessary, a dry shipper may be an alternative, which is provided for the transport of PBMC to the final storage site. Especially in multicenter clinical studies, it is important to minimize the artifacts from freezing and intermediate storage. In addition, the long-term storage conditions are crucial. Thus, the PBMC should be stored in controlled conditions with a permanent alarm and monitoring system.

In order to keep the quality of biobanks high, excellent management of the many biosamples is required. This requires complete documentation of the work processes in real time, including the tracking of aliquots and biosamples. Other important points are logistics management and cold chain monitoring. Large biobanks use modern laboratory information management systems (LIMS) to meet these requirements [2203]. These systems are advantageous for biobanks with multiple sites or multicenter studies. There are a variety of LIMS software that includes sample acquisition and sample storage with recorded sample and related factual information [2204–2206].

Additional features such as barcodes and barcode scanners are helpful to ensure that biosamples can be easily searched in biobanks. In addition to the individually coded tubes and racks, the LIMS also visually records the storage locations, thus ensuring a genealogy of the samples with process tracking. There are many barcode-coded tubes and the corresponding SBS racks on the market. Here, there is still a great need for investigations of the shelf life and permeability of the tubes. Since the tubes with PBMC are stored in nitrogen, they have to meet appropriate conditions. The coded tubes simplify handling by eliminating the need for time-consuming labeling. However, further purchases such as barcode scanners and other software will then be required.

11.6 *Experimental workflow and acquisition*

From the above discussion, there are clearly many different workflows possible with regard to sample banking. These vary from exclusive analysis of fresh samples to shipping, cryopreservation, and later batch analysis. Hybrid workflows are of course possible, with some assays done fresh, or aliquots of samples stimulated and/or fixed in real time for certain assays. Figure 242 shows a small selection of options and customizations available for PBMC isolation or whole blood stabilization, detailing the studies underlying these options/customisations [2198, 2207–2213, 2215]. In addition to the time of the possible processing steps, the different handling and cryopreservation media are also important.

In any case, once a sample banking workflow has been determined, it may be useful to test it using several control or pilot samples, prior to embarking on a large study. This will not only insure that the proposed logistics are workable, but can also give an idea of the variability to be expected, if, for example, replicate samples are drawn from the same healthy subject(s).

It is also worth considering acceptance criteria for large studies. These can be applied at multiple levels. For example, one might stipulate that fresh shipped samples that are not processed within 48 h of draw should be discarded. Or, that cryopreserved PBMC that do not yield a viability of >50% should not be further analyzed. While these types of rules will not eliminate technical variability in the results, they can at least reduce it, while at the same time saving reagents and technician time. The danger, of course, is that criteria that are too strict may result in loss of data that would still have been useful.

11.7 *Advantages*

As already detailed above, the advantages of sample banking can include a more efficient workflow, availability of samples for later, unforeseen assays, and better comparability between samples due to batching. In some cases, logistics strongly influence certain preferred banking workflows; for example, shipping blood to a central site in multicenter studies [2199]. But, because some FCM analytes are labile to shipping and/or cryopreservation, it may be necessary to set up hybrid schemes, where some assays are done fresh onsite, or at least some sample preparation is done fresh onsite (e.g., using Smart Tube or similar systems).

11.8 *Pitfalls*

As also outlined above, PBMC cryopreservation can result in preferential loss of certain cell types, markers, and functions. Well-known examples include loss of CD62L, certain chemokine receptors, and PD-1/PD-L1 with cryopreservation and thawing [861, 2196, 2197]; and loss of antigen-processing capabilities for functional assays. Restimulation assays are of course still possible after cryopreservation, particularly if using preprocessed antigens, i.e., peptides [638]. More globally, cryopreservation always results in some loss of cells versus fresh blood; and of course PBMC isolation results in loss of the granulocyte fraction.

11.9 *Top tricks*

While also mentioned above, we collect here certain generalizations that help to create high-quality sample banking studies for FCM.

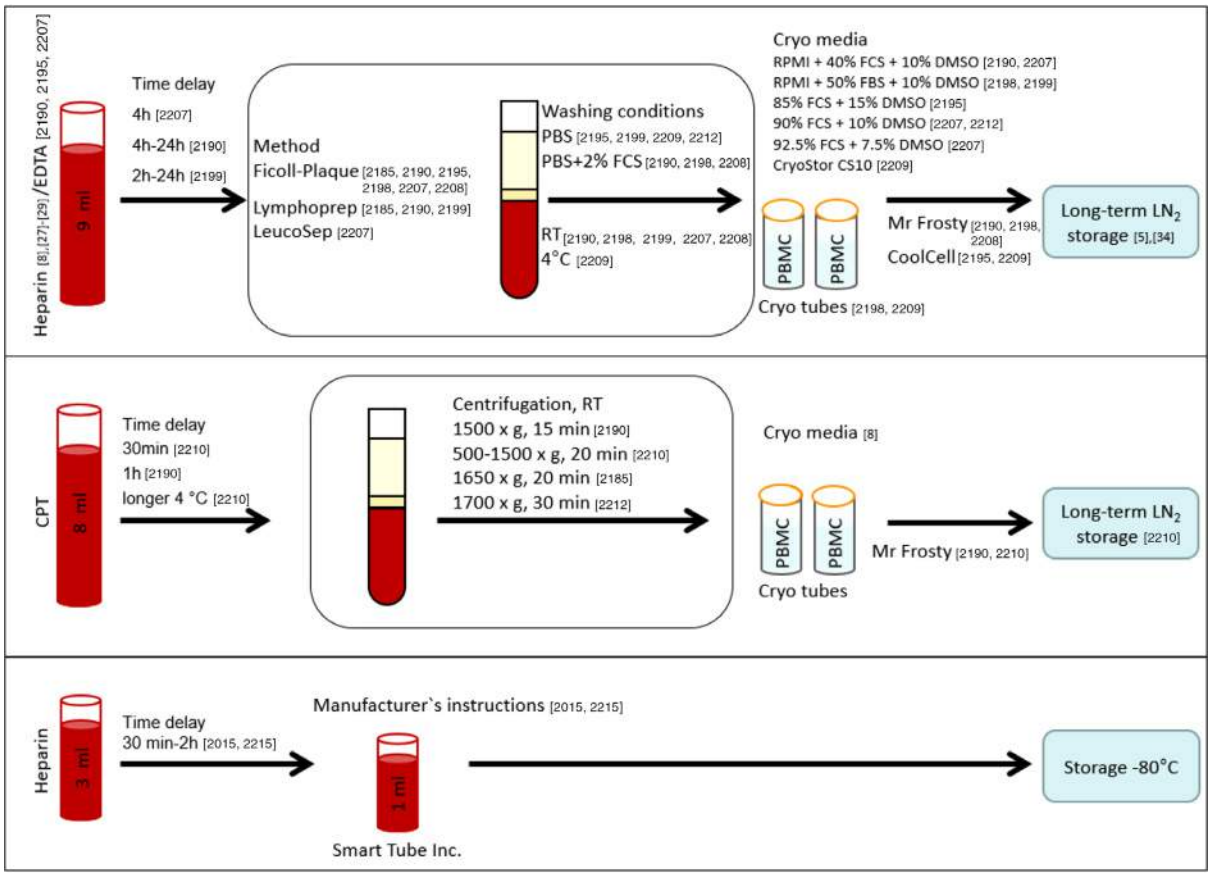

Figure 242. Brief overview of PBMC isolation or whole blood stabilization. References for each process are indicated.

1. Preanalytical variables, including time to processing, and choice of PBMC processing protocol, should be chosen according to the needs of the downstream assays, and should be tightly controlled.
2. If there are highly labile cells, markers, or functions that are key analytes for a given study, some level of fresh assays and/or fresh processing may be required.
3. Consider adopting a biobanking software, and create a logical scheme for sample annotation, prior to embarking on a banking study.
4. Equipment such as automated cell counters should be validated against manual methods. Although frequently biased with regards to accuracy, they may be preferable for their reproducibility across labs and operators.
5. Keep banked samples at a constant optimal temperature. For cryopreserved PBMC, use a liquid nitrogen tray when opening boxes to select samples. As much as possible, keep long-term samples separate from those that are actively being retrieved. Consider using nitrogen dry shippers for large or long (international) shipments. Use monitors and alarms to avoid undiscovered equipment failures.
6. Implement appropriate acceptance criteria (time limit to processing, viability post-thaw, etc.). These should help to reduce technical variability as well as wasted time and reagents; but they should not be so restrictive that samples are discarded that could still generate useful data.

12 High throughput screening

12.1 *Overview*

High-throughput screening is as a process by which a large number of samples are acquired in an automated fashion to identify molecules that exert biological activity on either a specific target or a cell population. Different technologies are used to detect the readout signal in a high-throughput screening assay such as automated microscopy, cell impedance measurement, time resolved fluorescence energy transfer (TR-FRET), or FCM. In this section, the use of high-throughput FCM (HTFC) will be described and examples for devices, screening assays, experimental setup, and data analysis as well as tricks and pitfalls will be shown.

12.2 *Introduction*

FCM has been used in almost every stage of the drug discovery process, including target identification and validation, lead and candidate selection, and safety studies for more than 30 years [2216].

This analytical technology has become very popular for drug development because of the possibility to analyze living cells out of a culture that is still available for further processing (e.g., nucleic acid extraction). However, only recently FCM has been applied also for primary high-throughput screenings. This might be due to the fact that for several years the drug screening field was dominated by target-based approaches, while cell based phenotypic assays were considered as too unspecific and risky [2217]. In addition, technical limitations of flow cytometers to process multiple samples did not make the technology very attractive for large screening campaigns. However, since microplate-based cell sampling and software capable of handling large data sets were developed the use of HTFC has become increasingly popular. In addition, affordable high quality HTFC devices were developed which also contributed to the popularity of HTFC not only in big pharma but also small companies and especially academic institutions. The possibility to use small sample and acquisition volumes and simultaneously monitor phenotypic responses of single cells in the presence of a large variety of compounds are major benefits of HTFC. The introduction of barcoding (See Chapter VIII Section 2 Barcoding) [1984] and the development of multiplex bead-based assays [2218] even allows measurement of secreted proteins or gene expression.

Recent development of laboratory automation even enable fully automated processes allowing cell culture, staining, washing, and measurement [2219]. The increasing popularity of this technology for modern drug discovery can be observed by the increasing diversity of applications in this field such as inhibition of non-homologous end joining in B cells [2220], identification of molecules inhibiting hantavirus cell entry [2221], Ab development [2222], or examination of CAR-T cell mediated cytotoxicity [2223].

12.3 *Principles of the technique being described*

HTFC is the combination of classical single cell multiparametric FCM with an autosampler delivering the sample to the FCM. The term high throughput refers to the number of samples being acquired and not to the number of cells being measured. Usually only short acquisition periods (1–3 s) are applied to ensure measurement of multiple samples in short time. Different plate formats (96, 384, or even 1536 well plates) can be handled by modern autosamplers. The preferred plate format for primary drug screenings depends on the format that the compound library is stored. Compatible plate formats are used to allow easy transfer of compounds from the storage plate to the assay plate. The most common screening format is 384-well plates, as most small molecule libraries are stored in this format. Almost all vendors of FCM offer machines capable of handling 96-well and 384-well plates. However, sampling of microvolumes (down to 1 μL) from 1536 well plates is so far only possible with the iQue screener (intellicyt). The acquisition time per sample can be individually adjusted which in turn influences the measurement time per plate. In the setup described below (Fig. 243), ten 384-well plates were measured per day resulting in a throughput of 3840 samples per day. However, it is still possible to increase the throughput when fully automated systems like liquid handling robotics are used. Other high-throughput flow cytometers (HTFCM) on the market are based on single sample acquisition and generation of individual FCM standard (FCS) files. They also come with optional washing steps in between the samples (e.g., MACS® QuantX, Miltenyi) to prevent sample carryover. Depending on the system, there are differences in speed and sample acquisition time but usually a 384-well plate can be measured in about 30 min. Data analysis can be performed with software shaped for high-throughput data analysis, e.g., Forecyt (intellicyt) or Genedata Screener (Genedata) that displays the samples in plate format and is designed to help the user to easily identify hits on a plate, calculate thresholds, Z-factor, and even combine and overlay results from different screening campaigns. However, it is also possible to analyze the samples with software like FlowJo (FlowJo, LLC), WinList, or even free (mostly R-based) FCM software [2077].

12.4 *Applications*

High-throughput screening technologies such as automated microscopy, cell impedance measurement, or TR-FRET mostly generate only a single readout. In contrast, HTFC offers the multiparameter analysis of particles and cells. This is especially useful for phenotypic screening assays where different cellular parameters (e.g., size, viability, surface molecule expression) or even different cell populations can be simultaneously analyzed to identify the most potent and less toxic hit compounds. HTFC can be performed using living cells, fixed cells, suspension cells, or even adherent cells [2224] and bead based assays. Examples for applications are Ab development [2222, 2225], toxicology [2226, 2227] and apoptosis studies [2228], analysis of protein phosphorylation [2003], identification of stem cell expanding compounds [2229], identification of immune enhancing [2230] or immune inhibiting compounds [2231], monitoring of chemotherapy side effects [2232], and characterization and cytotoxicity monitoring of engineered T cells [2223]. In addition, secreted molecules such as chemokines or cytokines as well as gene expression can be quantified using barcoded bead based multiplex assays [2233, 2234]. Specialized HTFCM can measure up to 500 analytes per sample in high throughput (e.g., FLEXMAP 3D, Luminex). Even the simultaneous analysis of cells and beads in one sample can be performed [2235]. Thus, the variety of different HTFC applications illustrates the flexibility this method offers for assay design and high-throughput screening. The HTFC assay described in Fig. 243 was designed to identify compounds inducing the expression of Foxp3–the master transcription factor of regulatory T cells. Therefore, spleen and lymph node cells from reporter mice were incubated with 40 000 small synthetic molecules (provided by the screening unit of the FMP Berlin) and the expression of enhanced green fluorescent protein (EGFP) under the control of the Foxp3 promotor was analyzed by FCM.

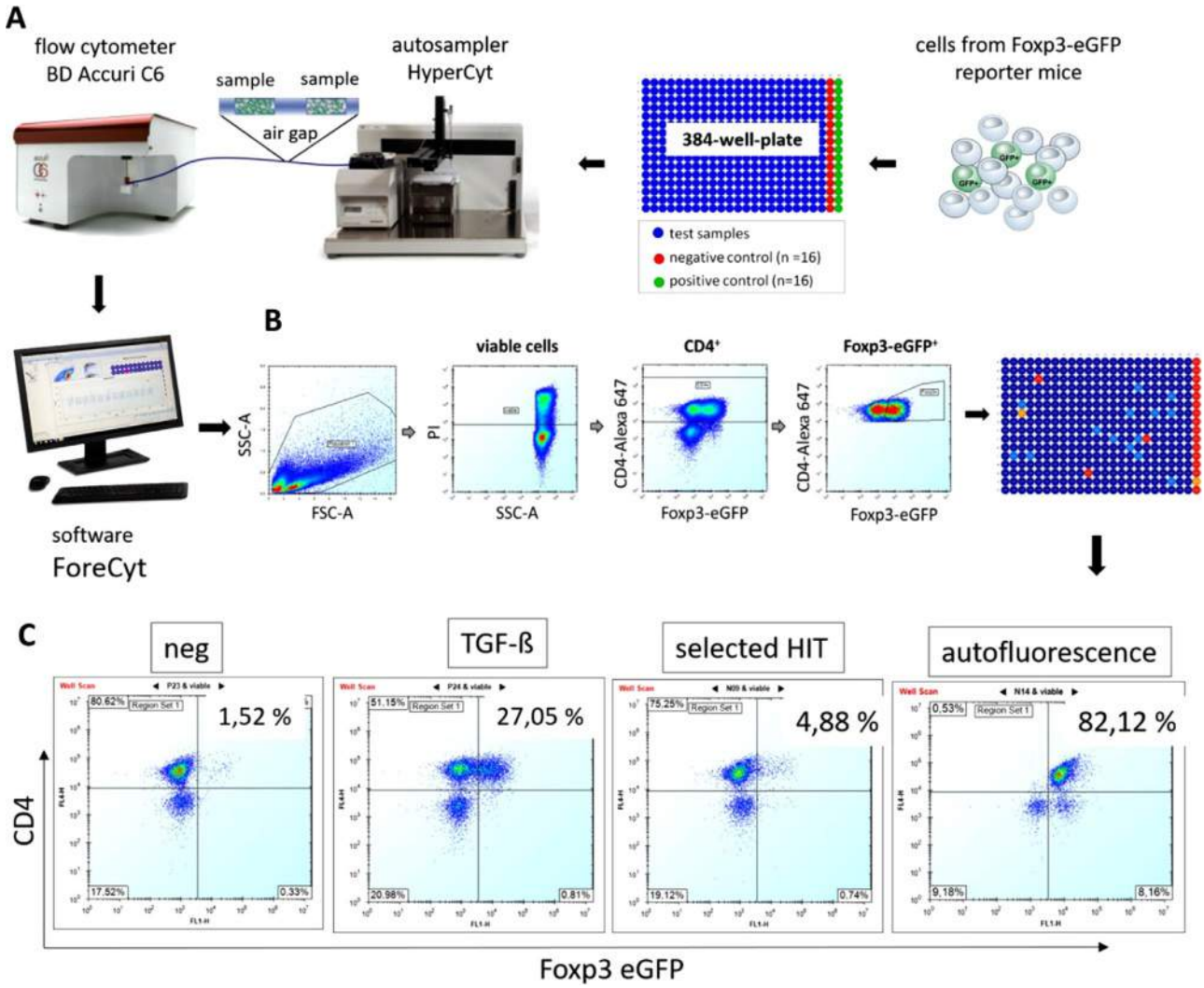

Figure 243. Experimental workflow, data deconvolution, and hit selection of an HTFC drug screen. (A) Primary immune cells from Foxp3-eGFP reporter mice are cultured in the presence of specific stimuli and compounds from a small molecule library. The autosampler is harvesting the cells from 384-plates and delivers it consecutively, without washing steps, to a connected cytometer. Air gaps in between samples created by position change of the sampling probe are necessary for sample deconvolution. (B) Data deconvolution to identify Foxp3-eGFP inducing hit compounds. Data of the entire 384-well plate is displayed. Hits and positive controls can be located on the plate heat map. (C) Single well analysis for hit verification, analysis of assay robustness, quality of controls, and exclusion of false positives (autofluorescence).

12.5 *Equipment*

To perform HTFC with reasonable throughput the assays should at least be set up in 96-well formats. Necessary hardware components are the autosampler, a FCM, and a computer with data analysis software. Several FCM offer already build in autosampler for 96- or even 384-well formats: iQue screener (intellicyt), MACS® Quant X (Miltenyi), ZE5 (BioRad), Cyte (ACEA Biosciences), Cytoflex (Beckman Coulter), and the spectral analyzer SA3800 (Sony). Other distributors offer compatible add-on autosampler for their devices like Attune (Thermo Fisher) or Beckton Dickinson instruments that can be easily connected. For the phenotypic assay described here, the HyperCyt® autosampler (intellicyt) [2236] connected to a FCM (Accuri) and a computer equipped with a specialized software capable of handling and analyzing the data (ForeCyt®) (Fig. 243A) was used.

12.6 *Experimental workflow and acquisition*

The assay described in Fig. 243 was performed in 384-well polypropylene U-bottom plates. Compounds were diluted in RPMI medium (10% FCS, 1% Pen/Strep, 1% Pyruvat, 2.5% HEPES, 0.5% Gentamycin, 0,01% Mercaptoethanol) and spotted on the assay plate. The final concentration of the screened compounds was 1 μM. Primary immune cells of Foxp3-eGFP reporter mice (DEREGxDo11.10) [2237] were isolated from spleen and lymph nodes and depleted of $CD8^+$ T cells by magnetic separation (Mil-

tenyi). Ovalbumin (1 μg/mL) and IL-2 (10 ng/mL) was added to the cell suspension for stimulation. The positive control additionally contained TGF-ß (5 ng/mL) as inducer of Foxp3 expression. The number of cells seeded per well was 3×10^5 cells. Experience showed that $CD8^+$ depleted cells from one animal are sufficient for up to four plates. The plate included 352 wells with compounds and 16 wells each for negative and positive controls (Fig. 243A). This number of controls is necessary to obtain statistical power for calculation of assay robustness (Z-factor). Incubation was performed at 37°C for 72 h and plates were subsequently centrifuged. The supernatant was discarded and staining solution containing CD4-Alexa647 mAb (GK 1.5; DRFZ) and PI (1 μg/mL) was added. The plates were shaken at 3000 rpm for 10 s on the plate shaker included in the HyperCyt autosampler and subsequently incubated for 15 min at 4°C with. Acquisition was performed right after incubation without washing. The acquisition time was set to 3 s, which results in approximately 1×10^4 recorded events per sample. Washing steps of 3 s were programmed after every 16 samples (1 column). The autosampler harvests the cells from 384-plates and delivers it consecutively, without washing steps, to a connected cytometer. When the sampling probe switches between individual wells, air gaps are created which interrupt the sample flow (Fig. 243A). As only one single FCS file is recorded for the whole plate these air gaps serve as reference point for the software to recognize individual samples and allocate them to the wells. Using these acquisition settings, the measurement time per plate was 37 min. The daily throughput was 3840 samples.

12.7 *Data analysis*

Following acquisition, the data are uploaded to the ForeCyt software where the data was processed and well gates were positioned automatically according to time and position of air gaps that separated the sample flow. The correct allocation of the well gates should be manually controlled to avoid misallocation and thereby misinterpretation of data. Gating of lymphocytes, live cells, $CD4^+$ T cell, and $Foxp3^+$ T cell populations was performed and percentages of $Foxp3^+$ cells are displayed in a 384-well heat map to facilitate hit identification (Fig. 243B). Frequencies of viable and Foxp3-$eGFP^+$ cells are exported to an excel sheet. Mean and SD of negative and positive controls are calculated and accordingly the Z-factor [2238] is calculated to obtain a measure of assay quality. Hit identification thresholds are set according to reporter expression (≥mean of negative control $+3x\sigma$) and cell viability (mean of negative control $-3x\sigma$). Hits passing the thresholds are again reanalyzed to exclude false positives (e.g., caused by autofluorescent compounds; Fig. 243C). The final hits are selected for further validation.

12.8 *Advantages*

- Speedy automated acquisition of hundreds of samples
- Simultaneous multiparameter analysis of cells (cellular size, viability, surface molecule expression)
- Multifactorial analysis [2077] of different cell populations in one sample in the presence of screening compounds
- Identification of toxic compounds already at screening stage of the drug discovery process helps to identify and focus on the right drug candidates
- Autosampler capable of acquiring samples from 96-, 384-, or even 1536-well plates help to drastically reduce the sample size which in turn reduces screening material (e.g. cells, less animals if primary cells are used), costs for reagents (Abs, buffers)
- False positive results resulting, e.g., from interaction of autofluorescent compounds with cells can be easily excluded which is not possible by, e.g., automated microscopic screenings
- label-free screenings are now possible with the use of spectral analyzers (e.g., SA3800, Sony).

12.9 *Pitfalls*

- Cells will accumulate at the well bottom if plates (especially 384- and 1536-well) are not properly shaken.
- Clogging of the device might occur but the software does always recognize and warn.
- Make sure that samples do not evaporate during measurement especially when working with very small volumes. Plate sealing helps and autosampler probe can perforate certain seals but make sure that the glue of the seals does not clog the probe. FCM manufacturers will help identifying the right seals.
- Check for unusual high signals. False positives might result from autofluorescent compounds sticking to cells.
- Check for carry over effect of the autosampler probe.

12.10 *Top tricks*

- Before starting the screen perform test runs to check the following: (1) quality of the assay by comparing negative and positive controls and calculate the Z-factor to determine the quality of the assay (SNR and signal to background ratio) [2238]. A Z-factor > 0.6 is desirable, (2) check for DMSO sensitivity of the cells. DMSO concentrations should be $<1\%$.
- The washing step after cell staining can be omitted that saves time and limits eventual loss of cells
- Determine carry over effect of autosampler probe to prevent intersample contamination. To prevent carry over include wells containing wash buffer in the assay well.
- To prevent clogging of the sampling probe or tubing QSol Buffer (intellicyt) can be used.
- Calibrate plate alignment and sampling probe depth before and if possible, also during screen to ensure proper sample uptake.
- Frequently shake the plate or mix the samples during the measurement to prevent cell accumulation at the well bottom.

– Frequently monitor data acquisition and sample flow during measurement to detect eventual problems (clogging of sampling probe, low event rate).
– Make sure to reserve enough space for positive and negative controls. On a 384-well plate it´s usually 16 positive and 16 negative controls that serve to calculate the assay robustness.
– Personalized R-based programs might help to process data as flow analysis software is often not designed to handle screening data and help with hit identification.

13 Core Facility setup and housekeeping/shared resource laboratory (SRL) management

Technologies and instrumentation are rapidly evolving and there is an increasing demand for sophisticated and high-priced technologies across the life sciences. Access to state-of-the-art infrastructure has become essential for success in scientific research. This has led to the development of Core Facilities also known as Shared Resource Laboratories (SRLs), core resources of institutions that provide highly skilled technology scientists and advanced instrumentation to enhance the scope and quality of biomedical research [2239]. The term "Shared Resource Laboratory" has been adopted to better define the role of shared instrumentation laboratories as a scientific partnership with researchers within an institution. SRLs and core facilities are called the prerequisite for breakthroughs in the life sciences, because they are collaborators who will not say "no," unless there are technical feasibility concerns [2240].

Cell sorters, high-end flow cytometers, imaging flow cytometers, and mass cytometers are usually placed in SRLs. There are two different approaches for setting up a shared resource laboratory: (i) a pool of existing instrumentation from different groups/principal investigators is put together into an SRL (bottom-up approach) or (ii) the management of an institution makes a strategic investment in central research infrastructure (top-down approach). In order to achieve the desired result—the many synergistic effects of a successful SRL—several points must be taken into consideration. Operational best practice manuals have been published recently for both FCM and advanced light microscopy SRLs, two classes of core facilities that share many challenges in common [2241, 2242]. In this section, we will give a short overview of important aspects for successful SRL management. Key topics for SRL management are staffing, education, finances, data management, quality assurance (QA)/quality control (QC), laboratory space, and safety/biosafety.

13.1 *Staffing*

An SRL needs a head or director to oversee and manage the facility, who consults with researchers and laboratory staff across a large range of disciplines with different level of technical expertise. The head should have a scientific background reflecting the need for scientific and research expertise in SRLs. In addition to the head, more personnel are needed to successfully operate a larger SRL, to ensure continuous operation and cover vacations, sick leave, and business trips. Cell sorters are commonly operated by sorter operators, who need to be highly qualified, knowledgeable, and service-oriented people. In an SRL, the ability to interact with people is as important as technical skill. A recent publication describes careers in SRLs and lists skills and qualifications, because SRL positions require certain common sets of skills [2243]. Among the most important qualifications are a love of learning, the ability to keep up with new technologies, and a passion for solving problems, such as troubleshooting equipment problems. SRL staff acts in a service/customer-support-type manner, and reacts to changing tasks and priorities throughout the day. Up to hundreds of people use an SRL, therefore an ability to work with individuals with very different personalities is required [2243]. Working in an SRL is a very rewarding job if one has the right skills, interests, talents, and service-oriented attitude. Determining staffing levels is a difficult challenge for SRLs. Key factors are the number and complexity of shared instruments, and the number of users needing support and training. The best practices for FCM SRLs published by the International Society for Advancement of Cytometry (ISAC) give some advice on this topic [2241]. A certain amount of SRL staff time should be reserved for consultation with users, educational activities, and optimization and development of new techniques. Such developments may be formally published as SRL Communications within the journal *Cytometry Part A*, a new publication format created to provide a vehicle for SRL-focused subjects [2244]. SRL staff members need ongoing continuing education, for example through regular attendance of conferences or courses, in order to optimally support users.

13.2 *Education*

In addition to the needs of SRL staff, the users of the SRL also require education. Depending on the institution, researchers with varying and diverse expertise levels will use the SRL. The first step with a new project should always be an initial consultation in which the project is discussed between the user and SRL staff. It is crucial to offer a training program, consisting of theoretical and practical education, which includes experimental planning and data analysis. If independent usage of equipment by users is a goal, users should be made aware of all required training steps, and facilities should implement measures to ensure users' competency, for example by checking the users' skills with a practical exam at the instrument. The users must understand that training is mandatory prior to instrument usage. They should be reminded that they are operating expensive equipment that is needed for numerous scientific projects, and therefore any instrument downtime due to careless handling will affect their own projects and also those of their colleagues. Instructions are best placed next to the instruments in a written form or as standard operating procedure (SOP). Each SRL should have user guidelines in which the main topics are clarified.

13.3 *Finances*

SRLs should provide high-quality, cost-effective services. Significant costs are associated with cytometry services; depending on the institution, different financial models are in place. Usually, SRLs charge usage fees, but some institutions cover costs under a central budget. Nevertheless, the preparation and periodic review of an annual operational budget is critical. The calculation of usage fees can be based on a full economic cost calculation; in this case, institutions and facility heads must consider which costs should be covered by SRL users and which costs will be subsidized by the institution. Ferrando-May et al. published an example cost calculation; although it is for a microscopy SRL, the approach is very similar for a flow cytometry SRL [2242]. Other publications show an approach for a cost accounting method [2245], and metrics for evaluating cell sorting services [2246]. Independent of whether usage fees are charged by a facility or not, the role of the SRL should be mentioned in scientific publications in the acknowledgements section, together with any grant numbers through which instruments have been purchased. This is not just a kind way of saying 'Thank you!' for the effort SRL staff has put into a published result. It very important that SRLs and SRL staff are formally acknowledged for their contributions, because the evaluation of SRL performance is often based on numbers of published acknowledgements.

13.4 *Data management*

Data management and data analysis are critical to the experiments performed in an SRL. It is in the interest of research institutions that data obtained in their SRLs complies with the highest scientific standards. If the flow cytometers are not operated by SRL staff, the users operate the instruments independently. Therefore, the large number of users with their diverse projects does not allow for a proper quality control by SRL staff. Thus, responsibility for data, including experimental design and compliance to scientific best practices, lies in the hands of the users and their PIs. To ensure the proper description of experiments, SRLs can offer proof-reading of methods parts of scientific publications. Transferring data off instrument PCs is the first step to accessing to data. Here, users should refrain from using USB devices (flash drives, external hard drives) due to the high risk of spreading computer viruses and malware. A centrally accessible file server is an option to overcome this problem. The facility should state clearly who has the responsibility to transfer and store data and when data will be deleted from SRL computers and file servers. In clinical environment, there may be additional regulations addressing data management.

13.5 *Quality assurance and quality control*

SRLs must monitor instruments to maintain optimal performance. In a multi-user environment such as an SRL, contamination, optical misalignment, damage, or careless handling can happen on a daily basis. Regular system checks and performance tracking must be common practice, and the quality control (QC) data should be stored and made available to the SRL users, if needed. It is important to perform preventative maintenance for the instruments. Here, maintenance contracts with instrument vendors can help minimize instrument downtime. QC criteria can be rather different depending on the equipment, but Barsky et al. give some advice on this topic [2241].

13.6 *Laboratory space*

SRLs should occupy highly visible space that has the same quality as research labs. The quality of laboratory space expresses the commitment of the institution to state-of-the-art technologies [2239]. Large instrumentation, such as cell sorters, image cytometers, or mass cytometers have special room requirements, especially in regard to temperature stability. Other important physical environmental factors are square footage, humidity, presence of vibrations, electricity, and gas supplies [2241, 2242]. SRL lab space should be designed and equipped in close collaboration with SRL staff, as reconstruction after installation is expensive and will always interfere with SRL operations. High quality lab space also makes it feasible to fulfil safety and biosafety requirements.

13.7 *Safety/Biosafety*

Biosafety regulations vary depending on regional authorities; nevertheless, the main goal is always to protect people from biological hazards, such as infectious diseases caused by human pathogens. The potential of cytometers and especially cell sorters to create aerosols during cell sorting procedures places SRL staff and users at risk of laboratory-associated infections (LAI). A risk assessment must be performed, resulting in a risk management solution, encompassing personal protective equipment, safe laboratory procedures, and laboratory design for containment [143]. Placing cell sorters in biosafety cabinets for aerosol containment is one method to reduce the risk to sorter operators [2247]. The Biosafety Committee of the International Society for Advancement of Cytometry (ISAC) published cell sorter biosafety standards [143] and offers additional information on the ISAC webpage (https://isac-net.org/page/Biosafety). In an SRL, users bring a diverse range of samples to be analyzed or sorted. It is very important that the SRL keep track of the biosafety levels of all samples, including genetically modified organisms. This can be achieved by asking users to fill out questionnaires about their samples before use in the SRL. An institutional biosafety committee can help to determine the rules how to handle potentially infectious samples. SRLs may need to keep records for regional authorities. There are many additional safety topics that must be considered, including laser safety, waste management, and protection from chemical hazards, although these topics can vary due to regional regulations. Emergency and disaster planning is described elsewhere [2248].

In addition to the resources cited above, the Shared Resource Lab section of CYTO University (CYTO U) offers a seven-part series of webinars on SRL best practices, four webinars on Finance 101, and webinars on a great many other topics related to establishing and operating an SRL. CYTO U is ISAC's online portal for on-demand, peer-reviewed cytometry education, a great educational resource (http://cytou.org).

Acknowledgements: Work in the laboratory of Dieter Adam is supported by the Deutsche Forschungsgemeinschaft (DFG, German Research Foundation)—Projektnummer 125440785 – SFB 877, Project B2.

Petra Hoffmann, Andrea Hauser, and Matthias Edinger thank BD Biosciences®, San José, CA, USA, and SKAN AG, Bale, Switzerland for fruitful cooperation during the development, construction, and installation of the GMP-compliant cell sorting equipment and the Bavarian Immune Therapy Network (BayImmuNet) for financial support.

Edwin van der Pol and Paola Lanuti acknowledge Aleksandra Gąsecka M.D. for excellent experimental support and Dr. Rienk Nieuwland for textual suggestions. This work was supported by the Netherlands Organisation for Scientific Research – Domain Applied and Engineering Sciences (NWO-TTW), research program VENI 15924.

Jessica G Borger, Kylie M Quinn, Mairi McGrath, and Regina Stark thank Francesco Siracusa and Patrick Maschmeyer for providing data.

Larissa Nogueira Almeida was supported by DFG research grant MA 2273/14-1. Rudolf A. Manz was supported by the Excellence Cluster "Inflammation at Interfaces" (EXC 306/2).

Susanne Hartmann and Friederike Ebner were supported by the German Research Foundation (GRK 2046).

Hans Minderman was supported by NIH R50CA211108.

This work was funded by the Deutsche Forschungsgemeinschaft through the grant TRR130 (project P11 and C03) to Thomas H. Winkler.

Ramon Bellmàs Sanz, Jenny Kühne, and Christine S. Falk thank Jana Keil and Kerstin Daemen for excellent technical support. The work was funded by the Germany Research Foundation CRC738/B3 (CSF).

The work by the Mei laboratory was supported by German Research Foundation Grant ME 3644/5-1 and TRR130 TP24, the German Rheumatism Research Centre Berlin, European Union Innovative Medicines Initiative - Joint Undertaking - RTCure Grant Agreement 777357, the Else Kröner-Fresenius-Foundation, German Federal Ministry of Education and Research e:Med sysINFLAME Program Grant 01ZX1306B and KMU-innovativ "InnoCyt", and the Leibniz Science Campus for Chronic Inflammation (http://www.chronische-entzuendung.org).

Axel Ronald Schulz, Antonio Cosma, Sabine Baumgart, Brice Gaudilliere, Helen M. McGuire, and Henrik E. Mei thank Michael D. Leipold for critically reading the manuscript.

Christian Kukat acknowledges support from the ISAC SRL Emerging Leaders program.

John Trowsdale received funding from the European Research Council under the European Union's Horizon 2020 research and innovation program (Grant Agreement 695551).

The following formed the writing committees for the indicated sections:

Andrea Cossarizza (Introduction: Guidelines for the use of flow cytometry and cell sorting in immunological studies (second edition)); Christoph Goettlinger (I.1 Fluidic system of a flow cytometer); Toralf Kaiser, Konrad von Volkmann (I.2 Optics and electronics); Toralf Kaiser, Mark Dessing (I.3 Flow cytometry, including flow cytometry cell sorting); Alan M. Stall (II.1 Compensation); Steffen Schmitt (II.2. Maintenance); James Wing (II.3 PMT voltage optimization); Hyun-Dong Chang, Andreas Radbruch (III.1 Controls: Determining positivity by eliminating false positives); Hyun-Dong Chang, Van Duc Dang, Andreas Radbruch (III.2 Titration: Determining optimal reagent concentration); Wolfgang Beisker (III.3 Preparation of single-cell suspensions); Gemma A. Foulds, Gabriele Multhoff, A. Graham Pockley (III.4 Dead cell exclusion, cell viability and sample freezing); Vincent Shankey, Sue Chow, David Hedley (III.5 Cell fixation and permeabilization for flow cytometric analyses); Srijit Khan, Yanling Liu, Leslie Y.T. Leung, Götz R.A. Ehrhardt (III.6 Variable Lymphocyte Receptor Antibodies); Marcus Eich (III.7 New antibody reagents); Steffen Schmitt (Pre-enrichment of low abundant cell populations prior to acquisition/cell sorting); Charlotte Esser, Liping Yu, Diether Recktenwald, Steffen Schmitt (IV.2 Parallel cell sorting); Joe Trotter, Toralf Kaiser, Sarah Warth, Désirée Kunkel, Martin Büscher, Christian Peth, Esther Schimisky, Leonie Wegener, Daryl Grummitt, John Foster (IV.3 Serial cell sorting); Toralf Kaiser (IV.4 Collecting cells); Petra Hoffmann, Andrea Hauser, Matthias Edinger (IV.5 Flow-Cytometric Cell Sorting under GMP Conditions); Sara De Biasi, Milena Nasi, Lara Gibellini, Marcello Pinti, Andrea Cossarizza (V.1 Rare cells: General rules); Derek Davies, Rachael Walker (V.2 Organisms, cells, organelles, chromosomes and extracellular vesicles); Lara Gibellini, Marcello Pinti, Anna Iannone, Milena Nasi, Sara De Biasi, Andrea Cossarizza (V.3 Mitochondria); Edwin van der Pol, Paola Lanuti (V.4 Extracellular vesicles); Alexander Scheffold, Andreas Grützkau (V.5 Surface parameters); A. Graham Pockley, Gabriele Multhoff (V.6 DNA synthesis, cell cycle and proliferation); Graham Pockley, Gemma A. Foulds, Gabriele Multhoff (V.7 Measuring cell death mechanisms); Rieke Winkelmann, Sabine Adam-Klages, Dieter Adam (V.7.3 Necroptosis); Rieke Winkelmann, Sabine Adam-Klages, Dieter Adam (V.7.4 Pyroptosis); Mar Felipo-Benavent, Guadalupe Herrera, Beatriz Jávega, Alicia Martínez-Romero, José-Enrique O'Connor, Francisco Sala-de-Oyanguren (V.8 Phagocytosis); Hanlin Zhang, Isabel Panse, Sharon Sanderson, Anna Katharina Simon (V.9 Autophagy); Laura G. Rico, Michael D. Ward, Jolene A. Bradford, Jordi Petriz (V.10 Reactive oxygen species production with minimal sample perturbation); Baerbel Keller, Marie Follo, Klaus

Warnatz (V.11 Intracellular Ca^{2+} mobilization by means of Indo-1 AM); Linda Schadt, Maries van den Broek, Susanne Ziegler, Glòria Martrus (V.12 mRNA); Derek Davies, Alfonso Blanco, Andrew Filby, Timothy P. Bushnell (V.13 Transcription factors); Jakob Zimmermann, Christina Stehle, Hyun-Dong Chang, Andreas Radbruch (V.14 Intracellular parameters); T. Vincent Shankey, Sue Chow, Lilly Lopez, David Hedley (V.15 Measurement of signal transduction pathways by flow cytometry); Katharina Pracht, Sophia Urbanczyk, Tobit Steinmetz, Hans-Martin Jäck, Dirk Mielenz (V.16 Assessing Lymphocyte metabolism through functional dyes); Alessio Mazzoni, Laura Maggi, Francesco Annunziato (V.17.1 Measurement of signal transduction pathways in human T cells); Steven L.C. Ketelaars, Anastasia Gangaev, Pia Kvistborg (V.17.2 Measuring antigen specific T cell responses); Matthias Schiemann, Immanuel Andrä, Kilian Schober, Dirk H. Busch (T cell assays-MHC multimers); Alexander Scheffold, Petra Bacher (Functional readouts); Alessio Mazzoni, Laura Maggi, Lorenzo Cosmi (V.17.6 Live cytokine-producing cell sorting with cytokine secretion assay™); Laura Maggi, Alessio Mazzoni, Francesco Liotta (V.17.7 Quantification of soluble cytokines with cytometric bead array); Thomas Schüler, Gerald Willimsky, Tristan Holland, Salvador Vento-Asturias, Natalio Garbi (V.17.8 Cytotoxicity); James Wing, Ilenia Cammarata, Vincenzo Barnaba, Shimon Sakaguchi (V.17.9 Treg suppression assays); Johanna E. Huber, Dirk Baumjohann (V.18 Adoptive T and B cell transfer as a read-out for antigen-specific immune responses in mice); Jessica G. Borger, Kylie M. Quinn, Mairi McGrath, Regina Stark (VI.1.1 Murine CD4 and CD8 T cells); Kylie M. Quinn, Luka Čičin-Šain, Katarzyna M. Sitnik (VI.1.5 Immune senescence (aging) in murine T cells); Michael Delacher, Juhao Yang, Markus Feuerer, Jochen Huehn (VI.1.6 Murine $Foxp3^+$ regulatory T cells); Immo Prinz, Anneke Wilharm, Inga Sandrock (VI.1.7 Murine γδ T cells); Heike Kunze-Schumacher, Andreas Krueger (VI.1.8 Murine NKT cells); Heike Kunze-Schumacher, Andreas Krueger (VI.1.9 Murine mucosal-associated invariant T (MAIT) cells); Immo Prinz, Joana Barros-Martins (VI.1.10 Murine intestinal intraepithelial T cells); Pleun Hombrink, Ester B.M. Remmerswaal (VI.1.11 Human CD4 and CD8 T cells); Anna Oja, Pleun Hombrink (VI.1.12 Human tissue resident memory T cells); Yotam Raz (VI.1.13 Immune senescence (aging) of human T cells); Kirsten A Ward-Hartstonge, Laura Cook, Dominic A Boardman, Sabine M Ivison, Jennie H. M. Yang, Eleni Christakou, Timothy I.M. Tree, Megan K Levings (VI.1.14 Human $FOXP3^+$ regulatory T cells); Anouk von Borstel, Martin S. Davey (VI.1.15 Human γδ T cells); Christopher M. Harpur, Dale I. Godfrey, Garth Cameron (VI.1.16 Human NKT cells); Garth Cameron, Nicholas A. Gherardin, Alexandra J. Corbett, Sidonia B. G. Eckle, James McCluskey, Dale I. Godfrey, Hui-Fern Koay (VI.1.17 Human mucosal-associated invariant T (MAIT) cells); Larissa Nogueira Almeida, Britta Frehse, Rudolf Armin Manz (VI.2.1 Murine B cells and their subsets, including Bregs); Thomas Weisenburger, Andreas Acs, Thomas H. Winkler (VI.2.2 Murine Germinal Center B cells); Annika Wiedemann, Andreia Lino, Thomas Dörner (VI.2.3 Human B cells and their subsets); Annika Wiedemann, Andreia C. Lino, H. Kristyanto, Hans U. Scherer, Thomas Dörner (VI.2.4 Human B cells recognizing defined (auto)antigens); Oliver Wirz, Willem van de Veen, Mübeccel Akdis (VI.2.5 Human regulatory B cells); Willem van de Veen, Oliver Wirz, Mübeccel Akdis (VI.2.6 Human immunoglobulin heavy chain isotypes); Sebastian Schulz, Katharina Pracht, Ljiljana Cvetkovic, Dirk Mielenz, Dorothea Reimer, Wolfgang Schuh, Hans-Martin Jäck (VI.3.1 Murine antibody-secreting plasmablasts and plasma cells); Antonia Niedobitek, Henrik E. Mei (VI.3.2 Human antibody-secreting cells); Daniela C Hernández, Christina Stehle, Andreas Diefenbach, James Di Santo, Chiara Romagnani (VI.4 Innate Lymphoid cells); Lorenzo Moretta, Linda Quatrini, Genny del Zotto (VI.5 Natural Killer (NK) cells); Regine J. Dress, Alicia Wong, Ahad Khalilnezhad, Wan Ting Kong, Charles-Antoine Dutertre, Florent Ginhoux (VI.6 Mononuclear phagocytes: Monocytes, macrophages and dendritic cells); Jonas Hahn, Christian Maueröder, Jasmin Knopf, Malgorzata Justyna Podolska, Luis Enrique Muñoz, Martin Herrmann (VI.7.1 Neutrophils, eosinophils and basophils); Immanuel Kwok, Leonard Tan, Maximilien Evrard, Lai Guan Ng (VI.7.2 Bone marrow and umbilical cord blood neutrophils); Philip E. Boulais, Paul S. Frenette (VI.8 Murine bone marrow stromal cells); Peter K. Jani, Julia Tornack, Wolfgang Bauer, Fritz Melchers, Susann Rahmig, Claudia Waskow (VI.9 Hematopoietic Stem Cells); Ramon Bellmàs Sanz, Jenny Kühne, Christine S. Falk (VI.10 Tumor cells); Katharina Kriegsmann, Michael Hundemer, Leo Hansmann (VI.11 Human plasma cells in multiple myeloma); Pascale Eede, Katja Kobow, Helena Radbruch (VI.12 Brain/neural cells); Katrin Neumann, Aaron Ochel, Gevitha Ravichandran, Gisa Tiegs, Sebastian Lunemann (VI.13 Cells from liver); Friederike Ebner, Kerstin H. Mair, Josephine Schlosser, Susanne Hartmann, Armin Saalmüller, Wilhelm Gerner (VI.14.1 Porcine cells); Kerstin H. Mair, Armin Saalmüller, Wilhelm Gerner (VI.14.2 Cross-reactive Ab clones); Yvan Saeys (Introduction and Artificial intelligence in flow cytometry); Tim Mosmann, Alice Yue, Sally Quataert, Jonathan Rebhahn, Ryan R. Brinkman (Cell-population analysis: Data preprocessing, manual and automated gating, and quality control); Thomas Höllt (Dimensionality reduction); Sofie Van Gassen (VII.1 Clustering); Natalie Stanley and Nima Aghaeepour (Integration of cytometric data into multiomics analysis) James V Watson, Diether Recktenwald, James Wing (VII.2 Statistics for flow cytometry); Susanne Melzer, Attila Tarnok (VII.3 Analysis presentation and publication (MIFlowCyt)); Josef Spidlen, Ryan R. Brinkman (VII.4 Data repositories: Sharing your data); Orla Maguire, Hans Minderman (VIII.1 Imaging Flow Cytometry); Henrik E. Mei, Michael D. Leipold, Holden T. Maecker (VIII.2 Barcoding in cytometric assays); Axel Ronald Schulz, Antonio Cosma, Sabine Baumgart, Brice Gaudilliere, Helen M. McGuire, Henrik E. Mei (VIII.3 Mass cytometry); J. Paul Robinson, Bartek Rajwa (VIII.4 Combinatorial cytometry); Claudia Haftmann, Florian Mair (VIII.5 High dimensional flow cytometry); Daniel Schraivogel, Dinko Pavlinic, Bianka Baying, Diana Ordonez, Anders Stahlberg, Vladimir Benes, Malte Paulsen (VIII.6 Single cell genomics and cytometry); Hyun-Dong Chang, Jakob Zimmermann, Susann Müller (VIII.7 Microbial cells); Marina Saresella, Ivana Marventano, Federica Piancone, Francesca LaRosa, Mario Clerici (VIII.8 Detailed and standardized methods to detect inflammasome assembly and activation

in immune cells (FlowSight AMNIS); Kata Filkor, Gergely Toldi (VIII.9 Multidrug resistance activity); Leo Hansmann, Livius Penter, Hans-Peter Rahn (VIII.10 Index sorting); Chantip Dang-Heine, Holden T. Maecker (VIII.11 Sample banking for flow cytometry); Stefan Frischbutter (VIII.12 High throughput screening); Christian Kukat (VIII.13 Core Facility setup and housekeeping /Shared Resource Laboratory (SRL) management).

Conflict of interest

Some of the authors of these guidelines work for companies manufacturing FCM equipment and reagents. The mention of a particular company's equipment or reagents does not imply endorsement of these products but are included as examples. The content of these guidelines is editorially independent of any company and has been peer-reviewed.

References

1 **Cossarizza, A., Chang, H.-D., Radbruch, A., Akdis, M., Andrä, I., Annunziato, F., Bacher, P. et al.**, Guidelines for the use of flow cytometry and cell sorting in immunological studies. *Eur. J. Immunol.* 2017. **47**: 1584–1797.

2 **Mack, J.**, Fulwyler Particle Separator. US patent US 3380584 A.

3 **Kachel, V., Fellner-Feldegg, H. and Menke, E.**, Hydrodynamic properties of flow cytometry instruments. In M. R. Melamed, T. Lindmo and M. L. Mendelsohn (Eds.), *Flow cytometry and sorting*, 2nd ed., Wiley, New York, NY, 1990, pp. 27–44.

4 **Crosland-Taylor, P. J.**, A device for counting small particles suspended in a fluid through a tube. *Nature* 1953. **171**: 37–38.

5 **Gucker, F. T., Jr., O'Konski, C. T., Pickard, H. B. and Pitts, J. N., Jr.**, A photoelectronic counter for colloidal particles. *J. Am. Chem. Soc.* 1947. **69**: 2422–2431.

6 **Van den Engh, G. J.**, Flow cytometer droplet formation system. US patent US 6861265 B1.

7 **Van den Engh, G. J.**, Particle separating apparatus and method. US patent US 5819948 A.

8 **Norton, P. O., Vane, D. R. and Javadi, S.**, Fixed mounted sorting cuvette with user replaceable nozzle. US patent US 7201875 B2.

9 **Doležel, J. and Göhde, W.**, Sex determination in dioecious plants *Melandrium album* and *M. rubrum* using high-resolution flow cytometry. *Cytometry* 1995. **19**: 103–106.

10 **Steen, H. B., Lindau, T. and Sorensen, O.**, A simple, high resolution flow cytometer based on a standard fluorescence microscope. In O. D. Laerum, T. Lindmo and E. Thorud (Eds.), *Proceedings of the IVth international symposium on flow cytometry (pulse cytophotometry)*, Bergen, Norway, 1980, pp. 31–33.

11 **Pinkel, D. and Stovel, R.**, Flow chambers and sample handling. In M. A., Van Dilla, P. N. Dean, O. D. Laerum, and M. R. Melame (Eds.), *Flow cytometry: Instrumentation and data analysis*, Academic Press, London, 1985, pp. 77–128.

12 **Kaduchak, G. et al.**, Ultrasonic analyte concentration and application in flow cytometry. US patent US 7340957 B2.

13 **Kaduchak, G. et al.**, System and method for acoustic focusing hardware and implementations. US patent US 8714014 B2.

14 **Ward, M., Turner, P., DeJohn, M. and Kaduchak, G.**, Fundamentals of acoustic cytometry. *Curr. Protoc. Cytometry* 2009. **53**: 1.22.1–1.22.12.

15 **Sweet, R. G.**, Fluid droplet recorder. US patent US 3596275 A.

16 **Göttlinger, C., Mechtold, B., Meyer, K. L. and Radbruch, A.**, Setup of a flow sorter. In Radbruch, A. (Ed.), *Flow cytometry and cell sorting*. Springer Laboratory, Berlin, Germany 1992, pp. 153–158.

17 **Petersen, T. W. and Van den Engh, G.**, Stability of the breakoff point in a high-speed cell sorter. *Cytometry Part A* 2003. **56**: 63–70.

18 **Kaiser, T., Raba, K., Scheffold, A. and Radbruch, A.**, A sheath-cooling system to stabilize side-streams and drop delay during long-term sorts for FACS-Aria® cell-sorter, http://fccf.drfz.de/uploads/pdf/poster_zentrallabor_A0.pdf

19 **Lawrence, W. G., Varadi, G., Entine, G., Podniesinski, E. and Wallace, P. K.**, Enhanced red and near infrared detection in flow cytometry using avalanche photodiodes. *Cytometry A* 2008. **73**: 767–776.

20 **Kester, W.**, Understand SINAD, ENOB, SNR, THD, THD+ N, and SFDR so you don't get lost in the noise floor. MT-003 Tutorial, 2009, http://www.analog.com/media/en/training-seminars/tutorials/MT-003.pdf

21 AD9240AS by Analog Devices | Data Acquisition, Arrow.com. [Online]. Available: https://www.arrow.com/de-de/products/ad9240as/analog-devices. [Accessed: 18-Jan-2017].

22 **Snow, C.**, Flow cytometer electronics. *Cytometry Part A* 2004. **57A**: 63–69.

23 **Asbury, C. L., Uy, J. L. and van den Engh, G.**, Polarization of scatter and fluorescence signals in flow cytometry. *Cytometry* 2000. **40**: 88–101.

24 **Shapiro, H. M.**, *Practical flow cytometry*, 4th ed., John Wiley & Sons, Inc., Hoboken, NJ 2003, pp. 184–197.

25 **Watson, D. A., Brown, L. O., Gaskill, D. F., Naivar, M., Graves, S. W., Doorn, S. K. and Nolan, J. P.**, A flow cytometer for the measurement of Raman spectra. *Cytometry A* 2008. **73A**: 119–128.

26 **Nolan, J. P., Condello, D., Duggan, E., Naivar, M. and Novo, D.**, Visible and near infrared fluorescence spectral flow cytometry. *Cytometry A* 2012. **83**: 253–264.

27 **Wade, C. G., Rhyne, R. H., Woodruff, W. H., Bloch, D. P. and Bartholomew, J. C.**, Spectra of cells in flow cytometry using a vidicon detector. *J. Histochem. Cytochem.* 1979. **27**: 1049–1052.

28 **Robinson, J. P.**, Multispectral cytometry: the next generation. *Biophoton. Int.* 2004, 36–40.

29 **Robinson, J. P., Rajwa, B., Gregori, G., Jones, V and Patsekin, V**, Multispectral cytometry of single bio-particles using a 32-channel detector. In T. Tuan Vo-Dinh, W. S. Grundfest, D. A. Benaron and G. E. Cohn, (Eds.), *Advanced biomedical and clinical diagnostic systems III*, 5692 ed. Springer, Berlin/Heidelberg, 2005, Pp. 359–365.

30 **Robinson, J. P., Rajwa, B., Patsekin, V., Gregori, G. and Jones, J.** *Multispectral detector and analysis system US patent US7280204 B2.*

31 **Grégori, G., Patsekin, V., Rajwa, B., Jones, J., Ragheb, K., Holdman, C., Robinson, J. P. et al.**, Hyperspectral cytometry at the single cell level using a 32 channel photodetector. *Cytometry A* 2012. **81A**: 35–44.

32 **Goddard, G., Martin, J. C., Naivar, M., Goodwin, P. M., Graves, S. W., Habbersett, R., Nolan, J. P. et al.**, Single particle high resolution spectral analysis flow cytometry. *Cytometry* 2006. **69A**: 842–851.

33 **Futamura, K., Sekino, M., Hata, A., Ikebuchi, R., Nakanishi, Y., Egawa, G., Kabashima, K. et al.**, Novel full-spectral flow cytometry with multiple spectrally-adjacent fluorescent proteins and fluorochromes and visualization of in vivo cellular movement. *Cytometry* 2015. **87**: 830–842.

34 **Feher, K., von Volkmann, K., Kirsch, J., Radbruch, A., Popien, J. and Kaiser, T.**, Multispectral flow cytometry: The consequences of increased light collection. *Cytometry* 2016. **89**: 681–689.

35 **Roederer, M.**, Distributions of autofluorescence after compensation: Be panglossian, fret not. *Cytometry A* 2016. **89**: 398–402.

36 **Szalóki, G. and Goda, K.**, Compensation in multicolor flow cytometry. *Cytometry A* 2015. **87**: 982–985.

37 **Novo, D., Grégori, G. and Rajwa, B.**, Generalized unmixing model for multispectral flow cytometry utilizing nonsquare compensation matrices. *Cytometry A* 2013. **83**: 508–520.

38 **Nguyen, R., Perfetto, S., Mahnke, Y. D., Chattopadhyay, P. and Roederer, M.**, Quantifying spillover spreading for comparing instrument performance and aiding in multicolor panel design. *Cytometry A* 2013. **83**: 306–315.

39 **Lee, J. A., Spidlen, J., Boyce, K., Cai, J., Crosbie, N., Dalphin, M., Furlong, J.**, et al. MIFlowCyt: the Minimum Information about a Flow Cytometry Experiment. *Cytometry A* 2008. **73**: 926–930.

40 **Tung, J. W., Parks, D. R., Moore, W. A. and Herzenberg, L. A.**, New approaches to fluorescence compensation and visualization of FACS data. *Clin. Immunol.* 2004. **110**: 277–283.

41 BD Cytometer Setup and Tracking Application Guide V3.0, 2013, BD Biosciences, San Jose, CA.

42 **Wood, J. and Hoffman, R.**, Evaluating fluorescence sensitivity on flow cytometers: an overview. *Cytometry* 1998. **33**: 256–259.

43 **Wood, J.**, Fundamental flow cytometer properties governing sensitivity and resolution. *Cytometry* 1998. **33**: 260–266.

44 **Hoffman, R. A.**, Standardization, calibration, and control in flow cytometry. *Curr. Protoc. Cytom.* 2005. **79**: 1.3.1–1.3.21.

45 **Wood, J. C. S.**, 2009, Establishing and maintaining system linearity. *Curr. Protoc. Cytom.* Chapter **1**: 1.4.1–1.4.14.

46 **Jett, J. H., Martin, J. C., Habbersett, R. C.**, Techniques for flow cytometer alignment. *Curr. Protoc. Cytom.* 2009. **Chapter 1**: 1.10.1–1.10.7.

47 **Perfetto, S. P., Chattopadhyay, P. K., Wood, J., Nguyen, R., Ambrozak, D., Hill, J. P. and Roederer, M.**, Q and B Values are Critical Measurements Required for Inter-Instrument Standardization and Development of Multicolor Flow Cytometry Staining Panels. *Cytometry* 2014. **85A**: 1037–1048.

48 **Perfetto, S. P., Ambrozak, D., Nguyen, R., Chattopadhyay, P. K. and Roederer, M.**, Quality assurance for polychromatic flow cytometry using a suite of calibration beads. *Nat. Protoc.* 2012. **7**: 2067–2079.

49 **Steen, H. B.**, Noise, Sensitivity, and Resolution of Flow Cytometers. *Cytometry* 1992. **13**: 822–830.

50 **Friend, M., Franklin, G. B. and Quinn, B.**, An LED pulser for measuring photomultiplier linearity. *Nucl. Instr. And Meth. A* 2012. **676**: 66–69.

51 **Giesecke, C., Feher, K., von Volkmann, K., Kirsch, J., Radbruch, A. and Kaiser, T.**, Determination of background, signal-to-noise, and dynamic range of a flow cytometer: a novel practical method for instrument characterization and standardization. *Cytometry* 2017. **91A**: 1104–1114.

52 Reference Manuals for discussed instruments: a) BD FACSCanto II Flow Cytometer Reference Manual, 2006, BD Biosciences, San Jose, USA; b) MACSQuant Instrument User Manual, V6, 2015, Miltenyi Biotec, Bergisch Gladbach, Germany; c) CyFlow Cube 6 Instrument Operating Manual, 2012, Partec GmbH, Germany; d) Attune NxT Acoustic Focusing Cytometer User Guide, 2015, Life Technologies, USA part of Thermo Fisher Scientific; e) Gallios Flow Cytometer Instructions for use, 2009, Beckman Coulter, USA

53 Flow Cell Care & Maintenance; Feb 2011, Precision Cells, Inc. http://ezinearticles.com/?Flow-Cytometry—Flow-Cell-Care-and-Maintenance&id=5898431

54 A Guide to Absolute Counting Using the BD Accuri C6 Flow Cytometer, Jan. 2012, BD Biosciences, Technical Bulletin.

55 BD FACSDIVA Software v 8.0 Reference Manual

56 **Maciorowski, Z., Chattopadhyay, P. K. and Jain, P.**, Basic Multicolor Flow Cytometry. *Curr. Protoc. Immunol.* 2017. **117**: 5.4.1–5.4.38.

57 **Maecker, H. T. and Trotter, J.**, Flow cytometry controls, instrument setup, and the determination of positivity. *Cytometry A* 2006. **69**: 1037–1042.

58 **Chase, E. S. and Hoffman, R. A.**, Resolution of dimly fluorescent particles: a practical measure of fluorescence sensitivity. *Cytometry* 1998. **33**: 267–279.

59 **Meinelt, E., Reunanen, M., Edinger, M., Jaimes, M., Stall, A., Sasaki, D. and Trotter, J.**, Standardizing Application Setup Across Multiple Flow Cytometers Using BD FACSDiva™ Version 6. Software. BD Biosciences Technical Bulletin. 2012.

60 **Roederer, M.**, Compensation in flow cytometry. *Curr. Protoc. Cytom.* 2002. **22**: 1.14.1–1.14.20.

61 **Biburger, M., Trenkwald, I. and Nimmerjahn, F.**, Three blocks are not enough—blocking of the murine IgG receptor FcgammaRIV is crucial for proper characterization of cells by FACS analysis. *Eur. J. Immunol.* 2015. **45**: 2694–2697.

62 **Maecker, H. T., Frey, T., Nomura, L. E. and Trotter, J.**, Selecting fluorochrome conjugates for maximum sensitivity. *Cytometry A* 2004. **62**: 169–173.

63 **Nüsse, M., Beisker, W., Kramer, J., Miller, B. M., Schreiber, G. A., Viaggi, S., Weller, E. M. et al.**, Measurement of micronuclei by flow cytometry. *Methods Cell Biol.* 1994. **42**: 149–158.

64 **Hengst, J., Theorell, J., Deterding, K., Potthoff, Dettmer, A., Ljunggren, H. G., Wedemeyer, H. and Björkström, N. K.**, High-resolution determination of human immune cell signatures from fine-needle liver aspirates. *Eur. J. Immunol.* 2015. **45**: 2154–2157.

65 **Johnson, S., Nguyen, V. and Coder, D.**, Assessment of cell viability. *Curr. Protoc. Cytom.* 2013.**64**: 9.2.1–9.2.26

66 **Edward, R. and Dimmick, I.**, Compensation-free dead cell exclusion: multi-beam excitation of the far-red DNA binding viability dye-DRAQ7.(TECH2P. 873). *J. Immunol.* 2014. **192**: 135.4

67 **Pieper, I. L., Radley, G., Chan, C. H., Friedmann, Y., Foster, G. and Thornton, C. A.**, Quantification methods for human and large animal leukocytes using DNA dyes by flow cytometry. *Cytometry A* 2016. **89**: 565–574.

68 **Reardon, A. J., Elliott, J. A. and McGann, L. E.**, Fluorescence as an alternative to light-scatter gating strategies to identify frozen-thawed cells with flow cytometry. *Cryobiology* 2014. **69**: 91–99.

69 **Hønge, B. L., Petersen, M. S., Olesen, R., Møller, B. K. and Erikstrup, C.** Optimizing recovery of frozen human peripheral blood mononuclear cells for flow cytometry. *PLoS One*. 2017. **12**: e0187440

70 **Alsayed, H., Owaidah, T. and Al Rawas, F.**, Validation of a modifiedcryopreservation method for leukemic blasts for flow cytometry assessment. *Hematol. Oncol. Stem Cell Ther.* 2008. **1**: 94–97.

71 **Chow, S., Hedley, D., Grom, P., Magari, R., Jacobberger, J. W. and Shankey, T. V.**, Whole blood fixation and permeabilization protocol with red blood cell lysis for flow cytometry of intracellular phosphorylated epitopes in leukocyte subpopulations. *Cytometry A*. 2005. **67**: 4–17.

72 **Woost, P. C., Solchaga, L. A., Meyerson, H. J., Shankey, T. V., Goolsby, C. L. and Jacobberger, J. W.**, High-resolution kinetics of cytokine signaling in human CD34/CD117-positive cells in unfractionated bone marrow. *Blood* 2011. **117**: e131–e141.

73 **Marvin, J., Swiminathan, S., Kraker, G., Chadburn, A., Jacobberger, J. W. and Goolsby, C.**, Normal bone marrow signal-transduction profiles: a requisite for enhanced detection of signaling dysregulations in AML. *Blood* 2011. **117**: e120–e130.

74 **Shankey, T. V., Forman, M. F., Scibelli, P., Cobb, J., Smith, C. M., Mills, R., Holdiway, K. et al.**, An optimized whole blood method for flow cytometric measurement of ZAP-70 protein expression in chronic lymphocytic leukemia. *Cytometry* 2006. **70**: 259–269.

75 **Jacobberger, J. W., Sramkowski, R. M., Frisa, P. S., Peng Ye, P., Gottlieb, M. A., Hedley, D. W., Shankey, T. V. et al.**, Immunoreactivity of STAT5 phosphorylated on tyrosine as a cell-based measure of Bcr/Abl kinase activity. *Cytometry* 2003. **54**: 75–88.

76 **Boehm, T., McCurley, N., Sutoh, Y., Schorpp, M., Kasahara, M. and Cooper, M. D.**, VLR-based adaptive immunity. *Annu. Rev. Immunol.* 2012. **30**: 203–220.

77 **Pancer, Z., Amemiya, C. T., Ehrhardt, G. R., Ceitlin, J., Gartland, G. L. and Cooper, M. D.**, Somatic diversification of variable lymphocyte receptors in the Agnathan sea lamprey. *Nature* 2004. **430**: 174–180.

78 **Velikovsky, C. A., Deng, L., Tasumi, S., Iyer, L. M., Kerzic, M. C., Aravind, L., Pancer, Z. et al.**, Structure of a lamprey variable lymphocyte receptor in complex with a protein antigen. *Nat. Struct. Mol. Biol.* 2009. **16**: 725–730.

79 **Han, B. W., Herrin, B. R., Cooper, M. D. and Wilson, I. A.**, Antigen recognition by variable lymphocyte receptors. *Science* 2008. **321**: 1834–1837.

80 **Luo, M., Velikovsky, C. A., Yang, X., Siddiqui, M. A., Hong, X., Barchi, J. J., Jr., Gildersleeve, J. C. et al.**, Recognition of the Thomsen-Friedenreich pancarcinoma carbohydrate antigen by a lamprey variable lymphocyte receptor. *J. Biol. Chem.* 2013. **288**: 23597–23606.

81 **Collins, B. C., Gunn, R. J., McKitrick, T. R., Cummings, R. D., Cooper, M. D., Herrin, B. R. and Wilson, I. A.**, Structural Insights into VLR Fine Specificity for Blood Group Carbohydrates. *Structure* 2017. **25**: 1667–1678.

82 **Chan, J. T. H., Liu, Y., Khan, S., St-Germain, J. R., Zou, C., Leung, L. Y., Yang, T. et al.**, A tyrosine sulfation-dependent HLA-I modification identifies memory B cells and plasma cells. *Sci. Adv.* 2018. **4**: eaar7653.

83 **Herrin, B. R., Alder, M. N., Roux, K. H., Sina, C., Ehrhardt, G. R., Boydston, J. A., Turnbough, C. L., Jr. et al.**, Structure and specificity of lamprey monoclonal antibodies. *Proc. Natl. Acad. Sci. USA.* 2008. **105**: 2040–2045.

84 **Haas, J., Roth, S., Arnold, K., Kiefer, F., Schmidt, T., Bordoli, L. and Schwede, T.**, The Protein Model Portal–a comprehensive resource for protein structure and model information. *Database* 2013. **2013**: bat031.

85 **Yu, C., Liu, Y., Chan, J. T., Tong, J., Li, Z., Shi, M., Davani, D. et al.**, Identification of human plasma cells with a lamprey monoclonal antibody. *JCI Insight* 2016. **1**: e84738.

86 **Alder, M. N., Rogozin, I. B., Iyer, L. M., Glazko, G. V., Cooper, M. D. and Pancer, Z.**, Diversity and function of adaptive immune receptors in a jawless vertebrate. *Science* 2005. **310**: 1970–1973.

87 **Yu, C., Ali, S., St-Germain, J., Liu, Y., Yu, X., Jaye, D. L., Moran, M. F. et al.**, Purification and identification of cell surface antigens using lamprey monoclonal antibodies. *J. Immunol. Methods* 2012. **386**: 43–49.

88 **Baker, M.**, Antibody anarchy: a call to order. *Nature* 2015. **527**: 545–551.

89 **Zhang, X., Calvert, R. A., Sutton, B. J. and Dore, K. A.**, IgY: a key isotype in antibody evolution. *Biol. Rev. Camb. Philos. Soc.* 2017. **92**: 2144–2156.

90 **Mucci, I., Legitimo, A., Compagnino, M., Consolini, R., Miglidaccio, P., Metelli, M. R. and Scatena, F.**, The methodological approach for the generation of human dendritic cells from monocytes affects the maturation state of the resultant dendritic cells. *Biologicals* 2009. **37**: 288–96.

91 **Delirezh, N. and Shojaeefar, E.**, Phenotypic and functional comparison between flask adherent and magnetic activated cell sorted monocytes derived dendritic cells. *Iran J. Immunol.* 2012. **9**: 98–108.

92 **Pribush, A., Meyerstein, D. and Meyerstein, N.**, Kinetics of erythrocyte swelling and membrane hole formation in hypotonic media. *BBABiomembrane* 2002. **1558**: 119–132.

93 **Tiirikainen, M. I.**, Evaluation of red blood cell lysing solutions for the detection of intracellular antigens by flow cytometry. *Cytometry* 1995. **20**: 341–348.

94 **Einwallner, E., Subasic, A., Strasser, A., Augustin, D., Thalhammer, R., Steiner, I. and Schwarzinger, I.**, Lysis matters: red cell lysis with FACS Lyse affects the flow cytometric enumeration of circulating leukemic blasts. *J. Immunol. Methods* 2013. **390**: 127–132.

95 **Lindahl, P. E.**, Principle of a counter-streaming centrifuge for the separation of particles of different sizes. *Nature* 1948. **161**: 648–649.

96 **McEwen, C. R., Stallard, R. W. and Juhos, E. T.**, Separation of biological particles by centrifugal elutriation. *Anal. Biochem.* 1968. **23**: 369–77.

97 **Pretlow, T. G. and Pretlow, T. P.**, Centrifugal elutriation (counterstreaming centrifugation) of cells. *Cell Biophys.* 1979. **1**: 195–210.

98 www.biologydiscussion.com/cell-biology/8-methods-involved-in-separation-of-whole-cells-with-diagram/3494

99 **Ferrone, S., Cooper, N. R., Pellegrino, M. A. and Reisfeld, R. A.**, Interaction of histocompatibility (HL-A) antibodies and complement with synchronized human lymphoid cells in continuous culture. *J. Exp. Med.* 1973. **137**: 55–68.

100 **Lustig, H. and Bianco, C.**, Antibody-mediated cell cytotoxicity in a defined system: regulation by antigen, antibody, and complement. *J. Immunol.* 1976. **116**: 253–60.

101 **Esser, C.**, Historical and useful methods of preselection and preparative scale cell sorting. In D. Recktenwald and A. Radbruch (Eds.), *Cell separation methods and applications*. Marcel Dekker Inc., New York/Basel/Hong Kong, 1998, pp. 1–14.

102 www.pluriselect.com

103 www.miltenyibiotec.com

104 **Thomas, T. E., Miller, C. L. and Eaves, C. J.**, Purification of hematopoietic stem cells for further biological study. *Methods.* 1999. **17**: 202–218.

105 **Van der Toom, E. E., Verdone, J. E., Gorin, M. A. and Pienta, K. J.**, Technical challenges in the isolation and analysis of circulating tumor cells. *Oncotarget* 2016. **7**: 62754–62766.

106 **Donnenberg, V. S. and Donnenberg, A. D.**, Identification, rare-event detection and analysis of dendritic cell subsets in bronchio-alveolar lavage fluid and peripheral blood by flow cytometry. *Front. Biosci.* 2003. **8**: s1175–s1180.

107 **Bacher, P. and Scheffold, A.**, New technologies for monitoring human antigen-specific T cells and regulatory T cells by flow-cytometry. *Curr. Opin. Pharmacol.* 2015. **23**: 17–24.

108 www.thermofisher.com/de/de/home/brands/product-brand/dynal.html

109 www.bdbiosciences.com/us/reagents/research/magnetic-cell-separation/other-species-cell-separation-reagents/cell-separation-magnet/p/552311

110 Recktenwald, D. and Radbruch, A. (Eds.), *Cell separation methods and applications*. Marcel Dekker Inc., New York/ Basel/ Hong Kong, 1998.

111 **Miltenyi, S. and Pflueger, E.**, High gradient magnetic cell sorting. In A. Radbruch (Ed.), *Flow cytometry and sorting*. Springer-Verlag, Berlin/Heidelberg, 1992, pp. 141–152.

112 **Ruffert, C.**, Magnetic bead—Magic bullet (review). *Micromachines* 2016. **7**: 21.

113 **McCloskey, K. E., Chalmers, J. J. and Zborowski, M.**, Magnetic cell separation: Characterization of magnetophoretic mobility. *Anal. Chem.* 2003. **75**: 6868–6874.

114 **Boyum, A.**, Isolation of leucocytes from human blood. Further observations. Methylcellulose, dextran, and ficoll as erythrocyteaggregating agents. *Scand. J. Clin. Lab. Invest. Suppl.* 1968. **97**: 31–50.

115 **Boyum, A.**, Isolation of lymphocytes, granulocytes and macrophages. *Scand. J. Immunol.* 1976. Suppl **5**: 9–15.

116 **Yeo, C., Saunders, N., Locca, D., Flett, A., Preston, M., Brookman, P., Davy, B. et al.**, Ficoll-Paque versus Lymphoprep: A comparative study of two density gradient media for therapeutic bone marrow mononuclear cell preparations. *Regen. Med.* 2009. **4**: 689–696.

117 **Boyum, A., Brincker, F. H., Martinsen, I., Lea, T. and Lovhaug, D.**, Separation of human lymphocytes from citrated blood by density gradient (NycoPrep) centrifugation: Monocyte depletion depending upon activation of membrane potassium channels. *Scand. J. Immunol.* 2002. **56**: 76–84.

118 **Kuhns, D. B., Priel, D. A., Chu, J. and Zarember, K. A.**, Isolation and functional analysis of human neutrophils. *Curr. Protoc. Immunol.* 2015. **111**: 7.23.1–7.23.16.

119 **Maqbool, M., Vidyadaran, S., George, E. and Ramasamy, R.**, Optimisation of laboratory procedures for isolating human peripheral blood derived neutrophils. *Med. J. Malaysia* 2011. **66**: 296–299.

120 **Bruyninckx, W. J. and Blancquaert, A. M.**, Isolation of horse mononuclear cells, especially of monocytes, on Isopaque-Ficoll neutral density gradient. *Vet. Immunol. Immunopathol.* 1983. **4**: 493–504.

121 **Pertoft, H.**, Fractionation of cells and subcellular particles with Percoll. *J. Biochem. Biophys. Methods* 2000. **44**: 1–30.

122 **Yu, L., Warner, P., Warner, B., Recktenwald, D., Yamanishi, D., Guia, A. and Ghetti, A.**, Whole blood leukocytes isolation with microfabricated filter for cell analysis, *Cytometry* 2011. **79A**: 1009–1015.

123 **Higuchi, A., Wang, C.-T., Ling, Q.-D., Lee, H. H.-C., Suresh Kumar, S., Chang, Y., Alarfaj, A. A. et al.**, A hybrid-membrane migration method to isolate high-purity adipose-derived stem cells from fat tissues. *Sci. Rep.* 2015. **5**: 10217.

124 **Huang, L. R., Cox, E. C., Austin, R. H. and Sturm, J. C.**, Continuous particle separation through deterministic lateral displacement. *Science* 2004. **304**: 987–990.

125 **Davis, J. A., Inglis, D. W., Morton, K. J., Lawrence, D. A., Huang, L. R., Chou, S. Y., Sturm, J. C. et al.**, Deterministic hydrodynamics: Taking blood apart, *Proc. Nat. Acad. Sci.* 2008. **103**: 14779–14784.

126 **Loutherback, K., D'Silva1, J., Liu, L., Wu, A., Austin, R. H. and Sturm, J. C.**, Deterministic separation of cancer cells from blood at 10 mL/min. *AIP Adv.* 2012. **2**: 042107.1–042107.7.

127 **D'Silva, J., Austin, H. and Sturm, C.**, Inhibition of clot formation in deterministic lateral displacement arrays for processing large volumes of blood for rare cell capture. *Lab Chip* 2015. **15**: 2240–2247.

128 **Civin, C. I., Ward, T., Skelley, A. M., Gandhi, K., Peilun Lee, Z., Dosier, C. R., D'Silva, J. L. et al.**, Automated leukocyte processing by microfluidic deterministic lateral displacement. *Cytometry A*. 2016. **89**: 1073–1083.

129 **Campos-González, R., Skelley, A. M., Gandhi, K., Inglis, D. W., Sturm, J. C., Civin, C. I. and Ward, T.**, Deterministic lateral displacement: the next-generation CAR T-cell processing? *SLAS Technol.* 2018. **23**: 338–351.

130 **Laurell, T., Petersson, F. and Nilsson, A.**, Chip integrated strategies for acoustic separation and manipulation of cells and particles. *Chem. Soc. Rev.* 2007. **36**: 492–506.

131 **Dykes, J., Lenshof, A., Åstrand-Grundström, I.-B., Laurell, T. and Scheding, S.**, Efficient removal of platelets from peripheral blood progenitor cell products using a novel micro-chip based acoustophoretic platform. *PLoS ONE* 2011. **6**: e23074.

132 **Urbansky, A., Ohlsson, P., Lenshof, A., Garofalo, F., Scheding, S. and Laurell, T.**, Rapid and effective enrichment of mononuclear cells from blood using acoustophoresis. *Sci. Rep.* 2017. **7**: 17161.

133 **Wysocki, L. J. and Sato, V. L.**, Panning for lymphocytes: A method for cell selection. *Proc. Natl. Acad. Sci. U S A* 1978. **75**: 2844–2848.

134 **Weiner, M. S., Bianco, C. and Nussenzweig, V.**, Enhanced binding of neuraminidase-treated sheep erythrocytes to human T lymphocytes. *Blood* 1973. **42**: 939–946.

135 **Indiviri, F., Huddlestone, J., Pellegrino, M. A. and Ferroni, S.**, Isolation of human T lymphocytes: Comparison between wool filtration and rosetting with neuraminidase (VCN) and 2-aminoethylisothiouronium (AET)-treated sheep red blood cells. *J. Immunol. Methods* 1980. **34**: 107–112.

136 **Lepe-Zuniga, J. L., Zigler, J. S. and Gery, I.**, Toxicity of light-exposed Hepes media. *J. Immunol. Methods* 1987. **103**: 145.

137 **Cowan, C. M. and Basu, S., Heng, B. C.**, Comparison of enzymatic and nonenzymatic means of dissociating adherent monolayers of mesenchymal stem cells. *Biol. Proc. Online* 2009. **11**: 161–169.

138 **Amaral, K., Rogero, M., Fock, R., Borelli, P. and Gavini, G.**, Cytotoxicity analysis of EDTA and citric acid applied on murine resident macrophages culture. *Int. Endod. J.* 2007. **40**(5): 338–343.

139 **Wiesman, U.**, Segregating cells—proteases in tissue culture. In Sterchi, E. E. and Stöcker, W. (Eds.), *Proteolytic enzymes: Tools and targets*. Springer, Berlin, Germany, 1999, pp. 298–311.

140 **Stovel, R. T.**, The influence of particles on jet breakoff. *J. Histochem. Cytochem.* 1977. **25**: 813–820.

141 **Pinkel, D. and Stovel, R.**, Flow chambers and sample handling. In Van Dilla, M. A., Dean, P. N., Laerum, O. D. and Melame, M. R. (Eds.), *Flow cytometry: Instrumentation and data analysis*, Academic Press, London, UK, 1985, pp. 77–128.

142 **Houtz, B., Trotter, J. and Sasaki, D.**, Tips on cell preparation for flow cytometric analysis and sorting. *BD FACService Technotes* 2004. **9**.

143 **Holmes, K. L., Fontes, B., Hogarth, P., Konz, R., Monard, S., Pletcher, Jr., C. H., Wadley, R. B. et al.**, International Society for the Advancement of Cytometry cell sorter biosafety standards. *Cytometry A* 2014. **85**: 434–453.

144 **van der Maaten, L. J. P. and Hinton, G. E.**, Visualizing high-dimensional data using t-SNE. *J. Mach. Learn. Res.* 2008. **9**: 2579–2605.

145 **McInnes, L., Healy, J and Melville, J.**, UMAP: uniform manifold approximation and projection for dimension reduction arXiv:1802.03426

146 **Aghaeepour, N, Simonds, E. F., Knapp, D. J. H. F., Bruggner, R. V., Sachs, K., Culos, A., Gherardini, P. F. et al.**, GateFinder: projection-based gating strategy optimization for flow and mass cytometry. *Bioinformatics* 2018. **34**(23): 4131–4133.

147 **Becht, E., Simoni, Y., Coustan-Smith, E., Maximilien, E., Cheng, Y., Ng, L. G., Campana, D. et al.**, Reverse-engineering flow-cytometry gating strategies for phenotypic labelling and high-performance cell sorting. *Bioinformatics* 2019. **35**: 301–308.

148 **Samusik, N., Irvine, A., Aghaeepour, A., Spidlen, J. and Trotter, J.** Computational Sorting with HyperFinder, CYTO 2019, Session Parallel 06, 24 June 2019.

149 **Bøyum, A., Løvhaug, D., Tresland, L. and Nordlie, E. M.**, Separation of leucocytes: improved cell purity by fine adjustments of gradient medium density and osmolality. *Scand. J. Immunol.* 1991. **34**: 697–712.

150 **Loos, H., Blok-Schut, B., van Doorn, R., Hoksbergen, R., Brutel de la Rivière, A. and Meerhof, L.**, A method for the recognition and separation of human blood monocytes on density gradients. *Blood* 1976. **48**: 731–742.

151 BD FACSAria user's guide, BD Biosciences, San Jose, USA, 2006.

152 **Wixforth, A.**, Acoustically driven programmable microfluidics for biological and chemical applications. *J. Lab. Automat.* 2006. **11**: 399–405.

153 **Kaiser, T., Raba, K., Sickert, M., Radbruch, A. and Scheffold, A.**, Integration of an ultrasonic wave device in a FACS-Aria cell sorter for continuous, noninvasive mixing of cell suspensions. Poster, Budapest, 2008 ISAC congress. https://doi.org/10.13140/RG.2.1.1760.2966

154 Radbruch, A. (Ed.), *Flow cytometry and cell sorting*, 2nd ed., Springer, Berlin/Heidelberg 2000.

155 **Freyer, J. P., Fillak, D. and Jett, J. H.**, Use of xantham gum to suspend large particles during flow cytometric analysis and sorting. *Cytometry* 1989. **10**: 803–806.

156 **Fu, L.-M., Yang, R.-J., Lin, C.-H., Pan, Y.-J. and Gwo-Bin, L.**, Electrokinetically driven micro flow cytometers with integrated fiber optics for on-line cell/particle detection. *Anal. Chim. Acta* 2004. **507**: 163–169.

157 **Telleman, P., Larsen, U. D., Philip, J., Blankenstein, G. and Wolff, A.**, Cell Sorting in Microfluidic Systems. In Jed Harrison, D. and van den Berg, A. (Eds.). *Micro total analysis systems '98*. Springer, Amsterdam, the Netherlands, 1998, pp. 39–44.

158 **Wang, X., Chen, S., Kong, M., Wang, Z., Costa, K. D., Li, R. A. and Sun, D.**, Enhanced cell sorting and manipulation with combined optical tweezer and microfluidic chip technologies. *Lab Chip* 2011. **11**: 3656–3662.

159 **Bhagat, A. A., Bow, H., Hou, H. W., Tan, S. J., Han, J. and Lim, C. T.**, Microfluidics for cell separation. *Med. Biol. Eng. Comput.* 2010. **48**: 999–1014.

160 **Chapman, G. V.**, Instrumentation for flow cytometry. *J. Immunol. Methods* 2000. **243**: 3–12.

161 **Abate, A. R., Agresti, J. J. and Weitz, D. A.**, Microfluidic sorting with highspeed single-layer membrane valves. *Appl. Phys. Lett.* 2010. **96**: 203509.

162 **Shemesh, J., Bransky, A., Khoury, M. and Levenberg, S.**, Advanced microfluidic droplet manipulation based on piezoelectric actuation. *Biomed. Microdevices* 2010. **12**: 907–914.

163 **Chen, C. H., Cho, S. H., Tsai, F., Erten, A. and Lo, Y. H.**, Microfluidic cell sorter with integrated piezoelectric actuator. *Biomed. Microdevices* 2009. **11**: 1223–1231.

164 **Wang, M. M., Tu, E., Raymond, D. E., Yang, J. M., Zhang, H., Hagen, N., Dees, B. et al.**, Microfluidic sorting of mammalian cells by optical force switching. *Nat. Biotechnol.* 2005. **23**: 83–87.

165 **Roederer, M.**, Spectral compensation for flow cytometry: visualization artifacts, limitations, and caveats. *Cytometry* 2001. **45**: 194–205.

166 Rockefeller University BD FACSAria2-3 Water-Cooled Sort Collection Integrated Tube Holder 5-15-;5-5 | NIH 3D Print Exchange. Available at: http://3dprint.nih.gov/discover/3dpx-002415. (Accessed: 20th April 2016)

167 **Sasaki, D. T., Tichenor, E. H., Lopez, F., Combs, J., Uchida, N., Smith, C. R., Stokdijk, W. et al.**, Development of a clinically applicable high-speed flow cytometer for the isolation of transplantable human hematopoietic stem cells. *J. Hematother.* 1995. **4**: 503–514.

168 **June, C. H., O'Connor, R. S., Kawalekar, O. U., Ghassemi, S., Milone, M. C.**, CAR T cell immunotherapy for human cancer. *Science* 2018. **359**: 1361–1365.

169 **Hoffmann, P., Eder, R., Boeld, T. J., Doser, K., Piseshka, B., Andreesen, R. et al.**, Only the CD45RA+ subpopulation of CD4+CD25high T cells gives rise to homogeneous regulatory T-cell lines upon in vitro expansion. *Blood* 2006. **108**: 4260–4267.

170 GMP EudraLex Volume 4, Part I, with guidance in Annex 1 on 'Manufacture of Sterile Medicinal Products' and Annex 2 on 'Manufacture of Biological active substances and Medicinal Products for Human Use'; https://ec.europa.eu/health/documents/eudralex/vol-4_de.

171 Good Manufacturing Practice for Advanced Therapy Medicinal Products, published in Part IV of Eudralex Volume 4; https://ec.europa.eu/health/documents/eudralex/vol-4_de

172 Reflection paper on classification of advanced therapy medicinal products. EMA/CAT/600280/2010 (ed. EMA) (EMA-CAT, http://www.ema.europa.eu/docs/en_GB/document_library/Regulatory_and_procedural_guideline/2012/04/WC500126681.pdf, 2012).

173 Commission Directive 2009/120/EC of 14 September 2009 amending Directive 2001/83/EC of the European Parliament and of the Council on the Community code relating to medicinal products for human use as regards advanced therapy medicinal product.

174 Regulation (EC) No 1394/ 2007 of the European Parliament and of the Council of 13 November 2007 on advanced therapy medicinal products and amending Directive 2001/83/EC and Regulation (EC) No 726/2004.

175 Guideline on process validation for finished products - information and data to be provided in regulatory submissions, EMA/CHMP/CVMP/QWP/BWP/70278/2012-Rev1. 27 February 2014: European Medicines Agency (EMA).

176 **USFDA**. *Guidance for industry. Process validation: General principles and practices*, U.S. Department of Health and Human Services Food and Drug Administration Washington, DC 2011.

177 ICH Q6B: Specifications: Test Procedures and Acceptance Criteria for Biotechnological / Biological Products, ICH Harmonised Tripartite Guideline. International Conference on Harmonisation of Technical Requirements for Registration of Pharmaceuticals for Human Use.

178 ICH Q2(R1): Validation of Analytical Procedures: Text and Methodology, ICH Harmonised Tripartite Guideline. International Conference on Harmonisation of Technical Requirements for Registration of Pharmaceuticals for Human Use.

179 **Leslie, D. S., Johnston, W. W., Daly, L., Ring, D. B., Shpall, E. J., Peters, W. P. and Bast, R. C., Jr.**, Detection of breast carcinoma cells in human bone marrow using fluorescence-activated cell sorting and conventional cytology. *Am. J. Clin. Pathol.* 1990. **94**: 8–13.

180 **Frantz, C. N., Ryan, D. H., Cheung, N. V., Duerst, R. E. and Wilbur, D. C.**, Sensitive detection of rare metastatic human neuroblastoma cells in bone marrow by two-color immunofluorescence and cell sorting. *Prog. Clin. Biol. Res.* 1988. **271**: 249–262.

181 **Ryan, D. H., Mitchell, S. J., Hennessy, L. A., Bauer, K. D., Horan, P. K. and Cohen, H. J.**, Improved detection of rare CALLA-positive cells in peripheral blood using multiparameter flow cytometry. *J. Immunol. Methods* 1984. **74**: 115–128.

182 **Visser, J. W. and De Vries, P.**, Identification and purification of murine hematopoietic stem cells by flow cytometry. *Methods Cell Biol.* 1990. **33**: 451–468.

183 **Cory, J. M., Ohlsson-Wilhelm, B. M., Brock, E. J., Sheaffer, N. A., Steck, M. E., Eyster, M. E. and Rapp, F.**, Detection of human immunodefi-

ciency virus-infected lymphoid cells at low frequency by flow cytometry. *J. Immunol. Methods* 1987. **105**: 71–78.

184 **Jensen, R. H. and Leary, J. F.**, Mutagenesis as measured by flow cytometry and cell sorting. In M. R. Melamed, M. L. Mendelsohn and T. Lindmo (Eds.) *Flow cytometry and sorting*, 2nd ed., Wiley-LISS, New York, NY, 1990.

185 **Cossarizza, A. and Cousins, D.**, Overcoming challenges in cellular analysis: multiparameter analysis of rare cells. *Science* 2015. **347**: 443.

186 **Gross, H. J., Verwer, B., Houck, D., Hoffman, R. A. and Recktenwald, D.**, Model study detecting breast cancer cells in peripheral blood mononuclear cells at frequencies as low as 10^{-7}. *Proc. Natl. Acad. Sci. U.S.A.* 1995. **92**: 537–541.

187 **Donnenberg, A. D. and Donnenberg, V. S.**, Rare-event analysis in flow cytometry. *Clin. Lab. Med.* 2007. **27**: 627–652.

188 **De Biasi, S., Bianchini, E., Nasi, M., Digaetano, M., Gibellini, L., Carnevale, G., Borghi, V. et al.**, Th1 and Th17 pro-inflammatory profile characterizes iNKT cells in virologically suppressed HIV^+ patients with low CD4/CD8 ratio. *AIDS* 2016. **30**: 2599–2610.

189 **Duda, D. G., Cohen, K. S., Scadden, D. T. and Jain, R. K.**, A protocol for phenotypic detection and enumeration of circulating endothelial cells and circulating progenitor cells in human blood. *Nat. Protoc.* 2007. **2**: 805–810.

190 **Mancuso, P., Antoniotti, P., Quarna, J., Calleri, A., Rabascio, C., Tacchetti, C. and Braidotti, P.**, Validation of a standardized method for enumerating circulating endothelial cells and progenitors: flow cytometry and molecular and ultrastructural analyses. *Clin. Cancer Res.* 2009. **15**: 267–273.

191 **Van Craenenbroeck, E. M., Conraads, V. M., Van Bockstaele, D. R., Haine, S. E., Vermeulen, K., Van Tendeloo, V. F. and Vrints, C. J.**, Quantification of circulating endothelial progenitor cells: A methodological comparison of six flow cytometric approaches. *J. Immunol. Methods* 2008. **332**: 31–40.

192 **Estes, M. L., Mund, J. A., Ingram, D. A. and Case, J.**, Identification of endothelial cells and progenitor cell subsets in human peripheral blood. *Curr. Protoc. Cytom.* 2010. **52**: 9.33.1–9.33.11.

193 **De Biasi, S., Cerri, S., Bianchini, E., Gibellini, L., Persiani, E., Montanari, G. and Luppi, F.**, Levels of circulating endothelial cells are low in idiopathic pulmonary fibrosis and are further reduced by anti-fibrotic treatments. *BMC Med.* 2015. **13**: 277.

194 **Cox, C., Reeder, J. E., Robinson, R. D., Suppes, S. B. and Wheeless, L. L.**, Comparison of frequency distribution in flow cytometry. *Cytometry* 1988. **9**: 291–298.

195 **Haight, F. A.**, *Handbook of the Poisson distribution*. John Wiley & Sons, New York, NY, 1967.

196 **Roederer, M.**, How many events is enough? Are you positive? *Cytometry* 2008. **73**: 384–385.

197 **Boyd, W. A., Smith, M. V. and Freedman, J. H.**, *Caenorhabditis elegans* as a model in developmental toxicology. *Methods Cell. Biol.* 2012. **889**: 15-24.

198 **Steffen, A., Ludwig, B., Krautz, C., Bornstein, S. and Solimena, M.**, Functional assessment of automatically sorted pancreatic islets using large particle flow cytometry. *Islet*. 2011. **3**: 67–270.

199 **Li, C. Y., Wood, D. K., Huang, J. H. and Bhatia, S. N.**, Flow-based pipeline for systematic modulation and analysis of 3D tumor microenvironments. *Lab. Chip*. 2013. **13**: 1969–1978.

200 **Coder, D. M.**, Assessment of cell viability. *Curr. Protoc. Cytom.* 2001. **15**: 9.2:9.2.1–9.2.14.

201 **Perfetto, S. P., Chattopadhyay, P. K., Lamoreaux, L., Nguyen, R., Ambrozak, D., Koup, R. A. and Roederer, M.** Amine reactive dyes: an effective tool to discriminate live and dead cells in polychromatic flow cytometry. *J. Immunol. Methods* 2006. **313**: 199–208.

202 **Zuba-Surman, E. K., Kucia, M. and Ratajczak, M. Z.**, Decoding the dots: the ImageStream system (ISS) as a novel and powerful tool for flow cytometric analysis. *Cent. Eur. J. Biol.* 2008. **3**: 1–10.

203 **Vindelov, L. L., Christensen, I. J. and Nissen, N. I.**, A detergent-trypsin method for the preparation of nuclei for flow cytometric DNA analysis. *Cytometry* 1983. **3**: 323–327.

204 **Hedley, D. W., Friedlander, M. L., Taylor, I. W., Rugg, C. A. and Musgrove, E. A.**, Method for analysis of cellular DNA content of paraffin-embedded pathological material using flow cytometry. *J. Histochem. Cytochem.* 1983. **31**: 1333–1335.

205 **Degtyarev, M., Reichelt, M. and Lin, K.**, Novel quantitative autophagy analysis by organelle flow cytometry after cell sonication. *PLoS One*. 2014. **9**: e87707

206 **Poot, M., Gibson, L. L. and Singer, V. L.**, Detection of apoptosis in live cells by MitoTracker CMXRos and SYTO dye flow cytometry. *Cytometry*. 1997. **27**: 358–364.

207 **Poot, M.**, Analysis of intracellular organelles by flow cytometry or microscopy. *Curr. Protoc. Cytom.* 2001. **14**: 9.4:9.4.1–9.4.24.

208 **Bailey, S. and Macardle, P. J.**, A flow cytometric comparison of Indo-1 to fluo-3 and Fura Red excited with low power lasers for detecting Ca(2+) flux. *J. Immunol. Methods* 2006. **311**: 220–225.

209 **Leverrier, S., Bergamaschi, D., Ghali, L., Ola, A., Warnes, G., Akgul, B. et al.**, Role of HPV E6 proteins in preventing UVB-induced release of pro-apoptotic factors from the mitochondria. *Apoptosis*. 2007. **12**: 549–560.

210 **Dolezel, J., Vrana, J., Safar, J., Bartos, J., Kubalakova, M. and Simkova, H.**, Chromosomes in the flow to simplify genome analysis. *Funct. Integr. Genomics*. 2012. **12**: 97–416.

211 **Davies, D. C., Monard, S. P. and Young, B. D.** Chromosome analysis and sorting by flow cytometry. In MG Ormerod (Ed.), *Flow cytometry: A practical approach*, 3rd edition, Oxford University Press, Oxford, U.K., 2000.

212 **Ng, B. L., Fu, B., Graham, J., Hall, C. and Thompson, S.**, Chromosome analysis using benchtop cell analysers and high speed cell sorters. *Cytometry A* 2018. **95**: 323–331.

213 **Rhys, H. I., Dell'Accio, F., Pitzalis, C., Moore, A., Norling, L. V. and Perretti, M.**, Neutrophil microvesicles from healthy control and rheumatoid arthritis patients prevent the inflammatory activation of macrophages. *EBioMedicine*. 2018. **29**: 60–69.

214 **Orozco, A. and Lewis, D.**, Flow cytometric analysis of circulating microparticles in plasma. *Cytometry A*. 2010. **77A**: 502–514.

215 **Zucker, R. M., Ortenzio, J. N. R., Boyes, W. K.**, Characterization, detection, and counting of metal nanoparticles using flow cytometry. *Cytometry A*. 2016. **89A**: 69–183.

216 **Morales-Kastresana, A., Telford, W., Musich, T. A., McKinnon, K., Clayborne, C., Braig, Z., Rosner, A. et al.**, Labeling extracellular vesicles for nanoscale flow cytometry. *Sci. Rep.* 2017. **7**: 1878

217 **Kastelowitz, N. and Yin, H.**, Exosomes and microvesicles: identification and targeting by particle size and lipid chemical probes. *ChemBioChem*. 2014. **15**: 923–928.

218 **Erdbrügger, U., Rudy, C. K., Etter, M. E., Dryden, K. A., Yeager, M., Kibanov, A. L. and Lannigan, J.**, Imaging flow cytometry elucidates limitations of microparticle analysis by conventional flow cytometry. *Cytometry A*. 2014. **85A**: 756–770.

219 **Marcoux, G., Duchez, A. C., Clouthier, N., Provost, P., Nigrovic, P. A. and Boilard, E.**, Revealing the diversity of extracellular vesicles using high-dimensional flow cytometry analyses. *Sci. Rep.* 2016. **6**: 35928

220 **Wallace, D. C.**, Mitochondria and cancer. *Nat. Rev. Cancer* 2012. **12**: 685–698.

221 **Wallace, D. C.**, Mitochondrial diseases in man and mouse. *Science* 1999. **283**: 1482–1488.

222 **Brand, M. D. and Nicholls, D. G.**, Assessing mitochondrial dysfunction in cells. *Biochem. J.* 2011. **435**: 297–312.

223 **Cottet-Rousselle, C., Ronot, X., Leverve, X. and Mayol, J. F.**, Cytometric assessment of mitochondria using fluorescent probes. *Cytometry A* 2011. **79**: 405–425.

224 **Lay, A. W. L. and Burton, A. C.**, Direct measurement of potential difference across the human red blood cell membrane. *Biophys. J.* 1969. **9**: 115–121.

225 **Perry, S. W., Norman, J. P., Barbieri, J., Brown, E. B. and Gelbard, H. A.**, Mitochondrial membrane potential probes and the proton gradient: A practical usage guide. *Biotechniques* 2011. **50**: 98–115.

226 **Petit, P. X., Susin, S. A., Zamzami, N., Mignotte, B. and Kroemer, G.**, Mitochondria and programmed cell death: Back to the future. *FEBS Lett.* 1996. **396**: 7–13.

227 **Rottenberg, H. and Wu, S.**, Quantitative assay by flow cytometry of the mitochondrial membrane potential in intact cells. *Biochim. Biophys. Acta* 1998. **1404**: 393–404.

228 **Johnson, L. V., Walsh, M. L. and Chen, L. B.**, Localization of mitochondria in living cells with rhodamine 123. *Proc. Natl. Acad. Sci. U.S.A.* 1980. **77**: 990–994.

229 **Troiano, L., Granata, A. R., Cossarizza, A., Kalashnikova, G., Bianchi, R., Pini, G., Tropea, F. et al.**, Mitochondrial membrane potential and DNA stainability in human sperm cells: a flow cytometry analysis with implications for male infertility. *Exp. Cell. Res.* 1998. **241**: 384–393.

230 **Ehrenberg, B., Montana, V., Wei, M. D., Wuskell, J. P. and Loew, L. M.**, Membrane potential can be determined in individual cells from the nernstian distribution of cationic dyes. *Biophys. J.* 1988. **53**: 785–794.

231 **Nicholls, D. G. and Ward, M. W.**, Mitochondrial membrane potential and neuronal glutamate excitotoxicity: Mortality and millivolts. *Trends Neurosci.* 2000. **23**: 166–174.

232 **Cossarizza, A., Baccarani-Contri, M., Kalashnikova, G. and Franceschi, C.**, A new method for the cytofluorimetric analysis of mitochondrial membrane potential using the J-aggregate forming lipophilic cation 5,5′,6,6′-tetrachloro-1,1′,3,3′;-tetraethylbenzimidazolcarbocyanine iodide (JC-1). *Biochem. Biophys. Res. Commun.* 1993. **197**: 40–45.

233 **Smiley, S. T., Reers, M., Mottola-Hartshorn, C., Lin, M., Chen, A., Smith, T. W., Steele, G. D. et al.**, Intracellular heterogeneity in mitochondrial membrane potentials revealed by a J-aggregate-forming lipophilic cation JC-1. *Proc. Natl. Acad. Sci. U.S.A.* 1991. **88**: 3671–3675.

234 **Reers, M., Smith, T. W. and Chen, L. B.**, J-aggregate formation of a carbocyanine as a quantitative fluorescent indicator of membrane potential. *Biochemistry* 1991. **30**: 4480–4486.

235 **Moudy, A. M., Handran, S. D., Goldberg, M. P., Ruffin, N., Karl, I., Kranz-Eble, P., DeVivo, D. C. et al.**, Abnormal calcium homeostasis and mitochondrial polarization in a human encephalomyopathy. *Proc. Natl. Acad. Sci. U.S.A.* 1995. **92**: 729–733.

236 **Perelman, A., Wachtel, C., Cohen, M., Haupt, S., Shapiro, H. and Tzur, A.**, JC-1: alternative excitation wavelengths facilitate mitochondrial membrane potential cytometry. *Cell Death Dis.* 2012. **3**: e430.

237 **De Biasi, S., Gibellini, L. and Cossarizza, A.**, Uncompensated polychromatic analysis of mitochondrial membrane potential using JC-1 and multilaser excitation. *Curr. Prot. Cytom.* 2015. **72**: 7.32.1–7.32.11.

238 **Troiano, L., Ferraresi, R., Lugli, E., Nemes, E., Roat, E., Nasi, M., Pinti, M. et al.**, Multiparametric analysis of cells with different mitochondrial membrane potential during apoptosis by polychromatic flow cytometry. *Nat. Protoc.* 2007. **2**: 2719–2727.

239 **Poot, M., Zhang, Y. Z., Kramer, J. A., Wells, K. S., Jones, L. J., Hanzel, D. K., Lugade, A. G. et al.**, Analysis of mitochondrial morphology and function with novel fixable fluorescent stains. *J. Histochem. Cytochem.* 1996. **44**: 1363–1372.

240 **Septinus, M., Seiffert, W. and Zimmermann, H. W.**, Hydrophobic acridine dyes for fluorescence staining of mitochondria in living cells. 1. Thermodynamic and spectroscopic properties of 10-n-alkylacridine orange chlorides. *Histochemistry* 1983. **79**: 443–456.

241 **Dickinson, B. C., Lin, V. S. and Chang, C. J.**, Preparation and use of MitoPY1 for imaging hydrogen peroxide in mitochondria of live cells. *Nat. Protoc.* 2013. **8**: 1249–1259.

242 **Mukhopadhyay, P., Rajesh, M., Hasko, G., Hawkins, B. J., Madesh, M. and Pacher, P.**, Simultaneous detection of apoptosis and mitochondrial superoxide production in live cells by flow cytometry and confocal microscopy. *Nat. Protoc.* 2007. **2**: 2295–2301.

243 **Mukhopadhyay, P., Rajesh, M., Yoshihiro, K., Hasko, G. and Pacher, P.**, Simple quantitative detection of mitochondrial superoxide production in live cells. *Biochem. Biophys. Res. Commun.* 2007. **358**: 203–208.

244 **Robinson, K. M., Janes, M. S., Pehar, M., Monette, J. S., Ross, M. F., Hagen, T. M., Murphy, M. P. et al.**, Selective fluorescent imaging of superoxide in vivo using ethidium-based probes. *Proc. Natl. Acad. Sci. U.S.A.* 2006. **103**: 15038–15043.

245 **Cossarizza, A., Ferraresi, R., Troiano, L., Roat, E., Gibellini, L., Bertoncelli, L., Nasi, M. et al.**, Simultaneous analysis of reactive oxygen species and reduced glutathione content in living cells by polychromatic flow cytometry. *Nat. Protoc.* 2009. **4**: 1790–1797.

246 **Gibellini, L., Pinti, M., Bartolomeo, R., De Biasi, S., Cormio, A., Musicco, C., Carnevale, G. et al.**, Inhibition of Lon protease by triterpenoids alters mitochondria and is associated to cell death in human cancer cells. *Oncotarget* 2015. **6**: 25466–25483.

247 **Hawkins, B. J., Madesh, M., Kirkpatrick, C. J. and Fisher, A. B.**, Superoxide flux in endothelial cells via the chloride channel-3 mediates intracellular signaling. *Mol. Biol. Cell* 2007. **18**: 2002–2012.

248 **Iuso, A., Scacco, S., Piccoli, C., Bellomo, F., Petruzzella, V., Trentadue, R., Minuto, M. et al.**, Dysfunctions of cellular oxidative metabolism in patients with mutations in the NDUFS1 and NDUFS4 genes of complex I. *Biol. Chem.* 2006. **281**: 10374–10380.

249 **Rezvani, H. R., Dedieu, S., North, S., Belloc, F., Rossignol, R., Letellier, T., de Verneuil, H. et al.**, Hypoxia-inducible factor-1alpha, a key factor in the keratinocyte response to UVB exposure. *J. Biol. Chem.* 2007. **282**: 16413–16422.

250 **van der Pol, E., Böing, A. N., Harrison, P., Sturk, A. and Nieuwland, R.**, Classification, functions, and clinical relevance of extracellular vesicles. *Pharmacol. Rev.* 2012. **64**: 676–705.

251 **van der Pol, E., Coumans, F. A. W., Grootemaat, A. E., Gardiner, C., Sargent, I. L., Harrison, P., Sturk, A. et al.**, Particle size distribution of exosomes and microvesicles determined by transmission electron microscopy, flow cytometry, nanoparticle tracking analysis, and resistive pulse sensing. *J. Thromb. Haemost.* 2014. **12**: 1182–1192.

252 **De Rond, L., Coumans, F. A. W., Nieuwland, R., Van Leeuwen, T. G. and van der Pol, E.**, Deriving extracellular vesicle size from scatter

intensities measured by flow cytometry. *Blood Coagul. Fibrinolysis* 2018. 1–14.

253 **van der Pol, E., de Rond, L., Coumans, F. A. W., Gool, E. L., Böing, A. N., Sturk, A., Nieuwland, R. et al.**, Absolute sizing and label-free identification of extracellular vesicles by flow cytometry. *Nanomed. Nanotechnol. Biol. Med.* 2018. **14**: 801–810.

254 **White, J. G.**, Platelet structure. In: Michelson AD, ed. *Platelets*. 2nd ed.Academic Press, San Diego, CA 2006:45–73.

255 **Arraud, N., Linares, R., Tan, S., Gounou, C., Pasquet, J. M., Mornet, S. and Brisson, A. R.**, Extracellular vesicles from blood plasma: determination of their morphology, size, phenotype and concentration. *J. Thromb. Haemost.* 2014. **12**: 614–627.

256 **Brisson, A. R., Tan, S., Linares, R., Gounou, C. and Arraud, N.**, Extracellular vesicles from activated platelets: a semiquantitative cryo-electron microscopy and immuno-gold labeling study. *Platelets*. 2017. **28**: 263–271.

257 **Dragovic, R. A., Gardiner, C., Brooks, A. S., Tannetta, D. S., Ferguson, D. J. P., Hole, P., Carr, B. et al.**, Sizing and phenotyping of cellulars vesicles using nanoparticle tracking analysis. *Nanomed. Nanotechnol. Biol. Med.* 2011. **7**: 780–788.

258 **van der Pol, E., Hoekstra, A. G., Sturk, A., Otto, C., van Leeuwen, T. G. and Nieuwland, R.**, Optical and non-optical methods for detection and characterization of microparticles and exosomes. *J. Thromb. Haemost.* 2010. **8**: 2596–2607.

259 **van der Pol, E., Sturk, A., van Leeuwen, T. G., Nieuwland, R. and Coumans, F. A. W.**, Standardization of extracellular vesicle measurements by flow cytometry through vesicle diameter approximation. *J. Thromb. Haemost.* 2018. **16**: 1236–1245.

260 **van der Pol, E., van Gemert, M. J. C., Sturk, A., Nieuwland, R. and van Leeuwen, T. G.**, Single vs. swarm detection of microparticles and exosomes by flow cytometry. *J. Thromb. Haemost.* 2012. **10**: 919–930.

261 **Chandler, W. L., Yeung, W. and Tait, J. F.**, A new microparticle size calibration standard for use in measuring smaller microparticles using a new flow cytometer. *J. Thromb. Haemost.* 2011. **9**: 1216–1224.

262 **Coumans, F. A. W., Brisson, A. R., Buzas, E. I., Dignat-George, F., Drees, E. E. E., El-Andaloussi, S., Emanueli, C. et al.**, Methodological guidelines to study extracellular vesicles. *Circ. Res.* 2017. **120**: 1632–1648.

263 **Yuana, Y., Böing, A. N., Grootemaat, A. E., van der Pol, E., Hau, C. M., Cizmar, P., Buhr, E. et al.**, Handling and storage of human body fluids for analysis of extracellular vesicles. *J. Extracell. Vesicles*. 2015. **4**: 29260.

264 **Witwer, K. W., Buzás, E. I., Bemis, L. T., Bora, A., Lässer, C., Lötvall, J., Nolte-'t Hoen, E. N. et al.**, Standardization of sample collection, isolation and analysis methods in extracellular vesicle research. *J. Extracell. Vesicles* 2013. **2**: 1–25.

265 **Lacroix, R., Judicone, C., Mooberry, M., Boucekine, M., Key, N. S., Dignat-George, F., Ambrozic, A. et al.**, Standardization of pre-analytical variables in plasma microparticle determination: results of the International Society on Thrombosis and Haemostasis SSC collaborative workshop. *J. Thromb. Haemost.* 2013. **11**: 1190–1193.

266 **Wachalska, M., Koppers-Lalic, D., van Eijndhoven, M., Pegtel, M., Geldof, A. A., Lipinska, A. D., van Moorselaar, R. J. et al.**, Protein complexes in urine interfere with extracellular vesicle biomarker studies. *J. Circ. biomarkers*. 2016. **5**: 4.

267 **Berckmans, R. J., Sturk, A., Schaap, M. C. and Nieuwland, R.**, Cell-derived vesicles exposing coagulant tissue factor in saliva. *Blood*. 2011. **117**: 3172–3180.

268 **Lippi, G., Salvagno, G. L., Montagnana, M., Franchini, M. and Guidi, G. C.**, Venous stasis and routine hematologic testing. *Clin. Lab. Haematol.* 2006. **28**: 332–337.

269 **Jy, W., Horstman, L. L., Jimenez, J. J. and Ahn, Y. S.**, Measuring circulating cell-derived microparticles. *J. Thromb. Haemost.* 2004. **2**: 1842–1843.

270 **Lippi, G., Salvagno, G. L., Montagnana, M., Poli, G. and Guidi, G. C.**, Influence of the needle bore size on platelet count and routine coagulation testing. *Blood Coagul. Fibrinolysis* 2006. **17**: 557–561.

271 **Piccin, A., Murphy, W. G. and Smith, O. P.**, Circulating microparticles: pathophysiology and clinical implications. *Blood Rev.* 2007. **21**: 157–171.

272 **Hefler, L., Grimm, C., Leodolter, S. and Tempfer, C.**, To butterfly or to needle: the pilot phase. *Ann. Intern. Med.* 2004. **140**: 935–936.

273 **Van Ierssel, S. H., Van Craenenbroeck, E. M., Conraads, V. M., Van Tendeloo, V. F., Vrints, C. J., Jorens, P. G. and Hoymans, V. Y.**, Flow cytometric detection of endothelial microparticles (EMP): effects of centrifugation and storage alter with the phenotype studied. *Thromb. Res.* 2010. **125**: 332–339.

274 **Rikkert, L. G., van der Pol, E., van Leeuwen, T. G., Nieuwland, R. and Coumans, F. A. W.**, Centrifugation affects the purity of liquid biopsy-based tumor biomarkers. *Cytometry A* 2018. **93**: 1207–1212.

275 **Stoner, S. A., Duggan, E., Condello, D., Guerrero, A., Turk, J. R., Narayanan, P. K. and Nolan, J. P.**, High sensitivity flow cytometry of membrane vesicles. *Cytometry A* 2016. **89**: 196–206.

276 **Böing, A. N., van der Pol, E., Grootemaat, A. E., Coumans, F. A. W., Sturk, A. and Nieuwland, R.**, Single-step isolation of extracellular vesicles by size-exclusion chromatography. *J. Extracell. Vesicles*. 2014. **3**: 23430.

277 **Yuana, Y., Bertina, R. M. and Osanto, S.**, Pre-analytical and analytical issues in the analysis of blood microparticles. *Thromb. Haemost.* 2011. **105**: 396–408.

278 **Biro, E., Sturk-Maquelin, K. N., Vogel, G. M. T., Meuleman, D. G., Smit, M. J., Hack, C. E., Sturk, A. et al.**, Human cell-derived microparticles promote thrombus formation in vivo in a tissue factor-dependent manner. *J. Thromb. Haemost.* 2003. **1**: 2561–2568.

279 **Simak, J. and Gelderman, M. P.**, Cell membrane microparticles in blood and blood products: Potentially pathogenic agents and diagnostic markers. *Transfus. Med. Rev.* 2006. **20**: 1–26.

280 **Trummer, A., De Rop, C., Tiede, A., Ganser, A. and Eisert, R.**, Recovery and composition of microparticles after snap-freezing depends on thawing temperature. *Blood Coagul. Fibrinolysis* 2009. **20**: 52–56.

281 **de Rond, L., van der Pol, E., Hau, C. M., Varga, Z., Sturk, A., van Leeuwen, T. G., Nieuwland, R. et al.**, Comparison of generic fluorescent markers for detection of extracellular vesicles by flow cytometry. *Clin. Chem.* 2018. **64**: 680–689.

282 **Baumgarth, N. and Roederer, M.**, A practical approach to multicolor flow cytometry for immunophenotyping. *J. Immunol. Methods*. 2000. **243**: 77–97.

283 **Chattopadhyay, P. K., Gaylord, B., Palmer, A., Jiang, N., Raven, M. A., Lewis, G., Reuter, M. A. et al.**, Brilliant violet fluorophores: a new class of ultrabright fluorescent compounds for immunofluorescence experiments. *Cytometry A* 2012. **81**: 456–466.

284 **Pieragostino, D., Lanuti, P., Cicalini, I., Cufaro, M. C., Ciccocioppo, F., Ronci, M., Simeone, P. et al.**, Proteomics characterization of extracellular vesicles sorted by flow cytometry reveals a disease-specific molecular cross-talk from cerebrospinal fluid and tears in multiple sclerosis. *Proteomics*. 2019. In press https://doi.org/10.1016/j.jprot.2019.103403

285 **Nolan, J. P. and Stoner, S. A.**, A trigger channel threshold artifact in nanoparticle analysis. *Cytometry A* 2013. **83**: 301–305.

286 **Arraud, N., Gounou, C., Turpin, D. and Brisson, A. R.** Fluorescence triggering: a general strategy for enumerating and phenotyping extracellular vesicles by flow cytometry. *Cytometry A* 2016. **89**: 184–195.

287 **Steen, H. B.**, Noise, sensitivity, and resolution of flow cytometers. *Cytometry* 1992. **13**: 822–830.

288 **Giesecke, C.**, **Feher, K.**, **von Volkmann, K.**, **Kirsch, J.**, **Radbruch, A. and Kaiser, T.**, Determination of background, signal-to-noise, and dynamic range of a flow cytometer: A novel practical method for instrument characterization and standardization. *Cytometry A* 2017. **91**: 1104–1114.

289 **Poncelet, P.**, **Robert, S.**, **Bouriche, T.**, **Bez, J.**, **Lacroix, R. and Dignat-George, F.**, Standardized counting of circulating platelet microparticles using currently available flow cytometers and scatter-based triggering: Forward or side scatter? *Cytometry A* 2016. **89**: 148–158.

290 **Hoen, E. N. M.**, **van der Vlist, E. J.**, **Aalberts, M.**, **Mertens, H. C. H.**, **Bosch, B. J.**, **Bartelink, W.**, **Mastrobattista, E. et al.**, Quantitative and qualitative flow cytometric analysis of nanosized cell-derived membrane vesicles. *Nanomed. Nanotechnol. Biol. Med.* 2012. **8**: 712–720.

291 **Lanuti, P.**, **Rotta, G.**, **Almici, C.**, **Avvisati, G.**, **Budillon, A.**, **Doretto, P.**, **Malara, N. et al.**, Endothelial progenitor cells, defined by the simultaneous surface expression of VEGFR 2 and CD 133, are not detectable in healthy peripheral and cord blood. *Cytometry A* 2016. **89**: 259–270.

292 **van der Vlist, E. J.**, **Nolte-'t Hoen, E. N. M.**, **Stoorvogel, W.**, **Arkesteijn, G. J. A. and Wauben, M. H. M.**, Fluorescent labeling of nano-sized vesicles released by cells and subsequent quantitative and qualitative analysis by high-resolution flow cytometry. *Nat. Protoc.* 2012. **7**: 1311–26.

293 **Osteikoetxea, X.**, **Sódar, B.**, **Németh, A.**, **Szabó-Taylor, K.**, **Pálóczi, K.**, **Vukman, K. V.**, **Tamási, V. et al.**, Differential detergent sensitivity of extracellular vesicle subpopulations. *Org. Biomol. Chem.* 2015. **13**: 9775–9782.

294 **Schwartz, A.**, **Gaigalas, A. K.**, **Wang, L.**, **Marti, G. E.**, **Vogt, R. F. and Fernandez-Repollet, E.**, Formalization of the MESF unit of fluorescence intensity. *Cytometry B Clin. Cytom.* 2004. **57**: 1–6.

295 **Wang, L.**, **Gaigalas, A. K.**, **Abbasi, F.**, **Marti, G. E.**, **Vogt, R. F. and Schwartz, A.**, Quantitating fluorescence intensity from fluorophores: practical use of MESF values. *J. Res. Natl. Inst. Stand. Technol.* 2002. **107**: 339.

296 **Wang, L. and Gaigalas, A. K.**, Development of multicolor flow cytometry calibration standards: assignment of equivalent reference fluorophores (ERF) unit. *J. Res. Natl. Inst. Stand. Technol.* 2011. **116**: 671.

297 **Welsh, J.**, **Kepley, J.**, **Rosner, A.**, **Horak, P.**, **Berzofsky, J. and Jones, J.**, Prospective use of high-refractive index materials for single molecule detection in flow cytometry. *Sensors*. 2018. **18**: 2461.

298 **Lacroix, R.**, **Robert, S.**, **Poncelet, P.**, **Kasthuri, R. S.**, **Key, N. S. and Dignat-George, F.**, Standardization of platelet-derived microparticle enumeration by flow cytometry with calibrated beads: results of the International Society on Thrombosis and Haemostasis SSC Collaborative workshop. *J. Thromb. Haemost.* 2010. **8**: 2571–2574.

299 **Lacroix, R.**, **Robert, S.**, **Poncelet, P. and Dignat-George, F.**, Overcoming limitations of microparticle measurement by flow cytometry. *Semin. Thromb. Hemost.* 2010. **36**: 807–818.

300 **Zhu, S.**, **Ma, L.**, **Wang, S.**, **Chen, C.**, **Zhang, W.**, **Yang, L.**, **Hang, W. et al.**, Light-scattering detection below the level of single fluorescent molecules for high-resolution characterization of functional nanoparticles. *ACS Nano*. 2014. **8**: 10998–11006.

301 **Welsh, J. A.**, **Horak, P.**, **Wilkinson, J. S.**, **Ford, V. J.**, **Jones, J. C.**, **Smith, D.**, **Holloway, J. A.**, **and Englyst, N. A.**, FCMPASS Software Aids Extracellular Vesicle Light Scatter Standardization. *Cytometry Part A*. 2019. https://doi.org/10.1002/cyto.a.23782

302 **Scheffold, A.**, **Radbruch, A. and Assenmacher, M.**, Phenotyping and separation of leukocyte populations based on affinity labelling. *Methods Microbiol.* 2002. **32**: 23–58.

303 **Bradbury, A. M. and Plückthun, A.**, Antibodies: validate recombinants once. *Nature*. 2015. **520**: 295.

304 **Jain, R. and Gray, D. H.**, Isolation of thymic epithelial cells and analysis by flow cytometry. *Curr. Protoc. Immunol.* 2014.**107**: 3.26.1–3.26.15.

305 **Grützkau, A.**, **Krüger-Krasagakes, S.**, **Baumeister, H.**, **Schwarz, C.**, **Kögel, H.**, **Welker, P.**, **Lippert, U. et al.**, Synthesis, storage, and release of vascular endothelial growth factor/vascular permeability factor (VEGF/VPF) by human mast cells: implications for the biological significance of VEGF206. *Mol. Biol. Cell.* 1998. **9**: 875–84.

306 **Santangelo, C.**, *Worthington Biochemical Corporation tissue dissociation guide*. Worthington Biochemical Corporation, Lakewood, NJ 2008.

307 **Wong, K. H. K.**, **Sandlin, R. D.**, **Carey, T. R.**, **Miller, K. L.**, **Shank, A. T.**, **Oklu, R.**, **Maheswaran, S. et al.**, The role of physical stabilization in whole blood preservation. *Sci. Rep.* 2016. **6**: 21023.

308 **Plate, M. M.**, **Louzao, R.**, **Steele, P. M.**, **Greengrass, V.**, **Morris, L. M.**, **Lewis, J.**, **Barnett, D. et al.**, Evaluation of the blood stabilizers TransFix and Cyto-Chex BCT for low-cost CD4 T-cell methodologies. *Viral Immunol.* 2009. **22**: 329–32.

309 **Hayashida, K.**, **Bartlett, A. H.**, **Chen, Y.**, **Park, P. W.**, Molecular and cellular mechanisms of ectodomain shedding. *Anat. Rec.* 2010. **293**: 925–37.

310 **Berhanu, D.**, **Mortari, F.**, **De Rosa, S. C. and Roederer, M.**, Optimized lymphocyte isolation methods for analysis of chemokine receptor expression. *J. Immunol. Methods*. 2003. **279**: 199–207.

311 **Kivisäkk, P.**, **Liu, Z.**, **Trebst, C.**, **Tucky, B.**, **Wu, L.**, **Stine, J.**, **Mack, M. et al.**, Flow cytometric analysis of chemokine receptor expression on cerebrospinal fluid leukocytes. *Methods* 2003. **29**: 319–325.

312 **Liu, H.**, **Rhodes, M.**, **Wiest, D. L.**, **Vignali, D. A.**, On the dynamic of TCR:CD3 complex cell surface expression and downmodulation. *Immunity* 2000. **192**: 1529–1534.

313 **Mueller, A.**, **Kelly, E. and Strange, P. G.**, Pathways for internalization and recycling of the chemokine receptor CCR5. *Blood* 2002.**99**: 785–791.

314 **Campana, S.**, **De Pasquale, C.**, **Carrega, P.**, **Ferlazzo, G. and Bonaccorsi, I.**, Cross-dressing: an alternative mechanism for antigen presentation. *Immunol. Lett.* 2015. **168**: 349–354.

315 **Anselmo, A.**, **Mazzon, C.**, **Borroni, E. M.**, **Bonecchi, R.**, **Graham, G. J. and Locati, M.**, Flow cytometry applications for the analysis of chemokine receptor expression and function. *Cytometry A* 2014. **85**: 292–301.

316 **Pockley, A. G.**, **Foulds, G. A.**, **Oughton, J. A.**, **Kerkvliet, N. I. and Multhoff, G.**, Immune cell phenotyping using flow cytometry. *Curr. Protoc. Toxicol.* 2015. **66**:18.8.1—18.8.34.

317 **Darzynkiewicz, Z.**, **Halicka, H. D. and Zhao, H.**, Analysis of cellular DNA content by flow and laser scanning cytometry. *Adv. Exp. Med. Biol.* 2010. **676**: 137–147.

318 **Hamelik, R. M. and Krishan, A.**, Click-iT assay with improved DNA distribution histograms. *Cytometry A*. 2009. **75**: 862–865.

319 **Krishan, A. and Hamelik, R. M.**, Click-iT proliferation assay with improved DNA histograms. *Curr. Protoc. Cytom.* 2010. Chapter 7:Unit7 36.

320 **Lyons, A. B. and Parish, C. R.**, Determination of lymphocyte division by flow cytometry. *J. Immunol. Methods* 1994. **171**: 131–137.

321 **Wersto, R. P.**, **Chrest, F. J.**, **Leary, J. F.**, **Morris, C.**, **Stetler-Stevenson, M. A. and Gabrielson, E.**, Doublet discrimination in DNA cell-cycle analysis. *Cytometry* 2001. **46**: 296–306.

322 **van Engeland, M.**, **Nieland, L. J.**, **Ramaekers, F. C.**, **Schutte, B. and Reutelingsperger, C. P.**, Annexin V-affinity assay: a review on an apoptosis detection system based on phosphatidylserine exposure. *Cytometry* 1998. **31**: 1–9.

323 **Gehrmann, M., Doss, B. T., Wagner, M., Zettlitz, K. A., Kontermann, R. E., Foulds, G. et al.**, A novel expression and purification system for the production of enzymatic and biologically active human granzyme B. *J. Immunol. Methods* 2011. **371**: 8–17.

324 **Gehrmann, M., Stangl, S., Kirschner, A., Foulds, G. A., Sievert, W., Doss, B. T. et al.**, Immunotherapeutic targeting of membrane HSP70-expressing tumors using recombinant human granzyme B. *PLoS One* 2012. **7**: e41341

325 **Abate, M, Festa, A, Falco, M, Lombardi, A, Luce, A, Grimaldi, A, Zappavigna, S et al.**, Mitochondria as playmakers of apoptosis, autophagy and senescence. *Semin Cell Dev Biol.* 2019. S1084-9521(18)30187-3.

326 **Shalini, S., Dorstyn, L., Dawar, S. and Kumar, S.**, Old, new and emerging functions of caspases. *Cell Death Differ*. 2015. **22**: 526–539.

327 **Galluzzi, L., Lopez-Soto, A., Kumar, S. and Kroemer, G.**, Caspases connect cell-death signaling to organismal homeostasis. *Immunity* 2016. **44**: 221–231.

328 **Van Opdenbosch, N and Lamkanfi, M**, Caspases in cell death, inflammation, and disease. *Immunity*. 2019. **50**: 1352–1364.

329 **Galluzzi, L., Vitale, I., Aaronson, S. A., Abrams, J. M., Adam, D., Agostinis, P., Alnemri, E. S. et al.**, Molecular mechanisms of cell death: recommendations of the Nomenclature Committee on Cell Death 2018. *Cell Death Differ*. 2018. **25**: 486–541.

330 **Galluzzi, L., Kepp, O., Chan, F. K. and Kroemer, G.**, Necroptosis: mechanisms and relevance to disease. *Annu. Rev. Pathol. Mech. Dis.* 2017. **12**: 103–130.

331 **He, S. and Wang, X.**, RIP kinases as modulators of inflammation and immunity. *Nat. Immunol.* 2018. **19**: 912–922.

332 **Frank, D. and Vince, J. E.**, Pyroptosis versus necroptosis: similarities, differences, and crosstalk. *Cell Death Differ*. 2019. **26**: 99–114.

333 **Weinlich, R., Oberst, A., Beere, H. M. and Green, D. R.**, Necroptosis in development, inflammation and disease. *Nat. Rev. Mol. Cell Biol.* 2017. **18**: 127–136.

334 **Fuchslocher Chico, J., Saggau, C. and Adam, D.**, Proteolytic control of regulated necrosis. *Biochim. Biophys. Acta* 2017. **1864**: 2147–2161.

335 **Newton, K. and Manning, G.**, Necroptosis and inflammation. *Annu. Rev. Biochem.* 2016. **85**: 743–763.

336 **Lin, Y., Devin, A., Rodriguez, Y. and Liu, Z. G.**, Cleavage of the death domain kinase RIP by caspase-8 prompts TNF-induced apoptosis. *Genes Dev*. 1999. **13**: 2514–2526.

337 **Feng, S., Yang, Y., Mei, Y., Ma, L., Zhu, D. E., Hoti, N., Castanares, M. et al.**, Cleavage of RIP3 inactivates its caspase-independent apoptosis pathway by removal of kinase domain. *Cell Signal.* 2007. **19**: 2056–2067.

338 **O'Donnell, M. A., Perez-Jimenez, E., Oberst, A., Ng, A., Massoumi, R., Xavier, R., Green, D. R. et al.**, Caspase 8 inhibits programmed necrosis by processing CYLD. *Nat. Cell Biol.* 2011. **13**: 1437–1442.

339 **Vandenabeele, P., Galluzzi, L., Vanden Berghe, T. and Kroemer, G.**, Molecular mechanisms of necroptosis: an ordered cellular explosion. *Nat. Rev. Mol. Cell Biol.* 2010. **11**: 700–714.

340 **Tait, S. W., Oberst, A., Quarato, G., Milasta, S., Haller, M., Wang, R., Karvela, M. et al.**, Widespread mitochondrial depletion via mitophagy does not compromise necroptosis. *Cell Rep*. 2013. **5**: 878–885.

341 **He, S., Huang, S. and Shen, Z.**, Biomarkers for the detection of necroptosis. *Cell Mol. Life Sci.* 2016. **73**: 2177–2181.

342 Ting, A. T. (Ed.), *Programmed necrosis—Methods and protocols*. Humana Press, New York, NY, 2018.

343 **Zargarian, S., Shlomovitz, I., Erlich, Z., Hourizadeh, A., Ofir-Birin, Y., Croker, B. A., Regev-Rudzki, N. et al.**, Phosphatidylserine externalization, "necroptotic bodies" release, and phagocytosis during necroptosis. *PLoS Biol.* 2017. **15**: e2002711.

344 **Gong, Y. N., Guy, C., Olauson, H., Becker, J. U., Yang, M., Fitzgerald, P., Linkermann, A. et al.**, Escrt-III acts downstream of MLKL to regulate necroptotic cell death and its consequences. *Cell* 2017. **169**: 286–300.

345 **Lee, H. L., Pike, R., Chong, M. H. A., Vossenkamper, A. and Warnes, G.**, Simultaneous flow cytometric immunophenotyping of necroptosis, apoptosis and RIP1-dependent apoptosis. *Methods* 2018. **134-135**: 56–66.

346 **Moriwaki, K., Balaji, S., Bertin, J., Gough, P. J. and Chan, F. K.**, Distinct kinase-independent role of RIPK3 in CD11c+ mononuclear phagocytes in cytokine-induced tissue repair. *Cell Rep*. 2017. **18**: 2441–2451.

347 **Pietkiewicz, S., Schmidt, J. H. and Lavrik, I. N.**, Quantification of apoptosis and necroptosis at the single cell level by a combination of Imaging Flow Cytometry with classical Annexin V/propidium iodide staining. *J. Immunol. Methods* 2015. **423**: 99–103.

348 **Giampietri, C., Starace, D., Petrungaro, S., Filippini, A. and Ziparo, E.**, Necroptosis: molecular signalling and translational implications. *Int. J. Cell Biol.* 2014. **2014**: 490275.

349 **Richter, J., Schlesner, M., Hoffmann, S., Kreuz, M., Leich, E., Burkhardt, B., Rosolowski, M. et al.**, Recurrent mutation of the ID3 gene in Burkitt lymphoma identified by integrated genome, exome and transcriptome sequencing. *Nat. Genet.* 2012. **44**: 1316–1320.

350 **Lüschen, S., Ussat, S., Scherer, G., Kabelitz, D. and Adam-Klages, S.**, Sensitization to death receptor cytotoxicity by inhibition of Fas-associated death domain protein (FADD)/caspase signaling - Requirement of cell cycle progression. *J. Biol. Chem.* 2000. **275**: 24670–24678.

351 **Falk, M., Ussat, S., Reiling, N., Wesch, D., Kabelitz, D. and Adam-Klages, S.**, Caspase inhibition blocks human T cell proliferation by suppressing appropriate regulation of IL-2, CD25, and cell cycle-associated proteins. *J. Immunol.* 2004. **173**: 5077–5085.

352 **Philipp, S., Sosna, J., Plenge, J., Kalthoff, H. and Adam, D.**, Homoharringtonine, a clinically approved anti-leukemia drug, sensitizes tumor cells for TRAIL-induced necroptosis. *Cell Commun. Signal*. 2015. **13**: 25.

353 **Aglietti, R. A. and Dueber, E. C.**, Recent insights into the molecular mechanisms underlying pyroptosis and gasdermin family functions. *Trends Immunol.* 2017. **38**: 261–271.

354 **Man, S. M., Karki, R. and Kanneganti, T. D.**, Molecular mechanisms and functions of pyroptosis, inflammatory caspases and inflammasomes in infectious diseases. *Immunol. Rev.* 2017. **277**: 61–75.

355 **Jorgensen, I., Rayamajhi, M. and Miao, E. A.**, Programmed cell death as a defence against infection. *Nat. Rev. Immunol.* 2017. **17**: 151–164.

356 **den Hartigh, A. B. and Fink, S. L.**, Pyroptosis induction and detection. *Curr. Protoc. Immunol.* 2018. e52.

357 **Zhang, Y., Chen, X., Gueydan, C. and Han, J.**, Plasma membrane changes during programmed cell deaths. *Cell Res.* 2018. **28**: 9–21.

358 **Yuan, J., Najafov, A. and Py, B. F.**, Roles of caspases in necrotic cell death. *Cell* 2016. **167**: 1693–1704.

359 **Sester, D. P., Zamoshnikova, A., Thygesen, S. J., Vajjhala, P. R., Cridland, S. O., Schroder, K. and Stacey, K. J.**, Assessment of inflammasome formation by flow cytometry. *Curr. Protoc. Immunol.* 2016. **114**: 14.40.11–14.40.29.

360 **Cui, J., Zhou, Z., Yang, H., Jiao, F., Li, N., Gao, Y., Wang, L. et al.**, MST1 suppresses pancreatic cancer progression via ROS-induced pyroptosis. *Mol. Cancer Res.* 2019. **17**: 1316–1325.

361 **Paddenberg, R., Wulf, S., Weber, A., Heimann, P., Beck, L. A. and Mannherz, H. G.**, Internucleosomal DNA fragmentation in cultured

cells under conditions reported to induce apoptosis may be caused by mycoplasma endonucleases. *Eur. J. Cell Biol.* 1996. **71**: 105–119.

362 **Zhang, D. W., Shao, J., Lin, J., Zhang, N., Lu, B. J., Lin, S. C., Dong, M. Q. et al.**, RIP3, an energy metabolism regulator that switches TNF-induced cell death from apoptosis to necrosis. *Science* 2009. **325**: 332–336.

363 **Pozarowski, P., Huang, X., Halicka, D. H., Lee, B., Johnson, G. and Darzynkiewicz, Z.**, Interactions of fluorochrome-labeled caspase inhibitors with apoptotic cells: a caution in data interpretation. *Cytometry A* 2003. **55**: 50–60.

364 **Darzynkiewicz, Z., Zhao, H., Dorota Halicka, H., Pozarowski, P. and Lee, B.**, Fluorochrome-labeled inhibitors of caspases: expedient in vitro and in vivo markers of apoptotic cells for rapid cytometric analysis. *Methods Mol. Biol.* 2017. **1644**: 61–73.

365 **Tran, T. A. T., Grievink, H. W., Lipinska, K., Kluft, C., Burggraaf, J., Moerland, M., Tasev, D. et al.**, Whole blood assay as a model for in vitro evaluation of inflammasome activation and subsequent caspase-mediated interleukin-1 beta release. *PLoS One* 2019. **14**: e0214999.

366 **Sokolovska, A., Becker, C. E., Ip, W. K., Rathinam, V. A., Brudner, M., Paquette, N., Tanne, A. et al.**, Activation of caspase-1 by the NLRP3 inflammasome regulates the NADPH oxidase NOX2 to control phagosome function. *Nat. Immunol.* 2013. **14**: 543–553.

367 **Fuchslocher Chico, J., Falk-Paulsen, M., Luzius, A., Ruder, B., Bolik, J., Schmidt-Arras, D., Linkermann, A. et al.**, The enhanced susceptibility of ADAM-17 hypomorphic mice to DSS-induced colitis is not ameliorated by loss of RIPK3, revealing an unexpected function of ADAM-17 in necroptosis. *Oncotarget* 2018. **9**: 12941–12958.

368 **Gordon, S.**, Phagocytosis: An Immunobiologic Process. *Immunity*. 2016. **44**: 463–475.

369 **Cooper, E. L., Kauschke, E. and Cossarizza, A.**, Digging for innate immunity since Darwin and Metchnikoff. *Bioessays* 2002. **24**: 319–333.

370 **Navarre, W. W. and Zychlinsky, A.**, Pathogen-induced apoptosis of macrophages: a common end for different pathogenic strategies. *Cell Microbiol.* 2000. **2**: 265–273.

371 **Savill, J.**, Recognition and phagocytosis of cells undergoing apoptosis. *Br. Med. Bull.* 1997. **53**: 491–508.

372 **Brown, G. C., Vilalta, A. and Fricker, M.**, Phagoptosis—cell death by phagocytosis plays central roles in physiology, host defense and pathology. *Curr. Mol. Med.* 2015. **15**: 842–851.

373 **Lunov, O., Syrovets, T., Loos, C., Beil, J., Delacher, M., Tron, K., Nienhaus, G. U. et al.**, Differential uptake of functionalized polystyrene nanoparticles by human macrophages and a monocytic cell line, *ACS Nano* 2011. **5**: 1657–1669.

374 **Valet, G., Jenssen, H. L., Krefft, M. and Ruhenstroth-Baued, G.**, Flow-cytometric measurements of the transmembrane potential, the surface charge density and the phagocytic activity of guinea pig macrophages after incubation with lymphokines. *Blut* 1981. **42**: 379–382.

375 **Dunn, P. A. and Tyrer, H. W.**, Quantitation of neutrophil phagocytosis, using fluorescent latex beads. Correlation of microscopy and flow cytometry. *J. Lab. Clin. Med.* 1981. **98**: 374–381.

376 **Bjerknes, R. and Bassøe, C. F.**, Human leukocyte phagocytosis of zymosan particles measured by flow cytometry. *Acta Pathol. Microbiol. Immunol. Scand. C.* 1983. **91**: 341–348.

377 **Lehmann, A. K., Sørnes, S. and Halstensen, A.**, Phagocytosis: measurement by flow cytometry. *J. Immunol. Methods* 2000. **243**: 229–242.

378 **Bassøe, C. F.**, Assessment of phagocyte functions by flow cytometry. *Curr. Prot. Cytom.* 2002. **21**: 9.19.1–9.19.22.

379 **Simons, E. R.**, Measurement of phagocytosis and of the phagosomal environment in polymorphonuclear phagocytes by flow cytometry. *Curr. Protoc. Cytom.* 2010. 9.31.1–9.31.10.

380 **Sokolovska, A., Becker, C. E. and Stuart, L. M.**, Measurement of phagocytosis, phagosome acidification, and intracellular killing of *Staphylococcus aureus*. *Curr. Protoc. Immunol.* 2012. **99**: 14.30.1–14.30.12.

381 **Elbim, C. and Lizard, G.**, Flow cytometric investigation of neutrophil oxidative burst and apoptosis physiological and pathological situation. *Cytometry Part A*. 2009. **75A**: 475–481.

382 **Thomason, J., Archer, T., Mackin, A., Stokes, J. and Pinchuk, L.**, Applications of flow cytometry in veterinary research and small animal clinical practice. *J. Vet. Med. Res.* 2014. **1**: 1004–1012.

383 **Keogh, M. J., Spoon, T., Ridgway, S. H., Jensen, E., Van Bonn, W. and Romano, T. A.**, Simultaneous measurement of phagocytosis and respiratory burst of leukocytes in whole blood from bottlenose dolphins (*Tursiops truncatus*) utilizing flow cytometry. *Vet. Immunol. Immunopathol.* 2011. **144**: 468–475.

384 **Frankenberg, T., Kirschnek, S., Häcker, H. and Häcker, G.**, Phagocytosis-induced apoptosis of macrophages is linked to uptake, killing and degradation of bacteria. *Eur. J. Immunol.* 2008. **38**: 204–215.

385 **Tartaro, K., VanVolkenburg, M., Wilkie, D., Coskran, T. M., Kreeger, J. M., Kawabata, T. T. and Casinghino, S.**, Development of a fluorescence-based in vivo phagocytosis assay to measure mononuclear phagocyte system function in the rat. *J. Immunotoxicol.* 2015. **12**: 239–246.

386 **Webb, C., McCord, K. and Dow, S.**, Neutrophil function in septic dogs. *J. Vet. Intern. Med.* 2007. **21**: 982–989.

387 **Rossi, G, Capitani, L., Ceciliani, F., Restelli, L. and Paltrinieri, S.**, Hyposialylated α1-acid glycoprotein inhibits phagocytosis of feline neutrophils. *Res. Vet. Sci.* 2013. **95**: 465–471.

388 **Moya, S. L., Gómez, M. A., Boyle, L. A., Mee, J. F., O'Brien, B. and Arkins, S.**, Effects of milking frequency on phagocytosis and oxidative burst activity of phagocytes from primiparous and multiparous dairy cows during early lactation. *J. Dairy Sci.* 2008. **91**: 587–595.

389 **Stent, G., Reece, J. C., Baylis, D. C., Ivinson, K., Paukovics, G., Thomson, M. and Cameron, P. U.**, Heterogeneity of freshly isolated human tonsil dendritic cells demonstrated by intracellular markers, phagocytosis, and membrane dye transfer. *Cytometry*. 2002. **48**: 167–176.

390 **Becker, S., Halme, J. and Haskill, S.**, Heterogeneity of human peritoneal macrophages: Cytochemical and flow cytometric studies. *J. Reticuloendothelial Soc.* 1983. **33**: 127–138.

391 **Jersmann, H. P. A., Ross, K. A., Vivers, S., Brown, S. B., Haslett, C. and Dransfield, I.**, Phagocytosis of apoptotic cells by human macrophages: analysis by multiparameter flow cytometry. *Cytometry A*. 2003. **51A**: 7–15.

392 **Linehan, E., Dombrowski, Y., Snoddy, R., Fallon, P. G., Kissenpfennig, A. and Fitzgerald, D. C.**, Aging impairs peritoneal but not bone marrow-derived macrophage phagocytosis. *Aging Cell*. 2014. **13**: 699–708.

393 **Fuller-Espie, S. L.**, Using flow cytometry to measure phagocytic uptake in earthworms. *J. Microbiol. Biol. Educ.* 2010. **11**: 144–151.

394 http://www.lgcstandards-atcc.org/

395 **Rothwell, D. J. and Doumas, B. T.**, The effect of heparin and EDTA on the NBT test. *J. Lab. Clin. Med.* 1975. **85**: 950–956.

396 **Li, W. and Chung, S. C.**, Flow cytometric evaluation of leukocyte function in rat whole blood. *In Vitro Cell Dev. Biol. Anim.* 2003. **39**(10):413–419.

397 **Ducusin, R. J., Sarashina, T., Uzuka, Y., Tanabe, S. and Ohtani, M.**, Phagocytic response of bovine polymorphonuclear leukocytes to different incubation conditions and following exposure to some effectors

of phagocytosis and different anticoagulants in vitro. *Can. J. Vet. Res.* 2001. **65**: 38–44.

398 **van der Maten, E., de Jonge, M. I., de Groot, R., van der Flier, M. and Langereis, J. D.**, A versatile assay to determine bacterial and host factors contributing to opsonophagocytotic killing in hirudin-anticoagulated whole blood. *Sci. Rep.* 2017.**7**: 42137.

399 **Sustrova, T., Ondrackova, P., Leva, L. and Sladek, Z.**, Isolation techniques of neutrophils and peripheral blood mononuclear cells for the comparative experiments in humans and pigs model organisms in flow cytometry. *Mendelnet* 2014. 516–521.

400 **Carneiro, C., Vaz, C., Carvalho-Pereira, J., Pais, C. and Sampaio, P.**, A new method for yeast phagocytosis analysis by flow cytometry. *J. Microbiol. Methods* 2014. **101**: 56–62.

401 **Murciano, C., Villamón, E., O'Connor, J. E., Gozalbo, D. and Gil, M. L.**, Killed candida albicans yeasts and hyphae inhibit gamma interferon release by murine natural killer cells. *Infect. Immun.* 2006. **74**: 1403–1406.

402 **Anding, K., Rost, J. M., Jacobs, E. and Daschner, F. D.**, Flow cytometric measurements of neutrophil functions: the dependence on the stimulus to cell ratio. *FEMS Immunol. Med. Microbiol.* 2003. **35**: 147–152.

403 **Chan, C. L., Rénia, L. and Tan, K. S. W., A simplified**, sensitive phagocytic assay for malaria cultures facilitated by flow cytometry of differentially-stained cell populations. *PLoS One.* 2012. **7**: e38523.

404 **Lee, C. Y., Herant, M. and Heinrich, M.**, Target-specific mechanics of phagocytosis: Protrusive neutrophil response to zymosan differs from the uptake of antibody-tagged pathogens. *Cell Sci.* 2011. **124**: 1106–1114.

405 **Salih, H. R., Husfeld, L. and Adam, D.**, Simultaneous cytofluorometric measurement of phagocytosis, burst production and killing of human phagocytes using *Candida albicans* and *Staphylococcus aureus* as target organisms. *Clin. Microbiol. Infect.* 2000. **6**: 251–258.

406 **Li, F., Yang, M., Wang, L., Williamson, I., Tian, F., Qin, M., Shah, P. K. et al.**, Autofluorescence contributes to false-positive intracellular Foxp3 staining in macrophages: a lesson learned from flow cytometry. *J. Immunol. Meth.* 2012. **386**: 101–107.

407 **Yáñez, A., Flores, A., Murciano, C., O'Connor, J. E., Gozalbo, D. and Gil, M. L.**, Signalling through TLR2/MyD88 induces differentiation of murine bone marrow stem and progenitor cells to functional phagocytes in response to *Candida albicans*. *Cell. Microbiol.* 2010.**12**: 114–128.

408 **Bicker, H., Höflich, C., Wolk, K., Vogt, K., Volk, H. D. and Sabat, R.**, A simple assay to measure phagocytosis of live bacteria. *Clin. Chem.* 2008. **54**: 5 911–915.

409 **Schreiner, L., Huber-Lang, M., Weiss, M. E., Hohmann, H., Schmolz, M. and Schneider, E. M.**, Phagocytosis and digestion of pH-sensitive fluorescent dye (Eos-FP) transfected *E. coli* in whole blood assays from patients with severe sepsis and septic shock. *J. Cell. Commun. Signal.* 2011. **5**: 135–144.

410 **Bajno, L. and Grinstein, S.**, Fluorescent proteins: powerful tools in phagocyte biology. *J. Immunol. Methods.* 1999. **232**: 67–75.

411 **Zawada, A. M., Rogacev, K. S., Schirmer, S. H., Sester, M., Böhm, M., Fliser, D. and Heine, G. H.**, Monocyte heterogeneity in human cardiovascular disease. *Immunobiology.* 2012. **217**: 1273–1284.

412 **Neaga, A., Lefor, J., Lich, K. E., Liparoto, S. F. and Xiao, Y. Q.**, Development and validation of a flow cytometric method to evaluate phagocytosis of pHrodo™ BioParticles® by granulocytes in multiple species. *J. Immunol. Methods.* 2013. **390**: 9–17.

413 **Schrijvers, D. M, Martinet, W., De Meyer, G. R. Y, Andries, L. Herman and Kockx, M. M.**, Flow cytometric evaluation of a model for phagocytosis of cells undergoing apoptosis. *J. Immunol. Methods* 2004. **287**: 101–108.

414 **Basiji, D. A., Ortyn, W. E., Liang, L., Venkatachalam, V. and Morrissey, P.**, Cellular image analysis and imaging by flow cytometry. *Clin. Lab. Med.* 2007. **27**: 653–670.

415 **Kapellos, T. S., Taylor, L., Lee, H., Cowley, S. A., James, W. S., Iqbal, A. J. and Greaves, D. R.**, A novel real time imaging platform to quantify macrophage phagocytosis. *Biochem. Pharmacol.* 2016. **116**: 107–119.

416 **Lu, S. M., Grinstein, S. and Fairn, G. D.**, Quantitative live-cell fluorescence microscopy during phagocytosis. *Methods Mol. Biol.* 2017. **1519**: 79–91.

417 **McFarlin, B. K., Williams, R. R., Venable, A. S., Dwyer, K. C.** and, **Haviland, D. L.**, Image-based cytometry reveals three distinct subsets of activated granulocytes based on phagocytosis and oxidative burst. *Cytometry A.* 2013. **83A**: 745–751.

418 **Pul, R., Morbiducci, F., Škuljec, J., Skripuletz, T., Singh, V., Diederichs, U., Garde, N. et al.**, Glatiramer acetate increases phagocytic activity of human monocytes in vitro and in multiple sclerosis patients. *PLoS One.* 2012. **7**: e51867.

419 **Boya, P., Reggiori, F. and Codogno, P.**, Emerging regulation and functions of autophagy. *Nat. Cell Biol.* 2013. **15**: 713–720.

420 **Cuervo, A. M. and Wong, E.**, Chaperone-mediated autophagy: roles in disease and aging. *Cell Res.* 2014. **24**: 92–104.

421 **Li, W. W., Li, J., Bao, J. K.**, Microautophagy: lesser-known self-eating. *Cell Mol. Life Sci.* 2012. **69**: 1125–1136.

422 **Mizushima, N., Yoshimori, T. and Ohsumi, Y.**, The role of Atg proteins in autophagosome formation. *Annu. Rev. Cell Dev. Biol.* 2011. **27**: 107–132.

423 **Zhang, H., Puleston, D. J. and Simon, A. K.**, Autophagy and immune senescence. *Trends Mol. Med.* 2016. **22**: 671–686.

424 **Pasquier, B.**, Autophagy inhibitors. *Cell Mol. Life Sci.* 2016. **73**: 985–1001.

425 **Mauthe, M., Orhon, I., Rocchi, C., Zhou, X., Luhr, M., Hijlkema, K. J., Coppes, R. P. et al.**, Chloroquine inhibits autophagic flux by decreasing autophagosome-lysosome fusion. *Autophagy* 2018. **14**: 1435–1455.

426 **Mauvezin, C., Nagy, P., Juhasz, G. and Neufeld, T. P.**, Autophagosome-lysosome fusion is independent of V-ATPase-mediated acidification. *Nat. Commun.* 2015. **6**: 7007.

427 **Klionsky, D. J., Abdelmohsen, K., Abe, A., Abedin, M. J., Abeliovich, H., Acevedo Arozena, A., Adachi, H. et al.**, Guidelines for the use and interpretation of assays for monitoring autophagy (3rd edition). *Autophagy* 2016. **12**: 1–222.

428 **Eng, K. E., Panas, M. D., Karlsson Hedestam, G. B. and McInerney, G. M.**, A novel quantitative flow cytometry-based assay for autophagy. *Autophagy* 2010. **6**: 634–641.

429 **Chikte, S., Panchal, N. and Warnes, G.**, Use of LysoTracker dyes: a flow cytometric study of autophagy. *Cytometry A* 2014. **85**: 169–178.

430 **Phadwal, K., Alegre-Abarrategui, J., Watson, A. S., Pike, L., Anbalagan, S., Hammond, E. M., Wade-Martins, R. et al.**, A novel method for autophagy detection in primary cells: impaired levels of macroautophagy in immunosenescent T cells. *Autophagy* 2012. **8**: 677–689.

431 **Puleston, D. J., Zhang, H., Powell, T. J., Lipina, E., Sims, S., Panse, I., Watson, A. S. et al.**, Autophagy is a critical regulator of memory CD8(+) T cell formation. *eLife* 2014. **3**: 03706.

432 **Watson, A. S., Riffelmacher, T., Stranks, A., Williams, O., De Boer, J., Cain, K., MacFarlane, M. et al.**, Autophagy limits proliferation and glycolytic metabolism in acute myeloid leukemia. *Cell Death Discov.* 2015. **1**: 15008.

433 **Clarke, A. J. and Simon, A. K.**, Autophagy in the renewal, differentiation and homeostasis of immune cells. *Nat. Rev. Immunol.* 2018. **19**: 170–183.

434 **Song, Y. M., Song, S. O., Jung, Y. K., Kang, E. S., Cha, B. S., Lee, H. C. and Lee, B. W.**, Dimethyl sulfoxide reduces hepatocellular lipid accumulation through autophagy induction. *Autophagy* 2012. **8**: 1085–1097.

435 **Caro, L. H., Plomp, P. J., Wolvetang, E. J., Kerkhof, C. and Meijer, A. J.**, 3-Methyladenine, an inhibitor of autophagy, has multiple effects on metabolism. *Eur. J. Biochem.* 1988. **175**: 325–329.

436 **Klionsky, D. J., Elazar, Z., Seglen, P. O. and Rubinsztein, D. C.**, Does bafilomycin A1 block the fusion of autophagosomes with lysosomes? *Autophagy* 2008. **4**: 849–850.

437 **Spielberg, S. P., Boxer, L. A., Oliver, J. M., Allen, J. M. and Schulman, J. D.**, Oxidative damage to neutrophils in glutathione synthetase deficiency. *Br. J. Haematol.* 1979. **42**: 215–223.

438 **Min-Wen, J. C., Jun-Hao, E. T. and Shyh-Chang, N.**, Stem cell mitochondria during aging. *Semin Cell Dev. Biol.* 2016. **52**: 110–118.

439 **Watanabe, R., Fujii, H., Shirai, T., Saito, S., Ishii, T. and Harigae, H.**, Autophagy plays a protective role as an anti-oxidant system in human T cells and represents a novel strategy for induction of T-cell apoptosis. *Eur. J. Immunol.* 2014. **44**: 2508–2520.

440 **Chen, L. M., Peng, F., Li, G. D., Jie, X. M., Cai, K. R., Cai, C., Zhong, Y. et al.**, The studies on the cytotoxicity in vitro, cellular uptake, cell cycle arrest and apoptosis-inducing properties of ruthenium methylimidazole complex [Ru(MeIm)4(p-cpip)](2.). *J. Inorg. Biochem.* 2016. **156**: 64–74.

441 **Alfadda, A. A. and Sallam, R. M.**, Reactive oxygen species in health and disease. *J. Biomed. Biotechnol.* 2012. **2012**: 936486.

442 **Ilkun, O. and Boudina, S.**, Cardiac dysfunction and oxidative stress in the metabolic syndrome: an update on antioxidant therapies. *Curr. Pharm. Des.* 2013. **19**: 4806–4817.

443 **Zhou, T., Chuang, C. C. and Zuo, L.**, Molecular characterization of reactive oxygen species in myocardial ischemia-reperfusion injury. *Biomed. Res. Int.* 2015. **2015**: 864946.

444 **Gabelloni, M. L., Sabbione, F., Jancic, C., Fuxman Bass, J., Keitelman, I., Iula, L., Oleastro, M. et al.**, NADPH oxidase derived reactive oxygen species are involved in human neutrophil IL-1beta secretion but not in inflammasome activation. *Eur. J. Immunol.* 2013. **43**: 3324–3335.

445 **Vogel, D. Y., Kooij, G., Heijnen, P. D., Breur, M., Peferoen, L. A., van der Valk, P., de Vries, H. E., Amor, S. and Dijkstra, C. D.**, GM-CSF promotes migration of human monocytes across the blood brain barrier. *Eur. J. Immunol.* 2015. **45**: 1808–1819.

446 **D'Autreaux, B. and Toledano, M. B.**, ROS as signalling molecules: mechanisms that generate specificity in ROS homeostasis. *Nat. Rev. Mol. Cell Biol.* 2007. **8**: 813–824.

447 **Ray, P. D., Huang, B. W. and Tsuji, Y.**, Reactive oxygen species (ROS) homeostasis and redox regulation in cellular signaling. *Cell Signal.* 2012. **24**: 981–990.

448 **Reth, M.**, Hydrogen peroxide as second messenger in lymphocyte activation. *Nat. Immunol.* 2002. **3**: 1129–1134.

449 **Nathan, C.**, Specificity of a third kind: reactive oxygen and nitrogen intermediates in cell signaling. *J. Clin. Invest.* 2003. **111**: 769–778.

450 **Nathan, C. and Cunningham-Bussel, A**, Beyond oxidative stress: an immunologist's guide to reactive oxygen species. *Nat. Rev. Immunol.* 2013. **13**: 349–361.

451 **Solaini, G., Baracca, A., Lenaz, G. and Sgarbi, G.**, Hypoxia and mitochondrial oxidative metabolism. *Biochim. Biophys. Acta.* 2010. **1797**: 1171–1177.

452 **Wang, L., Duan, Q., Wang, T., Ahmed, M., Zhang, N., Li, Y., Li, L. et al.**, Mitochondrial respiratory chain inhibitors involved in ROS production induced by acute high concentrations of iodide and the effects of SOD as a protective factor. *Oxid. Med. Cell Longev.* 2015. **2015**: 217670.

453 **Halliwell, B. and Gutteridge, J. M.**, Oxygen toxicity, oxygen radicals, transition metals and disease. *Biochem. J.* 1984. **219**: 1–14.

454 **Diacovich, L. and Gorvel, J. P.**, Bacterial manipulation of innate immunity to promote infection. *Nat. Rev. Microbiol.* 2010. **8**: 117–128.

455 **Nauseef, W. M.**, Biological roles for the NOX family NADPH oxidases. *J. Biol. Chem.* 2008. **283**: 16961–16965.

456 **Belaaouaj, A.**, Neutrophil elastase-mediated killing of bacteria: lessons from targeted mutagenesis. *Microbes Infect.* 2002. **4**: 1259–1264.

457 **Nathan, C. and Shiloh, M. U.**, Reactive oxygen and nitrogen intermediates in the relationship between mammalian hosts and microbial pathogens. *Proc. Natl. Acad. Sci. U.S.A.* 2000. **97**(16):8841–8848.

458 **Bogdan, C., Röllinghoff, M. and Diefenbach, A.**, Reactive oxygen and reactive nitrogen intermediates in innate and specific immunity. *Curr. Opin. Immunol.* 2000. **12**(1): 64–76.

459 **Nauseef, W. M.**, Nox enzymes in immune cells. *Semin. Immunopathol.* 2008. **30**(3): 195–208.

460 **Gonzalez-Navajas, J. M., Corr, M. P. and Raz, E.**, The immediate protective response to microbial challenge. *Eur. J. Immunol.* 2014. **44**: 2536–2549.

461 **Fang, F. C.**, Antimicrobial actions of reactive oxygen species. *MBio.* 2011. **2**: e00141–11.

462 **Rahal, A., Kumar, A., Singh, V., Yadav, B., Tiwari, R., Chakraborty, S. and Dhama, K.**, Oxidative stress, prooxidants, and antioxidants: the interplay. *Biomed. Res. Int.* 2014. **2014**: 761264.

463 **Schieber, M. and Chandel, N. S.**, ROS function in redox signaling and oxidative stress. *Curr. Biol.* 2014. **24**: R453–R462.

464 **Wu, Z., Zhao, Y. and Zhao, B.**, Superoxide anion, uncoupling proteins and Alzheimer's disease. *J. Clin. Biochem. Nutr.* 2010. **46**: 187–194.

465 **Baehner, R. L., Murrmann, S. K., Davis, J. and Johnston, R. B., Jr.**, The role of superoxide anion and hydrogen peroxide in phagocytosis-associated oxidative metabolic reactions. *J. Clin. Invest.* 1975. **56**: 571–576.

466 **Kohen, R. and Nyska, A.**, Oxidation of biological systems: oxidative stress phenomena, antioxidants, redox reactions, and methods for their quantification. *Toxicol. Pathol.* 2002. **30**: 620–650.

467 **Tafazoli, S. and O'Brien, P. J.**, Amodiaquine-induced oxidative stress in a hepatocyte inflammation model. *Toxicology* 2009. **256**: 101–109.

468 **Klebanoff, S. J., Kettle, A. J., Rosen, H., Winterbourn, C. C. and Nauseef, W. M.**, Myeloperoxidase: a front-line defender against phagocytosed microorganisms. *J. Leukoc. Biol.* 2013. **93**(2): 185–198.

469 **Okado-Matsumoto, A. and Fridovich, I.**, Assay of superoxide dismutase: cautions relevant to the use of cytochrome c, a sulfonated tetrazolium, and cyanide. *Anal. Biochem.* 2001. **298**: 337–342.

470 **Trevithick, J. R. and Dzialoszynski, T.**, A new technique for enhancing luminol luminescent detection of free radicals and reactive oxygen species. *Biochem. Mol. Biol. Int.* 1994. **33**: 1179–1190.

471 **Soh, N.**, Recent advances in fluorescent probes for the detection of reactive oxygen species. *Anal. Bioanal. Chem.* 2006. **386**: 532–543.

472 **Emmendorffer, A., Hecht, M., Lohmann-Matthes, M. L. and Roesler, J.**, A fast and easy method to determine the production of reactive oxygen intermediates by human and murine phagocytes using dihydrorhodamine 123. *J. Immunol. Methods* 1990. **131**: 269–275.

473 **Amini, P., Stojkov, D., Wang, X., Wicki, S., Kaufmann, T., Wong, W. W., Simon, H. U. et al.**, NET formation can occur independently of RIPK3 and MLKL signaling. *Eur. J. Immunol.* 2016. **46**: 178–184.

474 **Sheyn, U., Rosenwasser, S., Ben-Dor, S., Porat, Z. and Vardi, A.**, Modulation of host ROS metabolism is essential for viral infection of a

bloom-forming coccolithophore in the ocean. *ISME J*. 2016. **10**: 1742–1754.

475 **van Eeden, S. F., Klut, M. E., Walker, B. A. and Hogg, J. C.**, The use of flow cytometry to measure neutrophil function. *J. Immunol. Methods* 1999. **232**: 23–43.

476 **Fornas, O., Garcia, J. and Petriz, J.**, Flow cytometry counting of CD34+ cells in whole blood. *Nat. Med.* 2000. **6**: 833–836.

477 **Fornas, O., Domingo, J. C., Marin, P. and Petriz, J.**, Flow cytometric-based isolation of nucleated erythroid cells during maturation: an approach to cell surface antigen studies. *Cytometry* 2002. **50**: 305–312.

478 **Berridge, M. J., Lipp, P. and Bootman, M. D.**, The versatility and universality of calcium signalling. *Nat. Rev. Mol. Cell Biol.* 2000. **1**: 11–21.

479 **Feske, S., Okamura, H., Hogan, P. G. and Rao, A.**, Ca2+/calcineurin signalling in cells of the immune system. *Biochem. Biophys. Res. Commun.* 2003. **311**: 1117–1132.

480 **Gwack, Y., Feske, S., Srikanth, S., Hogan, P. G. and Rao, A.**, Signalling to transcription: store-operated Ca2+ entry and NFAT activation in lymphocytes. *Cell Calcium* 2007. **42**: 145–156.

481 **Trebak, M. and Kinet, J. P.**, Calcium signalling in T cells. *Nat. Rev. Immunol.* 2019. **19**: 154–169.

482 **Varga-Szabo, D., Braun, A. and Nieswandt, B.**, Calcium signaling in platelets. *J. Thromb. Haemost.* 2009. **7**: 1057–1066.

483 **Feske, S., Skolnik, E. Y. and Prakriya, M.**, Ion channels and transporters in lymphocyte function and immunity. *Nat. Rev. Immunol.* **12**: 532–547.

484 **Putney, J. W., Jr.**, A model for receptor-regulated calcium entry. *Cell Calcium* 1986. **7**: 1–12.

485 **Armstrong, D. L., Erxleben, C. and White, J. A.**, Patch clamp methods for studying calcium channels. *Methods Cell Biol.* 2010. **99**: 183–197.

486 **Hoth, M. and Penner, R.**, Depletion of intracellular calcium stores activates a calcium current in mast cells. *Nature* 1992. **355**: 353–356.

487 **Grynkiewicz, G., Poenie, M. and Tsien, R. Y.**, A new generation of Ca2+ indicators with greatly improved fluorescence properties. *J. Biol. Chem.* 1985. **260**: 3440–3450.

488 **Greimers, R., Trebak, M., Moutschen, M., Jacobs, N. and Boniver, J.**, Improved four-color flow cytometry method using fluo-3 and triple immunofluorescence for analysis of intracellular calcium ion ([Ca2+]i) fluxes among mouse lymph node B- and T-lymphocyte subsets. *Cytometry* 1996. **23**: 205–217.

489 **Minta, A. and Tsien, R. Y.**, Fluorescent indicators for cytosolic sodium. *J. Biol. Chem.* 1989. **264**: 19449–19457.

490 **Burchiel, S. W., Edwards, B. S., Kuckuck, F. W., Lauer, F. T., Prossnitz, E. R., Ransom, J. T. and Sklar, L. A.** Analysis of free intracellular calcium by flow cytometry: multiparameter and pharmacologic applications. *Methods* 2000. **21**: 221–230.

491 **Wendt, E. R., Ferry, H., Greaves, D. R. and Keshav, S.**, Ratiometric analysis of fura red by flow cytometry: a technique for monitoring intracellular calcium flux in primary cell subsets. *PLoS One* 2015. **10**:e0119532.

492 **Foerster, C., Voelxen, N., Rakhmanov, M., Keller, B., Gutenberger, S., Goldacker, S., Thiel, J. et al.**, B cell receptor-mediated calcium signaling is impaired in B lymphocytes of type Ia patients with common variable immunodeficiency. *J. Immunol.* **184**: 7305–7313.

493 **Dolmetsch, R. E., Lewis, R. S., Goodnow, C. C. and Healy, J. I.**, Differential activation of transcription factors induced by Ca2+ response amplitude and duration. *Nature* 1997. **386**: 855–858.

494 **Griesbeck, M., Ziegler, S., Laffont, S., Smith, N., Chauveau, L., Tomezsko, P., Sharei, A. et al.**, Sex differences in plasmacytoid dendritic cell levels of IRF5 drive higher IFNα production in women. *J. Immunol.* 2015. **195**: 5327–5336.

495 **Martrus, G., Niehrs, A., Cornelis, R., Rechtien, A., Garcı´a-Beltran, W., Löutgehetmann, M., Hoffmann, C. et al.**, Kinetics of HIV-1 latency reversal quantified on the single-cell level using a novel flow-based technique. *J. Virol. Sep.* 2016. **90**: 9018–9028.

496 **Baxter, A. E., Niessl, J., Fromentin, R., Richard, J., Porichis, F., Charlebois, R., Massanella, M. et al.**, Single-cell characterization of viral translation-competent reservoirs in HIV-infected individuals. *Cell Host Microbe* 2016. **20**: 368–380.

497 **Taghizadeh, R. R., Cetrulo, K. J. and Cetrulo, C. L.**, Collagenase impacts the quantity and quality of native mesenchymal stem/stromal cells derived during processing of umbilical cord tissue. *Cell Transplant.* 2018. **27**: 181–193.

498 **Martrus, G., Kautz, T., Lunemann, S., Richert, L., Glau, L., Salzberger, W., Goebels, H. et al.**, Proliferative capacity exhibited by human liver-resident CD49a+CD25+ NK cells. *PLoS One*. 2017. **12**:e0182532.

499 **Sun, H., Sun, R., Hao, M., Wang, Y., Zhang, X., Liu, Y., Cong, X.**, Effect of duration of ex vivo ischemia time and storage period on RNA quality in biobanked human renal cell carcinoma tissue. *Ann. Surg. Oncol.* 2016. **23**: 297–304.

500 **Garcia-Beltran, W. F., Hölzemer, A., Martrus, G., Chung, A. W., Pacheco, Y., Simoneau, C. R., Rucevic, M. et al.**, Open conformers of HLA-F are high-affinity ligands of the activating NK-cell receptor KIR3DS1. *Nat. Immunol. Sep.* 2016. **17**: 1067–1074.

501 **Thaler, B., Hohensinner, P. J., Krychtiuk, K. A., Matzneller, P., Koller, L., Brekalo, M., Maurer, G. et al.**, Differential in vivo activation of monocyte subsets during low-grade inflammation through experimental endotoxemia in humans. *Sci. Rep.* 2016. **6**: 30162.

502 **Krutzik, P. O. and Nolan, G. P.**, Intracellular phospho-protein staining techniques for flow cytometry: monitoring single cell signaling events. *Cytometry* 2003. **55**: 61–70.

503 **Pozarowski, P. and Darzykiewicz, Z.**, Analysis of cell cycle by flow cytometry. In A. H. Schönthal, (Ed.) *Checkpoint controls and cancer. Methods in molecular biology*, vol **281**. Humana Press, Totowa, NJ 2004, 301–311.

504 **Schmid, I. and Sakamoto, K. M.**, Analysis of DNA content and green fluorescent protein expression. *Curr. Protoc. Cytom.* 2001. **16**: 7.16.1–7.16.10.

505 **Lanier, L. L. and Warner, N. L.**, Paraformaldehyde fixation of hematopoietic cells for quantitative flow cytometry (FACS) analysis. *J. Immunol. Methods* 1981. **47**: 25–30.

506 **Filby, A., Seddon, B., Kleczkowska, J., Salmond, R., Tomlinson, P., Smida, M., Lindquist, J. A. et al.**, Fyn regulates the duration of TCR engagement needed for commitment to effector function. *The J. Immunol.* 2007. **179**: 4635–4644.

507 **Filby, A., Perucha, E., Summers, H., Rees, P., Chana, P., Heck, S., Lord, G. M. et al.**, An imaging flow cytometric method for measuring cell division history andmolecular symmetry duringmitosis. *Cytometry Part A* 2011. **79**: 496–506.

508 **Fan, J., Nishanian, P., Breen, E. C., McDonald, M. and Fahey, J. L.**, Cytokine gene expression in normal human lymphocytes in response to stimulation. *Clin. Diagn. Lab. Immunol.* 1998. **5**: 335–340.

509 **Löhning, M., Richter, A. and Stamm, T.**, Establishment of memory for IL-10 expression in developing T helper 2 cells requires repetitive IL-4 costimulation and does not impair proliferation. *Proc. Natl. Acad. Sci. U.S.A.* 2003. **100**: 12307–12312.

510 **Sanos, S. L., Vonarbourg, C., Mortha, A. and Diefenbach, A.**, Control of epithelial cell function by interleukin-22-producing RORgammat+ innate lymphoid cells. *Immunology* 2011. **132**: 453–465.

511 **Nussbaum, J. C., Dyken, S. J. and Moltke, J.**, Type 2 innate lymphoid cells control eosinophil homeostasis. *Nature* 2013. **502**: 245–248.

512 **Robinson, D., Shibuya, K., Mui, A., Zonin, F., Murphy, E., Sana, T., Hartley, S. B. et al.**, IGIF does not drive Th1 development but synergizes with IL-12 for interferon-gamma production and activates IRAK and NFκB. *Immunity* 1997. **7**: 571–581.

513 **Sattler, A., Wagner, U., Rossol, M., Sieper, J., Wu, P., Krause, A., Schmidt, W. A. et al.**, Cytokine-induced human IFN-γ-secreting effector-memory Th cells in chronic autoimmune inflammation. *Blood* 2009. **113**: 1948–1956.

514 **Zimmermann, J., Radbruch, A. and Chang, H. D.**, A Ca(2+) concentration of 1.5 mM, as present in IMDM but not in RPMI, is critical for maximal response of Th cells to PMA/ionomycin. *Eur. J. Immunol.* 2015. **45**: 1270–1273.

515 **Lohning, M., Richter, A., Stamm, T., Hu-Li, J., Assenmacher, M., Paul, W. E. and Radbruch, A.**, Establishment of memory for IL-10 expression in developing T helper 2 cells requires repetitive IL-4 costimulation and does not impair proliferation. *Proc. Natl. Acad. Sci. U. S. A.* 2003. **100**: 12307–12312.

516 **Assenmacher, M., Schmitz, J. and Radbruch, A.**, Flow cytometric determination of cytokines in activated murine T helper lymphocytes: Expression of interleukin-10 in interferon-gamma and in interleukin-4-expressing cells. *Eur. J. Immunol.* 1994. **24**: 1097–1101.

517 **Lorenz, H., Hailey, D. W., Wunder, C. and Lippincott-Schwartz, J.**, The fluorescence protease protection (FPP) assay to determine protein localization and membrane topology. *Nat. Protoc.* 2006. **1**: 276–279.

518 **Francis, G., Kerem, Z., Makkar, H. P. and Becker, K.**, The biological action of saponins in animal systems: a review. *Br. J. Nutr.* 2002. **88**: 587–605.

519 **Moller, B. K., Andresen, B. S., Christensen, E. I. and Petersen, C. M.**, Surface membrane CD4 turnover in phorbol ester stimulated T-lymphocytes. Evidence of degradation and increased synthesis. *FEBS Lett.* 1990. **276**: 59–62.

520 **Boyer, C., Auphan, N., Luton, F., Malburet, J. M., Barad, M., Bizozzero, J. P., Reggio, H. et al.**, T cell receptor/CD3 complex internalization following activation of a cytolytic T cell clone: evidence for a protein kinase C-independent staurosporine-sensitive step. *Eur. J. Immunol.* 1991. **21**: 1623–1634.

521 **Grupillo, M., Lakomy, R., Geng, X., Styche, A., Rudert, W. A., Trucco, M. and Fan, Y.**, An improved intracellular staining protocol for efficient detection of nuclear proteins in YFP-expressing cells. *Biotechniques* 2011. **51**: 417–420.

522 **Heinen, A. P., Wanke, F., Moos, S., Attig, S., Luche, H., Pal, P. P., Budisa, N. et al.**, Improved method to retain cytosolic reporter protein fluorescence while staining for nuclear proteins: transcription factor staining with retention of fluorescent proteins. *Cytometry* 2014. **85**: 621–627.

523 **Watson, M., Chow, S., Barsyte, D., Arrowsmith, C., Shankey, T. V., Minden, M. and Hedley, D.**, The study of epigenetic mechanisms based on the analysis of histone modification patterns by flow cytometry. *Cytometry* 2013. **85**: 78–87.

524 **Guha, M. and Mackman, N.**, LPS induction of gene expression in human monocytes. *Cell. Signal.* 2001. **13**: 85–94.

525 **Gantke, T., Sriskantharajah, S. and Ley, S. C.**, Regulation and function of TPL-2, an IκB kinase-regulated MAP Kinase Kinase. *Cell Res.* 2011. **21**: 131–134.

526 **Dufner, A. and Thomas, G.**, Ribosomal S6 kinase signaling and the control of translation. *Exp. Cell Res.* 1999. **253**: 100–109.

527 **Firaguay, G. F. and Nunès, J. A.**, Analysis of signaling events by dynamic phosphoflow cytometry. *Sci. Signal* 2009. **2**: pl3.

528 **West, M. A., Koons, A., Crandall, M., Skinner, R., Worley, M. and Shapiro, M. B.**, Whole blood leukocyte mitogen activated protein kinases activation differentiates intensive care unit patients with systemic inflammatory response syndrome and sepsis. *J. Trauma* 2007. **62**: 805–811.

529 **Donnelly, R. P. and Finlay, D. K.**, Glucose, glycolysis and lymphocyte responses. *Mol. Immunol.* 2015. **68**: 513–519.

530 **Caro-Maldonado, A., Wang, R., Nichols, A. G., Kuraoka, M., Milasta, S., Sun, L. D., Gavin, A. L. et al.**, Metabolic reprogramming is required for antibody production that is suppressed in anergic but exaggerated in chronically BAFF-exposed B cells. *J. Immunol.* 2014. **192**: 3626–3636.

531 **Warburg, O.** On the Origin of Cancer Cells. *Science* 1956. **123**: 309–14.

532 **Michalek, R. D., Gerriets, V. A., Jacobs, S. R., Macintyre, A. N., MacIver, N. J., Mason, E. F., Sullivan, S. A. et al.**, CD4+, cutting edge: distinct glycolytic and lipid oxidative metabolic programs are essential for effector and regulatory cell, T subsets. *J Immunol. Author.* 2012. **186**: 3299–3303.

533 **Berod, L., Friedrich, C., Nandan, A., Freitag, J., Hagemann, S., Harmrolfs, K., Sandouk, A. et al.**, De novo fatty acid synthesis controls the fate between regulatory T and T helper 17 cells. *Nat. Med.* 2014. **20**: 1327–1333.

534 **Hale, L. P., Braun, R. O. D. D., Gwinn, W. M., Greer, P. K., Dewhirst, M. W., Laura, P., Braun, R. O. D. D. et al.**, Hypoxia in the thymus: role of oxygen tension in thymocyte survival. *Am. J. Physiol. Heart Circ. Physiol.* 2002. **282**: H1467–H1477.

535 **Parmar, K., Mauch, P., Vergilio, J.-A., Sackstein, R. and Down, J. D.**, Distribution of hematopoietic stem cells in the bone marrow according to regional hypoxia. *Proc. Natl. Acad. Sci. U.S.A.* 2007. **104**: 5431–5436.

536 **Chandel, N. S., McClintock, D. S., Feliciano, C. E., Wood, T. M., Melendez, J. A., Rodriguez, A. M. and Schumacker, P. T.**, Reactive oxygen species generated at mitochondrial Complex III stabilize hypoxia-inducible factor-1alpha during hypoxia: a mechanism of O_2 sensing. *J. Biol. Chem.* 2000. **275**: 25130–25138.

537 **Bigarella, C. L., Liang, R. and Ghaffari, S.**, Stem cells and the impact of ROS signaling. *Development.* 2014. **141**: 4206–4218.

538 **Jang, K.-J., Mano, H., Aoki, K., Hayashi, T., Muto, A., Nambu, Y., Takahashi, K. et al.**, Mitochondrial function provides instructive signals for activation-induced B-cell fates. *Nat. Commun.* 2015. **6**: 6750.

539 **Barros, L. F., Bittner, C. X., Loaiza, A., Ruminot, I., Larenas, V., Moldenhauer, H., Oyarzún, C. et al.**, Kinetic validation of 6-NBDG as a probe for the glucose transporter GLUT1 in astrocytes. *J Neurochem.* 2009. **109**: 94–100.

540 **Zou, C., Wang, Y. and Shen, Z.**, 2-NBDG as a fluorescent indicator for direct glucose uptake measurement. *J. Biochem. Biophys. Methods* 2005. **64**: 207–215.

541 **Lam, W. Y., Jash, A., Yao, C. H., D'Souza, L., Wong, R., Nunley, R. M., Meares, G. P. et al.**, Metabolic and transcriptional modules independently diversify plasma cell lifespan and function. *Cell Rep.* 2018. **24**: 2479–2492.e6.

542 **Byersdorfer, C. A., Tkachev, V., Opipari, A. W., Goodell, S., Swanson, J., Sandquist, S., Glick, G. D. et al.**, Effector T cells require fatty acid metabolism during murine graft-versus-host disease. *Blood.* 2013. **122**: 3230–3237.

543 **Kolahi, K., Louey, S., Varlamov, O. and Thornburg, K.**, Real-time tracking of BODIPY-C12 long-chain fatty acid in human term placenta

reveals unique lipid dynamics in cytotrophoblast cells. *PLoS One*. 2016. **11**: e0153522.

544 **Muroski, M. E., Miska, J., Chang, A. L., Zhang, P., Rashidi, A., Moore, H., Lopez-Rosas, A. et al.**, Fatty acid uptake in T cell subsets using a quantum dot fatty acid conjugate. *Sci. Rep*. 2017. **7**: 5790.

545 **Xiao, B., Deng, X., Zhou, W. and Tan, E.-K.**, Flow cytometry-based assessment of mitophagy using MitoTracker. *Front. Cell. Neurosci*. 2016. **10**: 76.

546 **Avramidou, A., Kroczek, C., Lang, C., Schuh, W., Jäck, H.-M. and Mielenz, D.**, The novel adaptor protein Swiprosin-1 enhances BCR signals and contributes to BCR-induced apoptosis. *Cell Death Differ*. 2007. **14**: 1936–1947.

547 **Pracht, K., Meinzinger, J., Daum, P., Schulz, S. R., Reimer, D., Hauke, M., Roth, E. et al.**, A new staining protocol for detection of murine antibody-secreting plasma cell subsets by flow cytometry. *Eur. J. Immunol*. 2017. **47**: 1389–1392.

548 **Eruslanov, E. and Kusmartsev, S.** Identification of ROS using oxidized DCFDA and flow-cytometry. *Methods Mol. Biol*. 2010. **594**: 57–72.

549 **Kalyanaraman, B., Darley-Usmar, V., Davies, K. J. A., Dennery, P. A., Forman, H. J., Grisham, M. B., Mann, G. E. et al.**, Measuring reactive oxygen and nitrogen species with fluorescent probes: challenges and limitations. *Free Radic. Biol. Med*. 2012. **52**: 1–6.

550 **Hempel, S. L., Buettner, G. R., O'Malley, Y. Q., Wessels D. A. and Flaherty D. M.**, Dihydrofluorescein diacetate is superior for detecting intracellular oxidants: comparison with 2',7'-dichlorodihydrofluorescein diacetate, 5 (and 6)-caboxy-2',7'-dichlorodihydrofluorescein diacetate, and dihydrorhodamine 123. *Free Radic. Biol. Med*. 1999. **27**: 146–159.

551 Anon. Thermo Fisher. CellROX® Oxidative Stress Reagents: User manual. Available at: https://assets.thermofisher.com/TFS-Assets/LSG/manuals/mp10422.pdf

552 Anon. Thermo Fisher. MitoSOX™ Red mitochondrial superoxide indicator *for live-cell imaging* (M36008): User manual. Available at: https://assets.thermofisher.com/TFS-Assets/LSG/manuals/mp36008.pdf

553 **Tzur, A., Moore, J. K., Jorgensen, P., Shapiro, H. M. and Kirschner, M. W.**, Optimizing optical flow cytometry for cell volume-based sorting and analysis. *PLoS One*. 2011. **6**: 1–9.

554 **Stein, M., Dütting, S., Di, M., Bösl, M., Fritsch, K., Reimer, D., Urbanczyk, S. et al.**, A defined metabolic state in pre B cells governs B-cell development and is counterbalanced by Swiprosin-2/EFhd1. *Cell Death Differ*. 2017. **24**: 1239–1252.

555 **Henzi, T. and Schwaller, B.** Antagonistic regulation of parvalbumin expression and mitochondrial calcium handling capacity in renal epithelial cells. *PLoS One*. 2015. **10**: e0142005.

556 **Santarlasci, V., Maggi, L., Capone, M., Querci, V., Beltrame, L., Cavalieri, D., D'Aiuto, E. et al.**, Rarity of human T helper 17 cells is due to retinoic acid orphan receptor-dependent mechanisms that limit their expansion. *Immunity*. 2012. **36**: 201–214.

557 **Santarlasci, V, Mazzoni, A, Capone, M, Rossi, MC, Maggi, L, Montaini, G, Rossettini, B et al.**, Musculin inhibits human T-helper 17 cell response to interleukin 2 by controlling STAT5B activity. *Eur. J. Immunol*. 2017. **47**: 1427–1442.

558 **Altman, J. D., Moss, P. A., Goulder, P. J., Barouch, D. H., McHeyzer-Williams, M. G., Bell, J. I., McMichael, A. J. et al.**, Phenotypic analysis of antigen-specific T lymphocytes. *Science* 1996. **274**: 94–96.

559 **Newell, E. W., Klein, L. O., Yu, W. and Davis, M. M.**, Simultaneous detection of many T-cell specificities using combinatorial tetramer staining. *Nat. Methods* 2009. **6**: 497–499.

560 **Hadrup, S. R., Bakker, A. H., Shu, C. J., Andersen, R. S., van Veluw, J., Hombrink, P., Castermans, E. et al.**, Parallel detection of antigen-specific T-cell responses by multidimensional encoding of MHC multimers. *Nat. Methods* 2009. **6**: 520–526.

561 **Newell, E. W., Sigal, N., Nair, N., Kidd, B. A., Greenberg, H. B. and Davis, M. M.**, Combinatorial tetramer staining and mass cytometry analysis facilitate T-cell epitope mapping and characterization. *Nat. Biotechnol*. 2013. **31**: 623–629.

562 **Bentzen, A. K., Marquard, A. M., Lyngaa, R., Saini, S. K., Ramskov, S., Donia, M., Such, L. et al.**, Large-scale detection of antigen-specific T cells using peptide-MHC-I multimers labeled with DNA barcodes. *Nat. Biotechnol*. 2016. **34**: 1037–1045.

563 **Dolton, G., Zervoudi, E., Rius, C., Wall, A., Thomas, H. L., Fuller, A., Yeo, L. et al.**, Optimized peptide–MHC multimer protocols for detection and isolation of autoimmune T-cells. *Front Immunol*. 2018. **9**: 1378.

564 **Zhang, S. Q., Ma, K. Y., Schonnesen, A. A., Zhang, M., He, C., Sun, E., Williams, C. M. et al.**, High-throughput determination of the antigen specificities of T cell receptors in single cells. *Nat. Biotechnol*. 2018. **36**: 1156.

565 **Toebes, M., Coccoris, M., Bins, A., Rodenko, B., Gomez, R., Nieuwkoop, N. J., van de Kasteele, W. et al.**, Design and use of conditional MHC class I ligands. *Nat. Med*. 2006. **12**: 246–251.

566 **Luimstra, J. J., Garstka, M. A., Roex, M. C., Redeker, A., Janssen, G. M., van Veelen, P. A. and Neefjes, J.**, A flexible MHC class I multimer loading system for large-scale detection of antigen-specific T cells. *J. Exp. Med*. 2018. **215**(5): 1493–1504.

567 **Amore, A., Wals, K., Koekoek, E., Hoppes, R., Toebes, M., Schumacher, T. N., Rodenko, B. et al.**, Development of a hypersensitive periodate-cleavable amino acid that is methionine-and disulfide-compatible and its application in MHC exchange reagents for T cell characterisation. *ChemBioChem* 2013. **14**: 123–131.

568 **Choo, J. A., Thong, S. Y., Yap, J., van Esch, W. J., Raida, M., Meijers, R., Lescar, J. et al.**, Bioorthogonal cleavage and exchange of major histocompatibility complex ligands by employing azobenzene-containing peptides. *Angew. Chem. Int. Ed*. 2014. **53**: 13390–13394.

569 **Saini, S. K., Schuster, H., Ramnarayan, V. R., Rammensee, H.-G., Stevanović, S. and Springer, S.**, Dipeptides catalyze rapid peptide exchange on MHC class I molecules. *Proc. Natl. Acad. Sci. USA* 2015. **112**: 202–207.

570 **Kuball, J., Hauptrock, B., Malina, V., Antunes, E., Voss, R. H., Wolfl, M., Strong, R. et al.**, Increasing functional avidity of TCR-redirected T cells by removing defined N-glycosylation sites in the TCR constant domain. *J. Exp. Med*. 2009. **206**: 463–475.

571 **Kvistborg, P., Philips, D., Kelderman, S., Hageman, L., Ottensmeier, C., Joseph-Pietras, D., Welters, M. J. et al.**, Anti-CTLA-4 therapy broadens the melanoma-reactive CD8+ T cell response. *Sci. Transl. Med*. 2014. **6**: 254ra128.

572 **Kvistborg, P., Shu, C. J., Heemskerk, B., Fankhauser, M., Thrue, C. A., Toebes, M., van Rooij, N. et al.**, TIL therapy broadens the tumor-reactive CD8(+) T cell compartment in melanoma patients. *Oncoimmunology* 2012. **1**: 409–418.

573 **Rizvi, N. A., Hellmann, M. D., Snyder, A., Kvistborg, P., Makarov, V., Havel, J. J., Lee, W. et al.**, Mutational landscape determines sensitivity to PD-1 blockade in non-small cell lung cancer. *Science* 2015. **348**: 124–128.

574 **van Rooij, N., van Buuren, M. M., Philips, D., Velds, A., Toebes, M., Heemskerk, B., van Dijk, L. J. et al.**, Tumor exome analysis reveals neoantigen-specific T-cell reactivity in an ipilimumab-responsive melanoma. *J. Clin. Oncol*. 2013. **31**: e439–442.

575 **Schneck, J. P.**, Monitoring antigen-specific T cells using MHC-Ig dimers. *Immunol. Invest.* 2000. **29**: 163–169.

576 **Selin, L. K.**, **Vergilis, K.**, **Welsh, R. M. and Nahill, S. R.**, Reduction of otherwise remarkably stable virus-specific cytotoxic T lymphocyte memory by heterologous viral infections. *J. Exp. Med.* 1996. **183**: 2489–2499.

577 **Martinez, R. J.**, **Andargachew, R.**, **Martinez, H. A. and Evavold, B. D.**, Low-affinity CD4+ T cells are major responders in the primary immune response. *Nat. Commun.* 2016. **7**: 13848.

578 **Xiao, Z.**, **Mescher, M. F. and Jameson, S. C.**, Detuning CD8 T cells: down-regulation of CD8 expression, tetramer binding, and response during CTL activation. *J. Exp. Med.* 2007. **204**: 2667–2677.

579 **Bakker, A. H.**, Schumacher TNM. MHC multimer technology: current status and future prospects. *Curr. Opin. Immunol.* 2005. **17**: 428–433.

580 **McMichael, A. J. and O'Callaghan, C. A.**, A new look at T cells. *J. Exp. Med.* 1998. **187**: 1367–1371.

581 **Ogg, G. S.**, **King, A. S.**, **Dunbar, P. R. and McMichael, A. J.**, Isolation of HIV-1-specific cytotoxic T lymphocytes using human leukocyte antigen-coated beads. *AIDS* 1999. **13**: 1991–1993.

582 **Luxembourg, A. T.**, **Borrow, P.**, **Teyton, L.**, **Brunmark, A. B.**, **Peterson, P. A. and Jackson, M. R.**, Biomagnetic isolation of antigen-specific CD8+ T cells usable in immunotherapy. *Nat. Biotechnol.* 1998. **16**: 281–285.

583 **Xu, X. N.**, **Purbhoo, M. A.**, **Chen, N.**, **Mongkolsapaya, J.**, **Cox, J. H.**, **Meier, U. C.**, **Tafuro, S. et al.**, A novel approach to antigen-specific deletion of CTL with minimal cellular activation using alpha3 domain mutants of MHC class I/peptide complex. *Immunity* 2001. **14**: 591–602.

584 **Whelan, J. A.**, **Dunbar, P. R.**, **Price, D. A.**, **Purbhoo, M. A.**, **Lechner, F.**, **Ogg, G. S.**, **Griffiths, G. et al.**, Specificity of CTL interactions with peptide-MHC class I tetrameric complexes is temperature dependent. *J. Immunol.* 1999. **163**: 4342–4348.

585 **Daniels, M. A. and Jameson, S. C.** Critical role for CD8 in T cell receptor binding and activation by peptide/major histocompatibility complex multimers. *J. Exp. Med.* 2000. **191**: 335–346.

586 **Knabel, M.**, **Franz, T. J.**, **Schiemann, M.**, **Wulf, A.**, **Villmow, B.**, **Schmidt, B.**, **Bernhard, H. et al.**, Reversible MHC multimer staining for functional isolation of T-cell populations and effective adoptive transfer. *Nat. Med.* 2002. **8**: 631–637.

587 **Neuenhahn, M.**, **Albrecht, J.**, **Odendahl, M.**, **Schlott, F.**, **Dössinger, G.**, **Schiemann, M.**, **Lakshmipathi, S. et al.**, Transfer of minimally manipulated CMV-specific T cells from stem cell or third-party donors to treat CMV infection after allo-HSCT. *Leukemia* 2017. **31**: 2161–2171.

588 **Nauerth, M.**, **Weißbrich, B.**, **Knall, R.**, **Franz, T.**, **Dössinger, G.**, **Bet, J.**, **Paszkiewicz, P. J. et al.**, TCR-ligand koff rate correlates with the protective capacity of antigen-specific CD8+ T cells for adoptive transfer. *Sci. Transl. Med.* 2013. **5**: 192ra87.

589 **Nauerth, M.**, **Stemberger, C.**, **Mohr, F.**, **Weißbrich, B.**, **Schiemann, M.**, **Germeroth, L. and Busch, D. H.**, Flow cytometry-based TCR-ligand K off -rate assay for fast avidity screening of even very small antigen-specific T cell populations ex vivo. *Cytometry A* 2016. **89**: 816–825.

590 **Stemberger, C.**, **Dreher, S.**, **Tschulik, C.**, **Piossek, C.**, **Bet, J.**, **Yamamoto, T. N.**, **Schiemann, M. et al.**, Novel serial positive enrichment technology enables clinical multiparameter cell sorting. *PLoS One* 2012. **7**: e35798.

591 **Davis, D. M.**, **Reyburn, H. T.**, **Pazmany, L.**, **Chiu, I.**, **Mandelboim, O. and Strominger, J. L.**, Impaired spontaneous endocytosis of HLA-G. *Eur. J. Immunol.* 1997. **27**: 2714–2719.

592 **Effenberger, M.**, **Stengl, A.**, **Schober, K.**, **Gerget, M.**, **Kampick, M.**, **Müller, T. R.**, **Schumacher, D. et al.**, FLEXamers: a double tag for universal generation of versatile peptide-MHC multimers. *J. Immunol.* 2019. https://doi.org/10.4049/jimmunol.1801435

593 **Lund-Johansen, F.**, **Bjerknes, R. and Laerum, O. D.**, Flow cytometric assay for the measurement of human bone marrow phenotype, function and cell cycle. *Cytometry* 1990. **11**: 610–616.

594 **Vollers, S. S. and Stern, L. J.**, Class II major histocompatibility complex tetramer staining: progress, problems, and prospects. *Immunology* 2008. **123**: 305–313.

595 **James, E. A.**, **LaFond, R.**, **Durinovic-Bello, I. and Kwok, W.**, Visualizing antigen specific CD4+ T cells using MHC class II tetramers. *J. Vis. Exp.* 2009: 1–4.

596 **Scheffold, A.**, **Busch, D. H. and Kern, F.**, Detection of antigen-specific T-cells using major histocompatibility complex multimers or functional parameters. In Sack, U. (Eds.), *Cellular diagnostics*.KARGER, Basel 2008: 476–502.

597 **Chattopadhyay, P. K.**, **Gierahn, T. M.**, **Roederer, M. and Love, J. C.**, Single-cell technologies for monitoring immune systems. *Nat. Immunol.* 2014. **15**: 128–135.

598 **Chattopadhyay, P. K. and Roederer, M.**, A mine is a terrible thing to waste: high content, single cell technologies for comprehensive immune analysis. *Am. J. Transplant.* 2015. **15**: 1155–1161.

599 **Kvistborg, P.**, **Gouttefangeas, C.**, **Aghaeepour, N.**, **Cazaly, A.**, **Chattopadhyay, P. K.**, **Chan, C.**, **Eckl, J. et al.**, Thinking outside the gate: single-cell assessments in multiple dimensions. *Immunity* 2015. **42**: 591–592.

600 **Mahnke, Y. D. and Roederer, M.**, Optimizing a multicolor immunophenotyping assay. *Clin. Lab. Med.* 2007. **27**: 469–485.

601 **Newell, E. W. and Davis, M. M.**, Beyond model antigens: high-dimensional methods for the analysis of antigen-specific T cells. *Nat. Biotechnol.* 2014. **32**: 149–157.

602 **Bacher, P. and Scheffold, A.**, Flow-cytometric analysis of rare antigen-specific T cells. *Cytometry A* 2013. **83**: 692–701.

603 **Dimitrov, S.**, **Gouttefangeas, C.**, **Besedovsky, L.**, **Jensen, A. T. R.**, **Chandran, P. A.**, **Rusch, E.**, **Businger, R. et al.**, Activated integrins identify functional antigen-specific CD8(+) T cells within minutes after antigen stimulation. *Proc. Natl. Acad. Sci. USA* 2018. **115**: E5536–E5545.

604 **Kutscher, S.**, **Dembek, C. J.**, **Deckert, S.**, **Russo, C.**, **Korber, N.**, **Bogner, J. R.**, **Geisler, F. et al.**, Overnight resting of PBMC changes functional signatures of antigen specific T- cell responses: impact for immune monitoring within clinical trials. *PLoS One* 2013. **8**: e76215.

605 **Owen, R. E.**, **Sinclair, E.**, **Emu, B.**, **Heitman, J. W.**, **Hirschkorn, D. F.**, **Epling, C. L.**, **Tan, Q. X. et al.**, Loss of T cell responses following long-term cryopreservation. *J. Immunol. Methods* 2007. **326**: 93–115.

606 **Romer, P. S.**, **Berr, S.**, **Avota, E.**, **Na, S. Y.**, **Battaglia, M.**, **ten Berge, I.**, **Einsele, H. et al.**, Preculture of PBMCs at high cell density increases sensitivity of T-cell responses, revealing cytokine release by CD28 superagonist TGN1412. *Blood* 2011. **118**: 6772–6782.

607 **Wegner, J.**, **Hackenberg, S.**, **Scholz, C. J.**, **Chuvpilo, S.**, **Tyrsin, D.**, **Matskevich, A. A.**, **Grigoleit, G. U. et al.**, High-density preculture of PBMCs restores defective sensitivity of circulating CD8 T cells to virus- and tumor-derived antigens. *Blood* 2015. **126**: 185–194.

608 **Lamoreaux, L.**, **Roederer, M. and Koup, R.**, Intracellular cytokine optimization and standard operating procedure. *Nat. Protoc.* 2006. **1**: 1507–1516.

609 **Maecker, H. T.**, **Rinfret, A.**, **D'Souza, P.**, **Darden, J.**, **Roig, E.**, **Landry, C.**, **Hayes, P. et al.**, Standardization of cytokine flow cytometry assays. *BMC Immunol.* 2005. **6**: 13.

610 **Reddy, M.**, **Eirikis, E.**, **Davis, C.**, **Davis, H. M. and Prabhakar, U.**, Comparative analysis of lymphocyte activation marker expression and cytokine secretion profile in stimulated human peripheral blood

mononuclear cell cultures: an in vitro model to monitor cellular immune function. *J. Immunol. Methods* 2004. **293**: 127–142.

611 **Redmond, W. L., Ruby, C. E. and Weinberg, A. D.**, The role of OX40-mediated co-stimulation in T-cell activation and survival. *Crit. Rev. Immunol.* 2009. **29**: 187–201.

612 **Zaunders, J. J., Munier, M. L., Seddiki, N., Pett, S., Ip, S., Bailey, M., Xu, Y. et al.**, High levels of human antigen-specific CD4+ T cells in peripheral blood revealed by stimulated coexpression of CD25 and CD134 (OX40). *J. Immunol.* 2009. **183**: 2827–2836.

613 **Chattopadhyay, P. K., Yu, J. and Roederer, M.**, A live-cell assay to detect antigen-specific CD4+ T cells with diverse cytokine profiles. *Nat. Med.* 2005. **11**: 1113–1117.

614 **Frentsch, M., Arbach, O., Kirchhoff, D., Moewes, B., Worm, M., Rothe, M., Scheffold, A. et al.**, Direct access to CD4+ T cells specific for defined antigens according to CD154 expression. *Nat. Med.* 2005. **11**: 1118–1124.

615 **Bacher, P., Kniemeyer, O., Schonbrunn, A., Sawitzki, B., Assenmacher, M., Rietschel, E., Steinbach, A. et al.**, Antigen-specific expansion of human regulatory T cells as a major tolerance mechanism against mucosal fungi. *Mucosal. Immunol.* 2014. **7**: 916–928.

616 **Schoenbrunn, A., Frentsch, M., Kohler, S., Keye, J., Dooms, H., Moewes, B., Dong, J. et al.**, A converse 4-1BB and CD40 ligand expression pattern delineates activated regulatory T cells (Treg) and conventional T cells enabling direct isolation of alloantigen-reactive natural Foxp3+ Treg. *J. Immunol.* 2012. **189**: 5985–5994.

617 **Bacher, P., Heinrich, F., Stervbo, U., Nienen, M., Vahldieck, M., Iwert, C., Vogt, K. et al.**, Regulatory T cell specificity directs tolerance versus allergy against aeroantigens in humans. *Cell* 2016. **167**: 1067–1078.

618 **Wolfl, M., Kuball, J., Eyrich, M., Schlegel, P. G. and Greenberg, P. D.**, Use of CD137 to study the full repertoire of CD8+ T cells without the need to know epitope specificities. *Cytometry A* 2008. **73**: 1043–1049.

619 **Wolfl, M., Kuball, J., Ho, W. Y., Nguyen, H., Manley, T. J., Bleakley, M. and Greenberg, P. D.**, Activation-induced expression of CD137 permits detection, isolation, and expansion of the full repertoire of CD8+ T cells responding to antigen without requiring knowledge of epitope specificities. *Blood* 2007. **110**: 201–210.

620 **Brosterhus, H., Brings, S., Leyendeckers, H., Manz, R. A., Miltenyi, S., Radbruch, A., Assenmacher, M. et al.**, Enrichment and detection of live antigen-specific CD4(+) and CD8(+) T cells based on cytokine secretion. *Eur. J. Immunol.* 1999. **29**: 4053–4059.

621 **Manz, R., Assenmacher, M., Pfluger, E., Miltenyi, S. and Radbruch, A.**, Analysis and sorting of live cells according to secreted molecules, relocated to a cell-surface affinity matrix. *Proc. Natl. Acad. Sci. USA* 1995. **92**: 1921–1925.

622 **Jung, T., Schauer, U., Heusser, C., Neumann, C. and Rieger, C.**, Detection of intracellular cytokines by flow cytometry. *J. Immunol. Methods* 1993. **159**: 197–207.

623 **O'Neil-Andersen, N. J. and Lawrence, D. A.**, Differential modulation of surface and intracellular protein expression by T cells after stimulation in the presence of monensin or brefeldin A. *Clin. Diagn. Lab. Immunol.* 2002. **9**: 243–250.

624 **Bacher, P., Schink, C., Teutschbein, J., Kniemeyer, O., Assenmacher, M., Brakhage, A. A. and Scheffold, A.**, Antigen-reactive T cell enrichment for direct, high-resolution analysis of the human naive and memory Th cell repertoire. *J. Immunol.* 2013. **190**: 3967–3976.

625 **Bacher, P., Hohnstein, T., Beerbaum, E., Rocker, M., Blango, M. G., Kaufmann, S., Rohmel, J. et al.**, Human Anti-fungal Th17 Immunity and Pathology Rely on Cross-Reactivity against Candida albicans. *Cell* 2019. **176**: 1340–1355.e1315.

626 **Wehler, T. C., Karg, M., Distler, E., Konur, A., Nonn, M., Meyer, R. G., Huber, C. et al.**, Rapid identification and sorting of viable virus-reactive CD4(+) and CD8(+) T cells based on antigen-triggered CD137 expression. *J. Immunol. Methods* 2008. **339**: 23–37.

627 **Betts, M. R., Brenchley, J. M., Price, D. A., De Rosa, S. C., Douek, D. C., Roederer, M. and Koup, R. A.**, Sensitive and viable identification of antigen-specific CD8+ T cells by a flow cytometric assay for degranulation. *J. Immunol. Methods* 2003. **281**: 65–78.

628 **Betts, M. R. and Koup, R. A.**, Detection of T-cell degranulation: CD107a and b. *Methods Cell Biol.* 2004. **75**: 497–512.

629 **Dimitrov, S., Benedict, C., Heutling, D., Westermann, J., Born, J. and Lange, T.**, Cortisol and epinephrine control opposing circadian rhythms in T cell subsets. *Blood* 2009. **113**: 5134–5143.

630 **Dimitrov, S., Lange, T. and Born, J.**, Selective mobilization of cytotoxic leukocytes by epinephrine. *J. Immunol.* 2010. **184**: 503–511.

631 **Day, C. L., Seth, N. P., Lucas, M., Appel, H., Gauthier, L., Lauer, G. M., Robbins, G. K. et al.**, Ex vivo analysis of human memory CD4 T cells specific for hepatitis C virus using MHC class II tetramers. *J. Clin. Invest.* 2003. **112**: 831–842.

632 **Miltenyi, S., Muller, W., Weichel, W. and Radbruch, A.**, High gradient magnetic cell separation with MACS. *Cytometry* 1990. **11**: 231–238.

633 **Moon, J. J., Chu, H. H., Pepper, M., McSorley, S. J., Jameson, S. C., Kedl, R. M. and Jenkins, M. K.**, Naive CD4(+) T cell frequency varies for different epitopes and predicts repertoire diversity and response magnitude. *Immunity* 2007. **27**: 203–213.

634 **Obar, J. J., Khanna, K. M. and Lefrancois, L.**, Endogenous naive CD8+ T cell precursor frequency regulates primary and memory responses to infection. *Immunity* 2008. **28**: 859–869.

635 **Macey, M. G.**, *Flow cytometry: Principles and applications*. Humana Press, New York, NY, 2007.

636 **Krensky, A. M.**, The HLA system, antigen processing and presentation. *Kidney Int. Suppl.* 1997. **58**: S2–7.

637 **Kern, F., Faulhaber, N., Frommel, C., Khatamzas, E., Prosch, S., Schonemann, C., Kretzschmar, I. et al.**, Analysis of CD8 T cell reactivity to cytomegalovirus using protein-spanning pools of overlapping pentadecapeptides. *Eur. J. Immunol.* 2000. **30**: 1676–1682.

638 **Maecker, H. T., Dunn, H. S., Suni, M. A., Khatamzas, E., Pitcher, C. J., Bunde, T., Persaud, N. et al.**, Use of overlapping peptide mixtures as antigens for cytokine flow cytometry. *J. Immunol. Methods* 2001. **255**: 27–40.

639 **Eberl, G., Renggli, J., Men, Y., Roggero, M. A., Lopez, J. A. and Corradin, G.**, Extracellular processing and presentation of a 69-mer synthetic polypeptide to MHC class I-restricted T cells. *Mol. Immunol.* 1999. **36**: 103–112.

640 **Sherman, L. A., Burke, T. A. and Biggs, J. A.**, Extracellular processing of peptide antigens that bind class I major histocompatibility molecules. *J. Exp. Med.* 1992. **175**: 1221–1226.

641 **Alanio, C., Lemaitre, F., Law, H. K., Hasan, M. and Albert, M. L.**, Enumeration of human antigen-specific naive CD8+ T cells reveals conserved precursor frequencies. *Blood* 2010. **115**: 3718–3725.

642 **Campion, S. L., Brodie, T. M., Fischer, W., Korber, B. T., Rossetti, A., Goonetilleke, N., McMichael, A. J. et al.**, Proteome-wide analysis of HIV-specific naive and memory CD4(+) T cells in unexposed blood donors. *J. Exp. Med.* 2014. **211**: 1273–1280.

643 **Geiger, R., Duhen, T., Lanzavecchia, A. and Sallusto, F.**, Human naive and memory CD4+ T cell repertoires specific for naturally processed antigens analyzed using libraries of amplified T cells. *J. Exp. Med.* 2009. **206**: 1525–1534.

644 **Su, L. F., Kidd, B. A., Han, A., Kotzin, J. J. and Davis, M. M.**, Virus-specific CD4(+) memory-phenotype T cells are abundant in unexposed adults. *Immunity* 2013. **38**: 373–383.

645 **Annunziato, F., Romagnani, C. and Romagnani, S.**, The 3 major types of innate and adaptive cell-mediated effector immunity. *J. Allergy Clin. Immunol.* 2015. **135**: 626-635.

646 **Brugnolo, F., Sampognaro, S., Liotta, F., Cosmi, L., Annunziato, F., Manuelli, C., Campi, P. et al.**, The novel synthetic immune response modifier R-848 (Resiquimod) shifts human allergen-specific CD4+ TH2 lymphocytes into IFN-gamma-producing cells. *J. Allergy Clin. Immunol.* 2003. **111**: 380–388.

647 **Annunziato, F., Cosmi, L., Santarlasci, V., Maggi, L., Liotta, F., Mazzinghi, B., Parente, E. et al.**, Phenotypic and functional features of human Th17 cells. *J. Exp. Med.* 2007. **204**: 1849–1861.

648 **Cosmi, L., Maggi, L., Santarlasci, V., Capone, M., Cardilicchia, E., Frosali, F., Querci, V. et al.**, Identification of a novel subset of human circulating memory CD4(+) T cells that produce both IL-17A and IL-4. *J. Allergy Clin. Immunol.* 2010. **125**(1): 222-230.e1-4.

649 **Becattini, S., Latorre, D., Mele, F., Foglierini, M., De Gregorio, C., Cassotta, A., Fernandez, B. et al.**, T cell immunity. Functional heterogeneity of human memory $CD4^+$ T cell clones primed by pathogens or vaccines. *Science* 2015. **347**: 400–406.

650 **Mazzoni, A., Maggi, L., Siracusa, F., Ramazzotti, M., Rossi, M. C., Santarlasci, V., Montaini, G. et al.**, Eomes controls the development of Th17-derived (non-classic) Th1 cells during chronic inflammation. *Eur. J. Immunol.* 2019. **49**: 79–95.

651 **Mazzoni, A., Santarlasci, V., Maggi, L., Capone, M., Rossi, M. C., Querci, V., De Palma, R. et al.**, Demethylation of the RORC2 and IL17A in human CD4+ T lymphocytes defines Th17 origin of nonclassic Th1 cells. *J. Immunol.* 2015. **194**: 3116–3126.

652 **Mueller, S. N., Gebhardt, T., Carbone, F. R. and Heath, W. R.**, Memory T cell subsets, migration patterns, and tissue residence. *Annu. Rev. Immunol.* 2013. **31**: 137–161.

653 **Masopust, D. and Schenkel, J. M.**, The integration of T cell migration, differentiation and function. *Nat. Rev. Immunol.* 2013. **13**: 309–320.

654 **Murali-Krishna, K., Altman, J. D., Suresh, M., Sourdive, D. J., Zajac, A. J., Miller, J. D., Slansky, J. et al.**, *Immunity* 1998. **8**: 177–187.

655 **Masopust, D., Vezys, V., Marzo, A. L. and Lefrancois, L.**, Preferential localization of effector memory cells in nonlymphoid tissue. *Science* 2001. **291**: 2413–2417.

656 **Barber, D. L., Wherry, E. J. and Ahmed, R.**, *J. Immunol.* 2003. **171**: 27–31.

657 **Brunner, K. T., Mauel, J., Cerottini, J. C. and Chapuis, B.**, *Immunology* 1968. **14**: 181–196.

658 **Nagata, S. and Golstein, P.**, The Fas death factor. *Science* 1995. **267**: 1449–1456.

659 **Lopez, J. A., Susanto, O., Jenkins, M. R., Lukoyanova, N., Sutton, V. R., Law, R. H., Johnston, A. et al.**, *Blood* 2013. **121**: 2659–2668.

660 **Liu, L., Chahroudi, A., Silvestri, G., Wernett, M. E., Kaiser, W. J., Safrit, J. T., Komoriya, A. et al.**, Visualization and quantification of T cell-mediated cytotoxicity using cell-permeable fluorogenic caspase substrates. *Nat. Med.* 2002. **8**: 185–189.

661 **Bedner, E., Smolewski, P., Amstad, P. and Darzynkiewicz, Z.**, *Exp. Cell Res.* 2000. **259**: 308–313.

662 **Amstad, P. A., Yu, G., Johnson, G. L., Lee, B. W., Dhawan, S. and Phelps, D. J.**, *BioTechniques* 2001. **31**: 608–10, 612, 614, passim

663 **Sheehy, M. E., McDermott, A. B., Furlan, S. N., Klenerman, P. and Nixon, D. F.**, *J. Immunol. Methods* 2001. **249**: 99–110.

664 **Michonneau, D., Sagoo, P., Breart, B., Garcia, Z., Celli, S. and Bousso, P.**, *Immunity* 2016. **44**: 143–154.

665 **Aichele, P., Brduscha-Riem, K., Oehen, S., Odermatt, B., Zinkernagel, R. M., Hengartner, H. and Pircher, H.**, *Immunity* 1997. **6**: 519–529.

666 **Coles, R. M., Mueller, S. N., Heath, W. R., Carbone, F. R. and Brooks, A. G.**, Progression of armed CTL from draining lymph node to spleen shortly after localized infection with herpes simplex virus 1. *J. Immunol.* 2002. **168**: 834–838.

667 **Wabnitz, G. H., Balta, E., Schindler, S., Kirchgessner, H., Jahraus, B., Meuer, S. and Samstag, Y.**, The pro-oxidative drug WF-10 inhibits serial killing by primary human cytotoxic T-cells. *Cell Death Discov.* 2016. **2**: 16057.

668 **Wabnitz, G. H., Kirchgessner, H. and Samstag, Y.** Multiparametric analysis of molecular mechanism involved in the cytotoxicity of human CD8 T-cells. *J. Cell. Biochem.* 2017. **118**: 2528–2533.

669 **Mahnke, Y. D., Devevre, E., Baumgaertner, P., Matter, M., Rufer, N., Romero, P. and Speiser, D. E.**, Human melanoma-specific CD8(+) T-cells from metastases are capable of antigen-specific degranulation and cytolysis directly ex vivo. *Oncoimmunology* 2012. **1**: 467–530.

670 **Kurioka, A., Ussher, J. E., Cosgrove, C., Clough, C., Fergusson, J. R., Smith, K., Kang, Y. H. et al.**, MAIT cells are licensed through granzyme exchange to kill bacterially sensitized targets. *Mucosal. Immunol.* 2015. **8**: 429–440.

671 **Wing, K., Onishi, Y., Prieto-Martin, P., Yamaguchi, T., Miyara, M., Fehervari, Z., Nomura, T. et al.**, CTLA-4 control over Foxp3(+) regulatory T cell function. *Science* 2008. **322**: 271–275.

672 **McMurchy, A. N. and Levings, M. K.**, Suppression assays with human T regulatory cells: a technical guide. *Eur. J. Immunol.* 2012. **42**: 27–34.

673 **Cammarata, I., Martire, C., Citro, A., Raimondo, D., Fruci, D., Melaiu, O., D'Oria, V. et al.**, Counter-regulation of regulatory T cells by autoreactive CD8(+) T cells in rheumatoid arthritis. *J. Autoimmun.* 2019. **99**: 81–97.

674 **Walker, L. S.**, Regulatory T cells overturned: the effectors fight back. *Immunology* 2009. **126**: 466–474.

675 **Miyara, M., Yoshioka, Y., Kitoh, A., Shima, T., Wing, K., Niwa, A., Parizot, C. et al.**, Functional delineation and differentiation dynamics of human CD4+ T cells expressing the FoxP3 transcription factor. *Immunity* 2009. **30**: 899–911.

676 **Wing, J. B., Kitagawa, Y., Locci, M., Hume, H., Tay, C., Morita, T., Kidani, Y. et al.**, A distinct subpopulation of CD25(−) T-follicular regulatory cells localizes in the germinal centers. *Proc. Natl. Acad. Sci. USA* 2017. **114**: E6400–E6409.

677 **Roederer, M.**, Interpretation of cellular proliferation data: avoid the panglossian. *Cytometry A* 2011. **79**: 95–101.

678 **Grossman, W. J., Verbsky, J. W., Barchet, W., Colonna, M., Atkinson, J. P. and Ley, T. J.**, Human T regulatory cells can use the perforin pathway to cause autologous target cell death. *Immunity* 2004. **21**: 589–601.

679 **Koristka, S., Cartellieri, M., Arndt, C., Feldmann, A., Topfer, K., Michalk, I., Temme, A. et al.**, Cytotoxic response of human regulatory T cells upon T-cell receptor-mediated activation: a matter of purity. *Blood Cancer J.* 2014. **4**: e199.

680 **Pircher, H., Burki, K., Lang, R., Hengartner, H. and Zinkernagel, R. M.**, Tolerance induction in double specific T-cell receptor transgenic mice varies with antigen. *Nature* 1989. **342**: 559–561.

681 **Hogquist, K. A., Jameson, S. C., Heath, W. R., Howard, J. L., Bevan, M. J. and Carbone, F. R.**, T cell receptor antagonist peptides induce positive selection. *Cell* 1994. **76**: 17–27.

682 **Oxenius, A., Bachmann, M. F., Zinkernagel, R. M. and Hengartner, H.**, Virus-specific MHC-class II-restricted TCR-transgenic mice: effects on humoral and cellular immune responses after viral infection. *Eur. J. Immunol.* 1998. **28**: 390–400.

683 **Barnden, M. J., Allison, J., Heath, W. R. and Carbone, F. R.**, Defective TCR expression in transgenic mice constructed using cDNA-based alpha- and beta-chain genes under the control of heterologous regulatory elements. *Immunol. Cell. Biol.* 1998. **76**: 34–40.

684 **Murphy, K. M., Heimberger, A. B. and Loh, D. Y.**, Induction by antigen of intrathymic apoptosis of CD4+CD8+TCRlo thymocytes in vivo. *Science* 1990. **250**: 1720–1723.

685 **Kagi, D., Odermatt, B., Ohashi, P. S., Zinkernagel, R. M. and Hengartner, H.**, Development of insulitis without diabetes in transgenic mice lacking perforin-dependent cytotoxicity. *J. Exp. Med.* 1996. **183**: 2143–2152.

686 **Bettelli, E., Pagany, M., Weiner, H. L., Linington, C., Sobel, R. A. and Kuchroo, V. K.**, Myelin oligodendrocyte glycoprotein-specific T cell receptor transgenic mice develop spontaneous autoimmune optic neuritis. *J. Exp. Med.* 2003. **197**: 1073–1081.

687 **Mason, D. Y., Jones, M. and Goodnow, C. C.**, Development and follicular localization of tolerant B lymphocytes in lysozyme/anti-lysozyme IgM/IgD transgenic mice. *Int. Immunol.* 1992. **4**: 163–175.

688 **Phan, T. G., Amesbury, M., Gardam, S., Crosbie, J., Hasbold, J., Hodgkin, P. D., Basten, A. et al.**, B cell receptor-independent stimuli trigger immunoglobulin (Ig) class switch recombination and production of IgG autoantibodies by anergic self-reactive B cells. *J. Exp. Med.* 2003. **197**: 845–860.

689 **Allen, C. D., Okada, T., Tang, H. L. and Cyster, J. G.**, Imaging of germinal center selection events during affinity maturation. *Science* 2007. **315**: 528–531.

690 **Shih, T. A., Roederer, M. and Nussenzweig, M. C.**, Role of antigen receptor affinity in T cell-independent antibody responses in vivo. *Nat. Immunol.* 2002. **3**: 399–406.

691 **Garside, P., Ingulli, E., Merica, R. R., Johnson, J. G., Noelle, R. J. and Jenkins, M. K.**, Visualization of specific B and T lymphocyte interactions in the lymph node. *Science* 1998. **281**: 96–99.

692 **Litzenburger, T., Fassler, R., Bauer, J., Lassmann, H., Linington, C., Wekerle, H. and Iglesias, A.**, B lymphocytes producing demyelinating autoantibodies: development and function in gene-targeted transgenic mice. *J. Exp. Med.* 1998. **188**: 169–180.

693 **Bettelli, E., Baeten, D., Jager, A., Sobel, R. A. and Kuchroo, V. K.**, Myelin oligodendrocyte glycoprotein-specific T and B cells cooperate to induce a Devic-like disease in mice. *J. Clin. Invest.* 2006. **116**: 2393–2402.

694 **Jenkins, M. K. and Moon, J. J.**, The role of naive T cell precursor frequency and recruitment in dictating immune response magnitude. *J. Immunol.* 2012. **188**: 4135–4140.

695 **Buchholz, V. R., Schumacher, T. N. and Busch, D. H.**, T cell fate at the single-cell level. *Annu. Rev. Immunol.* 2016. **34**: 65–92.

696 **Stemberger, C., Huster, K. M., Koffler, M., Anderl, F., Schiemann, M., Wagner, H. and Busch, D. H.**, A single naive CD8+ T cell precursor can develop into diverse effector and memory subsets. *Immunity* 2007. **27**: 985–997.

697 **Baumjohann, D. and Ansel, K. M.**, Tracking early T follicular helper cell differentiation in vivo. *Methods Mol. Biol.* 2015. **1291**: 27–38.

698 **Paus, D., Phan, T. G., Chan, T. D., Gardam, S., Basten, A. and Brink, R.**, Antigen recognition strength regulates the choice between extrafollicular plasma cell and germinal center B cell differentiation. *J. Exp. Med.* 2006. **203**: 1081–1091.

699 **Boesch, M., Cosma, A. and Sopper, S.**, Flow cytometry: to dump or not to dump. *J. Immunol.* 2018. **201**: 1813.

700 **Beura, L. K., Hamilton, S. E., Bi, K., Schenkel, J. M., Odumade, O. A., Casey, K. A., Thompson, E. A. et al.**, Normalizing the environment recapitulates adult human immune traits in laboratory mice. *Nature* 2016. **532**: 512–516.

701 **Akondy, R. S., Monson, N. D., Miller, J. D., Edupuganti, S., Teuwen, D., Wu, H., Quyyumi, F. et al.**, The yellow fever virus vaccine induces a broad and polyfunctional human memory CD8+ T cell response. *J. Immunol.* 2009. **183**: 7919–7930.

702 **Schulz, A. R., Malzer, J. N., Domingo, C., Jurchott, K., Grutzkau, A., Babel, N., Nienen, M. et al.**, Low thymic activity and dendritic cell numbers are associated with the immune response to primary viral infection in elderly humans. *J. Immunol.* 2015. **195**: 4699–4711.

703 **van Leeuwen, E. M., de Bree, G. J., Remmerswaal, E. B., Yong, S. L., Tesselaar, K., ten Berge, I. J. and van Lier, R. A.**, IL-7 receptor alpha chain expression distinguishes functional subsets of virus-specific human CD8+ T cells. *Blood* 2005. **106**: 2091–2098.

704 **Zhou, L., Chong, M. M. and Littman, D. R.**, Plasticity of CD4+ T cell lineage differentiation. *Immunity* 2009. **30**: 646–655.

705 **Luckheeram, R. V., Zhou, R., Verma, A. D. and Xia, B.**, CD4(+)T cells: differentiation and functions. *Clin. Dev. Immunol.* 2012. **2012**: 925135.

706 **Zhu, J., Yamane, H. and Paul, W. E.**, Differentiation of effector CD4 T cell populations (*). *Annu. Rev. Immunol.* 2010. **28**: 445–489.

707 **Cua, D. J., Sherlock, J., Chen, Y., Murphy, C. A., Joyce, B., Seymour, B., Lucian, L. et al.**, Interleukin-23 rather than interleukin-12 is the critical cytokine for autoimmune inflammation of the brain. *Nature* 2003. **421**: 744–748.

708 **Murphy, C. A., Langrish, C. L., Chen, Y., Blumenschein, W., McClanahan, T., Kastelein, R. A., Sedgwick, J. D. et al.**, Divergent pro- and anti-inflammatory roles for IL-23 and IL-12 in joint autoimmune inflammation. *J. Exp. Med.* 2003. **198**: 1951–1957.

709 **Iwakura, Y., Ishigame, H., Saijo, S. and Nakae, S.**, Functional specialization of interleukin-17 family members. *Immunity* 2011. **34**: 149–162.

710 **Brown, D. M., Dilzer, A. M., Meents, D. L. and Swain, S. L.**, CD4 T cell-mediated protection from lethal influenza: perforin and antibody-mediated mechanisms give a one-two punch. *J. Immunol.* 2006. **177**: 2888–2898.

711 **Lord, G. M., Rao, R. M., Choe, H., Sullivan, B. M., Lichtman, A. H., Luscinskas, F. W. and Glimcher, L. H.**, T-bet is required for optimal proinflammatory CD4+ T-cell trafficking. *Blood* 2005. **106**: 3432–3439.

712 **Sundrud, M. S., Grill, S. M., Ni, D., Nagata, K., Alkan, S. S., Subramaniam, A. and Unutmaz, D.**, Genetic reprogramming of primary human T cells reveals functional plasticity in Th cell differentiation. *J. Immunol.* 2003. **171**: 3542–3549.

713 **Hirota, K., Yoshitomi, H., Hashimoto, M., Maeda, S., Teradaira, S., Sugimoto, N., Yamaguchi, T. et al.**, Preferential recruitment of CCR6-expressing Th17 cells to inflamed joints via CCL20 in rheumatoid arthritis and its animal model. *J. Exp. Med.* 2007. **204**: 2803–2812.

714 **Breitfeld, D., Ohl, L., Kremmer, E., Ellwart, J., Sallusto, F., Lipp, M. and Forster, R.**, Follicular B helper T cells express CXC chemokine receptor 5, localize to B cell follicles, and support immunoglobulin production. *J. Exp. Med.* 2000. **192**: 1545–1552.

715 **Hsieh, C. S., Macatonia, S. E., Tripp, C. S., Wolf, S. F., O'Garra, A. and Murphy, K. M.**, Development of TH1 CD4+ T cells through IL-12 produced by Listeria-induced macrophages. *Science* 1993. **260**: 547–549.

716 **Lighvani, A. A., Frucht, D. M., Jankovic, D., Yamane, H., Aliberti, J., Hissong, B. D., Nguyen, B. V. et al.**, T-bet is rapidly induced by

interferon-gamma in lymphoid and myeloid cells. *Proc. Natl. Acad. Sci. U S A* 2001. **98**: 15137–15142.

717 **Szabo, S. J., Kim, S. T., Costa, G. L., Zhang, X., Fathman, C. G. and Glimcher, L. H.**, A novel transcription factor, T-bet, directs Th1 lineage commitment. *Cell* 2000. **100**: 655–669.

718 **Le Gros, G., Ben-Sasson, S. Z., Seder, R., Finkelman, F. D. and Paul, W. E.**, Generation of interleukin 4 (IL-4)-producing cells in vivo and in vitro: IL-2 and IL-4 are required for in vitro generation of IL-4-producing cells. *J. Exp. Med.* 1990. **172**: 921–929.

719 **Swain, S. L., Weinberg, A. D., English, M. and Huston, G.**, IL-4 directs the development of Th2-like helper effectors. *J. Immunol.* 1990. **145**: 3796–3806.

720 **Zheng, W. and Flavell, R. A.**, The transcription factor GATA-3 is necessary and sufficient for Th2 cytokine gene expression in CD4 T cells. *Cell* 1997. **89**: 587–596.

721 **Ivanov, I. I., McKenzie, B. S., Zhou, L., Tadokoro, C. E., Lepelley, A., Lafaille, J. J., Cua, D. J. et al.**, The orphan nuclear receptor RORgammat directs the differentiation program of proinflammatory IL-17+ T helper cells. *Cell* 2006. **126**: 1121–1133.

722 **Baba, N., Rubio, M., Kenins, L., Regairaz, C., Woisetschlager, M., Carballido, J. M. and Sarfati, M.**, The aryl hydrocarbon receptor (AhR) ligand VAF347 selectively acts on monocytes and naive CD4(+) Th cells to promote the development of IL-22-secreting Th cells. *Hum. Immunol.* 2012. **73**: 795–800.

723 **Gerlach, K., Hwang, Y., Nikolaev, A., Atreya, R., Dornhoff, H., Steiner, S., Lehr, H. A. et al.**, TH9 cells that express the transcription factor PU.1 drive T cell-mediated colitis via IL-9 receptor signaling in intestinal epithelial cells. *Nat. Immunol.* 2014. **15**: 676–686.

724 **Chtanova, T., Tangye, S. G., Newton, R., Frank, N., Hodge, M. R., Rolph, M. S. and Mackay, C. R.**, T follicular helper cells express a distinctive transcriptional profile, reflecting their role as non-Th1/Th2 effector cells that provide help for B cells. *J. Immunol.* 2004. **173**: 68–78.

725 **Zhu, J., Jankovic, D., Oler, A. J., Wei, G., Sharma, S., Hu, G., Guo, L. et al.**, The transcription factor T-bet is induced by multiple pathways and prevents an endogenous Th2 cell program during Th1 cell responses. *Immunity* 2012. **37**: 660–673.

726 **Mosmann, T. R., Cherwinski, H., Bond, M. W., Giedlin, M. A. and Coffman, R. L.**, Two types of murine helper T cell clone. I. Definition according to profiles of lymphokine activities and secreted proteins. *J. Immunol.* 1986. **136**: 2348–2357.

727 **Harrington, L. E., Hatton, R. D., Mangan, P. R., Turner, H., Murphy, T. L., Murphy, K. M. and Weaver, C. T.**, Interleukin 17-producing CD4+ effector T cells develop via a lineage distinct from the T helper type 1 and 2 lineages. *Nat. Immunol.* 2005. **6**: 1123–1132.

728 **Grewal, I. S., Xu, J. and Flavell, R. A.**, Impairment of antigen-specific T-cell priming in mice lacking CD40 ligand. *Nature* 1995. **378**: 617–620.

729 **Liu, F. and Whitton, J. L.**, Cutting edge: re-evaluating the in vivo cytokine responses of CD8+ T cells during primary and secondary viral infections. *J. Immunol.* 2005. 5936–5940.

730 **Kirchhoff, D., Frentsch, M., Leclerk, P., Bumann, D., Rausch, S., Hartmann, S., Thiel, A. et al.**, Identification and isolation of murine antigen-reactive T cells according to CD154 expression. *Eur J Immunol* 2007. **37**: 2370–2377.

731 **Shore, D. A., Issafras, H., Landais, E., Teyton, L. and Wilson, I. A.**, The crystal structure of CD8 in complex with YTS156.7.7 Fab and interaction with other CD8 antibodies define the binding mode of CD8 alpha-beta to MHC class I. *J. Mol. Biol.* 2008. **384**: 1190–1202.

732 **Joshi, N. S., Cui, W., Chandele, A., Lee, H. K., Urso, D. R., Hagman, J., Gapin, L. et al.**, Inflammation directs memory precursor and short-lived effector CD8(+) T cell fates via the graded expression of T-bet transcription factor. *Immunity* 2007. **27**: 281–295.

733 **Kaech, S. M., Tan, J. T., Wherry, E. J., Konieczny, B. T., Surh, C. D. and Ahmed, R.**, Selective expression of the interleukin 7 receptor identifies effector CD8 T cells that give rise to long-lived memory cells. *Nat. Immunol.* 2003. 1191–1198.

734 **Obar, J. J., Jellison, E. R., Sheridan, B. S., Blair, D. A., Pham, Q. M., Zickovich, J. M. and Lefrancois, L.**, Pathogen-induced inflammatory environment controls effector and memory CD8+ T cell differentiation. *J. Immunol.* 2011. 4967–4978.

735 **Gerlach, C., Moseman, E. A., Loughhead, S. M., Alvarez, D., Zwijnenburg, A. J., Waanders, L., Garg, R. et al.**, The chemokine receptor CX3CR1 defines three antigen-experienced CD8 T cell subsets with distinct roles in immune surveillance and homeostasis. *Immunity* 2016. **45**: 1270–1284.

736 **Sosinowski, T., White, J. T., Cross, E. W., Haluszczak, C., Marrack, P., Gapin, L. and Kedl, R. M.**, CD8α+ dendritic cell trans presentation of IL-15 to naive CD8+ T cells produces antigen-inexperienced T cells in the periphery with memory phenotype and function. *J. Immunol.* 2013. **190**: 1936–1947.

737 **White, J. T., Cross, E. W. and Kedl, R. M.**, Antigen-inexperienced memory CD8(+) T cells: where they come from and why we need them. *Nat. Rev. Immunol.* 2017. **17**: 391–400.

738 **Chiu, B. C., Martin, B. E., Stolberg, V. R. and Chensue, S. W.**, Cutting edge: central memory CD8 T cells in aged mice are virtual memory cells. *J. Immunol.* 2013. **191**: 5793–5796.

739 **Quinn, K. M., Fox, A., Harland, K. L., Russ, B. E., Li, J., Nguyen, T. H. O., Loh, L. et al.**, Age-related decline in primary CD8(+) T cell responses is associated with the development of senescence in virtual memory CD8(+) T cells. *Cell Rep* 2018. **23**: 3512–3524.

740 **Tsukumo, S.-i., Unno, M., Muto, A., Takeuchi, A., Kometani, K., Kurosaki, T., Igarashi, K. et al.**, Bach2 maintains T cells in a naive state by suppressing effector memory-related genes. *Proc. Natl. Acad. Sci. USA* 2013. 10735–10740.

741 **Kaech, S. M. and Cui, W.**, Transcriptional control of effector and memory CD8+ T cell differentiation. *Nat. Rev. Immunol.* 2012. **12**: 749–761.

742 **Mackay, L. K., Minnich, M., Kragten, N. A., Liao, Y., Nota, B., Seillet, C., Zaid, A. et al.**, Hobit and Blimp1 instruct a universal transcriptional program of tissue residency in lymphocytes. *Science* 2016. **352**: 459–463.

743 **Mittrucker, H. W., Visekruna, A. and Huber, M.**, Heterogeneity in the differentiation and function of CD8(+) T cells. *Arch. Immunol. Ther. Exp.* 2014. **62**: 449–458.

744 **Frentsch, M., Stark, R., Matzmohr, N., Meier, S., Durlanik, S., Schulz, A. R., Stervbo, U. et al.**, CD40L expression permits CD8+ T cells to execute immunologic helper functions. *Blood* 2013. **122**: 405–412.

745 **van Stipdonk, M. J., Hardenberg, G., Bijker, M. S., Lemmens, E. E., Droin, N. M., Green, D. R. and Schoenberger, S. P.**, Dynamic programming of CD8+ T lymphocyte responses. *Nat. Immunol.* 2003. **4**: 361–365.

746 **Masopust, D., Murali-Krishna, K. and Ahmed, R.**, Quantitating the magnitude of the lymphocytic choriomeningitis virus-specific CD8 T-cell response: it is even bigger than we thought. *J. Virol.* 2007. **81**: 2002–2011.

747 **Mueller, S. N. and Mackay, L. K.**, Tissue-resident memory T cells: local specialists in immune defence. *Nat. Rev. Immunol.* 2016. **16**: 79–89.

748 **Behr, F. M., Chuwonpad, A., Stark, R. and van Gisbergen, K.**, Armed and ready: transcriptional regulation of tissue-resident memory CD8 T cells. *Front. Immunol.* 2018. **9**: 1770.

749 **Beura, L. K., Fares-Frederickson, N. J., Steinert, E. M., Scott, M. C., Thompson, E. A., Fraser, K. A., Schenkel, J. M. et al.**, CD4(+) resident

memory T cells dominate immunosurveillance and orchestrate local recall responses. *J. Exp. Med.* 2019.

750 **Autengruber, A., Gereke, M., Hansen, G., Hennig, C. and Bruder, D.**, Impact of enzymatic tissue disintegration on the level of surface molecule expression and immune cell function. *Eur. J. Microbiol. Immunol.* 2012. **2**: 112–120.

751 **Rissiek, B., Haag, F., Boyer, O., Koch-Nolte, F. and Adriouch, S.**, P2X7 on mouse T cells: one channel, many functions. *Front. Immunol.* 2015. **6**: 204.

752 **Rissiek, B., Lukowiak, M., Raczkowski, F., Magnus, T., Mittrucker, H. W. and Koch-Nolte, F.**, In vivo blockade of murine ARTC2.2 during cell preparation preserves the vitality and function of liver tissue-resident memory T cells. *Front. Immunol.* 2018. **9**: 1580.

753 **Stark, R., Wesselink, T. H., Behr, F. M., Kragten, N. A. M., Arens, R., Koch-Nolte, F., van Gisbergen, K. and van Lier, R. A. W.**, T RM maintenance is regulated by tissue damage via P2RX7. *Sci. Immunol.* 2018. **3**: eaau1022.

754 **Steinert, E. M., Schenkel, J. M., Fraser, K. A., Beura, L. K., Manlove, L. S., Igyarto, B. Z., Southern, P. J. et al.**, Quantifying memory CD8 T cells reveals regionalization of immunosurveillance. *Cell* 2015. **161**: 737–749.

755 **Anderson, K. G., Mayer-Barber, K., Sung, H., Beura, L., James, B. R., Taylor, J. J., Qunaj, L. et al.**, Intravascular staining for discrimination of vascular and tissue leukocytes. *Nat. Protoc.* 2014. **9**: 209–222.

756 **Nikolich-Žugich, J. and Čičin-Šain, L.**, Aging of the Immune System Across Different Species. In N. S. Wolf (Ed.), *The comparative biology of aging*, Springer Netherlands, Dordrecht, the Netherlands, 2010. pp. 353–376.

757 **Calado, R. T. and Dumitriu, B.**, Telomere dynamics in mice and humans. *Semin. Hematol.* 2013. **50**: 165–174.

758 **Cicin-Sain, L., Brien, J. D., Uhrlaub, J. L., Drabig, A., Marandu, T. F. and Nikolich-Zugich, J.**, Cytomegalovirus infection impairs immune responses and accentuates T-cell pool changes observed in mice with aging. *PLoS Pathog.* 2012. **8**: e1002849.

759 **Reese, T. A., Bi, K., Kambal, A., Filali-Mouhim, A., Beura, L. K., Burger, M. C., Pulendran, B. et al.**, Sequential infection with common pathogens promotes human-like immune gene expression and altered vaccine response. *Cell Host Microbe* 2016. **19**: 713–719.

760 **Pinchuk, L. M. and Filipov, N. M.**, Differential effects of age on circulating and splenic leukocyte populations in C57BL/6 and BALB/c male mice. *Immun. Ageing: I&A* 2008. **5**: 1–1.

761 **Yuan, R., Meng, Q., Nautiyal, J., Flurkey, K., Tsaih, S. W., Krier, R., Parker, M. G. et al.**, Genetic coregulation of age of female sexual maturation and lifespan through circulating IGF1 among inbred mouse strains. *Proc. Natl. Acad. Sci. USA* 2012. **109**: 8224–8229.

762 **Xu, W. and Larbi, A.**, Markers of T cell senescence in humans. *Int. J. Mol. Sci.* 2017. **18**: 1742.

763 **Lanna, A., Gomes, D. C., Muller-Durovic, B., McDonnell, T., Escors, D., Gilroy, D. W., Lee, J. H. et al.**, A sestrin-dependent Erk-Jnk-p38 MAPK activation complex inhibits immunity during aging. *Nat. Immunol.* 2017. **18**: 354–363.

764 **White, J. T., Cross, E. W., Burchill, M. A., Danhorn, T., McCarter, M. D., Rosen, H. R., O'Connor, B. et al.**, Virtual memory T cells develop and mediate bystander protective immunity in an IL-15-dependent manner. *Nat. Commun.* 2016. **7**: 11291.

765 **Marandu, T. F., Oduro, J. D., Borkner, L., Dekhtiarenko, I., Uhrlaub, J. L., Drabig, A., Kroger, A. et al.**, Immune protection against virus challenge in aging mice is not affected by latent herpesviral infections. *J. Virol.* 2015. **89**: 11715–11717.

766 **Sakaguchi, S., Sakaguchi, N., Asano, M., Itoh, M. and Toda, M.**, Immunologic self-tolerance maintained by activated T cells expressing IL-2 receptor alpha-chains (CD25). Breakdown of a single mechanism of self-tolerance causes various autoimmune diseases. *J. Immunol.* 1995. **155**: 1151–1164.

767 **Hori, S., Nomura, T. and Sakaguchi, S.**, Control of regulatory T cell development by the transcription factor Foxp3. *Science* 2003. **299**: 1057–1061.

768 **Fontenot, J. D., Gavin, M. A. and Rudensky, A. Y.**, Foxp3 programs the development and function of $CD4^+CD25^+$ regulatory T cells. *Nat. Immunol.* 2003. **4**: 330–336.

769 **Hill, J. A., Feuerer, M., Tash, K., Haxhinasto, S., Perez, J., Melamed, R., Mathis, D. et al.**, Foxp3 transcription-factor-dependent and -independent regulation of the regulatory T cell transcriptional signature. *Immunity* 2007. **27**: 786–800.

770 **Bennett, C. L., Christie, J., Ramsdell, F., Brunkow, M. E., Ferguson, P. J., Whitesell, L., Kelly, T. E. et al.**, The immune dysregulation, polyendocrinopathy, enteropathy, X-linked syndrome (IPEX) is caused by mutations of FOXP3. *Nat. Genet.* 2001. **27**: 20–21.

771 **Brunkow, M. E., Jeffery, E. W., Hjerrild, K. A., Paeper, B., Clark, L. B., Yasayko, S. A., Wilkinson, J. E. et al.**, Disruption of a new forkhead/winged-helix protein, scurfin, results in the fatal lymphoproliferative disorder of the scurfy mouse. *Nat. Genet.* 2001. **27**: 68–73.

772 **Bacchetta, R., Passerini, L., Gambineri, E., Dai, M., Allan, S. E., Perroni, L., Dagna-Bricarelli, F. et al.**, Defective regulatory and effector T cell functions in patients with FOXP3 mutations. *J. Clin. Invest.* 2006. **116**: 1713–1722.

773 **Klein, L., Robey, E. A. and Hsieh, C. S.**, Central CD4+ T cell tolerance: deletion versus regulatory T cell differentiation. *Nat. Rev. Immunol.* 2019. **19**: 7–18.

774 **Tanoue, T., Atarashi, K. and Honda, K.**, Development and maintenance of intestinal regulatory T cells. *Nat. Rev. Immunol.* 2016. **16**: 295–309.

775 **Thornton, A. M., Korty, P. E., Tran, D. Q., Wohlfert, E. A., Murray, P. E., Belkaid, Y. and Shevach, E. M.**, Expression of Helios, an Ikaros transcription factor family member, differentiates thymic-derived from peripherally induced Foxp3+ T regulatory cells. *J. Immunol.* 2010. **184**: 3433–3441.

776 **Weiss, J. M., Bilate, A. M., Gobert, M., Ding, Y., Curotto de Lafaille, M. A., Parkhust, C. N., Xiong, H. et al.**, Neuropilin-1 is expressed on thymus-derived natural regulatory T cells, but not mucosa-generated induced Foxp3+ Treg cells. *J. Exp. Med.* 2012. **209**: 1723–1742.

777 **Sefik, E., Geva-Zatorsky, N., Oh, S., Konnikova, L., Zemmour, D., McGuire, A. M., Burzyn, D. et al.**, Individual intestinal symbionts induce a distinct population of RORgamma+ regulatory T cells. *Science* 2015. **349**: 993–997.

778 **Ohnmacht, C., Park, J. H., Cording, S., Wing, J. B., Atarashi, K., Obata, Y., Gaboriau-Routhiau, V. et al.**, The microbiota regulates type 2 immunity through RORgammat+ T cells. *Science* 2015. **349**: 989–993.

779 **Akimova, T., Beier, U. H., Wang, L., Levine, M. H. and Hancock, W. W.**, Helios expression is a marker of T cell activation and proliferation. *PLoS One* 2011. **6**: e24226.

780 **Kim, B.-S., Lu, H., Ichiyama, K., Chen, X., Zhang, Y.-B., Mistry, N. A., Tanaka, K. et al.**, Generation of RORγt+ Antigen-Specific T Regulatory 17 Cells from Foxp3+ Precursors in Autoimmunity. *Cell Rep.* 2017. **21**: 195–207.

781 **Yang, J., Zou, M., Pezoldt, J., Zhou, X. and Huehn, J.**, Thymus-derived Foxp3+ regulatory T cells upregulate RORgammat expression under inflammatory conditions. *J. Mol. Med. (Berl)* 2018. **96**: 1387–1394.

782 **Delacher, M., Schreiber, L., Richards, D. M., Farah, C., Feuerer, M. and Huehn, J.**, Transcriptional Control of Regulatory T cells. *Curr. Topics Microbiol. Immunol.* 2014. **381**: 83–124.

783 **Owen, D. L., Mahmud, S. A., Sjaastad, L. E., Williams, J. B., Spanier, J. A., Simeonov, D. R., Ruscher, R. et al.**, Thymic regulatory T cells arise via two distinct developmental programs. *Nat. Immunol.* 2019. **20**: 195–205.

784 **Toker, A., Engelbert, D., Garg, G., Polansky, J. K., Floess, S., Miyao, T., Baron, U. et al.**, Active demethylation of the Foxp3 locus leads to the generation of stable regulatory T cells within the thymus. *J. Immunol.* 2013. **190**: 3180–3188.

785 **Thiault, N., Darrigues, J., Adoue, V., Gros, M., Binet, B., Perals, C., Leobon, B. et al.**, Peripheral regulatory T lymphocytes recirculating to the thymus suppress the development of their precursors. *Nat. Immunol.* 2015. **16**: 628–634.

786 **Cowan, J. E., McCarthy, N. I. and Anderson, G.**, CCR7 controls thymus recirculation, but not production and emigration, of Foxp3+ T cells. *Cell Rep.* 2016. **14**: 1041–1048.

787 **Panduro, M., Benoist, C. and Mathis, D.**, Tissue Tregs. *Annu. Rev. Immunol.* 2016. **34**: 609–633.

788 **Feuerer, M., Herrero, L., Cipolletta, D., Naaz, A., Wong, J., Nayer, A., Lee, J. et al.**, Lean, but not obese, fat is enriched for a unique population of regulatory T cells that affect metabolic parameters. *Nat. Med.* 2009. **15**: 930–939.

789 **Cipolletta, D., Feuerer, M., Li, A., Kamei, N., Lee, J., Shoelson, S. E., Benoist, C. et al.**, PPAR-gamma is a major driver of the accumulation and phenotype of adipose tissue Treg cells. *Nature* 2012. **486**: 549–553.

790 **Kolodin, D., van Panhuys, N., Li, C., Magnuson, A. M., Cipolletta, D., Miller, C. M., Wagers, A., Germain, R. N. et al.**, Antigen- and cytokine-driven accumulation of regulatory T cells in visceral adipose tissue of lean mice. *Cell Metab.* 2015. **21**: 543–557.

791 **Burzyn, D., Kuswanto, W., Kolodin, D., Shadrach, J. L., Cerletti, M., Jang, Y., Sefik, E. et al.**, A special population of regulatory T cells potentiates muscle repair. *Cell* 2013. **155**: 1282–1295.

792 **Arpaia, N., Green, J. A., Moltedo, B., Arvey, A., Hemmers, S., Yuan, S., Treuting, P. M. et al.**, A distinct function of regulatory T cells in tissue protection. *Cell* 2015. **162**: 1078–1089.

793 **Dombrowski, Y., O'Hagan, T., Dittmer, M., Penalva, R., Mayoral, S. R., Bankhead, P., Fleville, S. et al.**, Regulatory T cells promote myelin regeneration in the central nervous system. *Nat Neurosci* 2017. **20**: 674–680.

794 **Ali, N., Zirak, B., Rodriguez, R. S., Pauli, M. L., Truong, H. A., Lai, K., Ahn, R. et al.**, Regulatory T cells in skin facilitate epithelial stem cell differentiation. *Cell* 2017. **169**: 1119–1129 e1111.

795 **Delacher, M., Imbusch, C. D., Weichenhan, D., Breiling, A., Hotz-Wagenblatt, A., Trager, U., Hofer, A. C. et al.**, Genome-wide DNA-methylation landscape defines specialization of regulatory T cells in tissues. *Nat. Immunol.* 2017.

796 **Delacher, M., Schmidl, C., Herzig, Y., Breloer, M., Hartmann, W., Brunk, F., Kägebein, D. et al.**, Rbpj expression in regulatory T cells is critical for restraining TH2 responses. *Nat. Commun.* 2019. **10**: 1621.

797 **Carding, S. R. and Egan, P. J.**, Gammadelta T cells: functional plasticity and heterogeneity. *Nat. Rev. Immunol.* 2002. **2**: 336–345.

798 **Bonneville, M., O'Brien, R. L. and Born, W. K.**, γδ T cell effector functions: a blend of innate programming and acquired plasticity. *Nat. Rev. Immunol.* 2010. **10**: 467–478.

799 **Prinz, I., Silva-Santos, B. and Pennington, D. J.**, Functional development of gammadelta T cells. *Eur. J. Immunol.* 2013. **43**: 1988–1994.

800 **Heilig, J. S. and Tonegawa, S.**, Diversity of murine gamma genes and expression in fetal and adult T lymphocytes. *Nature* 1986. **322**: 836–840.

801 **Garman, R. D., Doherty, P. J. and Raulet, D. H.**, Diversity, rearrangement, and expression of murine T cell gamma genes. *Cell* 1986. **45**: 733–742.

802 **Pereira, P., Hermitte, V., Lembezat, M. P., Boucontet, L., Azuara, V. and Grigoriadou, K.**, Developmentally regulated and lineage-specific rearrangement of T cell receptor Valpha/delta gene segments. *Eur. J. Immunol.* 2000. **30**: 1988–1997.

803 **Mallick-Wood, C. A., Lewis, J. M., Richie, L. I., Owen, M. J., Tigelaar, R. E. and Hayday, A. C.**, Conservation of T cell receptor conformation in epidermal gammadelta cells with disrupted primary Vgamma gene usage. *Science* 1998. **279**: 1729–1733.

804 **Roark, C. L., Aydintug, M. K., Lewis, J., Yin, X., Lahn, M., Hahn, Y. S., Born, W. K. et al.**, Subset-specific, uniform activation among V gamma 6/V delta 1+ gamma delta T cells elicited by inflammation. *J. Leukoc. Biol.* 2004. **75**: 68–75.

805 **Goodman, T. and Lefrancois, L.**, Intraepithelial lymphocytes. Anatomical site, not T cell receptor form, dictates phenotype and function. *J. Exp. Med.* 1989. **170**: 1569–1581.

806 **Prinz, I., Sansoni, A., Kissenpfennig, A., Ardouin, L., Malissen, M. and Malissen, B.**, Visualization of the earliest steps of gammadelta T cell development in the adult thymus. *Nat. Immunol.* 2006. **7**: 995–1003.

807 **Koenecke, C., Chennupati, V., Schmitz, S., Malissen, B., Forster, R. and Prinz, I.**, In vivo application of mAb directed against the gammadelta TCR does not deplete but generates "invisible" gammadelta T cells. *Eur. J. Immunol.* 2009. **39**: 372–379.

808 **Sandrock, I., Reinhardt, A., Ravens, S., Binz, C., Wilharm, A., Martins, J., Oberdorfer, L. et al.**, Genetic models reveal origin, persistence and non-redundant functions of IL-17-producing gammadelta T cells. *J. Exp. Med.* 2018. **215**: 3006–3018.

809 **Ribot, J. C., deBarros, A., Pang, D. J., Neves, J. F., Peperzak, V., Roberts, S. J., Girardi, M. et al.**, CD27 is a thymic determinant of the balance between interferon-gamma- and interleukin 17-producing gammadelta T cell subsets. *Nat. Immunol.* 2009. **10**: 427–436.

810 **Haas, J. D., Gonzalez, F. H., Schmitz, S., Chennupati, V., Fohse, L., Kremmer, E., Forster, R. et al.**, CCR6 and NK1.1 distinguish between IL-17A and IFN-gamma-producing gammadelta effector T cells. *Eur. J. Immunol.* 2009. **39**: 3488–3497.

811 **Lombes, A., Durand, A., Charvet, C., Riviere, M., Bonilla, N., Auffray, C., Lucas, B. et al.**, Adaptive Immune-like gamma/delta T Lymphocytes Share Many Common Features with Their alpha/beta T Cell Counterparts. *J. Immunol.* 2015. **195**: 1449–1458.

812 **Itohara, S., Farr, A. G., Lafaille, J. J., Bonneville, M., Takagaki, Y., Haas, W. and Tonegawa, S.**, Homing of a gamma delta thymocyte subset with homogeneous T-cell receptors to mucosal epithelia. *Nature* 1990. **343**: 754–757.

813 **Shibata, K., Yamada, H., Hara, H., Kishihara, K. and Yoshikai, Y.**, Resident Vdelta1+ gammadelta T cells control early infiltration of neutrophils after Escherichia coli infection via IL-17 production. *J. Immunol.* 2007. **178**: 4466–4472.

814 **Papotto, P. H., Reinhardt, A., Prinz, I. and Silva-Santos, B.**, Innately versatile: gammadelta17 T cells in inflammatory and autoimmune diseases. *J. Autoimmun.* 2018. **87**: 26–37.

815 **Ohteki, T. and MacDonald, H. R.**, Major histocompatibility complex class I related molecules control the development of CD4+8- and CD4-8- subsets of natural killer 1.1+ T cell receptor-alpha/beta+ cells in the liver of mice. *J. Exp. Med.* 1994. **180**: 699–704.

816 **Makino, Y., Kanno, R., Ito, T., Higashino, K. and Taniguchi, M.**, Predominant expression of invariant V alpha 14+ TCR alpha chain in NK1.1+ T cell populations. *Int. Immunol.* 1995. **7**: 1157–1161.

817 **Wei, D. G., Curran, S. A., Savage, P. B., Teyton, L. and Bendelac, A.**, Mechanisms imposing the Vbeta bias of Valpha14 natural killer T cells and consequences for microbial glycolipid recognition. *J. Exp. Med.* 2006. **203**: 1197–1207.

818 **Lantz, O. and Bendelac, A.**, An invariant T cell receptor alpha chain is used by a unique subset of major histocompatibility complex class I-specific CD4+ and CD4-8- T cells in mice and humans. *J. Exp. Med.* 1994. **180**: 1097–1106.

819 **Bendelac, A., Lantz, O., Quimby, M. E., Yewdell, J. W., Bennink, J. R. and Brutkiewicz, R. R.**, CD1 recognition by mouse NK1+ T lymphocytes. *Science*. 1995. **268**: 863–865.

820 **Benlagha, K., Weiss, A., Beavis, A., Teyton, L. and Bendelac, A.**, In vivo identification of glycolipid antigen–specific T cells using fluorescent Cd1d tetramers. *J. Exp. Med.* 2000. **191**: 1895–1904.

821 **Matsuda, J. L., Naidenko, O. V., Gapin, L., Nakayama, T., Taniguchi, M., Wang, C. R., Koezuka, Y. et al.**, Tracking the response of natural killer T cells to a glycolipid antigen using CD1d tetramers. *J. Exp. Med.* 2000. **192**: 741–754.

822 **Moran, A. E., Holzapfel, K. L., Xing, Y., Cunningham, N. R., Maltzman, J. S., Punt, J. and Hogquist, K. A.**, T cell receptor signal strength in Treg and iNKT cell development demonstrated by a novel fluorescent reporter mouse. *J. Exp. Med.* 2011. **208**: 1279–1289.

823 **Savage, A. K., Constantinides, M. G., Han, J., Picard, D., Martin, E., Li, B., Lantz, O. et al.**, The transcription factor PLZF directs the effector program of the NKT cell lineage. *Immunity* 2008. **29**: 391–403.

824 **Kovalovsky, D., Uche, O. U., Eladad, S., Hobbs, R. M., Yi, W., Alonzo, E., Chua, K. et al.**, The BTB-zinc finger transcriptional regulator PLZF controls the development of invariant natural killer T cell effector functions. *Nat. Immunol.* 2008. **9**: 1055–1064.

825 **Benlagha, K., Kyin, T., Beavis, A., Teyton, L. and Bendelac, A.**, A thymic precursor to the NK T cell lineage. *Science* 2002. **296**: 553–555.

826 **Benlagha, K., Wei, D. G., Veiga, J., Teyton, L. and Bendelac, A.**, Characterization of the early stages of thymic NKT cell development. *J. Exp. Med.* 2005. **202**: 485–492.

827 **Pellicci, D. G., Hammond, K. J. L., Uldrich, A. P., Baxter, A. G., Smyth, M. J. and Godfrey, D. I.**, A natural killer T (NKT) cell developmental pathway iInvolving a thymus-dependent NK1.1(-)CD4(+) CD1d-dependent precursor stage. *J. Exp. Med.* 2002. **195**: 835–844.

828 **Wang, H. and Hogquist, K. A.**, CCR7 defines a precursor for murine iNKT cells in thymus and periphery. *Elife* 2018. **7**.

829 **Berzins, S. P., McNab, F. W., Jones, C. M., Smyth, M. J. and Godfrey, D. I.**, Long-term retention of mature NK1.1+ NKT cells in the thymus. *J. Immunol.* 2006. **176**: 4059–4065.

830 **Lee, Y. J., Holzapfel, K. L., Zhu, J., Jameson, S. C. and Hogquist, K. A.**, Steady-state production of IL-4 modulates immunity in mouse strains and is determined by lineage diversity of iNKT cells. *Nat. Immunol.* 2013. **14**: 1146–1154.

831 **Crosby, C. M. and Kronenberg, M.**, Tissue-specific functions of invariant natural killer T cells. *Nat. Rev. Immunol.* 2018. **18**: 559–574.

832 **Salou, M., Legoux, F., Gilet, J., Darbois, A., Du Halgouet, A., Alonso, R., Richer, W. et al.**, A common transcriptomic program acquired in the thymus defines tissue residency of MAIT and NKT subsets. *J. Exp. Med.* 2019. **216**: 133–151.

833 **Brigl, M., Tatituri, R. V. V., Watts, G. F. M., Bhowruth, V., Leadbetter, E. A., Barton, N., Cohen, N. R. et al.**, Innate and cytokine-driven signals, rather than microbial antigens, dominate in natural killer T cell activation during microbial infection. *J. Exp. Med.* 2011. **208**: 1163–1177.

834 **Velazquez, P., Cameron, T. O., Kinjo, Y., Nagarajan, N., Kronenberg, M. and Dustin, M. L.**, Cutting edge: activation by innate cytokines or microbial antigens can cause arrest of natural killer T cell patrolling of liver sinusoids. *J. Immunol.* 2008. **180**: 2024–2028.

835 **Salio, M., Silk, J. D., Jones, E. Y. and Cerundolo, V.**, Biology of CD1- and MR1-restricted T cells. *Annu. Rev. Immunol.* 2014. **32**: 323–366.

836 **Wang, H. and Hogquist, K. A.**, How lipid-specific T cells become effectors: the differentiation of iNKT subsets. *Front. Immunol.* 2018. **9**: 1450.

837 **Jungblut, M., Oeltze, K., Zehnter, I., Hasselmann, D. and Bosio, A.**, Standardized preparation of single-cell suspensions from mouse lung tissue using the gentleMACS dissociator. *J. Vis. Exp.* 2009.

838 **Liu, Y., Goff, R. D., Zhou, D., Mattner, J., Sullivan, B. A., Khurana, A., Cantu, C. et al.**, A modified alpha-galactosyl ceramide for staining and stimulating natural killer T cells. *J. Immunol. Methods* 2006. **312**: 34–39.

839 **Lee, Y. J., Wang, H., Starrett, G. J., Phuong, V., Jameson, S. C. and Hogquist, K. A.**, Tissue-specific distribution of iNKT cells impacts their cytokine response. *Immunity* 2015. **43**: 566–578.

840 **Ziętara, N., Łyszkiewicz, M., Witzlau, K., Naumann, R., Hurwitz, R., Langemeier, J., Bohne, J. et al.**, Critical role for miR-181a/b-1 in agonist selection of invariant natural killer T cells. *Proc. Natl. Acad. Sci. U S A.* 2013. **110**: 7407–7412.

841 **Winter, S. J., Kunze-Schumacher, H., Imelmann, E., Grewers, Z., Osthues, T. and Krueger, A.**, MicroRNA miR-181a/b-1 controls MAIT cell development. *Immunol. Cell. Biol.* 2019. **97**: 190–202.

842 **Treiner, E., Duban, L., Bahram, S., Radosavljevic, M., Wanner, V., Tilloy, F., Affaticati, P. et al.**, Selection of evolutionarily conserved mucosal-associated invariant T cells by MR1. *Nature* 2003. **422**: 164–169.

843 **Porcelli, S., Yockey, C. E., Brenner, M. B. and Balk, S. P.**, Analysis of T cell antigen receptor (TCR) expression by human peripheral blood CD4-8- alpha/beta T cells demonstrates preferential use of several V beta genes and an invariant TCR alpha chain. *J. Exp. Med.* 1993. **178**: 1–16.

844 **Tilloy, F., Treiner, E., Park, S. H., Garcia, C., Lemonnier, F., La Salle, H. de, Bendelac, A., Bonneville, M. et al.**, An invariant T cell receptor alpha chain defines a novel TAP-independent major histocompatibility complex class Ib-restricted alpha/beta T cell subpopulation in mammals. *J. Exp. Med.* 1999. **189**: 1907–1921.

845 **Rahimpour, A., Koay, H. F., Enders, A., Clanchy, R., Eckle, S. B. G., Meehan, B., Chen, Z. et al.**, Identification of phenotypically and functionally heterogeneous mouse mucosal-associated invariant T cells using MR1 tetramers. *J. Exp. Med.* 2015. **212**: 1095–1108.

846 **Reantragoon, R., Corbett, A. J., Sakala, I. G., Gherardin, N. A., Furness, J. B., Chen, Z., Eckle, S. B. G. et al.**, Antigen-loaded MR1 tetramers define T cell receptor heterogeneity in mucosal-associated invariant T cells. *J. Exp. Med.* 2013. **210**: 2305–2320.

847 **Koay, H. F., Gherardin, N. A., Enders, A., Loh, L., Mackay, L. K., Almeida, C. F., Russ, B. E. et al.**, A three-stage intrathymic development pathway for the mucosal-associated invariant T cell lineage. *Nat. Immunol.* 2016. **17**: 1300–1311.

848 **Cui, Y., Franciszkiewicz, K., Mburu, Y. K., Mondot, S., Le Bourhis, L., Premel, V., Martin, E. et al.**, Mucosal-associated invariant T cell-rich congenic mouse strain allows functional evaluation. *J. Clin. Invest.* 2015. **125**: 4171–4185.

849 **Salou, M., Franciszkiewicz, K. and Lantz, O.**, MAIT cells in infectious diseases. *Curr. Opin. Immunol.* 2017. **48**: 7–14.

850 **Corbett, A. J., Eckle, S. B., Birkinshaw, R. W., Liu, L., Patel, O., Mahony, J., Chen, Z. et al.**, T-cell activation by transitory neo-antigens derived from distinct microbial pathways. *Nature* 2014. **509**: 361–365.

851 **Olivares-Villagomez, D. and Van Kaer, L.**, Intestinal Intraepithelial Lymphocytes: Sentinels of the Mucosal Barrier. *Trends Immunol.* 2018. **39**: 264–275.

852 **Ma, H., Tao, W. and Zhu, S.**, T lymphocytes in the intestinal mucosa: defense and tolerance. *Cell Mol. Immunol.* 2019.

853 **Cheroutre, H., Lambolez, F. and Mucida, D.**, The light and dark sides of intestinal intraepithelial lymphocytes. *Nat. Rev. Immunol.* 2011. **11**: 445–456.

854 **Georgiev, H., Ravens, I., Papadogianni, G., Malissen, B., Forster, R. and Bernhardt, G.**, Blocking the ART2.2/P2X7-system is essential to avoid a detrimental bias in functional CD4 T cell studies. *Eur. J. Immunol.* 2018. **48**: 1078–1081.

855 **Konjar, S., Ferreira, C., Blankenhaus, B. and Veldhoen, M.**, Intestinal Barrier Interactions with Specialized CD8 T Cells. *Front. Immunol.* 2017. **8**: 1281.

856 **Chennupati, V., Worbs, T., Liu, X., Malinarich, F. H., Schmitz, S., Haas, J. D., Malissen, B. et al.**, Intra- and intercompartmental movement of gammadelta T cells: intestinal intraepithelial and peripheral gammadelta T cells represent exclusive nonoverlapping populations with distinct migration characteristics. *J. Immunol.* 2010. **185**: 5160–5168.

857 **Malinarich, F. H., Grabski, E., Worbs, T., Chennupati, V., Haas, J. D., Schmitz, S., Candia, E. et al.**, Constant TCR triggering suggests that the TCR expressed on intestinal intraepithelial gammadelta T cells is functional in vivo. *Eur. J. Immunol.* 2010. **40**: 3378–3388.

858 **Martina, M. N., Noel, S., Saxena, A., Rabb, H. and Hamad, A. R.**, Double negative (DN) alphabeta T cells: misperception and overdue recognition. *Immunol. Cell Biol.* 2015. **93**: 305–310.

859 **Gerlach, C., van Heijst, J. W., Swart, E., Sie, D., Armstrong, N., Kerkhoven, R. M., Zehn, D. et al.**, One naive T cell, multiple fates in CD8+ T cell differentiation. *J. Exp. Med.* 2010. **207**: 1235–1246.

860 **Appay, V., van Lier, R. A., Sallusto, F. and Roederer, M.**, Phenotype and function of human T lymphocyte subsets: consensus and issues. *Cytometry A* 2008. **73**: 975–983.

861 **Costantini, A., Mancini, S., Giuliodoro, S., Butini, L., Regnery, C. M., Silvestri, G. and Montroni, M.**, Effects of cryopreservation on lymphocyte immunophenotype and function. *J. Immunol. Methods* 2003. **278**: 145–155.

862 **van den Broek, T., Borghans, J. A. M. and van Wijk, F.**, The full spectrum of human naive T cells. *Nat. Rev. Immunol.* 2018. **18**: 363–373.

863 **Sallusto, F., Lenig, D., Mackay, C. R. and Lanzavecchia, A.**, Flexible programs of chemokine receptor expression on human polarized T helper 1 and 2 lymphocytes. *J. Exp. Med.* 1998. **187**: 875–883.

864 **Cosmi, L., Annunziato, F., Galli, M. I. G., Maggi, R. M. E., Nagata, K. and Romagnani, S.**, CRTH2 is the most reliable marker for the detection of circulating human type 2 Th and type 2 T cytotoxic cells in health and disease. *Eur. J. Immunol.* 2000. **30**: 2972–2979.

865 **Mahnke, Y. D., Beddall, M. H. and Roederer, M.**, OMIP-017: human CD4(+) helper T-cell subsets including follicular helper cells. *Cytometry A* 2013. **83**: 439–440.

866 **Ouyang, W., Ranganath, S. H., Weindel, K., Bhattacharya, D., Murphy, T. L., Sha, W. C. and Murphy, K. M.**, Inhibition of Th1 development mediated by GATA-3 through an IL-4-independent mechanism. *Immunity* 1998. **9**: 745–755.

867 **Kanhere, A., Hertweck, A., Bhatia, U., Gokmen, M. R., Perucha, E., Jackson, I., Lord, G. M. et al.**, T-bet and GATA3 orchestrate Th1 and Th2 differentiation through lineage-specific targeting of distal regulatory elements. *Nat. Commun.* 2012. **3**: 1268.

868 **Staudt, V., Bothur, E., Klein, M., Lingnau, K., Reuter, S., Grebe, N., Gerlitzki, B. et al.**, Interferon-regulatory factor 4 is essential for the developmental program of T helper 9 cells. *Immunity* 2010. **33**: 192–202.

869 **Maggi, L., Santarlasci, V., Capone, M., Peired, A., Frosali, F., Crome, S. Q., Querci, V. et al.**, CD161 is a marker of all human IL-17-producing T-cell subsets and is induced by RORC. *Eur. J. Immunol.* 2010. **40**: 2174–2181.

870 **Zielinski, C. E., Mele, F., Aschenbrenner, D., Jarrossay, D., Ronchi, F., Gattorno, M., Monticelli, S. et al.**, Pathogen-induced human TH17 cells produce IFN-gamma or IL-10 and are regulated by IL-1beta. *Nature* 2012. **484**: 514–518.

871 **Cosmi, L., Maggi, L., Santarlasci, V., Liotta, F. and Annunziato, F.**, T helper cells plasticity in inflammation. *Cytometry A* 2014. **85**: 36–42.

872 **Acosta-Rodriguez, E. V., Rivino, L., Geginat, J., Jarrossay, D., Gattorno, M., Lanzavecchia, A., Sallusto, F. et al.**, Surface phenotype and antigenic specificity of human interleukin 17-producing T helper memory cells. *Nat. Immunol.* 2007. **8**: 639–646.

873 **Gagliani, N., Amezcua Vesely, M. C., Iseppon, A., Brockmann, L., Xu, H., Palm, N. W., de Zoete, M. R., Licona-Limon, P. et al.**, Th17 cells transdifferentiate into regulatory T cells during resolution of inflammation. *Nature* 2015. **523**: 221–225.

874 **Jankovic, D., Kugler, D. G. and Sher, A.**, IL-10 production by CD4+ effector T cells: a mechanism for self-regulation. *Mucosal Immunol.* 2010. **3**: 239–246.

875 **Zhang, P., Lee, J. S., Gartlan, K. H., Schuster, I. S., Comerford, I., Varelias, A., Ullah, M. A. et al.**, Eomesodermin promotes the development of type 1 regulatory T (TR1) cells. *Sci. Immunol.* 2017. **2**: eaah7152.

876 **Gruarin, P., Maglie, S., De Simone, M., Haringer, B., Vasco, C., Ranzani, V., Bosotti, R., Noddings, J. S. et al.**, Eomesodermin controls a unique differentiation program in human IL-10 and IFN-gamma coproducing regulatory T cells. *Eur. J. Immunol.* 2019. **49**: 96–111.

877 **Basu, R., O'Quinn, D. B., Silberger, D. J., Schoeb, T. R., Fouser, L., Ouyang, W., Hatton, R. D. et al.**, Th22 cells are an important source of IL-22 for host protection against enteropathogenic bacteria. *Immunity* 2012. **37**: 1061–1075.

878 **Duhen, T., Geiger, R., Jarrossay, D., Lanzavecchia, A. and Sallusto, F.**, Production of interleukin 22 but not interleukin 17 by a subset of human skin-homing memory T cells. *Nat. Immunol.* 2009. **10**: 857–863.

879 **Morita, R., Schmitt, N., Bentebibel, S. E., Ranganathan, R., Bourdery, L., Zurawski, G., Foucat, E. et al.**, Human blood CXCR5(+)CD4(+) T cells are counterparts of T follicular cells and contain specific subsets that differentially support antibody secretion. *Immunity* 2011. **34**: 108–121.

880 **Glatman Zaretsky, A., Taylor, J. J., King, I. L., Marshall, F. A., Mohrs, M. and Pearce, E. J.**, T follicular helper cells differentiate from Th2 cells in response to helminth antigens. *J. Exp. Med.* 2009. **206**: 991–999.

881 **Oja, A. E., Vieira Braga, F. A., Remmerswaal, E. B., Kragten, N. A., Hertoghs, K. M., Zuo, J., Moss, P. A., van Lier, R. A., van Gisbergen, K. P. et al.**, The transcription factor Hobit identifies human cytotoxic CD4(+) T cells. *Front. Immunol.* 2017. **8**: 325.

882 **Hamann, D., Baars, P. A., Rep, M. H., Hooibrink, B., Kerkhof-Garde, S. R., Klein, M. R. and van Lier, R. A.**, Phenotypic and functional separation of memory and effector human CD8+ T cells. *J. Exp. Med.* 1997. **186**: 1407–1418.

883 **Appay, V., Dunbar, P. R., Callan, M., Klenerman, P., Gillespie, G. M., Papagno, L., Ogg, G. S. et al.**, Memory CD8+ T cells vary in differentiation phenotype in different persistent virus infections. *Nat. Med.* 2002. **8**: 379–385.

884 **Sallusto, F., Lenig, D., Forster, R., Lipp, M. and Lanzavecchia, A.**, Two subsets of memory T lymphocytes with distinct homing potentials and effector functions. *Nature* 1999. **401**: 708–712.

885 **van Aalderen, M. C., Remmerswaal, E. B., Verstegen, N. J., Hombrink, P., ten Brinke, A., Pircher, H., Kootstra, N. A., ten Berge, I. J. et al.**, Infection history determines the differentiation state of human CD8+ T cells. *J. Virol.* 2015. **89**: 5110–5123.

886 **van Leeuwen, E. M., Remmerswaal, E. B., Vossen, M. T., Rowshani, A. T., Wertheim-van Dillen, P. M., van Lier, R. A. and ten Berge, I. J.**, Emergence of a CD4+CD28- granzyme B+, cytomegalovirus-specific T cell subset after recovery of primary cytomegalovirus infection. *J. Immunol.* 2004. **173**: 1834–1841.

887 **Huster, K. M., Busch, V., Schiemann, M., Linkemann, K., Kerksiek, K. M., Wagner, H. and Busch, D. H.**, Selective expression of IL-7 receptor on memory T cells identifies early CD40L-dependent generation of distinct CD8+ memory T cell subsets. *Proc. Natl. Acad. Sci. U. S. A.* 2004. **101**: 5610–5615.

888 **Hand, T. W., Morre, M. and Kaech, S. M.**, Expression of IL-7 receptor alpha is necessary but not sufficient for the formation of memory CD8 T cells during viral infection. *Proc. Natl. Acad. Sci. USA* 2007. **104**: 11730–11735.

889 **Shay, T., Jojic, V., Zuk, O., Rothamel, K., Puyraimond-Zemmour, D., Feng, T., Wakamatsu, E. et al.**, Conservation and divergence in the transcriptional programs of the human and mouse immune systems. *Proc. Natl. Acad. Sci. USA* 2013. **110**: 2946–2951.

890 **Remmerswaal, E. B. M., Hombrink, P., Nota, B., Pircher, H., Ten Berge, I. J. M., van Lier, R. A. W. and van Aalderen, M. C.**, Expression of IL-7Ralpha and KLRG1 defines functionally distinct CD8(+) T-cell populations in humans. *Eur. J. Immunol.* 2019. **49**: 694–708.

891 **Intlekofer, A. M., Takemoto, N., Wherry, E. J., Longworth, S. A., Northrup, J. T., Palanivel, V. R., Mullen, A. C. et al.**, Effector and memory CD8+ T cell fate coupled by T-bet and eomesodermin. *Nat. Immunol.* 2005. **6**: 1236–1244.

892 **Kragten, N. A. M., Behr, F. M., Vieira Braga, F. A., Remmerswaal, E. B. M., Wesselink, T. H., Oja, A. E., Hombrink, P. et al.**, Blimp-1 induces and Hobit maintains the cytotoxic mediator granzyme B in CD8 T cells. *Eur. J. Immunol.* 2018. **48**: 1644–1662.

893 **Vieira Braga, F. A., Hertoghs, K. M., Kragten, N. A., Doody, G. M., Barnes, N. A., Remmerswaal, E. B., Hsiao, C. C. et al.**, Blimp-1 homolog Hobit identifies effector-type lymphocytes in humans. *Eur. J. Immunol.* 2015. **45**: 2945–2958.

894 **Kim, H. J., Barnitz, R. A., Kreslavsky, T., Brown, F. D., Moffett, H., Lemieux, M. E., Kaygusuz, Y. et al.**, Stable inhibitory activity of regulatory T cells requires the transcription factor Helios. *Science* 2015. **350**: 334–339.

895 **Sathaliyawala, T., Kubota, M., Yudanin, N., Turner, D., Camp, P., Thome, J. J., Bickham, K. L. et al.**, Distribution and compartmentalization of human circulating and tissue-resident memory T cell subsets. *Immunity* 2013. **38**: 187–197.

896 **Thome, J. J. C., Yudanin, N., Ohmura, Y., Kubota, M., Grinshpun, B., Sathaliyawala, T., Kato, T. et al.**, Spatial map of human t cell compartmentalization and maintenance over decades of life. *Cell* 2014. **159**: 814–828.

897 **Okhrimenko, A., Grün, J. R., Westendorf, K., Fang, Z., Reinke, S., von Roth, P., Wassilew, G. et al.**, Human memory T cells from the bone marrow are resting and maintain long-lasting systemic memory. 2014. **111**: 9229–9234.

898 **Watanabe, R., Gehad, A., Yang, C., Scott, L. L., Teague, J. E., Schlapbach, C., Elco, C. P. et al.**, Human skin is protected by four functionally and phenotypically discrete populations of resident and recirculating memory T cells. *Sci. Transl. Med.* 2015. **7**: 279ra39.

899 **Hombrink, P., Helbig, C., Backer, R. A., Piet, B., Oja, A. E., Stark, R., Brasser, G., Jongejan, A., Jonkers, R. E., Nota, B., Basak, O., Clevers, H. C., Moerland, P. D., Amsen, D., van Lier, R. A.** Programs for the persistence, vigilance and control of human CD8+ lung-resident memory T cells. *Nat. Immunol.* 2016. **17**: 1467–1478.

900 **Kumar, B. V., Ma, W., Miron, M., Granot, T., Guyer, R. S., Carpenter, D. J., Senda, T. et al.**, Human tissue-resident memory T cells are defined by core transcriptional and functional signatures in lymphoid and mucosal sites. *Cell Rep.* 2017. **20**: 2921–2934.

901 **Oja, A. E., Piet, B., Helbig, C., Stark, R., van der Zwan, D., Blaauwgeers, H., Remmerswaal, E. B. M. et al.**, Trigger-happy resident memory CD4+ T cells inhabit the human lungs. *Mucosal Immunol.* 2018. **11**: 654–667.

902 **Smolders, J., Heutinck, K. M., Fransen, N. L., Remmerswaal, E. B. M., Hombrink, P., Ten Berge, I. J. M., van Lier, R. A. W. et al.**, Tissue-resident memory T cells populate the human brain. *Nat. Commun.* 2018. **9**: 4593.

903 **Pascutti, M. F., Geerman, S., Collins, N., Brasser, G., Nota, B., Stark, R., Behr, F. et al.**, Peripheral and systemic antigens elicit an expandable pool of resident memory CD8$^+$ T cells in the bone marrow. *Eur. J. Immunol.* 2019. **49**: 853–872.

904 **Snyder, M. E., Finlayson, M. O., Connors, T. J., Dogra, P., Senda, T., Bush, E., Carpenter, D. et al.**, Generation and persistence of human tissue-resident memory T cells in lung transplantation. *Sci. Immunol.* 2019. **4**: eaav5581.

905 **Skon, C. N., Lee, J. Y., Anderson, K. G., Masopust, D., Hogquist, K. A. and Jameson, S. C.**, Transcriptional downregulation of S1pr1 is required for the establishment of resident memory CD8+ T cells. *Nat. Immunol.* 2013. **14**: 1285–1293.

906 **Steinert, E. M. et al.**, Quantifying memory CD8 T cells reveals regionalization of immunosurveillance. *Cell* 2015. **161**: 737–749.

907 **Kumar, B. V., Connors, T. J. and Farber, D. L.**, Human T Cell Development, Localization, and Function throughout Life. *Immunity* 2018. **48**: 202–213.

908 **Cepek, K. L. et al.**, Adhesion between epithelial cells and T lymphocytes mediated by E-cadherin and the alpha E beta 7 integrin. *Nature* 1994. **372**: 190–193.

909 **Cheuk, S., Schlums, H., Bryceson, Y. T., Eidsmo, L. and Tjernlund, A.**, CD49a Expression Defines Tissue-Resident CD8 + T Cells Poised for Cytotoxic Function in Human Skin. *Immunity* 2017. 1–14. https://doi.org/10.1016/j.immuni.2017.01.009

910 **Webb, J. R., Milne, K., Watson, P., DeLeeuw, R. J. and Nelson, B. H.**, Tumor-infiltrating lymphocytes expressing the tissue resident memory marker cd103 are associated with increased survival in high-grade serous ovarian cancer. *Clin. Cancer Res.* 2014. **20**: 434–444.

911 **Djenidi, F., Adam, J., Goubar, A., Durgeau, A., Meurice, G., de Montpréville, V., Validire, P. et al.**, CD8 $^+$ CD103 $^+$ Tumor–Infiltrating Lymphocytes Are Tumor-Specific Tissue-Resident Memory T Cells and a Prognostic Factor for Survival in Lung Cancer Patients. *J. Immunol.* 2015. **194**: 3475–3486.

912 **Koh, J., Kim, S., Kim, M. Y., Go, H., Jeon, Y. K. and Chung, D. H.**, Prognostic implications of intratumoral CD103+ tumor-infiltrating lymphocytes in pulmonary squamous cell carcinoma. *Oncotarget* 2017. **8**: 13762–13769.

913 **Ganesan, A.-P., Clarke, J., Wood, O., Garrido-Martin, E. M., Chee, S. J., Mellows, T., Samaniego-Castruita, D., Singh, D. et al.**, Tissue-resident memory features are linked to the magnitude of cytotoxic

T cell responses in human lung cancer. *Nat. Immunol.* 2017. **18**: 940–950.

914 **Oja, A. E., Piet, B., van der Zwan, D., Blaauwgeers, H., Mensink, M., de Kivit, S., Borst, J. et al.**, Functional heterogeneity of CD4+ tumor-infiltrating lymphocytes with a resident memory phenotype in NSCLC. *Front. Immunol.* 2018. **9**: 2654.

915 **Gu-Trantien, C. et al.**, CXCL13-producing T FH cells link immune suppression and adaptive memory in human breast cancer. *JCI Insight* 2017. **2**: 1–17.

916 **Thommen, D. D., Koelzer, V. H., Herzig, P., Roller, A., Trefny, M., Dimeloe, S., Kiialainen, A. et al.**, A transcriptionally and functionally distinct PD-1 + CD8 + T cell pool with predictive potential in non-small cell lung cancer treated with PD-1 blockade. *Nat. Med.* 2018.**24**.

917 **Simoni, Y. et al.**, Bystander CD8+ T cells are abundant and phenotypically distinct in human tumour infiltrates. *Nature* 2018. **557**: 575–579.

918 **Holt, P. G., Robinson, B. W., Reid, M., Kees, U. R., Warton, A., Dawson, V. H., Rose, A., Schon-Hegrad, M. et al.**, Extraction of immune and inflammatory cells from human lung parenchyma: evaluation of an enzymatic digestion procedure. *Clin. Exp. Immunol.* 1986. **66**: 188–200.

919 **Piet, B., de Bree, G. J., Smids-Dierdorp, B. S., van der Loos, C. M., Remmerswaal, E. B., von der Thüsen, J. H., van Haarst, J. M. et al.**, CD8+ T cells with an intraepithelial phenotype upregulate cytotoxic function upon influenza infection in human lung. *J. Clin. Invest.* 2011. **121**: 2254–2263.

920 **Clark, R. A., Chong, B., Mirchandani, N., Brinster, N. K., Yamanaka, K., Dowgiert, R. K. and Kupper, T. S.**, The Vast Majority of CLA + T Cells Are Resident in Normal Skin. *J. Immunol.* 2006. **176**: 4431–4439.

921 **Bektas, A., Schurman, S. H., Sen, R. and Ferrucci, L.**, Human T cell immunosenescence and inflammation in aging. *J. Leukoc. Biol.* 2017. **102**: 977–988.

922 **Costantini, E., D'Angelo, C. and Reale, M.**, The role of immunosenescence in neurodegenerative diseases. *Mediators Inflamm.* 2018. **2018**: 6039171.

923 **Franceschi, C., Capri, M., Monti, D., Giunta, S., Olivieri, F., Sevini, F., Panourgia, M. P. et al.**, Inflammaging and anti-inflammaging: a systemic perspective on aging and longevity emerged from studies in humans. *Mech. Ageing Dev.* 2007. **128**: 92–105.

924 **Derhovanessian, E., Maier, A. B., Hahnel, K., Zelba, H., de Craen, A. J., Roelofs, H., Slagboom, E. P. et al.**, Lower proportion of naive peripheral CD8+ T cells and an unopposed pro-inflammatory response to human Cytomegalovirus proteins in vitro are associated with longer survival in very elderly people. *Age (Dordr)* 2013. **35**: 1387–1399.

925 **Naylor, K., Li, G., Vallejo, A. N., Lee, W. W., Koetz, K., Bryl, E., Witkowski, J. et al.**, The influence of age on T cell generation and TCR diversity. *J. Immunol.* 2005. **174**: 7446–7452.

926 **Olsson, J., Wikby, A., Johansson, B., Lofgren, S., Nilsson, B. O. and Ferguson, F. G.**, Age-related change in peripheral blood T-lymphocyte subpopulations and cytomegalovirus infection in the very old: the Swedish longitudinal OCTO immune study. *Mech. Ageing Dev.* 2000. **121**: 187–201.

927 **Rubino, G., Bulati, M., Aiello, A., Aprile, S., Gambino, C. M., Gervasi, F., Caruso, C. et al.**, Sicilian centenarian offspring are more resistant to immune ageing. *Aging Clin. Exp. Res.* 2019. **31**: 125–133.

928 **Sanderson, S. L. and Simon, A. K.**, In aged primary T cells, mitochondrial stress contributes to telomere attrition measured by a novel imaging flow cytometry assay. *Aging Cell* 2017. **16**: 1234–1243.

929 **Arnold, C. R., Pritz, T., Brunner, S., Knabb, C., Salvenmoser, W., Holzwarth, B., Thedieck, K. et al.**, T cell receptor-mediated activation is a potent inducer of macroautophagy in human CD8(+)CD28(+) T cells but not in CD8(+)CD28(-) T cells. *Exp. Gerontol.* 2014. **54**: 75–83.

930 **Pellicano, M., Buffa, S., Goldeck, D., Bulati, M., Martorana, A., Caruso, C., Colonna-Romano, G. et al.**, Evidence for less marked potential signs of T-cell immunosenescence in centenarian offspring than in the general age-matched population. *J. Gerontol. A Biol. Sci. Med. Sci.* 2014. **69**: 495–504.

931 **Derhovanessian, E., Maier, A. B., Beck, R., Jahn, G., Hahnel, K., Slagboom, P. E., de Craen, A. J. et al.**, Hallmark features of immunosenescence are absent in familial longevity. *J. Immunol.* 2010. **185**: 4618–4624.

932 **Raz, Y., Guerrero-Ros, I., Maier, A., Slagboom, P. E., Atzmon, G., Barzilai, N. and Macian, F.**, Activation-induced autophagy is preserved in CD4+ T-cells in familial longevity. *J. Gerontol. A Biol. Sci. Med. Sci.* 2017. **72**: 1201–1206.

933 **Duggal, N. A., Pollock, R. D., Lazarus, N. R., Harridge, S. and Lord, J. M.**, Major features of immunesenescence, including reduced thymic output, are ameliorated by high levels of physical activity in adulthood. *Aging Cell* 2018. **17**.

934 **Senda, T., Dogra, P., Granot, T., Furuhashi, K., Snyder, M. E., Carpenter, D. J., Szabo, P. A. et al.**, Microanatomical dissection of human intestinal T-cell immunity reveals site-specific changes in gut-associated lymphoid tissues over life. *Mucosal Immunol.* 2019. **12**(2): 378–389.

935 **Thome, J. J., Bickham, K. L., Ohmura, Y., Kubota, M., Matsuoka, N., Gordon, C., Granot, T. et al.**, Early-life compartmentalization of human T cell differentiation and regulatory function in mucosal and lymphoid tissues. *Nat. Med.* 2016. **22**(1): 72–77.

936 **Seddiki, N., Santner-Nanan, B., Martinson, J., Zaunders, J., Sasson, S., Landay, A., Solomon, M. et al.**, Expression of interleukin (IL)-2 and IL-7 receptors discriminates between human regulatory and activated T cells. *J. Exp. Med.* 2006. **203**(7): 1693–1700.

937 **Kverneland, A. H., Streitz, M., Geissler, E., Hutchinson, J., Vogt, K., Boes, D., Niemann, N. et al.**, Age and gender leucocytes variances and references values generated using the standardized ONE-Study protocol. *Cytometry A* 2016. **89**(6): 543–564.

938 **Abbas, A. K., Benoist, C., Bluestone, J. A., Campbell, D. J., Ghosh, S., Hori, S., Jiang, S. et al.**, Regulatory T cells: recommendations to simplify the nomenclature. *Nat. Immunol.* 2013. **14**(4): 307–308.

939 **Himmel, M. E., MacDonald, K. G., Garcia, R. V., Steiner, T. S. and Levings, M. K.**, Helios+ and Helios- cells coexist within the natural FOXP3+ T regulatory cell subset in humans. *J. Immunol.* 2013. **190**(5): 2001–2008.

940 **Bin Dhuban, K., d'Hennezel, E., Nashi, E., Bar-Or, A., Rieder, S., Shevach, E. M., Nagata, S. et al.**, Coexpression of TIGIT and FCRL3 identifies Helios+ human memory regulatory T cells. *J. Immunol.* 2015. **194**(8): 3687–3696.

941 **Milpied, P., Renand, A., Bruneau, J., Mendes-da-Cruz, D. A., Jacquelin, S., Asnafi, V., Rubio, M. T. et al.**, Neuropilin-1 is not a marker of human Foxp3+ Treg. *Eur. J. Immunol.* 2009. **39**(6): 1466–1471.

942 **Duhen, T., Duhen, R., Lanzavecchia, A., Sallusto, F. and Campbell, D. J.**, Functionally distinct subsets of human FOXP3+ Treg cells that phenotypically mirror effector Th cells. *Blood* 2012. **119**(19): 4430–4440.

943 **MacDonald, K. G., Dawson, N. A., Huang, Q., Dunne, J. V., Levings, M. K. and Broady, R.**, Regulatory T cells produce profibrotic cytokines in the skin of patients with systemic sclerosis. *J. Allergy Clin. Immunol.* 2015. **135**(4): e946–e949.

944 **Pesenacker, A. M., Bending, D., Ursu, S., Wu, Q., Nistala, K. and Wedderburn, L. R.**, CD161 defines the subset of FoxP3+ T cells capable of producing proinflammatory cytokines. *Blood* 2013. **121**(14): 2647–2658.

945 **Ferreira, R. C., Rainbow, D. B., Rubio Garcia, A., Pekalski, M. L., Porter, L., Oliveira, J. J., Waldron-Lynch, F. et al.**, Human IL-6R(hi)TIGIT(-)

CD4(+)CD127(low)CD25(+) T cells display potent in vitro suppressive capacity and a distinct Th17 profile. *Clin. Immunol.* 2017. **179**: 25–39.

946 **Hoeppli, R. E., MacDonald, K. N., Leclair, P., Fung, V. C. W., Mojibian, M., Gillies, J., Rahavi, S. M. R. et al.**, Tailoring the homing capacity of human Tregs for directed migration to sites of Th1-inflammation or intestinal regions. *Am. J. Transplant* 2019. **19**: 62–76.

947 **Allan, S. E., Crome, S. Q., Crellin, N. K., Passerini, L., Steiner, T. S., Bacchetta, R., Roncarolo, M. G. et al.**, Activation-induced FOXP3 in human T effector cells does not suppress proliferation or cytokine production. *Int. Immunol.* 2007. **19**(4): 345–354.

948 **Pesenacker, A. M., Wang, A. Y., Singh, A., Gillies, J., Kim, Y., Piccirillo, C. A., Nguyen, D. et al.**, A regulatory T-cell gene signature is a specific and sensitive biomarker to identify children with new-onset type 1 diabetes. *Diabetes* 2016. **65**(4): 1031–1039.

949 **Spreafico, R., Rossetti, M., van den Broek, T., Jansen, N. J., Zhang, H., Moshref, M., Prakken, B., van Loosdregt, J., van Wijk, F. and Albani, S.**, A sensitive protocol for FOXP3 epigenetic analysis in scarce human samples. *Eur. J. Immunol.* 2014. **44**(10): 3141–3143.

950 **Rainbow, D. B., Yang, X., Burren, O., Pekalski, M. L., Smyth, D. J., Klarqvist, M. D., Penkett, C. J. et al.**, Epigenetic analysis of regulatory T cells using multiplex bisulfite sequencing. *Eur. J. Immunol.* 2015. **45**(11): 3200–3203.

951 **Liu, W., Putnam, A. L., Xu-Yu, Z., Szot, G. L., Lee, M. R., Zhu, S., Gottlieb, P. A. et al.**, CD127 expression inversely correlates with FoxP3 and suppressive function of human CD4+ T reg cells. *J. Exp. Med.* 2006. **203**(7): 1701–1711.

952 **Wang, J., Ioan-Facsinay, A., van der Voort, E. I., Huizinga, T. W. and Toes, R. E.**, Transient expression of FOXP3 in human activated nonregulatory CD4+ T cells. *Eur. J. Immunol.* 2007. **37**(1): 129–138.

953 **Wu, D., Han, J. M., Yu, X., Lam, A. J., Hoeppli, R. E., Pesenacker, A. M., Huang, Q. et al.**, Characterization of regulatory T cells in obese omental adipose tissue in humans. *Eur. J. Immunol.* 2019. **49**(2): 336–347.

954 **Dijke, I. E., Hoeppli, R. E., Ellis, T., Pearcey, J., Huang, Q., McMurchy, A. N., Boer, K. et al.**, Discarded human thymus is a novel source of stable and long-lived therapeutic regulatory T cells. *Am. J. Transplant* 2016. **16**(1): 58–71.

955 **Mason, G. M., Lowe, K., Melchiotti, R., Ellis, R., de Rinaldis, E., Peakman, M., Heck, S., Lombardi, G. et al.**, Phenotypic complexity of the human regulatory T cell compartment revealed by mass cytometry. *J. Immunol.* 2015. **195**(5): 2030–2037.

956 **Dawson, N. A. J., Lam, A. J., Cook, L., Hoeppli, R. E., Broady, R., Pesenacker, A. M. and Levings, M. K.**, An optimized method to measure human FOXP3(+) regulatory T cells from multiple tissue types using mass cytometry. *Eur. J. Immunol.* 2018. **48**(8): 1415–1419.

957 **Chen, X. and Oppenheim, J. J.**, Resolving the identity myth: key markers of functional CD4+FoxP3+ regulatory T cells. *Int. Immunopharmacol.* 2011. **11**(10): 1489–1496.

958 **Ward-Hartstonge, K. A. and Kemp, R. A.**, Regulatory T-cell heterogeneity and the cancer immune response. *Clin. Transl. Immunol.* 2017. **6**(9): e154.

959 **Groux, H., O'Garra, A., Bigler, M., Rouleau, M., Antonenko, S., de Vries, J. E. and Roncarolo, M. G.**, A CD4+ T-cell subset inhibits antigen-specific T-cell responses and prevents colitis. *Nature* 1997. **389**(6652): 737–742.

960 **Jeurink, P. V., Vissers, Y. M., Rappard, B. and Savelkoul, H. F.**, T cell responses in fresh and cryopreserved peripheral blood mononuclear cells: kinetics of cell viability, cellular subsets, proliferation, and cytokine production. *Cryobiology* 2008. **57**(2): 91–103.

961 **White, A. M. and Wraith, D. C.**, Tr1-like T cells—an enigmatic regulatory T cell lineage. *Front. Immunol.* 2016. **7**: 355.

962 **Tran, D. Q., Andersson, J., Wang, R., Ramsey, H., Unutmaz, D. and Shevach, E. M.**, GARP (LRRC32) is essential for the surface expression of latent TGF-beta on platelets and activated FOXP3+ regulatory T cells. *Proc. Natl. Acad. Sci. USA* 2009. **106**(32): 13445–13450.

963 **Wang, R., Kozhaya, L., Mercer, F., Khaitan, A., Fujii, H. and Unutmaz, D.**, Expression of GARP selectively identifies activated human FOXP3+ regulatory T cells. *Proc. Natl. Acad. Sci. USA* 2009. **106**(32): 13439–13444.

964 **Camisaschi, C., Casati, C., Rini, F., Perego, M., De Filippo, A., Triebel, F., Parmiani, G. et al.**, LAG-3 expression defines a subset of CD4(+)CD25(high)Foxp3(+) regulatory T cells that are expanded at tumor sites. *J. Immunol.* 2010. **184**(11): 6545–6551.

965 **Gagliani, N., Magnani, C. F., Huber, S., Gianolini, M. E., Pala, M., Licona-Limon, P., Guo, B. et al.**, Coexpression of CD49b and LAG-3 identifies human and mouse T regulatory type 1 cells. *Nat. Med.* 2013. **19**(6): 739–746.

966 **Raimondi, G., Shufesky, W. J., Tokita, D., Morelli, A. E. and Thomson, A. W.**, Regulated compartmentalization of programmed cell death-1 discriminates $CD4^+CD25^+$ resting regulatory T cells from activated T cells. *J. Immunol.* 2006. **176**(5): 2808–2816.

967 **Lam, A., MacDonald, J. K. N., Pesenacker, A. M., Juvet, S. C., Morishita, K. A., Bressler, B., iGenoMed, C. et al.**, Innate control of tissue-reparative human regulatory T cells. *J. Immunol.* 2019. 202: 2195–2209.

968 **Borsellino, G., Kleinewietfeld, M., Di Mitri, D., Sternjak, A., Diamantini, A., Giometto, R., Hopner, S. et al.**, Expression of ectonucleotidase CD39 by Foxp3+ Treg cells: hydrolysis of extracellular ATP and immune suppression. *Blood* 2007. **110**(4): 1225–1232.

969 **Deaglio, S., Dwyer, K. M., Gao, W., Friedman, D., Usheva, A., Erat, A., Chen, J. F. et al.**, Adenosine generation catalyzed by CD39 and CD73 expressed on regulatory T cells mediates immune suppression. *J. Exp. Med.* 2007. **204**(6): 1257–1265.

970 **Rissiek, A., Baumann, I., Cuapio, A., Mautner, A., Kolster, M., Arck, P. C., Dodge-Khatami, A. et al.**, The expression of CD39 on regulatory T cells is genetically driven and further upregulated at sites of inflammation. *J. Autoimmun.* 2015. **58**: 12–20.

971 **Baecher-Allan, C., Wolf, E. and Hafler, D. A.**, MHC class II expression identifies functionally distinct human regulatory T cells. *J. Immunol.* 2006. **176**(8): 4622–4631.

972 **Linsley, P. S., Brady, W., Urnes, M., Grosmaire, L. S., Damle, N. K. and Ledbetter, J. A.**, CTLA-4 is a second receptor for the B cell activation antigen B7. *J. Exp. Med.* 1991. **174**(3): 561–569.

973 **Qureshi, O. S., Zheng, Y., Nakamura, K., Attridge, K., Manzotti, C., Schmidt, E. M., Baker, J. et al.**, Trans-endocytosis of CD80 and CD86: a molecular basis for the cell-extrinsic function of CTLA-4. *Science* 2011. **332**(6029): 600–603.

974 **Norton, S. E., Ward-Hartstonge, K. A., McCall, J. L., Leman, J. K. H., Taylor, E. S., Munro, F., Black, M. A. et al.**, High-dimensional mass cytometric analysis reveals an increase in effector regulatory T cells as a distinguishing feature of colorectal tumors. *J. Immunol.* 2019. **202**: 1871–1884.

975 **Kleinewietfeld, M., Starke, M., Di Mitri, D., Borsellino, G., Battistini, L., Rotzschke, O. and Falk, K.**, CD49d provides access to "untouched" human Foxp3+ Treg free of contaminating effector cells. *Blood* 2009. **113**(4): 827–836.

976 **Santegoets, S. J., Dijkgraaf, E. M., Battaglia, A., Beckhove, P., Britten, C. M., Gallimore, A., Godkin, A. et al.**, Monitoring regulatory T cells in clinical samples: consensus on an essential marker set and gat-

ing strategy for regulatory T cell analysis by flow cytometry. *Cancer Immunol. Immunother.* 2015. **64**(10): 1271–1286.

977 **Dwyer, K. M., Hanidziar, D., Putheti, P., Hill, P. A., Pommey, S., McRae, J. L., Winterhalter, A. et al.**, Expression of CD39 by human peripheral blood CD4+ CD25+ T cells denotes a regulatory memory phenotype. *Am. J. Transplant* 2010. **10**(11): 2410–2420.

978 **Schuler, P. J., Schilling, B., Harasymczuk, M., Hoffmann, T. K., Johnson, J., Lang, S. and Whiteside, T. L.**, Phenotypic and functional characteristics of CD4+ CD39+ FOXP3+ and CD4+ CD39+ FOXP3neg T-cell subsets in cancer patients. *Eur. J. Immunol.* 2012. **42**(7): 1876–1885.

979 **Iellem, A., Colantonio, L. and D'Ambrosio, D.**, Skin-versus gut-skewed homing receptor expression and intrinsic CCR4 expression on human peripheral blood CD4+CD25+ suppressor T cells. *Eur. J. Immunol.* 2003. **33**(6): 1488–1496.

980 **Battaglia, A., Buzzonetti, A., Monego, G., Peri, L., Ferrandina, G., Fanfani, F., Scambia, G. et al.**, Neuropilin-1 expression identifies a subset of regulatory T cells in human lymph nodes that is modulated by preoperative chemoradiation therapy in cervical cancer. *Immunology* 2008. **123**(1): 129–138.

981 **Griseri, T., Asquith, M., Thompson, C. and Powrie, F.**, OX40 is required for regulatory T cell-mediated control of colitis. *J. Exp. Med.* 2010. **207**(4): 699–709.

982 **Seddiki, N., Cook, L., Hsu, D. C., Phetsouphanh, C., Brown, K., Xu, Y., Kerr, S. J. et al.**, Human antigen-specific CD4(+) CD25(+) CD134(+) CD39(+) T cells are enriched for regulatory T cells and comprise a substantial proportion of recall responses. *Eur. J. Immunol.* 2014. **44**(6): 1644–1661.

983 **Ivison, S., Malek, M., Garcia, R. V., Broady, R., Halpin, A., Richaud, M., Brant, R. F. et al.**, A standardized immune phenotyping and automated data analysis platform for multicenter biomarker studies. *JCI Insight* 2018. **3**(23).

984 **Fox, B. C., Bignone, P. A., Brown, P. J. and Banham, A. H.**, Defense of the clone: antibody 259D effectively labels human FOXP3 in a variety of applications. *Blood* 2008. **111**(7): 3897–3899.

985 **Pillai, V. and Karandikar, N. J.**, Attack on the clones? Human FOXP3 detection by PCH101, 236A/E7, 206D, and 259D reveals 259D as the outlier with lower sensitivity. *Blood* 2008. **111**(1): 463–464; author reply 464–466.

986 **Law, J. P., Hirschkorn, D. F., Owen, R. E., Biswas, H. H., Norris, P. J. and Lanteri, M. C.**, The importance of Foxp3 antibody and fixation/permeabilization buffer combinations in identifying CD4+CD25+Foxp3+ regulatory T cells. *Cytometry A* 2009. **75**(12): 1040–1050.

987 **Kaur, G., Goodall, J. C., Jarvis, L. B. and Hill Gaston, J. S.**, Characterisation of Foxp3 splice variants in human CD4+ and CD8+ T cells–identification of Foxp3Delta7 in human regulatory T cells. *Mol. Immunol.* 2010. **48**(1-3): 321–332.

988 **Mahnke, Y. D., Beddall, M. H. and Roederer, M.**, OMIP-015: human regulatory and activated T-cells without intracellular staining. *Cytometry A* 2013. **83**(2): 179–181.

989 **Terstappen, L. W., Meiners, H. and Loken, M. R.**, A rapid sample preparation technique for flow cytometric analysis of immunofluorescence allowing absolute enumeration of cell subpopulations. *J. Immunol. Methods* 1989. **123**(1): 103–112.

990 **Bonecchi, R., Bianchi, G., Bordignon, P. P., D'Ambrosio, D., Lang, R., Borsatti, A., Sozzani, S. et al.**, Differential expression of chemokine receptors and chemotactic responsiveness of type 1 T helper cells (Th1s) and Th2s. *J. Exp. Med.* 1998. **187**(1): 129–134.

991 **Gosselin, A., Monteiro, P., Chomont, N., Diaz-Griffero, F., Said, E. A., Fonseca, S., Wacleche, V. et al.**, Peripheral blood CCR4+CCR6+ and CXCR3+CCR6+CD4+ T cells are highly permissive to HIV-1 infection. *J. Immunol.* 2010. **184**(3): 1604–1616.

992 **Halim, L., Romano, M., McGregor, R., Correa, I., Pavlidis, P., Grageda, N., Hoong, S. J. et al.**, An atlas of human regulatory T helper-like cells reveals features of Th2-like Tregs that support a tumorigenic environment. *Cell Rep.* 2017. **20**(3): 757–770.

993 **Bowcutt, R., Malter, L. B., Chen, L. A., Wolff, M. J., Robertson, I., Rifkin, D. B., Poles, M. et al.**, Isolation and cytokine analysis of lamina propria lymphocytes from mucosal biopsies of the human colon. *J. Immunol. Methods* 2015. **421**: 27–35.

994 **Zheng, J., Liu, Y., Lau, Y. L. and Tu, W.**, γδ-T cells: An unpolished sword in human anti-infection immunity. *Cell. Mol. Immunol.* 2013. **10**: 50–57.

995 **Silva-Santos, B., Serre, K. and Norell, H.**, γδ T cells in cancer. *Nat. Rev. Immunol.* 2015. **15**: 23–38.

996 **Tanaka, Y., Sano, S., Nieves, E., De Libero, G., Rosa, D., Modlin, R. L., Brenner, M. B. et al.**, Nonpeptide ligands for γδ T cells. *Proc. Natl. Acad. Sci. USA* 1994. **91**: 8175–8179.

997 **Godfrey, D. I., Uldrich, A. P., McCluskey, J., Rossjohn, J. and Moody, D. B.**, The burgeoning family of unconventional T cells. *Nat. Immunol.* 2015. **16**: 1114–1123.

998 **Halary, F., Pitard, V., Dlubek, D., Krzysiek, R., de la Salle, H., Merville, P., Dromer, C. et al.**, Shared reactivity of Vδ2neg γδ T cells against cytomegalovirus-infected cells and tumor intestinal epithelial cells. *J. Exp. Med.* 2005. **201**: 1567–1578.

999 **Morita, C. T., Chenggang, J., Sarikonda, G. and Wong, H.**, Nonpeptide antigens, presentation mechanisms, and immunological memory of human Vγ2Vδ2 T cells: discriminating friend from foe through the recognition of prenyl pyrophosphate antigens. *Immunol. Rev.* 2007. **215**: 59–76.

1000 **Davey, M. S., Willcox, C. R., Hunter, S., Kasatskaya, S. A., Remmerswaal, E. B. M., Salim, M., Mohammed, F. et al.**, The human Vδ2+ T-cell compartment comprises distinct innate-like Vγ9+ and adaptive Vγ9- subsets. *Nat. Commun.* 2018. **9**: 1–14.

1001 **Riganti, C., Massaia, M., Davey, M. S. and Eberl, M.**, Human gammadelta T-cell responses in infection and immunotherapy: common mechanisms, common mediators? *Eur. J. Immunol.* 2012. **42**: 1668–1676.

1002 **Chien, Y. H., Meyer, C. and Bonneville, M.**, γδ T cells: first line of defense and beyond. *Annu. Rev. Immunol.* 2014. **32**: 121–155.

1003 **Davodeau, F., Peyrat, M. A., Hallet, M. M., Houde, I., And, H. V. and Bonneville, M.**, Peripheral selection of antigen receptor junctional features in a major human γδ subset. *Eur. J. Immunol.* 1993. **23**: 804–808.

1004 **Parker, C. M., Groh, V., Band, H., Porcelli, S. A., Morita, C., Fabbi, M., Glass, D. et al.**, Evidence for extrathymic changes in the T cell receptor gamma/delta repertoire. *J. Exp. Med.* 1990. **171**: 1597–1612.

1005 **Dimova, T., Brouwer, M., Gosselin, F., Tassignon, J., Leo, O., Donner, C., Marchant, A. et al.**, Effector Vγ9Vδ2 T cells dominate the human fetal γδ T-cell repertoire. *Proc. Natl. Acad. Sci. USA* 2015. **112**: E556–E565.

1006 **Willcox, C. R., Davey, M. S. and Willcox, B. E.**, Development and selection of the human Vγ9Vδ2$^+$T-cell repertoire. *Front. Immunol.* 2018. **9**: 1501.

1007 **Hunter, S., Willcox, C. R., Davey, M. S., Kasatskaya, Sofya, A., Jeffery, H. C., Chudakov, D. M. et al.**, Human liver infiltrating γδ T cells are composed of clonally expanded circulating and tissue-resident populations. *J. Hepatol.* 2018. **69**: 654–665.

1008 **Davey, M. S., Willcox, C. R., Baker, A. T., Hunter, S. and Willcox, B. E.**, Recasting human Vδ1 lymphocytes in an adaptive role. *Trends Immunol.* 2018. **39**: 446–459.

1009 **Davey, M. S., Willcox, C. R., Joyce, S. P., Ladell, K., Kasatskaya, S. A., McLaren, J. E., Hunter, S. et al.**, Clonal selection in the human Vδ1 T cell repertoire indicates γδ TCR-dependent adaptive immune surveillance. *Nat. Commun.* 2017. **8**: 1–15.

1010 **Ravens, S., Schultze-Florey, C., Raha, S., Sandrock, I., Drenker, M., Oberdörfer, L., Reinhardt, A. et al.**, Human γδ T cells are quickly reconstituted after stem-cell transplantation and show adaptive clonal expansion in response to viral infection. *Nat. Immunol.* 2017. **18**: 393–401.

1011 **Correia, D., Fogli, M., Hudspeth, K., Gomes da Silva, M., Mavilio, D. and Silva-Santos, B.**, Differentiation of human peripheral blood Vδ1+ T cell expressing the natural cytotoxicity receptor NKp30 for recognition of lymphoid leukemia cells. *Blood* 2011. **118**: 992–1001.

1012 **Bouet-Toussaint, F., Cabillic, F., Toutirais, O., Le Gallo, M., Thomas de la Pintiere, C., Genetet, N., Meunier, B. et al.**, Vγ9Vδ2 T cell-mediated recognition of human solid tumors. Potential for immunotherapy of hepatocellular and colorectal carcinomas. *Cancer Immunol. Immunother.* 2008. **57**: 531–539.

1013 **Mattarollo, S. R., Kenna, T., Nieda, M. and Nicol, A. J.**, Chemotherapy and zoledronate sensitize solid tumour cells to Vγ9Vδ2 T cell cytotoxicity. *Cancer Immunol. Immunother.* 2007. **56**: 1285–1297.

1014 **Almeida, A. R. M., Correia, D. V., Fernandes-Platzgummer, A., da Silva, C. L., Gomes da Silva, M., Anjos, D. R. and Silva-Santos, B.**, Delta one T cells for immunotherapy of chronic lymphocytic leukemia: clinical-grade expansion/differentiation and preclinical proof-of-concept. *Clin. Cancer Res.* 2016. **22**: 5795–5804.

1015 **Ryan, P. L., Sumaria, N., Holland, C. J., Bradford, C. M., Izotova, N., Grandjean, C. L., Jawad, A. S. et al.**, Heterogeneous yet stable Vδ2(+) T-cell profiles define distinct cytotoxic effector potentials in healthy human individuals. *Proc. Natl. Acad. Sci. USA* 2016. **113**: 14378–14383.

1016 **Kinjo, Y. and Ueno, K.**, iNKT cells in microbial immunity: recognition of microbial glycolipids. *Microbiol. Immunol.* 2011. **55**: 472–482.

1017 **Shissler, S. C., Bollino, D. R., Tiper, I. V., Bates, J. P., Derakhshandeh, R. and Webb, T. J.**, Immunotherapeutic strategies targeting natural killer T cell responses in cancer. *Immunogenetics* 2016. **68**: 623–638.

1018 **Godfrey, D. I., Le Nours, J., Andrews, D. M., Uldrich, A. P. and Rossjohn, J.**, Unconventional T cell targets for cancer immunotherapy. *Immunity* 2018. **48**: 453–473.

1019 **Pellicci, D. G. and Uldrich, A. P.**, Unappreciated diversity within the pool of CD1d-restricted T cells. *Semin. Cell. Dev. Biol.* 2018. **84**: 42–47.

1020 **Godfrey, D. I., MacDonald, H. R., Kronenberg, M., Smyth, M. J. and Van Kaer, L.**, NKT cells: what's in a name? *Nat. Rev. Immunol.* 2004. **4**: 231–237.

1021 **Thierry, A., Robin, A., Giraud, S., Minouflet, S., Barra, A., Bridoux, F., Hauet, T. et al.**, Identification of invariant natural killer T cells in porcine peripheral blood. *Vet. Immunol. Immunopathol.* 2012. **149**: 272–279.

1022 **Monzon-Casanova, E., Paletta, D., Starick, L., Muller, I., Sant'Angelo, D. B., Pyz, E. and Herrmann, T.**, Direct identification of rat iNKT cells reveals remarkable similarities to human iNKT cells and a profound deficiency in LEW rats. *Eur. J. Immunol.* 2013. **43**: 404–415.

1023 **Gansuvd, B., Hubbard, W. J., Hutchings, A., Thomas, F. T., Goodwin, J., Wilson, S. B., Exley, M. A. et al.**, Phenotypic and functional characterization of long-term cultured rhesus macaque spleen-derived NKT cells. *J. Immunol.* 2003. **171**: 2904–2911.

1024 **Yasuda, N., Masuda, K., Tsukui, T., Teng, A. and Ishii, Y.**, Identification of canine natural CD3-positive T cells expressing an invariant T-cell receptor alpha chain. *Vet. Immunol. Immunopathol.* 2009. **132**: 224–231.

1025 **Kawano, T., Cui, J., Koezuka, Y., Toura, I., Kaneko, Y., Motoki, K., Ueno, H. et al.**, CD1d-restricted and TCR-mediated activation of valpha14 NKT cells by glycosylceramides. *Science* 1997. **278**: 1626–1629.

1026 **Lopez-Sagaseta, J., Kung, J. E., Savage, P. B., Gumperz, J. and Adams, E. J.**, The molecular basis for recognition of CD1d/alpha-galactosylceramide by a human non-Valpha24 T cell receptor. *PLoS Biol.* 2012. **10**: e1001412.

1027 **Gadola, S. D., Dulphy, N., Salio, M. and Cerundolo, V.**, Valpha24-JalphaQ-independent, CD1d-restricted recognition of alpha-galactosylceramide by human CD4(+) and CD8alphabeta(+) T lymphocytes. *J. Immunol.* 2002. **168**: 5514–5520.

1028 **Le Nours, J., Praveena, T., Pellicci, D. G., Gherardin, N. A., Ross, F. J., Lim, R. T., Besra, G. S., Keshipeddy, S. et al.**, Atypical natural killer T-cell receptor recognition of CD1d-lipid antigens. *Nat. Commun.* 2016. **7**: 10570.

1029 **Gadola, S. D., Koch, M., Marles-Wright, J., Lissin, N. M., Shepherd, D., Matulis, G., Harlos, K. et al.**, Structure and binding kinetics of three different human CD1d-alpha-galactosylceramide-specific T cell receptors. *J. Exp. Med.* 2006. **203**: 699–710.

1030 **Brigl, M., van den Elzen, P., Chen, X., Meyers, J. H., Wu, D., Wong, C. H., Reddington, F. et al.**, Conserved and heterogeneous lipid antigen specificities of CD1d-restricted NKT cell receptors. *J. Immunol.* 2006. **176**: 3625–3634.

1031 **Uldrich, A. P., Le Nours, J., Pellicci, D. G., Gherardin, N. A., McPherson, K. G., Lim, R. T., Patel, O., Beddoe, T. et al.**, CD1d-lipid antigen recognition by the gammadelta TCR. *Nat. Immunol.* 2013. **14**: 1137–1145.

1032 **Kobayashi, E., Motoki, K., Uchida, T., Fukushima, H. and Koezuka, Y.**, KRN7000, a novel immunomodulator, and its antitumor activities. *Oncol. Res.* 1995. **7**: 529–534.

1033 **Morita, M., Motoki, K., Akimoto, K., Natori, T., Sakai, T., Sawa, E., Yamaji, K. et al.**, Structure-activity relationship of alpha-galactosylceramides against B16-bearing mice. *J. Med. Chem.* 1995. **38**: 2176–2187.

1034 **Nair, S. and Dhodapkar, M. V.**, Natural killer T cells in cancer immunotherapy. *Front. Immunol.* 2017. **8**: 1178.

1035 **Rossjohn, J., Pellicci, D. G., Patel, O., Gapin, L. and Godfrey, D. I.**, Recognition of CD1d-restricted antigens by natural killer T cells. *Nat. Rev. Immunol.* 2012. **12**: 845–857.

1036 **Miyamoto, K., Miyake, S. and Yamamura, T.**, A synthetic glycolipid prevents autoimmune encephalomyelitis by inducing TH2 bias of natural killer T cells. *Nature* 2001. **413**: 531–534.

1037 **Yu, K. O., Im, J. S., Molano, A., Dutronc, Y., Illarionov, P. A., Forestier, C., Fujiwara, N. et al.**, Modulation of CD1d-restricted NKT cell responses by using N-acyl variants of alpha-galactosylceramides. *Proc. Natl. Acad. Sci. USA* 2005. **102**: 3383–3388.

1038 **Schmieg, J., Yang, G., Franck, R. W. and Tsuji, M.**, Superior protection against malaria and melanoma metastases by a C-glycoside analogue of the natural killer T cell ligand alpha-Galactosylceramide. *J. Exp. Med.* 2003. **198**: 1631–1641.

1039 **Wun, K. S., Cameron, G., Patel, O., Pang, S. S., Pellicci, D. G., Sullivan, L. C., Keshipeddy, S. et al.**, A molecular basis for the exquisite CD1d-restricted antigen specificity and functional responses of natural killer T cells. *Immunity* 2011. **34**: 327–339.

1040 **Wun, K. S., Ross, F., Patel, O., Besra, G. S., Porcelli, S. A., Richardson, S. K., Keshipeddy, S. et al.**, Human and mouse type I natural killer T cell antigen receptors exhibit different fine specificities for CD1d-antigen complex. *J. Biol. Chem.* 2012. **287**: 39139–39148.

1041 **Freigang, S., Landais, E., Zadorozhny, V., Kain, L., Yoshida, K., Liu, Y., Deng, S. et al.**, Scavenger receptors target glycolipids for natural killer T cell activation. *J. Clin. Invest.* 2012. **122**: 3943–3954.

1042 http://tetramer.yerkes.emory.edu/reagents/cd1

1043 **Gumperz, J. E., Miyake, S., Yamamura, T. and Brenner, M. B.**, Functionally distinct subsets of CD1d-restricted natural killer T cells revealed by CD1d tetramer staining. *J. Exp. Med.* 2002. **195**: 625–636.

1044 **Sidobre, S. and Kronenberg, M.**, CD1 tetramers: a powerful tool for the analysis of glycolipid-reactive T cells. *J. Immunol. Methods* 2002. **268**: 107–121.

1045 **Boyson, J. E., Rybalov, B., Koopman, L. A., Exley, M., Balk, S. P., Racke, F. K., Schatz, F. et al.**, CD1d and invariant NKT cells at the human maternal-fetal interface. *Proc. Natl. Acad. Sci. USA* 2002. **99**: 13741–13746.

1046 **Thomas, S. Y., Hou, R., Boyson, J. E., Means, T. K., Hess, C., Olson, D. P., Strominger, J. L. et al.**, CD1d-restricted NKT cells express a chemokine receptor profile indicative of Th1-type inflammatory homing cells. *J. Immunol.* 2003. **171**: 2571–2580.

1047 **Aricescu, A. R., Lu, W. and Jones, E. Y.**, A time- and cost-efficient system for high-level protein production in mammalian cells. *Acta Crystallogr. D Biol. Crystallogr.* 2006. **62**: 1243–1250.

1048 **Ng, S. S., Souza-Fonseca-Guimaraes, F., Rivera, F. L., Amante, F. H., Kumar, R., Gao, Y., Sheel, M. et al.**, Rapid loss of group 1 innate lymphoid cells during blood stage Plasmodium infection. *Clin. Transl. Immunol.* 2018. **7**: e1003.

1049 http://www.enzolifesciences.com/BML-SL232/krn7000/

1050 https://avantilipids.com/product/867000

1051 **Boyum, A.**, Separation of leukocytes from blood and bone marrow. Introduction. *Scand. J. Clin. Lab. Invest. Suppl.* 1968. **97**: 7.

1052 **Lee, P. T., Benlagha, K., Teyton, L. and Bendelac, A.**, Distinct functional lineages of human V(alpha)24 natural killer T cells. *J. Exp. Med.* 2002. **195**: 637–641.

1053 **Montoya, C. J., Pollard, D., Martinson, J., Kumari, K., Wasserfall, C., Mulder, C. B., Rugeles, M. T. et al.**, Characterization of human invariant natural killer T subsets in health and disease using a novel invariant natural killer T cell-clonotypic monoclonal antibody, 6B11. *Immunology* 2007. **122**: 1–14.

1054 **Cameron, G., Pellicci, D. G., Uldrich, A. P., Besra, G. S., Illarionov, P., Williams, S. J., La Gruta, N. L. et al.**, Antigen Specificity of Type I NKT Cells Is Governed by TCR beta-Chain Diversity. *J Immunol* 2015. **195**: 4604–4614.

1055 https://www.miltenyibiotec.com/AU-en/products/macs-cell-separation/cell-separation-reagents/microbeads-and-isolation-kits/any-cell-type/anti-pe-microbeads.html

1056 **Rossjohn, J., Gras, S., Miles, J. J., Turner, S. J., Godfrey, D. I. and McCluskey, J.**, T cell antigen receptor recognition of antigen-presenting molecules. *Annu. Rev. Immunol.* 2015. **33**: 169–200.

1057 **Kjer-Nielsen, L., Patel, O., Corbett, A. J., Le Nours, J., Meehan, B., Liu, L., Bhati, M., Chen, Z. et al.**, MR1 presents microbial vitamin B metabolites to MAIT cells. *Nature* 2012. **491**: 717–723.

1058 **Kjer-Nielsen, L., Corbett, A. J., Chen, Z., Liu, L., Mak, J. Y., Godfrey, D. I., Rossjohn, J. et al.**, An overview on the identification of MAIT cell antigens. *Immunol. Cell. Biol.* 2018. **96**: 573–587.

1059 **Koay, H. F., Godfrey, D. I. and Pellicci, D. G.**, Development of mucosal-associated invariant T cells. *Immunol. Cell. Biol.* 2018.

1060 **Gherardin, N. A., Souter, M. N., Koay, H. F., Mangas, K. M., Seemann, T., Stinear, T. P., Eckle, S. B. et al.**, Human blood MAIT cell subsets defined using MR1 tetramers. *Immunol. Cell. Biol.* 2018. **96**: 507–525.

1061 **Le Bourhis, L., Martin, E., Peguillet, I., Guihot, A., Froux, N., Core, M., Levy, E., Dusseaux, M. et al.**, Antimicrobial activity of mucosal-associated invariant T cells. *Nat. Immunol.* 2010. **11**: 701–708.

1062 **Tang, X. Z., Jo, J., Tan, A. T., Sandalova, E., Chia, A., Tan, K. C., Lee, K. H. et al.**, IL-7 licenses activation of human liver intrasinusoidal mucosal-associated invariant T cells. *J. Immunol.* 2013. **190**: 3142–3152.

1063 **Dusseaux, M., Martin, E., Serriari, N., Peguillet, I., Premel, V., Louis, D., Milder, M. et al.**, Human MAIT cells are xenobiotic-resistant, tissue-targeted, CD161hi IL-17-secreting T cells. *Blood* 2011. **117**: 1250–1259.

1064 **Walker, L. J., Kang, Y. H., Smith, M. O., Tharmalingham, H., Ramamurthy, N., Fleming, V. M., Sahgal, N. et al.**, Human MAIT and CD8alphaalpha cells develop from a pool of type-17 precommitted CD8+ T cells. *Blood* 2012. **119**: 422–433.

1065 **Le Bourhis, L., Dusseaux, M., Bohineust, A., Bessoles, S., Martin, E., Premel, V., Core, M., Sleurs, D. et al.**, MAIT cells detect and efficiently lyse bacterially-infected epithelial cells. *PLoS Pathog.* 2013. **9**: e1003681.

1066 **Meermeier, E. W., Harriff, M. J., Karamooz, E. and Lewinsohn, D. M.**, MAIT cells and microbial immunity. *Immunol. Cell. Biol.* 2018.

1067 **Wang, H., D'Souza, C., Lim, X. Y., Kostenko, L., Pediongco, T. J., Eckle, S. B. G., Meehan, B. S. et al.**, MAIT cells protect against pulmonary Legionella longbeachae infection. *Nat. Commun.* 2018. **9**: 3350.

1068 **D'Souza, C., Chen, Z. and Corbett, A. J.**, Revealing the protective and pathogenic potential of MAIT cells. *Mol. Immunol.* 2018. **103**: 46–54.

1069 **Ussher, J. E., Bilton, M., Attwod, E., Shadwell, J., Richardson, R., de Lara, C., Mettke, E., Kurioka, A. et al.**, CD161++ CD8+ T cells, including the MAIT cell subset, are specifically activated by IL-12+IL-18 in a TCR-independent manner. *Eur. J. Immunol.* 2014. **44**: 195–203.

1070 **Ussher, J. E., Willberg, C. B. and Klenerman, P.**, MAIT cells and viruses. *Immunol. Cell. Biol.* 2018. **96**: 630–641.

1071 **van Wilgenburg, B., Scherwitzl, I., Hutchinson, E. C., Leng, T., Kurioka, A., Kulicke, C., de Lara, C., Cole, S., Vasanawathana, S. et al.**, MAIT cells are activated during human viral infections. *Nat. Commun.* 2016. **7**: 11653.

1072 **Loh, L., Wang, Z., Sant, S., Koutsakos, M., Jegaskanda, S., Corbett, A. J., Liu, L. et al.**, Human mucosal-associated invariant T cells contribute to antiviral influenza immunity via IL-18-dependent activation. *Proc. Natl. Acad. Sci. USA* 2016. **113**: 10133–10138.

1073 **Rouxel, O. and Lehuen, A.**, Mucosal-associated invariant T cells in autoimmune and immune-mediated diseases. *Immunol. Cell. Biol.* 2018. **96**: 618–629.

1074 **Gibbs, A., Leeansyah, E., Introini, A., Paquin-Proulx, D., Hasselrot, K., Andersson, E., Broliden, K. et al.**, MAIT cells reside in the female genital mucosa and are biased towards IL-17 and IL-22 production in response to bacterial stimulation. *Mucosal Immunol.* 2017. **10**: 35–45.

1075 **Dias, J., Boulouis, C., Gorin, J. B., van den Biggelaar, R., Lal, K. G., Gibbs, A., Loh, L. et al.**, The CD4(-)CD8(-) MAIT cell subpopulation is a functionally distinct subset developmentally related to the main CD8(+) MAIT cell pool. *Proc. Natl. Acad. Sci. USA* 2018. **115**: E11513–E11522.

1076 **Brozova, J., Karlova, I. and Novak, J.**, Analysis of the phenotype and function of the subpopulations of mucosal-associated invariant T cells. *Scand. J. Immunol.* 2016. **84**: 245–251.

1077 **Davanian, H., Gaiser, R. A., Silfverberg, M., Hugerth, L. W., Sobkowiak, M. J., Lu, L., Healy, K. et al.**, Mucosal-associated invariant T cells and oral microbiome in persistent apical periodontitis. *Int. J. Oral. Sci.* 2019. **11**: 16.

1078 **Mori, L., Lepore, M. and De Libero, G.**, The immunology of CD1- and MR1-restricted T cells. *Annu. Rev. Immunol.* 2016. **34**: 479–510.

1079 **Gherardin, N. A., McCluskey, J., Rossjohn, J. and Godfrey, D. I.**, The diverse family of MR1-restricted T cells. *J. Immunol.* 2018. **201**: 2862–2871.

1080 **Martin, E., Treiner, E., Duban, L., Guerri, L., Laude, H., Toly, C., Premel, V. et al.**, Stepwise development of MAIT cells in mouse and human. *PLoS Biol.* 2009. **7**: e54.

1081 **Sharma, P. K., Wong, E. B., Napier, R. J., Bishai, W. R., Ndung'u, T., Kasprowicz, V. O., Lewinsohn, D. A. et al.**, High expression of CD26 accurately identifies human bacteria-reactive MR1-restricted MAIT cells. *Immunology* 2015. **145**: 443–453.

1082 **Gold, M. C., Eid, T., Smyk-Pearson, S., Eberling, Y., Swarbrick, G. M., Langley, S. M., Streeter, P. R. et al.**, Human thymic MR1-restricted MAIT cells are innate pathogen-reactive effectors that adapt following thymic egress. *Mucosal Immunol.* 2013. **6**: 35–44.

1083 **Leeansyah, E., Ganesh, A., Quigley, M. F., Sonnerborg, A., Andersson, J., Hunt, P. W., Somsouk, M. et al.**, Activation, exhaustion, and persistent decline of the antimicrobial MR1-restricted MAIT-cell population in chronic HIV-1 infection. *Blood* 2013. **121**: 1124–1135.

1084 **Koppejan, H., Jansen, D., Hameetman, M., Thomas, R., Toes, R. E. M. and van Gaalen, F. A.**, Altered composition and phenotype of mucosal-associated invariant T cells in early untreated rheumatoid arthritis. *Arthritis Res. Ther.* 2019. **21**: 3.

1085 **Eckle, S. B., Birkinshaw, R. W., Kostenko, L., Corbett, A. J., McWilliam, H. E., Reantragoon, R., Chen, Z. et al.**, A molecular basis underpinning the T cell receptor heterogeneity of mucosal-associated invariant T cells. *J. Exp. Med.* 2014. **211**: 1585–1600.

1086 **Kurioka, A., Jahun, A. S., Hannaway, R. F., Walker, L. J., Fergusson, J. R., Sverremark-Ekstrom, E., Corbett, A. J. et al.**, Shared and distinct phenotypes and functions of human CD161++ Valpha7.2+ T cell subsets. *Front. Immunol.* 2017. **8**: 1031.

1087 **Ben Youssef, G., Tourret, M., Salou, M., Ghazarian, L., Houdouin, V., Mondot, S., Mburu, Y. et al.**, Ontogeny of human mucosal-associated invariant T cells and related T cell subsets. *J. Exp. Med.* 2018. **215**: 459–479.

1088 **Koay, H. F., Gherardin, N. A., Xu, C., Seneviratna, R., Zhao, Z., Chen, Z., Fairlie, D. P. et al.**, Diverse MR1-restricted T cells in mice and humans. *Nat. Commun.* 2019. **10**: 2243.

1089 NTCF, NIH Tetramer Core Facility: Human MR1 Tetramer Staining 2016. https://tetramer.yerkes.emory.edu/sites/default/files/shared/human_mr1_tetramer_staining.pdf

1090 NTCF, NIH Tetramer Core Facility: Tetramer Preparation - Addition of streptavidin, emory.edu 2010. https://tetramer.yerkes.emory.edu/support/protocols#10

1091 **Gherardin, N. A., Keller, A. N., Woolley, R. E., Le Nours, J., Ritchie, D. S., Neeson, P. J., Birkinshaw, R. W. et al.**, Diversity of T cells restricted by the MHC class I-related molecule MR1 facilitates differential antigen recognition. *Immunity* 2016. **44**: 32–45.

1092 **Dias, J., Leeansyah, E. and Sandberg, J. K.**, Multiple layers of heterogeneity and subset diversity in human MAIT cell responses to distinct microorganisms and to innate cytokines. *Proc. Natl. Acad. Sci. USA* 2017. **114**: E5434–E5443.

1093 **Lissina, A., Ladell, K., Skowera, A., Clement, M., Edwards, E., Seggewiss, R., van den Berg, H. A., Gostick, E. et al.**, Protein kinase inhibitors substantially improve the physical detection of T-cells with peptide-MHC tetramers. *J. Immunol. Methods* 2009. **340**: 11–24.

1094 **Wood, G. S. and Warnke, R.**, Suppression of endogenous avidin-binding activity in tissues and its relevance to biotin-avidin detection systems. *J. Histochem. Cytochem.* 1981. **29**: 1196–1204.

1095 **Harriff, M. J., McMurtrey, C., Froyd, C. A., Jin, H., Cansler, M., Null, M., Worley, A. et al.**, MR1 displays the microbial metabolome driving selective MR1-restricted T cell receptor usage. *Sci. Immunol.* 2018. **3**.

1096 **Lepore, M., Kalinichenko, A., Calogero, S., Kumar, P., Paleja, B., Schmaler, M., Narang, V. et al.**, Functionally diverse human T cells recognize non-microbial antigens presented by MR1. *Elife* 2017. **6**.

1097 **Tung, J. W., Mrazek, M. D., Yang, Y., Herzenberg, L. A. and Herzenberg, L. A.**, Phenotypically distinct B cell development pathways map to the three B cell lineages in the mouse. *Proc. Natl. Acad. Sci. USA* 2006. **103**: 6293–6298.

1098 **Manz, R. A., Hauser, A. E., Hiepe, F. and Radbruch, A.**, Maintenance of serum antibody levels. *Annu. Rev. Immunol.* 2005. **23**: 367–386.

1099 **Wen, L., Brill-Dashoff, J., Shinton, S. A., Asano, M., Hardy, R. R. and Hayakawa, K.**, Evidence of marginal-zone B cell-positive selection in spleen. *Immunity* 2005. **23**: 297–308.

1100 **Fillatreau, S. and Manz, R. A.**, Tolls for B cells. *Eur. J. Immunol.* 2006. **36**: 798–801.

1101 **Tornberg, U. C. and Holmberg, D.**, B-1a, B-1b and B-2 B cells display unique VHDJH repertoires formed at different stages of ontogeny and under different selection pressures. *EMBO J.* 1995. **14**: 1680–1689.

1102 **Ochsenbein, A. F., Fehr, T., Lutz, C., Suter, M., Brombacher, F., Hengartner, H. and Zinkernagel, R. M.**, Control of early viral and bacterial distribution and disease by natural antibodies. *Science* 1999. **286**: 2156–2159.

1103 **Stall, A. M., Adams, S., Herzenberg, L. A. and Kantor, A. B.**, Characteristics and development of the murine B-1b (Ly-1 B sister) cell population. *Ann. N. Y. Acad. Sci.* 1992. **651**: 33–43.

1104 **Kristiansen, T. A., Jaensson Gyllenbäck, E., Zriwil, A., Björklund, T., Daniel, J. A., Sitnicka, E., Soneji, S. et al.**, Cellular barcoding links B-1a B cell potential to a fetal hematopoietic stem cell state at the single-cell level. *Immunity* 2016. **45**: 346–357.

1105 **Pedersen, G. K., Li, X., Khoenkhoen, S., Ádori, M., Beutler, B. and Karlsson Hedestam, G. B.**, B-1a cell development in splenectomized neonatal mice. *Front. Immunol.* 2018. **9**: 1738.

1106 **Melchers, F., ten Boekel, E., Seidl, T., Kong, X. C., Yamagami, T., Onishi, K., Shimizu, T. et al.**, Repertoire selection by pre-B-cell receptors and B-cell receptors, and genetic control of B-cell development from immature to mature B cells. *Immunol. Rev.* 2000. **175**: 33–46.

1107 **Montecino-Rodriguez, E., Leathers, H. and Dorshkind, K.**, Identification of a B-1 B cell-specified progenitor. *Nat. Immunol.* 2006. **7**: 293–301.

1108 **Rajewsky, K.**, Early and late B-cell development in the mouse. *Curr. Opin. Immunol.* 1992. **4**: 171–176.

1109 **ten Boekel, E., Melchers, F. and Rolink, A.**, The status of Ig loci rearrangements in single cells from different stages of B cell development. *Int. Immunol.* 1995. **7**: 1013–1019.

1110 **Grawunder, U., Leu, T. M., Schatz, D. G., Werner, A., Rolink, A. G., Melchers, F. and Winkler, T. H.**, Down-regulation of RAG1 and RAG2 gene expression in preB cells after functional immunoglobulin heavy chain rearrangement. *Immunity* 1995. **3**: 601–608.

1111 **Rolink, A. and Melchers, F.**, Molecular and cellular origins of B lymphocyte diversity. *Cell* 1991. **66**: 1081–1094.

1112 **Lu, L., Smithson, G., Kincade, P. W. and Osmond, D. G.**, Two models of murine B lymphopoiesis: a correlation. *Eur. J. Immunol.* 1998. **28**: 1755–1761.

1113 **Hardy, R. R., Carmack, C. E., Shinton, S. A., Kemp, J. D. and Hayakawa, K.**, Resolution and characterization of pro-B and pre-pro-B cell stages in normal mouse bone marrow. *J. Exp. Med.* 1991. **173**: 1213–1225.

1114 **Melchers, F., Rolink, A., Grawunder, U., Winkler, T. H., Karasuyama, H., Ghia, P. and Andersson, J.**, Positive and negative selection events during B lymphopoiesis. *Curr. Opin. Immunol.* 1995. **7**: 214–227.

1115 **Ghia, P., ten Boekel, E., Sanz, E., de la Hera, A., Rolink, A. and Melchers, F.**, Ordering of human bone marrow B lymphocyte precursors by single-cell polymerase chain reaction analyses of the rearrangement status of the immunoglobulin H and L chain gene loci. *J. Exp. Med.* 1996. **184**: 2217–2229.

1116 **Allman, D., Lindsley, R. C., DeMuth, W., Rudd, K., Shinton, S. A. and Hardy, R. R.**, Resolution of three nonproliferative immature splenic B cell subsets reveals multiple selection points during peripheral B cell maturation. *J. Immunol.* 2001. **167**: 6834–6840.

1117 **Hao, Z. and Rajewsky, K.**, Homeostasis of peripheral B cells in the absence of B cell influx from the bone marrow. *J. Exp. Med.* 2001. **194**: 1151–1164.

1118 **Wells, S. M., Kantor, A. B. and Stall, A. M.**, CD43 (S7) expression identifies peripheral B cell subsets. *J. Immunol.* 1994. **153**: 5503–5515.

1119 **Hart, G., Flaishon, L., Becker-Herman, S. and Shachar, I.**, Ly49D receptor expressed on immature B cells regulates their IFN-gamma secretion, actin polymerization, and homing. *J. Immunol.* 2003. **171**: 4630–4638.

1120 **Kozmik, Z., Wang, S., Dörfler, P., Adams, B. and Busslinger, M.**, The promoter of the CD19 gene is a target for the B-cell-specific transcription factor BSAP. *Mol. Cell. Biol.* 1992. **12**: 2662–2672.

1121 **Li, Y. S., Wasserman, R., Hayakawa, K. and Hardy, R. R.**, Identification of the earliest B lineage stage in mouse bone marrow. *Immunity* 1996. **5**: 527–535.

1122 **Koni, P. A., Joshi, S. K., Temann, U.-A., Olson, D., Burkly, L. and Flavell, R. A.**, Conditional Vascular Cell Adhesion Molecule 1 Deletion in Mice: Impaired Lymphocyte Migration to Bone Marrow. *J. Exp. Med.* 2001. **193**: 741–754.

1123 **Kikuchi, K., Lai, A. Y., Hsu, C.-L. and Kondo, M.**, IL-7 receptor signaling is necessary for stage transition in adult B cell development through up-regulation of EBF. *J. Exp. Med.* 2005. **201**: 1197–1203.

1124 **Rolink, A., ten Boekel, E., Melchers, F., Fearon, D. T., Krop, I. and Andersson, J.**, A subpopulation of B220+ cells in murine bone marrow does not express CD19 and contains natural killer cell progenitors. *J. Exp. Med.* 1996. **183**: 187–194.

1125 **Osmond, D. G., Rolink, A. and Melchers, F.**, Murine B lymphopoiesis: towards a unified model. *Immunol. Today* 1998. **19**: 65–68.

1126 **Melchers, F., Haasner, D., Grawunder, U., Kalberer, C., Karasuyama, H., Winkler, T. and Rolink, A. G.**, Roles of IgH and L chains and of surrogate H and L chains in the development of cells of the B lymphocyte lineage. *Annu. Rev. Immunol.* 1994. **12**: 209–225.

1127 **Rolink, A., Streb, M., Nishikawa, S. and Melchers, F.**, The c-kit-encoded tyrosine kinase regulates the proliferation of early pre-B cells. *Eur. J. Immunol.* 1991. **21**: 2609–2612.

1128 **Tonegawa, S.**, Somatic generation of antibody diversity. *Nature* 1983. **302**: 575–581.

1129 **ten Boekel, E., Melchers, F. and Rolink, A. G.**, Precursor B cells showing H chain allelic inclusion display allelic exclusion at the level of pre-B cell receptor surface expression. *Immunity* 1998. **8**: 199–207.

1130 **Rumfelt, L. L., Zhou, Y., Rowley, B. M., Shinton, S. A. and Hardy, R. R.**, Lineage specification and plasticity in CD19- early B cell precursors. *J. Exp. Med.* 2006. **203**: 675–687.

1131 **Osmond, D. G.**, B cell development in the bone marrow. *Semin. Immunol.* 1990. **2**: 173–180.

1132 **Cancro, M. P.**, Peripheral B-cell maturation: the intersection of selection and homeostasis. *Immunol. Rev.* 2004. **197**: 89–101.

1133 **Oliver, A. M., Martin, F., Gartland, G. L., Carter, R. H. and Kearney, J. F.**, Marginal zone B cells exhibit unique activation, proliferative and immunoglobulin secretory responses. *Eur. J. Immunol.* 1997. **27**: 2366–2374.

1134 **Krzyzak, L., Seitz, C., Urbat, A., Hutzler, S., Ostalecki, C., Gläsner, J., Hiergeist, A. et al.**, CD83 modulates B cell activation and germinal center responses. *J. Immunol.* 2016. **196**: 3581–3594.

1135 **Dogan, I., Bertocci, B., Vilmont, V., Delbos, F., Mégret, J., Storck, S., Reynaud, C.-A. et al.**, Multiple layers of B cell memory with different effector functions. *Nat. Immunol.* 2009. **10**: 1292–1299.

1136 **Bell, J. and Gray, D.**, Antigen-capturing cells can masquerade as memory B cells. *J. Exp. Med.* 2003. **197**: 1233–1244.

1137 **Schittek, B. and Rajewsky, K.**, Maintenance of B-cell memory by long-lived cells generated from proliferating precursors. *Nature* 1990. **346**: 749–751.

1138 **Anderson, S. M., Tomayko, M. M., Ahuja, A., Haberman, A. M. and Shlomchik, M. J.**, New markers for murine memory B cells that define mutated and unmutated subsets. *J. Exp. Med.* 2007. **204**: 2103–2114.

1139 **Good-Jacobson, K. L., Song, E., Anderson, S., Sharpe, A. H. and Shlomchik, M. J.**, CD80 expression on B cells regulates murine T follicular helper development, germinal center B cell survival, and plasma cell generation. *J. Immunol.* 2012. **188**: 4217–4225.

1140 **Zuccarino-Catania, G. V., Sadanand, S., Weisel, F. J., Tomayko, M. M., Meng, H., Kleinstein, S. H., Good-Jacobson, K. L. et al.**, CD80 and PD-L2 define functionally distinct memory B cell subsets that are independent of antibody isotype. *Nat. Immunol.* 2014. **15**: 631–637.

1141 **Tomayko, M. M., Steinel, N. C., Anderson, S. M. and Shlomchik, M. J.**, Cutting edge: Hierarchy of maturity of murine memory B cell subsets. *J. Immunol.* 2010. **185**: 7146–7150.

1142 **Weisel, F. J., Zuccarino-Catania, G. V., Chikina, M. and Shlomchik, M. J.**, A temporal switch in the germinal center determines differential output of memory B and plasma cells. *Immunity* 2016. **44**: 116–130.

1143 **Weisel, F. and Shlomchik, M.**, Memory B cells of mice and humans. *Annu. Rev. Immunol.* 2017. **35**: 255–284.

1144 **Loder, F., Mutschler, B., Ray, R. J., Paige, C. J., Sideras, P., Torres, R., Lamers, M. C. et al.**, B cell development in the spleen takes place in discrete steps and is determined by the quality of B cell receptor-derived signals. *J. Exp. Med.* 1999. **190**: 75–89.

1145 **Carsetti, R., Köhler, G. and Lamers, M. C.**, Transitional B cells are the target of negative selection in the B cell compartment. *J. Exp. Med.* 1995. **181**: 2129–2140.

1146 **Baumgarth, N.**, The double life of a B-1 cell: self-reactivity selects for protective effector functions. *Nat. Rev. Immunol.* 2011. **11**: 34–46.

1147 **Haas, K. M., Poe, J. C., Steeber, D. A. and Tedder, T. F.**, B-1a and B-1b cells exhibit distinct developmental requirements and have unique functional roles in innate and adaptive immunity to S. pneumoniae. *Immunity* 2005. **23**: 7–18.

1148 **Hardy, R. R., Hayakawa, K., Parks, D. R., Herzenberg, L. A. and Herzenberg, L. A.**, Murine B cell differentiation lineages. *J. Exp. Med.* 1984. **159**: 1169–1188.

1149 **Pedersen, G. K., Àdori, M., Khoenkhoen, S., Dosenovic, P., Beutler, B. and Karlsson Hedestam, G. B.**, B-1a transitional cells are phenotypically distinct and are lacking in mice deficient in IκBNS. *Proc. Natl. Acad. Sci. USA* 2014. **111**: E4119–4126.

1150 **Herzenberg, L. A., Stall, A. M., Braun, J., Weaver, D., Baltimore, D., Herzenberg, L. A. and Grosschedl, R.**, Depletion of the predominant B-

cell population in immunoglobulin mu heavy-chain transgenic mice. *Nature* 1987. **329**: 71–73.

1151 **Shinall, S. M., Gonzalez-Fernandez, M., Noelle, R. J. and Waldschmidt, T. J.**, Identification of murine germinal center B cell subsets defined by the expression of surface isotypes and differentiation antigens. *J. Immunol.* 2000. **164**: 5729–5738.

1152 **Naito, Y., Takematsu, H., Koyama, S., Miyake, S., Yamamoto, H., Fujinawa, R., Sugai, M. et al.**, Germinal center marker GL7 probes activation-dependent repression of N-glycolylneuraminic acid, a sialic acid species involved in the negative modulation of B-cell activation. *Mol. Cell. Biol.* 2007. **27**: 3008–3022.

1153 **Grötsch, B., Brachs, S., Lang, C., Luther, J., Derer, A., Schlötzer-Schrehardt, U., Bozec, A. et al.**, The AP-1 transcription factor Fra1 inhibits follicular B cell differentiation into plasma cells. *J. Exp. Med.* 2014. **211**: 2199–2212.

1154 **Arnold, L. W., Pennell, C. A., McCray, S. K. and Clarke, S. H.**, Development of B-1 cells: segregation of phosphatidyl choline-specific B cells to the B-1 population occurs after immunoglobulin gene expression. *J. Exp. Med.* 1994. **179**: 1585–1595.

1155 **Rauch, P. J., Chudnovskiy, A., Robbins, C. S., Weber, G. F., Etzrodt, M., Hilgendorf, I., Tiglao, E. et al.**, Innate response activator B cells protect against microbial sepsis. *Science* 2012. **335**: 597–601.

1156 **Bouaziz, J.-D., Yanaba, K. and Tedder, T. F.**, Regulatory B cells as inhibitors of immune responses and inflammation. *Immunol. Rev.* 2008. **224**: 201–214.

1157 **Shen, P. and Fillatreau, S.**, Antibody-independent functions of B cells: a focus on cytokines. *Nat. Rev. Immunol.* 2015. **15**: 441–451.

1158 **Bermejo, D. A., Jackson, S. W., Gorosito-Serran, M., Acosta-Rodriguez, E. V., Amezcua-Vesely, M. C., Sather, B. D., Singh, A. K. et al.**, Trypanosoma cruzi trans-sialidase initiates a program independent of the transcription factors RORγt and Ahr that leads to IL-17 production by activated B cells. *Nat. Immunol.* 2013. **14**: 514–522.

1159 **Shen, P., Roch, T., Lampropoulou, V., O'Connor, R. A., Stervbo, U., Hilgenberg, E., Ries, S. et al.**, IL-35-producing B cells are critical regulators of immunity during autoimmune and infectious diseases. *Nature* 2014. **507**: 366–370.

1160 **Fillatreau, S.**, Pathogenic functions of B cells in autoimmune diseases: IFN-γ production joins the criminal gang. *Eur. J. Immunol.* 2015. **45**: 966–970.

1161 **Mizoguchi, A. and Bhan, A. K.**, A case for regulatory B cells. *J. Immunol.* 2006. **176**: 705–710.

1162 **Rosser, E. C. and Mauri, C.**, Regulatory B cells: origin, phenotype, and function. *Immunity* 2015. **42**: 607–612.

1163 **Maseda, D., Smith, S. H., DiLillo, D. J., Bryant, J. M., Candando, K. M., Weaver, C. T. and Tedder, T. F.**, Regulatory B10 cells differentiate into antibody-secreting cells after transient IL-10 production in vivo. *J. Immunol.* 2012. **188**: 1036–1048.

1164 **Kulkarni, U., Karsten, C. M., Kohler, T., Hammerschmidt, S., Bommert, K., Tiburzy, B., Meng, L. et al.**, IL-10 mediates plasmacytosis-associated immunodeficiency by inhibiting complement-mediated neutrophil migration. *J. Allergy Clin. Immunol.* 2016. **137**: 1487–1497.e6.

1165 **Matsumoto, M., Baba, A., Yokota, T., Nishikawa, H., Ohkawa, Y., Kayama, H., Kallies, A. et al.**, Interleukin-10-producing plasmablasts exert regulatory function in autoimmune inflammation. *Immunity* 2014. **41**: 1040–1051.

1166 **Blanc, P., Moro-Sibilot, L., Barthly, L., Jagot, F., This, S., de Bernard, S., Buffat, L. et al.**, Mature IgM-expressing plasma cells sense antigen and develop competence for cytokine production upon antigenic challenge. *Nat. Commun.* 2016. **7**: 13600.

1167 **Lino, A. C., Dang, V. D., Lampropoulou, V., Welle, A., Joedicke, J., Pohar, J., Simon, Q. et al.**, LAG-3 inhibitory receptor expression identifies immunosuppressive natural regulatory plasma cells. *Immunity* 2018. **49**: 120–133.e129.

1168 **Evans, J. G., Chavez-Rueda, K. A., Eddaoudi, A., Meyer-Bahlburg, A., Rawlings, D. J., Ehrenstein, M. R. and Mauri, C.**, Novel suppressive function of transitional 2 B cells in experimental arthritis. *J. Immunol.* 2007. **178**: 7868–7878.

1169 **Blair, P. A., Chavez-Rueda, K. A., Evans, J. G., Shlomchik, M. J., Eddaoudi, A., Isenberg, D. A., Ehrenstein, M. R. et al.**, Selective targeting of B cells with agonistic anti-CD40 is an efficacious strategy for the generation of induced regulatory T2-like B cells and for the suppression of lupus in MRL/lpr mice. *J. Immunol.* 2009. **182**: 3492–3502.

1170 **Miles, K., Heaney, J., Sibinska, Z., Salter, D., Savill, J., Gray, D. and Gray, M.**, A tolerogenic role for Toll-like receptor 9 is revealed by B-cell interaction with DNA complexes expressed on apoptotic cells. *Proc. Natl. Acad. Sci. USA* 2012. **109**: 887–892.

1171 **Bankoti, R., Gupta, K., Levchenko, A. and Stäger, S.**, Marginal zone B cells regulate antigen-specific T cell responses during infection. *J. Immunol.* 2012. **188**: 3961–3971.

1172 **Tedder, T. F.**, B10 cells: a functionally defined regulatory B cell subset. *J. Immunol.* 2015. **194**: 1395–1401.

1173 **Ding, Q., Yeung, M., Camirand, G., Zeng, Q., Akiba, H., Yagita, H., Chalasani, G. et al.**, Regulatory B cells are identified by expression of TIM-1 and can be induced through TIM-1 ligation to promote tolerance in mice. *J. Clin. Invest.* 2011. **121**: 3645–3656.

1174 **Xiao, S., Brooks, C. R., Sobel, R. A. and Kuchroo, V. K.**, Tim-1 is essential for induction and maintenance of IL-10 in regulatory B cells and their regulation of tissue inflammation. *J. Immunol.* 2015. **194**: 1602–1608.

1175 **Fillatreau, S.**, Natural regulatory plasma cells. *Curr. Opin. Immunol.* 2018. **55**: 62–66.

1176 **Mills, D. M. and Cambier, J. C.**, B lymphocyte activation during cognate interactions with CD4+ T lymphocytes: molecular dynamics and immunologic consequences. *Semin. Immunol.* 2003. **15**: 325–329.

1177 **Okada, T., Miller, M., Parker, I., Krummel, M. F., Neighbors, M., Hartley, S. B., O'Garra, A. et al.**, Antigen-engaged B cells undergo chemotaxis toward the T zone and form motile conjugates with helper T cells. *PLoS Biol.* 2005. **3**: e150.

1178 **MacLennan, I.**, Germinal centers. *Annu. Rev. Immunol.* 1994. **12**: 117–139.

1179 **Victora, G. D. and Nussenzweig, M. C.**, Germinal centers. *Annu. Rev. Immunol.* 2012. **30**: 429–457.

1180 **Nieuwenhuis, P. and Opstelten, D.**, Functional anatomy of germinal centers. *Am. J. Anat.* 1984. **170**: 421–435.

1181 **Wagner, S. and Neuberger**, Somatic hypermutation of immunoglobulin genes. *Annu. Rev. Immunol.* 1996. **14**: 441–457.

1182 **Li, Z., Woo, C. J., Iglesias-Ussel, M. D., Ronai, D. and Scharff, M. D.**, The generation of antibody diversity through somatic hypermutation and class switch recombination. *Genes Dev.* 2004. **18**: 1–11.

1183 **Wu, J., Qin, D., Burton, G., Szakal, A. and Tew, J.**, Follicular dendritic cell-derived antigen and accessory activity in initiation of memory IgG responses in vitro. *J. Immunol.* 1996. **157**: 3404–3411.

1184 **Yeh, C.-H. H., Nojima, T., Kuraoka, M. and Kelsoe, G.**, Germinal center entry not selection of B cells is controlled by peptide-MHCII complex density. *Nat. Commun.* 2018. **9**: 928.

1185 **Klaus, G., Humphrey, J., Kunkl, A. and Dongworth, D.**, The follicular dendritic cell: its role in antigen presentation in the generation of immunological memory. *Immunol. Rev.* 1980. **53**: 3–28.

1186 **Coico, R., Bhogal, B. and Thorbecke, G.**, Relationship of germinal centers in lymphoid tissue to immunologic memory. VI. Transfer of B cell memory with lymph node cells fractionated according to their receptors for peanut agglutinin. *J. Immunol.* 1983. **131**: 2254–2257.

1187 **Benner, R., Hijmans, W. and Haaijman, J.**, The bone marrow: the major source of serum immunoglobulins, but still a neglected site of antibody formation. *Clin. Exp. Immunol.* 1981. **46**: 1–8.

1188 **Dilosa, R., Maeda, K., Masuda, A., Szakal, A. and Tew, J.**, Germinal center B cells and antibody production in the bone marrow. *J. Immunol.* 1991. **146**: 4071–4077.

1189 **Meyer-Hermann, M., Deutsch, A. and Or-Guil, M.**, Recycling probability and dynamical properties of germinal center reactions. *J. Theor. Biol.* 2001. **210**: 265–285.

1190 **Oprea, M. and Perelson, A.**, Somatic mutation leads to efficient affinity maturation when centrocytes recycle back to centroblasts. *J. Immunol.* 1997. **158**: 5155–5162.

1191 **Oliver, A., Martin, F. and Kearney, J.**, Mouse CD38 is down-regulated on germinal center B cells and mature plasma cells. *J. Immunol.* 1997. **158**: 1108–1115.

1192 **Laszlo, G., Hathcock, K., Dickler, H. and Hodes, R.**, Characterization of a novel cell-surface molecule expressed on subpopulations of activated T and B cells. *J. Immunol.* 1993. **150**: 5252–5262.

1193 **Reichert, R., Gallatin, W., Weissman, I. and Butcher, E.**, Germinal center B cells lack homing receptors necessary for normal lymphocyte recirculation. *J Exp. Med.* 1983. **157**: 813–827.

1194 **Butcher, E. et al.**, Surface phenotype of Peyer's patch germinal center cells: implications for the role of germinal centers in B cell differentiation. *J. Immunol.* 1982. **129**: 2698–2707.

1195 **Davies, A., Forrester, J., Rose, M., Birbeck and Wallis, V.**, Peanut lectin binding properties of germinal centers of mouse lymphoid tissue. *Nature* 1980. **284**: 364.

1196 **Kraal, G., Weissman, I. and Butcher, E.**, Germinal centre B cells: antigen specificity and changes in heavy chain class expression. *Nature* 1982. **298**: 377–379.

1197 **Smith, K., Nossal, G. and Tarlinton, D.**, FAS is highly expressed in the germinal center but is not required for regulation of the B-cell response to antigen. *Proc. Natl. Acad. Sci. USA* 1995. **92**: 11628–11632.

1198 **Bourgois, A., Kitajima, K., Hunter, I. and Askonas**, Surface immunoglobulins of lipopolysaccharide-stimulated spleen cells. The behavior of IgM, IgD and IgG. *Eur. J. Immunol.* 1977. **7**: 151–153.

1199 **Monroe, J., Havran, W. and Cambier, J.**, B lymphocyte activation: entry into cell cycle is accompanied by decreased expression of IgD but not IgM. *Eur. J. Immunol.* 1983. **13**: 208–213.

1200 **Hathcock, K. et al.**, Identification of an alternative CTLA-4 ligand costimulatory for T cell activation. *Science* 1993. **262**: 905–907.

1201 **Freeman, G., Borriello, F., Hodes, R. J., Reiser, H., Hathcock, K. S., Laszlo, G., McKnight, A. J. et al.**, Uncovering of functional alternative CTLA-4 counter-receptor in B7-deficient mice. *Science (New York, N.Y.)* 1993. **262**: 907–909.

1202 **Freeman, G., Borriello, F., Hodes, R. J., Reiser, H., Gribben, J. G., Ng, J. W., Kim, J. et al.**, Murine B7-2, an alternative CTLA4 counter-receptor that costimulates T cell proliferation and interleukin 2 production. *J. Exp. Med.* 1993. **178**: 2185–2192.

1203 **Allen, C. D., Ansel, K. M., Low, C., Lesley, R., Tamamura, H., Fujii, N. and Cyster, J. G.**, Germinal center dark and light zone organization is mediated by CXCR4 and CXCR5. *Nat. Immunol.* 2004. **5**: 943–952.

1204 **Victora, G. D., Schwickert, T. A., Fooksman, D. R., Kamphorst, A. O., Meyer-Hermann, M., Dustin, M. L., Nussenzweig, M. C. et al.**, Germinal center dynamics revealed by multiphoton microscopy with a photoactivatable fluorescent reporter. *Cell* 2010. **143**: 592–605.

1205 **Anderson, K. C., Bates, M. P., Slaughenhoupt, B. L., Pinkus, G. S., Schlossman, S. F. and Nadler, L. M.**, Expression of human B cell-associated antigens on leukemias and lymphomas: a model of human B cell differentiation. *Blood* 1984. **63**: 1424–1433.

1206 **Stashenko, P., Nadler, L. M., Hardy, R. and Schlossman, S. F.**, Characterization of a human B lymphocyte-specific antigen. *J. Immunol.* 1980. **125**: 1678–1685.

1207 **LeBien, T. W. and Tedder, T. F.**, B lymphocytes: how they develop and function. *Blood* 2008. **112**: 1570–1580.

1208 **Sims, G. P., Ettinger, R., Shirota, Y., Yarboro, C. H., Illei, G. G. and Lipsky, P. E.**, Identification and characterization of circulating human transitional B cells. *Blood* 2005. **105**: 4390–4398.

1209 **Klein, U., Rajewsky, K. and Kuppers, R.**, Human immunoglobulin (Ig)M+IgD+ peripheral blood B cells expressing the CD27 cell surface antigen carry somatically mutated variable region genes: CD27 as a general marker for somatically mutated (memory) B cells. *J. Exp. Med.* 1998. **188**: 1679–1689.

1210 **Kuppers, R., Klein, U., Hansmann, M. L. and Rajewsky, K.**, Cellular origin of human B-cell lymphomas. *N. Engl. J. Med.* 1999. **341**: 1520–1529.

1211 **Agematsu, K., Hokibara, S., Nagumo, H. and Komiyama, A.**, CD27: a memory B-cell marker. *Immunol. Today* 2000. **21**: 204–206.

1212 **Agematsu, K., Nagumo, H., Yang, F. C., Nakazawa, T., Fukushima, K., Ito, S., Sugita, K. et al.**, B cell subpopulations separated by CD27 and crucial collaboration of CD27+ B cells and helper T cells in immunoglobulin production. *Eur. J. Immunol.* 1997. **27**: 2073–2079.

1213 **Odendahl, M., Jacobi, A., Hansen, A., Feist, E., Hiepe, F., Burmester, G. R., Lipsky, P. E. et al.**, Disturbed peripheral B lymphocyte homeostasis in systemic lupus erythematosus. *J. Immunol.* 2000. **165**: 5970–5979.

1214 **Mei, H. E., Wirries, I., Frolich, D., Brisslert, M., Giesecke, C., Grun, J. R. et al.**, A unique population of IgG-expressing plasma cells lacking CD19 is enriched in human bone marrow. *Blood* 2015. **125**: 1739–1748.

1215 **Pascual, V., Liu, Y. J., Magalski, A., de Bouteiller, O., Banchereau, J. and Capra, J. D.**, Analysis of somatic mutation in five B cell subsets of human tonsil. *J. Exp. Med.* 1994. **180**: 329–339.

1216 **Kikutani, H., Suemura, M., Owaki, H., Nakamura, H., Sato, R., Yamasaki, K., Barsumian, E. L. et al.**, Fc epsilon receptor, a specific differentiation marker transiently expressed on mature B cells before isotype switching. *J. Exp. Med.* 1986. **164**: 1455–1469.

1217 **Clark, E. A. and Lane, P. J.**, Regulation of human B-cell activation and adhesion. *Annu. Rev. Immunol.* 1991. **9**: 97–127.

1218 **Wu, Y. C., Kipling, D. and Dunn-Walters, D. K.**, The relationship between CD27 negative and positive B cell populations in human peripheral blood. *Front. Immunol.* 2011. **2**: 81.

1219 **Wei, C., Anolik, J., Cappione, A., Zheng, B., Pugh-Bernard, A., Brooks, J., Lee, E. H. et al.**, A new population of cells lacking expression of CD27 represents a notable component of the B cell memory compartment in systemic lupus erythematosus. *J. Immunol.* 2007. **178**: 6624–6633.

1220 **Jacobi, A. M., Reiter, K., Mackay, M., Aranow, C., Hiepe, F., Radbruch, A., Hansen, A. et al.**, Activated memory B cell subsets correlate with disease activity in systemic lupus erythematosus: delineation by expression of CD27, IgD, and CD95. *Arthritis Rheum.* 2008. **58**: 1762–1773.

1221 **Wehr, C., Eibel, H., Masilamani, M., Illges, H., Schlesier, M., Peter, H. H. and Warnatz, K.**, A new CD21low B cell population in the peripheral blood of patients with SLE. *Clin. Immunol.* 2004. **113**: 161–171.

1222 **Tedder, T. F., Zhou, L. J. and Engel, P.**, The CD19/CD21 signal transduction complex of B lymphocytes. *Immunol. Today* 1994. **15**: 437–442.

1223 **Jacobi, A. M. and Dorner, T.**, B-cell-directed therapy in patients with connective tissue diseases. *Dtsch. Med. Wochenschr.* 2012. **137**: 1755–1757.

1224 **Polikowsky, H. G., Wogsland, C. E., Diggins, K. E., Huse, K. and Irish, J. M.**, Cutting edge: redox signaling hypersensitivity distinguishes human germinal center B Cells. *J. Immunol.* 2015. **195**: 1364–1367.

1225 **Carrion, C., Guerin, E., Gachard, N., le Guyader, A., Giraut, S. and Feuillard, J.**, Adult bone marrow three-dimensional phenotypic landscape of B-cell differentiation. *Cytometry B Clin. Cytom.* 2019. **96**: 30–38.

1226 **Bernasconi, N. L., Traggiai, E. and Lanzavecchia, A.**, Maintenance of serological memory by polyclonal activation of human memory B cells. *Science* 2002. **298**: 2199–2202.

1227 **Giesecke, C., Meyer, T., Durek, P., Maul, J., Preiss, J., Jacobs, J. F. M. et al.**, simultaneous presence of non- and highly mutated keyhole limpet hemocyanin (KLH)-specific plasmablasts early after primary KLH immunization suggests cross-reactive memory B cell activation. *J. Immunol.* 2018. **200**(12): 3981–3992.

1228 **Liao, H. Y., Tao, L., Zhao, J., Qin, J., Zeng, G. C., Cai, S. W. et al.**, Clostridium butyricum in combination with specific immunotherapy converts antigen-specific B cells to regulatory B cells in asthmatic patients. *Sci. Rep.* 2016. **6**: 20481.

1229 **Ellebedy, A. H., Jackson, K. J., Kissick, H. T., Nakaya, H. I., Davis, C. W., Roskin, K. M. et al.**, Defining antigen-specific plasmablast and memory B cell subsets in human blood after viral infection or vaccination. *Nat. Immunol.* 2016. **17**(10): 1226–1234.

1230 **Kerkman, P. F., Fabre, E., van der Voort, E. I., Zaldumbide, A., Rombouts, Y., Rispens, T. et al.**, Identification and characterisation of citrullinated antigen-specific B cells in peripheral blood of patients with rheumatoid arthritis. *Ann. Rheum. Dis.* 2016. **75**: 1170–1176.

1231 **Murugan, R., Buchauer, L., Triller, G., Kreschel, C., Costa, G., Pidelaserra Marti, G. et al.**, Clonal selection drives protective memory B cell responses in controlled human malaria infection. *Sci. Immunol.* 2018. **3**(20): eaap8029.

1232 **Germar, K., Fehres, C. M., Scherer, H. U., van Uden, N., Pollastro, S., Yeremenko, N. et al.**, Generation and characterization of anti-citrullinated protein antibody-producing B-cell clones from rheumatoid arthritis patients. *Arthritis Rheumatol.* 2019. **71**: 340–350.

1233 **Kwakkenbos, M. J., Diehl, S. A., Yasuda, E., Bakker, A. Q., van Geelen, C. M., Lukens, M. V. et al.**, Generation of stable monoclonal antibody-producing B cell receptor-positive human memory B cells by genetic programming. *Nat. Med.* 2010. **16**(1): 123–128.

1234 **Giesecke, C., Frolich, D., Reiter, K., Mei, H. E., Wirries, I., Kuhly, R. et al.**, Tissue distribution and dependence of responsiveness of human antigen-specific memory B cells. *J. Immunol.* 2014. **192**(7): 3091–3100.

1235 **Kerkman, P. F., Kempers, A. C., van der Voort, E. I., van Oosterhout, M., Huizinga, T. W., Toes, R. E. et al.**, Synovial fluid mononuclear cells provide an environment for long-term survival of antibody-secreting cells and promote the spontaneous production of anti-citrullinated protein antibodies. *Ann. Rheum. Dis.* 2016. **75**(12): 2201–2207.

1236 **Kerkman, P. F., Rombouts, Y., van der Voort, E. I., Trouw, L. A., Huizinga, T. W., Toes, R. E. et al.**, Circulating plasmablasts/plasmacells as a source of anticitrullinated protein antibodies in patients with rheumatoid arthritis. *Ann. Rheum. Dis.* 2013. **72**(7): 1259–1263.

1237 **Hansen, A., Reiter, K., Dorner, T. and Pruss, A.**, Cryopreserved human B cells as an alternative source for single cell mRNA analysis. *Cell Tissue Bank* 2005. **6**(4): 299–308.

1238 **Townsend, S. E., Goodnow, C. C. and Cornall, R. J.**, Single epitope multiple staining to detect ultralow frequency B cells. *J. Immunol. Methods* 2001. **249**(1-2): 137–146.

1239 **Brooks, J. F., Liu, X., Davies, J. M., Wells, J. W. and Steptoe, R. J.**, Tetramer-based identification of naive antigen-specific B cells within a polyclonal repertoire. *Eur. J. Immunol.* 2018. **48**(7): 1251–1254.

1240 **Cornec, D., Berti, A., Hummel, A., Peikert, T., Pers, J. O. and Specks, U.**, Identification and phenotyping of circulating autoreactive proteinase 3-specific B cells in patients with PR3-ANCA associated vasculitis and healthy controls. *J. Autoimmun.* 2017. **84**: 122–131.

1241 **Frolich, D., Giesecke, C., Mei, H. E., Reiter, K., Daridon, C., Lipsky, P. E. and Dorner, T.**, Secondary immunization generates clonally related antigen-specific plasma cells and memory B cells. *J. Immunol.* 2010. **185**: 3103–3110.

1242 **Lighaam, L. C., Vermeulen, E., Bleker, T., Meijlink, K. J., Aalberse, R. C., Barnes, E. et al.**, Phenotypic differences between IgG4+ and IgG1+ B cells point to distinct regulation of the IgG4 response. *J. Allergy Clin. Immunol.* 2014. **133**(1): 267–270 e1-6.

1243 **Koning, M. T., Kielbasa, S. M., Boersma, V., Buermans, H. P. J., van der Zeeuw, S. A. J., van Bergen, C. A. M. et al.**, ARTISAN PCR: rapid identification of full-length immunoglobulin rearrangements without primer binding bias. *Br. J. Haematol.* 2017. **178**(6): 983–986.

1244 **Gatto, M., Wiedemann, A., Nomovi, N., Reiter, K., Schrezenmeier, E., Rose, T. et al.**, Circulating Pentraxin3-Specific B Cells Are Decreased in Lupus Nephritis. *Front. Immunol.* 2019. **10**: 29.

1245 **Odendahl, M., Mei, H., Hoyer, B. F., Jacobi, A. M., Hansen, A., Muehlinghaus, G., Berek, C. et al.**, Generation of migratory antigen-specific plasma blasts and mobilization of resident plasma cells in a secondary immune response. *Blood* 2005. **105**: 1614–1621.

1246 **Mei, H. E., Hahne, S., Redlin, A., Hoyer, B. F., Wu, K., Baganz, L. et al.**, Plasmablasts With a Mucosal Phenotype Contribute to Plasmacytosis in Systemic Lupus Erythematosus. *Arthritis Rheumatol.* 2017. **69**: 2018–2028.

1247 **Willemze, A., Trouw, L. A., Toes, R. E. and Huizinga, T. W.**, The influence of ACPA status and characteristics on the course of RA. *Nat. Rev. Rheumatol.* 2012. **8**(3): 144–152.

1248 **Katz, S. I., Parker, D. and Turk, J. L.**, B-cell suppression of delayed hypersensitivity reactions. *Nature* 1974. **251**: 550–551.

1249 **Neta, R. and Salvin, S. B.**, Specific suppression of delayed hypersensitivity: the possible presence of a suppressor B cell in the regulation of delayed hypersensitivity. *J. Immunol.* 1974. **113**: 1716–1725.

1250 **Wolf, S. D., Dittel, B. N., Hardardottir, F. and Janeway, C. A., Jr.**, Experimental autoimmune encephalomyelitis induction in genetically B cell-deficient mice. *J. Exp. Med.* 1996. **184**: 2271–2278.

1251 **Mizoguchi, A., Mizoguchi, E., Takedatsu, H., Blumberg, R. S. and Bhan, A. K.**, Chronic intestinal inflammatory condition generates IL-10-producing regulatory B cell subset characterized by CD1d upregulation. *Immunity* 2002. **16**: 219–230.

1252 **Fillatreau, S., Sweenie, C. H., McGeachy, M. J., Gray, D. and Anderton, S. M.**, B cells regulate autoimmunity by provision of IL-10. *Nat. Immunol.* 2002. **3**: 944–950.

1253 **van de Veen, W., Stanic, B., Wirz, O. F., Jansen, K., Globinska, A. and Akdis, M.**, Role of regulatory B cells in immune tolerance to allergens and beyond. *J. Allergy Clin. Immunol.* 2016. **138**: 654–665.

1254 **Wirz, O. F., Globinska, A., Ochsner, U., van de Veen, W., Eller, E., Christiansen, E. S., Halken, S. et al.**, Comparison of regulatory B cells in asthma and allergic rhinitis. *Allergy* 2019. **74**: 815–818.

1255 **van de Veen, W., Stanic, B., Yaman, G., Wawrzyniak, M., Sollner, S., Akdis, D. G., Ruckert, B. et al.**, IgG4 production is confined to human IL-

10-producing regulatory B cells that suppress antigen-specific immune responses. *J. Allergy Clin. Immunol.* 2013. **131**: 1204–1212.

1256 **Kaminski, D. A., Wei, C., Qian, Y., Rosenberg, A. F. and Sanz, I.**, Advances in human B cell phenotypic profiling. *Front. Immunol.* 2012. **3**: 302.

1257 **Carter, N. A., Rosser, E. C. and Mauri, C.**, Interleukin-10 produced by B cells is crucial for the suppression of Th17/Th1 responses, induction of T regulatory type 1 cells and reduction of collagen-induced arthritis. *Arthritis Res. Ther.* 2012. **14**: R32.

1258 **Parekh, V. V., Prasad, D. V., Banerjee, P. P., Joshi, B. N., Kumar, A. and Mishra, G. C.**, B cells activated by lipopolysaccharide, but not by anti-Ig and anti-CD40 antibody, induce anergy in CD8+ T cells: role of TGF-beta 1. *J. Immunol.* 2003. **170**: 5897–5911.

1259 **Tian, J., Zekzer, D., Hanssen, L., Lu, Y., Olcott, A. and Kaufman, D. L.**, Lipopolysaccharide-activated B cells down-regulate Th1 immunity and prevent autoimmune diabetes in nonobese diabetic mice. *J. Immunol.* 2001. **167**: 1081–1089.

1260 **Carter, N. A., Vasconcellos, R., Rosser, E. C., Tulone, C., Munoz-Suano, A., Kamanaka, M., Ehrenstein, M. R. et al.**, Mice lacking endogenous IL-10-producing regulatory B cells develop exacerbated disease and present with an increased frequency of Th1/Th17 but a decrease in regulatory T cells. *J. Immunol.* 2011. **186**: 5569–5579.

1261 **Schioppa, T., Moore, R., Thompson, R. G., Rosser, E. C., Kulbe, H., Nedospasov, S., Mauri, C. et al.**, B regulatory cells and the tumor-promoting actions of TNF-alpha during squamous carcinogenesis. *Proc. Natl. Acad. Sci. USA* 2011. **108**: 10662–10667.

1262 **Gray, M., Miles, K., Salter, D., Gray, D. and Savill, J.**, Apoptotic cells protect mice from autoimmune inflammation by the induction of regulatory B cells. *Proc. Natl. Acad. Sci. USA* 2007. **104**: 14080–14085.

1263 **Bankoti, R., Gupta, K., Levchenko, A. and Stager, S.**, Marginal zone B cells regulate antigen-specific T cell responses during infection. *J. Immunol.* 2012. **188**: 3961–3971.

1264 **Matsushita, T., Horikawa, M., Iwata, Y. and Tedder, T. F.**, Regulatory B cells (B10 cells) and regulatory T cells have independent roles in controlling experimental autoimmune encephalomyelitis initiation and late-phase immunopathogenesis. *J. Immunol.* 2010. **185**: 2240–2252.

1265 **Kalampokis, I., Yoshizaki, A. and Tedder, T. F.**, IL-10-producing regulatory B cells (B10 cells) in autoimmune disease. *Arthritis Res. Ther.* 2013. **15** (Suppl 1): S1.

1266 **Watanabe, R., Ishiura, N., Nakashima, H., Kuwano, Y., Okochi, H., Tamaki, K., Sato, S. et al.**, Regulatory B cells (B10 cells) have a suppressive role in murine lupus: CD19 and B10 cell deficiency exacerbates systemic autoimmunity. *J. Immunol.* 2010. **184**: 4801–4809.

1267 **Sheng, J. R., Quan, S. and Soliven, B.**, CD1d(hi)CD5+ B cells expanded by GM-CSF in vivo suppress experimental autoimmune myasthenia gravis. *J. Immunol.* 2014. **193**: 2669–2677.

1268 **Yang, M., Deng, J., Liu, Y., Ko, K. H., Wang, X., Jiao, Z., Wang, S. et al.**, IL-10-producing regulatory B10 cells ameliorate collagen-induced arthritis via suppressing Th17 cell generation. *Am. J. Pathol.* 2012. **180**: 2375–2385.

1269 **Yanaba, K., Yoshizaki, A., Asano, Y., Kadono, T., Tedder, T. F. and Sato, S.**, IL-10-producing regulatory B10 cells inhibit intestinal injury in a mouse model. *Am. J. Pathol.* 2011. **178**: 735–743.

1270 **Khan, A. R., Amu, S., Saunders, S. P., Hams, E., Blackshields, G., Leonard, M. O., Weaver, C. T. et al.**, Ligation of TLR7 on CD19(+) CD1d(hi) B cells suppresses allergic lung inflammation via regulatory T cells. *Eur. J. Immunol.* 2015. **45**: 1842–1854.

1271 **Amu, S., Saunders, S. P., Kronenberg, M., Mangan, N. E., Atzberger, A. and Fallon, P. G.**, Regulatory B cells prevent and reverse allergic airway inflammation via FoxP3-positive T regulatory cells in a murine model. *J. Allergy Clin. Immunol.* 2010. **125**: 1114–1124.e1118.

1272 **Yanaba, K., Bouaziz, J. D., Haas, K. M., Poe, J. C., Fujimoto, M. and Tedder, T. F.**, A regulatory B cell subset with a unique CD1dhiCD5+ phenotype controls T cell-dependent inflammatory responses. *Immunity* 2008. **28**: 639–650.

1273 **Xiao, S., Brooks, C. R., Zhu, C., Wu, C., Sweere, J. M., Petecka, S., Yeste, A. et al.**, Defect in regulatory B-cell function and development of systemic autoimmunity in T-cell Ig mucin 1 (Tim-1) mucin domain-mutant mice. *Proc. Natl. Acad. Sci. USA* 2012. **109**: 12105–12110.

1274 **Neves, P., Lampropoulou, V., Calderon-Gomez, E., Roch, T., Stervbo, U., Shen, P., Kuhl, A. A. et al.**, Signaling via the MyD88 adaptor protein in B cells suppresses protective immunity during Salmonella typhimurium infection. *Immunity* 2010. **33**: 777–790.

1275 **Dass, S., Vital, E. M. and Emery, P.**, Development of psoriasis after B cell depletion with rituximab. *Arthritis Rheum.* 2007. **56**: 2715–2718.

1276 **Goetz, M., Atreya, R., Ghalibafian, M., Galle, P. R. and Neurath, M. F.**, Exacerbation of ulcerative colitis after rituximab salvage therapy. *Inflamm. Bowel Dis.* 2007. **13**: 1365–1368.

1277 **Blair, P. A., Norena, L. Y., Flores-Borja, F., Rawlings, D. J., Isenberg, D. A., Ehrenstein, M. R. and Mauri, C.**, CD19(+)CD24(hi)CD38(hi) B cells exhibit regulatory capacity in healthy individuals but are functionally impaired in systemic Lupus Erythematosus patients. *Immunity* 2010. **32**: 129–140.

1278 **Das, A., Ellis, G., Pallant, C., Lopes, A. R., Khanna, P., Peppa, D., Chen, A. et al.**, IL-10-producing regulatory B cells in the pathogenesis of chronic hepatitis B virus infection. *J. Immunol.* 2012. **189**: 3925–3935.

1279 **Flores-Borja, F., Bosma, A., Ng, D., Reddy, V., Ehrenstein, M. R., Isenberg, D. A. and Mauri, C.**, CD19+CD24hiCD38hi B cells maintain regulatory T cells while limiting TH1 and TH17 differentiation. *Sci. Transl. Med.* 2013. **5**: 173ra123.

1280 **Iwata, Y., Matsushita, T., Horikawa, M., Dilillo, D. J., Yanaba, K., Venturi, G. M., Szabolcs, P. M. et al.**, Characterization of a rare IL-10-competent B-cell subset in humans that parallels mouse regulatory B10 cells. *Blood* 2011. **117**: 530–541.

1281 **Machado-Santos, J., Saji, E., Troscher, A. R., Paunovic, M., Liblau, R., Gabriely, G., Bien, C. G. et al.**, The compartmentalized inflammatory response in the multiple sclerosis brain is composed of tissue-resident CD8+ T lymphocytes and B cells. *Brain* 2018. **141**: 2066–2082.

1282 **Horikawa, M., Weimer, E. T., DiLillo, D. J., Venturi, G. M., Spolski, R., Leonard, W. J., Heise, M. T. et al.**, Regulatory B cell (B10 Cell) expansion during Listeria infection governs innate and cellular immune responses in mice. *J Immunol* 2013. **190**: 1158–1168.

1283 **Menon, M., Blair, P. A., Isenberg, D. A. and Mauri, C.**, A regulatory feedback between plasmacytoid dendritic cells and regulatory B cells is aberrant in systemic lupus erythematosus. *Immunity* 2016. **44**: 683–697.

1284 **Ramirez, J., Lukin, K. and Hagman, J.**, From hematopoietic progenitors to B cells: mechanisms of lineage restriction and commitment. *Curr. Opin. Immunol.* 2010. **22**: 177–184.

1285 **Hardy, R. R., Kincade, P. W. and Dorshkind, K.**, The protean nature of cells in the B lymphocyte lineage. *Immunity* 2007. **26**: 703–714.

1286 **Cerutti, A., Puga, I. and Cols, M.**, New helping friends for B cells. *Eur. J. Immunol.* 2012. **42**: 1956–1968.

1287 **Xu, Z., Zan, H., Pone, E. J., Mai, T. and Casali, P.**, Immunoglobulin class-switch DNA recombination: induction, targeting and beyond. *Nat. Rev. Immunol.* 2012. **12**: 517–531.

1288 **King, C., Tangye, S. G. and Mackay, C. R.**, T follicular helper (TFH) cells in normal and dysregulated immune responses. *Annu. Rev. Immunol.* 2008. **26**: 741–766.

1289 **Papavasiliou, F. N. and Schatz, D. G.**, Somatic hypermutation of immunoglobulin genes: merging mechanisms for genetic diversity. *Cell* 2002. **109** Suppl: S35–4.

1290 **Radbruch, A., Muehlinghaus, G., Luger, E. O., Inamine, A., Smith, K. G., Dorner, T. and Hiepe, F.**, Competence and competition: the challenge of becoming a long-lived plasma cell. *Nat. Rev. Immunol.* 2006. **6**: 741–750.

1291 **Honjo, T.**, Immunoglobulin genes. *Annu. Rev. Immunol.* 1983. **1**: 499–528.

1292 **Schatz, D. G. and Ji, Y.**, Recombination centres and the orchestration of V(D)J recombination. *Nat. Rev. Immunol.* 2011. **11**: 251–263.

1293 **Shan, M., Carrillo, J., Yeste, A., Gutzeit, C., Segura-Garzon, D., Walland, A. C., Pybus, M. et al.**, Secreted IgD amplifies humoral T helper 2 cell responses by binding basophils via galectin-9 and CD44. *Immunity* 2018. **49**: 709–724 e708.

1294 **Boonpiyathad, T., Meyer, N., Moniuszko, M., Sokolowska, M., Eljaszewicz, A., Wirz, O. F., Tomasiak-Lozowska, M. M. et al.**, High-dose bee venom exposure induces similar tolerogenic B-cell responses in allergic patients and healthy beekeepers. *Allergy* 2017. **72**: 407–415.

1295 **Kallies, A., Hasbold, J., Tarlinton, D. M., Dietrich, W., Corcoran, L. M., Hodgkin, P. D. and Nutt, S. L.**, Plasma cell ontogeny defined by quantitative changes in blimp-1 expression. *J. Exp. Med.* 2004. **200**: 967–977.

1296 **Nutt, S. L., Hodgkin, P. D., Tarlinton, D. M. and Corcoran, L. M.**, The generation of antibody-secreting plasma cells. *Nat. Rev. Immunol.* 2015. **15**: 160–171.

1297 **Bankoti, R., Ogawa, C., Nguyen, T., Emadi, L., Couse, M., Salehi, S., Fan, X. et al.**, Differential regulation of Effector and Regulatory T cell function by Blimp1. *Sci. Rep.* 2017. **7**: 12078.

1298 **Fukushima, P. I., Nguyen, P. K. T., O'Grady, P. and Stetler-Stevenson, M.**, Flow cytometric analysis of kappa and lambda light chain expression in evaluation of specimens for B-cell neoplasia. *Cytometry* 1996. **26**: 243–252.

1299 **Pelz, A., Schaffert, H., Diallo, R., Hiepe, F., Meisel, A. and Kohler, S.**, S1P receptor antagonists fingolimod and siponimod do not improve the outcome of experimental autoimmune myasthenia gravis mice after disease onset. *Eur. J. Immunol.* 2018. **48**: 498–508.

1300 **Chu, V. T., Fröhlich, A., Steinhauser, G., Scheel, T., Roch, T., Fillatreau, S., Lee, J. J. et al.**, Eosinophils are required for the maintenance of plasma cells in the bone marrow. *Nat. Immunol.* 2011. **12**: 151–159.

1301 **Wilmore, J. R., Jones, D. D. and Allman, D.**, Protocol for improved resolution of plasma cell subpopulations by flow cytometry. *Eur. J. Immunol.* 2017. **47**: 1386–1388.

1302 **Cantor, J., Browne, C. D., Ruppert, R., Féral, C. C., Fässler, R., Rickert, R. C. and Ginsberg, M. H.**, CD98hc facilitates B cell proliferation and adaptive humoral immunity. *Nat. Immunol.* 2009. **10**: 412–419.

1303 **Wrammert, J., Källberg, E., Agace, W. W. and Leanderson, T.**, Ly6C expression differentiates plasma cells from other B cell subsets in mice. *Eur. J. Immunol.* 2002. **32**: 97–103.

1304 **Smith, K. G. C., Hewitson, T. D., Nossal, G. J. V. and Tarlinton, D. M.**, The phenotype and fate of the antibody-forming cells of the splenic foci. *Eur. J. Immunol.* 1996. **26**: 444–448.

1305 **Manz, R. A., Thiel, A. and Radbruch, A.**, Lifetime of plasma cells in the bone marrow. *Nature* 1997. **388**: 133–134.

1306 **Zehentmeier, S., Roth, K., Cseresnyes, Z., Sercan, Ö., Horn, K., Niesner, R. A., Chang, H.-D. et al.**, Static and dynamic components synergize to form a stable survival niche for bone marrow plasma cells: cellular immune response. *Eur. J. Immunol.* 2014. **44**: 2306–2317.

1307 **Sanderson, R. D., Lalor, P. and Bernfield, M.**, B lymphocytes express and lose syndecan at specific stages of differentiation. *Cell Regul.* 1989. **1**: 27–35.

1308 **Arumugakani, G., Stephenson, S. J., Newton, D. J., Rawstron, A., Emery, P., Doody, G. M., McGonagle, D. et al.**, Early emergence of CD19-negative human antibody-secreting cells at the plasmablast to plasma cell transition. *J. Immunol.* 2017. **198**: 4618–4628.

1309 **Racine, R., Chatterjee, M. and Winslow, G. M.**, CD11c expression identifies a population of extrafollicular antigen-specific splenic plasmablasts responsible for CD4 T-independent antibody responses during intracellular bacterial infection. *J. Immunol.* 2008. **181**: 1375–1385.

1310 **Van Camp, B., Durie, B. G., Spier, C., De Waele, M., Van Riet, I., Vela, E., Frutiger, Y. et al.**, Plasma cells in multiple myeloma express a natural killer cell-associated antigen: CD56 (NKH-1; Leu-19). *Blood* 1990. **76**: 377–382.

1311 **Hoffmann, F. S., Kuhn, P.-H., Laurent, S. A., Hauck, S. M., Berer, K., Wendlinger, S. A., Krumbholz, M. et al.**, The immunoregulator soluble TACI is released by ADAM10 and reflects B cell activation in autoimmunity. *J. Immunol.* 2015. **194**: 542–552.

1312 **Pinto, D., Montani, E., Bolli, M., Garavaglia, G., Sallusto, F., Lanzavecchia, A. and Jarrossay, D.**, A functional BCR in human IgA and IgM plasma cells. *Blood* 2013. **121**: 4110–4114.

1313 **Yoshida, T., Mei, H., Dörner, T., Hiepe, F., Radbruch, A., Fillatreau, S. and Hoyer, B. F.**, Memory B and memory plasma cells. *Immunol. Rev.* 2010. **237**: 117–139.

1314 **Slifka, M. K., Antia, R., Whitmire, J. K. and Ahmed, R.**, Humoral immunity due to long-lived plasma cells. *Immunity* 1998. **8**: 363–372.

1315 **Jacobi, A. M., Mei, H., Hoyer, B. F., Mumtaz, I. M., Thiele, K., Radbruch, A., Burmester, G. R. et al.**, HLA-DRhigh/CD27high plasmablasts indicate active disease in patients with systemic lupus erythematosus. *Ann. Rheum. Dis.* 2010. **69**: 305–308.

1316 **Hoyer, B. F., Mumtaz, I. M., Loddenkemper, K., Bruns, A., Sengler, C., Hermann, K. G., Maza, S. et al.**, Takayasu arteritis is characterised by disturbances of B cell homeostasis and responds to B cell depletion therapy with rituximab. *Ann. Rheum. Dis.* 2012. **71**: 75–79.

1317 **Sarkander, J., Hojyo, S. and Tokoyoda, K.**, Vaccination to gain humoral immune memory. *Clin. Transl. Immunol.* 2016. **5**: e120.

1318 **Wrammert, J., Onlamoon, N., Akondy, R. S., Perng, G. C., Polsrila, K., Chandele, A., Kwissa, M. et al.**, Rapid and massive virus-specific plasmablast responses during acute dengue virus infection in humans. *J. Virol.* 2012. **86**: 2911–2918.

1319 **Mei, H. E., Frolich, D., Giesecke, C., Loddenkemper, C., Reiter, K., Schmidt, S., Feist, E. et al.**, Steady-state generation of mucosal IgA+ plasmablasts is not abrogated by B-cell depletion therapy with rituximab. *Blood* 2010. **116**: 5181–5190.

1320 **Huggins, J., Pellegrin, T., Felgar, R. E., Wei, C., Brown, M., Zheng, B., Milner, E. C. et al.**, CpG DNA activation and plasma-cell differentiation of CD27- naive human B cells. *Blood* 2007. **109**: 1611–1619.

1321 **Cocco, M., Stephenson, S., Care, M. A., Newton, D., Barnes, N. A., Davison, A., Rawstron, A. et al.**, In vitro generation of long-lived human plasma cells. *J. Immunol.* 2012. **189**: 5773–5785.

1322 **Mei, H. E., Yoshida, T., Sime, W., Hiepe, F., Thiele, K., Manz, R. A., Radbruch, A. et al.**, Blood-borne human plasma cells in steady state are derived from mucosal immune responses. *Blood* 2009. **113**: 2461–2469.

1323 **Kantele, A., Hakkinen, M., Moldoveanu, Z., Lu, A., Savilahti, E., Alvarez, R. D., Michalek, S. et al.**, Differences in immune responses

induced by oral and rectal immunizations with Salmonella typhi Ty21a: evidence for compartmentalization within the common mucosal immune system in humans. *Infect. Immun.* 1998. **66**: 5630–5635.

1324 **Medina, F., Segundo, C., Campos-Caro, A., Gonzalez-Garcia, I. and Brieva, J. A.**, The heterogeneity shown by human plasma cells from tonsil, blood, and bone marrow reveals graded stages of increasing maturity, but local profiles of adhesion molecule expression. *Blood* 2002. **99**: 2154–2161.

1325 **Caraux, A., Klein, B., Paiva, B., Bret, C., Schmitz, A., Fuhler, G. M., Bos, N. A. et al.**, Circulating human B and plasma cells. Age-associated changes in counts and detailed characterization of circulating normal $CD138^-$ and $CD138^+$ plasma cells. *Haematologica* 2010. **95**: 1016–1020.

1326 **Arce, S., Luger, E., Muehlinghaus, G., Cassese, G., Hauser, A., Horst, A., Lehnert, K. et al.**, CD38 low IgG-secreting cells are precursors of various CD38 high-expressing plasma cell populations. *J. Leukoc. Biol.* 2004. **75**: 1022–1028.

1327 **Jourdan, M., Caraux, A., Caron, G., Robert, N., Fiol, G., Reme, T., Bollore, K. et al.**, Characterization of a transitional preplasmablast population in the process of human B cell to plasma cell differentiation. *J. Immunol.* 2011. **187**: 3931–3941.

1328 **Mei, H. E., Schmidt, S. and Dorner, T.**, Rationale of anti-CD19 immunotherapy: an option to target autoreactive plasma cells in autoimmunity. *Arthritis Res. Ther.* 2012. **14** Suppl 5: S1.

1329 **Lokhorst, H. M., Plesner, T., Laubach, J. P., Nahi, H., Gimsing, P., Hansson, M., Minnema, M. C. et al.**, Targeting CD38 with daratumumab monotherapy in multiple myeloma. *N Engl J Med* 2015. **373**: 1207–1219.

1330 **Halliley, J. L., Tipton, C. M., Liesveld, J., Rosenberg, A. F., Darce, J., Gregoretti, I. V., Popova, L. et al.**, Long-lived plasma cells are contained within the CD19(-)CD38(hi)CD138(+) subset in human bone marrow. *Immunity* 2015. **43**: 132–145.

1331 **Landsverk, O. J., Snir, O., Casado, R. B., Richter, L., Mold, J. E., Reu, P., Horneland, R. et al.**, Antibody-secreting plasma cells persist for decades in human intestine. *J. Exp. Med.* 2017. **214**: 309–317.

1332 **Hacbarth, E. and Kajdacsy-Balla, A.**, Low density neutrophils in patients with systemic lupus erythematosus, rheumatoid arthritis, and acute rheumatic fever. *Arthritis Rheum.* 1986. **29**: 1334–1342.

1333 **Sato, S., Fujimoto, M., Hasegawa, M. and Takehara, K.**, Altered blood B lymphocyte homeostasis in systemic sclerosis: expanded naive B cells and diminished but activated memory B cells. *Arthritis Rheum.* 2004. **50**: 1918–1927.

1334 **Carrell, J. and Groves, C. J.**, OMIP-043: Identification of human antibody secreting cell subsets. *Cytometry A* 2018. **93**: 190–193.

1335 **Mesin, L., Di Niro, R., Thompson, K. M., Lundin, K. E. and Sollid, L. M.**, Long-lived plasma cells from human small intestine biopsies secrete immunoglobulins for many weeks in vitro. *J. Immunol.* 2011. **187**: 2867–2874.

1336 **Laurent, S. A., Hoffmann, F. S., Kuhn, P.-H., Cheng, Q., Chu, Y., Schmidt-Supprian, M., Hauck, S. M. et al.**, γ-Secretase directly sheds the survival receptor BCMA from plasma cells. *Nat. Commun.* 2015. **6**: 7333.

1337 **Kunkel, E. J. and Butcher, E. C.**, Plasma-cell homing. *Nat. Rev. Immunol.* 2003. **3**: 822–829.

1338 **Delogu, A., Schebesta, A., Sun, Q., Aschenbrenner, K., Perlot, T. and Busslinger, M.**, Gene repression by Pax5 in B cells is essential for blood cell homeostasis and is reversed in plasma cells. *Immunity* 2006. **24**: 269–281.

1339 **Medina, F., Segundo, C., Jimenez-Gomez, G., Gonzalez-Garcia, I., Campos-Caro, A. and Brieva, J. A.**, Higher maturity and connective tissue association distinguish resident from recently generated human tonsil plasma cells. *J. Leukoc. Biol.* 2007. **82**: 1430–1436.

1340 **Frigyesi, I., Adolfsson, J., Ali, M., Christophersen, M. K., Johnsson, E., Turesson, I., Gullberg, U. et al.**, Robust isolation of malignant plasma cells in multiple myeloma. *Blood* 2014. **123**: 1336–1340.

1341 **Spits, H., Artis, D., Colonna, M., Diefenbach, A., Di Santo, J. P., Eberl, G., Koyasu, S. et al.**, Innate lymphoid cells—a proposal for uniform nomenclature. *Nat. Rev. Immunol.* 2013. **13**: 145–149.

1342 **Vivier, E., Artis, D., Colonna, M., Diefenbach, A., Di Santo, J. P., Eberl, G., Koyasu, S. et al.**, Innate lymphoid cells: 10 years on. *Cell* 2018. **174**: 1054–1066.

1343 **Biron, C. A., Nguyen, K. B., Pien, G. C., Cousens, L. P. and Salazar-Mather, T. P.**, Natural killer cells in antiviral defense: function and regulation by innate cytokines. *Annu. Rev. Immunol.* 1999. **17**: 189–220.

1344 **Daussy, C., Faure, F., Mayol, K., Viel, S., Gasteiger, G., Charrier, E., Bienvenu, J. et al.**, T-bet and Eomes instruct the development of two distinct natural killer cell lineages in the liver and in the bone marrow. *J. Exp. Med.* 2014. **211**: 563–577.

1345 **Klose, C. S., Flach, M., Mohle, L., Rogell, L., Hoyler, T., Ebert, K., Fabiunke, C. et al.**, Differentiation of type 1 ILCs from a common progenitor to all helper-like innate lymphoid cell lineages. *Cell* 2014. **157**: 340–356.

1346 **Sojka, D. K., Plougastel-Douglas, B., Yang, L., Pak-Wittel, M. A., Artyomov, M. N., Ivanova, Y., Zhong, C. et al.**, Tissue-resident natural killer (NK) cells are cell lineages distinct from thymic and conventional splenic NK cells. *Elife* 2014. **3**: e01659.

1347 **Walker, J. A. and McKenzie, A. N.**, Development and function of group 2 innate lymphoid cells. *Curr. Opin. Immunol.* 2013. **25**: 148–155.

1348 **Montaldo, E., Juelke, K. and Romagnani, C.**, Group 3 innate lymphoid cells (ILC3s): origin, differentiation, and plasticity in humans and mice. *Eur. J. Immunol.* 2015. **45**: 2171–2182.

1349 **Spits, H. and Cupedo, T.**, Innate lymphoid cells: emerging insights in development, lineage relationships, and function. *Annu. Rev. Immunol.* 2012. **30**: 647–675.

1350 **Paclik, D., Stehle, C., Lahmann, A., Hutloff, A. and Romagnani, C.**, ICOS regulates the pool of group 2 innate lymphoid cells under homeostatic and inflammatory conditions in mice. *Eur. J. Immunol.* 2015. **45**: 2766–2772.

1351 **Ryon, J. J.**, Isolation of mononuclear cells from tonsillar tissue. *Curr. Protoc. Immunol.* 2001. Chapter 7: Unit 7 8.

1352 **Gasteiger, G., Fan, X., Dikiy, S., Lee, S. Y. and Rudensky, A. Y.**, Tissue residency of innate lymphoid cells in lymphoid and nonlymphoid organs. *Science* 2015. **350**: 981–985.

1353 **Hoyler, T., Klose, C. S., Souabni, A., Turqueti-Neves, A., Pfeifer, D., Rawlins, E. L., Voehringer, D. et al.**, The transcription factor GATA-3 controls cell fate and maintenance of type 2 innate lymphoid cells. *Immunity* 2012. **37**: 634–648.

1354 **Fuchs, A., Vermi, W., Lee, J. S., Lonardi, S., Gilfillan, S., Newberry, R. D., Cella, M. et al.**, Intraepithelial type 1 innate lymphoid cells are a unique subset of IL-12- and IL-15-responsive IFN-gamma-producing cells. *Immunity* 2013. **38**: 769–781.

1355 **Robinette, M. L., Fuchs, A., Cortez, V. S., Lee, J. S., Wang, Y., Durum, S. K., Gilfillan, S. et al.**, Transcriptional programs define molecular characteristics of innate lymphoid cell classes and subsets. *Nat. Immunol.* 2015. **16**: 306–317.

1356 **Serafini, N., Klein Wolterink, R. G., Satoh-Takayama, N., Xu, W., Vosshenrich, C. A., Hendriks, R. W. and Di Santo, J. P.**, Gata3 drives development of RORgammat+ group 3 innate lymphoid cells. *J. Exp. Med.* 2014. **211**: 199–208.

1357 **Moro, K., Yamada, T., Tanabe, M., Takeuchi, T., Ikawa, T., Kawamoto, H., Furusawa, J. et al.**, Innate production of T(H)2 cytokines by adipose tissue-associated c-Kit(+)Sca-1(+) lymphoid cells. *Nature* 2010. **463**: 540–544.

1358 **Neill, D. R., Wong, S. H., Bellosi, A., Flynn, R. J., Daly, M., Langford, T. K., Bucks, C. et al.**, Nuocytes represent a new innate effector leukocyte that mediates type-2 immunity. *Nature* 2010. **464**: 1367–1370.

1359 **Sawa, S., Cherrier, M., Lochner, M., Satoh-Takayama, N., Fehling, H. J., Langa, F. et al.**, Lineage relationship analysis of RORgammat+ innate lymphoid cells. *Science* 2010. **330**: 665–669.

1360 **Rankin, L. C., Groom, J. R., Chopin, M., Herold, M. J., Walker, J. A., Mielke, L. A. et al.**, The transcription factor T-bet is essential for the development of NKp46+ innate lymphocytes via the Notch pathway. *Nat. Immunol.* 2013. **14**: 389–395.

1361 **Klose, C. S., Kiss, E. A., Schwierzeck, V., Ebert, K., Hoyler, T., d'Hargues, Y., Goppert, N. et al.**, A T-bet gradient controls the fate and function of CCR6-RORgammat+ innate lymphoid cells. *Nature* 2013. **494**: 261–265.

1362 **Vonarbourg, C., Mortha, A., Bui, V. L., Hernandez, P. P., Kiss, E. A., Hoyler, T., Flach, M. et al.**, Regulated expression of nuclear receptor RORgammat confers distinct functional fates to NK cell receptor-expressing RORgammat(+) innate lymphocytes. *Immunity* 2010. **33**: 736–751.

1363 **Cella, M., Fuchs, A., Vermi, W., Facchetti, F., Otero, K., Lennerz, J. K. M., Doherty, J. M. et al.**, A human natural killer cell subset provides an innate source of IL-22 for mucosal immunity. *Nature* 2009. **457**: 722–725.

1364 **Mjosberg, J. M., Trifari, S., Crellin, N. K., Peters, C. P., van Drunen, C. M., Piet, B., Fokkens, W. J. et al.**, Human IL-25- and IL-33-responsive type 2 innate lymphoid cells are defined by expression of CRTH2 and CD161. *Nat. Immunol.* 2011. **12**: 1055–1062.

1365 **Bernink, J. H., Peters, C. P., Munneke, M., te Velde, A. A., Meijer, S. L., Weijer, K., Hreggvidsdottir, H. S. et al.**, Human type 1 innate lymphoid cells accumulate in inflamed mucosal tissues. *Nat. Immunol.* 2013. **14**: 221–229.

1366 **Hazenberg, M. D. and Spits, H.**, Human innate lymphoid cells. *Blood* 2014. **124**: 700–709.

1367 **Cupedo, T., Crellin, N. K., Papazian, N., Rombouts, E. J., Weijer, K., Grogan, J. L., Fibbe, W. E. et al.**, Human fetal lymphoid tissue-inducer cells are interleukin 17-producing precursors to RORC+ CD127+ natural killer-like cells. *Nat. Immunol.* 2009. **10**: 66–74.

1368 **Marquardt, N., Beziat, V., Nystrom, S., Hengst, J., Ivarsson, M. A., Kekalainen, E., Johansson, H. et al.**, Cutting edge: identification and characterization of human intrahepatic CD49a+ NK cells. *J. Immunol.* 2015. **194**: 2467–2471.

1369 **Vacca, P., Montaldo, E., Croxatto, D., Loiacono, F., Canegallo, F., Venturini, P. L., Moretta, L. et al.**, Identification of diverse innate lymphoid cells in human decidua. *Mucosal Immunol.* 2015. **8**: 254–264.

1370 **Montaldo, E., Vacca, P., Chiossone, L., Croxatto, D., Loiacono, F., Martini, S., Ferrero, S. et al.**, Unique eomes(+) NK cell subsets are present in uterus and decidua during early pregnancy. *Front. Immunol.* 2015. **6**: 646.

1371 **Teunissen, M. B., Munneke, J. M., Bernink, J. H., Spuls, P. I., Res, P. C., Te Velde, A., Cheuk, S. et al.**, Composition of innate lymphoid cell subsets in the human skin: enrichment of NCR(+) ILC3 in lesional skin and blood of psoriasis patients. *J. Invest. Dermatol.* 2014. **134**: 2351–2360.

1372 **Lim, A. I., Li, Y., Lopez-Lastra, S., Stadhouders, R., Paul, F., Casrouge, A., Serafini, N. et al.**, Systemic human ILC precursors provide a substrate for tissue ILC differentiation. *Cell* 2017. **168**: 1086–1100 e1010.

1373 **Wojno, E. D., Monticelli, L. A., Tran, S. V., Alenghat, T., Osborne, L. C., Thome, J. J., Willis, C. et al.**, The prostaglandin D(2) receptor CRTH2 regulates accumulation of group 2 innate lymphoid cells in the inflamed lung. *Mucosal Immunol.* 2015. **8**: 1313–1323.

1374 **Kim, S., Iizuka, K., Kang, H. S., Dokun, A., French, A. R., Greco, S. and Yokoyama, W. M.**, In vivo developmental stages in murine natural killer cell maturation. *Nat. Immunol.* 2002. **3**: 523–528.

1375 **Hayakawa, Y. and Smyth, M. J.**, CD27 dissects mature NK cells into two subsets with distinct responsiveness and migratory capacity. *J. Immunol.* 2006. **176**: 1517–1524.

1376 **Chiossone, L., Chaix, J., Fuseri, N., Roth, C., Vivier, E. and Walzer, T.**, Maturation of mouse NK cells is a 4-stage developmental program. *Blood* 2009. **113**: 5488–5496.

1377 **Bjorkstrom, N. K., Riese, P., Heuts, F., Andersson, S., Fauriat, C., Ivarsson, M. A., Bjorklund, A. T. et al.**, Expression patterns of NKG2A, KIR, and CD57 define a process of CD56dim NK-cell differentiation uncoupled from NK-cell education. *Blood* 2010. **116**: 3853–3864.

1378 **Lopez-Verges, S., Milush, J. M., Pandey, S., York, V. A., Arakawa-Hoyt, J., Pircher, H., Norris, P. J. et al.**, CD57 defines a functionally distinct population of mature NK cells in the human CD56dimCD16+ NK-cell subset. *Blood* 2010. **116**: 3865–3874.

1379 **Juelke, K., Killig, M., Luetke-Eversloh, M., Parente, E., Gruen, J., Morandi, B., Ferlazzo, G. et al.**, CD62L expression identifies a unique subset of polyfunctional CD56dim NK cells. *Blood* 2010. **116**: 1299–1307.

1380 **Sanos, S. L., Bui, V. L., Mortha, A., Oberle, K., Heners, C., Johner, C. and Diefenbach, A.**, ROR gamma t and commensal microflora are required for the differentiation of mucosal interleukin 22-producing NKp46(+) cells. *Nat. Immunol.* 2009. **10**: 83–91.

1381 **Satoh-Takayama, N., Vosshenrich, C. A. J., Lesjean-Pottier, S., Sawa, S., Lochner, M., Rattis, F., Mention, J. J. et al.**, Microbial flora drives interleukin 22 production in intestinal NKp46(+) cells that provide innate mucosal immune defense. *Immunity* 2008. **29**: 958–970.

1382 **Luci, C., Reynders, A., Ivanov, I. I., Cognet, C., Chiche, L., Chasson, L., Hardwigsen, J. et al.**, Influence of the transcription factor ROR gamma t on the development of NKp46(+) cell populations in gut and skin. *Nat. Immunol.* 2009. **10**: 75–82.

1383 **Fort, M. M., Cheung, J., Yen, D., Li, J., Zurawski, S. M., Lo, S., Menon, S. et al.**, IL-25 induces IL-4, IL-5, and IL-13 and Th2-associated pathologies in vivo. *Immunity* 2001. **15**: 985–995.

1384 **Price, A. E., Liang, H. E., Sullivan, B. M., Reinhardt, R. L., Eisley, C. J., Erle, D. J. and Locksley, R. M.**, Systemically dispersed innate IL-13-expressing cells in type 2 immunity. *Proc. Natl. Acad. Sci. USA* 2010. **107**: 11489–11494.

1385 **Walzer, T., Blery, M., Chaix, J., Fuseri, N., Chasson, L., Robbins, S. H., Jaeger, S. et al.**, Identification, activation, and selective in vivo ablation of mouse NK cells via NKp46. *Proc. Natl. Acad. Sci. USA* 2007. **104**: 3384–3389.

1386 **Carlyle, J. R., Mesci, A., Ljutic, B., Belanger, S., Tai, L. H., Rousselle, E., Troke, A. D. et al.**, Molecular and genetic basis for strain-dependent NK1.1 alloreactivity of mouse NK cells. *J. Immunol.* 2006. **176**: 7511–7524.

1387 **Del Zotto, G., Marcenaro, E., Vacca, P., Sivori, S., Pende, D., Della Chiesa, M., Moretta, F. et al.**, Markers and function of human NK cells in normal and pathological conditions. *Cytom. B Clin. Cytom.* 2017. **92**: 100–114.

1388 **Crinier, A., Milpied, P., Escaliere, B., Piperoglou, C., Galluso, J., Balsamo, A., Spinelli, L. et al.**, High-dimensional single-cell analysis identifies organ-specific signatures and conserved nk cell subsets in humans and mice. *Immunity* 2018.**49**: 971–986 e975.

1389 **Weizman, O. E., Adams, N. M., Schuster, I. S., Krishna, C., Pritykin, Y., Lau, C., Degli-Esposti, M. A. et al.**, ILC1 confer early host protection at initial sites of viral infection. *Cell* 2017.**171**: 795–808 e712.

1390 **Huntington, N. D., Tabarias, H., Fairfax, K., Brady, J., Hayakawa, Y., Degli-Esposti, M. A., Smyth, M. J. et al.**, NK cell maturation and peripheral homeostasis is associated with KLRG1 up-regulation. *J. Immunol.* 2007. **178**: 4764–4770.

1391 **Sciume, G., Hirahara, K., Takahashi, H., Laurence, A., Villarino, A. V., Singleton, K. L., Spencer, S. P. et al.**, Distinct requirements for T-bet in gut innate lymphoid cells. *J. Exp. Med.* 2012. **209**: 2331–2338.

1392 **Quatrini, L., Wieduwild, E., Escaliere, B., Filtjens, J., Chasson, L., Laprie, C., Vivier, E. et al.**, Endogenous glucocorticoids control host resistance to viral infection through the tissue-specific regulation of PD-1 expression on NK cells. *Nat. Immunol.* 2018. **19**: 954–962.

1393 **Herberman, R. B., Nunn, M. E., Holden, H. T. and Lavrin, D. H.**, Natural cytotoxic reactivity of mouse lymphoid cells against syngeneic and allogeneic tumors. II. Characterization of effector cells. *Int. J. Cancer* 1975. **16**: 230–239.

1394 **Herberman, R. B., Nunn, M. E. and Lavrin, D. H.**, Natural cytotoxic reactivity of mouse lymphoid cells against syngeneic acid allogeneic tumors. I. Distribution of reactivity and specificity. *Int. J. Cancer* 1975. **16**: 216–229.

1395 **Ljunggren, H. G. and Karre, K.**, In search of the 'missing self': MHC molecules and NK cell recognition. *Immunol. Today* 1990. **11**: 237–244.

1396 **Moretta, A., Bottino, C., Mingari, M. C., Biassoni, R. and Moretta, L.**, What is a natural killer cell? *Nat. Immunol.* 2002. **3**: 6–8.

1397 **Vivier, E., Tomasello, E., Baratin, M., Walzer, T. and Ugolini, S.**, Functions of natural killer cells. *Nat. Immunol.* 2008. **9**: 503–510.

1398 **Lopez-Botet, M., Perez-Villar, J. J., Carretero, M., Rodriguez, A., Melero, I., Bellon, T., Llano, M. et al.**, Structure and function of the CD94 C-type lectin receptor complex involved in recognition of HLA class I molecules. *Immunol. Rev.* 1997. **155**: 165–174.

1399 **Braud, V. M., Allan, D. S., O'Callaghan, C. A., Soderstrom, K., D'Andrea, A., Ogg, G. S., Lazetic, S. et al.**, HLA-E binds to natural killer cell receptors CD94/NKG2A, B and C. *Nature* 1998. **391**: 795–799.

1400 **Moretta, A., Bottino, C., Vitale, M., Pende, D., Biassoni, R., Mingari, M. C. and Moretta, L.**, Receptors for HLA class-I molecules in human natural killer cells. *Annu. Rev. Immunol.* 1996. **14**: 619–648.

1401 **Parham, P.**, MHC class I molecules and KIRs in human history, health and survival. *Nat. Rev. Immunol.* 2005. **5**: 201–214.

1402 **Moretta, A., Bottino, C., Vitale, M., Pende, D., Cantoni, C., Mingari, M. C., Biassoni, R. et al.**, Activating receptors and coreceptors involved in human natural killer cell-mediated cytolysis. *Annu. Rev. Immunol.* 2001. **19**: 197–223.

1403 **Vivier, E., Raulet, D. H., Moretta, A., Caligiuri, M. A., Zitvogel, L., Lanier, L. L., Yokoyama, W. M. et al.**, Innate or adaptive immunity? The example of natural killer cells. *Science* 2011. **331**: 44–49.

1404 **Raulet, D. H.**, Roles of the NKG2D immunoreceptor and its ligands. *Nat. Rev. Immunol.* 2003. **3**: 781–790.

1405 **Moretta, A., Sivori, S., Vitale, M., Pende, D., Morelli, L., Augugliaro, R., Bottino, C. et al.**, Existence of both inhibitory (p58) and activatory (p50) receptors for HLA-C molecules in human natural killer cells. *J. Exp. Med.* 1995. **182**: 875–884.

1406 **Wagtmann, N., Biassoni, R., Cantoni, C., Verdiani, S., Malnati, M. S., Vitale, M., Bottino, C. et al.**, Molecular clones of the p58 NK cell receptor reveal immunoglobulin-related molecules with diversity in both the extra- and intracellular domains. *Immunity* 1995. **2**: 439–449.

1407 **Sivori, S., Cantoni, C., Parolini, S., Marcenaro, E., Conte, R., Moretta, L. and Moretta, A.**, IL-21 induces both rapid maturation of human CD34+ cell precursors towards NK cells and acquisition of surface killer Ig-like receptors. *Eur. J. Immunol.* 2003. **33**: 3439–3447.

1408 **Freud, A. G. and Caligiuri, M. A.**, Human natural killer cell development. *Immunol. Rev.* 2006. **214**: 56–72.

1409 **Hu, P. F., Hultin, L. E., Hultin, P., Hausner, M. A., Hirji, K., Jewett, A., Bonavida, B. et al.**, Natural killer cell immunodeficiency in HIV disease is manifest by profoundly decreased numbers of CD16+CD56+ cells and expansion of a population of CD16dimCD56- cells with low lytic activity. *J. Acquir. Immune Defic. Syndr. Hum. Retrovirol.* 1995. **10**: 331–340.

1410 **Mavilio, D., Lombardo, G., Benjamin, J., Kim, D., Follman, D., Marcenaro, E., O'Shea, M. A. et al.**, Characterization of CD56-/CD16+ natural killer (NK) cells: a highly dysfunctional NK subset expanded in HIV-infected viremic individuals. *Proc. Natl. Acad. Sci. U. S. A.* 2005. **102**: 2886–2891.

1411 **Della Chiesa, M., Falco, M., Podesta, M., Locatelli, F., Moretta, L., Frassoni, F. and Moretta, A.**, Phenotypic and functional heterogeneity of human NK cells developing after umbilical cord blood transplantation: a role for human cytomegalovirus? *Blood* 2012. **119**: 399–410.

1412 **Pesce, S., Greppi, M., Tabellini, G., Rampinelli, F., Parolini, S., Olive, D., Moretta, L. et al.**, Identification of a subset of human natural killer cells expressing high levels of programmed death 1: a phenotypic and functional characterization. *J. Allergy Clin. Immunol.* 2017.**139**: 335–346 e333.

1413 **Caligiuri, M. A., Zmuidzinas, A., Manley, T. J., Levine, H., Smith, K. A. and Ritz, J.**, Functional consequences of interleukin 2 receptor expression on resting human lymphocytes. Identification of a novel natural killer cell subset with high affinity receptors. *J. Exp. Med.* 1990. **171**: 1509–1526.

1414 **Carson, W. E., Fehniger, T. A. and Caligiuri, M. A.**, CD56bright natural killer cell subsets: characterization of distinct functional responses to interleukin-2 and the c-kit ligand. *Eur. J. Immunol.* 1997. **27**: 354–360.

1415 **Frey, M., Packianathan, N. B., Fehniger, T. A., Ross, M. E., Wang, W. C., Stewart, C. C., Caligiuri, M. A. et al.**, Differential expression and function of L-selectin on CD56bright and CD56dim natural killer cell subsets. *J. Immunol.* 1998. **161**: 400–408.

1416 **Campbell, J. J., Qin, S., Unutmaz, D., Soler, D., Murphy, K. E., Hodge, M. R., Wu, L. et al.**, Unique subpopulations of CD56+ NK and NK-T peripheral blood lymphocytes identified by chemokine receptor expression repertoire. *J. Immunol.* 2001. **166**: 6477–6482.

1417 **Robertson, M. J.**, Role of chemokines in the biology of natural killer cells. *J. Leukoc. Biol.* 2002. **71**: 173–183.

1418 **Lima, M., Leander, M., Santos, M., Santos, A. H., Lau, C., Queiros, M. L., Goncalves, M. et al.**, Chemokine receptor expression on normal blood CD56(+) NK-cells elucidates cell partners that comigrate during the innate and adaptive immune responses and identifies a transitional NK-cell population. *J. Immunol. Res.* 2015. **2015**: 839684.

1419 **De Maria, A., Bozzano, F., Cantoni, C. and Moretta, L.**, Revisiting human natural killer cell subset function revealed cytolytic CD56(dim)CD16+ NK cells as rapid producers of abundant IFN-gamma on activation. *Proc. Natl. Acad. Sci. USA* 2011. **108**: 728–732.

1420 **Fauriat, C., Long, E. O., Ljunggren, H. G. and Bryceson, Y. T.**, Regulation of human NK-cell cytokine and chemokine production by target cell recognition. *Blood* 2010. **115**: 2167–2176.

1421 **Guma, M., Angulo, A., Vilches, C., Gomez-Lozano, N., Malats, N. and Lopez-Botet, M.**, Imprint of human cytomegalovirus infection on the NK cell receptor repertoire. *Blood* 2004. **104**: 3664–3671.

1422 **Malmberg, K. J., Beziat, V. and Ljunggren, H. G.**, Spotlight on NKG2C and the human NK-cell response to CMV infection. *Eur. J. Immunol.* 2012. **42**: 3141–3145.

1423 **Muccio, L., Bertaina, A., Falco, M., Pende, D., Meazza, R., Lopez-Botet, M., Moretta, L. et al.**, Analysis of memory-like natural killer cells in

human cytomegalovirus-infected children undergoing alphabeta+T and B cell-depleted hematopoietic stem cell transplantation for hematological malignancies. *Haematologica* 2016. **101**: 371–381.

1424 **Sivori, S., Falco, M., Marcenaro, E., Parolini, S., Biassoni, R., Bottino, C., Moretta, L. et al.**, Early expression of triggering receptors and regulatory role of 2B4 in human natural killer cell precursors undergoing in vitro differentiation. *Proc. Natl. Acad. Sci. USA* 2002. **99**: 4526–4531.

1425 **Vacca, P., Pietra, G., Falco, M., Romeo, E., Bottino, C., Bellora, F., Prefumo, F. et al.**, Analysis of natural killer cells isolated from human decidua: Evidence that 2B4 (CD244) functions as an inhibitory receptor and blocks NK-cell function. *Blood* 2006. **108**: 4078–4085.

1426 **Vacca, P., Vitale, C., Montaldo, E., Conte, R., Cantoni, C., Fulcheri, E., Darretta, V. et al.**, CD34+ hematopoietic precursors are present in human decidua and differentiate into natural killer cells upon interaction with stromal cells. *Proc. Natl. Acad. Sci. USA* 2011. **108**: 2402–2407.

1427 **Hanna, J., Goldman-Wohl, D., Hamani, Y., Avraham, I., Greenfield, C., Natanson-Yaron, S., Prus, D. et al.**, Decidual NK cells regulate key developmental processes at the human fetal-maternal interface. *Nat. Med.* 2006. **12**: 1065–1074.

1428 **Fehniger, T. A., Cooper, M. A., Nuovo, G. J., Cella, M., Facchetti, F., Colonna, M. and Caligiuri, M. A.**, CD56bright natural killer cells are present in human lymph nodes and are activated by T cell-derived IL-2: a potential new link between adaptive and innate immunity. *Blood* 2003. **101**: 3052–3057.

1429 **Ferlazzo, G., Thomas, D., Lin, S. L., Goodman, K., Morandi, B., Muller, W. A., Moretta, A. et al.**, The abundant NK cells in human secondary lymphoid tissues require activation to express killer cell Ig-like receptors and become cytolytic. *J. Immunol.* 2004. **172**: 1455–1462.

1430 **Merad, M., Sathe, P., Helft, J., Miller, J. and Mortha, A.**, The dendritic cell lineage: ontogeny and function of dendritic cells and their subsets in the steady state and the inflamed setting. *Annu. Rev. Immunol.* 2013. **31**: 563–604.

1431 **Ginhoux, F. and Guilliams, M.**, Tissue-resident macrophage ontogeny and homeostasis. *Immunity* 2016. **44**: 439–449.

1432 **Heidkamp, G. F. et al.**, Functional specialization of Dendritic cell subsets. *Encyclopedia of Cell Biology*, (Elsevier) 2016. 588–604.

1433 **Dress, R. J., Wong, A. Y. and Ginhoux, F.**, Homeostatic control of dendritic cell numbers and differentiation. *Immunol. Cell Biol.* 2018. **96**: 463–476.

1434 **Hoeffel, G. and Ginhoux, F.**, Fetal monocytes and the origins of tissue-resident macrophages. *Cell. Immunol.* 2018. **330**: 5–15.

1435 **Collin, M. and Ginhoux, F.**, Human dendritic cells. *Semin. Cell Dev. Biol.* 2019. **86**: 1–2.

1436 **Schlitzer, A., Sivakamasundari, V., Chen, J., Sumatoh, H. R., Schreuder, J., Lum, J., Malleret, B. et al.**, Identification of cDC1- and cDC2-committed DC progenitors reveals early lineage priming at the common DC progenitor stage in the bone marrow. *Nat. Immunol.* 2015. **16**: 718–728.

1437 **Guilliams, M., Dutertre, C. A., Scott, C. L., McGovern, N., Sichien, D., Chakarov, S., Van Gassen, S. et al.**, Unsupervised high-dimensional analysis aligns dendritic cells across tissues and species. *Immunity* 2016. **45**: 669–684.;

1438 **Dress, R. J., Dutertre, C. A., Giladi, A., Schlitzer, A., Low, I., Shadan, N. B., Tay, A. et al.**, Plasmacytoid dendritic cells develop from Ly6D+ lymphoid progenitors distinct from the myeloid lineage. *Nat. Immunol.* 2019. **20**: 852–864.

1439 **Rodrigues, P. F., Alberti-Servera, L., Eremin, A., Grajales-Reyes, G. E., Ivanek, R. and Tussiwand, R.**, Distinct progenitor lineages contribute to the heterogeneity of plasmacytoid dendritic cells. *Nat. Immunol.* 2018. **19**: 711–722.

1440 **Herman, J. S., Sagar and Grun, D.**, FateID infers cell fate bias in multipotent progenitors from single-cell RNA-seq data. *Nat. Methods* 2018. **15**: 379–386.

1441 **Hoeffel, G., Wang, Y., Greter, M., See, P., Teo, P., Malleret, B., Leboeuf, M. et al.**, Adult Langerhans cells derive predominantly from embryonic fetal liver monocytes with a minor contribution of yolk sac-derived macrophages. *J. Exp. Med.* 2012. **209**: 1167–1181.

1442 **Ginhoux, F., Tacke, F., Angeli, V., Bogunovic, M., Loubeau, M., Dai, X. M., Stanley, E. R. et al.**, Langerhans cells arise from monocytes in vivo. *Nat. Immunol.* 2006. **7**: 265–273.

1443 **Doebel, T., Voisin, B. and Nagao, K.**, Langerhans Cells - The Macrophage in Dendritic Cell Clothing. *Trends Immunol.* 2017. **38**: 817–828.

1444 **Ginhoux, F. and Jung, S.**, Monocytes and macrophages: developmental pathways and tissue homeostasis. *Nat. Rev. Immunol.* 2014. **14**: 392–404.

1445 **Geissmann, F., Jung, S. and Littman, D. R.**, Blood monocytes consist of two principal subsets with distinct migratory properties. *Immunity* 2003. **19**: 71–82.

1446 **Tamoutounour, S., Henri, S., Lelouard, H., de Bovis, B., de Haar, C., van der Woude, C. J., Woltman, A. M. et al.**, CD64 distinguishes macrophages from dendritic cells in the gut and reveals the Th1-inducing role of mesenteric lymph node macrophages during colitis. *Eur. J. Immunol.* 2012. **42**: 3150–3166.

1447 **Bain, C. C., Scott, C. L., Uronen-Hansson, H., Gudjonsson, S., Jansson, O., Grip, O., Guilliams, M. et al.**, Resident and pro-inflammatory macrophages in the colon represent alternative context-dependent fates of the same Ly6Chi monocyte precursors. *Mucosal Immunol* 2013. **6**: 498–510.

1448 **Heidkamp, G. F., Sander, J., Lehmann, C. H. K., Heger, L., Eissing, N., Heger, L., Baranska, A. et al.**, Human lymphoid organ dendritic cell identity is predominantly dictated by ontogeny, not tissue microenvironment. *Sci. Immunol.* 2016. **1**: pii: eaai7677.

1449 **Alcántara-Hernández, M., Leylek, R., Wagar, L. E., Engleman, E. G., Keler, T., Marinkovich, M. P., Davis, M. M. et al.**, High-Dimensional Phenotypic Mapping of Human Dendritic Cells Reveals Interindividual Variation and Tissue Specialization. *Immunity*. 2017. **47**: 1037–1050.e6.

1450 **See, P., Dutertre, C. A., Chen, J., Gunther, P., McGovern, N., Irac, S. E., Gunawan, M. et al.**, Mapping the human DC lineage through the integration of high-dimensional techniques. *Science* 2017. **356**: eaag3009.

1451 **Ziegler-Heitbrock, L., Ancuta, P., Crowe, S., Dalod, M., Grau, V., Hart, D. N., Leenen, P. J. et al.**, Nomenclature of monocytes and dendritic cells in blood. *Blood* 2010. **116**: e74–80.

1452 **Briseno, C. G., Haldar, M., Kretzer, N. M., Wu, X., Theisen, D. J., Kc, W., Durai, V. et al.**, Distinct transcriptional programs control cross-priming in classical and monocyte-derived dendritic cells. *Cell Rep* 2016. **15**: 2462–2474.

1453 **Fujiyama, S., Nakahashi-Oda, C., Abe, F., Wang, Y., Sato, K. and Shibuya, A.**, Identification and isolation of splenic tissue-resident macrophage sub-populations by flow cytometry. *Int. Immunol.* 2019. **31**: 51–56.

1454 **Crozat, K., Guiton, R., Contreras, V., Feuillet, V., Dutertre, C. A., Ventre, E., Vu Manh, T. P. et al.**, The XC chemokine receptor 1 is a conserved selective marker of mammalian cells homologous to mouse CD8alpha+ dendritic cells. *J. Exp. Med.* 2010. **207**: 1283–1292.

1455 **Gurka, S., Hartung, E., Becker, M. and Kroczek, R. A.**, Mouse conventional dendritic cells can be universally classified based on the mutu-

ally exclusive expression of XCR1 and SIRPalpha. *Front Immunol* 2015. **6**: 35.

1456 **Misharin, A. V., Morales-Nebreda, L., Mutlu, G. M., Budinger, G. R. and Perlman, H.**, Flow cytometric analysis of macrophages and dendritic cell subsets in the mouse lung. *Am. J. Respir. Cell Mol. Biol.* 2013. **49**: 503–510.

1457 **Chakarov, S., Lim, H. Y., Tan, L., Lim, S. Y., See, P., Lum, J., Zhang, X. M. et al.**, Two distinct interstitial macrophage populations coexist across tissues in specific subtissular niches. *Science* 2019. **363**.

1458 **Schlitzer, A., McGovern, N., Teo, P., Zelante, T., Atarashi, K., Low, D., Ho, A. W. et al.**, IRF4 transcription factor-dependent CD11b+ dendritic cells in human and mouse control mucosal IL-17 cytokine responses. *Immunity* 2013. **38**: 970–983.

1459 **Shaw, T. N., Houston, S. A., Wemyss, K., Bridgeman, H. M., Barbera, T. A., Zangerle-Murray, T., Strangward, P. et al.**, Tissue-resident macrophages in the intestine are long lived and defined by Tim-4 and CD4 expression. *J. Exp. Med.* 2018. **215**: 1507–1518.

1460 **Takenaka, S., Safroneeva, E., Xing, Z. and Gauldie, J.**, Dendritic cells derived from murine colonic mucosa have unique functional and phenotypic characteristics. *J. Immunol.* 2007. **178**: 7984–7993.

1461 **Johansson-Lindbom, B., Svensson, M., Pabst, O., Palmqvist, C., Marquez, G., Forster, R. and Agace, W. W.**, Functional specialization of gut CD103+ dendritic cells in the regulation of tissue-selective T cell homing. *J. Exp. Med.* 2005. **202**: 1063–1073.

1462 **Harusato, A., Geem, D. and Denning, T. L.**, Macrophage isolation from the mouse small and large intestine. *Methods Mol. Biol.* 2016. **1422**: 171–180.

1463 **Gross, M., Salame, T. M. and Jung, S.**, Guardians of the gut—murine intestinal macrophages and dendritic cells. *Front Immunol* 2015. **6**: 254.

1464 **Helft, J. and Merad, M.**, Isolation of cutaneous dendritic cells. *Methods Mol. Biol.* 2010. **595**: 231–233.

1465 **Benck, C. J., Martinov, T., Fife, B. T. and Chatterjea, D.**, Isolation of infiltrating leukocytes from mouse skin using enzymatic digest and gradient separation. *J Vis Exp* 2016: e53638.

1466 **Forni, M. F., Ramos Maia Lobba, A., Pereira Ferreira, A. H. and Sogayar, M. C.**, Simultaneous isolation of three different stem cell populations from murine skin. *PLoS One* 2015. **10**: e0140143.

1467 **Merad, M., Ginhoux, F. and Collin, M.**, Origin, homeostasis and function of Langerhans cells and other langerin-expressing dendritic cells. *Nat. Rev. Immunol.* 2008. **8**: 935–947.

1468 **Stutte, S., Jux, B., Esser, C. and Forster, I.**, CD24a expression levels discriminate Langerhans cells from dermal dendritic cells in murine skin and lymph nodes. *J. Invest. Dermatol.* 2008. **128**: 1470–1475.

1469 **Malissen, B., Tamoutounour, S. and Henri, S.**, The origins and functions of dendritic cells and macrophages in the skin. *Nat. Rev. Immunol.* 2014. **14**: 417–428.

1470 **Becht, E., McInnes, L., Healy, J., Dutertre, C. A., Kwok, I. W. H., Ng, L. G., Ginhoux, F. et al.**, Dimensionality reduction for visualizing single-cell data using UMAP. *Nat. Biotechnol.* 2019. **37**: 38–44.

1471 **McInnes, L., Healy, J., Saul, N. and Großberger, L.**, UMAP: uniform manifold approximation and projection. *J. Open Source Softw.* 2018. **3**: 861.

1472 **Ester, M., Kriegel, H. P., Sander, J. and Xu, X.**, A density-based algorithm for discovering clusters in large spatial databases with noise. In KDD'96 Proceedings of the Second International Conference on Knowledge Discovery and Data Mining. Portland, OR, 1996, pp. 226–231.

1473 **Levine, J. H., Simonds, E. F., Bendall, S. C., Davis, K. L., Amir el, A. D., Tadmor, M. D., Litvin, O. et al.**, Data-driven phenotypic dissection of AML reveals progenitor-like cells that correlate with prognosis. *Cell* 2015. **162**: 184–197.

1474 **Villani, A. C., Satija, R., Reynolds, G., Sarkizova, S., Shekhar, K., Fletcher, J., Griesbeck, M. et al.**, Single-cell RNA-seq reveals new types of human blood dendritic cells, monocytes, and progenitors. *Science* 2017. **356**: eaaah4573.

1475 **Dutertre, C.-A., Becht, E., Irac, S. E., Khalilnezhad, A., Narang, V., Khalilnezhad, S., Ng, P. Y. et al.**, Single-cell analysis of human mononuclear phagocytes reveals subset-defining markers and identifies circulating inflammatory dendritic cells. *Immunity* 2019. **51**: 573–589.e8.

1476 **Casanova-Acebes, M., Pitaval, C., Weiss, L. A., Nombela-Arrieta, C., Chevre, R., N, A. G., Kunisaki, Y., Zhang, D. et al.**, Rhythmic modulation of the hematopoietic niche through neutrophil clearance. *Cell* 2013. **153**: 1025–1035.

1477 **Maueroder, C., Mahajan, A., Paulus, S., Gosswein, S., Hahn, J., Kienhofer, D., Biermann, M. H. et al.**, Menage-a-Trois: the ratio of bicarbonate to CO_2 and the pH regulate the capacity of neutrophils to form NETs. *Front. Immunol.* 2016. **7**: 583.

1478 **Evrard, M., Kwok, I. W. H., Chong, S. Z., Teng, K. W. W., Becht, E., Chen, J., Sieow, J. L. et al.**, Developmental analysis of bone marrow neutrophils reveals populations specialized in expansion, trafficking, and effector functions. *Immunity* 2018. **48**: 364–379 e368.

1479 **Kim, M. H., Yang, D., Kim, M., Kim, S. Y., Kim, D. and Kang, S. J.**, A late-lineage murine neutrophil precursor population exhibits dynamic changes during demand-adapted granulopoiesis. *Sci. Rep.* 2017. **7**: 39804.

1480 **Zhu, Y. P., Padgett, L., Dinh, H. Q., Marcovecchio, P., Blatchley, A., Wu, R., Ehinger, E. et al.**, Identification of an early unipotent neutrophil progenitor with pro-tumoral activity in mouse and human bone marrow. *Cell Rep.* 2018. **24**: 2329–2341 e2328.

1481 **Geering, B., Stoeckle, C., Conus, S. and Simon, H. U.**, Living and dying for inflammation: neutrophils, eosinophils, basophils. *Trends Immunol.* 2013. **34**: 398–409.

1482 **Borregaard, N.**, Neutrophils, from marrow to microbes. *Immunity* 2010. **33**: 657–670.

1483 **Ley, K., Hoffman, H. M., Kubes, P., Cassatella, M. A., Zychlinsky, A., Hedrick, C. C. and Catz, S. D.**, Neutrophils: new insights and open questions. *Sci. Immunol.* 2018. **3**.

1484 **Ng, L. G., Ostuni, R. and Hidalgo, A.**, Heterogeneity of neutrophils. *Nat. Rev. Immunol.* 2019. **19**: 255–265.

1485 **Terstappen, L. W., Safford, M. and Loken, M. R.**, Flow cytometric analysis of human bone marrow. III. Neutrophil maturation. *Leukemia* 1990. **4**: 657–663.

1486 **Satake, S., Hirai, H., Hayashi, Y., Shime, N., Tamura, A., Yao, H., Yoshioka, S. et al.**, C/EBPbeta is involved in the amplification of early granulocyte precursors during candidemia-induced "emergency" granulopoiesis. *J. Immunol.* 2012. **189**: 4546–4555.

1487 **Theilgaard-Monch, K., Jacobsen, L. C., Borup, R., Rasmussen, T., Bjerregaard, M. D., Nielsen, F. C., Cowland, J. B. et al.**, The transcriptional program of terminal granulocytic differentiation. *Blood* 2005. **105**: 1785–1796.

1488 **Garley, M. and Jablonska, E.**, Heterogeneity among neutrophils. *Arch. Immunol. Ther. Exp.* 2018. **66**: 21–30.

1489 **Scapini, P., Marini, O., Tecchio, C. and Cassatella, M. A.**, Human neutrophils in the saga of cellular heterogeneity: insights and open questions. *Immunol. Rev.* 2016. **273**: 48–60.

1490 **Coffelt, S. B., Kersten, K., Doornebal, C. W., Weiden, J., Vrijland, K., Hau, C. S., Verstegen, N. J. M. et al.**, IL-17-producing gammadelta

T cells and neutrophils conspire to promote breast cancer metastasis. *Nature* 2015. **522**: 345–348.

1491 **Engblom, C., Pfirschke, C., Zilionis, R., Da Silva Martins, J., Bos, S. A., Courties, G., Rickelt, S. et al.**, Osteoblasts remotely supply lung tumors with cancer-promoting SiglecF(high) neutrophils. *Science* 2017. **358**: eaal5081.

1492 **Youn, J. I., Collazo, M., Shalova, I. N., Biswas, S. K. and Gabrilovich, D. I.**, Characterization of the nature of granulocytic myeloid-derived suppressor cells in tumor-bearing mice. *J. Leukoc. Biol.* 2012. **91**: 167–181.

1493 **McAlpine, C. S., Kiss, M. G., Rattik, S., He, S., Vassalli, A., Valet, C., Anzai, A. et al.**, Sleep modulates haematopoiesis and protects against atherosclerosis. *Nature* 2019. **566**: 383–387.

1494 **Grassi, L., Pourfarzad, F., Ullrich, S., Merkel, A., Were, F., Carrillo-de-Santa-Pau, E., Yi, G. et al.**, Dynamics of transcription regulation in human bone marrow myeloid differentiation to mature blood neutrophils. *Cell Rep.* 2018. **24**: 2784–2794.

1495 **Friedenstein, A. J., Chailakhjan, R. K. and Lalykina, K. S.**, The development of fibroblast colonies in monolayer cultures of guinea-pig bone marrow and spleen cells. *Cell Tissue Kinet.* 1970. **3**: 393–403.

1496 **Friedenstein, A. J., Chailakhyan, R. K., Latsinik, N. V., Panasyuk, A. F. and Keiliss-Borok, I. V.**, Stromal cells responsible for transferring the microenvironment of the hemopoietic tissues. Cloning in vitro and retransplantation in vivo. *Transplantation* 1974. **17**: 331–340.

1497 **Frenette, P. S., Pinho, S., Lucas, D. and Scheiermann, C.**, Mesenchymal stem cell: keystone of the hematopoietic stem cell niche and a stepping-stone for regenerative medicine. *Annu. Rev. Immunol.* 2013. **31**: 285–316.

1498 **Pinho, S. and Frenette, P. S.**, Haematopoietic stem cell activity and interactions with the niche. *Nat. Rev. Mol. Cell Biol.* 2019.

1499 **Chan, C. K., Chen, C. C., Luppen, C. A., Kim, J. B., DeBoer, A. T., Wei, K., Helms, J. A. et al.**, Endochondral ossification is required for haematopoietic stem-cell niche formation. *Nature* 2009. **457**: 490–494.

1500 **Mendez-Ferrer, S., Michurina, T. V., Ferraro, F., Mazloom, A. R., Macarthur, B. D., Lira, S. A., Scadden, D. T. et al.**, Mesenchymal and haematopoietic stem cells form a unique bone marrow niche. *Nature* 2010. **466**: 829–834.

1501 **Kunisaki, Y., Bruns, I., Scheiermann, C., Ahmed, J., Pinho, S., Zhang, D., Mizoguchi, T. et al.**, Arteriolar niches maintain haematopoietic stem cell quiescence. *Nature* 2013. **502**: 637–643.

1502 **Zhou, B. O., Yue, R., Murphy, M. M., Peyer, J. G. and Morrison, S. J.**, Leptin-receptor-expressing mesenchymal stromal cells represent the main source of bone formed by adult bone marrow. *Cell Stem Cell* 2014. **15**: 154–168.

1503 **Omatsu, Y., Sugiyama, T., Kohara, H., Kondoh, G., Fujii, N., Kohno, K. and Nagasawa, T.**, The essential functions of adipo-osteogenic progenitors as the hematopoietic stem and progenitor cell niche. *Immunity* 2010. **33**: 387–399.

1504 **Greenbaum, A., Hsu, Y. M., Day, R. B., Schuettpelz, L. G., Christopher, M. J., Borgerding, J. N., Nagasawa, T. et al.**, CXCL12 in early mesenchymal progenitors is required for haematopoietic stem-cell maintenance. *Nature* 2013. **495**: 227–230.

1505 **Mizoguchi, T., Pinho, S., Ahmed, J., Kunisaki, Y., Hanoun, M., Mendelson, A., Ono, N. et al.**, Osterix marks distinct waves of primitive and definitive stromal progenitors during bone marrow development. *Dev. Cell* 2014. **29**: 340–349.

1506 **Chan, C. K., Seo, E. Y., Chen, J. Y., Lo, D., McArdle, A., Sinha, R., Tevlin, R. et al.**, Identification and specification of the mouse skeletal stem cell. *Cell* 2015. **160**: 285–298.

1507 **Marecic, O., Tevlin, R., McArdle, A., Seo, E. Y., Wearda, T., Duldulao, C., Walmsley, G. G. et al.**, Identification and characterization of an injury-induced skeletal progenitor. *Proc Natl Acad Sci USA* 2015. **112**: 9920–9925.

1508 **Debnath, S., Yallowitz, A. R., McCormick, J., Lalani, S., Zhang, T., Xu, R., Li, N. et al.**, Discovery of a periosteal stem cell mediating intramembranous bone formation. *Nature* 2018. **562**: 133–139.

1509 **Dominici, M., Le Blanc, K., Mueller, I., Slaper-Cortenbach, I., Marini, F., Krause, D., Deans, R. et al.**, Minimal criteria for defining multipotent mesenchymal stromal cells. The International Society for Cellular Therapy position statement. *Cytotherapy* 2006. **8**: 315–317.

1510 **Suire, C., Brouard, N., Hirschi, K. and Simmons, P. J.**, Isolation of the stromal-vascular fraction of mouse bone marrow markedly enhances the yield of clonogenic stromal progenitors. *Blood* 2012. **119**: e86–95.

1511 **Pinho, S., Lacombe, J., Hanoun, M., Mizoguchi, T., Bruns, I., Kunisaki, Y. and Frenette, P. S.**, PDGFRalpha and CD51 mark human nestin+ sphere-forming mesenchymal stem cells capable of hematopoietic progenitor cell expansion. *J. Exp. Med.* 2013. **210**: 1351–1367.

1512 **Morikawa, S., Mabuchi, Y., Kubota, Y., Nagai, Y., Niibe, K., Hiratsu, E., Suzuki, S. et al.**, Prospective identification, isolation, and systemic transplantation of multipotent mesenchymal stem cells in murine bone marrow. *J. Exp. Med.* 2009. **206**: 2483–2496.

1513 **Houlihan, D. D., Mabuchi, Y., Morikawa, S., Niibe, K., Araki, D., Suzuki, S., Okano, H. et al.**, Isolation of mouse mesenchymal stem cells on the basis of expression of Sca-1 and PDGFR-alpha. *Nat. Protoc.* 2012. **7**: 2103–2111.

1514 **Worthley, D. L., Churchill, M., Compton, J. T., Tailor, Y., Rao, M., Si, Y., Levin, D. et al.**, Gremlin 1 identifies a skeletal stem cell with bone, cartilage, and reticular stromal potential. *Cell* 2015. **160**: 269–284.

1515 **Boulais, P. E., Mizoguchi, T., Zimmerman, S., Nakahara, F., Vivie, J., Mar, J. C., van Oudenaarden, A. et al.**, The majority of CD45(-) Ter119(-) CD31(-) bone marrow cell fraction is of hematopoietic origin and contains erythroid and lymphoid progenitors. *Immunity* 2018. **49**: 627–639, e626.

1516 **Morrison, S. J., Uchida, N. and Weissman, I. L.**, The biology of hematopoietic stem cells. *Annu. Rev. Cell. Dev. Biol.* 1995. **11**: 35–71.

1517 **Spangrude, G. J., Brooks, D. M. and Tumas, D. B.**, Long-term repopulation of irradiated mice with limiting numbers of purified hematopoietic stem cells: in vivo expansion of stem cell phenotype but not function. *Blood* 1995. **85**(4): 1006–1016.

1518 **Cheshier, S. H., Morrison, S. J., Liao, X. and Weissman, I. L.**, In vivo proliferation and cell cycle kinetics of long-term self-renewing hematopoietic stem cells. *Proc. Natl. Acad. Sci. USA* 1999. **96**(6): 3120–3125.

1519 **Calvi, L. M., Adams, G. B., Weibrecht, K. W., Weber, J. M., Olson, D. P., Knight, M. C., Martin, R. P. et al.**, Osteoblastic cells regulate the haematopoietic stem cell niche. *Nature* 2003. **425**(6960): 841–846.

1520 **Arai, F., Hirao, A., Ohmura, M., Sato, H., Matsuoka, S., Takubo, K., Ito, K. et al.**, Tie2/angiopoietin-1 signaling regulates hematopoietic stem cell quiescence in the bone marrow niche. *Cell* 2004. **118**(2): 149–161.

1521 **Zhang, J., Niu, C., Ye, L., Huang, H., He, X., Tong, W. G., Ross, J. et al.**, Identification of the haematopoietic stem cell niche and control of the niche size. *Nature* 2003. **425**(6960): 836–841.

1522 **Hofer, T., Busch, K., Klapproth, K. and Rodewald, H. R.**, Fate mapping and quantitation of hematopoiesis in vivo. *Annu. Rev. Immunol.* 2016. **34**: 449–478.

1523 **Carrelha, J., Meng, Y., Kettyle, L. M., Luis, T. C., Norfo, R., Alcolea, V., Boukarabila, H. et al.**, Hierarchically related lineage-restricted fates of

multipotent haematopoietic stem cells. *Nature* 2018. **554**(7690): 106–111.

1524 **Haas, S., Hansson, J., Klimmeck, D., Loeffler, D., Velten, L., Uckelmann, H., Wurzer, S. et al.**, Inflammation-induced emergency megakaryopoiesis driven by hematopoietic stem cell-like megakaryocyte progenitors. *Cell Stem Cell* 2015. **17**(4): 422–434.

1525 **Medvinsky, A., Rybtsov, S. and Taoudi, S.**, Embryonic origin of the adult hematopoietic system: advances and questions. *Development* 2011. **138**(6): 1017–1031.

1526 **Kajikhina, K., Melchers, F. and Tsuneto, M.**, Chemokine polyreactivity of IL7Ralpha+CSF-1R+ lympho-myeloid progenitors in the developing fetal liver. *Sci. Rep.* 2015. **5**: 12817.

1527 **Mikkola, H. K. and Orkin, S. H.**, The journey of developing hematopoietic stem cells. *Development* 2006. **133**(19): 3733–3744.

1528 **Majeti, R., Park, C. Y., Weissman, I. L.**, Identification of a hierarchy of multipotent hematopoietic progenitors in human cord blood. *Cell Stem Cell* 2007. **1**(6): 635–645.

1529 **Notta, F., Zandi, S., Takayama, N., Dobson, S., Gan, O. I., Wilson, G., Kaufmann, K. B. et al.**, Distinct routes of lineage development reshape the human blood hierarchy across ontogeny. *Science* 2016. **351**(6269): aab2116.

1530 **Cosgun, K. N., Rahmig, S., Mende, N., Reinke, S., Hauber, I., Schafer, C., Petzold, A. et al.**, Kit regulates HSC engraftment across the human-mouse species barrier. *Cell Stem Cell* 2014. **15**(2): 227–238.

1531 **Kiel, M. J., Yilmaz, O. H., Iwashita, T., Yilmaz, O. H., Terhorst, C. and Morrison, S. J.**, SLAM family receptors distinguish hematopoietic stem and progenitor cells and reveal endothelial niches for stem cells. *Cell* 2005. **121**(7): 1109–1121.

1532 **Papathanasiou, P., Attema, J. L., Karsunky, H., Xu, J., Smale, S. T. and Weissman, I. L.**, Evaluation of the long-term reconstituting subset of hematopoietic stem cells with CD150. *Stem Cells* 2009. **27**(10): 2498–2508.

1533 **Yilmaz, O. H., Kiel, M. J. and Morrison, S. J.**, SLAM family markers are conserved among hematopoietic stem cells from old and reconstituted mice and markedly increase their purity. *Blood* 2006. **107**(3): 924–930.

1534 **Pei, W., Feyerabend, T. B., Rossler, J., Wang, X., Postrach, D., Busch, K., Rode, I. et al.**, Polylox barcoding reveals haematopoietic stem cell fates realized in vivo. *Nature* 2017. **548**(7668): 456–460.

1535 **Busch, K., Klapproth, K., Barile, M., Flossdorf, M., Holland-Letz, T., Schlenner, S. M., Reth, M. et al.**, Fundamental properties of unperturbed haematopoiesis from stem cells in vivo. *Nature* 2015. **518**(7540): 542–546.

1536 **Gomez Perdiguero, E., Klapproth, K., Schulz, C., Busch, K., Azzoni, E., Crozet, L., Garner, H. et al.**, Tissue-resident macrophages originate from yolk-sac-derived erythro-myeloid progenitors. *Nature* 2015. **518**(7540): 547–551.

1537 **Tornack, J., Reece, S. T., Bauer, W. M., Vogelzang, A., Bandermann, S., Zedler, U., Stingl, G. et al.**, Human and Mouse Hematopoietic Stem Cells Are a Depot for Dormant Mycobacterium tuberculosis. *PLoS One* 2017. **12**(1): e0169119.

1538 **Spangrude, G. J., Heimfeld, S. and Weissman, I. L.**, Purification and characterization of mouse hematopoietic stem cells. *Science* 1988. **241**(4861): 58–62.

1539 **Ikuta, K. and Weissman, I. L.**, Evidence that hematopoietic stem cells express mouse c-kit but do not depend on steel factor for their generation. *Proc. Natl. Acad. Sci. USA* 1992. **89**(4): 1502–1506.

1540 **Morrison, S. J. and Weissman, I. L.**, The long-term repopulating subset of hematopoietic stem cells is deterministic and isolatable by phenotype. *Immunity* 1994. **1**(8): 661–673.

1541 **Okada, S., Nakauchi, H., Nagayoshi, K., Nishikawa, S., Miura, Y. and Suda, T.**, In vivo and in vitro stem cell function of c-kit- and Sca-1-positive murine hematopoietic cells. *Blood* 1992. **80**: 3044–3050.

1542 **Balazs, A. B., Fabian, A. J., Esmon, C. T. and Mulligan, R. C.**, Endothelial protein C receptor (CD201) explicitly identifies hematopoietic stem cells in murine bone marrow. *Blood* 2006. **107**: 2317–2321.

1543 **Osawa, M., Hanada, K., Hamada, H. and Nakauchi, H.**, Long-term lymphohematopoietic reconstitution by a single CD34-low/negative hematopoietic stem cell. *Science* 1996. **273**: 242–245.

1544 **Tornack, J., Kawano, Y., Garbi, N., Hammerling, G. J., Melchers, F. and Tsuneto, M.**, Flt3 ligand-eGFP-reporter expression characterizes functionally distinct subpopulations of CD150(+) long-term repopulating murine hematopoietic stem cells. *Eur. J. Immunol.* 2017. **47**: 1477–1487.

1545 **Zhou, S., Schuetz, J. D., Bunting, K. D., Colapietro, A. M., Sampath, J., Morris, J. J., Lagutina, I. et al.**, The ABC transporter Bcrp1/ABCG2 is expressed in a wide variety of stem cells and is a molecular determinant of the side-population phenotype. *Nat. Med.* 2001. **7**: 1028–1034.

1546 **Ergen, A. V., Jeong, M., Lin, K. K., Challen, G. A., Goodell, M. A.**, Isolation and characterization of mouse side population cells. *Methods Mol. Biol.* 2013. **946**: 151–162.

1547 **Lu, R., Neff, N. F., Quake, S. R. and Weissman, I. L.**, Tracking single hematopoietic stem cells in vivo using high-throughput sequencing in conjunction with viral genetic barcoding. *Nat. Biotechnol.* 2011. **29**: 928–933.

1548 **Bystrykh, L. V., de Haan, G. and Verovskaya, E.**, Barcoded vector libraries and retroviral or lentiviral barcoding of hematopoietic stem cells. *Methods Mol. Biol.* 2014. **1185**: 345–360.

1549 **Kawano, Y., Petkau, G., Stehle, C., Durek, P., Heinz, G. A., Tanimoto, K., Karasuyama, H. et al.**, Stable lines and clones of long-term proliferating normal, genetically unmodified murine common lymphoid progenitors. *Blood* 2018. **131**(18): 2026–2035.

1550 **Knapp, D. J., Hammond, C. A., Miller, P. H., Rabu, G. M., Beer, P. A., Ricicova, M., Lecault, V. et al.**, Dissociation of survival, proliferation, and state control in human hematopoietic stem cells. *Stem Cell Rep.* 2017. **8**(1): 152–162.

1551 **Yamamoto, R., Morita, Y., Ooehara, J., Hamanaka, S., Onodera, M., Rudolph, K. L., Ema, H. et al.**, Clonal analysis unveils self-renewing lineage-restricted progenitors generated directly from hematopoietic stem cells. *Cell* 2013. **154**(5): 1112–1126.

1552 **Uchida, N. and Weissman, I. L.**, Searching for hematopoietic stem cells: evidence that Thy-1.1lo Lin- Sca-1+ cells are the only stem cells in C57BL/Ka-Thy-1.1 bone marrow. *J. Exp. Med.* 1992. **175**(1): 175–184.

1553 **Murray, L., Chen, B., Galy, A., Chen, S., Tushinski, R., Uchida, N., Negrin, R. et al.**, Enrichment of human hematopoietic stem cell activity in the CD34+Thy-1+Lin- subpopulation from mobilized peripheral blood. *Blood* 1995. **85**(2): 368–378.

1554 **Civin, C. I., Strauss, L. C., Brovall, C., Fackler, M. J., Schwartz, J. F. and Shaper, J. H.**, Antigenic analysis of hematopoiesis. III. A hematopoietic progenitor cell surface antigen defined by a monoclonal antibody raised against KG-1a cells. *J. Immunol.* 1984. **133**(1): 157–165.

1555 **Goodell, M. A., Rosenzweig, M., Kim, H., Marks, D. F., DeMaria, M., Paradis, G., Grupp, S. A. et al.**, Dye efflux studies suggest that hematopoietic stem cells expressing low or undetectable levels of CD34 antigen exist in multiple species. *Nat. Med.* 1997. **3**(12): 1337–1345.

1556 **Kang, Y., Chao, N. J., Aversa, F.**, Unmanipulated or CD34 selected haplotype mismatched transplants. *Curr. Opin. Hematol.* 2008. **15**(6): 561–567.

1557 **Wang, J., Kimura, T., Asada, R., Harada, S., Yokota, S., Kawamoto, Y., Fujimura, Y. et al.**, SCID-repopulating cell activity of human cord

blood-derived CD34- cells assured by intra-bone marrow injection. *Blood* 2003. **101**(8): 2924–2931.

1558 **Bhatia, M., Bonnet, D., Murdoch, B., Gan, O. I. and Dick, J. E.**, A newly discovered class of human hematopoietic cells with SCID-repopulating activity. *Nat. Med.* 1998. **4**(9): 1038–1045.

1559 **Danet, G. H., Luongo, J. L., Butler, G., Lu, M. M., Tenner, A. J., Simon, M. C. and Bonnet, D. A.**, C1qRp defines a new human stem cell population with hematopoietic and hepatic potential. *Proc. Natl. Acad. Sci. USA* 2002. **99**(16): 10441–10445.

1560 **Herbein, G., Sovalat, H., Wunder, E., Baerenzung, M., Bachorz, J., Lewandowski, H., Schweitzer, C. et al.**, Isolation and identification of two CD34+ cell subpopulations from normal human peripheral blood. *Stem Cells* 1994. **12**: 187–197.

1561 **Bhatia, M., Wang, J. C., Kapp, U., Bonnet, D. and Dick, J. E.**, Purification of primitive human hematopoietic cells capable of repopulating immune-deficient mice. *Proc. Natl. Acad. Sci. USA* 1997. **94**(10): 5320–5325.

1562 **Notta, F., Doulatov, S., Laurenti, E., Poeppl, A., Jurisica, I. and Dick, J. E.**, Isolation of single human hematopoietic stem cells capable of long-term multilineage engraftment. *Science* 2011. **333**(6039): 218–221.

1563 **Fares, I., Chagraoui, J., Lehnertz, B., MacRae, T., Mayotte, N., Tomellini, E., Aubert, L. et al.**, EPCR expression marks UM171-expanded CD34(+) cord blood stem cells. *Blood* 2017. **129**(25): 3344–3351.

1564 **Iwasaki, H., Arai, F., Kubota, Y., Dahl, M., Suda, T.**, Endothelial protein C receptor-expressing hematopoietic stem cells reside in the perisinusoidal niche in fetal liver. *Blood* 2010. **116**(4): 544–553.

1565 **Galuzzi, L., Vacchelli, E., Bravo-San Pedro, J. M., Buqué, A., Senovilla, L., Baracco, E. E., Bloy, N. et al.**, Classification of current anticancer immunotherapies. *Oncotarget* 2015. **5**(24): 12472–12508.

1566 **Hanahan, D. and Weinberg, R. A.**, Hallmarks of cancer – the next generation. *Cell* 2011. **144**: 646–674. https://doi.org/10.1016/j.cell.2011.02.013

1567 **Lansdorp, P. M., Sutherland, H. J. and Eaves, C. J.**, Selective expression of CD45 isoforms on functional subpopulations of CD34+ hemopoietic cells from human bone marrow. *J. Exp. Med.* 1990. **172**: 363–366. https://doi.org/363-3660022-1007/90/07/0363/04

1568 **van Dongen, J. J. M., Lhermitte, L., Böttcher, S., Almeida, J., van der Velden, J. V. H., Flores-Montero, J., Rawstron, A. et al., on behalf of the EuroFlow Consortium (EU-FP6, LSHB-CT-2006-018708)**. EuroFlow antibody panels for standardized n-dimensional flow cytometric immunophenotyping of normal, reactive and malignant leukocytes. *Leukemia* 2012. **26**: 1908–1975.

1569 **Streitz, M., Miloud, T., Kapinsky, M., Reed, M. R., Magari, R., Geissler, E. K., Hutchinson, J. A. et al.**, Standardization of whole blood immune phenotype monitoring for clinical trials: panels and methods from the ONE study. *Transplant Res.* 2013. **2**(1): 17.

1570 **Alix-Panabières, C. and Pantel, K.**, Challenges in circulating tumour cell research. *Nat. Rev. Cancer* 2014. **14**: 623–631. https://doi.org/10.1038/nrc3820

1571 **Lopresti, A., Malergue, F., Bertucci, F., Liberatoscioli, M. L., Garnier, S., DaCosta, Q., Finetti, P. et al.**, Sensitive and easy screening for circulating tumor cells by flow cytometry. *JCI Insight.* 2019. 5: 128180. https://doi.org/10.1172/jci.insight.128180

1572 **Schumacher, T. and Schreiber, R. D.**, Neoantigens in cancer immunotherapy. *Science* 2015. **348**(6230): 69–74.

1573 **Grizzi, F., Mirandola, L., Qehajaj, D., Cobos, E., Figueroa, J. A. and Chiriva-Internati, M.**, Cancer-testis antigens and immunotherapy in the light of cancer complexity. *Int. Rev. Immunol.* 2015. **34**: 143–153. https://doi.org/10.3109/08830185.2015.1018418

1574 **Garrido, F., Aptsiauri, N., Doorduijn, E. M., Garcia Lora, A. M. and van Hall, T.**, The urgent need to recover MHC class I in cancers for effective immunotherapy. *Curr. Opin. Immunol.* 2016. **39**: 44–51. https://doi.org/10.1016/j.coi.2015.12.007

1575 **Raulet, D. H., Gasser, S., Gowen, B. G., Deng, W. and Jung, H.**, Regulation of ligands for the NKG2D activating receptor. *Annu. Rev. Immunol.* 2013. **31**: 413–441.

1576 **Sers, C., Kuner, R., Fak, C. S., Lund, P., Sueltmann, H., Braun, M., Buness, A. et al.**, Down-regulation of HLA Class I and NKG2D ligands through a concerted action of MAPK and DNA methyltransferases in colorectal cancer cells. *Int. J. Cancer* 2009. **125**(7): 1626–1639.

1577 **Luo, Z., Wu, R. R., Lv, L., Li, P., Zhang, L. Y., Hao, Q. L. and Li, W.**, Prognostic value of CD44 expression in non-small cell lung cancer: a systematic review. *Int. J. Clin. Exp. Pathol.* 2014. **7**(7): 3632–3646.

1578 **Paulis, Y. W., Huijbers, E. J., van der Schaft, D. W., Soetekouw, P. M., Pauwels, P., Tjan-Heijnen, V. C. and Griffioen, A. W.**, CD44 enhances tumor aggressiveness by promoting tumor cell plasticity. *Oncotarget* 2015. **6**(23): 19634–19646.

1579 http://www.cancerresearchuk.org/about-cancer/what-is-cancer/how-cancer-starts/types-of-cancer#carcinomas

1580 **Weng, Y. R., Cui, Y. and Fang, J. Y.**, Biological functions of cytokeratin 18 in cancer. *Mol. Cancer Res.* 2012. **10**(4); 485–493.

1581 **Appert-Collin, A., Hubert, P., Crémel, G. and Bennasroune, A.**, Role of ErbB receptors in cancer cell migration and invasion. *Front. Pharmacol.* 2015. https://doi.org/10.3389/fphar.2015.00283

1582 http://www.cancer.org/cancer/breastcancer/detailedguide/breast-cancer-breast-cancer-types

1583 **Park, J. W., Lee, J. K., Phillips, J. W., Huang, P., Cheng, D., Huang, J. and Witte, O. N.**, Prostate epithelial cell of origin determines cancer differentiation state in an organoid transformation assay. *Proc. Natl. Acad. Sci. USA* 2016. **113**: 4482–4487.

1584 http://screening.iarc.fr/colpochap.php?chap=2

1585 https://www.iarc.fr/en/publications/pdfs-online/pat-gen/bb2/bb2-chap1.pdf

1586 http://www.cancer.org/cancer/bladdercancer/detailedguide/bladder-cancer-what-is-bladder-cancer

1587 **Hruban, R. H. and Fukushima, N.**, Pancreatic adenocarcinoma: update on the surgical pathology of carcinomas of ductal origin and PanINs. *Modern Pathol.* 2007. **20**: 61–70.

1588 **DuBois, S. G., Epling, C. L., Teague, J., Matthay, K. K. and Sinclair, E.**, Flow cytometric detection of ewing sarcoma cells in peripheral blood and bone marrow. *Pediatr. Blood Cancer* 2010. **54**(1): 13–18. https://doi.org/10.1002/pbc.22245

1589 **Avey, D., Brewers, B. and Zhu, F.**, Recent advances in the study of Kaposi's sarcoma-associated herpesvirus replication and athogenesis. *Virol Sin.* 2015. **30**(2): 130-145. https://doi.org/10.1007/s12250-015-3595-2

1590 **Deel, M. D., Li, J. J., Crose, L. E. and Linardic, C. M.**, A Review: molecular aberrations within hippo signaling in bone and soft-tissue sarcomas. *Front Oncol.* 2015. **5**: 190. https://doi.org/10.3389/fonc.2015.00190

1591 **Sullivan, R. J.**, The role of mitogen-activated protein targeting in melanoma beyond BRAFV600. *Curr. Opin. Oncol.* 2016. **28**(2): 185–191.

1592 **Sucker, A., Zhao, F., Real, B., Heeke, C., Bielefeld, N., Maßen, S., Horn, S. et al.**, Genetic evolution of T cell resistance in the course of melanoma progression. *Clin. Canc. Res.* 2014. **20**(24): 6593–6604.

1593 **Lakshmikanth, T., Burke, S., Ali, T. H., Kimpfler, S., Ursini, F., Ruggeri, L., Capanni, M. et al.**, NCRs and DNAM-1 mediate NK cell recognition

and lysis of human and mouse melanoma cell lines in vitro and in vivo. *J. Clin. Invest.* 2009. **119**(5): 1251–1263. https://doi.org/10.1172/JCI36022

1594 **Binder, D. C., Davis, A. A. and Wainwright, D. A.**, Immunotherapy for cancer in the central nervous system: Current and future directions. *Oncoimmunology* 2015. **5**(2): e1082027.

1595 **Razavi, S. M., Lee, K. E., Jin, B. E., Aujla, P. S., Gholamin, S. and Li, G.**, Immune Evasion Strategies of Glioblastoma. *Frnt. Surg.* 2016. **3**: 11.

1596 **Seifert, M., Garbe, M., Friedrich, B., Mittelbronn, M. and Klink, B.**, Comparative transcriptomics reveals similarities and differences between astrocytoma grades. *BMC Cancer* 2015. **15**: 952.

1597 **Dranoff, G.**, Experimental mouse tumour models: what can be learnt about human cancer immunology? *Nat. Rev. Immunol.* 2012. **12**: 61–66. https://doi.org/10.1038/nri3129

1598 **Morton, J. J., Bird, G., Fefaeli, Y. and Jimeno, A.**, Humanized mouse xenograft models: narrowing the tumor-microenvironment gap. *Canc. Res.* 2016. **76**: 6153–6158.

1599 **Huntington, N. D., Xu, Y., Puthalakath, H., Light, A., Willis, S. N., Strasser, A. et al.**, CD45 links the B cell receptor with cell survival and is required for the persistence of germinal centers. *Nat. Immunol.* 2006. **7**(2): 190–198.

1600 **Oracki, S. A., Walker, J. A., Hibbs, M. L., Corcoran, L. M. and Tarlinton, D. M.**, Plasma cell development and survival. *Immunol. Rev.* 2010. **237**(1): 140–159.

1601 **Brynjolfsson, S. F., Persson Berg, L., Olsen Ekerhult, T., Rimkute, I., Wick, M. J., Martensson, I. L. et al.**, Long-lived plasma cells in mice and men. *Front. Immunol.* 2018. **9**: 2673.

1602 **Steensma, D. P., Gertz, M. A., Greipp, P. R., Kyle, R. A., Lacy, M. Q., Lust, J. A. et al.**, A high bone marrow plasma cell labeling index in stable plateau-phase multiple myeloma is a marker for early disease progression and death. *Blood* 2001. **97**(8): 2522–2523.

1603 **Bakkus, M. H., Heirman, C., Van Riet, I., Van Camp, B. and Thielemans, K.**, Evidence that multiple myeloma Ig heavy chain VDJ genes contain somatic mutations but show no intraclonal variation. *Blood* 1992. **80**(9): 2326–2335.

1604 **Kosmas, C., Stamatopoulos, K., Stavroyianni, N., Zoi, K., Belessi, C., Viniou, N. et al.**, Origin and diversification of the clonogenic cell in multiple myeloma: lessons from the immunoglobulin repertoire. *Leukemia* 2000. **14**(10): 1718–1726.

1605 **Pfeifer, S., Perez-Andres, M., Ludwig, H., Sahota, S. S. and Zojer, N.**, Evaluating the clonal hierarchy in light-chain multiple myeloma: implications against the myeloma stem cell hypothesis. *Leukemia* 2011. **25**(7): 1213–1216.

1606 **Hansmann, L., Han, A., Penter, L., Liedtke, M. and Davis, M. M.**, Clonal expansion and interrelatedness of distinct B-lineage compartments in multiple myeloma bone marrow. *Cancer Immunol. Res.* 2017. **5**: 744–754.

1607 **Hideshima, T., Nakamura, N., Chauhan, D. and Anderson, K. C.**, Biologic sequelae of interleukin-6 induced PI3-K/Akt signaling in multiple myeloma. *Oncogene* 2001. **20**(42): 5991–6000.

1608 **de Haart, S. J., van de Donk, N. W., Minnema, M. C., Huang, J. H., Aarts-Riemens, T., Bovenschen, N. et al.**, Accessory cells of the microenvironment protect multiple myeloma from T-cell cytotoxicity through cell adhesion-mediated immune resistance. *Clin. Cancer Res.* 2013. **19**(20): 5591–5601.

1609 **Hideshima, T., Bergsagel, P. L., Kuehl, W. M. and Anderson, K. C.**, Advances in biology of multiple myeloma: clinical applications. *Blood* 2004. **104**: 607–618.

1610 **Mitsiades, C. S., Mitsiades, N., Munshi, N. C. and Anderson, K. C.**, Focus on multiple myeloma. *Cancer Cell* 2004. **6**(5): 439–444.

1611 **Mitsiades, C. S., Mitsiades, N. S., Richardson, P. G., Munshi, N. C. and Anderson, K. C.**, Multiple myeloma: a prototypic disease model for the characterization and therapeutic targeting of interactions between tumor cells and their local microenvironment. *J. Cell. Biochem.* 2007. **101**(4): 950–968.

1612 **Bianchi, G. and Munshi, N. C.**, Pathogenesis beyond the cancer clone(s) in multiple myeloma. *Blood* 2015. **125**(20): 3049–3058.

1613 **Keats, J. J., Chesi, M., Egan, J. B., Garbitt, V. M., Palmer, S. E., Braggio, E. et al.**, Clonal competition with alternating dominance in multiple myeloma. *Blood* 2012. **120**(5): 1067–1076.

1614 **Lohr, J. G., Kim, S., Gould, J., Knoechel, B., Drier, Y., Cotton, M. J. et al.**, Genetic interrogation of circulating multiple myeloma cells at single-cell resolution. *Sci. Transl. Med.* 2016. **8**(363): 363ra147.

1615 **Lohr, J. G., Stojanov, P., Carter, S. L., Cruz-Gordillo, P., Lawrence, M. S., Auclair, D. et al.**, Widespread genetic heterogeneity in multiple myeloma: implications for targeted therapy. *Cancer Cell* 2014. **25**(1): 91–101.

1616 **Paino, T., Paiva, B., Sayagues, J. M., Mota, I., Carvalheiro, T., Corchete, L. A. et al.**, Phenotypic identification of subclones in multiple myeloma with different chemoresistant, cytogenetic and clonogenic potential. *Leukemia* 2015. **29**(5): 1186–1194.

1617 **Arroz, M., Came, N., Lin, P., Chen, W., Yuan, C., Lagoo, A. et al.**, Consensus guidelines on plasma cell myeloma minimal residual disease analysis and reporting. *Cytom. B Clin. Cytom.* 2016. **90**(1): 31–39.

1618 **Flores-Montero, J., de Tute, R., Paiva, B., Perez, J. J., Bottcher, S., Wind, H. et al.**, Immunophenotype of normal vs. myeloma plasma cells: Toward antibody panel specifications for MRD detection in multiple myeloma. *Cytom. B Clin. Cytom.* 2016. **90**(1): 61–72.

1619 **Jelinek, T. and Hajek, R.**, Monoclonal antibodies—a new era in the treatment of multiple myeloma. *Blood Rev.* 2016. **30**(2): 101–110.

1620 **Paiva, B., Puig, N., Cedena, M. T., de Jong, B. G., Ruiz, Y., Rapado, I. et al.**, Differentiation stage of myeloma plasma cells: biological and clinical significance. *Leukemia* 2017. **31**(2): 382–392.

1621 **Lisenko, K., Schonland, S., Hegenbart, U., Wallenwein, K., Braun, U., Mai, E. K. et al.**, Potential therapeutic targets in plasma cell disorders: a flow cytometry study. *Cytom. B Clin. Cytom.* 2017. **92**(2): 145–152.

1622 **Berliner, N., Ault, K. A., Martin, P. and Weinberg, D. S.**, Detection of clonal excess in lymphoproliferative disease by kappa/lambda analysis: correlation with immunoglobulin gene DNA rearrangement. *Blood* 1986. **67**(1): 80–85.

1623 **Smock, K. J., Perkins, S. L. and Bahler, D. W.**, Quantitation of plasma cells in bone marrow aspirates by flow cytometric analysis compared with morphologic assessment. *Arch. Pathol. Lab. Med.* 2007. **131**(6): 951–955.

1624 **Lokhorst, H. M., Laubach, J. and Nahi, H.**, Dose-dependent efficacy of daratumumab (DARA) as monotherapy in patients with relapsed or refractory multiple myeloma (RR MM). J Clin. Oncol. 2014. 32: abstract 8513.

1625 **Lammerts van Bueren, J., Jakobs, D. and Kaldenhoven, N.**, Direct in vitro comparison of daratumumab with surrogate analogs of CD38 antibodies MOR03087, SAR650984 and Ab79. In: *56th ASH Annual Meeting & Exposition*: Oral and Poster Abstracts, 2014.

1626 **Oberle, A., Brandt, A., Alawi, M., Langebrake, C., Janjetovic, S., Wolschke, C. et al.**, Long-term CD38 saturation by daratumumab interferes with diagnostic myeloma cell detection. *Haematologica* 2017. **102**(9): e368–e370.

1627 **Perincheri, S., Torres, R., Tormey, C. A., Smith, B. R., Rinder, H. M. and Siddon, A. J.**, Daratumumab interferes with flow cytometric evaluation of multiple myeloma. 2016. **128**(22): 5630–5630.

1628 **Malaer, J. D. and Mathew, P. A.**, CS1 (SLAMF7, CD319) is an effective immunotherapeutic target for multiple myeloma. *Am. J. Cancer Res.* 2017. **7**(8): 1637–1641.

1629 **Tellier, J., Shi, W., Minnich, M., Liao, Y., Crawford, S., Smyth, G. K. et al.**, Blimp-1 controls plasma cell function through the regulation of immunoglobulin secretion and the unfolded protein response. *Nat. Immunol.* 2016. **17**(3): 323–330.

1630 **Rawstron, A. C., Orfao, A., Beksac, M., Bezdickova, L., Brooimans, R. A., Bumbea, H. et al.**, Report of the European Myeloma Network on multiparametric flow cytometry in multiple myeloma and related disorders. *Haematologica* 2008. **93**(3): 431–438.

1631 **Paiva, B., Garcia-Sanz, R. and San Miguel, J. F.**, Multiple myeloma minimal residual disease. *Cancer Treat. Res.* 2016. **169**: 103–122.

1632 **Paiva, B., van Dongen, J. J. and Orfao, A.**, New criteria for response assessment: role of minimal residual disease in multiple myeloma. *Blood* 2015. **125**(20): 3059–3068.

1633 **Flores-Montero, J., Sanoja-Flores, L., Paiva, B., Puig, N., Garcia-Sanchez, O., Bottcher, S. et al.**, Next Generation Flow for highly sensitive and standardized detection of minimal residual disease in multiple myeloma. *Leukemia* 2017. **31**(10): 2094–2103.

1634 **Roschewski, M., Stetler-Stevenson, M., Yuan, C., Mailankody, S., Korde, N. and Landgren, O.**, Minimal residual disease: what are the minimum requirements? *J. Clin. Oncol.* 2014. **32**(5): 475–476.

1635 **Cahoy, J. D., Emery, B., Kaushal, A., Foo, L. C., Zamanian, J. L., Christopherson, K. S., Xing, Y. et al.**, A Transcriptome Database for Astrocytes, Neurons, and Oligodendrocytes: A New Resource for Understanding Brain Development and Function. *J. Neurosci.* 2008. **28**: 264–278.

1636 **Hawrylycz, M. J., Lein, E. S., Guillozet-Bongaarts, A. L., Shen, E. H., Ng, L., Miller, J. A., Van De Lagemaat, L. N. et al.**, An anatomically comprehensive atlas of the adult human brain transcriptome. *Nature* 2012. **489**: 391.

1637 **Mink, J. W., Blumenschine, R. J. and Adams, D. B.**, Ratio of central nervous system to body metabolism in vertebrates: its constancy and functional basis. *Am. J. Physiol. Regul. Integr. Comp. Physiol.* 1981. **241**: R203–R212.

1638 **Lake, B. B., Ai, R., Kaeser, G. E., Salathia, N. S., Yung, Y. C., Liu, R., Wildberg, A. et al.**, Neuronal subtypes and diversity revealed by single-nucleus RNA sequencing of the human brain. *Science* 2016. **352**: 1586–1590.

1639 **Bradl, M. and Lassmann, H.**, Oligodendrocytes: biology and pathology. *Acta Neuropathol.* 2010. **119**: 37–53.

1640 **Sofroniew, M. V. and Vinters, H. V.**, Astrocytes: biology and pathology. *Acta Neuropathol.* 2010. **119**: 7–35.

1641 **Bergström, T. and Forsberg-Nilsson, K.**, Neural stem cells: brain building blocks and beyond. *Ups. J. Med. Sci.* 2012. **117**: 132–142.

1642 **Ginhoux, F., Greter, M., Leboeuf, M., Nandi, S., See, P., Gokhan, S., Mehler, M. F. et al.**, Fate mapping analysis reveals that adult microglia derive from primitive macrophages. *Science* 2010. **330**: 841–845.

1643 **Goldmann, T., Wieghofer, P., Jordão, M. J. C., Prutek, F., Hagemeyer, N., Frenzel, K., Amann, L. et al.**, Origin, fate and dynamics of macrophages at central nervous system interfaces. *Nat. Immunol.* 2016. **17**: 797–805.

1644 **Kantzer, C. G., Boutin, C., Herzig, I. D., Wittwer, C., Reiß, S., Tiveron, M. C., Drewes, J. et al.**, Anti-ACSA-2 defines a novel monoclonal antibody for prospective isolation of living neonatal and adult astrocytes. *Glia* 2017. **65**: 990–1004.

1645 **Batiuk, M. Y., De Vin, F., Duque, S. I., Li, C., Saito, T., Saido, T., Fiers, M. et al.**, An immunoaffinity-based method for isolating ultrapure adult astrocytes based on ATP1B2 targeting by the ACSA-2 antibody. *J. Biol. Chem.* 2017. **292**: 8874–8891.

1646 **Lin, C.-C. J., Yu, K., Hatcher, A., Huang, T.-W., Lee, H. K., Carlson, J., Weston, M. C. et al.**, Identification of diverse astrocyte populations and their malignant analogs. *Nat. Neurosci.* 2017. **20**: 396.

1647 **Tsai, H.-H., Li, H., Fuentealba, L. C., Molofsky, A. V., Taveira-Marques, R., Zhuang, H., Tenney, A. et al.**, Regional astrocyte allocation regulates CNS synaptogenesis and repair. *Science* 2012. **337**: 358–362.

1648 **Guttenplan, K. A. and Liddelow, S. A.**, Astrocytes and microglia: models and tools. *J. Exp. Med.* 2018. **216**: 71–83.

1649 **Zhuo, L., Sun, B., Zhang, C. L., Fine, A., Chiu, S. Y. and Messing, A.**, Live astrocytes visualized by green fluorescent protein in transgenic mice. *Dev. Biol.* 1997. **187**: 36–42.

1650 **Nolte, C., Matyash, M., Pivneva, T., Schipke, C. G., Ohlemeyer, C., Hanisch, U.-K., Kirchhoff, F. et al.**, GFAP promoter-controlled EGFP-expressing transgenic mice: a tool to visualize astrocytes and astrogliosis in living brain tissue. *Glia* 2001. **33**: 72–86.

1651 **Kuzmanovic, M., Dudley, V. J. and Sarthy, V. P.**, GFAP promoter drives Muller cell-specific expression in transgenic mice. Invest. *Ophthalmol. Vis. Sci.* 2003. **44**: 3606–3613.

1652 **Cho, W., Hagemann, T. L., Johnson, D. A., Johnson, J. A. and Messing, A.**, Dual transgenic reporter mice as a tool for monitoring expression of glial fibrillary acidic protein. *J. Neurochem.* 2009. **110**: 343–351.

1653 **Regan, M. R., Huang, Y. H., Kim, Y. S., Dykes-Hoberg, M. I., Jin, L., Watkins, A. M., Bergles, D. E. et al.**, Variations in promoter activity reveal a differential expression and physiology of glutamate transporters by glia in the developing and mature CNS. *J. Neurosci.* 2007. **27**: 6607–6619.

1654 **Bardehle, S., Kruger, M., Buggenthin, F., Schwausch, J., Ninkovic, J., Clevers, H., Snippert, H. J. et al.**, Live imaging of astrocyte responses to acute injury reveals selective juxtavascular proliferation. *Nat. Neurosci.* 2013. **16**: 580–586.

1655 **Yang, Y., Vidensky, S., Jin, L., Jie, C., Lorenzini, I., Frankl, M. and Rothstein, J. D.**, Molecular comparison of GLT1+ and ALDH1L1+ astrocytes in vivo in astroglial reporter mice. *Glia* 2011. **59**: 200–207.

1656 **Gong, S., Zheng, C., Doughty, M. L., Losos, K., Didkovsky, N., Schambra, U. B., Nowak, N. J. et al.**, A gene expression atlas of the central nervous system based on bacterial artificial chromosomes. *Nature* 2003. **425**: 917–925.

1657 **Jung, S., Aliberti, J., Graemmel, P., Sunshine, M. J., Kreutzberg, G. W., Sher, A. and Littman, D. R.**, Analysis of fractalkine receptor CX(3)CR1 function by targeted deletion and green fluorescent protein reporter gene insertion. *Mol. Cell Biol.* 2000. **20**: 4106–4114.

1658 **Yona, S., Kim, K. W., Wolf, Y., Mildner, A., Varol, D., Breker, M., Strauss-Ayali, D. et al.**, Fate mapping reveals origins and dynamics of monocytes and tissue macrophages under homeostasis. *Immunity* 2013. **38**: 79–91.

1659 **Buttgereit, A., Lelios, I., Yu, X., Vrohlings, M., Krakoski, N. R., Gautier, E. L., Nishinakamura, R. et al.**, Sall1 is a transcriptional regulator defining microglia identity and function. *Nat. Immunol.* 2016. **17**: 1397–1406.

1660 **Hirasawa, T., Ohsawa, K., Imai, Y., Ondo, Y., Akazawa, C., Uchino, S. and Kohsaka, S.**, Visualization of microglia in living tissues using Iba1-EGFP transgenic mice. *J. Neurosci. Res.* 2005. **81**: 357–362.

1661 **Sasmono, R. T., Oceandy, D., Pollard, J. W., Tong, W., Pavli, P., Wainwright, B. J., Ostrowski, M. C. et al.**, A macrophage colony-stimulating factor receptor-green fluorescent protein transgene is expressed throughout the mononuclear phagocyte system of the mouse. *Blood* 2003. **101**: 1155–1163.

1662 **Dziennis, S., Van Etten, R. A., Pahl, H. L., Morris, D. L., Rothstein, T. L., Blosch, C. M., Perlmutter, R. M. et al.**, The CD11b promoter directs

high-level expression of reporter genes in macrophages in transgenic mice. *Blood* 1995. **85**: 319–329.

1663 **Yang, J., Hills, D., Taylor, E., Pfeffer, K., Ure, J. and Medvinsky, A.**, Transgenic tools for analysis of the haematopoietic system: knock-in CD45 reporter and deletor mice. *J. Immunol. Methods* 2008. **337**: 81–87.

1664 **Pillai, M. M., Hayes, B. and Torok-Storb, B.**, Inducible transgenes under the control of the hCD68 promoter identifies mouse macrophages with a distribution that differs from the F4/80 - and CSF-1R-expressing populations. *Exp. Hematol.* 2009. **37**: 1387–1392.

1665 **Iqbal, A. J., Mcneill, E., Kapellos, T. S., Regan-Komito, D., Norman, S., Burd, S., Smart, N. et al.**, Human CD68 promoter GFP transgenic mice allow analysis of monocyte to macrophage differentiation in vivo. *Blood* 2014. **124**: e33–e44.

1666 **Hägglund, M., Borgius, L., Dougherty, K. J. and Kiehn, O.**, Activation of groups of excitatory neurons in the mammalian spinal cord or hindbrain evokes locomotion. *Nat. Neurosci.* 2010. **13**: 246–252.

1667 **Blanco-Centurion, C., Bendell, E., Zou, B., Sun, Y., Shiromani, P. J. and Liu, M.**, VGAT and VGLUT2 expression in MCH and orexin neurons in double transgenic reporter mice. *IBRO Rep.* 2018. **4**: 44–49.

1668 **Daigle, T. L., Madisen, L., Hage, T. A., Valley, M. T., Knoblich, U., Larsen, R. S., Takeno, M. M. et al.**, A suite of transgenic driver and reporter mouse lines with enhanced brain-cell-type targeting and functionality. *Cell* 2018. **174**: 465–480.e422.

1669 **Martin, D., Xu, J., Porretta, C. and Nichols, C. D.**, Neurocytometry: flow cytometric sorting of specific neuronal populations from human and rodent brain. *ACS Chem. Neurosci.* 2017. **8**: 356–367.

1670 **Evrony, G. D., Cai, X., Lee, E., Hills, L. B., Elhosary, P. C., Lehmann, H. S., Parker, J. J. et al.**, Single-neuron sequencing analysis of L1 retrotransposition and somatic mutation in the human brain. *Cell* 2012. **151**: 483–496.

1671 **Cai, X., Evrony, G. D., Lehmann, H. S., Elhosary, P. C., Mehta, B. K., Poduri, A. and Walsh, C. A.**, Single-cell, genome-wide sequencing identifies clonal somatic copy-number variation in the human brain. *Cell Rep.* 2014. **8**: 1280–1289.

1672 **Girdhar, K., Hoffman, G. E., Jiang, Y., Brown, L., Kundakovic, M., Hauberg, M. E., Francoeur, N. J. et al.**, Cell-specific histone modification maps in the human frontal lobe link schizophrenia risk to the neuronal epigenome. *Nat. Neurosci.* 2018. **21**: 1126–1136.

1673 **Matevossian, A. and Akbarian, S.**, Neuronal nuclei isolation from human postmortem brain tissue. *J. Vis. Exp.* 2008. **1**: 914.

1674 **McCarthy, K. D. and De Vellis, J.**, Preparation of separate astroglial and oligodendroglial cell cultures from rat cerebral tissue. *J. Cell. Biol.* 1980. **85**: 890–902.

1675 **Barres, B. A., Hart, I. K., Coles, H. S. R., Burne, J. F., Voyvodic, J. T., Richardson, W. D. and Raff, M. C.**, Cell death and control of cell survival in the oligodendrocyte lineage. *Cell* 1992. **70**: 31–46.

1676 **Seiwa, C., Kojima-Aikawa, K., Matsumoto, I. and Asou, H.**, CNS myelinogenesis in vitro: myelin basic protein deficient shiverer oligodendrocytes. *J. Neurosci. Res.* 2002. **69**: 305–317.

1677 **Yang, Z., Watanabe, M. and Nishiyama, A.**, Optimization of oligodendrocyte progenitor cell culture method for enhanced survival. *J. Neurosci. Meth.* 2005. **149**: 50–56.

1678 **Robinson, A. P., Rodgers, J. M., Goings, G. E. and Miller, S. D.**, Characterization of oligodendroglial populations in mouse demyelinating disease using flow cytometry: clues for MS pathogenesis. *PLoS ONE* 2014. **9**: e107649.

1679 **Zhang, Y., Sloan, S. A., Clarke, L. E., Caneda, C., Plaza, C. A., Blumenthal, P. D., Vogel, H. et al.**, Purification and Characterization of Progenitor and Mature Human Astrocytes Reveals Transcriptional and Functional Differences with Mouse. *Neuron* 2016. **89**: 37–53.

1680 **Deng, Y., Kim, B., He, X., Kim, S., Lu, C., Wang, H., Cho, S. G. et al.**, Direct visualization of membrane architecture of myelinating cells in transgenic mice expressing membrane-anchored EGFP. *Genesis* 2014. **52**: 341–349.

1681 **Hughes, E. G., Kang, S. H., Fukaya, M. and Bergles, D. E.**, Oligodendrocyte progenitors balance growth with self-repulsion to achieve homeostasis in the adult brain. *Nat. Neurosci.* 2013. **16**: 668–676.

1682 **Sedgwick, J. D., Schwender, S., Imrich, H., Dörries, R., Butcher, G. W. and Ter Meulen, V.**, Isolation and direct characterization of resident microglial cells from the normal and inflamed central nervous system. *Proc. Natl. Acad. Sci. USA* 1991. **88**: 7438–7442.

1683 **Bennett, M. L., Bennett, F. C., Liddelow, S. A., Ajami, B., Zamanian, J. L., Fernhoff, N. B., Mulinyawe, S. B. et al.**, New tools for studying microglia in the mouse and human CNS. *Proc. Natl. Acad. Sci. USA* 2016. **113**: E1738–E1746.

1684 **Korin, B., Ben-Shaanan, T. L., Schiller, M., Dubovik, T., Azulay-Debby, H., Boshnak, N. T., Koren, T. et al.**, High-dimensional, single-cell characterization of the brain's immune compartment. *Nat. Neurosci.* 2017. **20**: 1300–1309.

1685 **Mrdjen, D., Hartmann, F. J. and Becher, B.**, High dimensional cytometry of central nervous system leukocytes during neuroinflammation. *Methods Mol. Biol.* 2017. **1559**: 321–332.

1686 **Ajami, B., Samusik, N., Wieghofer, P., Ho, P. P., Crotti, A., Bjornson, Z., Prinz, M. et al.**, Single-cell mass cytometry reveals distinct populations of brain myeloid cells in mouse neuroinflammation and neurodegeneration models. *Nat. Neurosci.* 2018. **21**: 541–551.

1687 **Mrdjen, D., Pavlovic, A., Hartmann, F. J., Schreiner, B., Utz, S. G., Leung, B. P., Lelios, I. et al.**, High-dimensional single-cell mapping of central nervous system immune cells reveals distinct myeloid subsets in health, aging, and disease. *Immunity* 2018. **48**: 599.

1688 **Böttcher, C., Schlickeiser, S., Sneeboer, M. a. M., Kunkel, D., Knop, A., Paza, E., Fidzinski, P. et al.**, Human microglia regional heterogeneity and phenotypes determined by multiplexed single-cell mass cytometry. *Nat. Neurosci.* 2019. **22**: 78–90.

1689 **Ecker, J. R., Geschwind, D. H., Kriegstein, A. R., Ngai, J., Osten, P., Polioudakis, D., Regev, A. et al.**, The BRAIN Initiative Cell Census Consortium: lessons learned toward generating a comprehensive brain cell atlas. *Neuron* 2017. **96**: 542–557.

1690 **Tham, C. S., Lin, F. F., Rao, T. S., Yu, N. and Webb, M.**, Microglial activation state and lysophospholipid acid receptor expression. *Int. J. Dev. Neurosci.* 2003. **21**: 431–443.

1691 **Pfenninger, C. V., Roschupkina, T., Hertwig, F., Kottwitz, D., Englund, E., Bengzon, J., Jacobsen, S. E. et al.**, CD133 is not present on neurogenic astrocytes in the adult subventricular zone, but on embryonic neural stem cells, ependymal cells, and glioblastoma cells. *Cancer Res.* 2007. **67**: 5727–5736.

1692 **Moussaud, S. and Draheim, H. J.**, A new method to isolate microglia from adult mice and culture them for an extended period of time. *J. Neurosci. Methods* 2010. **187**: 243–253.

1693 **Foo, L. C., Allen, N. J., Bushong, E. A., Ventura, P. B., Chung, W.-S., Zhou, L., Cahoy, J. D. et al.**, Development of a Method for the Purification and Culture of Rodent Astrocytes. *Neuron* 2011. **71**: 799–811.

1694 **Horst, A. K., Neumann, K., Diehl, L. and Tiegs, G.**, Modulation of liver tolerance by conventional and nonconventional antigen-presenting cells and regulatory immune cells. *Cell. Mol. Immunol.* 2016. **13**: 277–292.

1695 **Jenne, C. N. and Kubes, P.**, Immune surveillance by the liver. *Nat. Immunol.* 2013. **14**: 996–1006.

1696 **Thomson, A. W. and Knolle, P. A.**, Antigen-presenting cell function in the tolerogenic liver environment. *Nat. Rev. Immunol.* 2010. **10**: 753–766.

1697 **Crispe, I. N.**, Immune tolerance in liver disease. *Hepatology* 2014. **60**: 2109–2117.

1698 **Racanelli, V. and Rehermann, B.**, The liver as an immunological organ. *Hepatology*. 2006. **43**: S54–62.

1699 **Blom, K. G., Qazi, M. R., Matos, J. B., Nelson, B. D., DePierre, J. W. and Abedi-Valugerdi, M.**, Isolation of murine intrahepatic immune cells employing a modified procedure for mechanical disruption and functional characterization of the B, T and natural killer T cells obtained. *Clin. Exp. Immunol.* 2009. **155**: 320–329.

1700 **Gao, B., Radaeva, S. and Park, O.**, Liver natural killer and natural killer T cells: immunobiology and emerging roles in liver diseases. *J. Leukoc. Biol.* 2009. **86**: 513–528.

1701 **Niemeyer, M., Darmoise, A., Mollenkopf, H. J., Hahnke, K., Hurwitz, R., Besra, G. S., Schaible, U. E. et al.**, Natural killer T-cell characterization through gene expression profiling: an account of versatility bridging T helper type 1 (Th1), Th2 and Th17 immune responses. *Immunology* 2008. **123**: 45–56.

1702 **Pang, D. J., Neves, J. F., Sumaria, N. and Pennington, D. J.**, Understanding the complexity of γδ T-cell subsets in mouse and human. *Immunology* 2012. **136**: 283–290.

1703 **Golubovskaya, V. and Wu, L.**, Different subsets of T cells, memory, effector functions, and CAR-T immunotherapy. *Cancers* 2016. **8**(3): E36.

1704 **Davies, L. C., Jenkins, S. J., Allen, J. E. and Taylor, P. R.**, Tissue-resident macrophages. *Nat. Immunol.* 2013. **14**: 986–995.

1705 **Gordon, S. and Plüddemann, A.**, Tissue macrophages: Heterogeneity and functions. *BMC. Biol.* 2017. **15**: 53.

1706 **Gordon, S. and Taylor, P. R.**, Monocyte and macrophage heterogeneity. *Nat. Rev. Immunol.* 2005. **5**: 953–964.

1707 **Shortman, K. and Liu, Y. J.**, Mouse and human dendritic cell subtypes. *Nat. Rev. Immunol.* 2002. **2**: 151–161.

1708 **Meurens, F., Summerfield, A., Nauwynck, H., Saif, L. and Gerdts, V.**, The pig: a model for human infectious diseases. *Trends Microbiol.* 2012. **20**: 50–57.

1709 **Piriou-Guzylack, L. and Salmon, H.**, Membrane markers of the immune cells in swine: an update. *Vet. Res.* 2008. **39**: 54.

1710 **Dawson, H. D. and Lunney, J. K.**, Porcine cluster of differentiation (CD) markers 2018 update. *Res. Vet. Sci.* 2018. **118**: 199–246.

1711 **Saalmüller, A., Reddehase, M. J., Bühring, H.-J., Jonjić, S. and Koszinowski, U. H.**, Simultaneous expression of CD4 and CD8 antigens by a substantial proportion of resting porcine T lymphocytes. *Eur. J. Immunol.* 1987. **17**(9): 1297–1301.

1712 **Saalmüller, A., Weiland, F. and Reddehase, M. J.**, Resting porcine T lymphocytes expressing class II major histocompatibility antigen. *Immunobiology* 1991. **183**: 102–114.

1713 **Reutner, K., Leitner, J., Mullebner, A., Ladinig, A., Essler, S. E., Duvigneau, J. C., Ritzmann, M. et al.**, CD27 expression discriminates porcine T helper cells with functionally distinct properties. *Vet. Res.* 2013. **44**(1): 18.

1714 **Mair, K. H., Essler, S. E., Patzl, M., Storset, A. K., Saalmüller, A. and Gerner, W.**, NKp46 expression discriminates porcine NK cells with different functional properties. *Eur. J. Immunol.* 2012. **42**(5): 1261–1271.

1715 **Álvarez, B., Escalona, Z., Uenishi, H., Toki, D., Revilla, C., Yuste, M., Gómez del Moral, M. et al.**, Molecular and functional characterization of porcine Siglec-3/CD33 and analysis of its expression in blood and tissues. *Dev. Comp. Immunol.* 2015. **51**(2): 238–250.

1716 **Summerfield, A., Guzylack-Piriou, L., Schaub, A., Carrasco, C. P., Tâche, V., Charley, B. and McCullough, K. C.**, Porcine peripheral blood dendritic cells and natural interferon-producing cells. *Immunology* 2003. **110**(4): 440–449.

1717 **Escalona, Z., Álvarez, B., Uenishi, H., Toki, D., Yuste, M., Revilla, C., Gómez del Moral, M. et al.**, Molecular characterization of porcine Siglec-10 and analysis of its expression in blood and tissues. *Dev. Comp. Immunol.* 2015. **48**(1): 116–123. https://doi.org/10.1016/j.dci.2014.09.011

1718 **Sedlak, C., Patzl, M., Saalmüller, A. and Gerner, W.**, IL-12 and IL-18 induce interferon-γ production and de novo CD2 expression in porcine Γδ T cells. *Dev. Comp. Immunol.* 2014b. **47**(1): 115–122. https://doi.org/10.1016/j.dci.2014.07.007

1719 **Yang, H. and Parkhouse, R. M.**, Phenotypic classification of porcine lymphocyte subpopulations in blood and lymphoid tissues. *Immunology* 1996. **89**(1): 76–83.

1720 **Saalmüller, A., Hirt, W. and Reddehase, M. J.**, Porcine γ/δ T lymphocyte subsets differing in their propensity to home to lymphoid tissue. *Eur. J. Immunol.* 1990. **20**(10): 2343–2346.

1721 **Sinkora, M., Šinkorová, J. and Holtmeier, W.**, Development of γδ thymocyte subsets during prenatal and postnatal ontogeny. *Immunology* 2005. **115**(4): 544–555.

1722 **Wen, K., Bui, T., Li, G., Liu, F., Li, Y., Kocher, J. and Yuan, L.**, Characterization of immune modulating functions of γδ T cell subsets in a gnotobiotic pig model of human rotavirus infection. *Comp. Immunol. Microbiol. Infect. Dis.* 2012. **35**(4): 289–301.

1723 **Lee, J., Choi, K., Olin, M. R., Cho, S.-N. and Molitor, T. W.**, Γδ T cells in immunity induced by *Mycobacterium bovis* Bacillus Calmette-Guérin vaccination. *Infect. Immun.* 2004. **72**(3): 1504–1511.

1724 **Sedlak, C., Patzl, M., Saalmüller, A. and Gerner, W.**, CD2 and CD8α define porcine γδ T cells with distinct cytokine production profiles. *Dev. Comp. Immunol.* 2014. **45**: 97–106.

1725 **Yang, H. and Parkhouse, R. M.**, Differential expression of CD8 epitopes amongst porcine CD8-positive functional lymphocyte subsets. *Immunology* 1997. **92**(1): 45–52.

1726 **Olin, M. R., Choi, K. H., Lee, J. and Molitor, T. W.**, Γδ T-lymphocyte cytotoxic activity against *Mycobacterium bovis* analyzed by flow cytometry. *J. Immunol. Methods* 2005. **297**: 1–11.

1727 **Rodríguez-Gómez, I. M., Talker, S. C., Käser, T., Stadler, M., Reiter, L., Ladinig, A., Milburn, J. V. et al.**, Expression of T-Bet, eomesodermin, and GATA-3 correlates with distinct phenotypes and functional properties in porcine γδ T cells. *Front. Immunol.* 2019. **10**. https://doi.org/10.3389/fimmu.2019.00396

1728 **Summerfield, A., Rziha, H.-J. and Saalmüller, A.**, Functional characterization of porcine CD4+CD8+extrathymic T lymphocytes. *Cell. Immunol.* 1996. **168**(2): 291–296. https://doi.org/10.1006/cimm.1996.0078

1729 **Rodríguez-Gómez, I. M., Talker, S. C., Käser, T., Stadler, M., Hammer, S. E., Saalmüller, A. and Gerner, W.**, Expression of T-bet, eomesodermin and GATA-3 in porcine αβ T cells. *Dev. Comp. Immunol.* 2016. **60**: 115–126.

1730 **Talker, S. C., Käser, T., Reutner, K., Sedlak, C., Mair, K. H., Koinig, H., Graage, R. et al.**, Phenotypic maturation of porcine NK- and T-cell subsets. *Dev. Comp. Immunol.* 2013. **40**(1): 51–68.

1731 **Käser, T., Gerner, W., Hammer, S. E., Patzl, M. and Saalmüller, A.**, Detection of Foxp3 protein expression in porcine T lymphocytes. *Vet. Immunol. Immunopathol.* 2008. **125**(1–2): 92–101. https://doi.org/10.1016/j.vetimm.2008.05.007

1732 **Ebner, F., Rausch, S., Scharek-Tedin, L., Pieper, R., Burwinkel, M., Zentek, J. and Hartmann, S.**, A novel lineage transcription factor based

analysis reveals differences in T helper cell subpopulation development in infected and intrauterine growth restricted (IUGR) piglets. *Dev. Comp. Immunol.* 2014. **46**: 333–340.

1733 **Gerner, W., Denyer, M. S., Takamatsu, H.-H., Wileman, T. E., Wiesmüller, K.-H., Pfaff, E. and Saalmüller, A.**, Identification of novel foot-and-mouth disease virus specific T-cell epitopes in c/c and d/d haplotype miniature swine. *Virus Res.* 2006. **121**(2): 223–228.

1734 **Ebner, F., Schwiertz, P., Steinfelder, S., Pieper, R., Zentek, J., Schütze, N., Baums, C. G. et al.**, Pathogen-reactive T helper cell analysis in the pig. *Front. Immunol.* 2017. **8**: 565. https://doi.org/10.3389/fimmu.2017.00565

1735 **Stepanova, K. and Sinkora, M.**, Porcine γδ T lymphocytes can be categorized into two functionally and developmentally distinct subsets according to expression of CD2 and level of TCR. *J. Immunol.* 2013. **190**(5): 2111–2120. https://doi.org/10.4049/jimmunol.1202890

1736 **Gerner, W., Talker, S. C., Koinig, H. C., Sedlak, C., Mair, K. H. and Saalmüller, A.**, Phenotypic and functional differentiation of porcine Aβ T cells: current knowledge and available tools. *Mol. Immunol.* 2015. **66**(1): 3–13. https://doi.org/10.1016/j.molimm.2014.10.025

1737 **Holzer, B., Morgan, S. B., Matsuoka, Y., Edmans, M., Salguero, F. J., Everett, H., Brookes, S. M. et al.**, Comparison of heterosubtypic protection in ferrets and pigs induced by a single-cycle influenza vaccine. *J. Immunol.* 2018. **200**: 4068–4077.

1738 **Hayashi, Y., Okutani, M., Ogawa, S., Tsukahara, T. and Inoue, R.**, Generation of anti-porcine CD69 monoclonal antibodies and their usefulness to evaluate early activation of cellular immunity by flow cytometric analysis. *Anim. Sci. J.* 2018. **89**: 825–832.

1739 **Yang, W. C., Schultz, R. D. and Spano, J. S.**, Isolation and characterization of porcine natural killer (NK) cells. *Vet. Immunol. Immunopathol.* 1987. **14**(4): 345–356.

1740 **Denyer, M. S., Wileman, T. E., Stirling, C. M., Zuber, B. and Takamatsu, H. H.**, Perforin expression can define CD8 positive lymphocyte subsets in pigs allowing phenotypic and functional analysis of natural killer, cytotoxic T, natural killer T and MHC un-restricted cytotoxic T-cells. *Vet. Immunol. Immunopathol.* 2006. **110**: 279–292.

1741 **Walzer, T., Jaeger, S., Chaix, J. and Vivier, E.**, Natural Killer Cells: From CD3(-)NKp46(+) to post-genomics meta-analyses. *Curr. Opin. Immunol.* 2007. **19**(3): 365–372.

1742 **Mair, K. H., Müllebner, A., Essler, S. E., Duvigneau, J. C., Storset, A. K., Saalmüller, A. and Gerner, W.**, Porcine CD8αdim/-NKp46high NK cells are in a highly activated state. *Vet. Res.* 2013. **44** (March): 13. https://doi.org/10.1186/1297-9716-44-13

1743 **Forberg, H., Hauge, A. G., Valheim, M., Garcon, F., Nunez, A., Gerner, W., Mair, K. H. et al.**, Early responses of natural killer cells in pigs experimentally infected with 2009 pandemic H1N1 influenza A virus. *PLoS One* 2014. **9**(6): e100619. https://doi.org/10.1371/journal.pone.0100619

1744 **Jones, M., Cordell, J. L., Beyers, A. D., Tse, A. G. and Mason, D. Y.**, Detection of T and B cells in many animal species using cross-reactive anti-peptide antibodies. *J. Immunol.* 1993. **150**: 5429–5435.

1745 **Reutner, K., Leitner, J., Essler, S. E., Witter, K., Patzl, M., Steinberger, P., Saalmüller, A. et al.**, Porcine CD27: identification, expression and functional aspects in lymphocyte subsets in swine. *Dev. Comp. Immunol.* 2012. **38**(2): 321–331.

1746 **Sinkora, M., Stepanova, K. and Sinkorova, J.**, Different Anti-CD21 antibodies can be used to discriminate developmentally and functionally different subsets of B lymphocytes in circulation of pigs. *Dev. Comp. Immunol.* 2013. **39**(4): 409–418.

1747 **Kandasamy, S., Chattha, K. S., Vlasova, A. N., Rajashekara, G. and Saif, L. J.**, Lactobacilli and Bifidobacteria enhance mucosal B cell responses and differentially modulate systemic antibody responses to an oral human rotavirus vaccine in a neonatal gnotobiotic pig disease model. *Gut Microbes* 2014. **5**(5): 639–651. https://doi.org/10.4161/19490976.2014.969972

1748 **Braun, R. O., Python, S. and Summerfield, A.**, Porcine B cell subset responses to toll-like receptor ligands. *Front. Immunol.* 2017. **8**: 1044. https://doi.org/10.3389/fimmu.2017.01044

1749 **Summerfield, A., Auray, G. and Ricklin, M.**, Comparative dendritic cell biology of veterinary mammals. *Annu. Rev. Anim. Biosci.* 2015. **3**: 533–557.

1750 **Vu Manh, T.-P., Elhmouzi-Younes, J., Urien, C., Ruscanu, S., Jouneau, L., Bourge, M., Moroldo, M. et al.**, Defining mononuclear phagocyte subset homology across several distant warm-blooded vertebrates through comparative transcriptomics. *Front. Immunol.* 2015. **6**: 299.

1751 **Soldevila, F., Edwards, J. C., Graham, S. P., Stevens, L. M., Crudgington, B., Crooke, H. R., Werling, D. et al.**, Characterization of the myeloid cell populations' resident in the porcine palatine tonsil. *Front. Immunol.* 2018. **9**: 1800.

1752 **Auray, G., Keller, I., Python, S., Gerber, M., Bruggmann, R., Ruggli, N. and Summerfield, A.**, Characterization and transcriptomic analysis of porcine blood conventional and plasmacytoid dendritic cells reveals striking species-specific differences. *J. Immunol.* 2016. **197**(12): 4791–4806.

1753 **Maisonnasse, P., Bouguyon, E., Piton, G., Ezquerra, A., Urien, C., Deloizy, C., Bourge, M. et al.**, The respiratory DC/macrophage network at steady-state and upon influenza infection in the swine biomedical model. *Mucosal Immunol.* 2016a. **9**(4): 835–849. https://doi.org/10.1038/mi.2015.105

1754 **Chun, T., Wang, K., Zuckermann, F. A. and Rex Gaskins, H.**, Molecular cloning and characterization of a novel CD1 gene from the pig. *J. Immunol.* 1999. **162**(11): 6562–6571.

1755 **Nestle, F. O., Zheng, X. G., Thompson, C. B., Turka, L. A. and Nickoloff, B. J.**, Characterization of dermal dendritic cells obtained from normal human skin reveals phenotypic and functionally distinctive subsets. *J. Immunol.* 1993. **151**(11): 6535–6545.

1756 **Dutertre, C.-A., Wang, L.-F. and Ginhoux, F.**, Aligning bona fide dendritic cell populations across species. *Cell. Immunol.* 2014. **291**(1): 3–10. https://doi.org/10.1016/j.cellimm.2014.08.006

1757 **Chamorro, S., Revilla, C., Alvarez, B., Alonso, F., Ezquerra, A. and Domínguez, J.**, Phenotypic and functional heterogeneity of porcine blood monocytes and its relation with maturation. *Immunology* 2005. **114**(1): 63–71.

1758 **Ondrackova, P., Nechvatalova, K., Kucerova, Z., Leva, L., Dominguez, J. and Faldyna, M.**, Porcine mononuclear phagocyte subpopulations in the lung, blood and bone marrow: dynamics during inflammation induced by actinobacillus pleuropneumoniae. *Vet. Res.* 2010. **41**: 64.

1759 **Fairbairn, L., Kapetanovic, R., Beraldi, D., Sester, D. P., Tuggle, C. K., Archibald, A. L. and Hume, D. A.**, Comparative analysis of monocyte subsets in the pig. *J. Immunol.* 2013. **190**(12): 6389–6396. https://doi.org/10.4049/jimmunol.1300365

1760 **Ondrackova, P., Leva, L., Kucerova, Z., Vicenova, M., Mensikova, M. and Faldyna, M.**, Distribution of porcine monocytes in different lymphoid tissues and the lungs during experimental actinobacillus pleuropneumoniae infection and the role of chemokines. *Vet. Res.* 2013. **44**: 98.

1761 **Moreno, S., Alvarez, B., Poderoso, T., Revilla, C.Ezquerra, A., Alonso, F. and Dominguez, J.**, Porcine monocyte subsets differ in the expression of CCR2 and in their responsiveness to CCL2. *Vet Res.* 2010. **41**: 76.

1762 **Ezquerra, A., Revilla, C., Alvarez, B., Pérez, C., Alonso, F. and Domínguez, J.**, Porcine myelomonocytic markers and cell populations. *Dev. Comp. Immunol.* 2009. **33**(3): 284–298. https://doi.org/10.1016/j.dci.2008.06.002

1763 **Fernández-Caballero, T., Álvarez, B., Revilla, C., Zaldívar-López, S., Alonso, F., Garrido, J. J., Ezquerra, Á. et al.**, Phenotypic and functional characterization of porcine bone marrow monocyte subsets. *Dev. Comp. Immunol.* 2018. **81**: 95–104. https://doi.org/10.1016/j.dci.2017.11.012

1764 **Talker, S. C., Baumann, A., Tuba Barut, G., Keller, I., Bruggmann, R. and Summerfield, A.**, Precise delineation and transcriptional characterization of bovine blood dendritic-cell and monocyte subsets. *Front. Immunol.* 2018. **9**: 2505.

1765 **Sinkora, M. and Sinkorova, J.**, B cell lymphogenesis in swine is located in the bone marrow. *J. Immunol.* 2014. **193**(10): 5023–5032.

1766 **Maisonnasse, P., Bordet, E., Bouguyon, E. and Bertho, N.**, Broncho alveolar dendritic cells and macrophages are highly similar to their interstitial counterparts. *PLoS One* 2016b. **11**(12): e0167315. https://doi.org/10.1371/journal.pone.0167315

1767 **Bordet, E., Maisonnasse, P., Renson, P., Bouguyon, E., Crisci, E., Tiret, M., Descamps, D. et al.**, Porcine alveolar macrophage-like cells are pro-inflammatory pulmonary intravascular macrophages that produce large titers of porcine reproductive and respiratory syndrome virus. *Sci. Rep.* 2018. **8**(1): 10172. https://doi.org/10.1038/s41598-018-28234-y

1768 **Guilliams, M., Ginhoux, F., Jakubzick, C., Naik, S. H., Onai, N., Schraml, B. U., Segura, E. et al.**, Dendritic cells, monocytes and macrophages: a unified nomenclature based on ontogeny. *Nat. Rev. Immunol.* 2014. **14**: 571–578.

1769 **Bharat, A., Bhorade, S. M., Morales-Nebreda, L., McQuattie-Pimentel, A. C., Soberanes, S., Ridge, K., DeCamp, M. M. et al.**, Flow cytometry reveals similarities between lung macrophages in humans and mice. *Am. J. Respir Cell Mol Biol* 2016. **54**(1): 147–149. https://doi.org/10.1165/rcmb.2015-0147LE

1770 **Cai, Y., Sugimoto, C., Arainga, M., Alvarez, X., Didier, E. S. and Kuroda, M. J.**, In vivo characterization of alveolar and interstitial lung macrophages in rhesus macaques: implications for understanding lung disease in humans. *J. Immunol. (Baltimore, Md.: 1950)* 2014. **192**(6): 2821–2829. https://doi.org/10.4049/jimmunol.1302269

1771 **Yu, Y.-R. A., Hotten, D. F., Malakhau, Y., Volker, E., Ghio, A. J., Noble, P. W., Kraft, M. et al.**, Flow cytometric analysis of myeloid cells in human blood, bronchoalveolar lavage, and lung tissues. *Am. J. Respir. Cell Mol. Biol.* 2016. **54**(1): 13–24.

1772 **Marquet, F., Vu Manh, T.-P., Maisonnasse, P., Elhmouzi-Younes, J., Urien, C., Bouguyon, E., Jouneau, L. et al.**, Pig skin includes dendritic cell subsets transcriptomically related to human CD1a and CD14 dendritic cells presenting different migrating behaviors and T cell activation capacities. *J. Immunol.* 2014. **193**(12): 5883–5893.

1773 **Parra-Sánchez, H., Puebla-Clark, L., Reséndiz, M., Valenzuela, O. and Hernández, J.**, Characterization and expression of DEC205 in the CDC1 and CDC2 subsets of porcine dendritic cells from spleen, tonsil, and submaxillary and mesenteric lymph nodes. *Mol. Immunol.* 2018. **96**: 1–7.

1774 **Saalmüller, A., Pauly, T., Lunney, J. K., Boyd, P., Aasted, B., Sachs, D. H., Arn, S. et al.**, Overview of the second international workshop to define swine cluster of differentiation (CD) antigens. *Vet. Immunol. Immunopathol.* 1998. **60**(3–4): 207–228.

1775 **Leitner, J., Reutner, K., Essler, S. E., Popow, I., Gerner, W., Steinberger, P. and Saalmüller, A.**, Porcine SWC1 Is CD52—final determination by the use of a retroviral CDNA expression library. *Vet. Immunol. Immunopathol.* 2012. **146**(1): 27–34.

1776 **Pérez, C., Revilla, C., Alvarez, B., Chamorro, S., Correa, C., Domenech, N., Alonso, F. et al.**, Phenotypic and functional characterization of porcine granulocyte developmental stages using two new markers. *Dev. Comp. Immunol.* 2007. **31**(3): 296–306.

1777 **Saalmüller, A. and Aasted, B.**, Summary of the animal homologue section of HLDA8. *Vet. Immunol. Immunopathol.* 2007. **119**: 2–13.

1778 **Saalmüller, A., Lunney, J. K., Daubenberger, C., Davis, W., Fischer, U., Göbel, T. W. and Griebel, P. et al.**, Summary of the animal homologue section of HLDA8. *Cell. Immunol.* 2005. **236**: 51–58.

1779 **Cobaleda, C., Schebesta, A., Delogu, A. and Busslinger, M.**, Pax5: the guardian of B cell identity and function. *Nat. Immunol.* 2007. **8**: 463–470.

1780 **Brodie, T., Brenna, E. and Sallusto, F.**, OMIP-018: chemokine receptor expression on human T helper cells. *Cytometry A* 2013. **83**: 530–532.

1781 **Shaffer, A. L., Lin, K.-I., Kuo, T. C., Yu, X., Hurt, E. M., Rosenwald, A. and Giltnane, J. M. et al.**, Blimp-1 orchestrates plasma cell differentiation by extinguishing the mature B cell gene expression program. *Immunity* 2002. **17**: 51–62.

1782 **Bekeredjian-Ding, I. and Jego, G.**, Toll-like receptors—sentries in the B-cell response. *Immunology* 2009. **128**: 311–323.

1783 **Calame, K.**, Activation-dependent induction of Blimp-1. *Curr. Opin. Immunol.* 2008. **20**: 259–264.

1784 **Gerner, W., Käser, T. and Saalmüller, A.**, Porcine T lymphocytes and NK cells - an update. *Dev. Comp. Immunol.* 2009. **33**: 310–320.

1785 **Saalmüller, A., Werner, T. and Fachinger, V.**, T-helper cells from naive to committed. *Vet. Immunol. Immunopathol.* 2002. **87**: 137–145.

1786 **Bolzer, K., Käser, T., Saalmüller, A. and Hammer, S. E.**, Molecular characterisation of porcine Forkhead-box p3 (Foxp3). *Vet. Immunol. Immunopathol.* 2009. **132**: 275–281.

1787 **Rocchi, M. S., Wattegedera, S. R., Frew, D., Entrican, G., Huntley, J. F. and McNeilly, T. N.**, Identification of $CD4^{+}CD25^{high}$ $Foxp3^{+}$ T cells in ovine peripheral blood. *Vet. Immunol. Immunopathol.* 2011. **144**: 172–177.

1788 **Käser, T., Mair, K. H., Hammer, S. E., Gerner, W. and Saalmüller, A.**, Natural and inducible Tregs in swine: helios expression and functional properties. *Dev. Comp. Immunol.* 2015. **49**: 323–331.

1789 **Kwong, L. S., Thom, M., Sopp, P., Rocchi, M., Wattegedera, S., Entrican, G. and Hope, J. C.**, Production and characterization of two monoclonal antibodies to bovine tumour necrosis factor alpha (TNF-alpha) and their cross-reactivity with ovine TNF-alpha. *Vet. Immunol. Immunopathol.* 2010. **135**: 320–324.

1790 **Wattegedera, S. R., Corripio-Miyar, Y., Pang, Y., Frew, D., McNeilly, T. N., Palarea-Albaladejo, J. and McInnes, C. J. et al.**, Enhancing the toolbox to study IL-17A in cattle and sheep. *Vet. Res.* 2017. **48**: 20.

1791 **Pedersen, L. G., Castelruiz, Y., Jacobsen, S. and Aasted, B.**, Identification of monoclonal antibodies that cross-react with cytokines from different animal species. *Vet. Immunol. Immunopathol.* 2002. **88**: 111–122.

1792 **Franzoni, G., Kurkure, N. V., Edgar, D. S., Everett, H. E., Gerner, W., Bodman-Smith, K. B., Crooke, H. R. et al.**, Assessment of the phenotype and functionality of porcine CD8 T cell responses following vaccination with live attenuated classical swine fever virus (CSFV) and virulent CSFV challenge. *Clin. Vaccine Immunol.* 2013. **20**: 1604–1616.

1793 **Takamatsu, H. H., Denyer, M. S., Stirling, C., Cox, S., Aggarwal, N., Dash, P., Wileman, T. E. et al.**, Porcine γδ T cells: possible roles on the innate and adaptive immune responses following virus infection. *Vet. Immunol. Immunopathol.* 2006. **112**: 49–61.

1794 **Saeys, Y., Gassen, S. V. and Lambrecht, B. N.**, Computational flow cytometry: helping to make sense of high-dimensional immunology data. *Nat. Rev. Immunol.* 2016. **16**: 449–462.

1795 **Aghaeepour, N., Finak, G., The FlowCAP Consortium, The DREAM Consortium, Hoos, H., Mosmann, T. R., Brinkman, R. et al.**, Critical assessment of automated flow cytometry data analysis techniques. *Nat. Methods* 2013. **10**: 228–238.

1796 **Bashashati, A. and Brinkman, R. R.**, A survey of flow cytometry data analysis methods. *Adv. Bioinformatics* 2009. **2009**: 584603

1797 **O'Neill, K., Aghaeepour, N., Spidlen, J. and Brinkman, R. R.**, Flow cytometry bioinformatics. *PLoS Comput. Biol.* 2013. **9**: e1003365.

1798 **Aghaeepour, N., Chattopadhyay, P. K., Ganesan, A., O'Neill, K., Zare, H., Jalali, A., Hoos, H. et al.**, Early immunologic correlates of HIV protection can be identified from computational analysis of complex multivariate T-cell flow cytometry assays. *Bioinformatics* 2012. **28**: 1009–1016.

1799 **Aghaeepour, N., Nikolic, R., Hoos, H. H., and Brinkman, R. R.** Rapid cell population identification in flow cytometry data. *Cytometry Part A* 2011. **79A**: 6–13.

1800 **Finak, G., Bashashati, A., Brinkman, R. and Gottardo, R.**, Merging mixture components for cell population identification in flow cytometry. *Adv. Bioinformatics* 2009, 247646.

1801 **Mosmann, T. R., Naim, I., Rebhahn, J., Rebhahn, J., Datta, S., Cavenaugh, J. S., Weaver, J. M. and Sharma, G.**, SWIFT-scalable clustering for automated identification of rare cell populations in large, high-dimensional flow cytometry datasets, Part 2: Biological evaluation. *Cytometry A* 2014. **85**: 422–433.

1802 **Finak, G., Langweiler, M., Jaimes, M., Malek, M., Taghiyar, J., Korin, Y., Raddassi, K. et al.**, Standardizing flow cytometry immunophenotyping analysis from the human immunophenotyping consortium. *Sci. Rep.* 2016. **6**: 20686.

1803 **Qian, Y., Wei, C., Eun-Hyung Lee, F., Campbell, J., Halliley, J., Lee, J. A., Cai, J. et al.**, Elucidation of seventeen human peripheral blood B-cell subsets and quantification of the tetanus response using a density-based method for the automated identification of cell populations in multidimensional flow cytometry data. *Cytometry B Clin. Cytom.* 2010. **78**(Suppl 1): S69–S82.

1804 **Qiu, P., Simonds, E. F., Bendall, S. C., Gibbs, K. D., Bruggner, R. V., Linderman, M. D., Sachs, K. et al.**, Extracting a cellular hierarchy from high-dimensional cytometry data with SPADE. *Nat. Biotechnol.* 2011. **29**: 886–891.

1805 **Naim, I., Datta, S., Cavenaugh, J. S., Mosmann, T. R. and Sharma, G.**, SWIFT-scalable clustering for automated identification of rare cell populations in large, high-dimensional flow cytometry datasets, Part 1: Algorithm design, *Cytometry A* 2014. **85**: 408–421.

1806 **Leipold, M. D. and Maecker, H. T.**, Mass cytometry: protocol for daily tuning and running cell samples on a CyTOF mass cytometer. *J. Vis. Exp.* 2012. e4398.

1807 **Fletez-Brant, K., Spidlen, J., Brinkman, R. R., Roederer, M. and Chattopadhyay, P. K.**, flowClean: Automated identification and removal of fluorescence anomalies in flow cytometry data. *Cytometry A* 2016. **89**: 461–471.

1808 **Finak, G., Perez, J. M., Weng, A. and Gottardo, R.**, Optimizing transformations for automated, high throughput analysis of flow cytometry data. *BMC Bioinformatics*. 2010. **11**: 546.

1809 **Finak, G., Perez, J. M. and Gottardo, R.**, flowTrans: Parameter Optimization for Flow Cytometry Data Transformation. *R package version* 1.24.0. 2010.

1810 **Hahne, F., Khodabakhshi, A. H., Bashashati, A., Wong, C. J., Gascoyne, R. D., Weng, A. P., Seyfert-Margolis, V. et al.**, Per-channel basis normalization methods for flow cytometry data. *Cytometry A* 2010. **77**: 121–131.

1811 **Finak, G., Jiang, W., Krouse, K., Wei, C., Sanz, I., Phippard, D., Asare, A. et al.**, High–throughput flow cytometry data normalization for clinical trials. *Cytometry A* 2014. **85**: 277–286

1812 **Mair, F.**, Gate to the future: computational analysis of immunophenotyping data. *Cytometry A* 2019. **95**: 147–149.

1813 **Aghaeepour, N., Chattopadhyay, P., Chikina, M., Dhaene, T., Van Gassen, S., Kursa, M., Lambrecht, B. N. et al.**, A benchmark for evaluation of algorithms for identification of cellular correlates of clinical outcomes. *Cytometry* 2016. **89**: 16–21.

1814 **Weber, L. M. and Robinson, M. D.**, Comparison of clustering methods for high-dimensional single-cell flow and mass cytometry data. *Cytometry A* 2016. **89**: 1084–1096.

1815 **Li, H., Shaham, U., Stanton, K. P., Yao, Y., Montgomery, R. R. and Kluger, Y.**, Gating mass cytometry data by deep learning. *Bioinformatics* 2017. **33**: 3423–3430.

1816 **Ko, B. S., Wang, Y. F., Li, J. L., Li, C. C., Weng, P. F., Hsu, S. C., Hou, H. A. et al.**, Clinically validated machine learning algorithm for detecting residual diseases with multicolor flow cytometry analysis in acute myeloid leukemia and myelodysplastic syndrome. *EBioMedicine* 2018. **37**: 91–100.

1817 **Azad, A., Rajwa, B. and Pothen, A.**, Immunophenotype discovery, hierarchical organization, and template-based classification of flow cytometry samples. *Front. Oncol.* 2016. **6**: 188.

1818 **Finak, G., Frelinger, J., Jiang, W., Newell, E. W., Ramey, J., Davis, M. M., Kalams, S. A. et al.**, OpenCyto: An open source infrastructure for scalable, robust, reproducible, and automated, end-to-end flow cytometry data analysis. *PLoS Comput. Biol.* 2014. **10**: e1003806.

1819 **Malek, M., Taghiyar, M. J., Chong, L., Finak, G., Gottardo, R. and Brinkman, R. R.**, flowDensity: Reproducing manual gating of flow cytometry data by automated density-based cell population identification. *Bioinformatics* 2015. **31**: 606–607.

1820 **Lux, M., Brinkman, R. R., Chauve, C., Laing, A., Lorenc, A., Abeler-Dörner, L., Hammer, B. et al.**, flowLearn: fast and precise identification and quality checking of cell populations in flow cytometry. *Bioinformatics* 2018. **1**: 9.

1821 **Kalina, T., Flores-Montero, J., Lecrevisse, Q., Pedreira, C. E., van der Velden, V. H., Novakova, M., Mejstrikova, E., Hrusak, O. et al.**, Quality assessment program for Euro Flow protocols: Summary results of four-year (2010–2013) quality assurance rounds. *Cytometry A* 2015. **87**(2): 145–156.

1822 **Aghaeepour, N.**, FlowMeans: non-parametric flow cytometry data gating. R package version. 2010. 1(0).

1823 **Aghaeepour, N. and Simonds, E. F.**, GateFinder: projection-based gating strategy optimization for polychromatic and mass flow cytometry data. *Bioinformatics* 2018. **34**: 4131–4133.

1824 **Amir, E.-A. D., Davis, K. L., Tadmor, M. D., Simonds, E. F., Levine, J. H., Bendall, S. C., Shenfeld, D. K. et al.**, viSNE enables visualization of high dimensional single-cell data and reveals phenotypic heterogeneity of leukemia. *Nat. Biotechnol.* 2013. **31**: 545–552.

1825 **Samani, F. S., Moore, J. K., Khosravani, P. and Ebrahimi, M.**, Features of free software packages in flow cytometry: a comparison between four non-commercial software sources. *Cytotechnology*. 2014. **66**(4): 555–559.

1826 **Chen, T. J. and Kotecha, N.**, Cytobank: providing an analytics platform for community cytometry data analysis and collaboration. *Curr. Top. Microbiol. Immunol.* 2014. **377**: 127–157.

1827 **Roederer, M., Nozzi, J. L. and Nason, M. C.**, SPICE: Exploration and analysis of post-cytometric complex multivariate datasets. *Cytometry A.* 2011. **79**: 167–174.

1828 **Spidlen, J., Barsky, A., Breuer, K., Carr, P., Nazaire, M. D., Hill, B. A., Qian, Y. et al.**, GenePattern flow cytometry suite. *Source Code Biol. Med.* 2013. **8**: 14.

1829 **Brinkman, R. R., Aghaeepour, N., Finak, G., Gottardo, R., Mosmann, T. and Scheuermann, R. H.**, Automated analysis of flow cytometry data comes of age. *Cytometry A* 2016. **89**: 16–21.

1830 **Benjamini, Y. and Hochberg, Y.**, Controlling the False Discovery Rate - a Practical and Powerful Approach to Multiple Testing. *Journal of the Royal Statistical Society Series B-Methodological* 1995. **57**: 289–300.

1831 **Almudevar, A.**, Multiple hypothesis testing: a methodological overview. *Methods Mol. Biol.* 2013. **972**: 37–55.

1832 **Rebhahn, J. A., Roumanes, D. R., Qi, Y., Khan, A., Thakar, J., Rosenberg, A., Lee, F. E. et al.**, Competitive SWIFT cluster templates enhance detection of aging changes. *Cytometry A* 2016. **89**: 59–70.

1833 **Maaten, L. V. D. and Hinton, G.**, Visualizing data using t-SNE. *J. Mach. Learn. Res.* 2008. **9**: 2579–2605.

1834 **Aghaeepour, N., Jalali, A., O'Neill, K., Chattopadhyay, P. K., Roederer, M., Hoos, H. H. and Brinkman, R. R.**, RchyOptimyx: Cellular hierarchy optimization for flow cytometry. *Cytometry A* 2012. **81**: 1022–1030.

1835 **O'Neill, K., Jalali, A., Aghaeepour, N., Hoos, H. and Brinkman, R. R.**, Enhanced flowType/RchyOptimyx: a bioconductor pipeline for discovery in high-dimensional cytometry data. *Bioinformatics* 2014. **30**: 1329–1330.

1836 **Tong, D. L., Ball, G. R. and Pockley, A. G.**, gEM/GANN: a multivariate computational strategy for auto-characterizing relationships between cellular and clinical phenotypes and predicting disease progression time using high-dimensional flow cytometry data. *Cytometry* 2015. **87**: 616–623.

1837 **Gassen, S. V., Vens, C., Dhaene, T., Lambrecht, B. N. and Saeys, Y.**, FloReMi: flow density survival regression using minimal feature redundancy. *Cytometry A* 2015. **89**: 22–29.

1838 **Mair, F., Hartmann, F. J., Mrdjen, D., Tosevski, V., Krieg, C. and Becher, B.**, The end of gating? An introduction to automated analysis of high dimensional cytometry data. *Eur. J. Immunol.* 2016. **46**: 34–43.

1839 **LeCun, Y., Bengio, Y. and Hinton, G.**, Deep learning. *Nature* 2015. **521**: 436–444.

1840 **Rosenblatt, F.**, The Perceptron: a probabilistic model for information storage and organization in the brain. *Psychol. Rev.* 1958. **65**: 386–408.

1841 **Szegedy, C., Liu, W., Jia, Y., Sermanet, P., Reed, S. E., Anguelov, D., Erhan, D. et al.**, Going deeper with convolutions. 2015 IEEE Conference on Computer Vision and Pattern Recognition (CVPR), Boston, MA, 2015, pp. 1–9.

1842 **Gupta, P. J. Harrison, Wieslander, H., Pielawski, N., Kartasalo, K., Partel, G., Solorzano, L., Suveer, A. et al.**, Deep learning in image cytometry: a review. *Cytometry A* 2019. **95**: 366–380.

1843 **Eulenberg, P., Koehler, N., Blasi, T., Filby, A., Carpenter, A. E., Rees, P., Theis, F. J. et al.**, Reconstructing cell cycle and disease progression using deep learning. *Nat. Commun.* 2017. **8**: 463.

1844 **Behrmann, J., Etmann, C., Boskamp, T., Casadonte, R., Kriegsmann, J. and Maass, P.**, Deep learning for tumor classification in imaging mass spectrometry. *Bioinformatics* 2017. **1**: 1–10.

1845 **Arvaniti, E. and Claassen, M.**, Sensitive detection of rare disease-associated cell subsets via representation learning. *Nat. Commun.* 2017. **8**: 14825

1846 **Li, H., Shaham, U., Stanton, K. P., Yao, Y., Montgomery, R. R., Kluger, Y. et al.**, Gating mass cytometry data by deep learning. *Bioinformatics* 2017. **33**: 3423–3430.

1847 **Ornatsky, O. I., Kinach, R., Bandura, D. R., Lou, X., Tanner, S. D., Baranov, V. I., Nitz, M. and Winnik, M. A.**, Development of analytical methods for multiplex bio-assay with inductively coupled plasma mass spectrometry. *J. Anal. At. Spectrom.* 2008. **23**: 463–469.

1848 **Jolliffe, I. T.**, *Principal component analysis*, Springer Science & Business Media, Berlin, Germany 2002.

1849 **Bendall, S. C., Simonds, E. F., Qiu, P., Amir el, A. D., Krutzik, P. O., Finck, R., Bruggner, R. V. et al.**, Single-cell mass cytometry of differential immune and drug responses across a human hematopoietic continuum. *Science* 2011. **332**: 687–696.

1850 **Newell, E. W., Sigal, N., Bendall, S. C., Nolan, G. P. and Davis, M. M.**, Cytometry by time-of-flight shows combinatorial cytokine expression and virus-specific cell niches within a continuum of CD8+ T cell phenotypes. *Immunity* 2012. **36**: 142–152.

1851 **Kotecha, N., Krutzik, P. O. and Irish, J. M.**, Web-based analysis and publication of flow cytometry experiments. *Curr. Protoc. Cytom.* 2010. Chapter 10, Unit10.17.

1852 **Höllt, T. et al.**, Cytosplore: interactive immune cell phenotyping for large single-cell datasets. *Comput. Graphics Forum* 2016. **35**: 171–180.

1853 **Chen, H. et al.**, Cytofkit: a bioconductor package for an integrated mass cytometry data analysis pipeline. *PLoS Comput. Biol.* 2016. **12**: e1005112.

1854 **Kobak, D. and Berens, P.**, The art of using t-SNE for single-cell transcriptomics. *bioRxiv*. 2018. Available at: https://doi.org/10.1101/453449

1855 **Wattenberg, M., Viégas, F. and Johnson, I.**, How to use t-SNE effectively. *Distill* 2016. **1**(10). https://doi.org/10.23915/distill.00002

1856 **Belkina, A. C. et al.**, Automated optimal parameters for T-distributed stochastic neighbor embedding improve visualization and allow analysis of large datasets. *bioRxiv*. 2018.

1857 **Linderman, G. C., Rachh, M., Hoskins, J. G., Steinerberger, S. and Kluger, Y.**, Efficient Algorithms for t-distributed stochastic neighborhood embedding. *arXiv*. 2017. Available at: https://arxiv.org/abs/1712.09005

1858 **van der Maaten, L. J. P.**, Accelerating t-SNE using tree-based algorithms. *J. Mach. Learn. Res.* 2014. (15): 3221–3245.

1859 **Pezzotti, N., Lelieveldt, B. P. F., Van Der Maaten, L., Hollt, T., Eisemann, E., Vilanova, A. et al.**, Approximated and user steerable tSNE for progressive visual analytics. *IEEE Trans. Vis. Comput. Graph.* 2017. **23**: 1739–1752.

1860 **Linderman, G. C., Rachh, M., Hoskins, J. G., Steinerberger, S. and Kluger, Y.**, Fast interpolation-based t-SNE for improved visualization of single-cell RNA-seq data. *Nat. Methods* 2019. **16**(3): 243–245.

1861 **Pezzotti, N., Höll, T., Lelieveldt, T., Eisemann, E. and Vilanova, A.**, Hierarchical stochastic neighbor embedding. *Comput. Graphics Forum* 2016. **35**: 21–30.

1862 **van Unen, V., Höllt, T., Pezzotti, N., Li, N., Reinders, M. J. T., Eisemann, E., Koning, F. et al.**, Visual analysis of mass cytometry data by hierarchical stochastic neighbour embedding reveals rare cell types. *Nat. Commun.* 2017. **8**: 1740.

1863 **Linderman, G. C. and Steinerberger, S.**, Clustering with t-SNE, provably. *arXiv*. 2017. Available at: https://arxiv.org/abs/1706.02582

1864 **Shekhar, K. et al.**, Automatic classification of cellular expression by nonlinear stochastic embedding (ACCENSE). *Proc. Natl. Acad. Sci. USA* 2014. **111**: 202–207.

1865 **Murphy, R. F.**, Automated identification of subpopulations in flow cytometric list mode data using cluster analysis. *Cytometry*. 1985. **6**: 302–309.

1866 **Diggins, K. E., Gandelman, J. S., Roe, C. E. and Irish, J. M.**, Generating quantitative cell identity labels with marker enrichment modeling (MEM). *Curr. Protoc. Cytom.* 2018. **83**: 10.21.1–10.21.28.

1867 **Schadt, E. E., Lamb, J., Yang, X., Zhu, J., Edwards, S., Guhathakurta, D., Sieberts, S. K. et al.**, An integrative genomics approach to infer causal associations between gene expression and disease. *Nat. Genet.* 2005. **37**: 710–717.

1868 **Emilsson, V., Thorleifsson, G., Zhang, B., Leonardson, A. S., Zink, F., Zhu, J., Carlson, S. et al.**, Genetics of gene expression and its effect on disease. *Nature* 2008. **452**: 423–428.

1869 **Stegle, O., Teichmann, S. A. and Marioni, J. C.**, Computational and analytical challenges in single-cell transcriptomics. *Nat. Rev. Genet.* 2015; **16**: 133–145.

1870 **Bantscheff, M., Schirle, M., Sweetman, G., Rick, J. and Kuster, B.**, Quantitative mass spectrometry in proteomics: a critical review. *Anal. Bioanal. Chem.* 2007. **389**: 1017–1031.

1871 **Weston, A. D. and Hood, L.**, Systems biology, proteomics, and the future of health care: toward predictive, preventative, and personalized medicine. *J. Proteome Res.* 2004. **3**: 179–196.

1872 **Aghaeepour, N., Lehallier, B., Baca, Q., Ganio, E. A., Wong, R. J., Ghaemi, M. S., Culos, A. et al.**, A proteomic clock of human pregnancy. *Am. J. Obstet. Gynecol.* 2018. **218**: 347.e1–347.e14.

1873 **Patterson, A. D., Maurhofer, O., Beyoglu, D., Lanz, C., Krausz, K. W., Pabst, T., Gonzalez, F. J. et al.**, Aberrant lipid metabolism in hepatocellular carcinoma revealed by plasma metabolomics and lipid profiling. *Cancer Res.* 2011. **71**: 6590–6600.

1874 **Zhao, Y., Fu, L., Li, R., Wang, L. N., Yang, Y., Liu, N. N., Zhang, C. M. et al.**, Metabolic profiles characterizing different phenotypes of polycystic ovary syndrome: plasma metabolomics analysis. *BMC Med.* 2012. **10**: 153.

1875 **Chen, X., Liu, L., Palacios, G., Gao, J., Zhang, N., Li, G., Lu, J. et al.**, Plasma metabolomics reveals biomarkers of the atherosclerosis. *J. Sep. Sci.* 2010. **33**: 2776–2783.

1876 **Psychogios, N., Hau, D. D., Peng, J., Guo, A. C., Mandal, R., Bouatra, S., Sinelnikov, I. et al.**, The human serum metabolome. *PLoS One* 2011. **6**: e16957.

1877 **Bathe, O. F. et al.**, Feasibility of identifying pancreatic cancer based on serum metabolomics. *Cancer Epidemiol. Biomarkers Prev.* 2011. **20**: 140–147.

1878 **Zhang, A., Sun, H. and Wang, X.**, Serum metabolomics as a novel diagnostic approach for disease: a systematic review. *Anal. Bioanal. Chem.* 2012. **404**: 1239–1245.

1879 **Bouatra, S., Aziat, F., Mandal, R., Guo, A. C., Wilson, M. R., Knox, C., Bjorndahl, T. C. et al.**, The human urine metabolome. *PLoS One* 2013. **8**: e73076.

1880 **Kim, Y., Koo, I., Jung, B. H., Chung, B. C. and Lee, D.**, Multivariate classification of urine metabolome profiles for breast cancer diagnosis. *BMC Bioinformatics* 2010. **11**: S4.

1881 **Dethlefsen, L., McFall-Ngai, M. and Relman, D. A.**, An ecological and evolutionary perspective on human-microbe mutualism and disease. *Nature* 2007. **449**: 811–818.

1882 **Woodward, L. J., Anderson, P. J., Austin, N. C., Howard, K. and Inder, T. E.**, Neonatal MRI to predict neurodevelopmental outcomes in preterm infants. *N. Engl. J. Med.* 2006. **355**: 685–694.

1883 **Giesen, C., Wang, H. A., Schapiro, D., Zivanovic, N., Jacobs, A., Hattendorf, B., Schuffler, P. J. et al.**, Highly multiplexed imaging of tumor tissues with subcellular resolution by mass cytometry. *Nat. Methods* 2014. **11**: 417–422.

1884 **Halilaj, E., Hastie, T. J., Gold, G. E. and Delp, S. L.**, Physical activity is associated with changes in knee cartilage microstructure. *Osteoarthr. Cartil.* 2018. **26**: 770–774.

1885 **Jensen, P. B., Jensen, L. J. and Brunak, S.**, Mining electronic health records: towards better research applications and clinical care. *Nat. Rev. Genet.* 2012. **13**: 395–405.

1886 **Marbach, D., Costello, J. C., Küffner, R., Vega, N. M., Prill, R. J., Camacho, D. M., Allison, K. R. et al.**, Wisdom of crowds for robust gene network inference. *Nat. Methods* 2012. **9**: 796–804.

1887 **Elhalawani, H. et al.**, Machine Learning Applications in Head and Neck Radiation Oncology: Lessons From Open-Source Radiomics Challenges. *Front. Oncol.* 2018. **8**: 294.

1888 **Ritchie, M. D., Holzinger, E. R., Li, R., Pendergrass, S. A. and Kim, D.**, Methods of integrating data to uncover genotype-phenotype interactions. *Nat. Rev. Genet.* 2015. **16**: 85–97.

1889 **Feinberg, A. P.**, Epigenomics reveals a functional genome anatomy and a new approach to common disease. *Nat. Biotechnol.* 2010. **28**: 1049–1052.

1890 **Huang, S., Chaudhary, K. and Garmire, L. X.**, More Is Better: Recent Progress in Multi-Omics Data Integration Methods. *Front. Genet.* 2017. **8**: 84.

1891 **Bersanelli, M. et al.**, Methods for the integration of multi-omics data: mathematical aspects. *BMC Bioinformatics* 2016. **17**(Suppl 2): 15.

1892 **Li, Y., Wu, F-X. and Ngom, A.**, A review on machine learning principles for multi-view biological data integration. *Brief. Bioinformatics* 2018. **19**: 325–340.

1893 **Tini, G., Marchetti, L., Priami, C. and Scott-Boyer, M-P.**, Multi-omics integration-a comparison of unsupervised clustering methodologies. *Brief. Bioinformatics* 2017. bbx167

1894 **Shen, R., Olshen, A. B. and Ladanyi, M.**, Integrative clustering of multiple genomic data types using a joint latent variable model with application to breast and lung cancer subtype analysis. *Bioinformatics* 2009. **25**: 2906–2912.

1895 **Lock, E. F., Hoadley, K. A., Marron, J. S. and Nobel, A. B.**, Joint and individual variation explained (jive) for integrated analysis of multiple data types. *Ann. Appl. Stat.* 2013. **7**: 523–542.

1896 **Wang, B. et al.**, Similarity network fusion for aggregating data types on a genomic scale. *Nat. Methods* 2014. **11**: 333–337.

1897 **Nassar, H. and Gleich, D. F.**, in *Proceedings of the 2017 SIAM international conference on data mining*, In N. Chawla, W. Wang, (Eds) Society for Industrial and Applied Mathematics, Philadelphia, PA, 2017. pp. 615–623.

1898 **Lock, E. F., Dunson, D. B.**, Bayesian consensus clustering. *Bioinformatics* 2013. **29**: 2610–2616.

1899 **Lin, D., Zhang, J., Li, J., Calhoun, V. D., Deng, H. W. and Wang, Y. P.**, Group sparse canonical correlation analysis for genomic data integration. *BMC Bioinformatics* 2013. **14**: 245.

1900 **Holzinger, E. R., Dudek, S. M., Frase, A. T., Pendergrass, S. A. and Ritchie, M. D.**, ATHENA: the analysis tool for heritable and environmental network associations. *Bioinformatics* 2014. **30**: 698–705.

1901 **Ghaemi, M. S. et al.**, Multiomics modeling of the immunome, transcriptome, microbiome, proteome and metabolome adaptations during human pregnancy. *Bioinformatics* 2019. **35**: 95–103.

1902 **Singh, A. et al.**, DIABLO: an integrative approach for identifying key molecular drivers from multi-omic assays. *Bioinformatics* 2019. https://doi.org/10.1093/bioinformatics/bty1054

1903 **He, L., Yang, Z., Zhao, Z., Lin, H. and Li, Y.**, Extracting drug-drug interaction from the biomedical literature using a stacked generalization-based approach. *PLoS One* 2013. **8**: e65814.

1904 **Bendall, S. C., Davis, K. L., Amir, E.-A. D., Tadmor, M. D., Simonds, E. F., Chen, T. J., Shenfeld, D. K. et al.**, Single-cell trajectory detection uncovers progression and regulatory coordination in human B cell development. *Cell* 2014. **157**: 714–725.

1905 **Saelens, W., Cannoodt, R., Todorov, H. and Saeys, Y.**, A comparison of single-cell trajectory inference methods. *Nat. Biotechnol.* 2019. **37**: 547–554.

1906 **Treutlein, B., Lee, Q. Y., Camp, J. G., Mall, M., Koh, W., Shariati, S. A. M., Sim, S. et al.**, Dissecting direct reprogramming from fibroblast to neuron using single-cell RNA-seq. *Nature* 2016. **534**: 391–395.

1907 **Cannoodt, R., Saelens, W. and Saeys, Y.**, Computational methods for trajectory inference from single cell transcriptomics. *Eur. J. Immunol.* 2016. **46**: 2496–2506.

1908 **Rebhahn, J. A., Deng, N., Sharma, G., Livingstone, A. M., Huang, S. and Mosmann, T. R.**, An animated landscape representation of CD4+ T-cell differentiation, variability, and plasticity: insights into the behavior of populations versus cells. *Eur. J. Immunol.* 2014. **44**: 2216–2229.

1909 **Dean, P. N. and Jett, J. J.**, Mathematical analysis of DNA distributions derived from flow microfluorometry. *J. Cell. Biol.* 1974. **60**: 523–527.

1910 **Gray, J. W.**, Cell cycle analysis from computer synthesis of deoxyribonucleic acid histograms. *J. Histochem. Cytochem.* 1974. **22**: 642–650.

1911 **Watson, J. V.**, The application of age distribution theory in the analysis of cytofluorimetric DNA-histogram data. *Cell Tissue Kinet.* 1977. **10**: 157–169.

1912 **Watson, J. V., Chambers, S. H. and Smith, P. J.**, A pragmatic approach to the analysis of DNA histograms with a definable G1 peak. *Cytometry* 1987. **8**: 1–8.

1913 **Rosenblatt, J. I., Hokanson, J. A., McLaughlin, S. R. and Leary, J. F.**, Theoretical basis for sampling statistics useful for detecting and isolating rare cells using flow cytometry and cell sorting. *Cytometry* 1997. **27**: 233–238.

1914 **Poisson, S. D.**, *Recherches sur la probabilité des jugements en matière criminelle et en matière civile: précédées des règles générales du calcul des probabilités*. Bachelier, Paris, France, 1837.

1915 **Gosset, W. S.**, The probable error of a mean. *Biometrica* 1908. **6**: 1–25.

1916 **Fisher, R. A.**, *Statistical methods for research workers*. Oliver & Boyd, Edinburgh, U.K., 1925.

1917 **Watson, J. V.**, *Flow cytometry data analysis: basic concepts and statistics*, Cambridge University Press, Cambridge, UK, 2005.

1918 **Fisher, R. A. and Yates, F.**, *Statistical tables for biological, medical and agricultural research*. Oliver and Boyd, Edinburgh, UK, 1963. p. 86.

1919 **Snedecor, G. W.**, *Statistical methods* 4th ed., Iowa State College Press, Ames, Iowa, 1946.

1920 **Wilcoxon, F.**, Individual comparisons by ranking methods. *Biometrics Bull.* 1945. **1**: 80–83.

1921 **Mann, H. B. and Whitney, D. R.**, On a test of whether one of two random variables is stochastically larger than the other. *Ann. Math. Stat.* 1947. **18**: 50–60.

1922 **Siegel, S. and Castellón, N. J.**, *Non-parametric statistics for the behavioral sciences*, 2nd ed., McGraw-Hill, New York, NY, 1988, Chapter 6.

1923 **Young, I. T.**, Proof without prejudice: use of the Kolmogorov–Smirnov test for the analysis of histograms from flow systems and other sources. *J. Histochem. Cytochem.* 1977. **25**: 935–941.

1924 **Kendall, M. G.**, Rank and product-moment correlation. *Biometrika* 1949. **36**: 177–193.

1925 **Watson, J. V.**, Proof without prejudice revisited: Immunofluorescence histogram analysis using cumulative frequency subtraction plus ratio analysis of means. *Cytometry* 2001. **43**: 55–68.

1926 **Bocsi, J., Melzer, S., Dähnert, I. and Tárnok, A.**, OMIP-023: 10-color, 13 antibody panel for in-depth phenotyping of human peripheral blood leukocytes. *Cytometry A* 2014. **85**: 781–784.

1927 **Melzer, S., Zachariae, S., Bocsi, J., Engel, C., Löffler, M. and Tárnok, A.**, Reference intervals for leukocyte subsets in adults: Results from a population-based study using 10-color flow cytometry. *Cytometry B Clin. Cytom.* 2015. **88**: 270–281.

1928 **Nettey, L., Giles, A. J. and Chattopadhyay, P. K.**, OMIP-050: a 28-color/30-parameter fluorescence flow cytometry panel to enumerate and characterize cells expressing a wide array of immune checkpoint molecules. *Cytometry A* 2018. **93**:1094–1096.

1929 **Mazza, E. M. C., Brummelman, J., Alvisi, G., Roberto, A., De Paoli, F., Zanon, V, Colombo, F., Roederer, M. et al.**, Background fluorescence and spreading error are major contributors of variability in high-dimensional flow cytometry data visualization by t-distributed stochastic neighboring embedding. *Cytometry A* 2018. **93**:785–792.

1930 **Diggins, K. E., Ferrell, P. B. and Irish, J. M.**, Methods for discovery and characterization of cell subsets in high dimensional mass cytometry data. *Methods* 2015. **82**: 55–63.

1931 **Pierzchalski, A., Robitzki, A., Mittag, A., Emmrich, F., Sack, U., O'Connor, J. E., Bocsi, J. et al.**, Cytomics and nanobioengineering. *Cytometry B Clin. Cytom.* 2008. **74**:416–426.

1932 **Van Gassen, S., Callebaut, B., Van Helden, M. J., Lambrecht, B. N., Demeester, P., Dhaene, T. and Saeys, Y.**, FlowSOM: using self-organizing maps for visualization and interpretation of cytometry data. *Cytometry A* 2015. **87**: 636–645.

1933 **Elhmouzi-Younes, J., Palgen, J. L., Tchitchek, N., Delandre, S., Namet, I., Bodinham, C. L., Pizzoferro, K. et al.**, In depth comparative phenotyping of blood innate myeloid leukocytes from healthy humans and macaques using mass cytometry. *Cytometry A* 2017. **91**:969–982.

1934 **Loeffler, M., Engel, C., Ahnert, P., Alfermann, D., Arelin, K., Baber, R., Beutner, F. et al.**, The LIFE-Adult-Study: objectives and design of a population-based cohort study with 10 000 deeply phenotyped adults in Germany. *BMC Public Health* 2015. **15**: 691.

1935 **Moher, D., Glasziou, P., Chalmers, I., Nasser, M., Bossuyt, P. M., Korevaar, D. A., Graham, I. D. et al.**, Increasing value and reducing waste in biomedical research: who's listening? *Lancet* 2015. **387**: 1573–1586.

1936 **Taylor, C. F., Field, D., Sansone, S. A., Aerts, J., Apweiler, R., Ashburner, M., Ball, C. A. et al.**, Promoting coherent minimum reporting guidelines for biological and biomedical investigations: the MIBBI project. *Nat. Biotechnol.* 2008. **26**: 889–896.

1937 **Nies, K. P. H., Kraaijvanger, R., Lindelauf, K. H. K., Drent, R. J. M. R., Rutten, R. M. J., Ramaekers, F. C. S. and Leers, M. P. G.**, Determination of the proliferative fractions in differentiating hematopoietic cell lineages of normal bone marrow. *Cytometry A.* 2018. **93**:1097–1105.

1938 **Parks, D. R., Moore, W. A., Brinkman, R. R., Chen, Y., Condello, D., El Khettabi, F., Nolan, J. P. et al.**, Methodology for evaluating and comparing flow cytometers: a multisite study of 23 instruments. *Cytometry A* 2018. **93**:1087–1091.

1939 **Jaracz-Ros, A., Hémon, P., Krzysiek, R., Bachelerie, F., Schlecht-Louf, G. and Gary-Gouy, H.**, OMIP-048 MC: quantification of calcium sensors and channels expression in lymphocyte subsets by mass cytometry. *Cytometry A* 2018. **93**:681–684.

1940 **Leavesley, S. and Tárnok, A.**, Tycho Brahe's way to precision. *Cytometry A*. 2018. **93**:977–979.

1941 **Spidlen, J., Breuer, K. and Brinkman, R.**, Preparing a Minimum Information about a Flow Cytometry Experiment (MIFlowCyt) compliant manuscript using the International Society for Advancement of Cytometry (ISAC) FCS file repository (FlowRepository.org). *Curr. Protoc. Cytom.* 2012. Chapter 10: Unit 10.18.

1942 **Holzwarth, K., Köhler, R., Philipsen, L., Tokoyoda, K., Ladyhina, V., Wählby, C., Niesner, R. A. et al.**, Multiplexed fluorescence microscopy reveals heterogeneity among stromal cells in mouse bone marrow sections. *Cytometry A* 2018. **93**:876–888.

1943 **Roederer, M. and Tárnok, A.**, OMIPs–Orchestrating multiplexity in polychromatic science. *Cytometry A* 2010. **77**: 811–812.

1944 **Finak, G., Jiang, W. and Gottardo, R.**, CytoML for cross-platform cytometry data sharing. *Cytometry A* 2018. **93**: 1189–1196

1945 **O'Neill, K. and Brinkman, R. R.**, Publishing code is essential for reproducible flow cytometry bioinformatics. *Cytometry A* 2016. **89**: 10–11.

1946 Thomson Reuters. Collaborative Science - Solving the Issues of Discovery, Attribution and Measurement in Data Sharing. 2012. http://wokinfo.com/products_tools/multidisciplinary/dci/collaborative_science_essay.pdf

1947 **Piwowar, H. A. and Chapman, W. W.**, A review of journal policies for sharing research data. Proceedings ELPUB 2008 Conference on Electronic Publishing, 2008, http://elpub.scix.net/data/works/att/001_elpub2008.content.pdf

1948 **Fecher, B., Friesike, S. and Hebing, M.**, What drives academic data sharing? *PLoS One* 2015. **10**: e0118053.

1949 **Nicol, A., Caruso, J. and Archambault, É.**, Open Data Access Policies and Strategies in the European Research Area and Beyond. Science-Metrix, Inc. Produced for the European Commission DG Research & Innovation, 2013, http://www.science-metrix.com/pdf/SM_EC_OA_Data.pdf

1950 National Institute of Health. NIH Data Sharing Policy. http://grants.nih.gov/grants/policy/data_sharing/

1951 PLOS. PLOS' New Data Policy: Public Access to Data. http://blogs.plos.org/everyone/2014/02/24/plos-new-data-policy-public-access-data-2/

1952 **Spidlen, J., Breuer, K., Rosenberg, C., Kotecha, N. and Brinkman, R. R.**, FlowRepository: a resource of annotated flow cytometry datasets associated with peer-reviewed publications. *Cytometry A* 2012. **81**: 727–731.

1953 **Kong, Y. M., Dahlke, C., Xiang, Q., Qian, Y., Karp, D. and Scheuermann, R. H.**, Toward an ontology-based framework for clinical research databases. *J. Biomed. Inform.* 2011. **44**: 48–58.

1954 **Bhattacharya, S., Andorf, S., Gomes, L., Dunn, P., Schaefer, H., Pontius, J., Berger, P. et al.**, ImmPort: disseminating data to the public for the future of immunology. *Immunol. Res.* 2014. **58**: 234–239.

1955 **Brusic, V., Gottardo, R., Kleinstein, S. H., Davis, M. M.; HIPC steering committee**, Computational resources for high-dimensional immune analysis from the Human Immunology Project Consortium. *Nat. Biotechnol.* 2014. **32**(2): 146–148.

1956 U.S. Department of Health & Human Services. Summary of the HIPAA Privacy Rule. http://www.hhs.gov/sites/default/files/privacysummary.pdf

1957 **Vasilevsky, N. A., Minnier, J., Haendel, M. A. and Champieux, R. E.**, Reproducible and reusable research: are journal data sharing policies meeting the mark? *Peer J.* 2017. **5**: e3208.

1958 **Kay, D. B., Cambier, J. L. and Wheeless, L. L., Jr.**, Imaging in flow. *J. Histochem. Cytochem.* 1979. **27**: 329–334.

1959 **George, T. C., Basiji, D. A., Hall, B. E., Lynch, D. H., Ortyn, W. E., Perry, D. J., Seo, M. J. et al.**, Distinguishing modes of cell death using the ImageStream multispectral imaging flow cytometer. *Cytometry A* 2004. **59**: 237–245.

1960 **Pozarowski, P., Holden, E. and Darzynkiewicz, Z.**, Laser scanning cytometry: principles and applications-an update. *Methods Mol. Biol.* 2013. **931**: 187–212.

1961 **Stavrakis, S., Holzner, G., Choo, J. and deMello, A.**, High-throughput microfluidic imaging flow cytometry. *Curr. Opin. Biotechnol.* 2019. **55**: 36–43.

1962 **Nitta, N., Sugimura, T., Isozaki, A., Mikami, H., Hiraki, K., Sakuma, S., Iino, T. et al.**, Intelligent image-activated cell sorting. *Cell* 2018. **175**: 266–276.

1963 **Hritzo, M. K., Courneya, J. P. and Golding, A.**, Imaging flow cytometry: a method for examining dynamic native FOXO1 localization in human lymphocytes. *J. Immunol. Methods* 2018. **454**: 59–70.

1964 **Maguire, O., Collins, C., O'Loughlin, K., Miecznikowski, J. and Minderman, H.**, Quantifying nuclear p65 as a parameter for NF-kappaB activation: Correlation between ImageStream cytometry, microscopy, and Western blot. *Cytometry A* 2011. **79**: 461–469.

1965 **Maguire, O., Tornatore, K. M., O'Loughlin, K. L., Venuto, R. C. and Minderman, H.**, Nuclear translocation of nuclear factor of activated T cells (NFAT) as a quantitative pharmacodynamic parameter for tacrolimus. *Cytometry A* 2013. **83**: 1096–1104.

1966 **Stone, R. C., Feng, D., Deng, J., Singh, S., Yang, L., Fitzgerald-Bocarsly, P., Eloranta, M. L. et al.**, Interferon regulatory factor 5 activation in monocytes of systemic lupus erythematosus patients is triggered by circulating autoantigens independent of type I interferons. *Arthritis Rheum.* 2012. **64**: 788–798.

1967 **Trifonova, R. T. and Barteneva, N. S.**, Quantitation of IRF3 nuclear translocation in heterogeneous cellular populations from cervical tissue using imaging flow cytometry. *Methods Mol. Biol.* 2018. **1745**: 125–153.

1968 **Volk, A., Li, J., Xin, J., You, D., Zhang, J., Liu, X., Xiao, Y. et al.**, Co-inhibition of NF-kappaB and JNK is synergistic in TNF-expressing human AML. *J. Exp. Med.* 2014. **211**: 1093–1108.

1969 **Wan, C. K., Andraski, A. B., Spolski, R., Li, P., Kazemian, M., Oh, J., Samsel, L. et al.**, Opposing roles of STAT1 and STAT3 in IL-21 function in CD4+ T cells. *Proc. Natl. Acad. Sci. USA* 2015. **112**: 9394–9399.

1970 **Haridas, V., Ranjbar, S., Vorobjev, I. A., Goldfeld, A. E. and Barteneva, N. S.**, Imaging flow cytometry analysis of intracellular pathogens. *Methods* 2017. **112**: 91–104.

1971 **Pugsley, H. R.**, Quantifying autophagy: Measuring LC3 puncta and autolysosome formation in cells using multispectral imaging flow cytometry. *Methods* 2017. **112**: 147–156.

1972 **Lannigan, J. and Erdbruegger, U.**, Imaging flow cytometry for the characterization of extracellular vesicles. *Methods* 2017. **112**: 55–67.

1973 **Shenoy, G. N., Loyall, J., Maguire, O., Iyer, V., Kelleher, R. J., Jr., Minderman, H., Wallace, P. K. et al.**, Exosomes associated with human ovarian tumors harbor a reversible checkpoint of T-cell responses. *Cancer Immunol. Res.* 2018. **6**: 236–247.

1974 **Ploppa, A., George, T. C., Unertl, K. E., Nohe, B. and Durieux, M. E.**, ImageStream cytometry extends the analysis of phagocytosis and oxidative burst. *Scand J. Clin. Lab. Invest.* 2011. **71**: 362–369.

1975 **Henery, S., George, T., Hall, B., Basiji, D., Ortyn, W. and Morrissey, P.**, Quantitative image based apoptotic index measurement using multi-

spectral imaging flow cytometry: a comparison with standard photometric methods. *Apoptosis* 2008. **13**: 1054–1063.

1976 **Poh, S. E. P., Png, E. and Tong, L.**, Quantitative image analysis of cellular morphology using Amnis® ImageStreamX Mark II imaging flow cytometer: a comparison against conventional methods. *Single Cell Biol.* 2015. **4**: s1.

1977 **Balta, E., Stopp, J., Castelletti, L., Kirchgessner, H., Samstag, Y. and Wabnitz, G. H.**, Qualitative and quantitative analysis of PMN/T-cell interactions by InFlow and super-resolution microscopy. *Methods* 2017. **112**: 25–38.

1978 **Mace, T. A., Zhong, L., Kilpatrick, C., Zynda, E., Lee, C. T., Capitano, M., Minderman, H. et al.**, Differentiation of CD8+ T cells into effector cells is enhanced by physiological range hyperthermia. *J. Leukoc. Biol.* 2011. **90**: 951–962.

1979 **Maguire, O., Wallace, P. K. and Minderman, H.**, Fluorescent in situ hybridization in suspension by imaging flow cytometry. *Methods Mol. Biol.* 2016. **1389**: 111–126.

1980 **Blasi, T., Hennig, H., Summers, H. D., Theis, F. J., Cerveira, J., Patterson, J. O., Davies, D. et al.**, Label-free cell cycle analysis for high-throughput imaging flow cytometry. *Nat. Commun.* 2016. **7**: 10256.

1981 **Ortyn, W. E., Perry, D. J., Venkatachalam, V., Liang, L., Hall, B. E., Frost, K. and Basiji, D. A.**, Extended depth of field imaging for high speed cell analysis. *Cytometry A* 2007. **71**: 215–231.

1982 **Ortyn, W. E., Hall, B. E., George, T. C., Frost, K., Basiji, D. A., Perry, D. J., Zimmerman, C. A. et al.**, Sensitivity measurement and compensation in spectral imaging. *Cytometry A* 2006. **69**: 852–862.

1983 **Chester, C. and Maecker, H. T.**, Algorithmic tools for mining high-dimensional cytometry data. *J. Immunol.* 2015. **195**: 773–779.

1984 **Krutzik, P. O. and Nolan, G. P.**, Fluorescent cell barcoding in flow cytometry allows high-throughput drug screening and signaling profiling. *Nat. Methods* 2006. **3**: 361–368.

1985 **Bodenmiller, B., Zunder, E. R., Finck, R., Chen, T. J., Savig, E. S., Bruggner, R. V., Simonds, E. F. et al.**, Multiplexed mass cytometry profiling of cellular states perturbed by small-molecule regulators. *Nat. Biotechnol.* 2012. **30**: 858–867.

1986 **Behbehani, G. K., Thom, C., Zunder, E. R., Finck, R., Gaudilliere, B., Fragiadakis, G. K., Fantl, W. J. et al.**, Transient partial permeabilization with saponin enables cellular barcoding prior to surface marker staining. *Cytometry A* 2014. **85**: 1011-1019.

1987 **Mei, H. E., Leipold, M. D. and Maecker, H. T.**, Platinum-conjugated antibodies for application in mass cytometry. *Cytometry A* 2016. **89**: 292–300.

1988 **Mei, H. E., Leipold, M. D., Schulz, A. R., Chester, C. and Maecker, H. T.**, Barcoding of live human peripheral blood mononuclear cells for multiplexed mass cytometry. *J. Immunol.* 2015. **194**: 2022–2031.

1989 **Lai, L., Ong, R., Li, J. and Albani, S.**, A CD45-based barcoding approach to multiplex mass-cytometry (CyTOF). *Cytometry A* 2015. **87**: 369–374.

1990 **Akkaya, B., Miozzo, P., Holstein, A. H., Shevach, E. M., Pierce, S. K. and Akkaya, M.**, A simple, versatile antibody-based barcoding method for flow cytometry. *J. Immunol.* 2016.

1991 **Nassar, A. F., Wisnewski, A. V. and Raddassi, K.**, Automation of sample preparation for mass cytometry barcoding in support of clinical research: protocol optimization. *Anal. Bioanal. Chem.* 2017. **409**: 2363–2372.

1992 **Zunder, E. R., Finck, R., Behbehani, G. K., Amir el, A. D., Krishnaswamy, S., Gonzalez, V. D., Lorang, C. G. et al.**, Palladium-based mass tag cell barcoding with a doublet-filtering scheme and single-cell deconvolution algorithm. *Nat. Protoc.* 2015. **10**: 316–333.

1993 **Catena, R., Ozcan, A., Zivanovic, N. and Bodenmiller, B.**, Enhanced multiplexing in mass cytometry using osmium and ruthenium tetroxide species. *Cytometry A* 2016. **89**: 491–497.

1994 **Chevrier, S., Crowell, H. L., Zanotelli, V. R. T., Engler, S., Robinson, M. D. and Bodenmiller, B.**, Compensation of signal spillover in suspension and imaging mass cytometry. *Cell Syst.* 2018. **6**: 612–620.e615.

1995 **Fread, K. I., Strickland, W. D., Nolan, G. P. and Zunder, E. R.**, An updated debarcoding tool for mass cytometry with cell type-specific and cell sample-specific stringency adjustment. *Pac. Symp. Biocomput.* 2017. **22**: 588–598.

1996 **Zivanovic, N., Jacobs, A. and Bodenmiller, B.**, A practical guide to multiplexed mass cytometry. *Curr. Top. Microbiol. Immunol.* 2013.

1997 **Hartmann, F. J., Simonds, E. F. and Bendall, S. C.**, A universal live cell barcoding-platform for multiplexed human single cell analysis. *Sci. Rep.* 2018. **8**: 10770.

1998 **Yamanaka, Y. J., Szeto, G. L., Gierahn, T. M., Forcier, T. L., Benedict, K. F., Brefo, M. S., Lauffenburger, D. A. et al.**, Cellular barcodes for efficiently profiling single-cell secretory responses by microengraving. *Anal. Chem.* 2012. **84**: 10531–10536.

1999 **Schulz, A. R. and Mei, H. E.**, Surface barcoding of live PBMC for multiplexed mass cytometry. *Methods Mol. Biol.* 2019. **1989**: 93–108.

2000 **Simard, C., Cloutier, M. and Neron, S.**, Rapid determination of IL-6 specific activity by flow cytometry. *J. Immunol. Methods* 2014. **415**: 63–65.

2001 **Simard, C., Cloutier, M. and Neron, S., Feasibility study**: phosphospecific flow cytometry enabling rapid functional analysis of bone marrow samples from patients with multiple myeloma. *Cytometry B Clin. Cytom.* 2014. **86**: 139–144.

2002 **Krutzik, P. O., Clutter, M. R., Trejo, A. and Nolan, G. P.**, Fluorescent cell barcoding for multiplex flow cytometry. *Curr. Protoc. Cytom.* 2011. Chapter 6: Unit 6 31.

2003 **Krutzik, P. O., Crane, J. M., Clutter, M. R. and Nolan, G. P.**, High-content single-cell drug screening with phosphospecific flow cytometry. *Nat. Chem. Biol.* 2008. **4**: 132–142.

2004 **Frischbutter, S., Schultheis, K., Patzel, M., Radbruch, A. and Baumgrass, R.**, Evaluation of calcineurin/NFAT inhibitor selectivity in primary human Th cells using bar-coding and phospho-flow cytometry. *Cytometry A* 2012. **81**: 1005–1011.

2005 **Bernardo, S. M., Allen, C. P., Waller, A., Young, S. M., Oprea, T., Sklar, L. A. and Lee, S. A.**, An automated high-throughput cell-based multiplexed flow cytometry assay to identify novel compounds to target Candida albicans virulence-related proteins. *PLoS One* 2014. **9**: e110354.

2006 **Spurgeon, B. E., Aburima, A., Oberprieler, N. G., Tasken, K. and Naseem, K. M.**, Multiplexed phosphospecific flow cytometry enables large-scale signaling profiling and drug screening in blood platelets. *J. Thromb. Haemost.* 2014. **12**: 1733–1743.

2007 **Clark, M. A., Goheen, M. M., Spidale, N. A., Kasthuri, R. S., Fulford, A. and Cerami, C.**, RBC barcoding allows for the study of erythrocyte population dynamics and P. falciparum merozoite invasion. *PLoS One* 2014. **9**: e101041.

2008 **Becher, B., Schlitzer, A., Chen, J., Mair, F., Sumatoh, H. R., Teng, K. W. et al.**, High-dimensional analysis of the murine myeloid cell system. *Nat. Immunol.* 2014. **15**: 1181–1189.

2009 **McCarthy, R. L., Mak, D. H., Burks, J. K. and Barton, M. C.**, Rapid monoisotopic cisplatin based barcoding for multiplexed mass cytometry. *Sci. Rep.* 2017. **7**: 3779.

2010 **Schulz, A. R. and Mei, H. E.**, Cell-surface barcoding of live PBMC for multiplexed mass cytometry. In McGuire, H. and Ashhurst, T. (Eds.) *Methods in molecular biology*. Springer Nature, Basingstoke, UK 2019.

2011 **Willis, L. M., Park, H., Watson, M. W. L., Majonis, D., Watson, J. L. and Nitz, M.**, Tellurium-based mass cytometry barcode for live and fixed cells. *Cytometry A* 2018. **93**: 685–694.

2012 **Wu, X., DeGottardi, Q., Wu, I. C., Wu, L., Yu, J., Kwok, W. W. and Chiu, D. T.**, Ratiometric Barcoding for Mass Cytometry. *Anal. Chem.* 2018. **90**: 10688–10694.

2013 **Meng, H., Warden, A., Zhang, L., Zhang, T., Li, Y., Tan, Z., Wang, B. et al.**, A mass-ratiometry-based CD45 barcoding method for mass cytometry detection. *SLAS Technol.* 2019. 2472630319834057.

2014 **Irish, J. M., Myklebust, J. H., Alizadeh, A. A., Houot, R., Sharman, J. P., Czerwinski, D. K., Nolan, G. P. et al.**, B-cell signaling networks reveal a negative prognostic human lymphoma cell subset that emerges during tumor progression. *Proc. Natl. Acad. Sci. USA* 2010. **107**: 12747–12754.

2015 **Gaudillière, B., Fragiadakis, G. K., Bruggner, R. V., Nicolau, M., Finck, R., Tingle, M., Silva, J. et al.**, Clinical recovery from surgery correlates with single-cell immune signatures. *Sci. Transl. Med.* 2014. **6**: 255ra131.

2016 **Bandura, D. R., Baranov, V. I., Ornatsky, O. I., Antonov, A., Kinach, R., Lou, X., Pavlov, S. et al.**, Mass cytometry: technique for real time single cell multitarget immunoassay based on inductively coupled plasma time-of-flight mass spectrometry. *Anal. Chem.* 2009. **81**: 6813–6822.

2017 **Bendall, S. C., Nolan, G. P., Roederer, M. and Chattopadhyay, P. K.**, A deep profiler's guide to cytometry. *Trends Immunol.* 2012. **33**: 323–332.

2018 **Tanner, S. D., Baranov, V. I., Ornatsky, O. I., Bandura, D. R. and George, T. C.**, An introduction to mass cytometry: fundamentals and applications. *Cancer Immunol. Immunother.* 2013. **62**: 955–965.

2019 **Wong, M. T., Ong, D. E., Lim, F. S., Teng, K. W., McGovern, N., Narayanan, S., Ho, W. Q. et al.**, A high-dimensional atlas of human T cell diversity reveals tissue-specific trafficking and cytokine signatures. *Immunity* 2016. **45**: 442–456.

2020 **Zunder, E. R., Lujan, E., Goltsev, Y., Wernig, M. and Nolan, G. P.**, A continuous molecular roadmap to iPSC reprogramming through progression analysis of single-cell mass cytometry. *Cell Stem Cell* 2015. **16**: 323–337.

2021 **Nair, N., Mei, H. E., Chen, S. Y., Hale, M., Nolan, G. P., Maecker, H. T., Genovese, M. et al.**, Mass cytometry as a platform for the discovery of cellular biomarkers to guide effective rheumatic disease therapy. *Arthritis Res. Ther.* 2015. **17**: 127.

2022 **Mingueneau, M., Boudaoud, S., Haskett, S., Reynolds, T. L., Nocturne, G., Norton, E., Zhang, X. et al.**, Cytometry by time-of-flight immunophenotyping identifies a blood Sjogren's signature correlating with disease activity and glandular inflammation. *J. Allergy Clin. Immunol.* 2016. **137**: 1809–1821 e1812.

2023 **Olin, A., Henckel, E., Chen, Y., Lakshmikanth, T., Pou, C., Mikes, J., Gustafsson, A. et al.**, Stereotypic immune system development in newborn children. *Cell* 2018. **174**: 1277–1292.

2024 **Brodin, P., Jojic, V., Gao, T., Bhattacharya, S., Angel, C. J., Furman, D., Shen-Orr, S. et al.**, Variation in the human immune system is largely driven by non-heritable influences. *Cell* 2015. **160**: 37–47.

2025 **Pejoski, D., Tchitchek, N., Rodriguez Pozo, A., Elhmouzi-Younes, J., Yousfi-Bogniaho, R., Rogez-Kreuz, C., Clayette, P. et al.**, Identification of vaccine-altered circulating b cell phenotypes using mass cytometry and a two-step clustering analysis. *J. Immunol.* 2016. **196**: 4814–4831.

2026 **Leipold, M. D., Ornatsky, O., Baranov, V., Whitfield, C. and Nitz, M.**, Development of mass cytometry methods for bacterial discrimination. *Anal. Biochem.* 2011. **419**: 1–8.

2027 **Guo, Y., Baumgart, S., Stark, H. J., Harms, H. and Muller, S.**, Mass cytometry for detection of silver at the bacterial single cell level. *Front Microbiol.* 2017. **8**: 1326.

2028 **Yang, Y. S., Atukorale, P. U., Moynihan, K. D., Bekdemir, A., Rakhra, K., Tang, L., Stellacci, F. et al.**, High-throughput quantitation of inorganic nanoparticle biodistribution at the single-cell level using mass cytometry. *Nat. Commun.* 2017. **8**: 14069.

2029 **Abdelrahman, A. I., Ornatsky, O., Bandura, D., Baranov, V., Kinach, R., Dai, S., Thickett, S. C. et al.**, Metal-containing polystyrene beads as standards for mass cytometry. *J. Anal. At Spectrom.* 2010. **25**: 260–268.

2030 **Galli, E., Friebel, E., Ingelfinger, F., Unger, S., Nunez, N. G. and Becher, B.**, The end of omics? High dimensional single cell analysis in precision medicine. *Eur. J. Immunol.* 2019. **49**: 212–220.

2031 **Kimball, A. K., Oko, L. M., Bullock, B. L., Nemenoff, R. A., van Dyk, L. F. and Clambey, E. T.**, A beginner's guide to analyzing and visualizing mass cytometry data. *J. Immunol.* 2018. **200**: 3–22.

2032 **Cosma, A.**, A time to amaze, a time to settle down, and a time to discover. *Cytometry A* 2015. **87**: 795–796.

2033 **Chang, Q., Ornatsky, O. I., Siddiqui, I., Loboda, A., Baranov, V. I. and Hedley, D. W.**, Imaging mass cytometry. *Cytometry A* 2017. **91**: 160–169.

2034 **Zhao, Y., Uduman, M., Siu, J. H. Y., Tull, T. J., Sanderson, J. D., Wu, Y. B., Zhou, J. Q. et al.**, Spatiotemporal segregation of human marginal zone and memory B cell populations in lymphoid tissue. *Nat. Commun.* 2018. **9**: 3857.

2035 **Keren, L., Bosse, M., Marquez, D., Angoshtari, R., Jain, S., Varma, S., Yang, S. R. et al.**, A structured tumor-immune microenvironment in triple negative breast cancer revealed by multiplexed ion beam imaging. *Cell* 2018. **174**: 1373–1387 e1319.

2036 **Tricot, S., Meyrand, M., Sammicheli, C., Elhmouzi-Younes, J., Corneau, A., Bertholet, S., Malissen, M., Le Grand, R. et al.**, Evaluating the efficiency of isotope transmission for improved panel design and a comparison of the detection sensitivities of mass cytometer instruments. *Cytometry A* 2015. **87**: 357–368.

2037 **Rahman, A. H., Tordesillas, L. and Berin, M. C.**, Heparin reduces nonspecific eosinophil staining artifacts in mass cytometry experiments. *Cytometry A* 2016. **89**: 601–607.

2038 **Schulz, A. R., Stanislawiak, S., Baumgart, S., Grutzkau, A. and Mei, H. E.**, Silver nanoparticles for the detection of cell surface antigens in mass cytometry. *Cytometry A* 2017. **91**: 25–33.

2039 **Lin, W., Hou, Y., Lu, Y., Abdelrahman, A. I., Cao, P., Zhao, G., Tong, L. et al.**, A high-sensitivity lanthanide nanoparticle reporter for mass cytometry: tests on microgels as a proxy for cells. *Langmuir* 2014. **30**: 3142–3153.

2040 **Tong, L., Lu, E., Pichaandi, J., Zhao, G. and Winnik, M. A.**, Synthesis of uniform NaLnF4 (Ln: Sm to Ho) nanoparticles for mass cytometry. *J. Phys. Chem. C* 2016. **120**: 6269–6280.

2041 **Baumgart, S., Schulz, A. R., Peddinghaus, A., Stanislawiak, S., Gillert, S., Hirseland, H., Krauthauser, S. et al.**, Dual-labelled antibodies for flow and mass cytometry: a new tool for cross-platform comparison and enrichment of target cells for mass cytometry. *Eur. J. Immunol.* 2017.

2042 **Finck, R., Simonds, E. F., Jager, A., Krishnaswamy, S., Sachs, K., Fantl, W., Pe'er, D. et al.**, Normalization of mass cytometry data with bead standards. *Cytometry A* 2013. **83**: 483–494.

2043 **Schulz, A. R., Baumgart, S., Schulze, J., Urbicht, M., Grutzkau, A. and Mei, H. E.**, Stabilizing antibody cocktails for mass cytometry. *Cytometry A* 2019.

2044 **Kadic, E., Moniz, R. J., Huo, Y., Chi, A. and Kariv, I.**, Effect of cryopreservation on delineation of immune cell subpopulations in tumor specimens as determinated by multiparametric single cell mass cytometry analysis. *BMC Immunol.* 2017. **18**: 6.

2045 **Kleinsteuber, K., Corleis, B., Rashidi, N., Nchinda, N., Lisanti, A., Cho, J. L., Medoff, B. D. et al.**, Standardization and quality control for high-dimensional mass cytometry studies of human samples. *Cytometry A* 2016. **89**: 903–913.

2046 **Leipold, M. D., Obermoser, G., Fenwick, C., Kleinstuber, K., Rashidi, N., McNevin, J. P., Nau, A. N. et al.**, Comparison of CyTOF assays across sites: Results of a six-center pilot study. *J. Immunol. Methods* 2018. **453**: 37–43.

2047 **Sumatoh, H. R., Teng, K. W., Cheng, Y. and Newell, E. W.**, Optimization of mass cytometry sample cryopreservation after staining. *Cytometry A* 2017. **91**: 48–61.

2048 **Nicholas, K. J., Greenplate, A. R., Flaherty, D. K., Matlock, B. K., Juan, J. S., Smith, R. M., Irish, J. M. et al.**, Multiparameter analysis of stimulated human peripheral blood mononuclear cells: a comparison of mass and fluorescence cytometry. *Cytometry A* 2016. **89**: 271–280.

2049 **Baumgart, S., Peddinghaus, A., Schulte-Wrede, U., Mei, H. E. and Grutzkau, A.**, OMIP-034: comprehensive immune phenotyping of human peripheral leukocytes by mass cytometry for monitoring immunomodulatory therapies. *Cytometry A* 2017. **91**: 34–38.

2050 **Behbehani, G. K., Bendall, S. C., Clutter, M. R., Fantl, W. J. et al.**, Single-cell mass cytometry adapted to measurements of the cell cycle. *Cytometry A* 2012. **81**: 552–566.

2051 **Frei, A. P., Bava, F. A., Zunder, E. R., Hsieh, E. W., Chen, S. Y., Nolan, G. P. and Gherardini, P. F.**, Highly multiplexed simultaneous detection of RNAs and proteins in single cells. *Nat. Methods* 2016. **13**: 269–275.

2052 **Mavropoulos, A., Allo, B., He, M., Park, E., Majonis, D. and Ornatsky, O.**, Simultaneous detection of protein and mRNA in Jurkat and KG-1a cells by mass cytometry. *Cytometry A* 2017. **91**: 1200–1208.

2053 **Cheung, P., Vallania, F., Warsinske, H. C., Donato, M., Schaffert, S., Chang, S. E., Dvorak, M. et al.**, Single-cell chromatin modification profiling reveals increased epigenetic variations with aging. *Cell* 2018. **173**: 1385–1397 e1314.

2054 **Lumba, M. A., Willis, L. M., Santra, S., Rana, R., Schito, L., Rey, S., Wouters, B. G. et al.**, A beta-galactosidase probe for the detection of cellular senescence by mass cytometry. *Org. Biomol. Chem.* 2017. **15**: 6388–6392.

2055 **Edgar, L. J., Vellanki, R. N., Halupa, A., Hedley, D., Wouters, B. G. and Nitz, M.**, Identification of hypoxic cells using an organotellurium tag compatible with mass cytometry. *Angew Chem. Int. Ed. Engl.* 2014. **53**: 11473–11477.

2056 **Stern, A. D., Rahman, A. H. and Birtwistle, M. R.**, Cell size assays for mass cytometry. *Cytometry A* 2017. **91**: 14–24.

2057 **Rapsomaniki, M. A., Lun, X. K., Woerner, S., Laumanns, M., Bodenmiller, B. and Martinez, M. R.**, CellCycleTRACER accounts for cell cycle and volume in mass cytometry data. *Nat. Commun.* 2018. **9**: 632.

2058 **Budzinski, L., Schulz, A. R., Baumgart, S., Burns, T., Rose, T., Hirseland, H. and Mei, H. E.**, Osmium-labeled microspheres for bead-based assays in mass cytometry. *J. Immunol.* 2019. **202**: 3103–3112.

2059 **Bringeland, G. H., Bader, L., Blaser, N., Budzinski, L., Schulz, A. R., Mei, H. E., Myhr, K. M. et al.**, Optimization of receptor occupancy assays in mass cytometry: standardization across channels with QSC beads. *Cytometry A* 2019. **95**: 314–322.

2060 **Ornatsky, O. I., Lou, X., Nitz, M., Schafer, S., Sheldrick, W. S., Baranov, V. I., Bandura, D. R. et al.**, Study of cell antigens and intracellular DNA by identification of element-containing labels and metallointercalators using inductively coupled plasma mass spectrometry. *Anal. Chem.* 2008. **80**: 2539–2547.

2061 **Blair, T. A., Michelson, A. D. and Frelinger, A. L., 3rd**, Mass cytometry reveals distinct platelet subtypes in healthy subjects and novel alterations in surface glycoproteins in Glanzmann thrombasthenia. *Sci. Rep.* 2018. **8**: 10300.

2062 **Lee, B. H. and Rahman, A. H.**, Acquisition, Processing, and Quality Control of Mass Cytometry Data. *Methods Mol. Biol.* 2019. **1989**: 13–31.

2063 **Fienberg, H. G., Simonds, E. F., Fantl, W. J., Nolan, G. P. and Bodenmiller, B.**, A platinum-based covalent viability reagent for single-cell mass cytometry. *Cytometry A* 2012. **81**: 467–475.

2064 **Leipold, M. D. and Maecker, H. T.**, Phenotyping of live human PBMC using CyTOFTM mass cytometry. *bio-protocol* 2015. **5**: e1382.

2065 **Han, G., Spitzer, M. H., Bendall, S. C., Fantl, W. J. and Nolan, G. P.**, Metal-isotope-tagged monoclonal antibodies for high-dimensional mass cytometry. *Nat. Protoc.* 2018. **13**: 2121–2148.

2066 **Han, G., Chen, S. Y., Gonzalez, V. D., Zunder, E. R., Fantl, W. J. and Nolan, G. P.**, Atomic mass tag of bismuth-209 for increasing the immunoassay multiplexing capacity of mass cytometry. *Cytometry A* 2017. **91**: 1150–1163.

2067 **Horowitz, A., Strauss-Albee, D. M., Leipold, M., Kubo, J., Nemat-Gorgani, N., Dogan, O. C., Dekker, C. L. et al.**, Genetic and environmental determinants of human NK cell diversity revealed by mass cytometry. *Sci. Transl. Med.* 2013. **5**: 208ra145.

2068 **Leipold, M. D., Newell, E. W. and Maecker, H. T.**, Multiparameter phenotyping of human PBMCs using mass cytometry. *Methods Mol. Biol.* 2015. **1343**: 81–95.

2069 **Olsen, L. R., Leipold, M. D., Pedersen, C. B. and Maecker, H. T.**, The anatomy of single cell mass cytometry data. *Cytometry A* 2018.

2070 **Robinson, J. P., Patsekin, V., Holdman, C., Ragheb, K., Sturgis, J., Fatig, R., Avramova, L. V. et al.**, High-throughput secondary screening at the single-cell level. *J. Lab. Automat.* 2012. **18**: 85–98.

2071 **Robinson, J. P., Durack, G. and Kelley, S.**, An innovation in flow cytometry data collection & analysis producing a correlated multiple sample analysis in a single file. *Cytometry* 1991. **12**: 82–90.

2072 **Newell, E., Bendall, S., Hong, D., Lewis, D., Nolan, G. and Davis, M.**, Surveying the influenza-specific cytotoxic T cell response in humans and mice using mass-cytometry (CyTOF) and combinatorial tetramer staining. *Clin. Immunol.* 2010. **135**: S104–S104.

2073 **Rajwa, B., Venkatapathi, M., Ragheb, K., Banada, P. P., Hirleman, E. D., Lary, T. and Robinson, J. P.** Automated classification of bacterial particles in flow by multiangle scatter measurement and a support vector machine classifier. *Cytometry Part A* 2008. **73A**: 369–379.

2074 **Costa, E. S., Pedreira, C. E., Barrena, S., Lecrevisse, Q., Flores, J., Quijano, S., Almeida, J. et al.**, Automated pattern-guided principal component analysis vs expert-based immunophenotypic classification of B-cell chronic lymphoproliferative disorders: A step forward in the standardization of clinical immunophenotyping. *Leukemia* 2010. **24**: 1927–1933.

2075 **Dundar, M., Akova, F., Yerebakan, H. Z. and Rajwa, B.**, A non-parametric Bayesian model for joint cell clustering and cluster matching: identification of anomalous sample phenotypes with random effects. *BMC Bioinformatics* 2014. **15**: 314.

2076 **Bagwell, C. B., Hunsberger, B. C., Herbert, D. J., Munson, M. E., Hill, B. L., Bray, C. M. and Preffer, F. I.**, Probability state modeling theory. *Cytometry A* 2015. **87**: 646–660.

2077 **Robinson, J. P., Rajwa, B., Patsekin, V. and Davisson, V. J.**, Computational analysis of high throughput flow cytometry data. *Expert Opin. Drug Deliv.* 2012. **7**: 679–693.

2078 **Fulton, R. J., McDade, R. L., Smith, P. L., Kienker, L. J. and Kettman, J. R.** Advanced multiplexed analysis with the FlowMetrix system. *Clin. Chem.* 1997. **43**: 1749–1756.

2079 **Robinson, J. P., Patsekin, V., Gregori, G., Rajwa, B. and Jones, J.**, Multispectral flow cytometry: next generation tools for automated classification. *Microsc. Microanal.* 2005. **11**: 2–3.

2080 **Mair, F. and Prlic, M.**, OMIP-044: 28-color immunophenotyping of the human dendritic cell compartment. *Cytometry A*. 2018. **106**: 255.

2081 **Nolan, J. P. and Condello, D.**, Spectral flow cytometry. *Curr. Protoc. Cytom.* 2013. Chapter 1:Unit1.27–1.27.13.

2082 **Bagwell, C. B. and Adams, E. G.**, Fluorescence spectral overlap compensation for any number of flow cytometry parameters. *Ann. N. Y. Acad. Sci.* 1993. **677**: 167–184.

2083 **Roederer, M.**, Compensation is not dependent on signal intensity or on number of parameters. *Cytometry*. 2001. **46**: 357–359.

2084 **Perfetto, S. P., Chattopadhyay, P. K. and Roederer, M.**, Seventeen-colour flow cytometry: unravelling the immune system. *Nat. Rev. Immunol.* 2004. **4**: 648–655.

2085 **Mahnke, Y. D., Brodie, T. M., Sallusto, F., Roederer, M., Lugli, E.**, The who's who of T-cell differentiation: human memory T-cell subsets. *Eur. J. Immunol.* 2013. **43**: 2797–2809.

2086 **Herzenberg, L. A., Tung, J., Moore, W. A., Herzenberg, L. A. and Parks, D. R.**, Interpreting flow cytometry data: a guide for the perplexed. *Nat. Immunol.* 2006. **7**: 681–685.

2087 **Gerner, M. Y., Kastenmüller, W., Ifrim, I., Kabat, J. and Germain, R. N.**, Histo-cytometry: a method for highly multiplex quantitative tissue imaging analysis applied to dendritic cell subset microanatomy in lymph nodes. *Immunity*. 2012. **37**: 364–376.

2088 **Ashhurst, T. M., Smith, A. L. and King, N. J. C.**, *High-dimensional fluorescence cytometry*. John Wiley & Sons, Inc., Hoboken, NJ 2017. 5.8.1–5.8.38.

2089 **Picelli, S., Faridani, O. R., Björklund, A. K., Winberg, G., Sagasser, S. and Sandberg, R.**, Full-length RNA-seq from single cells using Smart-seq2. *Nat. Protoc.* 2014. **9**: 171–181.

2090 **Lafzi, A., Moutinho, C., Picelli, S. and Heyn, H.**, Tutorial: guidelines for the experimental design of single-cell RNA sequencing studies. *Nat. Protoc.* 2018. **13**: 2742–2757.

2091 **Macosko, E. Z., Basu, A., Satija, R., Nemesh, J., Shekhar, K., Goldman, M., Tirosh, I. et al.**, Highly parallel genome-wide expression profiling of individual cells using nanoliter droplets. *Cell*. 2015. **161**: 1202–1214.

2092 **Klein, A. M., Mazutis, L., Akartuna, I., Tallapragada, N., Veres, A., Li, V., Peshkin, L. et al.**, Droplet barcoding for single-cell transcriptomics applied to embryonic stem cells. *Cell*. 2015. **161**: 1187–1201.

2093 **Valihrach, L., Androvic, P. and Kubista, M.**, Platforms for single-cell collection and analysis. *Int. J. Mol. Sci.* 2018. **19**: 807.

2094 **Cao, J., Packer, J. S., Ramani, V., Cusanovich, D. A., Huynh, C., Daza, R., Qiu, X. et al.**, Comprehensive single-cell transcriptional profiling of a multicellular organism. *Science*. 2017. **357**: 661–667.

2095 **Bucevičius, J., Lukinavičius, G. and Gerasimaitė, R.**, The use of Hoechst dyes for DNA staining and beyond. *Chemosensors*. 2018. **6**: 18.

2096 **Smith, P. J., Blunt, N., Wiltshire, M., Hoy, T., Teesdale-Spittle, P., Craven, M. R., Watson, J. V. et al.**, Characteristics of a novel deep red/infrared fluorescent cell-permeant DNA probe, DRAQ5, in intact human cells analyzed by flow cytometry, confocal and multiphoton microscopy. *Cytometry*. 2000. **40**: 280–291.

2097 **Wlodkowic, D., Skommer, J. and Darzynkiewicz, Z.**, Flow cytometry-based apoptosis detection. *Methods Mol. Biol.* 2009. **559**: 19–32.

2098 **Belloc, F., Belaud-Rotureau, M. A., Lavignolle, V., Bascans, E., Braz-Pereira, E., Durrieu, F. and Lacombe, F.**, Flow cytometry detection of caspase 3 activation in preapoptotic leukemic cells. *Cytometry*. 2000. **40**: 151–160.

2099 **Shapiro, H. M.**, *Practical flow cytometry*. Wiley-Liss, Hoboken, NJ 2003.

2100 **Riddell, A., Gardner, R., Perez-Gonzalez, A., Lopes, T. and Martinez, L.**, Rmax: a systematic approach to evaluate instrument sort performance using center stream catch. *Methods*. 2015. **82**: 64–73.

2101 **Ziegenhain, C., Vieth, B., Parekh, S., Reinius, B., Guillaumet-Adkins, A., Smets, M., Leonhardt, H. et al.**, Comparative analysis of single-cell RNA sequencing methods. *Mol. Cell*. 2017. **65**: 631–643.

2102 **Semrau, S., Goldmann, J. E., Soumillon, M., Mikkelsen, T. S., Jaenisch, R. and van Oudenaarden, A.**, Dynamics of lineage commitment revealed by single-cell transcriptomics of differentiating embryonic stem cells. *Nat. Commun.* 2017. **8**: 243.

2103 **Patel, A. P., Tirosh, I., Trombetta, J. J., Shalek, A. K., Gillespie, S. M., Wakimoto, H., Cahill, D. P. et al.**, Single-cell RNA-seq highlights intratumoral heterogeneity in primary glioblastoma. *Science*. 2014. **344**: 1396–1401.

2104 **Lopez, R., Regier, J., Cole, M. B., Jordan, M. I. and Yosef, N.**, Deep generative modeling for single-cell transcriptomics. *Nat. Methods*. 2018. **15**: 1053–1058.

2105 **Bacher, R. and Kendziorski, C.**, Design and computational analysis of single-cell RNA-sequencing experiments. *Genome Biol.* 2016. **17**: 63.

2106 **Vallejos, C. A., Marioni, J. C. and Richardson, S.**, BASiCS: Bayesian analysis of single-cell sequencing data *PLoS Comput. Biol.* 2015. **11**: e1004333.

2107 **Anders, S. and Huber, W.**, Differential expression analysis for sequence count data. *Genome Biol.* 2010. **11**: R106.

2108 **Robinson, M. D. and Oshlack, A.**, A scaling normalization method for differential expression analysis of RNA-seq data. *Genome Biol.* 2010. **11**: R25.

2109 **Bullard, J. H., Purdom, E., Hansen, K. D. and Dudoit, S.**, Evaluation of statistical methods for normalization and differential expression in mRNA-Seq experiments. *BMC Bioinformatics*. 2010. **11**: 94.

2110 **Bacher, R., Chu, L-F, Leng, N., Gasch, A. P., Thomson, J. A., Stewart, R. M., Newton, M. et al.**, SCnorm: robust normalization of single-cell RNA-seq data. *Nat. Methods*. 2017. **14**: 584–586.

2111 **Lun, A. T. L., Bach, K. and Marioni, J. C.**, Pooling across cells to normalize single-cell RNA sequencing data with many zero counts. *Genome Biol.* 2016. **17**: 75.

2112 **Butler, A., Hoffman, P., Smibert, P., Papalexi, E. and Satija, R.**, Integrating single-cell transcriptomic data across different conditions, technologies, and species. *Nat. Biotechnol.* 2018. **36**: 411–420.

2113 **Abdi, H. and Williams, L. J.**, Principal component analysis. *Wiley Interdiscip. Rev. Comput. Stat.* 2010. **2**: 433–459.

2114 **Ståhlberg, A. and Bengtsson, M.**, Single-cell gene expression profiling using reverse transcription quantitative real-time PCR. *Methods*. 2010. **50**: 282–288.

2115 **Ståhlberg, A., Bengtsson, M., Hemberg, M. and Semb, H.**, Quantitative transcription factor analysis of undifferentiated single human embryonic stem cells. *Clin. Chem.* 2009. **55**: 2162–2170.

2116 **Kiselev, V. Y., Kirschner, K., Schaub, M. T., Andrews, T., Yiu, A., Chandra, T., Natarajan, K. N. et al.**, SC3: consensus clustering of single-cell RNA-seq data. *Nat. Methods*. 2017. **14**: 483–486.

2117 **Soneson, C. and Robinson, M. D.**, Bias, robustness and scalability in single-cell differential expression analysis. *Nat. Methods*. 2018. **15**: 255–261.

2118 **Koch, C. and Muller, S.**, Personalized microbiome dynamics—cytometric fingerprints for routine diagnostics. *Mol. Aspects Med*. 2018. **59**: 123–134.

2119 **Muller, S.**, Modes of cytometric bacterial DNA pattern: a tool for pursuing growth. *Cell Prolif.* 2007. **40**: 621–639.

2120 **Delgado-Baquerizo, M., Oliverio, A. M., Brewer, T. E., Benavent-Gonzalez, A., Eldridge, D. J., Bardgett, R. D., Maestre, F. T. et al.**, A global atlas of the dominant bacteria found in soil. *Science* 2018. **359**: 320–325.

2121 **Koch, C., Harnisch, F., Schroder, U. and Muller, S.**, Cytometric fingerprints: evaluation of new tools for analyzing microbial community dynamics. *Front Microbiol.* 2014. **5**: 273.

2122 **Zimmermann, J., Hubschmann, T., Schattenberg, F., Schumann, J., Durek, P., Riedel, R., Friedrich, M. et al.**, High-resolution microbiota flow cytometry reveals dynamic colitis-associated changes in fecal bacterial composition. *Eur. J. Immunol.* 2016. **46**: 1300–1303.

2123 **Vandeputte, D., Kathagen, G., D'Hoe, K., Vieira-Silva, S., Valles-Colomer, M., Sabino, J., Wang, J. et al.**, Quantitative microbiome profiling links gut community variation to microbial load. *Nature* 2017. **551**: 507–511.

2124 **Muller, S. and Nebe-von-Caron, G.**, Functional single-cell analyses: flow cytometry and cell sorting of microbial populations and communities. *FEMS Microbiol. Rev.* 2010. **34**: 554–587.

2125 **Lambrecht, J., Schattenberg, F., Harms, H. and Mueller, S.**, Characterizing microbiome dynamics—flow cytometry based workflows from pure cultures to natural communities. *J. Vis. Exp.* 2018.

2126 **Gunther, S., Hubschmann, T., Rudolf, M., Eschenhagen, M., Roske, I., Harms, H. and Muller, S.**, Fixation procedures for flow cytometric analysis of environmental bacteria. *J. Microbiol. Methods* 2008. **75**: 127–134.

2127 **Shi, L., Gunther, S., Hubschmann, T., Wick, L. Y., Harms, H. and Muller, S.**, Limits of propidium iodide as a cell viability indicator for environmental bacteria. *Cytometry A* 2007. **71**: 592–598.

2128 **Props, R., Rubbens, P., Besmer, M., Buysschaert, B., Sigrist, J., Weilenmann, H., Waegeman, W. et al.**, Detection of microbial disturbances in a drinking water microbial community through continuous acquisition and advanced analysis of flow cytometry data. *Water Res.* 2018. **145**: 73–82.

2129 **Stepanauskas, R., Fergusson, E. A., Brown, J., Poulton, N. J., Tupper, B., Labonte, J. M., Becraft, E. D. et al.**, Improved genome recovery and integrated cell-size analyses of individual uncultured microbial cells and viral particles. *Nat. Commun.* 2017. **8**: 84.

2130 **Jahn, M., Seifert, J., von Bergen, M., Schmid, A., Buhler, B. and Muller, S.**, Subpopulation-proteomics in prokaryotic populations. *Curr. Opin. Biotechnol.* 2013. **24**: 79–87.

2131 **Liu, Z., Cichocki, N., Hubschmann, T., Suring, C., Ofiteru, I. D., Sloan, W. T., Grimm, V. et al.**, Neutral mechanisms and niche differentiation in steady-state insular microbial communities revealed by single cell analysis. *Environ. Microbiol.* 2019. **21**: 164–181.

2132 **Koch, C., Gunther, S., Desta, A. F., Hubschmann, T. and Muller, S.**, Cytometric fingerprinting for analyzing microbial intracommunity structure variation and identifying subcommunity function. *Nat. Protoc.* 2013. **8**: 190–202.

2133 **Rogers, W. T. and Holyst, H. A.**, FlowFP: A Bioconductor Package for Fingerprinting Flow Cytometric Data. *Adv. Bioinformatics* 2009. 193947.

2134 **De Roy, K., Clement, L., Thas, O., Wang, Y. and Boon, N.**, Flow cytometry for fast microbial community fingerprinting. *Water Res.* 2012. **46**: 907–919.

2135 **Koch, C., Fetzer, I., Harms, H. and Muller, S.**, CHIC-an automated approach for the detection of dynamic variations in complex microbial communities. *Cytometry A* 2013. **83**: 561–567.

2136 **Schroder, K. and Tschopp, J.**, The inflammosomes. *Cell* 2010. **140**: 821–832.

2137 **Aachoui, Y., Sagulenko, V., Miao, E. A. and Stacey, K. J.**, Inflammasomemediated pyroptotic and apoptotic cell death, and defense against infection. *Curr. Opin. Microbiol.* 2013. **16**: 319–326.

2138 **Miao, E. A., Rajan, J. V. and Aderem, A.**, Caspase-1-induced pyroptotic cell death. *Immunol. Rev.* 2011. **243**: 206–214.

2139 **Jin, C. and Flavell, R.A.**, Molecular mechanism of NLRP3 inflammasome activation. *J. Clin. Immunol.* 2010. **30**: 628–631.

2140 **Lamkanfi, M.**, Emerging inflammasome effector mechanisms. *Nat. Rev. Immunol.* 2011. **11**: 213–220.

2141 **Vajjhala, P. R., Lu, A., Brown, D. L., Pang, S. W., Sagulenko, V., Sester, D. P., Cridland, S. O. et al.**, The inflammasome adaptor ASC induces procaspase-8 death effector domain filaments. *J. Biol. Chem.* 2015. 4;**290**: 29217–29230.

2142 **Man, S. M., Tourlomousis, P., Hopkins, L., Monie, T. P., Fitzgerald, K. A. and Bryant, C. E.**, Salmonella infection induces recruitment of Caspase-8 to the inflammasome to modulate IL-1beta production. *J. Immunol.* 2013. **191**: 5239–5246.

2143 **Agostini, L., Martinon, F., Burns, K., McDermott, M. F., Hawkins, P. N. and Tschopp, J.**, NALP3 forms an IL-1beta-processing inflammasome with increased activity in Muckle-Wells autoinflammatory disorder. *Immunity* 2004. **20**: 319–325.

2144 **Martinon, F., Agostini, L., Meylan, E. and Tschopp, J.**, Identification of bacterial muramyl dipeptide as activator of the NALP3/cryopyrin inflammasome. *Curr. Biol.* 2004. **14**: 1929–1934.

2145 **Sagulenko, V., Thygesen, S. J., Sester, D. P., Idris, A., Cridland, J. A., Vajjhala, P. R., Roberts, T. L., Schroder, K., Vince, J. E., Hill, J. M. Silke, J. and Stacey K. J.**, AIM2 and NLRP3 inflammasomes activate both apoptotic and pyroptotic death pathways via ASC. *Cell Death Differ.* 2013. **20**: 1149–1160.

2146 **Masumoto, J., Taniguchi, S., Ayukawa, K., Sarvotham, H., Kishino, T., Niikawa, N., Hidaka, E. et al.**, ASC, a novel 22-kDa protein, aggregates during apoptosis of human promyelocytic leukemia HL-60 cells. *J. Biol. Chem.* 1999. **274**: 33835–33838.

2147 **Franklin, B. S., Bossaller, L., De Nardo, D., Ratter, J. M., Stutz, A., Engels, G., Brenker, C. et al.**, The adaptor ASC has extracellular and 'prionoid' activities that propagate inflammation. *Nat. Immunol.* 2014. **15**: 727–737.

2148 **Baroja-Mazo, A., Martín-Sánchez, F., Gomez, A. I., Martínez, C. M., Amores-Iniesta, J., Compan, V., Barberà-Cremades, M. et al.**, The NLRP3 inflammasome is released as a particulate danger signal that amplifies the inflammatory response. *Nat. Immunol.* 2014. **15**: 738–748.

2149 **Venegas, C., Kumar, S., Franklin, B. S., Dierkes, T., Brinkschulte, R., Tejera, D., Vieira-Saecker, A. et al.**, Microglia-derived ASC specks cross-seed amyloid-β in Alzheimer's disease. *Nature* 2017. **552**: 355–361.

2150 **Pollard, K. M. and Kono, D. H.**, Requirements for innate immune pathways in environmentally induced autoimmunity. *BMC Med.* 2013. **11**: 100.

2151 **Master, S. L.**, Specific inflammasomes in complex diseases. *Clin. Immunol.* 2013. **143**: 223–228.

2152 **Rubartelli, A.**, Redox control of NLRP3 inflammasome activation in health and disease. *J. Leukoc. Biol.* 2012. **92**: 951–958.

2153 **Heneka, M. T., Kummer, M. P., Stutz, A., Delekate, A., Schwartz, S., Vieira-Saecker, A., Griep, A. et al.**, NLRP3 is activated in Alzheimer's disease and contributes to pathology in APP/PS1 mice. *Nature* 2013. **493**: 674–678.

2154 **Saresella, M., La Rosa, F., Piancone, F., Zoppis, M., Marventano, I., Calabrese, E., Rainone, V., Nemni, R. et al.**, The NLRP3 and NLRP1 inflammasomes are activated in Alzheimer's disease. *Mol. Neurodegener* 2016. **11**(1): 23.

2155 **Saresella, M., Piancone, F., Marventano, I., Zoppis, M., Hernis, A., Zanette, M., Trabattoni, D. et al.**, Multiple Inflammasome Complexes are Activated in Autistic Spectrum Disorders. *Brain Behav. Immun.* 2016. **57**: 125–133.

2156 **Piancone, F., Saresella, M., Marventano, I., La Rosa, F., Santangelo, M. A., Caputo, D., Mendozzi, L., Rovaris, M. et al.**, Monosodium urate crystals activate the inflammasome in primary progressive multiple sclerosis. *Front. Immunol.* 2018. **9**: 983.

2157 **Bandera, A., Masetti, M., Fabbiani, M., Biasin, M., Muscatello, A., Squillace, N., Clerici, M. et al.**, The NLRP3 Inflammasome is Upregulated in HIV-Infected ART-treated Individuals with Defective Immune Recovery. *Front. Immunol.* 2018. **9**: 214.

2158 **Nagar, A., DeMarco, R. A. and Harton, J. A.**, Inflammasome and caspase-1 activity characterization and evaluation: An imaging flow cytometer-based detection and assessment of inflammasome specks and caspase-1 activation. *J. Immunol.* 2019. **202**: 1003–1015.

2159 **Hooijberg, J. H. Broxterman H. J., Kool M., Assaraf Y. G., Peters G. J., Noordhuis P. and Scheper R. J.**, Antifolate resistance mediated by the multidrug resistance proteins MRP1 and MRP2. *Cancer Res.* 1999. **59**: 2532–2535.

2160 **Zeng, H. et al.**, Transport of methotrexate (MTX) and folates by multidrug resistance protein (MRP) 3 and MRP1: effect of polyglutamylation on MTX transport. *Cancer Res.* 2001. **61**: 7225–7232.

2161 **Volk, E. L., Farley, K. M., Wu, Y., Li, F., Robey, R. W. and Schneider, E.**, Overexpression of wild-type breast cancer resistance protein mediates methotrexate resistance. *Cancer Res.* 2002. **62**: 5035–5040.

2162 **Sarkadi, B. et al.**, Human multidrug resistance ABCB and ABCG transporters: participation in a chemoimmunity defense system. *Physiol Rev.* 2006. **86**: 1179–1236.

2163 **Lee, N. H.**, Pharmacogenetics of drug metabolizing enzymes and transporters: effects on pharmacokinetics and pharmacodynamics of anticancer agents. *Anticancer Agents Med. Chem.* 2010. **10**: 583–592.

2164 **Porcelli, L., Lemos, C., Peters, G. J., Paradiso, A. and Azzariti, A.**, Intracellular trafficking of MDR transporters and relevance of SNPs. *Curr. Top. Med. Chem.* 2009. **9**: 197–208.

2165 **Damiani, D. et al.**, The prognostic value of P-glycoprotein (ABCB) and breast cancer resistance protein (ABCG2) in adults with de novo acute myeloid leukemia with normal karyotype. *Haematologica* 2006. **91**: 825–828.

2166 **Georges, E., Tsuruo, T. and Ling, V.**, Topology of P-glycoprotein as determined by epitope mapping of MRK-16 monoclonal antibody. *J. Biol. Chem.* 1993. **268**: 1792–1798.

2167 **Vasudevan, S., Tsuruo, T. and Rose, D. R.**, Mode of binding of anti-P-glycoprotein antibody MRK-16 to its antigen. A crystallographic and molecular modeling study. *J. Biol. Chem.* 1998. **273**: 25413–25419.

2168 **Telbisz, A., Hegedüs, C., Özvegy-Laczka, C., Goda, K., Várady, G., Takáts, Z., Szabó, E. et al.**, Antibody binding shift assay for rapid screening of drug interactions with the human ABCG2 multidrug transporter. *Eur. J. Pharm. Sci.* 2012. **45**: 101–109.

2169 **Toldi, G. et al.**, Peripheral lymphocyte multidrug resistance activity as a predictive tool of biological therapeutic response in rheumatoid arthritis. *J. Rheumatol.* 2019. **46**: 572–578.

2170 **Micsik, T. et al.**, MDR-1 and MRP-1 activity in peripheral blood leukocytes of rheumatoid arthritis patients. *Diagn. Pathol.* 2015. **10**: 216.

2171 **Homolya, L., Holló, Z., Germann, U. A., Pastan, I., Gottesman, M. M., Sarkadi, B.** Fluorescent cellular indicators are extruded by the multidrug resistance protein. *J. Biol. Chem.* 1993. **268**: 21493–21496.

2172 **Cortada, C. M. et al.**, Lymphocyte P-glycoprotein variability in healthy individuals. *Medicina* 2009. **69**: 619–624.

2173 **Szerémy, P., Tauberné Jakab, K., Baráth, S., Apjok, A., Filkor, K., Holló, Z., Márki-Zay, J., Kappelmayer, J., Sipka, S., Krajcsi, P., Toldi, G.** Determination of reference values of MDR-ABC transporter activities in CD3+ lymphocytes of healthy volunteers using a flow cytometry based method. *Cytometry B Clin. Cytom.* 2018 https://doi.org/10.1002/cyto.b.21729. [Epub ahead of print].

2174 **Yu, L., Sa, S., Wang, L., Dulmage, K., Bhagwat, N., Yee, S. S., Sen, M. et al.**, An integrated enrichment system to facilitate isolation and molecular characterization of single cancer cells from whole blood. *Cytometry A* 2018. **93**: 1226–1233.

2175 **Hayashi, T., Shibata, N., Okumura, R., Kudome, T., Nishimura, O., Tarui, H. and Agata, K.**, Single-cell gene profiling of planarian stem cells using fluorescent activated cell sorting and its "index sorting" function for stem cell research. *Dev. Growth Differ.* 2010. **52**: 131–144.

2176 **Schulte, R., Wilson, N. K., Prick, J. C., Cossetti, C., Maj, M. K., Gottgens, B. and Kent, D. G.**, Index sorting resolves heterogeneous murine hematopoietic stem cell populations. *Exp. Hematol.* 2015. **43**: 803–811.

2177 **Wilson, N. K., Kent, D. G., Buettner, F., Shehata, M., Macaulay, I. C., Calero-Nieto, F. J., Sanchez Castillo, M. et al.**, Combined single-cell functional and gene expression analysis resolves heterogeneity within stem cell populations. *Cell Stem Cell* 2015. **16**: 712–724.

2178 **Busse, C. E., Czogiel, I., Braun, P., Arndt, P. F. and Wardemann, H.**, Single-cell based high-throughput sequencing of full-length immunoglobulin heavy and light chain genes. *Eur. J. Immunol.* 2014. **44**: 597–603.

2179 **Gee, M. H., Han, A., Lofgren, S. M., Beausang, J. F., Mendoza, J. L., Birnbaum, M. E., Bethune, M. T. et al.**, Antigen identification for orphan T cell receptors expressed on tumor-infiltrating lymphocytes. *Cell* 2018. **172**: 549–563.

2180 **Penter, L., Dietze, K., Bullinger, L., Westermann, J., Rahn, H. P. and Hansmann, L.**, FACS single cell index sorting is highly reliable and determines immune phenotypes of clonally expanded T cells. *Eur. J. Immunol.* 2018. **48**: 1248–1250.

2181 **Penter, L., Dietze, K., Ritter, J., Lammoglia-Cobo, M. F., Garmshausen, J., Aigner, F., Bullinger, L. et al.**, Localization-associated immune phenotypes of clonally expanded tumor-infiltrating T cells and distribution of their target antigens in rectal cancer. *Oncoimmunology* 2019. **8**: e1586409.

2182 **Higdon, L. E., Cain, C. J., Colden, M. A. and Maltzman, J. S.** Optimization of single-cell plate sorting for high throughput sequencing applications. *J. Immunol. Methods* 2019. **466**: 17–23.

2183 **Kleeberger, C. A., Lyles, R. H., Margolick, J. B., Rinaldo, C. R., Phair, J. P. and Giorgi, J. V.**, Viability and recovery of peripheral blood mononuclear cells cryopreserved for up to 12 years in a multicenter study. *Clin. Diagn. Lab. Immunol.* 1999. **6**: 14–19.

2184 **Ruitenberg, J. J., Mulder, C. B., Maino, V. C., Landay, A. L. and Ghanekar, S. A.**, VACUTAINER CPT and Ficoll density gradient separation perform equivalently in maintaining the quality and function of PBMC from HIV seropositive blood samples. *BMC Immunol.* 2006. **7**: 11.

2185 **Grievink, H. W., Luisman, T., Kluft, C., Moerland, M. and Malone, K. E.**, Comparison of three isolation techniques for human peripheral blood mononuclear cells: cell recovery and viability, population composition, and cell functionality. *Biopreserv. Biobank.* 2016. **14**: 410–415.

2186 **Disis, M. L., dela Rosa, C., Goodell, V., Kuan, L-Y, Chang, JCC, Kuus-Reichel, K., Clay, T. M. et al.**, Maximizing the retention of antigen specific lymphocyte function after cryopreservation. *J. Immunol. Methods* 2006. **308**: 13–18.

2187 **Weinberg, A., Song, L-Y, Wilkening, C., Sevin, A., Blais, B., Louzao, R., Stein, D. et al.**, Optimization and limitations of use of cryopreserved peripheral blood mononuclear cells for functional and phenotypic T-cell characterization. *Clin. Vaccine Immunol.* 2009. **16**: 1176–1186.

2188 **Bull, M., Lee, D., Stucky, J., Chiu, Y-L, Rubin, A., Horton, H. and McElrath, M. J.**, Defining blood processing parameters for optimal detection of cryopreserved antigen-specific responses for HIV vaccine trials. *J. Immunol. Methods.* 2007. **322**: 57–69.

2189 **Scheiermann, C., Kunisaki, Y. and Frenette, P. S.**, Circadian control of the immune system. *Nat. Rev. Immunol.* 2013. **13**: 190–198.

2190 **Tompa, A., Nilsson-Bowers, A. and Faresjö, M.**, Subsets of CD4+, CD8+, and CD25hi lymphocytes are in general not influenced by isolation and long-term cryopreservation. *J. Immunol.* 2018. **201**: 1799–1809.

2191 **Seale, A. C., de Jong, B. C., Zaidi, I., Duvall, M., Whittle, H., Rowland-Jones, S. and Jaye, A.**, Effects of cryopreservation on CD4+ CD25+ T cells of HIV-1 infected individuals. *J. Clin. Lab. Anal.* 2008. **22**: 153–158.

2192 **AssumpcióRomeu, M., Mestre, M., González, L., Valls, A., Verdaguer, J., Corominas, M., Bas, J. et al.**, Lymphocyte immunophenotyping by flow cytometry in normal adults. *J. Immunol. Methods* 1992. **154**: 7–10.

2193 **Lemieux, J., Jobin, C., Simard, C. and Néron, S.**, A global look into human T cell subsets before and after cryopreservation using multiparametric flow cytometry and two-dimensional visualization analysis. *J. Immunol. Methods* 2016. **434**: 73–82.

2194 **Wang, L., Hückelhoven, A., Hong, J., Jin, N., Mani, J., Chen, B., Schmitt, M. et al.**, Standardization of cryopreserved peripheral blood mononuclear cells through a resting process for clinical immunomonitoring—development of an algorithm. *Cytometry A.* 2016. **89**: 246–258.

2195 **Holland, M., Cunningham, R., Seymour, L., Kleinsteuber, K., Cunningham, A., Patel, T., Manos, M. et al.**, Separation, banking, and quality control of peripheral blood mononuclear cells from whole blood of melanoma patients. *Cell Tissue Bank.* 2018. **19**: 783–790.

2196 **De Boer, F., Dräger, A. M., Van der Wall, E., Pinedo, H. M. and Schuurhuis, G. J.**, Changes in L-selectin expression on CD34-positive cells upon cryopreservation of peripheral blood stem cell transplants. *Bone Marrow Transplant.* 1998. **22**: 1103–1110.

2197 **Campbell, D. E., Tustin, N. B., Riedel, E., Tustin, R., Taylor, J., Murray, J. and Douglas, S. D.**, Cryopreservation decreases receptor PD-1 and ligand PD-L1 coinhibitory expression on peripheral blood mononuclear cell-derived T cells and monocytes. *Clin. Vaccine Immunol.* 2009. **16**: 1648–1653.

2198 **Zhang, W., Nilles, T. L., Johnson, J. R. and Margolick, J. B.**, The effect of cellular isolation and cryopreservation on the expression of markers identifying subsets of regulatory T cells. *J. Immunol. Methods.* 2016. **431**: 31–37.

2199 **Posevitz-Fejfár, A., Posevitz, V., Gross, C. C., Bhatia, U., Kurth, F., Schütte, V., Bar-Or, A. et al.**, Effects of blood transportation on human peripheral mononuclear cell yield, phenotype and function: implications for immune cell biobanking. *PLoS One.* 2014. **9**: e115920.

2200 **Nemes, E., Kagina, B. M. N., Smit, E., Africa, H., Steyn, M., Hanekom, W. A. and Scriba, T. J.**, Differential leukocyte counting and immunophenotyping in cryopreserved ex vivo whole blood. *Cytometry A.* 2015. **87**: 157–165.

2201 **Maecker, H. T., McCoy, J. P.**, FOCIS Human Immunophenotyping Consortium, **Amos, M., Elliott, J., Gaigalas, A., Wang, L. et al.**, A model for harmonizing flow cytometry in clinical trials. *Nat. Immunol.* 2010. **11**: 975–978.

2202 **Burel, J. G., Qian, Y., Lindestam Arlehamn, C., Weiskopf, D., Zapardiel-Gonzalo, J., Taplitz, R., Gilman, R. H. et al.**, An integrated workflow to assess technical and biological variability of cell population frequencies in human peripheral blood by flow cytometry. *J. Immunol.* 2017. **198**: 1748–1758.

2203 **Bernemann, I., Kersting, M., Prokein, J., Hummel, M., Klopp, N. and Illig, T.**, [Centralized biobanks: a basis for medical research]. *Bundesgesundheitsblatt. Gesundheitsforschung. Gesundheitsschutz.* 2016. **59**: 336–343.

2204 **Labarga, A., Beloqui, I. and Martin, A. G.**, Information Management. *Methods Mol. Biol.* 2017. **1590**: 29–39.

2205 **Bendou, H., Sizani, L., Reid, T., Swanepoel, C., Ademuyiwa, T., Merino-Martinez, R., Meuller, H. et al.**, Baobab laboratory information management system: development of an open-source laboratory information management system for biobanking. *Biopreserv. Biobank.* 2017. **15**: 116–120.

2206 **Mate, S., Kadioglu, D., Majeed, R. W., Stöhr, M. R., Folz, M., Vormstein, P., Storf, H. et al.**, Proof-of-concept integration of heterogeneous biobank IT infrastructures into a hybrid biobanking network. *Stud. Health Technol. Inform.* 2017. **243**: 100–104.

2207 **Consuegra, I., Rodríguez-Aierbe, C., Santiuste, I., Bosch, A., Martínez-Marín, R., Fortuto, M. A., Díaz, T. et al.**, Isolation methods of peripheral blood mononuclear cells in spanish biobanks: an overview. *Biopreserv. Biobank.* 2017. **15**: 305–309.

2208 **Aziz, N., Margolick, J. B., Detels, R., Rinaldo, C. R., Phair, J., Jamieson, B. D. and Butch, A. W.**, Value of a quality assessment program in optimizing cryopreservation of peripheral blood mononuclear cells in a multicenter study. *Clin. Vaccine Immunol.* 2013. **20**: 590–595.

2209 **Ramos, T. V., Mathew, A. J., Thompson, M. L. and Ehrhardt, R. O.**, Standardized cryopreservation of human primary cells. *Curr. Protoc. Cell Biol.* 2014. **64**: A.3I.1-8.

2210 **Xiao, D., Ling, K. H. J., Custodio, J., Majeed, S. R. and Tarnowski, T.**, Quantitation of intracellular triphosphate metabolites of antiretroviral agents in peripheral blood mononuclear cells (PBMCs) and corresponding cell count determinations: review of current methods and challenges. *Expert Opin. Drug Metab. Toxicol.* 2018. **14**: 781–802.

2211 **Becher, F., Pruvost, A. G., Schlemmer, D. D., Créminon, C. A., Goujard, C. M., Delfraissy, J. F., Benech, H. C. et al.**, Significant levels of intracellular stavudine triphosphate are found in HIV-infected zidovudine-treated patients. *AIDS.* 2003. **17**: 555–561.

2212 **Corkum, C. P., Ings, D. P., Burgess, C., Karwowska, S., Kroll, W. and Michalak, T. I.**, Immune cell subsets and their gene expression profiles from human PBMC isolated by Vacutainer Cell Preparation Tube (CPT™) and standard density gradient. *BMC Immunol.* 2015. **16**: 48.

2213 **Angel, S., von Briesen, H., Oh, Y.-J., Baller, M. K., Zimmermann, H. and Germann, A.**, Toward optimal cryopreservation and storage for achievement of high cell recovery and maintenance of cell viability and T cell functionality. *Biopreserv. Biobank.* 2016. **14**: 539–547.

2214 **Angelo, M., Bendall, S. C., Finck, R., Hale, M. B., Hitzman, C., Borowsky, A. D., Levenson, R. M. et al.**, Multiplexed ion beam imaging of human breast tumors. *Nat. Med.* 2014. **20**: 436–442.

2215 **Smets, T., Stevenaert, F., Adams, H. and Vanhoof, G.**, Deep profiling of the immune system of multiple myeloma patients using cytometry by time-of-flight (CyTOF). *Methods Mol. Biol.* 2018. **1792**: 47–54.

2216 **Edwards, B. S. and Sklar, L. A.**, Flow cytometry: impact on early drug discovery. *J. Biomol. Screen* 2015. **20**: 689–707.

2217 **Moffat, J. G., Vincent, F., Lee, J. A., Eder, J. and Prunotto, M.**, Opportunities and challenges in phenotypic drug discovery: an industry perspective. *Nat. Rev. Drug Discov.* 2017. **16**: 531–543.

2218 **Vignali, D. A.**, Multiplexed particle-based flow cytometric assays. *J. Immunol. Methods* 2000. **243**: 243–255.

2219 **Joslin, J., Gilligan, J., Anderson, P., Garcia, C., Sharif, O., Hampton, J., Cohen, S. et al.**, A Fully automated high-throughput flow cytometry screening system enabling phenotypic drug discovery. *SLAS Discov.* 2018. **23**: 697–707.

2220 **Bredemeyer, A. L., Edwards, B. S., Haynes, M. K., Morales, A. J., Wang, Y., Ursu, O., Waller, A. et al.**, High-throughput screening approach for identifying compounds that inhibit nonhomologous end joining. *SLAS Discov.* 2018. **23**: 624–633.

2221 **Buranda, T., Gineste, C., Wu, Y., Bondu, V., Perez, D., Lake, K. R., Edwards, B. S. et al.**, A high-throughput flow cytometry screen identifies molecules that inhibit hantavirus cell entry. *SLAS Discov.* 2018. **23**: 634–645.

2222 **Wang, Y., Yoshihara, T., King, S., Le, T., Leroy, P., Zhao, X., Chan, C. K. et al.**, Automated high-throughput flow cytometry for high-content screening in antibody development. *SLAS Discov.* 2018. **23**: 656–666.

2223 **Martinez, E. M., Klebanoff, S. D., Secrest, S., Romain, G., Haile, S. T., Emtage, P. C. R. and Gilbert, A. E.**, High-throughput flow cytometric method for the simultaneous measurement of CAR-T cell characterization and cytotoxicity against solid tumor cell lines. *SLAS Discov.* 2018. **23**: 603–612.

2224 **Kaur, M. and Esau, L.**, Two-step protocol for preparing adherent cells for high-throughput flow cytometry. *Biotechniques* 2015. **59**: 119–126.

2225 **Chan, B. M., Badh, A., Berry, K. A., Grauer, S. A. and King, C. T.**, Flow cytometry-based epitope binning using competitive binding profiles for the characterization of monoclonal antibodies against cellular and soluble protein targets. *SLAS Discov.* 2018. **23**: 613–623.

2226 **Virginia Litwin, P. M.**, *Flow cytometry in drug discovery and development*. Wiley, Hoboken, NJ 2011.

2227 **Goni-de-Cerio, F., Mariani, V., Cohen, D., Madi, L., Thevenot, J., Oliveira, H., Uboldi, C. et al.**, Biocompatibility study of two diblock copolymeric nanoparticles for biomedical applications by in vitro toxicity testing. *J. Nanopart. Res.* 2013. **15**: 1–17.

2228 **Buenz, E. J., Limburg, P. J. and Howe, C. L.**, A high-throughput 3-parameter flow cytometry-based cell death assay. *Cytometry A* 2007. **71**: 170–173.

2229 **Boitano, A. E., Wang, J., Romeo, R., Bouchez, L. C., Parker, A. E., Sutton, S. E., Walker, J. R. et al.**, Aryl hydrocarbon receptor antagonists promote the expansion of human hematopoietic stem cells. *Science* 2010. **329**: 1345–1348.

2230 **Zhao, Z., Henowitz, L. and Zweifach, A.**, A multiplexed assay that monitors effects of multiple compound treatment times reveals candidate immune-enhancing compounds. *SLAS Discov.* 2018. **23**: 646–655.

2231 **Ding, M., Kaspersson, K., Murray, D. and Bardelle, C.**, High-throughput flow cytometry for drug discovery: principles, applications, and case studies. *Drug Discov. Today* 2017. **22**: 1844–1850.

2232 **Javarappa, K. K., Tsallos, D. and Heckman, C. A.**, A multiplexed screening assay to evaluate chemotherapy-induced myelosuppression using healthy peripheral blood and bone marrow. *SLAS Discov.* 2018. **23**: 687–696.

2233 **Nolan, J. P. and Mandy, F.**, Multiplexed and microparticle-based analyses: quantitative tools for the large-scale analysis of biological systems. *Cytometry A* 2006. **69**: 318–325.

2234 **Moeller, T., Brown, C., Muchow, M. and Yee, B.**, Transcript regulation of 18 ADME genes by prototypical inducers in human hepatocytes. *Drug Metab. Rev.* 2012. **44**: 79–80.

2235 **Liu, Z. and O'Rourke, J.**, Expediting antibody discovery with a cell and bead multiplexed competition assay. *SLAS Discov.* 2018. **23**: 667–675.

2236 **Young, S. M., Bologa, C., Prossnitz, E. R., Oprea, T. I., Sklar, L. A. and Edwards, B. S.**, High-throughput screening with HyperCyt flow cytometry to detect small molecule formylpeptide receptor ligands. *J. Biomol. Screen* 2005. **10**: 374–382.

2237 **Lahl, K., Loddenkemper, C., Drouin, C., Freyer, J., Arnason, J., Eberl, G., Hamann, A. et al.**, Selective depletion of Foxp3+ regulatory T cells induces a scurfy-like disease. *J. Exp. Med.* 2007. **204**: 57–63.

2238 **Zhang, J. H., Chung, T. D. and Oldenburg, K. R.**, A simple statistical parameter for use in evaluation and validation of high throughput screening assays. *J. Biomol. Screen* 1999. **4**: 67–73.

2239 **Moore, J. and Roederer, M.**, The flow cytometry shared resource laboratory: best practices to assure a high-quality, cost-effective partnership with biomedical research laboratories. *Cytometry A* 2009. **75**: 643–649.

2240 **Meder, D. et al.**, Institutional core facilities: prerequisite for breakthroughs in the life sciences: core facilities play an increasingly important role in biomedical research by providing scientists access to sophisticated technology and expertise. *EMBO Rep.* 2016. **17**: 1088–1093.

2241 **Barsky, L. W. et al.**, International Society for Advancement of Cytometry (ISAC) flow cytometry shared resource laboratory (SRL) best practices. *Cytometry A* 2016. **89**: 1017–1030.

2242 **Ferrando-May, E. et al.**, Advanced light microscopy core facilities: Balancing service, science and career. *Microsc. Res. Tech.* 2016. **79**: 463–479.

2243 **Brown, C. M.**, Careers in core facility management. *Cold Spring Harb. Perspect. Biol.* 2018. **10**(8).

2244 **Davies, D., Filby, A. and Lannigan, J.**, Shared Resource Laboratory (SRL) Communications—a new journal type. *Cytometry A* 2018.

2245 **Box, A. C., Park, J., Semerad, C. L., Konnesky, J. and Haug, J. S.**, Cost accounting method for cytometry facilities. *Cytometry A* 2012. **81**: 439–444.

2246 **Petrunkina, A. M.**, Algorithm and metrics for a standardized evaluation of cell sorting service delivery. *Cytometry A* 2013. **83**: 602–607.

2247 **Lennartz, K., Lu, M., Flasshove, M., Moritz, T. and Kirstein, U.**, Improving the biosafety of cell sorting by adaptation of a cell sorting system to a biosafety cabinet. *Cytometry A* 2005. **66**: 119–127.

2248 **Mische, S. and Wilkerson, A.**, Disaster and Contingency Planning for Scientific Shared Resource Cores. *J. Biomol. Tech.* 2016. **27**: 4–17.

2249 **Antal-Szalmás, P., Nagy, B. Jr, Debreceni, I. B. and Kappelmayer, J.**, Measurement of soluble biomarkers by flow cytometry. *EJIFCC* 2013. **23**: 135–142.

2250 **Commenges, D., Alkhassim, C., Gottardo, R., Hejblum, B. and Thiebaut, R.**, cytometree: a binary tree algorithm for automatic gating in cytometry analysis. bioRxiv. 2018 1:335554.

2251 **de Jager, W., te Velthuis, H., Prakken, B. J., Kuis, W. and Rijkers, G. T.**, Simultaneous detection of 15 human cytokines in a single sample of stimulated peripheral blood mononuclear cells. *Clin. Diagn. Lab. Immunol.* 2003. **10**: 133–139.

2252 **DiGiuseppe, J. A., Cardinali, J. L., Rezuke, W. N. and Pe'er, D.**, PhenoGraph and viSNE facilitate the identification of abnormal T-cell populations in routine clinical flow cytometric data. *Cytometry B Clin. Cytom.* 2018. **94**: 744–757.

2253 **Gomaa, A. and Boye, J.**, Simultaneous detection of multi-allergens in an incurred food matrix using ELISA, multiplex flow cytometry and liquid chromatography mass spectrometry (LC–MS). *Food Chem.* 2015. **175**: 585–592.

2254 http://www.cancer.net/cancer-types/sarcoma-soft-tissue/overview

2255 **Maggi, L., Cimaz, R., Capone, M., Santarlasci, V., Rossi, M. C., Mazzoni, A., Montaini, G. et al.**, Immunosuppressive activity of abatacept on circulating T helper lymphocytes from juvenile idiopathic arthritis patients. *Int. Arch. Allergy Immunol.* 2016. **171**: 45–53.

2256 **Maueröder, C., Chaurio, R. A., Dumych, T., Podolska, M., Lootsik, M. D., Culemann, S., Friedrich, R. P. et al.**, A blast without power—cell death induced by the tuberculosis-necrotizing toxin fails to elicit adequate immune responses. *Cell Death Differ.* 2016. **23**: 1016–1025.

2257 **Munoz, L. E., Maueroder, C., Chaurio, R., Berens, C., Herrmann, M. and Janko, C.**, Colourful death: six-parameter classification of cell death by flow cytometry–dead cells tell tales. *Autoimmunity* 2013. **46**: 336–341.

2258 **Salvioli, S., Ardizzoni, A., Franceschi, C. and Cossarizza, A.**, JC-1, but not DiOC6(3) or rhodamine 123, is a reliable fluorescent probe to assess AW changes in intact cells: implications for studies on mitochondrial functionality during apoptosis. *FEBS Lett.* 1997. **411**: 77–82.

Abbreviations: **7AAD**: 7-aminoactinomycin D · **ab**: antibody · **ADC**: analog-to-digital conversion · **ADCC**: antibody dependent cellular cytotoxicity · **AHR**: aryl hydrocarbon receptor · **AM**: acetoxymethyl · **AMPK**: 5AMP-activated protein kinase · **ANX-V**: annexin-V · **AO**: acridine orange · **APC**: allophycocyanin · **APD**: avalanche photodiodes · **APS**: ammonium peroxodisulfate · **ASCs**: antibody-secreting cells · **ATCC**: American type tissue collection · **ATGs**: autophagy related genes · **AxA5**: fluorophore-conjugated annexin A5 · **BafA**: bafilomycin A1 · **BAFF**: Bcell activating factor · **BCL6**: B-cell lymphoma 6 · **BD**: Becton Dickinson · **bDNA**: branched DNA technology · **BDS**: bright detail similarity · **BF**: brightfield · **BFA**: brefeldin A · **BISC**: Bioinformatics Integration Support Contract · **BM**: bone marrow · **BP**: band pass · **BrdU**: 5-bromo-2-deoxyuridine · **BSA**: bovine serum albumin · **BV**: brilliant violet · **CCCP**: carbonyl cyanide 3-chloro phenyl hydrazine · **CCDs**: charge-coupled devices · **CLL**: chronic lymphocytic leukemia · **cDCs**: classical DCs · **CDR**: complementarity determining regions · **CEA**: carcinoembryonal · **CECs**: circulating endothelial cells · **CFSE**: carboxyfluorescein succinimidyl ester · **CFU-F**: colony-forming units-fibroblasts · **CIMT**: cancer immunotherapy consortium · **CIP**: CIMT immunoguiding program · **CK**: cytokeratin 18 · **CM**: central memory · **cMOP**: common monocyte precursors · **CMV**: cytomegalovirus · **CS&T**: cytometer setup and tracking · **CSF**: cerebrospinal fluid · **CT**: cancer-testis · **CTCs**: circulating tumor cells · **CTL**: cytolytic cells · **CV**: coefficient of variation · **CW**: continuous wave · **Cy**: cyanine · **CyTOF**: Cytometry by Time-Of-Flight · **DAIT**: Division of Allergy, Immunology, and Transplantation · **DAMP**: danger-associated molecular patterns · **DAPI**: 4,6-diamidine-2-phenylindole · **DCF**: 2,7-dichlorofluorescein · **DCFDA**: 2-7-dichlorodihydrofluorescein diacetate · **DCs**: dendritic cells · **DCV**: dyecycle violet · **DHR**: dihydrorhodamine · **DIOC6**: 3,3-dihexyloxacarbocyanine iodide · **DLD**: deterministic lateral displacement · **DLP**: dichroic longpass · **DMSO**: dimethyl sulfoxide · **DNase**: deoxyribonuclease · **DNR**: dynamic detection range · **DPBS**: Dulbecco's phosphate buffered saline · **DPEC**: double positive effector cells · **E:T**: effector-to-target cell · **ECI 2015**: European Congress of Immunology ECI 2015 · **EdU**: 5-ethynyl-2-deoxyuridine · **EGFR**: epidermal growth factor receptor · **EM**: effector memory cells · **ENOBs**: effective number of bits · **ERK pathway**: extracellular-signal regulated kinase pathway · **ESCCA**: European Society for Clinical Cell Analysis · **FACS**: fluorescence activated cell sorting · **FBS**: fetal bovine serum · **Fc**: fragment of immunoglobulins · **FCCP**: carbonyl cyanide-4- (trifluoromethoxy)phenylhydrazone · **FCM**: flow cytometry · **FCS**: fetal calf serum · **FCS**: flow cytometry standard · **FDA**: fluorescein-diacetate · **FGFR**: fibroblast growth factor receptor · **FISH**: fluorescent in situ hybridization · **FITC**: fluorescein isothiocyanate · **FL1-10**: fluorescence channels · **FLIMs**: fluorescent life time measurements · **FMK**: fluoromethyl ketone · **FMO**: fluorescence minus one · **FOCIS**: Federation of Clinical Immunology Societies · **FOXP3**: forkhead box P3 · **FSC**: forward scatter · **GATA3**: GATA binding protein-3 · **GFP**: green fluorescent protein · **GUIs**: graphical user interfaces · **GZMB**: granzyme B · **HBSS**: Hank's balanced saline solution · **HCC**: hepatocellular carcinoma · **HCS**: hematopoietic progenitor cells · **HHV8**: human herpesvirus 8 · **HIPAA**: Health Insurance Portability and Accountability Act · **HIPC**: Human Immunology Project Consortium · **HIV**: Human immunodeficiency virus · **HLA**: human leukocyte antigen · **HSC**: hematopoietic stem cell · **HTS**: high throughput system · **IBD**: inflammatory bowel disease · **ICCS**: International Clinical Cytometry Society · **ICPC TOF-MS**: inductively-coupled plasma time of flight mass spectrometry · **IdU**: Iodo-2-deoxyuridine · **IFN**: interferon · **Ig**: immunoglobulin · **IL**: interleukin · **ILCs**: innate lymphoid cells · **ImmPort**: immunology database and analysis portal · **iono**: ionomycin · **IRF4**: interferon regulatory factor 4 · **ISAC**: International Society for Analytical Cytology · **ISR**: internal store release · **ITAM**: immune-receptor tyrosinebased activating motifs · **ITIM**: immune-receptor tyrosine-based inhibition motif · **KIRs**: killer Ig-like receptors · **KLH**: keyhole limpet hemocyanin · **KLRG1**: killer cell lectin-like receptor G1 · **K-S**: Kolmogorov-Smirnov statistic · **L/D**: live dead · **LCA**: leukocyte common antigen · **Lin**: lineage markers · **Lin−**: lineage-negative · **lncRNA**: long non-coding RNA · **LmP**: lamina propria · **LP**: long pass · **LPS**: lipopolysaccharide · **LRR**: leucine-rich repeat · **LRR-CT**: LRR C-terminal capping · **LRR-NT**: LRR N-terminal · **LTi**: lymphoid tissue-inducer cells · **mAb**: monoclonal antibody · **MAP kinase**: membrane activated protein kinase · **MARS-seq**: massive parallel single-cell RNA-seq · **mBCs**: memory B cells · **MCs**: mononuclear cells · **MdFI**: median fluorescence intensity · **MDP**: monocyte/macrophage-DC precursors · **MFI**: mean fluorescence intensity · **MHC**: major histocompatibility complex · **MIBBI**: minimum information for biological and biomedical investigations · **MIBI**: multiplexed ion beam imaging · **MIFloCyt**: minimum information about a flow cytometry experiment · **mitoPY**: mitochondria peroxy yellow-1 · **MitoSOX**: mitochondrial superoxide indicator · **MMM**: metal-minusmany · **MN**: monensin · **MoDC**: monocyte-derived DC · **MPEC**: memoryprecursor effector cells · **mRNA**: messenger RNA · **MSPCs**: mesenchymal stem and progenitor cells · **mt**: mitochondrial · **mtmP**: mitochondrial membrane potential · **mTOR**: mammalian target of rapamycin complex 1 · **NAO**: nonyl acridine orange · **NIAID**: National Institute of Allergy and Infectious Diseases · **NIH**: National Institutes of Health · **NIR**: near infrared · **NK**: natural killer · **NLOs**: non-lymphoid organs · **NSCLC**: non-small cell lung cancer · **NYSTEM Program**: New York State Department of Health Program · **OH**: hydroxyl radicals · **OMIP**: optimized multicolor immunofluorescence panels · **OVA**: ovalbumin · **OxPhos**: oxidative phosphorylation · **PI3K**: Phosphatidylinositol-4,5- bisphosphate 3-kinase · **PAMPs**: pathogen-associated molecular patterns · **PB**: peripheral blood · **PBMC**: peripheral blood mononuclear cells · **PBPC**: peripheral blood progenitor cell · **PBS**: phosphate buffered saline · **PD-1**: programmed cell death protein 1 · **PDGFR**: platelet-derived growth factor receptor · **PEA**: phosphatidylethanolamine · **PE**: phycoerythrin · **PerCP**: peridinin-chlorophyll · **PI**: propidium iodide · **PMA**: phorbol 12-myristate 13-acetate · **PMT**: photomultiplier tube · **PP**: phagocytosis product · **PS**: phosphatidylserine · **PVP**: polyvinylpyrrolidone · **PY(G)**: pyronin Y(G) · **RAR**: retinoic acid receptor · **RCC**: renal cell carcinoma · **Rho123**: rhodamine-123 · **RNase**: ribonuclease · **ROR-γt**: retinoic acid receptor-related orphan receptor gamma t · **RORγtfm**: RORγt fate mapping · **ROS**: reactive oxygen species · **RPMI 1640**: Roswell Park Memorial Institute 1640 · **RT**: room temperature · **SAPK/JNK pathway**: stress-activated protein kinase/c-jun n-terminal kinase · **SAW**: surface acoustic waves · **SB**: staining buffer · **SD**: standard deviation · **SE**: standard error · **SEB**: Staphylococcus enterotoxin B · **SERS**: surface enhanced Raman scattering · **SI**: small intestinal · **SIP**: sample injection port · **SLE**: systemic lupus erythematosus · **SLEC**: short-lived effector cells · **SLOs**: secondary lymphoid organs · **SMO**: signal-minus-one · **SNRs**: signal-tonoise ratios · **SOCE**: store-operated Ca2+ entry · **SOV**: spillover

value · **SP**: short pass · **SPADE**: Spanning-tree progression analysis of densitynormalized data · **β2m**: beta-2-microglobulin · **SSC**: side scatter · **SSM**: spillover-spreading matrix · **TAA**: tumor-associates antigens · **Tcon**: conventional T cells · **TCR**: T cell receptor · **TCRtg**: TCR-transgenic · **TdT**: terminal deoxynucleotidyltransferase · **Th cells**: T helper cells · **TIA**: transimpedance · **TM**: memory T lymphocytes · **TMRE**: tetramethylrhodamine · **TNF**: tumor necrosis factor · **TOF**: time-of-flight · **Treg**: regulatory T cells · **TRAIL**: TNF-related apoptosis-inducing ligand · **TSLP**: thymic stromal lymphopoietin · **t-SNE**: t-distributed stochastic neighbor embedding · **TUNEL**: TdT-mediated dUTP nick end labelling · **VA**: voltage · **ULK1**: Serine/threonine-protein kinase ULK1 · **UV**: ultraviolet · **Var**: variance · **VLR**: variable lymphocyte receptor · **Vps34**: vacuolar protein sorting34 · **WDM**: wavelength division multiplexer

Full correspondence: Prof. Andrea Cossarizza and Dr. Hyun-Dong Chang
e-mail: andrea.cossarizza@unimore.it; chang@drfz.de

